

DAMS AND RESERVOIRS UNDER CHANGING CHALLENGES

PROCEEDINGS OF THE INTERNATIONAL SYMPOSIUM ON DAMS AND RESERVOIRS
UNDER CHANGING CHALLENGES – 79 ANNUAL MEETING OF ICOLD, SWISS
COMMITTEE ON DAMS, LUCERNE, SWITZERLAND, 1 JUNE, 2011

Dams and Reservoirs under Changing Challenges

Editors

Anton J. Schleiss

*Laboratory of Hydraulic Constructions (LCH)
Ecole Polytechnique Fédérale de Lausanne (EPFL), Switzerland*

Robert M. Boes

*Laboratory of Hydraulics, Hydrology and Glaciology (VAW)
Swiss Federal Institute of Technology Zurich (ETH), Switzerland*



CRC Press

Taylor & Francis Group

Boca Raton London New York Leiden

CRC Press is an imprint of the
Taylor & Francis Group, an **informa** business

A BALKEMA BOOK

CRC Press/Balkema is an imprint of the Taylor & Francis Group, an informa business

© 2011 Taylor & Francis Group, London, UK

Typeset by Vikatan Publishing Solutions (P) Ltd., Chennai, India
Printed and bound in Great Britain by Antony Rowe (a CPI Group Company),
Chippenham, Wiltshire

All rights reserved. No part of this publication or the information contained herein may be reproduced, stored in a retrieval system, or transmitted in any form or by any means, electronic, mechanical, by photocopying, recording or otherwise, without written prior permission from the publisher.

Although all care is taken to ensure integrity and the quality of this publication and the information herein, no responsibility is assumed by the publishers nor the author for any damage to the property or persons as a result of operation or use of this publication and/or the information contained herein.

Published by: CRC Press/Balkema
P.O. Box 447, 2300 AK Leiden, The Netherlands
e-mail: Pub.NL@taylorandfrancis.com
www.crcpress.com – www.taylorandfrancis.co.uk – www.balkema.nl

ISBN: 978-0-415-68267-1 (Hbk)
ISBN: 978-0-203-80409-4 (eBook)

Table of contents

Preface	xiii
Organization	xv
Sponsors	xvii
<i>Theme A: Long-term behaviour of dams</i>	
Ermenek HEPP—dam and reservoir behavior during impounding <i>E. Üzüceck, R. Kohler, J. Linortner & S. Güven</i>	3
A new approach for large structures monitoring: SCANSITES 3D® <i>H. Lançon & S. Piot</i>	11
Maintenance and operation of aged dams <i>Y. Kita, S. Ariga & M. Katayama</i>	19
Estimation of rockfill dam behavior during impounding by elasto-plastic model <i>N. Tomida, N. Sato, H. Soda, S. Jikan, K. Ohmori & H. Ohta</i>	27
The investigation method of hydroelectric facilities by using digital camera <i>S. Wada & Y. Kono</i>	35
Situation and developing trend of defective reservoir reinforcing technology in China <i>G. Dashui & T. Jiexiong</i>	43
Long term behavior of the concrete dams drainage system and ageing phenomena <i>D. Stematiu, R. Sarghiuta & A. Constantinescu</i>	51
Unpredictable behaviour of a large arch dam in South Africa <i>L.C. Hattingh & C. Oosthuizen</i>	59
Performance of a high rockfill dam during construction and first impounding—Nam Ngum 2 CFRD <i>S. Moll & R. Straubhaar</i>	65
Intensified monitoring of Emosson arch dam during construction of Nant de Drance pump storage scheme <i>H. Stahl</i>	73
Dam embankment deformation and face slab movement monitoring of Nam Ngum 2 concrete face rockfill dam <i>P. Khamwongkhong & W. Mairaing</i>	79
Analysis on the operating performance of Sanbanxi CFRD <i>Z. Xu, G. Deng & C. Zhao</i>	91
Numerical modelling investigation of an existing crack within an arch-gravity dam <i>A. Mellal, A. Koliji & M. Balissat</i>	99

Distributed fiber optic temperature measurements in embankment dams with central core—new benchmark for seepage monitoring <i>M. Aufleger, M. Goltz, J. Dornstädter & O. Mangarovski</i>	107
Performance of dams affected by expanding concrete <i>F. Amberg</i>	115
Warning systems—basic components of Hidroelectrica’s emergency management system <i>I.D. Iacob & D. Zachia</i>	123
A risk based approach to dam safety management in New South Wales, Australia <i>P. Heinrichs</i>	129
Dam safety in Slovakia <i>P. Panenka & A. Kasana</i>	137
Improvement of safety of Swiss dams on the basis of experience <i>H. Pougatsch, R.W. Müller, T. Sonderegger & A. Kobelt</i>	145
Concept of safety and safety requirements for dams <i>P.A. Zielinski</i>	153
Alkali-Silica Reaction in Japan <i>H. Koga, T. Hyakutake, H. Watanabe & T. Sakamoto</i>	163
Experimental study on the detection and inhibition of alkali aggregate reactivity for dam concrete <i>C. Zhiqing, L. Xingping, Y. Jie, L. Shisheng, W. Ling & L. Han</i>	171
Expanding concrete in dams—long term challenges <i>R. Charlwood & K. Scrivener</i>	179
Re-assessment and treatment-design of an ASR-affected gravity dam <i>R. Leroy, L.I. Boldea, J-F. Seignol & B. Godart</i>	187
The integrity of old style post tensioned anchors in dams—a real dam safety issue <i>R. Herweynen</i>	195
Development of geomembrane systems for watertightness of dams in Europe <i>A.M. Scuero & G.L. Vaschetti</i>	203
Development of small hydropower plant utilizing pumped storage power plant’s dam <i>H. Watabe & N. Arai</i>	211
A study of the grouting at the bottom of the Yashio dam reservoir and the evaluation of the leakage by grouting <i>F. Kawashima, Y. Kimura & M. Nishigaki</i>	219
Filter design for the heightening of a high earth core rockfill dam <i>S. Messerklinger & R. Straubhaar</i>	229
Rock treatment around morning glory spillway of Sefidrud dam <i>A. Faghihimohaddess, R. Naghibian & A. Bashash</i>	239
Rehabilitation and upgrade of Giudea dam <i>G. Baldovin, E. Baldovin & G. Morelli</i>	247
Assessment of small gravity dam heightening <i>T. Hofmann, M. Wickenhäuser & W. Gabl</i>	255
Deriner double curvature arch dam—foundation consolidation and curtain grouting <i>K.A. Ross & M. Kaleli</i>	263

Application of grouting technique for stabilization of coarse materials—Karkkeh storage dam experience, Iran <i>M. Heidarzadeh, F. Eslamian & A. Mirghasemi</i>	271
Dam safety and operational efficiency improvements in Sri Lanka <i>A. Sorgenfrei & M. Friedrich</i>	279
Strengthening of Les Toules arch dam <i>A. Wohnlich & O. Müller</i>	287
<i>Theme B: Dams and climate change</i>	
Long-term behavior of the Yashio dam, asphalt faced rockfill dam <i>T. Tsukada, M. Doi, K. Yoshizawa & T. Kikuchi</i>	297
Some long-term problems associated with suffusion in the foundation of embankment dams <i>A. Soroush & P.T. Shourijeh</i>	305
RCC dams—is there a limit to the height? <i>M.R.H. Dunstan</i>	313
Numerical analysis of water reservoir dam—prediction of long term performance of Versetal dam (Germany) <i>M.M. Zimmerer, T. Schanz, Y. Lins & V. Bettzieche</i>	321
Dam and hydropower in a changing world <i>J. Jia, J. Ma & C. Zheng</i>	331
Sedimentation of Polish reservoirs—characteristics and significance of the phenomenon and procedures of its control <i>A. Kosik, J. Kloze & A. Wita</i>	339
Innovative sediment handling to restore reservoir capacity <i>H. Schüttrumpf & M. Detering</i>	345
Sediment management strategies for sustainable reservoir <i>T. Sumi & S.A. Kantoush</i>	353
An experimental study on turbid water coagulation method using natural coagulant <i>H. Umino & N. Hakoishi</i>	363
Burrowing-type sediment removal suction pipe for a sediment supply from reservoirs <i>T. Sakurai & N. Hakoishi</i>	371
Upper Missouri River mainstream reservoirs: Sedimentation and sustainability issues <i>M.J. Teal</i>	379
Flood retention in alpine catchments equipped with complex hydropower schemes—a case study of the upper Aare catchment in Switzerland <i>M. Bieri, A.J. Schleiss, F. Jordan, A.U. Fankhauser & M.H. Ursin</i>	387
Controlled sediment flushing of Cancano reservoir <i>P. Espa, M.L. Brignoli, A. Previde Prato, E. Castelli, G. Crosa, G. Gentili & F. Bondiolotti</i>	395
Sediment bypass tunnel design—review and outlook <i>C. Auel & R.M. Boes</i>	403
Numerical simulation of flow and sedimentation transport in the early stage of the Three Gorges Reservoir (TGR) <i>R. Huang, X. Zhang & Y. Huang</i>	413

Hybrid modeling of sediment management during drawdown of Räterichsboden reservoir <i>G. Möller, R.M. Boes, D. Theiner, A. Fankhauser, M. Daneshvari, G. De Cesare & A.J. Schleiss</i>	421
Aras transboundary river basin cooperation perspective <i>A. Heidari</i>	429
An example of sedimentation and proper management of flushing operation since 45 years: The Kashm El Girba reservoir on the Atbara river <i>C. Guilbaud, O. Cazaillet, P. Cochet & C. Odeyer</i>	437
Future glacier evolution and impact on the runoff regime in the catchments of Alpine reservoirs: The Aletsch area, Switzerland <i>D. Farinotti, A. Bauder, R.M. Boes, M. Huss, G. Jouvet & F. Widmer</i>	449
Decision Support System for the hydropower plants management: The MINERVE project <i>J.G. Hernández, A.J. Schleiss & J. Boillat</i>	459
Incorporating climate change scenarios into new operating rules for large reservoirs: A transnational assessment in the Meuse basin <i>B. Dewals, S. Detrembleur, P. Archambeau, S. Erpicum, M. Pirotton, G. Demny, T. Rose, C. Homann, J. Lange, N.P. Huber, M. Kufeld, B. Sinaba & H. Schüttrumpf</i>	469
The flexible flood control capacity exploration and its relevant extra benefit estimation of lower Jinsha River cascade reservoirs <i>J. Xu, J. Chen, Z. Yin & C. Yang</i>	479
Impact of climate change on the management of water resources in mountainous regions—case of the Lake Annecy basin in the French Alps <i>M. Cottet, C. Freissinet & B. Graff</i>	487
Optimized and adapted hydropower management considering glacier shrinkage scenarios in the Swiss Alps <i>S. Terrier, F. Jordan, A.J. Schleiss, W. Haeblerli, C. Huggel & M. Künzler</i>	497
Future challenges for dams under climate change <i>D.-K. Koh & J.-H. Park</i>	509
Study on rational control model for excess flood by utilizing rainfall prediction <i>A. Yamamoto, S. Mitsuishi, T. Ozeki & T. Sumi</i>	517
Effective flood control through integrated and collaborative dam operation at three dams in the upper Nabari River <i>T. Matsumura, H. Kamiya & N. Yoshida</i>	525
Global warming and design flood: The case study of Bagatelle dam, Mauritius <i>S. Le Clerc & H. Garros-Berthet</i>	533
Study on the Pan-basin optimization of West route engineering of South-to-North water transfer <i>J. Zhang, S. Peng, Y. Wang & H. Wang</i>	541
Impact of climate change on hydro-energy systems: An overview <i>R.P. Brenner</i>	551
The Upper Paunglaung RCC dam—design and construction <i>U. Myint Zaw, U. Thaug Han, Ch. Rohrer & K.M. Steiger</i>	559

Theme C: Dams and natural hazards

Damage to the Ishibuchi dam by the Iwate-Miyagi Nairiku earthquake in 2008 and seismic assessment <i>H. Yoshida, A. Nakamura, N. Matsumoto & T. Kasai</i>	569
Effects of vertical earthquake motions on deformation of Newmark sliding analysis <i>N. Matsumoto, T. Sasaki, K. Shimamoto, Y. Sugiura & H.Q. Zhao</i>	577
Earthquake-induced settlement analysis for rockfill dams using cumulative damage theory <i>Y. Yamaguchi, H. Satoh & K. Shimoyama</i>	585
Shaking table test of concrete dams with penetrated cracks and DEM analysis simulation <i>T. Iwashita, T. Kirinashizawa, Y. Yamaguchi, H. Kojima & Y. Fujitsuka</i>	595
Effects of the Iwate-Miyagi Nairiku earthquake in 2008, Japan, on a central clay core rockfill dam <i>T. Ohmachi & T. Tahara</i>	605
Seismic stability of a Peruvian tailings earth-rockfill dam with liquefiable foundation <i>M. Seid-Karbasi, H. Hawson & U. Atukorala</i>	613
Simplified methodology for estimating seismic coefficients for the pseudo-static slope stability analysis of earth dams <i>A.G. Papadimitriou, K.I. Andrianopoulos, G.D. Bouckovalas & K. Anastasopoulos</i>	621
Dam shape adaptation resulting from strong earthquake context <i>B. Tardieu, A. Si-Chaib, M. Marouk & M. Bibi</i>	629
Seismic safety of Chancy-Pougny dam <i>M. Ferrière, J.-P. Person, H. Charif, O. Vallotton, S. Rossier & P. Lestuzzi</i>	637
Behavior analysis of soil-structure interaction of a composite dam using geo-centrifuge test <i>J. Y. Lim & I.S. Ha</i>	645
Swiss expertise in North Africa focusing on flood protection <i>N. Nilipour & K. Essyad</i>	653
Risk assessment for the critical regimes of Chaira dam stilling basin <i>J. Tadjer & H.T. Falvey</i>	661
Design and hydraulic modelling of a fuse plug spillway <i>L. Schmocker, E. Rühli, V. Weitbrecht, R.M. Boes, P.A. Mayor & S.M. Springman</i>	669
Inflow Design Flood and dam safety <i>P.A. Zielinski</i>	677
Combinations of earthquake and flood hazards together with other factors <i>D.N.D. Hartford</i>	685
Measures to reduce dynamic plunge pool pressures generated by a free jet <i>Th. Berchtold & M. Pfister</i>	693
Impulse waves at Kühtai reservoir generated by avalanches and landslides <i>H. Fuchs, R.M. Boes & M. Pfister</i>	701
Numerical simulations of water waves due to landslides <i>Z. Jiang, J. Han & Z. Cheng</i>	709

Hazard and risk assessment of rock slide tsunamis in lakes and reservoirs <i>C. Harbitz, F. Løvholt, U. Domaas, S. Glimsdal & B. Romstad</i>	717
Characteristics study of Gorge reservoir landslide <i>X.L. Tang, X.L. Tang, D.Y. Liu & H.B. Feng</i>	725
Goescheneralp dam—impact of natural hazards on construction site and freeboard optimisation <i>T. Dietler</i>	733
Design and construction of asphalt facing in cold heavy snow region <i>S. Abe, H. Seto & H. Watanabe</i>	741
 <i>Theme D: Dams in a sound environment</i>	
Identification of hazardous zones for development of tourism industry: A case study in Taleghan dam catchment area <i>N. Ahmadi & H. Ahmadi</i>	753
How to maintain the bad reputation of dam projects <i>R. Zwahlen</i>	761
Measures for vegetation restoration on modification sites at Takizawa dam <i>N. Takemoto, Y. Takahashi & M. Hirose</i>	769
Building dams in a sound environment: Development of La Romaine HEP, situated in Northern Québec, Canada <i>B. Soucy, V. Alicescu & J.-P. Tournier</i>	777
Methodological approach and artificial intelligence application as a solution for environmental conflict related to large dams <i>S. Stevovic, M. Stamatovic & G. Ivanovic</i>	785
Introduction of cost-benefit evaluation of the environmental impacts and mitigation measures in hydropower production and water supply service sectors <i>A. Kryžanowski & M. Gorišek</i>	791
Environmentally rehabilitation of dam Bitdalen <i>A.M. Ruud & L. Lia</i>	799
The conservation measures on rare and endemic fish during the construction of cascaded hydropower projects in downstream of Jinsha River <i>X. Zhao, Z. Sun, Y. Chen, D. Wang & Y. Gao</i>	807
Application of MIKE 11 model in the prediction of water pollution accident in the Three Gorges Reservoir <i>Y. Fang & Y. Min</i>	813
Protection of the National Mayanghe Natural Reserve in development of Wujiang Panshui Hydropower Station <i>G. Jiang, H. Li & Y. Li</i>	821
Implement water diversion measures to ease the ecological water demand of the Yellow River Delta <i>X. Li, L. Sun & X. Meng</i>	829
Study on river ecological compensation of China <i>B. Ruan & Y. Fu</i>	835

Impacts of dam on Key Biodiversity Area in southwest China based on integrated map <i>L. Chong, P. Jing & W. Hao</i>	843
A model for the dry closure of tailings dams <i>J.L. Justo, P. Durand, M. Vázquez, A. Morales & F.A. Jiménez</i>	849
A holistic approach to reduce negative impacts of hydropeaking <i>W. Gostner, C. Lucarelli, D. Theiner, A. Kager, G. Premstaller & A.J. Schleiss</i>	857
The new Muttsee dam (Switzerland) <i>F. Tognola & M. Balissat</i>	867
Post-audit of Alqueva reservoir's water quality: Lessons learned with the comparison between forecast and reality <i>P.A. Diogo, A.C. Rodrigues, P.S. Coelho & M. Almeida</i>	875
Keyword index	883
Author index	885

Preface

This book contains 106 papers selected by the reviewers out of 170 accepted papers for the International Symposium on “Dams and Reservoirs under changing Challenges” held on June 1, 2011 during the 79th Annual Meeting of the International Commission on Large Dams in Lucerne, Switzerland.

In today’s globalized world, many things seem to be changing ever faster. Even for the very ancient art of building dams, the largest man-made structures of great longevity, some boundary conditions are indeed different nowadays from what they used to be. In particular, besides the technological part in the dam planning, construction, operation and maintenance processes, ICOLD’s mission to also adequately deal with the environment and related infrastructure has become increasingly important and challenging. In the frame of global climate change, altered water cycles as well as more extreme weather conditions and an increasing number of natural hazards clearly affect the safe and economical operation of dams and reservoirs. Moreover, emission-free hydropower production as the most important form of “liquid” solar energy and the provision of water for irrigation and potable water supply is becoming more and more important to meet the world’s fast growing demand for energy and food in a sustainable way.

These reflections led us to divide the symposium into four main themes, namely

- Long-term behaviour of dams
- Dams and climate change
- Dams and natural hazards
- Dams in a sound environment.

This book gives an overview on current case studies, design applications, construction, maintenance and operation experience as well as research and development activities related to the mentioned themes from around the world.

The editors gratefully acknowledge the contribution of the authors, the work of the reviewers and the support of the international scientific as well as the local organizing committees. Special thanks go to Dr. Michael Pfister (LCH) and Lukas Vonwiller, Jeannette Gabbi and Renata Müller (VAW) who managed the review process and the submission of the final papers and prepared the print-ready version of these Proceedings.

Moreover, the support and sponsorship of our partners and sponsors are kindly acknowledged.

Anton J. Schleiss
Laboratory of Hydraulic Constructions (LCH)
Ecole Polytechnique Fédérale de Lausanne (EPFL)
Conference chair and Chairman of the Swiss Committee on Dams

Robert M. Boes
Laboratory of Hydraulics, Hydrology and Glaciology (VAW)
Swiss Federal Institute of Technology Zurich (ETH)
Conference chair

Lucerne, June 2011

Organization

CONFERENCE CHAIRS

Prof. Dr. Anton J. Schleiss, *Switzerland*
Prof. Dr. Robert M. Boes, *Switzerland*

SECRETARY GENERAL

Dr. Bernard Joos, *Switzerland*

LOCAL ORGANIZING COMMITTEE

Marc Balissat, *Switzerland*
Dr. Peter Billeter, *Switzerland*
Hans Bodenmann, *Switzerland*
Dr. Roger Bremen, *Switzerland*
Dr. Peter Brenner, *Switzerland*
Ian Clarke, *Switzerland*
Dr. Georges Darbre, *Switzerland*
Dr. Walter Hauenstein, *Switzerland*
Dr. Harald Kreuzer, *Switzerland*
Laurent Mouvet, *Switzerland*
Dr. Bastian Otto, *Switzerland*
Andreas J. Siegfried, *Switzerland*
Karl Steiger, *Switzerland*
Dr. Martin Wieland, *Switzerland*

INTERNATIONAL SCIENTIFIC COMMITTEE

Prof. Dr. Markus Aufleger, *Austria*
André Carrère, *France*
Jean-Jaques Fry, *France*
Patrick Le Delliou, *France*
Michel-Marc Lino, *France*
Michel Poupert, *France*
Dr. Giovanni Ruggeri, *Italy*
Prof. Dr. Peter Rutschmann, *Germany*
Dr. Pietro Sembenelli, *Italy*
Prof. Dr. Peter Tschernutter, *Austria*
Prof. Dr. Silke Wieprecht, *Germany*
Prof. Dr. Gerald Zenz, *Austria*

PROCEEDINGS

Dr. Michael Pfister, *Switzerland*, Management of review process and proceedings
Lukas Vonwiller, *Switzerland*, Assistance to formatting

SECRETARIAL OFFICE

Rachel Niedermann, *Switzerland*

Sponsors

PARTNERS



MAIN SPONSORS



SPONSORS



CO-SPONSORS



Theme A: Long-term behaviour of dams



Grande Dixence Dam, Switzerland (285 m, 1961).

Ermenek HEPP—dam and reservoir behavior during impounding

E. Üzücek

Devlet Su İşleri (DSİ), Yucetepe, Ankara, Turkey

R. Kohler

Pöyry Energy GmbH, Salzburg, Austria

J. Linortner & S. Güven

Pöyry Energy GmbH, Ankara Branch Office, Ankara, Turkey

ABSTRACT: An Austrian—Turkish Consortium is constructing the hydro power plant Ermenek in Turkey for the Turkish State Hydraulic Works, DSİ. The project is located in the South of Turkey, at the Ermenek river, and has an installed capacity of 300 MW with an estimated annual energy output of 1000 GWh. The project consists of an arch dam, a large grout curtain, a pressure tunnel, a power house and appurtenant structures. The 218 m high double curved thin arch dam is located in a mega-block (Olistolith) of Nadire limestone. The highly karstified limestone is sealed at both sides of the dam by a huge grout curtain of 682.00 m². The performance of this grout curtain together with the drainage curtain in the vicinity of the dam abutment is of high importance for pore water pressure and consequently the dam stability. In addition the grout curtain should reduce the seepage to a minimum. Further on the tightness of the reservoir itself is of high interest due to the low water inflow (yearly average 42.3 m³/s) compared with the reservoir volume of 4600 mio m³.

1 INTRODUCTION

1.1 General

The concreting works for the dam started in September 2007 and could be finalized in October 2009. For the 218 m high dam, only 300,000 m³ of concrete and about 363,000 m³ of rock excavation were necessary due to the extreme steep and narrow gorge with a natural width at the base of 20 m and about 110 m at the crest. The thickness of the structure at the center line is at the dam's base 25 m and 7 m at the crest.

As the reservoir has a huge overall volume of about 4600 mio m³ it was necessary to start with the impounding already during the dam construction. Therefore, when concreting of the dam reached an elevation above 600 m a.s.l., i.e. 100 m below final crest elevation, the vertical contraction joints were grouted and the impounding started in August 2009. Due to the narrowness of the valley and the high water influx during the wet season the reservoir level increased rapidly after overtopping of the concrete cofferdam. The average increase between August 2009 and March 2010 was approximately 40 cm/day with a peak of 10 m/12 hours increase during an extraordinary flood (100 year flood event) in November 2009. By the end of September 2010 the lake reached the elevation of 625 m a.s.l., which is 135 m above foundation.

In summer-dry season the reservoir was gradually filling and the next increase of further rapid filling is expected in the winter-wet season between November 2010 and May 2011. Start of operation is expected for May/June 2011 depending on the water influx of the next coming months. The remaining additional amount of water volume for start of operation is

about 1300 mio m³. Maximum operation level can be reached only 2 years later according to longtime average influx values and the usage of water after start of operation.

The main items of interest which are influenced by the increase of the water level and mountain water table during impounding are:

- the stability of the dam and its abutments
- the tightness of the grout curtain
- the reservoir tightness itself

1.2 General geological conditions

The dam site is located in a large limestone body which is embedded in a sequence of flysch-type rock with alternating layers of sandstone and claystone. In the reservoir area the limestone is crossed by a major fault (F1) which also causes a downward displacement of the marl so that the permeable limestone (dam side) borders to impermeable Görmel marl along the F1 fault.

A second fault F2 runs parallel to F1-fault, but closer to dam site. An overview of the geological conditions at dam site is given in [figure 1](#).

In the course of the project execution the alignment of the grout curtain was re-considered once more and therefore further investigation (geophysical and hydro-geological investigations, boreholes, etc.) were executed at the right embankment to evaluate the behavior of fault F1. Finally it could be concluded that with the new alignment the grout curtain could be shortened and anchored into the impervious Flysch rock.

In the reservoir itself, detailed hydro-geological investigations were executed by the hydro-geological department of the client, to ensure that there will be no seepage out of the reservoir.

For the dam and for the wedge stability during the dam excavation detailed rock parameter studies were performed and detailed survey and mapping of the faults and joints in the concerned area was applied before and during the progress of the works. All information gained during the excavation of the grouting galleries and tunnel with a total length of more than ... km were taken into consideration for both wedge stability calculation and grout curtain design and application.

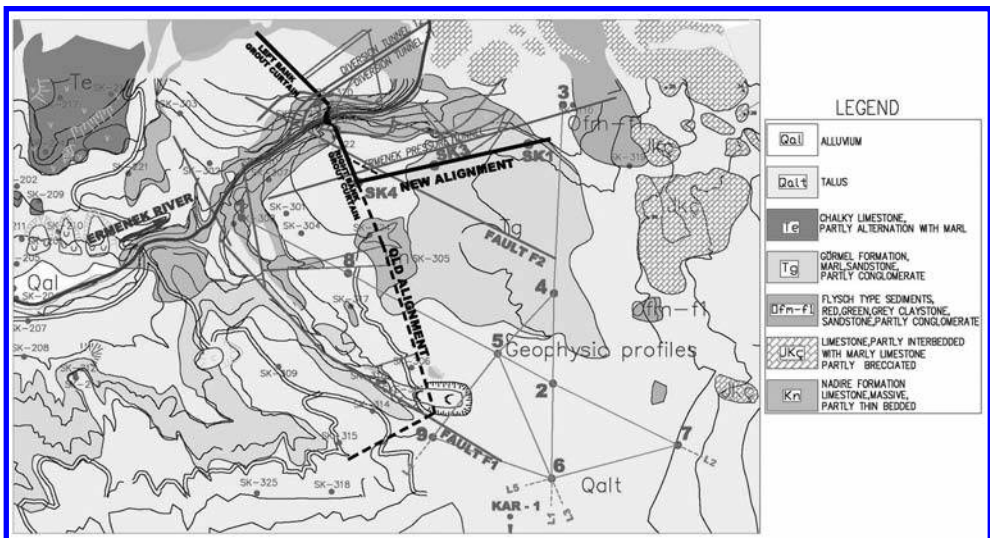


Figure 1. Geological overview at dam area.

2 EVALUATION OF THE DAM AND RESERVOIR BEHAVIOR AFTER START OF IMPOUNDING

2.1 Dam and abutments

The following picture shows the dam from a downstream view with the impounding stage in October 2010.

The grouting works in the vicinity of the dam were done in two steps: first step was consolidation grouting to improve the contact between concrete and rock and to homogenize the surrounding rock fissured due to blasting during excavation and as second step the grout curtain was drilled and injected. In addition link holes were executed in the abutments, to connect the grout curtain with the dam body concrete. In the vicinity of the dam the curtain was executed as double and partly triple row. Consolidation grouting holes and the link-holes were drilled from the inclined shafts, whereas the grout curtain was drilled from gallery to gallery. Subsequently [figure 3](#) shows the application of the grouting works in the dam abutment.

Finally a drainage curtain at both dam abutments was drilled at the air side with a drill-hole length of 20 m. This drainage curtain was drilled from the galleries as well as from



Figure 2. Picture of the dam from downstream taken in October 2010.

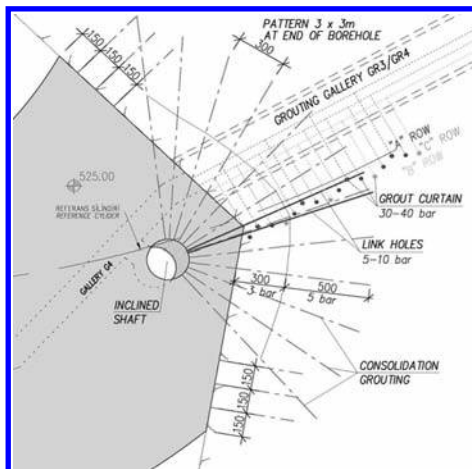


Figure 3. Application of consolidation and link hole grouting from inclined shaft.

the grouting chambers. The ones closer to the curtain are dewatering upwards, the others downwards (see figure 4). In order to observe and control the uplift pressure below the dam foundation drainage holes were drilled from the lower dam body gallery. By means of the drainage curtain in the vicinity of the dam the uplift pressure is controlled which is essential for the dam stability and also for the stability of the abutments. The total water seepage from the galleries and also from the dam abutments is measured by water flow gauging stations which are located at the gallery levels at both sides of the dam.

To monitor the deformation of the abutments, extensometers are installed at the gallery levels with depth of 5, 10, 20 and 30 m in downstream and upstream direction. Beside this the dam body is fully equipped with instrumentation of pendulum, clinometers, strain- and pressiometer, invar wires, temperature gauges, water level gauge, jointmeter, etc. (see Zenz et al. 2009).

Piezometer have been installed in addition at different levels and locations which also allow to monitor the development of the uplift pressure. The piezometer in the dam abutment at both sides have a staggered depth of 5, 15 and 30 m (see figures 4 and 5).

The evaluation of the measurement results at the Ermenek dam during the first two years of impounding, i.e. until reaching the minimum operation level of 660 m a.s.l., is done by Pöyry. As a first step Pöyry developed the work program for the measurements and focused on the improvement of the accuracy of different measuring devices. The evaluation of the records is done in 3 months intervals. So far no unusual behavior of the measured deformations and strains were observed at the dam body and abutment. The maximum deformations in the dam are actually around 3.3 mm which is below the calculated value of 4.7 mm.

From seepage point of view it can be stated that in the close vicinity of the dam (200 m on each side) the performance of the double row (-triple row) grout curtain is rather successful. No high seepage was encountered from the drainage curtain, neither in the grouting chambers nor in the gallery connection points with the dam body. Also the seepage in the gallery section is very low compared to the gallery sections with only single row curtain. In the double row curtain section only some holes are dripping and a few of them are slightly flowing.

The figures below show the locations of the piezometer and pore-water-pressures measured in the vicinity of the dam by the end of September 2010.

From uplift point of view it has to be stated that a few piezometers at the left bank showed rather high values which were already at the border of the design assumptions, in particular

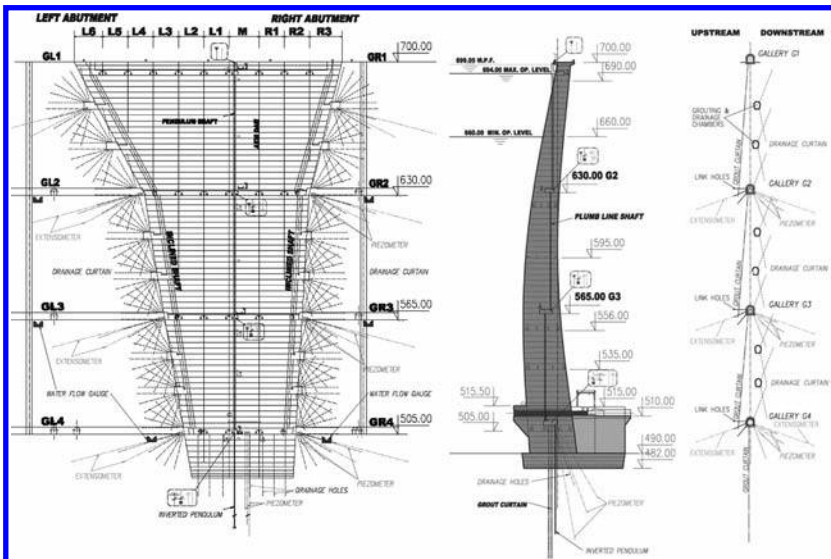


Figure 4. Dam instrumentation and drainage curtain.

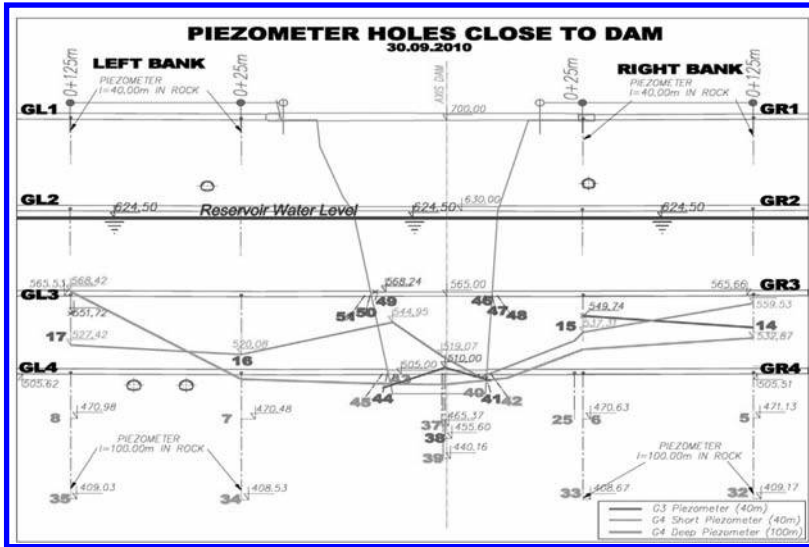


Figure 5. Piezometer measurements in the dam's vicinity.

the short (5 m) piezometer no. 43 and no. 49 next to the concrete-rock interface. Checkholes drilled into these intersection joints could not confirm the high uplift pressure. So the reason for these wrongly high recorded values might be found in the application of the piezometer installation. The uplift pressure at the dam foundation is below the design assumptions.

2.2 Application and tightness of the grout curtain

The grout curtain alignment was changed and shortened during project execution to a still remarkable total length of 2.2 km in order to anchor the curtain in the impermeable underlying flysch rocks (see chapter 1.2). About design and construction of the grout curtain it was reported in Linortner et al. (2009).

The limestone is a massive rock in moderately jointed condition. Especially at the left embankment and close to the contact to the underlying flysch rocks it could be noted that the degree of jointing is significantly lower than in general (see figure 6). In these areas it could be noted that the limestone is thickly bedded, but these bedding planes are closed and not karstified, therefore permeability and grout takes are low in these areas.

In general the rock is highly karstified. The intensity of karstification is slightly decreasing with depth. Even below the original groundwater level (of approximately 504 m) the rock is karstified, although approximately 100–150 m below the groundwater level the intensity of this process is significantly diminishing. The contact to the underlying flysch rocks is sharp, but it is not accompanied by increased karstification.

The karst cavities have been developed preferentially along the orthogonal joint system and the openings are often filled with soft clay with increased tendency of washing out closer to the surface of terrain. During grouting works it could be observed occasionally that the clay fillings have been pressed out to free surfaces from a depth of up to 70 m below gallery GR4. The fault F2 intersects the grout curtain two times, has a thickness of a few centimeters, at chainage 0 + 200 up to 1–2 decimeter, and is accompanied by parallel joints and faults of high persistence especially between chainage 470 and 770. This fault is associated with increased karstification and causes increased permeability of the rock mass so that additional sealing of the curtain had to be done.

The grout curtain is executed as an inclined curtain towards upstream from four galleries with about 70 m vertical distance, connected by link holes at the gallery levels. In general, it is a single row curtain with a final average spacing of 1.20 m. In the vicinity of the dam it is

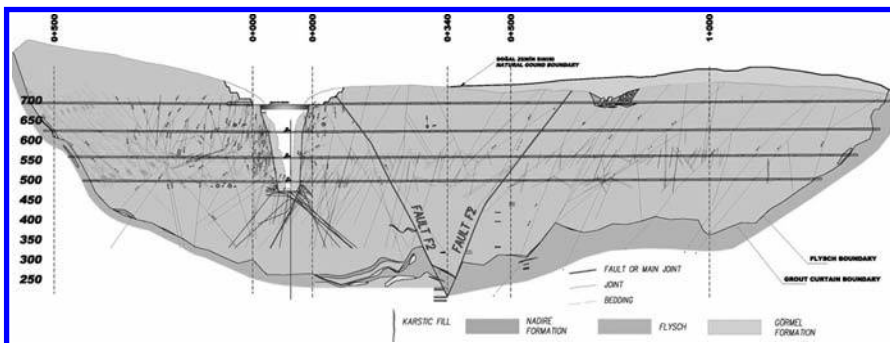


Figure 6. Geological section through the new grout curtain alignment.

executed as a double row curtain with reinforcing by a third row where necessary (based on the grout take in the first two rows). The average grout take in the grout curtain holes is 92 kg/m. The grout curtain was finalized in the lower two galleries before the impounding started. The grouting pressure applied was two times the final water pressure after full impounding.

Evaluation of the success of the grouting works was done during the grout curtain application by check holes with core recovery and Lugeon tests. The criteria for the Lugeon tests were defined by 1 to 2 Lugeon in the vicinity of the dam and 3 to 5 Lugeon in the other areas. Where these criteria could not be fulfilled additional grout holes were applied to strengthen the curtain.

Finally the drainage holes were drilled in each gallery with 12 m spacing and a depth of 10 m. For further control piezometer holes were applied, in the lower galleries with a depth of 40 and 100 m and in the upper galleries with 40 m. Prior to start of impounding the seepage and water pressure was recorded to be compared with the records during rising of the water level. Following figures show the increase of water seepage and the increase of water pressure in comparison with the rising water level in the reservoir within the first year of impounding. Total recorded seepage with end of September 2010 was recorded by 33 l/s which stays below the assumptions.

For comparison of the pressure, upstream and downstream of the grout curtain piezometer were installed, recorded and evaluated together with the piezometer installed in the galleries. The following figure shows a section about 300 m downstream of the dam through the grout curtain.

In the figure below it can be seen that the water pressure recorded downstream of the grout curtain is quit high and above the design assumptions. The reason for this is on the one hand side the high permeability along fault F2 which is also confirmed by the seepage measurements and on the other side the low permeability of the rock mass towards the gorge. To solve this problem strengthening of the grout curtain in the location of the fault and its branches is ongoing. Finally the water pressure will be released by drilling of additional drainage holes.

2.3 Tightness of the reservoir

At maximum operation level (694 m a.s.l.) the reservoir will have a surface area of 58.74 km² and a volume of 4582 mio m³. Compared to this huge reservoir, the mean water inflow of 42.3 m³/s is relatively low and therefore the tightness of the reservoir is very important. The hydrogeological investigations of the reservoir conditions were done by the geological and hydro-geological department of DSI. Mainly the geological formations and the springs surrounding the reservoir were mapped and evaluated. All springs are above the operation level of the reservoir indicating an impermeable basin. The question of waterloss out of the reservoir towards South along F1 was answered by the information gained from additional geological investigations like boreholes, seismic and

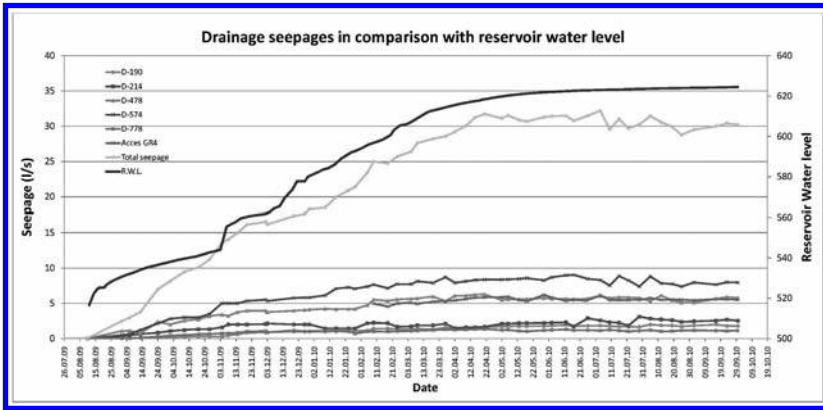


Figure 7. Seepage measurements in the galleries, single bigger seepages and total seepage.

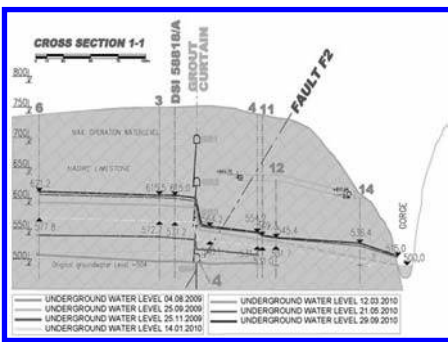


Figure 8. Section through the grout curtain.

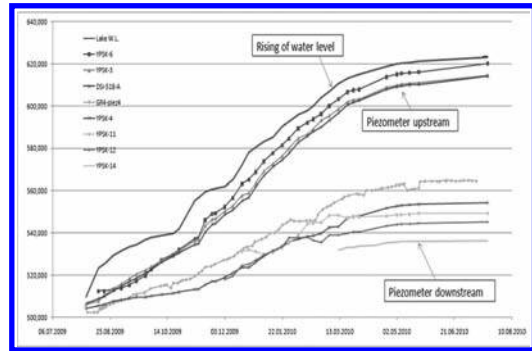


Figure 9. Development of the piezometer pressure.

hydro-geological investigations and lead to the decision that the grout curtain alignment was shortened as described in chapter 1.2.

In addition to the above mentioned investigations the contractor ordered a study at the UKAM—Hacettepe University/Ankara about possible waterloss along F1. For this study 15 wells in the concerned area were drilled and the water levels were measured during dry and wet season. Additionally to that the hydro chemical conditions (chemical analysis and electrical conductivity) have been evaluated and groundwater monitoring with tracer tests have been executed. The findings in this report did not give a clear picture but also not a clear indication of a risk for seepage towards South. Therefore Pöyry together with the local geological and hydro-geological experts A.&S. Altuğ prepared an additional study taking also the information's of the UKAM report into consideration. This study came to the conclusion that there is no indication for water loss along F1 and the chosen alignment of the grout curtain should be followed up.

Several piezometer have been installed on both embankments, up- and downstream of the grout curtain, in order to observe the increase of the groundwater level. The upstream ones show the development of the ground water table during impounding, the downstream ones give an indication of the tightness of the grout curtain. In the figure below the locations of those piezometer and some significant measurement records are shown. The general trend of bank filling can be seen from the contour lines of the groundwater level. This shape of the contour lines remained more or less constant during impounding which indicates also homogenous underground conditions in the reservoir.

The hydraulic gradient between reservoir and grout curtain is getting lower with increased reservoir filling which also indicates a gradual filling of the joint system in the banks upstream

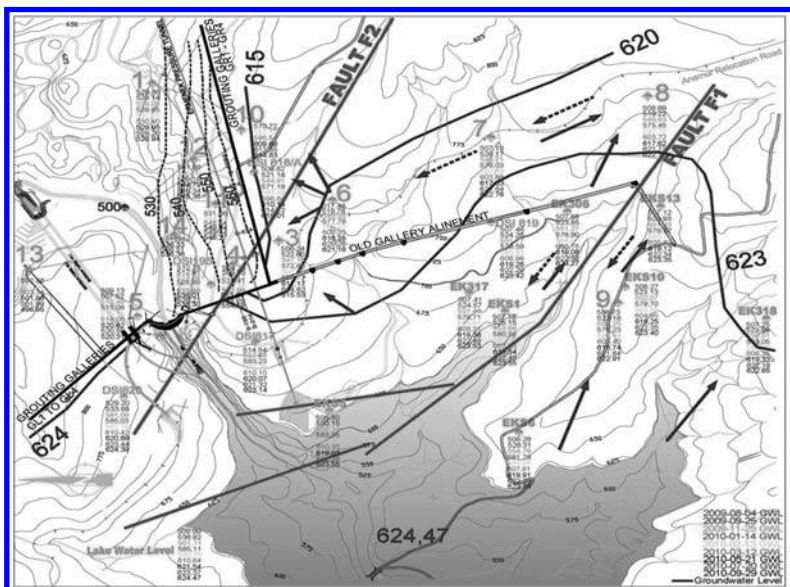


Figure 10. Field piezometer with flow directions.

of the grout curtain. This is demonstrated by the decreasing difference between the upstream piezometer and the reservoir water level as shown in figure 9. Furthermore it can be seen that the groundwater flow direction between several piezometer in the vicinity of fault F1 is changing in monthly intervals due to weather conditions which lead to increased groundwater inflow from the mountainside. This is a positive indication, as the extension of permeable rocks below the overlying Görmel marble could not be confirmed at every part of reservoir before impounding. Now it is confirmed that there is no seepage towards the South.

3 CONCLUSION

At this stage of the evaluation, October 2010, 135 m out of total 204 m are impounded. Impounding is still ongoing and start of operation is expected to be reached in May/June 2011.

So far the deformation behavior of the dam is within the expected range. For the tightness of the grout curtain and the reservoir the evaluation of the measuring results is an ongoing process. The pore pressures and seepages in the vicinity of the dam are within expected values. Higher seepages are encountered in the area of a fault zone crossing the grout curtain. The total seepage is below the assumptions, but the pressure at the downstream of the grout curtain is above the design assumptions in the area of F2. Therefore treatment of the grout curtain is ongoing in the concerned areas and additional drainage holes are ordered to be drilled. Bigger waterlosses out of the reservoir could not be recorded; even during the dry season in 2010 only smooth filling of the surrounded embankments was observed. So impounding can go on without any interruption.

REFERENCES

- Linortner J., Jung G., & Zenz G. 2009. Design and construction of the grout curtain for the Ermenek hydropower plant. Felsbau 5/2009.
- Zenz, G., Kohler, R., & Linortner J., 2009. Ermenek Dam-Construction, Instrumentation and start of Impounding, 2nd National Symposium and Exposition on Dam Safety, Eskişehir, May 2009.

A new approach for large structures monitoring: SCANSITES 3D®

H. Lançon & S. Piot

SITES Company, Rueil-Malmaison, France

ABSTRACT: Dams' monitoring needs to take care of walls' deformations and degradations. New technologies provide some modern tools to produce some detailed and numeric visual inspection and geometric surveys. The SCANSITES 3D® was developed to provide, in a multilayer file associated to a database, a high density survey and a detailed inspection. Two case studies show the method's results.

1 INTRODUCTION

Since decades, among the existing monitoring devices and methodologies, two are widely used for large dams' safety management: visual inspection and geometric survey. The first is usually carried out with empiric methods, and the second is realized using accurate but discrete methods such as geodetic micro-triangulation.

This paper introduces a new approach, using an exhaustive and numeric method called "SCANSITES 3D®".

The SCANSITES 3D® is based on a combination of the SCANSITES® method, which is an advanced tool to provide numeric defects inspection on large structures, and a new wide ranged Lidar technologies aiming to deliver geometric exhaustive mapping, and photogrammetric coverage.

In the first part of this paper, we will describe the SCANSITES® method, in a second part the Lidar coverage and in the third one, the photogrammetry. We will explain how the combination is performed and which data can be extracted on large structures. Before concluding, we will extend this paper with additional data which could be overlaid, such as thermographic pictures.

2 SCANSITES® OVERVIEW

By the past, many owners weren't completely satisfied with the traditional defects mapping process, using binoculars or rope access. The main drawback is the difficulty to produce a scaled defects map enabling an accurate and reproducible monitoring (crack evolution...). To answer this problem, the SCANSITES® was developed in 1990's. This system aims to produce a numeric defects mapping connected to a database which is working as a true real-time G.I.S. (Geographic Information System). It's composed of:

- An hardware tool with a robotized inspection head and its controllers (Fig. 1).
- A software suite including a database and several dedicated inspection tools.

The whole system is designed to operate in-field, without heavy carriage. Several dozens of dams have been surveyed by the SCANSITES® and SITES Company team across the world (Figs. 2, 3).



Figure 1. SCANSITES® head.

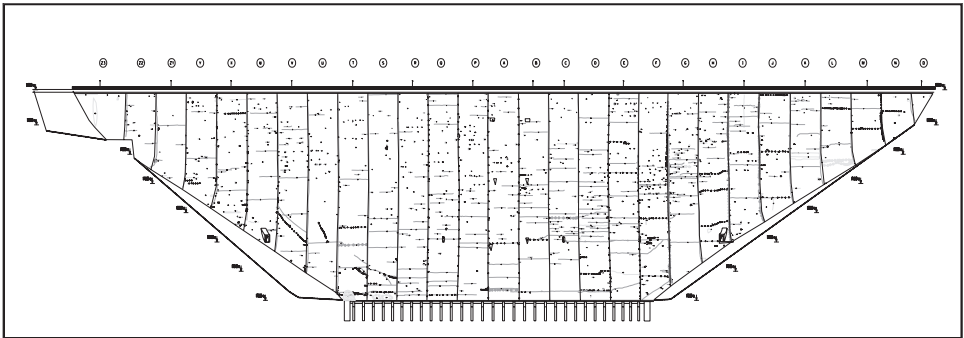


Figure 2. Defects mapping.

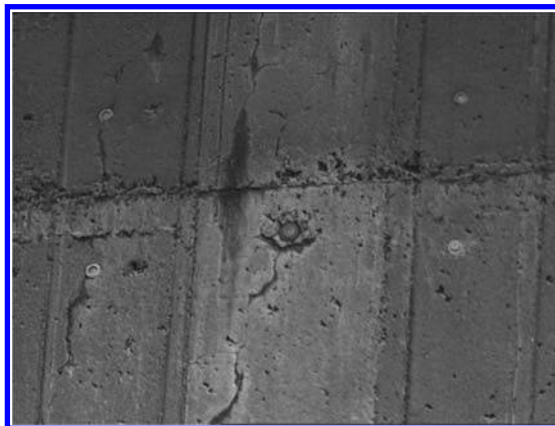


Figure 3. Picture of defect captured with SCANSITES®.

3 LIDAR OVERVIEW

The Lidar (Fig. 4) is a device which aims to produce some high density surveying in 3D coordinates. It's based on two angular coders and a remote electronic distance measurement device. The system works with enough velocity to acquire thousands of points each second. To cope with most of dams, a wide range Lidar is used. It is able to scan structure, up to 1000 meters onto surfaces, with less than 20% reflectivity.

The result of a Lidar survey, called "point cloud" (Fig. 5.), is usually composed of tens million points known in XYZ. The average density ranges from 1 point each 5 to 20 mm.

4 PHOTOGRAMMETRIC OVERVIEW

In this case, the photogrammetric coverage aims to deliver exhaustive and high definition pictures of the structure. The goal is to be able to produce a visual inspection, using 3D referenced pictures. The camera and lenses used can give a pixel equivalent to few millimeters onto the structure, which is enabling to detect the main defects. As photos' orientation is known, each photo can be projected on 3D mesh to texture it (Fig. 6). Next step is to project the textured 3D mesh on a primitive projection (plane, cone, and cylinder) to obtain a map. This projected image is called orthophotography.



Figure 4. Lidar in operation.

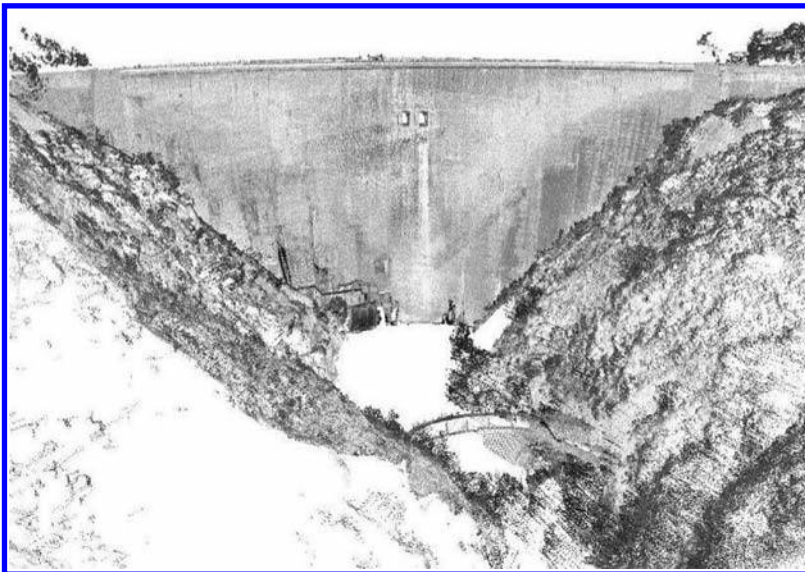


Figure 5. Point cloud of a dam.



Figure 6. High accuracy picture of degradation captured with the camera.

5 OPERATIONS

In this section, we will explain the different steps required to produce a SCANSITES 3D® survey. As said before, all data are known in a 3D referential. For that, the method can use the one established for the traditional survey (targets, pillars). In case where there is no available network, it is necessary to create one, based on singular points on the structure and determined with traditional survey operations.

Concerning the visual inspection, each dam's owner has its own requirements. It deals with defects, which have to be surveyed, and the associated classification. One of the most important parameter is the minimum opening for crack that needs to be surveyed. It mainly impacts the focal length used during the inspection (up to 4 meters!) and widely, the total number of defects stored. All those considerations enable to prepare the mission, mainly the database and the inspection software.

At this step, in-field operation can begin.

SCANSITES® and Lidar are set at different locations in order to cover the structure's surface. The high gain video camera and quality lenses of the SCANSITES® enable it to work with low ambient luminosity. The Lidar, as for it, can work without light.

With the Lidar, a complete scan is realized. Based on this point cloud, a triangular mapping (Fig. 7) is generated and converted in a 3D shape. The first use of this 3D shape is to enable the SCANSITES® to locate the defects in 3D.

With those incoming data, we proceed to the visual inspection. The technician scans the entire wall moving the inspection head with a joystick. When a defect is seen, it is caught. The 3D map is updated in real time with defects and the database is filled in, with its characteristics and coordinates.

In parallel to the scanning operation, a complete high definition photogrammetric coverage is done.

6 TREATMENTS

The treatments aim to produce, on a multilayer file, a map containing all defects caught, the geometric deflections and the photogrammetric coverage.

The first step is to compare the dam's 3D shape to the theoretical shape or to a previous survey. The 3D deflections are extracted, and a map is generated. Two ways of representation are possible. One is a coloured map: each colour depending on deflection value. The other way is to carry out a contour line representation.

The second step is to overlay the defects surveyed with the SCANSITES®, using the referential network.

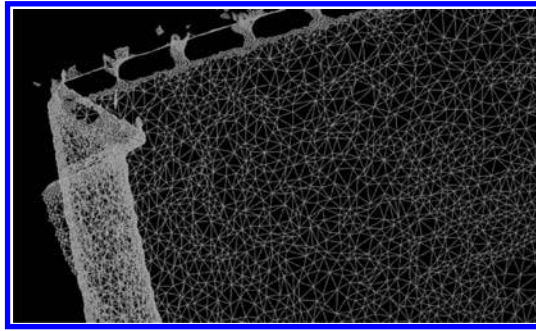


Figure 7. Triangular mapping.

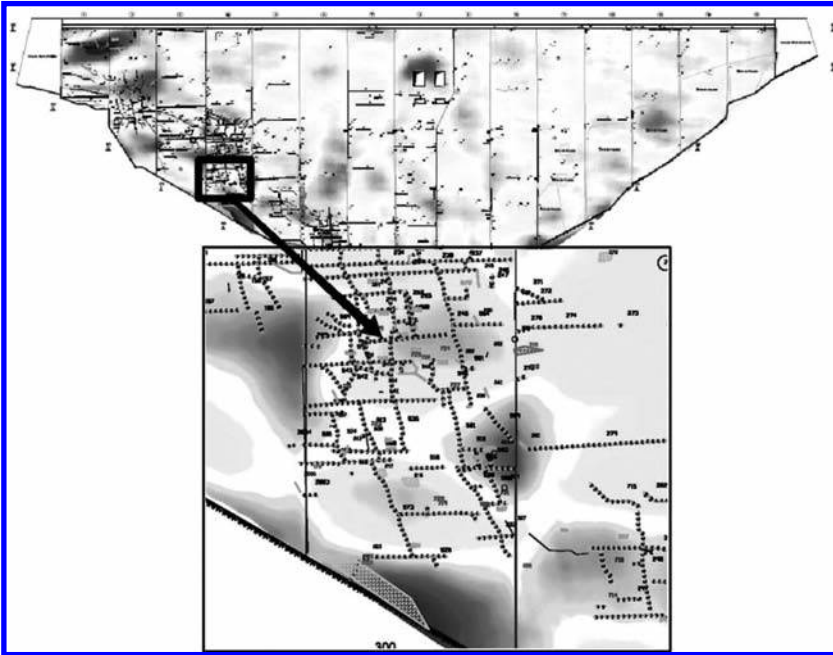


Figure 8. Map overlaying deflection/defects and magnifying.

The last step is to overlay the pictures directly on the structure's 3D shape enabling to produce an orthophotography. With that file, many views can be generated such as composite views: defects/deflections, defects/pictures, or thematic views (based on database queries).

6.1 Case study: dam N°1

The SCANSITES 3D® method was applied on a dam, located inside EU. Its main figures are 87 meters high and 180 meters long along the crest. The aim of this job was to connect the geometric deflections to the defects surveyed. Both upstream and downstream facings were monitored.

The Lidar survey required 12 million points, and the defect total quantity was near to 300.

The map (Fig. 8) shows a colored layer of the downstream facing deflections vs. defects drawing (mainly cracks).

6.2 Case study: dam N°2

The second case study concerns a dam also located in EU but slightly larger: 120 meters high and 250 meters long along the crest. The average distance between SCANSITES 3D® points of view and the downstream facing were about 200 meters (Fig. 9).

On this dam, two parts are distinguished: a sensitive part, located near to the banks and the bottom, and a common part which is the remainder.

The aim of the job is to get dam geometric deflection, a very accurate visual inspection onto the sensitive part, a less detailed inspection onto the common part and a global photo-grammetric coverage.

As carried out on the previous case study (Dam n°1), a Lidar point cloud was generated representing tens million points. In parallel, we covered the whole facing with pictures, projected it on 3D shape, and then on projection cylinder, for a total quantity exceeding 3 billion pixels (Fig. 10).

Concerning the visual inspection, the SCANSITES® was used for the sensitive part. For the common part, all defects were caught directly on the 3D textured model.



Figure 9. Lidar and SCANSITES® in operation.

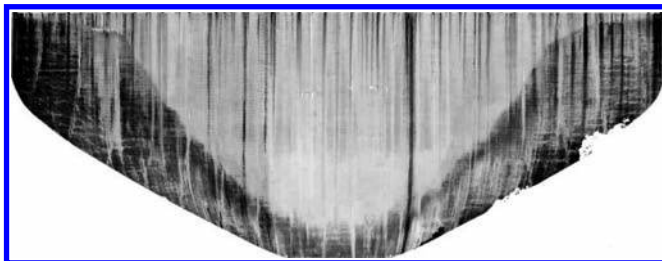


Figure 10. Orthophotography (cylindrical projection).

7 RESULTS

Concerning the visual inspection, the main difficulty for traditional methods, such as rope access or binocular inspection, is to produce a map enabling a good location of defects and their evolutions. SCANSITES 3D® provides some numerical results: a scaled defect map and defects database. The first result is to produce an accurate report emphasizes defects evolution between two inspections, and the number of defects classified by zone (Fig. 11). This is helpful for establishing an accurate bill of quantities for restoration works, like total crack length to be treated, total corroded bar amount for passivation treatment...

The Lidar coverage is a guideline for defects analysis, for instance to see if cracks are correlated, or not, with geometrical distortions.

Another interesting point is its use on parts covered of vegetal moss. Scanning one way we get structural information whereas visual inspection is inefficient. It is also helpful to know where a structural diagnosis has to focus on (with concrete sample or testing core for example).

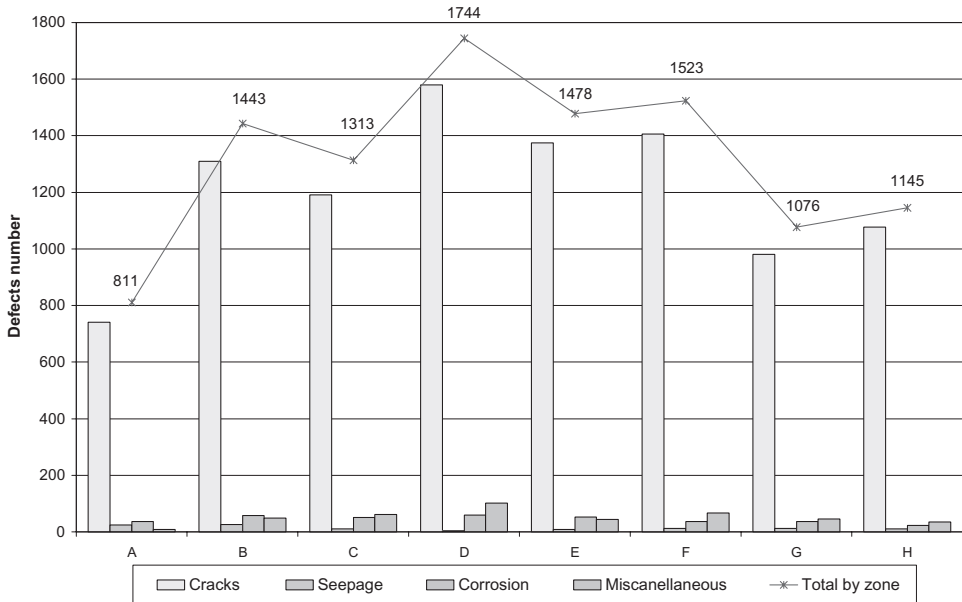


Figure 11. Number of defects by family and zone.

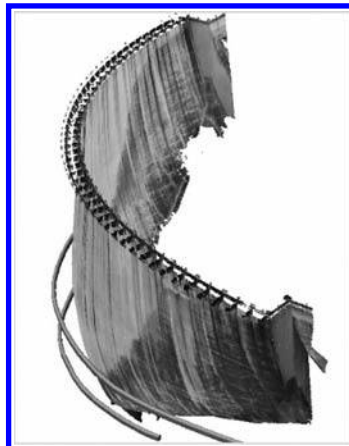


Figure 12. 3D textured shape of a downstream with a surveying of galleries.

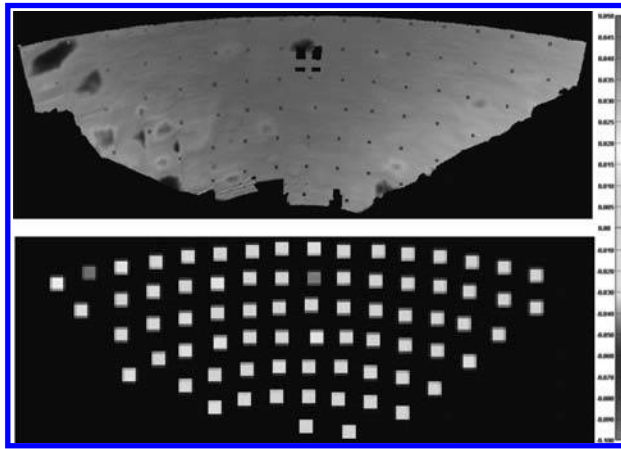


Figure 13. Scanner distortion map superposed to classical surveying targets, and classical surveying targets distortions.

As the accurate 3D shape of the dam is known, data for planning sensor installation or wells location can be easily computed (Fig. 12).

Traditional geometric survey uses theodolites and well-known microtriangulation methods. It presents the advantage to provide some results close to the best possible accuracy (near to 1 mm). However, the drawback is to be a “discrete” method, because it focuses on limited number of points, usually few tens (target, reflectors), not necessary placed on critical parts.

Even if SCANSITES 3D® is less accurate, the high density scan produces some surface definitions near to 3–4 mm uncertainty. Usually working with few millions points, it provides a global information. It widely improves the sensitivity of the geometric diagnosis, showing all details (Fig. 13).

The last advantage is these methods work on every structure, even if there is no surveying equipment such as targets.

All data (photo, geometric survey, defects maps, evolutions) are overlaid on a same file. The engineer gets a faster way to make his diagnosis compared to the fastidious data fusion imposed by separated reports.

The last result is to store all collected data in a database, offering efficient tools to measure the structure ageing and widely a “fleet” of structures.

All these jobs are performed without rope access, increasing dramatically the safety conditions.

8 CONCLUSION

We’ve presented a new and modern approach for visual inspection and geometric survey, here focused on dams, with the SCANSITES 3D®. This method is particularly adapted to every structure which needs the resuming of its monitoring program, because it provides an exhaustive inventory. It also permits to readjust an existing monitoring program by completing the lacks forgot by classical approach. Not only is this method adapted to concrete structures, but it can also be used on old constructed works, masonry-work, clay works. The correlations between the defects and deflections are finally some precious information to locate the areas where geodic surveying and sensors have to focus on. Moreover, besides useful results for the monitoring, the SCANSITES 3D® provides as-existing mappings which are often lacking on old structures. This method is widely applicable on large structures such as cooling towers but also skyscrapers, chimneys. The next step (in progress) is to overlay a high accuracy thermographic imagery survey. The aim is to study the possible gain in diagnosis, mainly on cracks.

Maintenance and operation of aged dams

Y. Kita, S. Ariga & M. Katayama

Electric Power Development Co., Ltd, Tokyo, Japan

ABSTRACT: In this paper, our approach for extending the lifetime of the aged dams is described. The main problems of the aged dams are structural deterioration and disappearance of records. The extraction work of the problem was conducted based on the failure mode analysis of the dam for structural deterioration. Consequently, there was no urgent problem connecting with the dam failure. But, it turned out that information such as monitoring records had not been used effectively enough for maintenance of dams. It was reconfirmed that the periodical check and the measurement were the most important for the operation and maintenance of the dam, and various approaches for the improvement of the dam safety have commenced.

1 DAMS OF EPDC

1.1 *History of EPDC*

EPDC (Electric Power Development Co.,Ltd.) was established in 1952 to accomplish the large-scale power generation projects suitable for a rapid increase in the power demand of Japan after World War II. The first large-scale electric power development that EPDC had handled was the Sakuma Dam of the concrete gravity type of 155.5 m in height in 1956. Then the domestic construction standard of a large-scale dam in Japan was not provided. So it was designed by adopting an overseas technology and the standard, and constructed by using imported construction equipments. Afterwards, the Okutadami Dam (concrete gravity type, 157.0 m, 1960) and the Miboro Dam (rock-fill with inclined impervious core, 131.0 m, 1961) which was called "Pyramid in the Orient" at that time were developed. The large-scale hydro power projects have been accomplished in a short term, and now EPDC subsequently owns and operates 48 Dams in Japan. The major EPDC dams show in [Table 1](#), and those locations in [Figure 1](#).

1.2 *Current situations and issues of hydro power plant*

Recently, Japan's economic growth is at low level after the high-growth period had been maintained after World War II, and also the expansion of the power demand has stagnated. The number of domestic new hydro power projects has decreased, and the scale is also smaller than before. However, the hydro power as renewable energy performs the key role in accordance with highlighting the value of global environment. Moreover, Japan's self-sufficiency ratio of the energy resources is the lowest in the advanced countries, and importance of the hydro power that is a pure domestic energy is quite high. Effective use of the existing hydro power is the national proposition in term of energy security.

The history of the hydro power development in Japan is so old that the half number of existing hydro power stations passed 60 years or more after construction, and various repair works, big and small, of the old hydro power plants are increasing in recent years. It is big problem for the electrical power companies in Japan how aged hydro power plants will be operated efficiently for a long time. The 73% of EPDC dams also passes 40 years or more ([Fig. 2](#)). The mission of EPDC is changing from the large-scale hydro power development into adequate maintenance to extend its dams' lifetime.

Table 1. Major EPDC dams.

Name	Type	Hight (m)	Crest Length (m)	Storage Capacity (m ³)	Since
Nukabira	Concrete-gravity	76.0	293.00	193,900,000	Jan-1956
Sakuma	Concrete-gravity	155.5	293.50	326,848,000	Apr-1956
Akiha	Concrete-gravity	89.0	273.40	34,703,000	Jan-1958
Kuromatagawa I	Concrete-gravity	91.0	276.00	42,845,220	Feb-1958
Tagokura	Concrete-gravity	145.0	462.00	494,000,000	May-1959
Kazaya	Concrete-gravity	101.0	329.50	130,000,000	Oct-1960
Okutadami	Concrete-gravity	157.0	480.00	601,000,000	Dec-1960
Miboro	Rock-fill	131.0	405.00	370,000,000	Jan-1961
Sakamoto	Aroh	103.0	256.30	87,000,000	Apr-1962
Ooshirakawa	Rock-fill	95.0	390.00	14,200,000	Dec-1963
Kuromatagawa II	Aroh	82.5	235.21	60,000,000	Jan-1964
Ikehara	Aroh	111.0	459.96	338,000,000	Sep-1964
Yanase	Rock-fill	115.0	202.00	104,625,000	Jun-1965
Misakubo	Rock-fill	105.0	258.00	30,000,000	May-1969
Kassa	Rock-fill	90.0	487.00	13,500,000	Jul-1978
Futai	Rock-fill	87.0	280.00	18,300,000	Jul-1978

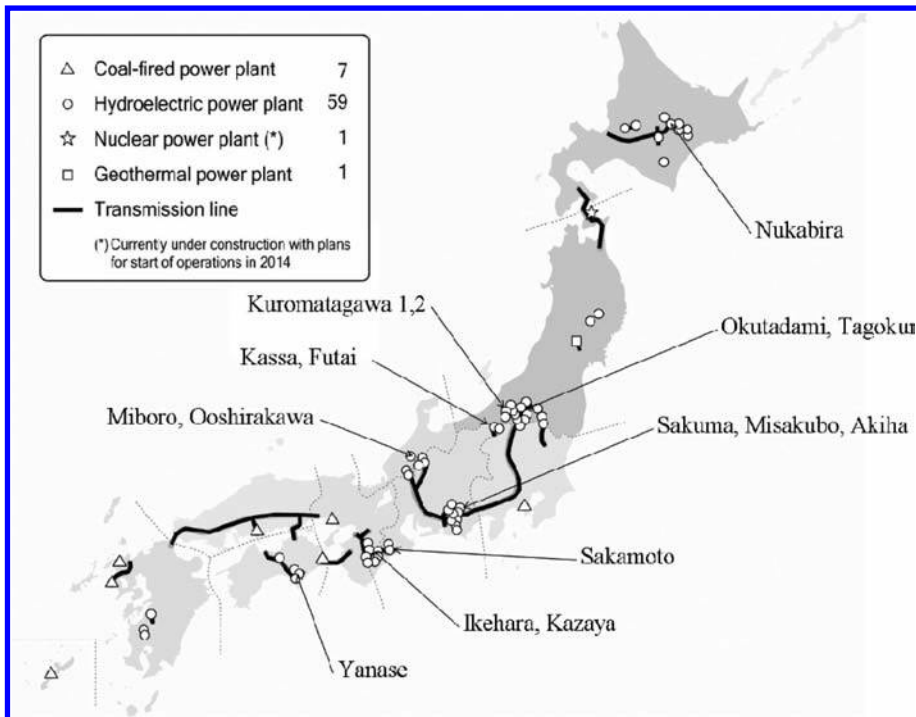


Figure 1. Locations of EPDC dams.

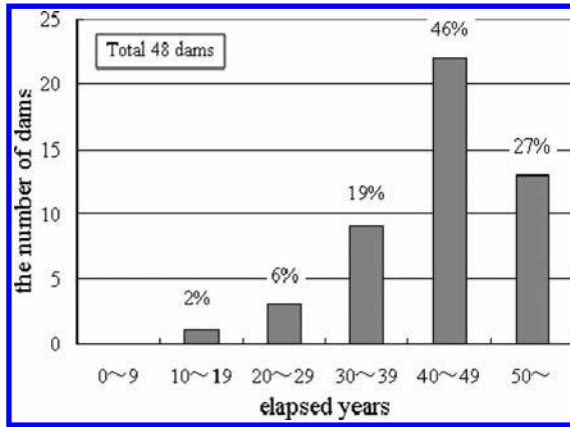


Figure 2. Elapsed years distribution of EPDC dams.

2 THE APPROACH FOR SAFETY MANAGEMENT OF DAM

2.1 Problems in safety management of dam

Although structural remarkable damage is not observed, partial deterioration of dams that EPDC manages begins to appear. For example, the water stop in construction joint deteriorated, and the surface materials of rock-fill dam weathered although those phenomena cause neither critical nor dysfunctional damage immediately. The dam has a complicated and organic function to store the river water, to generate the power utilizing the storage water, to supply the water to the industry, the public and for irrigation, and to control the flood. The steel structure such as the gates and the mechanical devices are maintained preventively based on the elapsed time. However, the fixed quantitative evaluation of the degradation phenomenon is difficult, because the dam is composed of various structures. It is necessary to understand that deterioration mechanism is different among each dam and it is important to make an appropriate diagnosis to an individual dam and to maintain it in the most effective way.

Moreover, when dealing with the aged deterioration, the problem is not only structural deterioration but also disappearance of information. The important information such as geological features and technological methods during construction was rarely recorded systematically at that time, and only a part of it was described explicitly in the construction records. A lot of information necessary for dam maintenance is disappearing as time goes by. That is the cause to make the dam safety management difficult.

2.2 The systematic approach for dam safety evaluation

The monitoring and the measurement are the most important work for managing the dam safety. The maintenance team at the site office has executed a repair work in a small-scale based on the daily monitoring and the measurement. On the other hand, a large-scale refurbishment has been conducted by the head office. Recently, as the deterioration of the most of dams is proceeding, it becomes more difficult for site office to evaluate the degree of deterioration and the most effective investment cost, which requires a high-level engineering judgment. Considering that situation, we are trying to create the system (Fig. 3) to manage the dam efficiently.

2.2.1 The risk analysis for dams

First of all, we tried to understand the current state of the dam, and to extract the risk connecting with the dam failure, then we referred the technique of the dam failure mode analysis used by Federal Energy Regulatory Commission (FERC)¹⁾, after comparing domestic and foreign standards. Secondly, we made the risk scenario (Fig. 4) taking into account the dam

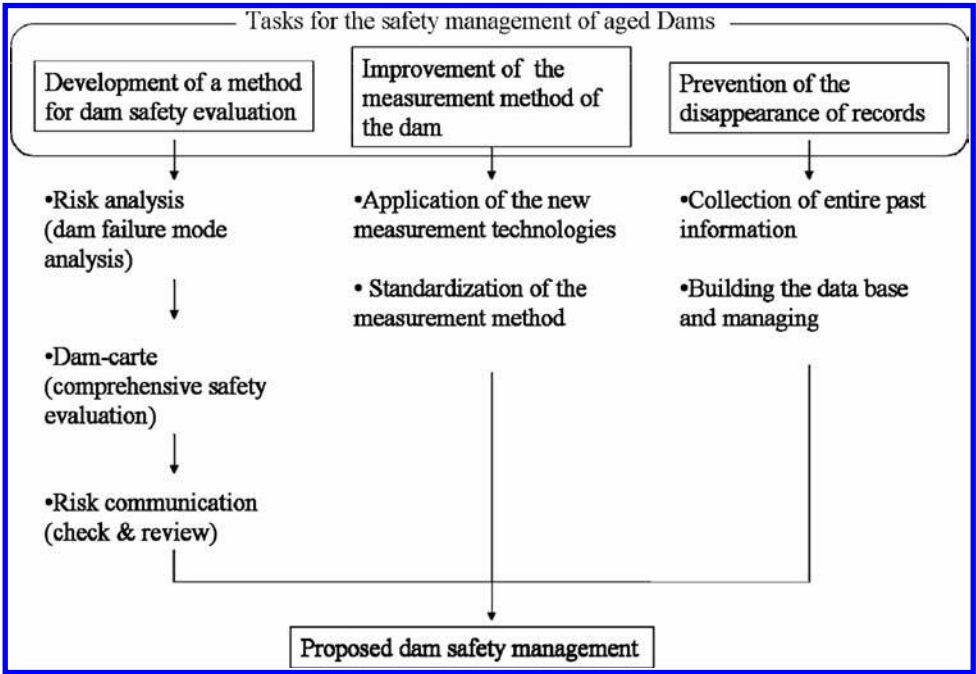


Figure 3. Approach for the safety management of dams.

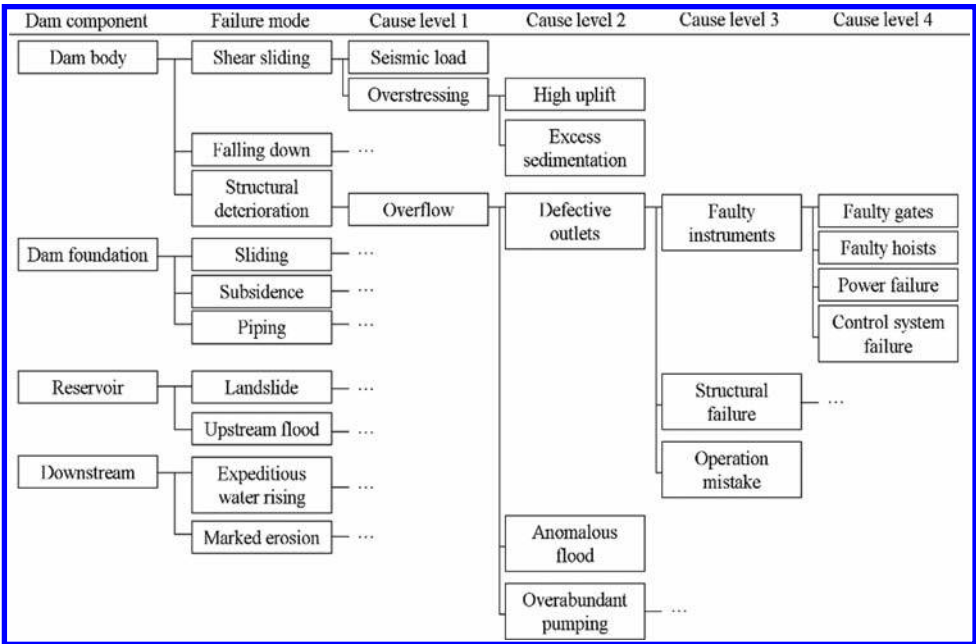


Figure 4. Tree diagram of dam failure mode and cause level.

failure modes and causes by each types of dam. According to the risk scenario, the chief engineer for each dam checks whether there is an event to meet the scenario or not. If there are any items to meet the scenario, they will collect and arrange the evidences, such as the pictures and the monitoring data. They can relate the events occurring in the dam to the dam failure mode, and can improve the knowledge of risk management by doing this analysis.

2.2.2 The dam-carte (comprehensive safety evaluation)

The dam-carte is the record of a series of information including the extracted problems by the risk analysis, the countermeasures, the progress, and the verification of the result. In the dam-carte, the extracted problems are prioritized according to the degree of influence and its emergency. And those problems are classified into two categories. One is the small-scale and a short term problem and the other is the large-scale and a mid/long term one. All of the related parties from the chief engineers for each dam to the engineers belonging to the head office have a common view through the dam-carte, and use it as the judging source for the capital investment.

2.2.3 The risk communication (check & review)

The risk communication is held to check the propriety of the dam-carte in order to make procedure, and to plan the countermeasures and those priorities. It is organized by the local managers, engineers in the regional offices, and the engineers at the head quarter including the external experts (Fig. 5).

2.3 Problems and countermeasures led from the result of risk analysis

2.3.1 Outline of the risk analysis result

As a result of the risk analysis done for 48 all dams that EPDC had, there was no critical problem connecting with the dam failure at the moment. However, it turned out that the dam measurement data that was the important information to evaluate the dam condition has not been verified enough so far. For instance, there was the volatility of the data seemed to be the movement of the reference point for the dam measurement, and the loss of the data caused by the plugging of the uplift measurement hole. Thus, there were some cases that the data was not verified regarding the reliability and the measurement method.

On the other hand, the steel structures such as the gate and the electrical control devices etc. were maintained periodically, so there was no problem to keep its quality.

2.3.2 The problems of the dam measurement

2.3.2.1 Seepage from the concrete dam

The total volume of the seepage from the concrete dam is measured together with the seepage from the joints and from the drain holes. The total amount of the seepage from some old dams over 50 years tended to increase gradually. It was too difficult to point out the reason of the increase when the measurement of the seepage from the joint and the drain holes was not separated. If it was separated as shown in Figure 6, it shows clearly that the seepage from the

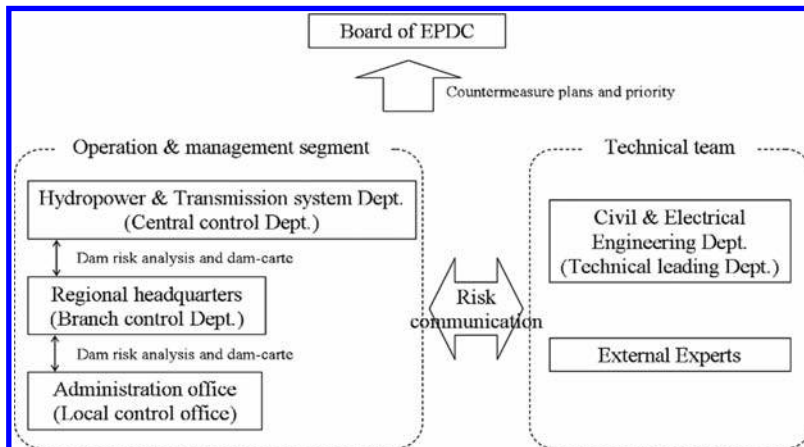


Figure 5. Risk communication in EPDC.

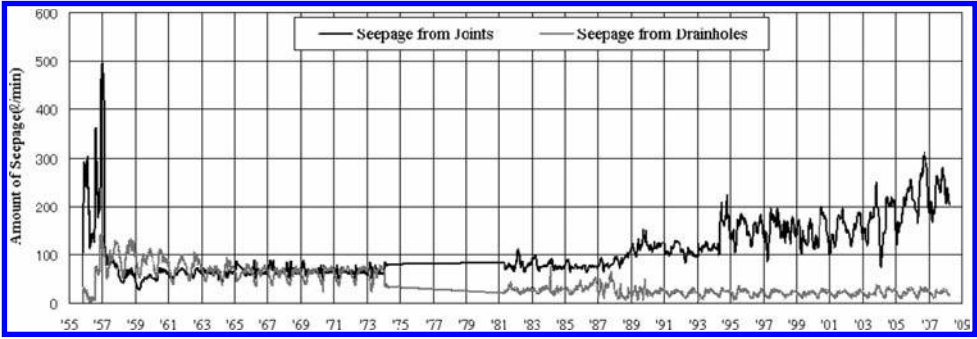


Figure 6. Seepage chart in a concrete-gravity dam.

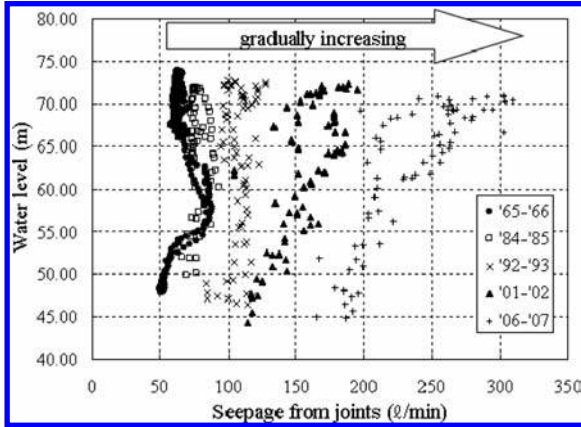


Figure 7. Correlation between seepage from joints and water level.

joints is gradually increasing, and one from the drain holes is decreasing. Figure 8 also shows the linear relation between the seepage from drain holes and the water level recently, so the hydraulic characteristic of the foundation of the dam is thought to be stable.

2.3.2.2 Uplift measurement

There were some cases where the uplift of a concrete-gravity dam showed “0”. In this case, it is necessary to check the reason why the instrument doesn’t react, for example, the breakdown of the meter, or the plugging of the drain holes. After the soundness of the devices is confirmed, it will be able to judge whether the uplift shows “0”, or the uplift water level doesn’t reach the top of the hole. An appropriate uplift measurement can be done only after those confirmation works are done.

2.4 Improvement of dam measurement

In case of the measurement of the dam displacement, it is necessary to treat the reference point as fixed point to survey a relative position and the movement of the dam. Several decades have passed since the dam construction, and there are some possibilities that the immobility of the reference point is doubted. Since the reference point is believed to be stable, the main reason of the dam displacement is thought to depend on the measurement error. However, the GPS technology is developed and prevailing, and an absolute position can be specified now. We are attempting to confirm the immobility of the reference point by using the GPS technology.

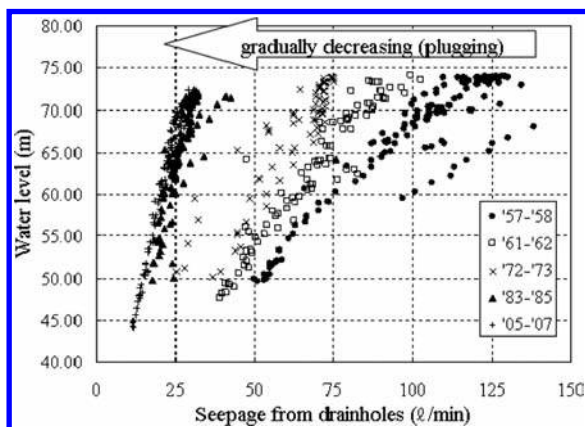


Figure 8. Correlation between seepage from drain holes and water level.



Figure 9. GPS installed on a rock-fill dam of EPDC.

Moreover, an industrial fiberscope can be applied to check the internal condition of the drain holes of the concrete dams, now. When it is plugged by the efflorescence and the function of the drain holes is damaged, measures to recover its function such as cleaning and the re-boring, etc. should be examined.

It is recognized again that it is important to understand that the original purpose of the measurement work is to confirm the stability of the dam, to detect the fault, and to maintain the appropriate environment for the measurement to reflect the dam's condition. And, we are trying to make an in-house standard of the dam measurement that shows the purpose of the dam measurement, the method, and the application of the new technologies.

2.5 Prevention of the disappearance of records

The development of the electronic information technology, information processing technology, and the telecommunication technology are improving the handling of the measuring data and the recorded information. Records of the past are uniformly managed and all information is shared among related parties through the data base system. This data base has a probability to make it more convenient to explore the similar events when some troubles are observed at any dams.

3 CONCLUSION

In Japan, after the age of large-scale infrastructure construction, it entered into the age of maintenance, when existing facilities should be maintained adequately for a long time. The dam is the compound and organic structure composed of the foundation, the dam body, and the associated equipment structure, and maintenance methods of dams are different from those of the mechanical and the steel structure. The improvement of the measurement technique makes it possible to specify the dam condition quantitatively and visibly which has not been observed so far. However, the monitoring is one of the most important works for the safety management for the dam. We have to change the consideration about the existing measurement methods, and to examine the new method in order to keep the dam safety. At the same time, we have to prevent the experiences accumulated so far from weathering, and aim to improve the maintenance technology as well as the construction technology.

REFERENCES

- Federal Energy Regulatory Commission: *Engineering Guidelines for the Evaluation of Hydropower Projects*, [Chapter 14](#), *Dam Safety Performance Monitoring Program*, July 1, 2005.
U.S. Dept. of the Interior Bureau of Reclamation: *Safety Evaluation of Existing Dams*, 1983.

Estimation of rockfill dam behavior during impounding by elasto-plastic model

N. Tomida, N. Sato, H. Soda & S. Jikan

Japan Water Agency, Saitama, Japan

K. Ohmori

Ridge Research Institute of Digital Geo-Environment, Kanazawa, Ishikawa, Japan

H. Ohta

Research and Development Initiative, Chuo University, Tokyo, Japan

ABSTRACT: Tokuyama dam is one of the largest rockfill dams in Japan, which JWA constructed across the Kiso River. Since width of the central core of Tokuyama dam was re-designed to be thinner than the original design. Therefore, evaluation of the safety of the core zone during the impounding period was carried out by both numerical analysis and observed data. In this report, following the actual construction process of embankment and impounding, an elasto-plastic soil/water coupled consolidation analysis is carried out to find the rise of pore water pressure and change of effective stress in the core zone. The safety level of the core zone during the impounding period was evaluated by Seed standard.

As a result, numerical analysis and observed data matched closely, which confirmed the validity of the analysis. The safety of the core zone during the impounding period was confirmed by both observed data and numerical analysis.

1 INTRODUCTION

Tokuyama dam is a multi-purpose dam constructed by JWA. It is one of the largest rockfill dams in Japan with the dam height of 161 m, the dam volume of 13,700,000 m³ and the gross storage capacity of 660,000,000 m³.

Figure 1 shows the location of Tokuyama dam. The construction work started in March, 2000, and completed in the end of November, 2005. The first impounding commenced on September 25, 2006. The water level in the reservoir reached surcharge water level on April 21, 2008, followed by the completion of the first impounding on May 5, 2008.

In Japan, the bottom width of the core zone of rockfill dams is normally around 40–50% (Ministry of Construction River division, 1987) of the dam height. The final design of Tokuyama dam applied thinner shape, and its bottom width of the core zone is 36% of the dam height. Due to adopting the thinner core zone than normal design, the stress reduction was concerned. So the appropriate estimation on safety against failure during the impounding period was necessary.

In this report, an elasto-plastic soil/water coupled consolidation analysis was carried out to simulate the physical behaviors within the dam body based on the actual construction process of embankment and impounding in Tokuyama dam. A comparison of the numerical analysis and observed data shows similarity, which proved the validity of elasto-plastic soil/water coupled consolidation analysis. The safety of the core zone during the impounding period was also estimated by using the results of this analysis.



Figure 1. Location of Tokuyama dam.

2 OUTLINE OF THE ANALYSIS

The analysis predicts the pore water pressure and minor principal stress of the core zone as the following procedures, in order to evaluate the safety level for hydraulic fracturing during the first impounding. Firstly, the rise and dissipation of pore water pressure of the core zone during the embankment is predicted. After that, the dam body behavior during impounding is analyzed in the initial conditions of the first impounding decided by the first prediction. During the impounding period, the elasto-plastic soil/water coupled consolidation analysis is carried out to estimate the rise of pore water pressure, the rise of osmotic pressure at the upper part of the dam body, the change of the effective stress and the dam body behavior. In the above analysis, the elasto-plastic soil/water coupled consolidation model is adapted as the model of the embankment material of dam.

The elasto-plastic soil/water coupled consolidation model employed a stress-distortion relationship (constitutive law) of Sekiguchi-Ohta model (Sekiguchi and Ohta, 1977) which can cover embankment material with anisotropy and predict the volume change of soil induced by compression stress and shear accurately. Figure 2 shows the conceptual diagram of elasto-plastic model. Table-1 shows main parameters used for analysis.

The analysis parameters of filter material and core material are set based on material test whereas that of rock material is based on both material test and observed data at site. The earth pressure coefficients at rest K_0 of each material is 0.7.

Figure 3 shows the relation between coefficient of permeability and void ratio of core material in Tokuyama dam. The coefficient of permeability of saturated soil obtained from consolidation test is 10 times larger than that of unsaturated soil obtained by consolidation test. The coefficient of permeability obtained from permeability test on embankment surface at site matches closely with that of saturated soil obtained by consolidation test. The coefficient of permeability used for the analysis is set based on the result of consolidation test of unsaturated soil, since the core material is unsaturated during embankment. The initial coefficient of permeability is obtained by consolidation test in which void ratio of the material was adjusted to the average void ratio in embankment area at site. Because the material of core with small void ratio tends to have lower permeability, coefficient of permeability is changed according to the change of void ratio obtained from the analysis, using the relationship between the coefficient of permeability and void ratio obtained from the consolidation test shown in dotted line in Figure 3. In the analysis, the coefficient of permeability is changed in every embankment stage.

Figure 4 shows the cross section of Tokuyama dam used for the analysis. Tokuyama Dam has the height of 161 m, upstream slope gradient of 1:3.0, downstream slope gradient of

A-B: Elastic territory
 (Embankment load < Compaction by the pre-compression stress P_c)
 B-C: Elasto-plastic territory
 (Embankment load \geq Compaction by the pre-compression stress P_c)
 C-D: Elastic territory
 (Decrease of the effective stress by the impound)

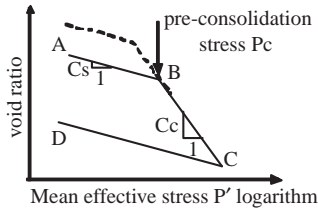


Figure 2. Conceptual diagram for elasto-plastic model.

Table 1. Material parameter for the analysis.

Category	Unit	Rock material	Filter material	Core material
Swell index (C_s)		0.0375	0.0033	0.0045
Compression index (C_c)		0.0860	0.0140	0.0215
Pre-consolidation stress (P_c)	(kPa)	820	920	132
Friction angle (ϕ')	(degree)	43.3	39.4	37.8
Coefficient of permeability	cm/sec	3.05×10^{-1}	8.0×10^{-4}	1.93×10^{-7}
Critical state parameter (M)		1.78	1.61	1.54
Irreversibility ratio (Λ)		0.564	0.764	0.791
Coefficient of dilatancy (D)		0.00317	0.00234	0.00928
Effective poisson ratio (ν')		0.412	0.412	0.412

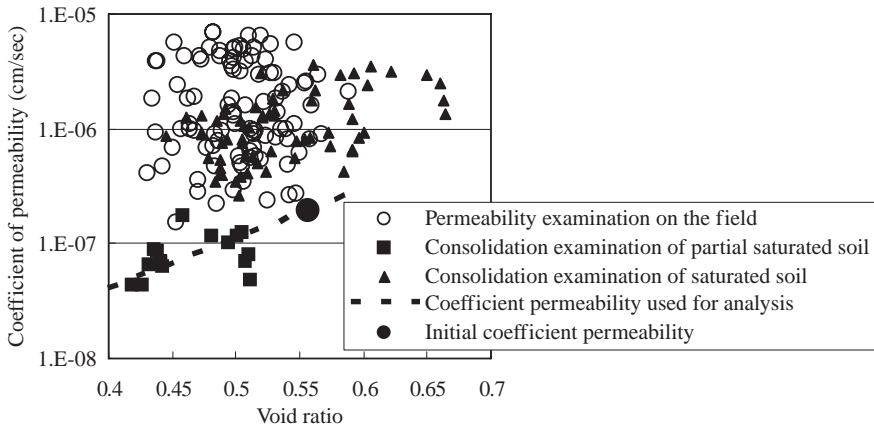


Figure 3. Relation between core material's coefficient permeability and void ratio.

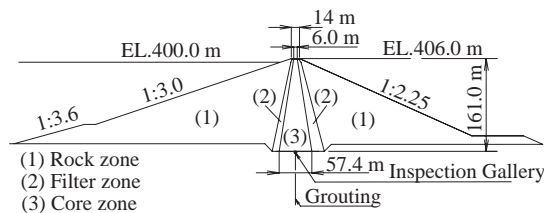


Figure 4. Cross-section.

1:2.25, and its symmetric core slope has a gradient of 1:0.16. The analysis is implemented for the dam body and the foundation. The analysis horizontal range is about the double of the base width and the vertical range is about the double of the dam height. The number of elements is 5524 in the finite elements method. As the boundary conditions, the horizontal displacement at the side of the foundation is 0 and that at the underside is fixed. As the hydraulic boundary conditions, the distribution load and hydrostatic pressure based on the reservoir level is set on the upper face of the dam. Also the vertical load based on the difference between the wet density and saturated density is set at the dam body under water. The pore water pressure at the lower rock zone is set as 0 during the embankment and impounding period. As the boundary conditions, the water pressure based on the reservoir level at the upper side of the foundation, the hydrostatic pressure at the lower side of the foundation and the undrained condition at the underside are set respectively.

In the embankment analysis, in order to represent the actual embankment process, the elements of dam body are accumulated successively based on the embankment process as shown in Figure 5.

In the impounding analysis, the effective stress is numerically predicted by an unsteady-state seepage analysis in saturated soils with a time dependent boundary condition of escalating water level in reservoir.

The fracturing pressure of the core zone is evaluated by “(Seed and Duncan, 1981)”. Seed suggests a quantitative evaluation method of hydraulic fracturing which defines the condition of soil destruction with crack by the following formula.

$$u_f = \sigma_3 + \sigma_t \quad (1)$$

where u_f = hydraulic fracturing pressure; σ_3 = minor principal stress in total stress; σ_t = tensile strength of soil.

In this report, the generation of hydraulic fracturing of core material is based on the Seed standard. Local safety factor against hydraulic fracturing (Fsh), is obtained by formula (2), neglecting tensile strength of soil to evaluate in a severer condition.

$$Fsh = (\sigma_3 + \sigma_t) / \Delta u \quad (2)$$

where Δu = pore water pressure.

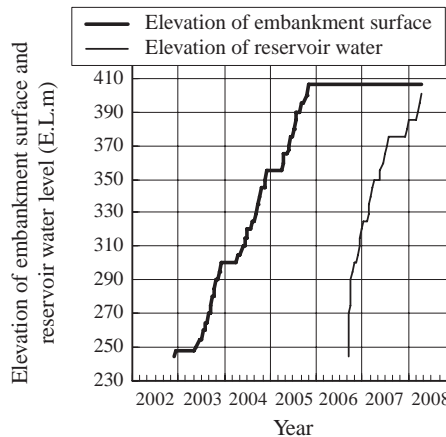


Figure 5. The process of embankment and impounding turned into a model by FEM analysis.

3 INVESTIGATION AND CONSIDERATION ON RESULT OF DAM BODY BEHAVIOR ANALYSIS COMPARED WITH ACTUAL VALUE

Figure 6 shows the comparison of settlement value at the same location between numerical result and data measured by settlement gauge A-2. The comparison shows close similarity when the water level reaches the maximum water level.

Figure 7 and Figure 8 show another comparison at the same location between numerical results and data measured by vertical earth pressure gauge, E-14 set up in the upper side of middle elevation of core zone and E-15 set up in the center part. The comparison of the value at E-14 between numerical results and data measured at site shows a close similarity, whereas that of E-15 does not. At E-15, earth pressure is numerically predicted larger by 30% than observed data.

Figure 9 and Figure 10 show a comparison of pore water pressure between numerical results and measured data at the time of maximum water level during the first impounding.

Residual pore water pressure exists after the completion of embankment, but the osmotic pressure in the core rises due to the impounding. Both observed data and numerical prediction show the dissipation of pore water pressure when the water level reaches the maximum water level, leaving the profile of pore water pressure high at the upper stream and low at the downstream.

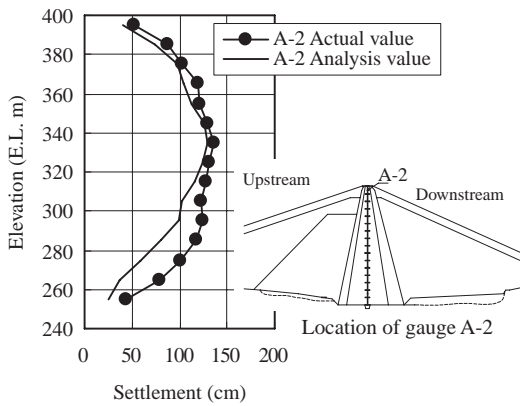


Figure 6. Actual value and analysis value by differential settlement gauge (Maximum water level).

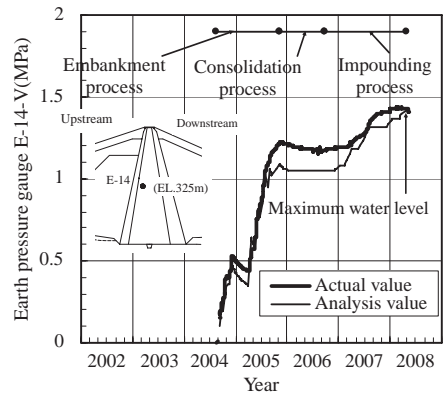


Figure 7. Chronological change of Vertical Earth Pressure.

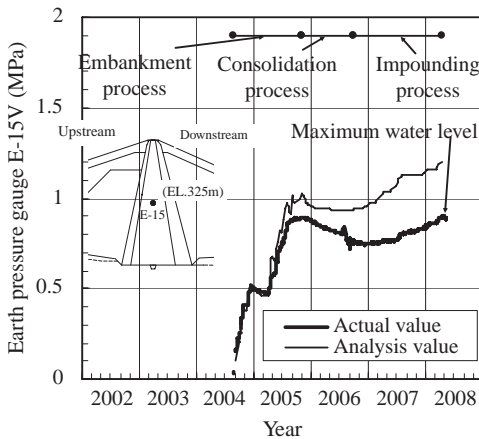


Figure 8. Chronological change of Vertical Earth Pressure.

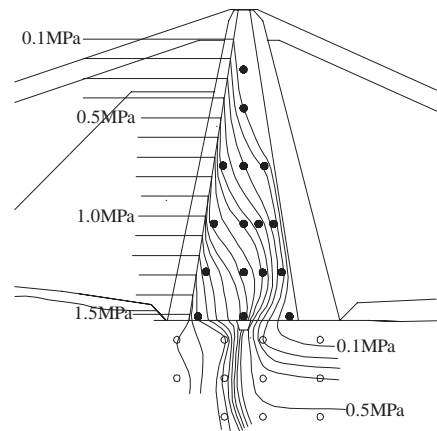


Figure 9. Distribution map of Pore water pressure on highest high-water level (actual value).

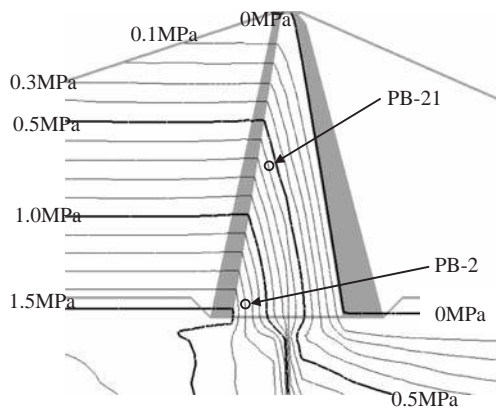


Figure 10. Distribution map of Pore water pressure on highest high-water level (analysis value).

Figure 11 and Figure 12 show a comparison of pore pressure at the same location between numerical prediction and observed data measured by pore pressure gauge at PB-21 set up in the upper side of middle elevation of core zone and PB-2 set up in the lower elevation. It shows similarity between numerical result and observed data of pore water pressure during the process of embankment and at the time of the maximum water level. Differences between numerical prediction and observed data are seen from November, 2005 to March, 2007. During this term, observed data tends to be larger than numerical prediction. The dissipation of water pressure is calculated by seepage analysis, on the assumption that the core is saturation. On the other hand, the core is unsaturated during this term, so the coefficient of permeability is small, seemingly resulted in the delay of dissipation of pore water pressure.

Figure 13 shows distribution contour of major effective principal stress at the end of embankment obtained by the embankment analysis. The generation of arching phenomena due to the difference of rigidity between core zone and filter zone leads the stress reduction in the core zone.

Figure 14 shows a comparison of the major principal stress σ_1 , minor principal stress σ_3 and pore water pressure at the same location between numerical prediction and data measured at E-14. Observed major principal stress σ_1 and minor principal stress σ_3 are calculated based on the data from trihedral earth pressure gauge. The numerical prediction is successful to simulate the qualitative trend of pore water pressure inside of the core, major principal stress in total stress σ_1 and the minor principal stress in total stress σ_3 , to increase parallel with the water level in the reservoir. Observed data and numerical prediction of minor principal stress σ_3 shows a close similarity. In addition to that, major principal stress in total stress σ_1 and minor principal stress in total stress σ_3 surpass pore water pressure in every point.

4 CONSIDERATION ON THE SAFETY AGAINST THE HYDRAULIC FRACTURING

Figure 15 shows the distribution contour of safety factor against hydraulic fracturing at the core zone obtained by the analysis at the time of the maximum water level. The safety factor against hydraulic fracturing becomes the smallest at the border of the core zone and the filter zone at the height of 1/3–2/3 of the dam height. The smallest safety factor is approximately 1.3.

On the other hand, Figure 16 shows both the safety factor against hydraulic fracturing in the core zone obtained from the observed data and that from the analysis. The smallest safety factor obtained by the observed data is 1.56, and that of numerical prediction is 1.42. Although observed data is a little larger than numerical prediction, safety factors in the core zone are nearly equal.

From these points, smallest safety factor against hydraulic fracturing at the core zone in Tokuyama dam is 1.56 based on observed value and 1.4 from numerical prediction, which confirms “safety factor ≥ 1.0 ” in every point.

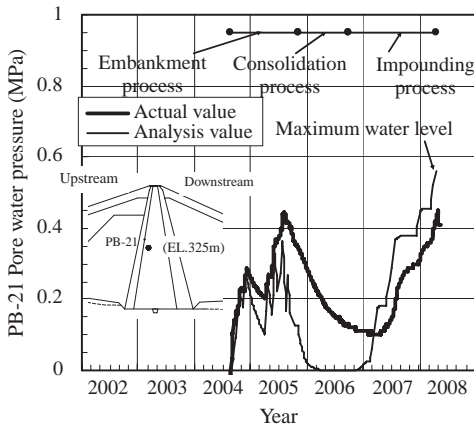


Figure 11. Chronological change of pore water pressure.

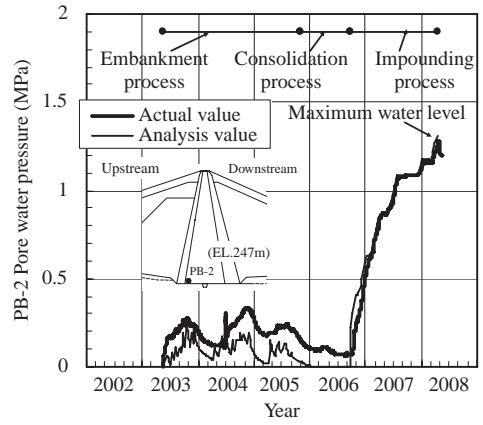


Figure 12. Chronological change of pore water pressure.

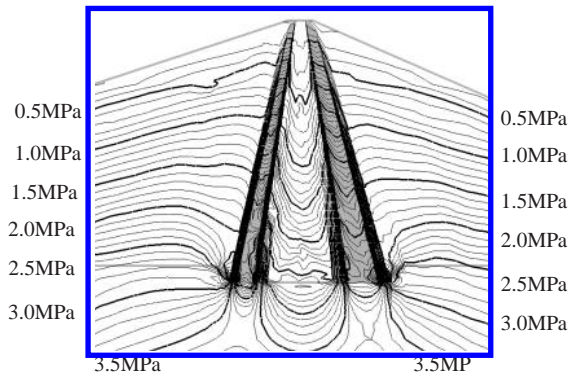


Figure 13. Distribution map of major effective principal stress when the embankment was completed (analysis value).

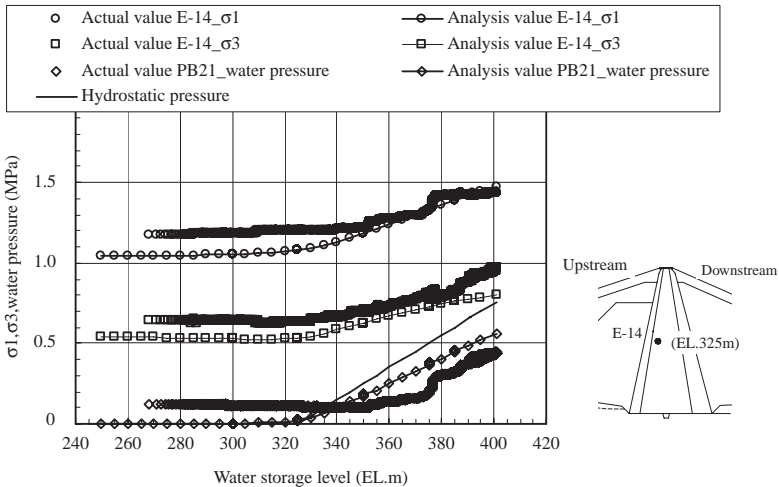


Figure 14. Chronological change of major, minor principal stress and Pore water pressure on E-14.

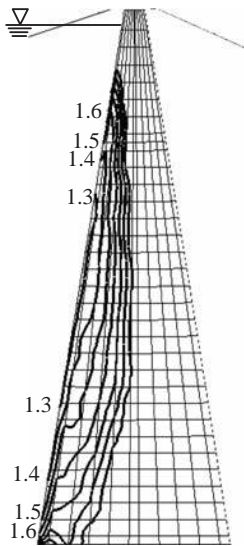


Figure 15. Distribution contour of safety factor against hydraulic fracturing in the core when the water level reached maximum water level (analysis value).

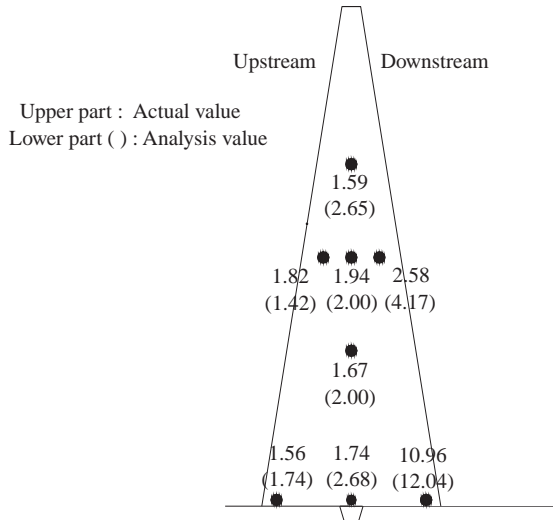


Figure 16. Safety rate against hydraulic fracturing of central core.

5 CONCLUSION

In this report, the numerical prediction of dam body behavior based on actual construction process of embankment and impounding in Tokuyama Dam is implemented by using elasto-plastic soil/water coupled consolidation analysis which can cover the rise and dissipation of pore water pressure and rise of osmotic pressure. As a result, the numerical prediction of settlement and vertical earth pressure from embankment to impounding are similar to that of observed data. The numerical prediction of pore water pressure is similar to that of observed data during the process of embankment and when impounding is completed. The numerical prediction is successful to simulate the qualitative trend of pore water pressure, major principal stress and minor principal stress in the core zone to increase parallel with the water level in the reservoir.

From these points, numerical prediction of dam body behavior in Tokuyama Dam is successful to prove the validity of elasto-plastic soil/water coupled consolidation analysis. The smallest safety factors against hydraulic fracturing at core zone in Tokuyama Dam are approximately 1.56 based on observed data and 1.4 based on numerical prediction. Safety against hydraulic fracturing is also confirmed since the smallest safety factors surpass 1.0 in both values.

Observed data during the first impounding did not show any abnormal phenomena in permeability and deformation of dam. The results of the numerical prediction matched with those observed data.

REFERENCES

- Ministry of Construction River division (Supervisor), 1987, Constructions of multi-purpose dam, 4th volume: 84. Tokyo: Dam Engineering Center foundation (in Japanese).
- Seed, B. & Duncan, J.M. 1981. The Teton Dam Failure- A Retrospective Review, Proc. of 10th ICS-MFE: 1-20.
- Sekiguchi, H. & Ohta, H. 1977. Induced anisotropy and time dependency in clays, Proc. of 9th ICS-MFE: 229-239.

The investigation method of hydroelectric facilities by using digital camera

S. Wada & Y. Kono

The KANSAI Electric Power Co., Inc., Osaka, Japan

ABSTRACT: In surface investigation of the concrete structures, an investigator has to often access a high place. In such a case, methods such as temporary scaffold and rope access are adopted. However, these methods are expensive, and dangerous. In recent years, the performances of a digital camera and image processing technology have accomplished remarkable progress. So the authors attempted to apply the photographic image measurement technique both for the surface of a dam and the concrete lining of a tunnel.

1 INTRODUCTION

The KANSAI Electric Power Co. (hereinafter called KEPCO), own 149 hydroelectric power plants in Japan and the total output of hydropower is about 8195 MW. KEPCO has Inspection and Monitoring System divided into three portions, such as patrol, inspection and deterioration diagnosis. The patrol is conducted daily and monthly, and the inspection is conducted annually. The deterioration diagnosis is conducted once in several years and we assess the conditions of facilities in total.

KEPCO conducts deterioration diagnosis at our concrete dams once every 10 years, and we conduct crack monitoring of the concrete structures in the deterioration diagnosis. In conventional investigation methods, investigators have to often access a high place. In such a case, methods such as temporary scaffold and rope access (Figure 1) are adopted. These methods, however, are expensive and time consuming, and danger is accompanied. Therefore, the improvement of the investigation methods is required.

Then, the authors developed a photographic image measurement system to check the surface of concrete, and KEPCO adopts the system in actual investigations since 2009.

This newly developed system is a combination technology of a total station and a digital camera (Tsugio et al. 2008). First, images taken with a digital camera are transformed into the images viewed from the front on the PC, based on three-dimensional coordinate data obtained by a total station. Secondly, the individual front view images are stitched into a total image of the structure. Finally, the crack locations, the crack total lengths and the crack widths are found from the stitched image.

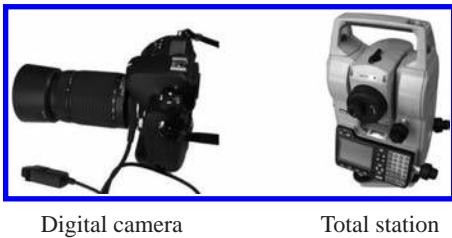
KEPCO has conducted the photographic image measurement at 16 dams and a waterway tunnel in 2009 and 2010. Authors report the investigation results here.

2 PRINCIPLE OF PHOTOGRAPHIC IMAGE MEASUREMENT TECHNIQUE

In the beginning, authors explain the principle of the image measurement technique. This technique provides synthesized front view images of the components of the structure. The technique uses images taken by high resolution digital camera and the coordinates measured by an automatic surveying instrument so called total station (Figure 2), and compensates angle, curvature and scale, then synthesizes images by image processing unit (Figure 3). Then the lengths of the cracks are measured by tracing the recognizable cracks on a synthesized



Figure 1. Dam surface inspection by rope access.



Digital camera

Total station



Figure 3. Image processing unit.

Figure 2. Image measurement equipment.

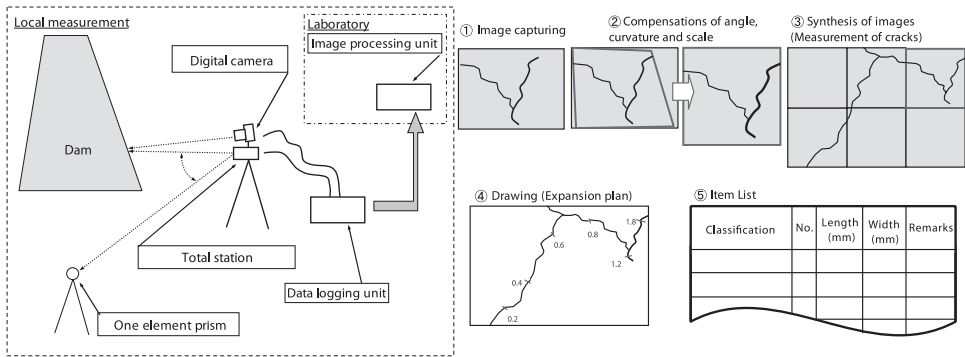


Figure 4. Flow of image measurement technique.

image displayed on a monitor and the widths of the cracks at the position that can be recognized on the cracks with the naked eye are evaluated (Figure 4). Main instruments of the system are a single-lens reflex digital camera, a non-prism total station (instrumental tolerance equals plus or minus 3 mm and plus or minus $[2 \times 10^{-5} \times \text{distance}]$), an image processing unit and a data logging unit (Table 1).

The quality of an image mainly depends on the resolution of the digital camera and the telephoto lens. When same area is captured, the quality of the image becomes higher if the digital camera is equipped with more pixels. The resolution of a pixel (the length of a side of a pixel) of the digital camera equipped with $2,900 \times 4,350$ pixels (12.6 million pixels) is around 1.4 mm when the rectangular surface of a concrete structure with the dimensions of $4 \text{ m} \times 6 \text{ m}$ is captured. Figure 5 shows an evaluation method of crack width. Since the individual pixel of the digital image usually has 256 gradation steps for each three primary color (RGB), the width of

Table 1. Specification of main equipments.

Equipment	Specification
Digital camera	Single-lens reflex digital camera: 12.6 million pixels
Telephoto lens	Autofocus (24–85, 80–400 mm)
(Non-prism) Total station	Instrumental tolerance: $[3 + \text{or} - 2 \times 10^{-5} \times \text{distance}] \text{ mm}$
Data logging unit	Note PC (CPU: Core Solo U1300, Memory: 1 GB, HDD: 60 GB)
Image processor unit	Desktop PC (CPU: Pen4, 3.2 GHz, Memory: 2 GB, HDD: 250 GB)

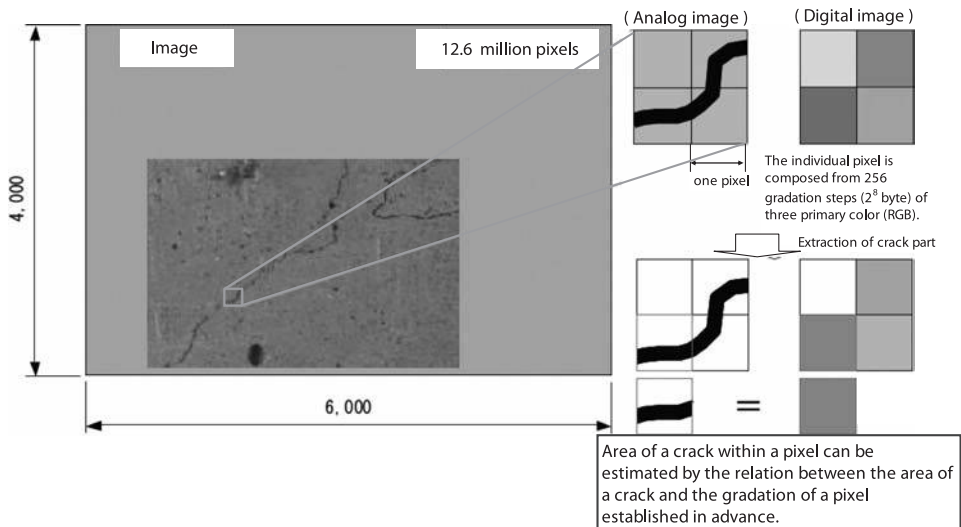


Figure 5. Evaluation method of crack width.

a crack which is narrower than the resolution can be measured if the relation between the ratio of the crack over to one pixel and the gradation level of the pixel is established (Hiroshi 2004).

In the case of using digital single-lens camera which is attached 400 mm telephoto lens, it is possible to identify the crack width of 0.2 mm if the image is taken 120 m away. The detection ratio of cracks of 0.2 mm width or wider is more than 90% by limiting the angle of view narrower than 7.3 m.

3 APPLICATION EXAMPLE OF PHOTOGRAPHIC IMAGE MEASUREMENT TECHNIQUE

3.1 Dam deterioration diagnosis

KEPCO conducts crack monitoring of the concrete structures in the dam deterioration diagnosis by using this photographic image measurement technique since 2009. KEPCO has already conducted the initial investigation in 16 dams out of 39 concrete dams owned by KEPCO. Here are the results to verify whether the photographic image measurement has an advantage over the conventional method by rope access.

The photographic image measurement technique was applied to aerial surfaces of two dams with a different size (surface areas of the two dams sum up to about 10,000 m² in all). Images were captured from where a captured image area was smaller than a rectangle of 4 m × 6 m, the angle to the subject was smaller than 45 degrees and distance from the subject was closer than 150 m. About 1,500 images of the two dams were captured in seven days. Figure 6 shows

distant view on the dam downstream side. Compensations of angle, curvature and scale were carried out to all the images, and these images were synthesized into several front view images. Cracks of 0.2 mm width or wider could be found individually while stains, concrete joints and formwork marks were checked on a monitor. Figure 7 shows an example of a sketch of cracks on a synthesized image after the compensation of angle, curvature and scale.

Moss and stain did not prevented any cracks from being found in the verification. Some painted concrete areas with reflection of sunlight prevent some cracks from being found. In such cases, images were captured again at other time considering the reflection of sunlight. Comparing all found crack lengths of the two dams with opening of 0.2 mm width or wider with those found by the conventional method, each deviation was within plus or minus 10% in about 97% of all cracks and the deviation of accumulated length of individual components of the dams varies from minus 2.1% to plus 6.2% (Table 2, Figure 8). The deviation of width of the cracks was within plus or minus 0.1 mm in about 98% of all cracks.

The photographic image measurement also has another advantage that degraded area is easily calculated because each pixel of a subject is accompanied with coordinates.



Figure 6. Distant view on the dam downstream side.



(Image processing area: about 378m² (The number of images:28))

Figure 7. Dam downstream side image after image processing.

Table 2. Comparison results of the crack of the two dams.

Crack	No.	Length (mm)		Deviation (%)	Maximum width (mm)		Deviation (%)
		Conventional method	Image measurement		Conventional method	Image measurement	
	1	8,100	8,006	-1.2	0.2	0.2	+0.0
	2	7,050	6,964	-1.2	0.2	0.2	+0.0
	3	2,750	2,981	+8.4	0.3	0.2	-33.3
	4	2,500	2,406	-3.7	0.2	0.2	+0.0
	5	2,500	2,393	-4.3	0.2	0.2	+0.0
	6	2,200	2,245	+2.1	0.2	0.2	+0.0
	7	2,200	2,245	+2.1	0.3	0.4	+33.3
	14	8,800	8,800	0.0	0.2	0.2	+0.0
	15	3,250	3,379	+4.0	0.2	0.2	+0.0
	16	5,050	4,886	-3.2	0.2	0.2	+0.0
	17	2,450	2,268	-7.4	0.3	0.2	-33.3
	18	2,700	2,883	+6.8	0.2	0.2	+0.0
	19	1,850	1,720	-7.0	0.2	0.2	+0.0
	20	3,300	3,328	+0.8	0.5	0.4	-20.0
Total / average		93,450	91,987	-1.6	0.275	0.240	-10.3

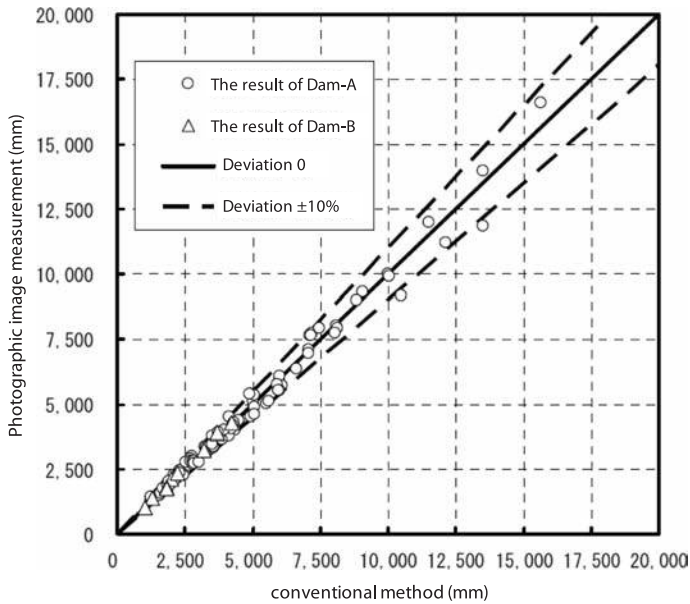


Figure 8. Comparison results of crack length.

The image measurement costs approximately 30% lower than the conventional method judging from the rough estimate of labor costs. Now we are conducting more detailed cost evaluation of the photographic image measurement.

We are also developing a database system with a retrieval function in which electronic data such as digital images and crack information are linked to drawings of the facilities. We expect the system help and save our maintenance work such as the comparison with the previous investigation.

3.2 Waterway tunnel inspection

Next, authors show an application example for a waterway tunnel inspection. The KANSAI Electric Power Group is engaged in an O&M consulting business of an overseas hydropower IPP, the San Roque Multi-purpose Project in Philippines, and in the waterway tunnel inspection of the San Roque power plant, the photographic image measurement has been conducted in 2009. Table 3 and Figure 9 show the outlines of the San Roque Dam and a longitudinal section profile of the waterway tunnel. Because the inside diameter of the waterway tunnel, which is pressure tunnel with concrete lining, is 8.5 m, it is necessary to set up a tall temporary scaffold for visual monitoring of cracks in order to observe the crown of the tunnel in detail. Since dewatering period of the waterway tunnel is a very short time, and a hatch of the waterway tunnel is less than 1 m in diameter from which inspection equipment are brought in. It is difficult to carry out enough research in a short time, so KEPCO introduced the photographic image measurement. The image measurements were carried out at sections where the bedrocks were weak and many cracks were found. Two locations were selected for the photographic image measurement, which were 29 m wide and 3 m high, 21 m wide and 3 m high respectively, with a total area of 150 m². Because the surface of the tunnel was stained with the mud, images were taken after cleaning the surface by high-pressure water washing. The measurement was completed in about three days. After bringing back the images to Japan, authors conducted image processing in our laboratory. Because the waterway tunnel has a simple circular cross section and the concrete surfaces had formwork marks, the image syntheses were relatively easy.

Table 4 and Figure 10 show comparison results of some of the data obtained from the image measurement in 2009 and 2010. As for the results of 2010, authors couldn't distin-

Table 3. Outlines of the San Roque Dam.

Item	Outline
Dam type	Center Core type Rock fill Dam
High (m)	200
Crest length (m)	1,130

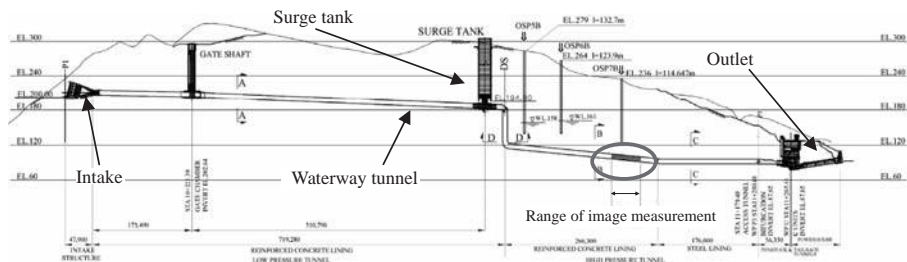


Figure 9. Longitudinal section profile of the waterway tunnel.

Table 4. Comparison of waterway tunnel crack data.

No.	Length (mm)		Deviation (%)	Maximum width (mm)		Deviation (%)
	2009	2010		2009	2010	
1	1167	1220	4.3	0.2	0.2	0.0
2	1138	1131	-0.6	0.6	0.6	0.0
3	1999	2030	1.5	0.4	0.4	0.0
4	1725	1691	-2.0	0.2	0.2	0.0
5	9959	9516	-4.7	0.8	0.8	0.0
6	1255	1178	-6.5	0.8	0.8	0.0
7	7150	7443	3.9	0.8	0.8	0.0
8	6995	8077	13.4	0.8	0.8	0.0
9	3940	4337	9.2	0.8	0.8	0.0
10	1765	1905	7.3	0.4	0.4	0.0
11	3084	3150	2.1	0.6	0.6	0.0
12	1833	1723	-6.4	0.2	0.2	0.0
13	-	954	-	-	0.4	-
Total/average	42010	44355	5.3	0.508	0.538	5.7

guish any change of crack width. But authors found slight progress of the length of the some cracks, and found one new crack. Seeing images of 2009 much more closely, authors could find a tiny sigh of a crack at the new crack position. Since the slight cracks were confirmed when images of the previous year were investigated in detail, it is assumed that the finding of the new crack is due to using a higher resolution camera (from 12.6 million pixels to 16.0 million pixels) or the different condition of the wall washing. Therefore, authors finally judge the tunnel keeps sound conditions.

Since the San Roque Power Plant, of which operation was started in 2003, is a relatively new power plant, significant degradation progress was not observed in the inspection. KANSAI could record the concrete condition at a relatively early stage. This data will be very useful at future stage in which degradation of the plant will advance.

The photographic image measurement at the San Roque waterway tunnel is the first-time experiment for KANSAI to conduct the measurement more than twice at the same point. We are firmly convinced that the database system is very useful by reconfirming as much as by comparing the past data.

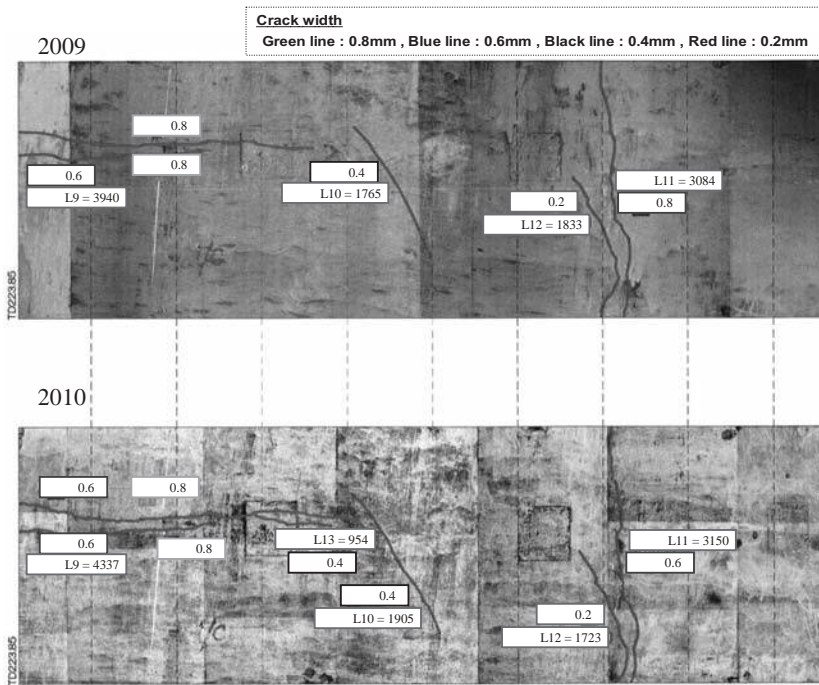


Figure 10. Result of waterway tunnel image analyses.

Authors have given on-the-job training of taking the images to the local civil engineer of the San Roque Multi-purpose Project. From now the local engineers will take and send the images to us and authors will conduct image processing in our laboratory. KANSAI can share the wide variety of the database both in Philippines and in Japan, and it makes the O&M more reliable and effective.

4 CONCLUSION

In this study, we have developed the photographic image measurement applying both for the surface of a dam and the concrete lining of a tunnel and have confirmed the availability with a certain level of the accuracy. We believe the new measurement ensures the safety of field works, the accuracy of observe data and economic efficiency.

With the information obtained from this new method, we are attempting to establish more reliable operation and maintenance of concrete structures. We are also going to pursuing more laborsaving method and expand applicable objects of the photographic image measurement by modifying the equipment and devising methodology of measurement and data processing.

We think a subject of future investigation is how to detect the depth of cracks, which is one of key factors to the soundness of concrete structures.

REFERENCES

- Hiroshi, K. 2004. Digital Imaging Process for Inspection, Diagnosis Concrete Structure. *Journal of the Japan Welding Society* 73(7): 510–513.
- Tsugio, Y., Yukihiro, K., Mashahiro, I. & Hiroshi, K. 2008. Dam Surface Investigation by Digital Camera. *Journal of Japan Society of Dam Engineers* 18(2): 118–125.

Situation and developing trend of defective reservoir reinforcing technology in China

G. Dashui & T. Jiexiong

Changjiang Institute of Survey, Planning, Design and Research, Wuhan, China

ABSTRACT: China has built more than 87,000 reservoirs, 40% of which are defective. In recent years, central government put huge amount of money into reinforcing projects from more than 7500 defective reservoirs, thus improving reservoir and dam safety situation throughout China. Through developing database information system of defective reservoirs reinforcement, and turning to mathematical statistics methods, our study systematically illustrates the characteristics and causes of diseases in certain aspects such as flood control, dam seepage, structural safety and seismic safety. We carry out statistics analyses on quantity, proportion and cost for reservoir reinforcing projects in China, according to size, dam type, structure, and disease form. Based on given examples, this article figures out technical features on dam reinforcing, summarizes various reinforcing methods, technical points, scope of application, and puts forward prospective direction for research and study in China.

1 GENERAL INSTRUCTIONS

According to “National Special Plan for Defective Reservoir Reinforcement”, China possesses 87,076 reservoirs at present, of which 508 are large reservoirs, 3209 medium-sized, 15,842 small (level one), and 67,517 small (level two). There are 38,019 defective reservoirs, of which 288 are large reservoirs, 2145 medium-sized, 9,133 small (level one) and 26,453 small (level two), accounting for 56.7%, 66.8%, 57.6%, 39.2% respectively.

Such a great number of defective reservoirs not only affect efficiency and benefit of reservoir, but also seriously threaten property safety and people’s life. Nowadays, defective reservoirs gradually become a significant weakness and potential safety hazard of the overall flood control system. Defective reservoir reinforcement is in critical need and urgency.

Because of large number and wide geographical distribution of defective reservoirs in China, engineering information management is a complicated and heavy work. Moreover, local capacity for defective reinforcement diversify quite a lot, so The Eleventh Five-Year National Technology Support Program launched a subject named Study on Technical Patterns on Information Management and Technology for Defective Reservoir Reinforcement,^[2] focusing on developing a engineering information management system for defective reservoir reinforcing projects, summarizing domestic technologies on defective reservoir reinforcing, and aiming to increase our comprehensive capacity in this field. This article gives a brief introduction of part of our research results.

2 GENERAL FEATURES OF DEFECTIVE RESERVOIRS IN CHINA

According to statistics, 95% of reservoirs in China are consisted of earth-rock dams,^[3] mostly built from the 1950s to the 1970s. Constrained technically and economically then,

low compaction, incomplete foundation clearance, ineffective seepage control treatment are rather common during dam construction, which left potential hazards of dam seepage, piping, soil erosion, contact scour, even dam crack, landslides and other problems after dam and reservoir was put into operation.

For stone masonry dam, concrete dam, spillway and aqueduct and so on, carbonization, crack, Re-bar exposure, peeling, scouring, lixiviation, leakage may appear due to the poor construction quality or imperfect foundation treatment with increasing years in operation. These problems actually affect structural and seepage control safety.

Generally speaking, causes of diseases in defective reservoirs can be summarized into following aspects:

1. Unsafety in flood control standard

Main problem is lower crest elevation or insufficient discharge capacity, that is, flood control standard can not meet requirement of relevant regulations. Statistical data^[4-5] from Chinese Ministry of Water Resources in 2004 shows that, 51 large, 196 medium-sized and 14,000 small reservoirs of the total defective reservoirs have this problem.

2. Unsafety in dam seepage control

Main problems are seepage in dam body or foundation; piping, erosion and contact scour in earth-rock dam; lixiviation in masonry and concrete dam. Statistical data^[5] (the 1st and 2nd batches of 26 defective reservoirs before 1998 not included, the same hereinafter) shows that, of the 46 homogeneous earth dams in large defective reservoirs, 10 have seepage risks; 17 have serious foundation seepage; 8 have by-pass seepage and contact seepage; and 11 have serious seepage at downstream dam slope. Of the 55 core-wall-dams in large defective reservoirs, 5 have seepage risks; 19 have serious foundation seepage; 9 have by-pass seepage and contact seepage; and 11 have quality problems in core wall. In addition, there are 16,000 small reservoirs which have seepage control problems.

3. Unsafety in Dam Structure

Main problem is structural strength and sliding stability of the dam cannot meet regulatory requirements. Statistical data^[6] shows that, of the 46 homogeneous earth dams in large defective reservoirs, 3 have insufficient cross-section size; 12 have unstable slope; and 14 have problems in slope protection form. Of the 55 core-wall-dams in large defective reservoirs, 13 have unstable slope; 7 have problems in slope protection form. In addition, there is a wide slotted concrete gravity dam and a stone masonry gravity dam having problem in sliding stability.

4. Unsafety in Anti-Seismic Standard

Main problem is anti-seismic standard for reservoir and dam cannot meet regulatory requirements. Statistical data^[4] shows that, 13 large defective reservoirs cannot meet anti-seismic requirements of relevant regulations. There are also a considerable number of medium-sized and small reservoirs have this problem.

5. Unsafety in Water-Delivering and Flood Discharge Structures

Main problem is structural strength and stability of water-delivering and flood discharge structures cannot meet regulatory requirements.

6. Unsafety in Metal Structures and Electromechanical Equipments

At most defective reservoirs, their metal structures and electromechanical equipments have been running for 30 to 50 years, over or close to the depreciation period. Aging and rust corrosion drive them out of normal operation, seriously affecting safety of the reservoir.

7. Inadequate Management Facilities

Most defective reservoirs do not have adequate hydrological measuring and reporting and dam monitoring systems, especially small reservoirs, which usually have no such facilities at all. Management facilities at many reservoirs are very old and out of date. There are low-level or even no highways for flood control use.

Table 1. Reinforcing cost for different structures unit: million RMB yuan.

Item	Scale		
	Large	Medium	Small
Dam Body	3046.85	1064.8	244.60
Dam Seepage Control	1640.77	420.18	90.22
Dam Related Structures	1406.08	644.60	154.37
Spillway	1337.60	475.63	83.97
Water-Delivering Structures	453.73	161.95	44.50

3 STATISTICS OF MODERN TECHNICAL PATTERNS ON DEFECTIVE RESERVOIR REINFORCEMENT IN CHINA

Based on specific information of 2311 defective reservoir reinforcing projects assigned by the Central Government collected from document literature,^[2] we established project management information databases for the above 2311 reservoirs and professional technical databases for another 206 reservoirs. Turning to modern statistic analysis methods, we summarize contemporary technical patterns in China on defective reservoir reinforcement as follows:

1. Of the above 2311 defective reservoirs already reinforced, 58 are large reservoirs, accounting for 2.5%; 744 medium-sized, 32.2%; 1509 small, 65.3%. Sorted by dam type, 93.3% are earth-rock dams, 5.6% stone masonry dams, and the rest concrete dams. Among earth-rock dams, homogeneous earth dam takes the largest proportion, that is, 66%; followed by clay core dam, 30%; clay sloping core dam and concrete face rock-fill dam accounts for 3.5%, 0.5% respectively.
2. Unit capacity reinforcing cost varies from one another for different scale of defective reservoir. The average cost is 0.17 RMB yuan for large reservoir, 0.45 RMB yuan for medium, and 0.67 RMB yuan for small. The total cost goes into different reinforcing items, with over 60% into dam seepage control and structure safety, 28% into spillway and 10% into water-delivering structures. See [Table 1](#).
3. Among all the reinforcing approaches for raising flood control standard, heightening of dam is the most widely used in specific projects, with a proportion of about 48%. Next are building wave wall and increasing discharge capacity, accounting for about 29% and 18%. Integration of heightening of dam and increasing discharge capacity take a proportion of 6%.
4. As for dam seepage control reinforcement approaches used in projects, concrete cut-off wall accounting for 52%; jet grouting cutoff wall 5%; geomembrane 3%; and foundation curtain grouting 36%. Principal measures dealing with seepage problems existing in concrete and stone masonry dams are adding new concrete slab and grouting.
5. For dam slope reinforcement, especially for upstream slope reinforcement of earth-rock dams, removing and rebuilding accounts for 46%; partly repairing 20%; partly rebuilding 12%; and no treatment 22%.
6. For spillway reinforcement, partly removing and rebuilding accounts for 73%; total discarding and rebuilding 4%; and no treatment 23%.
7. For water-delivering structures reinforcement, intake tower reinforcing or rebuilding accounts for 85%; tunnel reinforcing 66%; outlet energy dissipation structures reinforcing 10%; and metal structures and hoist equipments replacing or repairing 82%.

4 PHOTOGRAPHS AND FIGURES

4.1 *Increasing reservoir flood control capacity and heightening of dam*

In response to general features of unsafety in defective reservoir flood control, we take measures to improve reservoir flood control capacity that can be categorized into two major

classes: ① heighten the dam to increase reservoir flood storage capacity; ② expand scale of flood discharge structures to increase discharge capacity. In China, a number of large and medium-sized reservoirs have taken the above two approaches to increase their overall flood control capacity since “75.8” flood in the 1970s to the 1980s.

4.1.1 *Heighten the dam*

4.1.1.1 *Earth-rock dam*

1. Add wave wall

For dams which do not have wave walls, we prefer to add a new wave wall on the dam crest after we carry out calculation and make sure that dam body itself can meet basic requirements for normal operation. The wave wall is usually 1.0 to 1.2 meter tall.

2. Heighten the dam

Generally, it is favorable to heighten the dam on downstream slope without emptying reservoir or compromising operational benefit. However, supposed the dam slope was unstable, we should consider heightening the dam either at the upstream or downstream slope in view of dam slope stability condition.

4.1.1.2 *Concrete dam*

Heightening of concrete dam has two ways: ① pour concrete on dam crest, meanwhile increase dam cross section at upstream or downstream side; ② combine new concrete with old dam body and foundation through the vertical prestressed anchor cable. In order to guarantee bearing capacity of the joint structure, dig key seat, insert rebar and apply bonding adhesive at the concrete interface.

1. Increase dam cross section

Construction of Danjiangkou Water-Control Project is divided into two stages. The second stage serves for the South-to-North Water Transmission Project, with the main job of increasing dam cross section by 14.6 meter at downstream side. Affected by temperature changes, elastic modulus of new and old concrete diverse, and old concrete exert fairly big constraint force on new concrete, so there is great possibility that the joint structure would separate after construction. Original design for the first stage reserve key seats for later heightening at downstream dam slope, but dam face concrete carbonize as time pass by. During the second stage construction, we remove the carbonized concrete layer by 2 to 3 centimeter, dig new key seats where there is no seat reserved beforehand (new key seat size is 70 centimeter long, 40 centimeter wide, 30 centimeter deep; the downside forms an angle of 23.19° with original dam surface; and center interval of seats is 1.5 meter.), and insert anchor (diameter 25 millimeter, 4.5 meter long, 2 to 3 meter into old concrete, alternate with long and short anchor, interval distance 2×2 meter, mortar strength grade M20) at concrete interface for higher bond strength and better joint bearing performance. Still, we properly raise grade of new concrete to achieve relatively consistent elastic modulus of new and old concrete.

2. Heighten the dam with prestressed anchor cable

Fixing vertical prestressed anchors on the upstream side of a heightened dam can improve anti-sliding stability and anti-bending performance. In this way, there is no need lowering normal reservoir operational water level, and economic benefit will not decrease. We implemented this approach on Fengman Reservoir, resolving foundation seepage problems and heightening the dam by 1.2 meter. Shiquan Reservoir was adopted this way to solve the dam stability problems, while we heightened the dam 14.6 m. The Shiquan Reservoir is another example of this technology and its design flood standard was increased dramatically.^[7]

4.1.2 *Increase discharge capacity*

Besides exploring potential capability of flood discharge structures, we can also broaden or deepen original spillway or build a new one. For example, Miyun Reservoir in Beijing chose to build a new spillway. Another way is to build new emergency spillway. For example, Lucun Reservoir in Anhui builds two emergency spillways when reinforcing, which highly improve its flood control capacity.

4.2 Seepage treatment measures for earth-rock dam

Seepage is one of the primary diseases existing in defective earth-rock dams. We have multiple treatment measures such as concrete cut-off wall, high pressure jet grouting, fractured grouting, stable cream seriflux grouting, geomembrane, etc.^[2] This article just introduces three types of anti-seepage technologies.

1. Concrete cut-off wall

This methodology is to build a concrete cut-off wall along the axis of the earth-rock dam. The wall can be put inside dam body or stretch into the foundation for a certain depth, thus cut off seepage path inside dam body and foundation. Advantages of this method include: better adaptability to various geological conditions—applicable for both dam body and foundation reinforcement; no need to emptying the reservoir during construction; and construction of wall using displacement method, which is easier for monitoring construction quality than other methods. Disadvantages include: need of wider working platform for construction; need of lowering dam crest by excavation and fill it back to design elevation; and longer construction period and higher cost.

In China, we applied this technology for the first time to Tuolin Reservoir in Jiangxi, and then to Danjiangkou Reservoir. Earlier, Uzziah Kass drilling machine was widely used for cut-off wall construction, and it costs more time and money. As construction technique developed, hydraulic grab came into practice, increasing construction speed and reducing cost. Nowadays, cut-off wall gains extensive use in reservoir reinforcing projects. Take Hualiangting Reservoir in Anhui as an example. The dam is a clay core dam with upstream sand blanket. Due to poor construction quality, serious seepage was found in dam body. So we decided to build a concrete cut-off wall inside the clay core, stretching through sand layer into rock foundation by 1 meter. The wall is 540 meter long, 0.8 meter thick with an area of 25,470 square meter and maximum depth of 66.4 meter (see Figure 1). In order to form working platform, dam crest has to be lowered by 3.25 meter. Hydraulic grab was used for cut-off wall construction assisted by drilling machine. We made full use hydraulic grab's advantage of quick pore-creating. Hydraulic grab was used for dam body and drilling machine for foundation. The cut-off wall construction of this project commenced in December 2009 and finished in just four months. Flood season in 2010 has passed, and the reinforced dam does run well without any seepage problem.

2. High pressure jet grouting

This methodology contains following procedures: drill hole with drilling machine; put jet pipe life jet pipe (with water pipe, cement pipe and wind pipe inside) into the hole; spay high pressure fluid and shock soil (cement flow and soil are mixes together); lift jet pipe and leave the mixture to solidify. The main idea of this technology is to arrange drilling holes along the axis of earth-rock dam and grout in every single hole. Grouting coagulum in adjacent holes overlaps and forms a continuous cut-off wall, finally reaching the goal of anti-seepage.

High pressure jet grouting was initially carried out in silt and sand layers, though it extended successfully into gravel layer in recent years. Take Gongshang Reservoir in Henan as an example. The earth-rock dam is of poor construction quality, with deformation and cracks on dam body. Thirty meter width's pebbly sand layer under the dam was not cleared at all. Before

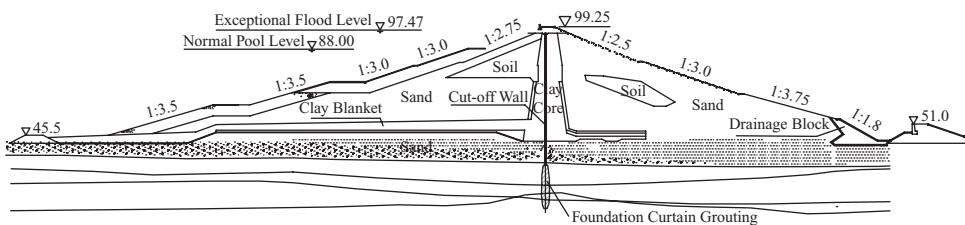


Figure 1. Sketch map of cut-off wall in Hualiangting Reservoir.

reinforcement, there was muddy water effusing at downstream dam toe—average leakage volume is 90 liter per second. In 1999, the dam was reinforced by jet grouting, and dam-toe leakage disappeared soon afterward. Advantages of this method include: no need of lowering dam crest to form wide working platform and fast construction speed. Disadvantages include: different technical parameters for different geological layers, which requires site tests and professional construction team with abundant experiences; Lower overall performance than concrete cut-off wall, for instance, difficulty of entering rock foundation, low strength in clay layer and poor durability; and high likelihood of cracking when depth exceeds 40 meter.

3. Stable cream seriflux grouting

This grouting technology is applied on coarse aggregate dam and foundation. The seriflux is liquid cement mixed with certain proportion of clay or bentonite, possesses greater viscosity and stability and is suitable for screw pump. Supported by this technology, we can build impervious curtain in rock-fill body or pebbly sand layer under macro porosity and high underground water flow rate. At Hongfeng Reservoir in Guizhou, the wood faced rock-fill dam is 416 meter long, with a maximum height of 52.5 meter. Its porosity reaches 38%. The wood face rotted after tens of years' operation, and serious seepage occurred. In order not to emptying the reservoir, we take stable cream seriflux grouting there. Based on site tests, four row of drilling holes were arranged inside the dam body to form a impervious curtain. The curtain is 4 and 14 meter thick on top and bottom respectively, and has achieved favorable performance. In 2009, Mopan Reservoir in Guangxi took this measure for its concrete faced rock-fill dam and it works very well.^[2]

4.3 *Dam slope stability and anti-seismic reinforcement of earth-rock dam*

1. Dam slope stability reinforcement

We usually gentle dam slope through either earth up or slope cutting, so as to increase slope stability of earth-rock dams. For steep slope at upstream side, lattice protection can be adopted. And as for slope instability caused by higher saturation at downstream side, cut-off wall may likely solve it.

Materials selected for upstream dam slope reinforcement should be rock block, rock ballast, gravel, sandy soil, which is more permeable than old dam slope ingredient and ensures quick drainage when lowering pool level. However, in some cases it is not allowed to emptying reservoir, and then we can choose rip-rap filling. When gentling downstream dam slope, we shall fill water permeable material at the bottom to lower saturation in dam body. At Lucun Reservoir in Anhui, our design for upstream dam slope reinforcement is partial rip-rap filling for slope under water, rough sand rolling filling for slope above water; for downstream slope, we use lattice protection. According to monitoring data during three years after reinforcement, we can judge that the dam slopes are all stable. At Qingshan Reservoir in Hubei, cut-off wall was built inside its dam to solve seepage problems of seepage and downstream slope instability.

2. Slope protection reinforcement

Upstream slope protection for earth-rock dam could be rock block, cast-in-place concrete and precast concrete, while downstream could be vegetation, lattice plus vegetation, rock block, cast-in-place concrete and precast concrete, etc. The Embankment dam upstream revetment to reinforce can use the revetment made in piece stone, cast-in-place concrete and precast concrete. If a reservoir is also a scenic spot, we shall choose prettified precast concrete for upstream slope, and prettified precast concrete or vegetation or lattice plus vegetation for downstream slope. Take Hualiangting Reservoir as an example. We specifically designed I-shaped precast concrete block (80 centimeter long, 30 centimeter wide, 20 centimeter thick) for its upstream dam slope. The reinforced dam slope does not only look nice, but also effectively resist waves.

3. Anti-seismic and anti earthquake liquefaction reinforcement on dam body

Liquefaction failure often occurs in sandy soil of poor denseness. Reinforcing methods for this kind of material include replacement, densification and weights. ① Replacement means

removing all sandy soil within liquefaction area and refill with anti liquefaction material like rock ballast. ② Densification means increasing density of sandy soil and its anti-liquefaction capability through vibratory percussion and compaction. ③ Weights means placing weights on surface of liquefaction area, so that it can help increase sandy effective stress and anti liquefaction capability of the sandy soil.

For instance, in the Reinforcing Project of Miyun Reservoir in 1977, without emptying the reservoir, upstream slope of Baihe earth dam was reinforced by removing the liquefaction layer, refilling with rock ballast, thickening blanket and part of sloping core.^[8] In 1998, still in Miyun Reservoir Reinforcing Project, again without emptying the reservoir, upstream slope of Chaohe earth dam was reinforced by rip-rap filling under water, replacing original sloping core with rock ballast above water. The rip-rap increased effective stress and anti liquefaction capability of the gravel layer, meanwhile, it helps gentle the slope and improve slope stability.^[8] For another example, clay core sandy shell dam of Hualiangting Reservoir have a maximum height of 58 meter, which have low density sandy soil upstream slope. The slope under water is highly likely to liquefy during a Richter scale 7 degree earthquake. After thorough study, we selected weights as reinforcement method that is placing 5.5 meter thick weights on upstream slope. In demand of water supply from local people around the reservoir, we decided not to empty the reservoir, keeping pool level at 66.5 meter elevation. The final solution is rip-rap filling for slope under water and rock ballast rolling filling for slope above water. After reinforcement, the risk of underwater slope liquefaction during 7 degree earthquake decreased a lot.^[9]

4.4 *Under-dam aqueduct reinforcement*

1. Replace under-dam culvert pipe with tunnel

At many reservoirs built earlier in China, their irrigating, generating and water-delivering structures were under-dam culverts. For different reasons such as dam body deformation, poor construction quality, deficient structure design, leakage and contact washing erosion appeared in lots of culvert, seriously threatening safety of the dam. Some culverts received reinforcement. Nevertheless, cracks did not disappear because there were deformations or current scour in dam body. Therefore, if there are leakage defects in under-dam culverts, the best disposal is to discard and block the old culvert, and build a new one at the bank.

2. Reinforced concrete lining

Adding reinforced concrete lining to the old tunnel can improve its structural and seepage safety. But this method asks for smaller tunnel cross section, slightly impacting carrying capacity. We shall pay attention to interface treatment of the old and new concrete. Inner diameter of tunnels in need of reinforcement should not be less than 2.5 meter, in case construction is impossible to proceed.

3. Steel liner

Through adding steel liner to old culverts or tunnels can improve their structural and seepage safety. By injecting cement mortar into gaps between the liner and tunnel wall, they can integrate. As the liner's roughness is relatively low, carrying capacity of the tunnel may not decrease after reinforcement. To avoid steel liner instability under high external water pressure, ribbed plate and anchorage rod can be added. Diameter of tunnel being reinforced shall not be less than 1 meter, in case it is impossible for construction.

4. High-strength carbon fiber sheet liner

Carbon fiber sheet is a tensile material with high strength and flexibility. Its ultimate tensile strength can reach up to 3,790 to 4,825 MPa, elastic modulus 220 to 235 GPa, and elongation over 1.4%. The thickness could be 0.111 or 0.167 millimeter. For tunnel concrete liner which can not meet crack resisting requirement under high internal water pressure, or have cracks and cavitations, we can paste 1 to 3 layers of carbon fiber sheet on inner surface of the tunnel to supplement its concrete strength and anti-seepage capability. For instance, at Qingshan Reservoir in Hubei, the power tunnel has a diameter of 3.5 meter and thickness

of 0.6 to 1 meter. Because of poor construction quality, cracks, scour erosion and leakage all appeared on the concrete liner, impacting safety of the tunnel itself and back massif. In view of the on-site construction conditions, we decided to use high strength carbon fiber sheet for tunnel reinforcing. Three layers of fiber sheet (0.167 millimeter thick) were pasted on lower flat and sloping sections, and two layers on upper flat and sloping sections.^[2]

5 FUTURE DEVELOPING TREND OF REINFORCING TECHNOLOGY FOR DEFECTIVE RESERVOIR IN CHINA

1. Nowadays, China has over 87,000 reservoirs, mostly built during the 1950s to the 1970s. And 44% of the reservoirs are defective, demanding more reinforcing and safety management work. Literature^[4] provides an engineering information system for defective reservoir reinforcing projects. The system has advantages of massive information processing, rapid processing speed, fine information share, easy querying and calling. It can be widely used in water administrative departments at different levels, which will improve reservoir reinforcing technology in China.
2. 95% of reservoirs in China contain earth dam. Upstream slope reinforcement is very common. Precast concrete block can better adapt to dam body deformation and prettify the slope. However, there is no requirement in regulation for precast concrete block design. Mechanically applying this technology may cause unnecessary problems. More research on this subject is needed to create systematic methodology for precast concrete slope protection and improve overall technical level.
3. Carbonization is an universal phenomenon for concrete structures in our defective dams. Currently, acrylic-emulsion cement mortar is frequently used dealing with this problem. But implementation is difficult and the ultimate appearance is imperfect. So we shall further research and develop systematic technology for treating concrete carbonization on hydraulic structures.
4. New reinforcing technologies such as fixing geomembrane, pasting steel plate and pasting carbon fiber sheet, are already used in defective reservoir reinforcing projects. Application of these technologies is still constrained by many environmental and working conditions. So further research and develop systematic technology to reduce cost and expand applied range of these technologies.

REFERENCES

- [1] Ministry of Water Resources of China, 2007. Special program of countrywide defective reservoir reinforcement [M].
- [2] TAN Jiexiong, Gao Dashui, 2010. Chiangjiang Institute of Survey, Planning, Design and Research. Special report on technical patterns on information management and technology for defective reservoir reinforcement. The Eleventh Five-Year National Technology Support Program, 2006BAC14B01.
- [3] Zhang Yanming., 2001. Professional technical paper collection on defective reservoirs and sluice in China [M]. Beijing: China Water Resource and Hydropower Press.
- [4] Zu Leiming, 2004. Safety management of defective reservoir in China [M]. Safety evaluation and reinforcement of hydro-engineering. Wuhan: Changjiang Press.
- [5] Shen Hailian, Zhang Hua, Xu Li, 2008. Present situation and reinforcing measures for small reservoirs in China [J]. *Water saving and irrigation*, 2008(8): 71–75.
- [6] Lv Guoliang, Cen Zhikang, Zheng Guangjun, 2009. Engineering design of Danjiangkou dam heightening works for South-to-North Water Transmission Project. *Yangtze River*, 2009(12): 81–84.
- [7] Gao Dashui., 2004. Application of prestressed anchorage technology and statistics of technical parameters [J]. *Journal of Yangtze River Scientific Research Institute*, 2004(6): 87–90.
- [8] Fu Lei, 2000. Anti-seismic design for earth dam of Chaohe Reservoir [J]. *Journal of Hydraulic Engineering*, 2008(8): 16–20. (in Chinese).
- [9] Gao Dashui, Ye Junrong, 2008. Study of anti-seismic performance and reinforcing measures for sandy shell dam of Hualiangting Reservoir. *Journal of Geotechnical Engineering*, 2008(12): 1921–1924.

Long term behavior of the concrete dams drainage system and ageing phenomena

D. Stematiu & R. Sarghiuta

Technical University of Civil Engineering Bucharest, Romania

A. Constantinescu

Freelance consultant

ABSTRACT: During service of a concrete dam the upstream watertightness and efficiency of the drains generally decrease. An ageing of the dam often entails ageing and clogging of the drains. The most common approach in assessing the decrease of the drainage efficiency is based on the monitoring of the uplift pressures and the seepage collected by drains. Several case studies of uplift evolution revealed by complex monitoring of dams have shown that the abnormal behavior can not be attributed entirely to the drainage clogging but also to site geology and foundation rock properties. Poiana Uzului dam is selected to underline the concept. The dam is a buttress dam, 80 m high that presented several behavior incidents as a consequence of the sudden uplift increases that in their turn were induced by tensile cracks in the grout curtain at the dam upstream toe and over passing of the drainage system capacity.

1 INTRODUCTION

An ageing of the dam often entails ageing and clogging of the drains. The most common approach in assessing the decrease of the drainage efficiency is based on the monitoring of the uplift pressures and the seepage collected by drains. However, the current approach does not cover all the particular conditions of a dam. Several cases from the Romanian dam portfolio present this particular behavior. Iron Gates overflowing gravity dam on Danube River has systematically lower uplift forces than assumed not as a consequence of the intensive drainage but due to the imperviousness of the rock as compared with the dam concrete. Golesti dam and the other dams on the Arges River cascade was provided with deep drainage drillings to control the pressure in sand layers underneath the first impervious foundation layer. Their active drainage has created in time some piping and the drainage closure did not affect the uplift pressures as expected. Poiana Uzului buttress dam has presented several behavior incidents as a consequence of the sudden uplift increases that in their turn were induced by tensile cracks in the grout curtain at the dam upstream toe and over passing of the drainage system capacity. Detailed analysis of the last dam may bring a new light on the traditional evaluation of uplift evolution.

Impoundment of the reservoir created by Poiana Uzului dam commenced in 1972. Although the dam structure allowed the operation of the reservoir up to the maximum water level during a 30 year period several incidents revealed by the monitoring system beginning with the year 1979 were caused by changes of the grout curtain and drainage system efficiency. A full set of constructive measures was established mainly aimed to improve the watertightness of the grout curtain, the drainage system hydraulic capacity and the dam-foundation interaction. The program was applied in stages monitoring the effects achieved.

2 POIANA UZULUI DAM

Poiana Uzului reservoir was performed in order to provide an active storage of $80 \times 10^6 \text{ m}^3$ for water supply in the downstream area. The dam is a concrete buttress one with a height of 80.4 m and a concrete volume of 70,000 m^3 . The dam is divided in 33 blocks out of which the three blocks in the central zone are overflowing. The buttress of each block is supported at the base b/a 15 m foundation pad, equal to the head width (Fig. 1). The pad is also used as a support for supplementary loading with fill material to provide the stability against sliding.

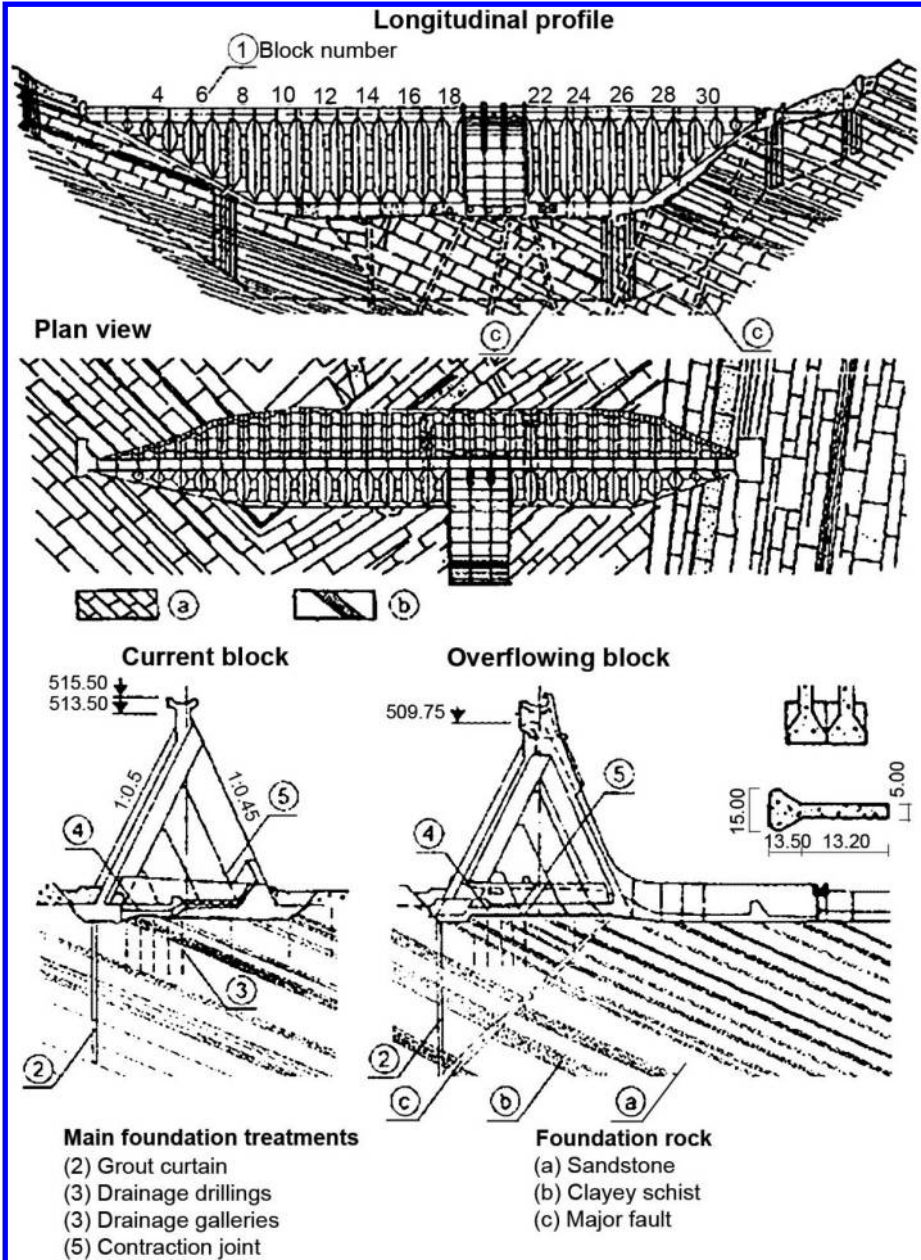


Figure 1. Poiana Uzului dam characteristics.

The buttress itself is divided into 13.2 m columns by means of construction joints oriented parallel to the downstream face. Consequently independent inclined columns transmit the load from the head of the buttress to the foundation ground. Visiting drainage galleries are provided along the contraction joints between the buttresses, at the foundation level in the upstream zone.

The concrete for the dam body was prepared with aggregates from a natural quarry formed of good quality sandstone. Due to the heterogeneity of the sand grain-size distribution about 40% of the sand was obtained by crushing. The cement content was of 250 kg/m³ and the water/cement ratio of 0.48. The laboratory tests carried out on site showed an average compressive strength of 17 MPa at 7 days and of 38 MPa at 180 days, with variation coefficients ranging between 8 and 12%. The particularly good results regarding the tensile strength—3.1 MPa in tension and 5.8 MPa in bending—should be underlined since they explain the reduced frequency of the cracks during construction (Stematiu, Constantinescu & Mircea, 1991).

The geology at the site consists of detrital sedimentary rocks: quartz feldspathic sandstones in metric layers with frequent intercalations of 2 ... 20 cm micashistous sandstones and several intercalations of 0.2 ... 4 m marly and clayey schist. Blocks of massive heavily fissured sandstone are encountered. The fissure matrix induces an increase of rock mass permeability and deformability. The site investigation has revealed a random variation of water takes in the range of 1 up to 10 lugeons, with very large values alternating to rather impervious zones. Two significant schist layers of some 3 m width are located at the base of right abutment. Six main faults accompanied by breccias with the thickness of 0.5 ... 1 m were identified during the foundation excavation.

The rock mass properties were obtained by geophysical investigations, permeability tests, compression tests as well as rock/rock and concrete/rock shear tests. The modulus of deformation ranged between 1000 and 4800 MPa about 50% of the total deformation being of elastic nature. Under the constant load of 2 ... 2.5 MPa the in time deformation stabilized in 6 ... 8 hours and the supplementary deformation level did not exceed 15%.

The watertightening of the foundation ground was performed all along the upstream toe and prolonged towards the abutment by 50 m. The grout curtain consists in three rows of drillings grouted with cement milk. During the watertightening grouting there occurred slurry pressure losses with total water circuit loss sometimes even accompanied by the cement slurry emerging to the surface. The cement uptake exceeded sometimes 1200 kg/m of drilling. The permeability-tests carried out during the grout curtain performance pointed out the existence of large discontinuities and the subsequent grouting required large cement quantities. A total of 40,000 m of drillings was performed with a mean cement uptake of 400 kg/m of drilling. The final imperviousness of the grout curtain was 1 lugeon on the upper half and up to 3 lugeons in the lower one. Mention should be made that near the right abutment, along blocks 11–14, the initial water take was significantly larger, up to 10 lugeons and the mean cement uptake was 595 kg/m of drilling.

A large number of drainage drillings was provided for uplift relief since the dam has a continuous pad foundation. Several 20 m deep drillings are located on each block, 12 ... 14 m downstream of the grout curtain. Additional five sub horizontal drillings of 40 ... 100 m length were provided in the both abutments, downstream the dam. The uplift relief is also achieved by the drainage galleries provided in between the blocks at the foundation level. The drainage galleries leave open the rock foundation along the block joint and on each side of it at the upstream end (T shape). A number of 3 ... 7 drainage drillings were performed for each gallery with a total number of 185 drillings for the whole dam. In 1977, after five years of reservoir operation 32 drainage drillings were added for the blocks 5 ... 12 located near the right abutment.

The monitoring system was designed according to the dam type and allowed a proper surveillance of the dam. Six direct pendulums and two inverted pendulums provide data concerning the relative and absolute displacements of the dam body. The rock mass displacements are measured by means of rockmeters. Survey measurements complete the total displacements monitoring and deformed markers provides inter-blocks relative movements.

Temperatures, strains and total stresses within the dam body are measured by electric transducers located in the block 11, at the base of right abutment and in the block 24 in the central zone. Uplift values are also monitored by means of pressure cells installed in the drainage drillings.

3 INCIDENTS CREATED BY LACK OF DRAINAGE

The dam on the whole presented an adequate behavior allowing the operation of the reservoir up to the maximum level. The measured values, i.e. displacements, strains, relative movements etc. are dependent on the reservoir water level and especially on the seasonal variation of temperatures. However, several abnormal phenomena and an incident were recorded. The large settlements at the downstream toe induced by continuous increase of the foundation ground settlements were pointed out by the multiple base borehole extensometer measurements especially in the downstream toe zone.

The flows drained by drillings present very small values and occur mainly in the right abutment. During the dam monitoring up to 1984, the sudden coming into operation of the drainage drillings was recorded in some years (1979, 1981) but it was considered no special phenomenon. At the end of April 1984, the increase of the flows collected by the drillings was significantly higher, drillings that were inactive came then into operation, water jet occurred directly from the rock in the drainage galleries at joints 516 and 10/11. Simultaneously with these seepage flow increase there were also recorded abnormal displacements of the blocks (Fig. 2). Upward movements and downstream displacements higher than the previous ones were recorded at the blocks located at the base of the right abutment. A sudden change of the displacement pattern (towards downstream) in relation to the general tendency (towards upstream) was also noticed (Constantinescu, Stematiu & Hapau, 2003).

They were rendered evident by the geodesic measurements and by pendulum monitoring data. The analysis of the 1984 phenomenon led to the conclusion that it was similar to the phenomena previously recorded but its amplitude was caused by an unfavorable combination

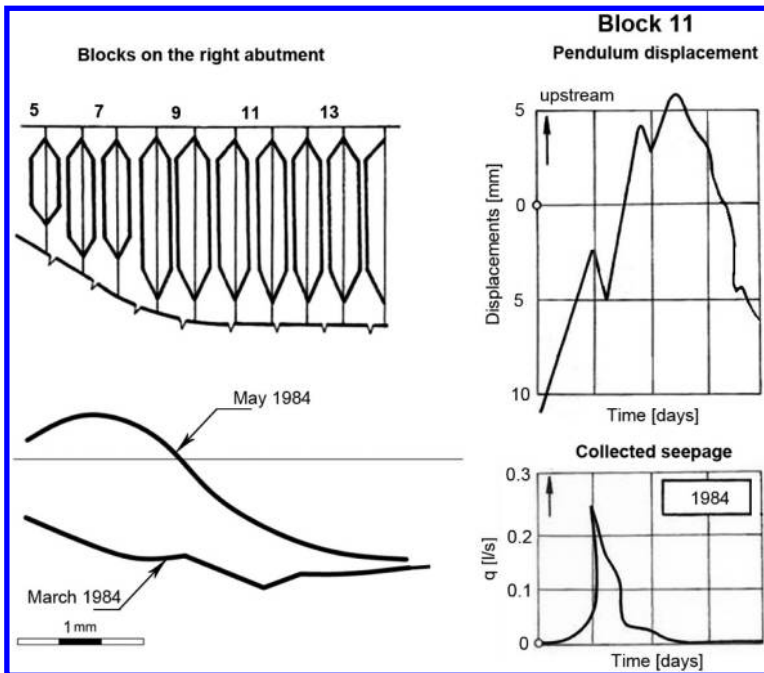


Figure 2. Change of the displacement pattern and increase of drainage flow in April 1984.

between the water load and the temperature variation. It should be noticed that the maximum water level of 1984 was exceeded in 1978 and 1983 without recording similar events. A particular role in causing the recorded phenomena was incumbent on the uplifts that occur in the foundation, due to the lack of draining capacity.

4 AGEING PHENOMENA

In the case of Poiana Uzului dam the ageing phenomena consist in loss of the grout curtain watertightness and a decrease of the drainage capacity encountered during the reservoir operation. The changes were noticed on the basis of the measurements provided by the monitoring system and by the incidents presented before.

The analysis of the dam behavior has revealed a stress dependent permeability of the foundation rock. This particular behavior was firstly pointed out by the correlation of the seepage flows with the buttress average temperature and not with the water level in the reservoir as usually happens (Stematiu & Ilie, 1992). The dependence of the drained flows on the reservoir water level is materialized only at reduced temperatures of the buttresses. For the same water level in the reservoir, the flows collected by the drainage system are larger only at reduced temperatures, when the stresses at the upstream toe decrease. From the structural point of view, tensile stresses do occur at the upstream toe of the dam under higher levels in the reservoir associated to lower temperatures in the concrete buttresses. Consequently the rock grouted fissures open. The foundation permeability increases and the drainage system are activated. Where the amount of seepage overcomes the drainage capacity the uplift increases and causes a sudden change of the displacement pattern. When the stress state in the upstream zone of the foundation is mainly compressive the fissures are closed and the seepage toward the drainage system is hindered. In between cycles of drainage reactivation a clogging of the drainage drillings occurs. Even after a large extension of the drainage system performed in 1988 similar phenomena took place (Fig. 3). The new drillings collected very

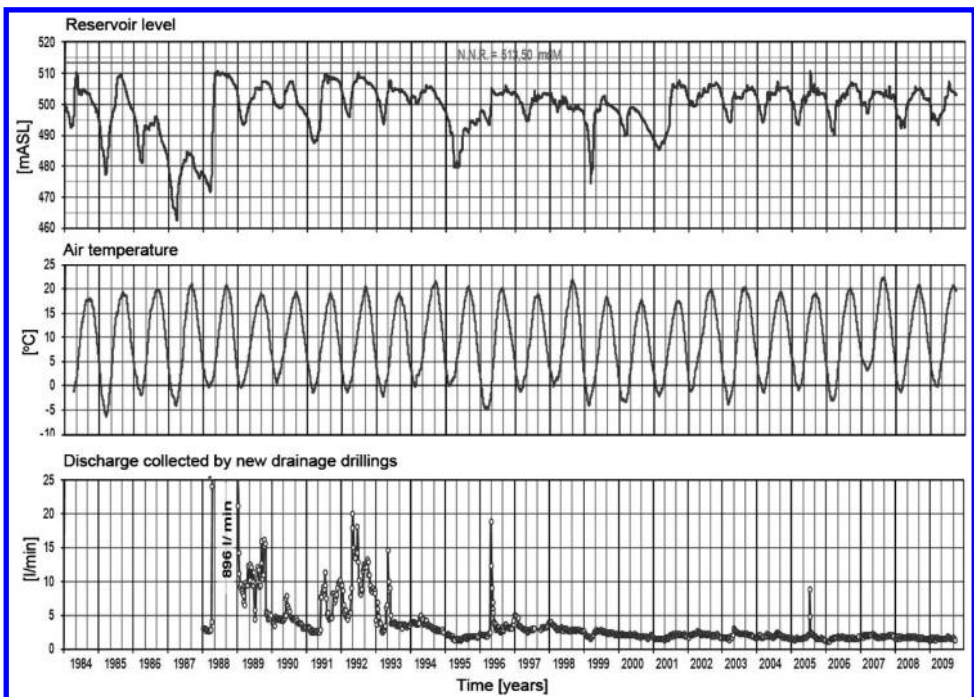


Figure 3. In time reducing the drainage flows.

high seepage flow rates and fine solid particles were carried out by the inflows. The seepage flow in the drainage gallery 8/9 has reached 4.5 ... 5.0 l/s while during the incident it was less than 0.9 l/s. Very soon the flow rates decreased and the collected seepage was clear.

The dam behavior incidents, evidenced at over 10 years from the first reservoir filling, point out once more the in time evolution induced by the unfavorable overlapping of the mechanical and thermal loadings after many cycles of the reservoir filling and emptying. The in time changes of the grout curtain watertightness and of the drainage condition are clearly an ageing phenomenon and a program of remedial works was established.

5 REMEDIAL WORKS

Subsequent to the events in April 1984 when the seepage flows collected by the drainage system increased about 30 times and were accompanied by a doubling of the horizontal displacements in the right abutment zone, a program of studies and remedial works was decided.

In a first phase, after the permeability tests using marked water rendered evident that seepages occur through the grout curtain, discharging at the upstream toe in the right abutment zone about 700 t of fly ashes performed an artificial clogging of the rock fissures. An immediate effect was obtained the seepage flows reducing significantly. After stabilizing the seepage the drainage system affected by clogging was reshaped.

In a second phase a complete program of remedial works was designed (ICOLD, 2000). It comprises (Fig. 4):

- a supplementary drainage system of the dam foundation;
- closure of preferential seepage paths through the grout curtain;

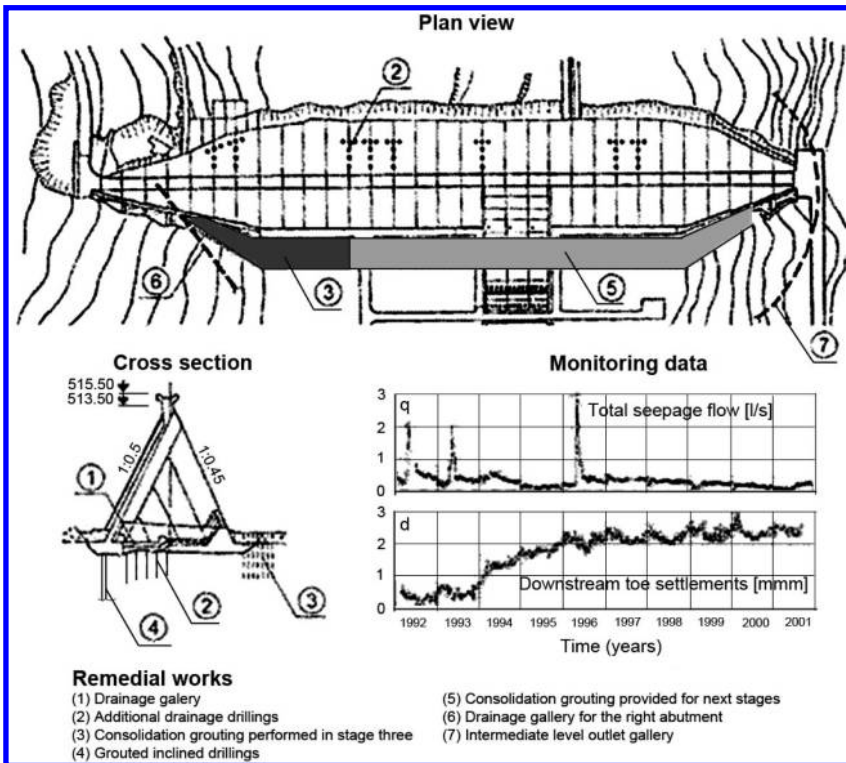


Figure 4. Remedial works program.

- consolidation grouting of the rock mass at the dam downstream toe;
- additional drainage of the left abutment;
- extension of the monitoring system dedicated to measurement of the uplift and rock deformation.

The extension of the drainage system was started immediately after the incident occurred in 1984. The first supplementary drainage drillings were performed in the blocks 8 and 9 where during the incident the water jet occurred directly from the rock. At the final stage of the drainage extension, 205 new drainage drillings were performed, with a total length of 6670 m. The total seepage flow has reached up to 11 l/s, ten times larger than before the drainage extension. The efficiency of this constructive measure is hard to evaluate in terms of dam behavior. In spite of a very large increase of the collected flows similar incidents with the one recorded in 1984 took place in 1988, 1992, 1993 and 1996.

The implementation of the uplift monitoring system was started concomitantly with the drainage extension. A total of 100 piezometric cells were installed in new drillings performed in the buttress concrete and partly in the rock. 37 cells were provided at the dam-foundation contact, 28 cells at a depth of 0.5 m under the buttress heads, 24 cells at a depth of 5 m in the rock under the buttresses and 11 cells were located at 30 m underneath the downstream toe.

The second stage of the remedial works was started in 1989 and was dedicated to cut down seepage that passes along the preferential channels through the grout curtain. Such channels have been identified by the tests performed with marked water and confirmed by the very large seepage flows collected by the drainage in the region of blocks 7 to 11. The channels closure was performed by means of 13 inclined grouted drillings that were assumed to intercept the main discontinuities. Some 3000 kg of cement was used. The results were very good, the seepage rate being cut down from 10 l/s before grouting to 1 l/s after the grouting.

The third stage was started in 1992 and consisted in consolidation grouting performed at the downstream toe of the buttresses. Due to the fact that stress state variation in the dam upstream zone are induced by temperature changes but amplified by the rock mass deformability it was decided to make the rock mass stiffer by injecting cement grout into the open fissures. Two main effects were expected. Firstly, the consolidation reduces the irrecoverable part of the deformations, and secondly, it increases the rock's modulus of elasticity. Since the abnormal behavior was recorded at the blocks 6–12, near the right abutment, the consolidation grouting were performed only for the downstream zone of these blocks. The works were performed between 1992 and 1995. A total of 207 drillings with a cement uptake in the range of 40 ... 80 kg/m of drilling were realized. The favorable effects are shown in [Figure 4](#). The irrecoverable settlement evolution was practically stopped and only elastic movements are recorded after the year 1996.

6 CONCLUDING REMARKS

The deterioration of drainage systems in dams may become apparent when for no other reason, the seepage volume decreases, usually slowly. Sometimes this is accompanied by an increase in the uplift pressure near the drains. Other drains in the vicinity may show increased discharges.

Experience shows that the piezometric pressure underneath a gravity dam is sometimes smaller than theoretically expected. This may be the result of fine material being washed from the reservoir into the joints in the rock below the dam, or another source of increased impermeability in the foundation.

Both for the deterioration of grout curtains and clogging of drains, only detailed and long-term monitoring results of seepage and uplift pressure, starting at the first impoundment of the dam, are a sufficiently reliable tool for the detection of deficiencies.

Poiana Uzului dam behavior incidents point out the in time evolution induced by the unfavorable overlapping of the mechanical and thermal loadings after many cycles of the reservoir filling and emptying. The in time changes of the grout curtain watertightness and

of the drainage condition is considered an ageing phenomenon and a program of remedial works was established.

The staged implementation of the program of remedial works has allowed a close monitoring of the effects achieved at the end of each stage and finally a review of the proposed program. Reservoir operation that prevents the unfavorable overlapping of the water pressure and thermal loadings proved to be a very efficient solution capable to eliminate the abnormal behavior of the dam.

REFERENCES

- Constantinescu, Al., Stematiu, D., Hapau-Petcu, S. 2003. Staged implementation of the remedial works program for Poiana Uzului buttress dam. Transactions of 21 Congress on Large Dams, Q82, R20, Montreal.
- ICOLD. 2000. Rehabilitation of dams and appurtenant works. Bulletin 119. Paris.
- Stematiu, D., Constantinescu, Al., Mircea, N. 1991. Cracking of Poiana Uzului buttress dam due to unusual structural behavior. *Proc. of Int. Conf. on "Dam Fractures"*, Boulder.
- Stematiu, D., Ilie, L. 1992. Safety assessment of Poiana Uzului dam based on monitoring data and backanalysis. *Proc. of Int. Symp. on "Monitoring Technology of Dam Safety"*. Hangzhou.

Unpredictable behaviour of a large arch dam in South Africa

L.C. Hattingh

Hattingh Anderson Associates, Pretoria, South Africa

C. Oosthuizen

Department of Water Affairs & Tshwane University of Technology, Pretoria, South Africa

ABSTRACT: The behaviour of the 88 m high Gariep Dam since 1972 is discussed as well as the various regression methods used to predict behaviour. An in-depth behaviour analysis performed in 2010 revealed that the majority of so-called “unpredictable” inelastic deformations occurred as a result of prolonged periods of low water levels. The observed stepped inelastic displacements as well as possible causes are briefly discussed. In conclusion, suggestions are made for the incorporation of duration-dependent inelastic and/or semi-plastic displacements (due to e.g. surface temperature, poro-plastic and swelling action) in regression models.

1 INTRODUCTION

The 88 m high Gariep Dam is located on the Orange River in South Africa (see [Figure 1](#)). The dam comprises of a double curvature arch in the river section changing to gravity sections on the flanks and has a reservoir capacity of more than 5 000 million cubic metres (the largest reservoir in the Republic of South Africa). The dam has been monitored since completion in 1972. Due its importance an effective monitoring system has been provided that was enhanced during the 1980's with an elaborate 3-D crack gauge system across joints and major cracks. A prediction model is part of the monitoring system to check the actual versus predicted behaviour of the structure on a weekly basis. The relative simple monitoring system includes 3D-crack gauges, pendulums as well as a geodetic survey system.

A hybrid mathematical/statistical regression model was compiled by the designers soon after first filling. At that stage there were already differences between the theoretical and actual behaviour. This regression model performed reasonably well for a number of years (requiring regular updating as can be expected). However, during the flood events of 1988 the model failed the test. The updating process proved to be laborious, and soon resulted in even more differences between expected and the actual behaviour.

The confidence levels in the particular regression model gradually dropped (to the extent that it was even doubted for loads that were not previously experienced). A neural network regression model was therefore developed during the late 1990s. Initially, the results seemed to be promising (Hattingh & Oosthuizen 1998), but soon proved to have the same deficiencies as the mathematical/statistical regression model (Hattingh 2002).

To address this problem a detailed behavioural analysis was performed in 2010 during the 5-yearly compulsory dam safety evaluation (Hattingh 2010). 5-Yearly inspections are required in terms of the South African Dam Safety Legislation that forms part of the National Water Act of 1998 (RSA 1998). The purpose of this analysis was firstly, to get a better understanding of the behaviour of the dam; and secondly, to develop a more reliable regression model for the long-term evaluation of the dam.

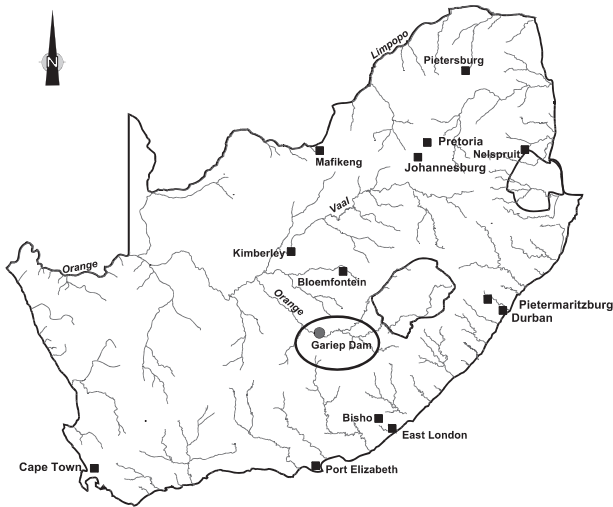


Figure 1. Location of Gariep Dam.

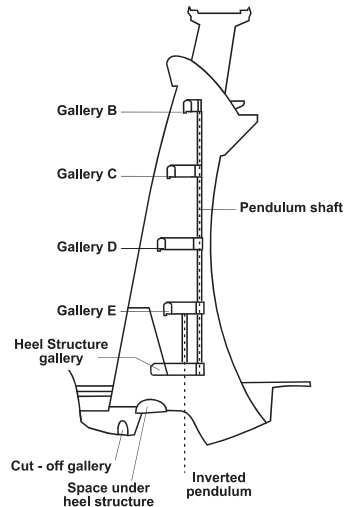


Figure 2. Section through block 1 (centre block).

2 RESULTS OF BEHAVIOUR ANALYSIS

2.1 *Pendulums*

The performance of the central part of the wall (mainly the double curvature arch) is monitored on a weekly basis by means of 7 pendulum systems (consisting of normal hanging pendulums in the concrete as well as inverted pendulums in the foundations). From these results the following were observed:

- As expected seasonal radial displacement of the structure is evident as well as the influence of water levels on the behaviour of the arch. No seasonal tangential displacement is observed; and
- Under “normal” conditions with the water levels not lower than 13 m below full supply level no abrupt inelastic radial displacement is evident. It is important to note that after the two prolonged periods of low water levels in the early and middle 1990s where the water level dropped to lower levels, it is clearly evident that some inelastic displacement in a downstream direction has occurred. This occurred gradually over a period of time—with a maximum inelastic displacement of 12 mm evident in Gallery B of block 1 i.e. the centre of the wall (see Figure 2 for a section through block 1 and Figure 4 for the radial pendulum displacements of Gallery B (top gallery) in the centre of the wall (block 1)). This observation is confirmed by the results of the geodetic survey system comprising triangulation levelling and traversing through selected galleries (see paragraph 2.2 below). This phenomenon could probably be attributed to the poro-plastic behaviour of the arch structure highlighting the importance of the effect of pore pressures in the concrete. This hypothesis is confirmed in the results of 3D-crack gauges (see paragraph 2.3 below).

2.2 *Geodetic survey*

The performance of the entire dam wall is also monitored on six monthly intervals by means of geodetic surveying done by geodetic surveyors of the Department of Water Affairs. From their results the following have been observed:

- Seasonal downstream displacements are clearly evident with the largest displacements as expected in the arch. The maximum displacement of 20 mm was observed on the bridge in the centre of the arch (see Figure 2);



Figure 3. Downstream view of Gariep Dam.

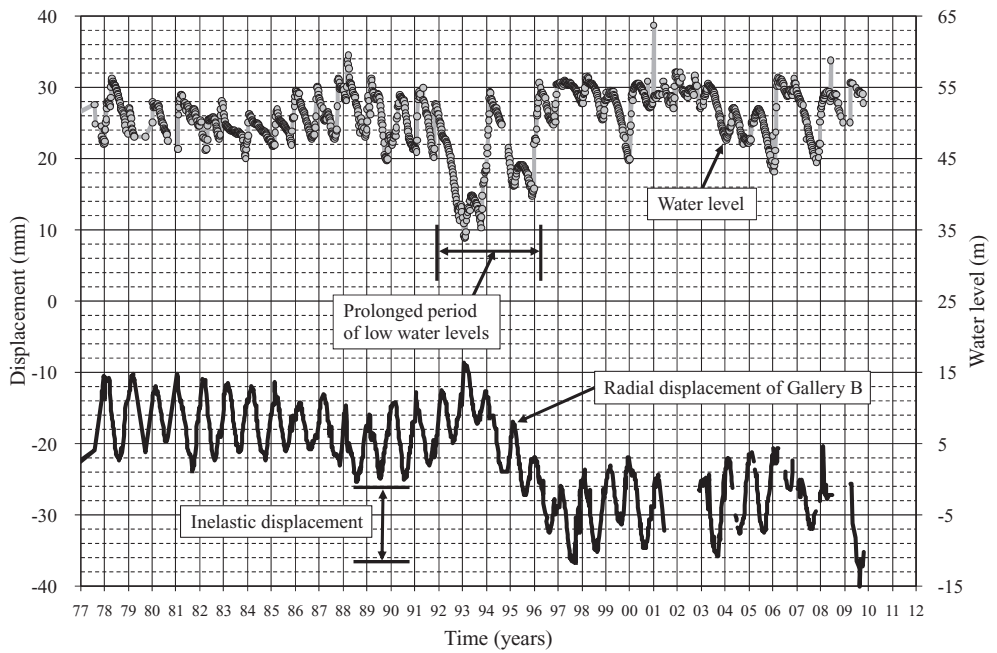


Figure 4. Radial pendulum displacement of Gallery B in the centre of the wall (block 1) (upstream movement is positive).

- The direct relationship between water levels and displacements, i.e. the behaviour of the arch, is also evident; and
- The same permanent (inelastic) downstream displacement after the two prolonged periods of low water levels in the early- and middle 1990s as shown by the pendulum results (see paragraph 2.1 above) is also evident.

2.3 3D-crack gauges

3D-crack gauges were installed in Galleries A, B and D across all the construction joints in 1992 and subsequently replaced in 2002 with DWAFF 2001 type 3D-crack-tilt gauges due to the fact that an electrolytic action between the back plate and the gauge that caused corrosion leading to false displacement readings. From the results of the 3D-crack gauges the following have been observed:

- No inelastic displacement is evident after the prolonged period of low water levels from the results of the 3D-crack gauges;
- This together with the fact that the radial displacements shows seasonal cyclical movements only at the extends of the gravity flanks as well as close to the spillway in the gallery flanking the spillway confirmed the primary arch action in the spillway section, additional “stiffness” in the left flank arch section as well as the additional stiffness created by the outlet works and chute spillways; and.
- The seasonal cyclical tangential displacements are decreasing in magnitude towards the centre of the wall confirming primary arch action in the spillway section as well as additional “stiffness” in the left flank arch section.

3 REGRESSION ANALYSIS

The hybrid mathematical/statistical regression model developed during the latest dam safety evaluation only uses two (2) independent variables/regressors—the water level and the date which was transformed to time of the year variable (s) as well as time since the start of the regression analysis (t). The water level was used in its basic form while the time of the year (s) was used to represent the cyclical nature of the seasonal displacements in the form of Sine (s) and Cosine (s). Inelastic displacements were modelled using the time since the start of the regression analysis (t) in the form of e^{-t} , $e^{-t/2}$, $e^{-t/4}$ and $e^{-t/8}$. This regression model is therefore basically similar to the hybrid mathematical/statistical regression model developed during the 1970s that used water level and the date as independent variables/regressors.

3.1 Pre- 1992 analysis

When a regression period from the end of construction to the beginning of 1992 (the start of the first prolonged period of low water levels) is used for calibration purposes, it is evident that the original regression model was unreliable for the period after 1992. See [Figure 5](#) for the regression results of the radial pendulum displacements of Gallery B in the centre of the wall. The residuals and the 95% prediction interval limits are also shown in the above-mentioned graph. The inelastic displacements as a result of the prolonged periods of low water levels are clearly visible. This regression model only made provision of a total inelastic displacement of 6 mm over a 30 year period (0.2 mm/year).

3.2 The 2010 analysis

When using a regression period from the end of construction to the beginning of 2003, it is evident that the proposed regression model predicts displacements most of the time within the 95% prediction interval limits for the residuals. See [Figure 6](#) for the regression results of

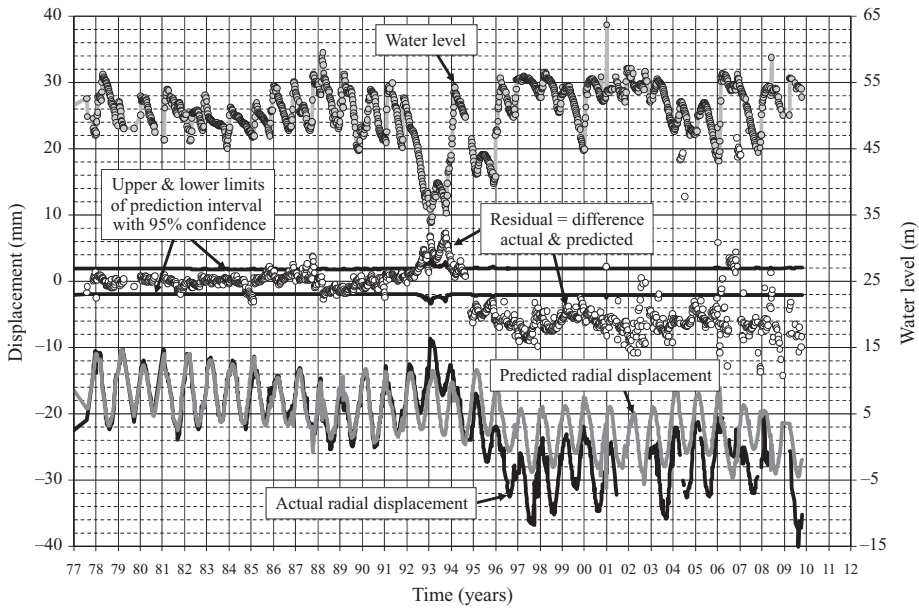


Figure 5. Regression results of pendulum displacement of Gallery B using a regression period from 1977 to 1992 (upstream movement is positive).

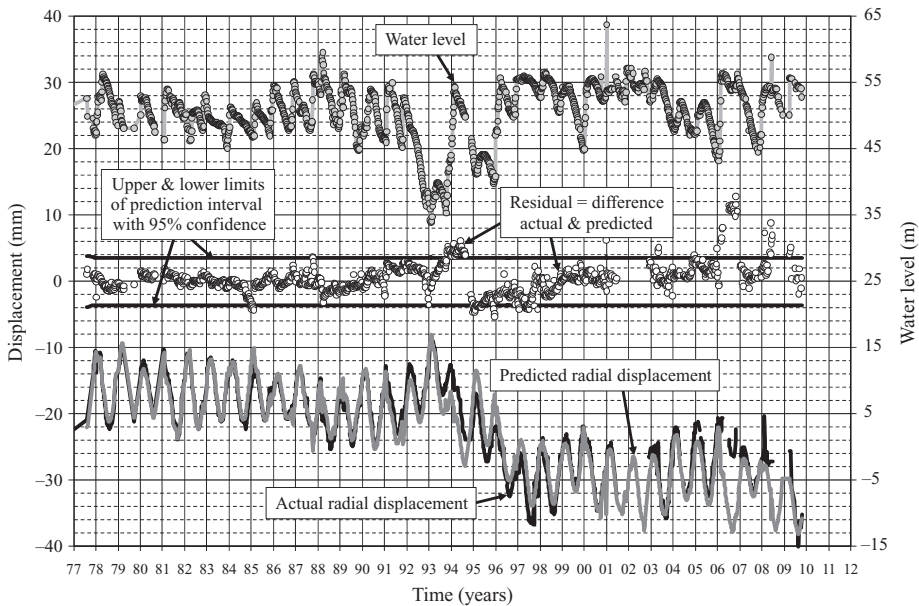


Figure 6. Regression results of pendulum displacement of Gallery B using a regression period from 1977 to 2003 (upstream movement is positive).

the radial pendulum displacements of Gallery B in the centre of the wall as well as the residuals and the 95% prediction interval limits. The improvement is mainly due to the regression model making provision of a total inelastic displacement of 14 mm over a 24 year period with the majority of the inelastic displacement taking place during the prolonged periods of low water levels.

4 CONCLUDING REMARKS

From the results of the monitoring system it is evident that inelastic deformations occurred especially in the central double curvature arch as a result of prolonged periods of low water levels. This was the main reason for the previous failure of the hybrid mathematical/statistical regression model developed in the 1970s as well as the neural network developed during the 1990s.

It must be mentioned that similar inelastic deformations are observed after prolonged periods of low water levels in several other concrete arch dams in South Africa. It is hypothesized that these inelastic deformations could be attributed to the poro-plastic behaviour of arch structures. This highlights the importance of pore pressure measurements in these dams. The importance of the results of 3D-crack gauges in making conclusions in this regard should also be emphasised.

Finally, the use of a simple hybrid mathematical/statistical regression model with only two independent variables/regressors (water level and the date as well as time since the start of the regression analysis) proved to be successful as it is predicts displacements most of the time within the 95% prediction interval limits for the residuals.

ACKNOWLEDGEMENTS

The authors wish to express their gratitude to all other present and past members of Sub-directorate Dam Surveillance that contributed in some or other way to the development of the above-mentioned paper. The opinions expressed are however those of the authors and do not necessarily reflect the views of the Department of Water Affairs.

REFERENCES

- Hattingh, L.C. & Oosthuizen, C. 1998. Surveillance of Gariep Dam using neural networks. *Proceed. Int. Symp. on New Trends and Guidelines on Dam Safety*, Barcelona, Spain, 17–19 June 1998.
- Hattingh, L.C. 2002. A critical review of the use of a neural network prediction model in the surveillance of a large dam. *Proceedings of the Conference called "Dam Engineering 2002"*. Singapore, 20–22 March 2002.
- Hattingh, L.C. 2010. *Gariiep Dam: Fourth Dam Safety Inspection Report*. Report No. 20/2/D350/02/D/1/22. Department of Water Affairs, Pretoria, South Africa.
- Republic of South Africa. 1998. *National Water Act. Act No 36 of 1998*. Government Printer. Republic of South Africa.

Performance of a high rockfill dam during construction and first impounding—Nam Ngum 2 CFRD

S. Moll & R. Straubhaar

Pöyry Energy Ltd., Zürich, Switzerland

ABSTRACT: The 182 m high Concrete Face Rockfill Dam (CFRD) is one of the main components of the Nam Ngum 2 (NN2) hydropower scheme in Lao PDR. Construction of the dam was essentially completed in March 2010 and reservoir impounding commenced subsequently. This paper presents the main dam design features comprising dam zoning, face slab design and instrumentation. Construction principles and rockfill properties are explained. The main observations from the dam monitoring during construction and impounding are presented. The dam deformations as monitored up to date are taken as basis for back-calculations of rockfill properties. A comparison of observed dam deformation behaviour with different rockfill deformation simulation and prediction models is made.

1 INTRODUCTION

1.1 *Nam Ngum 2 hydropower scheme*

The Nam Ngum 2 (NN2) hydropower scheme is located on the Nam Ngum river in Lao PDR, about 90 km north of the capital Vientiane and some 35 km upstream of the existing Nam Ngum 1 dam and powerhouse. With an installed capacity of 615 MW, the project will produce 2220 GWh per year energy for the Thai electricity grid. A significant component of the scheme is the 182 m high concrete face rockfill dam, with a volume of 9.7 M m³ and a crest length of 500 m. The dam impounds a reservoir with a volume of approximately 4900 M m³. A layout of the scheme is shown on [Figure 1](#).

Construction of the NN2 Project commenced in late 2005 and was essentially completed in the second half of 2010. Rockfill placement in the dam body started in January 2008 and was completed in November 2009. Construction of the face slab, which was divided into two stages, was performed from December 2008 to July 2009 and from November 2009 to February 2010. Reservoir impounding started mid of March 2010 with the closure of the diversion tunnels. The full supply level (FSL) will be reached at the end of the rainy season in November 2010. Commissioning of the first generating unit and synchronization to the Thai grid was achieved in August 2010. Full commercial operation of the plant is scheduled to start end of December 2010.

2 DAM DESIGN

2.1 *Dam foundation*

The dam is situated in a narrow valley and is founded on sedimentary rock of variable strength. The geological formations at the dam site consist of medium bedded to massive cliff-forming sandstone, interbedded with siltstone. Three easterly trending folds whose axes are nearly perpendicular to the Nam Ngum river are present at the dam site. The cliff-forming sandstone is generally slightly jointed and fractured, whereas the interbedded siltstone is

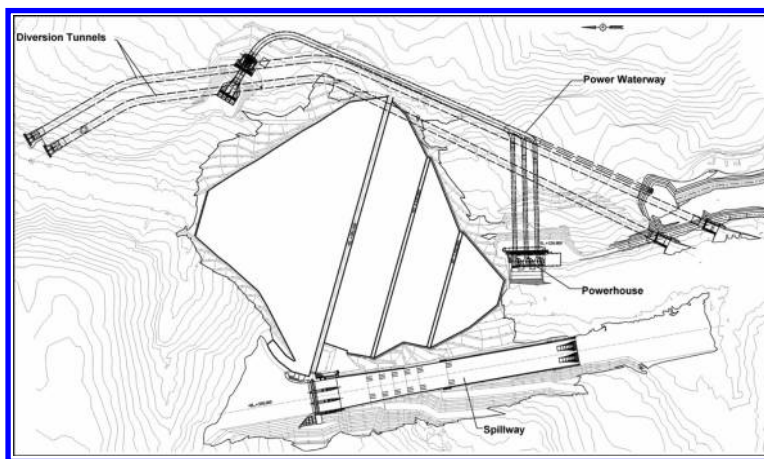


Figure 1. Project layout.

moderately to closely jointed. The typical quality of the foundation rock varies within the following limits:

- Sandstone: fresh, hard and slightly fractured, locally weathered and heavily fractured.
- Siltstone: fresh to weathered, soft and slaking.

Different foundation treatment measures have been carried out to cope with the foundation rock in particular in the upstream third of the dam.

2.2 Dam geometry and zoning

The dam has a maximum height of 182 m above the foundation at the deepest section. Both, upstream and downstream slope are inclined at 1v: 1.4 h (downstream incl. berms: 1v: 1.5 h). The dam crest is 500 m long and 12 m wide. The total dam volume is 9.7 M m³.

The dam was originally designed with a “traditional” zoning i.e. with face slab support and transition zone (2B, 3A), the main dam body of 2 rockfill zones (3B, 3C) with larger maximum size and higher lift thickness towards the downstream slope and a drainage zone (3D) at the dam bottom at the downstream 2/3 of the dam. An upstream fill (1A, 1B) is provided upstream of the face slab.

During construction it was observed that also rockfill of moderate quality and with an increased sand content was obtained from quarrying which could not always completely be separated and wasted. Therefore, the dam zoning was adjusted to permit also placement of lower quality rockfill in the central part of the dam embankment. The final dam zoning is shown on [Figure 2](#).

2.3 Rockfill characteristics and construction principles

For the construction of the dam quarried rock of sedimentary formations were available. The source material, consisting basically of sandstone and siltstone, has been investigated by drilling, quarry trials and laboratory testing. Of particular interest were large scale triaxial and compressibility tests, which have been carried out by the IWHR¹ in China. From the results of these tests material parameters were derived which were then taken as basis for 2-D and 3-D deformation analysis. The results of the laboratory tests and also visual observations indicated a high disintegration potential of the siltstone which could lead to high dam deformations. By using only sandstone for rockfill it was concluded that the dam deformation will be within acceptable and normal limits.

1. China Institute of Water Resources and Hydropower Research (IWHR), Department of Geotechnical Engineering.

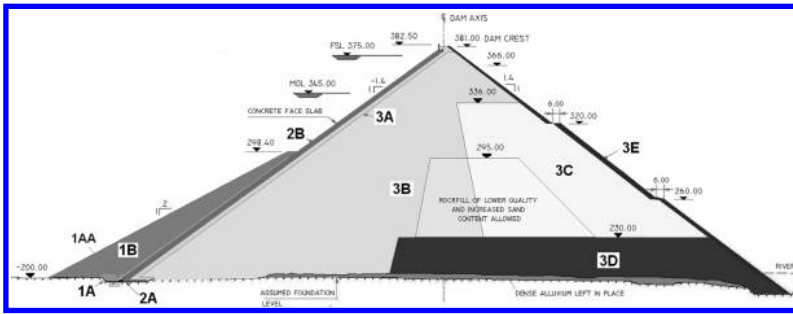


Figure 2. Dam zoning.

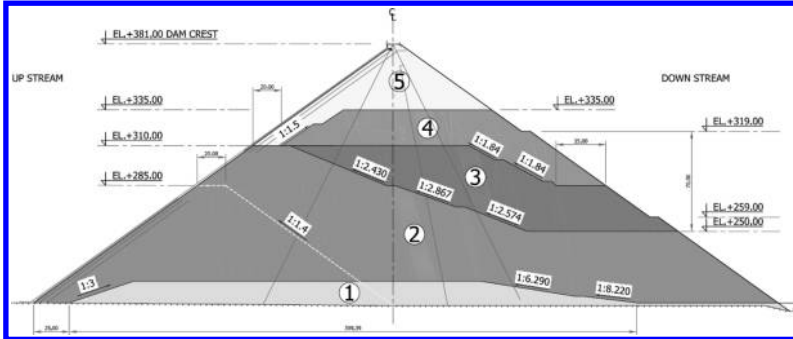


Figure 3. Dam construction stages.

For the rockfill fresh to moderately weathered sandstone was used whereby the lower quality material was placed in the central zone of the dam (see Ch. 2.2).

In general the used rockfill can be characterized as follows:

- The particle size is relatively large and particle shape is angular
- The gradation is often uniform and gap-graded, with lack of gravel-size particles
- Due to the gap-grading and increased sand content, water sluicing during placement leads to the development of a mud layer on the rockfill surface which needs to be removed
- The relative densities obtained after placement were generally adequate although areas of segregated fill occasionally occurred

The rockfill of the main dam body was placed in lifts of 0.8 m (zone 3B) and 1.2 m (zone 3C) thickness and compacted with 6–8 passes of 16 t vibrating roller compactors. The amount of water added to the fill was in the range of 100–150 l/m³.

The staging of construction is shown on [Figure 3](#). Construction of the first stage of the face slab (up to EL 293.4 masl) commenced after completion of the rockfill stage 2. During first stage face slab construction rockfill placement continued with stage 3 and 4.

The average rockfill placement rate was about 460,000 m³/month, with a maximum placement rate of 770,000 m³/month. The total volume of 9.7 M m³ was placed in 21 month.

2.4 Face slab design and construction

The dam is situated in a steep “V”-shaped valley. The concrete face slab has an area of about 88,000 m² and the valley shape factor is $A/H^2 = 2.7$. Considering this valley shape factor, increased movements of the face slab panels towards the river bed and resulting horizontal stresses in the central face slab panels were expected and considered in the design. [Figure 4](#) shows the valley shape factor of NN2 CFRD plotted on the graph developed by Pinto (2007).

With an assumed deformation modulus of 50 to 70 MPa the conditions at NN2 are about the same as at Campos Novos and Barra Grande CFRD where compression cracking of the face slab did occur.

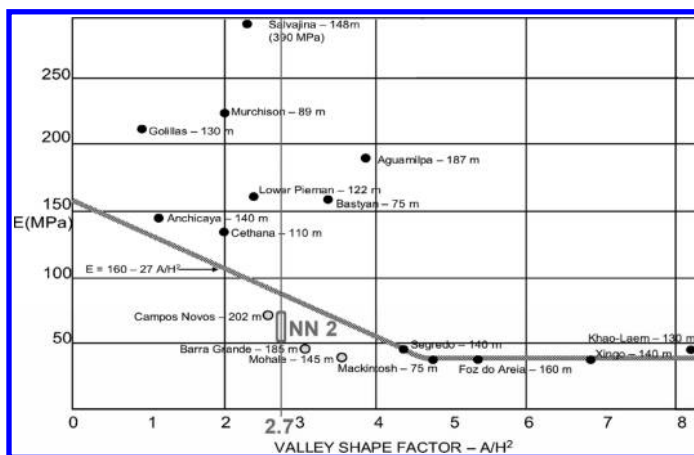


Figure 4. Graph deformation modulus vs. valley shape factor (after Pinto (2007)).

The face slab is designed with a thickness of $T = 0.3 + 0.003 H$. At the upper portion of the central slabs (above EL 293.4 masl) the thickness is somewhat increased to $0.4 + 0.0018 H$ to improve the resistance of the slab under compression. The face slab is constructed in panels of 15 m width. At the steep abutments the slab width is reduced to 7.5 m to cope with expected increased differential settlements along the relatively steep abutment slopes.

The vertical tension joints at the abutments are designed with bottom copper waterstop and GB®-surface waterstop², including corrugated waterstop, at the surface. An asphaltic bond breaker is applied on the concrete surface at the joint. The central joints are designed as compression joints with 20 mm thick compressible cork filler to allow some movement of the slabs towards the valley under compression. At the bottom a copper waterstop and at the surface a GB®-waterstop, without corrugated rubber waterstop, is provided. To maintain the designed slab thickness at the joints, the central loop of the copper waterstop is reduced and the chamfer at the slab surface is omitted. The perimeter joint is designed with copper waterstop at the bottom and GB®-waterstop system at the surface, including corrugated waterstop. A 20 mm thick bitumen painted wood filler is provided at the joint.

The face slab is constructed in two stages: Stage 1 up to EL 293.4 masl and stage 2 from EL 293.4 masl up to the top (connection to the parapet wall). The horizontal joint between the first and second stage of the face slab is constructed as movement joint with 20 mm joint filler board and bottom copper waterstop and surface GB®-waterstop. This joint will reduce the compressive stresses in slope direction.

Double layer reinforcement of total 0.4% in each direction is provided throughout the face slab. The reinforcement ratio is increased to 0.5% in each direction in an area of generally 20 m parallel to the plinth alignment and up to 40 m from the plinth at the very steep right abutment where higher stresses due to increased differential settlements are expected.

At the central slabs in an area of about 1/4 to 3/4 of the dam height, where the highest compressive forces will occur, additional stirrups are provided to prevent buckling of the upper and lower reinforcement under high compression. Anti-spalling reinforcement is provided along compression joints.

For the ease of construction the extruded curb method is used for the upstream face construction. Although constructed of lean concrete of low compressive strength (about 5 MPa), the deformability of the extruded curbs is significantly lower than that of the underlain zone 2B rockfill. Therefore, if the rockfill deforms and settles the relatively stiff curbs may not always follow the movements of the fill and potential voids may develop during dam construction.

When the concrete face is exposed to high water load (during impounding) the curbs may crack in areas of voids. In this case the concrete slab is subject to rapid deformations and high stresses.

2. GB® Waterstop Structure of Beijing IWHR-KHL Co. Ltd., China.

Therefore, the development of large voids beneath the concrete curbs must be avoided or already developed voids should be filled before impounding as e.g. done at Karahnjukar CFRD where extensive void grouting beneath the curbs and between face slab and curbs was performed.

To reduce the development of significant voids behind the curbs they should be as flexible as possible to be able to move with the rockfill deformations. In this respect cutting of the curbs into smaller pieces is promising. Therefore, at some recently constructed CFRDs in China the curbs were cut vertically at the locations of the face slab joints before construction of the face slab. At NN2 grooves were excavated into the extruded curbs during its construction on both sides along the vertical face slab joints to achieve predefined break lines in the curbs. During construction it was observed that several cracks in fact developed along these grooves.

After completion of the dam rockfill construction and during the construction of the second stage face slab exploratory holes were drilled through the face slab and curbs at defined locations. In these holes tests were performed to investigate if voids have developed between the face slab and the curbs or the curbs and the 2B fill which would have had to be grouted. No significant voids were, however, encountered.

3 INSTRUMENTATION AND MONITORING

3.1 Instrumentation concept

Instrumentation is provided to measure the behaviour of the dam during construction, reservoir impounding and long term operation. Emphasis is given towards monitoring seepage which could arise from imperfections of the face slab and from percolations through the dam foundation, and towards monitoring of embankment deformations. Seepage is indirectly monitored by piezometers installed upstream and downstream of the plinth and grout curtain, in the dam foundation and along the abutments. Seepage quantities are measured with a seepage weir at the dam toe. Deformations are mainly measured with settlement plates, embankment extensometers and inclinometers installed in the dam body and with joint-meters and tiltmeters installed at the face slab.

3.2 Monitoring and dam behaviour during construction

Dam deformations during construction were measured with hydrostatic settlement cells, fixed embankment extensometers and settlement gauges with combined inclinometer tubing. These instruments provided data of deformations along 3 sections within the dam body.

The maximum recorded construction settlement is 1.8 m, measured at both instrument levels EL 260 masl and EL 319 masl slightly downstream of the dam centre. The construction settlements measured with the instruments were used for calculating the deformation moduli during construction E_{rc} :

$$E_{rc} = \frac{\gamma Hd}{s} \quad (1)$$

where γ = unit weight of fill above settlement plate; H = height of fill above settlement plate; d = thickness of fill below settlement plate, s = recorded settlement of the settlement plate.

The back-calculated deformation moduli during construction are in the range of 70 MPa (upstream side) to 50 MPa (downstream side). Using these deformation moduli the dam settlements during construction were back-modelled using an elasto-plastic material model. The calculated dam settlements comply well with the measured settlement as shown on [Figure 5](#). The maximum dam settlement at the end of construction is about 2.2 m which corresponds to 1.2% of the dam height.

3.3 Monitoring and dam behaviour during first impounding

The first reservoir impounding started in March 2010 just after the completion of the second stage face slab construction and about 4 months after completion of the dam fill. Until December 2010 the reservoir was filled up to about 98% of the full supply level (FSL). Seepage quantities

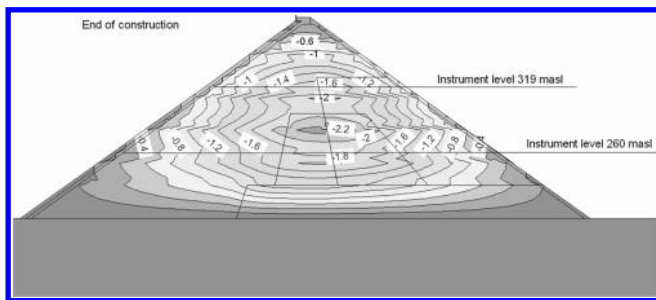


Figure 5. Dam settlements (in m) at the end of construction.

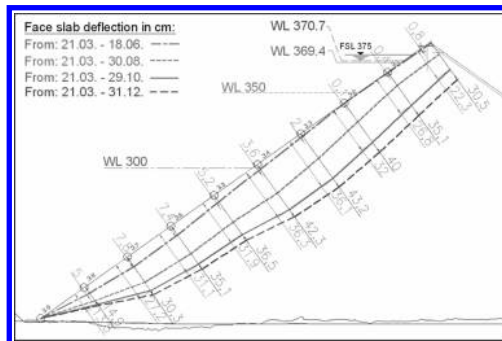


Figure 6. Face slab deflection derived from tiltmeter readings.

recorded with the seepage measuring weir have increased relatively linearly with the rise of the reservoir level until September 2010 when the reservoir level 360 masl (approx. 90% of FSL) was reached. Since then the recorded seepage quantity was stable at 80–90 l/s and it was suspected that the maximum capacity of the measuring system was somehow exceeded. After rectification works at the system had been performed a seepage quantity of about 300 l/s was measured.

Post-construction dam deformations generally occur due to the following reasons:

- Increased load from the reservoir
- Creep; softening of the rock due to wetting/water saturation

The increasing water load during reservoir impounding mainly acts on the dam face and causes the concrete face and the upstream part of the rockfill to deform. The face slab deflection is measured by tiltmeters (electro-levels) installed on the face slab and by geodetic survey of surface displacement points.

The face slab deflection at different reservoir levels as measured with the tiltmeters installed at a central face slab panel is shown on Figure 6. The face slab deflection has significantly increased after the water level exceeded EL 300 masl. At a reservoir level of 371 masl (corresponding to about 98% of FSL) the maximum face slab deflection since start of impounding is in the order of 43 cm and occurs at about half height of the dam.

From the deformation monitoring data of the downstream side of the dam body where the reservoir load has only little or no impact quite pronounced creep settlements are observed. Data from the settlement cells in the downstream part of the dam body and geodetic survey data of the downstream shell indicate a settlement rate of 20–40 mm/month.

4 DAM DEFORMATION PREDICTION AND BACK-CALCULATION

Several methods for predicting dam deformations during construction and first reservoir impounding exist. Such methods range from simplified deformation estimates based experience, up to mathematical modeling with various constitutive models.

For the Nam Ngum 2 dam 2-dimensional and 3-dimensional numerical stress and deformation analyses have been performed by IWHR³ prior to the construction of the dam. The analyses were performed using the non-linear hyperbolic material model. The used rockfill parameters were based on results from large scale triaxial tests carried out on samples from the quarry with gradations downscaled to suit the testing equipment. Additional calculations have been performed using adjusted rockfill properties. The used rockfill parameters are listed in Table 1.

In Table 2 the displacements obtained with the 3-dimensional analysis using the above sets of material parameters are summarized. It is noticed that the computed displacements are considerable lower than the actual displacements, indicating that the embankment materials behave softer than assumed based on triaxial testing.

It should be noted that the maximum settlement at the end of construction is observed in the central downstream part of the dam which is not much influenced by the water load acting on the concrete face.

After completion of the dam construction 2-dimensional numerical analyses have been performed using deformation moduli E_{rc} , back-calculated from the settlements measured with the instruments during construction. For the analysis an elasto-plastic constitutive model was used.

As shown in chapter 3.2 the back-calculated dam deformations at the end of construction coincide well with the monitored deformations (see chapter 3.2, Fig. 5). If the same parameters would be used for calculating the face slab deflections due to impounding, a value of 1.1 m would be obtained.

However, the deformation moduli to be used for estimating face deflection are normally higher. A simple and practical way of predicting the maximum face slab deflection is to consider the deformation modulus E_T of the rockfill evaluated in the direction of the face

Table 1. Material parameters used for numerical analyses.

Materials	γ_d (g/cm ³)	K	K_{ur}	n	R_f	K_b	m	c (kPa)	ϕ_0 (°)	$\Delta\phi$ (°)
Case 1: Zone 2B*	2.15	1600	3200	0.38	0.918	2800	-0.27	-	44.1	4.2
Zone 3A*	2.15	1040	2080	0.31	0.820	1000	-0.06	-	45.9	5.7
Zone 3B*	2.15	1000	2000	0.38	0.864	1680	-0.29	-	46.5	6.2
Zone 3C*	2.10	630	1260	0.37	0.802	520	0.0	-	45.1	5.4
Case 2: Zone 2B	2.15	1000	2000	0.35	0.918	500	0.20	-	44.1	4.2
Zone 3A	2.15	1000	2000	0.35	0.820	500	0.20	-	45.9	5.7
Zone 3B	2.15	630	1260	0.37	0.864	400	0.10	-	46.5	6.2
Zone 3C	2.10	630	1260	0.37	0.802	400	0.10	-	45.1	5.4

* Derived from triaxial test results.

Table 2. Results of 3-dimensional analyses.

Case	Case 1	Case 2
Settlement end of construction (cm)	96	140
Settlement after impounding (cm)*	98	149
Face slab deflection due to impounding (cm)	20	34

* Including construction settlements.

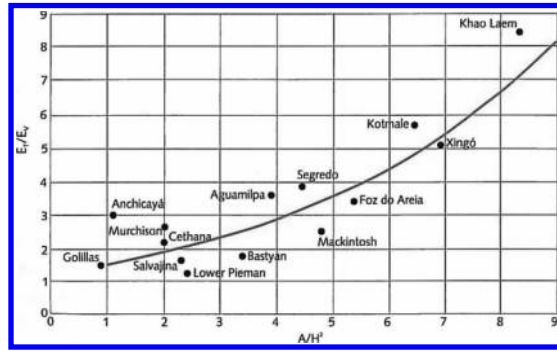


Figure 7. Ratio E_T/E_V as a function of A/H^2 (Pinto & Marques Filho (1998)).

slab movement, i.e. normal to the face slab, under the water load. Considering this transverse modulus the maximum face slab deflection D can be estimated:

$$D = \frac{\gamma_w H_w H_d}{E_T} \quad (2)$$

where γ_w = unit weight of water; H_w = height of water above face slab; H_d = thickness of fill below face slab (perpendicular to face slab), E_T = transverse rockfill modulus.

The transverse modulus E_T is higher than the vertical modulus E_V (E_V is equivalent to the modulus during construction E_{rc} as defined in Equation 1) due to a rotation of the principal stresses within the rockfill and rockfill consolidation during construction. Observed values are generally 1.5 to 5 times higher than the vertical modulus depending greatly on the valley shape factor A/H^2 , but certainly also on the creep characteristics of the rockfill. Knowing the vertical modulus E_V calculated from the measured settlements during construction E_T can be estimated using the graph developed by Pinto & Marques Filho (1998) (Fig. 7).

Considering the valley shape factor of $A/H^2 = 2$ and the vertical rockfill modulus $E_V = E_{rc} = 70$ MPa the maximum face slab deflection of the NN2 dam would be in the order of 65 cm occurring at about half of the dam height and full reservoir level.

5 CONCLUSION

The monitoring system of the Nam Ngum 2 dam has provided useful information on the deformation behavior of the dam. The maximum settlements at the end of construction are about 2.2 m which corresponds to 1.2% of the dam height. The measured maximum face slab deflection due to impounding up to 98% of FSL is 0.43 m. The maximum settlement may have reached a value corresponding to 1.5% of the dam height. The deformations will further increase with rising reservoir to full supply level and due to creeping of the rockfill. The deformation monitoring indicates a high rate of creeping.

Measured seepage quantities are in an acceptable range. At present the performance of the dam is good and the visual appearance is excellent.

The back-calculation of dam deformations and prediction of face slab deflection under consideration of deformations measured during construction give reasonable results. A reliable estimation of the in-situ rockfill properties, in particular its creep characteristics, remains the main challenge for deformation prediction.

REFERENCES

- Pinto, N.L.S. 2007. A challenge to very high CFRD dams: Very high concrete face compressive stresses. *5th International Conference on Dam Engineering*. Lisbon, February 2007.
- Pinto, N.L.S. & Marques Filho, P.L. 1998. Estimating the maximum face deflection in CFRDs. *The International Journal on Hydropower & Dams*. Issue 6, 1998: 28–31.

Intensified monitoring of Emosson arch dam during construction of Nant de Drance pump storage scheme

H. Stahl

AF-Consult (formerly Colenco Power Engineering), Baden, Switzerland

ABSTRACT: The access tunnel to the powerhouse cavern of Nant de Drance pump storage scheme, currently under construction, passes at a horizontal distance of some 800 m from Emosson arch dam. As a result of lessons learned from an incident in 1978, whereby the construction of an investigation gallery caused serious damage to the Zeuzier dam, the Emosson dam is under intensified monitoring with the aim of detecting any unexpected developments in due time in order to initiate timely corrective measures.

1 INTRODUCTION

In 1978 the Zeuzier arch dam, located in the western Swiss Alps, experienced major deformations leading to damage of the dam in the form of serious cracking and joint openings. The reservoir level had to be lowered and the hydropower plant was severely constricted for several years. Investigations of the cause indicated that an investigation gallery for a highway tunnel, which was under construction at some 1.5 km away from the dam was to blame. It was found that the tunnel had a draining effect on the rock mass forming the foundation of the dam, which resulted in surface settlements and subsequently deformations of the dam. Following this event, the possibility of surface deformation caused by tunnel excavations in the vicinity of existing dams needs to be addressed.

Emosson dam is a 180 m high arch dam in the western Swiss Alps, in the border region with France (Figure 1). It impounds a reservoir with a volume of 227 Mio m³, which is used for electricity production in a cascade of two power plants in Vallorcine (200 MW) and in La Bâtiаз (190 MW) operated by the dam owner Electricité d'Emosson SA. As with most of the Swiss mountain reservoirs, Emosson is operated as an annual storage scheme with a high water level in autumn and low water level in spring. It is filled with the melting snow and glaciers during the summer months to shift the energy production to the winter months, when the energy demand is high.

In 2008 construction works for the Nant de Drance pump storage scheme started. This 900 MW scheme consists of an underground connection of the Emosson reservoir to the higher reservoir of the Vieux-Emosson arch gravity dam, utilising Emosson reservoir as the lower basin of the pump storage scheme (Figure 2). Apart from the intake structure, to be constructed in the Emosson reservoir, the Emosson dam and reservoir are not directly affected by the works for the new scheme. However, the main access gallery to the powerhouse cavern passes at a horizontal distance of only 800 m from the dam and underpasses the reservoir.

2 BACKGROUND AND GOAL OF THE INTENSIFIED MONITORING

Following the experiences from Zeuzier arch dam, drainage of the rock mass due to the construction of the main access gallery to the powerhouse cavern of Nant de Drance pump storage scheme with subsequent surface deformation in the area of Emosson dam, cannot be ruled out.



Figure 1. Emosson arch dam (photo: Swiss Air Force).

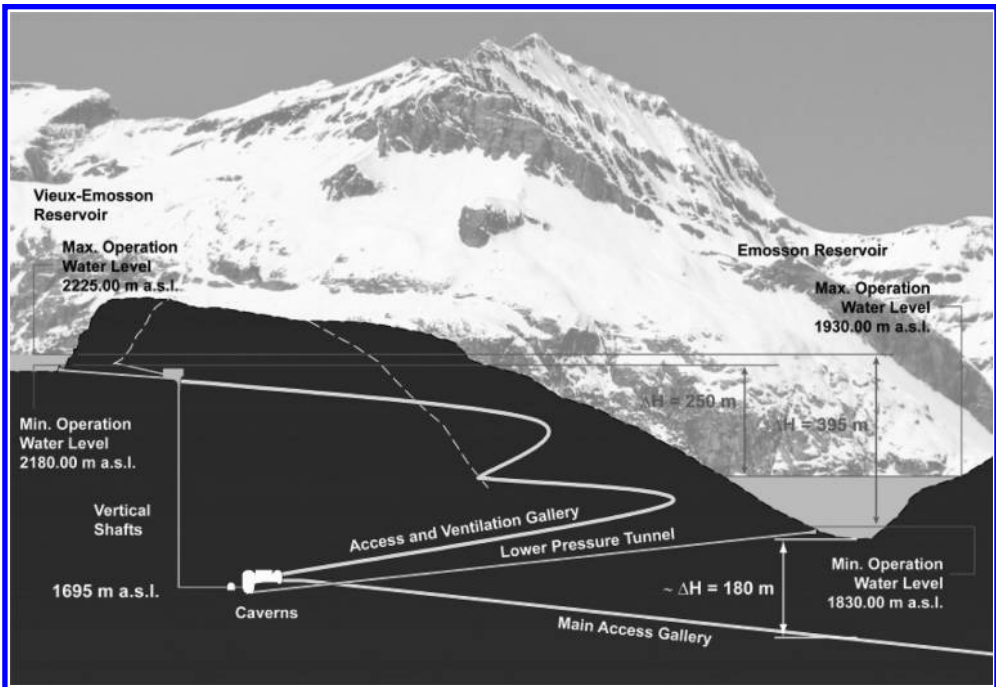


Figure 2. Nant de Drance pump storage scheme (Nant de Drance SA).

For this reason, the approval for the pump storage scheme, issued by the Swiss Federal Office of Energy (SFOE) is subject to the requirement to carry out measures to ensure the safety of Emosson dam during the entire construction period as well as thereafter. The measures that have been taken in this respect include the analysis of the hydrogeological situation in the area of the dam and main access gallery and the determination of the expected terrain deformation at the ground surface, in particular at the dam site. A 3-dimensional finite element model

for Emosson dam has been developed in order to evaluate the capacity of the dam to accept permanent ground surface deformations. The criterion adopted is to maintain elastic material behaviour independent from the reservoir level and temperature of the dam. It has been found that the dam can accept more than the expected terrain deformation at the dam site. Regardless, threshold values and alarm values with adequate safety factors have been defined with required measures to be taken in the event that these predefined values are reached.

The goal of the intensified monitoring is to ensure that the deformations of the dam and the surrounding area remain at all times within admissible limits. Based on the specific observations, any unexpected terrain deformations shall be detected immediately to allow for timely corrective measures to be taken in the tunnelling excavation works.

3 NORMAL MONITORING

The intensified monitoring as a consequence of the construction activities complements the normal monitoring activity which is continued as before. For the normal monitoring, surveillance of Emosson arch dam, which falls under the large dam's category, is under the supervision of the federal administration, represented by the SFOE and follows their specific regulations. This implies the application of the 4 levels of the dam surveillance system:

Level 1: dam owner. Activities by the dam owner include the regular visual inspections and instrument readings, tests and maintenance of all installations as well as general maintenance works.

Level 2: experienced civil engineer. The main tasks of the experienced civil engineer include the analysis and interpretation of the instrument readings and visual inspections, execution of an annual inspection visit to the dam and the preparation of an annual report on the behaviour and state of the dam.

Level 3: civil engineering expert and geological expert. The experts review the annual reports by the experienced civil engineer and, every 5 years, prepare an experts report, further analysing the dam behaviour and any developments during the last 5 years as well as giving recommendations.

Level 4: of the dam surveillance system is constituted by the SFOE, the supervising authority.

4 INSTALLATIONS AND MEASURES FOR THE INTENSIFIED MONITORING

In the intensified monitoring process the same engineers and experts as in the normal monitoring process are involved. This best allows for the integration of knowledge and experience gained over the past years. However, additional installations and measures have been introduced. These installations and measures can be structured as follows:

- monitoring of the wider area surrounding the dam;
- monitoring of the terrain around the dam;
- intensified monitoring of the dam.

4.1 *Monitoring of the wider area surrounding the dam*

The monitoring of the wider area surrounding the dam serves as early warning of changes, which could affect the dam. It essentially comprises precision levelling combined with GPS measurements.

The precision levelling consists of a series of levelling points along the access road to the dam, which is also crossed under by the access tunnel (see [Figure 3](#)). A zero measurement was carried out well before commencement of construction works. Through sequential measurement, settlement over the tunnel axis can be determined. As long as the settlements over the tunnel axis remain within pre-calculated boundary limits, then it can be assumed that the

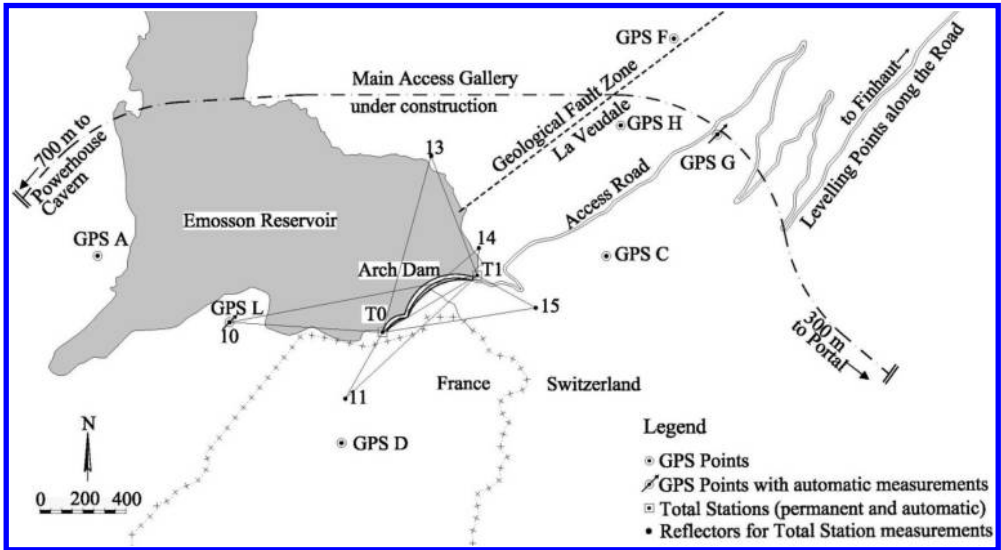


Figure 3. Instrumentation in the wider area surrounding the dam and in the terrain around the dam.

terrain deformations at the dam site also remain within prognosis and therefore below the threshold values.

For the early recognition of unexpected settlement a GPS point has been installed at the cross-over point between the surface precise levelling lines and the tunnel axis, which is automatically read several times per week (GPS G in Figure 3). Due to the fact that measurements need to be carried out also through the winter months in an area of high avalanche hazard, the GPS-measurement point has been housed in a specially constructed avalanche safe installation.

To increase the accuracy of the GPS measurements, a reference station has been positioned at a geologically stable site, which cannot be influenced by the construction works. This point serves equally as an altitude control point (GPS L in Figure 3).

A further GPS measurement point has been installed within the zone where the main access gallery crosses a geological fault zone. This point is measured manually periodically during the summer months when access is possible (GPS H in Figure 3). The GPS points of the normal monitoring array are measured annually during the construction period, as opposed to the normal 5 yearly measurement (GPS A, C, D and F in Figure 3, GPS point B further north, not shown in Figure 3).

In addition to the precise levelling and the GPS points, the following physical values are recorded and evaluated for the early recognition of deformation to the rock mass during the construction phase: drainage water volume from the tunnel drives, flow from regional springs as well as pressure measurements in the excavation boreholes for the powerhouse cavern.

4.2 Monitoring of the terrain around the dam

The intensified monitoring system of the terrain around the dam comprises automated total station measurements and an increased measurement of the external geodetic network for the dam.

From two permanently installed total stations T0 and T1 (see Figures 3 and 4), reflectors on both valley flanks are measured automatically several times a week, usually at night to minimize adverse atmospheric influences. From this network the deformation of the terrain around the dam can be calculated and compared with the threshold and alarm values.

The external geodetic network of the normal monitoring array, using additional survey pillars and reflector locations not shown in Figure 3, is measured with an increased frequency from the normal 5 year period up to an annual measurement during the construction period.



Figure 4. Protective cabin for the permanently installed total station T1 on the left bank (photo: Straub AG).

4.3 Intensified monitoring of the dam

Emosson dam contains a full array of instruments which are measured regularly. Therefore, installation of additional instruments or automatization of existing instruments has not been found necessary. Also, the frequency of the instrument readings and visual inspections is as under normal monitoring conditions.

However, in order to further monitor any deformation of the terrain around the dam, the measurement of the block-joints has been taken up again. The last complete measurement of the block joints was carried out in 1976 at the end of the dam's construction period. For this reason a zero reading of the original installation still in place was carried out prior to construction works. Repeat measurements are carried out annually under comparable circumstances with particular reference to reservoir level and concrete temperature.

5 DATA FLOW AND EVALUATION

A central data-base forms the key instrument for the administration of the large volume of data arising from the monitoring system. This data-base contains all measurements and allows for the graphical evaluation of the measurements. It affords remote access for all project engineers concerned via internet.

The data input into the project data base for the automatic readings and manual readings of the dam instruments is, as much as is feasible, automatic from the dam owner's data base and Level 2 engineer's database, where the data is stored as prior to the construction period. Due to the automatic import of data, the quality control of the data in the project data base is of great importance.

The automated total stations and GPS points are powered either by a solar power pack or are connected to the electrical power network. The measured data is transmitted via cable, WLAN or UMTS to a central control module located in an annex building to the dam, from which they are further transmitted via fibre optic cable and internet to a specialised land

surveying company for evaluation. After evaluation of the raw data, the calculated terrain deformations are filed in the project data base, where they are available to all concerned.

At the dam site, the valley undergoes a process of dilation and contraction corresponding to the water level in the reservoir. The rising water level during summer widens the valley. This deformation is reversible with the lowering of the reservoir level during winter. The deformation of the valley is approximately 10 mm between the maximum and minimum operation water level and can be measured with the pendulums located in both abutments and with the total stations. Based on the measurement series of the pendulums over the past 10 years prior to construction, a correlation between the reservoir level and the valley dilation and contraction respectively has been determined. This leads to an expected temporal value for the terrain deformation to which the deformation measured by total station can be compared to assess the actual measurement.

All things being equal, the data base is updated weekly. The frequency, however, can be increased to daily updating and evaluation if circumstances demand. An evaluation of the data of the dam instrumentation, along with that of the total station and GPS measurements, is carried out by a specialist engineer at AF-Consult at least weekly, in order that developments can be detected early.

A monthly report is submitted to the responsible Project representatives, for the dam owner and a panel of experts as well as the regulatory authorities indicating all occurrences, measurements that have been carried out and the state of measurements over the reporting period.

6 CONCLUSION

The additional installations and measures for the intensified monitoring have been operational since 2009 and are scheduled to remain in operation up to the end of the construction in 2016. The additional installations are working reliably and the newly introduced strategies within the action plan are well-rehearsed. With the measures taken, the responsible engineers are confident that the safety of the dam can be ensured throughout the construction period and thereafter.

Dam embankment deformation and face slab movement monitoring of Nam Ngum 2 concrete face rockfill dam

P. Khamwongkhong

Ramkhamhaeng University, Huamark, Bangkok, Thailand

W. Mairaing

Kasetsart University, Bangkok, Bangkok, Thailand

ABSTRACT: Nam Ngum 2 Hydroelectric Power Project is situated on upstream of existing Nam Ngum 1 reservoir and located approximately 93 km northeast of Vientiane, capital of Laos. The construction project was started on 2006 while the dam body began to embank on February 2008. It was started the reservoir impounding on March 2010. The dam embankment is Concrete Face Rockfill Dam (CFRD) of 182 m. high and crest length of 512 m. Construction of NN2 CFRD divided into 5 stages for embankment in order to incorporate with face slab construction. Concrete face slab is divided to two stages of construction, the first stage of face slab start from plinth to elevation +293 m ASL and the second stage of face slab continue to +377 m ASL. The first stage face slab started after compacted rockfill placement stage 1 and 2 to elevation +315 m ASL. The second stage face slab started when the upstream portion embanked up to the wave wall foundation. The dam site is located in a narrow valley with rather steep slopes ($A/H^2 = 2.66$) and complex geology. Nowadays dam behavior interpretation during the construction and initial stage of reservoir filling is proceeding to confirm the integrity on the dam and these would lead to the set up the safety or warning criteria for dam operation. The numbers of data during one year about 0.5 million records from extensive dam instruments more than 475 sensors would be summarized. In order to interpret the dam behaviors, GIS would be used for the analysis. The Hydrostatic Settlement Gauges, Fixed Embankment Extensometers, Incline Inclinometer and inclinometer with Magnetic Settlement Gauges were installed on tree section for measurement of internal displacements. In this paper, the behaviors during the construction and first filling are presented which are mainly for determination of dam deformation, face slab movement, the back analysis for material parameters and prediction of reservoir filling. The sandstone rockfill secant modulus during construction (E_{rc}), modified from Fitzpatrick et al. (1985), values varies in the 38–180 MPa range depending on the void ratio of the rockfill and the parent rock material from quarrying. The average values of 3B, 3C zone and for the whole dam are 151.40, 59.67 and 101.11 MPa respectively. The maximum settlements were observed during the construction period reached the values of 1.69 meters occurred in Zone 3C. The maximum settlement after construction for 10.5 months is 0.334% of the dam's height. The face slab shown deflections cause from impounding. The rockfill modulus on first filling of NN2 E_{rf} is 593 MPa.

1 INTRODUCTION

1.1 *Design of NN2 CFRD*

The dam is consisting of compacted rockfill found on a rock foundation, plinth, face slab and wave wall. Dam slopes for upstream and downstream are defined as 1V:1.4H to suit with available rockfill material. The rockfill materials are generally classified into three designated zones as follows: Zone 1 (1A and 1B) is concrete face slab protection zone in the upstream

of face slab, Zone 2 (2A and 2B) is concrete face slab supporting zone in the downstream of face slab, and Zone 3 (3A, 3B, 3C and 3D) is the rockfill zone, which is the major part of the rockfill material. (Sramoon et al., 2010)

1.2 *The structural geology at dam site*

Geological structure at the dam site is characterized by three easterly trending anticline folds whose axes are nearly perpendicular to the Nam Ngum River. The dam site is situated between the limbs of two local anticlines that strike nearly East-West across the river. Throughout the dam foundation area, the dip of bedding ranges from horizontal (0°) at the anticline axes to 65° on the limbs of the anticlines. Prominent slickenside are often developed on the bedding plane surface of the weaker, mudstone and siltstone beds, and indicates shear movement during folding. (Ngarmsirilertsgoon & Puangpatcharakul 2009).

2 DAM CONSTRUCTION DAM INSTRUMENTS AND DATA CORRECTION

2.1 *The dam construction*

The construction project was started on 2006 while the dam body began to embank on February 2008. The river bed was cleaned and the foundation was improved before the commencement of embankment work. The embankment constructed within 20 months. The dam has 182 m at elevation of 381 m assumed sea level above plinth foundation in riverbed. The crest length of dam is 512 m with 9 m width and the basement is 518.8 m. The total rockfill embankment volume is 10^7 m^3 and total area of the concrete face slab is $88,000 \text{ m}^2$.

The main dam embankment has mainly divided into 5 sequences in order to incorporate with the 2 stages of face slab construction sequences. The compacted sandstone rockfill has been controlled to achieve the dry unit weight more than 21.5 kN/m^3 and the maximum of void ratio 0.20. The 0.80 m lift thickness of 3B and 3C material has been employed depending on the maximum size of rockfill material. The steep abutment has treated by thin layer of rockfill/filter material in order to increase compressibility modulus. (Chalermnon et al., 2009).

During construction it was observed that also fine grained sandstone, porous or weathered sandstone of moderate quality is being obtained from quarrying which can not always completely be separated and wasted. Therefore the dam zoning was adjusted to permit also placement of lower quality rockfill in the central part of the dam embankment (3Bw and 3Cw). (Straubaar et al., 2009).

In [Figure 1](#), zoning and the sequence of rockfill placement are shown. Sequence 1 consists of Zone 3B and 3D, drainage, which was compacted the fresh and slightly to moderately weathered sandstone. The actual placement commenced on March 2008 of 10 m height start from downstream and left about 30 m at upstream path for construct the plinth at river bed. Sequence 2 started from April 2008 to January 2009, about 10 months. The placement of rockfill on the upstream was done to accommodate the construction of first stage face slab up to elevation 315 m asl, which corresponds to 115 m in height. Sequence 3 had to construct parallel with the first stage of face slab construction. Started from February to June 2009, about 5 months, and it is require to control the differential settlement and stress in rockfill between the zone by controlling the different height of embankment between upstream portion and downstream portion, not more than 40 m. Sequence 4 after completion of the first stage concrete face slab then start compacted the embankment till the elevation reach to the wave wall foundation. The work took about 5 months started from July to November 2009. Then strated the Sequence 5, the second stage face slab started commencement in December 2009 parallel with the earthfill and random fill placed on upstream face over the lower part of the face slab, Zone 1A and 1B, have also been compacted. After completion of the second stage face slab and the wave wall, the last portion of embankment above the wave wall foundation was constructed.

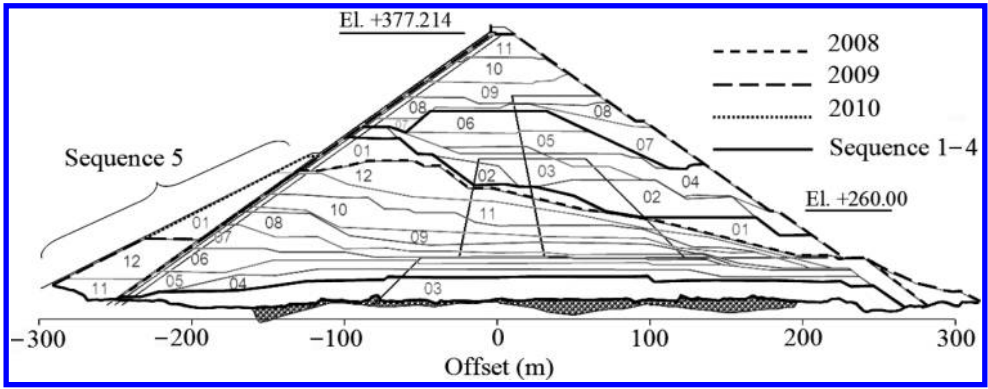


Figure 1. Sequence of rockfill placement.

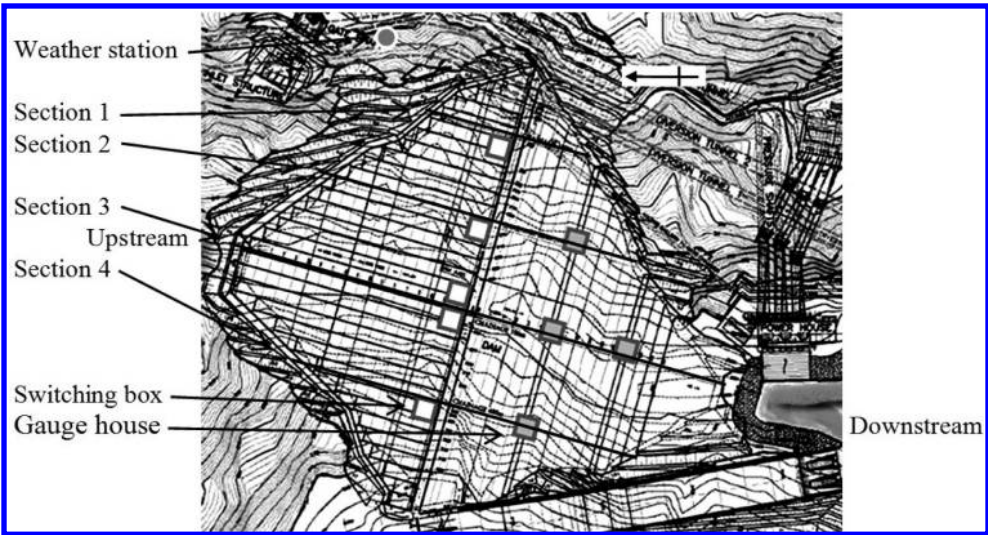


Figure 2. Layout of NN2 dam and dam instrument sections.

2.2 Dam instruments of NN2 CFRD

There are several kinds of dam instrument on NN2 dam; more than 475 sensors were installed. Most of the instruments were installed within dam body and on the face slab. Some instruments had been installed in dam foundation before filling of the dam embankment. [Figure 2](#) shows the layout of the Nam Ngum 2 dam and 4 main instrument sections. The total numbers of sensors are given on [Table 1](#). Instrumented data are reading and analyzed continuously to assess the performance of NN2 CFRD during construction, reservoir impounding and operation of the dam.

The deformation of rockfill embankment monitoring by the instruments which are installed at sections 2, 3 and 4. FEEs and HSCs indicated the deformation within rockfill embankment in horizontal and vertical respectively. PI indicates slope movement and instability. Magnetic settlement gages coupling with the inclinometer access tube detect the internal settlement of embankment. The network of 35 SM consists of 14 points on the upstream slope and 21 points on the crest and downstream slope of the embankment at points installed at three levels. Horizontal and vertical movements of the reference monuments are determined by geodetic observations.

Table 1. Summary of dam instruments installed at NN2 CFRD.

Instrumentation	Notation	Quantity	Location	
Surface Monuments	SM	14 21	Rockfill	Upstream slope Dam crest and Downstream slope
Inclinometer	PI	3 sets	Rockfill	Downstream berm
Magnetic Settlement Gauge	SG	41		
Hydrostatic Settlement Cell	HSC	22	Rockfill	Section 2–4
Fixed Embankment Extensometer	FEE	111	Rockfill	Section 2–4
Total Earth Pressure Cell	TPC	3	Rockfill	Section 3
Strong Motion Accelerometer	SMA	3	Rockfill	Crest, downstream berm and abutment
Weather Station	WS	1 set	Rockfill	Abutment
V-notch Measuring Weir	VW	1	Rockfill	Downstream toe
Open Standpipe Piezometer	OSP	7	Rockfill	Downstream of abutment and dam toe
Inclined Inclinometer	IIC	1	Face slab	Section 3
Electro Level (Tilt Meter)	EL	23	Face slab	Section 1–4
1 Dimensional Joint Meter	JM	4	Face slab	Parapet wall—face slab
2 Dimensional Joint Meter	2JM	10	Face slab	Between vertical joint
3 D (Perimetric) Joint Meter	PJM	13	Face slab	Along perimetric— construction joint
3D Concrete Strain Gauge	TSG	27	Face slab	Within concrete slab
Rebar Strain Gauge	RBSG	27	Face slab	Within concrete slab
Non Stress Strain Meter	RBSG	27	Face slab	Beneath concrete slab
Distributed Fiber Optic Temperature	DFOT	900 m	Plinth	Beneath concrete slab
Vibrating Wire Piezometer	VWP	35	Dam foundation	

In NN2, instrumentation interpretation to assess behavior and responses of the dam and appurtenant structures can be divided into five groups as follows: 1) dam embankment deformation, 2) concrete face slab movements, 3) seepage and leakage, 4) seismic response, and 5) instrumentation results for other structures. This paper will point out only dam embankment deformation and concrete face slab movement. The interpretation is for the instrumentation data up to 28 September 2010 which is about ten months after the completion of rockfill placement of the dam body to elevation 377 m, considered as the end of construction and initial impounding.

2.3 Data correction and error reduction

Interpretation of the monitoring data needed to realize on the data correction because all measurements involve some error. The measures by which error is defined should be considered as part of the dam behavior interpretations. By observed the field data it were found the cause of error such as changes of temperature, atmospheric pressure, change of reading station and drop of power supply. The type of errors used to define the correction in instrument measurement data including systematic error, human error and random error. In this paper, only two types of instruments will be use for example to explain the procedures of data correction and error reduction. There are HSC and EL. Figure 3 presents the located of HSCs in dam body and ELs positions on slab of NN2 dam. HSCs are devices placed in an embankment fill during construction to monitor settlement or heave at a discrete location within dam body. ELs were mounted on the dam's face slab on four sections to monitor slab deformation.

Pressure reading correction for HSC: The HSC consists of a pressure transducer and connected to a reference station by a twin tubing filled with water. The reference station consists

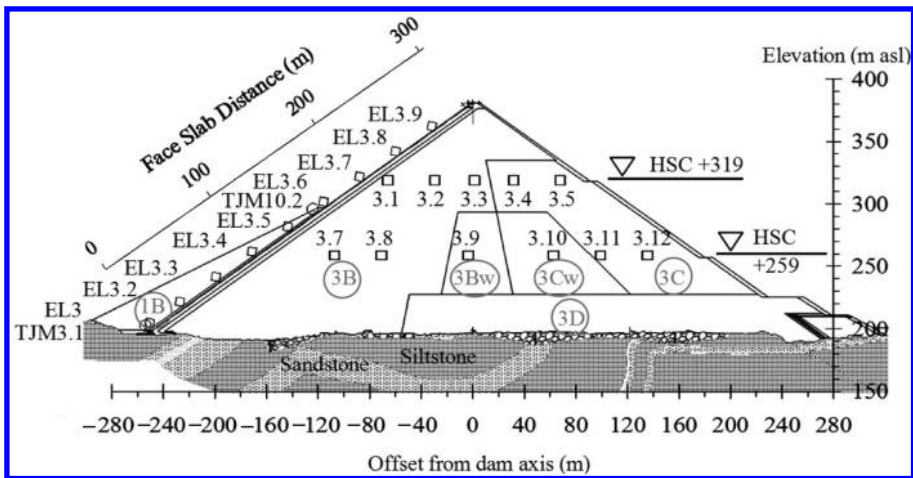


Figure 3. The located of HSCs, ELs and TJMs on typical section with rockfill zoning of the dam.

of a sealed liquid-filled reservoir open to atmospheric pressure and located at the gauge houses. The relationship between the height of water column and reading value is dependent on the barometric pressure at the reservoir and temperature of water in the system. The settlement is measured relatively to the elevation of the reservoir and the pressure at sensor had been corrected.

Data corrections for EL: ELs are used for monitoring changes in rotation at the surface of face slab which are interpretation with TJMs measurement the joint movement between face slab and plinth and also between 1st and 2nd stage face slab. It was found that the reading value is dependent on two major causes of the systematic errors including the variation of temperature at located ELs and change of reading station. The correction was done by finding the equation of relationship between rotation value and temperature for adjusting the reading values to the true values.

3 DAM EMBANKMENT DEFORMATION

3.1 Settlement of embankment

The settlements of the rockfill embankment across dam width recorded at the three sections of the dam by the HSC from 5 October 2008 to 28 September 2010. During the construction period, the accumulative settlements at Section 3 (deepest section) reached the values of 705 mm in Zone 3B, 955 mm in Zone 3Bw, 1690 mm in Zone 3Cw and 1252 mm in Zone 3C which recorded at the same level +258 m asl. The maximum settlement observed by HSC3.4 at level +319 is 1.89 m or 1.04% of dam's height. These settlements were compensating by the rockfill at placement which compacted during construction. Figure 4 show the contours of settlement in mm observed at the end of construction on 12 November 2009. It was found that the locations of maximum settlement are on the downstream zone where rockfills of lesser quality, Zone 3Cw and 3C, were used as opposed to 3B material in the center and upstream zones.

During 12 November 2009 to 18 March 2010 was the period of waiting for impounding and constructed the 1B zone. About 4 months, the maximum settlement was found at the same point with value of 250 mm or 0.138% of dam's height. The contour of settlement after construction observed during this period show in Figure 5a.

The reservoir impounding started on 18 March 2010, with water level at elevation +219.20, increasing quickly to level +315.03 on 18 July and to level +365.36 on 28 September 2010 (6.5 months). To monitor the behavior during the reservoir impounding, the displacements

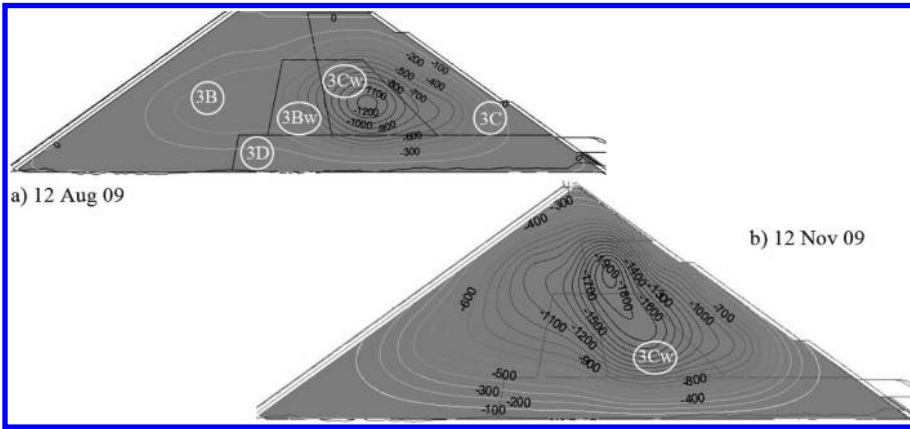


Figure 4. Contours of settlement (in mm) at maximum dam section during and at the end of construction.

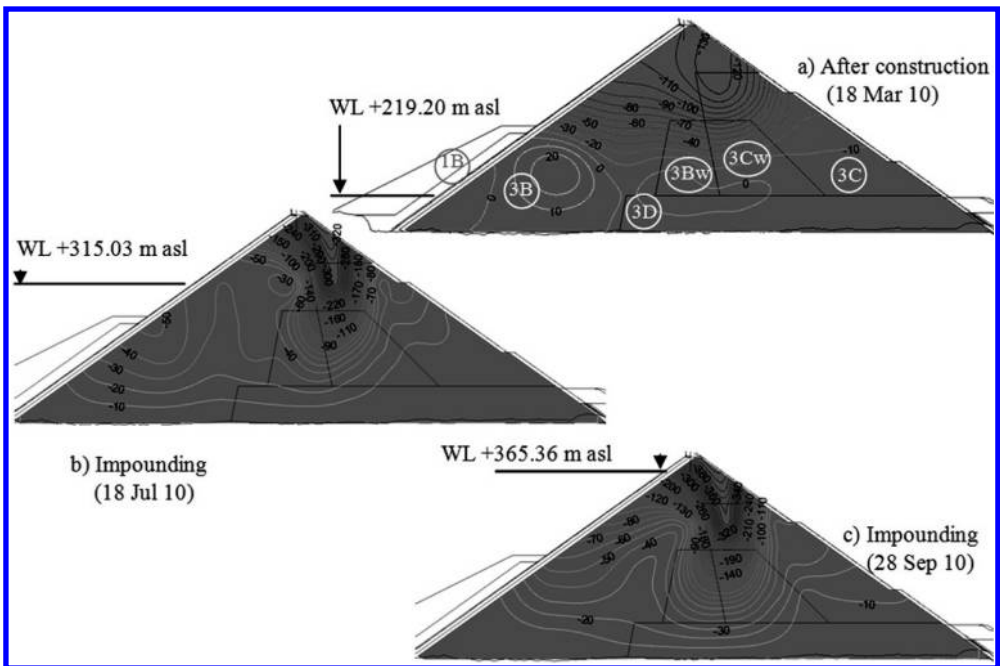


Figure 5. Contours of settlement (in mm) after construction and during impounding.

of the construction phase were reset to zero at 18 March 2010. The additional settlements were 604 mm or 0.194% of the dam's height. It was found that the major effect of rockfills settlement was the rockfills loading more than the impounding loading which show in Figure 5b–c. The impounding was cause the effect to settle of rockfill 3B zone on upstream of the dam while the center and downstream of the dam still remain settle by itself weight.

3.2 Lateral movement of embankment

Figure 6 shows the lateral movement of embankment. The upstream-downstream displacements monitor by Probe Inclinometers (PI) in Figure 6a show maximum lateral displacement

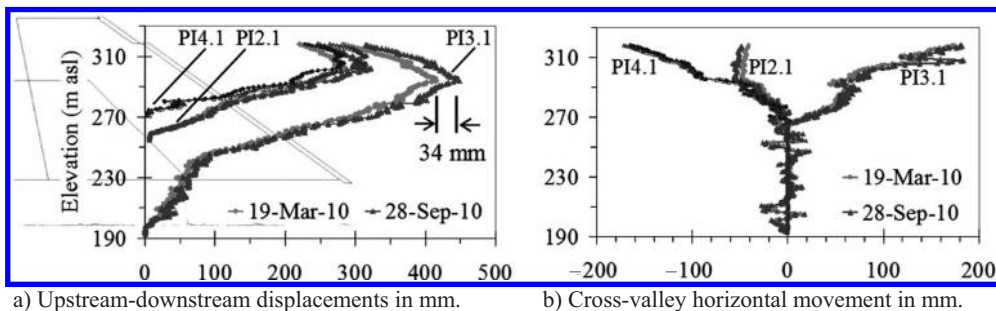


Figure 6. Lateral movement of embankment monitor by Probe Inclinometers (PI).

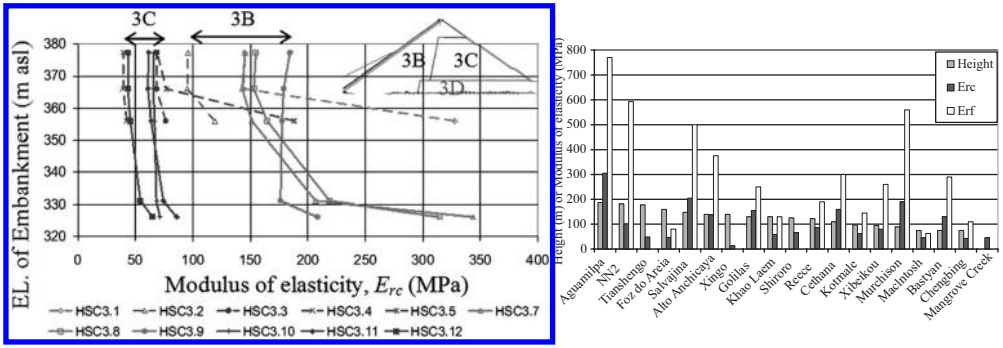
of 448.29 mm at elevation of +299.613 m (above the mid high of dam) toward the downstream direction. Compare with the baseline is the position of the casing on 18 March 2010, its detected downstream 33.91 mm, but the lower part below el +243 m (3D zone) remained stationary. With increasing reservoir level, the maximum movement toward the downstream at Sections 2 and 4 are 35.89 and 33.99 mm occurring at elevation of +307.034 and +311.479 m respectively.

The cross-valley horizontal movement during the construction period (up to 18 March 2010) and after construction (March to September 2010), are show in Figure 6b. The inclinometers were anchored into the bedrock. The PI showed zero movement at the interface between the rockfill and the bedrock. The post construction cross-valley movements as well as the settlements were significantly smaller than those that developed during construction.

3.3 The modulus of elasticity of rockfill

The rockfill modulus during construction (E_{rc}) values have been calculated from observed settlements of rockfill during construction of dam using HSCs measure with two layers of HSCs installed in section 3. The distribution of stress from the area transmitting a triangular stress and the secant moduli have been calculated from stress per strain by using elastic solution published in Poulos and Davis (1974). The E_{rc} of NN2 in MN/m² (MPa) were show in Figure 7 which can be seen that the rockfill materials should be divided to 4 groups. Group no 1 monitoring by HSC3.1 3.7 3.8 3.9, group no 2 by HSC3.2, group no 3 by HSC3.3 3.5 3.10 3.11 and group no 4 by HSC3.4 3.12 observed E_{rc} values are 145–180, 90–120, 62–75 and 38–50 MPa respectively. The observed results in term of E_{rc} values had been found that the rockfill in dam body ranging from 90 to 180 MPa in 3B zone and 38 to 75 MPa in 3C zone as also show the zoning description in Figure 7. The average E_{rc} calculated by ignoring the over-high values cause by the reading start after the settlement of rockfill lower part have been occurred so the data reading loss some settlement value, the lower settlement cause the higher E_{rc} . The average E_{rc} of 3B, 3C zone and for the whole dam are 151.40, 59.67 and 101.11 MPa respectively.

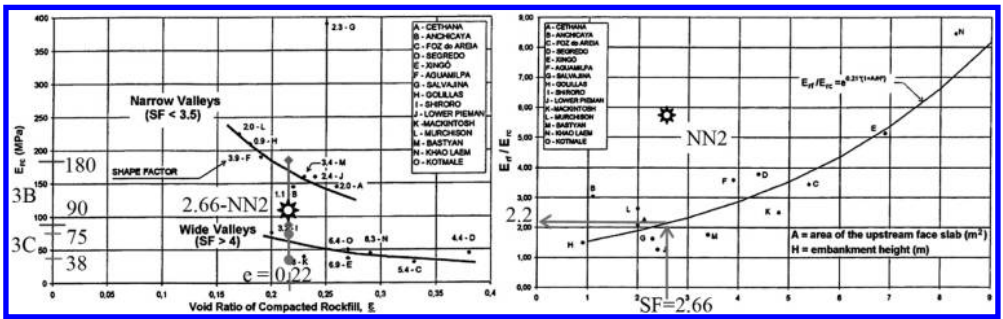
NN2 CFRD is located in a narrow valley with rather steep slopes having a valley shape factor (SF) equal to 2.66. From historical records of the performance of CFRDs constructed from well-compacted angular rockfills study by Pinto & Marques Filho (1998) (Figure 8a) they conclude that void ratio and valley shape are the dominant influences on the calculated two-dimensional deformation modulus during construction for narrow valleys because the valley shape affects the vertical stress. By comparison with other CFRDs in Figure 8a the average E_{rc} of NN2 is lower than trend line and also in 3C zone range. However, the range of E_{rc} in 3B zone is in the trend line of CFRDs in narrow valleys which are the SF less than 3.5. And the E_{rc} of weak sandstone and siltstone used in 3B zone of Salvajina dam recorded by Hunter (2003) show the value of 62 MPa and 55–60 MPa of weathered to fresh siltstone and sandstone in Mangrove Creek dam. Then the E_{rc} of NN2 is in rang value of sandstone material rockfills.



a) NN2 CFRD

b) CFRDs (ICOLD, 2004)

Figure 7. Rockfill modulus during construction in MN/m².



a) Deformation modulus during construction (E_{rc}) versus void ratio.

b) Ratio of deformation modulus on first filling to during construction (E_{rf}/E_{rc}) versus valley shape factor (SF).

Figure 8. The dominant influences on the calculated two-dimensional deformation modulus during construction. (modified from Pinto & Marques Filho 1998).

4 FACE SLAB MOVEMENT

4.1 Movements of face slab

The deformed shape of the concrete face slab on first impounding is strongly dependent on the water leveling as show in Figure 9. Before water level reach to the 2nd stage of face slab (+294) the lower part of face slab shown deflections cause from impounding while the second stage of face slab still settle with dam body. The deflections occurring on face slab were influenced by the water pressure. At the water level +365.36 m asl on September 2010, the maximum deflection occurred at about 52% of the embankment height with the values of 310.4 mm and reducing to 7.3 mm at the toe. For 2nd stage face slab, the deflection was also reducing toward the crest to 195.9 mm. From the elevation about +314 the deformation reducing with constant gradient while the face slab below this level is curve.

The rockfill modulus on first filling of NN2 E_{rf} calculated by the method of Fitzpatrick et al. (1985) is 593 MPa (the estimated value is 222.44 MPa). The rockfill moduli of NN2 are normal value compare with other CFRDs recorded by ICOLD (2004)

Figure 10 presents the contours of face slab deflection (in mm) during the first reservoir filling and can define the compression zone influence by water pressure. The maximum settlements along the elevations from the toe to top of face slab occurred in the middle way

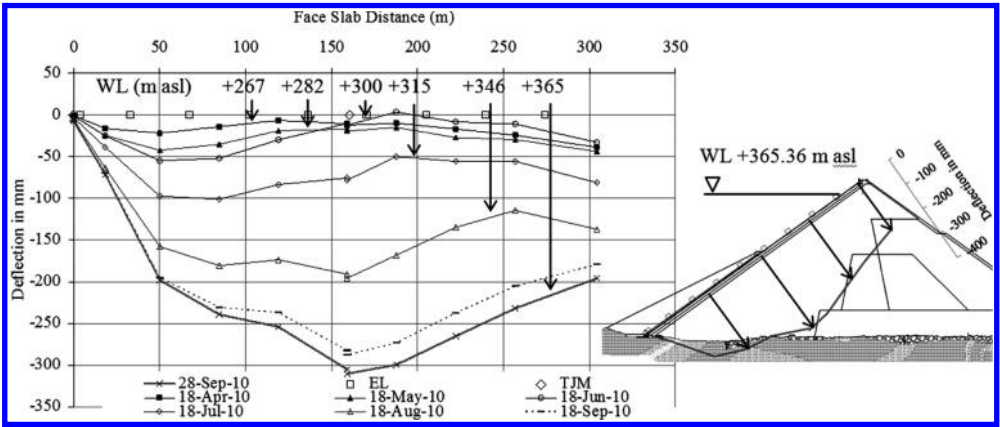


Figure 9. Movements of face slab at maximum dam section during first impounding. (Section 3).

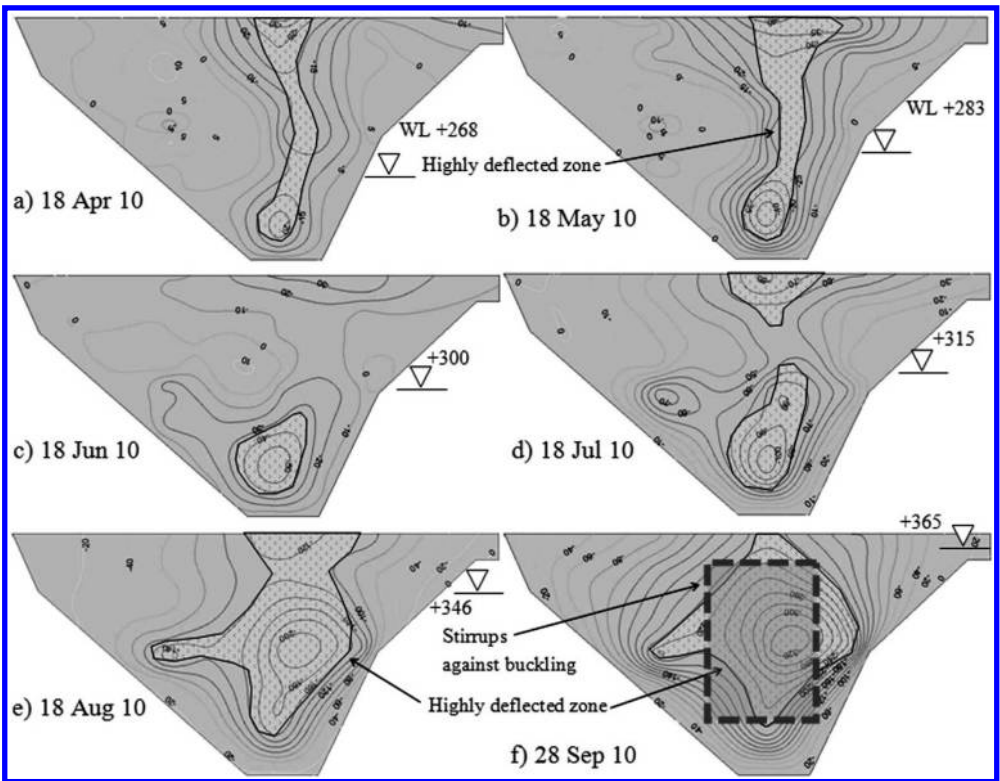


Figure 10. Contours of face slab deflection (in mm) during first impounding.

between left and right abutment. And close to the right abutment in the center of face slab at elevation about +294 m asl which cause from more steep slope on the right abutment. The increase in water pressure contacts on the surface of concrete face slab from May to September 2010 induce the differential settlement and cause the highly reflected zone in concrete in the area which the maximum settlement occurred. These highly reflected zones quite

agree with the area that design to use the steel stirrups against shearing by the designers. The area nearly the right abutment around the elevation of +294 m asl should be observe closely because of the potential to concrete bucking.

4.2 Joint movements

The movement of face slab along the plinth and the movement between 2nd and 1st stage of face slab monitor by the TJM and 2JM which installed at place during construction of the concrete face slab. The observed of movement in three directions are 1) the opening between the face slab and the plinth 2) the movement along the left and right abutment and 3) the settlement perpendicular to the face slab. Figure 11 showed movement along the plinth and between face slabs after construction. After construction and first filling, TJM4.2 and 4.4 (Figure 11a) show the opening on the right abutment while TJM1.2, 1.1, 2.1, 2.1, and 3.2 show the closing on the left abutment. TJM3.1 at the river bed show the face slab closing to plinth and TJM10.1–10.3 also show 2nd face slab closing to 1st stage face slab. After construction up to September 2010 the 2nd stage move down to closing to 1st stage face slab and it move at high rate (12.4 mm / month) when the water level higher than the elevation +346 (81% of dam high) on mid of July 2010. On September 2010 the maximum opening between 1st and 2nd face slab observed from TJM10.2 were 22.3 mm and between face slab and plinth were 7 mm from TJM4.2 on the right abutment. The maximum closing to the plinth were 12.8 mm occurred at TJM2.2 on the left abutment. At the toe of face slab observed by TJM3.1 it was

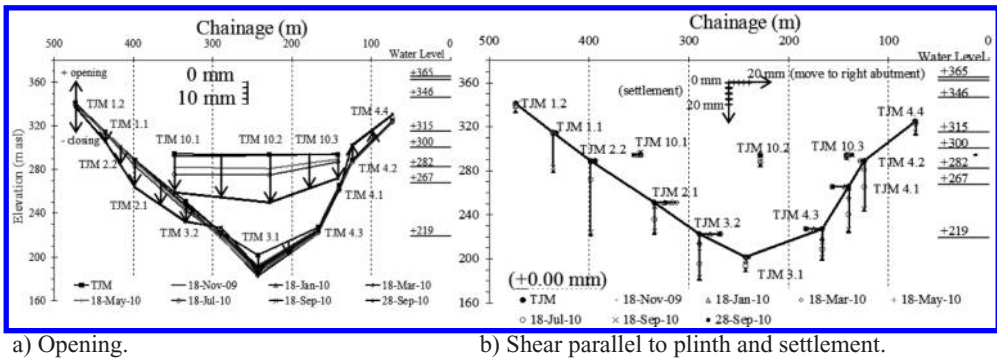


Figure 11. Three dimension jointmeter movement along the plinth and between face slab after construction.

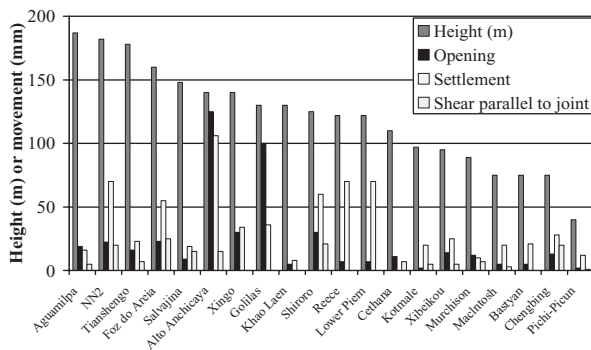


Figure 12. Face slab movement by jointmeters compare with other CFRDs record by ICOLD (2004).

found that at first the face slab closing to the plinth and after start impounding on March 2010 it was opening from the water pressure continue rising attack to the face slab and the nearly TJM3.2 and TJM4.3 on the left and right abutment also same behavior. These results confirm that was highly reflected zone occurred at the area around Chainage 0 + 180 to 260 and Elevation +230 to 290 m asl.

Figure 11b presented the movement parallel to plinth and the settlement perpendicular to the face slab. The face slab on both abutments moved toward the river channel and the values observed at TJM2.1, TJM3.2, TJM4.3 and TJM4.1 of 11.7, 20, 15.8 and 15.7 mm respectively, quite high compare with other area, cause from those located on the steep abutment. In term of settlement perpendicular to the face slab, it was settlement related to the plinth with higher value on the abutment. The maximum value occurred at TJM2.2, which located on the left abutment, is 70 mm. In Comparison to other CFRDs recorded by ICLOD (2004) in Figure 12, the TJM movement observed response on NN2 is normal value.

5 CONCLUSIONS

The dam embankment is Concrete Face Rockfill Dam (CFRD) of 182 m. High and crest length of 512 m. The dam site is located in a narrow valley with rather steep slopes ($SF=2.66$) and complex geology. The total rockfill embankment volume is 10^7 m³ and total area of the concrete face slab is 88,000 m². The main dam embankment has mainly divided into 5 sequences in order to incorporate with the 2 stages of face slab construction sequences. The embankment constructed within 20 months. More than 475 sensors were installed within dam body and on the face slab. By observed the field data it were found the causes of error and define the correction in instrument measurement data. The behaviors of NN2 during the construction and first filling were monitored for which are mainly dam deformation and face slab movement.

Deformation of the dam after reservoir impounding is cause by the water loading on the upstream face of the dam as well as by continuing creep due to the weight of the rockfill. The combined settlements were observed up to September 2010 at 2.5 meters while the settlement after construction was 0.854 meters. The locations of maximum settlement at the end of construction are on the downstream zone where rockfills of lower quality, Zone 3Cw and 3C, were used. The maximum settlement after construction for 10.5 months is 0.334% of the dam's height. The sandstone rockfill secant moduli during construction (E_{rc}) were modified from Fitzpatrick et al. (1985) method for finding the other points. The E_{rc} values varies in the 90–180 MPa range depending on the void ratio, the parent rock material from quarrying and the gradation of the rockfill. The average values of 3B and 3C zone are 151.40 and 59.67 MPa respectively.

The face slab shown deflections cause from impounding. The maximum deflection occurred at 52% of the embankment height at the point of starting 2nd stage face slab with the values of 310.4 mm. The rockfill modulus on first filling of NN2 E_{rf} is 593 MPa.

At the toe of face slab observed by TJM3.1 it was found that at first the face slab closing to the plinth and after start impounding on March 2010 it was opening from the water pressure continue rising attack to the face slab. The face slab on both abutments moved toward the river channel. The settlement perpendicular to the face slab was related to the plinth with higher value on the abutment, the maximum value is 70 mm occurred at TJM2.2 on the left abutment.

REFERENCES

- Chalermnon, W., et al. 2009. Construction of the Nam Ngum 2 CFRD. *The 1st international symposium on rockfill dams; Proc.intern. symp.*, 18–21 October 2009. China: Chendu.
- Fitzpatrick, M.D., et al. 1985. Design of concrete-faced rockfill dams. *Proceeding of the Symposium on Concrete Face Rockfill Dams—Design, Construction and Performance*, (Cooke & Sherard ed.) ASCE New York: 410–434. Detroit, Michigan.

- Hunter, G.J. 2003. The pre—and post-failure deformation behavior of soil slopes. PhD thesis, University of New South Wales; 2003.
- ICOLD, 2004. Concrete Faced Rockfill Dams, Concept Design and Construction.
- Ngarmsirilertsgoon, P. & Puangpatcharakul, S. 2009. Nam Ngum2 Hydroelectric Power Project Encountered Technical and Economical Challenges. *The 1st international symposium on rockfill dams; Proc. intern. symp.*, 18–21 October 2009. China: Chendu.
- Pinto, N.L.d.S. & Marques Filho, P.L. 1998. Estimating the maximum face slab deflection in CFRDs. *Hydropower & Dam*: No.6.
- Poulos, H.G. & Davis, E.H. 1974. Elastic Solutions for Soil & Rock Mechanics, Wiley & Sons, New York; 1974.
- Sramoon, A., et al. 2009. Design of Concrete Face Slab for 182 m High NN2 CFRD. *The 1st international symposium on rockfill dams; Proc.intern. symp.*, 18–21 October 2009. China: Chendu.
- Straubaar, R., et al. 2009. Design Considerations of A High Rockfill Dam Nam Ngum2 CFRD, LAO PDR. *The 1st international symposium on rockfill dams; Proc.intern. symp.*, 18–21 October 2009. China: Chendu.

Analysis on the operating performance of Sanbanxi CFRD

Xu Zeping, Deng Gang & Zhao Chun

China Institute of Water Resources and Hydropower Research, Beijing, China

ABSTRACT: The performance of Sanbanxi CFRD with dam height of 186.5 m was presented. Based on the observation data, different numerical analysis methods were applied to study the safety status of the dam. Furthermore, the mechanism of face slab rupture after reservoir impoundment was analyzed by back analysis. From the analysis, it could conclude that the general status of the stress and deformation of dam and face slab is basically acceptable. Safe operation of the dam could be achieved. The rupture of concrete face slab is mainly caused by relatively large deformation of upstream rockfill and the impact of local topography of the right abutment.

1 PROJECT INTRODUCTION

Sanbanxi Hydropower Station is situated in the middle reach of Qingshuijiang River, upstream of the main stream of Yuanshui River. The dam site is located in Jingping County, Guizhou Province, China. The normal storage water level of the reservoir is 475 m. The total storage capacity is $40.95 \times 10^8 \text{ m}^3$ and the installed capacity of the power station is 1000 MW. The project consists of concrete faced rockfill dam (main dam and auxiliary dam), right bank power generation system, left bank spillway and flood discharge tunnels. The maximum dam height of the concrete faced rockfill dam is 185.5 m (Chen & Li 2000). The general layout and typical section of CFRD are shown in Figure 1 and Figure 2.

The commencement of the project construction was July 1, 2002. River closure was conducted on Sept. 17, 2003. Rockfill dam construction was started on Nov. 15, 2003 and reservoir impoundment was started on Jan. 7, 2006. The first unit started power generation on July 25, 2006 and all the 4 units were put into operation on December in the same year.

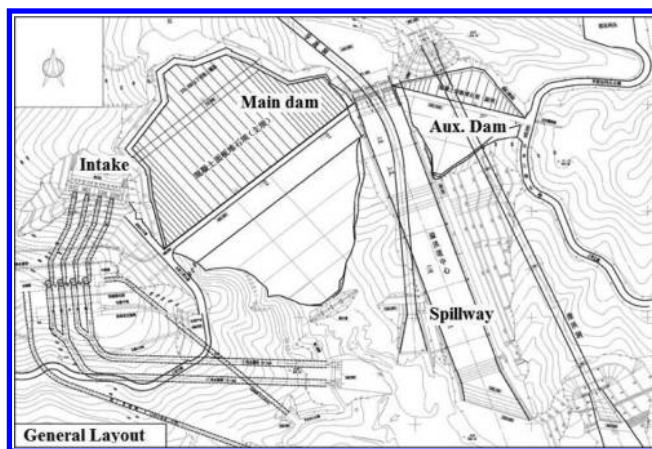


Figure 1. General layout of Sanbanxi hydropower project.

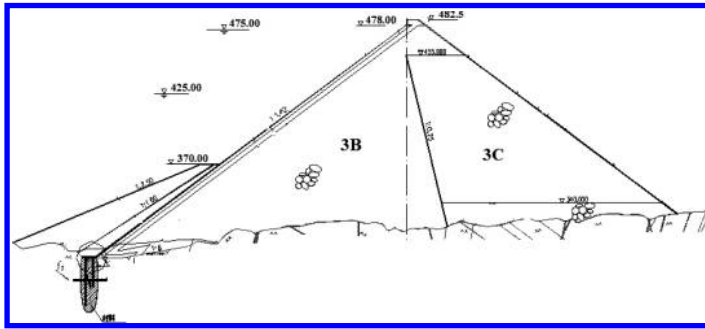


Figure 2. Typical cross section of the dam.

2 SAFETY MONITORING OF CFRD

2.1 Arrangement of instruments

The instrumentation for safety monitoring of Sanbanxi CFRD mainly include deformation of rockfill dam, stress and strain of concrete face slab, seepage through the dam, etc.

Dam deformation monitoring includes surface deformation of dam body, interior deformation of rockfill, displacement of joints (vertical joints and perimeter joint), deflection of concrete face slab, gaps between concrete face slab and rockfill. Strain and stress monitoring includes strain gauges on concrete, reinforcement metre on steel bar. Figure 3 shows the instruments arrangement for interior deformation monitoring of Section B-B (riverbed section).

2.2 Main results of instrumentation

The monitoring of interior deformation includes vertical displacement (settlement), horizontal displacement along river flow and horizontal displacement along dam axis. The instruments for observation are hydrostatic settlement cells, horizontal extensometers.

Vertical displacements were measured by hydrostatic settlement cells. Two sections were selected for deformation observation, which are: section A-A (Right 0 + 008.20 m) and Section B-B (Left +071.80 m). For each section, instruments were arranged on 4 levels, i.e. EL346 m, EL379 m, EL404 m, and EL445 m. From the observation data, the settlement of rockfill presents following features:

1. All the measured settlements are gradually increased with time. For Section A-A, the maximum settlement occurred at VSA2-4, EL404 m, 5 m downstream of the axis of the parapet wall. The measured value on Sept. 25, 2008 is 153.5 cm. For Section B-B, the maximum settlement occurred at VSB2-3, EL412 m, 36.9 m upstream of the axis of parapet wall. The measured value on Sept. 25, 2008 is 175.4 cm. The settlement measured at VSB2-3 is the maximum settlement of all the measuring points. The maximum settlement is about 0.95% of dam height.
2. From the time history graph of each measuring points, it could be noticed that the main part of settlement occurred in the period of rockfill compaction (before Sept., 2005). On Oct. 1, 2005, the settlement measured at VSB2-3 was 142.5 cm, account for 81.2% of its total settlement (175.4 cm). The settlement measured at VSA2-4 was 128.8 cm, account for 83.9% of its total settlement (153.5 cm). From June to July of year 2007, when reservoir water level firstly reached to 472.06 m, the speed of settlement development was increased.
3. The distribution of measured settlements of section B-B on Oct. 1, 2005 was shown in Figure 4. The maximum settlement area of the section is located between VSB2-3 and VSB2-2, below EL412 m. It could be noticed that the maximum settlement occurred in the area of upstream rockfill.

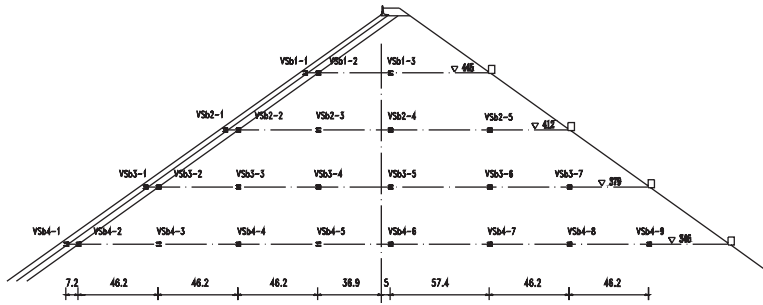


Figure 3. Instruments for observing interior deformation of rockfill (Section B-B).

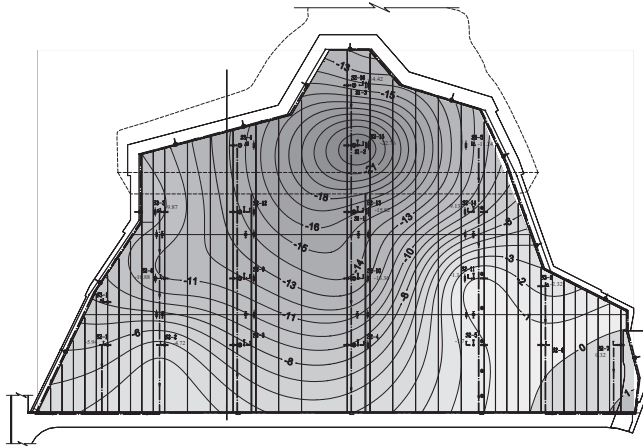


Figure 4. Distribution of the stress of face slab in the direction of upstream slope. Observation date: July 30, 2007, water level: 472.06 m, maximum compression stress: 22.76 MPa, maximum tensile stress: 0.32 MPa.

After reservoir impoundment, the measured strains and stresses of concrete face slab present following features:

1. The calculated stresses of all the measuring points are compression stress.
2. There are 7 sets strain gauges for the first stage concrete face slab. The calculated stresses in the direction of dam axis were $-20.55 \sim -4.86$ MPa. The maximum value occurred at the measuring point S2-13 on Sept. 6, 2007. The calculated stresses in the direction of upstream slope were $-24.14 \sim -10.12$ MPa. The maximum value occurred at the measuring point S2-15 on Oct. 13, 2006. On July, 2007, when reservoir water was in high level, the maximum stress of face slab in the direction of upstream slope reached to 24 MPa.
3. There are 5 set strain gauges for the second stage concrete face slab. The calculated stresses in the direction of dam axis were $-16.14 \sim -5.71$ MPa. The maximum value occurred at the measuring point S2-09 on Aug. 16, 2006. The calculated stresses in the direction of upstream slope were $-14.58 \sim -3.25$ MPa. The maximum value occurred at the measuring point S2-08 on Oct. 10, 2007.
4. There are 4 set strain gauges for the third stage concrete face slab. The calculated stresses in the direction of dam axis were $-0.97 \sim -7.76$ MPa. The maximum value occurred at the measuring point S2-02 on July 19, 2008. The calculated stresses in the direction of

upstream slope were $-10.73\sim-2.61$ MPa. The maximum value occurred at the measuring point S2-01 and on Oct. 26, 2006.

5. According to the measured data, the compression stress of concrete face slab in the direction of upstream slope is higher than the stress in the direction of dam axis. The maximum compression stress of concrete face slab occurred at S2-15 with the compression stress of 24 MPa in the direction of upstream slope. This stress has almost reached to the compressive strength of concrete.

Figure 4 shows the distribution of stresses in the direction of upstream slope of the whole face slab under the condition of high water level.

2.3 Rupture of concrete face slab after reservoir impoundment

The impounding of the reservoir of Sanbanxi hydropower station started on Jan. 2006. At the beginning, the reservoir water level was low, with the maximum water level of 435 m. The corresponding leakage is 30 L/s. When flood season came on June, 2007, reservoir water level was raised rapidly. At the end of July, reservoir water level reached to 472 m, 3 m below the normal storage level. After water level beyond 465 m, the measured leakage of the dam increased rapidly from 25 L/s to 150 L/s. On July 30, 2007, the measured leakage suddenly reached to 250 L/s. The maximum measured leakage was 315 L/s. After the flood season, reservoir water level fall down and the measured leakage decreased accordingly. On Jan., 2008, when reservoir water level dropped to 425 m (dead water level), the initial measured leakage was 150 L/s. Then it is further reduced to 100 L/s.

On Aug., 2007, several instruments on EL385 m and EL379 m of the face slab MB5 were disabled (Gou et al. 2009). It is presumed that some abnormal situations occurred in this area. On Jan, 2008, when reservoir water level dropped to the dead water level, under water inspection was conducted by divers. It was discovered that damages occurred on the horizontal construction joint between the first stage and the second stage face slab for the 12 continuous slabs on EL385 m. The length of the damage was 184 m. The concrete of face slab was ruptured and the reinforcement steel bar was exposed and bent. The waterstop of some vertical joints were destroyed. The maximum width of concrete rupture was 4 m and the maximum depth was 41 cm. The bottom layer concrete and steel bar were not damaged. The scope of concrete face slab rupture was shown in Figure 5 (Xu & Tan 2009).

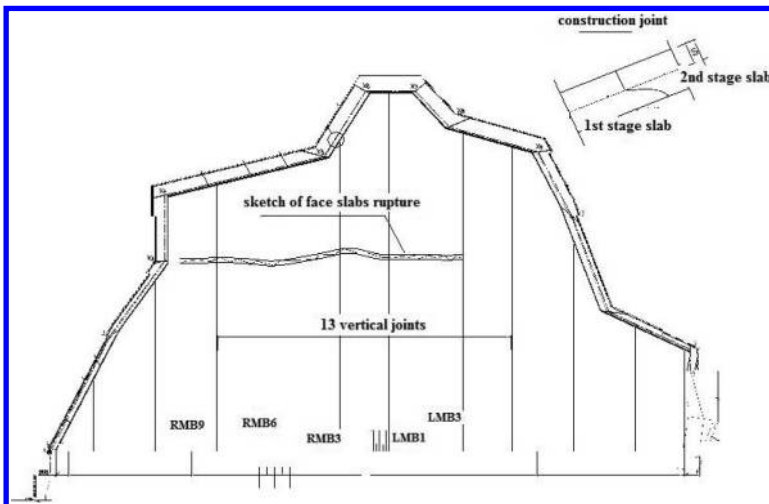


Figure 5. The position and scope of concrete face slab rupture.

3 BACK ANALYSIS OF THE STRESS AND DEFORMATION PROPERTIES

For studying the safety status of Sanbanxi CFRD, back analysis by using numerical analysis method was conducted to investigate the stress and deformation properties of the dam. The constitutive model for rockfill materials is Duncan's Hyperbolic Model (E-B model). The creep deformation is calculated by the empirical model suggested by IWHR (logarithmic attenuation function) (Xu 2004). The finite element mesh was shown in Figure 6. In the numerical analysis model, the whole dam was divided by 40 cross sections. The procedure of rockfill compaction was simulated by 23 layers and the construction of concrete face slab was simulated by 3 stages. After the completion of the second stage face slab, reservoir impoundment started. The procedure of reservoir impoundment was simulated by 37 steps load cases. In numerical analysis, the steps of rockfill construction and water load applying follow the real procedure of rockfill compaction and reservoir impoundment.

In the numerical analysis, the first phase analysis used parameters based on large scale laboratory triaxial test of rockfill materials, as shown in Table 1.

Based on the parameters obtained from laboratory triaxial test and by using the observed deformation data of rockfill, the adjusted parameters can be gotten from back analysis, as shown in Table 2. In the analysis by using the parameters from back analysis, the creep deformation of rockfill was considered. The parameters for creep deformation calculation were estimated by taking the reference of the creep deformation testing results of the similar materials.

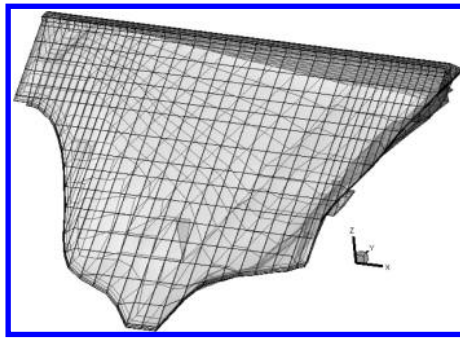


Figure 6. Finite element mesh for numerical analysis.

Table 1. Parameters of rockfill materials (laboratory triaxial test).

Material	ρ (kg/m ³)	ϕ_0 (°)	$\Delta\phi$ (°)	K	K_{ur}	n	R_f	K_b	M
2A	2200	56.0	11.7	1500	4500	0.57	0.936	770	0.09
3A	2170	58.1	13.3	1150	4500	0.55	0.903	650	0.14
3B	2150	56.0	12.0	1200	4500	0.35	0.900	500	0.10
3C	2130	52.7	10.7	900	2000	0.56	0.900	450	0.08

Table 2. Parameters of rockfill materials (back analysis).

Material	ρ (kg/m ³)	ϕ_0 (°)	$\Delta\phi$ (°)	K	K_{ur}	n	R_f	K_b	m
2A	2200	56.0	11.7	510	1020	0.57	0.94	265	0.09
3A	2170	58.1	13.3	495	990	0.55	0.90	225	0.14
3B	2150	56.0	12.0	500	1000	0.35	0.90	260	0.10
3C	2130	52.7	10.7	1000	2000	0.56	0.90	600	0.08

Table 3. Parameters of rockfill materials for creep deformation analysis.

Material	c_1 (%)	c_2 (%)	c_3
3B	0.03	0.45	1.6
3C	0.095	0.45	1.6

3.1 Results of the analysis by using parameters of laboratory test

With the numerical analysis by using rockfill parameters from laboratory test, the maximum vertical displacement (settlement) of rockfill when dam construction was just completed was 1.02 m, about 0.5% of dam height. The maximum settlement occurred at downstream part of rockfill, riverbed section, and middle height of the dam. Before reservoir impoundment, the distribution of horizontal displacement of rockfill at the time of dam construction completed was basically symmetrical to dam axis. The maximum horizontal displacement of upstream rockfill with its direction pointed to upstream was 16.5 cm. The maximum horizontal displacement of downstream rockfill with its direction pointed to downstream was 32.8 cm. The stress of rockfill was distributed related to the height of rockfill. The maximum stress located at the bottom of the dam, with the major principal stress of 3.8 MPa and the minor principal stress of 1.1 MPa. After reservoir impoundment, the distribution of horizontal displacement in the direction of river flow was significantly changed. The displacement towards upstream was reduced and the displacement towards downstream was increased. Under the action of water load, the settlement of rockfill was also increased. The maximum settlement of rockfill after reservoir impoundment was 1.05 m. At the same time, the stresses of rockfill were also slightly increased, with the maximum major principal stress of 4.1 MPa, the minor principal stress of 1.1 MPa. Figure 7 shows the settlement distribution of the dam after reservoir impoundment.

The maximum deflection of concrete face slab after reservoir impoundment was occurred at the central part of the face slab, with the value of 28.5 cm. The horizontal displacement of face slab presents the tendency of face slabs moving from both abutments towards the center of riverbed. From the distribution of the stresses, the face slab was subject compression stress both in the direction of dam axis and upstream slope. The slabs in riverbed sections are subject to compression stress in the direction of dam axis with the maximum value of 10 MPa, while the slabs in abutment area were subject to tensile stress. As the face slab was bent under the action of water load and the deformation of upstream rockfill, the middle and low part of the slabs were subject to compression stress in the direction of upstream slope, while the top of the slabs were subject to tensile stress. The maximum compression stress of face slabs in the direction of slope was 12 MPa. Figure 8 shows the distribution of the stresses of concrete face slab after reservoir impoundment.

3.2 Results of the analysis by using parameters of back analysis

The back analysis mainly took the reference of the observed data of rockfill deformation. In the mean time, the creep deformation of rockfill materials was also considered in the analysis. From the analysis by using the parameters from back analysis, when reservoir water level reached to 472.06 m, the maximum settlement of the dam was 1.81 m, about 0.98% of the dam height. This settlement value closed to the observed data. The maximum settlement occurred at the middle height of the dam, upstream rockfill. With the action of water load, the horizontal displacements of the most part of the dam were towards downstream direction, with the maximum value of 0.35 m. The maximum major principal stress was 3.0 MPa and the maximum minor principal stress was 0.8 MPa. For most part of the dam, the stress level was low.

When reservoir water level reached to 472.06 m, the maximum deflection of the face slab was 0.74 m. The position of the maximum deflection of face slab was near the construction joint of the first stage face slab and the second stage face slab (EL385 m), riverbed section. Corresponding to the position of the maximum deflection of the face slab, the maximum values of the major principal stress, minor principal stress, stress in the direction of dam axis and stress in the

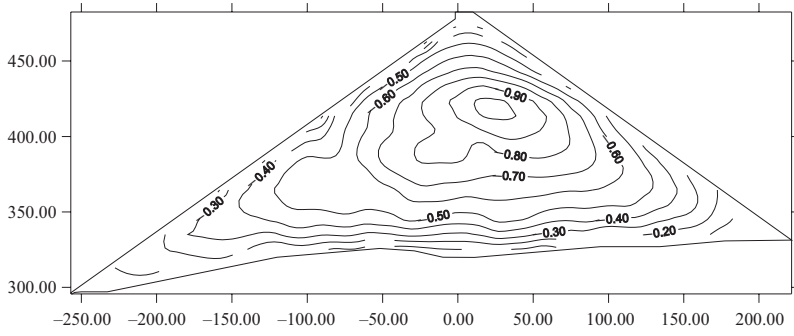


Figure 7. Settlement of the dam after reservoir impoundment (unit: m).

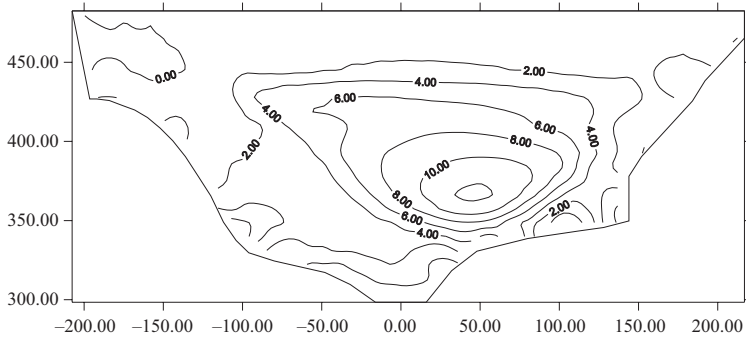


Figure 8. Stresses of face slab in the direction of upstream slope after reservoir impoundment (unit: MPa).

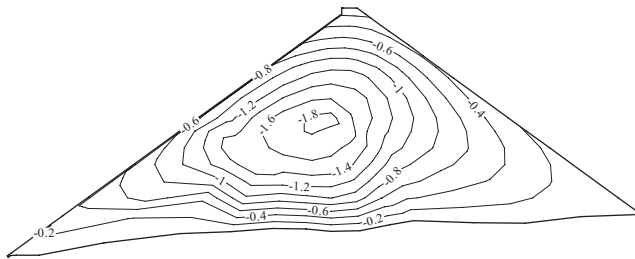


Figure 9. Settlement of the dam after reservoir impoundment (unit: m).

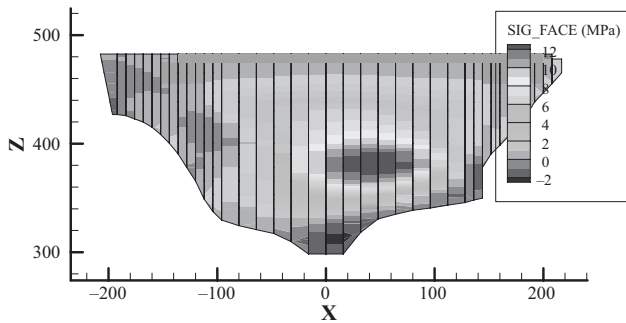


Figure 10. Stresses of face slab in the direction of upstream slope under high water level (unit: MPa).

direction of upstream slope were all occurred around EL385 m. The large stress concentration area covered area from the face slab Left MB3 to Right MB8, which was the similar location of the discovered concrete face rapture. From the results of computation, the values of major principal stress were rather high. It predicted the possibility of concrete damage in the area.

4 MAIN CONCLUSION ON THE SAFETY STATUS OF THE DAM

From instrument monitoring data and the numerical analysis, the distribution of stress and deformation of Sanbanxi CFRD presents the similar performance as other high CFRD. At present time, the maximum settlement of rockfill was less than 1% of dam height. The values of the deformation of rockfill and face slab, displacement of joints are within the acceptable range. Thus, the overall safety of the dam can be guaranteed.

From the comparison of the numerical analysis results by using rockfill parameters of laboratory test and the monitoring data of dam deformation, it is noticed that there are obvious difference in distribution of maximum settlement area. The observed maximum settlement occurred in upstream part of zone 3B. But the predicted maximum settlement from numerical analysis by using laboratory testing parameters occurred in zone 3C, downstream side of dam axis. The real performance of dam deformation presents a significant difference in settlement distribution with the predicted patterns in design stage. The back analysis based on monitoring data could well represent the real situation of dam operation.

According to the deformation monitoring data, the maximum settlement of rockfill occurred at upstream part of rockfill. As the deformation of upstream rockfill will have direct impact on the stress status of concrete face slabs, the consequence of this deformation tendency will lead to the increasing of the stress in the direction of upstream slope of the concrete face slab. According to the results of back analysis, on July 31, 2007, when reservoir water level reached the highest level, the stresses of the slabs (Left MB3 to Right MB8) in the area near EL385 m presented high values. It is very possible to be ruptured. The area predicted by back analysis is similar to the location of face slab rupture. If the face slab was not ruptured, the stresses of face slabs will further increased. The rupture of concrete face slab released the concentrated compression stress of the slab. Thus, if the deformation of rockfill is not developed, the rupture of face slab will not further extended.

The reasons for the maximum settlement occurred in upstream rockfill still need to be further investigated. From the results of back analysis, the low modulus of upstream rockfill could be one of the most important factors for the situation. Besides, the local topographic condition of the right abutment will also has certain impact on the stress concentration of face slab.

From present analysis, the main reason for face slab rupture should be the over large deformation of upstream rockfill. Besides, the connection manners of the construction joint and the arrangement of reinforcement steel bar will also contribute to the occurrence of concrete rupture.

From the results of numerical analysis, although there some problems in the distribution of rockfill deformation, the general deformation values of the dam are still acceptable. After the thorough rehabilitation of the ruptured area of concrete face slab, the dam can be safely operated. In future operation, the observation of deformation increment and dam leakage should be strengthened.

REFERENCES

- Chen Xialin, Li Nin, "Design of Concrete Faced Rockfill dam for Sanbanxi Hydroelectric Project", Proceedings of International Symposium on Concrete Faced Rockfill Dams, Sept., 2000, Beijing, China.
- Gou Xiaoli, Shen Hui, Wang Zhiyuan, Zhang Junrong, "Application of Dam Safety Monitoring Automation System on Safety Monitoring of Sanbanxi Hydropower Station", Modern Rockfill Dam-2009, China WaterPower Press, Beijing, 2009.
- Xu Runming, Tan Wensheng, "Summary of Face Slab Seepage Treatment in Sanbanxi Hydropower Station", China WaterPower Press, Beijing, 2009.
- Xu Zeping, "Research Works of IWHR on Numerical Analysis of CFRD—Past, Present and Future, Proceedings of the International Conference of Hydropower 2004, Vol. I, 2004, Yichang, China.

Numerical modelling investigation of an existing crack within an arch-gravity dam

A. Mellal, A. Koliji & M. Balissat
STUCKY Ltd., Renens VD, Switzerland

ABSTRACT: Numerical modelling investigations on a pre-existing crack within an arch-gravity dam are carried out. The purpose is to identify the crack path and behaviour and construct a reliable finite element model to analyse the dynamic behaviour of the dam and assess its seismic safety. Transient thermal and coupled thermo-mechanical analyses are performed using a three-dimensional finite element model of the dam including the identified crack. Calculated temperatures and displacements are compared to available thermometer and pendulum measurements. With the exception of an irreversible cumulative drift towards upstream, a generally good agreement is obtained between measurements and corresponding calculated values. Comparison of calculated crack opening time history and joint meter measurements shows a good agreement as well. Therefore, the proposed numerical model is considered to be reasonably representative of the dam behaviour and can be used to evaluate its dynamic response to earthquakes.

1 INTRODUCTION

Spitallamm Dam, an arch-gravity dam constructed in the 1928–1932 period on the Aare River in the Swiss Alps, features an evolving crack which has been thoroughly monitored for many years. The crack is visible on the downstream face of the dam about 10 m below the crest level and extends laterally over several blocks. According to borehole measurements, it propagates quasi-vertically within the dam. Most likely, the crack initiated after pressure grouting which caused debonding between face concrete and an intermediate “Trog” concrete zone (Fig. 1).

For the purpose of the assessment of dam’s seismic safety, a three-dimensional model of the dam, including a crack has been prepared. To be valid, it is essential that the numerical model reasonably reproduces main dam’s behaviour features. The aim of the present study is to evaluate the thermo-mechanical behaviour of the dam using the proposed finite element model and compare the obtained results to the available monitoring data.

The identification of the crack propagation mechanism and its path is first carried out by constructing a 3D finite element model of the dam and its foundation and evaluating the tensile stresses which indicate zones of potential crack initiation. In a second step, using frictional contact elements, a crack is introduced in the dam’s model in conformity with calculated stress pattern and on site observations. The validation of the numerical model is carried out through a comparative analysis between field measurements and calculated time histories of temperatures and displacements. For this purpose, transient thermal and thermo-mechanical finite element analyses are performed to evaluate the thermo-mechanical behaviour of the dam submitted to temperature and water level variations. Calculated time histories of temperatures, displacements and crack movements are compared to thermometer, pendulum and joint meter measurements, respectively. In a subsequent step, the calibrated finite element is used to analyse the dynamic behaviour of the fissured dam and to evaluate its seismic safety.

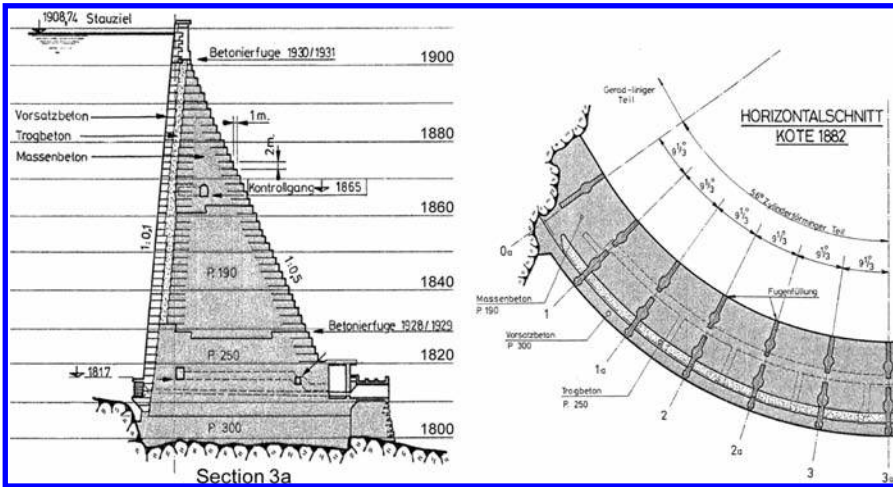


Figure 1. Spittalamm Dam—vertical and horizontal sections.

2 OBSERVATIONS—CRACK LOCATION AND EVOLUTION

The crack is visible on the downstream face of the dam at about 10 m below the crest level and extends laterally over 8 blocks, i.e. between vertical joints 1 and 5 (Fig. 2). Figure 3 shows a close view of the observed crack on the downstream face of the central block where joint meters are installed to monitor crack evolution in time. The major crack opening can be observed at the intersection of two concrete lifts at 1900.74 m level which corresponds to a construction joint (concreting stage).

In addition to usual pendulum measurements, inclinometer and Inkrex measurements are recorded at 4 different boreholes to precisely monitor dam's deformations (Balissat, 2006). Figure 4 shows boreholes' locations within the dam. Boreholes B1 and B2 are located in the central block respectively on upstream and downstream side. Boreholes B3 and B4 are located on the downstream side of right and left blocks respectively.

Inclinometer measurements in downstream boreholes B2, B3 and B4 reveal a discontinuity of upstream-downstream displacements at about 10 m below dam's crest, which corresponds to horizontal sliding along crack planes. This discontinuity is not present in recorded displacements at upstream borehole B1. This observation is important as it clearly indicates that the crack does not cross the whole dam thickness.

Moreover, according to Stucky (1968), pressure grouting executed in 1946, 1947 and 1948 through numerous boreholes on the upstream face to improve water tightness, has caused debonding between face concrete and "Trog" concrete zones and probably between "Trog" and mass concrete. From invar line measurements (Stucky 1968, Stucky 1978), vertical debonding between face concrete and "Trog" concrete propagates until level 1860 m, but this propagation can potentially go down to level 1830 m which is the lower bound of "Trog" concrete zone.

From visual observations and instrument measurements, the general spatial configuration of the crack is as follows:

- Quasi-horizontal propagation from downstream to upstream following construction joints at 1900.74 m and 1901.74 m
- Lateral extension over 8 blocks between joints 1 and 5
- Vertical debonding at face-"Trog" concrete interface between levels 1900 m and 1830 m

Monitoring of the crack shows a slow irreversible movement of the upper dam arch towards upstream (1–2 mm per year). This displacement is well controlled and stability checks indicate that the static safety of the dam crest is not impaired.

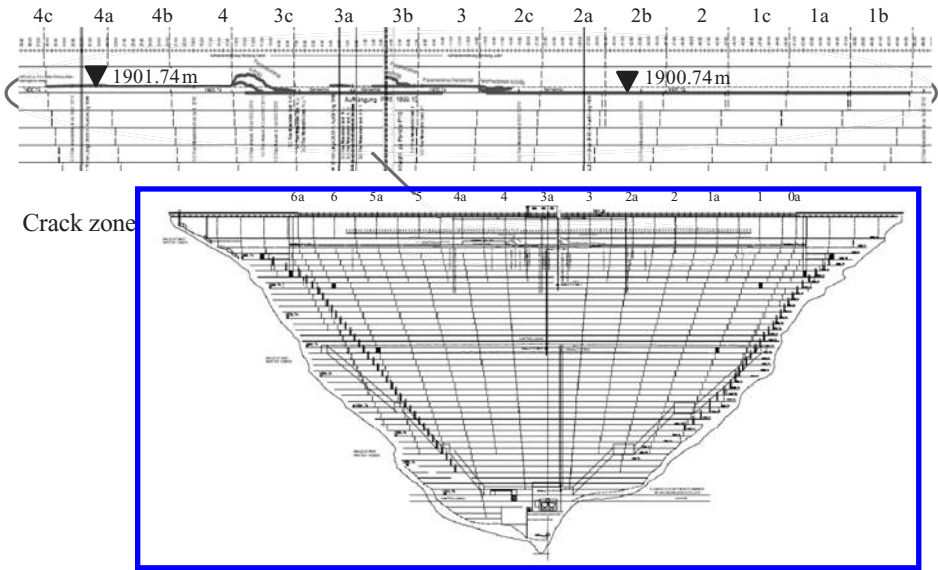


Figure 2. Lateral extension (red line) of the crack on the downstream face of Spittalamm Dam.

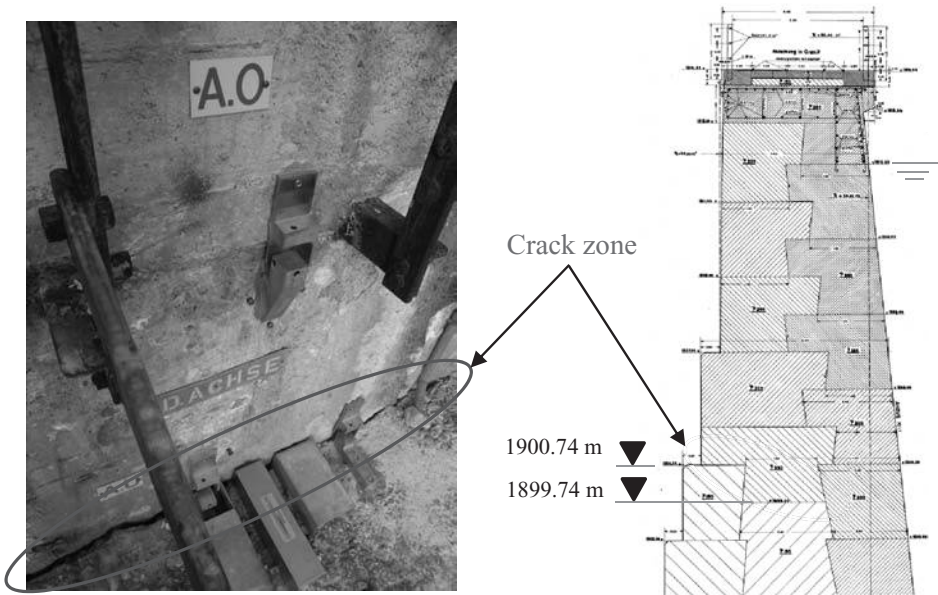


Figure 3. Location of the crack on the downstream face of Spittalamm Dam—close view.

3 FINITE ELEMENT MODEL OF THE DAM-FOUNDATION SYSTEM

To analyse the thermo-mechanical behaviour of Spittalamm Dam, including 3-D arching effects, a three-dimensional finite element model of the dam and its foundation is constructed based on available dam geometry and topographic data of the dam site. The modelling is carried out using the finite element code Z_Soil 3D v.2010.

Three material zones corresponding to face concrete, mass concrete and “Trog” concrete are defined in the dam model using 3D continuum elements. According to visual observations

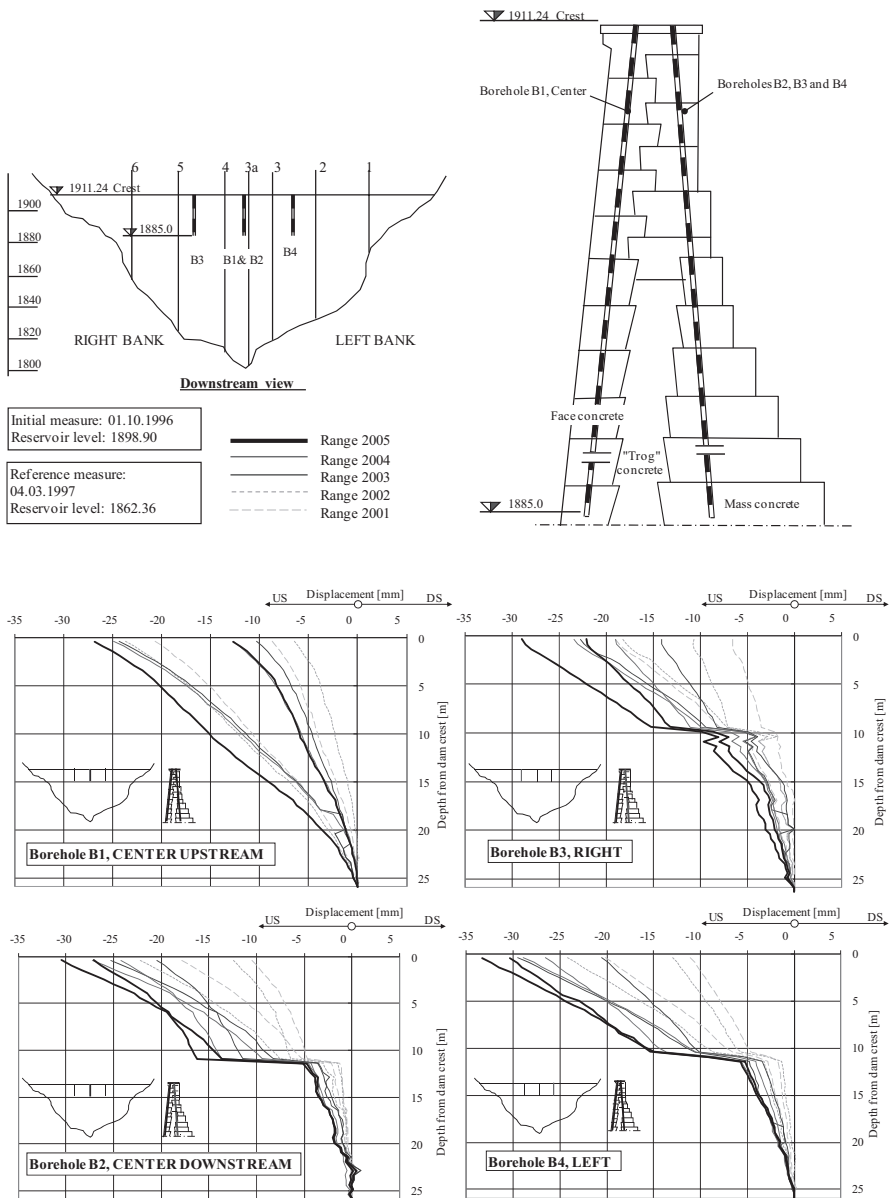


Figure 4. Position of boreholes (top) and inclinometer measurements at boreholes B1-B4 (bottom).

and measurements on the pre-existing crack, a three-dimensional crack is included in the numerical model, using frictional cohesionless contact elements. The geometrical configuration of the crack within the finite element model of the dam is illustrated in Figure 5.

Finite element analyses are carried out assuming linear elastic behaviour for both concrete and rock, whereas Mohr-Coulomb type constitutive model is considered for contact elements. Material properties are defined from available laboratory tests and similar materials. Table 1 summarizes mechanical and thermal parameters considered in the analyses.

A preliminary static stress analysis of the homogeneous non-fissured dam considering its self weight and hydrostatic pressure load at full reservoir level shows quasi-vertical tensile stresses on dam's downstream face at ~1900 m level, extending laterally over several blocks

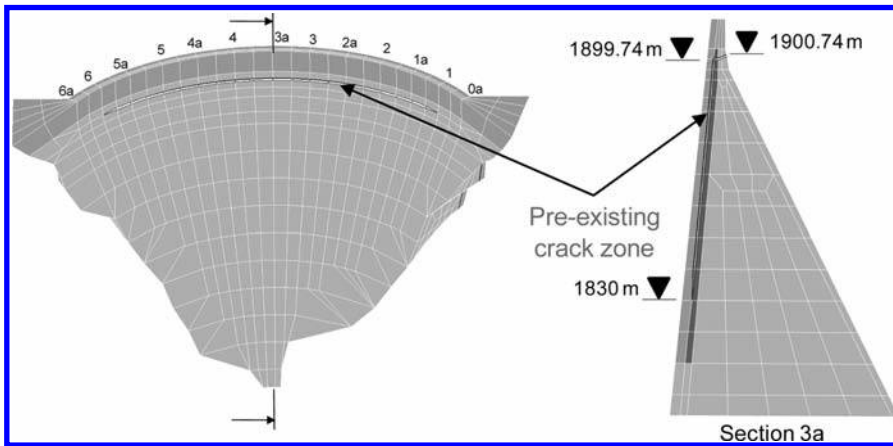


Figure 5. Three-dimensional finite element model of Spitallamm Dam including a crack.

Table 1. Thermo-mechanical material properties.

Parameter	Concrete	Rock
Elastic modulus, E (GPa)	30	30
Poisson ratio, ν	0.2	0.2
Heat conductivity (kW/m/day/ $^{\circ}\text{C}$)	241.9	259.2
Heat capacity (kW/m ³ / $^{\circ}\text{C}$)	2180	2160
Thermal dilatancy (1/ $^{\circ}\text{C}$)	0.87×10^{-5}	1×10^{-5}
Crack cohesion (kPa)	0	–
Crack friction angle ($^{\circ}$)	20	–

(sections 1 to 6). This result is consistent with the observations on the downstream face of the dam where a quasi-horizontal crack between blocks 1 and 5 is visible. Further analyses are performed considering activated pre-existing crack, with no initial opening gap.

4 THERMO-MECHANICAL ANALYSIS OF DAM BEHAVIOUR

4.1 Methodology

The thermo-mechanical analysis of Spitallamm Dam behaviour is conducted in two main steps. First, a transient thermal analysis is carried out to determine the time history of temperature fields within the dam and to compare simulation results to measured temperatures during the same time span. Then, the mechanical behaviour of the dam is simulated, considering dam's self weight, water level variations and thermal gradients resulting from temperature variations. Calculated displacements and crack opening evolution are compared to instruments' measurements, i.e. pendulum and joint meter, for the same time span.

4.2 Transient thermal analysis

A transient thermal analysis of the dam covering the period ranging from 1997 to 2008 is performed considering the following thermal boundary conditions:

- Daily air temperature on the crest and downstream face of the dam
- Daily air or water temperature on upstream face of the dam, depending on water level at the considered date
- Solar radiation on sun-exposed dam's faces

The input values of air and water boundary condition temperature are taken from the existing real time measured temperatures. Daily temperature fields in the dam are determined and time history of temperatures can be retrieved at any dam location.

4.3 Thermo-mechanical analysis

A transient thermo-mechanical analysis of the dam covering the period ranging from 1997 to 2008 is performed considering the following loading and boundary conditions:

- Dam’s self weight is applied in successive steps to simulate construction stages
- Hydrostatic pressure is applied on the upstream face according to water level variations
- Temperature gradients, determined from the transient thermal analysis, are applied simultaneously with water level variations

Daily stress and displacement fields in the dam are determined and correspondent time history can be retrieved at any dam location.

5 RESULTS AND COMMENTS

5.1 Temperatures

Figure 6 shows measured temperatures (Stucky 2010) at four locations in the dam body (thermometers T1, T2.1–T2.3) and time histories of calculated daily temperatures at the same locations. The comparison between measurements and calculated values shows a satisfactory agreement for the considered 12 years temperature cycles. Temperatures in other locations are also determined and compared to thermometers measurements (T3.1–T3.4, T4.1–T4.4) and a good agreement is obtained as well.

5.2 Displacements

Figure 7 shows pendulum measured upstream-downstream displacements below crack level (P15) and near dam’s crest (P16) (Stucky 2010). Corresponding calculated displacements are also shown in the same figure. Below the crack level, a good agreement between measured and calculated displacements for the whole considered period is generally obtained. Near the

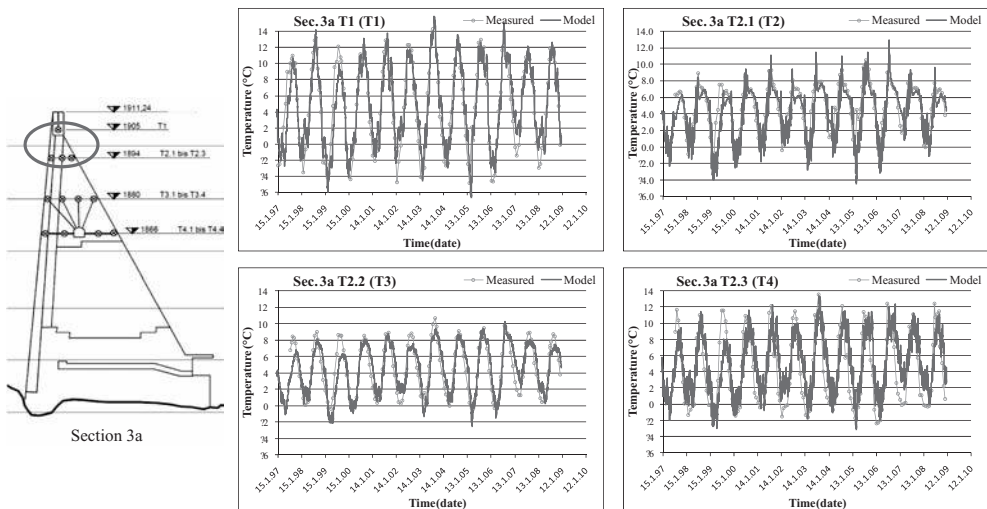


Figure 6. Calculated vs. measured concrete temperatures (thermometers).

crest, calculated displacements have similar amplitudes to measurements but the observed irreversible displacement towards upstream is not retrieved by the numerical model. This difference can be explained by the fact that by nature, the adjacent crack surfaces are not perfectly planar and may exhibit asperities and interlocks. Accordingly, interlocking mechanisms along these surfaces may prevent the crack from reversibly recovering its displacements. Other irreversible phenomena affecting long-term dam behaviour, such as creep or thermal reactions, may also be responsible for the observed drift. Once the crack opening occurs due to seasonal temperature and water level variations, the crack does not recover its initial state and leaves a permanent gap which increases at each yearly cycle.

Figure 8 shows obtained model's crest displacement assuming a linear drift representing the cumulative gap opening. From the upstream side, displacements cycles very closely fit the measurements. From the downstream side, however, the calculated peaks are lower than measurements. This latter issue can be explained by the fact that in the model, the crack completely closes at each cycle and no additional downstream displacement is possible; whereas in reality, cumulative annual residual gaps leave a freedom of dam's movement towards downstream.

5.3 Crack opening

Figure 9 shows a comparison between absolute crack opening obtained from joint meter measurements (Stucky 2010) and corresponding calculated relative displacements, assuming

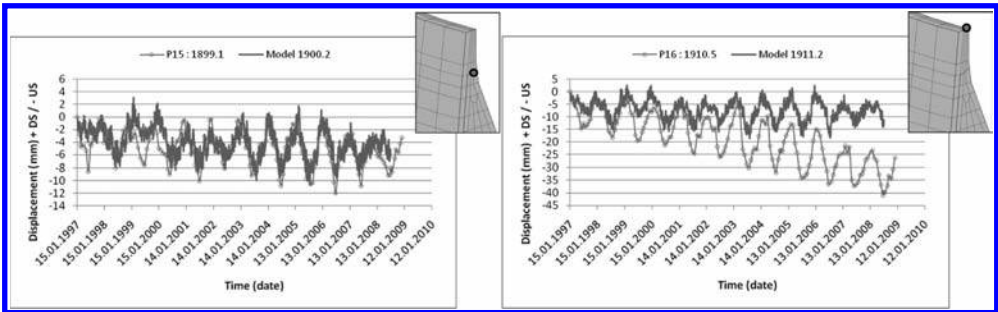


Figure 7. Calculated vs. measured displacements (pendulum).

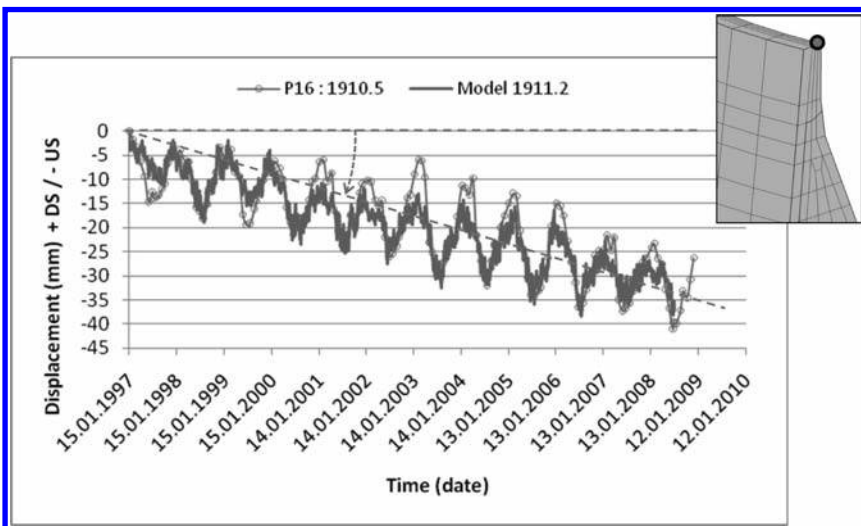


Figure 8. Calculated vs. measured crest displacements (pendulum)—linear irreversible drift assumption.

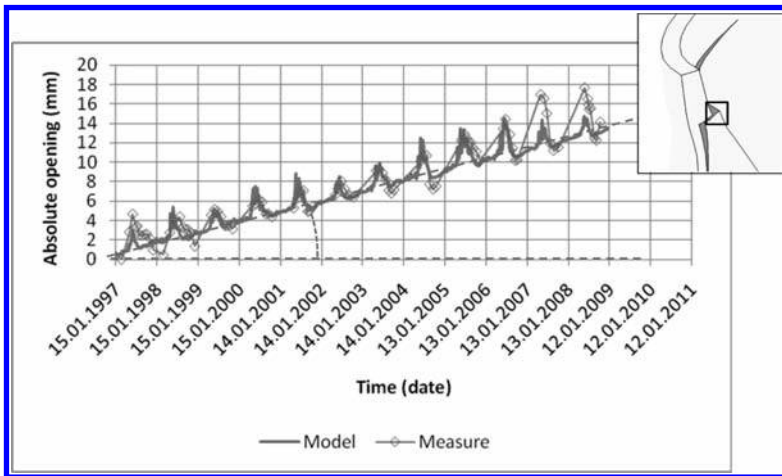


Figure 9. Calculated vs. measured crack opening (joint meter)—linear irreversible drift assumption.

a linear irreversible drift. Vector length is determined from upstream-downstream and vertical components, neglecting left-right horizontal component. A very close fit between measurements and calculations is obtained for the whole considered time span, except the two last cycles for which an amplitude increase of gap opening is observed. This evidence can be indicative of an evolution of the crack in the last years.

6 CONCLUSIONS

The thermal and thermo-mechanical behaviour of Spitallamm Dam is analysed by means of a three-dimensional finite element model of the dam, including the identified existing crack. Time histories of calculated temperatures, displacements and crack opening are compared to corresponding thermometer, pendulum and joint meter measurements. With the exception of an irreversible cumulative displacement towards upstream, all important features of dam behaviour, including cyclic crack opening-closing, have been reasonably represented by the numerical model. Therefore, it is concluded that the proposed finite element model is valid and appropriate to be used for the dynamic analysis of the fissured dam in order to evaluate its seismic safety and eventually to propose remedial solutions.

ACKNOWLEDGMENT

The presented study is part of a project funded by Kraftwerke Oberhasli AG (Switzerland). The authors wish to thank particularly M. Andres Fankhauser for providing all necessary data and for the fruitful discussions about investigations and results at different project stages.

REFERENCES

- Balissat, M. 2006. Stauanlage Spitallamm—Siebter Fünfjahresbericht, Gutachten 2005. Bericht Nr 1763/4003, Renens, September 2006.
- Stucky, A. 1968. Barrage de Spitallamm—Appréciation de la tenue du barrage actuel. Rapport no. 3641, Lausanne, le 31 janvier 1968.
- Stucky Ingénieurs-Conseils, 1978. Bericht über die Pruefung der Stauanlage Spitallamm—Fünfjahres-Kontrolle, 1974. Bericht Nr 5108 A, Lausanne, Juni 1978.
- Stucky SA, 2010. Spitallamm Sperre—Jahresbericht 2009, Messungen und Beobachtungen. Bericht Nr 1512/4014, Renens, den 30 Juni 2010.

Distributed fiber optic temperature measurements in embankment dams with central core—new benchmark for seepage monitoring

M. Aufleger & M. Goltz

Unit of Hydraulic Engineering, University of Innsbruck, Innsbruck, Austria

J. Dornstädter

GTC Kappelmeyer, Karlsruhe, Germany

O. Mangarovski

GD GRANIT a.d. Skopje, Macedonia

ABSTRACT: The Knezovo Dam is located in the upper stream of the Zletovica River, about 80 km east of the Macedonian capital Skopje. It is the main element of the Zletovica Basin Water Utilization Improvement Project, with the purpose of water supply, irrigation and power generation. The Knezovo Dam is an asphalt core rockfill dam with a maximum height of 82 m, a crest length of 270 m and a total dam embankment volume of 1,700,000 m³. The effective storage capacity is 22,500,000 m³. The instrumentation of the dam comprises among others piezometers, total pressure cells and extensometers. For leakage monitoring a leakage detection system based on fiber optic temperature measurements is installed directly downstream of the asphalt core. The paper deals with the measurement technique and design aspects of the leakage detection system. Furthermore results of laboratory tests are presented that prove the applicability of the monitoring system in the central part of embankment dams.

1 INTRODUCTION

Distributed Fiber Optic Temperature (DFOT) measurements are employed in several embankment dams to detect and localize leakage. The method has been successfully used during the last 15 years, and has continuously improved with regard to both monitoring and evaluation. The key feature of DFOT measurements is that the fiber optic cable is the sensor and the temperature can be measured along the entire length of the cable. For existing dams installations of the fiber optic cable in the dam toe, below a refurbished surface sealing or in existent standpipes, are the most common applications (Aufleger et al. 2007, Johansson and Sjödaahl, 2007). During the construction of new dams the cable can be installed at locations where monitoring will be most useful. So far the typical application has been the monitoring of the perimetric joint of embankment dams with surface sealing (Aufleger et al. 2005). For these applications the fiber optic cable is largely protected against mechanical loading due to deformation and stress in the dam. However, the monitoring system presented in this paper uses fiber optic cables installed in the D/S filter of a dam with central core to detect outflow areas. It is expected that the cables will be exposed to tensile forces and lateral pressure due to the deformations and the stresses in the dam. To evaluate the influence of deformations and stresses on the results of DFOT measurements, laboratory tests have been carried out in which realistic loads on the cable have been simulated. In the following conducted laboratory tests and their results are discussed and the design aspects of the leakage detection system as well as measuring results are presented.

2 LEAKAGE DETECTION USING TEMPERATURE MEASUREMENTS

The technology of distributed fiber optic temperature sensing offers the possibility to measure the temperature along fiber optical cables of a few kilometer length continuously with high accuracy. This technique possesses compared to conventional measuring methods a much higher information density and improves therefore considerably the evaluation of the temperature distribution in large structures. The method is based on the fact that the optical properties of the fiber are dependent on the ambient temperature. A highly developed measuring technique enables the analysis and evaluation of property changes with the result of a reliable temperature distribution along the fiber (Dakin et al. 1985).

In embankment dams and their foundation, the internal temperature field is dependent of the flow field. Temperature gradients can exist in the form of permanent or seasonal temperature differences, or in the form of significant temperature fluctuations at the probable source of seepage. If leakage is present, temperature anomalies will be transported into the structure by means of convection and will propagate throughout the earthen body, distorting the temperature field. Distributed measurements allow for a precise localization of the anomaly, delimiting quite precisely the area affected by leakage. The substantial prerequisite for leakage detection using absolute temperature measurements is a temperature difference between the reservoir water and the dam material.

The second approach to interpret temperature measurements is the active method or heat pulse method. The method is based on the thermal response of the cables surrounding to the additional heat and can indicate whether the cable is within a moist, a partially saturated or fully saturated medium, and whether seepage flow is present or not (Perzmaier 2007). Originally the active method was developed for applications where absolute temperature measurements were meaningless, which is the case if there are neither sufficient temperature gradients between reservoir water and location of temperature measurement (e.g. under facings) nor adequate seasonal temperature variations of the reservoir water.

By applying an electrical voltage to the electric conductors integrated in a hybrid fiber optic cable, the cable is heated up. The temperature increase depends on the thermal capacity and conductivity of the surrounding material (Fig. 1). In case of seepage water the conductive heat transport is superposed by the more effective convective heat transport. Thus, the heat input from the cable is transported away more quickly. Consequently, these sections show distinct anomalies in the temperature increase. Typically the analysis of the measurement data includes the evaluation of the temperature difference between the heated stage and a reference stage before heating.

3 LABORATORY TESTS

3.1 General

DFOT measurements provide a wide range of application for monitoring technical structures. In particular, the possibility of distributed monitoring of sealing elements and joints is of importance for hydraulic structures. Depending on the application and type of structure,

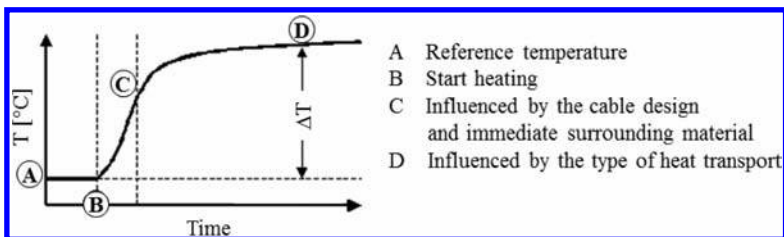


Figure 1. Temperature development inside the cable.

the conditions to which the cable is exposed vary considerably. For example, a fiber optic cable which is placed in the central part of a dam (Fig. 2, left) to monitor the sealing core is exposed to greater load caused by deformation of the dam and overburden pressure, than a cable placed underneath a surface sealing (Fig. 2, right).

In general ordinary fiber optic cables as used for telecommunication purposes are used for DFOT measurements. However, the specifications of these cables, which are based on standardized testing methods, give only limited information regarding applicability of the cables for installation in embankment dams. Furthermore, there was no experience from similar projects so far, how the results of DFOT measurements are affected if the cable is exposed to loads caused by overburden pressure and settlement. Therefore, to ensure the applicability of the proposed leakage detection system for embankment dams with central core laboratory tests were carried out at the University of Innsbruck. In several test series installation conditions and expected loads due to overburden pressure were simulated.

3.2 Description of laboratory tests

The laboratory tests for determination of the effects of pressure perpendicular to the cable axis on the results of DFOT measurements were carried out using the testing facility shown in Figure 3. The cable is installed in a 3.78 m long, 0.6 m wide and 0.6 m high reinforced steel box using different bedding materials. The load was applied forced-controlled using a fatigue testing machine with a capacity of 1,600 kN. This guaranteed constant loading during the different load steps. Different plungers were available for indirect loading.

In addition to the DFOT measurements, conventional temperature sensors (PT 100) were used. With the sensors the temperature in the steel box and the air temperature were recorded for the duration of the tests. Thus it was possible to check if the thermal boundary conditions remained constant. If changes in the ambient temperature occurred it was possible to consider their influence for the evaluation of the DFOT measurement data.

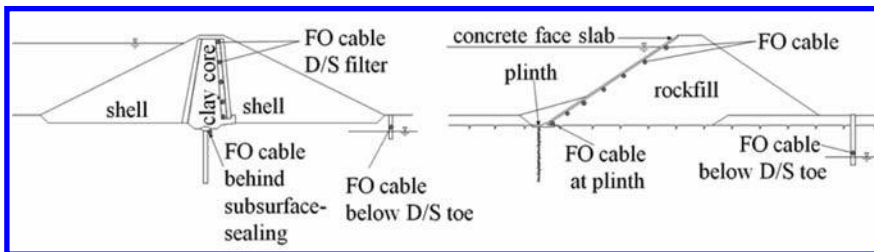


Figure 2. Application of DFOT measurements in embankment dams ECRD (left), CFRD (right).

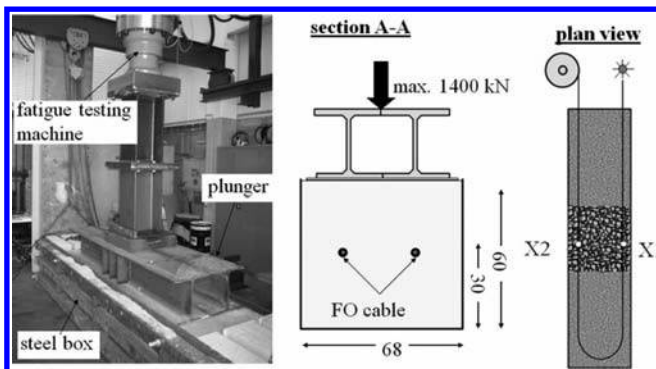


Figure 3. Setup for laboratory tests.

After installation of the cable in the soil material it took a certain time until stationary thermal conditions were reached which were necessary to start the tests. Before applying the load, reference measurements were conducted for about 10 minutes. The load was applied in load steps of 125 kN. Each load step took 6 minutes. After completion of the final load step the sample was unloaded.

3.3 Performed tests

The tests were carried out with a standard hybrid cable as shown in Figure 4. For the tests sand, gravel and sand-gravel mixes were used as bedding materials. To investigate the influence of particle shape both natural and processed material were used. The grading curves of the soils used as bedding material are shown in Figure 5.

3.4 Results of the laboratory tests

The evaluation of the results mainly focused on the measuring points just below the stamp. To determine the influence of pressure perpendicular to the cable axis on the DFOT measurement data, the temperature difference between the reference temperature measured in the unloaded state and the temperature measured in the loaded state was calculated and plotted against the applied load. Changes of the thermal boundary conditions during the tests were considered by means of the temperature data obtained from the conventional temperature sensors. Figure 6 exemplarily shows the results of the DFOT measurement depending on the applied load perpendicular to the cable axis.

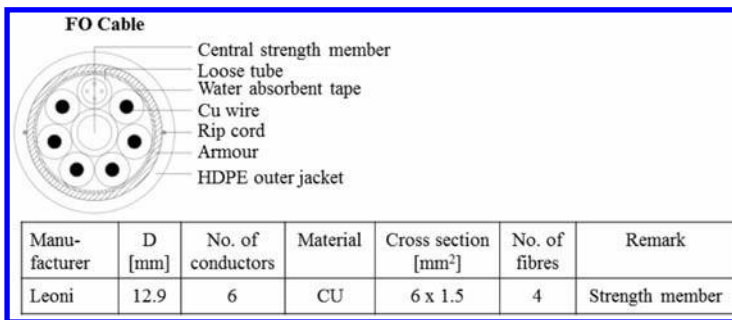


Figure 4. Fiber optic cable used for laboratory tests.

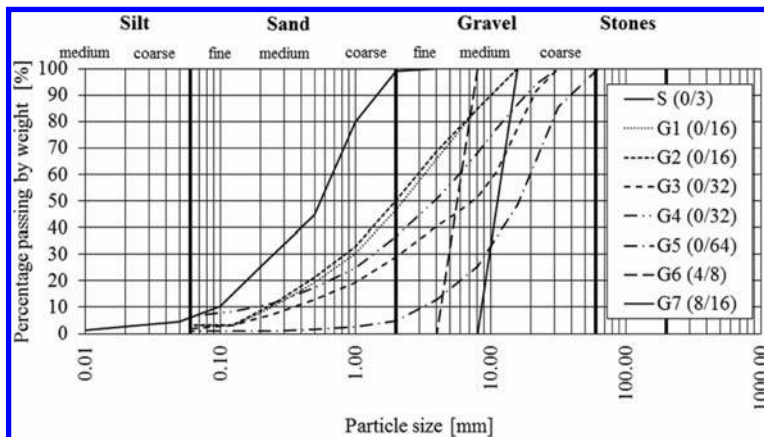


Figure 5. Grading curves of the soils used as bedding material.

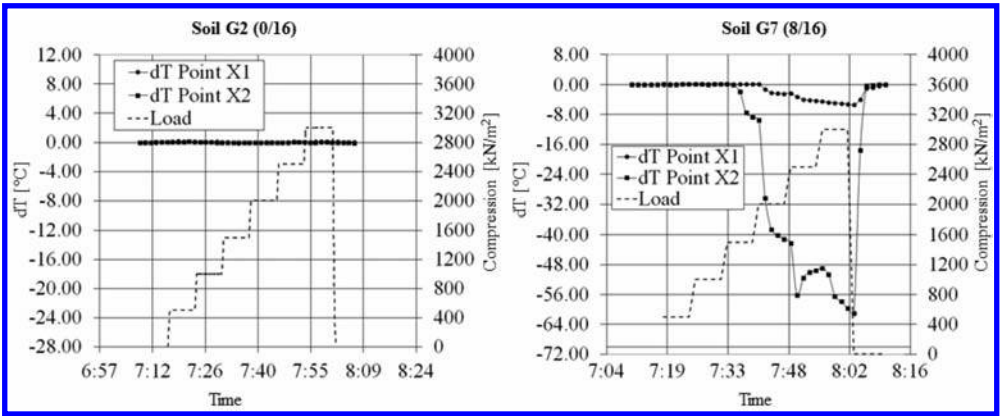


Figure 6. Results of laboratory tests for investigation of influence of lateral pressure.

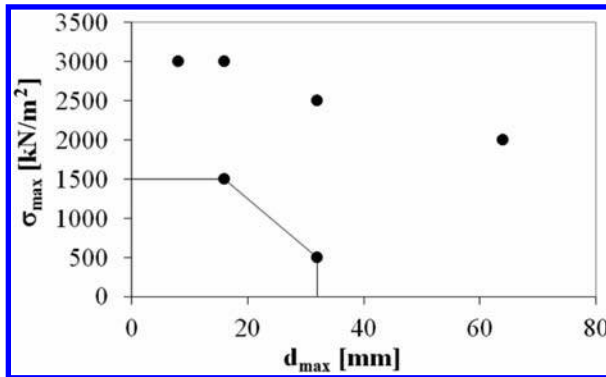


Figure 7. Maximum load without influencing the measurement results.

Because of the used bedding material in test P-7-B, which is a processed sand gravel mix 0/16, the temperature results are not affected by the applied load. In contrast, the results of the DFOT measurements for test P-10-B, which uses a uniform natural gravel 8/16, are affected significantly by the applied load.

Primarily the experiments provide knowledge of the maximum admissible load for a specific cable depending on the bedding material used. For the different test series bedding materials with a maximum particle size between 3 mm (S 0/3) and 64 mm (G5 0/64) were used. The test results show the influence of the maximum particle size of the bedding material. The decrease of the maximum permissible load without causing temperature anomalies for bedding materials with larger particle sizes was recognized.

The results of the laboratory tests show that pressure perpendicular to the cable axis can have significant influence on the measuring results of DFOT monitoring. In Figure 7 the maximum load without affecting the measurement results is plotted against the maximum particle size of the bedding material for the tested cable. Based on the results it is recommended to limit the maximum particle size of the bedding material to 16 mm and to use well graded material. Whilst bearing these recommendations in mind installation of fiber optic cable in dams with a height of up to 85 m should not cause problems regarding the reliability and accuracy of the measurements. As a result of the applied loads in some tests damages to the cable sheath occurred and high optical losses led to distortion of the measurement data. However, the applied loads did not cause the rupture of the optical fiber in any of the tests. By analyzing both, the raw data (optical losses) and the temperature data, temperature anomalies caused by mechanical loading can be detected.

4 KNEZOVO DAM

4.1 Project description

The Knezovo Dam is located in the upper stream of the Zletovica River, about 80 km east of the Macedonian capital Skopje. It is the main element of the Zletovica Basin Water Utilization Improvement Project, with the purpose of water supply, irrigation and power generation. The Knezovo Dam is an asphalt core rockfill dam with a maximum height of 82 m, a crest length of 270 m and a total dam embankment volume of 1,700,000 m³. The effective storage capacity will be 22,500,000 m³. According to the monitoring concept of the dam, a leakage detection system is installed to control the intactness of the sealing core. The leakage detection system is based on distributed fiber optic temperature measurements using the heat pulse method.

4.2 Leakage detection system

According to the design the monitoring system comprises only one cable, with measuring levels at the foundation level, at el. 1010 m.a.s.l, el. 1035 m.a.s.l and el. 1055 m.a.s.l. (Fig. 8). The cable was placed in the drainage and transition zone 2A downstream of the asphalt core. According to the specification, the maximum grain size for 2A material varied between 25 mm to 60 mm. To avoid damaging the cable during compaction of 2A material, uniform sand (CU ≤ 2) with a maximum grain size of 2 mm to 5 mm was used as cushion material around the cable. All necessary facilities such as measuring hut, reference section and power supply will be located on the right bank above the dam crest.

The cable used for the leakage detection system is a standard outdoor fiber optic hybrid cable. The main field of application of the cable is leakage detection in hydraulic engineering structures. The layout of the cable is similar to the cable used for the laboratory tests (Fig. 4), but it is considered to be more robust. It has a central supporting element, four copper conductors with a total cross-section of 6 mm². The external diameter is 17.0 mm. For the time being the DTS system used for the measurements is a mobile unit and only on site during measuring periods. However, it is planned to install a permanent monitoring system.

4.3 First measurements and simulation tests

To evaluate the change of seepage conditions in the dam due to impounding of the reservoir and during operation of the dam, reference measurements before filling the reservoir are necessary. The reference measurements were carried out when impounding of the reservoir was started (14-7-2010). The obtained temperature differences are shown in Figure 9.

In most parts of the dam the results of the reference measurement show no anomalies. Only at the lowest part of the dam the temperature differences indicate that the material

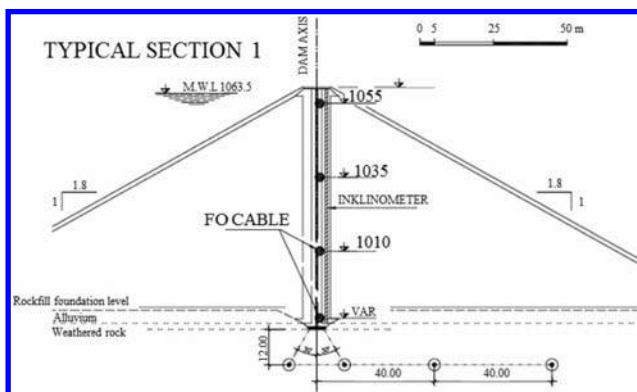


Figure 8. Allocation of the cable (cross section).

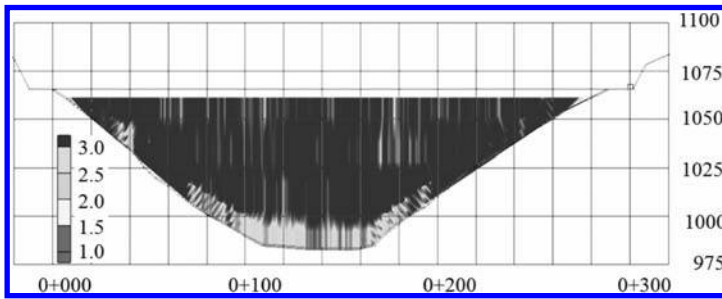


Figure 9. Results of reference measurement.



Figure 10. Leakage simulation test with 0.15 l/s.

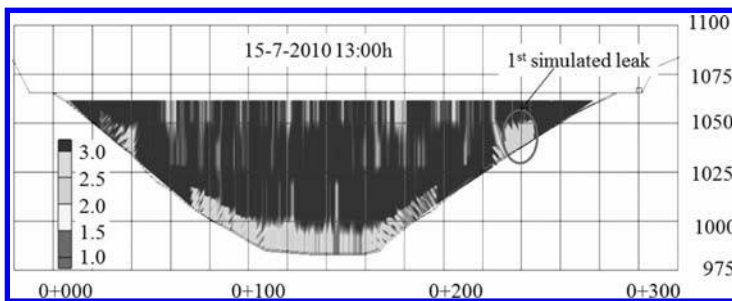


Figure 11. Results of leakage simulation test at 13:00 h.

around the cable is saturated or minor percolation is present. In general, the variations of the temperature differences are mainly caused by different thermal conductivities of the surrounding soil material. The thermal conductivity of a soil depends among others on mineralogical composition, the bulk density and the water content.

A leakage simulation test was carried out to check for proper operation of the installed system. For this purpose a water tank was placed at the dam crest. The amount of seepage was adjusted to approximately 0.15 l/s (Fig. 10, left) to prove the sensitivity of the system. Water was infiltrated at two different points (Fig. 10, right). The infiltration at the first location was started at 9:45 h and lasted for about 3 hours. Since it was assumed that the infiltrating water flows along the slope, infiltration was started at a second point at 13:30 h. This infiltration lasted for about 5 hours.

Figure 11 shows significant anomalies at the right slope between el. 1025 and el. 1050 which are caused by the infiltration at the first point. As already anticipated during the test, the infiltrating water runs off the slope causing an anomaly between St. 235 and St. 250. The anomaly increases with continuing infiltration. The anomaly caused by infiltration at the second point is shown in Figure 12. Further temperature anomalies are observed at the lower

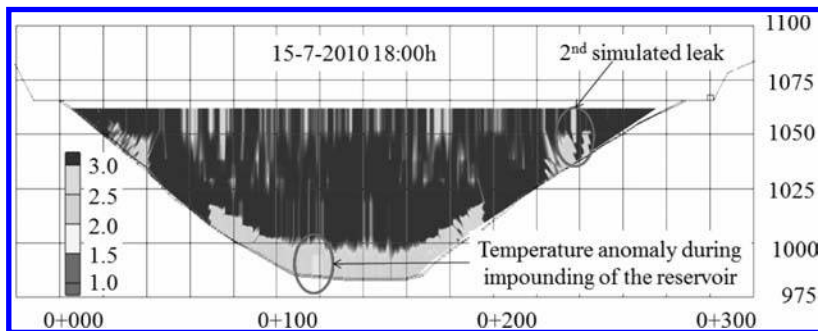


Figure 12. Results of leakage simulation test at 18:00 h.

part of the dam especially around St. 120. The anomalies intensify during the measurements. Both time characteristics and position suggest that the anomalies are caused by the increase of water level due to impounding of the reservoir.

5 CONCLUSIONS

The paper presents a leakage detection system based on distributed fiber optic temperature measurements for which the fiber optic cable is installed in the central part of the dam. Additionally information on the effect of deformation and stress in embankment dams on DFOT monitoring results are given.

In summary, it can be said that the fiber optic leakage detection system for the Knezovo dam is ready to use. Since the reference measurements were carried out at the beginning of impoundment, the results will serve as guide values to assess changes of the seepage conditions during impounding of the reservoir. The results of the leakage simulation test prove the proper operation of the system and the suitability of the system to detect small changes in the seepage behavior of the dam.

Laboratory tests were carried out at the University of Innsbruck, in which possible installation conditions and expected loads due to overburden pressure were simulated. Based on the results it is recommended to limit the maximum particle size of the bedding material to 16 mm and to use well graded material. As proved by the Knezovo dam installation of fiber optic cable in dams with a height of up to 85 m should not cause problems regarding the reliability and accuracy of the measurements.

REFERENCES

- Aufleger, M., Dornstädter, J., Strobl, T., Perzmaier, S., Conrad, M. & Goltz, M. 2007. 10 Jahre verteilte faseroptische Temperaturmessungen im Wasserbau. In Prof. Peter Rutschmann (ed.); Proceedings of the 7th ICOLD European Club Dam Symposium, September 17–19, Freising, Germany, Berichte des Lehrstuhls und der Versuchsanstalt für Wasserbau und Wasserwirtschaft TU München, Heft 115.
- Aufleger, M., Perzmaier, S., Dornstädter, J. & Schewe, L. 2005. A leakage detection system for concrete faced rockfill dams. In Chen Qian (ed.); Proceedings on symposium on concrete faced rockfill dams, September 19–26, Yichang, China.
- Dakin, J.P., Pratt, D.J., Bibby, G.W. & Ross, J.N. 1985. Temperature distribution measurements using Raman ratio thermometry. In: Fiber optic and laser sensors III. SPIE Vol. 566.
- Johannson, S. & Sjö Dahl, P. 2007. Experiences from seepage monitoring using distributed temperature sensing in optical fibers. In Prof. Peter Rutschmann (ed.); Proceedings of the 7th ICOLD European Club Dam Symposium, September 17–19, Freising, Germany, Berichte des Lehrstuhls und der Versuchsanstalt für Wasserbau und Wasserwirtschaft TU München, Heft 115.
- Perzmaier, S. 2007. Verteilte Filtergeschwindigkeitsmessung in Staudämmen. Berichte des Lehrstuhls und der Versuchsanstalt für Wasserbau und Wasserwirtschaft TU München, Heft 109.

Performance of dams affected by expanding concrete

Francesco Amberg

Lombardi Engineering Ltd., Switzerland

ABSTRACT: An increasing number of dams worldwide reveal permanent displacements due to concrete expansion occurrences. In most cases, concrete expansion occurs at a slow rate and becomes visible 20–30 years after construction. Thus, the phenomenon is generally at the initial stage of development, and apart from the measured displacements, no evidences are observed and the concrete quality is unaffected. Laboratory investigations might allow to detect the kind of chemical reaction, but it is still difficult to reproduce and predict its actual development. In few cases the rehabilitation of the dam was necessary to maintain the required safety conditions. In particular, cracks can arise as secondary effect since the concrete expansion and the related upstream drift can significantly change the equilibrium state and the stress distribution within the dam. The present work focuses on the behavior of dams affected by chemical expansion, the influence of the phenomenon on their safety is evaluated and several feasible remedial works are presented and discussed.

1 INTRODUCTION

Concrete swelling represents today the leading factor of dam ageing. After an initial period of a regular and reversible behavior of the dam, the above mentioned swelling mechanism provokes permanent deformations that progressively change the statical equilibrium of the structure.

The phenomenon is relatively slow, so that up to now, even in 60 years old dams, generally only observation of evolution has been sufficient. Apart from the measured displacements, in many dams no others evidences can be noticed. However the progressive ageing determines a reduction of their structural safety requiring sooner or later some remedial works. For single cases, a rehabilitation or reinforcement of the structure has already been undertaken.

The most common chemical reactions causing concrete swelling are alkali aggregate reaction (AAR) and sulfate reaction (ISA), which can also appear in combined form.

AAR is a reaction between the alkali of the cement (typical alkali content is 1%) and certain minerals included in the aggregates, as for example silica (SiO_2). The reaction occurs in presence of water (moisture of at least 80%), which in the case of dams does not seem to be a determining criterion. According to the ICOLD Bulletin 97, published in 1991, the term AAR includes three types of reactions: the most common alkali-silica reaction (ASR), the slow rate alkali-silicate reaction (ASSR) and the less frequent alkali-carbonate reaction (ACR). The AAR was first recognized in USA (Stanton 1940), but many dams built more recently are now still affected by this type of expansive phenomena. The main cause is that at beginning only few types of rock were considered to be reactive, while today the variety of reactive rocks increased considerably, here in particular the low reactive ones. The principal minerals related with the AAR are amorphous or poorly crystalline silica (opal and chalcedony) and strained quartz. These minerals are included in a wide variety of rocks: granite, granodiorite, rhyolite, dacite, andesite, basalt, obsidian, tuff, gneiss, schist, slate, quartzite, sandstone, siltstone, chert, silex, limestone, calc and dolomite can be mentioned as example.

ISA is a reaction between sulfates, present in aggregates or in water, and the cement paste, accompanied by the formation of expansive ettringite. ISA occurs often in correlation with

oxidation of pyrite and with the delete ettringite formation (DEF). ISA was known as “cement corrosion” since beginning of 20th century (Charlwood 2009), but due to the complexity of the process which is difficult to predict, ISA does nowadays still represent a problem.

From the practical point of view, for the engineers in charge with the safety of dams, the difference between the various kinds of expansive reaction is of low significance. Even though they might develop with different rapidity, the consequences on the structure and the possible remedial measures are rather similar. More relevant for the understanding of dam behavior is the kinetics of the reaction, which cause a variable expansion within the dam.

Distinctive consequences of AAR and ISA are concrete swelling, surface cracking and degradation of mechanical properties.

2 OBSERVED DAM BEHAVIOR

The behavior of a dam is monitored by specific instrumentation allowing to detect and follow the development of possible expansive phenomena, in some cases even long before cracks become visible. The concrete swelling leads to an increase in crest elevation. The value of rising allows a direct estimation of the expansion rate. This can vary from few $5 \mu\text{m}/\text{m}/\text{year}$ up to $200 \mu\text{m}/\text{m}/\text{year}$. Swelling of concrete might occur also more rapidly, but these cases have generally been able to be detected before dam construction. The observed expansion at the Mactaquac dam for example, with a rate between 50 and $150 \mu\text{m}/\text{m}/\text{year}$, can be identified as slow type (Hayward et al. 1991). It must be considered that the swelling tests performed to assess the presence of concrete swelling did not indicate any potential problem from AAR. At Chambon the crest rise of $3.6 \text{ mm}/\text{year}$ allowed to estimate an expansion rate of $70 \mu\text{m}/\text{m}/\text{year}$ in the upper part of the dam (Bister et al. 1991). In some particular cases a crest rising is more difficult to detect, even if the presence of concrete expansion is confirmed. At Pian Telesio (Amberg et al. 2009), for example, the upstream drift was able to mitigate the crest rising due to the shape of the vertical section, considerably inclined toward upstream. The estimated expansion rate in this case reaches only $10 \mu\text{m}/\text{m}/\text{year}$.

The expansion rate in vertical direction is often not uniform over the dam height. At Chambon the expansion in the upper part is higher than in the lower part. This was directly measured with level measurements on the crest as well as within galleries. A greater expansion in the upper part was also measured at Isola and Illsee. At Pian Telesio it was necessary to assume a greater expansion rate in the upper part in order to achieve for the structural analysis a similar distribution of permanent displacements as measured by the pendulums.

In arch dams, the presence of expansive phenomena induces an upstream drift. Said drift is governed by the expansion of the arches. In straight gravity dams, such an upstream drift can also be observed, but in these cases the mentioned drift is due to non uniform expansion within the wall thickness. In gravity dams the drift might also be downstream directed (e.g. Chambon).

In the Alpine region it is possible to observe a very slow upstream drift at crest elevation of various thin arch dams. The measured value of 0.5 to $1.0 \text{ mm}/\text{year}$ allows to estimate expansion rates of 5 to $10 \mu\text{m}/\text{m}/\text{year}$.

The current behavior of dams affected by extremely slow expansive phenomena is generally satisfactory since the swelling is at its initial state of progress, but small cracks do typically develop in those dams. Basically, it is possible to distinguish between two types of cracks: cracks induced directly by differential swelling and cracks induced indirectly by the structural response to the concrete expansion.

Cracks produced directly by differential swelling are visible in particular in the inspection galleries. Such type of cracks is present in various dams: e.g. Pian Telesio, Isola (Otto 2007) or Portodemouros (Pérez Rodríguez et al. 2010). These cracks are characterized by a relative continuity along the gallery, but they are often not visible or less visible on both dam faces. On the contrary, the typical diffuse cracking at the surface of structures affected by swelling is not visible in many dams.

Structural cracks, produced indirectly by expansion, appear typically along structural discontinuities, as for example at the transition between a straight gravity and a curved part like

at Illsee dam (Otto 2007), or along the foundation as peripheral cracks on the downstream face of arch dams, e.g. Serra (Leroy et al. 2010). In fact, the upstream drift in arch dams produces tensile stress at the downstream dam toe in case of low reservoir.

Summarizing, the typical phenomena observed in correlation with concrete expansion in dams are:

- Rising of dam height and horizontal permanent displacements (often upstream drift).
- Greater expansion in the upper part of the dam.
- Non uniform expansion within the dam body causing cracks in galleries which are less visible at both dam faces.
- Structural cracks due to the new equilibrium induced by permanent displacements.

In addition to visible cracks, the expansion can cause microcracking in the aggregates and the cement paste. The measurable consequence of this microcracking is a reduction of concrete quality, in particular strength and stiffness. Although, a concrete quality reduction can be observed in laboratory tests, for the dam safety this aspect seems to be of secondary importance. At Serra dam, with an estimated total expansion of almost 1100 $\mu\text{m}/\text{m}$ the concrete has excellent properties: the average compressive strength is 63 MPa and the average young's modulus 36 GPa (Amberg 2007). The dam was demolished by intense cracking along the foundation. Unchanged concrete properties could also be observed at the Pian Telesio dam, which required a rehabilitation, too.

3 EVALUATION OF OBSERVED BEHAVIOR

The measured displacements of dams affected by expansive phenomena generally show an initial period of normal behavior without signs of concrete swelling. This delayed start of the expansive reaction varies between some view years (first cracks in Portodemouros spillway appeared already 5 years after completion) up to a period of 30 years and more. The reasons for this delayed start can be various. First of all the swelling reaction effectively requires an initiation time before development. Second, the macroscopic swelling becomes visible only after a certain time period. The observed expansion may be influenced by the presence of pores within the concrete since the gel resulting from AAR might initially fill the voids. The reaction is active but any macroscopic effects do not occur at this stage. This could explain the behavior of the Illsee dam, built in two different stages: the first, up to an elevation of 2553 m a.s.l., was built in 1926/27, the second up to 2560 m a.s.l. in 1941/43. Permanent movements started around 1955, i.e. 25–30 years after construction of the original dam and 10–15 years after dam heightening. The old concrete, less compacted and thus more porous than the more recently placed one, suffers less from any expansive reaction, even with the same aggregates.

Other factors, which might contribute to the delayed start of swelling, are creep or thermal cooling and shrinkage at early age. In arch dams these factors cause downstream displacements that in an initial period can compensate the upstream drift due to expansion. Creep in particular can produce permanent displacements in large and thin arch dams up to 30 or 40 years after dam completion.

For extremely slow rate expansive phenomena in dams, i.e. less than 30 $\mu\text{m}/\text{m}/\text{year}$, it appears that the effect of moisture is of secondary importance for the reaction kinetics. This is, for example, proved by the relative moderate presence of surface cracking, which in structures affected by expansive phenomena is caused by a lower expansion at the surface, which is more dry, towards the internal part.

Another confirmation of the rather limited importance of moisture is the case of the Illsee gravity dam. In 1995/97 an impervious membrane was installed on the upstream dam face in order to reduce the moisture within the dam and so to prevent the further expansion. Until 10 years after rehabilitation no slowdown of the drift could be observed (Otto 2007).

The presence of internal cracks, observed in the inspection galleries but which were not found at the faces, clearly indicate a greater expansion near the surface than in the internal

part of a dam. The most probable reason, apart the confirmation that moisture cannot be relevant, is that the reaction at the faces is accelerated by the higher temperatures. Many dams located in south facing slopes are strongly subjected to solar radiation. The average yearly temperature downstream can be 4–5°C higher than at the upstream face, and the maximum temperature in summer might be even more than 10°C higher (due to impounding). The effect of temperature on the kinetics of chemical reaction is well recognized and was clearly verified by laboratory tests for concrete expansive reactions. The temperature dependency could also explain the greater expansion observed in the upper part relative to the lower part of many dams. In fact, in the upper, thinner part the concrete reaches higher temperatures.

Additional factors are also to be taken into considerations to explain a greater expansion near the faces of a dam than within the structure: a facing concrete with higher cement content, and thus higher alkali content, or a higher content of oxygen near the faces exposed to air, which is favorable for the ISA reaction (Aguado et al. 2007).

In gravity dams, the mitigating effect of compressive stress on the expansion can clearly be observed. In a straight gravity structure like Portodemouros spillway, for example, with a length of 130 m and a height of 10 m, the expansion rate in vertical direction is around 150 $\mu\text{m}/\text{m}/\text{year}$ while in horizontal direction it measures only 10 $\mu\text{m}/\text{m}/\text{year}$. The horizontal expansion is clearly hindered by the structure and therefore an increase of compressive stress is expected. If the horizontal expansion were the same as the vertical one, the horizontal compressive stress should increase yearly by some 4 MPa (with a typical Young's modulus of 30 GPa). The compressive strength should be reached after around 10 years. In 1983 in situ stress measurements have been performed by means of over-coring testing method. The results indicated compressive stress up to 5–6 MPa, thus clearly lower than the potential one.

In arch dams it is generally more difficult to give evidence for the effect of compressive stress, since the thin and curved structure is nearly free to expand upstream, in particular in periods of reduced reservoir level.

Since the chemical expansion is a slow load condition, creep is included in the structural behavior, where it plays an important role. In fact, similar results can be obtained using a model with stress dependency and a model without, but with creep. Creep must also be taken into account in laboratory tests, for example by performing tests with non reactive samples in order to quantify creep, which is to be subtracted from the outcome of expansion tests.

4 REQUIREMENTS FOR LABORATORY INVESTIGATIONS

Laboratory investigation have been principally conceived for accelerating the expansion reaction in order to obtain results at short time, to assess if the aggregates are reactive and thus not adequate to be used for a new construction. Laboratory investigations are therefore not intended to simulate the development with time of the actual reaction occurring in dams.

The existence of large dams affected by expansion phenomena, and in particular of cases with extremely slow rate expansion, is putting new challenges to laboratory investigations. Large dams cannot be simply demolished and replaced with a new construction and thus it is necessary to face with the consequences of the concrete swelling. The safety assessment for the actual condition and the evaluation of the static equilibrium for medium and long term behavior thus becomes of primary importance for optimizing the maintenance and the exploitation of such types of structures. For evaluating the behavior of a dam affected by expansive reaction, the structural engineer should get the main parameters that characterize the reaction within the specific concrete of the dam and for the specific boundary conditions.

In the laboratory tests the acceleration of the expansive reaction is necessary for practical reasons, in particular for the cases of extremely slow rate expansions, i.e. less than 20 $\mu\text{m}/\text{m}/\text{year}$ in the actual structure. Suitable results can be obtained by limiting said acceleration and by increasing the time of observation. This implies however others difficulties in order to assure carefully the control of the test over a long period (e.g. leaching of alkali).

The simulation of the reaction in laboratory and the identification of the main parameters influencing the expansion rate in the dam has to take into account different factors, such as:

- The already mentioned temperature, moisture and constraint.
- The alkali content in concrete, which depends also on the cement content.
- The dimension of the aggregates: smaller aggregates have a higher specific surface and therefore the reaction occurs more rapidly. In addition it can be mentioned that also the aggregate shape could influence the reaction: by using natural gravel of a schistose rock, the flattened aggregates tend to dispose horizontally within the concrete causing a possible higher vertical expansion than the horizontal one.
- The dimension and thickness of the structure: moisture needs more time to penetrate through a thick structure than in a thin one. For a dam it must also be considered that the water firstly infiltrates along cracks and joints and only subsequently diffuses through the concrete mass. The effect of the dimension can be observed at various dam sites, where the state of thin secondary structures, such as walls and piles, is often worse than that of the main dam body.

The qualitative influence of each factor is known, but the major problem is due to the fact that the quantitative effect is uncertain, here in particular the interaction between the different factors. The effect of moisture, for example, has probably not the same importance in a rapid expansion as in a very slow rate one. Each factor can significantly influence the reaction only in case it becomes the determining one that regulates the expansion rate, i.e. all the other factors would also allow a greater expansion.

A similar question may arise with respect to the deterioration of the concrete quality: the quality degradation is probably not the same in a slow rate expansion as in an accelerated one. The main problems of dams affected by expansive phenomena are not related to the deterioration of the concrete properties.

5 SAFETY ASSESSMENT AND DAM PERFORMANCE

A realistic simulation of the expansion in a structural analysis taking into account all the factors influencing the chemical reaction is theoretically possible. Recently various interesting constitutive models have been developed, e.g. Saouma & Perotti (2006), but the parameters required for these models are often difficult to determine. The analysis results have to be compared with the observed behavior as well as the visual appearance of the actual structure. The interpretation is in any case very difficult since a plausible result can be obtained in different ways.

A simple simulation of the non reversible displacement with a thermal uniform expansion in a linear elastic model clearly leads to an over estimation of stresses. The chemical expansion undoubtedly is in a certain manner auto-adaptive, i.e. the concrete expands, the shape changes, but the general state remains more or less acceptable. The visual appearance of the 60-years-old Molina gravity dam, in Switzerland, is satisfactory and does not show any particular signs of swelling, even if the estimated expansion has reached about 1100 $\mu\text{m}/\text{m}$. Stress variations due to concrete expansion can be reduced by including both, the mitigating effect of compressive stresses and/or creep in the simulation. The effect of stresses determine that in direction of high compressive stresses no expansion occurs, limiting any further increase of compressions, while in the direction of tensile stresses the free expansion reduces the tension with time. The expansion becomes anisotropic. Creep just reduces the effect of a permanent deformation applied to a hyperstatic structure, like a dam.

The structural behavior of a dam and thus its safety condition strongly depends on the non-uniform distribution of the expansion. If this aspect is not analyzed with sufficient reliability, the simulation of the expansion development with time becomes just a calculation exercise without real consequences for the safety evaluation.

Another way to assess the safety condition of a dam is to analyze the structure taking into account the actual observed condition: analyze the presence of observed cracks and define its

maximum acceptable extension or verify whether the possible additional compressive forces induced by the expansion can be supported by the dam and can be safely transferred to the abutments. This type of analysis is much easier as an exhaustive and refined simulation of the expansion and is in many cases equally effective for safety evaluations.

An essential question is how much expansion can be supported by a dam. There is no general answer, since every dam represents a unique case. Some order of magnitudes can however be proposed.

The compressive stress directly produced by the chemical expansion does not represent the main problem for concrete strength: concrete properties reduction appears to be of secondary role and compressive stress mitigate the expansion development. According to Charlwood et al. (1992) no expansion should occur by a compressive stress higher than 8 MPa. Compressive stresses can be a problem in case of geometrical discontinuities, i.e. spillway openings or abutment blocs, where the forces, that can not be supported, produce permanent displacements.

In vertical direction the expansion can more or less freely take place without major consequences. This statement is not generally valid since in narrow valleys it is possible to observe that the vertical expansion of the dam produces vertical displacements also within the rock mass. The dam equilibrium is changing: an increase of the vertical forces at the dam foot and a reduction towards both flanks is expected. This phenomenon might affect the stability at the dam shoulders.

A non-uniform distribution of vertical expansion across the wall thickness can produce horizontal cracks. The effect of these cracks on the dam stability has to be investigated. In some cases, however, it was possible to conclude that the presence of a cracks is acceptable, e.g. Pian Telesio or Isola (Malla & Wieland 1999). Obviously, the analysis has to consider any possible increase of the uplift pressure due to water seeping into the crack.

In arch dams the upstream drift induced by the expansion of the arches might cause the development of peripheral cracks at the downstream face along the foundation, even with a relatively slight expansion. In fact, it must be considered that the shape of a thin arch dam is already the result of an optimization process and that the action of unexpected load conditions may have some consequences on its performance. At the Roggiasca dam a peripheral crack is going to develop while the total estimated expansion reaches only 60–70 $\mu\text{m}/\text{m}$.

The presence of a crack might initially have little consequences on the dam stability, but it is clear that a fully regular behavior is preferable. An arch dam has generally large safety margins before stability problems can arise, but with the development of cracks these margins decrease. The Serra dam, for example, had to be replaced because of the presence of an important peripheral crack, where the expansion reached about 1100 $\mu\text{m}/\text{m}$.

Further examples can be taken from others type of imposed displacements on arch dams. At Kölnbrein dam (Lombardi 1991) the sum of measured joint opening at crest elevation produced by the grouting process reached about 400 mm. Compared to the crest length of 600 m, the equivalent expansion is 670 $\mu\text{m}/\text{m}$. The dam required an intensive rehabilitation before being taken into normal operation.

At the Zeuzier dam (Amberg & Lombardi 1982) the drainage induced settlement of the rock foundation caused by the excavation of a tunnel led since 1978 also to a valley closure. At crest elevation the final closure reached 75 mm and important cracks, up to 15 mm wide, developed on the downstream face along the foundation. The dam clearly required important rehabilitation works to assure a safe stability condition. The valley narrowing of 75 mm over a distance of 173 m is comparable with an expansion of 430 $\mu\text{m}/\text{m}$.

A last example presents the Pian Telesio dam. With a total expansion of almost 250 $\mu\text{m}/\text{m}$ the dam required a rehabilitation consisting in systematic slot cutting within the upper half of the dam. In case of low reservoir level during summer time, the compressive stress in vertical direction at the upstream dam heel reached values up to 15 MPa. The rehabilitation was proposed in order to prevent possible damages to the structure, since the concrete strength was relatively modest, i.e. around 20 MPa. This last case shows how, for arch dams, the unfavorable loading condition in case of expansive phenomena occur with low reservoir level.

6 REMEDIAL WORKS

Basically, there are two intervention categories: the first one aims to mitigate any expansion phenomenon while the second category acts on the effects of the reaction. The types of remedial works might be quite various.

In the first category it is possible to mention following remedial works:

- Installation of an impervious membrane on the upstream dam face in order to prevent the provision of water for the reaction. The effect of this type of intervention is uncertain: at Illsee no effect was observed, but at the Pracana buttress dam (Portuguese National Committee on Large Dams 2003) the effect of the upstream waterproofing turned out to be conducive. However, in this case the previous period of 12 years with empty reservoir has also played a role on the observed behavior. Probably in letting the concrete dry out.
- Reduction of temperature, for example through watering as proposed for the Portodemouros dam. Nevertheless, the effect of this measure was limited, both probably why the temperature decrease was not sufficient and additional water was provided.
- Increase of compressive stress by means of anchorages or additional masses. Theoretically a possible solution, but in practice, it is not feasible since the forces required to limit the expansion in a dam would be very high.

The possibilities to mitigate the reaction in an existing structure are therefore rather limited. A larger choice of remedial works is available to reinforce or to rehabilitate a dam damaged by expansion phenomena. These remedial works have more or less all a temporary character, because in order to reach an exhaustion of the reaction, a long time is often required. Possible remedial works are:

- Grouting of the cracks with cement grout or epoxy resins to enhance the structural continuity, reduce leakage or increase sliding safety on the lift joints.
- Improve the drainage and/or the grouting curtains to reduce uplift pressure and seepage.
- Sealing the upstream face with a membrane to avoid possible water inflow through cracks (e.g. Isola) causing flooding in the galleries or increase of the uplift pressure.
- Reinforcing using anchorages to assure the stability of a damaged dam.
- Slot cutting to relief the compressive stresses, in particular in cases where the expansion might have concentrated impacts along structural discontinuities, such as the transition between a gravity and a curved dam (e.g. Illsee) or near spillway openings. Slot cutting, however, has a limited impact on internal cracks, i.e. observed mainly in galleries and less on the faces, as can be typically encountered in gravity or arch-gravity dams. Slot cutting has never been achieved on a thin arch dam, but it can be assumed that its effects are rather conducive, in particular to avoid the progress of cracks along the foundation on the downstream face.

Finally, a possible remedial work, which is rather to be considered for the long term, is the replacement of a dam by a new structure or the partial change of the structure (e.g. moving of a spillway). These more extreme interventions, which are possible in certain cases, such as for the 20 m high Serra arch dam, have a long term character, provided the chemical expansion can be excluded in the new construction.

7 CONCLUSIONS

Alkali-Aggregate Reactions (AAR) and Internal Sulfate Attacks (ISA) are different types of chemical reactions that cause a concrete swelling. However, their impact on the structural behavior of dams is similar: delayed start of a slow rate expansive process that influences the dam equilibrium in time.

The concrete expansion is a very complex phenomena, which is influenced by many parameters: moisture, temperature, confinement, creep, alkali content, oxygen (for ISA), aggregate dimensions and shape, pore characteristics and discontinuities in dams, e.g. lift or

contraction joints. The effect of the different influencing factors is qualitatively known, but their precise interaction and the parameters to describe the actual expansion occurring in a dam are very difficult to reproduce in laboratory. The theoretical knowledge still needs to be significantly improved.

Concrete swelling represents a new loading case, which has not been considered in the structural design and which thus might lead to unfavorable conditions for the dam. The presence of expansion phenomena in concrete dams requires special consideration related to possible consequences during their service life, since no reliable methods are known to inhibit such kind of behavior. Thus, remedial works have generally a temporary character and need to be repeated after a certain period.

The problem is far from being completely solved, even if both the slowness of the reaction and a correct maintenance of the dam will certainly allow to maintain various affected dams in safe condition for still a long time.

REFERENCES

- Aguado, A., Serafim, G., Chinchón, S., López, C.M. & Agulló, L. 2007. Internal sulfate attack in dams, *ICOLD Workshop on Chemical expansion of concrete in dams and hydro projects*, Granada, 18–19 October 2007.
- Amberg, F. 2007. Recent experiences with expanding concrete in the alpine region, *ICOLD Workshop on Chemical expansion of concrete in dams and hydro projects*, Granada, 18–19 October 2007.
- Amberg, F., Bremen, R. & Brizzo, N. 2009. Rehabilitation of the Pian Telesio dam (It) affected by AAR-Reaction, *23rd Congress on large dams, Brasilia*; Q. 90, ICOLD.
- Amberg, W. & Lombardi, G. 1982. Comportement anormal du barrage-voûte de Zeuzier (Suisse)—Calculs statiques, *Wasser, Energie, Luft* 74. Jahrgang, Heft 3, Special Issue to ICOLD: 102–109.
- Bister, D., Bonnet, P., Denis, B., De Bauchamp, R., Dubois, P. & Goguel, B. 1991. Contribution au suivi des barrages en béton français sujets à gonflement ou retrait, application à des ouvrages adultes (Chambon, Vouglans) et au béton jeune (cas du BCR), *17th Congress on large dams, Vienna*; Q. 65 R. 7, ICOLD.
- Charlwood, R.G., Solimar, Z.V. & Curtis, D.D. 1992. A review of alkali-aggregate reactions in hydroelectric plants and dams, *Alkali-aggregate reactions in hydroelectric plants and dams; Proc. Intern. Conf.*, Fredericton, Canada.
- Charlwood, R.G. 2009. Predicting the long term behavior and service life of concrete dams, *Long term behavior of dams; Proc. 2nd Intern. Conf.*, Graz, 12–13 October 2009.
- Hayward, D.G., Thompson, G.A., Charlwood, R.G. & Steele, R.R. 1991. Remedial measures at the Mactaquac generating station, *17th Congress on large dams, Vienna*; Q. 65 R. 47, ICOLD.
- Leroy, R., Micoulet, G. & Tognola, F. 2010. Rehabilitation of Serra dam (Switzerland) affected by ASR, *Dam maintenance and rehabilitation; Proc. 2nd Intern. Congr.*, Zaragoza, 23–25 November 2010.
- Lombardi, G. 1991. Kölnbrein dam: an unusual solution for an unusual problem, *Water Power & Dam Construction* June 1991: 31–34.
- Malla, S. & Wieland, M. 1999. Analysis of an Arch-Gravity Dam with a Horizontal Crack, *Computer and Structures* Vol. 72, No. 1: 267–278.
- Otto, B. 2007. AAR and ISA at two dams in Switzerland, *ICOLD Workshop on Chemical expansion of concrete in dams and hydro projects*, Granada, 18–19 October 2007.
- Pérez Rodríguez, D.A., Pazo García, I., Alonso Muñoz, J.M. & Gonzalo Carracedo, A. 2009. La rehabilitación del aliviadero de la presa de Portodemouros, *Dam maintenance and rehabilitation; Proc. 2nd Intern. Congr.*, Zaragoza, 23–25 November 2010.
- Portuguese National Committee on Large Dams, 2003. Observed behavior and deterioration assessment of Pracana dam, *21st Congress on large dams, Montreal*; Q. 12 R. 12, ICOLD.
- Saouma, V. & Perotti, L. 2006. Constitutive Model for Alkali-Aggregate Reactions, *ACI Material Journal*, May–June 2006: 194–202.
- Stanton, T. 1940. The expansion of concrete through reaction between cement and aggregate, *Proceeding of American Society of Civil Engineer* Vol 66: 1781–1811.

Warning systems—basic components of Hidroelectrica's emergency management system

Irinel Daniela Iacob & Dragos Zachia

SC HIDROELECTRICA SA, Bucharest, Romania

ABSTRACT: The emergency management generated by: floods, dangerous meteorological phenomena, accidents to the hydro-technical constructions and accidental pollutions, are an activity of national interest considering the frequency and the impact that such kind of risks might have.

In Romania the protection against floods is a regulated domain in conformity with the Regulation concerning the management of the emergency situations generated by floods, dangerous meteorological phenomena, accidents to the hydro-technical constructions and accidental pollutions, approved through Order no. 638/12.05.2005 issued by the Ministry of Defense and Order no. 420/11.05.2006 issued by the Ministry of Environment and Water Management.

The owners, any title they might have, of dams and of such other hydro-technical constructions of which damage or destruction can endanger the population and its material goods, social objectives and production capacities or can prejudice the environment, must keep them, repair them, and operate them accordingly, endow these works with such systems required for their construction behavior monitoring activity, install systems for warning the population in case of danger, and organize the surveillance, intervention, and rehabilitation activity as in accordance with the regulations approved through the authorizations of water management, flood protection planning and of such other risk situations, and according to such other regulation documentation in force.

SC Hidroelectrica SA is the major power producer in Romania and one of the most important owners of dams in the country. Of 107 dams administered by Hidroelectrica, 96 fulfill one of the conditions required for the warning system, namely: Thalweg-crest height >10 m;

Water volume >10 million m³; The downstream localities and objectives are located at distances lower than 10 km away from the dam section.

Concerning risk management, Hidroelectrica has implemented its own risk management system. During the period of 1999–2010, Hidroelectrica has carried out and envisaged to carry out a number of 29 warning systems.

This column aims at emphasizing the data concerning the sizing and the architecture of the warning systems carried out by Hidroelectrica.

1 INTRODUCTION

The dam safety concept includes four major types of action: 1. dam design and execution, in accordance with the technical norms on structures safety; 2. ensuring an appropriate monitoring system, depending on dam type, and complying with the frequency of measurements as required under the construction behavior monitoring documentation; 3. drawing up and complying with the reservoir's operation regulation regarding the normal operation mode and special operation conditions; 4. action plans in case of emergency situations.

The first three elements are well known, dedicated extensive literature being available in the field. However, emergency action methods are less known. This is because the alarm-warning population evacuation systems are, in some countries, under military or civil authority

control, due to the fact that they are exposed to high risks. This article aims to bring forward the experience of Hidroelectrica, the largest energy generator in Romania, as regards the design and operation of alarm-warning systems.

2 LEGAL PROVISIONS ON THE ALARM-WARNING SYSTEMS

In Romania, the action plan in case of disasters is a legal obligation. The issuer of the safe operation agreement may impose requirements regarding the standards and norms to be observed as regards the constructions quality and safety, the alarm-warning system for the downstream localities, and other requirements that lead to population and environment protection.

Holders of any title, construction of dams and other hydro whose damage or destruction may threaten its people and material goods, social objectives and the productive capacity or harm the environment are required to install alarm systems, warning the population in case of danger and organize oversight, intervention and rehabilitation under regulations approved by the water management permits, flood plans and hazardous weather warning, alarm plans and objectives of the villages downstream from dams in accidents to them.

3 DIMENSION AND ARCHITECTURE OF SYSTEMS

3.1 *Dimensions of the systems*

The alarm systems mounted at Hidroelectrica's plants were sized depending on the potentially flooded area, as it results from dam or dikes breaking calculation. The potential situation taken into account at calculation was a full reservoir, 100% breaking and 50% average damage, in accordance with the technical requirements in force in Romania.

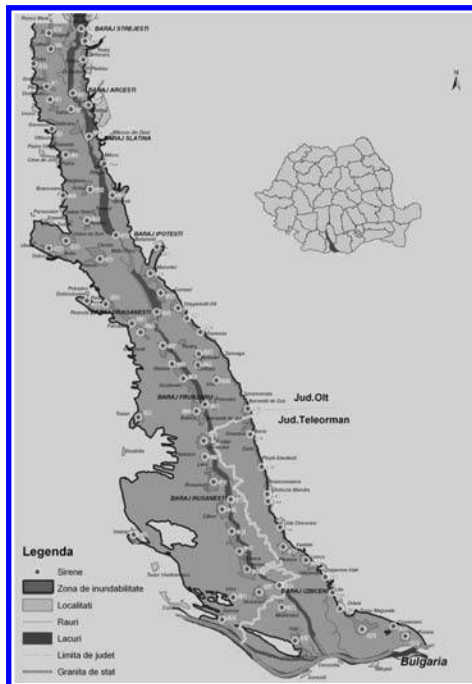


Figure1. Flood wave in case of accident at Vidra Dam.

The sirens were set in localities or locations covered by the flood wave (full lake and 100% breaking). The siren power and height at which it is mounted on the pillar were determined so that the siren service area to cover the populated areas.

Regarding the dams which are not located near towns, various powers of sirens have been used to cover the downstream areas where maintenance works are performed or in case evacuation equipment is maneuvered to prepare for discharge.

The main components of an alarm-warning system are the control centre, the retranslation systems and the electronic siren.

3.2 *Architecture of systems*

The control centre of the alarm-warning system performs the functions of collection, analysis and control of data linked to the alarm-warning system. The equipment of the control center has the following functions: self-tests the alarm system and displays the deviations; stores all events and activities and generates reports on demand; unlimited configuration of sirens participating in an alarm (one siren, groups of or all sirens); selects the type of alarm to be used; displays the status of each siren participating in the alarm.

The centre allows extension of number of posts (sirens), when the towns are expanding and connection with other alarm centers connect to the National Integrated System).

Access to system resources is based on a hierarchical password system, the control centre making available any reports on system status.

The control centers of the alarm system are located at the operation dispatch centers within Hidroelectrica's subsidiaries.

The sirens can be operated by radio waves (main option) or GSM (secondary option).

Alarm dispatch centers are directly connected to the County Inspectorates for Emergency Situations through mobile radio stations.

The retranslation system is a transceiver used in terrestrial wireless networks to retransmit the signal transmitted by a station to another station, located at far distance, which can not be directly communicated with.

The electronic sirens can be operated: locally and wirelessly. Local activation (which is made directly to sirens) may be performed using at least 4 different types of signals and public notices playing a tape or from a microphone. Related to the remote activation, an interface



Figure 2. Hydropower plant, control center.



Figure 3. Electronic siren.

unit provides signal activation. There is the possibility to make public announcements, as well as to transmit information to the control center on the status of components.

The electronic siren provides the following functions: broadcasts scheduled alarms; broadcasts texts read using a microphone or pre-registered texts; transmits 7 different alarm signals; functions in the event of energy disruption (are equipped with dual power supply); self-testing of the entire equipment of siren, including “mute” testing of the speakers; local and remote operation (control center).

The alarm-warning system is powered from the 220 V mains and, for proper operation, the system is equipped with batteries that can provide seven days running time.

To protect the alarm-warning system related equipment and to avoid accidents at the equipment mounted near schools, town halls, cultural centers etc., protection fences have been erected.

4 FUNCTIONS OF THE ALARM-WARNING SYSTEM

The alarm-warning system developed by Hidroelectrica can be used for the other types of contingencies (earthquakes, chemical or nuclear accidents, fire, war etc.), not only for accidents occurring at hydro constructions. It may issue the following signals: air alarm signal, disaster alarm signal, pre-alarm signal, alarm termination signal, live verbal announcements from a microphone, pre-registered announcements or any other sound.

5 ALARM-WARNING SYSTEMS DEVELOPED BY HIDROELECTRICA

As shown above, the Romanian law requires action to be taken so as to mitigate damages downstream dams, to protect property and population in case of extreme floods.

Of the 107 dams administered by Hidroelectrica, 96 dams meet the legislative requirements regarding alarm-warning systems: thalweg to crown height to be more than 10 m; water volume of more than 10 million m³; the existence of settlements and property downstream, at less than 10 km from the dam section.

Table 1. Alarm-warning systems developed by Hidroelectrica.

Item	Alarm-warning system	No. of sirens	Control center of alarm system*	Status
1.	Downstream Vidraru Dam	15	SH Curtea de Arges	in operation
2.	Downstream Portile de Fier I Dam	7	SH Portile de Fier I	in operation
3.	Downstream Portile de Fier II Dam	5	SH Portile de Fier II	in operation
4.	Downstream Candesti Dam	4	SH Buzau	in operation
5.	Downstream the dams located on the Upper Olt River basin	14	SH Sibiu	in operation
6.	Downstream Negovanu Dam	10	SH Sibiu	in operation
7.	Downstream Vidra Dam, Lotru River	10	Lotru Plant	in operation
8.	Downstream Vidra Dam, Middle Olt River	46	Ramnicu Valcea	in operation
9.	Downstream Vidra, Lower Olt River	72	SH Slatina	in operation
10.	Downstream the dams located on the Somesul Mic River basin	10	SH Cluj	in operation
11.	Downstream Dragan Dam	60	SH Oradea	in operation
12.	Downstream Vadeni Dam	7	SH Targu Jiu	in operation
13.	Downstream Motru Dam	9	SH Targu Jiu	in operation
14.	Downstream Vaja and Tismana Dams	12	SH Targu Jiu	in operation
15.	Downstream Valea Sadului Dam	16	SH Targu Jiu	in operation
16.	Downstream Herculane Dam	4	Herculane HPP	in operation
17.	Downstream Cerna Dam	3	Herculane HPP	in operation
18.	Downstream Poiana Rusca Dam	11	Ruieni HPP	in operation
19.	Downstream Poiana Marului Dam and Zervesti Polder	22	Ruieni HPP	in operation
20.	Downstream Poiana Marului Dam-extension	53	Ruieni HPP	in operation
21.	Downstream Poneasca and Gura Golumbului Dam	9	Ruieni HPP	in operation
22.	Downstream Gura Apelor Dam	9	SH Hateg	in operation
23.	Downstream Oasa and Cugir Dam	8	SH Sebes	in operation
24.	Downstream Izvorul Muntelui Dam—Neamt county	52	SH Bistrita	in operation
25.	Downstream Izvorul Muntelui Dam—Bacau county	48	SH Bistrita	in operation
26.	Downstream Izvorul Muntelui Dam—Vrancea county	51	SH Bistrita	in progress
27.	Downstream Izvorul Muntelui Dam—Galati Dam	39	SH Bistrita	in progress
28.	Downstream Izvorul Muntelui Dam—Braila county	36	SH Bistrita	in progress
29.	Downstream Rastolita Dam	17	Rastolita HPP	design phase
	Total no. of sirens	659		

*SH—Hydropower Subsidiary; *HPP—Hydropower plant.

Over 1999–2010, Hidroelectrica developed 20 alarm-warning systems and plans to further implement 8 new alarm systems.

6 CONCLUSIONS

The floods affecting many countries and the climate changes which have been increasingly felt in the last 10 years, as well as better involvement in what social responsibility involves, led to a new approach in addressing flood risk.

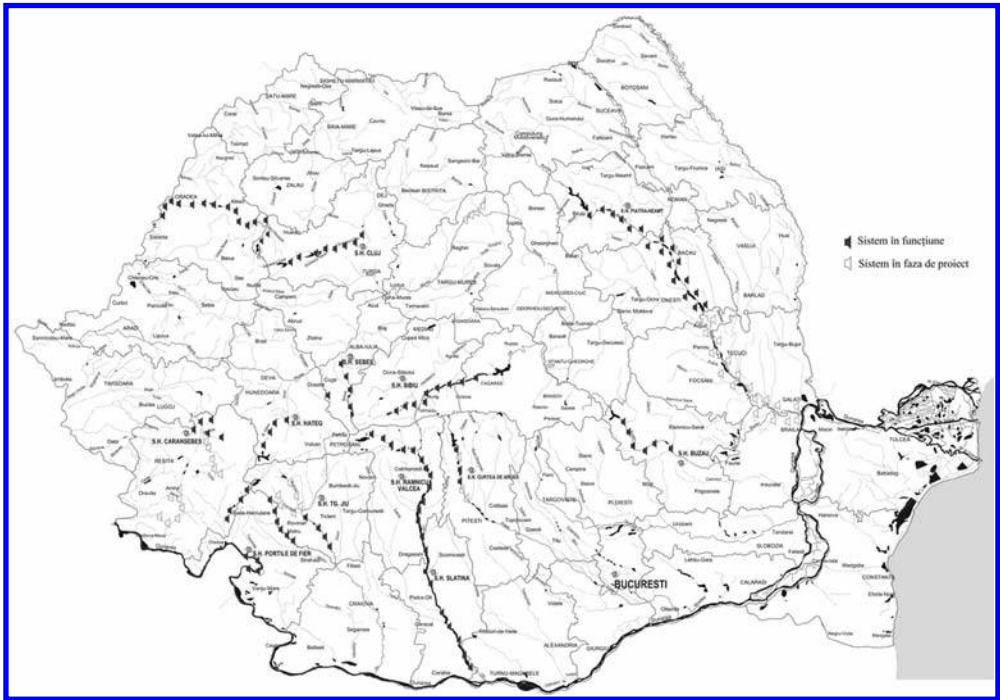


Figure 4. Alarm-warning systems developed by Hidroelectrica.

In Romania, the entity which administers a hydro-technical construction has the responsibility to draw up and submit, for approval, the protection against floods plans to the Ministerial Committee for Emergency Situations.

An important role in implementing a sound alarm system and determine the population and property evacuation areas and routes is assigned to the local Inspectorates for emergency situations; the owners and designers collaborate with these Inspectorates and obtain the required permits.

For an efficient alarm-warning system, that uses sirens and mobile devices, it is necessary to monitor the risk factors and, when the threshold is exceeded, transmit the data to the dispatch center located at the hydropower development, as well as interconnecting the dispatcher with the control centers of the local Inspectorates for Emergency Situations for joint management of risk situations.

As a conclusion, we believe that the flood risk management involves application of policies, procedures and practices with the aim to minimize and even eliminate the risks. Activities such as risk identification, analysis and evaluation, must be supported through a risk factors monitoring system and a flood protection plan.

REFERENCES

- Arnold V.I., *Metodele matematice ale mecanicii clasice*, Editura Științifică și Enciclopedică, Bucharest, 1980.
- Mauthe A., Hutchison D., Coulson G. & Namuye S., "Multimedia Group Communications Towards New Services", in *Distributed Systems Eng.*, vol. 3, no. 3, Sept. 1996, pp. 197–210.
- Soviany Cristina, *Embedding Data and Task Parallelism in Image Processing Applications*, PhD Thesis, Technische Universiteit Delft, 2003.

A risk based approach to dam safety management in New South Wales, Australia

P. Heinrichs

Dams Safety Committee, Sydney, NSW, Australia

ABSTRACT: The Dam Safety Committee (DSC) operates under the Australian New South Wales (NSW) Dams Safety Act 1978 to ensure the safety of dams. DSC prescribes dams whose failure could have significant effect on community interests particularly loss of life. A dam owner is responsible for the safety of a dam and must meet the DSC's requirements. An Owner must submit his conclusions on dam safety or proposals for safety improvements to the DSC for review. In 2006 the New South Wales Government endorsed the DSC's Risk Management Policy Framework for Dam Safety, which allowed the DSC to shift from the old standard based approach to a less prescriptive risk based approach. The DSC's new approach is goals-based regulation. Its requirements define the minimum level of safety that will adequately protect the community. A dam owner must keep the risks of a dam under review and demonstrate that risks are tolerable and As Low as Reasonably Practicable (ALARP). This eliminates the need for safety improvements with very low cost effectiveness.

1 INTRODUCTION TO DAMS SAFETY COMMITTEE

In the 1970's, international concern at failures of dams led to the Australian National Committee on Large Dams (ANCOLD) raising the need for dam safety regulation. Against this background, the NSW Government enacted the Dams Safety Act in 1978, and constituted the NSW Dams Safety Committee (DSC) under that Act in 1979.

The DSC consists of nine part-time members with eight experienced in dam engineering and the ninth in mining experience. The DSC is required to "formulate measures to ensure the safety of dams" in NSW. It "prescribes" those dams whose failure could threaten downstream life, cause extensive property or environmental damage, or have a severe impact on the public welfare. Currently there are 363 prescribed dams in NSW. The Committee adopts an ongoing "watchdog" role to ensure the owners of those dams conform to appropriate safety requirements throughout the life of those dams. This will ensure that the risks of uncontrolled loss of the storages, with consequent community and environmental effects, will be tolerably low. In this context, a "safe" dam is taken to be one that complies with the DSC's current requirements. Since the Committee's establishment, 47 deficient dams have been modified for safety improvement at a total cost of well over \$1 Aus Billion.

The DSC's approach to dam safety is goals-based, with its prime goal being that dams meet the DSC requirements set out in its guidance sheets. These goals include:

- Risks to community are identified, assessed and properly managed, reduced when necessary, and are kept under review through the life of a dam;
- Needed safety improvements are undertaken as soon as reasonably practicable.

It is the for dam owner to determine how he achieves these goals and to demonstrate to the DSC they have been achieved, or will be achieved following improvements in their dams or safety management practices.

Table 1. Consequence categories.

Population at Risk (PAR)	Severity of damage and loss			
	Negligible	Minor	Medium	Major
<1	Very Low	Very Low	Low	Significant
1 to 10	Low	Low	Significant	High C
10 to 100		Significant	High C	High B
100 to 1000			High A	High A
>1000				Extreme

2 DSC'S REQUIREMENTS

The DSC's requirements are based on the Consequence Category of the dam, which in turn is based on potential damage if the dam was to fail. The categories are evaluated on the Population at Risk and the level of damage from the matrix in [Table 1](#) below.

The Major requirements of the DSC are that all Extreme, High and Significant Consequence Category dams, along with Low Consequence Category dams over 15 m high, are prescribed under the Act.

For all prescribed dams the DSC requires Surveillance Reports after the first substantial filling (or one year after completion, whichever is first), and subsequently at intervals not exceeding five years. The type and content of report depends on the dam's Consequence Category above. These reports provide the DSC the necessary data on prescribed dams. Also, through regular DSC inspections, and discussions with dam owners, communication lines are developed and maintained.

Safety Reviews are required at regular intervals or where Surveillance Reports indicate a dam may be unsafe. They provide a vital input for any decisions on remedial measures and involve a conclusive reassessment of dam safety using the latest methodologies and information.

3 DAM OWNER REQUIREMENTS

The DSC also obtains its basic information through a series of requests sent out to dam owners at various stages in the development of a dam. For new dams, the DSC's initial objective is to ensure that they are designed and constructed according to appropriate engineering standards and safety criteria. Thus, owners and designers must provide details of proposed dams for the DSC's consideration at an early stage. After construction, dam safety is monitored by owners arranging for:

- Proper operation and maintenance of their dams by trained personnel
- Regular surveillance by trained personnel and annual inspections by a dams Engineer
- Dam safety emergency plans for dams whose failure could cause loss of life;
- Ongoing assessment of dam behaviour on the basis of surveillance information
- Periodic review of the dam's compliance with current DSC requirements
- Review of all dam information and assessments by experienced personnel
- Actions, in response to dam assessments, to ensure the dams are safe

Given that the safety of a dam is affected by many variables (e.g. changes in downstream development, new assessment methods and criteria) the DSC will not "sign-off" on a dam's safety but will judge whether a dam meets current safety criteria. However, if the DSC considers a dam is unsafe, or may become unsafe, it may give notice, under S.18 of the Dams Safety Act 1978, (and if necessary seek an injunction) requiring the dam owner to take such actions as necessary to ensure the dam's safety.

4 DSC RISK MANAGEMENT FRAMEWORK

Until the early 21st century the DSC had taken a ‘Standards-based’ (SBA) approach to dam safety, wherein risks to dams were controlled by following established design, loading, and event rules and which ensures the risk of dam failure is very low. However, this changed in 2006 when the NSW Government signed-off on the Risk Management Policy Framework for Dam Safety, which shifted the focus to a ‘risk-based’ approach.

4.1 *The DSC normal safety requirements*

The DSC’s normal safety level requirements or “starting points” are those levels of safety derived from the “Standards Based Approach (SBA)”. If a dam satisfies the SBA it will be generally acceptable to the DSC. The SBA is the conservative (safer) end of any ANCOLD range. For dams where the SBA starting point is not complied with the DSC requires compliance with its DSC Public Safety Guidelines.

4.1.1 *Flood capacity for dams*

Under the SBA if a dam complies with the requirements of [Table 2](#) below it will generally satisfy the DSC. However, if it does not comply the owner must demonstrate compliance with the Public Safety Guidelines.

4.1.2 *DSC public safety guidelines*

4.1.2.1 *Risk to the individual*

Where the adequacy of safety is judged on the DSC public safety risk Guidelines, the DSC requirement for the long-term is that risk to the individual be below the limit of tolerability to the extent dictated by the ALARP (As Low As Reasonably Practical) principle.

For existing dams, the DSC’s limit of tolerability is 1 in 10,000 per annum. For proposed dams and major augmentations, the DSC’s limit of tolerability is 1 in 100,000 per annum. For all dams and major augmentations, the DSC’s negligible risk is 1 in 1,000,000 per annum. The DSC regards this negligible level of risk as so low that it is not worth searching for further reduction.

4.1.2.2 *Societal risk*

Where safety is judged on the DSC public safety risk guidelines, the DSC requirement for the long- term is that societal risk be below the limit of tolerability shown at [Figure 1](#) as

Table 2. Starting point Acceptable Flood Capacity (AFC).

FCC rating	Flood or AEP
Extreme	Probable Maximum Flood, (PMF), (reservoir full)
High A	Probable Maximum Precipitation Design Flood, (PMPDF) (reservoir full)
High B	Max of AEP (Annual Exceedance Probability) of PMPDF, or 10^{-6} not necessary to use PMP Design Flood, as PMPDF was used in the previous row for HIGH A
High C	Max of AEP of PMPDF, or 10^{-5}
Significant	10^{-4}
Low	10^{-2} to 10^{-3}
Very Low	No requirements

Note: PMPDF is an abbreviation of Probable Maximum Precipitation Design Flood which is derived by applying the Probable Maximum Precipitation (PMP) to the catchment with the storage and catchment at statistically average conditions, that is The PMPDF (flood) has the same Annual Exceedance Probability as the PMP (rainfall) and may be up to an order of magnitude less than the PMF.

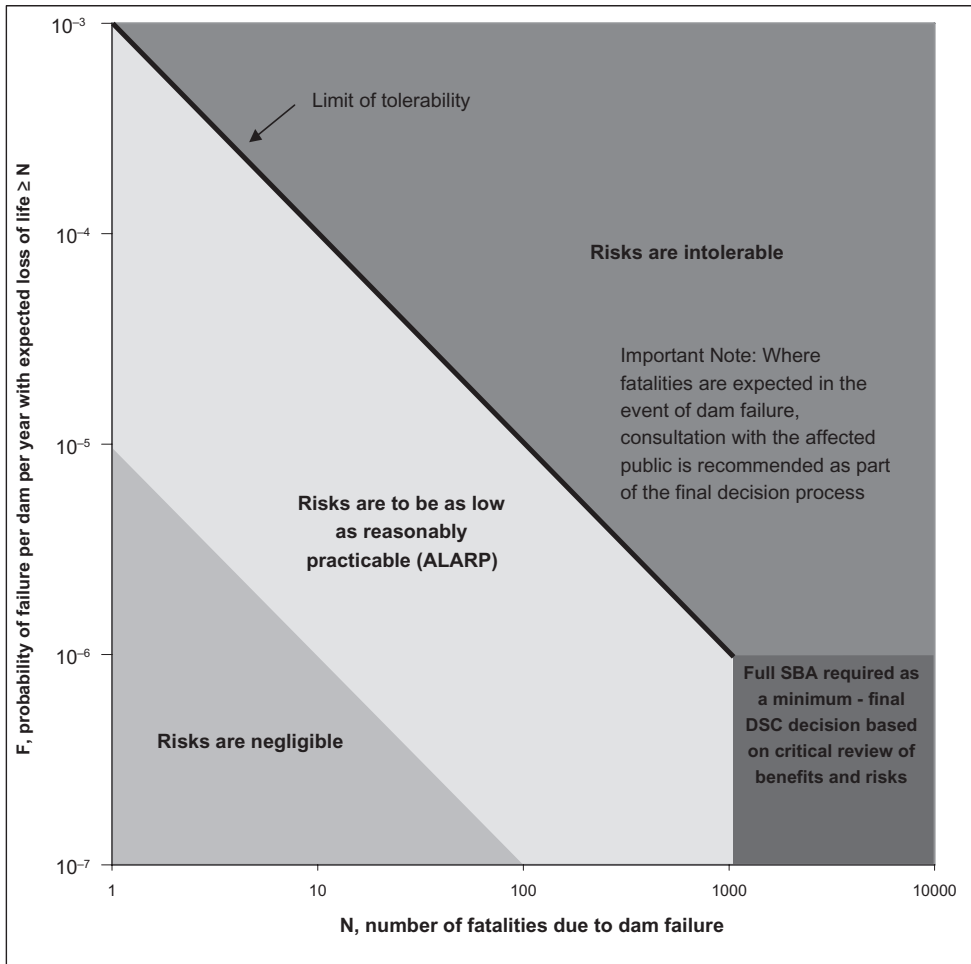


Figure 1. DSC societal risk requirements: existing dams.

dictated by the ALARP principle. For societal risk, the DSC has adopted a negligible level, two orders lower than the limit of tolerability. The DSC regards the negligible level of risk as acceptably low.

Where the societal risk from dam failure is within the intolerable region the risks are intolerable in nearly all circumstances. Within the intolerable region, the higher the risk plots on the graph and the further to the right, the more difficult it would be for an owner to persuade the DSC that the benefits of the dam justify acceptance of the risks.

The DSC requires owners to demonstrate that risks to the individual and societal risk are ALARP. The DSC will judge the owner's case for ALARP on:

- The disproportion between the sacrifice (money, time, trouble and effort) in making the safety improvement and the risk reduction that is achieved
- The level of risk in relation to the limit of tolerability and the negligible risk
- The cost-effectiveness of safety improvements, one indicator is Cost to Save a Statistical Life(CSSL)
- Any relevant recognized good practice; and
- Societal concerns revealed by the owner's consultation with the community
- To justify a progressive improvement or the need for a staged upgrade program.

Table 3. Progressive improvement of safety.

Stage	Aims	Indicative timeframe for completion of safety improvements
Short-term or Interim	<ul style="list-style-type: none"> To maximize safety, in a cost-effective manner, whilst planning proceeds for the later stages of improvements. 	<ul style="list-style-type: none"> For a structural fix- as soon as reasonably practicable, but generally not longer than 2 years. Program to be agreed with DSC For a non—structural fix, such as operating restrictions, warning and evacuation plans—as soon as reasonably practicable, but generally not longer than 1 year. Program to be agreed with DSC
Medium-term	<ul style="list-style-type: none"> To reach a low but not ultimate level of risk To reach risk levels below the limit of tolerability 	<ul style="list-style-type: none"> As soon as reasonably practicable, but generally not longer than 10 years. Program to be agreed with DSC
Long-term	<ul style="list-style-type: none"> To satisfy the DSC starting point deterministic safety level To have risks below the limit of tolerability to the extent required by the ALARP principle To satisfy national and international practice, if appropriate 	<ul style="list-style-type: none"> As soon as reasonably practicable, but generally not longer than 20 years. Program to be agreed with DSC

5 MEETING DAM SAFETY REQUIREMENTS

A dam owner may use risk assessment to support submissions to the DSC on dam safety. In undertaking risk assessment owners are to follow the ANCOLD Guidelines on Risk Assessment, October 2003. Situations where a need for risk assessment could arise are

- To review the risks to, or posed by, a dam
- To better clarify the safety status of a dam, especially where the SBA provided no or limited guidance (e.g. piping risk)
- Where there is doubt that the DSC’s starting point SBA will meet the DSC public safety risk guidelines;
- To justify a shift from the DSC normal level of safety, subject to DSC agreement;

A dam owner is to bring risks into compliance with the DSC’s safety requirements as soon as reasonably practicable, is to keep the residual risks under review and is to maintain risks as low as reasonably practicable over time, having regard to future technology, scientific knowledge, and other relevant considerations of the day.

Safety improvements required by the DSC may be implemented progressively where that would promote more effective risk reduction for the community as regards risks from dams, but in such cases progressive implementation is subject to DSC review. For guidance on acceptable progressive improved to a deficient dams’ safety an owner may refer to [Table 3](#) below. The DSC also requires the dam owner consult with the community and other stakeholders as input to decision-making on significant dam safety matters.

6 DEMONSTRATION OF SAFETY

The process of demonstrating a dam’s safety starts with submission of a 5-year Surveillance report which assesses if the dam meets the DSC requirements or does not meet the requirements, or the safety status is uncertain. In the later two cases, or if the dam is older than

15 years in its present state, a safety review will be required. The safety review covers the scenarios of all hazards, load states and failure modes on a risk based approach for comparison with the DSC's public safety risk guidelines.

Any safety review prepared for the DSC for Extreme or High Consequence category dam, must have an independent peer review. The peer reviewer must be a senior practitioner widely recognised for their knowledge and experience with the particular dam safety issues. In a safety review, if the dam meets compliance with the Standards Based Approach or any other recognised standard or good practice, including the starting point fall back flood capacity, this provides adequate demonstration of the dam's long term safety.

6.1 *Failure modes analysis*

A failure modes analysis is an essential part of a safety review and involves:

- Listing all elements of a dam, whose failure to function could affect its safety
- Listing all ways in which the element may fail to function as intended
- Rating the likelihood that the element will fail to function as intended
- Rating the consequences for the safety of the dam if the element fails to function
- Then build up the failure mechanisms using logic systems such as event or fault trees
- Decide which failure modes are plausible to require analysis

6.2 *Risk assessment*

A Risk assessment is required by DSC where there are aspects not adequately addressed by traditional standards or good practice or where an owner wishes to demonstrate that less costly safety improvements, than those required by standards or good practice, would adequately protect public safety. For the risk assessment the failure consequences are estimated in terms of Potential Loss of Life (PLL) determined based on the results of a dambreak analysis. The estimation of failure probability must comply with mathematics of probability and individual probabilities are to be assessed, challenged, debated and those reasoning in support of the estimated risks are to be documented.

When the risks analysis is complete the total estimated risk and the PLL are entered into [Figure 1](#) and if the best estimate of societal risk is in the negligible region DSC is satisfied. If the best estimate of societal risk is in the intolerable region the DSC requires the societal risk be reduced as soon as reasonably practicable in a short-term, and/or medium-term improvement to at least the limit of tolerability. If the best estimate of societal risk is in the region of tolerability review the DSC requires the risk to be reduced to the negligible level on a program agreed with the DSC unless the owner can demonstrate that a higher risk is tolerable. To be tolerable, the risk must be ALARP. The urgency for improvement is significantly lower than for risks in the intolerable region. Without improvement, or a demonstration that the existing risk is tolerable, the dam does not meet DSC requirements.

If the best estimate of societal risk is lower than the limit of tolerability and the estimated loss of life exceeds 1000—the DSC requirement is that, the dam complies with all relevant standards—including PMF capacity, and with currently recognized defensive design measures. If improvement is needed it is to be made as soon as reasonably practicable. Without compliance the dam does not meet DSC requirements.

When a dam falls below the DSC's requirements the owner must demonstrate that his recommended options for upgrading the dam has reduced the risk to tolerable levels either in a staged approach or in a single upgrade as per [Table 3](#) above.

7 CONCLUSIONS

As a result of the State Government's approval of the new Policy of Risk Based approach to dam safety, there are small additional costs to dam owners and the DSC, but implementing

risk-based safety policies is more cost-effective and will deliver a greater overall reduction in risks to life, property and community interests.

The Benefits of this new risk-based approach include:

- A less prescriptive, more flexible, holistic goals-based approach to dam safety
- A more consistent relationship of dam safety levels to dam failure consequences;
- A greater emphasis on dam owner responsibility for dam safety;
- The introduction of a concept of progressive improvement of dam safety to better apply the available resources to reducing risks to the community

Finally it ensures the elimination of safety improvements with very low cost-effectiveness through the adoption of less stringent requirements for the flood capacity of dams that threaten small populations of less than 1000 people. This frees-up resources to address intolerable risks on other dams, whilst still retaining an almost negligible risk of failure in line with levels accepted for facilities such as Airports, nuclear reactors and petrochemical plants.

ACKNOWLEDGEMENT

The author wishes to acknowledge the assistance of the Dams Safety Committee and in particular the Chairman of the Committee Mr. Brian Cooper in the preparation of the paper and for its permission to prepare this paper.

REFERENCES

- Dams Safety Committee, 2010, Acceptable Flood Capacity for Dams, DSC 3B.
- Dams Safety Committee, 2010, Background to DSC Risk Policy Context DSC 1B.
- Dams Safety Committee, 2010, Demonstration of Safety for Dams, DSC 2D.
- Dams Safety Committee, 2010, DSC Background Functions and Operations DSC1A.

Dam safety in Slovakia

P. Panenka & A. Kasana

Vodohospodárska výstavba š.p., Bratislava, Slovakia

ABSTRACT: System of technical and safety supervision of water works in Slovakia has been well established for decades. This system is based on legal preconditions and long-term experience and defines duties and responsibilities of designers, builders, owners and operators of water works. Already within the preparation of water work it is classified into one of four categories based on the amount of potential property damages and/or personnel casualties caused by their destruction or dysfunction. All types of water works are categorized. Category is determined by the Ministry of environment, which also authorizes the only state organization to execute technical and safety supervision over most relevant water works (Ist and IInd category—these are on the ICOLD list of Slovak dams, too). State enterprise Vodohospodárska výstavba, š.p. (Watermanagement construction s.e.) which has to employ experts with qualification for technical and safety supervision has been authorized organization since 1978.

1 INTRODUCTION

Ministry of Environment of the Slovak Republic is responsible for the legislative frame of the system, which has to provide safety of waterworks in Slovakia. Waterworks—water constructions are defined as all constructions which could cause impoundment or retention of water. It means especially dams, weirs, small dams and ponds, flood dikes and polders, lock chambers, hydropower plants and tailing dams, too. Professional technical and safety supervision of water work is a professional activity aimed at early detection of its safety threats. Supervision is based on measurements and monitoring, concurrently warns in advance risks of failures or crashes and proposes the necessary steps to remedy.

The Act Nr. 364/2004 Coll. of Law (Water Act) and Gov. Decree Nr. 458/2005 Coll. Of Law (Decree On Professional Technical and Safety Supervision on Water Constructions) are the basic documents governing duties and responsibilities of designers, builders, owners and operators of water works. They define notably:

- Owner or operator of water structure is responsible of its safety (investor or builder is responsible during its construction or reconstruction).
- Investor of the water work has the duty to order the professional review for categorization of the construction already during its preparation. This review contains all potential threats and possible damages of the construction breakdown.
- Category of every water construction is determined by the Ministry of Environment of the Slovak Republic.
- Every owner or builder of any water work is responsible for providing technical and safety supervision on his own costs.
- Owner of water construction has to employ person with qualification for technical and safety supervision for supervision providing or in the case of 1st or 2nd category water works to ensure supervision by the authorized state owned organization.
- Conditions for certification of qualified person for technical and safety supervision.

2 STATE OWNED ORGANIZATION AUTHORIZED FOR PROVIDING TECHNICAL AND SAFETY SUPERVISION

Since 1978 Watermanagement construction s.e. has been state owned organization authorized for providing technical and safety supervision on all 1st and 2nd category water works in accordance with the Water Act. The founder of this state enterprise is the Ministry of Environment of Slovak Republic. Watermanagement construction s.e. is an organization that was public investor of almost all large dams, hydro power stations and weirs constructed in Slovakia after World War II. Section of technical and safety supervision (TSS) was built continually and today it consists of four departments: TSS and operating dispatching, Supervision on tailing dams and special analyses, Geodetical measuring and last but not least Geomonitoring.

Primary role of the TSS section consists of periodic data capture from measuring on water structures, their processing and archiving, evaluating and interpreting of water structure owner's monthly reports. Another operation is performing of control measuring and special analyses, mainly geodetic measurements, videoscropy of boreholes and drainage, pump and slug tests, measuring of leakage and seepage, geophysical survey, logging conductometry and thermometry, surficial geophysical measurements of resistivity and induced polarization, analyses of silt content and turbidity, non-destructive defectoscopy on technological equipment and terrestrial laser scanning. Results are used in stability reviews, assessment of limit and critical values and complete surveys of technical and safety state of water construction.

Special task of the authorized organization is preparing reviews for the categorization of water structures.

3 RISK FACTORS AND CATEGORIZATION OF WATER CONSTRUCTIONS

Every water construction is classified into one of four categories based on the amount of potential property damages and/or personnel casualties caused by their destruction or dysfunction. All types of water works are categorized. Reviews for the categorization contain a proposal for the category of water structure and inventory compliance with the categorization criteria. Category is determined by the Ministry of environment. The categorization is based



Figure 1. Pumping hydropower station Čierny Váh—3D laser scanning of asphalt-concrete surface of upper reservoir.

on an estimation of the risk factor implied by the existence of water structure. Together with generated benefits water works also cause the danger for the area under it. Danger arising from the existence of water structure, especially the threat of dam failure and release of its potential energy and also impaired technical condition of water structure in terms of safety increase the possibility of its failure.

Estimation of the risk factor is the sum of all direct and consequential damages and losses, including human life, which could occur in a water structure crash with maximal volume of reservoir. The level of the potential danger depends on population density, economic and industrial estates in the land affected by water structure and its economic importance.

Categorization solves the following main tasks:

- Rate risk based upon the type and size of water construction,
- Definition of the threatened area, depending on its morphology,
- Estimation of direct and indirect damage,
- Economic value to assess the damage and losses of the benefits,
- Determination of benefit loss on the disposal of water works operation,
- Standard procedure for assessing damage caused by pollution of surface water and ground-water and agricultural land, in case of tailing dams breakdown.

4 SYSTEM OF TECHNICAL AND SAFETY SUPERVISION OF WATER WORKS IN SLOVAKIA

Performance of technical and safety supervision to monitor and evaluate the appropriate category on the water structure and its technical condition, in particular:

- Static and dynamic stability of water structure or its parts, including weirs and technological parts,
- Spatial changes in water structure as a whole against its surroundings,
- Deformation of subsoil and water structure itself, a mutual shift and deformations of individual parts of structures and cracks in structural materials,
- Physical and mechanical characteristics of construction materials and subsoil materials and the properties of waste disposal affecting the stability and safety of tailing dams,
- Mode of groundwater, surface water and leakage, particularly the water pressure, seepage connection, direction and velocity of water, partial and total amount of leakage, water spring up in the area of water structure and its surroundings,
- The functionality of protective, sealing, filtration and drainage elements of water structure and its subsoil, hydraulic gradient in structural and subsoil materials and filter stability,
- Environmental influences on the technical condition of water structure and its technological equipment, especially the effects of weather (frost and surge), on reservoir banks, landslides and slips in the vicinity of water structure, aggressive effects of air and water in the aquifer, the impact of groundwater and leakage, effects of construction work around the water structure, earthquakes, undermining, the effects of operating vibration, road shock, vegetation and animals, and unauthorized intervention of third parties,
- The impact of operation on the technical condition of water structure and its technological equipment, especially the effects of water manipulation in the reservoir, mechanical and other effects of the discharged water and drifting materials, wear and possible consequences of failure and closure structures of weirs, overflow and locks,
- Flow conditions of outlet equipment and facilities in comparison with the original forecasts considered in project design, for example, the flow at the upper watercourse affected with new constructions, failure or abolition of the existing constructions, change of drainage situation in river basins, vegetation and crossing of ice roadblock.

Supervision is carried out especially by monitoring the above events and facts and data processing on them, but also analyzing and evaluating the results of all observations and measurements in relation to determine the limits and critical values, as well as conditions in the approved project.



Figure 2. Liptovská Mara Dam—technical and safety supervision found a lack of efficacy of the injection sealing curtain, subsequently bedrock was sealed.



Figure 3. Rockfill Dam Ružín I, where was inadequate capacity of safety spillway found, subsequently side safety spillway with bypass tunnel was built.

The range of supervision for prepared water works is specified already before building permit is issued and then the Project of measurements follows. It means at the stage of preparation already. On this basis the supervision is performed during construction of water works, especially measuring equipment is installed to assess the actual measurements. The period of construction or reconstruction of the water work is reviewed by qualified expert in partial or total reviews—depending on length of construction time.

After completion of the construction and evaluation of supervision during this period the water work is put into the verification operation. Verification operation of water structure starts with the first tension of water structure with impoundment of water and includes



Figure 4. Lock chamber of Waterwork Gabčíkovo—inspection and repairing of dilatation.

operational situations in the range that could affirm expectations in the approved project and safety and reliable function of water structure. Later the period of permanent performance follows—by tailing dams after deposition and the construction phase begins long-term existence of a tailing dam. Also in this period the reviews from technical and safety supervision periodically (mostly annually) are issued. Every review contains description of water work, her history, list of measuring equipment, list of monitored phenomenon with its awaited limits and critical limits, summary of measuring results during reviewed period, special analysis, resultant survey and remedy proposition (if needed). Reviews are sent to owners and local authorities. Authorized organization issues Informative report about a state of technical safety of most relevant water works in Slovakia (1st and 2nd category). This report is presented to Ministry of Environment twice a year.

5 FEW NOTES ABOUT MONITORING RESULTS

5.1 *Dam Ružín I*

Construction: 1963–1968 Length of the dam crest: 350 m Volume of reservoir:
59 mil · m³

Height of dam above the terrain/above the foundations: 57 m/63 m

Purpose: water supply, hydropower production, regulation of discharges, flood protection, recreation

The hydraulic structure Ružín I was built on the river Hornád. The rock subsoil, created by cracked granodiorite that is effloresced on the surface and by layers of mylonite, is sealed by a grout curtain. The depth of the curtain varies from 25 to 30 metres. An important asset of the dam is in its use of the hydropotential of the water. The evaluation of hydrological data confirmed that in operation the discharges of Q_{100} were increased from 500 to 655 m³ · s⁻¹ and Q_{1000} from 700 to 890 m³ · s⁻¹. That was the reason why an additional uncontrolled side spillway and bypass gallery with a capacity of 125 m³ · s⁻¹ were built (1991–1993). The tunnel has length 446 m and diameter 4,0 m. After floods in 2010 we could state, that thanks increased capacity of safety spillway did not come to breakdown—operational volume of reservoir was exceeded.



Figure 5. Additional uncontrolled side spillway and its use during floods in 2010.

5.2 Dam Liptovská Mara

Construction: 1967–1975 Length of the dam crest: 1225 m Volume of reservoir: 361.9 mil · m³

Height of dam above the terrain/above the foundations: 45 m/52.5 m

Purpose: hydropower production, flood protection, regulation of discharges, recreation, fish breeding

Liptovská Mara Reservoir is the largest Slovak reservoir. In the profile of the dam, in the right bank of the valley, the Vlačiansky landslide can be found and approximately 200 m far from the dam, the Veľkomarský landslide is located. Both landslides have been subject to continuous observation since the beginning of the preparation of dam construction and during the operation various measuring and treatments have been done, especially geodetical positional a vertical measuring, surveillance on amount of water from horizontal drains and measuring in inclinometer bore-hole.

6 CONCLUSIONS

Every owner or builder of any water work is responsible for providing of technical and safety supervision on his own costs, i.e. notably arranging of measuring equipments, providing measuring and sending its results to authorized organization (for 1st and 2nd category) for analysis monthly at least. Authorized organization has no right to realize its remedy proposals and therefore is not responsible for damages caused with false operating or breakdown of water work, but its main responsibility is to warn in time—not only owner but local authority and Ministry of Environment, too.

Although first efforts of permanent monitoring and analyzing of technical safety of dams began in beginning of 20th century in former Czechoslovakia, first legislative norms were not approved until seventieth. The current system of technical and safety supervision used in the Slovak Republic has a number of shared elements of the system used in the Czech Republic (these systems evolved together from 1975 to 1992). The major difference is that in Slovakia the activity of authorized organization remained in state hands and only in within one organization. Thanks to this the dam safety has priority over commercial profit for the

supervision performance and all historical and present data are archived at state's disposal. The level of supervision on 1st and 2nd category hydraulic structures is almost identical in both countries, but in Slovakia is unlike Czech significantly less small dams and performance of technical and safety supervision could focus more on safety of protective dikes.

Although the surveillance system in Slovakia is functional and successful, it has several minor deficiencies which will be removed in the coming years:

- Increase the level of supervision and state water authorities over the safety of 3rd and 4th category water works.
- Increase the number of professionally qualified persons for the performance of technical and safety supervision.

The accurate coordination of technical and safety supervision between owners, authorized organization and local authorities or Ministry of Environment is not a single gain of this system. There was no serious crash, breakdown or accident on 1st and 2nd category water works in Slovakia during 35 years of legally performed technical and safety supervision.

REFERENCES

- Bednárová, E. et al. 2010. Dam construction in Slovakia. Originalities. Milestones. Attractions. Bratislava: Kuskus.
- Bednárová, E. & Minárik, M. 2007. Grouting Curtains in the Subsoil of Dams. Water Management and Hydraulic Engineering; Proc. 10th intern. symp., Šibenik, 4.–9.9.2007. Zagreb: National and University Library.
- Kopecký, M. & Antolová, D. 2010. Návrh komplexného monitoringu zosuvov na pravostrannom zaviazaní hrádze VS Liptovská Mara; Proc.: Medzinárodná odborná konferencia o bezpečnosti vodných stavieb, Bratislava, 12.–14.10.2010. Bratislava: Vodohospodárska výstavba š.p.

Improvement of safety of Swiss dams on the basis of experience

H. Pougatsch, R.W. Müller, T. Sonderegger & A. Kobelt

Civil Engineers ETH, Former Dam Safety Officials, Switzerland

ABSTRACT: Besides appropriate design and construction, an efficient monitoring system is a key element of dam safety. Measurements and visual inspections are an important means to detect any unusual behaviour or condition of a dam and, in such a case, to take proper action. This paper presents some interesting cases that led to a substantial improvement of the dam surveillance system in Switzerland and confirmed the importance of continuous monitoring, particularly the necessity for regular visual inspections.

1 INTRODUCTION

Starting in the middle of the 20th century, Switzerland experienced a remarkable development in dam construction due to a growing need for electric power. A large number of hydropower plants were built and Swiss engineers acquired considerable expertise in the design, construction and surveillance of dams. The authors of this paper want to point out the positive results of an effective surveillance of dams on the basis of some well-known and documented events. The presented cases encompass effects of abnormal foundation behaviour, the ageing processes, stability questions, as well as extreme floods. Some improvements are also described.

2 UPLIFT, SEEPAGE AND DRAINAGE

2.1 *Foundation and seepage*

The 115 m high Albigna hollow gravity dam was built between 1957 and 1959. The reservoir, with a capacity of 71 hm³, had been operated for nearly 20 years without problem, when in 1977 several springs appeared from rock joints on the left side of the valley, some distance downstream of the dam. Additionally, seepage discharge increased in the hollow joints of the dam. This continuously increasing discharge originated from the reservoir.

Investigations and inspections of the upstream dam foundation revealed that a crack in the rock ran almost parallel to the heel of the dam. Deformations of the foundation rock were detected and measured using a sliding micrometer. This continuous extensometer revealed a second fissure, found somewhat upstream from the first crack. The cyclic opening of the first and active crack was approximately 8 mm for a reservoir fluctuation of around 100 m (Fig. 1). Additional rock extensometers were installed to determine precisely the position and extension of the crack and to monitor its movements. Piezometer measurements to a depth of 60 m below foundation level complemented the investigation and surveillance instrumentation (Kovari & Peter 1983).

Measurements and analytical investigations suggested that the initial crack in the rock at the upstream heel of the dam dated from the first filling, when a slight downstream deformation of the dam was observed. With time, the crack depth propagated to about 40 m. Once the crack had crossed the grout curtain, seepage from the reservoir was able percolate through the rock and emerge as downstream springs (Bossoney & Balissat 2005).

The area of the crack in the rock surface and at the heel of the dam was protected by means of a seal membrane. The problem was the bridging of the crack in regard to its active

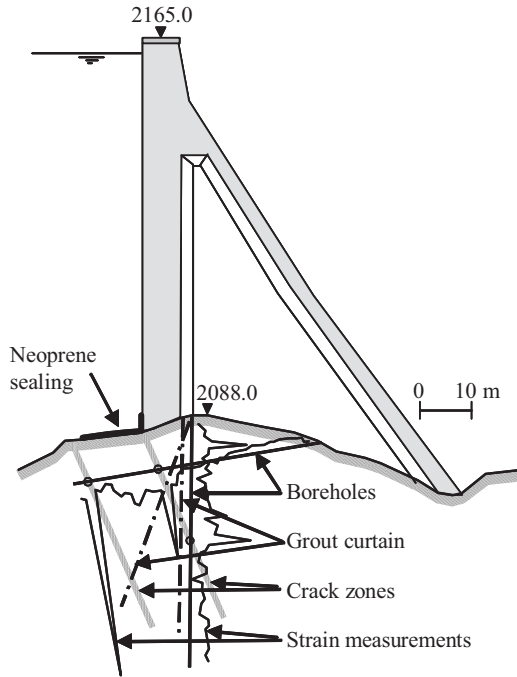


Figure 1. Albigna hollow gravity dam cross section. Foundation investigations and position of the fissure zones and the neoprene sealing.

condition and the high prevailing hydrostatic pressure. The solution consisted in the sealing of the zone close to the upstream heel of the dam by means of a stretchable neoprene membrane. Additionally, a series of boreholes were drilled to drain the foundation rock, and particularly the active crack. Nearly 30 years later, the behaviour of the dam still remains satisfactory and the measures taken proved to be appropriate.

2.2 Large-scale drainage of a rock mass

At the beginning of December 1978, the regular control measurements of the pendulums of the 156 m high Zeuzier arch dam indicated that the deformations were obviously different from those previously observed for elastic behaviour of the structure. The dam crest began moving upstream, even though the reservoir was nearly full. The results of the geodetic deformation measurements carried out in spring 1979 indicated large settlements and movements of the crown cantilever in upstream direction as well as a narrowing of the abutments. As a consequence of these deformations, opening of vertical joints in the upper part of the upstream face and the development of perimetral cracks on the downstream face were observed (Fig. 2). To gain more information, numerous special measuring instruments were installed in the foundation and the geodetic network was substantially extended. In addition, measurement frequency was increased. Further, several hypotheses (tectonic, seismic, hydrogeologic) were formulated. Analysis of the extended geodetic measurements revealed that the unusual dam deformations were the result of a general settlement of the ground, with a lateral extension in the order of 2 to 3 km. The drainage of the rock mass caused by the excavation of an exploration adit was the origin of the ground settlements. During the excavation of this adit, a number of considerable water inrushes (up to 1000 l/s) were observed, and settlements started immediately after such inrushes. There was a close coincidence between the exceeding deformations of the dam and the volume of drainage water resulting from tunneling. The development of a mathematical model to analyse the behaviour of a fissured, elastic

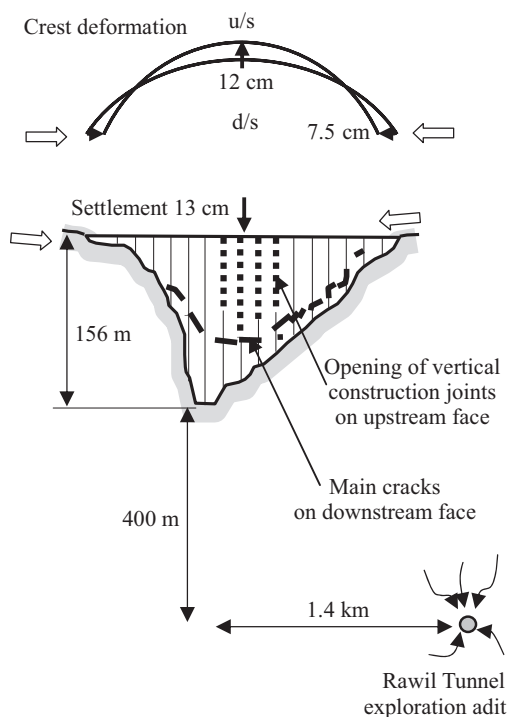


Figure 2. Zeuzier arch dam. Deformations due to drainage induced settlements of the rock mass caused by excavation of an exploration adit.

and saturated rock massif (“FES model”) clearly proved that the drilling of the exploration adit was the cause of the ground settlements (Lombardi 1992).

The case of Zeuzier clearly underlines the importance of having a continuous surveillance, using a widespread monitoring system and performing immediate analysis of the acquired data. Furthermore, geodetic measurements were the essential means of explaining the deformation at Zeuzier Dam (Biedermann et al. 1982, Pougatsch 1990).

Underground works (galleries, tunnels, caverns) can influence the hydrogeologic conditions by draining extended rock zones. Consequently, if such works are planned within a distance of 3 to 4 km of a dam, preventive measures (improvement of monitoring system, increase of measurement frequency) must be taken. Therefore, such measures were recently taken in connection with the excavation of the new Lötshberg and Gotthard Alpine railway tunnels in Switzerland, which were constructed in the vicinity of several large arch dams. In these cases, deformations could be controlled and kept well below critical limits (Pougatsch & Müller 2002).

3 SWELLING

3.1 Identifying swelling of concrete

Illsee Dam has been constructed in two stages in 1926–27 and 1941–43 and consists of an arch dam and an adjacent gravity dam with an angled crest line (Fig. 3). Due to seepage through the porous concrete, various sealing works were carried out between 1932 and 1966. Geodetic deformation measurements, performed since 1946, revealed strange permanent deformations characterized by an upstream displacement of the arch dam and a downstream displacement of the gravity dam. In view of these surprising results, the stability of the geodetic survey points was initially drawn into question. In connection with a periodical safety assessment performed later on, the hypothesis of concrete swelling was proposed.

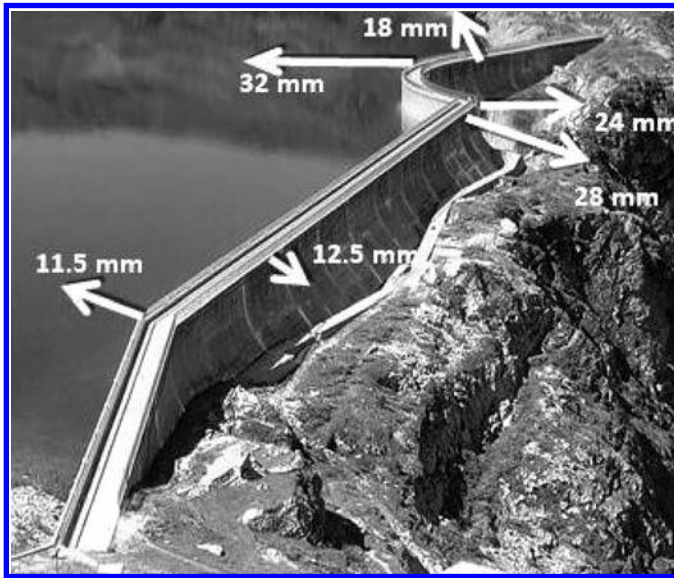


Figure 3. Illsee Dam. Permanent displacements measured by geodetic survey.

Subsequent petrographic and chemical analyses confirmed the existence of swelling due to alkali-aggregate reaction. Illsee Dam was the first case where a specific and comprehensive study of concrete swelling was carried out in Switzerland (Sinniger et al. 1991).

3.2 *Consequences of swelling*

Swelling is a slow chemical process developing in the concrete, which is driven by water and produces irreversible displacements of the structure. This phenomenon has a negative impact on the mechanical properties of the concrete. Vertical deformations give an initial, but insufficient indication of swelling. To unequivocally identify swelling, an adequate monitoring system is required; the one installed at Illsee Dam has been significantly enhanced. Generally, a rather long measurement period is necessary. Additionally, in situ and laboratory tests must be executed. Swelling further produces well marked cracks or finely distributed superficial fissures. Therefore, visual inspection is also of paramount importance (CSB 1997).

3.3 *Remedial measures*

For dam construction, materials are generally taken from nearby borrow areas in order to keep hauling distance short and thereby save costs. When there is a risk of alkali-aggregate reaction fly-ash or pozzolan cement can be used to avoid future trouble. For example, concrete used for the Hongrin twin arch dams (constructed 1963–67, H = 125 m and 90 m) was made with pozzolan cement, whereas fly ash cement has been retained for the recent reconstruction of Serra Dam (first constructed 1952, H = 22 m).

There are also solutions for fighting the consequences rather than avoiding the causes, such as protection against humidity or releasing of stresses by sawing the concrete. At Illsee Dam a geomembrane has been placed on the entire upstream face to stop seepage and thereby slow down the swelling process. The attempt failed because of continued seepage through the dam foundation. However, with additional sealing works in the foundation, seepage could be reduced. The Lago Bianco reservoir has two gravity dams. At Lago Bianco South Dam (constructed 1912–14, heightened in 1942, H = 26 m) a sealing system consisting of several layers of a polyurethane coating has been applied (Rüesch & Scherrer 2001).

A more radical solution consists in partly or entirely demolishing the dam, depending on its size. In the case of Lago Bianco North Dam ($H = 15$ m) the upper part of the dam has been demolished and reconstructed. At Serra Dam the solution consisting in the construction of a new dam downstream was preferred.

4 MASS MOVEMENTS

4.1 Overview

Visual inspections including both the dam and the reservoir slopes are a matter of routine in the Alps, where landslides, rockfalls as well as snow and ice avalanches are frequent natural hazards. Such mass movements, when sliding into a reservoir, can generate surge waves of considerable height that can overtop the dam, causing a dam failure, and thus jeopardize the downstream riparian population. Recently, a report was published (Heller 2008) which is a useful tool for dam safety engineers to quantify mass movement generated impulse waves. It is well known that the filling and drawdown of reservoirs can trigger such mass movements.

4.2 Landslide, rockfall

In 1963, a mass of some 250 hm^3 started to move during the first filling of the reservoir of the Vajont arch dam (Italy). It slid into the reservoir, generating a huge surge wave which overtopped the dam and caused a large number of casualties. Following this catastrophe, geologists were engaged to undertake a complete slope stability analysis for the major Swiss reservoirs in operation at that time. Such examinations are now made within the framework of the periodic safety assessments. It is essential that the geologists establish reference files which include all pertinent geological documents. Periodically taken photographs may also prove very useful in identifying any morphological changes in the surrounding area of the reservoir.

Triggering of a new landslide or reactivation of an old one can be caused by a change in hydrogeologic conditions (snowmelt or infiltration of water). In two cases in Switzerland the staff of the dam operator discovered landslides during their inspection work, namely at Mauvoisin and at Godey reservoirs (Schenk 2006). Subsequently, monitoring systems (geodetic measurements, inclinometers in boreholes) were installed and are still in operation. After evaluating the potential danger in case of a slide into the reservoirs and establishing an emergency action plan, water level limitations have been imposed for as long as the active zones remain instable. In both mentioned cases, drainage systems were executed to improve stability.

4.3 Snow and ice avalanches

A large number of dams are located in the Swiss Alps, where the accumulation of snow can be considerable. The danger of avalanches sliding into a reservoir or over a dam must not be neglected. Therefore, several reservoirs in the Alps are subject to water level limitations during the winter to provide a storage reserve in case of such events.

The movements of the glaciers threatening reservoirs are observed by means of various methods (e.g. position measurements of benchmarks, or using terrestrial, photogrammetric, GPS or laser scanning methods). Complete filling of the reservoir is then only permitted once it is confirmed that such a glacier presents no danger of calving.

5 FLOODS

5.1 General

Floods are phenomena that can be severe and occur quickly. On a global scale, many dams are quoted in the literature that were seriously damaged by overtopping (damage at the crest, erosion of abutments, erosion at the downstream toe), which in some instances led to their collapse.

One must keep in mind that during a flood various incidents can occur: blockage of the dam access road, breakdown of power supply, blockage or clogging of spillways and outlets, flooding of power plant and service building. It is therefore essential that the dam operating personal is on site to watch closely the inflow and the water level of the reservoir, and take action whenever required.

Important floods are not rare in Switzerland, and several investigations were carried out to study their causes and their consequences. Numerous incidents were also observed, among which two are described in the following.

5.2 Consequences of heavy floods

5.2.1 Palagnedra 1978

During severe floods, important quantities of debris can be transported. During the 7/8 August 1978 flood in southern Switzerland, the openings of the spillway of Palagnedra arch gravity dam (constructed 1950–1952, $H = 72$ m) were clogged by a tremendous quantity of driftwood as [Figure 4](#) shows. To avoid recurrence of such a major incident, the spillway was modified and a new road bridge was constructed downstream ([Fig. 5](#)).

After the floods of 1978, the pertinent design criteria were revised in Switzerland. A systematic re-evaluation of the flood conditions of all dams was carried out and led to the modification of a number of dams to increase discharge capacities. Measures taken were modifications of spillways, the heightening of dam crests to increase freeboard height, or the construction of new orifices. In 1987 again, severe floods, many of them carrying high debris load, occurred in Switzerland. When a study was made of the cause of these floods and their transport of driftwood, it was found that the maximum length of floating tree trunks in Alpine rivers was about 10 m. Therefore, to avoid clogging, it was concluded that the width of spillway openings should not be less than 10 m.

5.2.2 Wichelsee 2005

The small Wichelsee barrage, consisting of a weir with contiguous left side embankment, impounds the Sarner Aa River, which drains the catchment of Lake Sarnen as well as its intermediate catchment ([Fig. 6](#)).

The weir is equipped with a low level outlet with a capacity of $110 \text{ m}^3/\text{s}$ and with a 12 m wide overflow vertical lift gate. In closed position the capacity of this lift gate amounts to $20 \text{ m}^3/\text{s}$ when the water level reaches the embankment crest level. The total capacity of the two outlets amounts to $130 \text{ m}^3/\text{s}$, which corresponds to the estimated design flood level. The same discharge capacity can also be reached by raising the lift gate by 1.9 m.

During the extreme storm of 22/23 August 2005, the reservoir level of Wichelsee increased rapidly, and in this situation the responsible staff decided to lift the main gate to get more spilling capacity. Unfortunately—and symptomatically for such conditions—power supply



Figure 4. Palagnedra Dam. Spillway clogged with debris during 1978 flood.



Figure 5. Bridge and piers were removed from spillway. New bridge constructed downstream.



Figure 6. Wichelsee Weir with (1) bottom outlet, (2) lift gate and (3) adjacent embankment dam after passage of the flood of 2005.

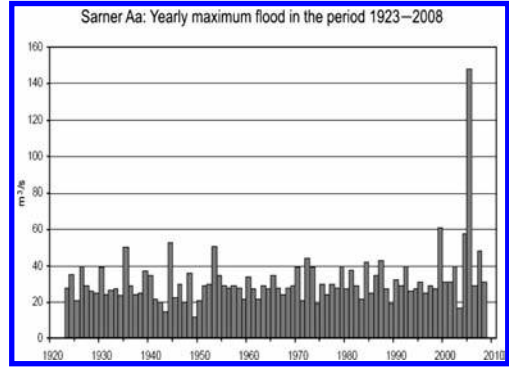


Figure 7. Maximum yearly flood of Sarner Aa River which flows into Wichelsee Reservoir.

failed during the flood, and an attempt to move the gate by manpower failed as well, due to mechanical blockage. As a consequence of this, the dam was overtopped, fortunately without severe damage.

The analysis of the flood showed that the Lake Sarnen peak outflow had been $150 \text{ m}^3/\text{s}$ in 2005, which is more than twice the maximum measured value in more than 80 years (Fig. 7). As a consequence and based on comprehensive hydrological studies, the design flood was recalculated and significantly increased. The new design flood is now $190 \text{ m}^3/\text{s}$ and the safety check flood has been increased to $290 \text{ m}^3/\text{s}$. Therefore, the embankment was equipped with an ancillary baffled chute spillway.

This event shows unambiguously that ungated spillways are safer than regulated ones in the event of extreme floods and should be preferred whenever possible. The determination of the design flood must be carried out taking into account the changes in behaviour of occasionally complex hydrological systems under extreme conditions, which are most likely due to climate change. In the case described above, the usual flood attenuation effect of Lake Sarnen failed due to extreme inflow.

6 CONCLUSIONS

Even after many years of satisfactory behaviour of a dam, unusual situations can occur at any time, and it is important to be able to detect quickly any abnormal behaviour and to look for the causes. Such abnormalities can consist of fast or slow increase of deformation, water pressure or seepage. Therefore, dam surveillance is a necessity and a permanent challenge, and must cover the dam body, its foundation and the surrounding area. The monitoring system is an essential element of the surveillance of dam behaviour, with special emphasis on visual inspections (CSB 2000, CSB 2006). Furthermore, immediate analysis of acquired data is strongly recommended.

It is advisable to periodically examine and, when required, adjust the current practice, taking into account experience gained from recent incidents. In some of the cases presented above, the monitoring system has had to be considerably extended, especially for the purpose of monitoring the behaviour of the foundation. As geodesy can play an important role to detect and explain the causes of widespread ground deformations, many existing geodetic networks have been significantly extended in recent years.

One must keep in mind that during a flood various incidents can occur, such as the breakdown of power supply or a mechanical blockage of gates or outlets. In such cases the presence of the dam surveillance staff is important to observe the situation on site and to take all action required. A visual inspection after any flood occurrence is mandatory.

Summarizing, the safety of dams is essentially based—besides appropriate design and construction—on an adequate monitoring system, where visual inspections play a paramount role to detect any unusual situation.

REFERENCES

- Biedermann, R. et al. 1982. Comportement anormal du barrage-voûte de Zeuzier. Abnormal behaviour of Zeuzier arch dam. *wasser energie luft—eau énergie air, Special issue to the 14th ICOLD Congress, Rio de Janeiro, Brazil*, 74(3): 65–112. Baden, Switzerland.
- Bossoney, C. & Balissat, M. 2005. Uncertainty about origin of permanent deformations on existing concrete dams. *Proc. 73rd Annual Meeting of ICOLD, Tehran, Iran May 1–6, 2005 Paper No.: 149-S4*.
- CSB. 1997. Surveillance de l'état des barrages et check lists pour les contrôles visuels. *Comité suisse des barrages—Swiss Committee on Dams*, Switzerland (in French).
- CSB. 2000. Comité suisse des barrages—Swiss Committee on Dams: Concrete of Swiss Dams: Experiences and Synthesis. *wasser energie luft—eau énergie air* (92)7/8: 205–233. Baden, Switzerland.
- CSB. 2006. Comité suisse des barrages—Swiss Committee on Dams: Dam Monitoring Instrumentation/ Dispositif d'auscultation des barrages (Part 1 and 2). *wasser energie luft—eau énergie air*, (98)2: 143–180. Baden, Switzerland.
- Heller, V. 2008. *Landslide generated impulse waves: Prediction of near field characteristics*. In H.-E. Minor (ed.), *Mitteilungen* 204. Versuchsanstalt für Wasserbau, Hydrologie und Glaziologie (VAW) ETH. Zürich.
- Kovari, K. & Peter, G. 1983. Continuous strain monitoring in the rock foundation of a large gravity dam. *Rock Mechanics and Rock Engineering*; Vol. 16, No. 3, Aug. 1983: 157–171. Vienna: Springer.
- Lombardi, G. 1992. The FES rock mass model—Part 1 and Part 2: Some examples. *Dam Engineering*; Vol III, Issue 1: 49–76 and Issue 3: 201–221.
- Pougatsch, H. 1990. Le barrage de Zeuzier. Rétrospective d'un événement particulier. *wasser energie luft—eau énergie air*, (82)9: 195–208. Baden, Switzerland (in French).
- Pougatsch, H. & Müller, R.W. 2002 Alp Transit und die Talsperren. Sicherheit ist oberstes Gebot. *wasser energie luft—eau énergie air*, (94)9/10: 273–276. Baden, Switzerland (in German).
- Rüesch, C. & Scherrer, I. 2001. Neues Abdichtungssystem für Staumauern. *wasser energie luft—eau énergie air*, (93)11/12: 319–321. Baden (in German).
- Schenk, T. 2006. Staudamm Godey und seine Umwelt. *wasser energie luft—eau énergie air*, (98)4: 277–280. Baden, Switzerland (in German).
- Sinniger, R. et al. 1991. Ageing of dams—Swiss experience. *Proc. 17th ICOLD Congress*, Vienna, Austria, Q.65(R.10): 159–186.

Concept of safety and safety requirements for dams

P.A. Zielinski

Ontario Power Generation, Toronto, Ontario, Canada

ABSTRACT: A key problem explored in the paper is what should be a rational basis for making societal choices for life safety decisions. The philosophy applied by traditional engineering also known as a “factor of safety” approach relies on designing the structures to survive under some extreme loads resulting from so called “maximum credible events”. Explicit consideration of risk helps in establishing a better, rational basis for decisions involving life safety but the road to effective and efficient decision-making mechanism requires significant effort in identifying and quantifying all risks present. This concentrates on development of risk assessment criteria and supporting attributes necessary for the proposed framework to be fully operational. Some aspects of ‘risk measuring’ related to assessment of consequences to life safety are discussed.

1 INTRODUCTION

A significant portion of regulatory activities in the area of dam safety related to life safety issues are quite often portrayed imprecisely as ‘life saving measures’, when in fact what they intend to do is to prevent premature death and only attempt to extend life. Individuals can design and implement risk-reduction strategies on their own but in certain cases when the control of the life safety risks is beyond their reach only a collective action in the form of the regulation initiated by the government can reduce these risks to the levels that are sufficiently low. Although any risk-reduction action contributes to the prevention of premature death it also involves costs and the economic consequences of its implementation can vary substantially from case to case. Thus the crucial problem facing the decision-makers is how to compare the monetary costs of risk-reduction measures with non-monetary benefits in the form of avoided premature loss of life.

Abelson (Abelson 2007) in his paper pointed out that Australia spends about one-sixth of its GDP on all forms of life and health protection and these actions cause a substantial diversion of resources away from other goods and services. That leads to the question whether this level of expenditure on health and safety is appropriate or whether it is too large or too small. Abelson concludes that in order to assess such issues properly quantitative measures of the value of life and health and safety are needed.

A key problem which needs to be explored further is what should be a rational basis for making societal choices for life safety decisions. The decisions have always been made by defining more or less conservative safety standards and by using considerable amount of judgment and experience. The philosophy applied by traditional engineering also known as a “factor of safety” approach relied on designing the structures to survive under some extreme loads resulting from so called “maximum credible events”. Explicit consideration of risk can be helpful in establishing a better, rational basis for decisions involving life safety but the road to effective and efficient decision-making mechanism requires significant effort in identifying and quantifying all risks present. This paper does not attempt to address all the complex problems of risk estimation and concentrates instead on development of risk assessment criteria and supporting attributes that are necessary if the proposed framework is to be fully operational. Thus, some aspects of risk measuring which assess the consequences to life safety

will be discussed here, but not these which are related to assigning probabilities. The judgment of acceptability of identified risks (judgment of safety) is a separate issue. An efficient, elegant and logically consistent framework for making these judgments has been established using risk informed approach (HSE 2001) and it is briefly characterized in Section 3.

At the end, the effort of constructing an appropriate framework will be judged as successful if the framework can deliver the answer to the question: is the risk acceptable? It may seem that the question was quite simply answered long time ago by Lowrance 1976 who stated that “A thing is safe if its risks are judged to be acceptable”. Lowrance interpretation of what constitutes safety was important because it clearly formulated the idea that nothing can be absolutely free of risk and thus there is no absolute safety. The implications of this statement are quite clear: since all activities involve some degree of risk it is more appropriate to talk about the degrees of safety and that someone has to define the boundaries of acceptability and also that someone has to formulate the criteria for that decision.

2 SETTING OF STANDARDS IN DAM SAFETY

Ball & Barrett 2009 trace introduction of general standards back to the beginnings of industrial revolution when the developing industries realized benefits from having manufactured items that were interchangeable and with known material properties. Development of technical standards consolidating existing knowledge followed and in the last two decades the standards setting activities expanded into the areas of management and business processes. These activities are usually coordinated at the international and national levels but there are also parallel activities at the industry sectors, professional associations and at the organization levels. It should be pointed out that the nature of activities changed with this expansion—from very focused and prescriptive to broadly encompassing and guiding documents (see Figure 1).

In the dam safety area the setting of standards cannot be initiated before a simple but often elusive and misleading question is answered: how safe is safe enough? An inappropriate answer to this question is that no risk to safety should be tolerated (Derby & Keeney 1981). This simple but unfortunate statement is an expression of the so-called “zero-risk” policy and it has been pervading the field of dam safety for many decades. As an example, inflow design

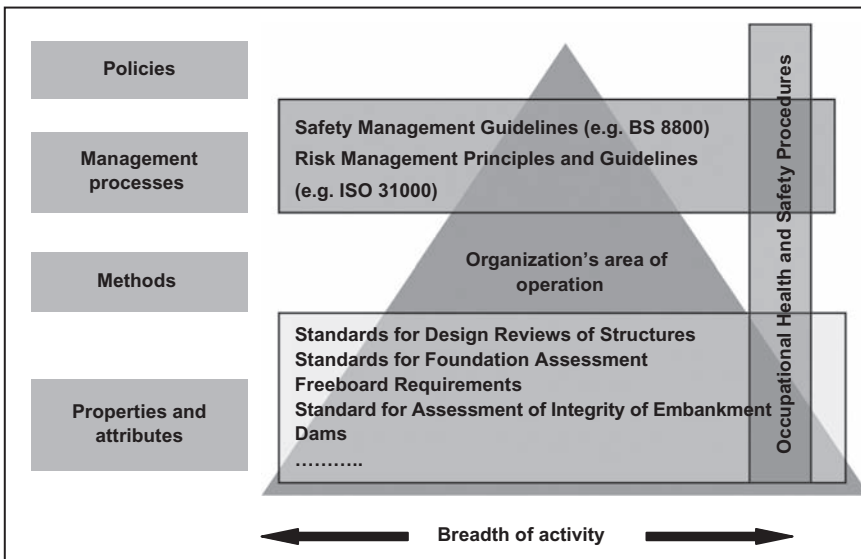


Figure 1. Impact of setting standards.

flood selection criteria for dams in many North American jurisdictions call for the Probable Maximum Flood (PMF) in these cases when there is a potential for a loss of life as a result of dam failure. Whether a particular PMF estimate constitutes the actual physical limit for the flood at a particular location is not relevant (it can be in fact either lower or higher than the actual limit). What is relevant is the concept of selecting the physically limiting event as a safety standard—no other engineering activity calls for such a stringent and conservative standard.

Subsequently introduced dam safety standard of Maximum Credible Earthquake (MCE) for seismic criteria was clear manifestation of the same school of thought and only very recently has begun the retreat leaving the room for probabilistic type of criteria based on ground motions that represent the best estimate ground motions for the specified annual exceedance probability (also often characterized by return periods).

Reviewing zero-risk policies in other regulatory fields may provide some necessary perspective. The famous Delaney Clause, named after its sponsor New York Congressman Jim Delaney, was an addition to the U.S. Federal Food, Drug, and Cosmetic Act of 1938 (Asch 1990). Delaney proposed in 1958 a rigid, zero risk standard that prohibited any amount of food additives or pesticides found to cause cancer from being added to processed food. This clause meant that no amount of a carcinogenic additive could be present in food, no matter how small a risk that substance might have posed. The zero-risk standard did not permit the incorporation of new analytical methods capable of assessing the risk and potency of carcinogens. Thus a paradox was created—the Delaney Clause was intended to protect the public but instead banned the introduction of new pesticides that could actually pose less risk than other pesticides. The zero-risk standard of the Delaney Clause made carcinogenic additives illegal, without regard to other characteristics of product use, such as other health risks or benefits. Recognizing that the total ban of Delaney Clause was zero-risk policy that actually caused higher risks to health and safety, the Congress after repeated attempts to fix the problem by amending the Clause, repealed it in 1996.

It is also interesting that in other areas of civil engineering where exposure to natural and human-made hazards can lead to significant loss of life, the concept of complete protection associated with conservative standards derived as physical limits of catastrophic events has never been accepted. As examples one may consider Canadian Building Code (NBCC 1995) which prescribes a ground motion with 2500-year return period ($4 \cdot 10^{-4}$ annual exceedance probability) as a standard for apartment buildings or Canadian Highway Bridge Design Code which defines an earthquake with return period of 1000 years (10^{-3} annual exceedance probability) as the most severe ground motion to be considered. Thus, these areas of civil engineering chose the safety requirements that do not attempt to offer unlimited protection; on the contrary they state that the residual risk exists and although it is relatively small it is clearly a non-zero risk.

3 RISK-INFORMED DECISION-MAKING FRAMEWORK

The section provides the origins and brief description of UK Health and Safety Executive (HSE) Framework for Decision-Making in the Presence of Uncertainty (HSE 2001). The centre of the framework, the concept of ALARP (As Low as Reasonably Practicable), was explicitly formulated for the first time as a result of a court case (Edwards versus The National Coal Board) in United Kingdom, in 1949.

The concept of ALARP is in its essence based on a legal principle that is aimed at controlling the level of risk associated with a hazardous activity. At the present, ALARP is used as a fundamental concept to all safety regulations in the United Kingdom in that it allows the costs to be taken into account when determining to what level the risk has to be, reduced. ALARP is also referred to in a number of Australian statutes, which are aimed at protection of the public from hazardous facilities. A number of guidelines issued by Australian regulators in various industrial sectors refer to UK Health and Safety Executive concept of ALARP (HSE 2001). Australian National Committee on Large Dams (ANCOLD) provides

explanation how ALARP principle can be applied in the context of dam safety in Australia (ANCOLD 2003).

A dam owner who decides to demonstrate dam safety with the help of this framework has to conduct the safety assessment in such a way as to ensure that all measures necessary to avert risk must be taken until the cost of these measures is disproportionate to the risk which would be averted. As a result, the risk must be reduced to a level which is ALARP. The ALARP principle provides practical means for assessing the tolerability of risk by establishing that if the cost of reducing a risk outweighs the benefit, then the risk may be considered tolerable.

The proper framing of the issue of how to interpret and apply the ALARP principle when life safety is being considered begins with the realization that any decision on proportionality of action requires the characterization of risks involved. The risk has to be characterized either qualitatively or quantitatively in order to describe how it arises and how it impacts those who may be affected.

Within this tolerability of risk framework introduced by HSE 2001, it is recognized that there are levels of risk that cannot be tolerated and which would be found unacceptable by the public. These risks have to be reduced regardless of the costs involved in risk reduction and the benefits from the presence of the dam, unless there are exceptional reasons to continue the operation. The risks within this zone are considered as so high that the continuing operation of the dam cannot be allowed.

In the zone of broadly acceptable risks the risks are generally regarded as insignificant and are comparable to the risks people face in their daily lives and consider as trivial. Further reduction of broadly acceptable risks is not required although the dam owner may decide that reduction is reasonably practicable and may implement additional measures reducing the risks to even lower levels.

The third zone represents these risks that people are prepared to tolerate in order to receive certain benefits. The benefits can be numerous and may include employment opportunities, maintenance of general social infrastructure (electricity production, water supply), recreation, etc. The willingness to tolerate the risks is however conditional and the conditions can be derived from the principles discussed in detail in HSE 2001.

The application of ALARP concept requires that the costs of implementation of risk reduction measures and related benefits be compared. In the case of life safety the benefits can be interpreted as avoided consequences (fatalities). In order to perform the comparison both costs and benefits have to be expressed using the same metric and a monetary valuation of both can be an obvious and practical candidate.

4 VALUATION OF LIFE

Valuation of human life and health resulting in assigning monetary values to lives lost has always been a very controversial topic. It is positioned within philosophical, ethical, moral and political context and as such has always been a subject of controversies and heated debates. The common argument of the opponents of this approach is that human life is irreplaceable and as such has infinite value. They also often argue that even consideration of the concept is highly unethical and should be abandoned.

4.1 *Ethical considerations*

Lenz 2006 and Ersdal & Aven 2007 provide quite detailed discussion of ethical and moral difficulties arising when making decisions affecting life safety, especially when these decisions are carried out with the help of risk based methods. The subject of making right or good decisions belongs essentially to the domain of philosophy and ethics but a basic summary of moral systems underpinning ethical decision-making can be helpful in understanding why risk-informed decision-making in dam safety has been met with opposition from a large segment of the dam engineering profession.

First of the two main ethical theories relevant to the subject is deontology which postulates the existence of some a priori moral obligations which either forbid or permit action. The term deontology originates from Greek words ('deon'—duty and 'logos'—science) and can be translated as 'science of duty'. The original theory was introduced at the end of the 18th century by a German philosopher Immanuel Kant who formulated what is now known as Kant's categorical imperative. Deontological ethical systems focus on adherence to independent moral rules or duties. From the perspective of decision-making the most significant aspect of deontological ethical systems is that the principles are separated from any potential consequences which may result from following those principles. Thus deontologists believe that there are right and wrong decisions regardless of consequences. In risk-informed decision-making environment, this position may lead to the conclusion that nobody has the right to expose a person to a certain risk, even if such decision is beneficial to the society as a whole. Lenz 2006 also points out that Kant's categorical imperative lead to the concept of 'intangibility of human life' and the principle of 'infinite value of human life' which has always been part of Judeo-Christian belief system and is now embedded into constitutional laws of most Western countries. According to deontologists intangibility of human life is a fundamental concept that cannot be further derived by rational means (e.g. analysis or optimization). Some sub-divide deontologist into two subgroups: absolute and moderate. Dam safety decision-maker who belongs to the absolute group would say that it is always wrong, whatever the consequences, to deliberately endanger an innocent person. The moderate deontologist would say that it is wrong to deliberately endanger an innocent person unless doing so is necessary to save at least, for example, 10 innocent lives.

The other major stream of ethical theories is commonly called 'consequentialism'. Consequentialism opposes deontology and in judging actions takes into account their consequences. One of the best known forms of consequentialism is the utilitarianism introduced also at the end of the 18th century by an English philosopher Jeremy Bentham. While Bentham's theory stressed the importance of cultural and spiritual aspects, the modern utilitarianism serves as the philosophical foundation for the economic utility theory. It should be pointed out that some forms of utilitarianism deny the principle of infinite value of life and the equality reasoning derived from this principle. From the perspective of risk-informed decision-making, the utilitarianist would require that the consequences of various choices or alternatives can be measured in some form of utility (Ersdal 2007). Referring back to the illustration of a dam safety decision-maker in the previous paragraph, the utilitarianist would say that whether an action, such as deliberately endangering an innocent person, is wrong depends solely on its consequences. The correct action would be the one which maximizes overall utility.

4.2 *Background and justification*

Putting aside for a moment emotive aspects of valuation of life concept, it can be said that safety always has a price, it is not the only thing people value and sometimes there are other things that they value even more than safety. If there are limits on what people are prepared or willing to pay for safety (and often these limits are imposed on people by economic constraints) then the reality forces us to put a value on life and thus help in creating a coherent and consistent mechanism capable of providing some guidance on what should be reasonably spend on safety improvements. It is being recognized that, given limited financial resources and the need for their efficient allocation, if the valuation of life is not made explicitly then it will be made implicitly by allocating the funds for safety improvements in a certain way. Thus, any decision which affects health and safety risk levels implicitly places a value on human lives and health.

The concept of 'value of life' has been introduced first by Schelling 1968 who very clearly articulated the distinction between statistical and identified life and wrote that "it is not the worth of human life that I shall discuss, but of 'life-saving', of preventing death. And it is not a particular death, but a statistical death".

HSE 2001 report pointed out that this useful concept is often misrepresented and "it is often misunderstood to mean that a value is being placed on a life. This is not the case. It is

simply another way of saying what people are prepared to pay to secure a certain averaged risk reduction. A VPF of £1,000,000 corresponds to a reduction in risk of one in a hundred thousand being worth about £10 to an average individual. VPF therefore, is not to be confused with the value society, or the courts, might put on the life of a real person or the compensation appropriate to its loss". The term VPF or Value of Preventing Fatality is a term approximately equivalent to the term VSL, Value of Statistical Life.

The general idea is that when a risk reduction option (potentially producing benefit of 'saving lives' or preventing fatalities) is available this requires putting a monetary value on achieving a reduction in the risk of death. Thus the intention of defining the value of statistical life (VSL) is to provide a measure capable of reflecting the marginal change in risk level for a large number of individuals but not specific, identified individuals. In everyday-life society and individuals face choices that involve tradeoffs between accepting physical risk in return for financial and non-financial benefits. The choices made can reveal our willingness to exchange financial gratification for the risk of physical harm. As eloquently explained by Ashenfelter 2006, the ratio of the wealth we are willing to accept in exchange for a small change in the probability of a fatality is expressed in units of 'dollars per death,' or the dollar value of a fatality. It is for this reason that this trade-off is often called the value of a 'statistical' life.

It has been pointed out (Hammit and Treich, 2007) that the major weakness of the VSL concept is that it is inadequate in situations where the threat is to identifiable individuals or when changes to individual risks across the threatened population are large. However, since the quantified risk is only one of the elements informing decision-making process, society or the institutions/individuals acting or its behalf may choose that the gains in equity, moral, ethical and political objectives may trump the loss of efficiency and decide appropriately.

What are the alternatives to the VSL in terms of improving efficiency of just decision-making? Jones-Lee 1989 concluded that the following alternative options available for decision-makers have serious deficiencies that handicap their usefulness in efficient and equitable decision-making.

1. Ignore the estimates of VSL because the safety effects of risk-reduction measures are incommensurable with the other costs and benefits.

It is undeniable that increase in safety benefits is inherently different than most of the other benefits but it is also true that the requirements to improve safety have to compete with other goals of allocating finite resources. If the measures of safety improvement are lacking then there is no rational way to judge to what extent the safety should outweigh other goals, short of either ignoring safety entirely or assigning the highest priority to it regardless the cost. The latter would result in assigning either zero or infinite value to the value of life.

2. Apply informal judgment for weighing safety benefits against other benefits and costs.

Informal, subjective judgment leads to inconsistencies not only between different decision-makers but also for different assignments of a single decision-maker. Since the decisions made are based on judgment, they cannot be evaluated or scrutinized in any meaningful way.

3. Define safety standards or targets.

Two major weaknesses of this approach are: (i) no sound fundamentals and clear criteria on establishing of what are the levels of safety to be achieved and, (ii) lack consistency between the standards and cost of meeting them, which in terms of life safety leads to inconsistencies in considered implicitly value of life and in inefficiencies in resources allocation.

4. Use cost-effectiveness analysis.

The analysis is aimed at either maximization of achieving improvement to life safety goal within a predetermined budget or at minimization of expenditures required to achieve a prescribed level of life safety. It cannot however help in considerations of what is the appropriate size of the budget, and consequently what is justifiable level of life safety that should be achieved.

5. Apply decision analysis approach.

The approach based on defining a multi-attribute utility function (reflecting value judgments of the decision-maker on trade-offs between different consequences and choice between their

probability distributions) has an inherent mutual incompatibility of three fundamental value judgments. These judgments are related to: (i) desirability to minimize expected loss of life, (ii) desirability of an equitable distribution of risk of life loss amongst the population, and (iii) desirability of avoiding catastrophic loss of life.

Examination of the alternatives reveals that their limitations are substantial, that they are incapable of providing structured, logical and accountable approach to decision-making and as result could lead to poor allocation of limited resources. Introduction of the VSL into decision-making mechanism, although not free of shortcomings, can provide rational, transparent and efficient basis to the entire process.

4.3 International studies

A study conducted by the Australian Government (ASCC 2008) provides the findings from the literature review of VSL estimates from 17 Australian and 227 international studies conducted between 1973 and 2007. Selected results are in the [Tables 1, 2 and 3](#), below. All values are converted to 2006 Australian dollars.

Table 1. Australia—VSL estimates, in million A\$.

Year of study	Min	Max	Point	Comments
Health Sector				
2006			2.88	
Transport Sector				
2006			3.00	Civil Aviation Safety Authority
2006			1.99	Bureau of Transport Economics
2000			1.55	
Environmental Protection				
1992	0.86	1.43	1.15	1.15 is a mean value
1994			7.21	
Other (Consumer choice, crime and fire safety)				
2007			17.65	
1990			1.50	
2003			2.18	
2000	3.66	5.41	4.67	4.67 is a mean value

Table 2. International VSL estimates, in million A\$.

Country	Year of study	Min	Max	Mean
Health Sector				
US/Canada	1973–2000	0.20	9.00	4.32
US	1973–2000	0.20	8.69	4.27
Canada	2000	2.69	9.00	4.52
US/Canada	Post 1990	2.69	9.00	5.00
Transport Sector				
Multiple	1973–2007	0.24	50.83	8.19
US	1973–2006	0.24	50.83	6.39
Multiple	Post 1990	0.24	50.83	8.34
Environmental Protection				
Multiple	1981–2006	0.14	132.85	11.96
US	1981–2006	0.85	13.61	7.48
US	1985–1999	2.69	10.26	8.53
Other (Consumer choice, crime and fire safety)				
Multiple	1973–2007	0.66	84.70	10.50
US	1977–2007	1.02	42.27	11.77
Multiple	Post 1990	1.02	42.27	8.03

Table 3. Ranges of VSL estimates by country, in million A\$.

Country	Number of studies	Health	Transport	Environment	Other	Total	Mean*
Australia	17	1.2–2.9	1.3–5.4	0.9–7.2	1.5–17.7	0.9–17.7	5.7
Austria	5				5.4–13.2	5.4–13.2	9.0
Canada	17	2.7–9.0	0.7–41.1		3.7–14.5	0.7–41.1	7.3
Denmark	2		1.3–1.9		6.6–8.7	1.3–8.7	4.3
France	2		1.5–35.8		5.1–7.3	1.5–35.8	11.9
Japan	4				8.2–12.2	8.2–12.2	17.8
New Zealand	10		1.1–21.4		2.8–4.2	1.1–21.4	5.3
South Korea	6				0.7–1.3	0.7–1.3	1.5
Sweden	7		2.1–44.1		2.1–6.8	2.1–44.1	5.6
Switzerland	5		1.4–1.7		7.3–12.9	1.4–12.9	7.7
Taiwan	7				1.4–1.9	1.4–1.9	1.7
UK	26		1.0–34.0	31.4	1.4–41.3	1.0–41.3	8.8
US	117	0.2–8.7	0.2–50.8	1.1–13.6	1.0–42.3	0.2–50.8	7.1
Multiple	17		0.2–50.8	0.1–132.9	0.7–84.7	0.1–132.9	7.5

* Mean value calculated including VSL estimates for occupational health and safety.

4.4 Canadian studies and practice

Transport Canada (TC 1994) has been assigning monetary values to fatalities avoided in order to reflect a “widespread recognition of a need for guidance on what should be spent to reduce the risks of transportation accidents”. Transport Canada guide on benefit-cost analysis states that “there has been extensive research world-wide to find a solid basis for such guidance, i.e., to determine the amount that society is willing to invest to reduce the statistically predicted number of accidental deaths in transport. Of course, this is a different concept from what would be spent to save a particular individual whose life might be at risk at a particular time.”

Based on a review of international studies and practices, Transport Canada recommends using \$1.5 million (1991 dollars) as the value of a fatality avoided in all modes of transport.

(Dionne and Lanoie 2004) study supported by Ministère des Transports du Québec performed comprehensive analysis of large number of available studies related to valuation of statistical lives and provided the following estimates. The best studies in the transport sector have a relatively narrow range of \$4.3 million to \$6.7 million, with the average value of \$5.2 million (all in 2000 CAD \$). The authors recommend that in the cost-benefit analyses, the Canadian Federal and Provincial transport authorities should value a statistical life at \$5 million (2000, CAD \$) and use values of \$3 million and \$7 million for sensitivity analyses.

Treasury Board of Canada (TBCS 2007) in its Canadian Cost-Benefit Guide recognizing that since policies on health and safety are expected to reduce the risk of premature death, the benefits of these reductions needs to be measured and recommends the value of statistical life as an appropriate measure that can be derived from the aggregation of many small risks over an exposed population. The Guide quotes the figure of \$5.2 million (from a report prepared in 1999 for Environment Canada and Health Canada) and recommends that it be adjusted for inflation. Consequently, all Government departments are expected to use the value of \$ 6.11 million (in 2004 CAD \$) as the VSL after adjusting it for inflation.

Most recently, Government of Canada (PRI 2009) provided a report (commissioned by Environment Canada and Health Canada as part of the development of the Air Quality Valuation Model) which strongly links government and regulatory efforts in areas of environmental protection, transportation safety and consumer products safety with practical ability to estimate monetary values of reductions in mortality risks. The report recommends the following primary VSL estimates for Canadian Policy Analyses (in 2007 CAD \$): low—\$3.5 million, central—\$6.5 million and, high—\$9.5 million.

Table 4. Estimates of VSL in Canadian practice, in CAD \$ million.

Source of VSL Estimate	Reference Year	Low	Mean	High	Mean 2009 prices
Transport Canada	1991		1.5		2.1
Dionne and Lanoie—Transports du Québec	2000	3.0	5.0	7.0	6.0
Health Canada	2002	3.5	5.8	11.7	6.6
Treasury Board of Canada	2004		6.11		6.7
Government of Canada—PRI	2007	3.5	6.5	9.5	6.7

Current Health Canada regulatory proposal (HC 2010) recommends the use of the VSL as an approach that allows the analysts to estimate the economic value of health and safety initiatives that are expected to prevent fatalities. The value recommended is \$5.8 million (in 2002 CAD \$) as a central value with \$3.5 million and \$11.7 million as low and high values, respectively. The proposal indicates that these values are consistent with the figures which Health Canada has been using in other assessments.

A summary of an existing practice in using VSL for decision-making in Canada is displayed in Table 4. The point values of these estimates (with the exception of Transportation Canada estimate) are spread over a surprisingly narrow interval between 5.0 and 6.5 CAD \$ million. When the VSL values are expressed in 2009 prices the spread is further reduced resulting in the interval of 6.0 to 6.7 CAD \$ million.

At the time of writing this paper the author was unaware of any explicit initiatives of Federal or Provincial regulators and legislators in Canada who are responsible for risk management activities in the area of life safety. Limited review of Provincial government's publications did not identify any documents providing the guidance on resources allocation decision-making in situations where human lives are at risk. It seems that explicit criteria how the resources should be allocated and how the benefits of preventing fatalities should be measured are not present in existing documents.

This hypothesis is not surprising. Most of the world governments (and this includes federal and provincial governments in Canada) are lacking general policies on risk management of hazardous activities. It is very common almost everywhere that if there are some policies developed by specific sectors, they are usually developed in isolation, are usually incoherent between the sectors and are very often not transparent. It should not be doubted that such policies are in place everywhere. This is how the decisions on which diseases and to what extent is funded in health care or the decisions which roads are upgraded to reduce fatalities or many others are being made in all Provinces at all times. In view of this, the fact that 'some' guidance on selecting inputs to cost-benefit analyses with regard to life safety is provided by Canadian federal government is encouraging. Hopefully this will serve as an example and encouragement to other legislators and regulators to follow.

5 CONCLUSIONS

Risk assessment is at the present being slowly but steadily accepted as the approach that permits more comprehensive and more complete assessment of safety in a variety of hazardous industries. Philosophy of decision-making with respect to safety of dams is also beginning to acknowledge that risk-informed approach can offer superior insights into all aspects of dam safety. Qualitative forms of risk assessment support the identification and analysis of important safety issues that are not treatable in any form by traditional approach to safety assessment. Fully quantitative dam safety risk analyses are still being hampered by analytic difficulties and general lack of necessary supporting information and data. However risk-informed approach will not go away, and the methodology and analytic techniques will continue to be further developed and perfected.

There is another aspect of risk-informed decision-making that extends beyond analytic capacity. This aspect relates to making safety choices in an explicit and transparent manner. Potential for a loss of life always brings the question of societal risk acceptability. Even if one agrees with the principle that human life is invaluable, the reality is that the resources are always limited and a reduction of specific risks causes that the investments have to be diverted from other essential societal needs. Thus the concepts of societal affordability and societal risk acceptability are always competing with each other. Traditional approach to defining decision-making criteria for life safety was based on the premise that “it would not be acceptable, on moral grounds, to put a monetary value on human life in calculation of damage” (Lafitte 1993). It seems that with the opportunities created by introduction of risk-informed decision-making approach this premise should be reconsidered and valuation of loss of statistical life should be included as an important tool in making dam safety decisions.

REFERENCES

- Abelson, P. 2007. Establishing a monetary value for lives saved: issues and controversies. *Proc. of the Conference on Delivering Better Quality Regulatory Proposals Through Better Cost-Benefit Analysis*. The Office of the Best Practice Regulation, Australian Government.
- ANCOLD (Australian National Committee on Large Dams). 2003. Guidelines on risk assessment.
- ASCC (Australian Safety and Compensation Council). 2008. The health of nations: the value of a statistical life.
- Asch, P. 1990. Food safety regulation: is the Delaney clause the problem or symptom? *Policy Sciences*. 23(2): 97–110.
- Ashenfelter, O. 2006. Measuring the value of statistical life: problems and prospects. *The Economic Journal*, 116(510):10–23.
- Ball, D.J. and Barrett, M. 2009. Standards setters and public risk. Report prepared for UK Risk & Regulation Advisory Council.
- CSA (Canadian Standards Association). 2006. Canadian highway bridge design code. CAN/CSA-S6.
- Derby, S.L. and Keeney, R.L. 1981. Risk analysis: understanding “How safe is safe enough?” *Risk Analysis*. 1(3): 217–224.
- Dionne, G. and Lanoie, P. 2004. Public choice about the value of a statistical life for cost-benefit analysis. *Journal of Transport Economics and Policy*. 38(2): 197–205.
- Ersdal, G. and Aven, T. 2007. Risk-informed decision-making and its ethical basis. *Reliability Engineering & System Safety*. 93(2): 197–205.
- Hammitt, J.K. and Treich, N. 2007. Statistical vs. identifies lives in benefit-cost analysis. *Journal of Risk and Uncertainty*, 35(1): 45–66.
- HC (Health Canada). 2010. Economic evaluation of Health Canada’s regulatory proposal for reducing fire risks from cigarettes. Health Canada website <http://www.hc-sc.gc.ca/hc-ps/pubs/tobac-tabac/evaluation-risks-risques/index-eng.php> accessed March 14, 2010.
- HM Treasury. 1996. The setting of safety standards – a report by an interdepartmental group and external advisers. Crown Copyright.
- HSE (Health and Safety Executive). 2001. Reducing risk protecting people - HSE’s decision making process. HM Stationery Office. London.
- Jones-Lee, M.W. 1989. The economics of safety and physical risk. Basil Blackwell, Oxford.
- Lafitte, R. 1993. Probabilistic risk analysis of large dams: its value and limits. *Water Power & Dam Construction*. 44(3): 13–16.
- Lenz, A. 2006. Acceptability of civil engineering decisions involving human consequences. Ph.D. thesis. Technischen Universität München.
- Lowrance, W.W. 1976. Of acceptable risk: science and the determination of safety. Kaufman. Los Altos, CA.
- NBCC. 1995. National Building Code of Canada, National Research Council of Canada.
- PRI (Policy Research Initiative). 2009. Economic valuation of mortality risk reduction: review and recommendations for policy and regulatory analysis. Government of Canada, Research Paper, PRI Project Regulatory Strategy.
- Schelling, T. 1968. The life you save may be your own. In Chase, S.B. (ed.), *Problems in Public Expenditure Analysis*. Brookings Institution, Washington, DC.
- TBCS (Treasury Board of Canada Secretariat). 2007. Canadian cost-benefit analysis guide—regulatory proposals.
- TC (Transport Canada). 1994. Guide to benefit-cost analysis in Transport Canada. TP 11875E.

Alkali-Silica Reaction in Japan

H. Koga, T. Hyakutake & H. Watanabe
Public Works Research Institute, Tsukuba, Japan

T. Sakamoto
Japan Commission of Large Dams, Tokyo, Japan

ABSTRACT: Alkali-Silica Reaction (ASR) has attracted considerable attention since the 1980s as one of the main causes of concrete deterioration in Japan. Defects caused by ASR are seen in various reinforced concrete structures such as viaduct piers, but there are no reports of ASR deterioration of large concrete dams. Possible reasons for the absence of ASR in large dams include low cement content and usage of fly ash blended cement compared with other concrete structures in Japan. On the other hand, deterioration of general concrete structures in Japan has significantly decreased since 1987 when provisional mitigation methods for ASR were introduced. However ASR is still seen in some concrete structures excluding dams despite the application of mitigation methods. In this paper, the results of long-term outdoor exposure test of concrete specimens with low total alkali are introduced to promote awareness of ASR.

1 DETERIORATION OF CONCRETE STRUCTURES DUE TO ASR IN JAPAN

1.1 *Deleterious rock types associated with ASR*

Various types of rocks are used as aggregate for concrete in Japan due to the region's complex geotectonic environment and many of the types used can cause ASR in concrete. The Public Works Research Institute (PWRI) collected samples of aggregate from quarries throughout Japan and examined their alkali reactivity using the ASTM C 289 standard test method. The results are shown in [Figure 1](#) (Wakizaka 1998). Volcanic rock, especially andesite, is widely used in Japan. The andesite contains cristobalite, tridymite and volcanic glass, which can have significantly high alkali reactivity. Chert, which contains cryptocrystalline quartz, is another typical aggregate with high alkali reactivity. Other sedimentary rocks, such as sandstone can also cause ASR.

Deleterious and potentially deleterious aggregates are distributed throughout Japan (Wakizaka 1998). Hence, deterioration due to ASR can occur almost anywhere in the region.

1.2 *Deterioration due to ASR and mitigation measures*

Alkali-silica reaction (ASR) has attracted considerable attention since the 1980s as one of the main causes of concrete deterioration in Japan. Defects caused by ASR are seen in various reinforced concrete structures such viaduct piers.

From the data on bridge inspections conducted by the Ministry of Land, Infrastructure, Transport and Tourism (MLIT), it is estimated that 2% of bridges built before 1987 are affected by ASR ([Fig. 2](#), Kawano & Koga 2005). Cracking due to ASR was mainly observed in piers and abutments.

A report on ASR deterioration states that there has been a dramatic reduction in damage since 1987 when provisional measures for ASR mitigation set by the Ministry of Construction became effective. Provisional mitigation methods consisted of the following four options: (1) Use of certified safe aggregate, (2) Use of low alkali portland cement, (3) Use of blended cement with controlling effect, and (4) Control of the total alkali content in the concrete.

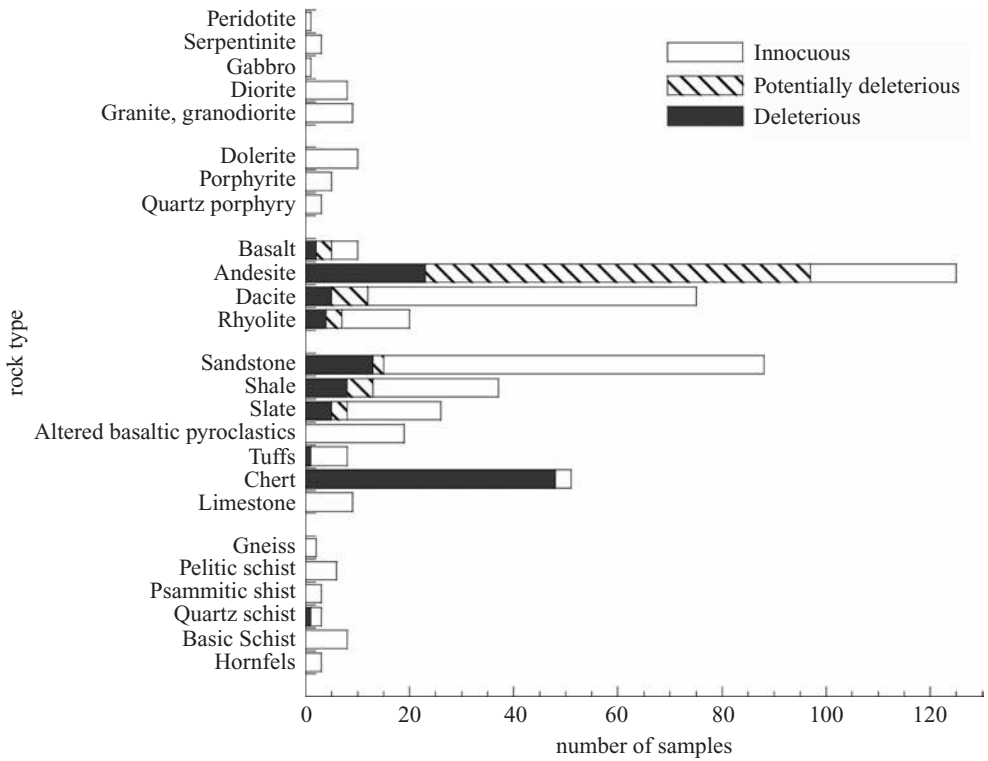


Figure 1. Reactivity of aggregates in Japan (from Wakizaka 1998).

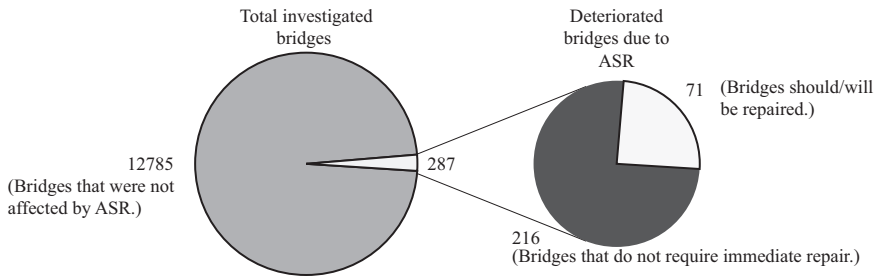


Figure 2. Number of highway bridges with deterioration due to ASR (Kawano & Koga 2005).
 * This figure was drawn using only the data on bridges managed by MLIT.

These measures were revised in 1989 and 2002. In the revised 2002 version, reference allowing the use of low-alkali portland cement was deleted mainly because of its limited marketability. One of the alternatives listed in Table 1 shall be chosen to prevent ASR, according to the revision in 2002.

2 MIX DESIGN OF DAM CONCRETE IN JAPAN

ASR is a major deterioration factor in Japan and its effects are seen in many different structures. However, there have been no reports of ASR causing damage to Japan's large dams. For instance, Kobayashi (1986) reported the absence of ASR deteriorated dams as

Table 1. Mitigation methods for ASR in Japan.

Control of the total alkali content in the concrete	The alkali content (based on Na ₂ O _{eq}) per cubic meter of concrete must be 3.0 kg or less. Portland cement with known alkali content should be used.
Use of blended cement with controlling effect	Use of blast-furnace cement conforming to JIS R 5211 or portland fly-ash cement conforming to JIS R 5213 or the use of binding material with verified suppressing effect on ASR added to portland cement In this case, blast-furnace slag in the blast-furnace cement should be 40% or more in mass and fly-ash in the fly-ash cement should be 15% or more in mass.
Use of certified innocuous aggregate	Use of aggregates that have been certified as innocuous according to alkali-silica reactivity tests (chemical method or mortar-bar method)

Table 2. Typical mix proportions of concrete used in large dams (Kano et al. 2005).

Type of dam	Type of concrete	Name of dam	Completion year	Gmax (mm)	W/B (%)	s/a (%)	Quantity of materials per unit volume of concrete (kg/m ³)				Type of cement**	
							W	B*	S	G		
Gravity Dam	Inner (conventional block)	Ikari	1956	150	62.9	27.8	104	170	584	1520	M	
						56.8	26.2	114	200	535	1508	
		Sonohara	1964	150	56.3	25	90	160	540	1627	BB	
		Shimokubo	1967	150	75.8	27	114	150	570	1565	BB	
						68.6	27	110	160	568	1581	
		Ishidegawa	1972	150	69	24.5	110	160	523	1672	BB	
		Ohishi	1978	150	68.7	23	110	160	490	1650	M	
		Ohdo	1982	150	65	24	98	150	521	1662	M	
		Hitokura	1983	150	75	27.1	105	140	612	1657	BB	
		Kyuragi	1987	150	72.5	25	116	160	535	1616	BB	
		Inner (ELCM)	Nunome	1991	150	88	26	115	130	560	1617	M+F
			Miharu	1997	150	80	23	112	140	501	1725	M+F
			Hinachi	1998	150	87.8	26	114	130	533	1580	M+F
			Nakasujigawa	1998	150	73.3	29	110	150	615	1527	M+F
	Inner (RCD)	shimajigawa	1981	80	87.5	34	105	120	752	1482	O+F	
		Tamagawa	1990	150	73	30	95	130	657	1544	M+F	
		Mano	1991	80	85.8	33	103	120	735	1520	M+F	
		Nunome	1991	150	79.2	27	95	120	608	1670	M+F	
		Miyagase	1998	150	73.1	30	95	130	652	1568	M+F	
	Exterior	Ikari	1956	150	48.7	25.2	112	230	535	1508	M	
		Sonohara	1964	150	42.5	23	85	200	474	1563	BB	
		Shimokubo	1967	150	52.4	25	110	210	516	1570	BB	
		Ishidegawa	1972	150	48	23.5	105	220	494	1662	BB	
		Ohishi	1978	150	50	23	110	220	436	1610	M	
		Ohdo	1982	150	50	23	105	210	483	1631	M	
		Hitokura	1983	150	50	25.3	105	210	549	1657	BB	
		Kyuragi	1987	150	54.5	23	120	220	477	1608	BB	
Tamagawa		1990	150	48	22	115	240	440	1572	M+F		
Miyagase		1998	150	50	26	108	216	537	1535	M+F		
Arch	Naruko	1958	150	55.3	26	105	190	528	1504	M		
	Amagase	1964	150	48.6	26.2	107	220	528	1525	M		

(Continued)

Table 2. (Continued).

Yagisawa	1967	150	46	25	105	230	495	1504	M
Hoheikyo	1972	150	47.6	24	100	210	490	1527	M
Managawa	1977	150	51	26.5	107	210	550	1543	M
Kawaji	1983	150	43	25	100	230	520	1615	M+F

*B: binder; total of cement and admixture materials, such as blast furnace slag and fly-ash.

** Abbreviation used as types of cement; M: moderate heat portland cement, BB: blast furnace -slag cement, O: ordinary portland cement, F: fry-ash.

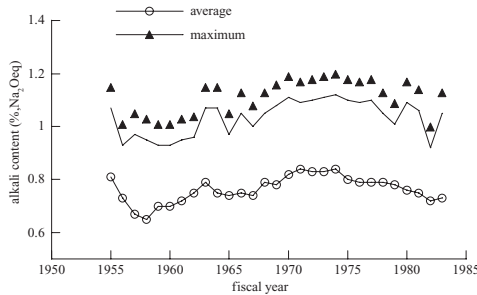


Figure 3. Alkali content of ordinary portland cement in Japan (Japan Cement Association, 1983).

the result of a document based survey of over 400 Japanese concrete dams with a height of 15 m or more.

The reason for this is considered to be the minimal amount of cement used in large dams in Japan. Typical mix proportions of concrete used in Japanese dams are listed in Table 2 (Kano et al. 2005). The amount of binder for dam concrete was usually set at less than 230 kg/m³.

On the other hand, the maximum total amount of alkali in ordinary portland cement produced between 1955 and 1984 was approximately 1.2% (Na₂Oeq) according to Fujii (1949) and a report by the Japan Cement Association (1983, Fig. 3). Alkali content of cement has been reduced since the 1980s due to growing concern over ASR (Kobayashi, 1986). Although there was no detailed information on the alkali content of moderate heat portland cement, it is estimated to be almost the same as that of ordinary portland cement.

The total alkali content of dam concrete, therefore, should be less than 2.6 kg per cubic meter of concrete. In addition, the use of fly-ash or blast-furnace slag cement has been common in dam concrete since the 1980s. The ratio of fly-ash in the mass of blended cement is usually between 20% and 40%, which should be enough to control ASR.

3 RECENT RESEARCH TOPICS ON ASR IN JAPAN

3.1 Examples affected by ASR in recent concrete structures

According to visual observations of recently built concrete structures in Japan, the number of the structures affected by ASR has decreased significantly, however, the problem has not been eliminated.

Although, it is difficult to identify the main cause of ASR in recent structures, a defect in the mitigation method using certified safe aggregate has been pointed out in several reports. For instance, Hayashi et al. (2009) reported the deterioration of a prestressed concrete bridge. ASR of the bridge was caused by opal and chalcedony produced by hydrothermal alteration in andesite, but this aggregate was judged as innocuous by the mortar-bar method normalized as the Japanese Industrial Standard testing method (JIS A 1146). Yoshizawa & Okazaki (2009) reported the deterioration of an expressway viaduct caused by fine aggregate that was certified as innocuous by the mortar-bar method. In each of these cases, ASR was caused by

a small amount of a substance having high reactivity and the ASR risk could not be accurately judged by the JIS mortar-bar method.

On the other hand, a number of researchers have stated that the control of total alkali content at 3.0 kg/m³ or less would not necessarily mitigate ASR. For instance, Katayama et al. (2008) reported the deterioration of structures in the Okinawa Expressway where total alkali content of concrete is estimated at between 2.2 and 3.5 kg/m³ depending on the structures. They also pointed out that alkali reactivity of crypto- to microcrystalline quartz contained in imported sand and sea-dredged sand from Okinawa cannot be detected by the mortar-bar method or chemical method (JIS A 1146 & 1145). Hayashi et al. (2009) reported that the total alkali content of concrete used for the prestressed concrete bridge mentioned above was 2.6 kg/m³ according to the concrete manufacturer. Obana & Torii (2008) reported ASR in prestressed concrete pavement having an estimated alkali content of 2.2 kg/m³.

3.2 Twenty-two-year exposure test

3.2.1 Test procedures

In 1987, the PWRI initiated exposure tests on concrete specimens in which various types of coarse aggregate of Japan were mixed. Ninety-five samples of coarse aggregate, about two-thirds of which were volcanic rocks, were collected throughout Japan. The purpose of the research test was to provide data for the development of improved ASR mitigation measures.

The mix proportion for the concrete specimens is shown in Table 3. Four specimens were made for each coarse aggregate: two specimens with 3 kg/m³ and two specimens with 5 kg/m³ of total alkali content in concrete. The alkali content of specimens was controlled by adding NaOH to the mixing water.

The specimens are prisms with dimensions of 150 mm in width and depth, and 800 mm in height. Two re-bars 13 mm in diameter were embedded in each specimen as reinforcement. A third part of the specimen was buried in the ground as shown in Figure 4. The specimens were exposed for 22 years in the test field, unsheltered grassland, of PWRI (Tsukuba, Japan).

Table 3. Mix proportion of concrete used for exposure test.

Gmax (mm)	W/C (%)	s/a (%)	Quantity of materials per unit volume of concrete (kg/m ³)			
			W	C	S*	G**
25	50	44	177	354	780	from 866 to 1114

* Innocuous crushed limestone was used as fine aggregate in all specimens.

** Amount of coarse aggregate was varied depending on the density.



Figure 4. Outdoor exposure condition.

Table 4. Tentative results of visual observation.

Alkali content in concrete	Number of samples possibly affected by ASR		
3 kg/m ³ (Na ₂ Oeq)	Total:	8	
	Andesite:		6
	Dacite:		1
	Dolerite:		1
5 kg/m ³ (Na ₂ Oeq)	Total:	38	
	Andesite:		21
	Sandstone:		5
	Dacite:		4
	Slate:		2
	Rhyolite:		1
	Basalt:		1
	Dolerite:		1
	Shale:		1
	Hornfels:		1
Andesitic pyroclastic rocks:		1	

Table 5. Results of petrographic observation.

Sample	Appearance	Petrographic observation		
		Rock types	Substances that have reactivity	ASR stage*
A	Cracking	Andesite 1	Cristobalite Volcanic glass	4
		Andesite 2	Volcanic glass	2 or 3
		Pelitic schist	Cryptocrystalline quartz	None
B	Cracking	Andesite	Tridymite Volcanic glass	4
C	No cracking	Andesite	Cristobalite Volcanic glass	2

* ASR stages are judged based on the classification by Katayama et al. (2008).

stage 1: Formation of reaction rims and exudation of ASR sol/gel around the reacted aggregate.

stage 2: Formation of gel-filled cracks within the reacted aggregate.

stage 3: Propagation of gel-filled cracks from the reacted aggregate into the surrounding cement paste.

stage 4: Migration of ASR gel into air voids.

3.2.2 Visual observation after approximately 22 years

In 2009, we conducted visual observation of cracks on the specimens and estimated whether or not ASR was the major cause. When there were differences in the condition of two specimens made with the same aggregate and total alkali content, it was estimated as a possible deteriorated case.

The tentative results of visual observation are shown in Table 4. Eight samples of coarse aggregate were suspected of causing ASR. Cracking on specimens with 3 kg/m³ alkali content was less significant than that on specimens with 5 kg/m³ alkali content.

3.2.3 Detailed examination of three selected specimens

Petrographic investigation was carried out using three specimens having 3 kg/m³ alkali content in the concrete. The results are shown in Table 5. Samples A and B that consist of crushed andesite stone contain cristobalite, tridymite and volcanic glass. In sections of concrete with

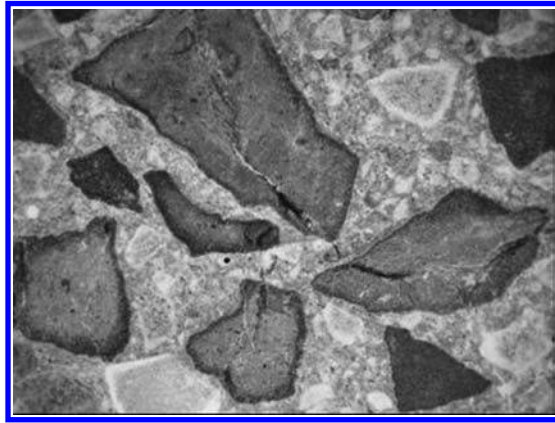


Figure 5. Cracks observed in a section (Sample A).

Samples A and B, the formation of reaction rims and cracks filled with ASR gel were identified, which is characteristic of ASR (Fig. 5).

Sample C also caused significant cracking in specimens with 5 kg/m^3 alkali content. However, in specimens with 3 kg/m^3 alkali content, while there is slight evidence of reaction by petrographic investigation, there is no significant cracking to indicate expansion of concrete. It is judged that the reactivity of Sample C was sufficiently mitigated by controlling the total alkali content at $\text{Na}_2\text{O}_{\text{eq}} 3.0 \text{ kg/m}^3$.

However, it is difficult to explain why there is a difference in ASR stages between Samples A, B and C in the concrete with $\text{Na}_2\text{O}_{\text{eq}} 3 \text{ kg/m}^3$ total alkali content.

4 CONCLUSION

Despite the wide distribution of aggregates with high alkali reactivity, there are no reports of ASR deterioration in Japanese large dams. It is assumed that this is due to the small amount of cement used in dam concrete and the use of fly-ash or blast-furnace slag cement. However, recent research has shown that some aggregates can cause expansion of concrete even at a total alkali content of less than $\text{Na}_2\text{O}_{\text{eq}} 3.0 \text{ kg/m}^3$. To ensure the success of ASR mitigation, further research is necessary on all concrete structure including large dams whose alkali content of concrete is relatively small.

REFERENCES

- Fijii, K. 1949. Excessive expansion of concrete due to reaction between cement and aggregate (3). *Cement and Concrete*, 32: 20–31 (J).
- Hayashi, K., Yamada, K., Kouno, K. & Ooba, M. 2009. Diagnosis of deterioration by ASR in a pre-stressed concrete bridge. *Proceedings of the 64th JSCE Annual Meeting*, V-099 (J).
- Japan Cement Association. 1983. JCA's opinion on the alkali aggregate reaction (J).
- Kano, S., Morihama, K. & Katahira, H. 2005. Properties of dam concrete. In Japan Dam Engineering Center ed. *Construction of Multi-Purpose Dams*, 5: 1–28 (J).
- Katayama, T., Oshiro, T., Sarai, Y., Zaha, K. & Yamato, T. 2008. Late-expansive ASR due to imported sand and local aggregates in Okinawa Island, southwestern Japan. *Proceedings of the 13th International Conference on Alkali-Aggregate Reaction in Concrete*, 862–873.
- Kawano, H. & Koga, H. 2005. Current status of deterioration of road bridges due to ASR. *Civil Engineering Journal*, 47(12): 66–71 (J).
- Kobayashi, S. 1986. Tests on dams; Testing methods and countermeasures against alkali-aggregate reaction; Official notice of the Ministry of Construction and its application. *Engineering for Dams*, 4(3): 34–45 (J).

- Obana, Y. & Torii, K. 2008. Case studies on deterioration of ASR-affected PC and PCa members. *Proceedings of the Japan Concrete Institute*, 30(1): 1065–1070 (J).
- Wakizaka, Y. 1998. Reactivity of rocks and minerals in alkaline solution. *Journal of Research; Public Works Research Institute*, 34.
- Yoshizawa, M. & Okazaki, K. 2009. Alkali reactivity of fine aggregate causing deterioration of PC bridge superstructure due to ASR. *Proceedings of the 64th JSCE Annual Meeting*, V-109 (J).

Experimental study on the detection and inhibition of alkali aggregate reactivity for dam concrete

C. Zhiqing, L. Xingping, Y. Jie, L. Shisheng & W. Ling

Hydrochina Kunming Engineering Corporation, Kunming, Yunnan province, China

L. Han

Yunnan University, Kunming, Yunnan province China

ABSTRACT: In this paper, the alkali silica reactivity (ASR) and alkali carbonate reactivity (ACR) of different aggregates are determined by means of petrographic test, accelerated autoclave test method, accelerated mortar bar test, mortar length method, rock column test and concrete prism test. In addition, fly ash (F), lava ash (H) and the mixture of iron-ore slag & ground limestone power (TL) are used to inhibit the ASR of potential aggregate. The results show that the alkali aggregate reactivity is closely associated with the lithological and mineral composition; the expansion rate of mortar at each age can be decreased by mixing the mineral admixture, the effect of inhibition against mortar expansion is enhanced with the incremental mixing of F and H; the inhibition effect of F against the alkali aggregate reactivity is the most distinct as the ASR expansion rate can be effectively controlled within the specification for the non-alkali reactivity of aggregate with the mixture of fly ash up to 25%, the inhibition effect of lava ash is less distinct, and of TL power is a little poor.

1 INSTRUCTIONS

With the ceaseless construction of hydraulic power projects, China has become one of the country with the most dams in the world, as concrete is the material used the most in a dam project, its durability draws more and more attention. AAR (alkali aggregate reactivity) is regarded as the “unbeatable enemy” of concrete durability, so the protection from AAR has become one of the most important issues for dam concrete projects (Oi 2006).

AAR is divided into ASR (alkali silica reactivity) and ACR (alkali carbonate reactivity), and AAR is mainly controlled by two measures: the first is to use non-active aggregate, and it is the safest and most reliable way to prevent AAR, but there are not so many types of aggregate for selecting as active aggregates are widely distributed and practical application is limited by field conditions and cost; the second is to inhibit AAR with mineral admixtures or additives in the usage of the active aggregate. This paper relates to the experimental study of the detection and inhibition of concrete AAR.

2 RAW MATERIAL AND TEST METHOD

2.1 *Raw material*

Cements used in the experiment are Dianxi Hongta Grade 42.5 moderate-heat portland cement and Jianfeng Grade 42.5 P-I portland cement, and the alkali contents are respectively 0.52% and 0.65%; the mineral admixtures are Grade 2 fly ash (F) manufactured by Yunnan Huadian (Kunming) Corporation, lava ash (H) manufactured by Jiangteng Lava Ash Corporation and the mixture of iron-ore slag & limestone powder (TL, weight ratio = 5:5)

manufactured by Desheng Steel & Iron Corporation; the experiment is performed with metamorphic volcanic breccia, ash rock, slate and limestone aggregates.

2.2 Test method

The test is performed according to Test Code for Aggregates of Hydraulic Concrete (DL/T 5151–2001) and A Rapid Test Method of Determining the Alkali Reactivity of Sands and Rocks (CECS 48: 93). Petrographic test method, accelerated autoclave test, accelerated mortar bar test, mortar length method, rock column test and concrete prism test are performed for the AAR study, and AAR inhibition effect test and accelerated mortar bar test are used to compare the AAR inhibition of different proportions of mineral admixtures.

The mortar length test is performed with Grade 42.5 moderate-heat portland cement, the accelerated autoclave test, accelerated mortar bar test and concrete prism test are performed with Grade 42.5 P-I portland cement, and cement is replaced by mineral admixtures in the same amount.

3 AAR TEST

AAR experimental study is performed with 9 aggregates by 6 methods, in which, ASR is tested by accelerated mortar bar, mortar length and accelerated autoclave, and ACR is tested by rock column. See Table 1 and Figures 1–5 for the test result.

Table 1. AAR test result.

SN	Aggregate	Petrographic test		ASR			ACR	
		Alkali mineral name	Content (%)	Accelerated autoclave test	Accelerated mortar bar test	Mortar length test	Rock column test	Concrete prism test
1	Volcanic breccia	Stress quartz	19	Non active	Non active	Non active	/	/
2	Volcanic breccia	Felsitic felsic (chalcedony), particle quartz	7	Non active	Potentially active	Non active	/	/
3	Ash rock	Stress and particle quartz, felsitic fescic (or silicoide)	18	Non active	Non active	Non active	/	/
4	Ash rock	Felsitic quartz and siliceous rock	25	Non active	Potentially active	Non active	/	/
5	Ash slate	Felsitic quartz and siliceous rock	30–40	Active	Potentially active	Non active	/	/
6	Ash slate	Felsitic and crack quartz in acid effusive rock	30	Active	Potentially active	Non active	/	/
7	Limestone	Microcrystalline dolomite, quartz and chalcedony	17	Non active	Non active	Non active	Non active	Non active
8	Dolomitic limestone	Microcrystalline dolomite and self-generated quartz	18	Non active	Non active	Non active	Non active	Non active
9	Dolomitic limestone	Microcrystalline dolomite and quartz	25	Non active	Potentially active	Non active	Non active	Potentially active

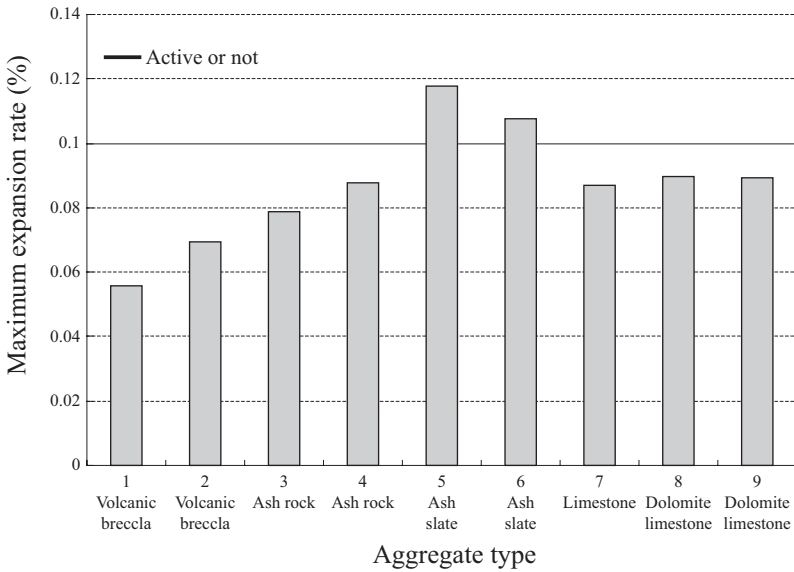


Figure 1. Maximum mortar expansion rate (accelerated autoclave test).

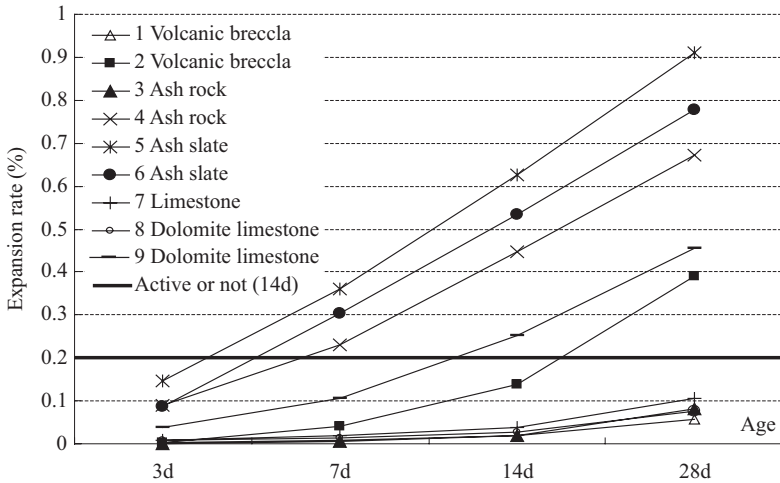


Figure 2. Mortar expansion rate—time increasing curve (accelerated mortar bar test).

The test result shows:

1. Alkali active minerals exist in quartz, microcrystalline dolomite and chalcedony, etc, with the content ranging from 7% to 40%. The AAR rate is higher with more Alkali active minerals composed, and in general, the potential AAR shall be strictly examined if the content of alkali active minerals is more than 20%.
2. The accelerated autoclave test for the 2 groups of ash slate with the highest content of alkali active minerals (more than 30%) shows the maximum expansion rates are both 0.1% above, and thus these two groups are determined as the ASR aggregate. The other 7 groups are not determined as the ASR aggregate, but four of them are presented with a critical expansion rate of 0.08% above for each.
3. The accelerated mortar bar test shows a favorable conformity with the engineering practical test result for the siliceous aggregate especially the slow-expanding siliceous aggregate (Duyou et al. 1998) and particularly the aggregate which reacts slowly and expands only in the later

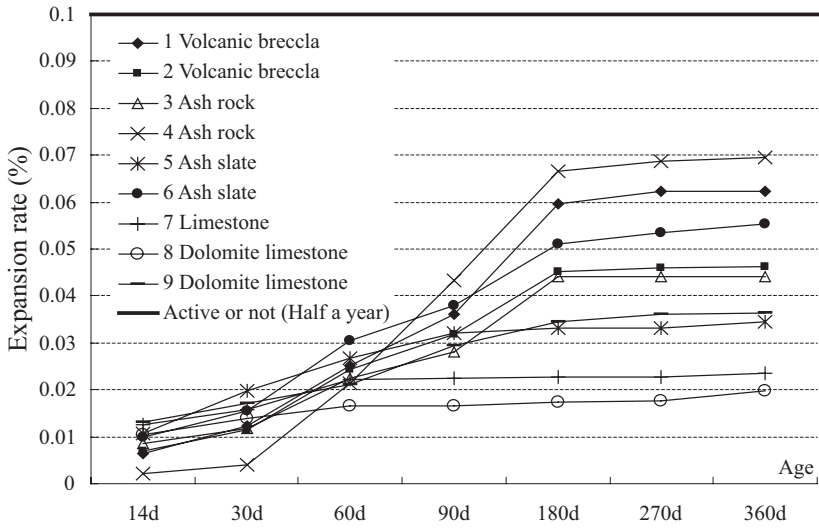


Figure 3. Mortar expansion rate—time increasing curve (mortar length method).

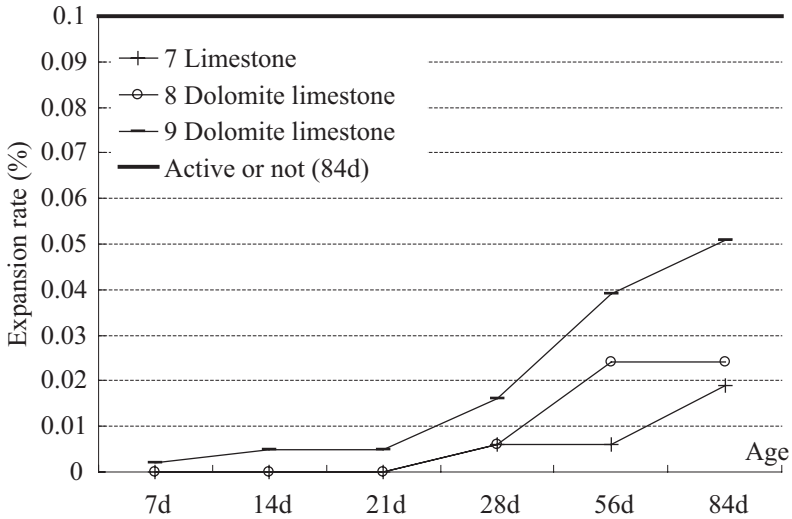


Figure 4. Rock column expansion rate—time increasing curve (rock column test).

phase. In the test, the expansion rate of each group of mortar is kept increasing sharply and is not stabilized at the 28th day. The expansion rate of 4 groups is above 0.2% at the 14th day, in which, the ash slate group containing 30%–40% alkali active minerals has expanded for 0.62% at the 14th day, 1 group of volcanic breccia has expanded for 0.1%–0.2% at the 14th day, and up to 0.39% at the 28th day. These 5 groups are all determined as the potential active aggregate (ASR). As the accelerated mortar bar test is performed in strict conditions, so the mortar expansion rate obtained is the maximum of all. Some aggregates which are deemed not active may still exceed the critical expanding rate, so this method is very effective for aggregate selection other than any basis for aggregate rejection (Berube et al. 1992, Mullick et al. 1996).

4. Mortar length method is applicable for some highly active and rapid-expanding ASR aggregates. In the test, the mortar expansion rate increases slowly in the first 30 days, sharply from the 30th day to the 180th day, and is stabilized after the 180th day. All the 9 groups are expanded for 0.015%–0.067% within 180 days which is below the critical value of 0.10%.

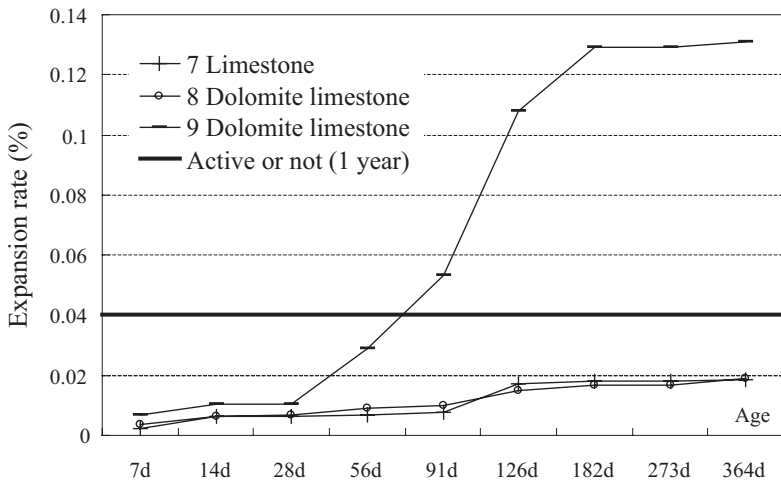


Figure 5. Concrete expansion rate—time increasing curve (concrete prism test).

5. Rock column test is made to measure the length change of carbonate aggregate in an alkali solution, and is used for determining whether the concrete aggregate has ACR. 3 groups of limestone aggregate expands slowly in the alkali solution within the first 21 days, sharply from the 28th day, and is stabilized at 0.019%–0.051% within 84 days which is below the critical value of 0.1%.
6. Concrete prism test is used for ASR and ACR aggregates. 2 groups of dolomitic limestone aggregate concrete expands a little and slowly, and is only expanded for 0.018% within 1 year, and thus they are determined as non-active aggregate. The other group expands slowly within the first 28 days, sharply from the 28th day, gradually stabilized after the 182nd day, and expands for 0.131% within 1 year which is much higher than the critical value of 0.04%.

AAR is closely associated with the aggregate lithological and mineral composition, and is varying with activity and content of minerals. The current 6 test methods are applicable for different AAR aggregate, each kind of aggregate shall be tested by the suitable method and the AAR shall be determined by several test methods comprehensively.

4 AAR INHIBITION TEST

AAR inhibition effect test and accelerated mortar bar test are made for a comparison to study the AAR inhibition effect of different mineral admixtures of F, H and TL. The test is made according to Test Code for Aggregates of Hydraulic Concrete (DL/T 5151–2001).

4.1 AAR inhibition effect test

In this test, highly active quartz glass sand with a SiO_2 content of 99.0% is used as the aggregate, and shaping and length measuring are realized with the same mortar to determine the inhibition effect of the mineral admixture. If the expansion rate of the test sample is decreased by more than 75% at the 14th day and is lower than 0.05% at the 56th day, it will be determined as that the admixture in the corresponding amount is effective in AAR inhibition. See Figure 6 for the test result. In the figure, JZ, F25%, H50% and TL60% respectively said without mineral admixture, 25% of fly ash, 50% of lava ash and 60% of TL power, following the same.

The test result shows that: (1) The expansion rate of mortar at each stage is decreased when 25%, 50% and 60% of F, H and TL are respectively admixed; and it decreases with the increasing of mineral admixture at the same type and condition. (2) In the same amount of mineral admixture, the expansion rate of F mortar decreases the most and reaches 83.8%,

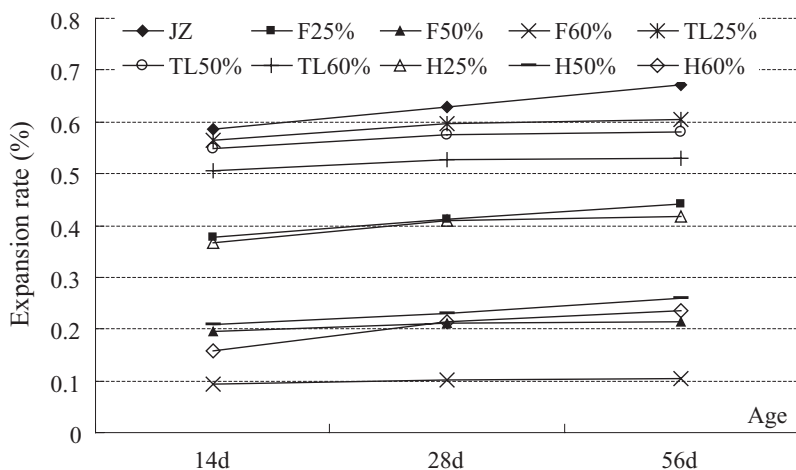


Figure 6. Mortar expansion rate—time increasing curve (AAR inhibition effect test).

and the AAR inhibition effect is the best; the expansion rate of H mortar decreases no so large (73.1% at maximum), and the inhibition effect of TL is the poorest (13.6% at the minimum). (3) The inhibition effect of the inhibiting material is evaluated by a strict standard, and in the test only the expansion rate of 60% fly-ash mortar sample has decreased for 75% at least on the 14th day but exceeded 0.05% on the 56th day. Therefore, none of the three mineral admixtures in the respective amounts complies with the standard for inhibition effect.

4.2 Comparison test for AAR inhibition of different mineral admixtures

The test is made by the accelerated mortar bar method with dolomitic limestone aggregate, and the test result is shown in Table 2 and Figure 7.

The result of accelerated mortar bar test shows that: (1) Dolomitic limestone is determined as a potential active aggregate (ASR), and the mortar expansion rate decreases respectively at each stage if F, H and TL at the respective amounts of 25%, 50% and 60% are admixed into the mortar. (2) In the same admixture condition, the one with the best inhibition effect against ASR is F, with the second best effect is H and the poorest is TL, complying with the AAR inhibition effect test result. (3) When the mineral admixture amount of F reaches 25%, the expansion rate of mortar can be reduced by 93.3% within the control range for the non-active aggregate, the inhibition effect improves with the increasing amount of the admixture, and the effect is not still obvious if the admixture amount reaches up to or over 50%. (4) The mortar expansion rate will be controlled within 0.1% after the 14th day only when the H admixture amount reaches 50%, and at this time it also shows an inhibition effect against ASR; the mortar expansion rate is still 0.1% above even if the admixture amount of TL reaches 60% and the inhibition effect is not favorable. This result is closely associated with the mineral composition and reactivity of the 3 aggregates.

The inhibition effect of the mineral admixture against ASR is mainly the physical dilution and adsorption for alkali and the reaction with $\text{Ca}(\text{OH})_2$ to reduce the alkali content and improve the compactness, etc (Duyou et al. 1999). Fly ash can be reacted with the alkali and $\text{Ca}(\text{OH})_2$ in the concrete to effectively reduce the content of OH^- in the concrete mortar, lighten the alkali corrosion against the active aggregate and inhibit ASR (Dingyan et al. 2008). In addition, not all admixtures have the inhibition effect against ASR, as the inhibition effect is determined by the effective alkali content, CaO content, fineness, pozzolanic activity and admixture amount, etc (Chenzhi et al. 2006, Kazuaki et al. 1989), so a careful and scientific analysis shall be made before practical application.

Table 2. Mortar expansion decreasing rate (Comparison test for AAR inhibition).

Test SN	Mineral admixture		Mortar expansion decreasing rate (%)				
	Name	Amount (%)	3d	7d	14d	28d	56d
JZ	/	0	0	0	0	0	0
F25%	F	25	89.5	93.3	92.8	91.3	89.7
F50%		50	100.6	99.9	99.8	99.3	98.9
F60%		60	121.5	102.1	100.2	99.3	98.9
Mean value			103.9	98.4	97.6	96.7	95.8
TL25%	TL	25	55.2	44.1	31.7	17.1	13.1
TL50%		50	23.8	26.4	28.6	24.4	21.7
TL60%		60	4.1	8.5	15.8	25.6	26.4
Mean value			27.7	26.3	25.3	22.3	20.4
H25%	H	25	22.1	27.3	31.0	43.3	49.0
H50%		50	37.2	45.2	68.6	75.9	78.5
H60%		60	45.1	71.1	85.2	86.6	88.6
Mean value			34.8	47.9	61.6	68.6	72.1

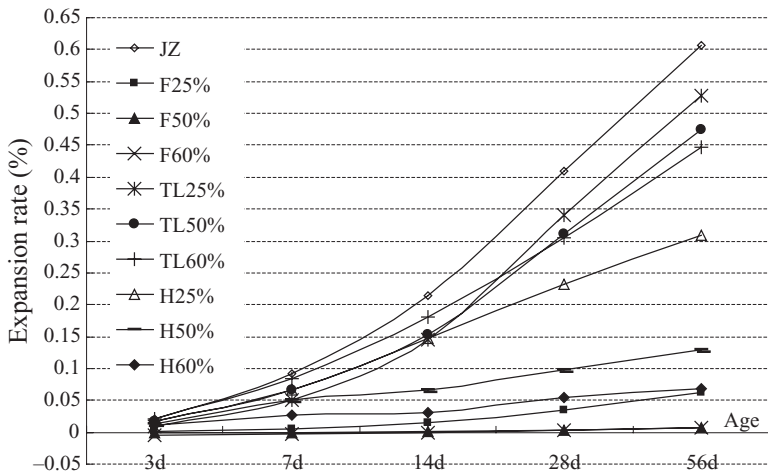


Figure 7. Expansion rate—time increasing curve after admixing (accelerated mortar bar test).

5 CONCLUSION

1. AAR is closely associated with the aggregate lithological and mineral composition, the alkali reactivity test method shall be selected as per the aggregate property, and AAR shall be determined by several test methods comprehensively.
2. The mortar expansion rate at each stage can be decreased by admixing fly ash, lava ash and mixture of iron-ore slag & limestone powder, and the effect improves with the increasing of the admixture amount.
3. The AAR inhibition effect of fly ash is the best, as the expansion rate of ASR can be controlled within the specified range only by admixing 25% of fly ash, the inhibition effect of lava ash is not so good, and of the mixture of iron-ore slag & limestone powder is the poorest.

REFERENCES

- Berube, M.A. et al. 1992. Effectiveness of the accelerated mortar bar method, ASTM C9-Proposal P214 or for assessing potential AAR in Quebec(Canada). *Proceeding of the 9th international conference on AAR in concrete, London*. 1:92–101.

- Chenzhi, Zhang & Ai qin, Wang. 2006. Study on the problems of mineral admixture on alkali-aggregate reaction. *China Concrete and Cement Products* 5(10):5–8.
- Dingyan, Wu et al. 2008. Research on alkali activity and inhibition with fly ash of aggregate. *Concrete* 219(1):69–72.
- Duyou, Lu et al. 1998. A review on the testing methods for indentifying the ask reactivity of aggregate. *Journal of Nanjing University of Chemical Technology* 20(4):86–92.
- Duyou, Lu et al. 1999. Study on the methods for inhibiting ASR. *China Concrete and Cement Products* 2(4):14–17.
- Kazuaki, Ukita et al. 1989. Effect of Classified Fly Ash on Alkali Aggregate Reaction. *Proceedings of 8th International Conference on Alkali-Aggregate Reaction, Kyoto*. 259–264.
- Mullick, A.K. & Wason, R.C. 1996. NBRI test on aggregates containing strained quartz. Shayan A. Eds, *Proceeding of 10th ICAAR, CSIRO divison of building construction and engineering, Australia: Melbourne*. 340–347.
- Qi, Yin. 2006. An experimental study on the expansion mechanism of alkali-silica reaction in concrete. *China Civil Engineering Journal* 39(8):76–80.

Expanding concrete in dams—long term challenges

R. Charlwood

Robin Charlwood & Associates, Seattle, WA, USA
Chairman, ICOLD Committee on Concrete Dams

K. Scrivener

Ecole Polytechnique Federal de Lausanne, Lausanne, Switzerland
Editor, Cement and Concrete Research, Elsevier Publications

ABSTRACT: Over 100 large dams and hydroelectric projects have been identified to be seriously affected by expanding concrete reactions in terms of dam safety and operations and in an increasing number of cases, the expansion appears to be continuing unabated. This paper will address the definition and characterization of the various underlying chemical mechanisms that are claimed to be affecting many dams and then identify of mechanisms affecting very long term alkali-silica reactions, the most common expansive reaction. Examples of long term expansion driven deformation will be shown where the rate of expansion is continuing unabated after forty or more years even with very low alkali content cements. The relative roles of alkali supply from various sources including the original cement, alkali “recycling” as the gels transform, and alkali release from certain aggregates will be discussed and long term effects identified.

1 INTRODUCTION

Only a few years ago an ICOLD paper stated that nearly 10% of concrete and masonry dams damaged by ageing undergo expansion. Recent experience suggests this figure is higher as many cases of dam expansion have been reported lately and it must also be noted that the phenomenon can also occur even if it is not directly apparent. Over 100 large dams and hydroelectric projects have been identified to be seriously affected by various forms of expansive chemical reactions in the concrete impacting dam safety and operations. Given the realization that most dams will be required to continue to operate well into the future, way beyond the 30 to 50 year service life that was initially considered, these long term behavior issues are going to become increasingly important.

Most of these reactions are an “alkali-aggregate reaction” (AAR) but other less well recognized chemical reactions appear to playing an important role as well. The characteristics of these “other reactions” and opportunities for prevention in new structures or management in existing structures are not as well understood as those of AAR.

Another key aspect, that is becoming increasingly apparent in existing structures, is that in many cases the reactions and associated expansions are continuing unabated after 40 or more years. The magnitude and duration of the residual expansion can be a key factor in estimating the remaining service life of a dam and is very difficult to estimate in the cases where expansion is continuing. The notion that with AAR the alkali source was the cement is now realized to be only part of the story, in many cases alkalis become available from certain reactive aggregates with time. This will clearly affect the duration of the reactions and in many cases will cause the reaction to continue effectively indefinitely. However, in new structures, where potentially reactive aggregates are being used, supplementary cementitious materials (SCMs) (such as pozzolans), if used in sufficient quantities, should still be effective by increasing the amount of alkalis fixed by the cement hydrates and so lowering the pH of

the pore solution, such that the reactivity of the aggregates (and consequently their release of alkalis) is minimized although this needs to be confirmed as discussed below.

Upon reviewing the current state of knowledge of expansion phenomena, it can be concluded that greater knowledge is required on several of the fundamental processes involved in concrete expansion and how it can be avoided or managed if they are present. Deficiencies in the knowledge and the treatment of chemical expansion phenomena include the following topics which were identified in the Workshop on Expanding Concrete in Dams held in Granada, Spain (ICOLD/SPANCOLD 2007) and summarized in *Hydropower and Dams* (Charlwood & Buil, 2008) are the subject of a new ICOLD Bulletin currently under preparation by the ICOLD Committee on Concrete Dams and ongoing work by the RILEM-ACS sub-committee (RILEM-ACS, 2010):

- Chemical reaction development and expansion mechanisms.
- Laboratory testing and analyses of materials.
- Reliable mathematical models for diagnosis and control.
- Practical procedures for determination of model parameters.
- Methods for estimation of residual long term expansion in affected dams.
- Techniques for long term rehabilitation of affected dams.
- Preventative measures of phenomena for new dams including the long term effectiveness of SCMs.

This paper will focus on two important fundamental long term issues from this list that are associated with continued operation of dams and hydro-electric projects:

- Definition and characterization of the underlying chemical mechanisms that are claimed to be affecting many dams: Alkali-Aggregate Reactions (AAR) including alkali-silica reactions (ASR) and alkali-carbonate reactions (ACR); Sulfate related deteriorations including external sulphate attack, Thaumasite formation, and internal sulphate attack (ISA) including, pyrite oxidation and delayed ettringite formation (DEF).
- Identification of mechanisms affecting very long term ASR expansion: Examples of long term expansion driven deformation will be shown where the rate of expansion is continuing unabated after forty or more years even with very low alkali content cements. The relative roles of alkali supply from various sources including the original cement, alkali “recycling” as the gels transform, and alkali release from certain aggregates will be discussed. Whereas the alkali supply from the cement may start early and be limited in duration, those coming from recycling or release from certain aggregates may become available in significant quantities later, and can cause the ASR to start very slowly and show as expansion much later and continue essentially indefinitely, even if the precautions of using low alkali cements were taken. The expected long term behaviour of concretes using SCMs in the presence of alkali release also raises some questions which will also be briefly addressed.

2 EXPANSIVE CHEMICAL REACTIONS IN CONCRETE DAMS

This section outlines the mechanisms behind processes which cause expansion in concrete and outlines their relevance for massive concrete dam structures.

2.1 *Alkali aggregate reaction*

By far the most relevant process leading to the expansion of concrete in dams is alkali aggregate reaction, AAR. There are two main types of AAR: ASR (alkali silica reaction) and ACR (alkali carbonated reaction) although the later is disputed to be also a form of ASR due to fine inclusions of silicate in the carbonate rocks (Katayama 2010).

In ASR, the alkaline pore solution of the cement pastes attacks reactive siliceous material in the aggregates, producing an alkali silica gel which imbibes water and swells. As gel usually forms inside the aggregate the gel cracks the aggregate, which in turn causes expansion and

cracking of the surrounding cement paste. The level of expansion strain before the appearance of visible surface cracks is usually around 0.04%. Frequently alkalis are leached from the surface regions, and then the differential expansion of the core concrete compared to the surface can lead to conspicuous cracks opening on the surface, the “map” or “pattern” cracking, that is often an obvious indicator of ASR.

The main parameters affecting ASR are temperature, pH of the pore solution, mineralogy of the aggregates and composition of the cement pastes (presence of pozzolans, etc). The relationship of reaction rate with temperature has been widely shown to follow the Arrhenius relationship shown in Equation 1 below.

$$\text{Rate} = R_{\text{ref}} \exp(-E_a/RT) \quad (1)$$

where R_{ref} = a pre-exponent factor; E_a = activation energy; R = universal gas constant; and T = absolute temperature.

However, high temperatures (60°C and above) may lead to additional effects, discussed in the paragraphs on pH and mineralogy below. The relationship is agreed to hold for temperatures up to around 38°C–50°C. Several publications give figures for the activation energy of typical mass concretes of around 40–50 kJ/mol, which is considered to correspond to the rupture of silanol bonds. As a very rough approximation it may be assumed that the reaction rate doubles for every 10°C increase in temperature. For a given concrete the activation energy can be determined by running expansion tests at at least 3 temperatures in the range in which the relation is considered valid.

The dependence on pH is less well established. Much early work focused on the existence of an “alkali threshold” (expressed in kg/m³ of concrete) and this was initially assumed to be in the range 3–4 kg/m³. However longer term tests, involving exposure of large blocks and field studies indicate that this “threshold” is much lower than values derived from short term laboratory testing and may be 1.5 kg/m³ or less. Lower alkali levels extend the induction period, before expansion is apparent and slow its rate and therefore tests need to be of long enough duration (without loss of alkalis through leaching) to recognize these factors. At ambient temperatures the alkalis ions (Na⁺ and K⁺) in solution are effectively balanced by OH⁻ ions so there is a direct relation between the alkali content and pH. As the temperature is raised above about 50°C there is an increase in the concentration of sulfate ions which partially balance the alkali ions, leading to a decrease in pH for the same alkali content. This could explain why lower expansions may be seen in high temperature testing (although the rapid leaching of alkalis at higher temperatures is also a factor). The questions of alkali content and pH are further complicated by the binding of alkali in the ASR gel and also in the cement hydrates; by the “recycling” of alkalis as ASR gel transforms to C-S-H when it comes into contact with the paste, so releasing alkalis. Yet another factor is that some rock minerals (e.g. feldspars) may release alkalis as they react: This may be of considerable importance in dams, which have slowly reacting rock types which show a long induction period and continue to react without apparent slowing down.

The dependence on mineralogy is complex owing in the main to the very large variety of minerals found in the earth’s crust. Broadly speaking the reactivity of a mineral increases as its crystal structure becomes more disorganized allowing easier penetration of the alkaline pore solution into the mineral structure.

2.2 Sulfate attack

The other group of reactions leading to expansion is caused by sulfate ions. The expansion is caused by the formation of ettringite. Generally it is described as due to the fact that the volume of ettringite is greater than the reacting phases. However, this is not correct. When all the reacting species, including water are considered the formation of ettringite leads to an overall decrease in volume. If the water needed for the reaction has to come from outside the system then it can be considered that there is a volume increase, but this alone is not sufficient to cause expansion. If this was the case the formation of other hydrates, such as

C-S-H in low water to cement ratio pastes, where water comes from outside would also give expansion, which is not observed. Furthermore all cementitious materials contain a considerable amount of porosity, in which the ettringite can form harmlessly. For expansion to occur, ettringite must form under conditions of super-saturation and in a region where its growth is confined by other phases. Indeed it is important to note that the fine ettringite normally formed as a product of cement hydration, slowly re-crystallizes into large crystals in pores over time. Thus the observation of large ettringite crystals is a common and normal feature of old concrete exposed to water.

The most common form of “sulfate attack” occurs on concretes in contact with water containing high concentrations of sulfate ions. The relatively high concentrations of sulfate ions needed to produce external sulfate attack are unlikely to be found in dams, except possibly in foundations. However, even in such cases, this form of degradation is a progressive phenomenon, starting from the surface, with successive layers being degraded and disintegrating so it would not lead to massive expansion of the whole structure.

Thaumasite formation may sometimes occur as the final stage of external sulfate attack. Once all the available aluminate has reacted to form ettringite. The sulfate ions, together with carbonate ions, may lead to the formation of Thaumasite. Due to the presence of silicate in its structure in place of the aluminate in ettringite, Thaumasite formation leads to decompositions of the main binding phase, C-S-H and the concrete disintegrates into a “mush”. Thaumasite formation is very slow, although it seems to be favored by low temperatures. The only serious cases of Thaumasite formation have occurred in very poor quality concrete with water/cement ratios in the range 0.8 and above. Thaumasite formation is the final stage of degradation in sulfate attack and as such is a progressive surface phenomenon, which will not produce massive expansion.

Following the above arguments “external” sulfate attack (ESA) can be effectively ruled out as a cause of massive expansion in structures such as dams.

Internal sulfate attack (ISA) can arise from sulfate provided by the aggregate or due to elevated temperatures ($>70\text{--}80^\circ\text{C}$) during initial hydration. The latter is often referred to as delayed ettringite formation or DEF and will be discussed first. The solubility of ettringite increases with temperature and with the concentration of alkalis in the pores solution. Therefore, instead of ettringite forming as a primary hydration product, monosulfate is formed and higher than normal levels of sulfate are absorbed on the C-S-H phase. When the concrete returns to lower temperatures sulfate is released by the C-S-H phase and reacts with the monosulfate to form ettringite. In some situations this ettringite formation may be expansive. To prevent DEF the maximum temperature should be limited. Some standards require a maximum temperature below 60°C , but this is certainly very much on the safe side. Experience shows that very few cements show problems at temperatures below 80°C . In dams measures are always taken to restrict maximum temperatures to avoid problems of thermal cracking so temperatures high enough to produce problems of temperature induced DEF should be unlikely. Field cases of heat induced delayed ettringite formation in in-situ concrete have arisen only when concrete with a high cement content ($>400\text{ kg/m}^3$) was cast in summer in large masses.

The other form of internal sulfate attack which certainly has caused problems in dams is due to release of sulfate from rock containing iron sulfides. Ironmonosulfide (pyrrhotite, FeS) and irondisulfide (pyrite, FeS_2) may both oxidise to give iron oxide and sulfate ions. These sulfate ions may then react with the cement paste to give ettringite. Large deposits of ettringite may certainly be found in affected concrete, however it is not yet clear, whether expansion is related to ettringite formation as the degree of supersaturation and restraint are likely to be small or to the formation of iron oxides within composite rocks, which also entails an increase in volume and cracking of the aggregates. Aggregates containing iron sulphide show rusty deposits on the surface, although rusty deposits do not always come from iron sulfides.

2.3 Comparisons

From the above discussion, it is clear that by far the most common form of expansive process affecting dams is Alkali Aggregate reaction. Apart from this a much smaller number of cases

may be attributed to iron sulfide containing rocks. Heat induced delayed ettringite formation should not occur if proper precautions have been taken to avoid thermal cracking. External sulfate attack will not give large scale expansions and is not a realistic possibility in dams other than peraps foundations.

3 LONG TERM EXPANSION BEHAVIOR

Some of the early cases of ASR that were reported in the USA (USCOLD, 1995) (with aggregate types shown in brackets), such as Stewart Mountain (rhyolitic, andesitic volcanics), Gene Wash (andesite, rhyolite) and Copper Basin (andesite, rhyolite) dams showed rapid initial expansion and then a slowing and ending of expansion after about 25 years. This limited period of expansion was interpreted to be due to the supply of alkalis being readily available from the cement and once this is used up, the reaction and related expansion ceases. However, as discussed below, when alkali silica gels come into contact with cement pastes, they will react with calcium ions to give the normal calcium silica hydrate (C-S-H) binding phase and in so doing the alkalis will be released.

Laboratory tests commonly show an “S-shaped” expansion versus time curve but this is realized to be due to the fact that alkalis are slowly washed out of small laboratory specimens and expansion usually stops, for this reason, after only a few years.

However, there have been an increasing number of cases of ASR where SCMs were not used and expansion is continuing after 40 years or more years, such as at Fontana (greywacke—USA), Hiwassee (greywacke—USA) and Roanoke Rapids (granitic-gneiss—USA), R.H. Saunders (limestone—Canada) and Mactaquac (greywacke—Canada), Chambon (gneiss—France), Kariba (granitic gneiss—Zambia/Zimbabwe) and Cahora Bassa (granite, porphyritic gneiss—Mozambique) dams. There have also been some cases exhibiting features of both AAR and of ISA such as San Esteban (granite, diabase, gneiss and shale with some pyrite—Spain).

In the 1980's tests were being done at some projects where expansion was continuing to measure free alkali content of the concrete (using test procedure ASTM C114 for instance). It was found that the amount of alkalis was sometimes at least the same or even greater than the initial alkali loading from the cements. This led to the recognition that in some cases alkalis were also being supplied by the aggregates. Two informative papers were published (Berube et al. 2002; and Constantiner & Diamond 2003) identifying the potential role of certain aggregates to supply alkalis. Berube's tests involved measuring the pickup of alkalis in various alkali solutions and were on both finely ground aggregate particles and also on concrete cores from dams. Berube showed that in several cases the amount of alkalis present in the concrete mix could be at least as much as that in the cement component. Constantiner and Diamond measured the alkali content in pore solutions in concrete and confirmed presence of the alkali supply from certain aggregates.

The role that such an alkali supply can play in the long term behavior of dams clearly warrants serious attention in terms of the duration of remaining expansion, perhaps effectively for ever, and whether or not such a supply can overpower the preventative value of using SCMs to reduce the initial alkali loading. These issues are the subject of the next section.

4 ACTION OF SCMs IN PREVENTING EXPANSION DUE TO ASR

The use of supplementary cementitious materials (SCMs) such as fly ash or other pozzolans to reduce the effects of ASR appears to have been a successful strategy to date in many cases, Lower Notch dam (greywacke-siltstone—Canada) for instance. The role of SCMs in alkali silica reaction has been recently reviewed by Thomas (Thomas 2011). SCMs work primarily by reducing the alkalinity of the pore solution over and above what would occur by simple dilution. This is brought about by the fact that the pozzolanic reaction lowers the calcium to silicon ratio in the C-S-H phases, which increases its capacity to fix alkalis. Although it is the impact on pore solution composition, brought about by the changes in C-S-H which is the

major factor, there are some aspects of the action of SCMs which are less clear. For example additions of silica fume seem, lower the pore solution pH over the first month, but the pH may subsequently rise to reasons which are not known. Furthermore, SCMs containing aluminum, such as fly ash and metakaolin seem to be more efficient in suppressing ASR, even though they do not lower the pore solution alkalinity as efficiently as silica fume.

Our lack of understanding of these details and inadequacy of test methods for concrete compositions, makes it difficult to determine how much addition of SCM is needed to suppress ASR with a given aggregate. Fortunately with dams, where the requirement for strength is not high one can make large substitutions of cement with SCMs (to be on the safe side) and such additions also make a positive contribution to minimizing temperature rise during hydration

5 IMPLICATIONS FOR THE LONG TERM FUTURE OF DAMS

Field experience and long terms tests on large blocks indicate that the alkali content in concrete needed to trigger ASR with reactive aggregates is much lower than the 3 kg/m^3 , which is often regarded as a safe limit. This limit of 3 kg/m^3 came from laboratory tests where alkalis leached out over time. This may be a reasonable limit for thin structural elements, where leaching may also occur. However in massive dams, leaching of alkalis is insignificant except in the outer surface layers and as is clear from the numerous field cases expansion may occur at alkali loadings less than half then 3 kg/m^3 . In addition to the initial alkali loading it is also clear that alkalis can be released from certain reactive aggregates, especially feldspar-rich ones. Bérubé et al. (2002) showed that such release may contribute around 1 kg/m^3 in mature concrete cored from dams. At present there does not seem to be a good test method to measure the amount of alkalis likely to come from aggregates.

For new concrete the addition of SCMs, such as fly ash seems to be the best solution to avoid problems from ASR. The reliability of test methods is roughly in proportion to their duration—short tests being the least reliable and long term tests the most reliable. However with dams, there is usually enough time to plan long terms tests at a very early stage during the feasibility and design phases. Thomas et al. (2009) describe the strategy being employed to verify the mix design for the replacement of the Mactaquac dam, which may have to be replaced in the next 10–20 years. In this case they may have to use known reactive aggregates and will compensate using SCMs. The study program is including some very long term tests.

As noted above, our present understanding of the chemistry of the behavior of SCMs suggests that they should also perform in the long term in cases where alkalis are available from certain aggregates. This aspect is worthy of further investigation.

For existing structures there may be two situations, one where no SCMs were used and one where they are present. In the former case, it appears that alkali supply from certain aggregates can certainly supply sufficient alkalis to sustain ASR for the indefinite future. Research to date (Berube et al. 2002) has indicated the total amounts of alkalis that may be available in certain aggregates. However, the available data does not provide data on the rates of release of these alkalis. It is debatable whether or not we need this rate data. On the one hand, it may provide a basis to assess whether the observed rates of expansion will be maintained, accelerate or slow down and whether the reactions will continue to the extent that significant structural deterioration of the concrete will occur. In some cases where expansion has continued for 40 or more years, and alkali supply from the aggregates is occurring, there are some subtle signs that the rate may be starting to slow down. In most cases a knowledge of the remaining service life of the project, is it another 20 years, another 50 years, or longer, is a very important financial and economic issue. The most reliable measure of the reaction rate is the expansion rate as measured by high accuracy instrumentation, but an understanding of the alkali supply kinetics would certainly help.

There have been a number of computer models of ASR behavior which use an “S” curve of expansion rate versus time. These intrinsically assume that at some time the reaction and associated expansion will cease. If alkalis are supplied from the aggregates then this modeling assumption may not be appropriate.

In the case where SCMs were used, supplementary alkali supply may not be a problem if the pozzolans sufficiently fix the alkalis, but as in the case of new concrete, this aspect needs further study to be sure.

6 CONCLUSIONS AND LONG TERM CHALLENGES

6.1 *Conclusions*

- Reactions:
 - There are several expansive reactions that may occur in concrete in dams.
 - Alkali Silica Reaction (ASR) is the most frequent for of Alkali-Aggregate Reaction (AAR) although some cases of Alkali Carbonate Reaction (ACR) have been suggested but the actual mechanism is debatable.
 - Internal Sulfate Attack (ISA) in the form of Delayed Ettringite Formation (DEF) need only be considered in cases where high temperatures may have occurred during initial hydration.
 - In some other ISA cases the release of sulfate from rock containing iron sulfides may cause ettringite formation but it is not yet clear, whether expansion in such cases is related to ettringite formation or to the formation of iron oxides within composite rocks.
 - The relatively high concentrations of sulfate ions needed to produce external sulfate attack (ESA) are unlikely to be found in dams, except possibly in foundations. However, even in such cases, this form of degradation is a progressive phenomenon, starting from the surface, with successive layers being degraded and disintegrating so it would not lead to massive expansion of the whole structure.
 - Thaumasite formation may sometimes occur as the final stage of external sulfate attack. Thaumasite formation is the final stage of degradation in sulfate attack and as such is a progressive surface phenomenon, which will not produce massive expansion in dams.
- Alkali “resupply” from certain aggregates
 - Certain feldspars can contribute equal total amounts of alkalis compared to the initial loading from the cement
 - The time scale or rate of supply of alkalis from the aggregates is not known at this time. However, this is a factor that affects the future rates and durations of expansion and would be helpful to know.
 - Based on our present somewhat limited understanding of the long term kinetics, it appears that SCMs should continue to be effective in minimizing ASR, even in cases where alkalis will continue to be supplied by the aggregate but this point warrants further investigation.

6.2 *Long term challenges*

- There is a need to be able to reliably predict the remaining service life of existing dams with significant ASR or ISA considering periods of 50 years or more.
- Alkali supply from certain aggregates clearly plays a significant role in the long term behavior. Berube et al. in 2002 provided a useful listing of aggregates that have the potential to supply alkalis.
- It would be helpful to be able to quantify the rates of release of such alkalis to better predict future behavior and possible structural deterioration of the concrete.
- Computer modeling of future behavior of dams where alkalis are being supplied by the aggregates should recognize the possibility of the reaction continuing indefinitely and not slowing down according to an “S” curve of expansion versus time.
- Tests should be done as early as possible, ideally at the feasibility stage of new projects to allow sufficient time to be confident of long term behavior. Tests should include expansion tests as well as tests for alkali supply.
- It appears that SCMs will continue to be effective as a means to minimize ASR with reactive aggregates, even in cases where alkalis will continue to be supplied by certain aggregates but this long term behavior needs to be better understood.

REFERENCES

- ASTM C 114 Section 17.2, Standard Test Methods for Chemical Analysis of Hydraulic Cement—Water-Soluble Alkalies. ASTM International, 100 Barr Harbor Drive, PO Box C700, West Conshohocken, PA, 19428–2959 USA.
- Berube, M-A., Duchesne, J., Dorion, J.F. & Rivest, J. 2002. Laboratory assessment of alkali contribution by aggregates to concrete and application to concrete structures affected by alkali-silica reactivity. *Cement and Concrete Research*, 32, 1215–1227.
- Charlwood, R. & Buil Sanz, J.M. 2008. Chemical expansion of concrete in dams and hydro-electric projects, Workshop Report, Hydropower and dams, Issue Three.
- Constantiner, D. & Diamond, S., 2003. Alkali release from feldspars into pore solutions. *Cement and Concrete Research*, 33, 549–554.
- ICOLD/SPANCOLD, 2007. Workshop on Chemical Expansion of Concrete in Dams and Hydro-Electric Projects, ICOLD Committee on Concrete Dams and Hydro 2007, Granada, <http://www.dam-research.org/Granada-2007/index.html>
- Katayama, T., 2010. The so-called alkali-carbonate reaction (ACR)—Its mineralogical and geochemical details, with special reference to ASR *Cement and Concrete Research*, 40, 643–675.
- RILEM-ACS, 2010, Technical Committee on Alkali Aggregate Reaction in concrete structures: performance testing and appraisal. <http://www.rilem.net/tcDetails.php?tc=ACS>.
- Thomas, M.D.A., Beaman, N., Sean Hayman, S. & Gilks, P. 2010. *Proceedings ICAAR*, Trondheim, Norway.
- USCOLD, 1995. Proceedings of the Second International Conference on Alkali-Aggregate Reactions in Hydroelectric Plants and Dams, Chattanooga, TN, October 22–27, 1995. United States Committee on Large Dams, Denver, CO. USA.

Re-assessment and treatment-design of an ASR-affected gravity dam

R. Leroy

Alpiq Suisse SA, Lausanne, Switzerland

L.I. Boldea

Stucky, Renens, Switzerland

J.-F. Seignol & B. Godart

Université Paris Est—LCPC, Structures and Bridges Department, Paris, France

ABSTRACT: This study focuses on a gravity dam in which abnormal crest displacements due to Alkali-silica reaction (ASR) have been monitored for 50 years. The polygonal shape of the dam amplifies the effect of concrete expansion in the bends and could result in excessive stresses.

The aim of this paper is to present the numerical re-assessment of this dam, as well as a predictive simulation of its behaviour, taking into account the ASR effects.

The dam is described in the first part, as well as the visual disorders due to ASR and their monitoring. The numerical model is then introduced. It represents ASR effect as a prescribed expansion linked to the moisture and stress states. The third part focuses on the simulation of the dam behaviour and on the comparison between numerical results and in-situ measurements. The last part is devoted to the numerical assessment of the dam treatment by slot-cutting.

1 INTRODUCTION

Dam managers have sometimes to face internal swelling reaction in their structure (Charlwood 2007). The main problem induced by these pathologies lies in the change occurring in the material stress-state, with potential consequences on structural reliability. Hence, evaluation of the modified stress-state is the main goal of structure re-assessment based on numerical modeling. But the numerical tool may also allow to design and dimension treatment solutions such as reducing internal stresses by slot-cutting.

These questions are illustrated in this paper by the case-study of Salanfe dam, a gravity dam in which Alkali-Silica Reaction (ASR) was proven and the displacement of which are monitored for several years.

Material investigations and structure monitoring are first described, focusing on the ASR-induced displacements. The structure modeling and its fitting on in-situ data are then presented. Last, the numerical tool aimed at dimensioning the slot-cutting is introduced.

2 THE DAM AND ITS PATHOLOGY

2.1 *Salanfe gravity dam*

The Salanfe Dam is situated, near the city of Martigny (Valais) at an altitude of 1925 m. ASL on the Salanfe Plateau in Swiss Alps. It is used to produce hydroelectricity from the waters of the Salanfe and Sauffla Rivers.

Salanfe is a concrete dam classified in the gravity-dam category, according to its profile. The upstream face is vertical and the downstream face has a slope of 1:0.742 to the 1915.60 m

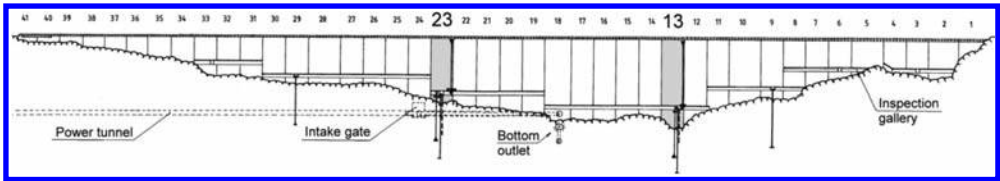


Figure 1. Upstream developed elevation.

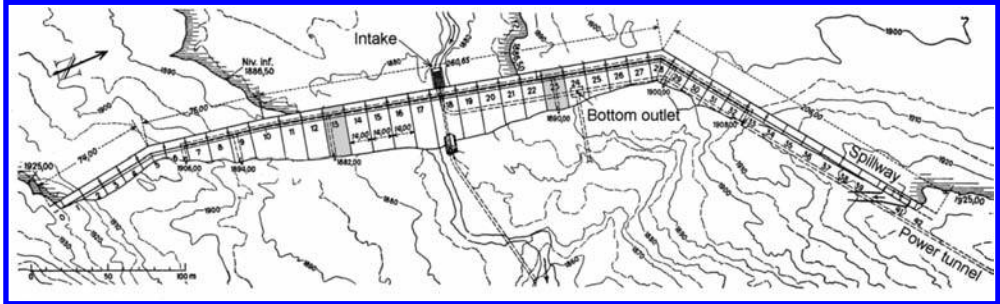


Figure 2. Plan view.

level, then 1:0.2 to the crest. The crest length can be divided into 4 straight sections: a central part which is 260.65 m long, the right wing composed of 2 sections of respectively 74 m and 76 m, and the left wing measuring 206 m. The total length at the crest is 616.65 m; the maximum height above the foundations is 52 m. The dam consists of 42 blocks which are for the most part 14 m long and separated by construction joints.

The core of the dam is in P150 concrete; P250 concrete is used in the crest starting from level 1915.60, as well as in the downstream face for a thickness of 2.50 m and in the upstream face for a thickness of 1.50 m.

Inspection galleries measuring 2 m wide by 2.5 m high are located at various levels between levels 1882.00 and 1908.00 from block 6 to 33. They are accessed from the downstream face via seven transversal galleries as well as via vertical shafts positioned to the construction joints.

2.2 Deformation monitoring

The dam is equipped with several monitoring systems as pendulums and extensometers and since 1993, with a geodetic and leveling network to follow the evolution and deformations. The results of those equipments allow to detect disorders so that the engineers can intervene to correct the problem in due time. The dam has constantly been deformed by the hydrostatic load, the effects of seasonal thermal variations and since 1970 by the effects of the swelling within the concrete.

The measurements (Fig. 3) show irreversible displacements of the crest, upstream and towards the right bank for block 13. This drift started soon after the dam was built and then accelerated in the 1970s. Since the dam was commissioned, the total irreversible downstream-upstream displacement is approximately 35 mm.

The upstream drift of the crest is amplified by the bends giving an “arched” form to the plan. This situation is typical of arch dams where swelling of the concrete leads to an increase in the length of the arch, which is only possible outwards, namely upstream.

Figure 4 shows the vertical displacements of the crest. As for the downstream-upstream movements, these displacements have continued over time. In 17 years the elevation has reached 35 mm at points 125 and 127. It has also doubled in the last ten years, compared to reference state.

The swelling in the main part of the dam between blocks 11 and 27 pushes the extremities of this part in opposite directions. Detailed inspections exhibited cracks in the galleries and on the downstream face (Fig. 5).

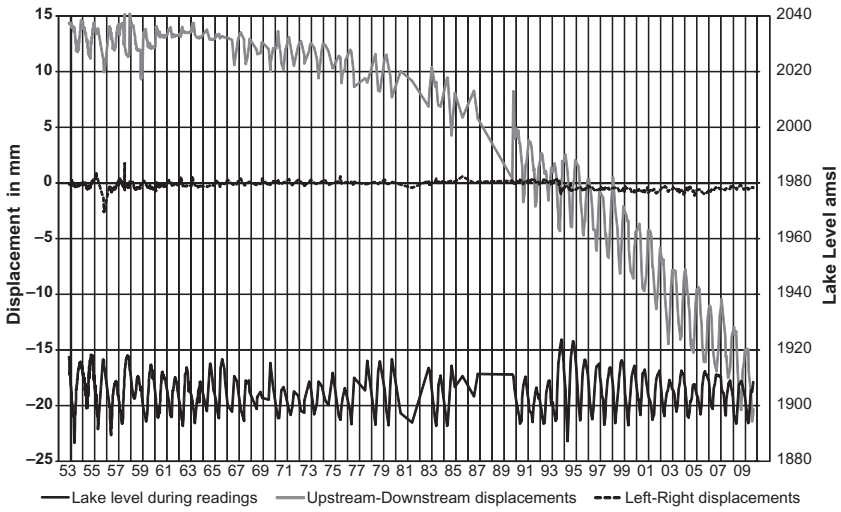


Figure 3. Displacements of block 13 monitored by pendulum.

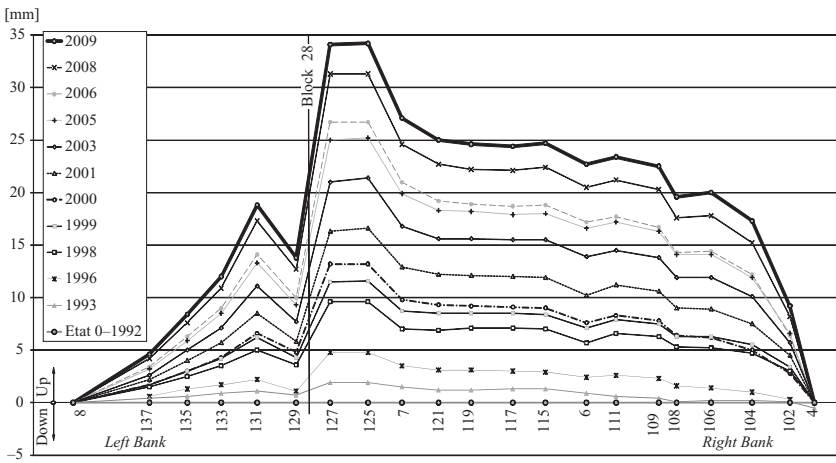


Figure 4. Vertical displacements (in mm) from 1993 to 2009 measured by geodesy.

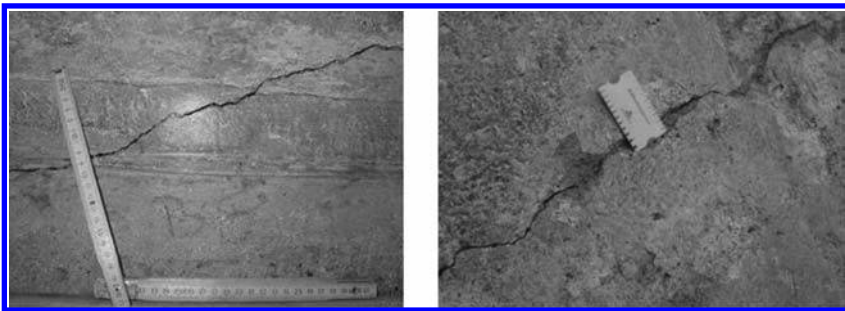


Figure 5. Cracks in the side wall of the inspection gallery (left) and in the downstream face, right angle to the left-bank elbow (right).

2.3 Alkali-silica reaction and its consequences on the dam

Having observed relatively important cracking, particularly around the left bank bend, as well as irreversible upstream displacements of the structure, it has been decided to analyze the condition of the concrete so as to ascertain whether or not it is being subject to alkali-silica reaction.

In 2001 the presence of ASR was confirmed by petrographic analysis and electronic microscopy. In 2009 deeper inquiries were made by LCPC to confirm the pathology. An alkali content up to 4 kg/m³ was found in the samples, which is above the 3 kg/m³ threshold value recommended to prevent ASR (LCPC 1994).

As for the cement paste, examination showed that the binding agent is relatively porous with micro-cracks, which makes the concrete quite permeable. Finally, the examination identified a pathogenic swelling reaction, specifically intense ASR. The diagnosis of the concrete microstructure was carried out on 6 core samples using scanning electron microscopy. This testing confirmed the presence of widespread microporosity in the concrete. Both types of concrete suffer from ASR presenting different facies (mammilated gel, cracked gel). The presence of ASR gel has been systematically confirmed in each sample, characteristic of widespread contamination.

The occasional presence of secondary ettringite can be found in the vacuoles or in the form of thin layers between the cement paste and aggregates. This concomitance has previously been observed in structures damaged by ASR. However, in this case the swelling is not due to delayed ettringite formation but rather to the ASR gel.

The investigation has established the development of ASR, the presence of numerous cracks in the cement paste and often decohesive interfaces between the binding agent and the aggregates. This pathology has systematically been found in all the examined samples.

To complete this diagnosis, we advised testing the residual expansion of the concrete using LPC 44 method (LCPC 1997). Monitoring longitudinal deformation as done in this testing would allow to evaluate the free swelling potential of the concrete.

3 NUMERICAL MODEL FOR ASR-AFFECTED STRUCTURES

The numerical model used to assess ASR-affected concrete structures is implemented in the ALKA modulus in FEM-software CESAR-LCPC. Concrete constitutive model considers ASR effect as a prescribed chemical strain ε_χ in linear relation with chemical extent ξ associated to the reaction responsible for the gel formation within the porous network of the cement paste. The kinetics of this phenomenon is modeled by the time-dependency of ξ , according to Larive's law:

$$\xi(t) = \frac{1 - \exp(-t/\tau_c)}{1 + \exp\left(\frac{\tau_l - t}{\tau_c}\right)}, \quad (1)$$

in which the parameters τ_c and τ_l are, respectively, characteristic and latency times, and the chemo-elastic behavior of concrete is then described by

$$\varepsilon = \varepsilon_e + \varepsilon_\infty \cdot \xi(t), \quad (2)$$

with ε_∞ the maximum free expansion of the ASR-affected concrete. The term ε_e represents the elastic strain, obtained from stress-state by Hooke's law, and can be easily replaced by elastoplastic strain if necessary.

Thermo-hydral state ($T;h$) influences ASR through coupling laws. High temperature is responsible for lower τ_c and τ_l according to Arrhenius' law whereas high value of h (high moisture content) increases both expansion amplitude ε_∞ and kinetics.

To take these coupling into account, the chemo-mechanical computation with ALKA modulus is based on the results of two previous modeling with CESAR-LCPC, one aimed at assessing the temperature field in the structure, the other one consisting in solving the

transient non-linear moisture-diffusion equation governing the evolution of h in the porous network of the structure.

4 SIMULATION OF THE DAM BEHAVIOUR

4.1 Preliminary tests on 2D-models

Preliminary tests were realized on 2D-models representing one “section” of the dam (Fig. 6). They lead to the following conclusions:

- although the dam was built with different concrete mix-design (with various cement quantities), the global behavior was best represented by considering an homogeneous expansion potential;
- the ASR-induced deformation and its kinetics are poorly influenced by temperature variations and temperature-field heterogeneity, as long as these variations remain in a reasonable range (tests were conducted with mean temperature varying from 4 to 8°C according to locations);
- global upward and upstream crest displacement is better obtained with homogeneous moisture field in the dam.

Nevertheless, the 2D-models seem unable to correctly represent the real structure behavior, since a large part of the observed displacement is due to the “arched” shape of the dam, as explained above.

4.2 Numerical model for the dam

The dam finite-element three-dimensional model was developed with the finite element software CESAR-LCPC.

The mesh is composed of 28,589 quadratic elements (20-node hexahedron, 15-node pentahedron, and 10-node tetrahedron) for a total of 128,861 nodes (see Fig. 7).

The height of the supporting ground below is, at the lowest point of the dam, 98.5 m. The maximum height of the dam is 51.5 m.

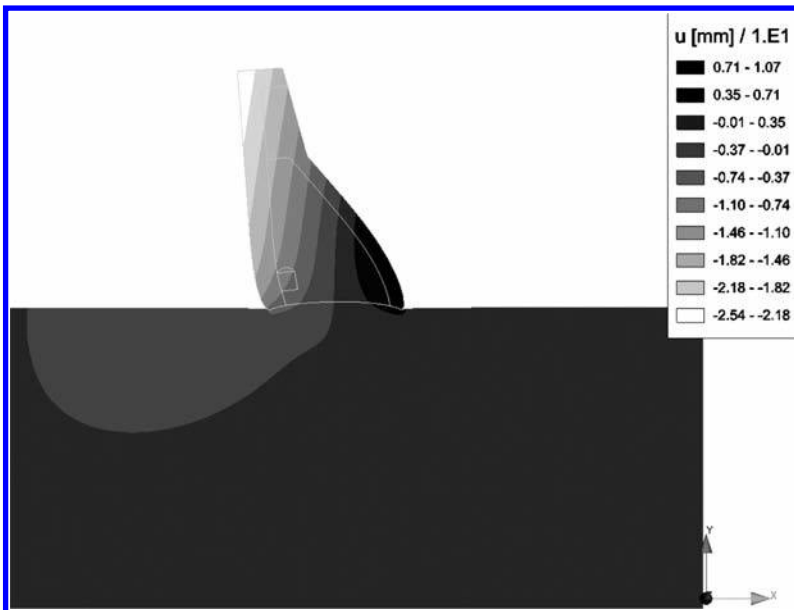


Figure 6. Deformation of a 2D-slice of the dam after 40 years with upstream-downstream displacement mapping (navy blue represents upstream displacement above 20 mm).

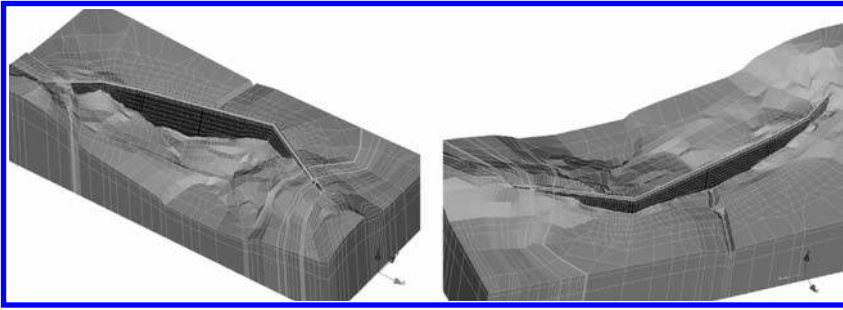


Figure 7. Views of the mesh representing Salanfe dam and the surrounding rock (left, downstream; right, upstream).

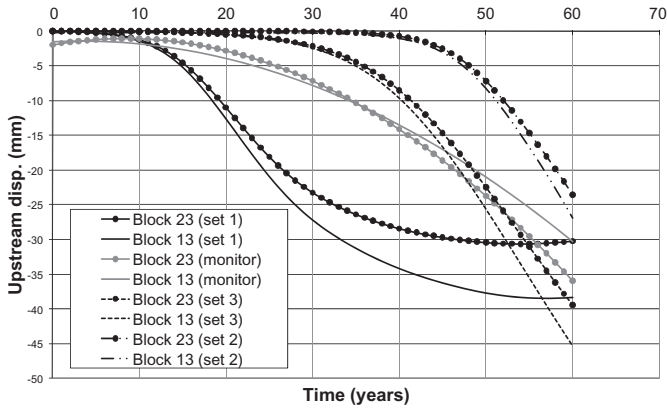


Figure 8. Downstream displacement at the crest of the dam (monitoring vs different computations).

The rock around the dam is considered to be of uniform quality and therefore consisting of a single material. Modeling shows realistic blockage created by the surrounding rock (Fig. 7).

The body of the dam is separated into several groups to allow to take into account the various different qualities of concrete, if necessary. The mesh of the dam alone consists of 64,733 nodes, and 13,944 quadratic elements.

4.3 Model fitting

For the lack of results on material core samples drilled—autumn 2009—out of the structure (the residual expansion test LPC 44 lasts about one year), fitting of the models has been based on monitoring data. The aim is to assess correct values for the three parameters τ_c , τ_l and ε_∞ introduced in Equations 1 and 2.

Resulting from previous results on 2D-models, the temperature and moisture fields in the structure are considered as homogeneous. More than 30 parameters sets for $(\varepsilon_\infty, \tau_c, \tau_l)$ are tested in a 60-year-long modeling of the ASR-development and the computed crest displacement in blocks 13 and 23 are compared to the upstream-downstream displacements monitored on the dam (note that on the Figure 8, data from monitoring have been smoothed to get rid of the small variations due to water level, etc.).

Figure 8 represents some comparison for 3 sets (the characteristic and latency times are given here for a reference temperature of 38°C, corresponding to LPC 44 test conditions, and transformed by Arrhenius' law to agree with the real temperature in the structure):

- set 1: $\varepsilon_\infty = 0.20\%$, $\tau_c = 180$ days, $\tau_l = 200$ days;
- set 2: $\varepsilon_\infty = 0.35\%$, $\tau_c = 220$ days, $\tau_l = 700$ days;
- set 3: $\varepsilon_\infty = 0.35\%$, $\tau_c = 350$ days, $\tau_l = 600$ days.

Based on these comparisons, the set number 3 is considered as the best representation of the dam behavior. It shall also be noticed that, without any results of residual expansion tests, the end of the phenomenon cannot be fairly assessed. This fitting shall be reconsidered with the residual expansion tests are finished.

5 NUMERICAL DESIGN FOR THE DAM TREATMENT

5.1 Slot-cutting

The first aim of this rehabilitation project is to reestablish an acceptable level of stress and deformation so as to guarantee the safety of the dam in all circumstances. Sawing the upper part of the dam to release stress and decrease the arching effect which has been amplified by the elbow in the dam is a good option to achieve this goal. The sawing technique using a diamond wire has already proven successful on other dams such as Mactaquac in Canada (Curtis 2000) or Chambon Dam in France and Pian Tessio in Italy.

As Salanfe is a gravity dam needing no arch effect to function, there is no need to inject the joints. However, it is preferable to maintain sufficient stress after sawing to keep the joints closed by arch effect.

The rehabilitation project does not take into account any other solution to limit or prevent future development of ASR; however, injecting some cracks in the galleries should be expected.

Complementary measures can be examined in a successive phase of dam rehabilitation. It may be necessary to repeat a similar process depending on the evolution of the reaction and its effects on the structure.

5.2 Numerical tool for slot-cutting

If the effectiveness of such a technique is generally agreed (Hull 2007), several practical questions need answers: how many slot-cutting shall be done? Where are the most pertinent localization? How long shall they be? At which periodicity shall the operation be repeated? Will the compressive stress remain light enough to ensure a closure of the slot-cutting?

A numerical model of the dam, taking into account ASR-development is a good tool to answer these different questions. In this aim, specific contact elements able to represent slot-cutting of controlled width have been introduced in ALKA modulus and will soon be used to model different repair scenarii for Salanfe dam.

The Figure 9 represents the evolution of computed transverse stress in a test-case dam block (which is purely academic and not representative of Salanfe dam) after a 10 mm-wide slot-cutting.

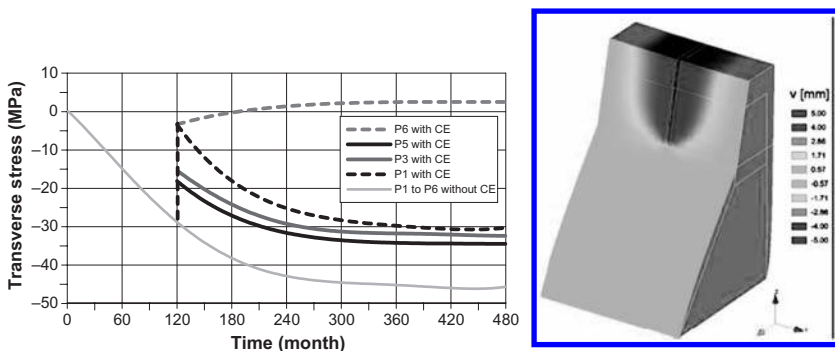


Figure 9. Transverse stress versus time at different heights (P1 is the top of the slot-cutting, P6 its bottom) and transverse displacement mapping just after slot-cutting.

6 CONCLUSION

This paper has presented an on-going investigation on an ASR-affected gravity dam. The use of monitoring data to fit numerical model was emphasized. The experience acquired during this study also leads to the following conclusions:

- The importance of material tests, first to confirm the nature of the pathology, then to evaluate its amplitude.
- The interest of 2D-models to quickly test some simple assumptions, but their limitation in correctly reproducing the real behavior of complex structures such as Salanfe dam.
- The need for residual expansion tests to fit the last part of the chemo-mechanical constitutive model.
- The role of numerical model with specific contact elements to assess treatment solutions.

In addition, the predictive numerical model comparing the “in situ” measurements will help the dam manager to maintain the performance of the powerplant. Stopping the facility for repair involves high costs economically and socially speaking.

REFERENCES

- Charlwood, R. 2007. Special Workshop on Chemical Expansion of Concrete in Dams & Hydro-electric Projects. Granada, <http://www.dam-research.org/Granada-2007/index.html>
- Curtis, Dan D. 2000. Analysis and structure response to recent slot cutting at Mactaquac Generating Station. In: M.A. Bérubé, B. Fournier, B. Durand (Eds.), Proceedings of the 11th International Conference on Alkali-Aggregate Reaction in Concrete: 1283–1291. Québec City.
- Hull, K. 2007. Center-Hill Dam. Mitigating Effects of Alkali-Aggregate Reaction with Vertical Slots. In Special Workshop on Chemical Expansion of Concrete in Dams & Hydro-electric Projects. <http://www.dam-research.org/Granada-2007/index.html>
- Humbert, P & Dubouchet, A & Fezans, G & Remaud, D. 2005. CESAR-LCPC, un progiciel de calcul dédié au génie civil. Bulletin des laboratoires des ponts et chaussées 256–257, 7–37.
- Larive, C. 1998. Apports combinés de l’expérimentation et de la modélisation à la compréhension de l’alcali-réaction et de ses effets mécaniques. OA28, collection ERLPC. Paris: LCPC.
- LCPC. 1994. Recommandations pour la prévention des désordres dus à l’alcali-réaction. Paris: LCPC.
- LCPC. 1997. Alcali-réaction du béton—Essai d’expansion résiduelle sur béton durci, Projet de méthode d’essai LPC 44. Paris: LCPC.
- Li, Kefei & Coussy, Olivier. 2002. Concrete ASR degradation: from material modelling to structure assessment. Concrete Science and Engineering 4: 35–46.
- Omikrine-Metalsi, O & Aïtsi, M & Rigobert, S & Toutlemonde, F & Seignol, J-F & Boldea, L-I. 2010. Integration of contact elements and creep in RGIB-modulus of the FE-program Cesar-LCPC. Application to structures affected by internal swelling reactions. In Hydro 2010 International Conf & Exhibition. Lisbonne.
- Seignol, J-F & Ngo, T-T & Toutlemonde, F. 2006. Modelling of the coupling between moisture and alkali-silica reactant in concrete. In Meschke, de Borst, Mang and Bićanić (Eds.), Computational Modelling of Concrete Structures. 639–646. Mayrhofen: Taylor & Francis.
- Seignol, J-F & Boldea, L-I & Leroy, R & Godart, B & Hammerschlag, J-G. 2009. Hydro-power structure affected by alkali-aggregate reaction: a case-study involving numerical re-assessment. In Chang, Meyer and Bićanić (Eds.), Computational Technologies in Concrete Structures. 155 (full paper on CD-Rom). Jeju, Korea: Techno-Press.
- Ulm, F-J & Coussy, O & Li, K & Larive, C. 2000. Thermo-chemo-mechanics of ASR expansion in concrete structures. J. Eng. Mech. 126 (3): 233–242.

The integrity of old style post tensioned anchors in dams—a real dam safety issue

R. Herweynen

Entura (previously Hydro Tasmania Consulting), Hobart, Tasmania, Australia

ABSTRACT: The integrity of post-tensioned anchors is a significant dilemma facing dam safety engineers worldwide. Hydro Tasmania, the largest dam owning authority in Australia, has seven major dams which were designed and constructed in the 1950–70s with fully grouted, post-tensioned anchors. The method used was leading edge in its day, and enabled significant savings in concrete. However, these anchors only defence against corrosion was the grout column, rather than the two barriers that modern permanent anchors have.

In 1999, Hydro Tasmania commenced its dam portfolio risk assessment, which highlighted safety deficiencies with Catagunya dam due to the unknown integrity of its post-tensioned anchors. It was recognised that this was potentially a bigger issue than just Catagunya dam. Rather than abandon all of these anchors as other dam owners have done, due to their lack of conformance to current standards, Hydro Tasmania endeavoured to develop an investigation program to assess their integrity.

The investigation and assessment undertaken at Catagunya dam indicated the likelihood that some corrosion of the anchors was occurring; as a result a decision was made in 2004 to cease reliance on the anchors, and in 2009–10 major upgrade works occurred. This paper presents the Catagunya dam journey, providing other dam owners with this knowledge.

1 INTRODUCTION

1.1 *General issue*

In contrast to modern post tensioned anchors, which have double corrosion protection, anchors installed in the 1950s–1980s had no corrosion protection, other than grout, to the tendon steel. For these anchors the stressing length was generally grouted once installation was complete, with no access for future monitoring or restressing. There are many dams around the world which depend on these types of anchors for their stability and, given the low degree of corrosion protection, the integrity of these anchors is a growing concern worldwide.

This growing concern internationally has led to the U.S. National Research Programme being funded by private industry and trade/professional associations, with support from dam-related bodies in North America, to conduct a national study on stressed anchors (McInerney et al. 2007). To date they have noted that “permanent anchors have been routinely installed in North America since the mid 1960s. They continue to perform well in a variety of environments, applications and ground conditions. No failures have been found which can be directly attributed to corrosion protection failure.” However, they also note “that there is currently no way to judge the current acceptability of the hundreds of anchors installed with bare steel (wire and strand) up until the early 1990s. This is a dilemma facing dam safety engineers worldwide, and the logical, conservative view is to assume they have no value and to replace the anchoring using Class I protection”, i.e. double corrosion protection.

1.2 *Specific issue for Hydro Tasmania*

Hydro Tasmania, the largest dam owning authority in Australia, has seven major dams which were designed and constructed in the 1950–70s with fully grouted, post-tensioned anchors,

Table 1. Hydro Tasmania dams with old style post-tensioned anchors.

Dam	Anchor details
Catagunya*	412 anchors, 102 H.T. parallel strand 5 mm diameter wires, installed 1959–1961.
Meadowbank	155 anchors, 72 galvanised H.T. parallel stranded 7 mm wires, installed 1962–1968.
Cluny	95 anchors of 72 H.T. parallel stranded wires of 7 mm diameter, plus 47 anchors of 12/12.7 mm strand installed 1964–1967.
Repulse	36 anchors, 72 H.T. parallel stranded wires of 7 mm diameter, installed 1966–1968.
Clark	400 anchors, H.T. strand of 12.7 mm diameter, installed 1964.
Devils Gate	90 anchors of 42 wires of parallel strand 7 mm diameter wires, plus 43 anchors of 6/12.5 mm monostrand installed 1964–1969.
Lake Margaret	150 anchors, Freyssinet multiwire cable, 12 wires of 7 mm diameter, installed 1974.

* Highest priority dam due to anchors providing a significant proportion of the stabilizing force.

where the grout column is the only barrier against corrosion. These dams are shown in [Table 1](#) below. Although the method used was leading edge in its day, and enabled significant savings in concrete by replacing some of the gravity mass with post-tensioned anchors, the lack of knowledge on the integrity of these anchors poses a dam safety concern.

In addition to this, Hydro Tasmania has similar types of anchors holding down spillway crests, power station draft tubes and power station crane beams. Therefore this concern spans more than just its dam assets, and is a critical asset management issue moving forward.

2 AUSTRALIAN DAM EXPERIENCES

2.1 *Hume Dam (Cooper & Rodd 1987)*

Hume consists of a 51 m high, 318 m long concrete gravity dam flanked by earth embankments. The dam was completed in 1936. However, in the mid 50s, the storage was enlarged and the dam strengthened using post tensioned ground anchors. Following reviews in the 1980s, the following factors led to a pessimistic view of the existing post tensioned anchors:

- construction reports indicating difficulties in ensuring satisfactory grouting;
- cable strands subject to seepage due to imperfect waterproof grouting;
- presence of sulphides in the storage water and the aggressiveness of these to steel; and
- variability in steel properties with possibilities of stress corrosion.

Offsetting the above were factors which could lead to a more optimistic view:

- tight joints in rock and good quality concrete;
- high pressures used in waterproof grouting;
- cables stressed to only 60% UTS; and
- generally satisfactory behaviour of two test cables which were not protective grouted.

Considering the above and after consultations with local and international experts, it was concluded that:

- the existing theoretical prestressing force could not be relied upon in the long term;
- the existing post tensioning should not be included in stability analyses; and
- a new post tensioning system, consisting of cables having a secure form of corrosion protection, being load monitorable and restressable, should be installed within 5 years.

As a result of these conclusions, a decision was made to install new anchors with double corrosion protection, load monitorable and restressable. This occurred in the mid 1980s.

2.2 *Stanwell Dam (Himsley & Heinrichs 1997)*

Stanwell Dam was a 6 m high concrete gravity dam built in 1915 and post-tensioned in 1977. The post-tensioning consisted of seventeen cables consisting of six strands of 12.7 mm diameter wires, and fourteen cables consisting of eight strands. The cables were initially

grouted into the foundation with typical bond lengths of 5 m to 6.5 m and free lengths, in the foundation and dam, of up to 11 m. After curing of the grout in the bond length zone, the cables were post-tensioned. The free lengths were then grouted.

In the early 1990s it was noted that two of the anchor blocks on the dam had “cracked off” indicating failure of those post-tensioning cables. A decision was taken to decommission the dam in 1996, which involved the complete demolition and removal of the dam allowing inspection of the condition of the post-tensioning strands within the dam structure.

The grouted cables within the dam wall generally appeared to be in good condition with minimal corrosion. A six meter length of cable was also drilled out of the foundation and showed minimal evidence of corrosion after 20 years in service. At the top of some cables, immediately below the anchorage lock off plates, the grout had settled and cracking in the top of the anchor blocks had allowed water ingress to initiate significant corrosion (and sometimes failure) at those locations.

2.3 *Tenterfield Dam (Himsley & Heinrichs 1997)*

Tenterfield Dam was a 11 m high concrete gravity dam built in 1930 and raised 1.8 m in 1974. Stability was provided by 97 post-tensioning cables consisting of 12×12.7 mm. The cables in the free lengths were enclosed in greased sheaths and the cable grouting undertaken in one operation. The cables were not designed to be monitorable or restressable.

Five representative anchors were tested for their current lift off load capacity. All anchorages exposed were found to be in excellent condition. In addition, the lift off loads registered for four of the five anchorages indicated post tensioning losses in the order of 5 to 10% of the original lock off loads, which would be within the normal expected range. However, the fifth test revealed a loss of 32% of prestress from lock-off loading, causing concern for the anchors.

Corrosion potential measurements were taken at the five cable locations to indicate any likelihood of corrosion. This was done by attaching an earthwire to the anchorage head and measuring the difference between the anchorage head and a Cu/CuSO₄ half-cell submerged in the storage adjacent to the dam wall. A significantly higher reading was obtained at the questionable cable compared with the other four cable locations. As a result it was decided to drill a small hole down each of the remaining cable head locations, so all anchors could be tested. Three cables tested over the generally accepted criteria for active corrosion.

If a correlation exists between the potential measurements and loss of prestress at the cable locations, the results indicate that only a small number of cables may have significant loss of prestress (i.e. 4%). This compares with the check load monitoring test results where 1 in 5 cables tested had significant loss. As a precursor to any decision on upgrading the dam, a risk assessment was planned to be undertaken to determine the dam's stability under varying levels of post tensioning loading.

2.4 *Catagunya Dam*

In 1999, Hydro Tasmania commenced its dam portfolio risk assessment, which highlighted safety deficiencies with Catagunya Dam due to the unknown integrity of its post tensioned anchors. It was recognised that this was potentially a bigger issue than just Catagunya dam, with six other dams having significant numbers of post tensioned anchors. Rather than abandon all of these anchors because they do not meet current standards for permanent anchors, Hydro Tasmania endeavored to develop a methodology for assessing their integrity, with Catagunya dam as the pilot dam. Entura performed the bulk of the analysis, and an expert panel was set up to assist in developing the methodology and provide advice throughout the process.

3 CATAGUNYA DAM INVESTIGATION CASE STUDY

3.1 *Dam and anchor description*

Catagunya Dam is located on the Derwent River in the southeast of Tasmania, Australia. It is the third in a cascade of six dams forming the lower Derwent hydropower development.

Catagunya Dam was constructed from 1957–1961, is 49 m high and has a crest length of approximately 280 m. Design and preliminary construction work were commenced early in 1957 for a mass concrete gravity dam. However, following a visit to Europe in 1957 by the Hydro Electric Commission's Chief Civil Engineer, the option of a post-tensioned concrete gravity dam was seriously considered. As a result it was estimated that a post-tensioned dam provided a saving at Catagunya in the order of 20 per cent of that for a conventional gravity dam (Wilkins & Fidler 1959). As a result of the cost advantage, a decision was made to construct Catagunya Dam as a post-tensioned concrete dam, where removed concrete volume was replaced by 412 no. \times 200 ton capacity, high tensile steel cables anchored to the dolerite foundation rock. At the time Catagunya was the highest post-tensioned concrete dam in the world.

The post-tensioned anchors used at Catagunya Dam were two-stage fully grouted and bonded anchors, where the grout column was the only defense against corrosion. It was recognized at the time of construction that these anchors would have a finite life and at some point they would need to be replaced. Based on current standards, these types of anchors would be classified as temporary anchors, since modern day permanent anchors have at least two barriers against corrosion, and are monitorable.

3.2 *Large scale testing at Meadowbank dam*

Meadowbank dam followed the construction of Catagunya dam. Due to bedding plane features within the foundation at Meadowbank dam, large scale insitu shear testing occurred within the foundation. A decision was made to install some test post-tensioned anchors as per the Catagunya dam specification within the Meadowbank dam foundation and drill one of these large diameter holes next to the anchor so that the integrity of the grout column could be inspected. This resulted in the shock discovery that the grout column could have some significant voids in its length, as shown in the photograph taken of this test anchor in [Figure 1](#).

3.3 *Safety Review and Portfolio Risk Assessment*

Following a Comprehensive Safety Review and the Portfolio Risk Assessment for Catagunya dam in the late 1990s, the integrity of the post-tensioned anchors was highlighted as a key safety deficiency for the dam. As a result, a strategy was developed in early 2000 to try to ascertain the condition of the post-tensioned anchors. Along with reviewing the existing data, undertaking a literature review and assessing the adequacy of the existing instrumentation, an investigation program was developed consisting of insitu groundwater sampling and analysis, corrosion studies in the laboratory and insitu corrosion testing (Herweynen & Hughes 2002).

3.4 *Resistivity measurements*

At the time of construction, 26 anchors had electrical wires connected to both ends so that the resistance of the anchor could be measured with time (only 24 can be read). The idea was that if corrosion occurred the resistance would increase due to loss of cross section of the steel. Readings were taken annually for the first four years following construction, and thereafter at two-yearly intervals. The downside of this system was that the steel spacers



Figure 1. Section of test anchor installed using the Catagunya dam specification.

between the wires provides a bridge for the electrical current and thus a significant loss in cross-sectional area would be required before a change in resistance occurred.

Based on a detailed review of this data, it was concluded that 4 out of the 24 anchors being read (i.e. 17%) were critical based on the slope of the resistance vs time curve showing an increase in resistance, corresponding to likely corrosion.

3.5 *In situ groundwater sampling*

An important part of the strategy developed was to determine the corrosivity of the groundwater in the vicinity of the anchors. In mid 2001, the installation of piezometers beneath all thirteen of the post-tensioned dam blocks provided inclined holes from which water samples could be taken. The method of collecting the water samples was critical to avoid contamination of the sample (Herweynen & Hughes 2002).

The ground water varied considerably across the valley with pH values as low as 6.4 and as high as 12. The dissolved oxygen level was also generally low. Although the results showed a wide variation of conditions, they indicated that most holes in the spillway section of the dam have conditions leading to low susceptibility to corrosion. Generally, the pH values are low where there was either a low grout take or relatively high flow rates which may have destroyed the alkaline environment through leaching.

3.6 *Laboratory testing*

As part of the groundwater sampling, four samples were chosen to represent the wide variety of water chemistry encountered across the valley; one sample was taken from the left abutment, one from the right and two from the spillway, for further laboratory testing by CAPCIS Ltd in the UK. The samples were analysed for composition and the overall corrosion risk was assessed in accordance with DIN 50 929 Part 3.

Although one sample had a pH of 11.6 and another had a pH of 7.2, in all cases the analysis in accordance with DIN 50 929 indicated a general corrosion rate of 0.01 mm/year. DIN 50 929 Part 3 does not take into account the passivating effects of pH values above 10 or totally cover the effects of dissolved oxygen, and therefore this rate of corrosion is likely to be overstated for the zones of higher pH ground water. However, at this rate of corrosion, a 5 mm wire could reduce to a 4 mm wire, a 36% reduction in cross-sectional area, within 50 years.

Corrosion measurements were carried out on samples of the anchor wire exposed to water from the spillway section (pH 11.6) and the right abutment (pH 7.2), representing a best and worse case scenario. Working electrodes were prepared for the tests for three different conditions; ungrouted electrode in the water sample, grouted electrode in the water sample and “coupled” where the grouted and ungrouted electrodes are connected via a zero resistance ammeter. The coupled test was designed to show the effect of a galvanic couple that occurs when grout has cracked to allow direct exposure of the metal to water at a limited location.

If only corrosion of the outer wires is considered, the loss of cross sectional area of the entire anchor over 40 years is 31% for the low pH water, and 19% for the high pH water. For the coupled cases this increases to 35% and 19% respectively. The conclusion drawn from the laboratory testing is that some corrosion is likely to have occurred (Herweynen & Hughes 2002).

3.7 *In situ testing*

Following completion of the laboratory corrosion studies, CAPCIS Ltd was asked to carry out *in situ* corrosion testing of three anchors within the dam, located in good, bad and average conditions based on ground water testing. The testing at Catagunya dam was the first time that this technique had been used on a dam anywhere in the world. The *in situ* corrosion testing technique is known as potentiostatic polarisation testing and requires that an electrical connection be made to the anchor being tested. By passing a low power dc current between the anchor and the measurement probe, the corrosion rate at the time of testing can be measured. In this study, the electrical connection was made to the anchors using the existing electrical resistance installation. In order to take measurements at intervals along the entire length of

each selected anchor, it was necessary to core a hole close to and parallel to each of them. The holes were 122 mm in diameter and drilled to close tolerances within the concrete and rock.

Although it was difficult to interpret the data obtained from this insitu testing, and some of the conclusions seemed counter intuitive, the results did support the conclusion that some degree of corrosion of the anchors was likely to be occurring (Herweynen & Hughes 2002). The estimated loss of corrosion was worst in the left abutment anchor, where if uniform corrosion is occurring we would have a loss of diameter of 1.0 ± 0.5 mm over 40 years. If localized corrosion is occurring the loss of cross-section would be greater.

3.8 *Heightened monitoring*

Based on the information gathered, there was growing evidence that some corrosion has likely occurred and that the anchors should not be relied upon in the long term. As a result, in the short term, Hydro Tasmania implemented a prudent dam safety management strategy of heightened monitoring and redrilling of drain holes to ensure adequate drainage for dam stability. The additional instrumentation that was added at Catagunya dam in 2001 was nineteen vibrating wire piezometers and nine tiltmeters (Herweynen & Hughes 2002).

3.9 *Decision on Catagunya dam anchors*

A definitive conclusion on the condition of the cables at Catagunya dam cannot be drawn based on the results of both the laboratory and insitu testing. However, there is sufficient evidence to conclude that some of the anchors are corroding. Based on the range of ground water conditions in the three blocks tested using the insitu testing method, and the fact that corrosion was obtained in all three of the anchors tested, some corrosion in all anchors must be assumed.

Although there was additional investigation that could have been pursued (e.g. exhuming a couple of anchors), it became apparent that the likelihood of a successful outcome that would assure the integrity of the anchors and could be applied across the entire structure was not high enough to warrant the additional cost and time. As a result, a decision was made in 2004 to make the existing anchors redundant in the medium term.

As a result of this conclusion, the project moved on to the next phase of option development to determine the best solution for achieving the result of making the existing anchor redundant (Herweynen et al. 2009).

4 CATAGUNYA DAM RESTORATION PROJECT

4.1 *Options study and design*

In 2005, Hydro Tasmania embarked on an options study to determine the best method to restore the long term dam stability to acceptable limits for the long term. The required solution was intended to not only resolve the issue of anchor deterioration but also to upgrade the flood rating for the dam.

Based on preliminary design work a buttress solution was recommended and approved for detailed design. The preliminary design utilised a simplified, 2-dimensional, rigid body model, including crack analysis. As part of the detailed design a finite element model was developed to refine the preliminary design. However, this model did not support the simplified analysis and further non-linear finite element analysis demonstrated that the proposed passive buttress design solution was not technically feasible without adding some active loading (i.e. jacks or post-tensioned anchors). The options were reconsidered and the adopted solution was to replace the original anchors with new modern anchors, with a high degree of corrosion protection.

The new anchors adopted are the largest post tensioned anchor loading currently used for a dam in the world. This along with the existing post tensioned anchors and the tight geometry of the dam, which has a significant cantilever ogee crest, provided significant challenges with the design of this dam upgrade. Some of the key design challenges included:

- Appropriate level of modeling and analysis to be able to make sound decisions.
- Congestion due to the tight geometry of the original design.

- Anchor head block detail to ensure the loads would be adequately secured and dispersed into the dam body.
- Crest cantilever support to ensure that structural integrity was retained during construction and later in service. Innovative installation of carbon fibre reinforcement was used.
- Strain compatibility. It was important to ensure the structural contribution of new and old working together.
- Existing anchor degradation. The design needed to ensure that stability compliance was achieved for complete to zero effectiveness over time.
- Maintaining operability of the dam and power station during construction.
- Achieving an effective long term maintainable solution.

For more details on the options study and design refer to past papers specifically on this topic (Herweynen et al. 2009, Harman et al. 2010).

4.2 Construction challenges and solutions

The stability of Catagunya dam has been restored using 92 modern, large diameter and corrosion protected, post-tensioned anchors that can be monitored for deterioration. A number of challenges were addressed during implementation (Cubit et al. 2010), including:

- Installing more than half the anchors within an operating spillway, utilising a limited construction window over the summer months.
- Providing access for drilling equipment and installation of the anchors well below the spillway crest on a 54° degree slope, 25 m above the riverbed, and demobilising these platforms sufficiently to allow floods to pass during the winter months.
- Replacing severed surface reinforcement with 9 m long carbon fibre rods.

In order to gain access to the spillway of Catagunya dam for installation of the temporary access platform brackets on the spillway and the carbon fibre tensile reinforcing on the spillway face, a purpose designed and built travelling gantry was suspended from the spillway crest. This gantry had five working deck levels (refer to [Figure 2](#)).

Two 200 m long temporary platforms were constructed to access the spillway (refer to [Figure 2](#)). The upper platform was designed to provide access for drilling and installation of anchors. The lower platform was to give direct access to the anchor hole locations.

With the unique cross-section of Catagunya dam, tensile reinforcing is required on the top surface of the downstream face of the spillway to support the large cantilevered ogee spillway crest. This steel was to be severed as the large diameter holes for the spillway headblocks were cored, so a replacement was required prior to coring. A major innovation of the project was the design and installation of carbon fibre reinforcing into the spillway face to provide this tensile reinforcing. The 9 m long carbon fibre rods were installed in the face of the spillway by sawing a 9 m long, 15 mm wide, and 90 mm deep slot in the concrete. In each of these slots, 6 carbon fibre rods were installed, bonded together and to the concrete with epoxy adhesive.

Anchors installed within the spillway were required to be constructed within the current profile. Coring of 1.2 m diameter holes into the slope, 3 m into the dam was undertaken to

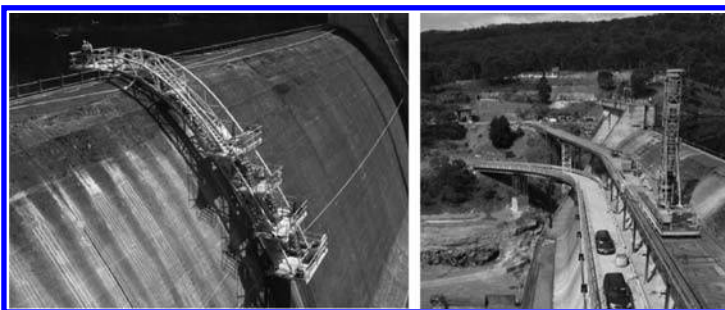


Figure 2. Construction photographs of Catagunya dam restoration project.

install the precast reinforced concrete headblocks to distribute the loads into the structure. Drilling was undertaken using a 350 mm downhole hammer drilling rig. The longest drill hole was 78 m through the concrete and into the dam foundation.

The modern post-tensioned anchors were fabricated on site using specialist equipment to open and grease the cables, and then install into a 20 mm HDPE sleeve over the free length. The bond length is cleaned back and left bare, with all 91 lengths of cable twisted into an hour glass shape to increase the bond with the dolerite foundation rock. The complete anchor is installed into a part corrugated, part smooth polyethylene sheath within the anchor hole, and grouted into the hole. Once the grout reaches its strength, a purpose built 2200 tonne capacity hydraulic jack is used to load the anchor to over 70% of its minimum breaking load.

4.3 Long term maintenance

The newly installed post tensioned anchors will be monitored every five years by Hydro Tasmania, with the first of these to be undertaken in early 2011. To undertake these tests, the travelling gantry, used during construction, was modified to carry all load monitoring equipment.

5 CONCLUSION

There is currently no way to judge the current performance of old style post-tensioned anchors installed between the 1950–1980s, where the only defense against corrosion is the grout column. This is a significant dilemma facing dam safety engineers worldwide as there are many concrete dams with these types of anchors providing an important stabilising force. As a result, a number of dam owners have chosen to replace the anchoring with modern post-tensioned anchors, having double corrosion protection and can be monitored for deterioration.

As a result of owning a number of post tensioned dams constructed in the 1950–70s, Hydro Tasmania embarked on an extensive investigation program at Catagunya dam to try to ascertain the condition of these old style anchors. The conclusion of these investigations was that some corrosion has occurred, however, the absolute magnitude and extent of this corrosion could not be concluded. Based on this the anchors in Catagunya dam could not be relied upon in the long term and were therefore replaced.

The conclusion eventually reached at Catagunya dam is similar to other experiences in Australia. It is the author's view that old style post-tensioned anchors pose a real dam safety issue, especially given that the risk, unless addressed, will increase with time. All dams, whose stability depends on these old style anchors, should be assessed as a high priority.

REFERENCES

- Cooper, B.W. & Rodd, R.J. 1987. Post tensioned strengthening of Hume dam. *Seminar—Use of cement and concrete in dams; ANCOLD and Concrete Institute of Australia, Sydney, 5 May 1987.*
- Cubit, T., Swindon, A. & Tanner, D. 2010. Innovations in resolving construction challenges on the Catagunya dam restoration project. *Proc. ANCOLD conf., Hobart, 3–5 November 2010.*
- Harman, T., Herweynen, R. & Ghosh, M. 2010. Analysis and design challenges associated with Catagunya dam restoration project. *Proc. ANCOLD conf., Hobart, 3–5 November 2010.*
- Herweynen, R., Harman, T. & Swindon, A. 2009. Catagunya post tensioned dam—the challenge of old style anchors. *23rd ICOLD Congress on Large Dams, Q.90, R.53, Brasilia, 2009.*
- Herweynen, R. & Hughes, A. 2002. Catagunya dam—corrosion assessment of fully grouted post-tensioned anchors. *Proc. ANCOLD conf., Adelaide, 19–25 October 2010.*
- Himsley, N. & Heinrichs, P. 1997. Recent NSW investigations into post tensioning longevity. *Proc. ANCOLD conf., Perth and Kununurra, 13–17 October 1997.*
- McInerney, S., Bruce, D.A. & Black, J. 2007. Comparison of New Zealand and North American dam anchoring practices. *Proc. NZSOLD/ANCOLD conf., Queenstown, 19–21 November 2007.*
- Wilkins, J.K. & Fidler, J. 1959. Design of Catagunya dam. *Civil Engineering Transactions, The Institute of Engineers, Australia, September 1959.*

Development of geomembrane systems for watertightness of dams in Europe

A.M. Sciuero & G.L. Vaschetti
Carpi Tech, Balerna, Switzerland

ABSTRACT: Europe has been a pioneer in impervious geomembrane systems for long-term waterproofing of dams. Most innovations, both for rehabilitation and for new construction, have been performed on European territory, or have been developed by European designers. This paper presents some significant recent or historical projects that are representative of the possible numerous applications of geomembrane systems to the rehabilitation of existing dams and to the construction of new dams.

1 INTRODUCTION

1.1 *Pioneer applications of geomembranes*

More than 50 years have elapsed since the first installations of a geomembrane on a dam. The first applications took place in new embankment dams because many of these dams, being too permeable, required a separate element to provide imperviousness. In many cases, geosynthetic barrier systems were more economical and easier to install than traditional impervious materials such as clay, cement concrete or bituminous concrete (Cazzuffi et al. 2010).

Europe has been a pioneer in developing the use of geomembranes in dams: the first geomembrane installations on dams were made at in 1959 at Contrada Sabetta rockfill dam in Italy, and in 1960 at Dobsina earthfill dam in Slovakia. With only two exceptions (Terzaghi rockfill dam in Canada and Atbashinsk rockfill dam in Kirgikistan) up to the early 1980ies all geomembrane applications on dams were made in Europe, as well as all first applications of geomembranes on concrete dams (ICOLD, 2010): on some arch dams in Austria in the early 1980ies, on gravity dams in Germany (Heimbach 1974) and Italy (Lago Miller 1976). In RCC dams, while USA pioneered the application of covered geomembranes (Carrol Ecton 1984), Europe started the application of exposed geomembranes at Riou dam in France, in 1990.

1.2 *Present geomembrane applications*

Impervious geomembranes are now an established technique for long-term waterproofing of all types of dams. Possibly, the credibility of synthetic materials had been established by the good performance of embedded PVC waterstops in a very large number of concrete dams worldwide. A geomembrane placed on the upstream face of a dam or inside a dam can be considered, from a conceptual viewpoint, as one wide waterstop sealed at the abutments and the bottom.

The range of applications has dramatically increased, and geomembranes are now used in a variety of projects all over the world, on dams as well as in hydraulic tunnels, canals, reservoirs both for rehabilitation and for new construction, in the dry or underwater. Europe has witnessed practically all innovations, either because the installations have been performed on European territory, or because the solutions and technologies, although applied elsewhere, have been developed by European designers. The examples that follow are not exhaustive of the large range of solutions available. They just intend to give an overview of some significant applications, for which details can be found in the cited references.

2 REHABILITATION OF CONCRETE DAMS

2.1 *Rehabilitation of the upstream face: Silvretta, Austria 2010–2011*

Silvretta is a gravity dam owned by Vorarlberger Illwerke AG and used for power production. The main dam, completed in 1948, is 80 m high upon foundations and has 4 inspection galleries. The main dam and the saddle dam forming the 40,000,000 m³ storage are located in the Alps at 2032 m altitude, with frequent freeze-thaw cycles. Temperatures vary from –30°C to +30°C, maximum compact ice thickness is 90 cm, maximum snow/ice layers thickness is 2 m. In the last decade, the combined action of frost and ice and of seeping water caused severe damage to the dam, and the deterioration of the concrete rapidly progressed.

Within the rehabilitation works that started in 2009 and will end in 2011, including waterproofing and placing new concrete on the crest, foundation treatment, grouting and renewal of instrumentation, rehabilitation works at the outlet and intake valves, Illwerke took the decision of installing an exposed PVC geomembrane system on the main dam and on the saddle dam. Silvretta is the first exposed PVC geomembrane project on an Austrian dam. The final design is the result of extensive research carried out by Illwerke on available rehabilitation systems, and of evaluation of performance data from previous similar applications.

The objectives of the waterproofing system are to stop water infiltrating into the dam body via existing or future cracks and fissures, to protect the dam against frost and seepage water damages, to drain infiltration and condensation water, and to allow monitoring of the waterproofing system. Site specific peculiarities are the bad conditions of the surface concrete, a particularly tight (only three springtime months) window for installation, and demanding climate with risk of snowfall also in summer. The decision was taken to design the geomembrane system so as to follow the dewatering program foreseen for the general rehabilitation works. As a result the system has to be installed in two separate campaigns. In the first campaign in 2010, when the water level was maintained at elevation 1995 m, the entire saddle dam has been lined, in total about 1680 m², and the main dam has been lined from crest down to elevation 2001 m, in total about 10,340 m². In 2011 the reservoir will be totally dewatered allowing lining the remaining part of the main dam, in total about 5940 m².

The new liner is Sibelon CNT 3750, a geocomposite consisting of a 2.5 mm thick PVC geomembrane heat-laminated to a 500 g/m² anti-puncture geotextile. The geocomposite was selected based on precedents having more than 20 years successful performance. To minimize the civil works and the delays due to adverse climatic conditions, it was decided to make extensive use of geosynthetic materials instead than of traditional surface preparation methods. After hydro-jet cleaning, removal of unstable parts and re-profiling by shotcrete mortar, two geosynthetics have been placed under the PVC geocomposite: one geogrid to provide support over the remaining cavities and cracks, and one thick anti-puncture geotextile, 2000 g/m², acting as a cushion against excessive irregularities.

The geocomposite is mechanically anchored to the dam face with Carpi patented tensioning system designed to resist wind velocity of 180 km/h, and at boundaries with flat batten strips. The submersible perimeter seals are made with stainless steel batten strips compressing the PVC geocomposite on a regularizing resin, with the aid of rubber gaskets and stainless steel splice plates to distribute the compression and achieve watertightness against water in pressure. The depth of the anchor bolts for the tensioning profiles and for the watertight perimeter anchorage was based on the results of the pull-out resistance tests carried out on the face concrete. The top seal, made with stainless steel batten strips, is not airtight, to establish atmospheric pressure in the drainage system and avoid suction. The drainage system is divided in 6 separate vertical compartments to allow monitoring the performance in sections. Drained water is discharged in the bottom gallery by transverse discharge pipes, one pipe for each compartment.

Installation was carried out from travelling platforms suspended at crest, and from scaffolding in the areas not accessible by the platforms and for works under winter conditions, as shown in [Figure 1](#). To allow performing all tasks including welding in adverse climatic conditions and minimizing idle time, the scaffolding was equipped with a shelter.



Figures 1, 2 and 3. At left Silvretta dam: from right to left control of surface, installation of vertical profiles, of support geogrid, of anti-puncture geotextile, of PVC geocomposite, and sheltered scaffolding at left abutment. At middle and right Illsee dam: exposed PVC geocomposite installed on an anti-puncture geotextile (white material) on rock masonry, and on a geonet (black material) on concrete.

2.2 Rehabilitation of a dam subject to Alkali-Aggregate-Reaction (AAR): Illsee, Switzerland 1996/1997

Illsee is a 25 m high gravity dam in the Swiss Alps, at altitude 2320 m a.s.l., with temperatures ranging from -30°C to $+35^{\circ}\text{C}$, freeze-thaw cycles in the order of 100 per year, and maximum ice thickness 1.0 m. The dam, now owned by Illsee Turttmann AG, is used for power production.

Displacements that could not be related to hydrostatic or thermal stresses were ascertained as being caused by AAR. Installation of a new impervious layer on the upstream face was deemed mandatory to stop water penetration inside the dam. A drained PVC geomembrane system was preferred to shotcrete and to reinforced concrete solutions for its superior performance in cold climates and its draining capability.

The waterproofing liner and the anchorage system are the same adopted at Silvretta. A drainage geonet was installed on the concrete face of the dam. As shown in Figure 2, at the bottom part of the arched section of the dam, where the existing surface is sharp rock masonry, instead of the geonet (the black material) a 2000 g/m^2 anti-puncture geotextile (the white material) was installed under the PVC geocomposite to protect it against the sharp rocks.

At bottom, there is a double perimeter seal: the primary seal is placed at the bottom of the upstream face, and the secondary seal is placed underneath it. The double seal system allows separating the water drained from the upstream face from the water drained from foundations, and reducing the water head on the primary seal.

From its completion in 1997, the geomembrane system has been providing continuous good performance. Since the owner is now considering the possibility of performing slot cutting to relieve tension stresses in the concrete, the presence of the PVC geomembrane system will allow restoring watertightness at the upstream face by simple removal of the geomembrane in the area of the slot, and by repositioning and welding a geomembrane strip after the slot has been made. This procedure was adopted at Chambon dam in France, where as stated by the owner (De Beauchamp & Bourdarot 1998) “The membrane proved very useful during sawing works for it avoided any later leakage near slot cuts usually affected by much cracking. The last membrane asset is that the membrane can be cut and repaired very easily for sawing and recurring sawing”.

2.3 Rehabilitation of a critical section: Toules, Switzerland 2010

The same waterproofing system described for rehabilitation of the entire upstream face can be used to rehabilitate only critical areas of the dam surface. An example is Toules double curvature arch dam, 86 m high and located at 1811 m altitude in the Swiss Alps. The dam, owned by Forces Motrices du Grand-St-Bernard, is used for power production and was erected over a pre-existing dam about 30 m high.

Some diagonal cracking was observed in blocks 10 and 14, at the joint between the old dam and the new dam. The cracks were treated with products of the paint type, which were not effective. To avoid that further deterioration could increase water seepage inside the cracks, and to ensure watertightness and safety of the dam in respect to under-pressures and seismic events, a geomembrane system was installed on bloc 14, from elevation 1755 to elevation 1750.

Site specific challenges at Toules were the presence of strong intermittent winds in the valley, difficult access to the staging area, due to the curvature of the dam and to the fact that installation had to be performed with reservoir at elevation 1740, and bad climate. The option selected was to perform installation working on hanging sheltered fixed scaffolding erected in front of the entire intervention area and anchored with brackets to the upstream face of the dam at elevation 1756, and to use a travelling platform suspended at a crane on the crest to daily transport the workers down to the staging area at block 14, and to quickly transport the workers off the dam when wind speed exceeded 25 km/h.

The waterproofing system, covering a rectangular area 23 m long and 5 m high for a total of 115 m², consists of a 2.5 mm thick PVC geomembrane heat-laminated to a 500 g/m² anti-puncture geotextile, secured to the dam by vertical tensioning profiles at 3.70 m spacing, and confined by a watertight perimeter seal of the compression type. Where the top and bottom watertight perimeter seals cross the vertical joints of the dam, a treatment was made to avoid water by-passing the seal at the joints. The treatment, performed by a Swiss specialty contractor, consisted in drilling on both sides of the joints 12 mm holes, inclined at 45 degrees in respect to the dam face, down to reach the waterstops. The holes were filled with a solvent-free, low viscosity fine injection acrylic resin.

Waterproofing works started on March 29 2010, and by contract had to be completed within 9 days. Completion date was April 6 2010.

2.4 Rehabilitation of a crack underwater: Platanovyssi, Greece 2002

Platanovyssi is an example of a similar concept as the one adopted at Toules, but with installation performed underwater. Platanovyssi, at 95 meters of height, is the highest RCC dam in Europe. Completed in 1998 and owned by PPC (Public Power Corporation), the dam was designed with a high cement content RCC mix. Carpi external waterstop system was installed on the contraction joints between blocks during construction of the dam.

In 1999, at first impounding, an approximately 20 m long crack developed at station 98+40 (left part of the upstream face) of the dam. The system selected for waterproofing the crack in 2002 is the same external waterstop that had been installed on the vertical contraction joints in 1998, with some modifications due to the lower hydraulic load (20 m instead than 95 m) they must sustain. Repair works were scheduled for spring 2002. Due to an unusually dry season, the owner could not afford to lose the volume of the water to empty the reservoir in order to work in dry conditions. In addition to that restriction, when Platanovyssi is emptied the pumped storage scheme of Thissavros cannot operate, with serious implications to the production system. Most of the repair works therefore had to be accomplished underwater.

The waterproofing liner, a 2.5 mm thick PVC geomembrane heat-laminated to a 500 g/m² anti-puncture geotextile, is supported over the cracks by 2 support layers of the same material, to avoid that under the water head the waterproofing liner intrudes into the crack and is damaged. The external waterstop following the path of the crack (Fig. 5) is confined by the same watertight perimeter seal already described. Underwater installation was performed by a Dutch specialist contractor in association with Carpi, from a diving pontoon, with turbines shut. Detailed information can be found in a previous paper by the same authors (Scuero & Vaschetti 2006).



Figures 4, 5, 6 and 7. Scheme of the areas waterproofed at Toules dam (left) and Platanovyssi dam (middle, artist's impression from the upstream side). At right, the waterproofing system installed from fixed sheltered scaffolding at Toules (top) and underwater at Platanovyssi (bottom).

3 REHABILITATION OF EMBANKMENT DAMS

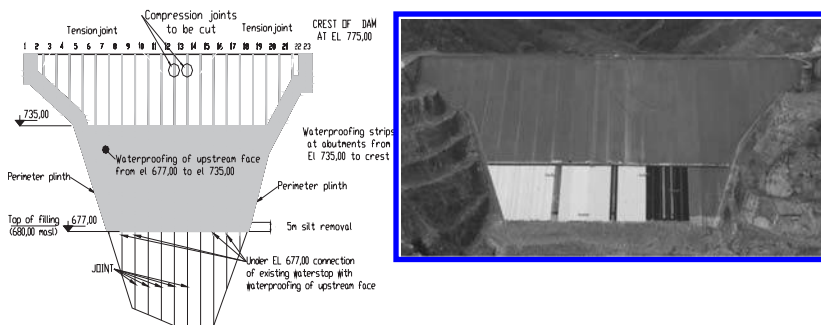
3.1 Rehabilitation of a CFRD: Messochora, Greece 2010

Messochora is an example of different waterproofing systems applied on different sections of a dam to achieve different objectives. Owned by the same owner of Platanovyssi, Messochora is a 150 m high CFRD; the peripheral joint and the joints between slabs have a traditional embedded copper waterstop + neoprene rod and filler + external waterstop consisting of mastic filler confined by a neoprene membrane. In the lower 55 m the face slabs are covered by a silty fill.

Although the dam was completed in 1996, and the powerhouse in 2000, the reservoir has never been impounded due to environmental assessment re-evaluation procedures. As impoundment kept being delayed, the steel plates installed on the waterstops as a protection measure were lifted and torn by the wind, exposing the neoprene membrane confining the mastic filler, and jeopardising the efficiency of the waterstop. In view of foreseen imminent impounding, PPC intended to restore watertightness at the joints, and to avoid water infiltration in the area where the anticipated settlement of the dams following impounding would cause the face slabs to deform under the pressure of water, and localized compression stresses to develop in the concrete, causing cracking and spalling.

These objectives were achieved by installing a full face waterproofing system in the lower half of the upstream face that is not covered by the backfill, from elevation 677 to elevation 735, and in a 15 m wide section following the peripheral joint at the abutments, and by installing Carpi external waterstop on all joints between slabs, from elevation 735 up to crest level (Fig. 8). The existing external waterstops have been cut flush the face slabs. A 5 cm wide groove has been cut at two of the five central compression joints to allow movements and avoid compression cracking.

The full face waterproofing system is the same described for Silvretta, and similar to one of which PPC had previous successful experience at Thissavros pressure tunnel. The external waterstop is similar to the one selected by PPC for the contraction joints and for crack repair at Platanovyssi dam. At elevation 735, at elevation 677, and all around the 15 m wide strips at the abutments, the geocomposite is fastened by the same watertight seal used for the external waterstops. An extra strip of geocomposite is left extending outside the top seal at elevation 735 and at the peripheral joint, in order to allow connecting the geocomposite to a new geocomposite which may be added in the future to cover the whole face in case the top slabs crack. At elevation 677 the existing waterstops are connected to the full face system to minimize water infiltration from the section below that has no liner. The existing backfill is removed from elevation 680 to elevation 675 to allow extending the geomembrane system to elevation 677, and connecting it to the waterstops below. Details on the design, on the installation and on the present status of works can be found in recent literature (Thanopoulos et al. 2010).



Figures 8 and 9. Arrangement of the new waterproofing system at Messochora dam: full face waterproofing from elevation 677 to elevation 735, waterproofing of peripheral and vertical joints from elevation 735 to crest. Two central compression joints were cut to avoid compression cracking.

3.2 Rehabilitation of a dam with bituminous concrete facing: Winscar, UK 2001

Winscar is an example of cost effective repair of bituminous concrete facings. Owned by Yorkshire Water Services and used for water supply, the dam is a 53 m high compacted rock-fill with a two-layer membrane of dense bituminous concrete covering the 25,000 m² upstream face. A cement grout curtain extends beneath the upstream toe to depths of up to 70 m.

In January 2001 the seepage rate exceeded the capacity of the drainage system and a leak appeared at the downstream toe of the dam with an estimated flow of about 15 l/s. The maximum rate of leakage was 6000 m³/day. Inspection after drawdown of the reservoir revealed over 60 small defects that had not been visible when minor repairs were done in 1996. It was decided to empty the reservoir completely and to refurbish the dam with the objective of securing the reliability of the resource for the next 40 years. This goal was to be achieved by the installation of an appropriate, well-proven and robust waterproofing system over the existing bituminous concrete face and by reinforcement of the grout curtain. The target was to reduce overall leakage to an insignificant level at economic cost.

The two retained options among various solutions were 1) removal of part of the existing facing and its replacement with a dense bituminous concrete membrane over a bituminous bound drainage layer and 2) installation of a drained tensioned geomembrane liner over the existing face of the dam. Priced tenders were sought from contractors for both alternatives, and a tender evaluation workshop was held to rank the tenders. The tender evaluation process, the selected drained tensioned exposed geomembrane system, risk sharing and capital cost, and project management, are discussed by Clayton et al. (2003). The geomembrane option was adopted.

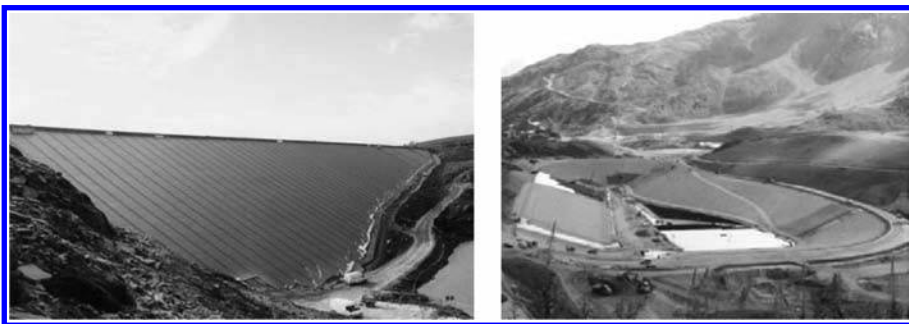
The construction schedule was very challenging, because of the fast-track nature of the project. Three standard 2.10 m wide PVC geocomposite rolls were then welded in a pre-fabrication yard to construct wider panels in order to maximise quality and minimise installation time on site. The liner was installed between August and December 2001, including 2 + 3 weeks interruptions to perform works on the grout curtain.

As reported by the owner (Clayton et al. 2003) “The geocomposite liner has performed well since impounding was resumed in December 2001. Flow from the primary compartment, which covers the original asphaltic concrete facing, is barely measurable. Flow from the secondary compartment is greater but less than 0.1 l/s”.

4 NEW CONSTRUCTION

4.1 World's first double geomembrane system on a dam: Les Arcs, France 2008

Adret des Tuffes—Les Arcs is the largest reservoir for production of artificial snow in Europe. The owner is Société Les Montagnes de l'Arc (SMA), the Designer and Engineer is EDF-CIH (Electricité de France—Hydro Engineering Centre). The reservoir is created by a main 230 m long earthfill dam having a height of 21.1 m above foundations, and by an upstream earthfill



Figures 10 and 11. At left Winscar dam, rehabilitation of bituminous concrete facing, exposed PVC geomembrane. At right Les Arcs reservoir, new construction, double geomembrane system, covered.

dam 8 m high. Due to its size and to its importance in respect to public safety, the reservoir falls under the jurisdiction of the French Permanent Technical Committee for Dams (CTPB).

The original design envisaged for the slopes and bottom of the reservoir a double geomembrane system with two separate drainage systems, one for the primary geomembrane and one for the secondary geomembrane. After award of tender, in consideration of the demanding environment (altitude 2214.4 m, cold temperatures and high possibility of rain and snow even in summer) and of the short installation time (three months only), the contractor proposed an alternative design using, instead of the two granular drainage layers foreseen by original design, two layers of synthetic materials that would facilitate completion of works within the allotted period. EDF-CIH requested extensive testing of the system in three independent laboratories, and verification of constructability on four 60 m long and 4 to 6 m wide testing embankments for the slopes, and two 10 m long and 6 m wide testing areas for the bottom. After successful results of testing the alternative solution was approved.

The quite innovative waterproofing and drainage system, as described by Delorme et al. (2009) is formed exclusively by synthetic materials: a draining geocomposite as secondary drainage layer, a thinner membrane to separate the two drainage systems, a draining geocomposite as primary drainage layer, a PVC geocomposite as primary waterproofing liner (2.0 mm thick PVC geomembrane heat-laminated to a 500 g/m² anti-puncture geotextile), and a gravel and riprap cover to blend the system in the landscape.

4.2 *World's first exposed geomembrane on an RCC dam: Riou, France 1990*

Riou, 20 m high and owned by EDF, was the first RCC dam adopting an exposed PVC geocomposite as waterproofing element. The Sibelon CNT 3750 geocomposite is fastened to the upstream face by tensioning profiles having configuration similar to the ones adopted for rehabilitation. The profiles have been attached to the permanent steel formworks used for construction of the dam (Fig. 12).

After 20 years of service the system is performing very well. Since 1990, the number of RCC dams waterproofed with geomembranes has been steadily increasing.

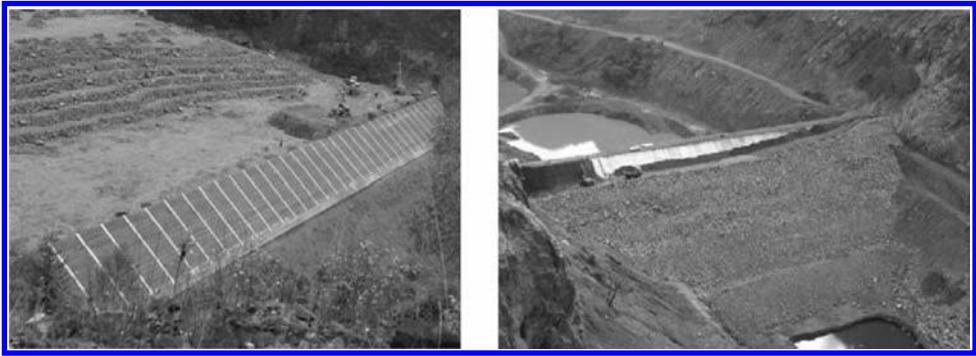
4.3 *Applications of European design and technology in new fill dams*

Latest developments of geomembrane systems are related to construction of new fill dams. The new design and technologies have been developed in Europe. One system is related to an upstream exposed PVC geomembrane that is anchored to the dam with PVC geomembrane wings embedded in the dam itself while it is under construction, to construct a Geomembrane Face Rockfill Dam (GFRD), as pictured in Figure 13.

The system of the upstream exposed PVC geomembrane anchored with PVC wings has been adopted in 2008 for the 20 m high raising of Sar Cheshmeh tailings dam in Iran (Noske 2009),



Figures 12 and 13. At left Riou RCC dam, new construction, exposed geomembrane. At right Sar Cheshmeh tailings dam in Iran, upstream exposed PVC geomembrane anchored with PVC wings.



Figures 14 and 15. At left installation of anchor wings for exposed upstream PVC geomembrane at Runcu 149 m high GFRD. At right Gibe III 50 m high upstream cofferdam in Ethiopia, central zigzag geomembrane core.

which will be followed by further 20 m raising. The same system is in 2010 under installation at Runcu 149 m high rockfill dam (Fig. 14).

Geomembranes are used also as central impervious core, replacing clay or bituminous concrete cores. An example of central zigzag geomembrane is Gibe III 50 m high upstream cofferdam in 2009 (Pietrangeli et al. 2009), pictured in Figure 15.

5 CONCLUSIONS

Modern geomembrane systems can address practically all projects requiring waterproofing of old and new dams, totally or partially, in the dry or underwater. Their successful performance in more than half a century testifies this established technology, that can technically and cost effectively substitute more traditional methods.

REFERENCES

- Cazzuffi, D., Giroud, J.P., Scuro, A. & Vaschetti, G. 2010. Geosynthetic barriers systems for dams, *Keynote Lecture, 9th International Conference on Geosynthetics, Guarujá, 23–27 May 2010*.
- Claydon, J., Stevens, I., Carter, I. & Wilson, G. 2002. Wincar dam membrane repairs: financial arrangements and risk management. *Proc. ICOLD International Congress, Montréal, 16–20 June 2003*.
- De Beauchamp, T. & Bourdarot, E. 1998. Earthquake and membrane at the Chambon dam, *Proc. SpanCOLD Symposium on the Safety of Dams, Barcelona, 17–19 June, 1998*.
- Delorme, F., Lochu, A., Kraemer, P., Scuro, A., Vaschetti, G., Prost, S. & Recalcati, P.G. 2009. Retenue d'altitude de l'Adret des Tuffes: conception et mise en œuvre d'un Double Dispositif d'Étanchéité par Géomembrane intégralement en géosynthétiques", *Proc. Rencontres géosynthétiques, Nantes, 1–3 April 2009*.
- ICOLD, the International Commission on Large Dams 2010. Bulletin 135. *Geomembrane sealing systems for dams—Design principles and return of experience*. Paris, December 2010.
- Noske, C. 2009. Geocomposite faced rockfill—an innovative approach to tailings dam waterproofing in the absence of clay, *Newsletter of Australian Centre for Geomechanics, Vol. 32, May 2009*.
- Pietrangeli, G., Pietrangeli, A., Scuro, A. & Vaschetti, G. 2009. Gibe III: a zigzag geomembrane core for a 50 m high rockfill cofferdam in Ethiopia, *Proc. 1st International Symposium on Rockfill Dams, Chengdu, 11–14 October 2009*.
- Scuro, A. & Vaschetti, G. 2006. Platanovyssi RCC dam: the underwater rehabilitation, *Proc. Hydro 2006—Maximising the benefits of hydropower, Porto Carras, 25–28 September 2006*.
- Thanapoulos, Y., Scuro, A. & Vaschetti, G. 2010. Exposed Geomembrane Systems at Messochora Concrete Face Rockfill Dam. *Proc. II Int. Congress on Dam Maintenance & Rehabilitation, Zaragoza, 23–25 November 2010*.

Development of small hydropower plant utilizing pumped storage power plant's dam

H. Watabe & N. Arai

Tokyo Electric Power Company, Tokyo, Japan

ABSTRACT: The Kazunogawa dam, which is the lower dam of the Kazunogawa pumped storage power plant, is a concrete gravity dam with a height of 105.2 m, and its reservoir has an effective storage capacity of 8.3 million m³. In the Kazunogawa hydropower plant, discharge outlet structures were installed in the Kazunogawa dam to discharge the river inflow downstream for river conservation measures. In order to utilize the river inflow and the dam head effectively, Tokyo Electric Power Company Co., Inc. (TEPCO) decided to construct the Tsuchimurogawa hydropower plant, which has a maximum output of 350 kW with an effective head of 89.94 m at a maximum discharge of 0.5 m³/s, just downstream of the Kazunogawa dam. It began commercial operations in December 1999. The development of the small hydropower plant utilizing the pumped storage power plant's dam makes it possible to prevent areas of water scarcity and allows for the effective use of renewable energy.

1 INTRODUCTION

TEPCO has been engaged in the development of pumped storage power generation in order to ensure high quality and a stable power supply. TEPCO's Kazunogawa hydropower plant is located near the Tokyo metropolitan area where electricity consumption is high.

The general layout of the Kazunogawa project is shown in [Figure 1](#). The Kazunogawa hydropower plant is a pure pumped storage power plant with an effective 714 m head with a maximum discharge of 280 m³/s and a maximum generation output of 1600 MW with four motor-generators. [Table 1](#) describes the features of the upper dam and the lower dam.

In order to utilize the discharging river inflow and the dam head effectively, TEPCO decided to construct the Tsuchimurogawa hydropower plant, which has a maximum output of 350 kW with an effective head of 89.94 m at a maximum discharge of 0.5 m³/s, just downstream of the Kazunogawa dam. It began commercial operations in December 1999.

After completion, the plant produced a total power generation capacity of around 12,000 MWh, and reduced CO₂ emissions by approximately 11,000 tons, which was calculated based on the capacity of the coal thermal power plants.

In this paper, the planning and the design of the small hydropower plant including the electrical equipment will be reported on.

2 INFLOW AND DISCHARGE IN THE KAZUNOGAWA DAM

The Kazunogawa dam is a concrete gravity dam with a height of 105.2 m, and its reservoir has an effective storage capacity of 8.3 million m³. In the Kazunogawa hydropower plant, after completing the designated storage to the reservoir, the storage of water from the river inflow into the reservoir has not been permitted by the government due to river conservation measures.

Therefore, some discharge outlet structures were installed in the Kazunogawa dam to discharge the river inflow downstream. The relationship between the river inflow into the reservoir and the discharge of it downstream is shown in [Figure 2](#).

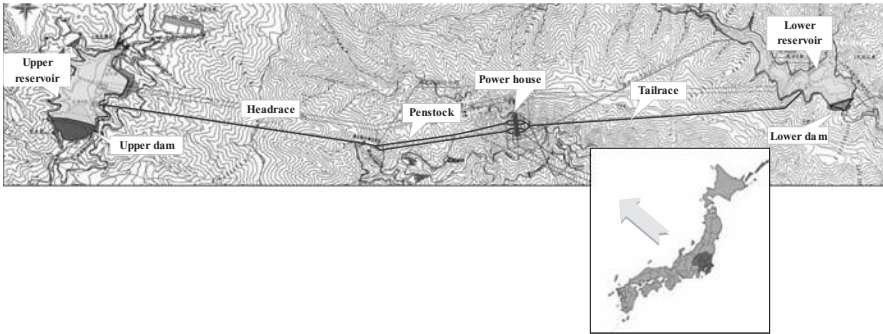


Figure 1. The location and the general layout of the Kazunogawa project.

Table 1. The features of the dams of the Kazunogawa project.

Item	Upper dam	Lower dam
Dam type	Rockfill (Centre core)	Concrete gravity
Height (m)	87	105
Crest length (m)	494	264
Volume (m ³)	4.11 million	0.62 million
Effective storage capacity (m ³)	8.30 million	8.30 million

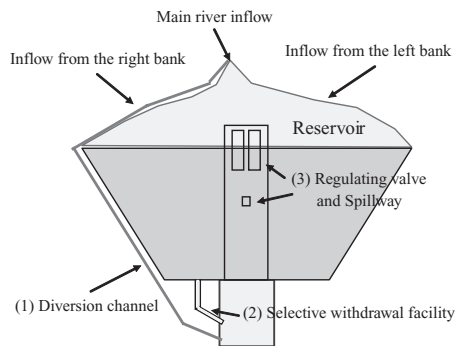


Figure 2. Inflow into the reservoir and its discharge into the downstream in the Kazunogawa dam.



Photo 1. Overview of the Kazunogawa dam and the reservoir.

Their functions are as follows:

1. Diversion channel
The inflow from the main river and the right bank has been discharged from the diversion channel. The maximum discharge is 0.25 m³/s, which was calculated based on the mean inflow for ten years in the Kazunogawa dam.
2. Selective withdrawal facility
The selective withdrawal facility, whose maximum discharge capacity is 2.0 m³/s calculated based on the mean inflow for ten years in the Kazunogawa dam was installed to discharge the inflow from the left bank. This facility is used as the intake of the Tsuchimurogawa hydropower plant, which produces 350 kW with a maximum turbine discharge of 0.5 m³/s.
3. Regulating valve and spillway
When the inflow into the reservoir exceeds 2.25 m³/s or there is a flood, the water is discharged from the regulating valve and the spillway. The design flood is 480 m³/s based on the Creager's curve of the Kazunogawa dam site, whose catchment area has 13.5 km².

3 OVERVIEW OF THE TSUCHIMUROGAWA HYDROPOWER PLANT

The features of the Tsuchimurogawa hydropower plant are shown in [Table 2](#). The development of the Tsuchimurogawa hydropower plant utilizing the Kazunogawa dam makes it possible to prevent areas of water scarcity from forming and allows for the effective use of renewable energy. Further, it is possible to reduce the costs and shorten the construction period by utilizing the existing discharge outlet structure as shown in [Figures 3 and 4](#).

Table 2. The features of the Tsuchimurogawa hydropower plant.

Generation type	Dam and Run-of-river type
Maximum output (kW)	350
Maximum turbine discharge (m ³ /s)	0.5
Effective head (m)	89.94
Annual energy generation (MWh)	1,225

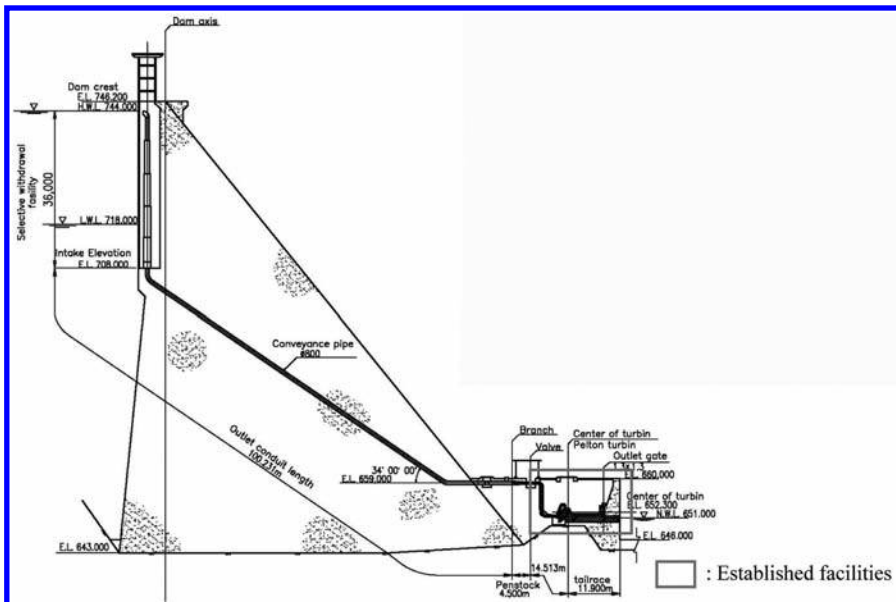


Figure 3. Overview of the Tsuchimurogawa hydropower plant.

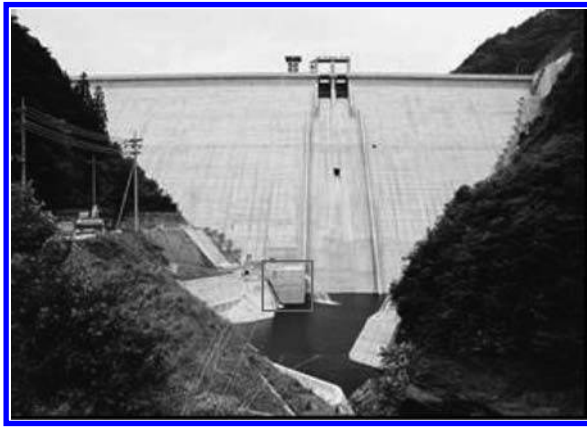


Photo 2. Overview of the Kazunogawa dam and the location of the Tsuchimurogawa hydropower plant.

	1997		1998			1999			
	Oct.	Jan.	Apr.	Jul.	Oct.	Jan.	Apr.	Jul.	Oct.
Penstock, Other equipment			■						
Turbine- generator			Inlet valve ■					Turbine-generator ■	
Test for Opera- tion								Commercial operation ▼ ■	
(Reference) Kazunogawa dam	Construction of dam ■		Stored water in reservoir ■			Test before stored water ■		Commercial operation ▼ Test for electrical facilities ■	

Figure 4. Construction schedule of the Tsuchimurogawa hydropower plant.

4 PLANNING AND DESIGN OF FACILITIES

4.1 Planning of the waterway route

Since the development planning of the Tsuchimurogawa hydropower plant was carried out during the construction of the Kazunogawa hydropower plant, it is possible to utilize the discharge outlet structure of the Kazunogawa dam as the intake effectively and ensure in advance that the area of the power house is just downstream. Further, the waterway route was determined to be the shortest distance from the intake to the power house in order to reduce the friction loss in the penstock.

From an environmental perspective, it is necessary to prevent areas of water scarcity so that the location of the outlet was selected in the stilling pool of the Kazunogawa dam.

As a result of these efforts, the decision of the waterway route called for the reduction of the construction costs and the shortening of the construction period.

4.2 Optimization of the development scale

Empirically, the optimum development scale of the run-of-river generation type becomes the load factor from 40% to 65% based on the common operation manner in Japan.

The comparison of the economic efficiency was carried out via the three cases, which were the turbine discharge of 0.44 m³/s, 0.50 m³/s and 0.52 m³/s respectively, as shown in Table 3.

As a result, the optimum development scale was determined to be 350 kW with a turbine discharge of 0.5 m³/s at the Tsuchimurogawa hydropower plant.

Table 3. The comparison for the optimum development scale.

Cases Items	Turbine discharge (m ³ /s)		
	0.44	0.50	0.52
Load factor (%)	50	47	45
Maximum output (kW)	300	350	360
Annual energy generation (MWh)	1,146	1,225	1,236
Economic effectiveness	1.02	1.00	1.01

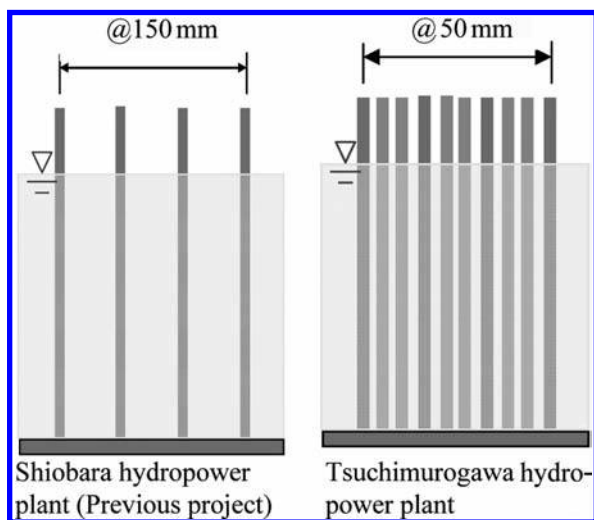


Figure 5. Overview of the screen bar space for the selective withdrawal facility.

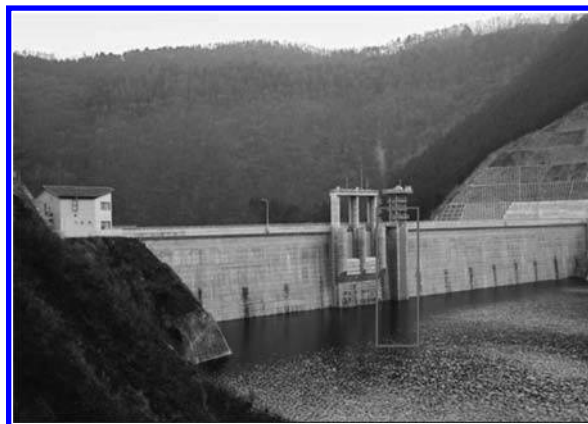


Photo 3. The intake of the Tsuchimurogawa hydropower plant from the upstream of the Kazunogawa dam.

4.3 Design of the screen bar space for the selective withdrawal facility

Since it is necessary to prevent an inflow of reservoir rubbish in order to prevent turbine trouble, a screen, whose bar space is narrower than the previous project, was installed in the selective withdrawal facility as shown in [Figure 5](#).

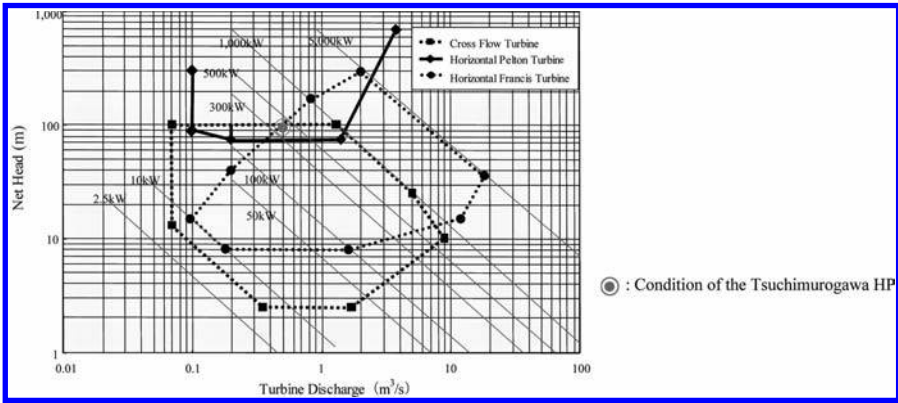


Figure 6. The application chart of the small-size hydro turbine.

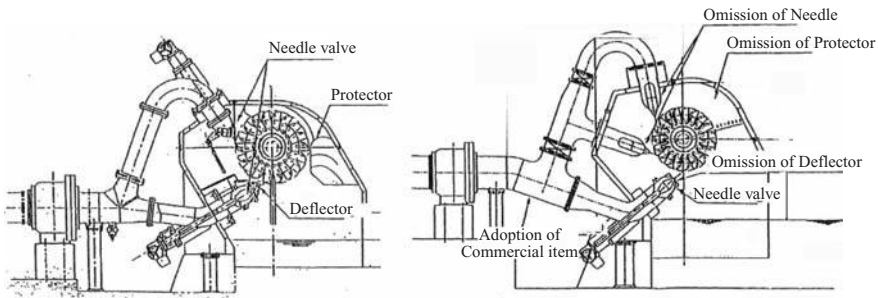


Figure 7. The comparison between the conventional type and the new type of the pelton turbine.

4.4 Design of the electrical equipment

4.4.1 Selection of the turbine type

The application chart of the small-size hydro turbine which is the relationship between the head and the turbine discharge is shown in Figure 6. According to this figure, the three turbine types, that are the cross flow turbine, the horizontal pelton turbine and the horizontal francis turbine, meet the conditions of the Tsuchimurogawa hydropower plant.

As a result of the comparison of economic efficiency, maintenance conditions and so on, given that the horizontal pelton turbine was superior to the others, we decided to adopt it.

4.4.2 Design of the electrical equipment

Generally, the horizontal pelton turbine is used for small generation capacity, and the numbers of runners and the jets of it have various combinations. The pelton turbine can regulate the output by changing the number of nozzles during the operation, and high efficiency operations can be obtained even in the low turbine discharge area.

In designing the turbine, research has been carried out by TEPCO and an electrical manufacturer in order to reduce the construction costs through improving the specifications.

As a result, the new simplified pelton turbine was applied to the Tsuchimurogawa hydropower plant as shown in Figure 7.

The special features of the new simplified pelton turbine are as follows:

1. Reduction of the two needle valves among the three one

To improve the turbine efficiency, the single runner and three jets pelton turbine was determined. It is possible for the designed structure to regulate the output utilizing a one needle valve and two conventional valves. As a result, the needle valve, which has a complicated structure, was decreased from three to one.

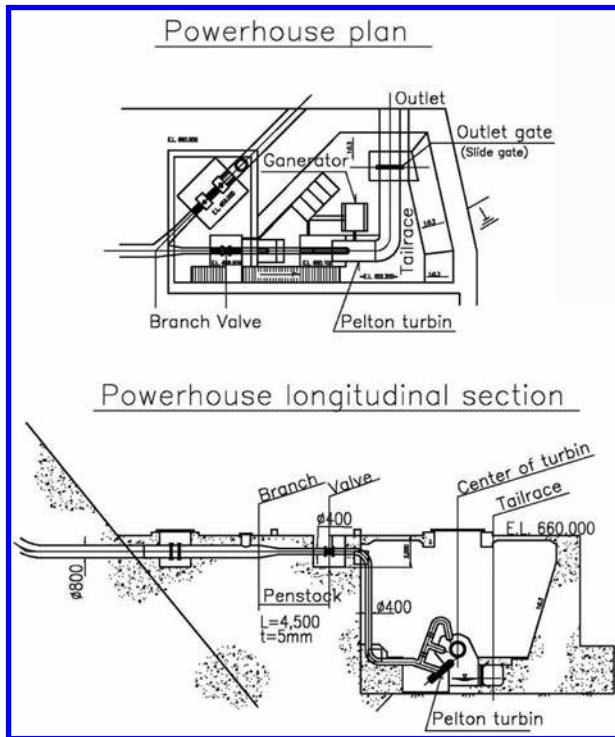


Figure 8. Overview of the new simplified pelton turbine.

2. Omission of the deflector

At Load interception, the deflector must change the direction of the jet water to rev down the turbine-generator. During its working, the needle valve is closed in order to suppress the water pressure rise in the penstock. In this project, the application of the new turbine-generator, this is proof against a rev up at load interception, made it possible to leave the deflector out.

3. Omission of the protector

The protector is generally installed to prevent the jet water from flying in all directions due to deflector changes at the load interception and hit the runner again. With regards to the aforementioned, the application of the new turbine-generator is proof against the rev up at load interception making it possible to omit the protector.

4. Adoption of the commercial equipment

The branch between the nozzle with a needle valve and the nozzle without needle valves was adopted by the commercial equipment due to satisfying the requirements.

The new simplified pelton turbine is shown in Figure 8. Further, its installation is described as shown in Photo 4.

5 RESULTS OF OPERATIONS

The Tsuchimurogawa hydropower plant began commercial operations in December 1999.

After completion, the plant produced a total power generation capacity of around 12,000 MWh, and reduced CO₂ emissions by approximately 11,000 tons, which was calculated based on the capacity of coal thermal power plants as shown in Figure 9.

In accordance with this figure, the plant was operated according to the original plan until 2006. However, since the operating conditions of the Kazunogawa reservoir has been

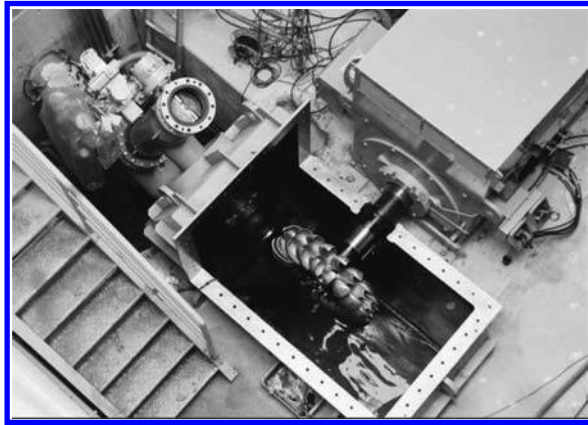


Photo 4. Installation of the new simplified pelton turbine of the Tschimurogawa hydropower plant.

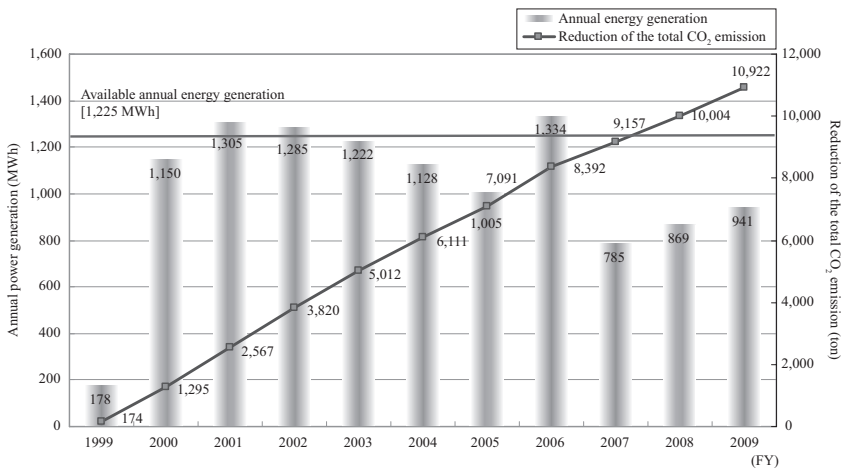


Figure 9. The results of the operations after completion.

changed under keeping closed to the low water level of the Kazunogawa dam, the plant has been affected by that.

6 CLOSING REMARKS

TEPCO is implementing a variety of activities to expand the utilization of renewable energy.

The development of a small hydropower plant utilizing the pumped storage power plant's dam makes it possible to prevent areas of water scarcity and allows for the effective use of renewable energy. Further, it is possible to reduce the costs and shorten the construction period by utilizing the existing discharge outlet structure and a simplified design of the turbine-generator.

Based on these results, the Togawa hydropower plant, which has a maximum output of 240 kW with a 50.55 m effective head at a maximum discharge of 0.6 m³/s just downstream of the Imaichi pumped storage power plant, will be completed by 2011.

REFERENCE

New Energy Foundation, Japan, 1996. *Guide Manual for Development Aid Programs and Studies of Hydro Electric Power Projects.*

A study of the grouting at the bottom of the Yashio dam reservoir and the evaluation of the leakage by grouting

F. Kawashima & Y. Kimura

Tokyo Electric Power Company, Tokyo, Japan

M. Nishigaki

Faculty of Environmental Science and Technology, Okayama University, Okayama, Japan

ABSTRACT: In the Yashio dam reservoir, there is a network of fissures which assumed open fissures of the high dip angle that has the hydrothermal alternation and a large-scale bedrock creep regarded as the main generation factor of the subject in deeper areas. As a result of the test grouting which we performed before the construction for leakage stoppage, we utilized an injection pressure and a limit sedimentation velocity of cement particles and performed effective grouting for fissures of the big width at the bedrock of the bottom of the reservoir filled with water. Further, we confirmed that the leak had been reduced. In this article, we have conducted a qualitative consideration of the grouting mechanism.

1 INTRODUCTION

The Yashio dam reservoir is the upper reservoir of the Shiobara pumped storage power plant (Cf. [figure 1](#)). An upper reservoir is generally made in the vicinity of mountaintop area to get a large head. Leakage tends to be a problem at such spot, because the permeability coefficient is high and the groundwater level is low. The original ground is thin at the right bank of the reservoir, and a lot of porphyrite has been distributed. In addition, the Groundwater level is generally low and falls to the right bank from the left bank in the reservoir. Given the concern for the leakage of the brooks in the Hokikawa River's drainage system from the right bank in the reservoir, we carried out construction to stop the leakage (Cf. [figure 2,3](#)). We conducted grouting from the grouting tunnel which we made in the right bank of the reservoir to the rim grouting tunnel in the right bank of the dam, and made a curtain to stop the leakage. As a result of the borehole of addition and extension based on the initial ponding results, the depth of the borehole in the curtain for leakage stoppage came to around 200–400 m, and the interval became 1.5–12 m (Cf. [figure 4](#)).

The additional grouting had some effect. However, since there was still much leakage, we investigated the place that was deeper than the curtain by the check borehole. As a result, there was not the convergence of permeability coefficient to the deep part direction, and points more than 10~100 Lu was distributed locally. All the tracers that we cast into a part of the point where permeability coefficient is high were confirmed in the brooks in Hokikawa river's drainage system (Cf. [figure 5,6](#)).

As a result of a diving investigation (We sprinkled the bentonite beforehand and investigated the trace of crater occurrence brought about by seepage water), we carried out the grouting in the bottom of Ichinosawa which has a lot of "Craters" ("Craters" is a dent in the bottom area created by seepage water) (Cf. [figure 7](#), photo 1). Since the leakage was decreased quite substantially, we expected that the accumulation of solid particles would naturally block fissures and discontinued the leakage stoppage work at that juncture (Cf. [figure 5](#)).

We conducted an investigation and test grouting in the bottom of the reservoir filled with water afterwards, because more leakage reduction was necessary (Cf. [figure 8](#)). Grouting

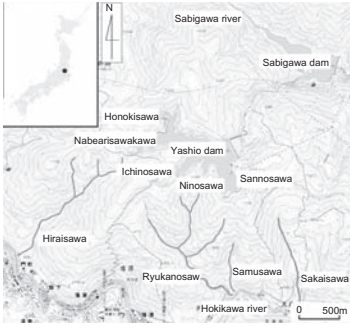


Figure 1. Map of Yashio dam and surroundings.

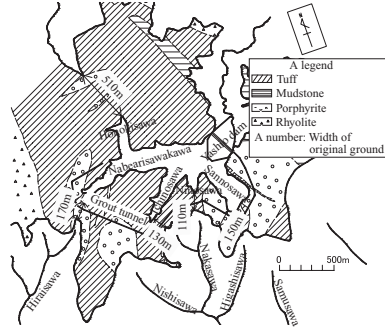


Figure 2. Planimetric map of geological features around Yashiodam.

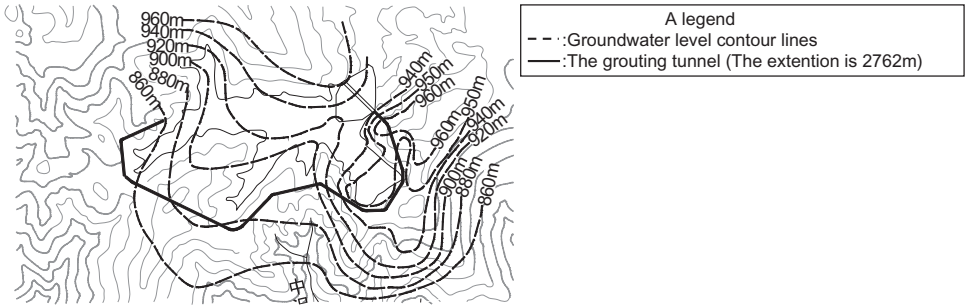


Figure 3. Groundwater level contour lines.

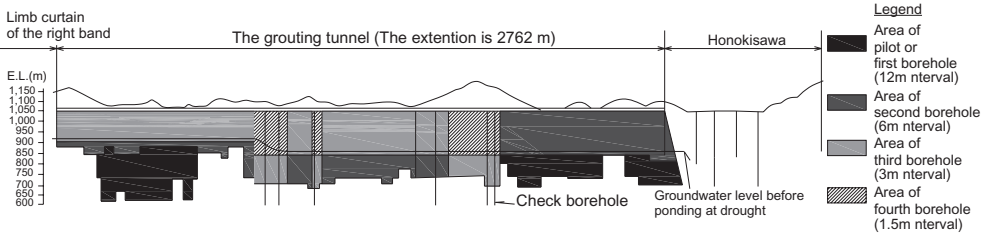


Figure 4. Development of curtain grouting for leakage stoppage.

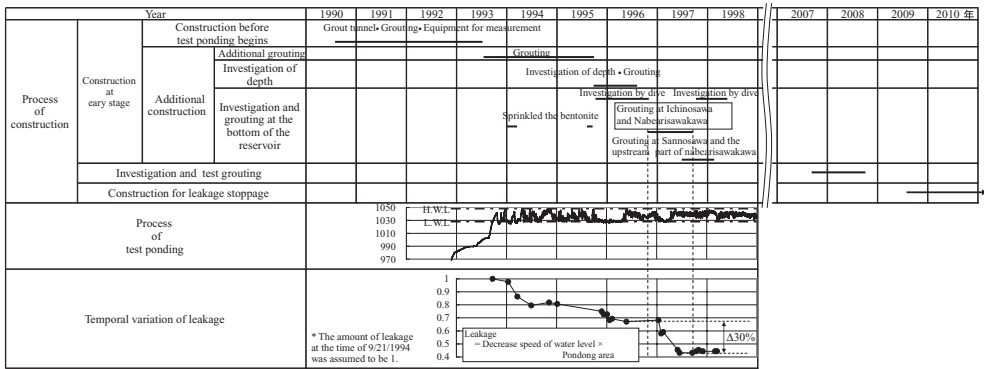


Figure 5. Construction process and the effect of leakage stoppage.

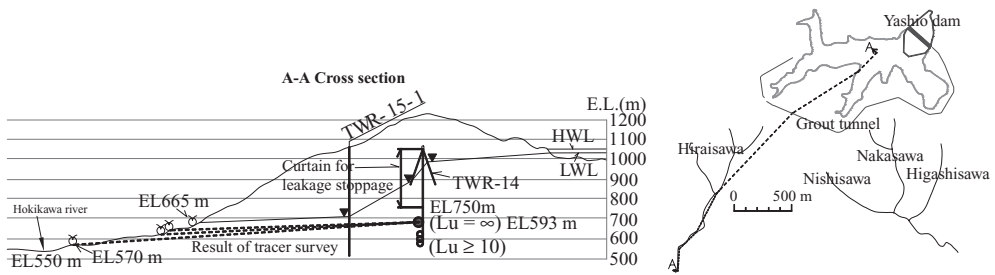


Figure 6. One example of results of the investigation of the depth at the curtain for leakage stoppage.

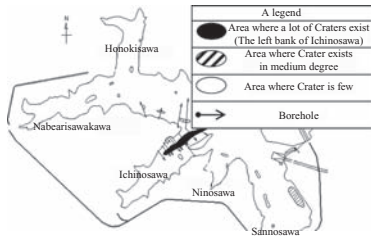


Figure 7. Results of the dive survey of the bottom of the reservoir.

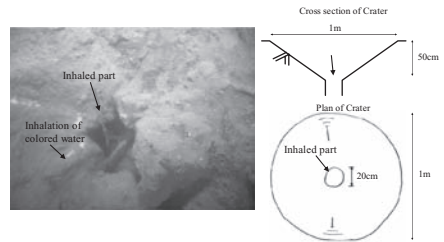


Photo 1. A crater sample.

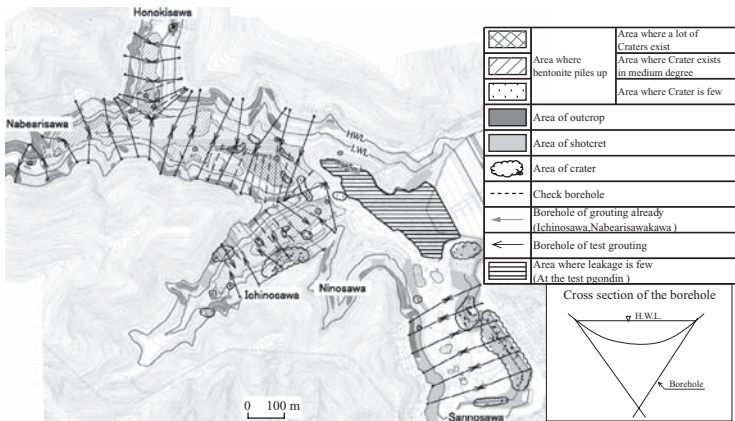


Figure 8. Layout drawing of the boreholes for test grouting.

was conducted in earnest due to remarkable reduction leakage. A characteristic of carrying out the grouting is what the seepage velocity utilizes as well as the injection pressure now to perform effective grouting.

In this article, we show the results of the test grouting, a confirmation result of the improvement degree of bedrock by checking the borehole, the changed situation of the leakage and the groundwater level. Further, we will qualitatively consider the mechanism of the grouting at the bottom of the reservoir filled with water. In addition, the Hydraulics and Geology characteristics of the foundation rock that such grouting is possible was concluded in a report in an annual symposium of No. 78 of 2010 ICOLD (“A STUDY FOR THE BEHAVIOR OF GROUND-WATER FLOW ALONG THE OPEN FISSURES WITH HIGH DIP ANGLES”).

2 THE HYDRAULICS AND GEOLOGICAL CHARACTERISTICS OF THE FOUNDATION ROCK

We show below the main point of the Hydraulics and Geological characteristic of the foundation rock at the bottom of the reservoir.

(Permeability coefficient)

- A high place of permeability coefficient more than 100 Lu has been distributed over the whole area (About 2% number of the investigated stage), and the permeability coefficient and depth are not correlated with each other.

(Open fissures)

- There were open fissures (Width more than 1 mm) in the whole area. The open fissures tends to excel in these high angle open fissures that were more than it at about 60°.
- The surface of the open fissures of the boring core changed to a brown color and varies to brown from the fissures to the bedrock inside.
- As a result of restoring the boring core's both sides as much as possible, they were exactly fitting. (They were fitted without displace, or were fitted if they were displaced.) It is thought that open fissures was caused by the tensile stress because there is no streak on boring core's both side.
- Because the Yashio dam reservoir is located at the edge of the caldera, the factor that the tensile stress produced is regarded as being due to the large-scale bedrock creep from the gravity instability of the caldera wall.
- The main factor of the leakage is the network of fissures continuing on to a deep area to the subject in the open fissures of the high dip angle. It is thought that the hydrothermal alternation and a large-scale bedrock creep were the main factors, and the open fissures of the high dip angle were created.

(The characteristic of the groundwater flow)

- As a result of the tracer investigation that we carried out between the “Craters” and the test borehole, that is all for about 1 cm/s of the seepage velocity. Further, we confirmed that the seepage velocity (About 4 cm/s or less) of the plumb direction excelled.

3 THE RESULTS OF GROUTING AT THE BOTTOM OF THE RESERVOIR

We show below the specifications, the results and the effect of the test grouting at the bottom of reservoir.

3.1 *The specifications of the test grouting*

The method was the stage grouting, and we used the blast furnace cement. An initial mixing of cement paste was assumed to be C:W = 1:6–1:0.8 according to the lugeon value ahead of the grouting. The injection pressure was set according to the thickness of the original ground, 0.3–3.0 MPa. Moreover, when the rise of the injection pressure was not admitted because of the efficiency of the grouting, mixing was switched to high density promptly. And the grouting was continued for as long a time as possible (For about 10 hours or less).

3.2 *The results and the effects of the test grouting*

1. The results of the test grouting

The amount of all the cement of the grouting was about 29,000 t. There were 120 st in stages where a large amount of grouting was done that was 10 t/m or more, and the maximum value was 108 t/m. In a part of those stages (There were 42 stages), they were injected without a rise of the injection pressure in early period of injection.(However, injection pressure finally rose to a regulated value at those stages.) (Cf. [table 1](#), [figures 9](#), [10](#)). The open fissures of the

Table 1. Result of the test grouting.

Place	A number of stage (st)	Injection results										Quantity of Cement injection (t)
		Lugion value before injection				Quantity of unit cement injection						
		Average*1) (Lu)	Loss probability of 10Lu (%)	Loss probability of 100Lu (%)	MAX (Lu)	Loss probability(%)				MAX (t/m)		
10t/m	10t/m patarn 1*2)	50t/m	50t/m patarn 1*2)	Average (t/m)								
Ichinosawa, Nabearisawakawa, Honokisawa	1,821	>15	35 (639st)	2 (30st)	∞	3	6 (106st)	2 (39st)	<1 (9st)	<1 (9st)	108	27,188
Sannosawa	521	>12	27 (139st)	2 (12st)	∞	1.4	3 (14st)	<1 (3st)	<1 (1st)	<1 (1st)	71	3,600
Total	2,342	>14	33 (778st)	2 (42st)	∞	2.6	5 (120st)	2 (42st)	<1 (10st)	<1 (10st)	108	30,788

*1) ∞ Lu is removed in average (∞:23st).

*2) patarn 1: Stage where grouting without injection pressure among.

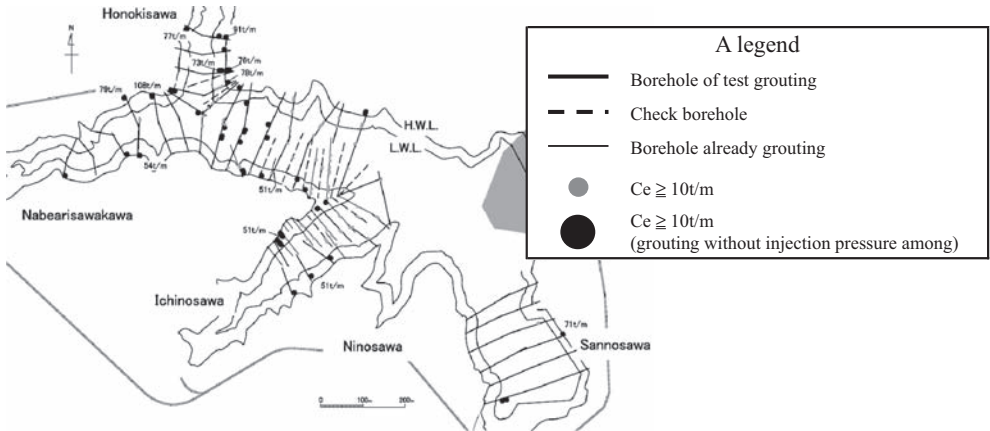


Figure 9. Distribution of the stage with a large amount of grouting.

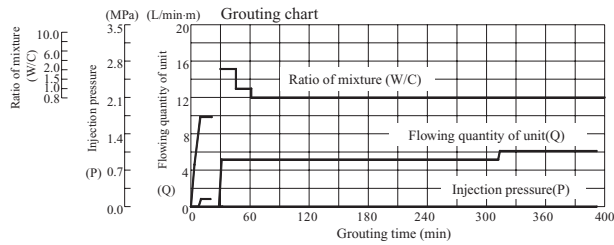


Figure 10. One example of the stage of grouting minus injection pressure.

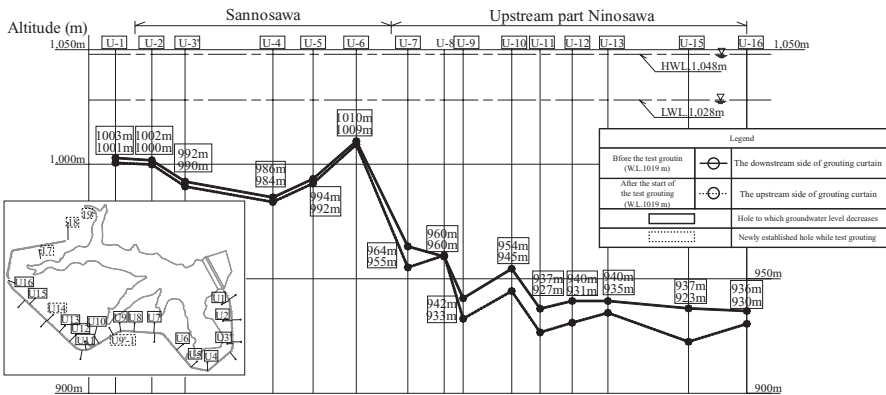


Figure 11. Groundwater level distribution along the curtain.

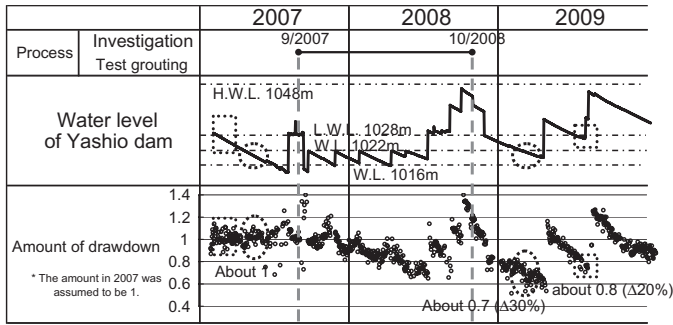


Figure 12. Changed situation of reservoir water level.

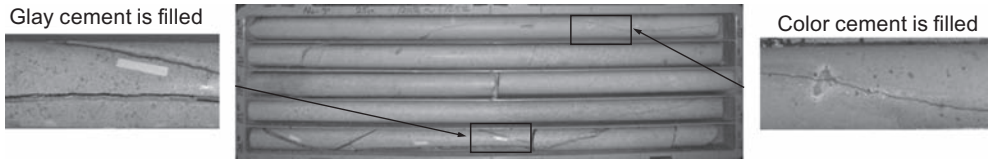


Photo 2. One example of a situation of filled cement.

high dip angle was admitted in these stages where grouting without injection pressure among them. As for such a grouting pattern, it is estimated that the grouting was previously done toward the depth direction by grouting directly into these open fissures.

2. The effectiveness of the test grouting

The groundwater level of the reservoir surround was widely decreased by the test grouting. The leakage was decreased by about 30% of the water level of the reservoir though it still has an influence. (Cf. figure 11, 12)

4 RESULTING CONFIRMATION OF IMPROVED SITUATION VIA BOREHOLE VERIFICATION

After the test grouting, we investigated the improved situation by checking the boreholes (11 totals) (Cf. figure 8). We injected the cement paste mixed the color powder into the check borehole, because it was possible to distinguish from cement injected from the other boreholes. (Cf. photo 2).

We arranged the result of the investigation under the following three conditions. The first condition is the water level of reservoir when adjacent boreholes of the check borehole was injected (The water level of reservoir is about EL.1020 m or about EL.1040 m). The second condition is the altitude or injection pressure (More than EL.1020 m: Injection pressure is 0.3~1.0 MPa, Fewer than EL.1020 m: Injection pressure is 1.0~3.0 Mpa). The third condition is the distance from the adjacent borehole. (Cf. Table 2).

If the injected stage nearby the check borehole is below the water level of the reservoir, in a check borehole where the distance from the near borehole is about 20 m or less, the open fissures are almost filled with cement covering a width of 3 mm or more (filled ratio is about 90%).

However, if the injected stage nearby the check borehole is above the water level of the reservoir, even if it is the same as the aforementioned injection pressure, open fissures of 3 mm or more in their width are not so filled with cement. (filled ratio is about 20%).

As shown above, the correlativity is high in the improvement degree of the bedrock by grouting and the water level of the reservoir after grouting. The cement reaches horizontally from the borehole within the range of about 20 m by grouting in the stage below the water level of

Table 2. Cement filling into open fissures in checking the borehole.

Water level of reservoir when the adjacent borehole grouting		About WL. 1,040m			About WL. 1,020m		
Distance with check borehole and the adjacent		10 – 15m	15 – 20m	20m –	– 10m	15 – 20m	20m –
Injection pressure		0.3 – 1.0MPa	0.3 – 1.0MPa	0.3 – 1.0MPa	0.3 – 1.0MPa	0.3 – 1.0MPa	0.3 – 1.0MPa
	Number of check borehole	1	3	1	3	1	3
Stages that are shallower than E.L.1020m	W. Fissures width (mm)	[Bar chart]		[Bar chart]	[Bar chart]	[Bar chart]	[Bar chart]
	Number of fissures	0 0 0 0 0 0 0	13 6 1 1 1 1	2 5 1 0 1 0	2 0 0 1 0 0	25 14 10 7 6	38 10 1 5 4
Cement filling results to open fissures in check borehole	Injection pressure	1.0MPa	1.0MPa	1.0MPa	1.0 – 3.0MPa	1.0 – 3.0MPa	1.0 – 3.0MPa
	Number of check borehole	1	3	2	2	1	5
Stages that are deeper than E.L.1020m	W. Fissures width (mm)	[Bar chart]		[Bar chart]	[Bar chart]	[Bar chart]	[Bar chart]
	Number of fissures	5 2 0 0 1 1	5 1 4 4 1 4	4 6 1 5 3 7 6	6 1 1 1 0 0	1 6 0 1 0 0	2 6 9 5 5 2 6 14 2 0
Cement filling rate of open fissures ($\pm 3\%$) (The distance from the adjacent hole is about 20m or less.)		[Bar chart]		[Bar chart]		[Bar chart]	
		Water level of reservoir when the adjacent borehole grouting		Water level of reservoir when the adjacent borehole grouting		Water level of reservoir when the adjacent borehole grouting	
		About WL. 1,040m		About WL. 1,020m		About WL. 1,020m	
		Stages that are shallower than about 1020m		47/51 – 92%		6/13 – 46%	
		Stages that are deeper than about 1020m		63/69 – 91%		6/7 – 86%	
		[Legend]		[Legend]		[Legend]	

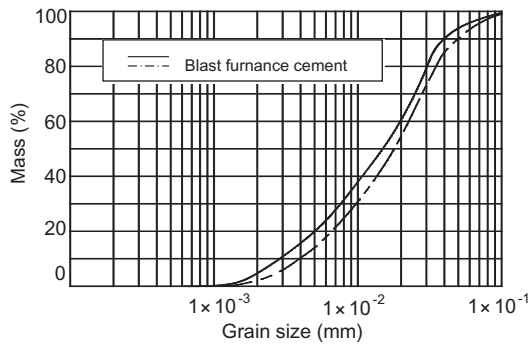


Figure 13. Grain-size distribution of cement particles.

the reservoir and according to the specification of the grouting. Further, it can be thought that grout cement is almost filled most of extreme open fissures that width is 3 mm or more.

5 THE MECANISM OF THE GROUTING AT THE BOTTOM OF RESERVOIR FILLED WITH WATER

It is believed that the grouting was effective because the reservoir was filled with water. This mechanism has been considered as follows. At first, the mechanism of the grouting that undertook the influence was first occupied only to the injection pressure. At last, the effect of the grouting where the reservoir was filled with water in addition to the influenced injection pressure was considered.

5.1 The specifications of the test grouting

The concept of the mechanism in which the open fissures are filled with grout cement is shown below. The relation between the distance “r” to the point and flow velocity “V” in the point is shown as follows if it is thought that cement extends in the open fissures (Parallel horizontal monotony is assumed, width:a) from the borehole like a concentric circle (Injection flowing quantity:Q).

$$V = Q/(2\pi ra) \tag{1}$$

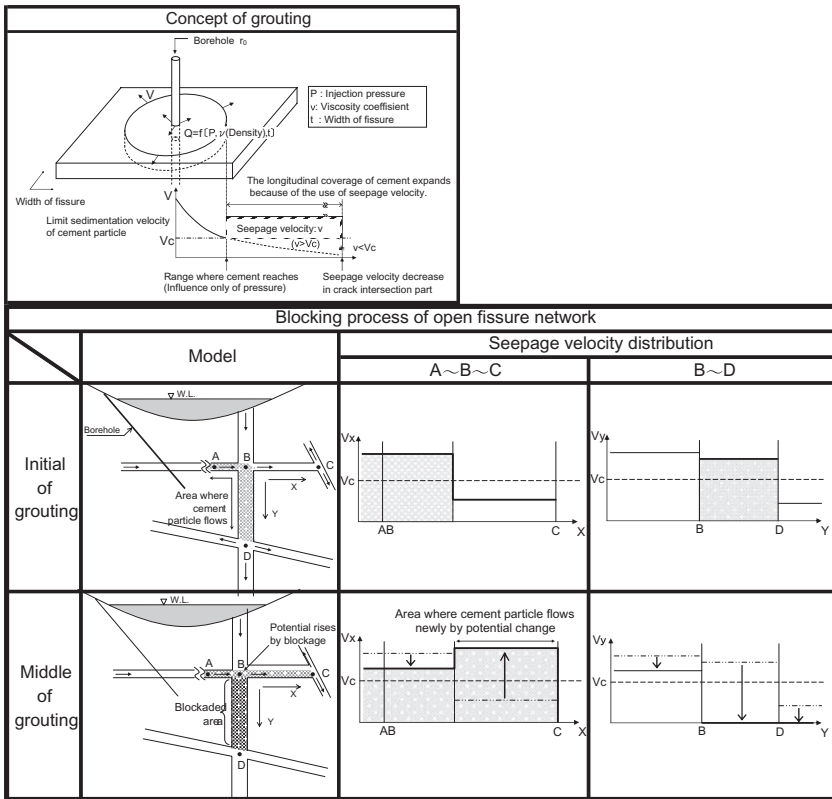


Figure 14. Concept of grouting at the bottom of the reservoir filled with water.

When r grows, V becomes small. It subsides because it came below the limit subsidence velocity of the cement particles. Further, the subsidence of the cement particles progresses toward the borehole, and the fissures were blocked at the end (Cf. figure 14).

The blast furnace cement was used for this grouting (Brain: $3000 \text{ cm}^2/\text{g}$ or more). It became $D_{10} = \text{about } 3\text{--}4 \text{ }\mu\text{m}$ if the effective diameter of the cement particles are 10% diameter. Further, if the specific gravity of the cement particles is assumed to be 3.2 g/cm^3 , it becomes that the limit subsidence velocity (The limit velocity of JUSTIN) of the cement particles becomes about 0.8 cm/s . That is, it is thought that the subsidence of the cement particles and the blockage of the crack progress toward “A” when the flow velocity of cement paste reaches the point where it becomes about 0.8 cm/s or less.

5.2 The grouting at the bottom of the reservoir filled with water

It was roughly 1 cm/s or more as a result of the investigating seepage velocity in the bottom of the reservoir. The seepage water, that velocity was more than the limit sedimentation velocity of the cement particle, wash out the tip of the cement paste. So the subsidence of the cement particle is controlled, and transported with the seepage water further far away. And it is thought that the cement particles subside due to a flow velocity decrease such as the intersection parts on the network of the open fissures, and blockage proceeds to the upstream. It is thought that the potential changes brought about by blocking the open fissures according to the shape of the network of the open fissures, the hydraulic gradient grows, the flow seepage velocity become fast, and there were fissures that were newly filled with cement too (Cf. figure 14).

6 CONCLUSION

In the Yashio dam reservoir, there is a network of fissures which assumes open fissures at a high dip angle that the hydrothermal alternation and a large-scale bedrock creep are regarded as a main generation factor of the subject in deeper areas.

① The grouting at the bottom of the reservoir filled with water is being executed now. As a result of the test grouting executed prior to this, the range of reaching cement was comparatively large (About 15–20 m horizontally) though the injection pressure was about 1.0 MPa or less when the grouting was executed below the water level of the reservoir. Further, cement paste was almost filled to fissures with a width of 3 mm or more, and a decrease of comparatively big leakage was able to be confirmed.

② The seepage velocity of the water investigated at the bottom of the reservoir was approximately 1 cm/s or more (About 4 cm/s or less). The test grouting blockaded the open fissures effectively, the seepage velocity more than the limit subsidence speed of the cement particles in addition to the injection pressure.

③ Such a grouting is effective for the network of open fissures that has a moderate seepage velocity. It is possible that the injection doesn't settle according to the forms of the path of infiltration such as extremely fast seepage flow velocities and continuous, single open fissures. Therefore, at the stage of selection of construction method, the investigation of the state of groundwater and the open fissures in the bedrock is important.

This time, utilization of the injection mechanism was qualitatively considered, we will clarify the experimental aspects of the mechanism and analyze it in the future.

REFERENCES

- Fumiharu, Kawashima. 2010. A study for the behavior of groundwater flow along the open fissures with high dip angles, *ICOLD*.
- Miyuki, Miyata. 1985. Research that concerns design and construction of leakage stoppage of fill dam in bedrock. *Thesis for a degree of Kyoto University*.
- Toru, Onogami. 1989. Analysis of old environment by plant group at pleistocene in Shiobara, Tochigi. *Report of Geological Survey of Japan No. 269*.

Filter design for the heightening of a high earth core rockfill dam

S. Messerklinger & R. Straubhaar

Poyry Energy Ltd., Switzerland

ABSTRACT: The 155 m high Goescheneralp earth-core rockfill dam will be heightened by 8 m with the aim of increasing the reservoir storage volume by 14.5% to 87 Mio m³. Therefore, the filter materials of the existing dam were reviewed and filter materials for the dam heightening were designed. In this paper the existing Goescheneralp dam is briefly described and filter test data are presented. The design of the dam heightening is presented and discussed. Emphasis is given to the filter materials including a comprehensive review of state-of-the-art filter criteria.

1 INTRODUCTION

The Goescheneralp hydropower storage scheme is composed of a 155 m high earthcore-rockfill dam (ECRD) with a crest length of 560 m; a 7.2 km long headrace tunnel; a 1.1 km penstock and a powerhouse situated in an underground cavern equipped with 4 Pelton turbines each with an installed capacity of 41 MW (Fig. 1a, see Eggenberger, 1953). The scheme was commissioned in 1962 after seven years of planning and design including thorough geotechnical laboratory and site investigations and five years of construction.

The scheme is located in the Alpine region in the central part of Switzerland in the Canton of Uri (Fig. 1b). The direct catchment area is 42.3 km². 10.2 km tunnels and 4 water intakes increase the catchment area to totally 90.2 km² of which ~30% are glaciated. An average annual inflow of 196 Mio m³ is used for producing 251 GWh. The scheme was designed as seasonal storage plant where the 76 Mio m³ reservoir was used for the winter production. Nowadays, the use has shifted to peak energy production throughout the year.

Since the year 1954, when the concession of the scheme was obtained from the authorities, a heightening of the dam by around 10 m was already considered. In several feasibility studies the dam heightening was evaluated until a study performed in 2008 pointed out that the so-called “small solution” with the placement of additional rockfill solely on the u/s side is the most economical design. The maximum possible heightening with this design was evaluated to be around 7.5 m. With the assessment of the necessary freeboard to be 4.5 m (Dietler, 2010) the reservoir elevation is going to be increased by 8 m. Respecting requests for the landscape and the tourism in the region, concrete elements and other structural features on the dam crest were not considered for the dam heightening. The review of the filter materials of the existing dam and the design of a filter for the dam heightening is the main subject of this paper.

2 THE GOESCHENERALP EARTH-CORE-ROCKFILL DAM

2.1 *The geology*

The Goescheneralp valley was formed in “Aare granite” during the last ice ages. Fluvio-glacial material composed of gravel and blocks with interlayers of sand, fine-sand and peat were deposited on the valley bottom with varying thickness of up to 70 m (Fig. 2b). Along the valley sides slope talus accumulated. For the dam foundation it was decided to excavate

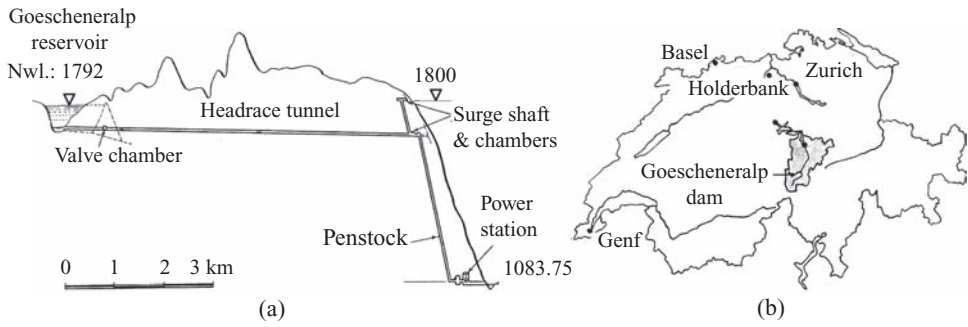


Figure 1. (a) Section of the Goescheneralp hydropower scheme; (b) Map of Switzerland.

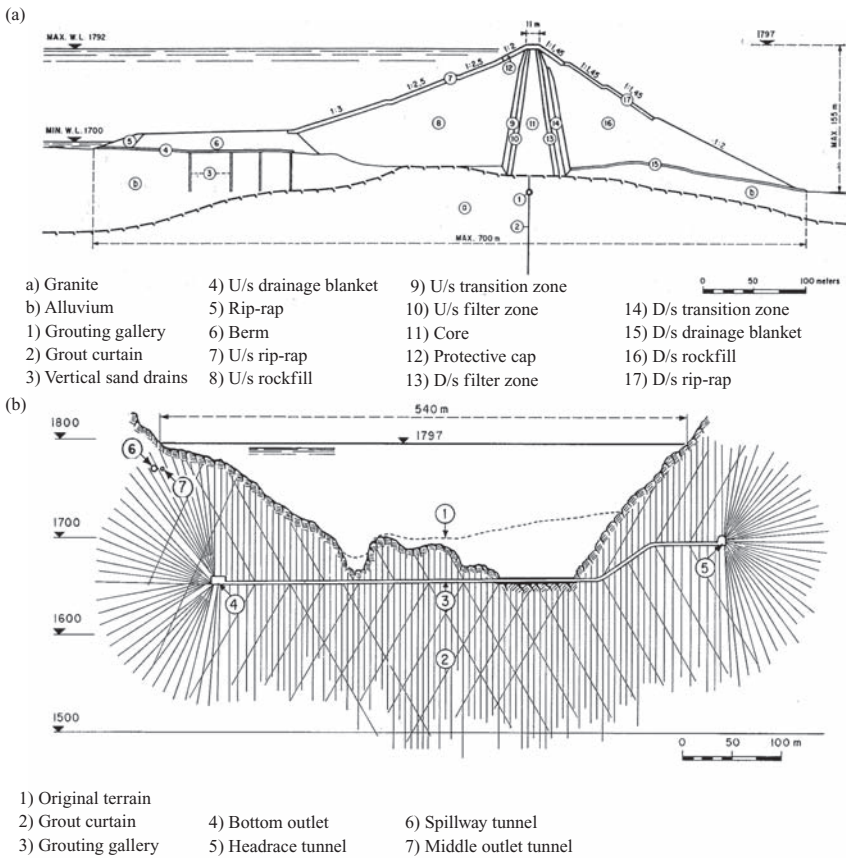


Figure 2. (a) Cross and (b) Longitudinal dam section; (adopted from Gil, 1963).

the deposits and to find the core and filter zones on bedrock. The rockfill shoulders are founded on overburden and in the area of interlayers of fine-sand and peat, sand drains were installed (Fig. 2a).

2.2 The grout curtain

A grouting gallery is situated on the dam axis from which the grout curtain composed of one row of borings at a spacing of 6 m was installed to a depth of up to 180 m below rock surface

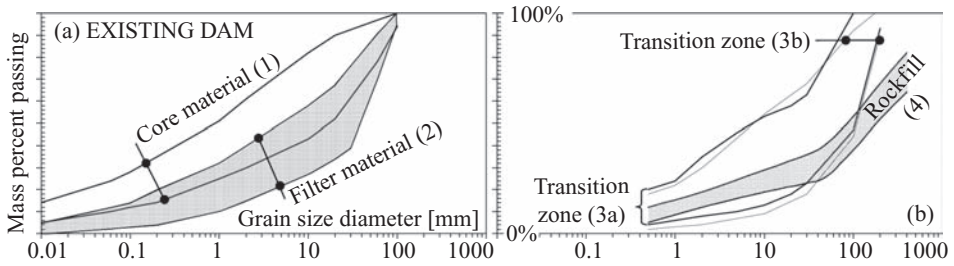


Figure 3. Dam materials of the existing Goescheneralp dam (Dam zoning see Fig. 2 and 5).

(Fig. 2b). At the contact between the earthcore and the rock contact-grouting was performed. The contact surface of the rock abutments and the core zone was smoothed. Uneven zones were filled with concrete and open joints were covered with mortar before two transition zones of core material with reduced grain size and increased clay content were placed.

2.3 The earth core

The slope talus did not have a sufficient content of fines in order to provide core material with adequately low permeability. Hence it was decided to add fine-grained material to the in-situ available slope talus. However, fine-grained materials such as clays were not available from natural resources in the Goescheneralp valley or from other locations near the site. Therefore, clays from several borrow areas in USA, Italy and Switzerland were investigated with respect to sealing efficiency and chemical stability in the Goescheneralp hydro-geological environment.

After a thorough study, Opalinus clay powder from Holderbank (140 km distance from the site, Fig. 1b) was chosen to be added at a mass percent of 11–16% to the granular material from the site. The industrially milled Opalinus clay is composed of ~50% clay minerals (mainly Kaolinite, Illite and Chlorite) and ~50% grains (mainly Mica, Quartz and Calcite). The clay has a flocculated structure with floc diameters of 0.007–0.1 mm. Its typical liquid limit is ~45% and the Plasticity Index is ~20%. For the granular components of the core material the in-situ available deposits were separated into three fractions of 0–30/30–100/100–200 mm. The fine fractions were dried and the coarse fractions were restocked with crushed components before the material was mixed with Opalinus clay powder in a stationary mixing plant. The material was placed at the wet side of the optimum water content in layers of 30 cm, compacted with 6 passes. The symmetrical central core has a thickness at the base of ~45 m and 5.5 m at the crest (el. 1794, Fig. 2).

2.4 The dam materials

The core is enclosed by u/s and d/s filter zones, each with a thickness of 1.5 m at the top and 4 m at the bottom side. The filter material (2, Fig. 3a) was produced in the same way as the granular components of the core material by separating the fraction <200 mm into three sub-fractions, drying, restocking and mixing them before transporting to the site and placing at the optimum water content in layers of 30 cm and compacting with 6 passes. The gradation of the filter material was chosen on the base of filter tests (see Sec. 4). The filter is surrounded by transition zones. On the u/s side is one transition zone (3a, Fig. 3) with a thickness of 2–6.6 m. On the d/s side there are two transition zones (3a and 3b) with thicknesses of 2–6.6 m. The transition zone (3b) acts as a drainage to (3a) and to the rockfill (4/6). The rockfill consists of slope talus excavated along the right valley flank. Blocks with a diameter of >1.5 m or a volume of >1 m³ were visually separated. During placement in layers of 2.5 m, 150 l water per 1 m³ rockfill was added. The dam slopes are protected by u/s and d/s rip-rap layers of 2–3.5 m thickness. Today the d/s surface is covered with grass (Fig. 2).

3 REVIEW OF FILTER DESIGN CRITERIA

Filter design had some development within the last 70 decades which may have been initiated by Terzaghi during his investigations on the hydro-mechanical soil behaviour which finally resulted in his consolidation theory (Terzaghi & Fröhlich, 1936) where he also recognized that seepage forces can lead to particle transport. Bertram (1940) under the supervision of Karl Terzaghi and Arthur Casagrande performed filter tests and proposed the filter criterion $D_{15\text{filter}}/D_{85\text{score}} \leq 6$ which was modified to $D_{15\text{coarse-side filter}}/D_{85\text{fine-side core}} \leq 4$ and extended by the drainage criterion $D_{15\text{fine-side filter}}/D_{85\text{coarse-side core}} \geq 4$ (Terzaghi & Peck 1948).

Since then a number of theoretical and experimental studies were performed. Particular attention was drawn to the topic with a number of excessive seepage or even dam failure events caused by inappropriate coarse filters (Vaughan 1970, Vestad 1976, Wood 1976, Ripley 1984). However, it should be pointed out that also a large number of incidents were caused by local anomalies such as: (i) Arching of the core across the abutments or irregularities in the foundation; (ii) Open joints and fissures in the core foundation due to insufficient grouting; (iii) Material segregation at zone boundaries or during placement along the rock foundation; (iv) Cracks in the dam caused by differential settlements. Therefore, appropriate filter design and appropriate construction method and site supervision are equally important. However, the following topics presented in this paper will mainly focus on filter design. For ECRD's, nowadays, it is generally agreed on that the following aspects should be considered: (a) Filter requirement; (b) Internal stability; (c) Self healing; (d) Segregation; (e) Drainage capacity; (f) Durability/Change in gradation.

3.1 Filter requirement

Based on data of the “filter test” (Sherard et al. 1984a), of the “slot test” (Sherard et al. 1984b) and the “no erosion filter test” (Sherard & Dunnigan, 1985) the design criteria for critical filters was presented in Sherard & Dunnigan (1985) and further discussed in Sherard & Dunnigan (1989). This design is nowadays state-of-the-Art and recommended by a number of regulations and codes (e.g. EM 1110-2-2300). For the core material only, the minus 4.76 mm fraction is considered and the mass content of fines ($M\% < 0.075$ mm) is determined, which defines the base soil group and the corresponding filter criterion. Four base soil groups are distinguished.

From the investigations of the Balderhead dam failure (Vaughan et al., 1970) a different approach for filter design was followed by Vaughan & Soares (1982) who stated “... that the effectiveness of a filter may be defined by its permeability with more generality than by its grading ...”. From filter tests with materials subjected to base soil slurries they proposed the following correlation between permeability (k in m/s) and the filtered particle size (δ in μm) $k = 6.1\text{E-}6 \cdot \delta^{1.42}$ where the particle size of the clayey base soil is represented by the clay particle size for clays with dispersive structure and by the clay floc size for clays with flocculated structure, respectively. For some cases the filter criteria recommended by Sherard & Dunnigan (1989) and Vaughan & Soares (1982) give similar filter gradations (Ross, 1992), however, generally the latter criterion gives the finer filters.

A different approach to filter design was followed by Silveira (1965) who simulated the filter with spherical grains of different size and calculated the pore diameter distribution curve and the travel distance of a particle based on the mass gradation curve using a probabilistic approach for the arrangement of particles around a pore. The results show that the void distribution curve has a similar shape as the gradation curve shifted by 1 log cycle. The approach was improved by Ziems (1968) using the number of particles curve instead of the mass gradation curve which resulted in even finer void distribution curves. This approach was followed and extended by Whittmann (1979) and Muckenthaler (1989) who developed criteria for critical hydraulic gradients which are applied for the erosion assessment in homogenous dams.

3.2 Internal stability

The issue of internal stability of materials can be described best following the definition given in Kenney & Lau (1985): “Internal stability of a granular material results from its ability to

prevent loss of its own small particles due to disturbing forces such as seepage and vibration.” They further specify three necessary conditions required for a soil fabric to be internally unstable and to allow small particles to relocate within the pore space: (a) Particle is not incorporated in a stress transfer chain (stressed particles are to some extent fixed in position). (b) Pore diameters are large enough. Pore size increases with increasing ϕ_{\min} and uniformity (Wittmann, 1979). (c) Seepage forces acting on a particle are high enough. Hydraulic gradients required to move a particle (i_{crit}) depend mainly on the particle diameter and has a minimum for particles of ~ 0.2 mm (Muckenthaler, 1989). For smaller particles stabilizing adhesion forces act. For ECRDs, condition (c) is always given for either the core or the filter or for both zones, as the main idea of the core of a dam is to dissipate the potential energy of the seepage water into thermal energy via friction. Condition (a) and (b) are to some extent contradictory. To fulfil condition (a), the material should be composed of a small number of particles with rather uniform size while to fulfil condition (b), the material should be composed of well graded material with particles from all fractions. After the formation of a number of sinkholes in the core zone of coarse, broadly graded soils, Sherard (1979) concluded that these soils are internally unstable and recommended the retention ratio criterion, which was initially proposed by DeMello (1975), to verify that the finer portion of a material is compatible to the coarser portion with respect to filter requirements. However, Milligan (2003) points out that the plasticity of the fines is an important aspect for the internal stability of broadly graded soils. It was shown that most sinkhole incidents reported by Sherard (1979) occurred in soils with fines of low plasticity. Filter tests are a good tool to verify the internal stability of a chosen filter gradation and are in particular important for broadly graded and gap graded soils.

3.3 *Self healing*

The filter material should not have real or apparent cohesion. Cracks which may eventually form through the core should not further propagate through the filter and remain open in the filter zone. The commonly agreed criterion is a content of non-plastic fines (<0.075 mm) of less than 5% and a successful sand castle test (Vaughan & Soares, 1982). However, for example Muckenthaler (1989) shows that adhesion forces start to act for particles as large as 0.2 mm. And for filter zones in the unsaturated state, depending on the degree of saturation, even larger particles will be affected by suction/apparent cohesion. Further it has to be assured that chemical or biological processes induced by the seepage water and/or the filter material do not result in cementation at the particle contacts. Therefore, similar compressibility for core, filter and rockfill materials placed at optimum density on a smooth rock foundation might be the best measure in reducing the necessity of filters to have perfect self-healing abilities.

3.4 *Segregation*

With the findings of Milligan (1999, 2003), that an increased content of sand can reduce segregation for well and broadly graded materials, provided the material is wetted prior to placement, the gradation limit curve (Fig. 7, Milligan line) was developed and it was highlighted that the coefficient of uniformity is an unsuitable parameter for assessing segregation, as it does not consider particles larger than d_{60} which are the most likely to segregate. These findings support the suggestions given by Ripley (1986), that segregation criteria should restrict the ϕ_{\max} and should give a sufficient content of sand fraction. This is also confirmed by laboratory investigations given in Sutherland (2002). Hence, it is commonly agreed that wet materials with gradations on the fine side of the Milligan line are not prone to segregate.

3.5 *Drainage*

The Terzaghi drainage criterion remains state-of-the-Art. However, the drainage abilities of a filter have the least priority. In case the drainage criterion is not fulfilled with the filter, the next adjacent zone has to provide drainage abilities.

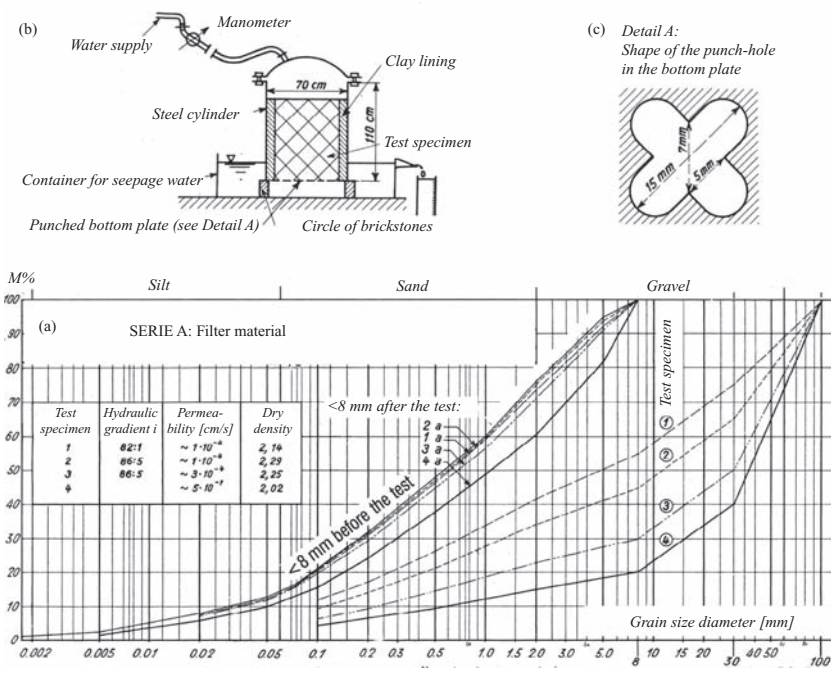


Figure 4. Filter tests for the existing dam: (a) Results for the Filter material; (b) Section of the test apparatus; (c) Punch-hole in the bottom-plate.

4 FILTER TESTS FOR MATERIALS OF THE EXISTING GOESCHENERALP DAM

The tests were performed in a steel cylinder (Fig. 4b) with a diameter of 70 cm, a height of 110 cm, a perforated plate at the bottom side (Fig. 4c) and a cap on the top side. The wall of the pot was lined with clay before the wetted test specimen was placed inside in layers of 20–30 cm compacted statically with a 15 kg stamper to the given dry densities of 2–2.3 g/cm³ (Fig. 4a). Water pressure representing hydraulic gradients of up to 89 were applied and the permeability was measured. Tested were filter and transition materials with different gradations. Presented is test series A (Fig. 4a, Serie A: specimen No. 1–4). For all materials tested within a series the gradation of the fraction <8 mm was kept the same (Fig. 4a: <8 mm before the test). After the test, the gradation of the remaining fraction <8 mm (Fig. 4a: <8 mm after test) was determined and is plotted in Fig. 4a. The comparison of gradations <8 mm before and after the test indicates the degree of internal stability.

The results show that in broadly graded materials of specimen 1 and 2 less erosion of fines occurred. This was explained by the reduced pore diameters for well graded soils. For uniform soils the pore diameter increase and the small fraction of fines is washed through the pore grid formed by the coarse particles. Conclusions of the filter tests were: (a) The behaviour of a material with respect to internal erosion is dependent on the shape of the gradation curve. For materials with convex gradation curves, the erosion is expected to be higher. (b) For the materials which are susceptible to internal erosion, the permeability is 10–1000 times higher than for materials which are not susceptible to internal erosion. (c) When the water pressure is applied suddenly to the specimen the amount of eroded material is larger than when the pressure is increased slowly.

4.1 Application of the Sherard (1979) and the Kenney & Lau (1985, 1986) criterion

Applying the criterion after Sherard (1979)—the sub-fractions of a soil should be a filter to each other which is assessed by the Retention ratio ($R_r = d_{15 \text{ coarse fraction}} / d_{85 \text{ fine fraction}} \leq 5$)—confirms the

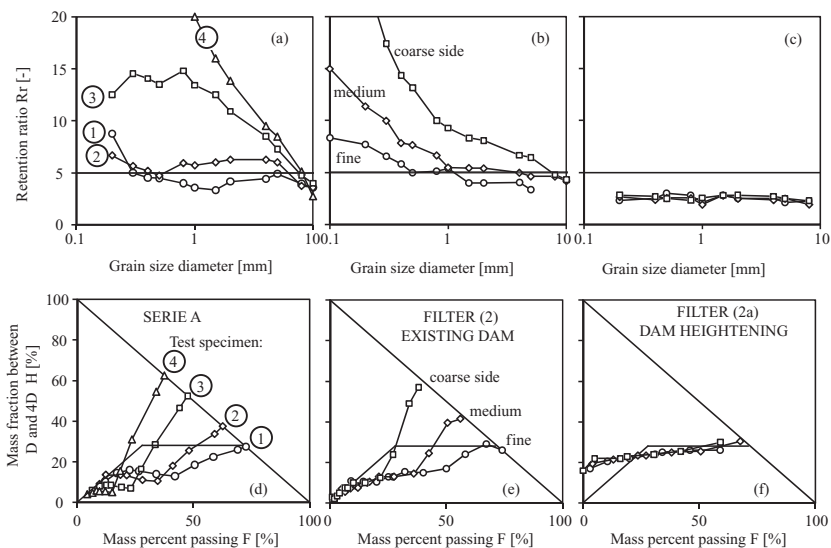


Figure 5. Criterion of (a)–(c) Sherard (1979) & (d)–(f) Kenney & Lau (1985) applied on filters.

findings of the filter tests that materials 1 and 2, are internally stable (Fig. 5a). However, when applying the criterion of Kenney & Lau (1985, 1986)—the curve of F (mass percent passing) versus H (mass percent between grain diameter D and $4D$) is above the boundaries of $H \geq F$ for $0 < F < 28\%$ and $H > 28\%$ for $28\% < F$ —none of the materials is seen to be stable (Fig. 5e).

4.2 Discussion of filter test results

The conclusion (a) of the filter tests agrees with findings of Sherard (1979), where he postulated a retention ratio (R_r) of <5 for stable materials (which is the case for broadly-graded soils). This conclusion is contrary to findings of Kenney and Lau (1985 & 1986) who consider a uniform material with $C_u < 12$ to be internally stable. However, following the three conditions needed for internally stable materials given in Kenney and Lau (1985) one can conclude that there are two types of materials which are internally stable. These are (i) those of broad gradation, with small pore spaces which do not allow a significant amount of particles to move (however, for this type of material it is important to have good self-healing abilities as in case of an open crack there are a larger number of particles available to be eroded) and (ii) those of uniform gradation where a major number of particles is involved in stress transfer chains and where the pores formed by the uniform particles are too small to be passed by particles of the same size. However, for this type of soil the pore space formed is comparable high with respect to its filter abilities for the core.

5 FILTERS FOR THE HEIGHTENING OF THE GOESCHENERALP DAM

For the dam heightening the protective cap on the dam crest as well as the top part of the existing core material will be removed (Fig. 6) before the dam crest is built up with new material. The contact between the existing and the new core material will be inclined to avoid a predefined horizontal surface through the core (Fig. 6). The core will be surrounded by a 1.5–2.8 m (horizontally measured) thick filter zone (2a) which was designed according to state of the art filter criteria (see Annex). The application of the full range of state of the art filter criteria allows for safe filter design (to satisfy filtration, self filtration, durability and drainage criteria) as well as for the selection of a material which can easily be placed (to meet segregation and self-healing criteria).

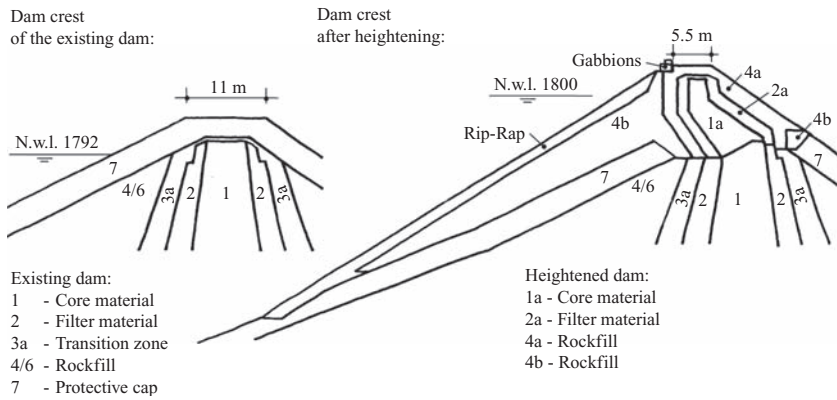


Figure 6. Dam crest of the existing and the heightened dam.

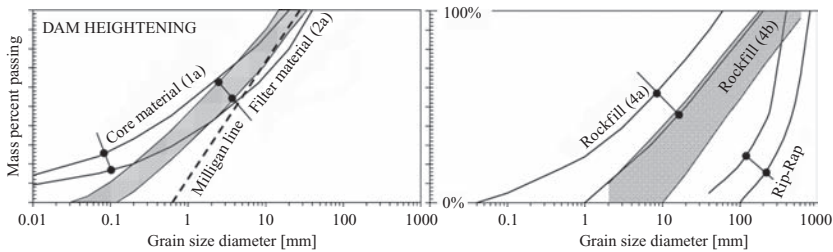


Figure 7. Dam materials for the heightening.

6 SUMMARY AND CONCLUSION

The existing Goeschenalp dam was designed more than half a century ago. At that time the filter was designed based on the retention criterion, certainly the most important criterion in filter design, which ensures that the fine particles cannot migrate into the filter, and lead to increasing seepage and erosion. Already at that time the internal stability (self filtration) of the filter materials was tested in the laboratory and this allowed broadly graded filter and transition materials, with gradation curve shapes similar to those of the core and the rockfill shoulders to be selected. These materials worked well. However, recent filter design does not only consider above mentioned criteria of filtration and self filtration or durability and drainage, additional emphasis is given to segregation of filter materials during placement and to self healing abilities during deformations. The broadly graded materials, such as used in the existing dam, certainly have a high segregation potential which needed particular care and local corrective measures during placement. Nowadays, because the construction period is in general shorter and man-power is more expensive, local corrective measures have to be avoided because these are costly and time consuming. Current filter design also gives more attention to the self healing abilities of the filter materials. Although this may not be a key requirement for comparable stiff materials, such as used in the Goeschenalp dam, it is good that the filter materials for the dam heightening fulfill this criterion. Finally, it can be concluded that the filters used in the existing dam are fully adequate and that the properties of the filter materials for the dam heightening are somewhat more conservative and that they fulfill all currently recommended filter criteria (see also Annex). However, for the construction of the dam heightening and in particular the filter zone, which is the main defense line against seepage and erosion, thorough site supervision will still be essential.

ACKNOWLEDGEMENT

The permission of Kraftwerk Göschenen AG to publish this paper is gratefully acknowledged. Thanks are also due to H. Wyss and E. Rothenfluh (Centralschweizerische Kraftwerke).

REFERENCES

- Bertram, G.E. 1940. An Experimental Investigation of Protective Filters. *Harvard Soil Mech. Series No.7*.
- DeMello, F. 1975. Some lessons from unsuspected, real and factitious problems in earth dam engineering in Brazil. *6th Regional Conf. On Soil Mech. & Found. Eng.*, South Africa (11): 304ff.
- Dietler, T. 2010. Heightening of Göschenalp Dam—Impact of Natural Hazards on Construction Site and Freeboard Optimisation. *79th Annual ICOLD Meeting*, Lucerne.
- Eggenberger, W. 1953. The Göschenalp rockfill dam project. *3rd ICSMFE Zurich*, (3): 296–301.
- Gilg, B. 1963. Die Setzungen des Staudammes Göschenalp. *Europ. Baugrundtagung*, Wiesbaden.
- Kenney, T.C. & Lau, D. 1985. Internal stability of granular filters. *Can. Geotech. J.* (22): 215–225.
- Kenney, T.C. & Lau, D. 1986. Internal stability of granular filters—Reply. *Can. Geotech. J.* (23): 420–423.
- Milligan, V. 1999. A historical perspective of the development of the embankment dam. *Proc. 2nd Annual Conf. Canadian Dam Association*. Edmonton, Alberta, Canada.
- Milligan, V. 2003. Some uncertainties in embankment dam engineering. *ASCE*. 129(9): 785–797.
- Muckenthaler, P. 1989. Hydraulische Sicherheit von Staudämmen. *Dissertation*. Techn. Univ. München.
- Ripley, C.F. 1984. Discussion of Progress in rockfill dams. *J. Geotech. Eng.*, 114(2): 236–240.
- Ross, K. 1992. Design & construction of the core filter for Carsington dam. *Dams & Reservoirs*. 2: 19–23.
- Sherard, J.L. 1979. Sinkholes in dams of coarse, broadly graded soils. *13th ICOLD Conf.*: 25–35.
- Sherard, J.L., Dunnigan, L.P. & Talbot, J.R. 1984a. Basic properties of sand and gravel filters. *J. Geot. Eng.* 110(6): 684–700.
- Sherard, J.L., Dunnigan, L.P. & Talbot, J.R. 1984b. Filters for silts & clays. *J. Geot. Eng.* 110(6): 701–718.
- Sherard, J.L. & Dunnigan, L.P. 1985. Filters and leakage control in embankment dams. *Proc. Symp. On Seepage and Leakage from Dams and Impoundments*. ASCE, New York: 1–29.
- Sherard, J.L. & Dunnigan, L.P. 1989. Critical filters for impervious soils. *J. Geot. Eng.* 115(7): 546–566.
- Silveira, A. 1965. An analysis of the problem of washing through in protective filters. *6th ICSMFE, Montreal*. 2: 551–555.
- Sutherland, K.J. 2002. Quantifying and controlling segregation in earth dam construction. *MASc Thesis*. University of Toronto. Department Civil Engineering.
- Terzaghi, K. & Fröhlich, O.K. 1936. Theorie der Setzungen von Tonschichten: Eine Einführung in die analytische Tonmechanik. Deuticke, Leipzig.
- Terzaghi, K. & Peck, R.B. 1948. Soil Mechanics in Engineering Practice, *John Wiley & Sons*, New York.
- Vaughan, P.R. & Soares, H.F. 1982. Design of filters for clay cores of dams. *J. Geot. Eng.* 108(1): 17–31.
- Vaughan, P.R., Kluth, D.J., Leonard, M.W. & Pradoura, H.H.M. 1970. Cracking and erosion of the rolled clay core of Balderhead dam and the remedial works adopted for its repair. *10th ICOLD*, Q.36-R.5.
- Vestad, H. 1976. Viddalsvath dam. A history of leakages and investigations. *12th ICOLD*, Q.45-R.22.
- Wittmann, L. 1979. The process of soil-filtration—its physics and the approach in engineering practice. *7th ECSMFE, Brighton* (1): 303–310.
- Wood, D.M., Kjaernsli, B. & Hoeg, K. 1976. Thoughts concerning the unusual behaviour of Hyttejuvet dam. *12th ICOLD*, Q.45-R.23.
- Zeller, J. 1957. Erdbauliche Untersuchungen für den Staudamm Göschenalp. *Schweiz. Bauztg.* 75: 18f.
- Ziems, J. 1968. Beitrag zur Kontakterosion nichtbindiger Erdstoffe. *Dissertation*. Techn. Univ. Dresden.

ANNEX

Annex. Assessment of the filters of the Göschenalp dam.

Criteria	Existing dam	Dam heightening
Filter requirement	Criteria of Sherard & Dunnigan (1989): $d_{15\text{filter}} < 2.2 \text{ mm}$ and Vaughan & Soares (1982): $k \leq 1 \cdot 10^{-4} \text{ m/s}$ are fulfilled; Fig. 4 .	Criteria of Sherard & Dunnigan (1989): $d_{15\text{filter}} < 2.5 \text{ mm}$ and Vaughan & Soares (1982): $k \leq 1 \cdot 10^{-4} \text{ m/s}$ are fulfilled & filter tests were successfully performed.

(Continued)

Annex. (Continued).

Criteria	Existing dam	Dam heightening
Self filtration	Self filtration (internal stability) was confirmed by filter tests (see Fig. 4)	Filter fulfills Sherard (1979) and Kenney & Lau (1985, 1986) criteria.
Self Healing	Criteria of fine content <5% not fulfilled. However, dam material with high compression modulus, placed at opt. density of 2–2.3 g/cm ³ on smooth dam foundation resulted in small settlements and minor differential displacements. Drainage measurements confirm that leakages through the core is unlikely.	Filter fulfills the criteria of fines content <5% and the design forms an equally stiff dam body throughout the zones.
Durability	The crest settlements (<20 cm at the crest, since 1977) confirm that the slope talus of Aare granite is a durable material.	The material has in the existing dam proven to be durable.
Segregation	Criteria which are applied nowadays and allow for fast dam construction with reduced necessity in site supervision are not fulfilled. However, at the time of construction an extensive site supervision program combined with a thorough investigation on the optimum material placement methods (Zeller, 1957) allowed for the construction of a homogenous dam body.	The average filter gradation curve fulfills the Milligan (1999) segregation criteria. However, thorough site supervision will still be conducted.
Drainage	Drainage of core and filter layers is provided by a separate zone (3b).	Drainage is provided by rockfill (4a).

Rock treatment around morning glory spillway of Sefidrud dam

A. Faghihimohaddess, R. Naghibian & A. Bashash
Yekom Consulting Engineers, Iran

ABSTRACT: Sefidrud Dam is a Concrete Buttress Dam completed in 1962. The height of the dam is 106 m above the foundation with its crest length of 425 m. In recent years after about 48 years of operation, some damages on steel lining of vertical bend of one of spillway shafts is seen. These damages include inflation of steel lining and consequently increase in volume of leaking water. The damage point is located on outer side of the bend. To investigate reasons of these damages some boreholes were drilled around the spillway to investigate possible causes and extend of the damages, its effects and to conclude proper treatment methods. Investigations show weathered and poor quality of rock mass around the spillway shaft as well as minor cracks in concrete lining which caused water pressure be applied directly on steel lining and the damages appeared. To start repair works on the steel lining in the damaged areas it was necessary to reduce volume of infiltration to an acceptable volume. For this purpose a series of boreholes around the spillway shaft were designed, drilled and injected with cement grout. Grout paste and grout method were designed according to requirements of such delicate structure also the treatment were conducted accordingly. This paper presents geotechnical investigations conducted to conclude causes of damages and rehabilitation method to reduce infiltration of reservoir water from cracked joints of steel lining.

1 INTRODUCTION

1.1 *Sefidrud dam*

The Sefidrud dam is a 106 m high buttress dam with a crest length of 425 m and a crest elevation of 276.25 m ASL (meter above sea level). The dam is located on the confluence of the Ghezel-Owzan and the ShahRud, about 70 km south of the provincial capital of Rasht. Construction took place between 1958 and 1962. The dam body is composed of 32 buttresses, of 14 m width and two gravity type abutments. The gravity section on the left bank comprises a two-bay mid-level spillway of 2000 m³/s capacity. There are five bottom outlets, (three on left and two on the right) providing water for irrigation and sediment flushing during the flood season. Total capacity of the bottom outlets is 1000 m³/s. Further flow shall pass through two morning glory spillways each with 1,920 m³/s capacity located at left bank. The general layout of the dam is shown in [figure 1](#).

1.2 *Spillways*

Based on designer calculations (Etco-Ofer Consulting Engineers) final capacity of each morning glory is 960 m³/sec. In this case effective head over spillway crest shall be 2.25 m.

1.3 *Damages to the spillway*

In late 2003 (after more than 40 years of service) during visual inspections of dam apparatus, inflation in steel lining of one of morning glories was seen. Because of remote location of

the bend inspections are irregular and time of development of the inflation is uncertain. The inflation part located at outer-top part of the vertical bend. The damage was seen only in spillway no. 1 which comparing with the other one is located further from dam body.

During the operation of the Sefidrud dam, both morning glory spillways had similar operation conditions and both experienced a severe earthquake. The earthquake had a magnitude of 7.2 in Richter scale and occurred in the 25 kilometers downstream of dam body on June 21, 1990.

Longitudinal section of the morning glory spillway and location of the damages area are shown in figure 2.

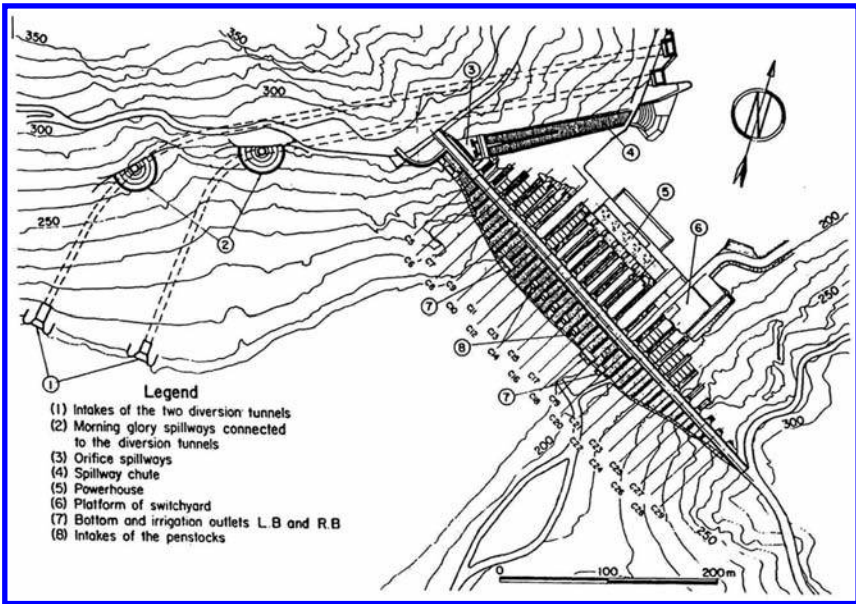


Figure 1. General layout of Sefidrud dam.

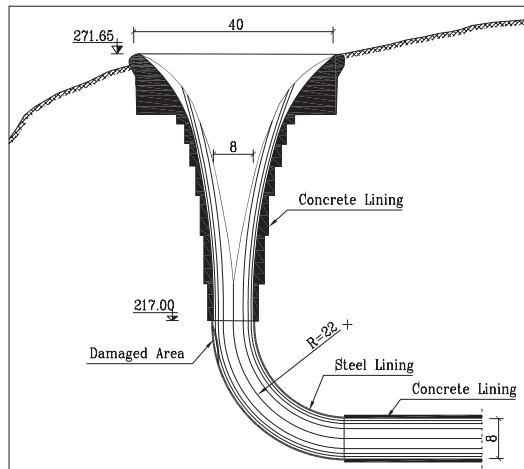


Figure 2. Longitudinal section of morning glory spillway and location of damaged area.

2 GEOLOGY OF THE SITE

2.1 Rock formations

Geological maps of the reservoir and the dam site show that the area includes faults. Trends of faults are mostly east-west or south-east north-west.

The dam had been constructed nearby a huge east-west fault. The fault passes through the upstream of the dam body (about 250 meters from dam axis).

Rocks in the area near the dam body forms two major groups, first group includes undivided intermediate to basic volcanic rocks (upper volcanic) of late Eocene age and second group includes light pink intermediate to acid brecciate volcanic crystal tuff quartz, trachy-andesite and crystal lithic tuff. These rock formations are from Alborz Plateau's Magmatic era same as Paleogene era. The two rock formations are separated by a contact fault in the areas near the dam's axis.

2.2 Rock quality

Observation of rock quality around the spillways reveals that around the morning glory spillways it could be varied from point to point in a wide range. It is observed that the morning glory no. 2 is located in an intact rock zone; the other morning glory is located in a fractured zone. These zones are separated by a straight line which can be seen both in situ and satellite images. The interface surface has azimuth of 10–12 degrees to the north and 80–85 degrees slope to horizon.

Extent of the fractured zone below the reservoir level is uncertain because of weathering of top surface of the rock, although it is likely that the zone extended well below spillway's vertical bend. Figure 3 shows the surface between fractured and intact zones.

2.3 Geotechnical investigations

To determine geotechnical condition of rock foundation around the damaged spillway a series of boreholes were design around the spillway. The boreholes were designed to be drilled in two stages. First stage included drilling of 5 boreholes to investigate the rock quality, determine the permeability of rock mass in rock mass by conducting Water Pressure Test Lugeon tests) and moreover using those holes for cement grouting if required. The second stage included drilling of 17 more boreholes for consolidating the rock mass by cement grouting.

The boreholes were arranged precisely to acquire the basic and necessary geotechnical rock mass data all around the morning glory especially areas near the damaged area by creating a net around the morning glory. The boreholes should be drilled close enough to the structure to show the extension of fractured zone around it. Boreholes were designed to reach minimum distance of 3 m from steel cover.



Figure 3. Fractured and intact zone and morning glory spillways.

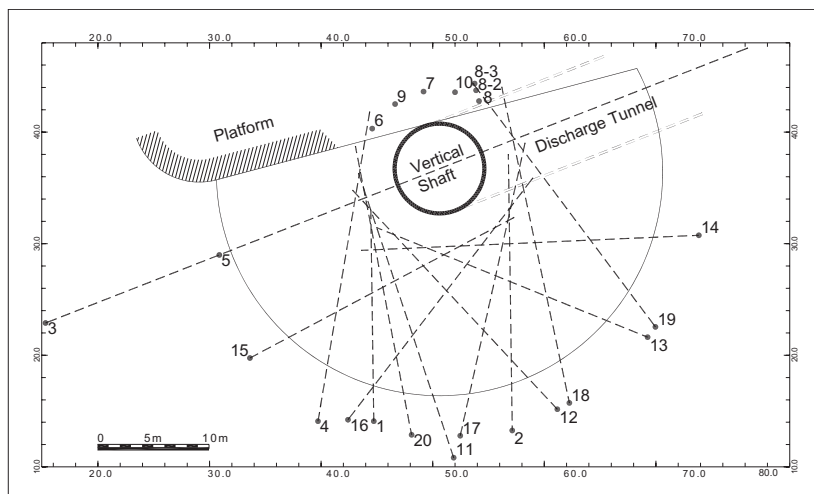


Figure 4. Layout of boreholes around the morning glory no. 1.

Although drilling through the concrete mass around the steel lining wasn't primary intention of the designer but many of boreholes were passed through the unexpected massive concrete which was used to fill spaces around the morning glory between the structure and excavated rock shaft. Length of the boreholes varied from 45 to 100 meters depends on their location and/or inclination. Layout of the boreholes around the morning glory spillway is shown in [figure 4](#).

Main reasons of drilling primary boreholes were to investigate following parameters:

- Rock formation
- Quality and soundness of rock mass
- Extent of the fractured zone
- Permeability of rock mass around the morning glory
- Quality and soundness of concrete after 40 years of service

3 GEOTECHNICAL CONDITION OF ROCK MASS

Obtained results from primary boreholes shows that most parts of the rock mass around the morning glory are fractured severely. Rock quality in the levels below the vertical bend and discharge tunnel increases significantly.

3.1 *Rock quality*

Due to obtained borehole cores the rock mass around the morning glory includes Trachyte, Trachy-Andesite and Andesite, which formed a mixed rock mass around the vertical shaft. Disordered rock units all around the morning glory No.1 is a good index of faulting.

The rock quality behind the damaged area is poor and the rock is fractured. It is unlikely that the fractures to be formed due to the 1990's earthquake because if the fractures had been formed due to earthquake forces, the forces would destroy the structure completely and we should had the same poor rock mass around the other morning glory in the vicinity of the morning glory no.1. Moreover, field observations confirm that the fractures are not originated by the earthquake. Therefore it is vivid that the rock quality was poor even long before construction of the vertical shaft and the morning glory. Due to mixed formation of rocks around the vertical shaft, it is impossible to recognize extent of the fault line around the shaft.

Permeability tests conducted in boreholes show that the rock mass around the morning glory is permeable and the Lugeon values vary from 1 to 15 and even ∞ in some segments.

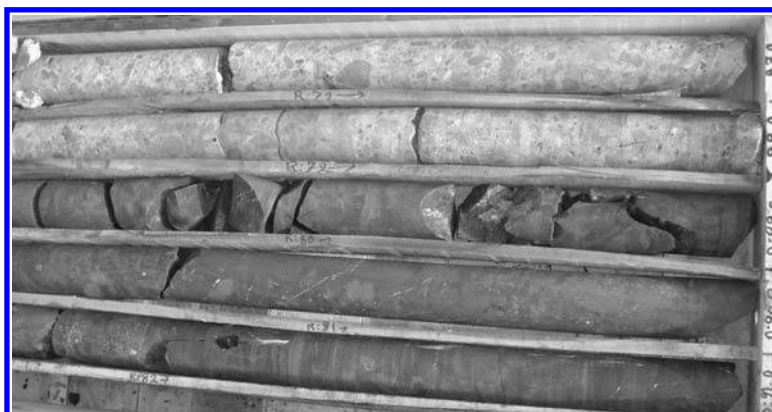


Figure 5. Quality of rock (bottom rows) and concrete (top rows) around morning glory.

3.2 Concrete quality

It must be noticed that significant lengths of the boreholes passes through unexpected concrete masses, concerning the designing plans and sections, some seems to be structural concrete and mostly seems as massive concrete used to fill void areas (excavated poor quality rock mass) behind the structure. This point confirms poor quality of rock mass around the vertical shaft which caused significant extent of the concrete mass around the vertical shaft to be filled during construction.

Boreholes passed through concrete masses shows that the concrete behind the steel lining is also cracked. Intensity of these cracks is different comparing the fractures in the rock mass. Cracks in concrete are more uncommon. Different intensity of cracks in concrete and fractures in rock masses especially longitudinal cracks indicate that the fractures may be caused by different reasons. It is clear that cracks in the concrete mass are formed after construction of the morning glory and it is likely that these cracks are formed due to earthquake forces. A sample of concrete and rock quality obtained from boreholes is shown in [figure 5](#).

3.3 Hypothesis of damages

Although available data about history of events during construction is very limited, it can be rationally discussed that the poor quality of rock mass were observed during construction and massive concrete fills were used to treat the rock quality and create a stable mass around the morning glory. Also poor quality of the concrete mass filling must be considered.

Cracks to concrete mass were formed after construction and during operation period of the dam due to external forces. The main origin of these external forces can be the 1990's earthquake. Due to absence of other geotechnical activities in the area, this earthquake is the most appropriate reason for damages in the concrete mass.

After formation of the cracks in the concrete mass the water pressure can easily shift to steel lining and create the inflations of the damaged areas. Also small structural deformation of the structure due to earthquake forces can increase intensity of stresses in the steel lining and intensify deformation of damaged area.

4 TREATMENT OF ROCK QUALITY

Due to nature of the damages rehabilitation work divided in two stages. First stage includes treatment of rock mass and improvement of permeability and structural properties of rock mass, and second stage includes repair of structural damages. A special arrangement for drilling and grouting of second group of boreholes were designed. As mentioned before the boreholes were designed in a manner to cover all areas around the morning glory's shaft near

the damaged area. Also a new cement paste was designed and used to ensure success of the treatment operations.

4.1 *Grout mix design*

To treat a better portion of rock mass around each borehole it was crucial to increase efficiency radius of each borehole. Relatively thin cement paste was used to achieve this goal. One part cement with 6% of cement's weight bentonite clay mixed in three parts water was used as concrete paste mix. It is not allowed to change the mix ratios and use of a thicker paste during grouting of each segment. Even when the grout absorbed easily, the grouting process must be continued until the time that the grout absorption stops.

4.2 *Grouting pressure*

There are many theoretical and empirical methods for selection of grouting pressure. For example, American designers prefer minimum grouting pressure not more than 5 bars and vary range of grout mixing portions is accepted, while French designers allow grouting pressure more than 50 to 100 bars, and German designers accept pressure range of 5 to 30 bars.

Kunert show that information about effective pressure on grouting in anisotropic and heterogen rocks is not enough. Therefore the grouting pressure may vary in different conditions and it is better to be determined according to in situ tests. According to new findings it is impractical to find a trend between grouting pressure and preferred results of grouting. In some areas very high or very low pressures may be used to achieve the goal.

Regarding of quality of rock around the morning glory and short distance of grouting area to morning glory grout pressure equal to 10 bars were selected. By this pressure, absorption of grout into rock mass assured and back pressure to steel lining shall be small enough to prevent development of the damaged area.

4.3 *Grout order*

In order to increase absorption of grout to rock mass and prevention of creation of residual pressures in grouted areas, the grouting was designed in an upward order. By this method 5 m segments of borehole were grouted from bottom to top of the boreholes. By this grouting method, good penetration of grout paste between rock cracks is assured.

It must be noted that due to obstruction of morning glory most of boreholes are drilled inclined and in nearest point to the morning glory passed in vicinity of the damaged area. Also lengths of grouting boreholes drilled to a depth at least 10 meter below damaged area. To decrease procedure's time only lowest 20–25 meter of boreholes were grouted. By this method at least 10 meters above and below the damaged area has been grouted.

5 OBSERVATIONS AND IMPROVEMENTS

To verify success of grouting procedure different criteria were considered. These criteria include improvement of permeability properties of rock mass, observation of grout paste in adjacent boreholes and measurement of leakage water from damaged cracks of the steel lining.

5.1 *Improvement of permeability properties*

In situ permeability tests (Lugeon test) of four last boreholes were considered to verify improvement of permeability properties of rock mass around the morning glory. These boreholes were drilled and tested when adjacent boreholes were drilled and grouted.

Lugeon values of boreholes in vicinity of the damaged area varied between 1–15 before grouting although $lu = \infty$ were measured in three segments of three different boreholes. Lugeon values near the damaged area vary between 0–2 after grouting.

5.2 Observation of grout paste

Absorption of the grout paste in rock crack was one of main concerns of the treatment method. Grout paste was observed between rock cracks in different segments of lower depths of boreholes 11, 12, 15, 17 and 20. These observations confirm good absorption of grout paste in rock fractures.

5.3 Measurement of leakage from steel lining cracks

Discharge of leaking water from steel lining crack were measured by a weir located at lowest point of vertical bend. Monitoring and measurement of the leakage discharge started one year before start of grouting operation and it is continuing by date. For comparison of results a two year period measurements were used, in which the first year is before treatment operations and the next year is during and after the operations. Values of measured discharges before and after treatments and water surface elevation (WSE) in dam's reservoir are shown in figure 6.

Comparison of leakage discharge shows significant decrease in leakage values although water surface elevation in adjacent years is different. Water surface elevation (WSE) in 2008–09 period is about 10 meter less than water level in 2009–10 period, but leakage values in 2008–09 period is much more than leakage discharge in 2009–10 period. To compare leakage decrease regarding to water surface elevation, variation of leakage values versus water surface elevation is shown in figure 7.

Also linear regression relation between leakage discharge and water surface elevation before and after treatment works has calculated and shown in figure 7. It can be assumed that leakage discharge decrease can be estimated as ratio of two slopes of regression lines. Considering slopes of two regression lines (0.00778 and 0.00190) decrease of leakage discharge can

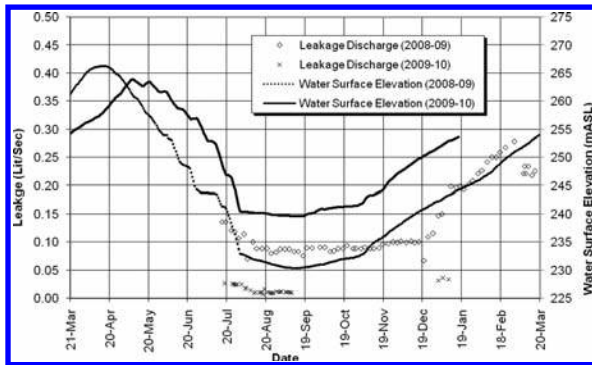


Figure 6. WSE and leakage variation before and after grouting treatment.

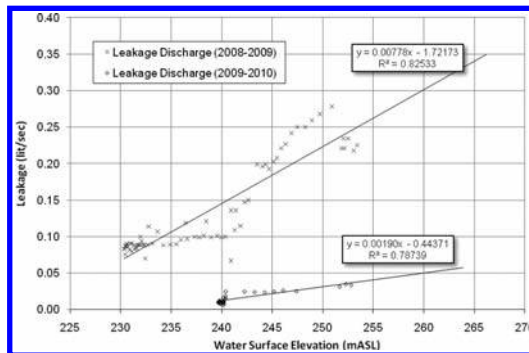


Figure 7. Relation between leakage discharge and water surface elevation.

be estimated about 75% ($0.00190/0.00778 = 24.4\%$). It must be remembered that water level in time period before treatments is higher than water level in period after treatments therefore the decrease ration is a conservative value.

6 CONCLUSION

Concerning to damages to steel lining of vertical bend of morning glory spillway of Sefidrud dam, 22 boreholes around the spillway has been drilled, investigated and treated. Regarding to the obtained data from boreholes and logs it is been concluded that the poor quality of rock mass around the morning glory can be a very significant factor on start of the damages. Second factor on extension and increase of the damages was 1990's earthquake in the area, which caused structural damages to concrete masses behind the steel lining. These damages were not seen because of steel cover. About 14 years after the earthquake the damages were surfaced.

Rehabilitation of damages was divided into two main parts. First stage consists of treatment of rock mass around the morning glory and making a good basis for second stage of treatments which includes rehabilitation of the damaged lining.

To ensure absorption of cement paste into rock mass around the borehole a high water content cement paste were designed and a modified grouting method was used. Later drilled boreholes show excellent penetration of the grout into rock mass, also obtained results show significant decrease in leakage water from steel lining cracks as well as achieving treatment goals.

REFERENCES

- Ewert, F.K. 1985. *Rock Grouting: with emphasis on dam sites*. German (Switzerland): Springer Verlag.
- Faghihimohaddess, A. 2008. *Sefidrud Dam rehabilitation project: Summary of studies*. Tehran: Yekom Consulting Engineers.
- Karbala, M.A. & Katibeh, H. 2009. *Cement paste grouting in rock (in Farsi)*. Tehran: Tarava.
- Mouvet, L. 2008. *Sefidrud Dam rehabilitation project: Review of rehabilitation report "Morning glory spillway rehabilitation report"*. Renens: Stucky.
- Naghbian, R. & Faghihimohaddess, A. 2007. *Sefidrud Dam rehabilitation project: Morning glory spillway rehabilitation report*. Tehran: Yekom Consulting Engineers.
- Nonveiller, E. 1989. *Grouting: theory and practice*. Amsterdam: Elsevier

Rehabilitation and upgrade of Giudea dam

G. Baldovin, E. Baldovin & G. Morelli

Geotecnica Progetti s.r.l., Milano-Roma, Italy

ABSTRACT: The Dam and the Impound of Giudea, for the water supply of Pistoia Municipality, were completed and accepted at the end of 1973. They were interested in 1990 by some local slides, which obliged to empty the reservoir. As the occurred phenomena were attributed to the degradation of the clayey materials, the dam rehabilitation design outlines include the substitution of the collapsed soil with other of better characteristics, the disposal of a protected waterproof geomembrane on the upstream face and the dam crest raising, in order to fit the Italian Dam Code in force. Meantime the bottom outlet and the draw-off pipes will be located in a new tunnel on the right bank. In the impound, the left bank of the reservoir will be reinforced in the weathered zones with a gravelly embankment. The seismic hazard and the safety assessments of the dam have been finalized according to the state of art.

1 INTRODUCTION

The Giudea Impound, located in Gello site in the Pistoia Municipality, was conceived in the 60's for the water supply of the town.

The plant, finally accepted at the end of 1973, operated regularly until 1990, when the occurrence of some slides obliged to empty the reservoir. After a preliminary study phase, the Municipal Administration appointed the design of the rehabilitation measures of the impound and the contextual upgrade of the works, according to the Italian Dam Code in force.

In 1993 a cofferdam was built upstream of the embankment, in order to make some preliminary arrangements at the foot of the dam, so allowing a provisional partial impound of about 65000 m³ (see Fig. 2). The Final Design for the complete rehabilitation of the reservoir was approved by the National Regulatory Agency at the end of 1996.

In 2007 the seismic safety assessments of the dam and the appurtenant works in the upgraded lay-out have been developed.

Meanwhile a new quarry area of gravelly and silty-sandy materials for the remodelling of the embankment and the reinforcement of the left bank of the reservoir has been investigated and characterized under the geotechnical profile. It is located in the Primavera Lakes zone, adjacent to Ombrone Pistoiese River, about one kilometre South of the city, where the coordinated construction of an important Expansion Impound for flood control is planned.

2 GENERAL ELEMENTS ABOUT THE WORKS AND THE FIRST PHASE OF OPERATION

The Giudea Impound is an “outside the river-bed” basin, located at the foot of the Apennines North-West of Pistoia, at the head of a valley determined by Rio dei Fontanacci Stream; it is used to modulate and store the winter and spring flows of a near stream.

The reservoir, which originally had an useful capacity of about 660,000 m³, is placed in a formation of shaley clays inglobing sandstones and strongly weathered and fractured grey limestones.

The availability of semi-pervious materials in the immediate surroundings and the relative deformability of the foundation grounds oriented the original design towards an homogeneous



Figure 1. Giudea impound—evidence upstream shell slides (2007).

embankment dam about 32 m high, realized with compacted shaley clays and protected upstream with a rip-rap layer and downstream with a filtering foot blanket. The embankment was built between 1965 and 1970 and regularly accepted in 1975. The crest, 6 m large and 295 m long, was at 150.06 m a.s.l. elevation, with normal water level at 147.76 m a.s.l. The net freeboard resulted 1.8 m. Being the impound “outside the river-bed”, the spillway was conceived for relatively modest discharges: having an overflowing sill 10.8 m long on the right bank, with a 0.5 m water head it was able to evacuate a $6.8 \text{ m}^3/\text{s}$ discharge.

The bottom outlet and the draw-off consisted of two side by side steel pipes, respectively 450 mm and 400 mm ϕ , which passed, in a special concrete embedding, under the dam abutment.

In 1990 autumn, without any evident premonitory signal, at first on the upstream shell of the dam (Fig. 1), then on the left bank of the reservoir, several some meters thick rotational slides interested the slope.

Some deformations appeared indeed on the upstream face, with the formation of several fractures and a general lowering of the profile from the upstream edge of the crest until about 137 m a.s.l., that is for the superior 13 m, and with a more or less remarkable raising at the inferior elevations; movements on the face occurred also later.

After some provisional stabilization works at the foot, the phenomenon practically stopped.

Since the preliminary studies, the reason of the failures seemed to be connected with the weathering of the embankment material, argillites and their alteration blanket, in contact with the water of reservoir.

A wide experimental investigation, with the intervention also of Prof. P. Colombo, confirmed that the slides happened in a phase of draw-down and that for such a condition the slope of the upstream face was inadequate to the actual reduced shear strength of the shell fill.

3 REHABILITATION WORKS DESIGN

The concept design involves the substitution of the displaced fill with material of better characteristics and the transfer of the dam watertightness function from the body of the embankment (original design) to an impervious geomembrane on the upstream face. In that way all the dam body, including both the new “rehabilitated zone” and the old embankment, still consisting of clayey material, is preserved from the contact with the water.

The reinforcement of the left bank of the reservoir, in the loosened zones, with a gravelly embankment adequately profiled (Fig. 2), is considered as well.

With the new design outlines, in addition to upgrade the works according to the in force Italian Dams Code, it is possible to increase the useful capacity of the reservoir up to about 802000 m^3 . Furthermore, with an important modification of the original lay-out, the bottom outlet and the draw-off pipes will be located in a dedicated new tunnel, with horseshoe section of 2.40 m, which will cross the right side, without interfering with the dam, and will convey

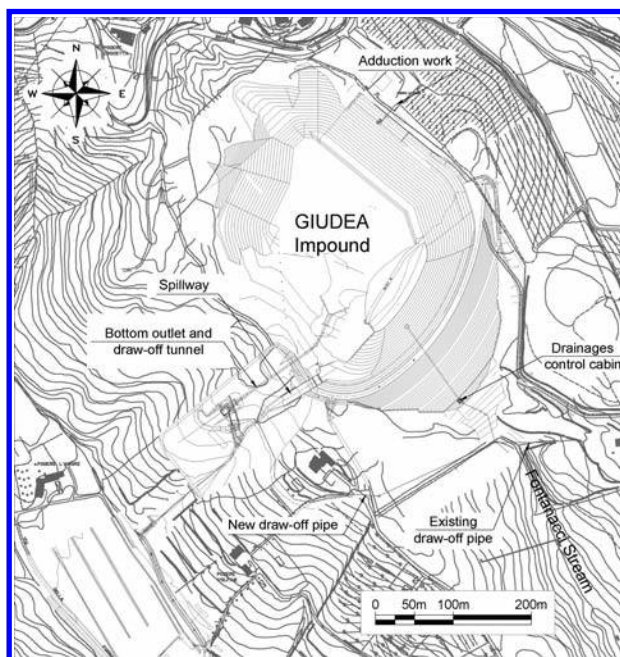


Figure 2. Giudea impound—general lay-out.

the water to the contiguous Tazzera Stream valley. As it is shown in the typical cross section (Fig. 3), the new crest elevation is 153.40 m a.s.l., with a raising of 3.34 m, and the net freeboard now results 3.45 m; the maximum height of the dam above the downstream foot is 33.40 m.

The lay-out of the dam reproduces the upstream concave shape of the original embankment: the new axis is displaced 6.60 m downstream and the overall crest is 395 m long.

The new embankment has a zoned section. On the upstream face an impervious PVC geomembrane, 1.5 mm thick, is interposed between two polypropylene continuous filament 350 g/m² geotextile sheets and ends in the waterproof “plug” located at the foot of the face. The watertight “package” lays on a 50 cm thick draining layer constituted by alluvial gravel of small size and is protected by a layer of selected gravelly material, 90 cm thick, and by a limestone rip-rap, 60 cm thick, formed by quarry elements.

In the typical cross section, which inglobes the pre-existing embankment, adequately profiled, four main zones can be identified:

- the upstream impervious toe plug;
- the upstream shell in gravelly alluvia;
- the upper central zone in gravelly silt;
- the downstream shell constituted by gravelly alluvia.

The wide impervious “plug” at the upstream foot connects the geomembrane and the foundation watertight clay formation. It will be formed with silts coming from Primavera Lakes adequately selected and compacted, partly added with 8% bentonite powder. Between the geomembrane and the existing embankment, preliminarily modelled with arrangement excavations, a new upstream shell about 8 m thick is realized in alluvial material of good mechanical characteristics selected from the gravels of the named Lakes.

The upper central zone is of alluvial origin and represents a semi-pervious barrier against the hypothetical remarkable filtrations in case of any breakage of the geomembrane; the material comes from the cultivation of the surface silty layer (70%) of Primavera Lakes mixed with the gravels below (30%). The downstream shell is formed with clean alluvia; the covering thickness of the old shell is between 4 and 9 m. The face is protected by a 40 cm thick layer of grassy vegetable soil. The shell itself rests on a draining blanket which, joining the remaining

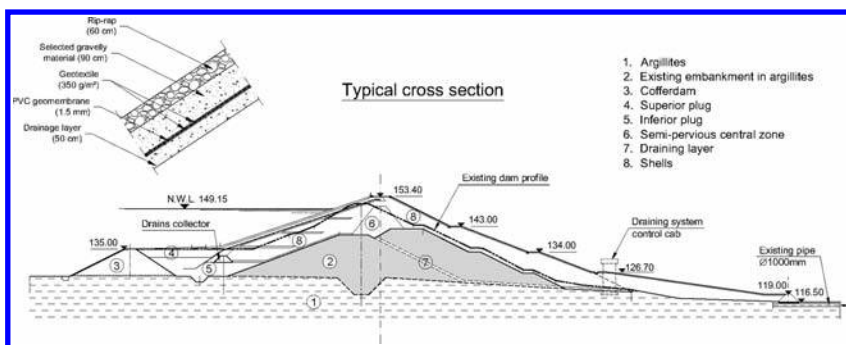


Figure 3. Giudea dam—cross section.

part of the original oblique drain, keeps low the level of the saturation curve and removes any water filtration of different origin. In the upstream shell, both the draining layer upon which the geomembrane is located and the blanket at the interface with the existing embankment, discharge into a drains collector. It conveys through the existing steel pipes ϕ 450 and ϕ 400 mm of the original bottom outlet and draw-off, which have been verified with an endoscopic investigation and supplied with discharge limiters; the seepage waters flow to a new measure and control cabin, equipped with a gauge station, immediately downstream of the dam. In the same cabin also the waters in case coming from the downstream oblique drain and draining blanket, already belonging to the old embankment, are collected.

4 GEOLOGICAL AND GEOTECHNICAL OUTLINES

4.1 *Geology of the area*

The foundation and the reservoir of Giudea Dam fall within a typical hilly landscape shaped in the argillites and siltstones of the Sillano Formation, a geological unit referred to the Upper Cretaceous-Lower Eocene. The unit tectonically overlies the Marmoreto Marls Formation (Upper Oligocene-Lower Miocene), constituted by prevailing layered brown calcilitites and light coloured silty marls, which outcrops on the NW bank of the reservoir almost above the maximum water level. Lithologically the Sillano Formation is predominantly composed of weak highly tectonized shaley clayey materials showing a complex structural pattern of numerous shears and faults, which determine a chaotic structure of blocks and fragments of limestones, sandstones and marls, with dimensions ranging from decimetres to several meters, included in a mainly clayey matrix. The formation occupies almost all the reservoir area and its very low permeability ensures appropriate watertight conditions for the reservoir banks.

The geomorphology of the area surrounding the Giudea Impound is marked by the presence of local slides and instability phenomena of the slopes, generally modest in scale, but widely involving the argillites. In these phenomena are included the mentioned small episodes, which have marginally involved, during the past operations of the basin, some local sectors of the reservoir banks, inducing limited mobilizations of the shallow weathered strata of the argillites.

4.2 *Geotechnical characterization of the dam foundation grounds*

The geotechnical characterization of Sillano argillites, which constitute the foundation of Giudea Dam, is the result of various geological and geotechnical campaigns, carried out starting from the earliest stages of the design work.

Indeed in the dam area a series of boreholes with undisturbed core sampling for physical-mechanical laboratory analysis, several trenches and exploratory shallow wells have been performed. The argillites show the structural features typical of the “complex structural formations” widely outcropping in the Apennines Chain. According to the classification originally proposed by ESU (1977) for those types of formations, Sillano argillites can be

attributed to types B2 and B3, corresponding to clayey strongly tectonized rock masses with a chaotic structure, including irregular clasts and fragments of more competent rocks.

In detail, the boreholes carried out in the foundation grounds of Giudea Dam have identified the presence, beneath a superficial layer of eluvial clay about $3 \div 4$ m thick, of weathered grey-brown argillites, gradually passing to the underlying dark-grey unweathered argillites, located around 10 to 12 m deep from ground level. A summary of the physical and mechanical properties derived from the geotechnical investigations for these lithotypes is shown in [Table 1](#).

4.3 *Geotechnical characteristics of the existing embankment and of the soils to be used for the rehabilitation*

The existing embankment, mainly formed by compacted clay materials derived from the excavations of the argillites in the dam section, was the subject of various geotechnical investigation and studies. In 2006–2007, also the alluvial deposits in the area of Primavera Lakes were investigated, in view of their use in some internal zones of the new Giudea Embankment and for the reinforcement of the left side of the reservoir. That area, covering approximately 6.5 hectares, is situated some kilometres SE of the dam site, at the confluence of Tazzera/Torbecchia and Ombrone Rivers. The materials consist of recent and terraced alluvial sediments constituted by a superficial layer, few meters thick, of sandy silts lying on gravelly-sandy deposits, partly affected by the natural ground water level. In detail, the materials composition corresponds to prevailing low gravelly silts with sands (silt 61–68%, sand 30–34%, gravel 0–7%) in the superficial part of the deposits, passing to underlying gravel and pebbles and sandy gravels (pebbles 24–69%, gravel 13–60%, sand 4–21%, fine fraction 1–20%).

The investigations carried out on the existing embankment and in the Primavera Lakes area have included numerous shallow wells and boreholes with sampling, at various depths, for laboratory analyses. The basic geotechnical parameters derived on the basis of investigations and tests conducted on these materials are summarized in [Table 2](#).

4.4 *Dynamic characterization of the foundation grounds and of the existing embankment materials*

The reconstruction of the seismic P and S waves speeds within the foundation grounds and the existing embankment of Giudea Dam is derived from the results of geophysical investigations.

In particular, a down-hole test was performed in a vertical hole, 30 m deep, drilled in the dam foundation argillites, at the foot of the downstream slope of the existing embankment. It has found average values of V_p equal to 920 m/s and over 2500 m/s, respectively for the weathered more superficial argillites and for the unweathered deeper ones. The corresponding average speeds V_s grow from 280 m/s to $520 \div 800$ m/s. $V_{s_{30}}$ parameter is equal to 506 m/s.

Furthermore some MASW tests, based on the measure of the propagation speed of the Rayleigh superficial seismic waves, were carried out from various positions through the body of the existing embankment, allowing the reconstruction of V_s profiles, in one and two dimensions. They were executed, respectively, from the dam crest road and from the downstream banks of the embankment, around levels 143 and 135 m a.s.l., and oriented according to the longitudinal direction of the dam. The results of the MASW tests in the existing embankment body show the presence, next to the crest of the embankment, of a low speed seismic zone, characterized by values of V_s between 120 and 150 m/sec, where a probable state of relaxation

Table 1. Physical-mechanical characteristics of foundation argillites.

Lithology	γ_d [KN/m ³]	W [%]	<2 μ [%]	PI [%]	c' [KN/m ²]	ϕ' [°]
Weathered argillites	17.5 \div 20	11 \div 30	34 \div 36	17 \div 18	1.4 \div 5	22 \div 29.5
Unweathered argillites	17.5 \div 20	12 \div 15	17 \div 18	17 \div 18	25.5 \div 59	22.5 \div 27

γ_d = dry unit weight; W = natural water content; <2 μ = passing%; PI = Plastic Index; c' = drained cohesion; ϕ' = drained shear strength angle.

Table 2. Geotechnical characteristics of the dam materials.

Dam materials	γ_u [kN/m ³]	γ_{sat} [kN/m ³]	c' [kN/m ²]	ϕ' [°]
Existing embankment	20.0	20.5	10	20
Cofferdam	20.0	22.0	0.0	30
Plug at upstream foot	19 ÷ 20	20.5 ÷ 21.5	0.0 ÷ 1.0	20 ÷ 32
Semi-pervious central zone	20.0	21.5	0.0	25
Shells and reinforcement embankment	20.0	22.0	0.0	32

exists. Deeper the speeds tend to increase up to values of the order of 350 to 450 m/s, despite local decreases, probably due to lack of uniformity of the materials in the construction phase.

5 WORKS SEISMIC SAFETY ASSESSMENTS

Being Pistoia Municipality classified as second seismic category, in 1995 both the dam and the reinforcement embankment on left side were positively verified with the pseudostatic method, according to the Italian Dams Code, even in the rapid draw-down condition following a breakage in the waterproof lining.

In 2007 limit states seismic analyses have been developed, assuming the following return times:

- ultimate limit state (SLU), with important damages, but without uncontrolled release of water: 1000 years;
- collapse limit state (SLC) with irretrievable damages and uncontrolled release of water: >2500 years.

6 SEISMIC HAZARD EVALUATION

The study has taken into account the historical and instrumental seismicity of a big area containing the site and the maxima effects observed in the municipal territory, making reference to the parametric catalogue of the Italian earthquakes (WORKING GROUP CPTI, 2004). The biggest macroseismic intensity values observed in Pistoia City are included between VIII and IX MCS degrees, as consequence of local earthquakes.

For the seismic hazard evaluation CORNELL (1968) methodology has been adopted.

The source zones have been identified with reference to the ZS9 simplified model, proposed by the Working Group for the compilation of the seismic risks map of INGV.

A recurrence law has been associated to each source zone according to the Gutenberg-Richter algorithm, using the above mentioned parametric catalogue of the Italian earthquakes.

In the study the attenuation laws proposed by SABETTA *et al.* (1996), on the basis exclusively of Italian data, have been adopted.

Taking into consideration all the seismic zones, the peak values of the ground motion (PGA and PGV) and the spectral values of acceleration (PSA) have been calculated, as a function of the return time, for a position in the middle of the crest.

The reference vibratory motions have been finally defined by comparing the results of the hazard evaluation with the values supplied in 2006 by INGV in S1 project for Civil Protection and prudentially adopting their envelope. For the site 0.21 and 0.28 g peak acceleration values and the response spectra summarized in Figure 4 have been so adopted, respectively for 975 and 2475 years return times. It was then selected a set of six artificial accelerograms in accordance with the reference motions, obtained assuming a couple of magnitude and distance values respectively between 5.6 and 5.9 and between 10 and 15 km.

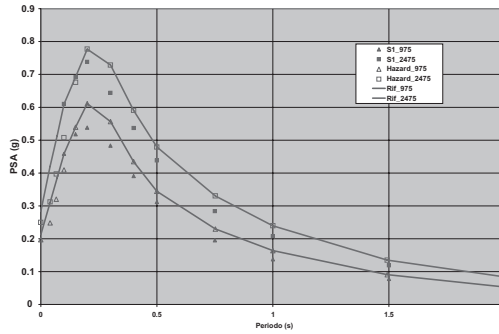


Figure 4. Response spectrum of reference vibratory motions (red: 2475 years, blue: 975 years).

7 DAM DYNAMIC ANALYSIS

For Giudea Dam the high degree of compaction specified for the construction of the granular shells, in addition to the nature of the abutments formation and of the materials of the existing embankment, excludes the occurrence of liquefaction phenomena or the reduction of strength under cyclic loads. It was then developed a dynamic analysis, considering the effective seismicity of the area together with the deformability and the strength mechanical characteristics of the materials.

7.1 Preliminary static analysis

The static analysis of the dam has been developed using a 2D model in plane deformation with elasto-plastic behaviour of the materials, taking into account the temporal evolution of the geometry and of the contour conditions.

The mesh, which represents the maximum height section, is formed by 1476 elements interconnected in 1554 nodes and has been drawn reproducing accurately the geometric and geotechnical features of the embankment.

In the numerical model the sequence of the phases has been reproduced distinguishing the construction of the original body and that of the other zones of the new embankment until the crest elevation. Due to the watertight upstream face, the impound effect has been introduced through simple nodal forces applied at the upstream contour.

7.2 Dynamic geotechnical parameters

The speed values V_s obtained with the MASW tests have been worked out for the existing embankment. As the new shells present a bigger stiffness, in their case at the same stress conditions an increase of about 15% of the V_s has been assumed.

For the foundation the V_s measures executed in the down-hole test have been used.

In absence of laboratory tests results, the materials have been divided in two categories (granular and cohesive), adopting literature G/G_0 and damping D curves versus shear strains.

7.3 Linear equivalent dynamic analysis

Firstly the dynamic analysis has been developed with a linear equivalent model in full reservoir conditions, using the same mesh as in the static simulation.

The application of the reference motion with 2475 years return time determines peak values generally inferior to 0.5 g, with a maximum of 0.8 g near the crest.

A big reduction of the shear modulus is located in the shells, with 20% of the value of G_0 ; in limited zones the G modulus drops near 10% of G_0 . In the pre-existing embankment they result 40–50% of the initial ones. With reference to the shear strains, besides the shells the

isolines 0.20% and 0.30% interest a more consistent part of the dam and about at 1/3 of the maximum height strain values near 0.40% are reached in a relevant zone.

For that reason also a non-linear model was developed (ISHIHARA (1968)).

7.4 *Permanent displacements*

On the basis of the results of the linear equivalent model the permanent displacements of the embankment for the design seismic events have been calculated with NEWMARK (1965) method. For the seism with return time of 2475 years the maximum displacement along the face direction is about 1.9 m (vertical component 0.73 m). Those values concern the nodes near to the crest; more modest entities characterize other zones of the embankment.

7.5 *Non-linear dynamic analysis*

The estimates executed with the non-linear model for the same return time show a maximum permanent settlement of 2.0 m (1.3 m in vertical direction) only in the downstream node of the crest. For the upstream node a vertical settlement of about 0.6 m is obtained. In other zones of the embankment much lower values are determined.

Resulting the maxima displacements largely inferior to the available net freeboard of 3.45 m, the watertightness of the embankment is then ensured.

With regard to this, it is meaningful the about 0.5 m calculated value of the final settlement in the central zone of secondary waterproofing: the relative top elevation would pass from 150.00 m a.s.l. to 149.50 m a.s.l., still superior to the normal water level (149.15 m a.s.l.).

8 CONCLUSIONS

The planned co-ordinated realization of an Expansion Impound on Ombrone River in Primavera Lakes zone and rehabilitation and upgrade of Giudea Impound represent an interesting example of synergy on the territory in the direction of the works sustainability.

The rehabilitation design of Giudea Dam, besides to eliminate the contact of the basin with the clayey material of the upstream face, primary reason of the occurred failures, introduces the zoning of the embankment, realizing with the existing body, suitably raised, an auxiliary watertightness in the central part in case of breakage of the superficial geomembrane.

In the new asset all the elements of waterproofing are associated with proper draining systems and their hypothetical losses are checked inside a downstream cabin. It is also verified that the safety of the works is warranted also in the most severe seismic conditions.

ACKNOWLEDGEMENTS

The Authors thank Consorzio di Bonifica Ombrone Pistoiese, who made the publication of this paper possible.

BIBLIOGRAPHY

- Cornell, C.A. 1968. Engineering Seismic Risk Analysis. BSSA 58, p. 1583–1606.
- Esu, F. 1977. Behaviour of slopes in structurally complex formations. In. AGI International Symposium “The Geotechnics of Structurally Complex Formations”. Capri 1977, Vol. II, p. 292–304.
- Gruppo di lavoro CPTI 2004. Catalogo Parametrico dei Terremoti Italiani, versione 2004 (CPTI04). INGV, Bologna. <http://emidius.mi.ingv.it/CPTI/>
- Ishihara, K. 1982. Evaluation of soil properties for use in earthquake response analysis. Num. Mod. Geom., R. Dungar, G.N. Pande and J.A. Studer (eds.).
- Newmark, N.M. 1965. Effects of Earthquakes on Dams and Embankments. Geotechnique, Vol. 15, No 2.
- Sabetta, F. & Pugliese, A. 1996. Estimation of response spectra and simulation of nonstationary earthquake ground motion. Bull. Seism. Soc. Am. 86, p. 337–352.

Assessment of small gravity dam heightening

T. Hofmann

Wächter AG Bauingenieure (Formerly STUCKY Ltd.), Zurich, Switzerland

M. Wickenhäuser

STUCKY Ltd. Renens, Switzerland

W. Gabl

BKW FMB Energie AG, Bern, Switzerland

ABSTRACT: This paper addresses the particular challenges of the heightening concept of an existing concrete dam in the Swiss Alps. It focuses on the heightening alternatives and on the logistic challenges related to the alpine character of the construction site without any access road.

1 INTRODUCTION

The Kummenbord gravity dam is situated at 2100 m a.s.l. and is part of the Gommer Kraftwerke hydropower scheme in the Swiss Alps. To increase the reservoir capacity from 160,000 m³ to 1,000,000 m³ it is planned to heighten the existing dam by 10.5 m and extend it by 90 m. The increase of the reservoir capacity requires additionally the construction of a saddle dam closing a tributary valley. The height of the earth-fill dam is 10 m with a total length of 160 m.

The paper focuses on the particular challenge of the heightening concept of the existing concrete dam related to the alpine character. Another particularity of the dam is the integrated top station of the cable car in the dam body. Further, logistic challenges are discussed since the site can only be reached by a cable car.

2 FOUNDATION CHARACTERISTICS

The project area is located in the Monte Leone gneiss. Essential information on its local characteristics was determined by field investigations and laboratory tests carried out in 2008. Amongst others, the deformation modulus, shear strength, permeability, joint and fault characteristics and the thickness of the superficial soil and loose rock cover were determined. The mean compressive strength of the bedrock amounts to $\sigma_c = 95.6$ MPa, the mean tensile strength amounts to $\sigma_{t, \perp \eta} = 9.7/5.1$ MPa. The bedrock permeability is $K = 3.10^{-7}$ m/s.

Due to the favorable bedrock fault and joint direction and their steep angle in the project area they have no significant influence on the stability of the dam.

Following to the Swiss standard for dam category II, the maximum horizontal peak for the ground acceleration to consider is $a_h = 0.39$ g whereas the vertical acceleration adds up to $a_v = 0.26$ g corresponding to an earthquake hazard with a return period of 5000 years.

3 DESIGN CRITERIA

The concept of the heightening should be in accordance with following requirements:

- maintenance of operation of the hydropower scheme, therefore
- maintenance the full supply level in the reservoir
- maintenance the service chamber in operation
- maintenance the flood control function
- maintenance of all outlet devices
- maintenance of operation of the cable car

4 HEIGHTENING ALTERNATIVES

To determine the best technical and economical solution for the dam heightening, the following four alternatives were examined.

4.1 *Enlarging the dam section on the downstream face (gravity dam)*

The dam is heightened by enlarging the existing dam by a conventional gravity dam on the downstream face. With a downstream face slope of 0.9/1.0 (H/V) the width at the dam toe measures 15.0 m. The total volume of concrete totals some 14,000 m³. The excavation volume amounts to 5000 m³.

To guarantee a monolithic behavior of the heightened dam, the existing dam will be anchored with the new dam body.

As a major advantage, this solution enables the construction of an internal gallery between existing and new concrete.

The drawbacks of this solution consist in the integration of the top cable car station and the service chamber in the dam body.

4.2 *Enlarging the dam section on the downstream face using prestressed anchors*

In order to reduce the need of space on the downstream side of the existing dam and to minimize the concrete volume, a heightening solution using prestressed anchors was examined. The enlargement of the dam the section on the downstream face is strengthened with 70 prestressed anchors drilled from the crest of the dam. The tendons are anchored at the crest level and at depth to the bedrock foundation. The width at the dam toe measures only 9.0 m. The total volume of concrete and excavation material amount to 9000 m³ and 2500 m³, respectively.

Prestressing provides an additional vertical load. The resultant prestressed load of the anchors improves significantly the overturning and sliding stability.

The relatively thin dam body would result in a small excavation and concrete volume, significantly less than for a conventional gravity dam (see 4.1). The thin dam body would also simplify the integration of the cable car station and the service chamber.

Although total construction cost would be approximately 20% lower than for the gravity dam solution, the prestressed anchors require continuous maintenance including readjustment or even replacement. The cost for maintenance and partially replacement during the assumed life time of 80 years exceed the initial savings in capital investment cost.

4.3 *Enlarging the dam section on the upstream face*

The existing dam is heightened by enlarging the existing dam by a conventional gravity dam on the upstream face. This alternative would present the advantage to maintain the existing outlet devices and station of the cable car. Furthermore, the joint between the old and the new concrete is put under pressure during static loads. Finally, the existing concrete, even though in fairly good condition, would have been covered and protected by new concrete.

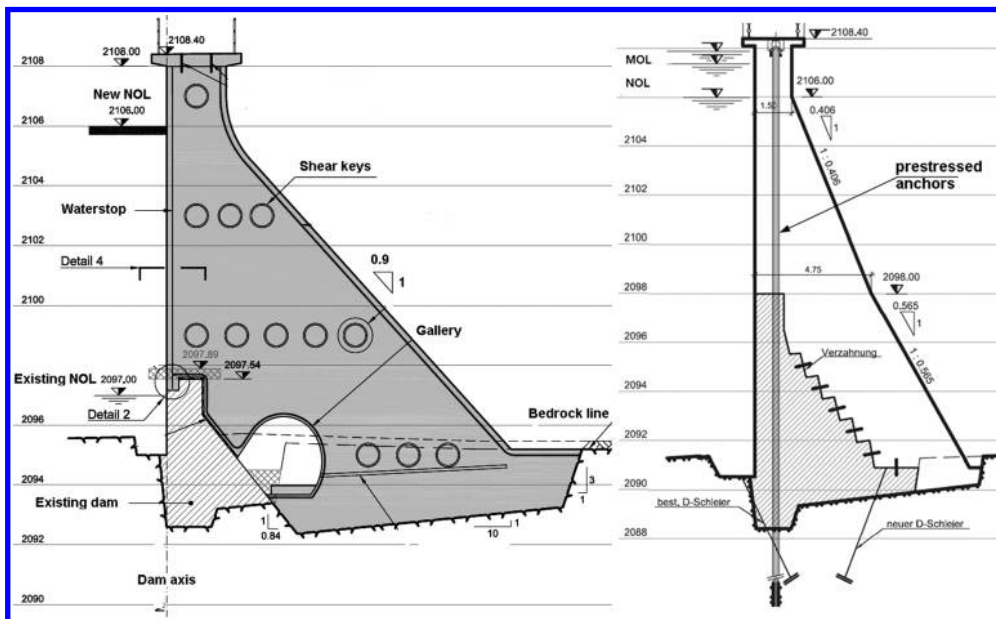


Figure 1. Left: typical cross section of the downstream gravity dam heightening. Right: typical cross section of the heightening using prestressed anchors. (Not to scale).

The major inconvenience of the solution consists to maintain full reservoir level at all times. This would only be possible by a cofferdam inside the existing reservoir. Further, the intake structures would need major adjustments.

4.4 Placing an embankment dam on the downstream side

This solution provides an embankment dam on the downstream side with an upstream and downstream slope of 1:1.75 and with an asphaltic concrete membrane on the upstream face.

The major advantage of this solution is the relatively simple construction method and the fact that relatively few materials must be transported to the site.

The inconvenients are the high space requirement, the complex adaptation works of the outlet devices, water intake and the top station of the cable car and particularly the lost profit. Considering a construction time of two years, the lost profit amounts to 4 to 5 mio. CHF due to the adjustments of the outlet devices and the service chamber. This amount equals roughly a third of the total investment cost.

4.5 Selected solution

Comparing all technical and economic issues, the heightening of the Kummensbord dam is chosen to be a conventional gravity dam on the downstream face (see 4.1). This solution presents fewest risks, either technical or economic.

The selected solution is presented in the following chapters.

5 HEIGHTENING CONCEPT

5.1 General layout

The elevation of the heightened dam crest is 2108 m a.s.l. topping the existing crest by 10.5 m. The total height of the dam is to be 20.5 m. The length of the dam is extended by 90 m from

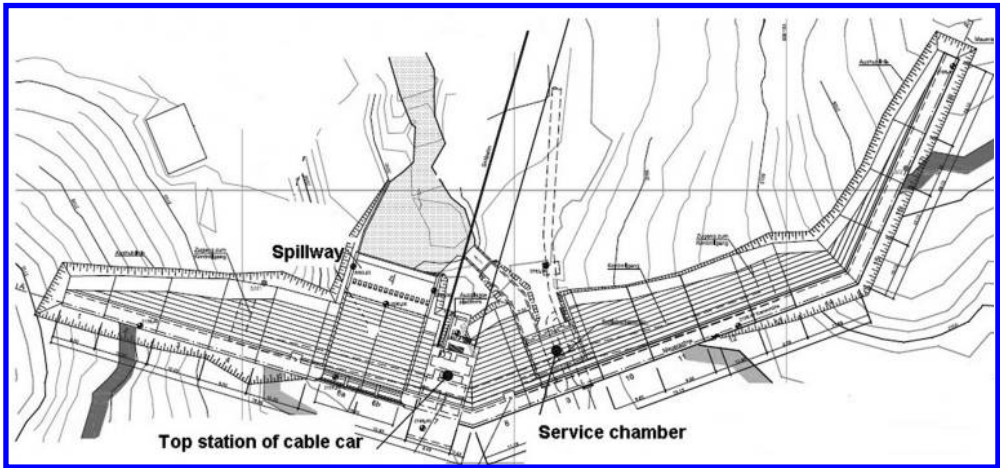


Figure 2. General situation of heightened dam.

110 to 200 m. The dam presents a vertical upstream face and a downstream face with a slope 1V:0.9 H. The dam crest width measures 2.0 m (bridge enlargement to 3.0 m). The dam base width is determined to be 15.0 m.

Along the existing downstream toe, a longitudinal inspection and drainage gallery is placed in the dam body between existing and new concrete. The gallery also provides a sheltered access from the station of the cable car to the service chamber as well as to the dam crest.

Parts of the existing dam structure (e.g. crest, flood protection outlet) will be demolished before placing the new concrete. Anchor rods drilled and cast in the existing concrete will stabilize the joint between old and new concrete and guarantee for a monolithic connection. To minimize relative movements between the independent dam blocks and to improve overall dam stability, shear keys are placed in the vertical joints of the heightened dam.

5.2 Stability and internal stresses

The stability analysis is performed on a 2-D model of the dam-foundation-reservoir model, whereas the stress and strain analysis is carried out by means of the finite-element method using the program Z-Soil.

The calculations present maximum tensile stresses at the downstream dam toe of 3.1 MPa and 2.6 MPa for dynamic and static load cases, respectively. The maximum tensile strength of the concrete is 4.0 MPa. The maximum tensile stresses in the existing dam body are also localized at the downstream dam toe. However, due to the additional vertical load the tensile stresses in the existing dam body are significantly reduced. The compression stresses are increased accordingly but remain low. The maximum tensile stresses and shear stress in the joint between the existing and new concrete amount to 0.5 MPa and 0.4 MPa which is acceptable for the anchor rods.

Thermal conditions during the construction phase are of major importance for the maximum stresses. Due to the relatively small dam body, the thermal stresses exceed clearly the stresses due to static and dynamic loads. Since the maximum values for tensile stresses are located at the surfaces the tensile strength of the concrete does not have to respect the maximum values. However, to reduce cracking formation at the surface and to assure a frost-resistance and water tightness a compressive strength of the new concrete of 25 MPa has been chosen.

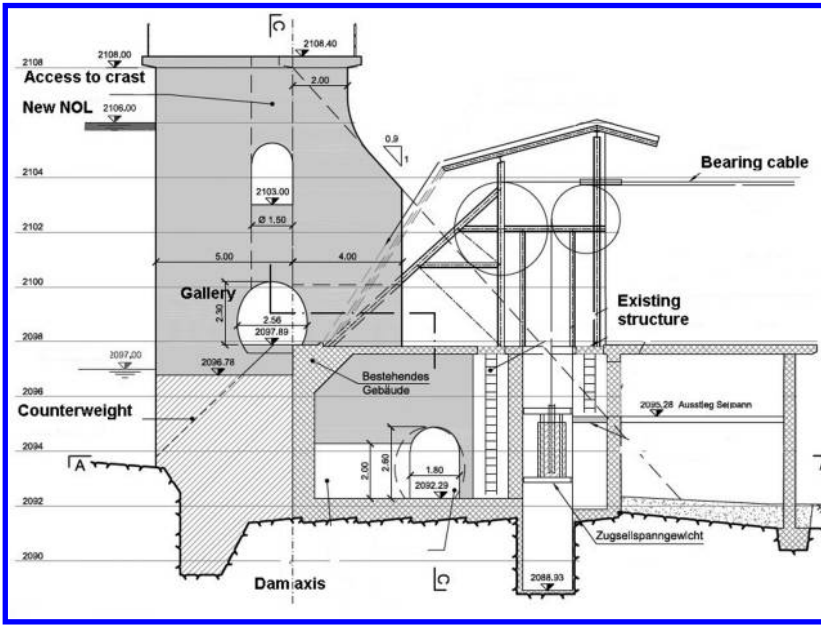


Figure 3. Section of cable car top station.

5.3 Integrated top station of the cable car

One important boundary condition of the project is to maintain operation of the existing cable car during the entire construction phase. Figure 3 shows the new layout of the dam and integrated station.

To respect the overturning stability of this block, either prestressed anchors or an enlargement of the upstream face have to be designed. Considering the drawbacks of the anchors (see 4.2) the most interesting solution is to enlarge the block on the upstream face by 2 m. This solution can be completed easily since the counterweight of the cable car serves as foundation for the enlargement. Other parts of the existing structure are adapted and integrated the heightened dam.

6 LOGISTICS

6.1 Means of transport to the construction site

Besides the design criteria for the dam itself, one of the most critical factors of the Kummnbord heightening project resides in the logistic challenge. Without any access road, the construction site cannot be reached by any road vehicle. Furthermore, a temporary access road would exceed the total budget for the project is therefore not an option. In conclusion, the construction site can only be reached by a cable car.

The existing cable car presents a maximum capacity of 6 tons. It is intended to keep in operation the existing cable car for passenger transport during the construction.

It is planned to install a temporary cable car with a capacity of about 12 to 15 tons for material transport. Any construction machine and construction material (including any site installations such concrete plant, etc.) need to be hauled to the valley station of the cable car, transhipped from the road vehicle to a special cable car transportation rig. Any heavy or oversize construction machine has to be disassembled for transportation.

The road up the valley station of the cable car also presents some delicate passages such as the Ernen village crossing and the single-lane tunnel leading to the Binn village. Those bottlenecks make transport of oversize loads impossible.

The aggregates for the concrete plant and the saddle earthfill dam can be extracted on site. However, specific treatment is necessary to optimize the concrete mixture. The binding material has to be transported from the valley to the site.

6.2 *Site installations*

The general concept for the dam heightening and construction is based on two installation sites. The gravel pit and material treatment zone will be situated on the present reservoir shore, entirely beneath the future water level. It will be reached by two access roads from the top station of the cable car. The concrete plant and the contractor's general installations will also be located on the future reservoir floor. Due to the danger of avalanches, these installations have to be protected or disassembled for the winter break.

The proper installations for the dam heightening will be located downstream the existing dam. It is planned to install three tower cranes for concrete works. The dam site installations also include wastewater treatment facilities, helicopter landing place, office containers, and staff canteen.

6.3 *Concrete plant*

An important issue of the planning of the site installation and construction schedule is the decision whether the concrete is produced on site or delivered from the valley. The advantages of a production on site are: use of aggregates from the site, characteristics of the concrete adapted to the specific requirements, less concrete additives required, the production is independent of the cable car and there is no or less risk of supply shortage.

On the other hand the drawbacks are: installation of a complete concrete plant on site is necessary, additional storage capacity is required, preliminary tests and a continuous quality control is needed.

Considering all aspects, neither the production on site nor the transport from the valley turns out as distinct best option. However, in respect to the tight construction schedule and to avoid delays due to long transportation route with the cable car as bottleneck, the production on site has been considered as favorable.

6.4 *Construction schedule*

The particular challenge of the construction concept is the alpine character of the site. Due to the high altitude (2100 m a.s.l.) construction works are only possible between June and October. Favorable weather conditions like early snow melting or late onset of winter would extend this period from May until November.

It is planned to conduct all works within two construction seasons. The year before starting construction works, the temporary cable car and most of the site installations should be installed.

During the first construction season, all demolition works on the existing dam and excavation works should be carried out. By the end of the first construction season, site conditions should be established ready for placing concrete. If possible, the first foundation concrete blocks can already be finished.

In the second construction season, all concrete works should be carried out. The site installations, the capacity of the concrete plant and the transportation system are designed to guarantee a continuous process without considerable interruption. The grouting works are carried out in parallel with the concrete works and should be finished by the end of the second year.

The removal of the site installation and temporary cable car is planned at the beginning of the following year.

7 SUMMARY

The Kummenbord reservoir expansion from actual 160,000 m³ to 1,000,000 m³ requires the heightening of the existing Kummenbord dam from 10 m to 20.5 m. The total length of the concrete gravity dam will reach approximately 200 m.

Among the several studied heightening solutions, a downstream extension with a gravity dam section has been chosen. The dam crest width measures 2.0 m, the base width 15 m. The downstream face features a slope of 0.9/1.0 (H/V). Anchor rods between the existing and new concrete provide for monolithic behavior of the heightened dam. An inspection and drainage gallery along the existing downstream provides access to the service chamber and the dam crest. The concrete volume to place totals some 14,000 m³. The total excavation volume (Monte Leone gneiss and loose rock) amounts to some 5000 m³.

The major technical requirements include the maintenance of operation of the reservoir, the integration of the service chamber and the cable car station, and the maintenance of the flood control and outlet devices.

Amongst the numerous technical requirements, the logistics represent a major challenge for the construction. With no access road, all site installations and construction materials (except for gravel) need to be transhipped and transported by a temporary cable to the construction site on 2100 m a.s.l.

ACKNOWLEDGEMENTS

The authors express their appreciation to Bernhard Truffer, Technical Director at Gommerkraftwerke AG, for his support.

REFERENCE

STUCKY SA (2009): Bauprojekt, Vergrößerung Ausgleichsbecken Kummenbord.

Deriner double curvature arch dam—foundation consolidation and curtain grouting

K.A. Ross

Pöyry Energy AG, Zurich, Switzerland

M. Kaleli

Dolsar Engineering Ltd, Ankara, Turkey

ABSTRACT: The depth of consolidation grouting below the dam was expected to be 30 m over the full area of the dam footprint during the initial design stages; however, the depth was later reduced to a minimum of 10 m on the upper right and left banks of the dam (whilst maintaining a depth of 30 m in the river bed area). During the initial design stages, the envisaged depth of the grout curtain was approximately 2/3 of the reservoir depth (circa 160 m). Primary holes were foreseen at intervals of 24 m, and higher order holes were expected to be routinely drilled to full depth, giving a final hole to hole spacing of 3 m. After completion of one grout curtain test panel, the depth of all holes was decreased significantly, and the depth routinely drilled to with a hole to hole spacing of 3 m was reduced to only 1/5 of the reservoir depth (50 m).

1 INTRODUCTION

Deriner Dam has a height of 249 m from the lowest foundation level, and has a crest length of 720 m. It consists of 40 blocks with a width of 18 m, and a maximum upstream to downstream block length of 55 m at the base of the crown cantilever section. The area of the dam footprint is approximately 48,500 m².

The design of the dam foundation grouting works commenced in 1991, ten years prior to the commencement of any construction activities on site. Modifications to the design were initially made in 2003 and 2005, as the dam excavation progressed.

An extensive grout mix trial programme was undertaken in 2005 and 2 grout mixes satisfying all design criteria were identified.

In 2006, one foundation consolidation grouting test area and two curtain grouting test panels were executed. These tests provided information that enabled the design of the grouting works to be optimised.

2 GEOLOGY

The bedrock in the dam foundation consists mainly of tectonically disrupted quartz diorite, mainly coarse grained and partly granodiorite, with varying thicknesses of intrusive dykes. Numerous diabase dykes outcrop in the dam site and provide key discontinuities inside the granitic rock. The contacts of the main dykes are strongly tectonized with schistose zones up to 3 m in width, and tend to be more jointed than the granitic bedrock due to their weaker resistance to tectonic action.

3 GROUT MIX TRIAL PROGRAMME

The grout mix trial programme was performed using different sources of cements, plasticisers, super-plasticisers, accelerators and bentonite. It was necessary to identify a stable grout mix with the characteristics given in [Table 1](#).

During the mix trials, water cement ratios of 0.6, 0.7, 0.8, 0.9 and 1.0 were used, with and without admixtures. After using Type 1 Portland cement in the initial trials, extra fine cement was introduced (which will enhance the penetration of the grout into fine fissures during dam foundation grouting). The specification for extra fine cement required a Blaine value in excess of 3500 cm²/g, and 100% and 98% passing the 0.08 mm and 0.04 mm sieves respectively.

The amounts of admixtures used for each water/cement ratio are given in [Table 2](#).

After completion of the extensive trials, the grout mix designs given in [Tables 3](#) and [4](#) were chosen for all rock grouting work.

Table 1. Required grout mix characteristics.

Grout mix characteristic	Requirement
Viscosity	30 ± 2 seconds (Marsh Cone)
Sedimentation	Maximum 5% after 2 hours
Density	Minimum 1.5 g/cm ³
Compressive strength	Minimum 15 MPa after 28 days
Setting time	Initial after 8 to 10 hours

Table 2. Quantities of admixture used in trial grout mixes.

Admixture	Percentage by weight of cement								
	0.3	0.5	1.0	1.1	1.2	1.5	1.8	2.0	3.0
Plasticiser	0.3	0.5							
Super-plasticiser	1.0	1.1	1.2	1.5	1.8	2.0	3.0		
Bentonite	0.5	0.8	1.0	2.0					

Table 3. Grout mixes chosen for dam foundation grouting.

Mix	Water/cement ratio	Super-plasticiser (% of cement)	Accelerator (% of cement)	Density (g/cm ³)	Sedimentation (% after 2 hours)
M1	0.8	1.1	0.0	1.543	2.0
M2	0.8	1.1	2.0	1.577	1.2

Table 4. Grout mixes chosen for dam foundation grouting.

Mix	Viscosity (Secs)	Setting time		Compressive strength at 7 days (kg/cm ²)
		Initial (hr:min)	Final (hr:min)	
M1	32.1	11:50	16:55	156.3
M2	32.3	07:05	10:45	139.3

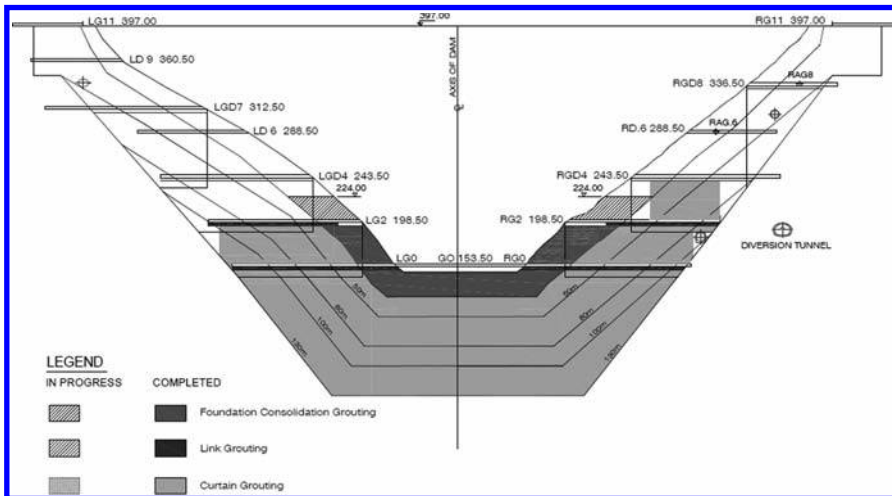


Figure 1. Status of dam foundation consolidation and curtain grouting.

4 PROGRESS OF FOUNDATION GROUTING

The current status of dam foundation consolidation and curtain grouting is presented in [Figure 1](#). All consolidation and curtain grouting required below the lowest dam and rock gallery has been completed. Both consolidation and curtain grouting works remain ongoing on both dam abutments.

5 FOUNDATION GROUTING METHODOLOGY

5.1 *Drilling and grouting*

All holes were drilled by rotary methods, with diameters between 56 mm (cored holes) and 48 mm. Upstage grouting methods were used in 5 m long stages from the bottom to the top of the holes. Downstage methods were only permitted in holes prone to collapse, or where other conditions prevailed that made upstage methods prohibitive. The maximum allowable hole deviation is 3% of the hole depth. Grouting holes were drilled from rock grouting galleries, rock access galleries, dam galleries and from the ground surface immediately upstream and downstream of the dam faces.

5.2 *Water pressure tests*

Water pressure tests were performed in the cored primary holes and check holes. The water test pressures and relevant depths are given in [Table 5](#).

5.3 *Acceptance criteria*

The fundamental requirements for acceptance of any stage in a consolidation or curtain grouting hole are listed below:

- Cement take of 45 kg/m above 50 m depth.
- Cement take of 60 kg/m between 50 m and 80 m depth.
- Cement take of 80 kg/m below 80 m depth.
- Lugeon value of 5.

Table 5. Water test pressures and depths.

Depth (m)	WPT pressure (bar) for consolidation	WPT pressure (bar) for curtain
0-5	2-4-2	2-4-2
5-10	3-6-3	3-6-3
10-20	3-6-8-6-3	3-6-10-6-3
>20	3-6-10-6-3	3-6-10-6-3

Table 6. Refusal criteria.

Depth (m)	Grout absorption (litre/m/min)
0.0-5.0 & 5.0-10.0	0.2
10-15.0 & 15.0-20.0	0.3
20.0-25.0 & 25.0-30.0	0.4
>30	0.5

Table 7. Refusal pressures.

Depth (m)	Refusal pressure (bar) for consolidation	Refusal pressure (bar) for curtain
0.0-5.0	3	5
5.0-10.0	5	10
10.0-20.0	8	30
20.0-30.0	12	30
>30.0	-	30

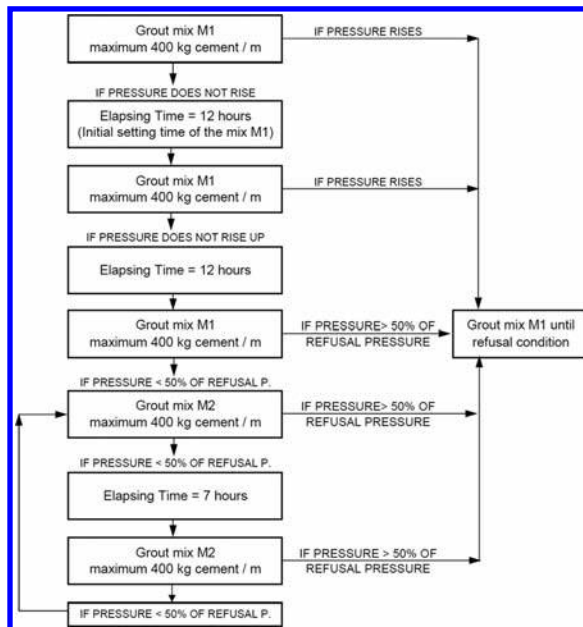


Figure 2. Flow chart for foundation grouting.

In the event that the cement take or Lugeon value exceeded the above magnitudes, higher order holes are drilled to one stage below the relevant stage, on both sides of the hole. The 5 Lu acceptance criteria relates to primary and check holes only, where water tests are required.

5.4 *Refusal criteria and pressure*

The execution of grouting in any stage was considered complete if the take was less than the values given in [Table 6](#).

The refusal pressures applicable to the criteria given in [Table 6](#) are given in [Table 7](#).

5.5 *Flow chart*

For the execution of foundation consolidation and curtain grouting, the flow chart shown in [Figure 2](#) was used.

6 FOUNDATION CONSOLIDATION GROUTING

6.1 *Purpose*

The principle purpose of consolidation grouting is to improve the quality of the foundation immediately below the dam, and to a shallow depth (up to 30 m). Improvements include enhancing the rock mass strength and elastic properties, providing more uniform parameters, reducing settlements and increasing water tightness.

6.2 *Test area*

A consolidation grouting test area at the centre of the dam close to the downstream face was specified to enable the proposed equipment and methodology to be tested. The results of the grouting work would also give an indication of the foundation permeability within the envisaged limits of the consolidation grouting bulb.

The test area measured 24 m by 24 m, and included a grid of primary holes at 12 m intervals, followed routinely by secondary holes which reduced the hole to hole spacing to 6 m. Tertiary holes were drilled and grouted and if the acceptance criteria had not been met. The depths of all holes were between 30 m and 38 m.

A total of 5 cored primary holes were drilled with a diameter of 56 mm. The remaining primary holes, as well as the secondary and tertiary holes were drilled using rotary rigs, but without core recovery. Following completion of the above holes, inclined check holes were drilled (cored) with a diameter of 56 mm. Hole deviations were measured during drilling.

6.3 *Test area results*

Water pressure tests were carried out in primary, tertiary and check holes. Thirty stages in primary holes were tested to get an indication of pre-grouting permeability. When the grouting was close to completion, 33 stages were tested in tertiary and check holes.

The average cement take in the primary holes was 108.8 kg/m, but this reduced to 29.6 kg/m in the tertiary holes. The percentage of water pressure test stages giving Lugeon values above 5 decreased from 56% to 24%.

6.4 *Drilling locations*

Holes for foundation consolidation grouting are required from the excavated surface close to the upstream and downstream face of the dam, from galleries inside the dam (approximately parallel to the foundation surface), and from access galleries excavated in rock inside the dam abutments.

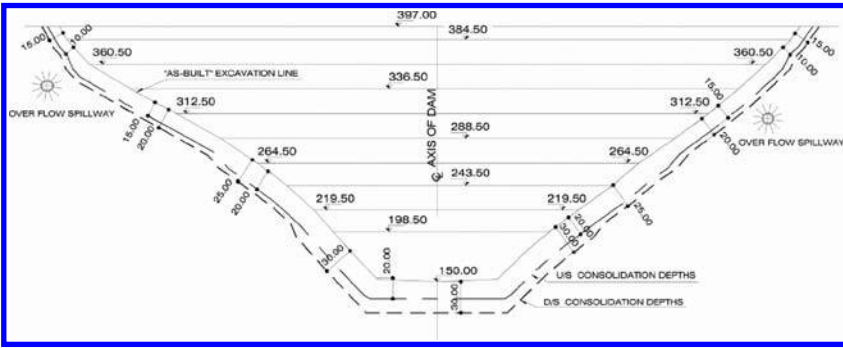


Figure 3. Depths of consolidation grouting holes.

6.5 Extent of consolidation grouting zone

The upstream extent of the consolidation grouting zone (in plan) is 10 m, apart from a short length close to the dam crest where the extent is reduced to 6 m on both abutments. On the downstream side of the dam, the extent of the “bulb” in plan is between 15 m and 30 m, and always equals the “bulb” depth.

Figure 3 shows the depths of the consolidation grouting below the upstream and downstream faces of the dam. The depth of the bulb is shallower below the upstream face due to the lower stress levels that will be imposed by the dam.

6.6 Hole size and pattern

The diameters of cored and non-cored consolidation grouting holes are 56 mm and 48 mm respectively. Fans of holes were drilled to provide a grid of holes with a maximum spacing of 3 m at the concrete/rock interface. These holes penetrated the rock by 1 m. The deeper consolidation grouting holes provide a grid with a maximum hole spacing of 6 m at a depth of 20 m below the dam.

6.7 Consolidation grouting test results

Below the lowest dam gallery, the percentage of takes above 45 kg/m reduced from 31% in the primary holes to 5% in the secondary holes.

Water pressure tests were carried out (after completion of secondary holes) in 45 intermediate tertiary and quaternary holes. The Lugeon values in 62 of the 226 stages exceeded the 5 Lu criteria, and additional quaternaries holes were drilled and grouted accordingly.

7 FOUNDATION CURTAIN GROUTING

7.1 Purpose

The principle purposes of curtain grouting are to limit seepage losses through the dam foundation, and to minimise uplift pressures below the dam.

7.2 Drilling locations and orientations

All holes required for curtain grouting are drilled from rock or dam galleries. The grout curtain holes are drilled vertically on a single row, and in a single plane, from the lowest dam/rock gallery. Between the rock galleries, the holes are inclined to enable them to pass on the upstream side of the gallery below. The curtain is closed by a fan of link holes drilled in the upstream direction from the lower gallery, see Figure 4.

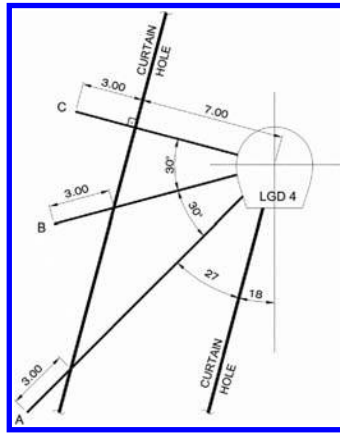


Figure 4. Layout of grout curtain link holes.

7.3 Test panels

Two grout curtain test panels were executed from rock galleries in the lower dam abutments. The initial test panel was executed in the lowest rock gallery on the left abutment of the dam, and consisted of 5 primary holes spaced at 12 m, followed by secondary and tertiary holes using the “split spacing” method. All holes were systematically drilled to a depth of 160 m (approximately 2/3 of the maximum reservoir depth). Higher order holes and check holes were subsequently drilled until the test panel was deemed satisfactorily complete in accordance with the specified criteria. The second test panel was drilled between the lowest two rock galleries on the right abutment of the dam.

7.4 Conclusions from initial test panels

The test panel results, which were considered to be representative of the central part of the dam foundation, indicated a distinct change in grout take at a depth of 30 m for all 32 holes. In this upper zone, cement takes ranged between 0 and 450 kg/m (measure in one 5 m stage only). Below a depth of 30 m, no cement takes exceeded 45 kg/m in any stage. This result was verified by inspection of the cores taken from the primary holes (which indicated “impermeable rock” below 30 m).

Low Lugeon values (less than 5) and low grout takes were also observed where the test panel passed through several “major faults” and “prominent joint sets” shown on the surface geological maps.

It was therefore considered safe to assume that the permeability (transmissivity) of the rock mass is very low. In high quality igneous rock formations (low percentage of open joints), the objective of the grout curtain generally changes its priority from reducing an initially already low transmissivity, to limiting piezometric levels and uplift forces downstream of the curtain and below the dam. These priorities are achievable with a grout curtain of shallow depth, typically less than 50% of the maximum hydrostatic head.

7.5 Extent of curtain grouting zone

Following consideration of the results of the test panels, the depths of the holes for the main grout curtain were specified as follows:

- Primary holes: 24 m spacing, maximum depth 130 m (53% of reservoir depth).
- Secondary holes: 24 m spacing, maximum depth 100 m (40% of reservoir depth).
- Tertiary holes: 12 m spacing, maximum depth 80 m (33% of reservoir).
- Quaternary holes: 6 m spacing, maximum depth 50 m (20% of reservoir depth).

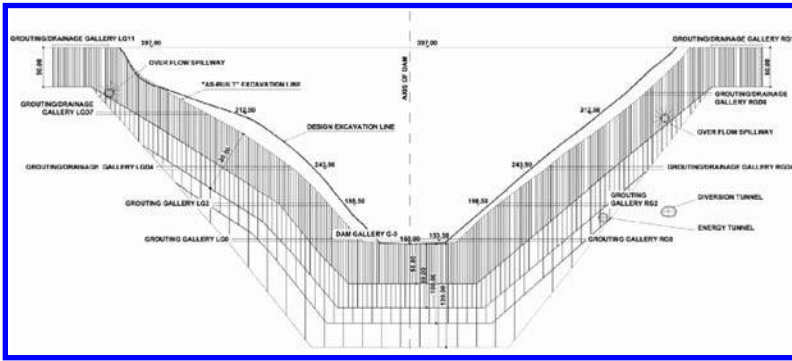


Figure 5. Extent of grout curtain holes.

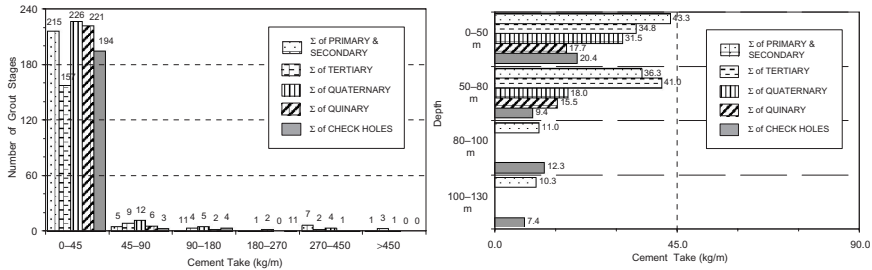


Figure 6. Summary of curtain grouting results from lowest gallery.

All holes were systematically drilled to their full depth, giving a final hole to hole spacing to a depth of 50 m below the dam of 3 m. In the event that any hole gave a high grout take (in excess of the acceptance criteria of 45 kg/m of cement), the higher order holes were drilled to one stage below the high take location.

The extents of the grout curtain holes are shown in [Figure 5](#).

7.6 Results of curtain grouting

Summaries from the curtain grouting results, for the area of the foundation directly below the lowest gallery in the dam (which took the most grout to date) are given in [Figure 6](#).

8 CONCLUSIONS

The extensive mix trials performed identified optimal stable grout mixes with a water/cement ratio of 0.8, using 1.1% of super-plasticiser (by weight of cement). Consolidation grouting test results provide evidence of a satisfactorily treated foundation to a maximum depth of 30 m. Results from the execution of the grout curtain fully vindicate the decision to substantially reduce the depth of the secondary and higher order holes, by consistently showing a negligible number of grout stages with cement takes in excess of 45 kg/m.

ACKNOWLEDGEMENT

The work of the authors in relation to foundation consolidation and curtain grouting below Deriner Dam was performed with the expert guidance of Dr Harald Kreuzer, Dam Expert, whose significant contribution to the Project led to the decisions made and the conclusions reached. The authors thank Dr Harald Kreuzer for his significant input to the Project.

Application of grouting technique for stabilization of coarse materials—Karkheh storage dam experience, Iran

M. Heidarzadeh

Faculty of Civil Engineering, Tarbiat Modares University, Tehran, Iran

F. Eslamian

Mahab Ghodss Consulting Engineers, Tehran, Iran

A. Mirghasemi

Faculty of Civil Engineering, University of Tehran, Tehran, Iran

ABSTRACT: This paper summarizes results and experiences obtained from stabilization of relatively coarse materials of drain using grouting technique in the Karkheh dam, southwest Iran. The grouting works performed at the Karkheh dam were part of the prerequisites for development of the dam's complementary cut-off wall. Since the dam was completed, the execution of the new cut-off wall from the dam crest was inevitable. Hence, one of the main difficulties associated with the development of the new wall was trenching and execution of plastic concrete wall through relatively coarse materials of the drain in the dam body. A full scale platform consisting actual drain materials was constructed and underwent various tests. Results of the testing program revealed that a Water/Cement mix ratio of 1/(1.5–2) can successfully stabilize the drain materials. After finalizing the technical characteristics of grouting, the method was applied on the drain materials of the Karkheh dam body. The results were satisfactory and the materials were stabilized successfully so that the cut-off wall was executed without any technical problem.

1 INTRODUCTION

Compared to other fields of civil engineering, grouting technique is a relatively new practice and still many new experiments and researches are needed for its development. In the past two centuries, this technique has been used in many civil works including permeability reduction, improvement of mechanical properties and soil stabilization.

Especially, this method has been widely applied in the field of dam engineering with the emphasis on water sealing of many dam foundations. Although considerable improvements have been introduced into the field of grouting of medium to fine materials in the recent decades, there are many unknowns in the grouting of coarse materials. A tentative review of international efforts in this field reveals that very little work has been performed or at least published in the grouting of coarse materials. Therefore, in this paper we report and analyze application of grouting technique for stabilization of coarse materials of drain at the Karkheh dam site, southwest of Iran. The grouting practice was employed in order to facilitate the execution of the dam's complementary cut-off wall. Part of this new cut-off wall should be performed through the dam body, and hence the stabilization of drain material was a must.

During each drilling and trenching activity, it is necessary to apply an appropriate drilling fluid in order to stabilize the trenching walls. In the trenching of drain materials, since the medium is highly permeable, the excessive slurry loss will occur, and thus it is necessary to reduce the permeability of the medium before trenching through grouting. In the next sections, at first a short review of the Karkheh dam project will be presented, and then the experiment procedure and results of the grouting practice in the drain materials of the Karkhe dam body will be discussed.

2 KARKHEH PROJECT AND THE LOCATION OF GROUTING

Karkheh storage dam is the largest dam in Iran in view of reservoir water capacity with about 7400 million cubic meters of water at the maximum water level. Karkheh dam and hydro-power project is located on the Karkheh river, the third largest one in Iran in terms of flow discharge. Karkheh is an earth core rock-fill dam having height of 127 m and 3030 m length (MGCE, 1998). The Karkheh Dam provides about 4 billion cubic meter of regulated water to irrigate 320,000 hectares of downstream farmlands (MGCE, 1998 and Mirghasemi et al., 2004). **Figure 1** presents the general plan of the Karkheh project. A plastic concrete cutoff wall was considered as the dam water sealing system. In addition to the dam main cutoff wall, another cutoff wall can be seen in **Figure 1** which was performed at the north and east of the powerhouse to decrease seepage at the slope overlooking the powerhouse (Heidarzadeh et al., 2006). **Figure 2** shows the height and extension of the dam main cut-off wall.

When reservoir filling started in 2001, water seepage from dam foundation and abutments were higher than had been anticipated before. As a result of such excessive seepage at the relatively high reservoir water elevation, uplift pressure and hydraulic gradient of the discharged water from the dam foundation increased. By increasing the reservoir water elevation and arriving at the elevation 210.50 in March 2004, the necessity for taking remedial measures became evident. A series of remedial measures were implemented to increase the safety factor of the dam among which was the extension of the main cut-off wall both at the right and left banks of the dam (cut-off walls 11-a, 11-b, 11-c, and 11-d in **Figure 1**). The main objective of this measure was to keep the foundation uplift and hydraulic gradient of the discharged water within the acceptable limits (IWPDC, 2004).

The general plan of the mentioned complementary cut-off walls is shown in **Figure 1**. The execution of the complementary cut-off wall was a unique experience in this field and was associated with many technical difficulties which required most update engineering techniques and equipments. Among most important encountered difficulties were, connection between the new and old cut-off wall, trenching and execution of plastic concrete wall through relatively coarse materials including drain and filter, approaching the old cut-off wall, and finally construction of the connecting panel.

In this paper we discuss the procedure used for execution of the powerhouse connection cut-off wall (cut-off entitled 11-b in **Fig. 1**). The dam cross section at the location of this cut-off is shown in **Figure 2**. Also, **Figure 3** shows the soil grading curve of the materials to be treated.

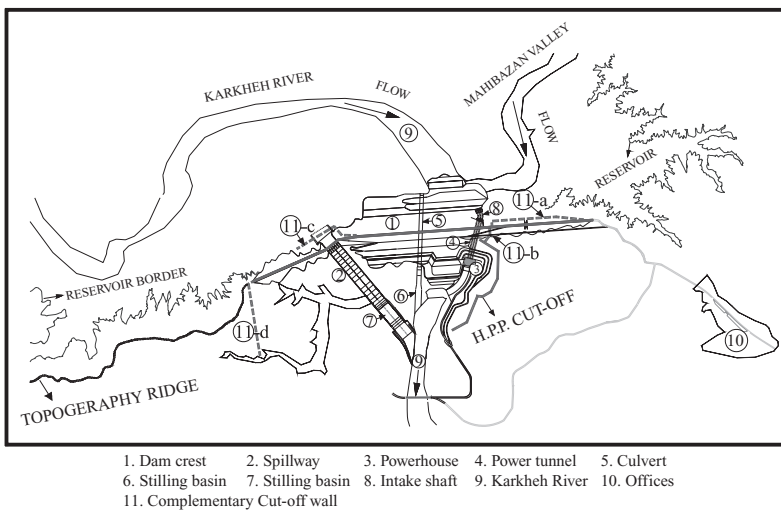


Figure 1. General plan of Karkheh dam and hydropower project. Thick solid and dashed lines represent the old and new cut-off wall respectively.

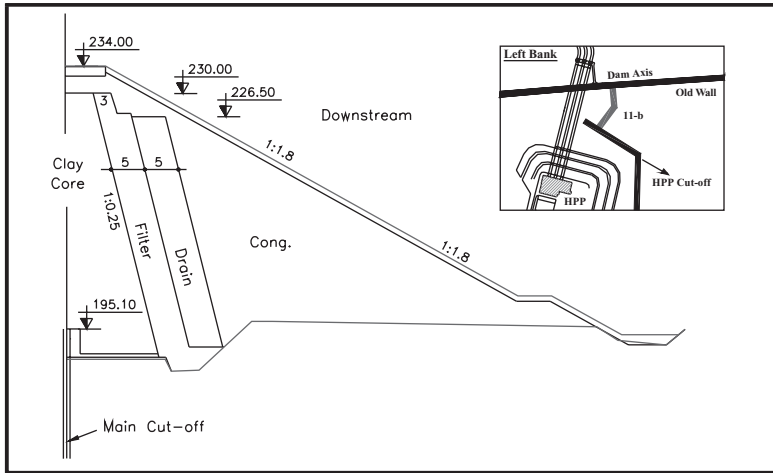


Figure 2. The section of the Karkheh dam body at the location of the powerhouse connection cut-off wall (cut-off entitled 11-b in Fig.1).

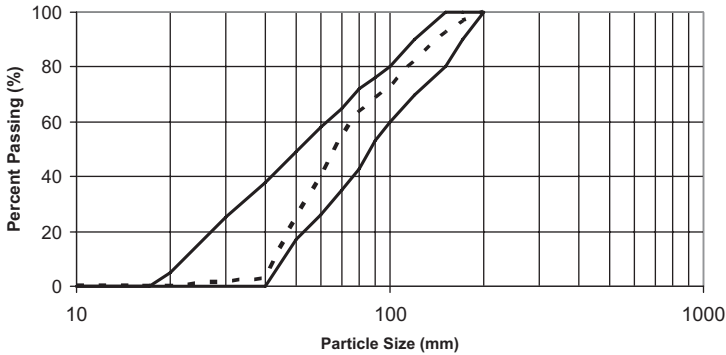


Figure 3. The grain size curve of the drain material.

3 CUT-OFF EXECUTION IN DRAIN

Execution of cut-off wall through coarse material of drain is associated with many difficulties and to the authors's knowledge such practice has not been experienced in the field of dam engineering or at least is not published. The main challenges in the trenching and execution of cut-off wall in drain arises from excessive slurry loss due to its high permeability as inferred from Figure 3. This could cause serious consequences including:

- Excessive slurry loss in one hand makes the execution of the wall impossible and in the other hand is followed by many risks. Slurry loss may cause the trench to collapse. In this case the expensive trench-cutter will be buried at depths of the dam foundation and a huge economical damage will be created.
- The excessive slurry loss through drain will pollute these materials and thus prevents it from its vital role for safe passage of seeped water.

Regarding above, special protective measure should be employed in order to prevent excessive slurry loss and also to stabilize the drain material. To reach this goal, the grouting technique was the only possible option. As discussed earlier, there were no experience in this field and thus, extensive trial grouting was done to reach appropriate grout mix design, grouting-hole pattern, required grouting pressure and other related issues. In the next sections, the results of experiments are discussed.

4 TRIAL GROUTING PLATFORM AND RESULTS

Using the dam's actual materials, a trial platform with the dimensions of 20 × 20 m was constructed in the site. Figure 4 shows the plan and two cross sections of the platform along with the test holes arrangement on it. As shown, 8 grouting holes along with 8 test holes in a triangular pattern were used for trial grouting.

All grouting and test holes were drilled to depth of about 5.5–6 m. All of the holes were water-flushed rotary-drilled. Based on Figure 4, the D holes were injected with cementitious grouts with a water:cement proportion of 1:2 along with 10% by volume of bentonite, 1% of sodium silicate, and 0.5% of TEA (Tri Ethanol Amine). The mix design used for grouting in DF holes was the same as the D holes with the exception that the water:cement proportion was 1:1.5. The down-hole method was applied for grouting in the holes. Since no tube-e-manchette was used in the holes, the application of down-hole grouting technique was inevitable. To maximize the efficiency of the process, the grouting was performed in certain intervals such as 1 m, and re-drilling was used. To prevent possible excessive grout take, the grouting pressure was kept below 5 bar throughout the grouting process. Figure 5 presents examples of the amount of grout take in some of the grouting holes. We note that we kept the volume of the required grout in each stage constant since the medium to be grouted was uniform.

To assess the effectiveness of the grouting program, the water pressure tests were conducted at the intermediate holes (test holes). In the case of back water flow from these holes, it could be inferred that the grouting was successful. However, water take reveals that still

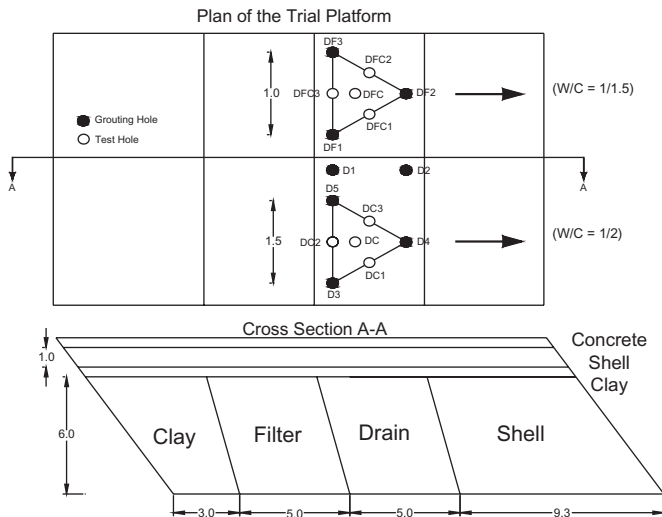


Figure 4. Plan and a cross section of the trial platform for grouting of drain. Dimensions are in meters.

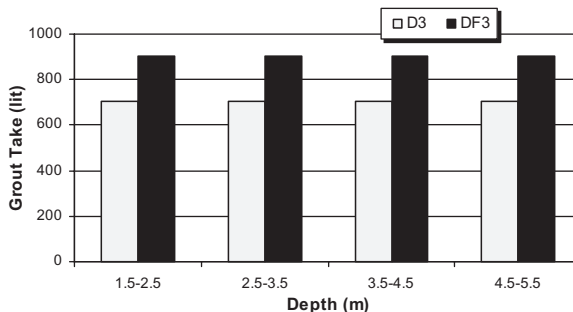


Figure 5. Amount of grout take in D3 and DF3.

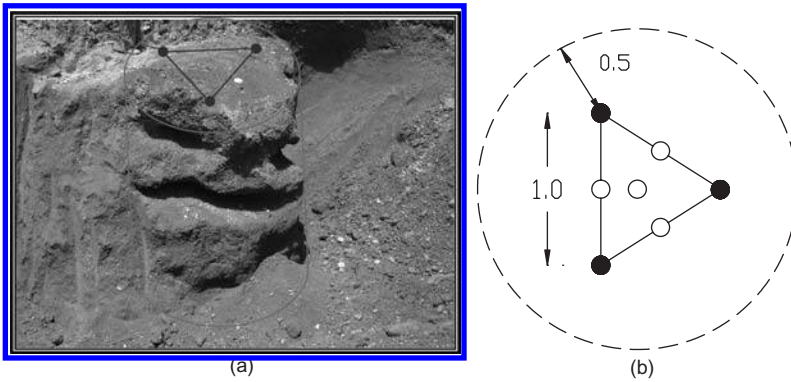


Figure 6. The stabilized drain around the D grouting holes (a) and the inferred stabilization pattern from it (b). Dimensions are in meters.

there were unfilled voids in the medium. As a whole, the water pressure tests in the intermediate holes revealed that each grouting hole was capable of stabilizing a distance of about 0.5 m of its axis creating a stabilized circle with the diameter of 1 m around its axis.

The above pattern was confirmed through trenching of the trial platform after 48 hours (Figure 6a). The creation of a stable cylinder with the radius of about 0.5 m around the D holes is evident in Figure 6a. According to this actual observation, we were able to determine the stabilization pattern as Figure 6b. However, Figure 6a shows that some parts of the drain remains untreated indicating that at least two rows of grouting lines are necessary for complete stabilization of the medium. In conclusion, the main findings of the trial grouting can be summarized as follows:

1. A cement grout with the water: cement proportion of 1:1.5 to 1:2 along with a 1 to 1.5 m hole spacing is appropriate for grouting of drain materials
2. Application of at least two grouting rows is necessary to achieve a uniformly treated medium
3. The grouting pressure should be limited to about 5 bar
4. The amount of grout take is about 700–900 lit/m

5 APPLICATION OF THE METHOD AND ACTUAL RESULTS

After successful application of the cement grouting technique in the stabilization of the drain materials at the trial platform, we apply this method at the drain of the dam body. Before proceeding towards this, it is necessary to design the grouting plan. The main considerations for designing the grouting plan are:

- To limit the grouting range in the desired range
- To prevent excessive grout take
- To completely stabilize the medium without leaving untreated parts

Due to the above considerations, three circles as well as a row of grout holes were used as shown in Figure 7 including P series at the outer side, T series at the middle, Q series at the inner side, and a row of holes in the center of Q series. The role of P holes is to produce a limited environment to introduce the subsequent grouting of T and Q holes. It is evident that the excessive grout takes in the grouting of P holes is very likely, thus it is very important to perform these grouting with relatively low grouting pressures and close hole-spacing.

A hole spacing of 1 m along with the relatively dense grout having W/C ratio of 1/1.5 was applied to the P holes. Throughout the process of grouting in P holes, the exerting pressure was below 5 bars and amount of grout take was carefully controlled. Figure 8 presents examples of grout take in two adjacent holes from P series. P13 was grouted prior to P12.

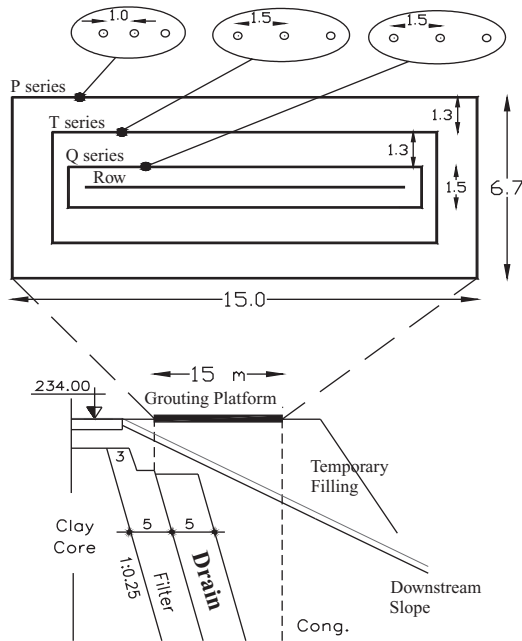


Figure 7. Grouting holes and their location in the dam body. All dimensions are in meters.

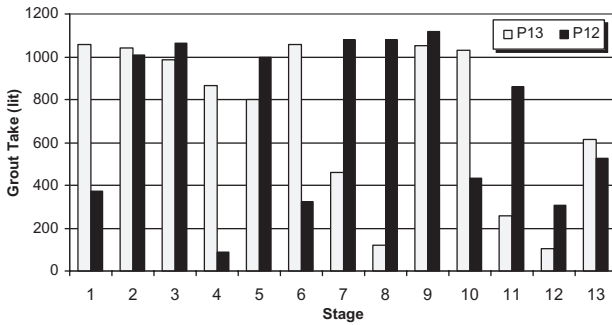


Figure 8. Examples of grout take in two adjacent holes from P series.

As can be seen, the average grout take in each stage is about 1000 lit except for some special stages which can be attributed to the possible local complexities. However, whenever the grout take in one stage is very little, the amount of grout take in the neighboring stage is high. This emphasizes that at least two rows of grouting is necessary.

Table 1 presents the details of mix design used for grouting. As can be seen, the W/C ration in the row grouting was reduced to 1/(0.75). The reason was to prevent the high compressive strength of the grouted medium. Since the grouted area was going to be trenched by a special trench-cutter, it is very important that the strength of the medium to be in the acceptable range. However, since the P, T, and Q series were grouted before the row grouting, we were certain that the excessive grout take would not occur.

Figures 9 and 10 present examples of grout take in two adjacent holes from T and Q grouting holes respectively. T6 and Q7 were grouted before T7 and Q6 respectively. These Figures reveal that excepting some limited stages, the total grout take in the T and Q holes is reduced which can be attributed to the effect of grouting in P holes.

After the grouting practice was completed, the supporting walls were executed through the drain since the medium was impermeable enough and there was not the risk of slurry loss.

Table 1. Details of mix design used for grouting.

Hole name	W/C	B ¹ (% of cement)	S ² (% of cement)	CaCl ³ (% of cement)	TEA ⁴ (% of cement)
P	1/1.5	1	1	0.2	0.05
T & Q	1/1.5	0.5	1	0.2	0.05
Row	1/0.75	3	3	0.3	0.05

¹Bentonite; ²Sodium Silicate; ³Calcium Chloride; ⁴Teri Ethanol Amin.

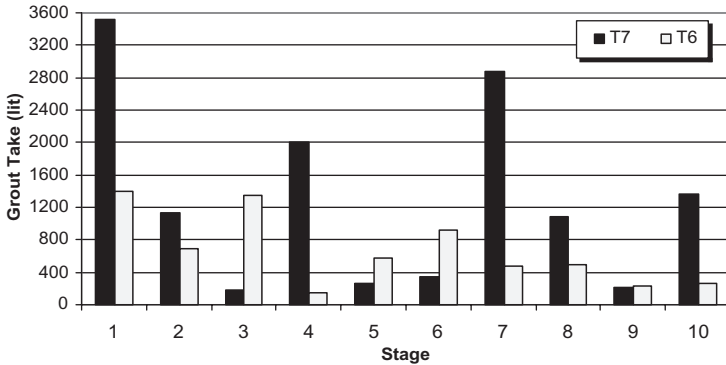


Figure 9. Examples of grout take in two adjacent holes from T series.

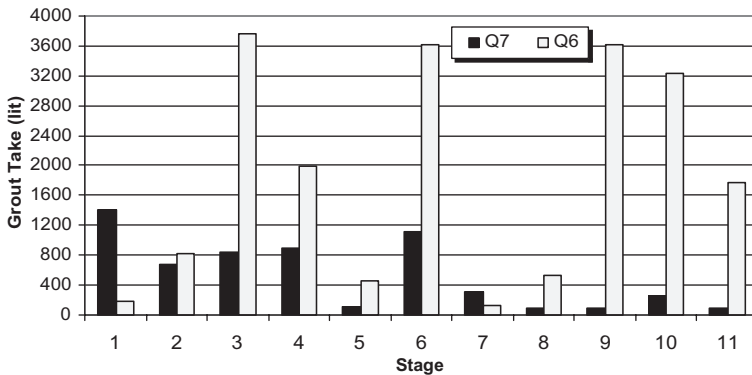


Figure 10. Examples of grout take in two adjacent holes from Q series.

Observations during the execution of the supporting walls showed that the grouting practice was successful in stabilization of drain. Table 2 presents records of slurry loss during the cut-off execution. It is clear that the rates of slurry loss are quite slow indicating the performance of grouting. However, Table 2 demonstrates that the rate of slurry loss in Panel SPEH (1–6) is considerable. This panel is a contact panel at the interface of drain and shell zones. Generally, high rate of slurry loss in these interface zones is expected.

5.1 The method of drilling and grouting

Drilling in the drain was one of the challenges encountered during the project. The challenge was associated with the removal of the cuttings from the hole in the shell material. It was observed that the water-flushing was not capable of removing the cuttings and thus, a relatively dense drilling fluid was employed. This fluid was a solution of bentonite and water

Table 2. Rates of slurry loss during the execution of supporting wall.

Panel name	Level of slurry loss (m)	Rate (Cm/min)
SPEH(1-4)	11.5	5
	13	6
	17	6
	25	4
SPEH(1-5)	22	1
SPEH(1-6)	20	23

with the proportion of B/W = 1/10. All of the drilling works were of rotary type. In summary, the drilling and grouting of the holes were composed of the following steps:

1. Drilling of the hole until the top of the drain material using a dense drilling fluid (as discussed above)
2. Installing a steel casing with the diameter of 131 mm until the top of the drain material and applying a weak grout around it
3. Leaving the hole for at least 24 hr for strength gaining
4. Drilling of the drain to the diameter of 96 mm with the interval of 1 m and using water-flushing
5. Grouting of the drilled section in the 30 cm intervals

We note that, in our method, the grouting was performed through a dropper at the head of the driller. This allowed us to perform the grouting without removing the driller from the hole.

6 CONCLUSIONS

Grouting technique was employed to stabilize and to reduce the high permeability of the drain material of the Karkheh dam body. Based on the full scale trial grouting and actual application of the method, the following conclusions can be made:

1. A cement grout with the water: cement proportion of 1:1.5 to 1:2 along with a 1 to 1.5 m hole spacing is appropriate for grouting of the Karkheh-type drain materials.
2. Application of at least two grouting rows is necessary to achieve a uniformly treated medium.
3. The grouting pressure should be limited to about 5 bar.
4. To prevent excessive grout take, the application of at least two rows of circle grouting is necessary. In this pattern, the outer circle includes close hole-spacing along with a relatively dense grout.
5. The amount of grout take in the Karkheh-type drain materials is about 900 lit per stage of grouting.

REFERENCES

- Heidarzadeh, M., Mirghasemi, A.A., Eslamian, F., Niroomand, F. and Etemad Zadeh, S.M. 2006. Construction of Pressure Relief wells Under Flowing Artesian Conditions, Karkheh Storage Dam-Iran. 74th Annual Meeting of ICOLD, May 2006, Barcelona, Spain.
- Iran Water and Power Resources Development Company (IWPDC), 2004. Technical Meeting Memorandum in Germany, 1-5 November 2004, Munich, Germany.
- Mahab Ghodss Consulting Engineers (MGCE), 1998. Karkheh project technical report of dam body and foundation, 138 pages, Tehran, Sep. 1998.
- Mirghasemi, Ali, A., Pakzad, M. and Tarkeshdooz, N. 2004. Rehabilitation of Karkheh dam foundation after four years of impounding. Proceedings, 72nd ICOLD annual meeting, Seoul, South Korea.

Dam safety and operational efficiency improvements in Sri Lanka

A. Sorgenfrei & M. Friedrich

Pöyry Energy Ltd., Zürich, Switzerland

ABSTRACT: Many of the dams in Sri Lanka are ageing and suffer from various structural deficiencies and shortcomings in their operation and maintenance procedures. To overcome these inadequacies, the Dam Safety and Water Resources Project (DSWRPP) was initiated in August 2008, with the assistance of World Bank financing. The project includes the rehabilitation of 32 major dam structures that show signs of risk or deterioration. This paper describes the present situation of dams in Sri Lanka and their current deficiencies. The main focus lies in the description of the various activities to be treated under DSWRPP, which approaches the basic dam safety elements; these include the upgrade of structural safety, dam monitoring and maintenance, and lastly emergency planning. The activities are explained in detail together with examples of remedial measures carried out during the dam safety project.

1 INTRODUCTION

1.1 *Dams in Sri Lanka*

The irrigation systems, hydropower generation schemes and water supply networks of Sri Lanka include reservoirs impounded by approximately 350 medium and large dams, and over 12,000 small dams. Eighty of the medium and large dams are higher than 5 m and have reservoir capacities of more than 3 million cubic meters, i.e. they are defined as large structures according to ICOLD's classification. The large dams can be further classified in the Sri Lankan context as ancient, recent or modern dams.

Ancient dams which were built by ancient kings several hundred years ago are mostly earth fill dams which fell into disuse over the years and subsequently became inoperable. The Government of Sri Lanka, newly independent in 1948, recognised the benefits of these ancient dams, as had the previous British rulers of the Island, and rehabilitated and upgraded many dams and irrigation schemes to various degrees.

Recent dams were constructed starting from the middle of the 20th century. At this time mostly earthfill or rockfill dams were developed for the purposes of hydropower production, irrigation and flood control at locations where no ancient structures previously existed.

Modern dams were built starting from 1970 under the Mahaweli Development Program, the largest comprehensive river basin development ever implemented in Sri Lanka. Concrete gravity and arch dams, as well as earth and rockfill dams were built to the latest design and construction standards and technology.

To summarise, four main types of dam are currently in operation in Sri Lanka: homogenous earthfill dams, rockfill dams, concrete gravity dams and one large double curvature concrete arch dam. There are no privately owned dams, neither does an agency exist which is mandated and responsible for adherence to the available dam safety regulations. The large dams are owned and operated by mainly four state agencies, namely the Irrigation Department (ID), the Mahaweli Authority of Sri Lanka (MASL), the Ceylon Electricity Board (CEB) and the National Water Supply and Drainage Board (NWSDB). Further large dams are owned by the Northern Provincial Council (PC/N) and the Eastern Provincial Council (PC/E).

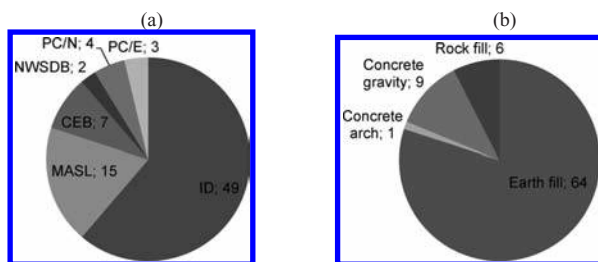


Figure 1. Ownership (a) and type of dam (b) of 80 large dams (according to ICOLD's classification) in Sri Lanka.

1.2 Present situation

The ageing and inadequate maintenance of many Sri Lankan dams is resulting in various structural deficiencies and shortcomings in their operation becoming evident as well as in defects of their monitoring facilities. A World Commission on Dams consultation was held in Sri Lanka in 1998 and highlighted the need to give prompt attention to the safety of Sri Lankan dams. Following the recommendations presented at this event, the World Bank supported the Government of Sri Lanka in carrying out a safety assessment of large dams that documented the deficiencies. The study confirmed the need for urgent action, which is to include improvements to the structures, to ensure the safety of the personnel, to protect the public, as well as safeguarding the environmental objectives of these valuable assets.

The failure of Kantale dam in January 1986 and the devastation caused by the tsunami in Sri Lanka in December 2004 further deepened the need and urgency for the country to protect the public from further disasters, including dam failures.

2 DAM SAFETY AND WATER RESOURCES PLANNING PROJECT

2.1 General

The Dam Safety and Water Resources Project (DSWRPP) was initiated in August 2008, with the assistance of World Bank financing. The main objective of the project is to improve the development and management of water resources within Sri Lanka, reduce the risk of water induced hazards to the public and enhance the sustainability of water related investments. There are three main components of the project, namely: (1) dam safety and operational efficiency improvement, (2) updating and modernising the existing Hydro Meteorological Information System (HMIS) and (3) multi-sector water resource planning.

The dam safety and operational efficiency improvement component is designed to emphasize the rehabilitation of structural deficiencies and to mitigate the risk to public safety of dams in a sustainable manner. Hence, all of the 80 large dams, based on the ICOLD classification, were ranked according to risk indexes obtained from the Portfolio Risk Assessment (PRA) methodology. It was concluded that there are 32 major dam structures which show signs of high risk deficiencies and therefore require full rehabilitation. The 32 dams at high risk are located as indicated in Figure 2. For all large dams, basic safety facilities are to be provided under DSWRPP.

2.2 Dam safety concept

DSWRPP approaches the following basic dam safety elements: (i) structural safety, (ii) dam monitoring and dam maintenance, and (iii) emergency planning.

i. *Upgrading of structural safety*: Minimizing the risks calls for appropriate design and construction of a dam, and this means that the original design has to be reviewed to ensure that the structural and operational safety is guaranteed according to current internationally accepted criteria and design concepts.

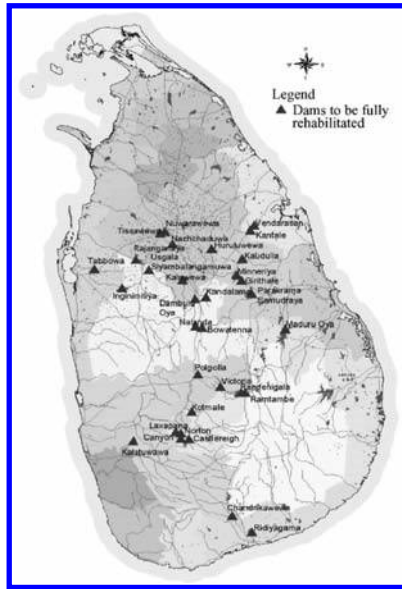


Figure 2. Location of 32 dams to be fully rehabilitated under DSWRPP.

ii. *Dam monitoring and dam maintenance*: Risk can be minimized but never totally eliminated even if a dam has been designed and constructed according to the latest state of knowledge. Therefore, it is necessary to detect any signs of abnormal behaviour and damage during operation of the dam as early as possible, so that corrective measures can be taken in good time. In order to achieve this, periodic inspections of all the dams, as well as periodic evaluations, are essential.

iii. *Emergency planning*: In case of an identified hazard to a dam the situation is managed according to the emergency planning concept. It is important that the measures to be taken be prepared in advance and are specified in an Emergency Action Plan (EAP). The potential flooded areas, in case of a dam break, have to be determined, and the results presented in a flood inundation map, which allows evacuation of the affected population from the flooded area to be planned and alarm measures and devices to be specified.

2.3 Project activities

DSWRPP is designed to address major structural deficiencies and institutional shortcomings, so as to ensure the safety of the dams and their appurtenant structures in the future. [Table 1](#) allocates typical project activities to the basic dam safety elements described above.

3 UPGRADE OF STRUCTURAL SAFETY

3.1 Typical deficiencies observed

Typical deficiencies observed on inspected dams in Sri Lanka can be divided into two categories, defined in terms of material factors, and associated with the further development of engineering know-how, respectively.

Material factors contributing to ageing include:

- Damage due to weathering, erosion and seepage.
- Wear of hydro-mechanical and instrument equipment through misuse, age and inadequate maintenance.
- Loss of serviceability after prolonged operation.
- Damage from natural events including floods, earthquake or landslides.
- Damage from vandalism and civil unrest.

Table 1. Project activities to be treated under DSWRPP.

Dam safety element	Project activities
Upgrading of the structural safety	Review of existing data, documentation and previous studies Inspection of dam, spillway and appurtenant structures. Preparation of a conceptual design of the remedial works.
Upgrading of the structural safety	Location/evaluation of missing but essential data for detailed design analysis (organization of latest hydrological data, performance of topographic surveys, geotechnical or concrete investigations, outlet inspections, etc.). Preparation of detailed design of civil and hydro-mechanical rehabilitation works. The tasks include, among others, the performance of hydrological and hydraulic studies with the intention to determine the adequacy of the existing spillways and assessment of the existing freeboard. Additionally and where required, stability analyses of dams and other structural components as well as a revised risk assessment to be carried out subsequently. Preparation of Tender Documents for the rehabilitation measures.
Dam monitoring and dam maintenance	Provision of basic safety facilities which consider prime requirements to monitor and to maintain the dam and appurtenant structures. Analysis, evaluation and interpretation of instrumentation data and upgrading of monitoring systems on dams. Preparation of reports on the behaviour of the dams based on a comprehensive safety inspection. The objective is to use this report as a template for periodical reports on dam behaviour in the future. Preparation of Operation & Maintenance manuals of rehabilitated and upgraded dams.
Emergency planning	Simulation of flood inundation and preparation of flood inundation maps. Preparation of Emergency Action Plans (EAP), including hazard and emergency classification, installation of warning systems and emergency communication and notification charts.

The further development of engineering know-how includes the following:

- Overcoming deficiencies resulting from design and construction procedures based on earlier standards and guidelines; an example is the definition of flood peaks and required freeboard margins.
- Overcoming the effects of any changes needed in operating conditions; an increase of the full supply level of the reservoir, for example.
- Studies for improvement of understanding and effects of natural impacts, such as improved ability to predict the magnitude of floods and, in that respect, to assess the adequacy of spillway capacities, or the better understanding of earthquake magnitudes.
- Consideration of the influence of changes in the vicinity of the dam, such as increased settlement of population in the immediate neighbourhood of dams and spillways or the construction of public roads immediately below the dam toe.
- Improvement of present understanding of dam failure scenarios so as to enable the performance of site-specific rehabilitation measures to be defined in accordance with current safety criteria.

3.2 Ageing of earth dams

The ageing process commonly affects not only the dam foundations but also the dams themselves, and a major objective of rehabilitation of observed ageing deficiencies of embankment dams is to overcome the following typical scenarios:

- Instability associated with internal erosion of the embankment materials, its abutments or its foundation, by leakage of water into an outlet sluice or seepage from the reservoir.
- External erosion caused by the failure or distress of the upstream slope protection (e.g. rip rap, concrete slabs) as a result of subsidence or wave impact/run-up.

- Slope instability caused by shear failure within the embankment, resulting from inadequate shear strength (high pore water pressure within the fill is the most important reason for loss of shear strength).
- Instability due to external erosion of the downstream embankment caused by overtopping of the embankment. This can occur because of insufficient spillway capacity and effects of seepage.

3.3 Ageing of concrete dams

All concrete dams age during their normal operation lives. Poor design, lack of maintenance and, in particular, lack of proper surveillance to notice early signs of deterioration increase the impact of ageing, which can also take place in the foundation rock mass and dam body. The major observed ageing scenarios of concrete dams are:

- Water percolation through the dam body; this is one of the main factors of ageing as dissolution of the cementitious fraction generally results in a decrease in mechanical strength and water tightness.
- Ageing of construction and foundation material influences the life of a concrete dam. Typical reasons are chemical processes causing, for example, swelling due to alkali aggregate reactivity, sulphate attack or leaching. Ageing is also caused by physical and mechanical processes such as drying-wetting cycles, non-uniform foundation movements or cracking due to seismic action. Biological processes can add to the deterioration of the concrete; examples are the growth of plants in cracks and drainage holes.
- Most concrete structures reveal minor cracks which can affect their functioning, durability and the appearance of the structure. Some of the possible causes for cracking are changes in the uplift forces, settlement of foundation, aggressive water, alkali-aggregate reaction in the concrete, seismic action, thermal stresses.

3.4 Examples of applicable remedial measures

The dams discussed under the heading “Upgrading of structural safety” have various characteristics (e.g. dam type, height, foundation parameters, age, function). Consequently, their deficiencies and necessary remedial measures are many and vary.

The majority of the dams to be treated in Sri Lanka are homogenous earthfill dams. Here the main deficiencies, among others, are inadequate spillway capacities, unstable cross sections which also include insufficient upstream and downstream slope gradients and crest widths, eroded upstream dam faces, seepage along the dam toe and insufficient monitoring equipment. The measures needed to rehabilitate the defects of such dams (mainly ancient earthfill embankments are affected) include but are not limited to raising of crest level, filling and re-profiling of upstream and downstream slopes, construction of toe drains, filters and loading berms.

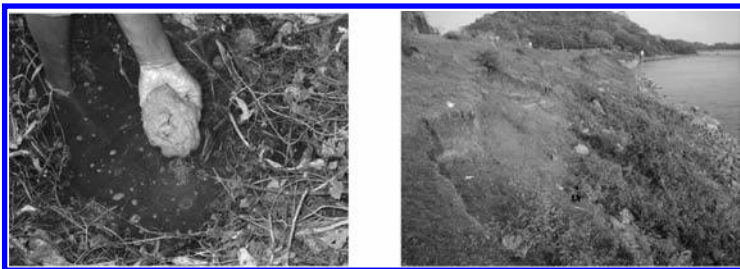


Figure 3. Ageing mechanisms at embankment dams: Sand boiling along the toe of Nachchaduwa dam (left), where extensive water-logged areas are seen when the reservoir is full; Upstream slope instability at Huruluwewa dam due to lack of wave protection (right).

Besides the more common measures, specific rehabilitation works are required at certain dams. One example is the rehabilitation of sluice barrels for irrigation water release located in the existing embankments. The resulting problems are erosion of the concrete structure and leakage into and/or along the contact of the outer face of the sluice barrel with the surrounding compacted fill material. Depending on the extent of the damage, localised repair works are foreseen. In the case of Tabbowa dam such measures were considered to be inadequate as the one of the sluices was in desolate condition. Only demolition followed by reconstruction was found to be an adequate solution.

The spillways of the dams under investigation vary from modern to very old structures, with gated or ungated overflows, of which some also lack routine maintenance and repair works. In addition, natural overflow and breaching sections are in some cases provided. The capacity adequacy is one of the main issues when determining the safety of an existing dam structure. For all dams, a hydrological study was carried out to upgrade the design values according to internationally accepted standards. Based on the results obtained, the capacity of the spillways was investigated, and it could be shown that various structures could be damaged during the occurrence of major floods. In the case of Chandrikawewa dam and spillway, for example, it was determined that, with the current layout of the natural spillway, the dam structure will be overtopped by a Probable Maximum Flood (PMF). To ensure the safety of the dam structure also during such extreme flood events, the discharge of the natural spillway was increased by additional excavation, constructing a clearly defined sill and additional retaining walls along the downstream channel.

The deficiencies of the inspected concrete dams vary significantly from those of the embankment dams, due mainly to the age of the structures. Most of the older concrete dams were built in the 1950s, and such structures age in a different way from embankments. One of the main problems regarding the older concrete dams of Sri Lanka, which were visited during these project inspections, is the lack of data, such as construction details and drawings. Despite the available information, another problem the owners have to face is the lack of specific information on the structure and its behaviour, which must be handed down from one generation of operators to the next. Nonetheless, most of the concrete gravity dams require only minor rehabilitation work. The main concern regarding these structures is the lack and/or the aging of instrumentation.

4 DAM MONITORING AND DAM MAINTENANCE

4.1 *Dam monitoring system*

The ancient dams as well as those built up to the middle of the last century were mostly never provided with monitoring devices while the main problem faced by the modern dams is the malfunctioning of their instruments and a lack of spare parts.

Within the terms of the DSWRPP, it is proposed to provide a minimum of monitoring equipment for those dams which have no instrumentation devices at all. For the old embankment dams such as Tissawewa this includes the installation of standpipe piezometers at critical sections of the dam plus the measurement of seepage outflow by means of V-notch weirs. For the concrete dams built recently, borehole piezometer and seepage measurement in the galleries have to be implemented as a minimum. In both cases, proper survey levelling systems need to be installed along the crests and the abutments.

The modern dams owned by the MASL are generally well equipped and well maintained. However, ageing of the structure as a whole also influences the status of available instrumentation. Modern dams such as Randenigala, Rantembe or Kotmale, which are less than thirty years old, are affected by the continuous decay of various monitoring devices. One problem faced by the owners of these dams is the lack of spare parts and the difficulty of obtaining new parts for the existing monitoring equipment. In the case of these particular dams the approach regarding the upgrading of the instrumentation system is to determine which instruments are essential for evaluating the behaviour of the dam. Further, all instruments that may have malfunctioned during their lifetime need checking to confirm that their data is still reliable. This allows the instruments needed in the future to be identified, and their need for repair, replacement or upgrade to be determined.

Providing instrumentation devices and obtaining measurement data can only be considered as the first step. To ensure that measurements are taken continuously and reliably in the future, appropriate procedures for each dam have to be provided to the owner and must also include staff training regarding the proper use and reading of the instrument systems.

4.2 *Instrumentation data analysis*

A difficulty encountered for the relatively well equipped modern dams is the inadequate evaluation to date of the available data for all of those dams for which instrumentation databases are maintained. However, the tasks involved in the evaluation of these databases vary to a large extent, and it is clear that, for the appropriate evaluation of measurement data, various types of information are needed. This relates not only to detailed information regarding the monitoring devices but also to detailed knowledge of irregular events during the monitoring period. In particular, the latter information is often almost impossible to obtain. In this respect it is of utmost importance to ensure the understanding and knowledge of the various devices with data evaluation being incorporated in the general operation procedures. This must include also the need for the responsible engineers at site to check continuously and follow up in detail any irregular behaviour of the dam that is observed, so that appropriate procedures can be set up in the course of the project.

4.3 *Basic safety facilities*

Many of the dams included in the DSWRPP lack the basic facilities necessary to operate and monitor the dam structures in an appropriate manner, and for this reason, all 80 large dams in Sri Lanka have been upgraded with basic facilities, as follows:

- Roads to and at the dam site and reservoirs must be accessible during all weather conditions. In this respect access roads have to be widened and provided with a durable surface protection.
- Basic equipment and instrumentation devices to survey and monitor the behaviour of the dam; this includes computational facilities to process and evaluate measured data.
- Equipment for basic maintenance and repair works.
- Emergency power supply equipment.
- Lighting facilities for use during normal and emergency conditions on spillways and major civil structures.
- Communication facilities to dam sites.

Providing the dam sites with these basic facilities is a prime requirement for the safe operation and monitoring of the structures, and is certain to have a positive effect on the future planning and execution of maintenance procedures.

4.4 *Operation & Maintenance manuals*

Operation & Maintenance (O&M) manuals are unfortunately only available for a few of the Sri Lankan dams included in the DSWRPP. Therefore, for each of the 32 dams at high risk, effective and ongoing operation and maintenance procedures have to be determined and included in new O&M manuals. These manuals have to contain not only instructions about the operation of the structure and the emergency planning, but also details of routine maintenance work and the programme of instrumentation reading and data evaluation. Detailed and comprehensive maintenance documentation will be an important aid to reduce the need for expensive future rehabilitation work.

5 EMERGENCY PLANNING

The Emergency Action Plan (EAP) which forms part of the DSWRPP is intended to help dam owners, operators and emergency officials to minimize the consequences of flooding

caused by uncontrolled release of water from the reservoir. The EAP guides the responsible personnel in identifying, monitoring, responding to, and mitigating emergency situations. It outlines “who does what, where, when, and how” in emergency situations or other unusual occurrence affecting the safety of the dam and downstream areas. The EAP should be updated regularly and after important emergency events. Basically, the dam owners are responsible for maintaining a safe dam by means of safety monitoring, operations manual, maintenance, repair and rehabilitation. In the case of an emergency, they must immediately notify the authorities in charge and start the evacuation of the affected population.

The basis for excavation planning is a dam breach flood wave analysis which shows the inundated area for the worst case failure scenario, i.e. the sudden failure of the dam. In addition, the arrival time of the flood wave, flow velocities and water depth are results obtained from the EAP analysis which consists generally of two classifications:

Hazard classification: Determination of the hazard level that could affect the safety of the dam as can be associated with natural events and processes (e.g. floods, internal erosion). This includes the operation of safety relevant hydro-mechanical equipment (e.g. gate jamming, failure of monitoring equipment) and with damages caused deliberately (e.g. vandalism, sabotage).

Emergency classification: Determination of the level of severity of an incident or the unusual behaviour of a monitoring instrument or of a mechanical/electrical component. Three levels to be defined for this classification: internal alert, developing situation and imminent situation.

Communication and notification is treated both internally and externally. Externally means communication with local and regional authorities, responsible for the execution of emergency actions. Notification charts which show the flow of information among parties and executive staff have been prepared to facilitate notification. Internally, the necessary measures are carried out by a team composed of members of the operating staff.

6 CONCLUSION

Under the DSWRPP, the dams at high risk in Sri Lanka have to be upgraded to assure their structural safety, adequate dam safety monitoring, dam maintenance and emergency planning. Skills and knowledge to carry out the required operation and maintenance activities in the future have to be taught but this must be enhanced. Further, institutional strengthening to develop the knowledge and interest of staff and to support regular maintenance is of utmost importance. To educate and train the staff of an organization responsible for the infrastructure is certainly more effective than providing expensive aid to undertake a rehabilitation project on structures after they have started to deteriorate. Regulation should typically require the following issues:

- Dams and reservoirs have to be provided with sufficient monitoring equipment to allow the basic assessment of the behaviour of the structure and its foundation.
- Monitoring equipment must be maintained and kept in good condition.
- Measurement data should be routinely evaluated, comparing the readings with the long term behaviour.
- A regular inspection of the dams, the reservoirs and the downstream area should be made on a periodical basis.
- Where unusual and unexpected behaviour of the structure is noted, the inspection of an independent expert is recommended.

A regular regime of inspection and reporting, coupled with a maintenance programme to treat signs of deterioration quickly and effectively, may reduce or even preclude the need for future rehabilitation work.

REFERENCE

Ministry of Agriculture Development & Agrarian Services of Sri Lanka (2008): *Project Implementation Plan of Dam Safety and Water Resources project (DSWRPP)*.

Strengthening of Les Toules arch dam

A. Wohnlich & O. Müller

STUCKY S.A., Renens, Switzerland

ABSTRACT: The paper addresses the case of Les Toules arch dam, which is a 86 meters high double curvature arch dam located in Switzerland. The dam enjoys a very slender shape out of any common values for such type of dam.

Since first impounding in 1964, continuous monitoring as well as observations revealed some specific long-term behavior concerns. In 2003, upgraded seismic regulations and recommendations of the Swiss Federal Office of Energy (FOE), in charge of dam safety in Switzerland required the dam owners to reassess the safety of their structures.

In this context, a project was started for safety enhancement and strengthening works at Les Toules arch dam. Comprehensive studies of the existing dam structure and its behavior were carried out. The final solution comprises a unique downstream strengthening in the form of abutment thickening, transferring the load from over-loaded cantilevers to the thickened arches, creation of shear keys in the vertical joints, local foundation treatment, and some other, secondary rehabilitation works.

1 INTRODUCTION

Les Toules double curvature arch dam is located in Switzerland close to the southern border with Italy, in Canton of Valais. The Owner of the dam is Forces Motrices du Grand-St-Bernard. The main dam characteristics are outlined in [Chapter 2](#).

The causes for the strengthening works are presented in [Chapter 3](#) and the main results of studies about the existing dam are presented in [Chapter 4](#). The final selected strengthening solution is discussed in [Chapter 5](#). The rehabilitation works started in 2008 and shall be completed by spring 2011; some specificities of the job site are exposed in [Chapter 6](#), with a particular emphasis on dam concrete and grouting works. The current monitoring system of the dam will be upgraded as outlined in [Chapter 7](#).

2 PARTICULAR DAM CHARACTERISTICS

The dam was built in 1960–64 and is actually the heightening of a first, single curvature arch dam built in 1958 as illustrated in [Figure 1](#) below.

The dam is 86 m high and the crest across the valley is 460 m long. The concrete volume is 235,000 m³. The ratio between crest length and dam height is 5.35, which is far beyond common values for double curvature arch dams. The dam enjoys a particular design, with a slender shape, a high vertical curvature toward downstream and no shear keys. An internal so-called prepaht joint exists at the contact between the initial dam (1958) and the heightened dam (1964).

3 CAUSES FOR THE STRENGTHENING WORKS

3.1 *Efficiency of the prepaht joint*

The prepaht joint discussed in [Chapter 2](#) above consists of gravel to be grouted before reservoir impounding. However, watertightness problems occurred as well as several horizontal

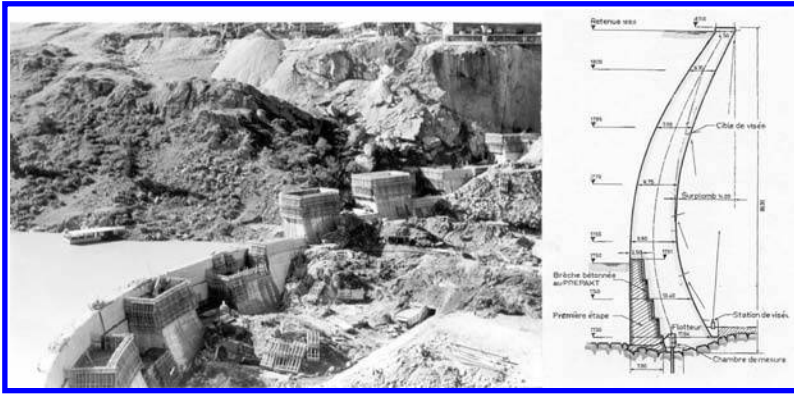


Figure 1. Construction of Les Toules arch dam in two stages—picture (left) and cross-section (right).

cracks on the upstream face. Remedial grouting works of the joint could lower but not stop the leakage inflows observed in the foot gallery. From 1993, an extensometer was placed between both dam and a constant opening of 0.05 mm/year has been recorded, demonstrating that the joint was actually not working properly. In case of high reservoir level, an increase of water inflows, as well as cracks opening are observed. Such behavior as well as a possible degradation of the joint with time plus the difficulty of performing a reliable remedial action lead to the conclusion that strengthening measures shall be taken to ensure long-term safety.

3.2 Localized and irreversible displacements towards downstream

The dam foundation lies on gneiss and mica schist rocks, forming alternate subvertical strips almost parallel to the valley. The gneiss appears to have better mechanical properties and to be more rigid than the mica schist; thus the dam rests on an alternate series of rock formations which have variable properties and stiffness, especially on the left bank in the vicinity of dam blocs 5 to 7, where small irreversible displacements toward downstream are observed since first reservoir impounding and beginning of operation. This displacement amounts to 4 mm, which occurred over the past 30 years. A local stability analysis was performed and showed, first of all, that the required factor of safety was barely ensured in the static case and, secondly, in case of a seismic event, the factor of safety drops dramatically. The constant increase with time of this displacement as well as the stability analysis performed call for remedial works at that particular location.

3.3 Upgraded seismic recommendations

Les Toules dam was designed in the late 1950s with the knowledge and tools of earthquake engineering of that time. Due to limited knowledge on seismic hazard of the country, most of the old dams in Switzerland have been designed for a peak ground acceleration (PGA) of 0.10 g.

As per the recommendations of the Swiss Federal Office of Energy (FOE) (2003), the PGA of a dam site should be determined based on the seismic hazard map of the country published in 1977. The map provides seismic intensity isolines for seismic events with return periods of 1000 and 10,000 years, which is then transformed in PGA.

Based on the dam classification in Switzerland, the recommended method gives a PGA of 0.33 g which is 3.3 times higher than the original design earthquake of the dam.

To be more specific and relevant, a seismic hazard study was carried out in order to determine a more precise PGA based on local faults and site geology and select three proper recorded earthquakes corresponding with local conditions. The seismic hazard study of the site was performed according to deterministic and probabilistic approaches and resulted in a horizontal PGA of 0.28 g and 0.19 g for the vertical component.

4 DESIGN STUDIES OF ARCH DAM STRENGTHENING

4.1 *Static and dynamic analyses of existing dam*

Before launching detailed analyses, calibration of the finite elements model had to be fulfilled for both static and dynamic behavior of the dam based on concrete test results and measurements. The static calibration was simulated by means of an analytical transient thermal solution proposed by Stucky & Derron (1957) considering three plumb-lines at three different blocs and mechanical characteristics of concrete and rock foundation. The behavior of the prepacked joint separating both construction phases of the existing dam was studied in two modes: a) joint fully open; b) perfect contact, i.e. monolithic behavior.

The dynamic calibration of the dam was carried out on the basis of natural frequencies and also mode shapes, both obtained by ambient and forced vibration test of the dam. The dynamic modulus of the dam concrete and the behavior of the construction joints could be inferred from the approach and used for the time-history dynamic analysis of the dam.

Full static and dynamic analyses of the existing dam allowed verifying the safety of the structure based on the FOE recommendations.

The static analysis showed relatively high vertical tensile stresses on the upstream face of the dam for full reservoir load case. These stresses were mostly found at the heel of the cantilevers and on the banks, and reached up to 5 MPa for full reservoir combined winter temperature load case. Such high vertical tensions for static load case could produce cracks on the upstream face of the dam, an opening of the dam/foundation contact, or decompressing of the foundation on the heel of the dam. To some extent, all these phenomena have been observed at Les Toules arch dam. The compressive stresses were also significant but acceptable with a maximum value of 12 MPa for static load cases.

The results of the dynamic analysis showed that the dam would experience very high tensile stresses in case of a seismic event. The maximum tensile stress obtained with the final elements model was about 12 MPa in the same zone as the tensions occur due to static load cases. Such high vertical tensions confirmed the necessity of the dam strengthening. In addition, high horizontal tensions were obtained in the central part of the upper arches, which could trigger significant opening of the radial joints. These joints enjoy a helical geometry but without any shear keys, which is unfavorable to withstand large joint opening and therefore, the dynamic stability of the upper parts of the cantilevers was of concern and had to be considered in the strengthening concept.

4.2 *Strengthening alternative study*

To remedy the different critical items as identified in the analysis of the existing dam, many solutions were envisaged and investigated in the framework of an extensive alternative study:

- Thickening of the dam section (upstream, downstream, thrust blocks)
- Buttresses
- Implementation of a seismic belt
- Use of prestressed anchors.

Even solutions with no interference with the dam were considered:

- Lowering the maximal operation level
- Building a new dam downstream of the existing dam.

Finally it was found that reinforcing the dam on its downstream face by addition of two lateral strengthening (abutment thickening) on each bank, together with shear columns in the central portion of the arch was the most optimized solution, in particular since it does not involve any job in the upstream face (inside the reservoir). With that, the power scheme can be operated during the reinforcement works, although under modified operating rules.

In-depth static and dynamic analyses of the strengthened arch dam were performed, showing that for the static cases, the high tensile stresses observed in the upstream face of the

existing dam are reduced by 45% for the critical load case of full reservoir combined with winter temperature. By reinforcing the arches in both banks, the cantilevers are effectively unloaded and the arch effect accordingly increased. The compressive stresses calculated in the strengthened dam remain in the same magnitude as for the existing dam, although for some specific load cases, a stress reduction in the range of 30% is observed.

The dynamic analysis confirmed that the increase of the dam rigidity by thickening of the arches leads to increased values of natural frequencies. A comparison of the results obtained for the existing dam and for the strengthened dam shows a reduction of the tensile stresses by 30%.

5 DESCRIPTION OF SELECTED STRENGTHENING SOLUTION

Figures 2 and 3 show the downstream face of the dam and three cross-sections of the existing dam together with the reinforcement. The strengthening of the dam is shown with dark grey, whilst the existing dam is shown with hatches.

To respond to seismic requirements, the thickening of abutments in both the left and right banks allows the transfer of the load from over-loaded cantilevers to thickened arches. Both abutment thickenings are designed with galleries located at the interface of both old and new structures. During the construction, the galleries serve as access and to implement the concrete post-cooling system, dam contraction joint grouting and rock foundation treatment

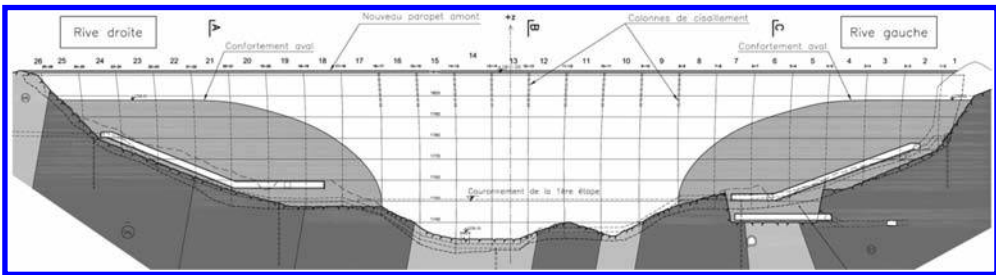


Figure 2. Downstream face of dam with strengthening solution.

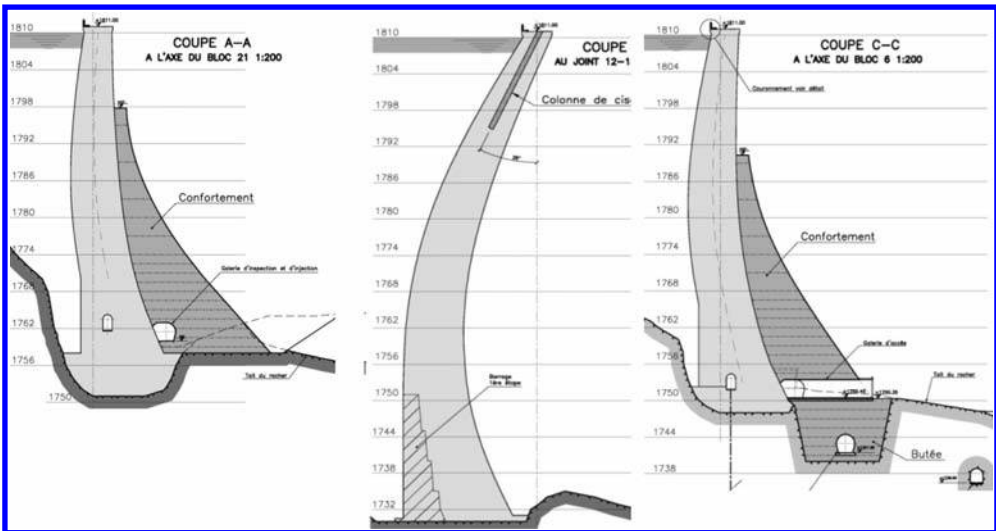


Figure 3. Cross-sections of existing dam with strengthening solution. Left: Bloc 21 with abutment thickening; Center: Shear keys from the crest; Right: Bloc 6 with abutment thickening and a 10 m deepening into the rock foundation.

(consolidation grouting and drainage). On completion of the reinforcement works and during operation, the galleries serve mainly to access the monitoring equipment. The bounding between the existing dam and the strengthening is performed by a proper hydrodemolition with high pressure rotating water jets (2500 bars) and with diameter 25 mm steel anchor bars grouted into the existing dam. The density of the steel anchors is 4 pieces/m² in a 3 m wide belt in the edge of the contact surface, and 1 piece/m² anywhere else.

Still for seismic purposes and along with these two 30,000 m³ concrete volumes added on the downstream face of the existing dam, it was found necessary to lock together the central cantilevers, from bloc 8 to bloc 17, so as to prevent the blocs to move independently one from each other in case of earthquake. Nine so-called shear columns are designed for that purpose. To behave properly, they have to be thoroughly aligned and centered in the helical plan of each dam joint and are made of heavily reinforced concrete. The columns are 16 m deep (diameter 700 mm), bored into the existing dam concrete.

Locally in the area of blocs 5, 6 and 7 (left bank), where the weakest geological layer prevails (mica schist rock), the dam abutment stability analysis of the existing dam revealed that the dam foundation was too shallow and not sufficiently deeply founded into the rock mass Cekerevac & Wohnlich (2009). To comply with the design requirements, a 10 m deepening of the dam foundation is designed (Figure 3, right), bridging the weak mica schist layer between both stronger, neighbor gneiss layers.

Following the construction of both dam thickenings as shown in Figures 2 and 3, proper foundation treatment including a 15 m deep consolidation grouting and drainage holes is implemented.

In addition to these works, a 1 m high reinforced concrete parapet wall is designed in substitution of the existing steel barrier. This measure allows the increase of the water head by 1 m for the ungated, free-flow spillway located on the left bank, thus substantial increase of the discharge capacity to better accommodate the PMF flow condition.

6 SPECIFICITIES OF JOB SITE

6.1 Concrete works

The aggregates and sand necessary to produce the dam concrete are sourced from the quarry located between 1780 and 1810 m.a.s.l. in the reservoir bed, upstream of the dam at the river mouth. It is to be noted that the existing dam was also built with aggregates and sand extracted from the same quarry. The long term behavior of the existing dam concrete was checked and found satisfactory.

The thermo-mechanical analysis showed that the maximal concrete temperature should not exceed 35°C, so as to keep the stresses below the tensile strength of the concrete.

Night concreting, permanent pre-cooling of aggregates with water mist and shady stock-piles, limited concrete lift volumes and installation of post-cooling pipes system each 3 m are the pre-and post-cooling measures implemented in order to comply with the maximal temperature authorized for the concrete works. During summer, when fresh concrete temperature is too high and causes the exceeding of the maximal authorized peak temperature, additional cooling pipes are placed, thus reducing to 1.5 m the spacing between two successive post-cooling layers.

In accordance with the strengths requirements computed from both statical and dynamical analyses and in order to fulfill the temperature elevation requirements, two different types of concrete with different cement contents are used for the abutment thickenings. In 2008, extensive concrete investigations were performed to fix the most suitable concrete mixes to comply with the technical requirements. Final mixes are: 190 kg/m³ of cement and 110 kg/m³ of fly ash, with 1.2% of plasticizer (concrete type I). For concrete type II, a reduction by 15 kg of cement is balanced with an increase by 15 kg of fly ash. The cement has low hydration heat. The maximal size aggregate is 80 mm. Cubic compressive strength requirements (20 × 20 × 20 cm) were set as shown in the following table.

Table 1. Required compressive strengths.

Mass concrete	28 days [MPa]	365 days [MPa]
Type I	30	50
Type II	25	37

Routine tests are ensured by the site laboratory installed by the Contractor and samples are taken on a daily basis.

The specificity of the site in mountainous conditions at 1800 m.a.s.l compels the Contractor to concentrate the works from April to October, the job site being without safe access in winter time. Considering this tight schedule, the decision of the Contractor to work with two 9 hours shifts—a day shift for formwork and preparatory works and a night shift for concrete works—becomes an evidence. A concrete placement rate of 40 m³/h is required. Concrete is placed with a 95 m high tower crane (630 tons meters) as shown in [Figure 4](#).

The stringent requirements regarding compressive strength and maximal allowable concrete temperature made the concrete mixes definition a sensitive technical issue. However, concrete works could be completed in time and satisfactory results have been recorded.

6.2 Contraction joint grouting

The contraction joint grouting of the abutments thickenings enjoys a particular design. Since the right and left abutment thickenings are not linked, there is no general prestressing effect with balanced arch forces, similar to a conventional arch dam. Moreover, considering the particular thin shape of the thickening, special care is required for the joint grouting procedure.

In spring 2010, contraction joint grouting of the right abutment thickening was performed. A continuous monitoring of displacement was carried out, with 24 deformeters installed in the galleries and on the downstream face of the thickening. The maximal allowed displacement was set to 1 mm, with an automatic warning in case of overrunning. Maximal pressures at the grouting point and at the upper vent hole were calculated in order to prevent the adjacent bloc from sliding or creating tensile stresses on the basis of the bloc due to overturning.

Grouting pressure was limited to 5 bars at the grouting point. Primary joint grouting system (grooves installed at the bottom of the grouting panel) and secondary system (captain valves distributed on the joint surface) were installed within the vertical panel. Due to grout losses within the rock foundation at the bottom of some lowest compartments, the use of the primary system was not sufficient for the grout to reach the top of the panel, thus the secondary system was used. In all cases, control grouting through the secondary system was performed. The maximal joint opening reached 0.75 mm and the average grout absorption reached 4.8 kg/m² of joint.

The grouting of the left bank contraction joints is scheduled in spring 2011, right before starting the reservoir impounding.

6.3 Contact and consolidation grouting

Consolidation grouting works performed in 1964 showed an average grout take of 37 kg/m of drillhole. In 2010, Foundation treatment with performance of consolidation grouting was carried out under the right and left bank abutments thickenings. Such operation, going down to 15 m below dam thickening foundation, aims at increasing and homogenizing the rock mass characteristics, reducing permeability and treating the contact zone between concrete and rock mass.

The grout take of the works performed in 2010 is of 8 kg/m of drillhole, which means around 4 times less than the absorption observed in 1964. However surprising, such difference could be explained either by a greater care taken in 2010 for rock foundation excavation, or by



Figure 4. Downstream views of the dam during strengthening works.

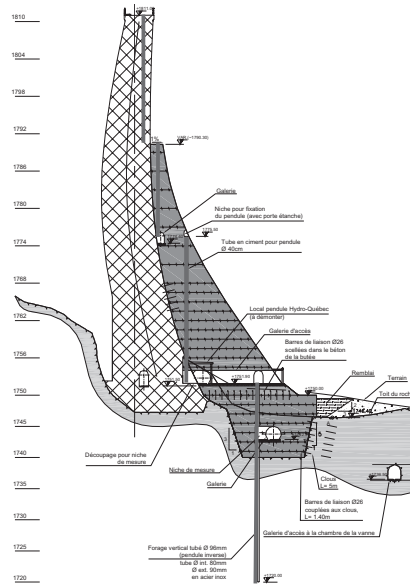


Figure 5. Plumbline section at bloc 6.

a different grouting methodology (grout pressure, refusal criteria, drillhole spacing, grout mix characteristics). In 1964, few data were available, but it is known that an unstable grout mix was used, whereas a stable grout mix (less than 2% of bleeding after 2 hours) was used in 2010.

Even for such very low takes, appreciable differences could be recorded. For example, grout take under the local deepening was 25% less than this of primary holes. Moreover, the grout take under the local deepening at blocs 5–7 (where the rock characteristics are lower than in any other part of the foundation) was 40% higher than elsewhere. Finally, the Lugeon tests performed in checkholes after completion of consolidation grouting showed an average value of 1.1 Lugeon, that is 5 times lower than the average values of tests performed prior to grouting within the same holes.

7 UPGRADED MONITORING

In the frame of the strengthening project, the monitoring equipment of the existing dam needs to be adapted to the new layout, and it is taken advantage of the project to upgrade

it and to increase the general quality of monitoring. In particular, no complete plumblin section is available in the existing dam (from dam crest down to rock foundation). Since dam construction in the 60's, the movements of dam by combination of two methods: (1) in the rock foundation by means of inverted plumblines; (2) for the dam structure itself by means of optical distance measuring equipment from remote survey stations installed in the vicinity of the dam site.

This will be substituted by two complete plumblin sections installed in blocs 6 and 19. [Figure 5](#) below shows the plumblin section at bloc 6, which also illustrates the section with local deepening into the rock foundation. From dam crest downwards, a first plumblin is bored into the existing dam (from 1811 down to 1790 masl); then two plumblines are installed in the strengthening structure (from 1790 down to 1774 masl, and from 1774 down to 1751 masl); finally an inverted plumblin is installed in the concrete deepening and the rock foundation from 1751 down to 1720 masl.

The strengthening project also includes the implementation of concrete thermometers, deformaters at the contact between old and new concrete and at dam vertical contraction joints to monitor the grouting operation, and piezometers and drainage network in the rock foundation to control the uplift pressure in that area.

8 CONCLUSION

Due to very specific and local conditions described in the paper, Les Toules double curvature arch dam enjoyed a unusual design in the 1950s and experienced particular behavior during the past 40 years of operation. However, due to the advent of up-graded seismic directives issued by the FOE, it was found necessary in 2005 to increase the safety of the dam by reinforcing the structure. In-depth studies were performed, first by the back-analysis of the existing dam, which allowed identifying the critical items to be addressed. On this basis, a strengthening project was developed, which mainly considers the construction of two, 30,000 m³ concrete volume, dam thickenings added onto the downstream face of the existing dam.

The construction started in 2008 and is scheduled to be completed in time in 2011. Common technical items belonging to dam technology have been implemented, but needed to be adapted to the particular site and strengthening work type; among others the hydropower scheme is still being operated during construction, and the job site must cope with rather extreme weather condition.

ACKNOWLEDGEMENTS

The authors are grateful to the Forces Motrices du Grand-St-Bernard (FGB) for allowing publication of this paper.

REFERENCES

- Cekerevac C., Wohnlich A. (2009). *Reassessment of dam foundation stability—The case of three Swiss dams*. 2nd International Conference, Long Term Behaviour of Dams, Graz, October 2009, pp. 733–738.
- Stucky A., Derron M.-H. (1957). *Problèmes thermiques posés par la construction des barrages-réservoirs*.
- Swiss Federal Office of Energy (2003). *Sécurité des ouvrages d'accumulation. Documentation de base pour la vérification des ouvrages d'accumulation aux séismes*.

Theme B: Dams and climate change



Mauvoisin Dam, Switzerland (250 m, 1957/1991).

Long-term behavior of the Yashio dam, asphalt faced rockfill dam

T. Tsukada & M. Doi

Tokyo Electric Power Company, Tokyo, Japan

K. Yoshizawa & T. Kikuchi

Tokyo Electric Power Company, Tochigi, Japan

ABSTRACT: The 90.5 m high 15 year old Yashio dam, which was completed in 1995, is the upper dam of Tokyo Electric Power Company's Shiobara pumped storage power plant. There has been no leakage through the asphalt facing, and leakage through the foundation and exterior deformation of the dam body has been stable. We have measured the deformation of the asphalt facing utilizing a clinometer mounted on a vehicle towed from the crest of the dam. In addition, we have investigated the aging of the asphalt facing at the exposure test yard which was installed near the dam site on the same elevation level of the dam. We estimate that the asphalt facing was performed adequately after the aging.

1 INTRODUCTION

The Yashio dam, the 90.5 m high rockfill dam with asphaltic concrete facing was constructed by the Tokyo Electric Power Co., Inc. This dam is used as an upper dam for the Shiobara Pumped Storage Power Plant (900MW). The Yashio dam has been operating for 15 years, and we have confirmed that the behavior of the dam has been stable via many measurements and inspections. In addition, we have investigated the aging of the asphalt facing at the exposure test yard which was installed near the dam site on the same elevation level of the dam. We paved asphaltic concrete on the slope of the test yard with same material of the dam's facing. Thus, we can investigate the aging of the facing without having to directly analyze the facing of the dam itself. We estimate that the asphalt facing was performed adequately after aging. In this paper, the evaluation of the long-term behaviour of the exterior deformation and the leakage, and the aging of the asphalt facing of the Yashio dam will be described in detail.

2 OUTLINE OF THE YASHIO DAM

Given the tremendous water pressure, the facing of the Yashio dam was designed as a double-deck structure having an impermeable layer in each upper and lower portion. An intermediate drainage layer has been installed in order to clearly detect water leakage. The facing have a total of seven layers and 37 cm thickness. The surface of the facing has been covered with a thin layer of asphalt mastic so as to protect it from damage which can be caused by ultraviolet, frost and snowfall. Three types of grain sizes were used: a coarse one (max. size of aggregate is 20 mm) in the macadam and levelling layers; a fine one (max. size of aggregate is 13 mm) in the impermeable layers; and an open one (max. size of aggregate is 25 mm) in the intermediate drainage layer. An outline of the Yashio dam is given in [Table 2.1](#), the plan of the dam is shown [Figure 2.1](#), and the typical cross section is shown in [Figure 2.2](#). The structure of the facing is shown in [Figure 2.3](#), the standard mix proportion of the asphaltic concrete for facing is shown in [Table 2.2](#).

Table 2.1. The outline of Yashio dam.

Name of dam	Yashio Dam
Name of river	Nabearisawa river, Naka river system
Purpose of dam	Hydropower generation (Pumped storage)
Type of dam	Rockfill dam with asphalt facing (AFRD)
Height of dam	90.5 m
Length of dam crest	263 m
Volume of dam	2,109,000 m ³
Catchment area	2.0 km ²
Reservoir area	0.47 km ²
Total storage volume	11,900,000 m ³
Year of completion	1995

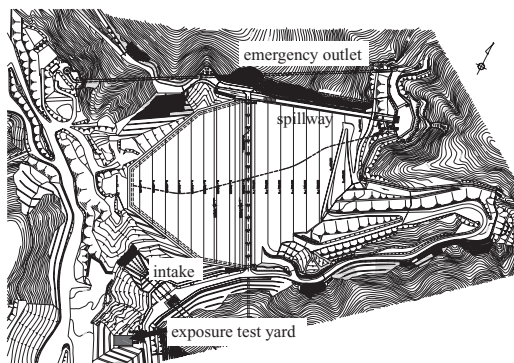
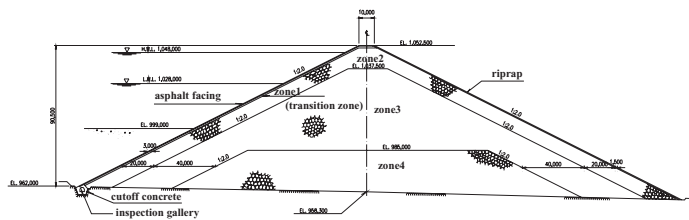


Figure 2.1. The plan of Yashio dam.



		Max. size (mm)	Density (g/cm ³)		Angle of internal friction	Cohesion
			Dry	Wet		
Zone 1	porphyrite	300	2.04	1.95	43	0
Zone 2	porphyrite	1,000	2.04	1.95	43	0
Zone 3	porphyrite	1,000	2.04	1.95	42	0
Zone 4	tuff	1,000	1.96	1.85	38	0

Figure 2.2. The standard cross section of Yashio dam.

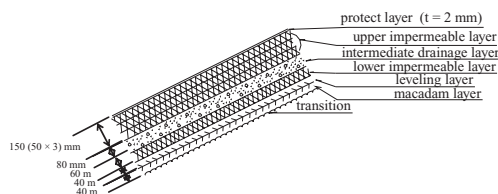


Figure 2.3. The structure of the facing.

Table 2.2(1). The standard mix proportion of the asphaltic concrete for facing.

		Content per unit weight (kg/ton)							
		Aggregate							
Grade	Max size of aggregate (mm)	Asphalt	Crushed stone		Crushed sand		Fine sand	Filler	Addition
			20-13	13-5	5-2.5	2.5-0	2.5-0	Stone dust	
Coarse	20	50	171	304	228	190	—	57	—
Open	25	40	399	292	197	—	48	24	—
Fine	13	85	—	166	267	275	83	115	8

Table 2.2(2). The standard mix proportion of the asphalt mastic for protect layer.

Content per unit weight (kg/ton)			
Asphalt		Filler	
Straight	Blown	Stone dust	Addition
185	185	580	50

3 THE RESULT OF THE MEASUREMENTS

3.1 Leakage

The leakage seeping through the facing and the bedrock are guided respectively to the inspection gallery. The drainage layer and the rock material of the dam body are connected with the inspection gallery with the drainpipes respectively. They are measured separately by the weir installed at eight points in the gallery. The flowing quantity is measured with the automatic measuring system. The leakage measurement equipment is shown in Figure 3.1. The leakage through the upper impermeable layer has been almost zero. Even though a slight amount of leakage through the seams and hair cracks of the inspection gallery concrete was measured for the period of the initial filling, it was stopped up. We installed drain pipes in the inspection gallery at the side of the dam body so that the backing pressure should not act on the facing. The amount of flowing quantity from these drain pipes was 10 liter/min. for the period of the initial filling, but it decreased and is about 5 liter/min. now. Moreover, it is judged that there is no danger of backing pressure or piping fracture occurring in the dam, because there has been no fine-grained fraction in the water. The flowing quantity from the dam body side drain in the inspection gallery is shown in Figure 3.2.

3.2 Exterior deformation of the dam body

The exterior deformation of the dam body is measured by external targets. The external targets set up at 15 points on the crest and the downstream side of the dam, and 26 points on the upstream of the dam. The 12 points under the LWL on the upstream were able to be measured only for the period of initial filling and 14 points were able to be measured in the event of a drawdown. The arrangement of the external targets is shown in Figure 3.3.

The maximum horizontal displacement towards the direction of the upstream was about 30 mm at No. 13 (near the center of the dam crest) and 25 mm at No. 3 (in the middle of the downstream at the left bank) towards the direction of the downstream. The maximum vertical displacement is about 150 mm at No. 12. We estimate that it has been stable because its increase has been 2 mm a year over the past five years. Further, we estimated that the vertical displacement near the center of the dam crest caused the horizontal displacement towards the direction of the upstream. The horizontal displacement towards the direction

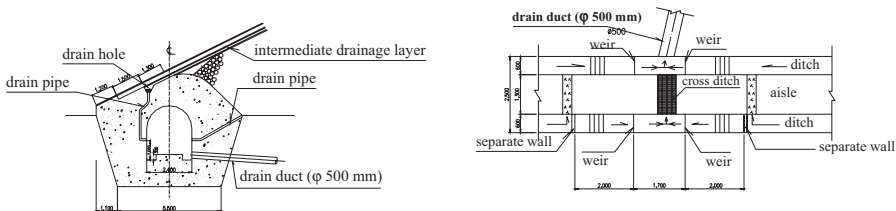


Figure 3.1. The leakage measurement equipment.

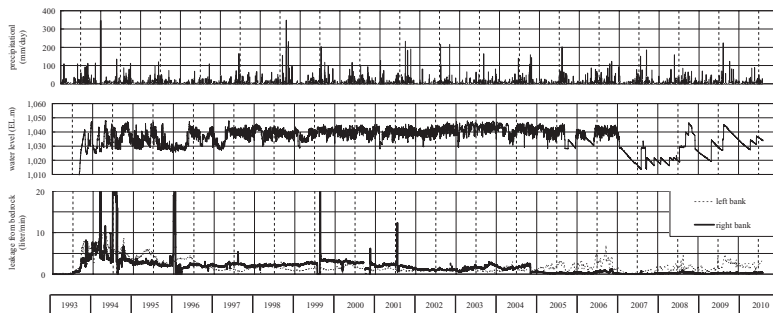


Figure 3.2. Flowing quantity from the dam body side drain.

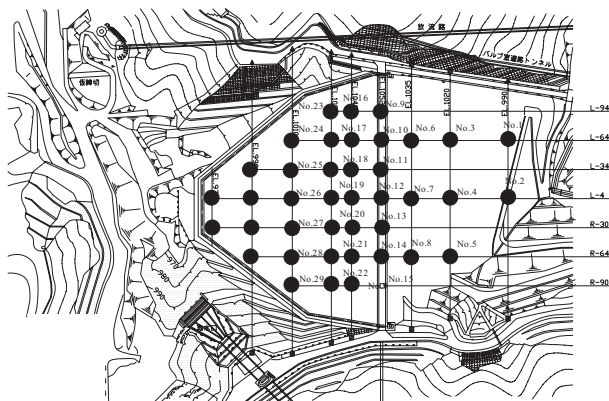


Figure 3.3. The arrangement of the external targets.

of the upstream of No. 13 increased along with the water level rising in the period of the initial filling. Further, it had decreased gradually for 10 years since five or six years after the water level reached the HWL. Now that the horizontal displacement toward the direction of the upstream of No. 13 is 20 mm. Similar behavior has been shown at other points on the dam crest, and it has been evaluated that the displacement towards the direction of the upstream was caused mainly by the influence of the vertical displacement of the upstream side of the dam by hydraulic pressure. The horizontal and vertical displacements are shown in Figures 3.4 and 3.5. Further, the distribution of the horizontal displacement and the vertical displacements in the dam central cross section is shown in Figure 3.6.

3.3 Deformation distribution of the facing

The deformation of the facing has been measured utilizing a clinometer mounted on a vehicle towed from the crest of the dam. We have measured the deformation of the facing at the center line of the upstream of the dam. The outline of the clinometer mounted on a vehicle is shown in Figure 3.7.

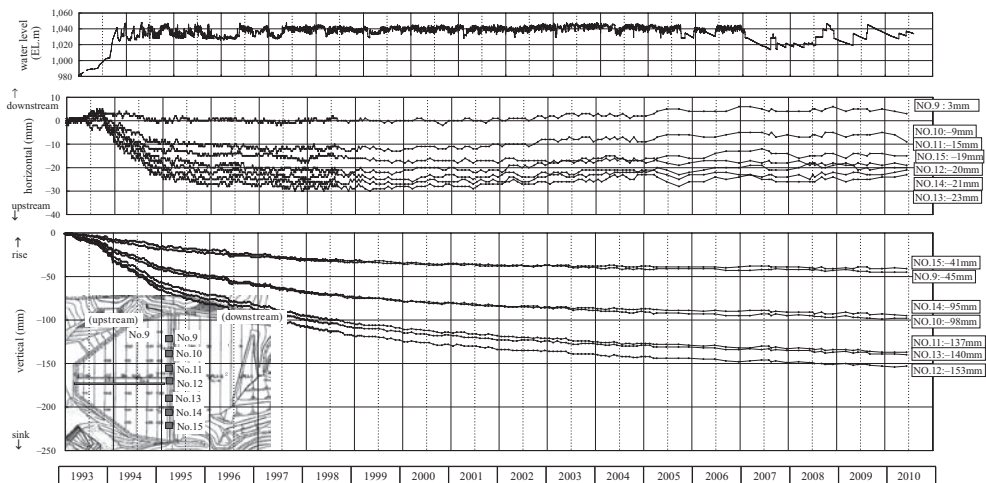


Figure 3.4. The exterior deformation measurement results (dam crest).

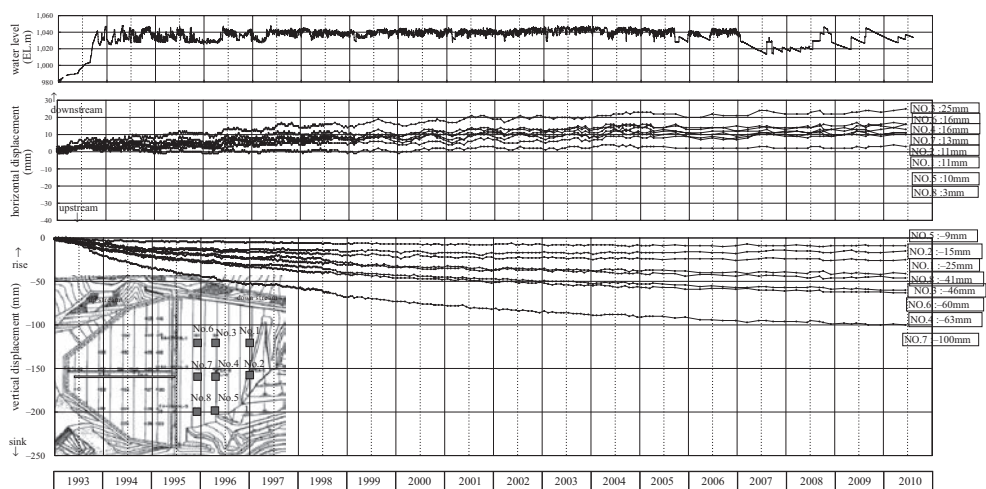


Figure 3.5. The exterior deformation measurement results (downstream surface).

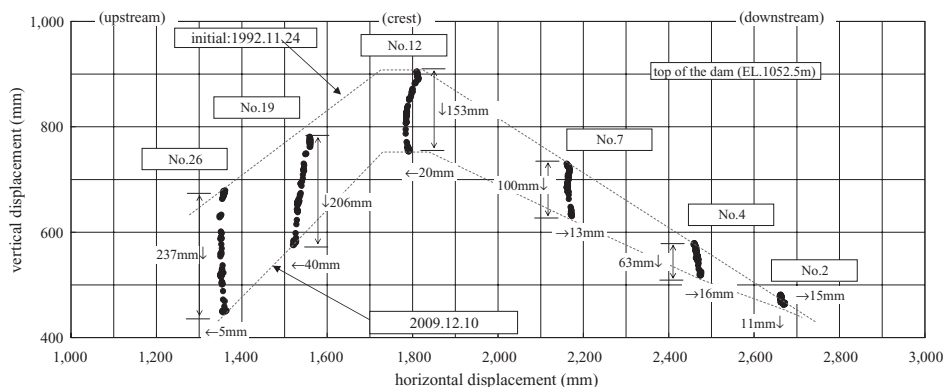


Figure 3.6. The distribution of the horizontal displacement and the vertical displacement in the dam central cross section.

The deformation of the facing is calculated by measuring the tilt angle with a clinometer and the distance between the measurements (1 m). We have observed it by the difference, converted to a perpendicular displacement of the upstream slope, between the each measurement and the initial value that was measured before the initial filling. The maximum displacement is about 400 mm at about 80 m from the bottom of the facing. The measurement results are shown in Figure 3.8. The deformation of the facing had increased according to the water rising in the initial filling, and have showed little elastic behavior according to water rising and the descent and creep deformation since the water level reached HWL. However, the deformation has been stable in recent years. The increase of the maximum displacement of the facing has gradually decreased. We evaluated that there is no problem with the stability of the facing, because the increase ratio of the maximum displacement is small and the increase of the displacement of the joint part of the facing with the inspection gallery concrete has been almost zero in recent years because the maximum tensile strain by hydraulic pressure occurs at the joint part of the facing with the inspection gallery concrete. The tensile strain at the joint part of the facing with the inspection gallery which is calculated by the deformation measurement result is about 0.5% or less, it is small enough for the yield strain of the asphaltic concrete of about 5% at the temperature of 5°C and the strain rate of 5×10^{-5} 1/sec. 5°C is the lowest water temperature of the reservoir, and the strain rate of 5×10^{-5} 1/sec is the lowest strain rate of the test machine(actual strain rate during the initial filling was about 1×10^{-10} 1/sec).

The yield strain of the asphaltic concrete depends on the temperature and the strain rate. The larger the strain rate becomes, the smaller the yield strain becomes. The relation between the yield strain and the temperature and the strain rate is shown in Figure 3.9.

We estimated that the facing is stable because the calculated tensile strain is smaller than the yield strain under the test conditions of a larger strain rate at the same temperature.

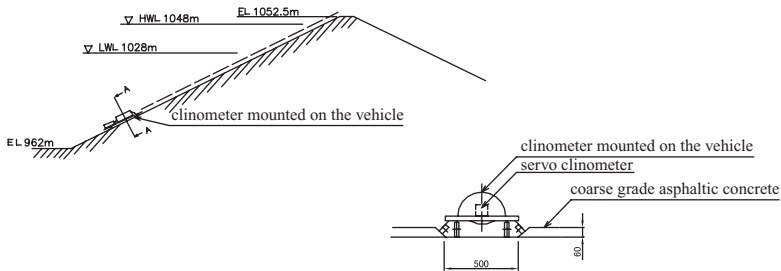


Figure 3.7. The outline of the clinometer mounted on a vehicle.

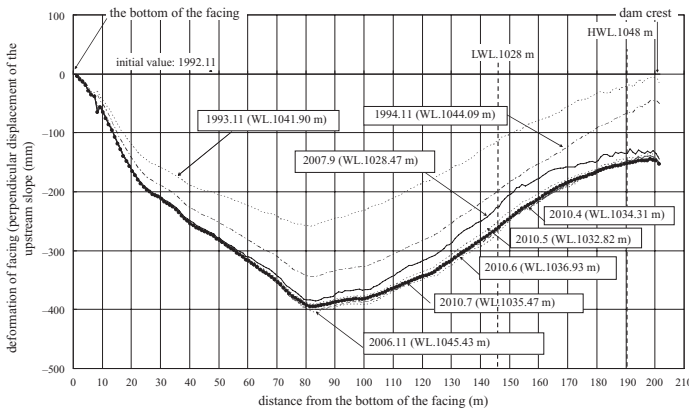


Figure 3.8. The deformation of the facing.

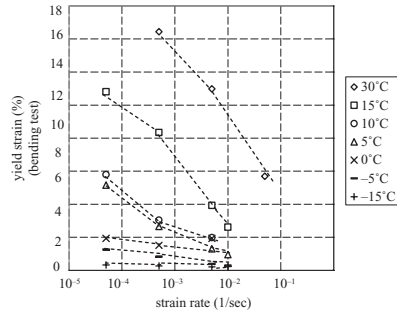


Figure 3.9. The relation between yield strain and temperature and strain rate.

4 THE AGING OF THE ASPHALTIC CONCRETE FACING

4.1 *The feature of the aging of the asphaltic concrete facing*

The asphaltic concrete is influenced by such factors as ultraviolet rays in the passing age which changes its mechanical properties. We set the exposure test pieces near the dam before the construction of the dam, and investigated the asphaltic concrete's property changes after aging. The test pieces were exposed for five years, the mechanical examination, and the basic physical properties test (such as the penetration and softening point) of the asphalt extracted from the test piece were executed. We made test pieces of fine grade asphaltic concrete with and without the protective layer made out of asphalt mastic. The results of the physical properties tests are shown in Figures 4.1 to 4.3.

The property changes of the test pieces with the protective layer were comparatively large for the first few years. The penetration became small and the softening point rose up and the yield bending tensile strain became small, but after that they didn't change that much. In other words, asphaltic concrete hardens after few years, but after that, there are no changes, if it was coated with a protective layer. The bending test condition of -15°C is the lowest temperature of the dam site and the strain rate of 1×10^{-2} 1/sec is the one during the earthquake in Figure 4.3.

The amount of the tensile strain occurring on the facing during earthquakes was calculated using the two-dimensional dynamic response by means of the finite element method was about 0.1%, it is enough smaller than yield tensile strain.

4.2 *The exposure test yard*

At the Yashio dam, test paving was conducted before the construction of the facing of the dam. We planned to use this test yard as an exposure test yard for the investigation of the changes of the asphaltic concrete facing after aging in the future. We installed an exposure test yard near the dam site on the same elevation level of the dam. We paved asphaltic concrete on the slope of the test yard with the same material of the dam's facing. The slope inclination and direction of the test yard are the same as the dam's one. Thus, we can investigate the aging of the facing without having to directly analyze the facing of the dam itself. We have extracted a sampling from the exposure test yard and executed an investigation 0, 1, 2, 5, 10 years after the paving. The location of the exposure test yard is shown in Figure 2.1.

4.3 *The results of the investigation of the aging of the asphalt facing at the exposure test yard*

We have conducted various investigations and tests shown as follows by using the test piece samples taken from the exposure test yard.

(1) Density test, (2) Penetration test, (3) Softening point test, (4) Chemical composition analysis, (5) Bending test, (6) Permeability test.

The results of the investigations are almost similar to the aforementioned former exposure tests results. The results of the bending test from this test yard are shown in Figure 4.4 as one

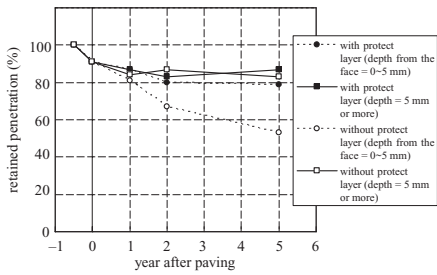


Figure 4.1. The retained penetration after aging.

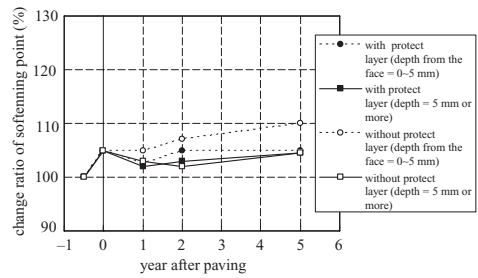


Figure 4.2. The change of softening point.

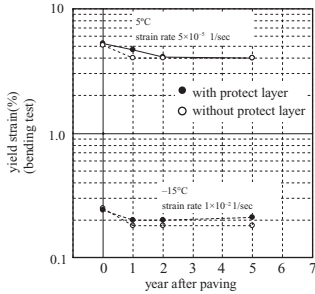


Figure 4.3. The change of yield strain.

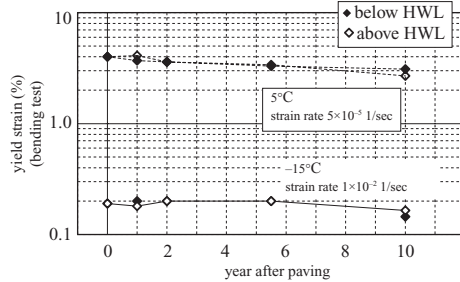


Figure 4.4. The change of yield strain after exposure.

of the examples. We have confirmed that the decrease of the yield bending tensile strain of the asphaltic concrete was small and that it had enough deformation performance about ten years after paving because we estimate that the tensile strain which occur during the earthquake is 0.06%. And we will continue investigating the change of the properties of the facing in the future, because they have tended to be a little hardened by aging.

5 CONCLUSION

We estimate that the asphalt facing is performing adequately after aging as follows.

- The leakage through the upper impermeable layer has been almost zero.
- The amount flowing from these drain pipes was 10 liter/min. for the period of the initial filling, but it decreased and is about 5 liter/min. now. Moreover, it has been judged that there is no danger of backing pressure or piping fracture in the dam, because there has been no fine-grained fraction in the water.
- We estimate that it has been stable because its increase has been 2 mm a year over the past five years.
- We evaluated that there is no problem with the stability of the facing, because the increase ratio of the maximum displacement is small and the increase of the displacement of the joint part of the facing with the inspection gallery concrete has been almost zero in recent years. Further, there were not large changes observed in the asphaltic concrete with a protective layer after a few years.

REFERENCES

- Kiyoshi.Ishii, Minoru.Kamijyo, 1988, Design for asphaltic concrete facing of Sabigawa upper dam, *ICOLD, San Francisco, 1988.*
- Yoshihisa.Hibino, Hideo.Suzuki & Yoshinori.Mori, 1999, Maintenance of asphaltic concrete facing of Yashio dam, *Electric Power Engineering, No. 279, January 1999.* Tokyo: Electric Power Civil Engineering Association.

Some long-term problems associated with suffusion in the foundation of embankment dams

A. Soroush

Amirkabir University of Technology (Tehran Polytechnic), Tehran, Iran
Member of Directorate Board of Iranian National Committee on Large Dams (IRCOLD), Iran
Chairman of Iranian Geotechnical Society (IGS), Iran

P.T. Shourijeh

Amirkabir University of Technology (Tehran Polytechnic), Tehran, Iran
Member of Iranian National Committee on Large Dams (IRCOLD), Iran
Member of Iranian Geotechnical Society (IGS), Iran

ABSTRACT: Suffusion may cause unavoidable changes in porosity, permeability, pore pressure distribution and mechanical behavior of soils, which in turn influence the stability/safety of earth dams and other hydro-geotechnical structures consisted-of, or constructed-on such soils. Open-framework gravels, alluvial sediments and glacial tills are samples of soils prone to suffusion. This paper present a systematic experimental program, aimed at studying changes of soil properties caused by suffusion. The tested soils are typical alluvial sediments. The state of the art seepage tests instigate suffusion in soils while monitoring changes in void ratio. Tri-axial experiments on the post-suffusion soils highlight changes in mechanical properties. The results reveal the complex interaction between hydraulic behavior, physical properties, and mechanical behavior of suffusive soils.

1 INTRODUCTION

The suffusion phenomenon, that is the migration of small particles through the coarse skeleton of internally unstable soils, may generate serious problems for embankment dams and other hydro-geotechnical structures. In internal suffusion, fine particles moving in the soil structure are prevented from exiting the soil layer, the total solid mass of the soil remains unchanged and the local permeability and void ratio are altered. In zones evacuated by loose particles, local permeability and void ratio increases, whereas in zones where loose small particles accumulate, local permeability and void ratio decreases. On the other hand, in the event of external suffusion small loose transported particles leave the soil layer. Thus, overall permeability and void ratio of the soil increase, which may cause serious problems regarding seepage and stability conditions of structures overlying the soil.

Many earth dams are founded on broadly graded and concave upward alluviums, for which suffusion may cause damage or even eventuate to failure (CFGB, 1997; Fell et al., 2005). During impounding and operation of the dam, such soils as foundation materials, are subjected to water heads and gradients significantly higher than those experienced by the soils during their history of formation and deposition/sedimentation. Therefore, the potential for suffusion in these soils is twofold: their internally unstable fabric and being subjected to comparatively high seepage forces.

Skempton & Brogan (1994) alluded to the abundance of alluvial sediments that are susceptible to suffusion, [Figure 1a](#), and noted the serious piping problems associated with these soils, especially in relation to embankment dams. [Figure 1b](#) illustrates some typical gradations of alluvial foundations for embankment dams, constructed or under construction in

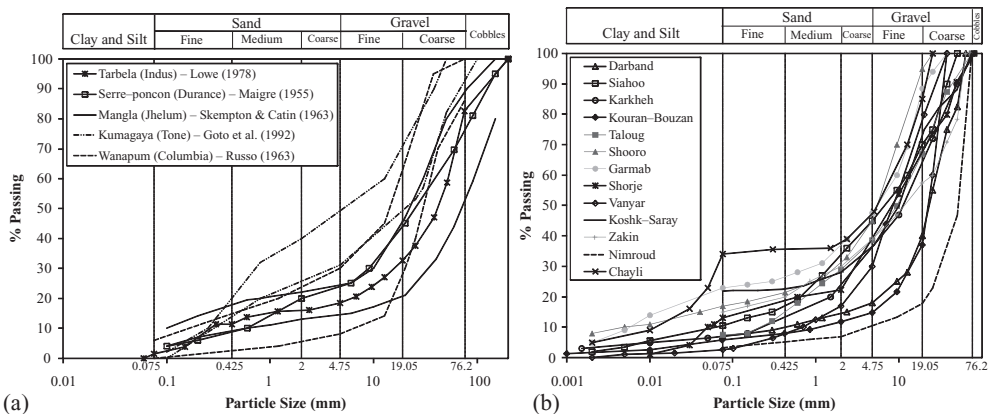


Figure 1. (a) Some alluvial sediment recognized as internally unstable by Skempton & Brogan (1994), and (b) typical gradations of some Iranian alluviums.

Iran. When suffusion occurs within the foundation of a dam, increased seepage and progressive weakening of the foundation may result in crest settlement, or development of pipes or sinkholes in the embankment or its foundation.

Many researchers have investigated the multi faceted phenomena of internal instability and suffusion. Antecedent studies have focused mainly on; (1) assessing the internal stability of soils and establishing recognition criteria (Kezdi 1969, Kenney & Lau 1985, Wan & Fell 2008), and (2) determining the critical threshold gradient whereat suffusion commences (Skempton & Brogan 1994, Li 2008). Nonetheless, little is available concerning suffusion effects on the mechanical behavior/properties of soils. Wolski et al. (2000) reported case histories where changes in mechanical properties of sandy soils as a consequence of erosion, mainly in the form of suffusion, had developed and argued that erosion may change the propensity of sandy soils to flow liquefaction. Sterpi (2003) conducted a systematic experimental program for measuring variations in density and mechanical behavior of a sandy soil subjected to suffusion. Apart from the limited studies mentioned, there is a lack of insight into the mechanical behavior of soils subjected to suffusion.

This treatment presents preliminary results of an ongoing experimental investigation of suffusion and its influence on the mechanical properties of soils.

2 FABRIC OF INTERNALLY UNSTABLE SOILS

The vulnerability to suffusion is controlled by soil's internal geometrical condition (fabric). The conceptual visualization of granular, cohesionless soil fabrics is illustrated in Figure 2. Two different fabrics can be distinguished as follows:

- Clast-supported fabric; coarser particles nest in contact building a skeleton or primary fabric, while finer particles are accommodated in voids formed between the coarser particles. The skeleton of clasts defines the overall soil volume, sustains mechanical loads and is dominant in shear strength mobilization.
- Matrix supported fabric; finer particles occupy a larger portion of the soil volume and coarser particles float in a fine matrix or binder. Therefore, finer particles are preponderant in carrying mechanical loads and governing the shear strength.

In general internally unstable soils, potentially prone to suffusion, have clast-supported fabrics. Hence, in the event of suffusion where finer particles are eroded a considerable increase in the void ratio along with limited (if any) volumetric strain would be plausible.

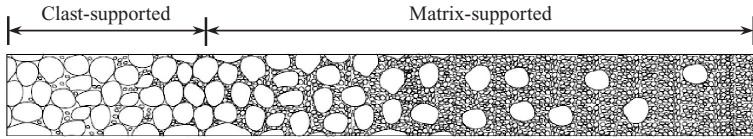


Figure 2. Conceptual visualization of clast-supported and matrix supported fabrics.

3 PERMEAMETER TESTS

3.1 Soils/gradations

Considering the typical gradations of Iranian alluvium (cf. Fig. 1), two concave upward gradations, i.e. S1 and S2, were defined for testing. As illustrated in Figure 3, the soils tested are artificially blended, broadly graded mixtures of rounded to sub-rounded sand and gravel aggregates. The fines content ($\% < 75 \mu\text{m}$) comprises ground silica powder; having no plasticity. It is assumed that the soils represent natural alluvial deposits from the prospect of particle shape and composition. Table 1 presents specifications of the gradations.

Internal stability assessment for the soils by methods of Burenkova (1993) and Li & Fannin (2008), Figure 4, reveals that the soils are internally unstable and susceptible to suffusion.

3.2 Apparatus and testing scheme

The test apparatus/system incorporated in this study, replicates the test setup developed by Moffat (2005) and used by Li (2008). The main cylinder of the apparatus is 100 cm high having an internal diameter of 23 cm. A unidirectional (up/down) seepage flow with gradients ranging from 0.5 to 150 may be applied to specimens up to 60 cm in length. The setup is equipped with a pneumatic actuator capable of applying vertical surcharge pressure (from 5 to 1000 kPa) to the specimen's top surface. The vertical surcharge is measured and controlled by a load cell, while any specimen deformation as a result of erosion is measured by the LVDT (Linear Variable Differential Transformer). Hydraulic head at different elevations is monitored by an array of pressure transducers. The system control and data logging is performed by closed-loop software. Figure 5 depicts the apparatus. Further details concerning the apparatus and test procedure are available in Shourijeh (2010).

The specimen reconstitution and test procedures are as follows:

- The soil specimen, 23 cm in diameter and 38 cm high, is carefully placed in eight moisturized layers. Roding and tamping (if necessary) is used for specimen compaction. The soil is located over a wire mesh (6.73 mm for soil S2 and 9.52 mm for S1).
- A surcharge pressure of 25 kPa is applied slowly to the specimen's top surface.
- The specimen is saturated very slowly, with an infinitesimal upward flow in a scheme similar to ASTM D2434.
- A downward flow is exerted to the specimen while the surcharge is preserved constantly. The flow gradient is increased in unit steps (equal to one) from 1 to 10, and each gradient level is maintained for 30 minutes.
- During seepage the effluent rate is measured and the erosion product is collected.

The mesh apertures are selected as to permit high external suffusion from the soils. The influent stepwise increase enables gradual erosion by suffusion, without subjecting the specimen to a sudden flushing, which may lead to clogging. The maximum gradient, i.e. 10, is much higher than gradients usually experienced in foundations of embankment dams, and therefore compensates for the limited test duration, circa 5 hours, in contrast to the life span of embankment dams.

The specimen subject to a constant surcharge pressure and experiencing suffusion undergoes volumetric strain accompanied by void ratio changes, which are determined by measurements of the specimen's surface settlement and amount (mass) of eroded particles.

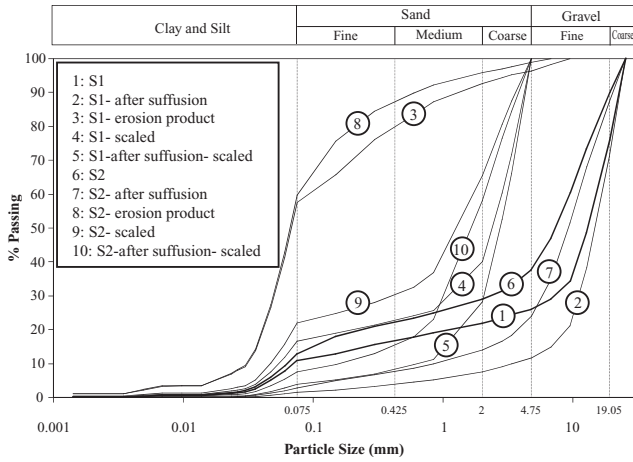


Figure 3. Gradations tested in the permeameter.

Table 1. Specifications of tested soils.

Soil	Original				After suffusion			
	% <math><75\ \mu\text{m}</math>	% <math><4.75\ \text{mm}</math>	C_u	USCS*	% <math><75\ \mu\text{m}</math>	% <math><4.75\ \text{mm}</math>	C_u	USCS
S1	11	26	215	GP-GM	1.6	11.7	5	GP
S2	13	37.7	150	GM	2.9	24	13	GP

*Unified Soil Classification System.

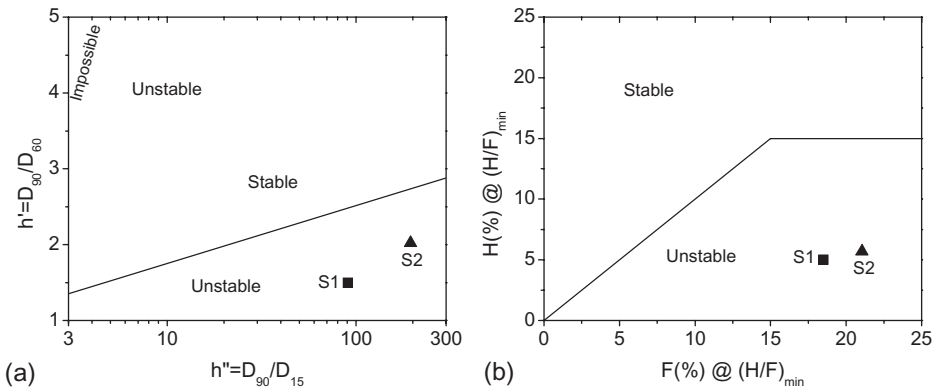


Figure 4. Internal stability assessment for tested gradations, via methods of (a) Burenkova (1993) and (b) Li & Fannin (2008).

No vibration was imparted to the apparatus during the tests. It should be noted that a specimen subjected to suffusion in permeameter tests is usually extracted in several layers and the gradation of each layer is defined (Kenney & Lau 1985, Wan and Fell 2004). In this study however, the specimen is considered as one layer after the test, that is to say the specimen is dealt as a single soil element. This reasonably represents field performance of alluvial deposits.

3.3 Suffusion tests results

Visual inspection of suffusion tests suggested that the rate of erosion was overall decreasing as time elapsed, albeit temporary increases in erosion were observed during each increase of



Figure 5. Photograph of permeameter test apparatus and setup.

the gradient. Results of the tests are reported in [Tables 1](#) and [2](#), and illustrated in [Figure 3](#). Both soils, S1 and S2, experienced a high amount of erosion during suffusion and the remnant gradation differed significantly from the original soil, inasmuch as the soil classification had changed (cf. [Table 1](#)). As expected a large proportion of the erosion product comprises fines (i.e. minus $75\ \mu\text{m}$), however, fine to medium sand particles are also abundantly eroded.

As a result of suffusion both S1 and S2 experience considerable increase in void ratio (e). The physical reason is that the erodible fraction of internally unstable soil evacuates voids between coarser particles comprising the soil's skeleton (primary fabric).

While the volumetric strain (ϵ_v) associated with suffusion was negligible for S1, it was close to 5% for soil S2, implying that the primary fabric (skeleton) of S2 was more compressible than S1. Noticing that; both S1 and S2 were tested in a similar manner, had identical initial void ratios, and experienced almost equal erosion, suggests that the volumetric strain observed for S2 is probably related to the finer gradation of S2 in comparison to S1.

4 MECHANICAL TESTS

4.1 *Methodology, apparatus and gradations*

With the changes in void ratio and gradation observed in permeameter tests for soils S1 and S2, it is anticipated that mechanical behavior/parameters should have been altered. Triaxial tests on soils before and after suffusion were executed to define the effects of suffusion on mechanical properties. A closed-loop digitally servo-controlled triaxial apparatus, capable of performing static and dynamic triaxial tests, was employed for this research.

A 7 cm diameter specimen can be seated in the triaxial cell. As stated by Jamiolkowski et al. (2005) the ratio of specimen diameter to maximum grain size should be more than 5 and preferably higher than 8. Hence soils S1 and S2, both before and after suffusion, should be scaled for triaxial testing. The parallel gradation technique (Lowe 1964) was used for scaling the gradations. In this method the gradation is shifted parallel to the logarithmic abscissa (i.e. particle size), hence gradation's shape, that is the foremost important factor controlling internal stability, remains unchanged. In [Figure 3](#) gradations scaled to the maximum size of 4.75 mm are illustrated.

Triaxial specimens are prepared by the under-compaction method (Ladd 1978) in 6 layers. A key assumption is made here, and that is the void ratio of soils before and after suffusion (cf. [Table 2](#)) is also valid for scaled gradations with the maximum size of 4.75 mm.

Consolidated drained (CD) triaxial tests were performed, for which detailed phases, viz. saturation, consolidation and shearing, are well known and will not be discussed here for brevity.

Table 2. Volumetric and density changes for soils S1 and S2 in suffusion.

Soil	Before suffusion		After suffusion		During suffusion		
	γ_d (gr/cm ³)	e (%)	γ_d (gr/cm ³)	e (%)	Mass erosion (%)	Δe (%)	$\Delta \epsilon_V$ (%)*
S1	1.89	36.4	1.59	61.2	17	24.9	0.29
S2	1.89	37.1	1.65	56.4	18.4	19.3	4.74

* Positive for volume reduction.

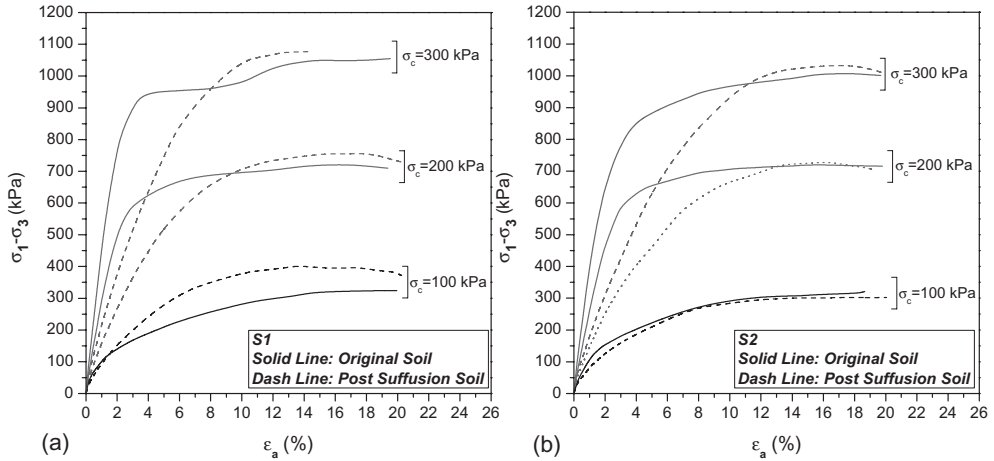


Figure 6. Stress-strain variation in triaxial CD test for soils; (a) S1 and (b) S2.

4.2 Triaxial tests results

The results of consolidated drained triaxial tests on scaled S1 and S2 (before and after suffusion), in terms of principal stress difference versus axial strain, are illustrated in Figure 6. As seen, at any confining pressure the strength of soils before and after suffusion is more or less similar and close in peak value. However, the original soils are stiffer and have a higher elastic modulus, i.e. $(E_{50\%})^{sec}$, for the linear part of stress-strain curve, which is attributed to the higher void ratio of post-suffusion specimens (cf. Table 2).

According to Table 3 the friction angle (ϕ) at peak strength is slightly higher after suffusion. The consequences of suffusion on mechanical properties of soils can be interpreted through the following notions:

- i. After suffusion the soil has lost finer particles and becomes coarser, tending to have a higher friction angle, and more strength.
- ii. The friction angle is dominated by soil's coarser particles. Coarser particles (i.e. primary fabric) are essentially remnant through suffusion; hence the friction angle should remain unchanged. This perception has been validated by triaxial tests on a gap-graded soil by Khalili et al. (2010).
- iii. After suffusion the void ratio is higher in comparison to the original soil. Thus, a lower friction angle and less strength/stiffness are projected.

A complicated interaction of the foregoing effects is at play in defining mechanical properties of soils subjected to suffusion. Of course, contribution of each mentioned effect depends on initial soil gradation, seepage forces, and to some extent confining pressure of soil during suffusion.

Table 3. Mechanical parameters of scaled S1 and S2 before and after suffusion.

Soil	Before suffusion			After suffusion		
	$e_{con.}$ (%)*	ϕ (°)**	$(E_{50\%})^{sec.}$ (Mpa)***	$e_{con.}$ (%)	ϕ (°)	$(E_{50\%})^{sec.}$ (Mpa)
S1	35	39.5	43	57	40.8	17
S2	35	38.8	36	52	39.2	13

* Void ratio for triaxial specimen after consolidation and before shearing.

** Friction angle in degrees.

*** Secant Young's modulus for 50% of peak strength.

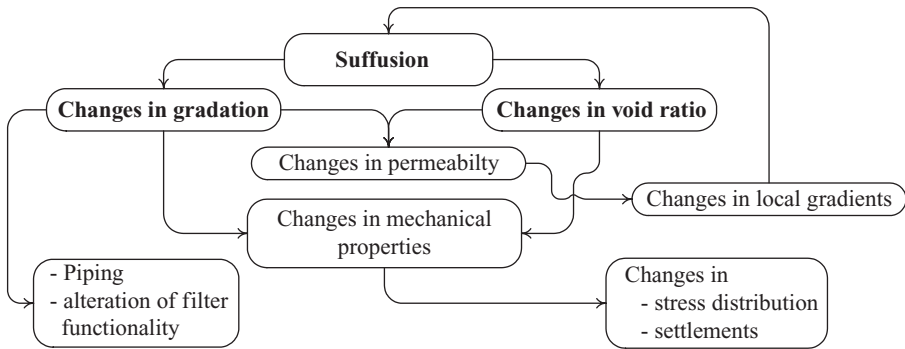


Figure 7. Flow diagram for major effects of suffusion.

5 CONCLUDING REMARKS

Heretofore, suffusion has been addressed chiefly from the viewpoint of piping and progression of internal erosion in foundations of embankment dams that may eventuate to dam breach or malfunctioning of seepage control strategies. Aside from piping related problems, suffusion may result in unavoidable changes of void ratio and fabric, mechanical behavior, and strength parameters of soils. This is especially disquieting bearing in mind that suffusion is slow in nature, and its development in embankment foundations may be out of sight for a long time.

The experimental results of this study show that internally unstable soils may experience a mass erosion of near 20% by suffusion. Furthermore, suffusion may lead to void ratio increase as high as 25%, and elastic modulus decrease up to 60%. Alterations of gradation and void ratio lead to permeability changes, which in turn effect pore pressure distribution and may eventuate to repetitive suffusion in soil layers.

Figure 7 introduces a flowchart addressing the consequences of suffusion. It is prudent to consider plausible and sound variations in mechanical and volume change properties of soils subjected to suffusion, in stress and settlement analysis dealing with the long term stability and performance of embankment dams and other hydro-geotechnical structures.

ACKNOWLEDGMENTS

The authors would like to express their appreciation to the Applied Research Office of the Iran Water Resources Management Company (IWRMC) for financially supporting this study through project DAM1-84002.

REFERENCES

- ASTM D2434. 1996. Standard Test Method for Permeability of Granular Soils (Constant Head), *Annual Book of ASTM Standards*, Vol. 04.09, ASTM Philadelphia, USA.
- Burenkova, V.V. 1993. Assessment of suffusion in non-cohesive and graded soils, *Proceedings of the First International Conference "Geo-Filters"*, Karlsruhe, Germany, 20–22 October 1992, *Filters in Geotechnical and Hydraulic Engineering*, Brauns, Heibbaum & Schuler (eds), 1993, 357–360, Rotterdam: Balkema.
- CFGB. 1997. Internal Erosion: Typology, Detection, Repair, *Barrages and Reservoirs*, No. 6., Comité Français des Grands Barrages, Le Bourget-du-lac Cedex.
- Fell, R., MacGregor, P., Stapledon, D. & Bell, G. 2005. *Geotechnical Engineering of Dams*, London: Taylor & Francis Group.
- Goto, S., Suzuku, Y., Nishio, S. & Ohoka, H. 1992. Mechanical properties of undisturbed Tone-River gravel obtained by in-situ freezing method. *Soils and Foundations*, 32 (1):15–25.
- Jamiolkowski, M., Kongsukprasert, L. & Lo Presti, D. 2005. Characterization of gravelly geo-materials, In *Proceedings of the Fifth International Geotechnical Conference*, Cairo, Egypt, 12 January 2005: 1–27.
- Kenney, T.C. & Lau, D. 1985. Internal stability of granular filters, *Canadian Geotechnical Journal*, 22(2): 215–225.
- Kézdi, Á. 1969. Increase of protective capacity of flood control dikes (in Hungarian), *Department of Geotechnics*, Technical University of Budapest, Report No. 1.
- Khalili, A., Wijewickreme, D. & Wilson G.W. 2010. Mechanical response of highly gap-graded mixtures of waste rock and tailing, Part I: Monotonic shear response, *Canadian Geotechnical Journal*, 47(5): 552–565.
- Ladd, R.S. 1978. Preparing test specimen using under compaction, *Geotechnical Testing Journal*, ASTM, 1(1): 16–23.
- Li, M. 2008. Seepage-induced failure of widely graded cohesion-less soils, *PhD thesis*, Department of Civil Engineering, The University of British Columbia, Vancouver, B.C.
- Li, M. & Fannin, R.J. 2008. Comparison of two criteria for internal stability of granular soil, *Canadian Geotechnical Journal*, 45(9): 1303–1309.
- Lowe, J. 1964. Shear Strength of Coarse Embankment Dam materials, *Proceedings 8th International Congress on Large Dams*, 2: 745–761.
- Lowe, J. 1978. *Foundation design: Tarbela Dam*. Mexico City: Mexican Society for Soil Mechanics.
- Maigre, R. 1955. Rétaliation par injection d'un écran imperméable en matériel alluvionnaire. *Proc. 5th Congr. Large Dams, Paris*, 1:757–801.
- Moffat, R. 2005. Experiments on the internal stability of widely graded cohesionless soils, *PhD thesis*, The University of British Columbia, Vancouver, B.C.
- Russo, R.S. La. 1963. Wanapum development: slurry trench and grouted cut-off. *Grouts and drilling muds in engineering practice*, 196–201. London: Butterworth.
- Shourijeh, P.T. 2010. An investigation of internal erosion and its influence on the mechanical properties of soils, *PhD thesis*, Amirkabir University of Technology, in Persian.
- Skempton, A.W. & Brogan, J.M. 1994. Experiments on piping in sandy gravels, *Geotechnique*, 44(3): 449–460.
- Skempton, A.W. & Catin, P. 1963. A full-scale alluvial grouting test at the site of Mangla Dam. *Grouts and drilling muds in engineering practice*, 131–135. London: Butterworth.
- Sterpi, D. 2003. Effects of the Erosion and Transport of Fine Particles due to Seepage Flow, *International Journal of Geomechanics*, 3(1): 111–122.
- Wan, C.F. & Fell, R. 2004. Experimental investigation of internal instability of soils in embankment dams and their foundations, *UNICIV Report No. R-429*, October 2004, School of Civil and Environmental Engineering, University of New South Wales, Australia.
- Wan, C.F. & Fell, R. 2008. Assessing the potential of internal instability and suffusion in embankment dams and their foundations, *Journal of Geotechnical and Geoenvironmental Engineering*, ASCE, 134(3): 401–407.
- Wolski, W., Lipiński, M.J., Fürstenberg, A. & Barański, T. 2000. "Influence of internal erosion on safety of old dams", *Proceedings of GeoFilters 2000, Filters and Drainage in Geotechnical and Environmental Engineering*, Wolski & Mlynarek (eds), Warsaw, Poland, 5–7 June 2000, Balkema, Rotterdam, 357–364.

RCC dams—is there a limit to the height?

M.R.H. Dunstan

Malcolm Dunstan & Associates, Hayford Hall, Buckfastleigh, Devon, UK

ABSTRACT: There are now some 470 RCC dams either complete or under construction around the World. A greater proportion of these dams are very high dams (more than 100 m high) than any other form of dam construction. By the end of 2009 there were two completed RCC dams more than 200 m high—Longtan (217 m) and Guangzhao (201 m), both in China. There is also a third dam, Gigel Gibe III (240 m) in Ethiopia that is under construction and at least a further four or five dams that have been designed and are waiting to start construction. The paper describes Longtan, the largest RCC completed to date, and discusses what are the limits to the height both in terms of the requirements of the RCC and also in terms of the economics of the construction methodology.

1 RCC DAMS IN 2010

At the end of 2009 there were at least 471 RCC dams (over 15 m in height) either complete or under construction (with the RCC due to start by the end of 2010). The total volume of RCC placed in these dams was a little under 165 Mm³ and the total volume of the dams (including the traditional immersion-vibrated concrete) was just over 230 Mm³.

These dams have been completed in 49 countries and are under construction in a further four (Ghana, El Salvador, Iraq and Panama). The number of RCC dams in each country is shown in [Table 1](#). It can be seen that China has by far the most dams, nearly 150, whereas the next countries, Japan and the USA, have only 45 to 50 each. The spread of the dams around the World by Continent is shown in [Figure 1](#). Nearly half all the RCC dams are in Asia and it is here where the highest and largest RCC dams are being constructed.

The first RCC dams were constructed during the early 1980s but during the first half of that decade very few RCC dams were constructed. During the second half of the 1980s as confidence in the methodology grew, the number of RCC dams being completed each year increased to circa 15. This number remained the same until the mid 2000s when again there has been a definite surge to about 25 dams per year. Whether this increase will be maintained only time will tell. Nevertheless the number of dams under construction seems to indicate that it will. At the same time there has been an increase in the size of the RCC dams being constructed. This is shown in [Figure 2](#). From the early RCC dams in the 1980s until 1990 the average size of RCC dam had remained relatively constant with an average height of circa 40 to 50 m and an average volume of circa 150,000 m³. However since 1990 there has been a steady increase in the size and the average RCC dam is now nearly 100 m high with a volume approaching 1 Mm³.

At the end of 2009, 17.6% of all RCC dams were 100 m or higher. This compares to an overall average for all dam types of 2.7%. Thus significantly more high dams are constructed of RCC than other forms of dam construction.

2 DESIGN PHILOSOPHY

The number of RCC dams, either complete or under construction at the end of 2009, designed as high-paste content RCC dams (i.e. with a cementitious content in excess of 150 kg/m³),

Table 1. Number of RCC dams that were complete or under construction at the end of 2009 in each country.

Country	Complete	U. construction	Total
Algeria	3	1	4
Angola	1	0	1
Argentina	1	1	2
Australia	12	2	14
Belize	1	0	1
Bolivia	1	0	1
Brazil	36	0	36
Burkina Faso	1	0	1
Canada	2	0	2
Chile	2	0	2
China	135	11	146
Colombia	2	0	2
Costa Rica	1	1	2
Dominican Rep.	3	0	3
El Salvador	0	1	1
Eritrea	1	0	1
France	6	0	6
French Guyana	1	0	1
Ghana	0	1	1
Greece	4	3	7
Honduras	2	0	2
India	3	0	3
Indonesia	1	1	2
Iran	3	6	9
Iraq	0	1	1
Japan	47	1	48
Jordan	3	0	3
Jordan/Syria	1	0	1
Kazakhstan	1	0	1
Kyrgyzstan	1	0	1
Laos	1	1	2
Malaysia	1	3	4
Mexico	10	2	12
Mongolia	1	0	1
Morocco	17	4	21
Myanmar	1	1	2
Oman	1	0	1
Pakistan	1	1	2
Panama	0	1	1
Peru	4	1	5
Philippines	1	0	1
Portugal	1	0	1
Romania	2	0	2
Russia	1	0	1
South Africa	14	2	16
Spain	23	1	24
Thailand	3	0	3
Tunisia	2	0	2
Turkey	3	2	5
UAE	2	0	2
USA	43	2	45
Venezuela	1	0	1
Vietnam	4	8	12
TOTAL	412	59	471

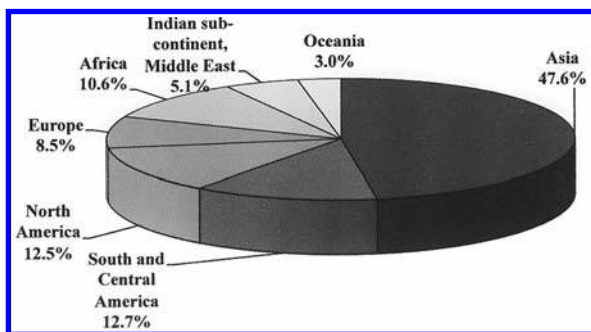


Figure 1. Percentage of RCC dams that were complete or under construction at the end of 2009 in each Continent.

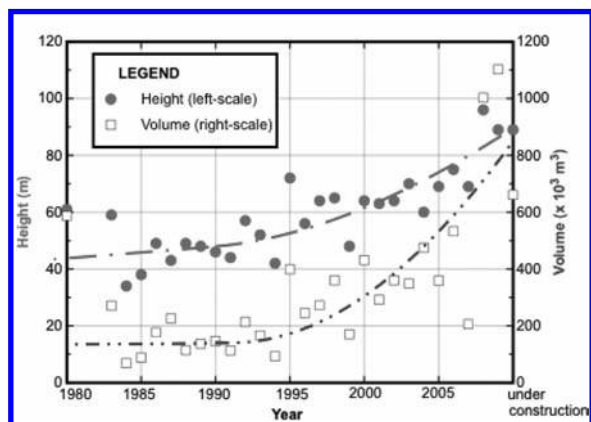


Figure 2. Average height and volume of RCC dams completed each year.

medium-paste content RCC dams (ie with a cementitious content between 100 and 149 kg/m^3), RCD dams (that are unique to Japan), lean RCC dams (ie with a cementitious content less than 99 kg/m^3) and hard-fill dams (with symmetrical sloping faces (Londe & Lino, 1992)) are shown in Figure 3.

It can be seen that 55% of all RCC dams contain high-paste content RCC. This percentage has been increasing ever since RCC dams were first constructed. For example the data used in ICOLD Bulletin N°126 (ICOLD, 2003) was gathered in 1996 and the percentage was then 43.3% and in 2002 (Dunstan, 2003) the percentage was 47.4%. Consequently it seems the percentage of RCC dams containing high-paste content RCC is increasing at an even faster rate.

Nevertheless Figure 3 does not give a true picture of the situation because it only relates to the number of dams and the volume of the RCC placed in these dams has varied from 3000 to 6.5 Mm^3 . Figure 4 shows the percentage of the volume of RCC placed using each design philosophy (without RCD dams because they are unique to Japan and also without the RCC dams for which the design philosophy is not known). In simple terms 75% of all RCC placed to date in dams is high-paste content RCC, circa 12.5% is medium-paste content RCC and circa 12.5% is lean RCC or hard fill. Unless there is a very good reason, it seems high-paste content RCC is the optimum solution for the great majority of RCC dams.

Sometimes there is a misconception that high-paste content RCCs have a ‘wet’ consistency. Indeed they are very much more workable than other forms of RCC, usually in a range of Loaded VeBe times of 8 to 12 seconds whereas a medium-paste content RCC will usually have a Loaded VeBe time of circa 15 to 20 seconds and most lean RCCs (and hard-fill RCC) will have a Loaded VeBe time in the range of 30 to 50 seconds, ie effectively outside the range of the test. Table 2 shows the average mixture proportions of the RCCs designed with the different design philosophies.

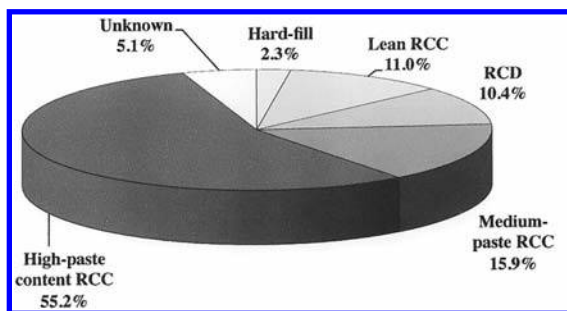


Figure 3. Percentage of RCC dams that were complete or under construction at the end of 2009 using various different design philosophies.

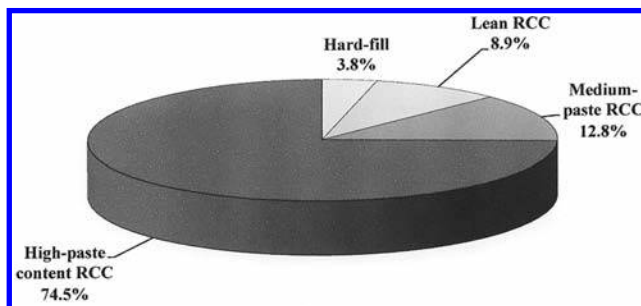


Figure 4. Percentage of the volume of RCC placed in dams that were complete or under construction at the end of 2009 using various different design philosophies.

Table 2. Average mixture proportions of RCCs designed with various design philosophies.

	Mixture proportions of the paste (kg/m ³)				Water/ cementitious ratio
	Cement	Pozzolan	Total	Water	
Hard-fill	60	14	74	135	1.83
Lean RCC	67	11	79	122	1.55
RCD	86	36	122	94	0.77
Medium-paste content RCC	78	40	117	116	0.99
High-paste content RCC	88	107	195	111	0.57

It is clear from [Table 2](#) that as the cementitious content increases and the RCC becomes more workable, the average water content actually decreases. This is because of the ‘ball-bearing’ effect of the high content of pozzolan in the mix. Nevertheless the most important figures in [Table 2](#) are the water/cementitious ratios. This drops from 1.5 to 2.0 for the lean RCCs (and the RCC used in hard-fill dams) to circa 1.0 for medium-paste content RCC to circa 0.75 for RCD and to 0.50 to 0.60 for high-paste content RCC. The average Portland cement contents in all the different forms of RCC does not vary significantly and are generally in the range of 60 to 90 kg/m³. The big differences are in the pozzolan contents that range from very low in the lean RCCs to significantly more than the Portland cement content in the high-paste content RCC.

3 LARGE RCC DAMS

3.1 Highest and largest RCC dams

The ten highest completed RCC dams at the end of 2009 are shown in Table 3 and the ten with the largest volume in Table 4. Perhaps surprisingly only four, Longtan, Guanyinyan, Jin'anqiao (all in China) and Son La (Vietnam) are in both Tables. All but two of the highest dams (see Table 3) are in Asia and all but three of the largest dams (see Table 4) are also in Asia. This again shows the importance of the development of RCC dams in that part of the World.

3.2 Longtan

Taking into account all factors, i.e. height, volume, reservoir capacity and installed capacity, Longtan ($h = 217$ m, volume = 7.5 Mm^3 , reservoir capacity = $27,270 \text{ Mm}^3$, installed capacity = 6300 MW ($9 \times 700 \text{ MW}$)) is the largest RCC dam so far completed, indeed it is probably one of the ten largest dams ever constructed. The 1st-Stage RCC at Longtan (4.623 Mm^3) was started on 8 October 2004 and was completed on 20 June 2007, less than three years later. Figure 5 shows a series of photographs taken from approximately the same position located upstream of the dam. Figure 5A was taken about a month before the start of the placement of the RCC in the upstream cofferdam (circa 80 m high and containing

Table 3. Details of the ten highest RCC dams completed by the end of 2009.

Dam	Country	Height (m)	Length (m)	Volume ($\times 10^3 \text{ m}^3$)		Cementitious content (kg/m^3)		Type of pozzolan
				RCC	Total	Cement	Pozzolan	
Longtan	China	217	849	4952	7458	86	109	(F)
Guangzhou	China	201	412	820	2870	71	87	(F)
Miel I	Colombia	188	345	1669	1730	85–160	0	(-)
Guanyinyan	China	168	1250	6473	9364			(F)
Jin'anqiao	China	156	640	2400	3600	96	117	(F)
Miyagase	Japan	156	400	1737	2060	91	39	(F)
Urayama	Japan	156	372	1294	1750	91	39	(F)
Ralco	Chile	155	360	1596	1640	116	41	(N)
Takizawa	Japan	140	424	810	1670	84	36	(F)
Son La	Vietnam	139	900	2700	4800	60	160	(F)

Table 4. Details of the ten dams completed by the end of 2009 with the largest volumes of RCC.

Dam	Country	Height (m)	Length (m)	Volume ($\times 10^3 \text{ m}^3$)		Cementitious content (kg/m^3)		Type of pozzolan
				RCC	Total	Cement	Pozzolan	
Guanyinyan	China	168	1250	6473	9364			(F)
Longtan	China	217	849	4952	7458	86	109	(F)
Tha Dan	Thailand	95	2600	4900	5400	90	100	(F)
Son La	Vietnam	139	900	2700	4800	60	160	(F)
Yeywa	Myanmar	135	680	2473	2843	75	145	(N)
Jin'anqiao	China	156	640	2400	3600	96	117	(F)
Beydag	Turkey	96	800	2350	2650	60	30	(F)
Taum Sauk	USA	49	2060	2250	2300	59	59	(F)
Baise	China	130	734	1995	2672	80	132	(F)
Beni Haroun	Vietnam	118	714	1690	1900	82	143	(F)

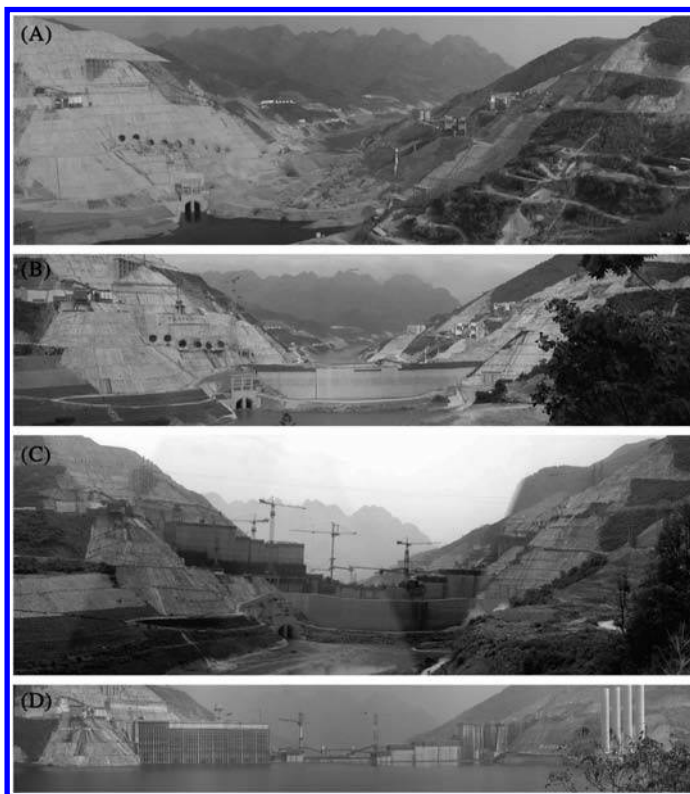


Figure 5. (A) View of the Longtan site from upstream in February 2004; (B) View of the Longtan site from upstream in February 2005; (C); View of the Longtan site from upstream in May 2006; (D) the Longtan site from upstream in November 2006.

0.25 Mm³ of RCC). [Figure 5B](#) was taken about seven months after the start of the placement of the RCC—the dam is still hidden behind the cofferdam. [Figure 5C](#) was taken less than a year after [Figure 5B](#) and the dam is now well above the cofferdam. [Figure 5D](#) shows the reservoir partially impounded with the RCC to be completed some seven months later.

The average rate of placement at Longtan was just under 143,000 m³/month. Although such a rate of placement resulted in the dam being completed some five months early (and several hundred million dollars worth of power being generated ahead of schedule), if the RCC had been better designed (as it was towards the top of the dam), if the placement had been better planned and if the dam had been designed for RCC placement, it is almost certain that the RCC would have been placed significantly faster. The maximum monthly placement was 400,755 m³. With a well-designed and well-constructed RCC dam, the peak month is between 1.60 and 1.95 times the average rate of placement. On this basis, the average rate of placement at Longtan could be been 235,000 m³/month. The peak day at Longtan was 18,475 m³—this figure is commensurate with the maximum monthly placement of 400,755 m³.

4 IN-SITU PROPERTIES

4.1 Grande Dixence

Grande Dixence is the highest concrete gravity dam (and the third highest dam) in the World. The dam was completed in 1961 and has been in operation for nearly 50 years. It is 285 m high and has a crest length of 695 m and a volume of circa 6 Mm³. The reservoir is relatively

Table 5. The ten completed RCC dams with the best-reported in-situ properties.

Dam	Core compressive strength (MPa)		Direct tensile strength across joints (MPa)		Cohesion at joints (MPa)	
	@ 91 days	@ 365 days	@ 91 days	@ 365 days	@ 91 days	@ 365 days
Shapai	28.3		2.05			
Satsunaigawa	25.9				4.10	
Platanovryssi	29.6		1.77		4.04	
Mano	17.3				3.20	
Beni Haroun	22.8		1.53			
Olivenhain		21.9		1.54		
Daguangba	19.3		1.32			
Changuinola 1 ^[1]	24.3		1.26	1.40		
Mianhuatan		33.3		1.40		2.55
Upper Stillwater ^[2]		38.5		1.40		1.90

^[1] Results from Full-Scale Trial—dam not completed, ^[2] A rather poor-quality sandstone aggregate was used that lead to an unusual relationship between the tensile and compressive strength.

small at 401 Mm³. There is no spillway. There is therefore a precedent for a concrete gravity dam with a height approaching 300 m. The concrete from Grande Dixence had an average cylinder (300 × 450 mm) compressive strength of 16.4 MPa at 90 days, a strength exceeded by over 50% of all RCC in dams and by the great majority of all high-paste contents RCCs.

4.2 In-situ properties of RCC dams

Table 5 contains details of the ten RCC dams that have the best-reported in-situ properties—there are almost certainly other RCC dams with equal, or even better, properties than those that have been reported.

Average in-situ static vertical direct tensile strengths across joints up to 2.0 MPa have been reported as well as average cohesions up to 4.0 MPa. Both these properties are more than sufficient for a concrete gravity dam with a height of approaching 300 m. All the core compressive strengths in Table 5 are in excess of the cylinder compressive strengths found at Grande Dixence, the majority well in excess.

5 RATE OF PLACEMENT

The rate of placement of RCC dams is one of the great advantages of the method of construction. Table 6 contains details of the ten fastest RCC dams (also included in the Table is Beydag, a hard-fill dam constructed very rapidly in Turkey. As the Quality Control of hard-fill dams does not have to be at the same level as other RCC dams, the very rapid and efficient placement cannot really be compared to the other RCC dams in the Table and thus there are 11 not ten dams in the Table).

Longtan is the fastest RCC dam to date with an average rate of placement of circa 143,000 m³/month. With a more efficient design and construction methodology, this might have increased to an average rate of placement of circa 235,000 m³/month using the same plant and equipment (see Section 3.2).

Of the dams in Table 6 (excluding Beydag), eight were high-paste content RCC dams and two, Taum Sauk and Al Wehdah, were medium-paste content RCC dams. There are no RCD dams or lean RCC dams in the Table, indeed there are only two lean RCC dams in the top fastest 30 RCC dams and there are no RCD dams.

There are essentially no technical problems with the placement at an average rate of 250,000 m³/month. It is not particularly difficult to mix such a quantity on a regular basis,

Table 6. The ten (& Beydag) completed RCC dams with the fastest average rates of placement.

Dam	Country	RCC placement		Height (m)	RCC vol. (x 10 ³ m ³)	Placement time (months)	Monthly placement (m ³)		Max. day (m ³)
		Start	Finish				Average	Peak	
Longtan	China	08-Oct-04	20-Jun-07	192	4623	32.4	142758	400755	18475
Upper Stillwater	USA	01-Sep-85	10-Aug-87	91	1125	9.0	125324	204430	8415
Tha Dan	Thailand	01-Mar-01	02-Jul-04	95	4900	40.1	122266	201490	13280
Olivenhain	USA	06-Feb-02	31-Oct-02	97	1070	8.8	121895	224675	12250
Beydag	Turkey	25-Jul-06	20-Apr-08	96	2350	20.9	112566	165000	
Beni Haroun	Algeria	18-Oct-98	31-May-00	121	1690	16.4	102860	175000	9100
Taum Sauk	USA	10-Oct-07	30-Nov-09	49	2250	25.7	87516		
Son La	Vietnam	11-Jan-08	26-Aug-10	139	2700	31.5	85725	200075	9980
Ralco	Chile	13-Jan-02	10-Oct-03	155	1596	20.9	76449	147600	6860
Al Wehdah	Jordan/Syria	19-Feb-05	19-Sep-06	94	1426	19.0	75172	123860	6185
Yeywa	Myanmar	07-Feb-06	15-Dec-08	134	2472	34.3	72173	147320	7555

nor it is difficult to transport it or to place it. If the dam is particularly large, it can be split into Sections and each Section can be constructed independently of each other. For example of the ten RCC dams in Table 6, five were constructed in Blocks. Of the others, 3.5 were placed horizontally in single layers, 1.0 was placed using the slope/layer method (Forbes et al., 1999) (actually two dams both of which were placed half horizontally and half with the slope/layer method) and 0.5 using split-level construction (Shelke et al., 2007).

The rate of placement is usually not determined by technical factors but almost always by the supply of materials. When 400,000 m³ was placed in a month at Longtan, this required 80,000 tonnes of cementitious materials to be delivered, peaking at 3500 tonnes in a day (some 140 trucks) and nearly 1 M tonnes of aggregate. At such a rate of placement, the Project becomes purely a logistical exercise.

6 CONCLUSIONS

There is no technical reason why a 300 m high RCC could not be completed very shortly. There is the precedent of Grande Dixence and the in-situ properties of modern RCC dams are superior to those of that dam. Nevertheless it would be sensible to progress in stages from the completion of the 217 m high Longtan dam to a number of dams circa 240 m high (e.g. Gigel Gibe II in Ethiopia and Ta Sang in Myanmar) to further dams circa 260 to 270 m high.

There is probably a limit to the average rate of placement of the RCC in the dam of circa 250,000 m³/month but this is limited by the delivery of materials rather than by the ability to mix, transport and place the RCC.

REFERENCES

- Dunstan, M.R.H. 2003. The state-of-the-art of RCC dams in 2003—an update of ICOLD Bulletin N°126. Special Lecture N°1 in Proceedings of the Fourth International Symposium on Roller-Compacted Concrete (RCC) Dams, Madrid, Spain.
- Forbes, B.J., Yang, L., Tang, G. & Yang, K. 1999. Jiangya dam, China: Some interesting techniques developed for high-quality RCC construction. Proceedings of International Symposium on Roller-compacted concrete dam, China RCC '99, Chengdu, China.
- ICOLD. 2003. Roller-compacted concrete dams—State of the art and case histories. Bulletin N°126, ICOLD, Paris.
- Londe, P. & Lino, M. 1992. The faced symmetrical hardfill dam: a new concept for RCC. *Water Power and Dam Construction*, London.
- Shelke, V.C., Sapre, S.D. & Dunstan, M.R.H. 2007. Construction of the first RCC dam in India at Ghatghar, Proceedings of the 5th International Symposium on RCC dams 'Celebration for 30 years' application of RCC in dams', Guiyang, China.

Numerical analysis of water reservoir dam—prediction of long term performance of Versetal dam (Germany)

M.M. Zimmerer

Varocon—Geo Engineering, Weimar & Bochum, Germany

T. Schanz & Y. Lins

Ruhr-Universität Bochum, Grundbau, Boden—und Felsmechanik, Bochum, Germany

V. Bettzieche

Ruhrverband, Essen, Germany

ABSTRACT: In this study the long term settlement behaviour of a rock fill dam is predicted by means of numerical simulation (FEM). The measured ongoing deformations since operation of the Verse Dam lead to the conclusion, that a creep type process takes place. Thus a visco elastic plastic model was chosen for the simulation. In a sensitivity analysis the sensitivity of the model response (deformations) with respect to the material model parameters was analysed. The study included the strength parameters from the Mohr-Coulomb failure criterion, the basic stiffness parameters and some advanced parameters. The sensitivity analysis showed a significant influence of the stiffness and creep parameters on the mechanical behaviour of the dam. Using an optimisation tool and deformation measurements carried out and/or horizontal measurements as reference values optimum set of parameter was derived. The optimum set of parameters was used to predict the deformations and the stability of the dam for the coming years.

1 INTRODUCTION

The Ruhrverband operates the Verse Dam and Reservoir with a storage volume of 33 Mio · m³. The Verse Dam was built in the 30's of last century and is located in the Märkischer Kreis District, in the southeast of Lüdenscheid on the northwestern flank of the Ebbe hills (Germany). In addition to its main reservoir impounded by a rockfill dam, the Verse Reservoir includes a preliminary reservoir impounded by a dam. The water is primarily discharged from the reservoir through a power plant at the foot of the Verse Dam.

Together with other reservoirs the Versetal Dam ensures to supply water to the Ruhr area and neighbouring areas. For routine the stability of the dam is calculated frequently using modified lamella (limit equilibrium) approach. Additionally extensive observations and measurements including horizontal as well as vertical deformations and water level fluctuations are carried out since the dam started operation in the 50's. Additional to the limit state calculations the relation between these measured deformations and the mobilization of factor of overall safety of the dam is of paramount interest for the upcoming years (e.g. for the next 10 years).

The measurement points and the measurements are given in [Figures 1](#) and [2](#). The measurements include vertical as well as horizontal measurements that are continuously taken along the dam crest, in the concrete core and on the dam at the air side since the operation of the dam in the 50's.

2 NUMERICAL MODEL

In this study the long term deformation behaviour of the Versetal Dam is predicted by means of numerical simulation. Therefore the finite element program PLAXIS was used. A multi step

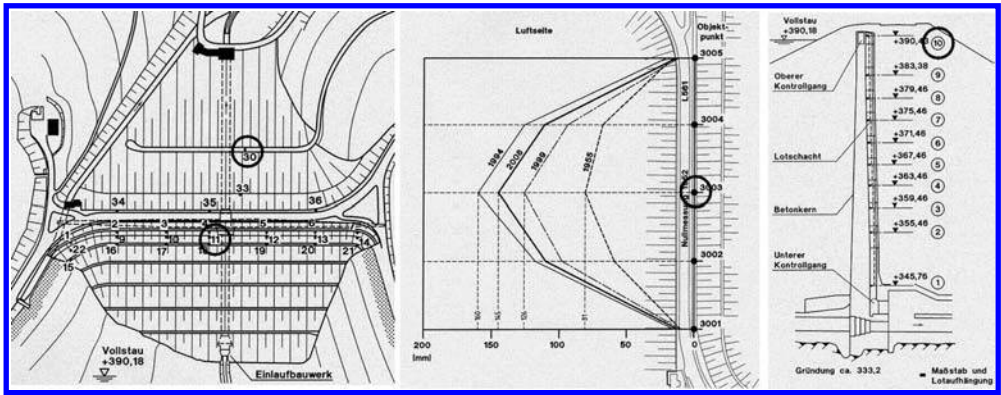


Figure 1. Measurement points.

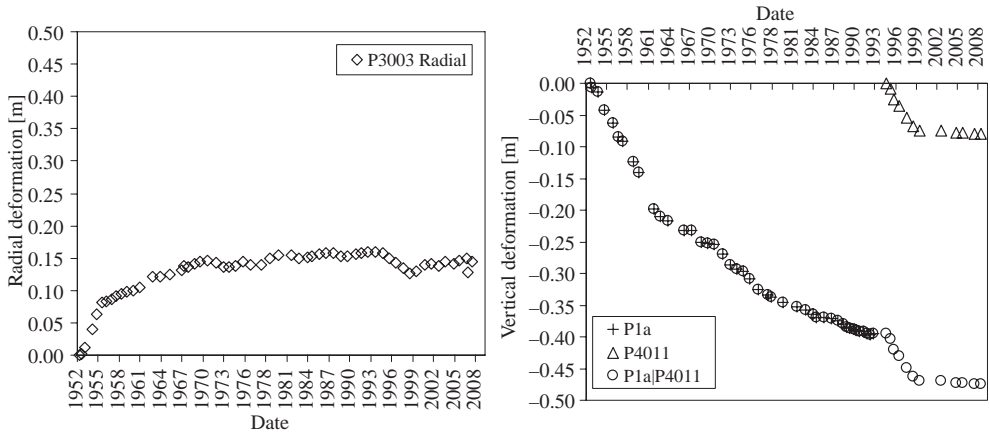


Figure 2. Measurements.

approach was followed in the following manner: In a first step a numerical model of the Versetal Dam was developed using Finite Element Method (FEM). The numerical model includes the geometry of the dam, material parameters, and initial as well as boundary conditions.

2.1 Geometry of the dam, boundary and initial condition

For the numerical simulation of the Versetal Dam a cross section in the middle of the dam was used. In the middle of the dam the maximum loadings as well as deformations due to increasing and decreasing water level were measured. The numerical model used for the FEM simulations and the generated mesh is given in Figure 3. The width of the dam is at the bottom ≈ 290 m and at the top ≈ 16 m. The dam is ≈ 54 m in height. The dam is a rock fill type dam including a concrete core as well as a clay core, a sealing body and a rock fill and was founded on the bedrock that is located below the soil of the valley.

The numerical simulation was carried out using 6-node triangular elements. The boundaries were fully fixed ($u_x = u_y = 0$) at the basement and roller conditions ($u_x = u_y = \text{free}$) were chosen for the vertical sides. Initial conditions (i.e. pore-water pressure and effective stress) were derived using a K_0 -procedure (i.e. $K_0 = 1 - \sin \phi$).

2.2 Construction phases

The numerical simulation was carried out in several construction phases starting with the construction of the dam in 1938, the impounding of the dam in several phases as well as the

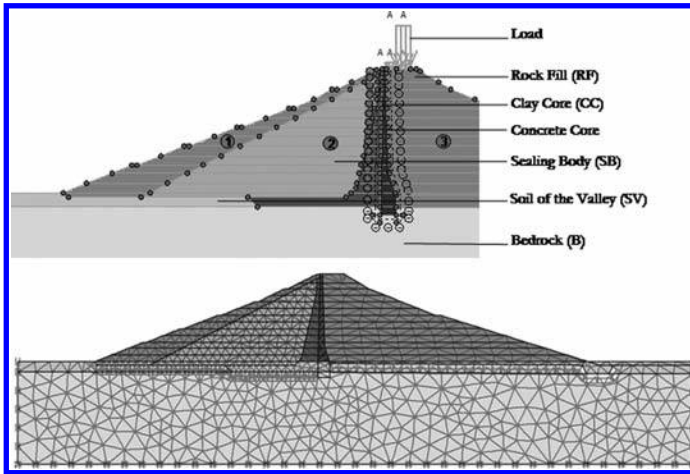


Figure 3. Model of Versetal Dam (top) and the generated mesh (bottom).

period of the operation of the dam from 1955 up to 2009. The deformations of the dam and the bearing capacity were predicted for the upcoming 10 years. All phases were calculated as consolidation phases. In detail the construction phases are described below:

1. *Construction of the dam*: The construction of the dam is divided into 15 steps and takes place over 13 years from 1938 to 1951.
2. *Impounding of the dam*: The impounding of the dam takes place over 4 years from 370.80 m above the sea level to 382.84 m and then to 389.00 m above the sea level.
3. *Operation of the dam*: The operation of the dam consists of the numerical simulation of significant water levels beginning from the operation of the dam up to 2009. The up and downturns of the water level measured by the Ruhrverband and the approximate water levels for the numerical simulation are given in [Figure 4](#).
4. *Prediction*: The prediction of the deformation and the bearing capacity of the dam were predicted for 10 years using the average water level.

2.3 Material models and parameters

The used finite element code provides different material models, e.g. the Mohr-Coulomb Model, the Hardening Soil Model, the Jointed Rock Model or the Soft Soil Model as well as the Soft Soil Creep Model, for the simulation of geotechnical applications.

The Mohr-Coulomb Model is a elastic-plastic material model. In the model it is assumed that the stiffness of the material (i.e. the stiffness of the soil) is constant distributed along the depth. But this is in general not the case for the material behaviour of soils. The Mohr-Coulomb Model is mostly used for numerical modelling of the mechanical behaviour of a soil in a first approach only.

A more realistic material model for the simulation of the behaviour of different type of soils is the Hardening Soil Model. When soil is subjected to primary loading it shows a decrease in stiffness and irreversible plastic strains develop and in contrast to the Mohr-Coulomb Model the Hardening Soil Model includes the stress dependent stiffness behaviour of the soils, i.e. the hardening of the soil is taken into account. Besides some Mohr-Coulomb material parameters additional input parameters as the stiffness modulus $E_{oed,ref}$, unloading and reloading stiffness modulus E_{ur} (derived from one dimensional compression tests) as well as the stiffness E_{50} (derived from triaxial tests) are required for the Hardening Soil Model. All required input parameters are summarised in [Table 1](#).

Whereas the Hardening Soil Model is not considering viscose effects as for instance creep or relaxation of a soil, the Soft Soil Creep Model takes this phenomenon into account.

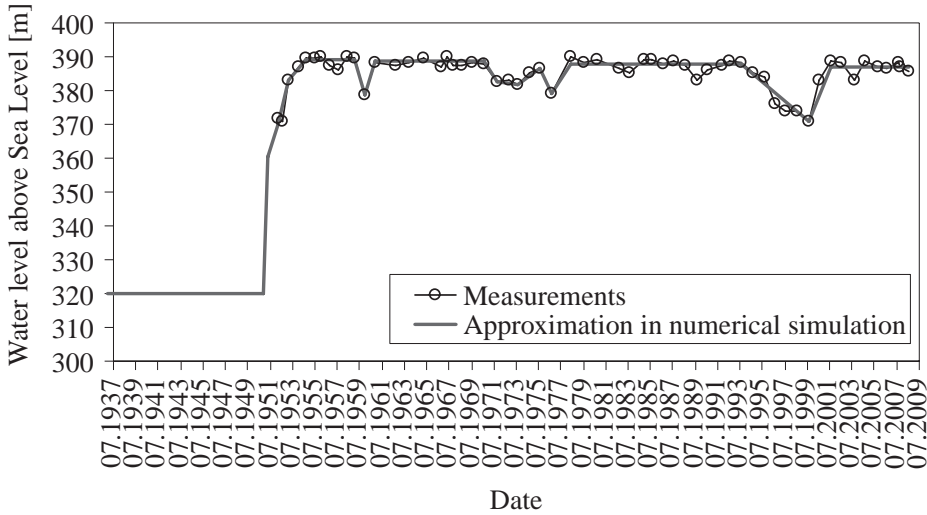


Figure 4. Measured water level in the reservoir and approximation of water level in numerical simulation.

Table 1. Soil parameters used for numerical simulation including Hardening Soil Model and Soft Soil Creep Model parameters.

Typ	B Drained	CC Undrained	SB Undrained	RF Drained	SV Undrained
General soil parameters					
γ_{unsat} [kN/m ³]	26	19.5	18	22	20
γ_{sat} [kN/m ³]	26	19.5	20	22	20
k_x [m/d]	0.0864	0.0009	0.8643	8.6430	0.8643
k_y [m/d]	0.0864	0.0009	0.8643	8.6430	0.8643
c_{ref} [kN/m ²]	3000	5	1	1	2
ϕ [°]	37.5	28.75	33	37.5	35
ψ [°]	0	0	0	0	0
ν [-]	0.2	0.2	0.2	0.2	0.2
Hardening Soil Model Parameters					
$E_{50,ref}$ [kN/m ²]	333300	3333	16666	16666	16660
$E_{oed,ref}$ [kN/m ²]	333300	3333	16666	16666	16660
$E_{ur,ref}$ [kN/m ²]	923076	10000	50000	46453	50000
M [-]	0.5	0.9	0.8	0.5	0.5
Soft Soil Creep Model parameters					
λ [-]	–	0.030 0	0.006 0	0.0060	–
κ [-]	–	0.020 0	0.004 0	0.0043	–
μ [-]	–	0.0012	0.0012	0.0012	–

This material model was primarily developed for the numerical simulation of deformation process of foundations or slopes. Some material parameters of the Soft Soil Creep model are related to the material parameters of the Hardening Soil Model:

- Modified compression index κ^* (derived from Hardening Soil parameters: $E_{ur,ref} \approx 2p^{ref}/\kappa^*$)
- Modified swelling index λ^* (derived from Hardening Soil parameters: $E_{ur,ref} = p^{ref}/\lambda^*$)
- Modified creep index μ^*
- Poisson's ratio for unloading and reloading path ν^*

- Stress ratio in a state of normal consolidation $\sigma'_{xx}/\sigma'_{yy} - K_0^{NC}$
- Parameter M

In a first step the numerical simulation was carried out using the Hardening Soil Model, because this model includes stress dependent stiffness and may differ between loading, reloading and unloading of the soil. In case of the Versetal dam the reloading and unloading of the soil is mainly caused by the changes of the water level in the Verse reservoir.

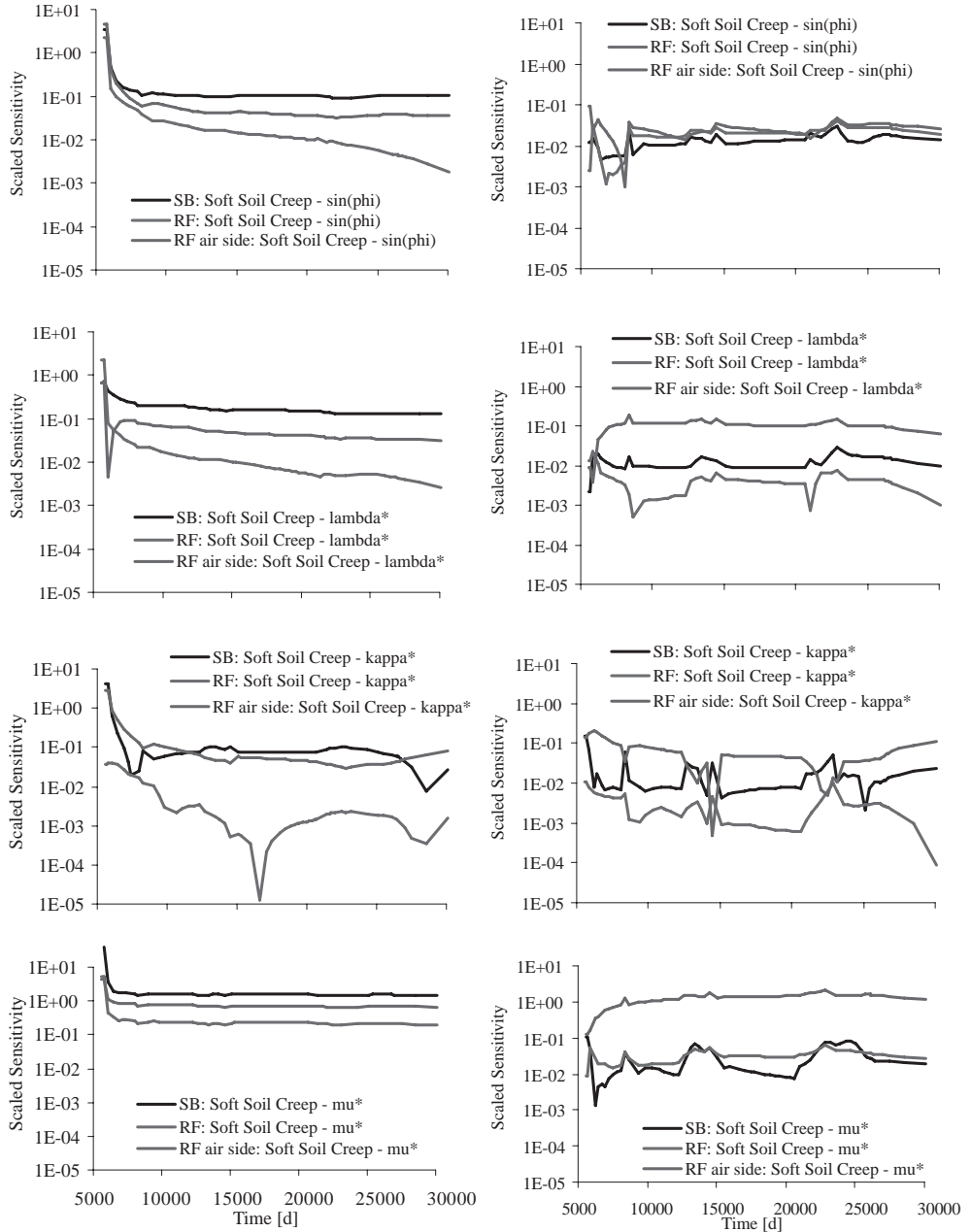


Figure 5. Scaled sensitivity (SS^+) of material parameters relating to vertical deformation in P 11 (left side) and horizontal deformation in P 3003 (right side).

But the deformation measurements along the dam performed by the Ruhrverband Essen show ongoing, continuous deformations since the operation of the dam in 1955 until 2009. That is after the consolidation of the dam (the numerical simulations using the Hardening Soil Model show, that the excess pore water pressure in the cohesive soil layers were reduced to zero after the construction of the dam) deformations are not finished yet. It seems that ongoing deformations are caused by stress redistribution due to the cyclic loading of the water level changes. Additional explanation is given by breakage of gravel due to cyclic infiltration in inherent micro-cracks. This phenomenon was approximated in further numerical simulations by using analogues Soft Soil Creep Model.

3 SENSITIVITY ANALYSIS

To evaluate the importance of model parameters (e.g. geometry, material parameters) and their influence of the results of the numerical simulations (e.g. deformations, displacement) a sensitivity analysis is carried out. In the sensitivity analysis the value of one model parameter or several model parameters are changed and its or their influence on the target value is derived (i.e. the target value is overestimated or underestimated).

In geotechnical applications sensitivity analysis is a tool to identify the value and the type of influence of material model parameters (e.g. stiffness, permeability, shear strength) to selected soil properties. Also the sensitivity analysis is used to determine the material parameters that may be identified based on the set of available data or measurements (e.g. field measurements or laboratory measurements).

In this study sensitivity was analyzed using a normalized scaled sensitivity analysis SS^+ . The normalized scaled sensitivity analysis indicates the amount of information provided by the i -th observations y_i for the estimation of j -th parameter d_j according to Eq. 1

$$SS^+ \text{ with the elements } ss_{i,j}^+ = \frac{d_j}{y_i} \frac{\partial y_i}{\partial d_j} \quad (1)$$

The results of the sensitivity analysis for the sensitivity of the Soft Soil Creep parameters λ , κ , φ and μ of the sealing body, the clay core and the rock fill (at the water side and the air side) are given in Figure 5.

The sensitivity results according to the vertical deformations in P11 (see left Figure 5) show, that the material model parameters λ , κ , φ and μ of the sealing body have the most significant influence on the mechanical behaviour (i.e. vertical deformations) followed by the rock fill (at the air side). The influence of the creep index μ is most important.

The sensitivity results according to the horizontal deformations in P3003 (see right Figure 5) show, that the material model parameters λ , κ , φ and μ of the rock fill (at the side of the air) have the most significant influence on the horizontal deformations. The most important influence was found for the creep index μ .

4 MODEL CALIBRATION

In the actual case the model calibration is done by using inverse analysis and optimisation procedures. To use optimisation procedures or algorithms we need a definition of the objective function $F(d)$ with the unknown model parameters d .

4.1 Objective function

In physics or engineering optimisation methods are used to interpret measurements from field or laboratory tests by changing constitutive material model or geometry model parameters of an analytical or numerical boundary value problem. The parameter modification is done until the model results fit the experimental data. The quality of the fit can be expressed

by the squared sum of all differences $f_i(d)$ between the numerical model $y_i(d_1, d_2, \dots, d_n)_{calc}$ and the experimental data $y_{i, meas}$ e.g.

$$F(d) = \frac{1}{n} \sum_{i=1}^n f_i^2(d) \omega_i \quad \text{and} \quad f(d) = y_{i, meas} - y_i(d_1, d_2, \dots, d_m)_{calc} \quad (2)$$

And a more advanced formulation can be found by scaling the squared differences $f_i(d)$ with the mean squared value of all observations

$$F(d) = \sqrt{\frac{\sum_{i=1}^n f_i^2(d)}{\sum_{j=1}^n y_{i, meas}^2}} \omega_i \quad \text{for } m \text{ measurements series} \quad F_{total}(d) = \frac{1}{m} \sum_{j=1}^m F_j(d) \quad (3)$$

Here

F : is the value of objective function

$i = 1, \dots, n$ number of measurements in each test series

ω : factor of weighting

$j = 1, \dots, m$ number of test series.

Basically the objective function can be any formulation describing somehow the quality of the calibrated model. A weighting of single measurements can be done using weighting factor ω .

4.2 Inverse analysis and model calibration

The optimization problem in its general formulation reads: minimize $f(d)$, subject to constraints $c_j \leq d_j \leq C_j$, for all j where $f(d)$ is a proper measure of the disagreement between model prediction and experimental observations, called objective function.

The optimisation can be done using either gradient procedures or evolutionary algorithms. In this case we used the well known particle swarm algorithm (Kennedy & Eberhard 1995) together with a surrogate model

$$y(d)_{calc} = \hat{y}(d, \beta) + \hat{\varepsilon} \quad (4)$$

for the Verse Dam in which the numerical finite element model is approximated by fully quadratic formulations $\hat{y}(d, \beta)$ for each time step t in Points 11 and 3003. β are the coefficients for a fully quadratic approximation, $\hat{\varepsilon}$ indicates the error between the finite element model and the surrogate model.

Based on the information of the soil investigation report, due to the lack of information regarding the creep index μ of the sealing body and the rock fill and due to the high sensitivity of the creep index μ on the numerical model response (see Figure 5) we focused on the calibration of the creep index μ and selected the stiffness and friction parameters from the soil investigation report.

Two cases have been analysed to verify the influence of number of available test data on the quality of the calibrated numerical model. Case one considers only the vertical settlements in point 11 and the horizontal deformation in point 3003 until the year 1980, the second case considers these recordings until 2009. Both calibrated models have been compared in Table 3.

To validate the calibrated model the desired model responses in P11 and P3003 are plotted together with the calculated and measured deformation in P30 which has not been part of the objective function in Equation 4 and 6. Figure 6 shows excellent agreement between the numerical model and the field measurements. Both calibrated creep indices μ have marginal differences in Variations V1 and V2 and no influence on the factor of safety M_{sf} (see Table 2).

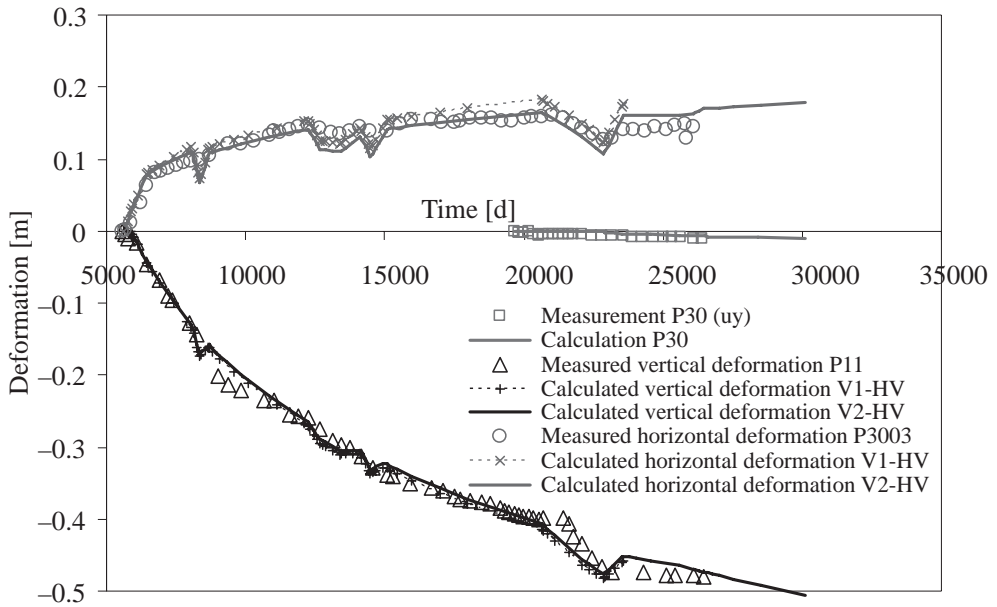


Figure 6. Comparison of vertical and horizontal measured results and calculated results in Point 11, Point 3003 and Point 30.

Table 2. SSC parameter resulting from optimisation, stability (factor of safety) and prediction of deformation.

Variation	V1-HV	V2-HV	Trend
Observation used until	1980	2009	
SB μ^* [-]	0.001546833	0.001661657	↑
RF μ^* [-]	0.000859106	0.000723486	↓
Msf (ignore undrained behaviour (D)) [-]	1.62	1.60	↓
Msf (undrained behaviour (UD)) [-]	1.39	1.39	→
u_y P11 [m] at $t = 30.000$ d	-0.515	-0.506	↑
u_x P3003 [m] at $t = 30.000$ d	0.205	0.168	↑

5 INFLUENCE OF THE ERROR OF OBSERVATION ON THE PREDICTION OF THE FACTOR OF SAFETY MSF

In finite element calculation the factor of safety Msf is calculated by reducing the shear strength parameters ϕ and c until a minimum shear strength is obtained (Brinkgreve et al. 2002).

$$\sum Msf = \frac{\tan \phi_{input}}{\tan \phi_{reduced}} = \frac{c_{input}}{c_{reduced}} \quad (5)$$

To analyse construction and operation dependent (cycling water level) stability of the dam we evaluated the factor of safety Msf after each modelled construction stage. Figure 7 indicates that (1) the operation of the dam (since 1952) and (2) its ongoing deformation has no influence on the global stability. If we assume, that only the creep behaviour influences the ongoing deformation and not cyclic loading and unloading conditions a closer look to Equation 5 emphasises this conclusion.

To investigate if it is possible to observe the long term settlement and deformation behaviour of the dam by using GPS equipment we had to assess if we can conclude on the

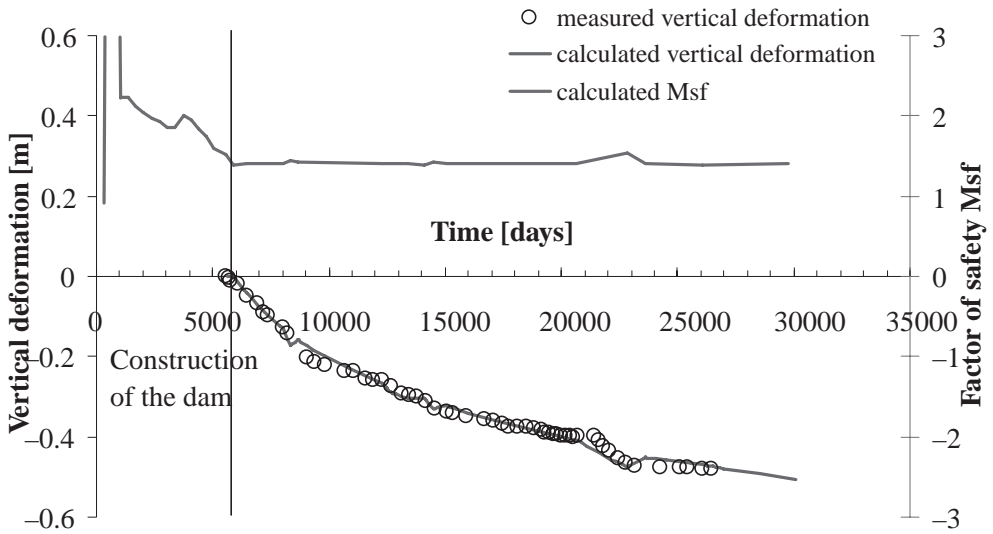


Figure 7. Vertical observations and calculated results in P11 vs. calculated Msf.

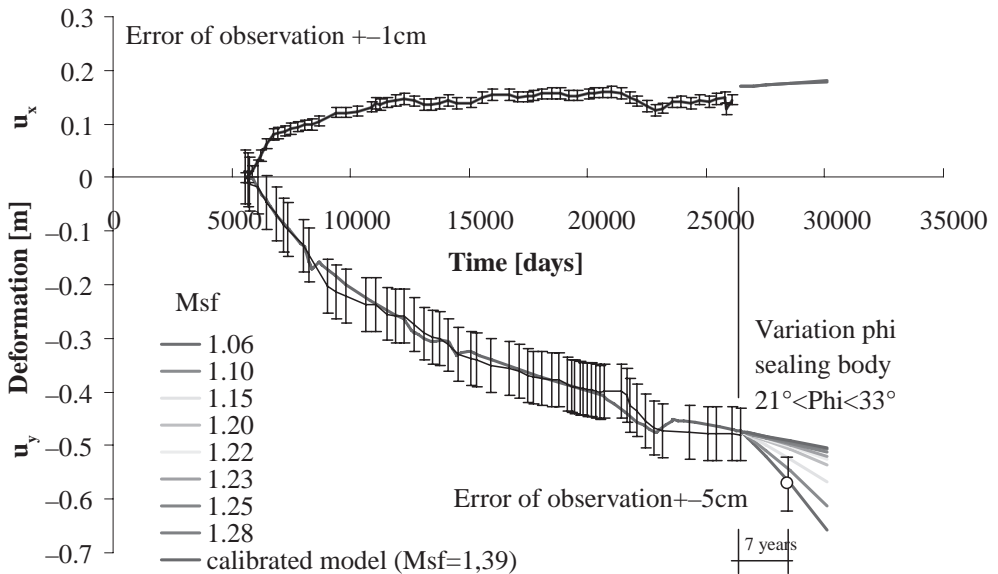


Figure 8. Calculated vertical and horizontal deformation, possible error of observation and factors of safety Msf for varying ϕ of the sealing body.

stability of the dam by exceeding a certain error of observation (vertical u_y or horizontal deformation u_x). Therefore we simulated material damaging in terms of reduction of the shear strength parameter.

ϕ in three possible damage zones (1 to 3, see Figure 3) and evaluated (1) the corresponding factor of safety Msf and (2) the corresponding deformation u_y and u_x .

The possible error of observation for vertical and horizontal measurement equipment (e.g. GPS) has been plotted together with the calibrated model response and the measured data (Fig. 8). In this figure ϕ of the sealing body (2) has been reduced from today on until a minimal stability has been obtained ($Msf \leq 1.0$). Its reduction leads to increasing vertical

deformation in Point 11. It has only marginal influence on the horizontal deformation in Point 3003.

Taking into account a possible error of observation (± 5 cm for vertical GPS recordings), after minimum seven years we could conclude on some damage in the dam that could lead to stability problems (failure).

6 CONCLUSIONS

To assess the influence of the error of observation on the determination of the stability of the Verse Dam it was essential to identify in situ soil material model to simulate the real deformation behaviour of the dam.

The primary used material models “Mohr Coulomb” or “Hardening Soil” for the Verse Dam construction (except the concrete core) were not able to simulate ongoing deformations due to viscose soil-fluid interaction and creep behaviour due to internal stress relocation caused by oscillating water levels. It is suggested to use a constitutive model which considers creep as an analogue.

In the demonstrated example of the Verse Dam model, the finite element method, together with the soft soil creep model, is appropriate to simulate the observed vertical and horizontal deformation.

The calibration of the numerical model of the dam has been done using the Soft Soil Creep Model. The vertical deformation observations of Point 11 and the horizontal deformation observations in Point 3003 have been part of the objective function. For the calibration the particle swarm algorithm has been used. To accelerate the optimisation procedure the numerical finite element model has been replaced by a fully quadratic approximation (surrogate model) in Points 11 and 3003.

With the observations until 1980 we succeeded in calibrating the numerical model. Using the observations until today only leads to marginal improvement.

Analysing the influence of the error of observation on the prediction of the stability shows that it is not possible to conclude on the stability if the error of observation measurement is large (e.g. vertical GPS measurement) compared to the expected increasing deformation.

To assess if the locations of observations can be improved such that it is possible to conclude on the stability of the structure it is recommended to analyse the numerical model using a node-based sensitivity analysis (Schanz et al. 2007, Zimmerer 2010).

ACKNOWLEDGEMENT

The sensitivity and inverse analysis has been performed using the inhouse software VARO²PT of VAROCON. For further details contact info@varocon.com.

REFERENCES

- Brinkgreve, R., Al-Khoury, R., Bakker, K., Bonier, P., Brand, P., Broere, W., Burd, H., Soltys, G. and Vermeer, P. (2002). *PLAXIS: Finite element code for soil and rock analyses (version 8.6)*. Rotterdam: Balkema.
- Kennedy, J. and Eberhard, R. (1995). Particle Swarm Optimization. In *Proc. IEEE Int'l Conf. on Neural Networks, Perth Australia*, pp. 1942–1948.
- Schanz, T., Zimmerer, M.M., Datcheva, M. and Lobers, S. (2007). Design of Soil Investigation Programs Using Sensitivity Analysis. In *Proc. International Conference VSU' 2007*, pp. IX-72–78.
- Zhang, Z.F., Ward, A.L. and Gee, W.G. (2003). Estimating Soil Hydraulic Parameters of a Field Drainage Experiment Using Inverse Technique. *Vadose Zone Journal* 2, 201–211.
- Zimmerer, M.M. (2010). Identifikation konstitutiver Parameter von weichen feinkörnigen Böden, Beitrag zum Konsolidationsverhalten von Ton. Ph.D. Thesis, Bauhaus-Universität Weimar.

Dam and hydropower in a changing world

J. Jia

International Commission on Large Dams (ICOLD), Paris, France
China Institute of Water Resources and Hydropower Research, Beijing, China
China National Committee on Large Dams (CHINCOLD), Beijing, China

J. Ma & C. Zheng

China Institute of Water Resources and Hydropower Research, Beijing, China
China National Committee on Large Dams (CHINCOLD), Beijing, China

ABSTRACT: The role of dam and reservoir in sustainable development has been widely highlighted and accepted by international community. Based on comparative study, the water storage per capita, hydropower generation per capita have close relationship with HDI (Human Development Index) proposed by UN. Hydropower, as the main benefit from dam and reservoir, is the best choice in life span Payback ration compared with any other power production. Finally, the way forward for better developing and managing water resources has been suggested.

1 HYDROPOWER IS THE BEST CHOICE IN PAYBACK RATION COMPARED WITH OTHER POWER

During the past century, multi-purpose dams and reservoirs have provided an opportunity for drought protection, flood mitigation, water provision for rural and urban need, navigation, recreation as well as energy. Moreover, its comprehensive advantage on water and energy utilization is popped out gradually with successive occurrence on energy crisis, water crisis, food crisis and climate change etc.

Water storage is energy storage. It has played an important role in modern power systems. Currently, hydropower generation accounts for approximate 20% of world electricity (EIA, 2008), which is the second dominating power after the fossil fuel (Fig. 1).

Among various types of energies hydropower has the highest energy pay back and lowest green house gas emission. The use of energy payback emerged with the oil crisis occurred in the early 1970s. After the oil crisis, the energy agenda began to change significantly, resulting in issues like energy independence, air quality, and later, climate change (Gagnon 2008). Many countries started to explore oil substitutes. One of the key problems that became apparent was the selection of efficient energy options for growing future demand. To identify appropriate solutions, policy-makers need to consider life-cycle assessments before taking decisions. Such life-cycle assessments must include energy payback as a central component. Energy payback may be a somewhat indirect measure of overall impact, and it provides a useful perspective on the origins of the real-world impacts. Therefore, the concept of energy payback was used to evaluate energy options in the form of Net Energy Analysis (NEA) by comparing the “net energy” for different energy options on a life-cycle basis.

One way to compare different energy options is to calculate the so-called life cycle Energy Payback Ratio. This is the ratio of total energy produced during that system’s normal lifespan to the energy required to build, maintain and fuel the system. The Energy Payback Ratio of

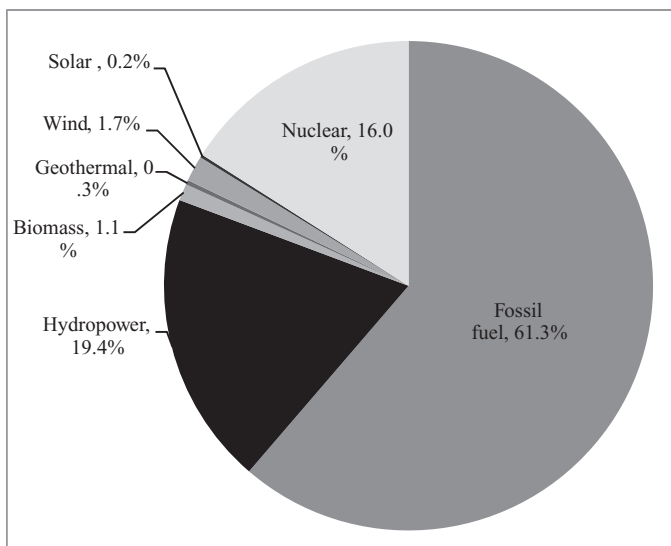


Figure 1. Power generation by type.

a power plant is defined as the total energy produced over the lifetime of the plant divided by the energy needed to build, operate, fuel, and decommission it. White & Kulcinski (1999) proposed a simple equation for calculating the Energy Payback Ratio, EPR,

$$EPR = \frac{E_{nL}}{(E_{matL} + E_{conL} + E_{opL} + E_{decL})} \quad (1)$$

in which, E_{nL} is the net electrical energy produced over a given plant lifetime L ; E_{matL} is total energy invested in materials used over a plant lifetime L ; E_{conL} is total energy invested in construction for a plant with lifetime L ; E_{opL} is total energy invested in operating the plant over the lifetime L ; E_{decL} is total energy invested in decommissioning a plant after it has operated for a lifetime L . A high ratio indicates a good performance.

According to Gagnon (2005), the energy payback ratio of different modes of energy development is about: 208–280 for hydropower with reservoir, 170–267 for hydropower run of river, 18–34 for wind power, 3–5 for biological energy, 3–6 for solar energy, 14–16 for nuclear energy, 2.5–5.1 for traditional thermal power and only 1.6–3.3 for thermal power in CO_2 capture or storage technology (Fig. 2).

Hydropower is also a source of energy causing the least greenhouse gas emission (Fig. 3). As World Energy Council (2004) calculation CO_2 emission per GWh is about 941–1022 t for traditional thermal power, 649–787 t for diesel, 220–300 t for thermal power in CO_2 capture or storage technology, 38–121 t for solar energy, 51–90 t for biological energy, 10–33 t for hydropower with reservoir, 9–20 for wind energy, 6–16 t for nuclear energy, and 3–4 t for hydropower run of river, the least emission.

2 DAM AND HYDROPOWER DEVELOPMENT HAVE CLOSE RELATIONSHIP WITH HDI

Not only the comprehensive advantages that the dam and hydropower have, but also the tight relation they have with socio-economic development. The idea initiated from Berga (2008) and Jia. They thought the per capita of storage capacity possessed and hydropower generation by the country was closely related to the socioeconomic development. Follow the idea,

Energy Payback Ratio

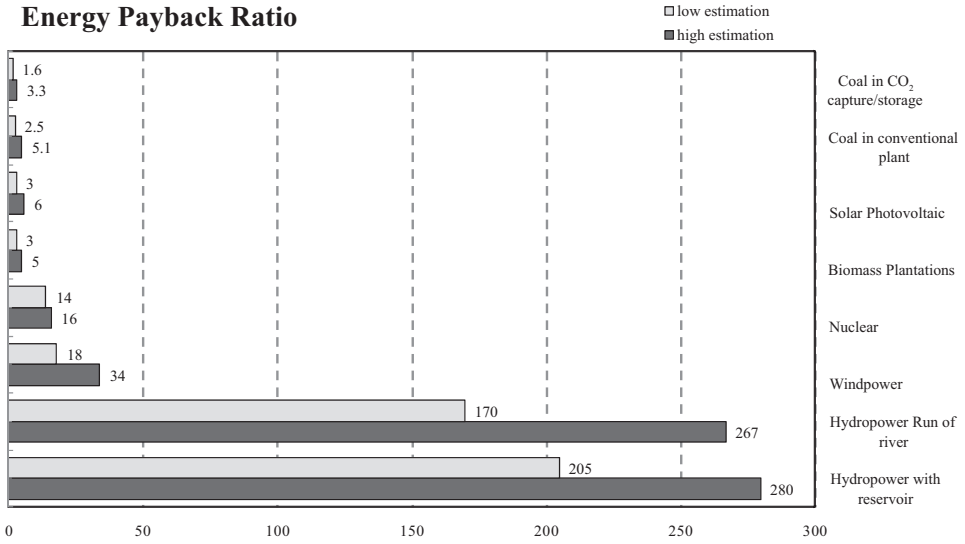


Figure 2. Energy payback ratio by type.

CO₂ emission (tons/per GWh electricity)

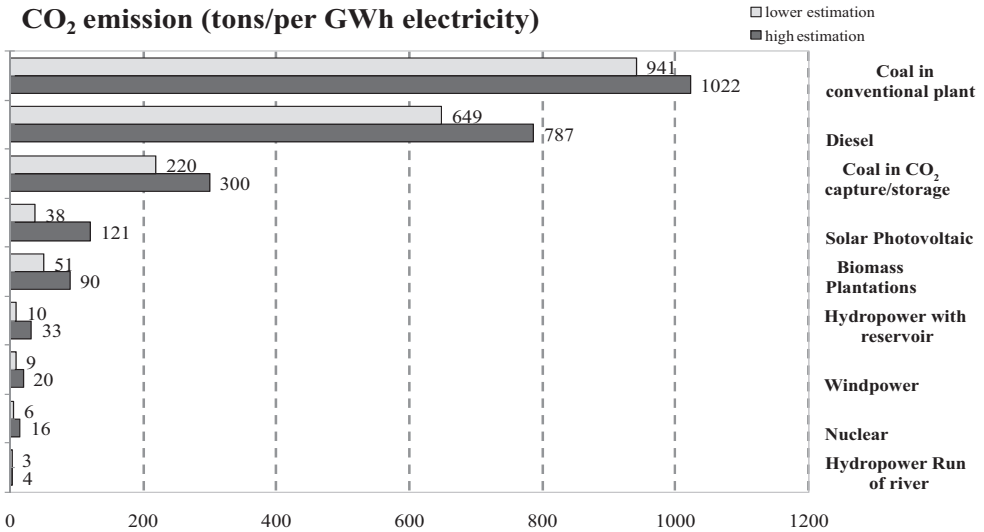


Figure 3. Greenhouse gas emission by type.

we compare and analyze per capita storage capacity index, per capita hydropower generation index and the human development index (HDI) about more than 100 countries. The result clearly indicates how dam/reservoir and hydropower development are related to socio-economic development.

HDI, the weighted average of the per capita GDP, health and education which reflect the quality of human development, is an overall index used to measure the level of socio-economic development in the UN member countries. This index avoids the disadvantage that the per capita GDP is used as the sole index for measuring human development. HDI is a value ranging from 0 to 1, the closer it is to 1, the higher the human development level is. The countries with HDI higher than 0.9 are mostly developed countries, e.g. Australia (0.970), United States (0.956), UK (0.947), those with HDI in the range of 0.8 to 0.9 are relatively developed

countries, e.g. Argentina (0.866), Russia (0.817), Brazil (0.813), while those with HDI below 0.5 are mostly less developed Asian and African countries, e.g. Rwanda (0.46), Burkina Faso (0.389) and Afghanistan (0.352).

As shown by the human development and dam/reservoir and hydropower development data of over 100 countries in 2007 (United Nation, 2009, Editorial Board, 2008), the countries with HDI above 0.9 had a per capita storage capacity of 2,924 m³, a per capita hydro-power generation of 1461 Kwh, those with HDI in the range of 0.8 to 0.9 had 2,476 m³ and 982 Kwh, those with HDI in the range from 0.7 to 0.8 had 571 m³ and 350 Kwh, those with HDI in the range of 0.6 to 0.7 had 212 m³ and 106 Kwh, and those with HDI in the range of 0.5 to 0.6 had 173 m³ and 86 Kwh only (Figs. 4, 5). As seen from this fact, developed countries have a solid ground for securing water and energy safety and coping with the changing water storage facilities, but developing countries still have a long way to go as limited by financial, technical and human resources. As for a given country, despite exceptions, e.g. Israel with HDI of 0.935 and a per capita storage capacity of 27 m³, and Zambia with 0.481 and 1072 m³ respectively, the level of dam development in a country or region is directly proportional to the level of human development. It is coincide with result of United Nation (2006) that the global distribution of water infrastructure is inversely related to the global distribution of water insecurity risks.

Due to the varying extent effect, global change represents different impacts and consequences to countries in different stages of development. As Blair (2008) pointed out in his report the change in climate is the same whether the emissions originate in New York or Shanghai. And of course, the most vulnerable to the impact of climate change live in the poorest area of the world. Likewise, the poor or undeveloped countries that have not caused, are not causing and will not cause significantly more greenhouse gas emissions are responsible for the cost of climate change. They are most easily subject to the effect of climate change and their adaptability is the most vulnerable. Countries in different stages of development have different objectives and priorities of water storage facilities, and also different concerns. For less developed countries, the consequence of global change is often catastrophic to the extent that, due to the inadequate storage capacity, subsequent extreme weather events occur frequently and bring about worse disasters. The construction of water storage facilities is

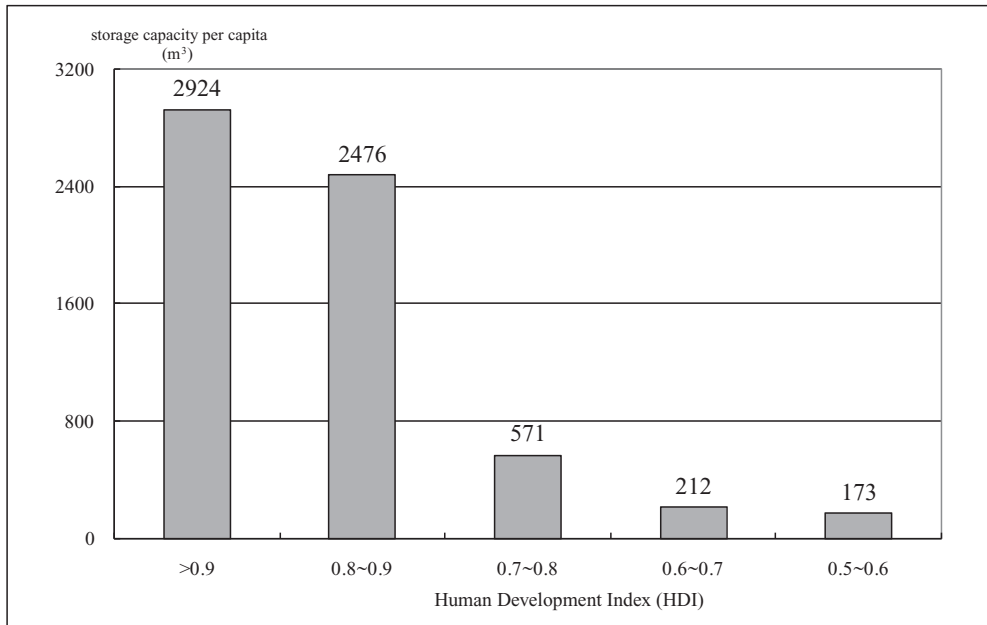


Figure 4. Relationship between per capita storage capacity and HDI.

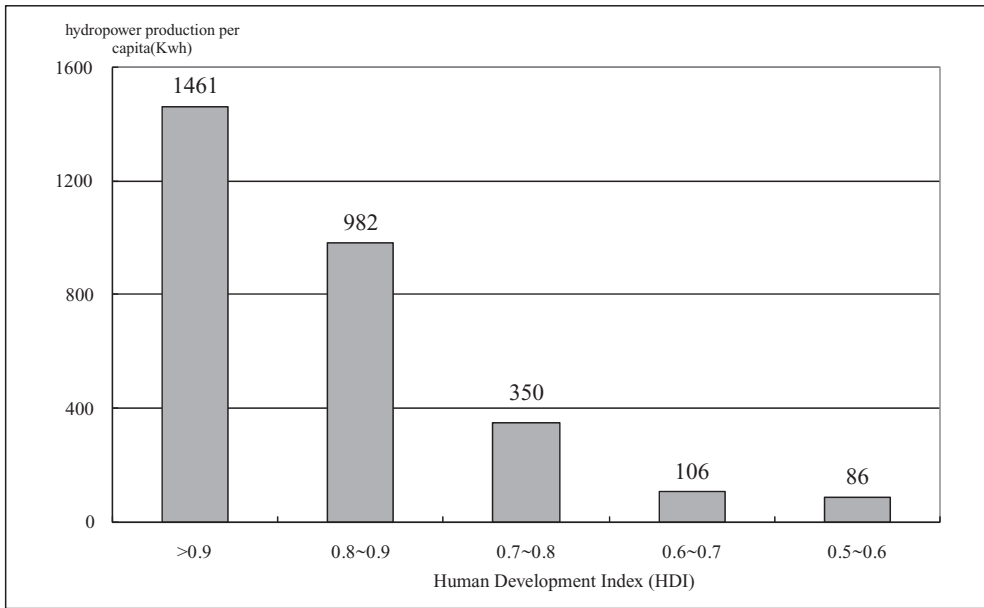


Figure 5. Relationship between per capita hydropower generation and HDI.

a crucial matter relating to their surviving and getting rid of poverty. Just as stated in the World Declaration on Hydropower Development (2008), a reliable electricity supply, taken for granted in many parts of the world, can be a life-saving commodity in the less developed African nations. In general, both energy and water needs are critical in these nations, so the obvious multiple benefits of hydro schemes (particularly when storage reservoirs are included) are of special significance in Africa. The effects of extreme climatic conditions (large-scale floods and regular droughts) that Africa suffers from can be vastly mitigated by dam/reservoir schemes. Naturally the supply of clean drinking water and irrigation water to enhance food security, are major additional benefits of hydro schemes. Thus the development of water and hydropower resources is of special significance for developing countries, especially the African countries, and one of the most urgent tasks to improve the livelihood.

3 THE LONG-TERM SAFETY OF LARGE DAMS IS THE FOUNDATION FOR DAM AND HYDROPOWER DEVELOPMENT

Today, sustainable development and sustainability of the life in many parts of the world continue to be threatened by the scarcity of supplies of water, food and energy. 1.1 billion people are still lacking the access to safe drinking water, 2.4 billion people are without the service of sanitation and 2.0 billion people are waiting for the electricity supply. Water storage infrastructure is a practice involving water security and energy security. We still need to build more and more dams and reservoirs on one hand; we need to keep the old ones working normally on the other. Even though a lot of modern and advanced technologies have been developed, we are still facing challenge issues. The accident of Sayano-Shushenskaya happened on 17th Aug, 2009 as a result of 76 people's death attracted worldwide attention. According to one report, the chain of events that commenced with turbine cover holding down bolts suffering progressive metal fatigue and finally failing, could have lead to a major catastrophe. Actually, a large percent of dam failure happened due to neglect of monitoring and maintenance. Much attention paid by society on safety of large dams alarms us that the long-term safety of large dams is foundation for dam and hydropower development.

Consideration needs to be given during the design, construction and operation stage to obtain long-term safety of large dams.

- Safety of dams is not only a technical issue, but also a social issue. We are responsible for technical part and at the same time we have to pay much attention on social responsibility.
- Aging and possible problems of the dam and rehabilitation measures should be considered during design, construction and operation stage. The owner, designer and contractor must never forget that the dam will probably still be there hundreds of years into the future. The structure and materials must last that long or can be rehabilitated.
- Evaluation of Long-term safety of a dam, considering all factors which will affect behavior of the dam, may make for decision making when developing rehabilitation program.
- Life span of a dam and its components may be different. The service life of a well-designed, well-constructed and well-maintained and monitored dam can easily reach 100 years. However, hydromechanical elements such as gates and their motors have to be replaced after 30 to 50 years. The life-span of penstocks is 40 to 60 years. Regular Repair and replacement of aged components is critical for security of the whole dam project.
- For risk management, Emergency Action Plan should take all possible factors which may affect dam safety into account. Failures associated with the powerhouse can put the dam at risk. Very often, this will be the result of a failure at the powerhouse cutting off power supply or communication to important safety devices such as spillway gates and penstock guard gates. Consideration also needs to be given to political, economic crisis or natural disasters, such as earthquake, and who will guarantee security of the dam and people downstream when it happens.

In this new century, the construction and operation of a dam and reservoir can no longer be considered as a purely scientific and technical matter. To minimize misunderstandings about dams and ensure support for further development at a global level, long-term safety of large dams is fundamental and critical.

4 NEW ERA OF WATER STORAGE INFRASTRUCTURE CONSTRUCTION AND HYDROPOWER DEVELOPMENT IS COMING

The world is changing. Population growth and economic development turn to be the prime driving power that stimulates the ever-increasing demand for resources and energy. Water is a basic natural resource, but also a strategic economic resource, and it has an important influence on the environment. The world's population is growing by about 80 million people a year, implying increased freshwater demand of about 64 billion m³ a year. In 2030, 47% of world population will be living in areas of high water stress (UNESCO, 2009). In the meanwhile, the increasing on extreme climatic events including flood and drought induced by climate change further intensified the difficulties for water allocation and utilization.

As one of outstanding constraints we are facing now, climate change necessitates us to take actions. On the one hand, we need to actively push forward the strategic adjustment of the structure of energy supply, change the leading role of fossil fuel in the structure and reduce greenhouse gas emissions; on the other hand, we need security measures against the consequence of global climate change. Naturally, enlarging the storage and the regulating capacity are regarded as a core and key engineering measure. The consensus on the role of dam and reservoir in adaption of climate change has been conducted in a wide range by international community. More and more people are recognizing water infrastructure is essential to achieve sustainable development. Insufficient water storage facilities will delay our ability to respond to climate change and to meet the Millennium Development Goals.

The supporter and opponent on constructing large water storage facility can back to sit together to discuss the issues on global development in a friendly manner, which reflects that development requirement is the foundation for forming consensus.

The transition is causing a new era on dam and reservoirs construction and hydropower development. Many of the infrastructure investments and other steps taken as a result of the dam will help individual country deal with climate change and economic crisis. Till now, about 165 countries already clarified to further develop the hydropower. The proposed installed capacity already comes to the 33.8 TW. Up to now, the attention on hydropower in developed countries already moved to the rehabilitation, reinforcement on constructed hydropower plants to strength flood relief facilities for increasing the capability on flood control, or adjust its regulating target or mode for the purpose of ecosystem protection and restoration, such as in the countries in north America and Europe. For the developing world, many countries stipulated ambitious plan which will finish the assignment on hydropower development before 2025, such as the countries in Asia and South America. For the less developing country, such as the countries in Africa, although they have abundant hydropower potential and have the intention on hydropower development, due to the limitation on investment, technical or political aspects, these countries still face much difficulties or barriers on the process for developing hydropower. At present, there are 1200 dams under the construction. Among them more than 370 dams is above 30 m high. The majority is distributed in 55 countries in Asian and South American countries.

REFERENCES

- Berga, L. 2008. Dam for sustainable development, in Proceedings of high-level International Forum on Water Resources and Hydropower: 1–6. Beijing, China.
- Blair, T. and Climate Group, 2008. Breaking the climate deadlock: A global deal for our low-carbon future.
- Editorial Board, 2008. Word Atlas & Industry Guide 2008. The International Journal on Hydropower and Dams, London, UK.
- EIA, 2008. Energy Information Administration International Statistics Database, <http://www.eia.doe.gov/>.
- Gagnon, L. 2005. Energy Payback Ratio. Hydro-Québec, Montreal.
- Gagnon, L. 2008. “Civilisation and energy payback.” *Energy Policy*, **36**(9): 3317–3322.
- Leyland, B., Debate is needed on the long-term safety of large dams 2010. ICOLD, Pairs.
- UNESCO, 2009. The United National World Water Development Report-Water in a Changing World. UNESCO, New York, USA.
- United Nation. 2006. United Nation Human Development Report-2006, United Nation, New York, USA.
- United Nation, Human Development Report 2009. Overcoming barriers: Human mobility and development, United Nation, 2009.
- White, S.W., and Kulcinski, G.L. 1999. “Birth to Death” analysis of the energy payback ratio and CO₂ gas emission rates from coal, fission, wind and DT fusion electrical power plants. UWFDM-1063, University of Wisconsin-Madison.
- World Declaration Dams & Hydropower, 2008. Paris, France.
- World Energy Council, 2004. Comparison of energy systems using life cycle assessment a special report for world energy council, London, UK.

Sedimentation of Polish reservoirs—characteristics and significance of the phenomenon and procedures of its control

A. Kosik, J. Kloze & A. Wita

Institute of Meteorology and Water Management, Warsaw, Poland

ABSTRACT: Water reservoirs are subjected to sedimentation process during the operation. The intensity of the phenomenon is variable and depends on many factors such as location and climatic conditions. The number and hence the total capacity of reservoirs in Poland is insufficient and totals slightly above 4% of average annual run-off, instead of the desired 10%. It became necessary to estimate the scale of accumulation and its control in operating reservoirs as well as to assess the technical and economical abilities to regain the lost retention capacity. Data on location, technical and operation parameters and test results of 51 selected Polish reservoirs meeting the given criteria were gathered and analyzed. The total initial capacity of the reservoirs was $2.857 \cdot 10^6 \text{ m}^3$ and the operation period was ranging from 3 to 105 years. Periodical bathymetric measurements are considered to be the best procedures to control the intensity of the process. Among 51 analyzed reservoirs there were 3 characteristic groups:

- reservoirs with the capacity based on current bathymetric measurements,
- reservoirs with the capacity measured in previous years,
- reservoirs with the capacity never measured before.

For each of the groups the scale of the sedimentation and the retention capacity was calculated using different methods with a different degree of accuracy. For chosen objects the course of the sedimentation process during the operation and changes of the intensity indicators were analyzed as well zones of intensive debris accumulation were marked out. For chosen objects grain size analysis is being done as well as chemical and biological analysis concerning the potential usability for economy.

1 INTRODUCTION

In 2010 floods occurred in Poland a few times. They covered the catchment areas of the two largest Polish rivers; The Vistula and The Oder. The results have clearly shown how important water reservoirs to fight such phenomena, with their ability to capture and store at least a part of flood waves. The number and hence the capacity of dam reservoirs in Poland is insufficient. Their total capacity is slightly over 4% of average annual run-off while it is estimated that it should reach 10% of the number. The situation becomes even worse because the reservoirs during operation are losing their initial capacity. The effect is caused by accumulation process of the dragged and floated sediment, transported by the rivers.

In Poland, as in many other countries, there are difficulties with construction of new dam reservoirs, main reasons being unfavorable geological conditions, dense population and the reluctance of local communities towards this kind of investments. One of the ways to improve the disadvantageous situation can be to regain the lost reservoir capacity as a result of sediments accumulation.

2 RESEARCH OF CHANGING CAPACITY OF RESERVOIRS IN POLAND

In 2009 a research was started aiming at estimation of accumulation size and its control in operating reservoirs and recognition of technical and economical possibilities of retrieval of the lost retention capacity. 51 selected reservoirs meeting the following criteria were analyzed:

- maximum reservoir capacity at the beginning of the operation was $5 \cdot 10^6 \text{ m}^3$ or more,
- the reservoir was created by a dam constructed on a natural stream,
- the reservoir has a retention function.

The total initial maximum capacity of the reservoirs was $2.857 \cdot 10^6 \text{ m}^3$ and their operation period ranges from 3 to 105 years.

The manner considered to be the best in Poland to control the intensity of the accumulation process are periodical bathymetric measurements. Unfortunately, there were not conducted systematically in most cases, following the relevant procedures and with required caution. Among 51 reservoirs there were three characteristic groups:

- 14 reservoirs with the capacity based on current bathymetric measurements,
- 14 reservoirs with the capacity measured in previous years,
- 23 reservoirs with the capacity never measured before.

It was also stated that one object was controlled in a proper way with satisfying frequency of average 6 years and 5 reservoirs are controlled frequently enough (an average of 5–6 years, the biggest gap in measurements was 19 years). Two reservoirs were controlled systematically until two new objects were built upstream. The rest of the reservoirs were rarely controlled or never at all.

For each of the reservoirs its current total capacity was determined. The method depended on the group mentioned above that the object belonged to. For the first group of reservoirs the results of the present bathymetric measurement (done in 2008–2010) were considered fully reliable. For the reservoirs of the second group calculations were done using Gontcharov equation based on the Orth and Shamov formula (CLIMAT, 2010):

$$Z_t = V_0 \cdot \left\{ 1 - \left[1 - \frac{Z_1}{V_0} \right]^t \right\} \quad (1)$$

where Z_t = volume of sediments in reservoir after t year in m^3 ; V_0 = initial capacity of reservoir in m^3 ; Z_1 = average annual accumulation in the initial stage of reservoir operation in m^3 ; t = time in years.

In the equation the numerical value of Z_1 —average annual accumulation in the initial stage of operation, was chosen so that the calculated accumulation was the same as the last bathymetrical measurement. Then, using the calculated Z_1 value, probable sediment volume was calculated since the beginning of the operation until 2008. The way of conduct was illustrated in Figure 1. For the reservoirs of the third group, e.g. those that have never been measured, a suspected volume of accumulated sediment was calculated using the indicators of surface denudation of the basin, determined for separate regions of Poland on maps compiled by Reiner (1959), Dębski (1959) and Barański (1986). The average annual reservoir accumulation calculated this way was marked on a map of denudation intensity of the area above the reservoir with the catchment area shape and partial basin surfaces were assigned to the separate denudation indicators. The product of the part of basin surface corresponding to the given denudation class and the intensity indicator were added up. Having determined the average annual reservoir accumulation and knowing the number of years of operation, the total capacity loss was estimated like in the case of group 2 reservoirs.

Two of the studied reservoirs have increased their total capacity from $82.80 \cdot 10^6 \text{ m}^3$ to $200.42 \cdot 10^6 \text{ m}^3$ due to the intensive aggregate extactio. It has been estimated that the rest of 49 reservoirs with the total initial capacity of $2674.67 \cdot 10^6 \text{ m}^3$ during the operation which

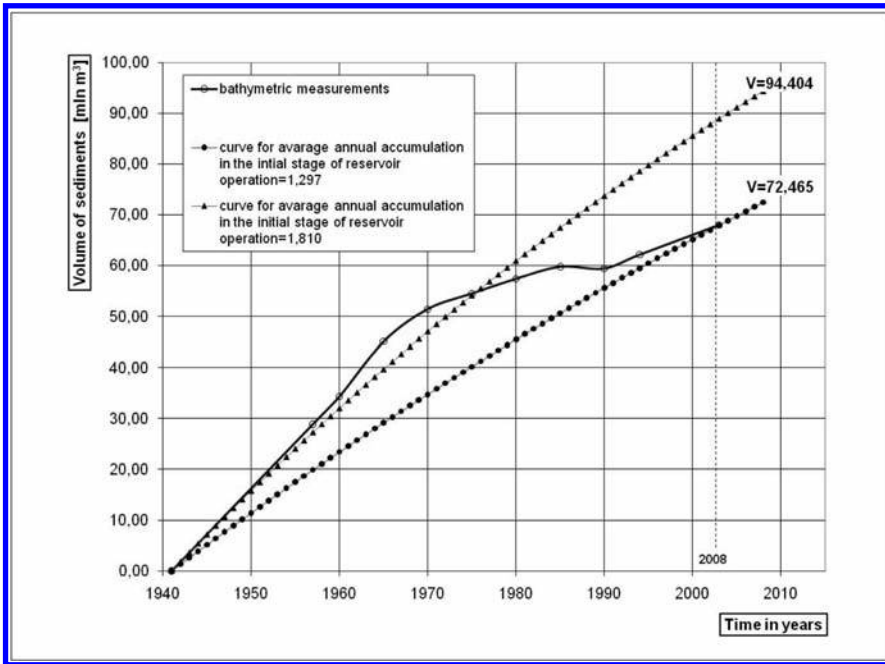


Figure 1. The method of calculating the current debris volume accumulated in Rożnów reservoir.

lasted on average 45.2 years have lost as a result of accumulation $159.92 \cdot 10^6 \text{ m}^3$, comprising 6% of their capacity. It gives an annual loss of $3.53 \cdot 10^6 \text{ m}^3$ which is extremely significant for the water economy in Poland.

The research of accumulation dynamics of water reservoirs and the location of the debris inside was based, where the bathymetric measurements' results were provided, on the capacity curve analysis. The changes in its flow in the years 1942–2003 for the most intensively accumulating Polish big reservoir of Rożnów were shown in Figure 2.

The changes happening in the reservoir are also well illustrated by the cross sections done in different years of its operation (Fig. 3) as well as distribution of d_{50} in the cross section determined in grain size analysis of the sediment samples (Fig. 4).

In order to restrain the accumulation in dam reservoirs a lot of measures is taken, among which it is worth to mention anti-sediment dams (Fig. 5) combined with river flow correction by means of sills as well as building small reservoirs directly over the big reservoir which aim at restraining the sediment transported by the river (Winter, 2000).

The sediment accumulated in the reservoir accumulates unevenly on its bottom causing the capacity loss in separate strata to be varied. For a few selected objects capacity loss curves have been generated, Sulejów reservoir serves as an example in Figure 6.

3 THE FIRST STAGE STUDY CONCLUSIONS

Reservoirs under study are located in different regions in Poland, thus in different geomorphological and hydrological conditions, and their catchment areas are cultivated up to a different extent. The accumulation proceeds a different intensity. Depending on the quantity of this indicator, the objects where field study was present can be divided into three groups:

- Group I—reservoirs with an intense accumulation, whose average annual accumulation is over $500 \cdot 10^3 \text{ m}^3/\text{year}$. The condition is met by Rożnów reservoir with the value ranging from $2150 \cdot 10^3 \text{ m}^3/\text{year}$ to $470 \cdot 10^3 \text{ m}^3/\text{year}$, the average being $1300 \cdot 10^3 \text{ m}^3/\text{year}$.

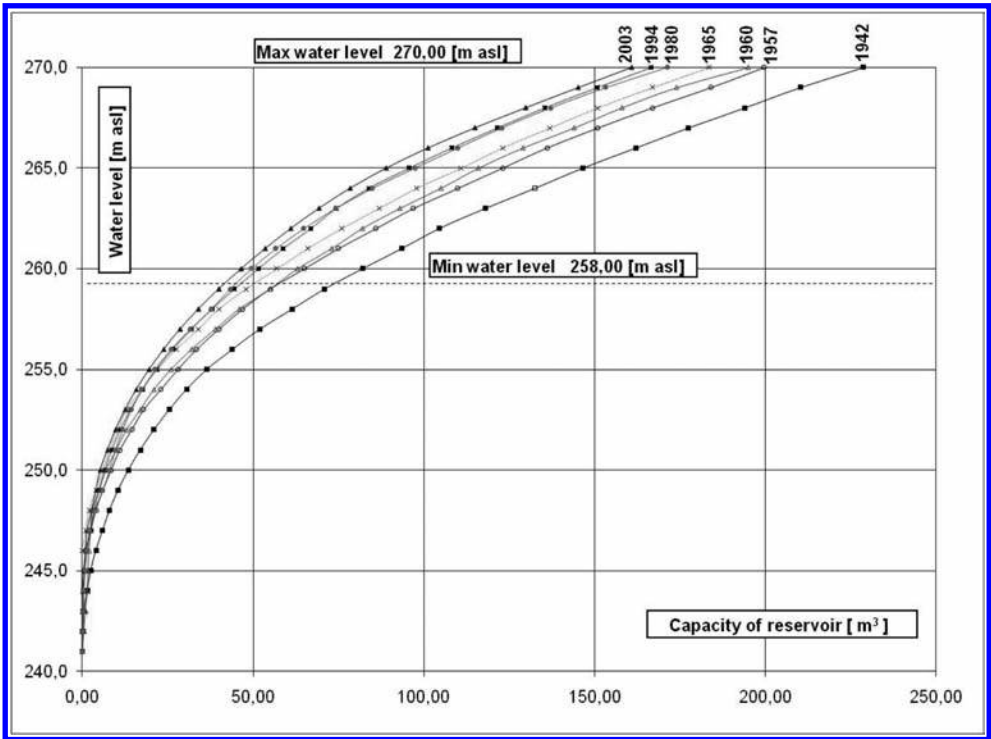


Figure 2. Capacity curves of Rożnów reservoir between 1942 and 2003.

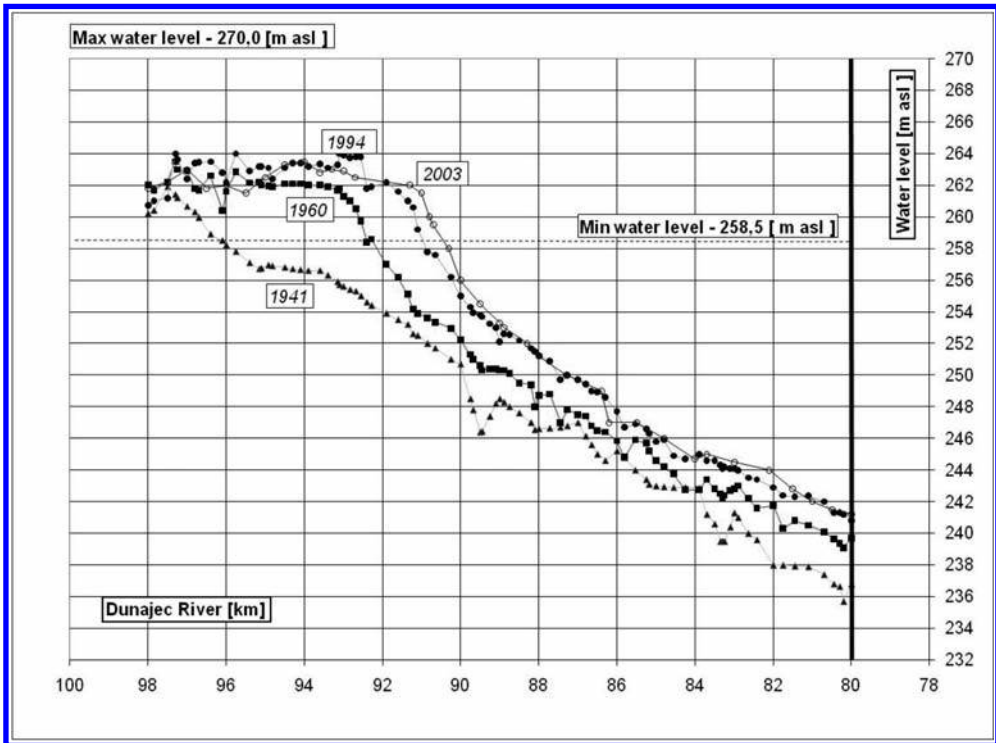


Figure 3. Cross sections of Rożnów reservoir in the Dunajec river between 1941 and 2003.

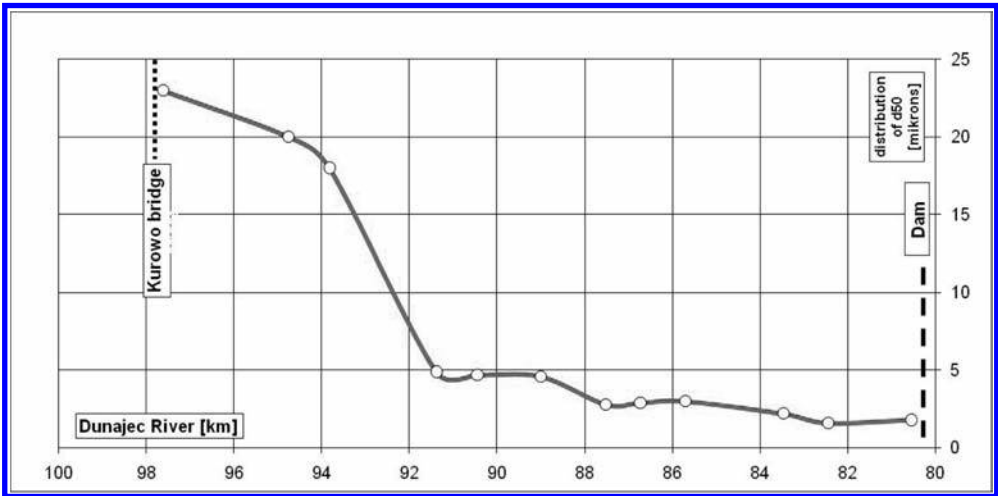


Figure 4. Distribution of d_{50} debris diameter in the cross section of Rożnów reservoir.

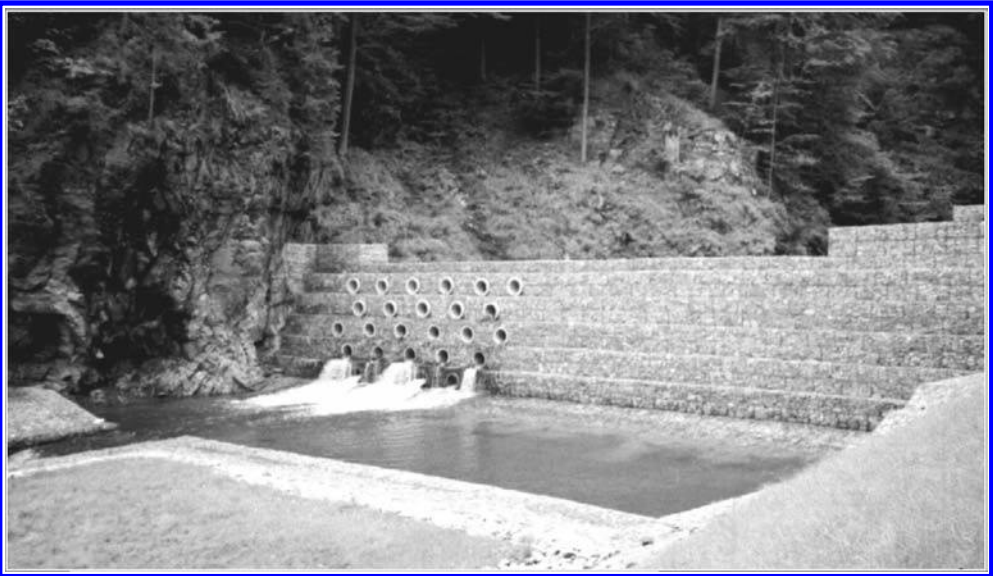


Figure 5. Anti-sediment dam Wilczka—Międzygórze (CLIMAT, 2010).

- Group II—reservoirs with a moderate accumulation between 500 and $100 \cdot 10^3 \text{ m}^3/\text{year}$. Examples of these are Dobczyce reservoir $345 \cdot 10^3 \text{ m}^3/\text{year}$, Goczałkowice reservoir $175 \cdot 10^3 \text{ m}^3/\text{year}$ or Tresna reservoir $170 \cdot 10^3 \text{ m}^3/\text{year}$.
- Group III—reservoirs with small accumulation a. e. lower than $100 \cdot 10^3 \text{ m}^3/\text{year}$. The examples are Sulejów reservoir $99 \cdot 10^3 \text{ m}^3/\text{year}$, Turawa reservoir $76 \cdot 10^3 \text{ m}^3/\text{year}$, Jeziorsko reservoir $38 \cdot 10^3 \text{ m}^3/\text{year}$.

For the catchment area of the three groups mentioned above indicators of average annual surface denudation were calculated and are as follows: for the first it is $280 \text{ m}^3/\text{km}^2$, for the second group it is $160 \text{ m}^3/\text{km}^2$, and for the third group is not more than $60 \text{ m}^3/\text{km}^2$.

The sediment samples collected from the bottom of ten reservoirs considered to be relevant are under chemical and biological study to determine their quality and especially the content of heavy metals and dangerous organic substances. Results of the study will serve

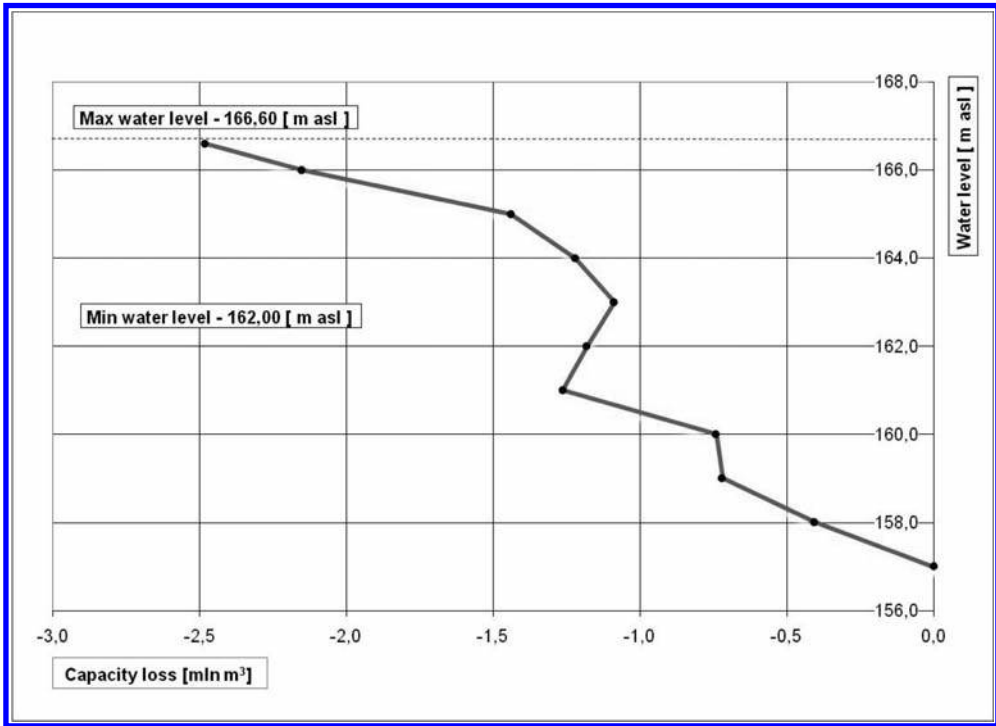


Figure 6. Capacity loss curve in Sulejów reservoir between 1973 and 2008.

a basis for making the decision about the possibilities to utilize the sediments in the case of removing them from the reservoir to regain lost retention capacity. A monitoring programme of reservoir capacity will also be developed including a detailed schedule of bathymetric measurements determining the criteria applied to the equipment used for the measurements, their methodology, required accuracy and the manner of data processing.

REFERENCES

- Brański J., Atlas Hydrologiczny Polski (Hydrological Atlas of Poland), tom II. Warszawa 1986.
- CLIMAT project—"The influence of climate change on environment, economy and society". Task 8: Prevention of degradation of polish water reservoirs. Stages I, III, IV. IMGW Warsaw 2010.
- Dębski K., Próba oszacowania denudacji na obszarze Polski. (Attempt to estimate denudation in Poland). Prace i Studia Komitetu Gospodarki Wodnej, tom II, część I. Warszawa 1959.
- Reniger A., Zagadnienie erozji gleb w Polsce (Problems of soil erosion in Poland). Prace i Studia Komitetu Gospodarki Wodnej, tom III, część I. Warszawa 1959.
- Winter G. & Winter J., Sediment in mountain streams—a case study of Wilczka Stream and Międzygórze Reservoir. 10th International Conference on Transport & Sedimentation of Solid Particles. Edited by J. Sobota. (Part 2). Wrocław 2000.

Innovative sediment handling to restore reservoir capacity

H. Schüttrumpf

*Institute for Hydraulic Engineering and Water Resources Management, University of Technology
Aachen, Aachen, Germany*

M. Detering

DB Sediments, Duisburg, Germany

ABSTRACT: Almost every reservoir is affected by sedimentation. WCD estimated that each year around 1% of worldwide storage capacity is lost due to this effect. Even the actual new build of reservoirs does not level out overall storage decrease. Dredging and disposing reservoir sediment is extremely expensive. On the other hand the caused lack of sediment downstream of reservoirs leads to erosion damages, substrate deficits and ground water problems. An innovative technical approach makes reservoirs permeable for sediment on a very cost effective basis. The application does not affect reservoir management and is performed during daily reservoir operation. The process restores overall sediment transport to a near nature state with overall benefits to ecology and the rivers morphological state, giving the operator back the desired reservoirs operational range. The new technical sediment management approach is transferable on almost any range of plants, small to large and run-of-river to pump storage.

1 SEDIMENTOLOGICAL BACKGROUND

The general effects of reservoir sedimentation are known to a wide audience. Already decades ago the range of this worldwide problem has been assessed (Mahmood 1987). The World Commission of Dams estimates that annually 0.5 to 1% of global storage volume is lost by sedimentation. Without further action one quarter of all dams in the next 25 to 50 years will lose their storage function by sedimentation (WCD 2000).

Sedimentation is still probably the most serious technical problem faced by the dam industry (McCully 1996). Given this scale it is surprising what little attention is often given to the field of sediment monitoring, control and operational solutions.

1.1 *Benefits of sediment*

Sediment is not a merely evil. Like water and organisms also sediment is an essential ingredient of every river. This solid fraction mostly is of natural origin and finds its way via erosion processes into the water body. Starting at the rivers source solid components usually begin their career as eroded massive rock. Transport processes changes rock size first to gravel size bedload and furthermore to fine-grained sediment. This sediment settles at the river floor. Depending on the local current this sediment does also come loose again by erosion effects. In middle and lower parts of natural rivers sedimentation and erosion usually balance each other and effectively prevent river beds from erosion damages (Fig. 1). Sediment deposition at and beyond coastal estuaries is required to preserve groundwater from becoming brackish.

1.2 *Morphological changes*

A natural river changes its morphology fundamentally when installing a dam or other barrage across a river section. Permeability is still given for water and mostly for aquatic life by

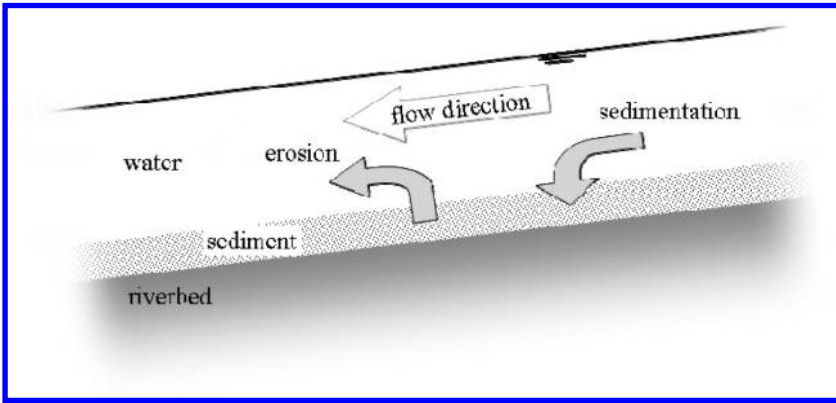


Figure 1. Sedimentation/Erosion equilibrium in natural rivers.

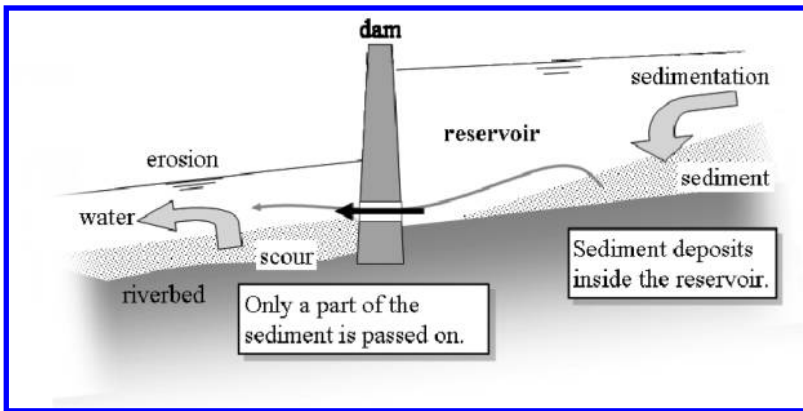


Figure 2. Reservoirs change the sediment balance profoundly.

discharge elements and if applicable fish ladders. The extended cross-section upstream of a barrage leads to low current velocities and therefore to profoundly more sedimentation while erosion is minimized. Gravel size sediment usually forms a delta at the reservoirs upper end. Finer fractions down to clay particle size settle down at the reservoirs floor by density currents. Therefore a barrage often is a massive barrier for sediment transport (GWSP 2000). Many reservoirs are affected by massive sedimentation and consequently a loss of storage volume (Fig. 2). The same is true for pump storage reservoirs in a similar way.

Largely extracting the sediment from the river at the concerned reservoir also leads to massive changes downstream. By trapping sediment in its tributary reservoirs, the German river Rhine alone—which certainly does not represent a major sediment carrier concerning worldwide average—is facing an annual sediment deficit of 2.5 million tons and thus is eroding its river bed level by 30 mm each year. To heal only major riverbed erosion damages an annual mass of approximately 1 million tons of soil is dropped into the Rhine at its middle and lower reaches, causing significant expense.

1.3 Operational consequences

Operational restrictions for reservoir users caused by sedimentation do not come overnight. They increase gradually over long time periods, usually years. Therefore many operators get used to live with these restrictions and consider them as normal, though they are not. Even worse, they grow over time if no counteraction is taken. Foreseen dead storage capacity to

store a bulk of sediment below the actively operated reservoir range often does not fully apply because sediment does not tend to settle plain but accumulates within the foreseen active storage volume.

2 SOLUTION ATTEMPTS SO FAR

In many cases of sediment issues action is taken not until problems are in far progressed stage. Previously conducted solutions attempts are briefly outlined below.

2.1 Former procedures

2.1.1 Opening the base outlet

Sedimentation processes usually start at the up-stream entrance into the reservoir which typically is the most distant point from the dam axis. As sedimentation increases the settled sediments eventually reach the dam. To prevent the dams discharge elements from plugging the operator is now forced to flush the base outlets periodically (e.g. every six months). If neglected the equipment will become inoperable within short term because the sediment will cover the gear. The tremendous runoff generated by opening the outlets erodes the sediment right upstream of the intake. The eroded sediment is transported downstream in short time and at a high rate (Fig. 3).

Performing this method is quite simple and requires no further physical facilities. However, with this technique a tremendous quantity of water for power generation or water supply is lost. Furthermore, significant amounts of sediment are moved into the downstream river section in a very short time period. This can lead to negative morphological and ecological effects.

Anyway, the method is applicable only when sedimentation already reached the dam line. Opening the base outlet then only leads to a dissipation of sediments in close vicinity of the outlets. The overall operative range of the reservoir is not restored.

2.1.2 Manual dredging

Another procedure is manual removal of sediments. Here the sediment is excavated by suction dredgers, hydraulic excavators or—after lowering the reservoirs water level and initial draining—wheel loaders (Fig. 4). After the often expensive removal and transport the sediment has to be stored on separate drainage fields for years or decades in order to reduce the water content. Thereafter it may be used as covering material for simple ground work applications. The relatively high percentage of organic ingredients (usually 2 ... 30%) prevents a use as a ground construction material even after dredging. In many cases, landfill is required.

The procedure allows for a thorough cleaning of reservoirs, but at exorbitant costs. Expenses consist of sediment dredging activities, plant/reservoir shutdown of several months as well as transport and dump expenditures which are in a million dollar range even at small reservoirs.

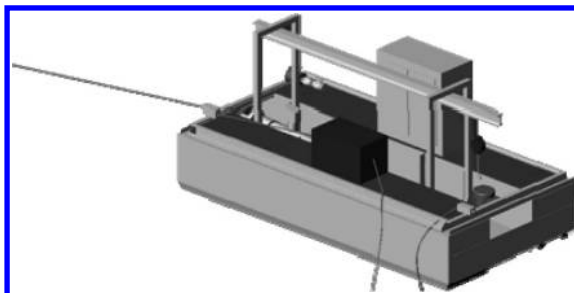


Figure 3. Sediment transfer vessel (electrically driven).

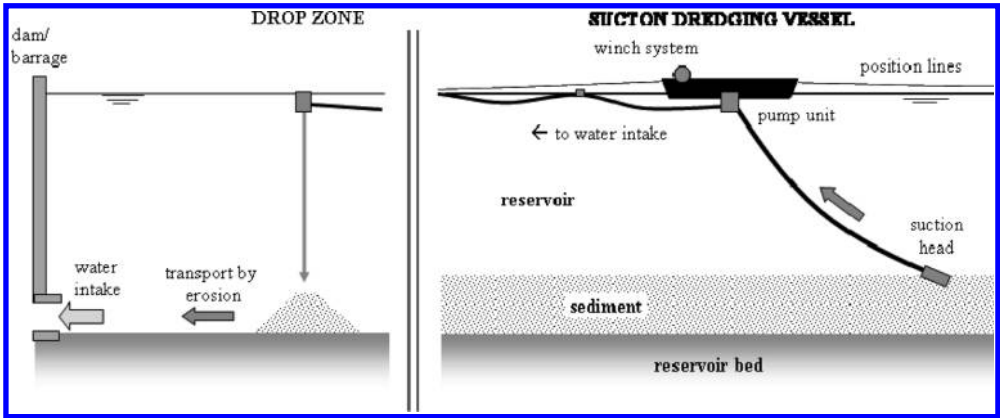


Figure 4. Sediment transfer.

2.1.3 Sludge dredging and disposal downstream

This method involves several suction dredging campaigns where sediment is dug, transferred over the barrage and dumped downstream (Fig. 5). For good reason this is not allowed in many countries. The loss of great amounts of flushing water for power production or irrigation may be even acceptable. The short-time transfer of large sediment quantities into the downstream river section however causes a massive intrusion into the river morphology and ecology.

2.2 Direct impact on river morphology

When opening the base outlet the downstream riverbed is often blocked for months. In any case the morphology is changed significantly. With manual removal, the sediment is extracted permanently from the water body. This leads to increased erosion in the lower reaches and therefore also affects the river, albeit with opposite effect.

Dredging and disposal downstream usually is not compatible with river morphology due to the large amounts that need to be transferred in a short period of time. So all previously described existing methods are problematic in a morphological point of view.

2.3 Ecological aspects

Via morphological effects also ecological topics are directly concerned in all described dredging methods. In addition the emptying of the reservoir required for a manual dredging leads to a destruction of the current reservoir's fish population. With sludge dredging and direct disposal downstream the underwater benthos structure is widely destroyed within a few days. Opening the base outlet or even failing to do any maintenance on the reservoir and risking siltation ends in a profoundly long-term change of the developed ecosystems. Some coastal river deltas already face salt water infiltration into ground water reservoirs by missing fresh sediment coverage.

2.4 Legal constraints

The above presented methods usually require permission by local or regional authorities before starting any physical activity. For permission the authorizing body will take into account appropriate guidelines as European Water Framework Directive or U.S. sediment acts. Usually the facility owner has to expect more or less extensive obligations for project execution even if permission is granted.

When digging the sediment and extracting it from the water body the contractor or plant operator usually becomes owner of the removed material. If critical ingredients are detected,

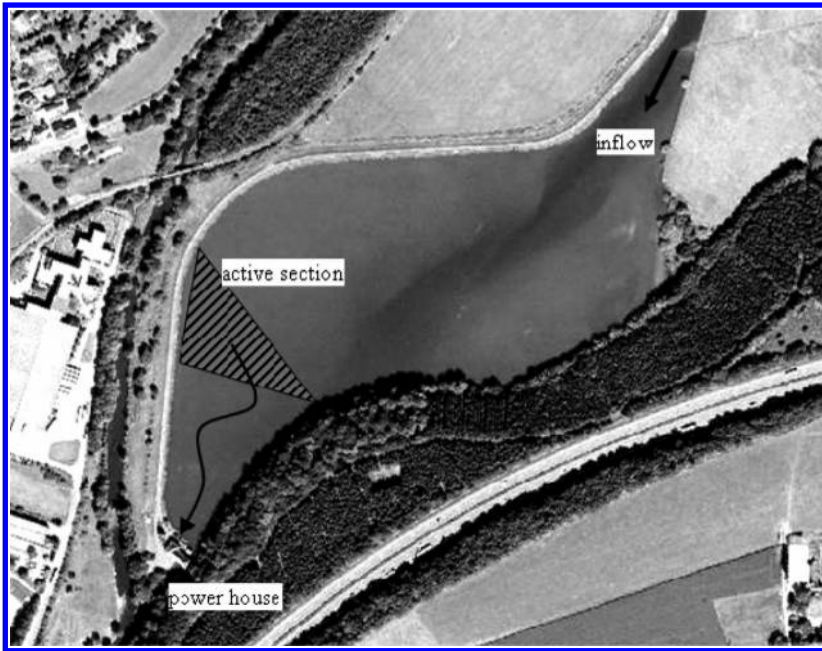


Figure 5. Sectional treatment of reservoir (Ehreshoven II reservoir/Germany).

the extracted sediments have to be dumped as contaminated material at enormous expense. This also applies in the case that the critical components found are of endogenous and thus natural origin (e.g. certain heavy metals).

2.5 *Economic evaluation*

The opening of the base outlet initially appears as a cheap solution. However, the above-mentioned constraints have to be taken into account. If opening the base outlet seems to be a suitable solution, the degree of sedimentation is already far advanced with often severe operational restrictions on reservoir management. The base problem and also the operational restrictions are not resolved by this method as are resulting financial implications. Both will continue because sediment is eroded only in the up-stream area near to the barrages outflow, not at the far end of the reservoir where most sediment is found. In addition it has to be taken care that no damage compensation liabilities are caused when discharging large quantities of sediment downstream in a short period of time.

The latter aspect also is valid for suction dredging with direct disposal into the downstream river section. For this reason, this variant in most cases is not licensable or generally unlawful.

Excavation of sediment from the reservoir usually is exorbitant expensive due to high direct construction costs, enormous disposal expenditures and long plant/reservoir downtime. For this reason, operators choose this option usually only when threatened by plant/reservoir loss.

3 INNOVATION

As a promising alternative to the previous discussed methods a new approach is paving its way. According to Water Framework Directives or Sediment Acts a barrage should not only be penetrable for water and fish, but also for sediment. The general approach is to bring the balance of sedimentation and erosion in a river back to a naturally acceptable or aspired degree to provide a sustainable and permanent solution.

3.1 *Required hardware*

The process is set up by devices allowing continuous and controlled transfer of sediment within the reservoir in a relatively small scale but permanent mode. Key element is an automatically working vessel with a suction dredging system installed that can be diesel or preferably electric driven (Fig. 6). To allow for an exact positioning the vessel is directed by tractor cables. Sediments are loosened by a suction head, pumped towards the reservoir's outlet and dumped in front of the outflow elements. The vessel gradually strikes the reservoir floor until the complete surplus sediment is removed.

The newly dumped sediments are eroded by the hydraulic discharge and therefore carried out of the reservoir, passing turbines or outlet valves (Fig. 7). Both types of outflow elements are able to handle water flow with some degree of sediment load. The sediment transfer rate can be adapted to the outflow rate and parameters to guarantee a compatible process speed. For an environmentally sound project implementation the time span should be set to months or years, depending on local conditions. A commercially competitive project performance is still assured by a high degree of automation.

The process is also applicable in pump storage reservoirs. When starting up a new pump storage plant, the newly created upper basin does not contain any sediment. After several years of operation the owner will frequently find a substantial degree of sedimentation, often limiting the plants operational parameters and commercial benefit. By using the process described here the initial state can be restored in an environmental friendly and commercially effective way.

As mentioned above the sediment leaves the reservoir via the usual outflow organs consisting of turbines, spillways, weirs etc. Wear on the discharge elements (e.g. turbine blades) remains within normal range unless you increase sediment content to a considerably higher level. Anyway, process benefit should easily outrange slightly higher rehab costs or useful turbine blade coating. It is also possible to limit transferred sediment particle size to compatible dimensions e.g. to max. 2 mm or max. 63 mm or to pass finer sediment through turbines and larger particles through other outlets.

Special care should be given to the turbines shaft main sealing. In many hydro power facilities a seal flushing with clear water already is installed. In these cases usually nothing else has to be done to prevent the seal from additional wear. At older turbines it is easy to add this feature or the operator simply accepts a slightly higher wear on the sealing.

3.2 *Impact on river morphology*

When attaching a dam to a natural waterway the river morphology changes considerably. By inventing the described method the natural morphology is widely restored, using the formerly unused suspended load carrying capacity. During the time span required for the reservoirs surplus sediment removal the concentration of solid components in the outflow will be slightly higher than long time average. Even this is a natural condition as sediment processes often are not continuous. Natural sediment layers of several meters are absolutely common and may be washed away in a single flood.

The scale of the 'removal time span' depends on sediment characteristics such as grain size/specific surface, organic constituents, salinity, cation exchange capacity, pH-Value and temperature and has to be adapted to local constraints (Schweim 2005). Assessment of these and other aspects is part of ongoing research within the Institute for Hydraulic Engineering and Water Resources Management at German Aachen University of Technology. Project results are going to be available within 2011.

3.3 *Ecological benefit*

Before starting the permanent sediment transfer the relevant ecological aspects have to be determined for the reservoir and the downstream river. The process has a positive impact on changes in storage volume. Periodically striking the reservoir floor with the suction dredging

tools however affects the benthos structure. This is similar to natural erosion. As the suction dredging never affects the overall floor at once and the process is stretched on a wide time span the reservoirs ecosystem should compensate the interference even better than natural erosion events (Fig. 8).

At the beginning of a sediment transfer the downstream river will experience a higher than average but not unnatural sediment concentration. When transitional effects fade out the river will be set back to a natural sediment equilibrium. This is the aspired ecological state where natural conditions are restored and many regulatory frameworks fulfilled.

The ecological benefit ranges far downstream, restoring the desired nutrition properties of sediment and also reestablish the flux of terrestrial sediment to the global coastal ocean.

3.4 *Legal aspects*

In many countries the method requires no riparian permission of local authorities because it represents a way of maintaining the hydraulic system, the active sediment transfer takes place only inside the reservoir, a natural condition is restored and the appropriate sediment acts/water directives are fulfilled. Due to these benefits the process has actively been supported by authorities so far.

In fact, the effects provided by the described process are asked for in many ecological programs. The ‘European Water Framework Directive’ identified Sediment deficit as a major problem and in its Annex 5 actively promotes sediment permeability for rivers in their entire length including reservoirs. In any way the operator should consult the relevant administrative bodies in advance. The same procedure is significant for patent legislation (PCT 2008).

3.5 *Economic advantages*

Since sediment is simply transferred back to the natural flow using an intelligent mechanism, no disposal or dump costs occur. Even the necessary technical facilities are relatively small and cost effective. The process benefit is achieved by continuous small and sustainable changes on a large timescale instead of large interventions in a short period. The cost of the necessary components is a fraction of the cost of conventional methods. Plant shut-down is limited to a few hours for equipment installation instead of months for excavation works. The former storage volume and operating range is restored within some months or few years—permanently.

For these reasons, in many applications the method is economically very attractive, even if no immediate action in terms of solving sediment problems is obligatory. Additional benefit can be gained if the above described improvement of the ecological status is financially honored as in Germany’s Renewable Energies Act (EEG).

For reservoirs that are almost inoperable due to sedimentation the operator should first think of restoring the existing facility by sediment transfer instead of placing an additional new reservoir, the latter including major construction work and flooding of additional land.

4 OPERATIONAL RESTRICTIONS

The process can be applied on almost any reservoir size. Of course equipment needs to be adjusted for different dimensions. For small applications fully automated vessels are available which completely fit into a 20’-container. Large applications require sectional built vessels with manned operation. Actual equipment is able to deal with water depths up to 20 m though no real constriction consists that would restrict operational range. Tests with up to 160 m water depth have already been performed with successful results.

For most hydro stations sediment abrasion is not a topic concerning machinery, but only within the reservoir. Nevertheless hydro operators faced with heavily sediment loaded waters may fear additional wear on plant installations, especially on turbine equipment. Factors to

sediment abrasion and erosion are multiple, ranging from involved materials to particle size and shape (Neopane 2010). Little is known about critical sediment loads yet while at the same time modern coatings like Wolframcarbide gives reliable surface protection if applied properly.

From a practical perspective additional wear is not a topic unless sediment ration exceeds 1000 mg/l, Francis heads range more than 200 m or Pelton turbines are involved. Even then in most cases cost savings on reservoir operation will more than level out additional wear on turbine equipment.

5 CONCLUSIONS

With the presented method a transfer of sediment is performed in a very elegant way. Ecological permeability of dams is improved and sediment problems in reservoirs are not only eliminated, but permanently resolved. The procedure is in line with and supported by U.S. Sediment Acts, European Water Framework Directive and similar guidelines. Moreover, the process is very cost effective, so that a fast spreading can be expected—a rare and ideal combination of economical and ecological benefit. A rising number of applications will give the chance to analyze additional aspects which will be especially interesting for river sciences.

REFERENCES

- GWSP 2009. Sediment trapping by large dams on The Digital Water Atlas as an activity of the Global Water System Project (GWSP). <http://atlas.gwsp.org>. Bonn: Center for Development Research (ZEF).
- Mahmood, K. 1987. Reservoir Sedimentation: Impact, Extent and Mitigation, Technical Paper 71. Washington DC: World Bank.
- McCully, P. 1996. Silenced Rivers: The Ecology and Politics of Large Dams. London: Zed Books.
- Neopane, H.P. 2010. Sediment Erosion in Hydro Turbines. Trondheim: Norwegian University of Science and Technology (NTNU), Faculty of Engineering Science and Technology.
- PCT 2008. Int. Appl. PCT/EP2008/002507, nat. Appl. 102007016679.8.
- Schweim 2005. Modellierung und Prognose der Erosion feiner Sedimente, Technische Hochschule Aachen, Lehrstuhl und Institut für Wasserbau und Wasserwirtschaft: Mitteilungen 141, ISBN 3-8322-4206-6. Aachen: Shaker.
- WCD 2000. The Report of the World Commission on Dams; London/Sterling: Earthscan Publications.

Sediment management strategies for sustainable reservoir

T. Sumi & S.A. Kantoush

Disaster Prevention Research Institute, Kyoto University, Goka-sho, Uji-shi, Japan

ABSTRACT: The worldwide sediment management techniques consist of three basic strategies: sediment yield reduction, sediment routing, and sediment removal. The paper focuses on reservoir sustainability by considering the following points. One is how we should choose suitable sediment management options under the consideration of each sedimentation conditions. In that case, annual water and sediment inflow volumes comparing to reservoir storage volumes are the key factors for the selection. The other is how we can design suitable volumes to be discharged from reservoirs. Combination of excavation and sediment replenishment option is now becoming common in Japan. Recently these projects are still in trial stage with limited percentages of sediment replenishment ranging between 0.1 to 10% of annual reservoir sedimentation. Case study at Nunome dam is a good example of comprehensive sediment management and it contributes positively to rebuilt sand bars, mitigate the armouring of river bed, and management of reservoir sedimentation.

1 INTRODUCTION

Sustainability of reservoirs and downstream reaches below dams are threatened by reservoir sedimentations. The objective of water and sediment incorporation is to manipulate the river-reservoir system to achieve sediment balance while maximizing the beneficial reservoir storage and minimizing downstream environmental impacts. Several methods for sediment management are available and have been implemented in practice. At the same time, an attempt to return the excavated and dredged sediment to the downstream river (hereafter we all ‘sediment replenishment’) has been undertaken aiming at balancing sediment inflow and outflow sediment budget. An understanding of channel geomorphic responses to various sediment replenishment technique and natural disturbances is important for effective management, conservation, and rehabilitation of rivers and streams to accommodate multiple, often conflicting, needs. For example, channel changes may have implications for various needs including water supply, infrastructure, navigation, and habitat.

1.1 *Sedimentation rates*

Today’s worldwide annual mean loss of storage capacity due to sedimentation is already higher than the increase of the capacity by construction of new reservoirs (Boillat et al., 2003). Thus, sustainable use of the reservoirs is not guaranteed on the long term. The time evolution over the last century of the water storage capacity and volume losses due to reservoir sedimentation in Japan, Switzerland and France are presented in [Figure 1a](#). These reservoirs are now facing a critical question of sedimentation. To maintain the existing dams and their facilities over the long term becomes an essential policy issue. Because of the following reasons: sedimentation is proceeding more than expected in many dams; the share of the dams having a design life of more than 50 years, such as multi-purpose dams where maintaining storage capacity is absolutely necessary, will rapidly increase in the future; and due to social changes in environment-conscious trend and an era of low-growth economy.

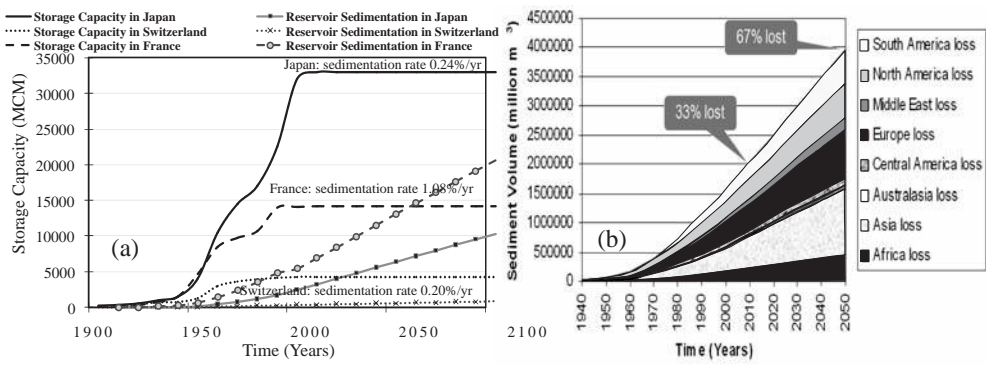


Figure 1. (a) Development and estimated evolution of installed water storage capacity and volumes lost due to reservoir sedimentation; (b) Global reservoir sedimentation rates (Basson, G. 2009).

Figure 1a shows the relationship between the changes in the reservoir storage capacity and the storage capacity loss due to sedimentation in Japan. While the storage capacity is being increased by the construction of new dams, it is being lost by an average rate of 0.24%/year. The figure shows that the average in Switzerland about 0.2% of the storage capacity and in France is 1.08%.

There are no accurate data on the rates of reservoir sedimentation worldwide, but it is commonly accepted that about 1–2% of the worldwide storage capacity is lost annually (Jacobsen, 1999). A detailed collection of sedimentation rates in regions all over the world can be found in Figure 1b. The volumes of water-storage capacity lost due to reservoir sedimentation and the volumes of installed water-storage capacity in the world are presented in Figure 1b. The graph shows the evolution over the last century, and the predicted future development.

1.2 Influences of sediment deficit on downstream reaches below dams

Reservoir construction and operation can have a substantial effect on the stability of the river channel downstream from the dam (Sumi and Kantoush, 2010). Reservoirs can trap and permanently store virtually the entire sediment load delivered from the upstream basin (Petts, 1979; Williams and Wolman, 1984). Thus, immediately downstream from a dam, a river's sediment load is greatly reduced. In addition, typical downstream changes in the flow regime include a reduction in the magnitude of peak flows and a possible increase in the magnitude of low flows (Williams and Wolman, 1984). In response, the downstream river may adjust in an attempt to re-establish an approximate equilibrium between the channel and the discharge and sediment load being transported. Possible adjustments include channel-bed erosion or deposition, channel widening or narrowing, and changes in channel pattern or shape. Downstream impacts develop through discontinuity in downstream gradients, e.g., sediment supply, water quality, temperature, flow and sediment regimes. Sediment deficit is not only an environmental issue but also a socio-economic problem, for instance due to loss of reservoir capacity. Morphological effects on the river channel (e.g., Kondolf and Matthews, 1993; Kantoush et al., 2010) that includes riverbed incision, riverbank instability, upstream erosion in tributaries, groundwater over drafting, damage to bridges, embankments and levees (e.g., Kondolf, 1997; Batalla, 2003), and changes in channel width.

1.3 Objectives

The main purpose is to explain, how to select appropriate sediment management strategy in each reservoir according to sedimentation conditions within reservoir and in downstream

reaches. The other is how we can design suitable volumes to be discharged from dam reservoirs. In this paper, the results of study in Japan that used sediment replenishment strategy to investigate the geomorphic responses of channels to disturbances are presented. The examples provided demonstrate the use of sediment excavation and replenishing to downstream reaches to reduce sedimentation in reservoir and improve downstream reaches. Given that currently about 20 reservoirs in Japan are excavated and sediments were supplied, the techniques described here may have utility for sediment replenishment and geomorphic response investigations nationally.

2 SUSTAINABILITY OF RESERVOIRS

2.1 Concept and economical feasibility

The concept of sustainability applied to agriculture developed, ground water development, and road engineering. The essential concept of sustainable development is that the welfare of future generation should logically figure into the project decision-making. Reservoirs arguably represent today's class of non-sustainable infrastructure. The objective of reservoir sedimentation management is to minimize the adverse effect that sediment deposition in a reservoir has on its usability. The sustainability of reservoir should seek to balance sediment



Figure 2. Concept of a sustainable reservoir.

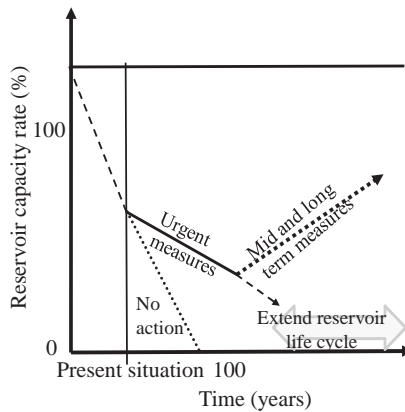


Figure 3. Illustration of prolongation of reservoir lifetime.

inflow and outflow across the reservoir while maximize the long-term benefits, the concept of sustainability is shown in Figure 2. The optimization of sediment removal methods as a dam group is inexpensive if a dam group was linked with each other for sediment management. This may involve strategies to minimize sediment inflow, enhance sediment release, or combination of several countermeasures for coarse and fine sediments. Examples of each facilities and proper maintenance sustainable reservoir management under the limited budget are presented. Technically, efficient economically and environmentally countermeasures, the coordinating sediment management of multiple reservoirs in a river basin, are discussed. The main development patterns for reservoirs and sustainable development are summarized in Figure 2.

The latter essentially implies that the current generation uses resources in a consumptive manner, leaving the problems of dealing with its remains to future generations without providing resources to do so. Integrated models of sediment flow and morphological dynamics in both regulated and free flowing rivers are necessary. Integration of different skills and approaches through provision of effective reservoir sediment management system to prolong the reservoir lifetime as illustrated in Figure 3, should allow the research to obtain some significant advances in the understanding of dam impacts.

Requiring a reservoir life measured in terms of thousands years instead of decades will demand new methods of analyzing costs and benefits. For all these reasons, developing new techniques to evacuate the fine and coarse sediment to maintain the functionality, and at the same time ecologically rehabilitating the involved landscape would be economically and environmentally beneficial for all types of reservoirs.

3 SEDIMENT CONTROL STRATEGIES

3.1 Classifications of sediment management techniques

Controlling reservoir sedimentations means in fact the control of sediment deposition in reservoir. It consists of three basic strategies:

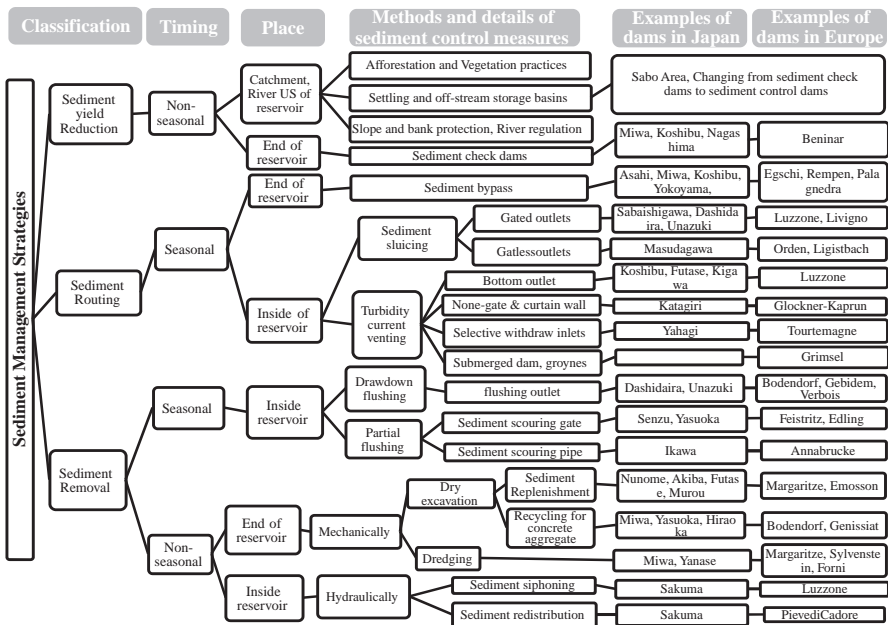


Figure 4. Classification of strategies of sediment control in Japanese and European reservoirs.

1. Sediment yield reduction: to reduce sediment inflow to reservoirs. Apply erosion control techniques to reduce sediment yield from tributary catchments.
2. Sediment routing: to pass sediment inflow around or through the reservoir by techniques such as sediment bypass, partial drawdown sluicing and turbidity release.
3. Sediment removal: to remove accumulated sediment by drawdown flushing, dredging and excavation by mechanically or hydraulically techniques.

Figure 4 shows how sediment management is undertaken and classified. And some representative dams and examples from Europe and Japan, which exercise sediment management, are listed up.

4 SEDIMENT REPLENISHMENT TECHNIQUE

There are two techniques to reduce the amount of transported sediment: 1) countermeasure to control sediment discharge which covers entire basin including the construction of erosion control dams; and 2) countermeasure to forcibly trap sediment by constructing check dams at the end of reservoirs. In the technique with sediment trap, a low dam is constructed at the end of reservoir as to deposit transported sediment, mainly bed load of relatively coarse grain size. The accumulated sediment can be excavated on land except for flood time, and the removed sediments have been utilized effectively as concrete aggregate. As of 2000, the check dams have been constructed at 57 out of the dams under jurisdiction of Ministry of Land, Infrastructure, Transport and Tourism (MLIT).

4.1 *Sediment replenishment projects in Japan: Volume and grain size*

In Japan, it is common practice to remove accumulated coarse sediment by excavation and dredging, and to make effective use of the removed sediment. Sediment replenishment method is one of new measures of sediment management. In this method, trapped sediment is periodically excavated and then transported to be placed temporarily downstream of the dam. In a manner decided according to the sediment transport capacity of the channel and the environmental conditions. Therefore, the sediment is returned to the channel downstream in the natural flooding processes. The procedure of the experiments consists of four steps: (1) extracting mechanically the accumulated sediment at check dam; (2) transporting it by truck to downstream river; (3) placing the sediment with specific geometry, and (4) monitoring flow, sediment, and environmental parameters.

Recently, sediment replenishment tests have been carried out in 20 dams in Japan. Okano et al. (2004) summarized sediment replenishment projects in Japanese Rivers. Kantoush et al. (2010) investigated the morphological evolution and corresponding flow field during replenishment experiments in Uda River, Japan. Sediment treatment system is applied by Sumi et al. (2009), to produce appropriate grain sized material with less turbidity. Seto et al. (2009) analyzed sediment replenishment effects on the downstream river of Yahagi dam.

Sediment replenishment volume and grain size are recognized as key factors for a successful management in the river basin to create and maintain physical habitats, aquatic and riparian ecosystems. Figure 5 shows the relationship between the annual excavated sediment volumes from reservoirs and annual reservoir sedimentation volumes within reservoir (Sumi and Fujita, 2009). Percentages of sediment replenishment are very limited ranging between 0.1 to 10% of annual reservoir sedimentation since these projects are still in trial stage. Figure 6 shows the grain size distributions of replenished sediment which are very much different in each dam because of the location to take sediment out from reservoirs. In Miharu and Nunome dams, relatively fine sediments are dredged in upstream secondary reservoirs for trapping nutrient rich sediments. Others are mainly excavating coarse sediments from conventional check dams.

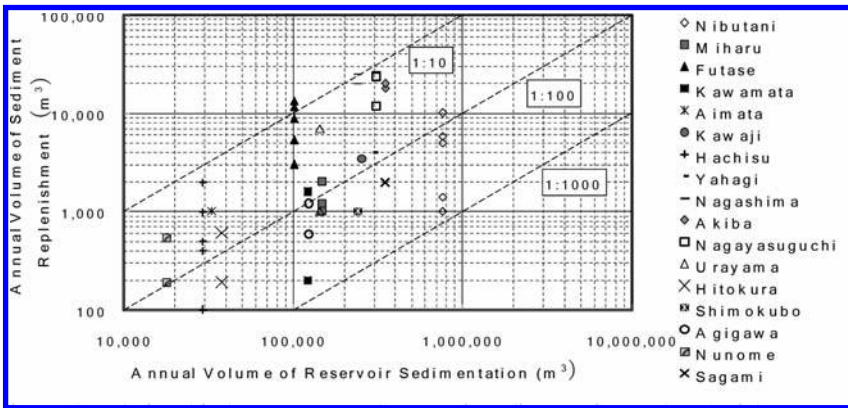


Figure 5. Relationship between annual reservoir sedimentation and replenishment volumes in Japan.

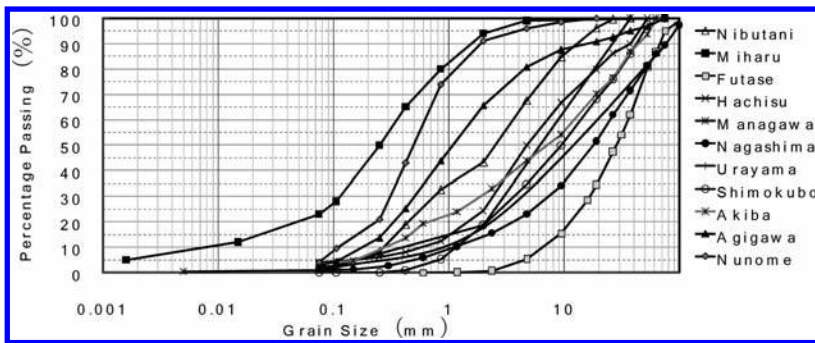


Figure 6. Grain size distributions of sediment replenishment.

4.2 Case study of Nunome dam actual sediment replenishment tests

Since 2004, six experiments of sediment replenishment projects with different sediment volumes are undertaken below Nunome dam. Tracking the history and performance of these projects is helping to understand the evolution of sandbars. Table 1 summarizes the replenishment history, flushing flow and sediments characteristics. The volume of placed sediment is limited to several hundreds of cubic meters each time. To implement this method, consideration has to be given to environmental problems in the lower river basins, to the occurrence of turbid water, and to safety risks due to sediment deposition in the channel. The data in Table 1 indicates that there is a need to increase the amount of the supplied sediments in Nunome River every year. The replenished sediment is placed at such an elevation; in order to reduce the turbidity during normal flow period. The top of the sediment is adjusted so that the sediment is completely submerged during flood at several times a year and all sediment is eventually transported downstream (Figure 7).

The evolving of bed topography and grain size distribution is monitored, along with water surface, velocities and rate of sediment transport at the downstream end of the Nunome River. Figure 8 shows the remained sediment of 2008 and during the heavy rain with peak discharge of $81 \text{ m}^3/\text{s}$. When the discharge exceeds $8 \text{ m}^3/\text{s}$, the erosion starts and about 40 m^3 of sediments are transported. Figure 8 shows the photos of field tests phases. All of the remained sediments are removed, and then new dredge sediments are placed.

Table 1. History of the sediment replenishment tests downstream of Nunome dam.

Year	Setting sediment period	Flood period	Volume of remained sediment (m ³)	Volume of placed sediment (m ³)	Volume of eroded sediment (m ³)
2004	28-9-2004	29-9-2004	0	190	190
2005	9-8-2005	4, 5-10-2005	0	540	80
2006	NA	19, 21-7-2006	460	0	370
2007	9-8-2007	23, 29-8-2007	90	720	810
2008	27-6-2008	8-7-2008	0	100	35
	7-8-2008	5, 19-9-2008	0*	100	100
	12-11-2008	NA	0	500	0
2009	NA	2-8-2009	500	0	500
	2-10-2009	7, 8-10-2009	0	500	500

* The remained 65 m³ sediment is removed.
 NA: No placed sediment or No flood occurred.

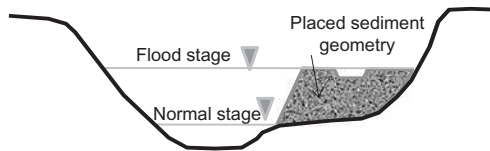


Figure 7. Concept of sediment replenishment.

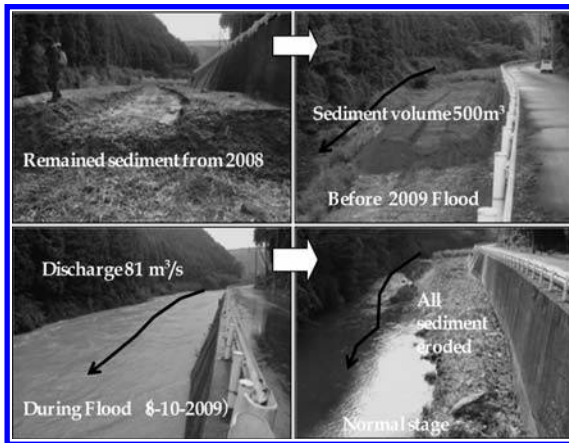


Figure 8. Evolution of replenishment experiments.

By using satellite images and aerial photos, a map of Nunome River in 2009 is constructed for 1 km below the dam. The river channel, island, point bars, and vegetation area are identified and distinguished as shown in Figure 9. The downstream reach of the dam, first 150 m from dam, experienced the greatest change in channel structure and loss of bars and islands. The replenishment processes are efficient to restore the bed load transport and the associated habitat by coupling reintroduction with floodplain habitat restoration. In Figure 9 along the Nunome River, several cross sections are identified to survey after replenishment. Newly depositions over sand bars and in the river channel are shown in Figure 9.

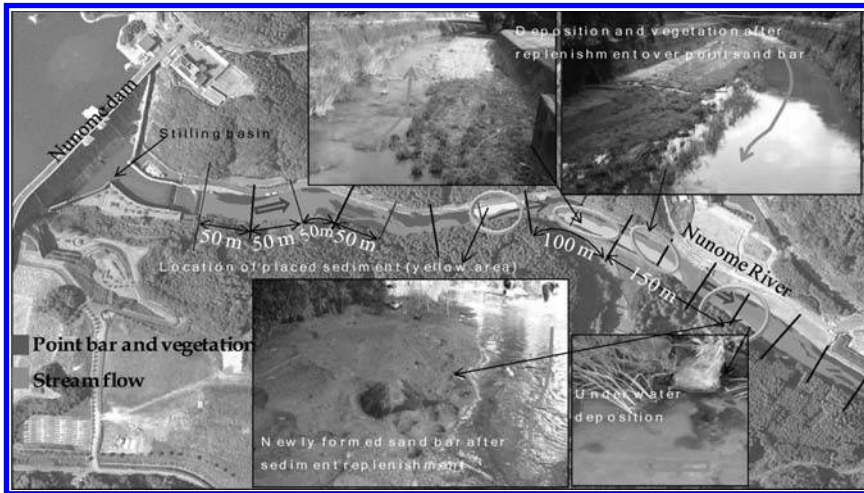


Figure 9. Aerial photographs of Nunome dam with the downstream reach of Nunome River. Morphological changes and the self forming sand bar due to sediment replenishment below the dam (14-10-2009).

Moreover, a completely new sand bar is formed after 600 m from dam. With the field experiments the processes are directly visible, and will be used for validation of numerical models.

5 SUITABLE SELECTION OF SEDIMENT MANAGEMENT TECHNIQUE

Figure 10 shows flow chart for setting up sediment management strategy. Firstly, we have to pick up dams for sediment management (1) and select high priority dams (2). We should consider design life cycle for redevelopment project for these dams to calculate investment cost and benefit (3). Based on past record of reservoir sedimentation, we can estimate future expected sediment inflow to the reservoir (4). Here, stochastic approach considering extreme flood events is recommended to assess long term sediment yield and transport process (Sumi and Kantoush, 2010).

After that, we should consider parallel studies; one is to design necessary reservoir capacity volume for maintaining original functions of dams (5) and design necessary sediment supply volume to realize it (6). The other is to design sound river environment described representatively such as by river bed elevation, grain size and morphological dynamics (7) and design necessary sediment supply volume and grain size (8).

Finally, we should combine these two needs and decide appropriate scenario to discharge sediment from dams (9). If there do not exist suitable scenarios, we should go back to (3). Based on the proposed scenarios, we can select optimal sediment management measures from several possible options such as reservoir flushing, sediment replenishment, bypass tunnel etc. (10). If technical significant problems may arise, we should modify the scenario.

Selected sediment management measure should be evaluated by benefit/cost analysis (11) and, if the project is not economically feasible, we should revise the project from the master planning stage. Sediment management of reservoirs is very much complicated project which will affect reservoir sustainability and also maintaining downstream river health. So we should start to implement step by step basis (12) by conducting filed monitoring under the adaptive management concept (13). Sediment replenishing case study at Nunome dam is a part of comprehensive sediment management in upper Kizu river basin containing five multi-purpose dams (Sumi et al., 2009). We are now starting to clarify how to sustaining reservoir functions and how to improve river environment at the same time by coordinating operation.

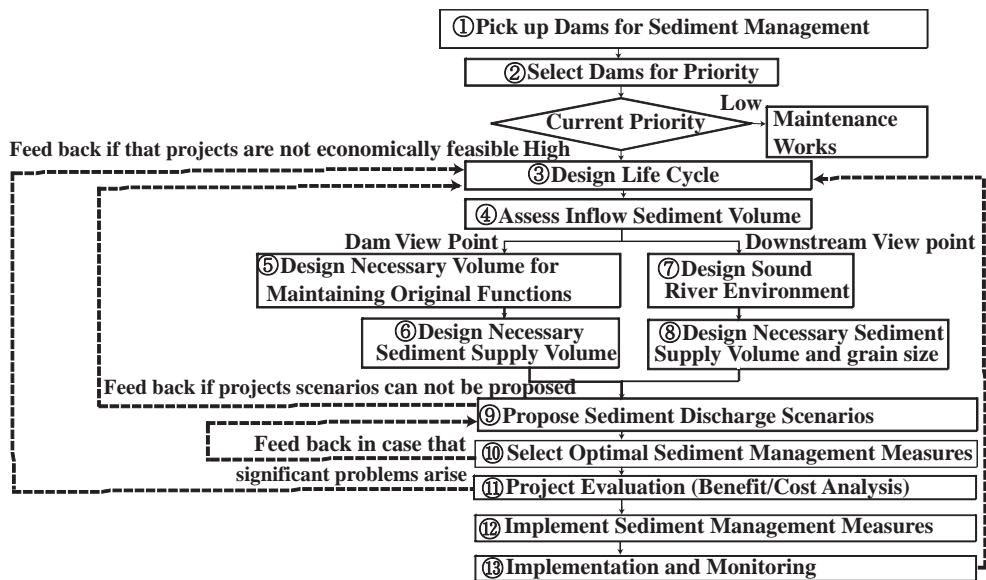


Figure 10. Flowchart for setting up sediment management strategy.

6 CONCLUSIONS AND DISCUSSIONS

Assessing issues, depending on each case, of dam security, sustainable management of water resources and sediment management in a sediment transport system, we have to draw up an effective sediment management plan with a limited budget and take specific action. It is necessary to find out appropriate combination of flow and sediment release which can meet demands of various functions based on data of hydrology, water quality, river morphology and ecosystem, etc. Furthermore, the integrated sediment management approach should be considered in sediment routing system which covers not only river basin but also connecting coastal area. Since suitable sediment replenishment volumes and grain sizes are key parameters to design effective management strategy, these values should be decided from two points of view of reservoir sustainability and downstream environmental improvements. Regarding to the case study of Nunome by replenishing sand at different locations of the Nunome River within the downstream reaches, the replenishment directs future supplements for a more widespread dispersal of suitable sand for fish habitat including spawning beds.

REFERENCES

- Basson, G., 2009. General Report of Q. 89. 23rd Congress of ICOLD, Brasilia, Brazil.
- Batalla, R.J., 2003. Sediment deficit in rivers caused by dams and instream gravel mining. A review with examples from NE Spain. *Cuaternario y Geomorfología* 17 (3-4):79-91.
- Boillat, J.-L., Oehy, Ch., and Schleiss, A., 2003. Reservoir sedimentation management in Switzerland. 3rd World Water Forum, Japan, pp. 143-158.
- Kantoush, S.A., Sumi, T., Kubota, A., and Suzuki, T., 2010. The impacts of sediment replenishment below dams on flow behavior and bed morphology of river channel and river mouth. First International Conference, Coastal Zone management, River Deltas and Low Land Coastlines, Alexandria, Egypt, 2010.
- Kantoush, S.A., and Sumi, T., Kubota, A., 2010. Geomorphic response of rivers below dams by sediment replenishment technique. In. Proc. River Flow 2010, Germany, 8-10 September 2010, pp. 1155-1163.
- Kondolf, G.M., 1997. Hungry water: effects of dams and gravel mining on river channels. *Environmental Management* 21 (4), 533-551.

- Okano, M., Kikui, M., Ishida, H., and Sumi T., 2004. Reservoir sedimentation management by coarse sediment replenishment below dams. 9th International Symposium on River Sedimentation, Yichang, China, Volume II, 1070–1078.
- Petts, G.E., 1979. Complex response of river channel morphology subsequent to reservoir construction. *Progress in Physical Geography*, 3, pp. 329–362.
- Seto, K., Sakamoto, T., and Suetsugi, T., 2009. Sediment control measures and improvement effects of physical condition and environment by sediment flushing—a case study in the Yahagi dam. 23rd Congress of ICOLD, Brasilia, Brazil, Q. 89–R. 3.
- Sumi, T., and Kantoush, S.A., 2010. Integrated Management of Reservoir Sediment Routing by Flushing, Replenishing, and Bypassing Sediments in Japan River Basins. 8th International Symposium on EcoHydraulics (ISE 2010), COEX, Seoul, Korea, 12–16 September 2010.
- Sumi, T., and Kantoush, S.A., 2010. Stochastic sediment deposition process of large reservoirs in Japan. 11th International Symposium on River Sedimentation, Stellenbosh, South Africa.
- Sumi, T., Kobayshi, K., Yamaguchi, K., and Takata, Y., 2009. Study on the applicability of the asset management for reservoir sediment management. 23rd Congress of ICOLD, Brasilia, Brazil, Q. 89–R. 4.
- Sumi, T., and Fujita, M., 2009. Current status and future challenges of sediment replenishment to downstream river. *Advanced in River Engineering, JSCE*, Vol. 15.
- Williams, G.P., and Wolman, M.G., 1984. Downstream effects of dams on Alluvial Rivers. US Geological Survey Professional Paper 1286.

An experimental study on turbid water coagulation method using natural coagulant

H. Umino & N. Hakoishi

Public Works Research Institute, Tsukuba, Ibaraki, Japan

ABSTRACT: Long term persistent turbidity is a major problem in the water reservoirs of Japan. Coagulation, especially under conditions where all of the water is turbid, is expected to be an effective countermeasure. We examined the use of natural coagulants or soil colloids, which can be deposited in the reservoirs, with the objective of clarifying their coagulation performance and developing an effective coagulation method for turbid water. The experiments conducted in this study provided three important findings. The first is that effective removal of turbid water can be achieved by coagulation treatment that consists of distributing the coagulant and circulating the mixture of turbid water with coagulant. The second is that the pH of the allophane solution water should be adjusted to be acidic if the distribution procedure is omitted. The third is that the allophane has limited coagulation performance, which can be estimated by measuring the zeta potential.

1 INTRODUCTION

We demonstrated through several experiments that the turbid components of reservoir water could be coagulated by natural materials. Long term persistent turbidity is a major water quality problem in Japan's reservoirs. Selective intake facilities and fences for controlling turbid water flow have been employed as countermeasures against this problem. However, the effects of conventional countermeasures are limited, and if all of the water in a reservoir turns turbid, as can occur after large flood inflows or large-scale water circulation, the only solution is to wait for the particulate matter to settle.

Coagulation is expected to be an effective countermeasure in such circumstances where all of the water is turbid. Treatment of deposited sediments, however, can present a serious problem when artificial coagulants are used. Here, we examine the use of natural coagulants or soil colloids, which can be deposited in the reservoir.

2 LONG TERM PERSISTENCE OF TURBID WATER IN A RESERVOIR

Long term persistence of turbid water in a reservoir can occur after large-scale inflows. In September 2007 in Japan, especially in the Kanto Region, persistent turbidity had developed in several reservoirs. We selected the Kawaji Dam reservoir for our observations. The location of the dam is shown in [Figure 1](#).

The monitoring data of turbidity at the Kawaji Dam reservoir is shown in [Figure 2](#). In Kawaji Dam, turbidity was automatically and daily monitored for every 1 meter deep. The observation device was a production of the Tsurumi Seiki Co., Ltd. The measurement of turbidity was based on formazin and the scattered/transmitted light method was adopted. For example, the device indicates 100 degree for the 100 mg/L formazin solution. The large scale inflow was happened on 7th of September 2007. Before the incident, the turbidity was less than 5 degree in surface layer and less than 10 degree in middle layer. After the incident,

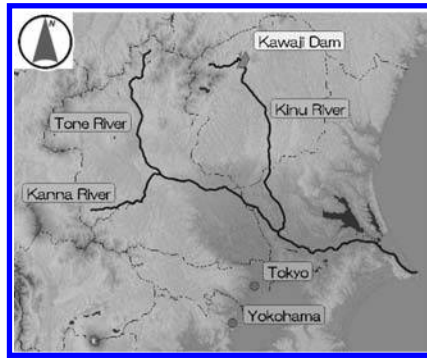


Figure 1. Location of Kawaji Dam.

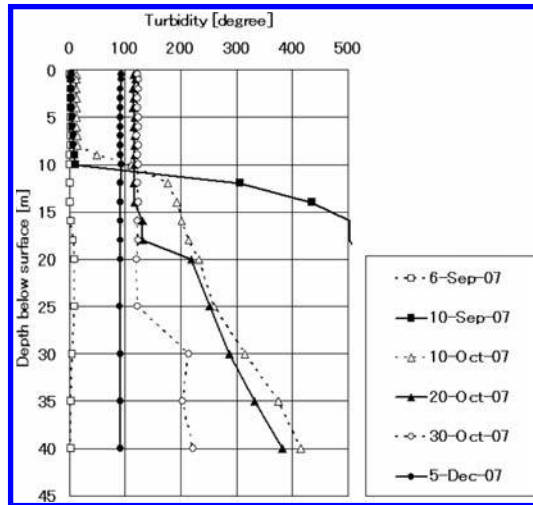


Figure 2. Change in degree of turbidity (Kawaji Dam Reservoir/formazin based).

the surface layer turned clear, on the other hand, extremely turbid water still remained in the middle layer and bottom layer.

It is regarded that the circulation of all the layers in the reservoir started between the 10th and 20th of October 2007. Prior to that time, the degree of turbidity was low in the surface layer, and turbidity was not a problem as long as the surface intake remained effective. In October, the temperature declined and the surface of the reservoir cooled. This cooling of the surface layer caused full circulation, because the water density of the surface layer and the other layers became almost the same. At the time of observation in December, turbidity had persisted for more than one and a half months since this mixing of the water layers. Waiting for dilution brought by clear water inflow was the only strategy to be taken at that time. Considered the artificial coagulation treatment, the target degree after coagulation should be set at 5 to 10 degree corresponding with the turbidity of the day before incident.

3 PREPARATION FOR EXPERIMENTS

3.1 Selection of coagulant

Allophane, a natural soil colloid, was used in this experiment (Fig. 3). Among natural soil colloids, kaolin, allophane and imogolite have large specific surface and they could be used as

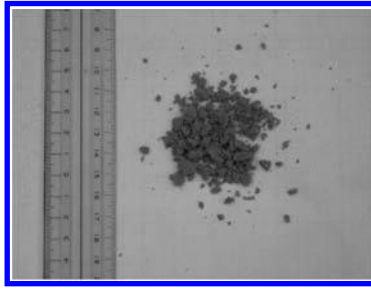


Figure 3. Allophane used in the experiment.

coagulant. In this study, we selected allophane as a coagulant because of its high performance in coagulation; moreover, it was easily obtained. Allophane is present at high levels in weathered volcanic ash and volcanic soils. Volcanic soils are widely distributed in the Hokkaido, Tohoku, and Kyushu regions of Japan and are easily obtained. Moreover, coagulation with allophane is considered to minimize the environmental impact on reservoirs and downstream rivers. Allophane is used in several industries. It is a porous material suitable for application as a drying or adsorption agent. Allophane is colloidal particle and has a character of distribution and coagulation according with the pH condition. The distributed allophane particles are surrounded by plus electric charge and it is easy to adsorb soil particles because soil particles ordinarily have the minus electric charge. In view of its absorbing characteristics, we considered that it would be capable of coagulating particulate matter in water.

3.2 *Production of turbid water*

Turbid water and sediment were sampled from the Kawaji Dam reservoir. As part of the preparations for the laboratory experiment, turbidity was adjusted to the prearranged degree by adding pure water. In addition, turbid water was artificially produced by using sediment collected from the bottom of the reservoir. The procedure for production was as follows:

1. Sediment was stirred into pure water and large particles were filtered off (mesh size of the filter: 7 μm) and the filtrate was extracted. Supersonic distribution was applied during filtering to accelerate distribution.
2. Filtrate was poured into a bucket and left undisturbed for 24 h.
3. The top clear layer of filtrate was collected and the turbidity and temperature were arranged.

All of the above procedures were conducted in an air-conditioned laboratory.

3.3 *Preliminary experiment*

We conducted a preliminary experiment to determine the quantity of coagulant that would be suitable for the turbidity of samples. It was reported that 90 to 180 mg-dry/L had been enough for the turbidity of 55 to 85 NTU (nephelometric turbidity unit) in Kawaji Dam reservoir (Umino et al. 2008). Referred the former paper, the concentration of coagulant was set 90 mg-dry/L in Case 3.1, 150 mg-dry/L in Case 3.2 and 180 mg-dry/L in Case 3.3 for the sample of 50 NTU. As the coagulation treatment, both supersonic distribution of coagulant and circulation of the mixture of turbid water and coagulant were adopted.

The results are shown in Figure 4. Hack 2100P Turbidity Meter was used for the observation of formazin based turbidity. The target degree of turbidity was set at less than 5 NTU at 30 min after the coagulation treatment, which corresponded to the ordinary turbidity of surface layer in Kawaji Dam reservoir. We found that the degree of turbidity declined with time. Thirty minutes after coagulation treatment, the turbidity was 5.3 NTU in Case 3.1, 4.5 NTU in Case 3.2 and 5.8 NTU in Case 3.3. There was little difference between the three cases.

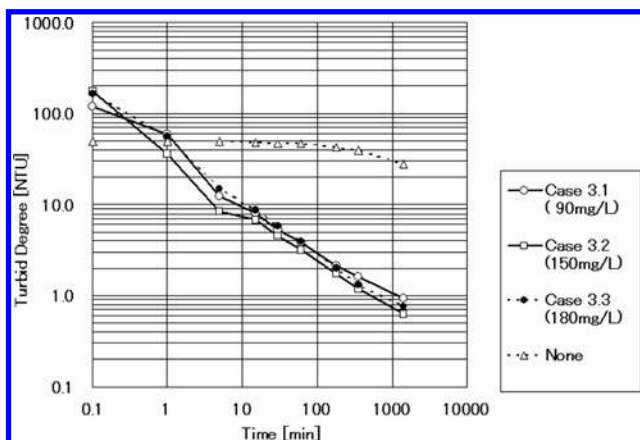


Figure 4. Change in degree of turbidity (preliminary experiment).

In contrast, there was hardly any change in turbidity in the case without coagulation treatment (Case 3.4). The appropriate concentration of coagulant for water with an initial turbidity of 50 NTU was considered to be 90 mg-dry/L, so we adopted this rate for the main experiment.

4 STANDARD COAGULATION TREATMENT IN WATER TANK

In an earlier paper, we reported that allophane was useful for the treatment of turbid water. Moreover, we reported that the distribution of coagulant and circulation were indispensable for effective coagulation (Umino et al. 2008). Here, we have expanded on the earlier study, changing from settling cylinders to water tanks, in order to demonstrate that the former reported procedures are effective at any size of experiment.

4.1 Procedure

We used artificial turbid water in the experiment. For the conditions of coagulation treatment, the quantity of coagulant was decided by the results of the preliminary experiment and the duration of distribution was arranged for two cases. The change in turbidity after the coagulation treatments was observed. The experimental procedure was as follows:

1. Artificial turbid water was created using sediment from the Kawaji Dam reservoir. The target initial degree of turbidity was set at 50 NTU.
2. A water tank was prepared and the artificial turbid water was poured into the tank to a volume of 500 liters.
3. A sample of 50 liters of turbid water was removed from the water tank to a bucket, and a predetermined quantity of coagulant was added to the bucket. The concentration of coagulant was 90 mg-dry/L.
4. The mixture of sampled water and coagulant was returned to the water tank, and then the coagulant and artificial turbid water were distributed by supersonic wave distributor (1,200 W, 28 kHz) for 12 min (Case 4.1) or 24 min (Case 4.2) while circulation was underway.
5. The mixture of artificial turbid water and coagulant was left undisturbed and the change in degree of turbidity was observed at 6 points in the water tank.

4.2 Results

The results of the experiment are shown in Figure 5. The target degree of turbidity was set at less than 5 NTU at 1440 min after the coagulation treatment, corresponding to the ordinary

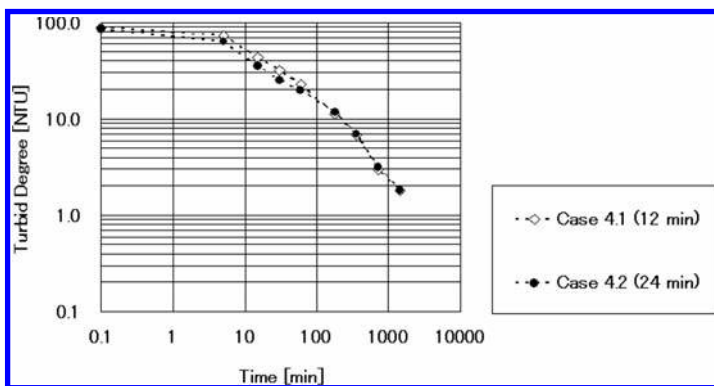


Figure 5. Change in degree of turbidity (water tank).

turbidity of surface layer in Kawaji Dam reservoir. The differences of turbidity among 6 points were little for each case so that the average of 6 points was plotted on the figure.

At 1440 min after coagulation treatment, the turbidity was 1.8 NTU in both cases and the target degree was achieved. Under these experimental conditions, 12 min of distribution was sufficient for coagulation treatment. We increased the size of the experiment from settling cylinders to a water tank, and have also confirmed that the distribution of coagulant and circulation of turbid water/coagulant mixture are effective as a coagulation treatment.

5 DISTRIBUTION OF COAGULANT UNDER ACID CONDITIONS

Allophane is a natural soil colloid, the distribution and coagulation characteristics of which vary with the pH of the colloid solution. In practical applications, it would be difficult to distribute the coagulant. We examined the possibility of chemically distributing the coagulant while adjusting the pH of the colloid solution to reduce the distribution load.

5.1 Procedure

We conducted an experiment to examine the distribution performance of allophane solution along with the pH conditions. Three samples of allophane solution were prepared as the coagulant and agitation was adopted as the coagulation treatment. After treatment, the changes in turbidity degree were observed to evaluate the efficiency of allophane solution. The experimental procedure was as follows:

1. Medium-sized beakers were prepared and 1 L of turbid water was poured into each one.
2. A 50-mL sample of turbid water was taken from each beaker and placed into a small beaker. Predetermined allophane solution was added. The pH of the allophane solution was adjusted to 4 (Case 5.1) and 5 (Case 5.2) by adding acetic acid solution. In addition, allophane solution without pH adjustment was also examined (Case 5.3). The concentration of coagulant was 150 mg-dry/L for each case.
3. The mixture of turbid water and allophane solution was returned to each medium-sized beaker and then agitated by stirring apparatus for 3 min to accelerate coagulation of the turbid particles.
4. The mixture of turbid water and allophane solution was left undisturbed and the change in degree of turbidity was observed at 4 cm below the surface.

5.2 Results

The experimental results are shown in Figure 6. The target degree of turbidity was set at less than 5 NTU at 30 min after the coagulation treatment.

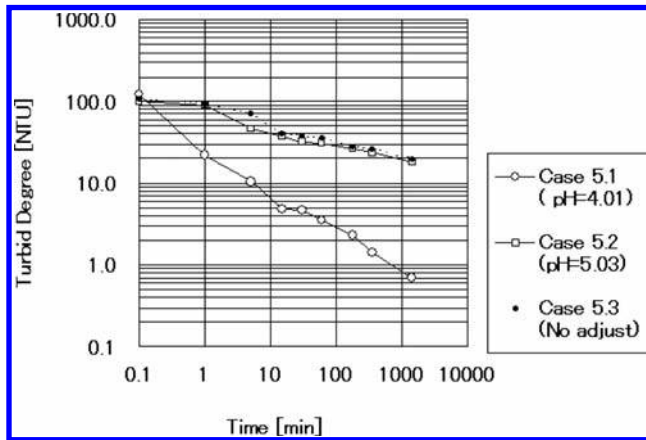


Figure 6. Change in degree of turbidity (pH adjustment).

We found that the degree of turbidity declined with time. After 30 min, the turbidity was 4.7 NTU in Case 5.1, 31.9 NTU in Case 5.2 and 37.6 NTU in Case 5.3. The target degree was attained only in Case 5.1. By adjusting the pH condition of the allophane solution to be acidic, instead of applying supersonic distribution, effective performance of coagulation was achieved. From the results of the experiment, pH of the allophane solution should be adjusted to around 4 if the distribution procedure is omitted.

On the other hand, there is a risk of affecting the water environment in the reservoir by spraying the mixture of allophane and acetic acid solution. It is estimated that the pH condition of the reservoir water could become acidic. Possible effects on the reservoir environment are yet to be evaluated.

6 VERTICAL TRANSMISSION OF COAGULATION IN SETTLING CYLINDERS

As mentioned above, allophane proved useful for the treatment of turbid water; moreover, the distribution of coagulant and circulation were indispensable for effective coagulation. If we consider the practical application of the coagulation treatment, the vertical transmission of coagulation effects should be realized because the coagulation treatment would be executed at the surface layer of the reservoir water. Here, we determine the vertical transmission of coagulation effects by conducting a continuous experiment using settling cylinders.

6.1 Procedure

The purpose of the experiment was to clarify the transmission of coagulation effects from the surface to the bottom of the reservoir along the vertical axis. We conducted a continuous coagulation experiment using a settling cylinder 2.2 m in length. The shape of the settling cylinder is shown in Figure 7. The sample was artificial turbid water created using sediment. The change in turbidity after the coagulation treatment was observed. The procedure for the primary experiment, Case 6.1, was as follows:

1. Artificial turbid water was prepared with turbidity of 50 NTU.
2. A settling cylinder was prepared and the artificial turbid water was poured into the cylinder up to a depth of 2.0 m.
3. A sample of 25 liters of turbid water was removed from the settling cylinder to a bucket, and the coagulant was added. The concentration of coagulant was 90 mg-dry/L.
4. The mixture of sampled water and coagulant was returned to the settling cylinder, and then the coagulant and artificial turbid water were distributed by a supersonic wave distributor (600 W, 28 kHz) for 12 min while circulation was underway.

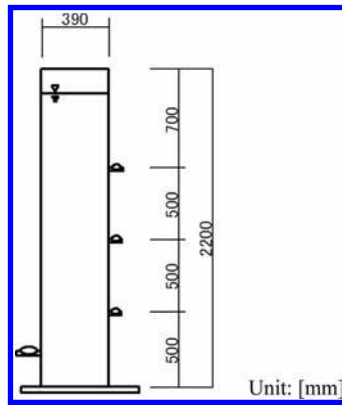


Figure 7. Shape of settling cylinder.

5. The mixture of artificial turbid water and coagulant was left undisturbed and the change in degree of turbidity was observed at 4 points in the settling cylinder.

After the completion of Case 6.1, sediment composed of allophane and turbid particles was collected from the bottom of the settling cylinder and placed in another settling cylinder, to which artificial turbid water was added for the preparation of Case 6.2. The purpose of this case was to evaluate the coagulation potential of sediment. The ratio of sediment and turbid water in volume was 1:9. for this case. Only circulation was conducted as the coagulation treatment in case 6.2, but it showed poor performance in coagulation, so that both distribution and circulation were conducted in Case 6.3. Both Case 6.2 and Case 6.3 simulated the coagulation conditions for the depth of 2 to 4 m below the surface

After the completion of Case 6.3, sediment was collected and placed in another settling cylinder. Then, Case 6.4 was started by adding turbid water. The coagulation treatment for Case 6.4 was the same as for Case 6.3. Case 6.4 simulated the coagulation conditions for the depth of 4 to 6 m below the surface. The treatment for each case is summarized in [Table 1](#).

6.2 Results

The results of the experiment are shown in [Figure 8](#). The target degree of turbidity was set at less than 5 NTU at 1,440 min after the coagulation treatment. The degrees of turbidity in this figure are the means of the four observation points in the settling cylinder.

At 1,440 min after coagulation treatment, the turbidity was 4.0 NTU in Case 6.1, 35.8 NTU in Case 6.2, 4.7 NTU in Case 6.3 and 40.8 NTU in Case 6.4. Both Case 6.1 and Case 6.3 achieved the target degree. This means that the sediment from Case 6.1 had sufficient coagulation ability because Case 6.3 showed good performance. On the other hand, the sediment from Case 6.3 had little coagulation ability because Case 6.4 showed poor performance. Moreover, the result for Case 6.4 suggests that the effects of coagulation could not be transmitted further than 4 m below the surface of the reservoir.

We measured the zeta potential ([Table 2](#)) and found that the allophane had positive potential and the artificial turbid water had negative potential. It was regarded that the particles of turbid water could be coagulated through electrical adsorption. The coagulation ability could be estimated by measuring the zeta potential of sediment composed of allophane and turbid particles.

Finally, it was considered that the allophane has limited coagulation performance; moreover, the effects of coagulation could be transmitted only 2 to 4 m below the reservoir surface if the surface layer was coagulated. An effective coagulation method that can transmit the effects of coagulation from the surface to the deep layers of the reservoir needs to be developed.

Table 1. Specifications for coagulation treatment.

Case	Coagulant	Distribution	Circulation
Case 6.1	Allophane	12 min	12 min
Case 6.2	Sediment from Case 6.1	None	12 min
Case 6.3	Sediment from Case 6.1	12 min	12 min
Case 6.4	Sediment from Case 6.3	12 min	12 min

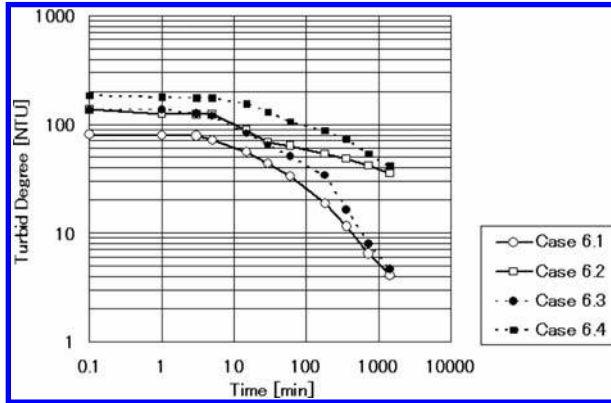


Figure 8. Change in degree of turbidity (continuous experiment).

Table 2. Zeta potential of allophane, turbid water and sediment.

Sample	Zeta potential [mV]
Wet allophane	2.0
Artificial turbid water	-23.3
Sediment (Case 6.1)	-11.4
Sediment (Case 6.3)	-20.5
Sediment (Case 6.4)	-19.7

7 CONCLUSIONS

We examined the use of natural coagulants or soil colloids, which can be deposited in the reservoirs, as an effective countermeasure for persistent turbidity under conditions where all the water in the reservoir is turbid. The experiments conducted in the study yielded three important findings. The first is that effective coagulation can be achieved by coagulation treatment that consists of distributing the coagulant and circulating the mixture of turbid water with coagulant. The second is that the pH of the allophane solution water should be adjusted to be acidic if the distribution procedure is omitted. The third is that the allophane has limited coagulation performance, which can be estimated by measuring the zeta potential.

REFERENCE

Umino, H. & Hakoishi, N. 2008. Turbid water treatment in a reservoir using natural coagulant, The 5th EADC International Symposium on Co-existence of Environment and Dams; Proc. Symp., Yokohama, October 2008. Yokohama: Japan.

Burrowing-type sediment removal suction pipe for a sediment supply from reservoirs

T. Sakurai & N. Hakoishi

Public Works Research Institute, Tsukuba, Ibaraki, Japan

ABSTRACT: In our work on sediment supply measures using flexible suction pipes, we developed the “burrowing-type sediment removal suction pipe method”, which employs a U-bend flexible pipe with a water intake at the upstream end, a permeable sheet and sediment suction holes at the bent part of the pipe. The suction pipe is initially set on the surface of deposited sediment. After the start of discharge, the pipe is expected to suck sediment and gradually burrow into the sediment using the differential water head energy. We carried out an experimental study on the sediment supply characteristics of the suction pipe using physical models and non-cohesive sediment materials. As a result of the model experiments, we confirmed that the suction pipe can supply sediment at almost the expected performance and we established the process of sediment supply and the influence of discharge rate and sediment particle size on the sediment supply characteristics.

1 INTRODUCTION

The construction of a dam can interrupt the transport of sediment through the river. Decreased sediment supply downstream causes environmental problems related to the riverbed such as degradation, armoring, and fewer opportunities to renew the riverbed material. Furthermore, sedimentation causes a reduction in the reservoir storage capacity. Therefore, measures are required for sediment supply from the reservoir. In consideration of the conditions and time variation of the downstream riverbed environment, it is desirable to be able to control the timing of sediment supply and the quantity and quality (mainly particle size) of supplied sediment.

In the past, besides traditional measures such as excavating and dredging, sediment flushing with water level drawdown (Kanazawa 2005) and sediment bypassing (Enomura 2005, Kataoka & Tada 2005) were developed and used in Japan. However, the conditions for applying these measures are restricted and it is difficult to control the exact quantity and quality of the discharging sediment by these methods. We have been working to develop new sediment supply measures using the differential water head energy between the upstream and downstream areas of the dam. We have also been researching methods that use flexible suction pipes.

As a result of earlier studies (Sakurai et al. 2006, Sakurai et al. 2007), we proposed the “burrowing-type sediment removal suction pipe method”.

In this study, we experimentally investigated the sediment supply characteristics of the burrowing-type sediment removal suction pipe using a small scale model (pipe diameter: 60 mm, sediment thickness: 0.6 m), a medium scale model (pipe diameter: 100 mm, sediment thickness: 2.0 m) and non-cohesive sediment materials. As a result of the model experiments, we confirmed that the suction pipe can supply sediment at almost the expected performance and we established the process of sediment supply and the influences of the discharge rate and sediment particle size on the sediment supply characteristics.

2 BURROWING-TYPE SEDIMENT REMOVAL SUCTION PIPE

Figure 1 illustrates the shape of the burrowing-type sediment removal suction pipe. It is a U-bend flexible pipe that has a water intake at the upstream end, a permeable sheet, and sediment suction holes at the bent part of the pipe.

Figure 2 shows the sediment discharge process of the burrowing-type sediment removal suction pipe. The pipe is initially set on the surface of deposited sediment. After the start of discharge, the pipe is expected to suck sediment through the sediment suction holes at the bent part and gradually burrow into the sediment using the differential water head energy.

After sediment discharge using the pipe, sedimentation should form a conical shape pocket. It is difficult to discharge large amounts of sediment by one facility. However, there are many dam reservoirs in Japan that have a mean annual sedimentation volume of less than several tens of thousands of cubic meters. This measure will be useful for achieving sediment transport balance in these reservoirs that have small sedimentation. When the repose angle of the sediment in the water is assumed to be 30° , in order to discharge ten thousand cubic meters of sediment, it is necessary to dig about 15 m for the depth and 26 m for the radius of the conical shape.

The operation method presently considered for the sediment removal suction pipe is as follows: 1) The sediment is transported to an area near the dam, not during the flood season. 2) The pipe is set up on the transported sediment before the flood season. 3) Discharge of the sediment is carried out during a flood by operating a gate installed at the end of the pipe. 4) After sediment discharge, the pipe is removed for maintenance. 5) The above processes are repeated every year. Here, sediment discharge is carried out during a flood in order to supply sediment downstream, similar to natural conditions, considering the downstream river environment.

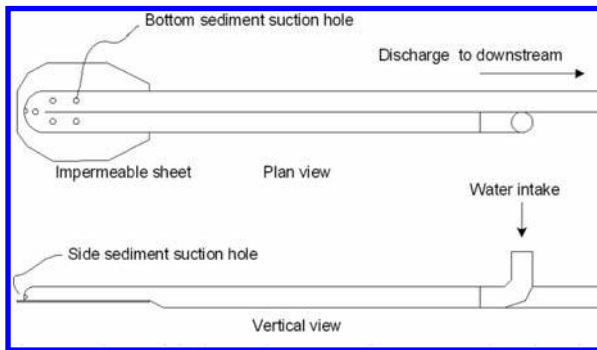


Figure 1. Shape of the burrowing-type sediment removal suction pipe.

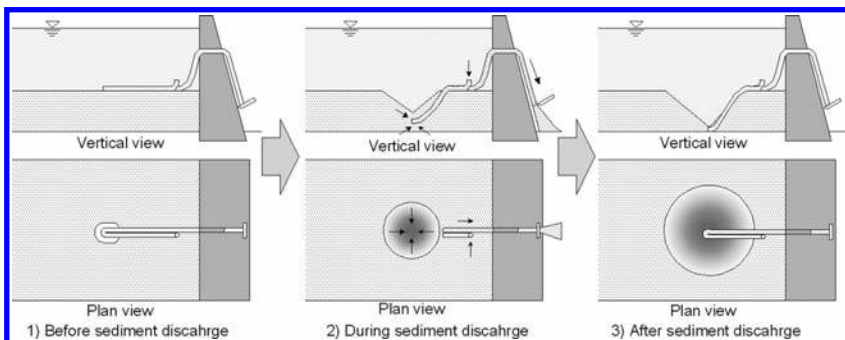


Figure 2. Sediment discharge process of the sediment removal suction pipe.

3 EXPERIMENTAL METHOD

3.1 Small scale model test

Tests were conducted on a small scale hydraulic model to examine the sediment discharge characteristics of the sediment removal suction pipe. An outline of the experimental facility is shown in Figure 3. The water tank used in the tests was 4.5 m long, 2.5 m wide and 1.3 m high. The tank has a rectangular weir to maintain the water level. An outlet pipe is installed at the downstream wall with a discharge control gate at the end of the pipe.

The experimental procedure was as follows: 1) Sediment was placed at a height of 0.6 m in the water tank. 2) The sediment removal suction pipe, shown in Figure 4, was set up on the sediment. 3) Water was pumped into the tank at a constant discharge rate (45 L/s). The water level in the tank was kept almost constant by overflowing from the weir. 4) Sediment discharge was started by opening the gate at the end of the pipe. 5) We observed the sediment discharge situation and measured the water level in the tank, pressure head in the pipe, discharge rate and sediment discharge rate.

The diameter of the sediment removal suction pipe used in the small scale model tests was 60.5 mm. If it is assumed that the pipe diameter in practical use ranges from 0.5 to 1.0 m, the model scale would be 1/16.5 to 1/8.3.

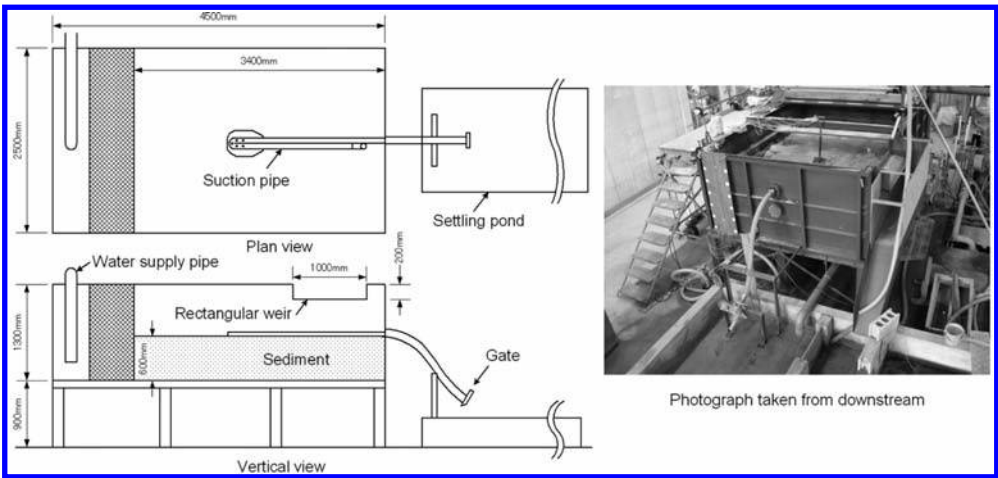


Figure 3. Outline of the experimental facility for small scale model tests.

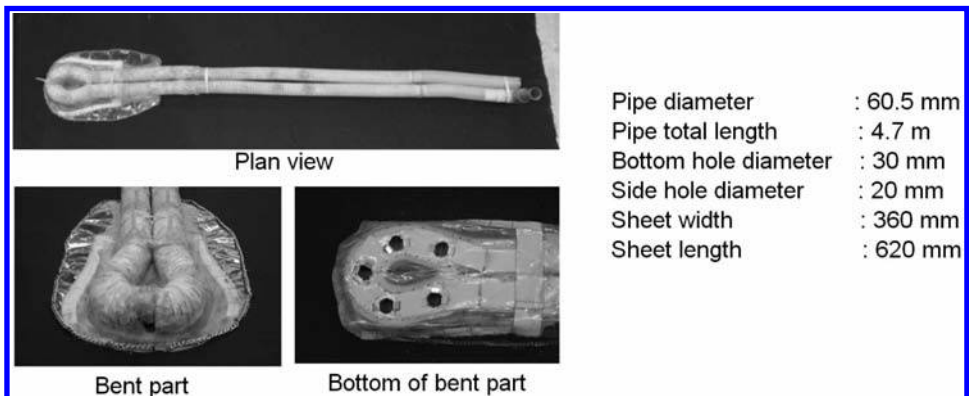


Figure 4. Outline of small scale model of the burrowing-type sediment removal suction pipe.

As the experimental sediment material, we used silica sand at three different particle sizes. The grain size distribution of the sand is shown in Figure 5. The model tests were carried out under the conditions of three different gate openings. The total number of experimental test cases reached nine due to the combination of sediment size and gate opening. The experimental conditions are listed in Table 1.

3.2 Medium scale model test

A test on medium scale hydraulic model was carried out to examine the sediment discharge characteristics of the sediment removal suction pipe under conditions closer to those of the actual facilities. An outline of the experimental facility is shown in Figure 6. The water tank is 7.5 m long, 7.5 m wide and 3.5 m high. The sediment removal suction pipe used in the medium scale model test is basically the same shape as the small scale model pipe (100 mm pipe diameter, 9.4 m pipe total length, 50 mm bottom hole diameter, 33 mm side hole diameter, 600 mm sheet width and 1000 mm sheet length).

The experimental procedure is also similar to that for the small scale model tests. The differences are as follows: 1) Sediment height was 2.0 m. 2) Water supply discharge rate was 47 L/s. 3) We changed the gate opening during the test depending on the sediment discharge situation. 4) The experimental sediment material was sand mixed particle size. The grain size distribution of the sand is shown in Figure 5.

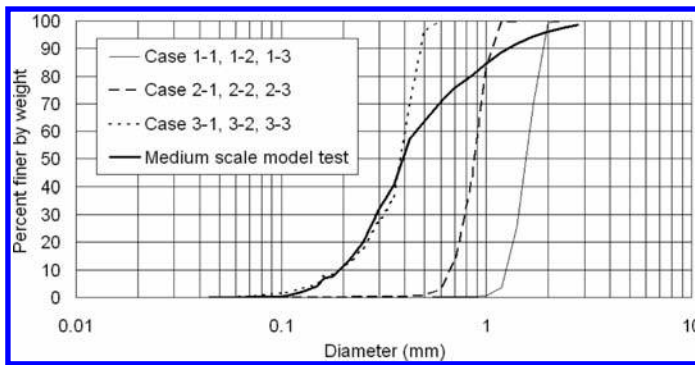


Figure 5. Grain size distribution of sediment material used for model tests.

Table 1. Experimental conditions of small scale model tests.

Case	Mean diameter of sediment Dm (mm)	Gate opening G (%)	Discharge rate Q (L/s)	Mean velocity (in pipe) V (m/s)	Test duration T (min)
1-1	1.56	24	3.32	1.17	80
1-2		18	3.05	1.08	150
1-3		12*	2.50	0.88	120
2-1	0.89	24	3.32	1.17	150
2-2		18	3.05	1.08	150
2-3		12	2.50	0.88	120
3-1	0.36	24	3.32	1.17	150
3-2		18	3.05	1.08	150
3-3		12	2.50	0.88	180

*Initially, the gate opening was set at 18%. After the pipe was buried, the gate opening was set at 12%.

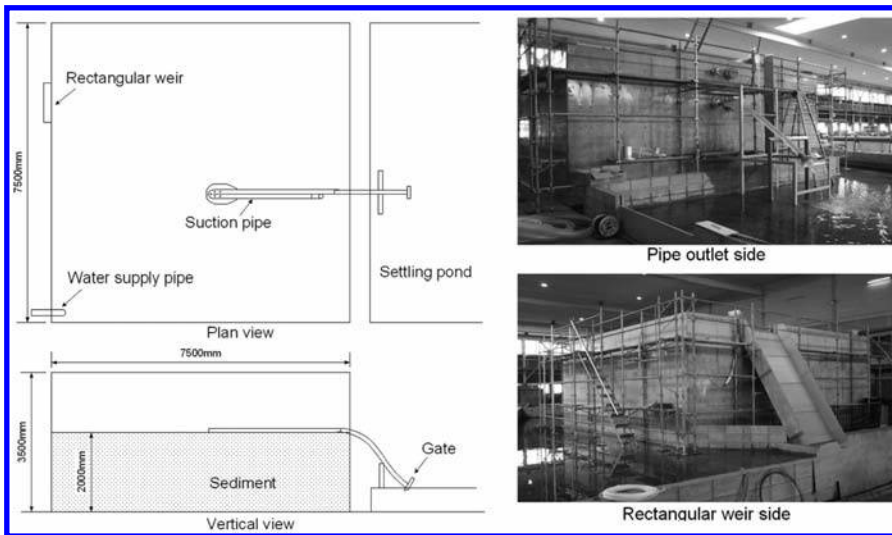


Figure 6. Outline of the experimental facility for medium scale model test.

4 EXPERIMENTAL RESULTS

4.1 *Experimental results for small scale model test*

Figure 7 shows photographs of the shape of sedimentation after sediment discharge in Case 1–2 and Case 3–2. These photographs were taken after drainage of the water tank. Figure 8 illustrates the longitudinal form of sedimentation after sediment discharge in all cases of small scale model tests. It was confirmed that the conical shape void space in sedimentation was made by sediment discharge using the burrowing-type sediment removal suction pipe. Figures 7 and 8 indicate that the conical shape tends to become long in the flow direction in the case using sediment material with a small particle size.

As an example, the time series for discharge rate and sediment concentration of discharged water in Case 1–1 is shown in Figure 9. The sediment concentration was obtained by analysis of sampled water. The sediment concentration is a volume concentration and is estimated by “sediment volume/(water volume + sediment volume)”. In addition, sediment volume is without void volume.

As shown in Figure 9, after the bent part was buried, the sediment concentration increased. Then, after the bent part reached the bottom of the water tank, the sediment concentration decreased. It is considered that the sediment concentration increases from the time when the bent part is buried to the time when the bent part reaches the bottom, because both the bottom suction holes and side suction hole suck the sediment. After the bent part reaches the bottom, it is difficult for the bottom suction holes to suck the sediment, so the sediment concentration decreases. After the bent part reached the bottom, the sediment concentration maintained a certain value for a certain time. The discharge rate became smaller when the sediment concentration became larger, and it became larger when the sediment concentration became smaller. It is considered that the energy loss in the pipe increases as the sediment concentration increases.

The sediment discharge process in Case 1–1 described above is basically similar to the other cases. The experimental results for all cases are summarized in Table 2. The larger the flow rate and the smaller the sediment particle diameter, the larger the maximum sediment concentration becomes. It was difficult to determine the explicit influence of the discharge rate and sediment particle size on the sediment concentration during stable conditions.

Before conducting the model tests, we estimated the total removed sediment volume with the void part at about 0.52 m³ (depth of conical shape: 0.55 m, repose angle of sediment in

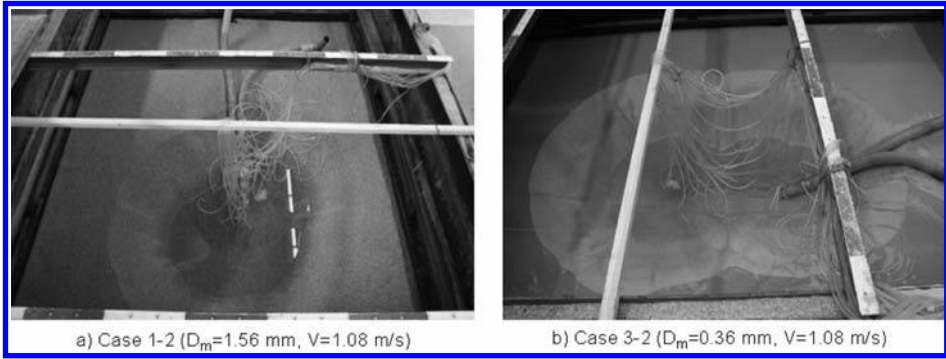


Figure 7. Shape of sedimentation after sediment discharge in small scale model tests.

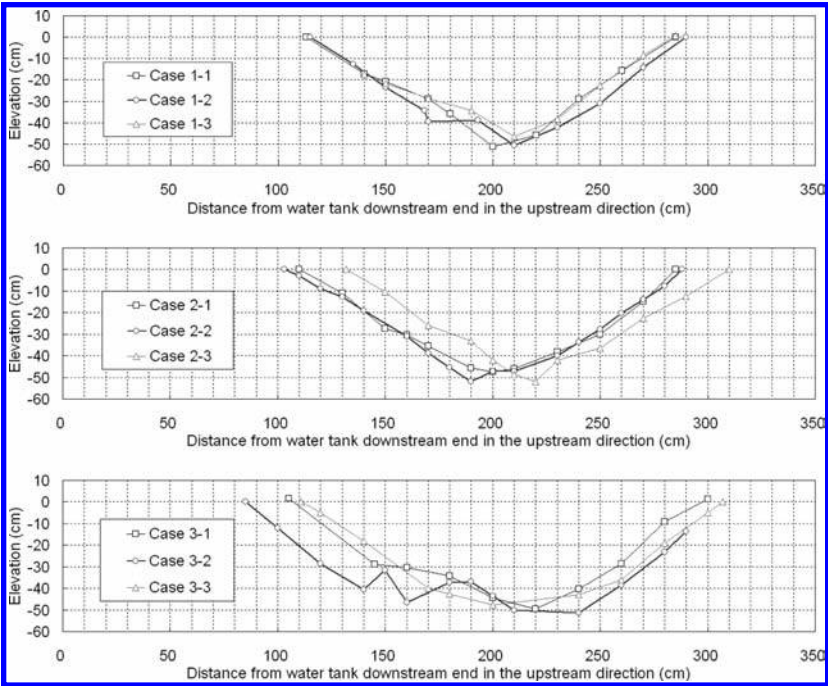


Figure 8. Longitudinal form of sedimentation after sediment discharge in small scale model tests.

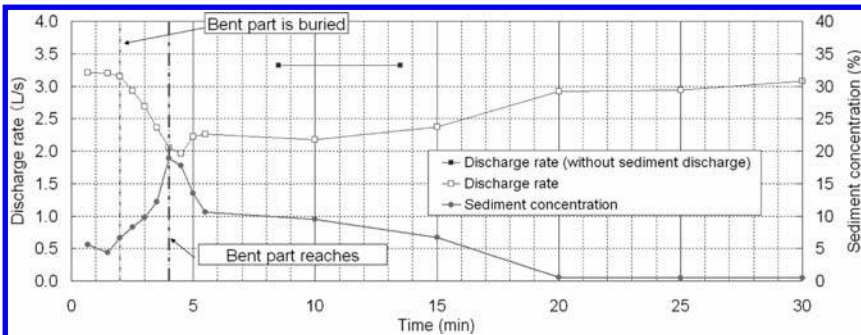


Figure 9. Time series of discharge rate and sediment concentration in Case 1-1.

water: 30°, radius of conical shape: 0.95 m). As shown in Table 2, the experimental results for the total removed sediment volume are close in value to the estimation. It was confirmed that the sediment removal suction pipe can supply sediment at almost the expected performance in the small scale model tests.

4.2 Experimental results for medium scale model test

The shape and section form of sedimentation after sediment discharge in the medium scale model test are shown in Figure 10. As in the small scale model tests, a conical shape was made in the medium scale model test. The total removed sediment volume with the void part was about 7.1 m³. We expected the depth of the conical shape to be 1.9 m, but the actual depth was about 1.3 m. Even though there was still a layer of sediment about 0.6 m thick on the bent part of pipe, the sediment removal suction pipe could not suck the sediment.

The time series for discharge rate and sediment concentration is illustrated in Figure 11. The maximum sediment concentration was 9.3% and occurred at 43 min after the start of the test at the 25% gate opening. The bent part of the pipe reached the bottom of the water tank at 105 min, after which the sediment concentration became smaller.

Before 330 min, trouble with air accumulation in the pipe occurred several times. Precautions will have to be taken in the actual facility. The sediment concentration became very small at 330 min. We considered that the reason for this was suction hole blockage by debris or space around the hole by arch action of sediment. However, we could not confirm the

Table 2. Experimental results for small scale model tests.

Case	Bent part was buried Time (min)	Bent part reached bottom Time (min)	Total removed sediment (with void part) (m ³)	Maximum sediment concentration (%)	Sediment concentration during stable situation (%)
1-1	2.0	4.0	0.49	18.9	8.9
1-2	3.0	6.5	0.52	11.4	5.4
1-3	—	6.0*	0.47	9.7	3.0
2-1	1.5	2.5	0.50	23.3	4.5
2-2	1.5	3.5	0.57	22.2	3.7
2-3	4.5	10.0	0.43	13.5	5.1
3-1	4.5	6.0	0.53	32.4	5.3
3-2	3.5	5.0	0.73	26.2	5.5
3-3	11.0	15.0	0.48	13.2	4.6

*The time was measured from when the bent part was buried.

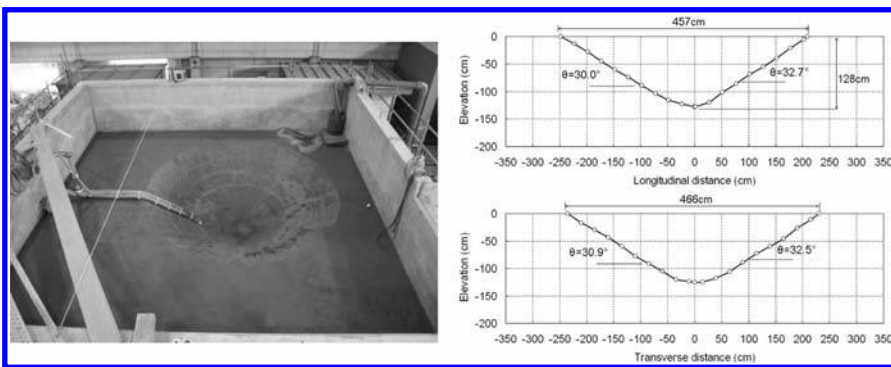


Figure 10. Shape and section form of sedimentation after sediment discharge in medium scale model test.

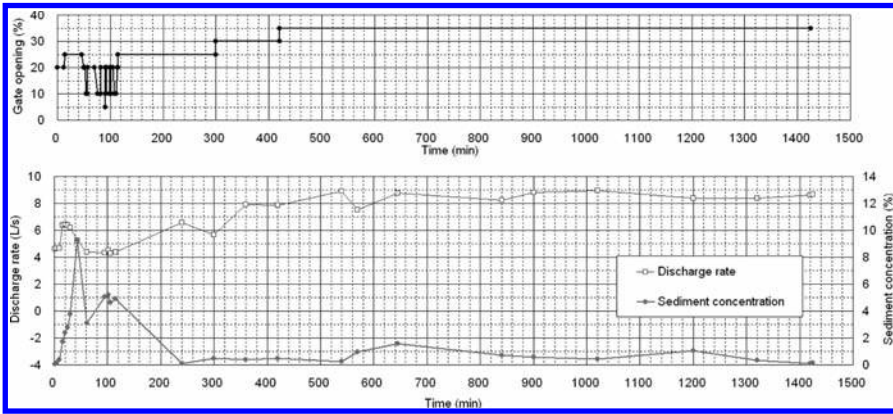


Figure 11. Time series of discharge rate and sediment concentration in medium scale model test.

reason. We tried applying vibration to the pipe after which the sediment discharge restarted and continued for a while. We repeated this process, but finally the sediment discharge could not be restarted by vibration at 1425 min. We identified new challenge from the results of the medium scale model test.

5 CONCLUSIONS

1. We proposed the “burrowing-type sediment removal suction pipe method” for sediment supply from reservoirs and carried out small scale experimental model tests on the pipe (pipe diameter: 60 mm, sediment thickness: 0.6 m). As a result, we confirmed that the suction pipe can supply sediment at almost the expected performance and we established the process of sediment supply and the influence of discharge rate and sediment particle size on sediment supply characteristics in the small scale model tests.
2. We carried out a medium scale experimental model test (pipe diameter: 100 mm, sediment thickness: 2.0 m) to examine the sediment discharge characteristics of the sediment removal suction pipe under conditions closer to those of actual facilities. As a result, the suction pipe could supply sediment until the bent part of the pipe reached the bottom, but after that it was difficult to continue stable sediment supply. We identified a new challenge from the results of the medium scale model test.

REFERENCES

- Enomura, Y. 2005. Sediment management measures at the Miwa dam, *International Symposium on Sediment Management and Dams Proceedings of the 2nd EADC Symposium, Tokyo*, pp. 67–72.
- Kanazawa, H. 2005. Comprehensive sediment management in the Kurobe river, *International Symposium on Sediment Management and Dams Proceedings of the 2nd EADC Symposium, Tokyo*, pp. 35–46.
- Kataoka, K. & Tada, T. 2005. Reservoir sedimentation management at the Asahi dam, *International Symposium on Sediment Management and Dams Proceedings of the 2nd EADC Symposium, Tokyo*, pp. 145–152.
- Sakurai, T., Hakoishi, N., Kashiwai, J., Izumiya, T. & Kubo, Y. 2007. Development of sediment measures from reservoir for restoration of riverbed environment—sheet and suction pipe sediment discharge facility, *International Symposium on Modern Technology of Dams Proceedings of the 3rd EADC Symposium, Chengdu*.
- Sakurai, T., Kashiwai, J. & Kubo, Y. 2006. Sediment discharge facility using sheet and pipe, *Civil Engineering Journal*, Vol. 48, No. 12, pp. 30–35 (in Japanese).

Upper Missouri River mainstream reservoirs: Sedimentation and sustainability issues

M.J. Teal

WEST Consultants, Inc., San Diego, California, USA

ABSTRACT: General sedimentation issues of the Upper Missouri River reservoirs are examined, with special attention given to two of the reservoirs that have been studied by the author over the last decade: Lake Sharpe (impounded by Big Bend Dam) and Lewis and Clark Lake (impounded by Gavins Point Dam). Delta build-up has and continues to cause problems in both of these areas. Sediment yield (inflows) to the lakes, including major tributary contributions, was estimated via different methods and numerical sediment transport modeling was performed in which the models were calibrated based on the historical cross section data. Estimates were made of progression of the deltas into the lakes, and future effects on water surface profiles and groundwater elevations around and upstream of the reservoirs.

1 INTRODUCTION

1.1 *Background*

The Missouri River is one of the world's longest rivers at 3770 km and as the largest tributary of the Mississippi River by area drains 1,400,000 square km of central North America including portions of 9 U.S. states and 2 Canadian provinces (Fig. 1). The river's mainstream system of dams is composed of six large earth embankments, which impound a series of lakes that extend for 2023 km from Gavins Point Dam near Yankton, South Dakota to the headwaters of Ft. Peck Lake north of Lewiston, Montana. The dams were constructed by the U.S. Army Corps of Engineers on the mainstream of the Missouri River for flood control, navigation, irrigation, power, water supply, water quality control, recreation and wildlife enhancement between 1937 and 1963. At the top of their carryover and multiple use pools, the lakes behind these six dams provide nearly 4000 km² of water surface and extend a total length of 1200 km. The reservoirs contain an aggregate storage space of 90.8×10^9 m³, more than three times the average annual flow of the Missouri River at Sioux City, Iowa. Approximately 10 million people live within the Missouri River watershed, mostly concentrated in urban centers.

1.2 *Impacts of dams related to sediment issues*

All of the mainstream dams effectively trap inflowing sediment from upstream sources. This trapping leads to the common results of delta building at the upstream end of reservoirs and erosion in the reaches immediately downstream of the dams. The former impact leads to increases in flood frequency and groundwater levels in upstream areas, while the latter leads to bed lowering and/or widening in downstream reaches. The remainder of this paper will examine specific studies related to sedimentation issues in which the author has participated.



Figure 1. Missouri River Basin location map (courtesy U.S. Army Corps of Engineers).

2 CHANNEL WIDENING AND BANK STABILIZATION

The dams and reservoirs on the upper Missouri River have caused a lowering of the streambed in the open reaches downstream from the dams. They have also caused continuing bank erosion, modification of the annual cycle of erosion and accretion, and widening of the channel in some locations. The U.S. Congress created the Section 33 program with the expressed purpose of allowing the U.S. Army Corps of Engineers (USACE) to assist affected landowners in alleviating these effects through a variety of measures. These measures include maintaining or rehabilitating existing bank stabilization structures, constructing new bank stabilization structures, purchasing affected property and monetary compensation.

USACE prepared a Programmatic Environmental Impact Statement (PEIS) to evaluate the potential degree or level of implementation of alternative measures to alleviate the identified problems, and their expected impacts, including cumulative environmental impacts. Since this was a programmatic PEIS, the study used a “broad-brush” approach including expert opinion and making general observations about the problems, alternatives, and impacts.

The purpose of the overall hydraulic and sedimentation portion of the PEIS was to estimate potential changes over time to the quantity and density of habitat features in several reaches of the upper Missouri River due to Section 33 program bank stabilization. Specifically, the purpose of the study was to document changes in habitat features, and erosion or deposition that occurred in the open channel reaches downstream of Ft. Peck, Garrison, Ft. Randall, and Gavin Point Dams. For purposes of the study, habitat features included sandbars, islands, chutes, backwaters, and attached sandbars. Because there is almost no bank stabilization in the in the Fort Peck reach (Biedenharn et al. 2001), study results from this reach were considered as a baseline for naturally occurring changes over the time period under consideration. Results from the other reaches, where revetment is present, were compared to those from the Ft. Peck reach to estimate changes in habitat features and erosion/deposition induced by bank stabilization.

The hydraulic and sedimentation portion of the PEIS addressed, based on existing information, the causes and effects of sedimentation along the river. This included the increase in sediment at the upper ends of the reservoirs. The role of bank stabilization related to sedimentation was identified and evaluated separately to the extent possible. This study attempted

to develop statistical relationships for the rates of erosion and reservoir sedimentation. The PEIS did not include analysis or discussion on the operation of the Missouri River dams and their effects on streambank erosion. The period of study was from the mid 1950's to 2000 for the Ft. Peck reach and from the mid 1970's to 2000 for the three downstream reaches.

3 LEWIS AND CLARK LAKE PREDICTIONS

3.1 *Background*

This study (WEST 1998) was part of the Omaha District's continuing operations and maintenance activities associated with the Missouri River mainstem dams and in particular with the operations of Fort Randall and Gavins Point Dams. Sedimentation at the mouth of the Niobrara River and downstream in Lewis and Clark Lake had increased the water surface elevations in both the Missouri River and tributaries from approximately Greenwood, South Dakota to Lewis and Clark Lake. This increase impacted farm/ranch land, residential property, recreational facilities, and infrastructure. The objective of this project was to document past aggradation and predict future aggraded conditions. This information was used to determine impacted areas where real estate acquisition might be required, was provided to state and county road/highway departments for design and scheduling of repairs and realignments, and was provided to environmental and natural resource specialists for habitat evaluation and recreational development.

3.2 *Hydraulic modeling*

The hydraulic analyses for the Missouri River were conducted in two phases. The first phase involved preparing the geometric data (cross sections), preparing hydraulic models with the geometric data, and calibrating the models to existing gage records. The second phase, after the sedimentation modeling had been completed, involved generating water surface profiles for certain frequency flows. HEC-2, a USACE steady-state one-dimensional hydraulic model was used for these analyses.

3.3 *Sediment transport modeling*

The calibrated hydraulic (HEC-2) models were converted to sediment transport (HEC-6, a one-dimensional movable boundary, open channel flow model designed to simulate stream bed profile changes over fairly long time periods) models. The 1955 model, hereafter called the "base conditions" model, was prepared and executed using the hydrologic record at the dams for the period 1955–1995. The average bed elevation for each cross section at each of the calibration years was compared to the average bed elevation of the measured cross section for the same year. Adjustments were made to the base conditions model such that the computed average bed elevations would approach the measured ones. Once the base conditions model was calibrated, it was executed to predict future conditions.

3.3.1 *Development of geometry and hydraulics*

Channel geometry and hydraulics were obtained from the HEC-2 models. However, because the base conditions model would be executed for a simulation period of ninety years (1955–1995 for calibration, 1995–2045 for future conditions) certain changes were made to the cross section geometry. The principal change made was adding overbank and upland areas to cross sections that, when surveyed in 1955, only included the main channel area. Deposition over time in the Missouri has caused water surface elevations to rise. In many cases this caused the computed water surface elevations to be higher than the highest surveyed ground point. To overcome the deficiency in the 1955 cross sections, points were added for the overbank and/or upland areas in one of two ways. The first, and most preferable, was to add points from the same cross section surveyed in a different year where the

overbank areas were included in the survey. The second manner of obtaining more points was to see where contours on a 7.5 minute topographic map crossed the cross section drawn on the map.

3.3.2 *Sediment parameters*

One major and one minor sediment inflow source enter the study reach of the Missouri River. The Niobrara River delivers most of the inflowing sediment to the study reach. Some sediment will also enter the reach from Fort Randall Dam at the upstream limit although the amount was expected to be minor. Sediment inflow from other tributaries and bank retreat was ignored.

Initial inflowing sediment amounts both from the Niobrara River and through Ft. Randall Dam were taken from sediment rating curves presented in the Niobrara Sedimentation Impacts Study (RCE 1993). Some modifications were made to these curves during the calibration phase.

Sediment gradations for flows entering the study reach at Fort Randall Dam were set to 97–99 percent very fine sand and 1–3 percent fine sand based on estimates of suspended sediment in Lake Francis Case just upstream of the dam. Inflowing sediment gradations for the Niobrara River were computed as follows. An HEC-6 model was created for the first three ranges of the Niobrara River. The original RCE (1993) inflowing load curve was used and gradations were assumed for a given flow. Using the Toffaleti (Vanoni 1975) transport method, the model was executed using steady flow and the outflowing sediment gradation noted. This was then entered as the new inflowing gradation and the program executed again. This procedure was repeated a few times for each selected flow until the inflowing and outflowing gradations appeared to converge. The resulting gradations were then used in the Missouri River HEC-6 models.

Bed material sampling data was provided by USACE and gradations applied to appropriate cross sections within the model.

3.3.3 *Hydrology*

Flow hydrographs are simulated in HEC-6 by a series of steady flow analyses. Mean daily flows at both Fort Randall and Gavins Point Dams, and mean daily water surface elevation at Gavins Point Dam were provided by USACE for the calibration period 1955–1995. Mean daily flows for the Niobrara River near Verdel were obtained from published U.S. Geological Survey (USGS) records.

3.3.4 *Calibration and verification*

After the base conditions model and the calibration year models were assembled and the hydraulics checked, the process of calibration began. This process involved adjustments to the base conditions model such that the resulting computed average bed elevations and sediment volumes would approximate measured values. The period 1955–1975 was used for calibration of model parameters, while the period 1975–1995 was used for verification. Important calibration parameters included movable bed limits and ineffective flow areas. Roughness values were typically not adjusted as these had already been calibrated to observed water surface elevations.

3.4 *Future predictions*

Once the base conditions sediment model was calibrated, the work of predicting future conditions could begin. Hydrology was developed for future conditions (described below), and the model was executed to yield results for 10, 20, 30, 40 and 50 years into the future (past the last calibration year of 1995, i.e., to 2005, 2015, 2025, 2035, and 2045).

Because of uncertainty in future weather conditions and associated releases from the dams along the Missouri River, hydrologic records were developed for three future conditions: “normal flow,” basically a repetition of the past 50-year record; “high flow,” where the twenty-year period with the highest average daily flow was repeated two and one half times to make fifty years of record; and “low flow,” where the twenty-year period with the lowest average daily flow was repeated two and one half times to make fifty years of record.

Computed channel geometry 10, 20, 30, 40, and 50 years into the future, obtained with the HEC-6 calibrated model, was imported into HEC-RAS to develop water surface profiles. For each of these projection years, profiles were developed for the 10-, 25-, 50-, and 100-year flow events. Results showed that water surface elevations for the areas affected by active delta building in Lewis and Clark Lake would increase by about 0.3 m over fifty years for all flow events. Water surface elevations in the middle area of the study reach, from Springfield to Greenwood were expected to increase by 0.3 to 1 m over the following fifty years for all flow events. The largest increases were expected to occur in the area extending several kilometers upstream and downstream from the Niobrara River confluence.

4 BIG BEND RESERVOIR PREDICTIONS

4.1 *Background*

Closure of Big Bend Dam in 1963 resulted in changes in the river and the formation of a delta in the headwaters of Lake Sharpe. The rising bed profile has, in turn, raised water surface elevations near the cities of Pierre and Fort Pierre, South Dakota. This problem is exacerbated by ice cover during the winter season. Aggradation in Lake Sharpe is of particular concern because it has the potential to constrain power generation at Oahe Dam during critically cold periods. USACE commissioned this study (WEST 1999) to predict future bed and flood levels. Predicted floodplain areas were used to in consideration of buy-outs of existing properties.

The Missouri River drains approximately 630,600 square kilometers above Big Bend Dam. The study reach extended upstream along the Missouri River to Oahe Dam near Pierre, South Dakota. At Big Bend Dam normal operating pool level Lake Sharpe is approximately 130 km long and has 320 km of shoreline.

The principal tributary flowing into Lake Sharpe is the Bad River, whose confluence with the Missouri River is at Ft. Pierre, South Dakota, approximately 10 km downstream of Oahe Dam. The Bad River, draining approximately 8000 square kilometers, is also the major source of sediment inflows to Big Bend Reservoir.

4.2 *Hydraulic modeling*

Hydraulic models provided the basis for later sediment transport calculations. These models (HEC-2 and HEC-RAS) were constructed to reflect the best available cross-section ground points, the location of channel banks, areas of ineffective flow, and the hydraulic roughness of the channel. Three hydraulic models were prepared to simulate conditions in 1968, 1983, and 1997. The 1968 model was created to use as the “base conditions” model. The sediment model developed from this hydraulic model would be calibrated and later used to predict future conditions. The 1983 and 1997 models would be used in the calibration/verification process.

Manning roughness coefficients from the District’s 1983 model were deemed applicable to the 1968 model as well. Bank stations and ineffective flow areas were determined based on the 1983 and 1997 models, topographic maps (most developed in 1973), and engineering judgment.

WEST prepared 1983 and 1997 condition hydraulic models based upon models provided by USACE. Corrections and modifications made to these models principally dealt with reach lengths, cross section orientation, bank stations, and ineffective flow areas.

4.3 *Sediment transport modeling*

The calibrated hydraulic (HEC-2) models were converted to HEC-6T sediment transport models (Thomas 1999). The 1968 model (the base conditions model) was prepared and executed using the hydrology for the periods 1968–1983 and 1983–1997. Adjustments were

made to the base conditions model such that the computed average bed elevations would reasonably approximate the measured ones. Once the base conditions model was calibrated, it could be executed to predict future conditions.

4.3.1 *Sediment parameters*

One major and several minor sediment inflow sources enter the study reach of the Missouri River. The Bad River delivers most of the inflowing sediment to the study reach. Some sediment will also enter the reach from local tributaries. An accurate model required (a) an estimate of the amount of sediment entering the reach at each defined inflow point for different tributary discharges (i.e. a sediment rating curve); and (b) the sediment gradation of the inflows for each discharge on the sediment rating curve.

A sediment budget was first prepared to help determine the amounts of sediment entering the system at various inflow points. It was assumed that no sediment enters from Oahe Dam upstream or passes through Big Bend Dam downstream. Hence, the components of the sediment inflow are the Bad River, other smaller tributaries, and bank erosion. The sediment inflow should approximately equal the measured deposition in the reservoir; in this case the rate differed by about 8 percent.

4.3.2 *Bad River inflowing sediment loads*

The USGS has collected suspended sediment samples from the Bad River near Fort Pierre since about 1950. WEST obtained measured values for water years 1972 through 1996 and plotted these values using log-log scales. A two-segment line graphically fit through the cloud of measured values provided the best approximation of the suspended sediment rating. The break between the two line segments was at 8.5 cu. m\^s, approximately bankfull discharge for the lower Bad River.

In order to compute the total inflowing sediment load, the bedload must be added to the suspended load. Bedload can be calculated using sediment transport equations. However, these equations are usually most applicable to streams with predominantly coarse particles (sands and gravels). Because particles in the Bad River are generally fine, bed material load equations are more applicable. Therefore, it was decided that the total load would be computed by adding the bed material load (computed using transport equations) and the wash load (computed as a percentage of the measured load).

The measured suspended load contains both wash load (particles finer than 0.062 mm) and bed material load. Based on the percentage of grain sizes in the measured suspended load finer than 0.062 mm, as reported by the USGS, an average value of 98% of the measured suspended load was considered wash load (measured values ranged from 94% to 100%). The other 2% would therefore correspond to bed material load.

Bed material load transport equations generally need particle information and hydraulic variables as input parameters. The sediment information is usually a representative grain size or sizes while the hydraulic variables can include velocity, shear stress, depth and width. Hydraulic variables were computed for the Bad River for a series of discharges by constructing an HEC-RAS hydraulic model using cross section (range) geometry provided by the District. However, no sediment sample information could be located for the Bad River to estimate a median grain size to use with most of the equations under consideration. Therefore, a unique approach was taken to estimate the inflowing bed material load.

First, unmeasured bed sediment load was estimated using measured suspended load values using Colby's Method (Vanoni 1975). Once the unmeasured bed material load was estimated, it was added to the fraction of the measured load assumed to consist of bed material (2% of total load, as mentioned above). In this manner, a bed material sediment rating curve was developed for a series of discharges. It is important to note that no grain size information was needed to develop the rating curve.

Second, transport equations considered applicable to fine-grained, small streams like the Bad River were employed using the hydraulics previously calculated and assumed grain sizes. Bed material rating curves were developed for these relations.

Third, various total load curves (bed material amount from the previous step plus 98% of the measured suspended load) were integrated with mean daily flow records for the Bad River. This produced an estimate of sediment discharge by water discharge increment and total annual sediment yield.

Fourth, the various transport relation results were compared to the Colby results for different grain sizes. The relation giving best results for the water discharge range where over 70% of the annual sediment transport occurs was the Yang (1984) sand and gravel method using $D_{50} = 0.5$ mm.

Fifth, a sediment gradation from the Missouri River at the confluence of the Bad River was adopted as representative of the Bad River bed gradation. The median grain size of this gradation is 0.463 mm, close to the 0.5 mm used with the Yang sand and gravel transport formula. Sediment transport by size class was then determined based on this gradation and the previously computed hydraulics. For consistency, the total load rating curve computed using the Yang sand and gravel formula was used for the input to HEC-6T (as previously stated, the results were very close to those from the Colby method).

4.3.3 *Bad River inflowing sediment gradation*

Gradations of inflowing bed material sediment discharge from the Bad River for several discharges were obtained using the Yang sand and gravel transport equation by size class as previously described. To estimate size fractions of the cohesive particles, USGS water quality data collected between 1972 and 1987 were used. Gradations showed no significant change or pattern at different river discharges. Therefore, 37 gradations were averaged to obtain a single clay and silt sediment gradation curve for all discharges. This information, when combined with the bed material gradations described above, produced total fractions.

The sum of sediment inflow from tributaries other than the Bad River and contributions from bank erosion was estimated at 1.6×10^6 t/year. This additional amount was distributed among the tributaries in the HEC-6T model based on plots of cumulative volume of deposition in the reservoir. These amounts should not be misconstrued as actual sediment loading from these streams, but rather understood as a synthetic device used to model distributed sediment flows (non-point sources) into the reservoir.

4.4 *Future predictions*

Once the base conditions sediment model was calibrated, the work of predicting future conditions could begin. Hydrology was developed for future conditions, and the model was executed to yield results for 10, 20, 30, 40 and 50 years into the future (past the last calibration year of 1997, i.e., to 2007, 2017, 2027, 2037, and 2047). The only change made to the calibrated base model was replacement of the historic hydrology with future hydrology. Average bed elevations were computed for the future conditions, and the resulting geometry at each of the five projection years was converted to an HEC-2 file to compute water surface elevations. Typical results are presented in [Figure 2](#). A sensitivity analysis of the results to inflowing sediment load and transport method was also performed although not presented herein.

4.5 *Additional scenarios*

As a continuation of the previous work, WEST analyzed methods to increase sediment flushing, i.e. to move deposited sediments deeper into the reservoir (WEST 2000). The calibrated and verified HEC-6T model was modified to assess the consequences of lowering pool elevations in Lake Sharpe. In addition, the existing model was modified to simulate what effect the installation of a series of dikes would have on delta formation in the headwaters of the lake.

4.5.1 *Model modification*

The HEC-6T model of the Missouri River from Oahe Dam to Big Bend Dam was modified to reflect three alternative lower pool elevations on Lake Sharpe, approximately 1, 2, and 3 m lower than current normal pool levels. For the calibration period 1968 through 1997, the pool

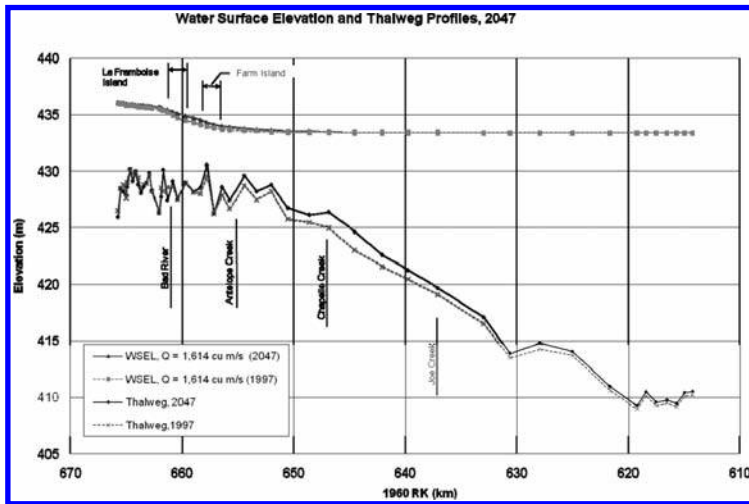


Figure 2. Beginning and projected future water surface and thalweg profile plots.

elevations were identical to the previous model, with the reservoir pool varying according to historical data from Big Bend Dam. Starting in the 1998 water year, the water surface on Lake Sharpe at Big Bend Dam was fixed at each of the three specified pool elevations through the end of the simulation (the year 2047).

Additional simulations were made with spur dikes added to the model near the delta formation zone at the headwaters of the reservoir. Dikes were assumed to be spaced at a distance equivalent to twice the dike length. This spacing is based upon literature review and previous experience.

4.5.2 Conclusions

This analysis showed that lowering pool elevations would more effective than installing spur dikes in the headwaters of the reservoir. Lowering the pool elevation on the reservoir should significantly reduce the magnitude of the predicted increase in water surface elevations on the Missouri River over the simulation period. Spur dikes had a very localized effect, and increased the predicted increases in upstream water surface elevations.

REFERENCES

- Biedenbarn, D.S., Soileau, R.S., Hubbard, L.C., Hoffman, P.H., Thorne, C.R., Bromley, C.C., & Watson, C.R. 2001. *Missouri River—Fort Peck Dam to Ponca State Park Geomorphological Assessment Related to Bank Stabilization*. U.S. Army Engineer Research and Development Center, Coastal and Hydraulics Laboratory, Vicksburg, MS.
- Resource Consultants and Engineers, Inc. 1993. *Niobrara River Sedimentation Impacts Study, Phase II*, prepared for USACE, Omaha District, Omaha, NE.
- Thomas, William A. March 1999. *HEC-6T, Sedimentation in Stream Networks, User's Manual*, Mobile Boundary Hydraulics, Clinton, MS.
- Vanoni, V.A (ed.). 1975. *Sedimentation Engineering*. ASCE Manual of Practice Number 54, American Society of Civil Engineers, New York, NY.
- WEST Consultants, Inc. June 1998. *Missouri River Fort Randall Dam to Gavins Point Dam and Ponca Creek Aggradation Assessment*. Prepared for the USACE Omaha District.
- WEST Consultants, Inc. September 1999. *Missouri River Oahe Dam to Big Bend Dam Aggradation Assessment*. Prepared for the USACE Omaha District.
- WEST Consultants, Inc. January 2000. *Missouri River Oahe Dam to Big Bend Dam Aggradation Assessment—Analysis of Lower Lake Sharpe Pools*. Prepared for the USACE Omaha District.
- Yang, C.T. 1984. Unit Stream Power for Gravel. *Journal of Hydraulic Engineering*, 110(12):1783–1797.

Flood retention in alpine catchments equipped with complex hydropower schemes—a case study of the upper Aare catchment in Switzerland

M. Bieri & A.J. Schleiss

Ecole Polytechnique Fédérale de Lausanne (EPFL), Laboratory of Hydraulic Constructions (LCH), Lausanne, Switzerland

F. Jordan

e-dric.ch Ingénieurs Conseils, Epalinges, Switzerland

A.U. Fankhauser & M.H. Ursin

Kraftwerke Oberhasli AG (KWO), Innertkirchen, Switzerland

ABSTRACT: The simulation of run-off in alpine catchment areas is an important issue for the optimal operation of hydropower plants for normal flow conditions, but also during flood events. A semi-lumped numerical approach combines hydrological modelling and operation of hydraulic elements. It allows simulation of operating mode of complex storage hydropower plants and its impacts on the downstream river system for different scenarios. The modelling of the upper Aare catchment with the Oberhasli hydropower scheme in Switzerland is presented. The effect of the existing reservoirs and their management, taking into account preventive turbinning, on flood routing in the Aare River upstream of Lake Brienz is presented for the 2005 and 1987 flood events. The enhancement project KWOplus, which contains a considerable increase of storage volume in the main reservoir as well as in turbinning capacity, is estimated.

1 INTRODUCTION

During the flood event of August 2005, the Aare River upstream Lake Brienz in Switzerland inundated the whole valley between Meiringen and Brienzwiler. The peak flow of 444 m³/s is the highest ever measured discharge in Brienzwiler, corresponding statistically to a return period of about 100 years. About half of the river catchment is used for hydropower generation. In order to evaluate the influence of the plant on flood retention, a flow prediction model was developed for the complex Oberhasli hydropower scheme.

For run-off estimations in catchment areas, production and routing of flow are calculated by numerical models. The semi-distributed conceptual code *Routing System* (Dubois 2005) is appropriate for hydrological forecast in high mountainous catchment areas. It is based on a conceptual glacio-hydrological model (Schaeffli et al. 2005). Tri-dimensional rainfall, temperature and evapotranspiration distributions are used for simulating the hydrological processes. The model is able to simulate glacier melt, snow pack constitution and melt, soil infiltration and run-off. The advantage of this object-oriented modelling tool is the integration of flood routing in rivers as well as hydraulic structures such as water intakes, water transfer tunnels, reservoirs with water releasing structures as well as powerhouses. It was successfully applied for several alpine catchments in Switzerland, for example in the Wallis Canton (Jordan 2007).

First the hydrographs of the 1987 and 2005 flood events were accurately simulated. The calibrated and verified model was then used to study the influence of the initial water level

in the main reservoirs on the outflow of the catchment area for the flood of 2005 (Bieri et al. 2010). The contribution of the hydraulic scheme to flood routing was analysed through simulations without reservoirs and power plants. For the 2005 flood event, the peak flow without reservoirs was reduced by about 20%. Therefore the retention effect of the Oberhasli hydropower scheme is confirmed.

Storage hydropower plants have an important effect on flood routing. The potential of active flood management of the Oberhasli scheme is highlighted and discussed for several scenarios, taking into account different flow prediction times, water levels in the four main lakes as well as the enhancement project KWOpplus.

2 THE UPPER AARE RIVER BASIN

2.1 Upper Aare River basin

The upper Aare River, also called Hasliaare, springs in the glaciers of Unteraar and Oberaar at the altitude of 2000 m a.s.l. and flows nowadays through several artificial reservoirs (Oberaar, Grimsel, Räterichsboden), in which the main part of the water is temporarily retained to be turbined in the power plants of Grimsel, Handeck and Innertkirchen. In Innertkirchen the water is given back to the Aare River immediately downstream the confluence with the Gadmerwasser, the river draining the eastern part of the catchment area. After the Aare Gorge the Aare River reaches the main valley of Meiringen and enters Lake Brienz at Brienzwiler. The surface of the upper Aare River basin is 554 km², where 21% was glaciated in 2003. The hydrologic regime of the river is therefore glacial. The average annual discharge is 35 m³/s.

2.2 Today's hydropower scheme

At the end of the 19th century, the area of the Grimsel and Sustenpass was recognized as particularly appropriate for hydropower production. Heavy rainfalls, large retention areas, solid granitic underground as well as substantial slopes provide optimal conditions for a hydropower storage scheme. The first concrete dams were built by the Kraftwerke Oberhasli AG (KWO) between 1925 and 1932. Since then, a complex scheme with nine power plants and eight reservoirs has been constructed (Fig. 1a). The largest reservoirs are the lakes Oberaar (57 Mm³), Grimsel (94 Mm³), Gelmer (13 Mm³) and Räterichsboden (25 Mm³).

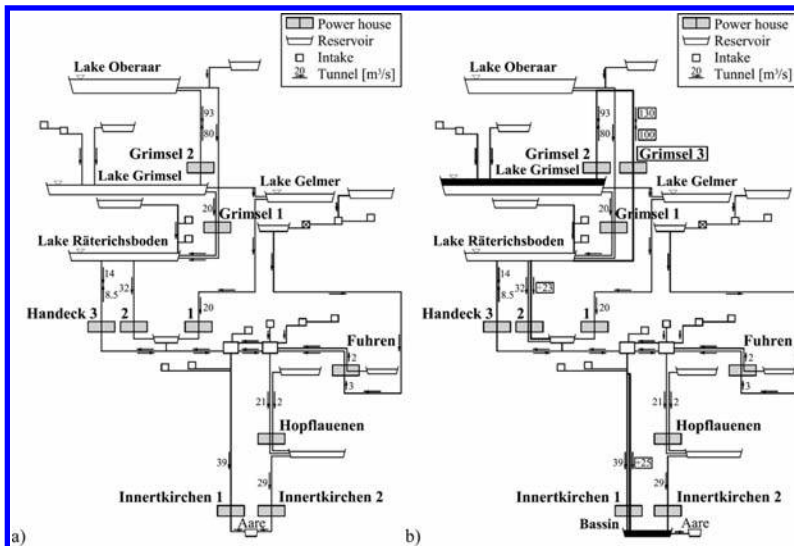


Figure 1. The complex Oberhasli hydropower scheme: a) Today; b) Upgraded scheme of KWOpplus.

2.3 Upgraded scheme KWOpplus

In the upgrading program KWOpplus, a large number of technical, economic and ecological improvements of the actual scheme is foreseen (Fig. 1b). An increase in storage capacity of Lake Grimsel up to 170 Mm³ is achieved by a heightening of the dam by 23 m. Power generation can be optimised through a better distribution of the water during the year. In parallel, the enhanced power plants Handeck 2 and Innertkirchen 1 will be able to turbine, respectively 23 m³/s and 25 m³/s more than today, which corresponds to a total power increase of 240 MW. The new 600 MW pump storage plant Grimsel 3, using the water from the two existing lakes Oberaar and Räterichsboden, has a turbinning capacity of 130 m³/s and pumping capacity of 100 m³/s. The enhancement project KWOpplus is planned for construction between 2013 and 2019.

3 MODELLING

3.1 Data sources

For the simulations several input datasets are needed. The meteorological data are available from the Federal Office of Meteorology and Climatology. On the one hand, temperature and rainfall data are collected every ten minutes by an automatic monitoring network (ANETZ) all over Switzerland. On the other hand, a large number of gauging stations (NIME) measure the daily rainfall. Five stations of the first type and nine of the second are used as input data points in and around the Hasliaare catchment (Fig. 4). The discharge is measured every ten minutes on the Aare River in Brienzwiler by the Federal Office of Environment (BAFU) (Fig. 2).

The KWO made available the hydraulic characteristics of the hydropower scheme, operation rules and historical data from the last 30 years of exploitation. The datasets allow calculation of the inflow of the ten sub-catchments operated by KWO (Fig. 2). Electricity prices are real spot market values from the European Energy Exchange (EEX).

3.2 Calibration and validation

The catchment area of the Aare River upstream Lake Brienz is modelled for the configuration of 2003. The 41 sub-catchments are divided in 96 glacial and 243 non glacial elevation bands. For each band, precipitation and temperature are interpolated from the 14 meteorological stations. The basic hydrological formulas as well as the calibration process are explained generically in García Hernández et al. (2007) and specifically in Bieri et al. (2010).

The model was pre-calibrated over a 12 month period for the ten sub-catchments exploited by KWO (Fig. 5a) as well as the natural catchment area upstream of the gauging station of BAFU. In a second step, the model was calibrated by the extreme flood event of August 2005 and validated for the flood of August 1987. The peak flow of the Aare River in 2005, reaching 444 m³/s (called measured discharge) is the highest value ever measured in Brienzwiler, corresponding

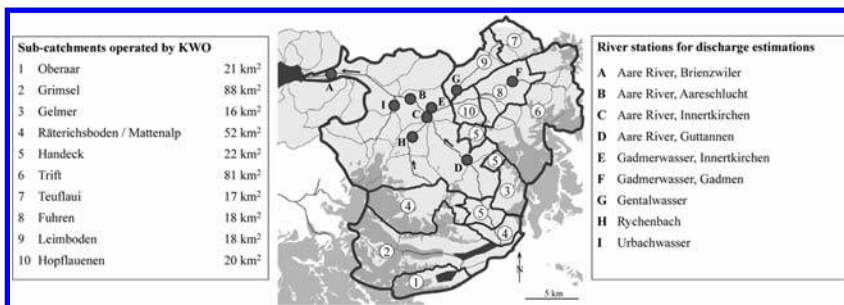


Figure 2. The upper Aare River basin with sub-catchments operated by KWO and river stations used for discharge estimations.

statistically to a return period of about 100 years (Fig. 3a). Because of lateral flooding, the entire discharge could not be measured at the gauging station. A post-analysis of the event, however, allowed an estimation of the real peak and a reconstruction of the hydrograph (called estimated discharge). Flooding is not simulated with *Routing System*. For this reason, the model was calibrated using the adapted hydrograph with a peak discharge of 520 m³/s (Fig. 2). The 1987 flood event produced only insignificant inundation. With minor adaptations of coefficients, the measured and simulated outflow in Brienzwiler are comparable (Fig. 3b).

The simulations were started at the beginning of the hydrological year in order to obtain parameters independent from the initial conditions. The results were compared to the inflow from the sub-catchments, to the observed outflow in Brienzwiler and to the peak flow estimations in terms of Nash coefficient, water volume ratio r_{vol} and peak flow ratio r_{peak} .

During calibration and verification of the model, rainfall patterns of all available meteorological stations were compared to generated discharges. As for the Hasliaare catchment, the most relevant Grimsel station was not operational in 1987, therefore the rainfall of Ulrichen is plotted instead (Fig. 3b). Both flood events show coherence between rainfall and discharge. Even if the simulated flood of 1987 generates too high values at an early stage.

3.3 Scenarios

A particularity of the two simulated floods is the quite different distribution of rainfall. During the flood event of 2005 (Fig. 4a), maximum rainfall was measured in the north-eastern part of the river basin, where only small reservoirs are situated. For the event of 1987, the gravity centre of the precipitations is in the east (Fig. 4b).

Preventive operation consists of lowering the reservoir levels by turbinng or water release by bottom outlets before the flood peak is achieved. By avoiding outflow from the reservoirs

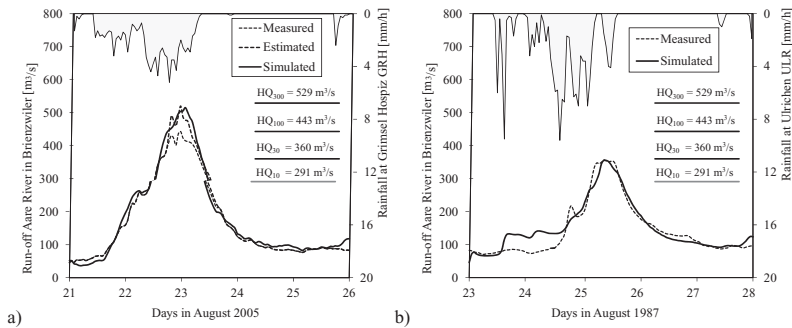


Figure 3. Modelling: a) Calibration with 2005 flood event (Nash = 0.98, r_{vol} = 1.03, r_{peak} = 0.99); b) Verification with 1987 flood event (Nash = 0.90, r_{vol} = 1.05, r_{peak} = 1.00).

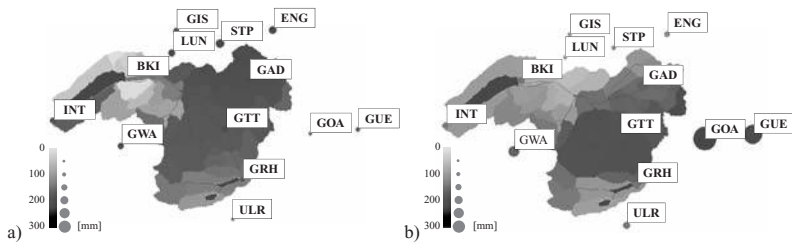


Figure 4. Accumulated rainfall: a) during 2005 flood event (between 21st and 26th of August 2005); b) during 1987 flood event (between 23rd and 28th of August 1987).

during maximal flow period, peak discharge in the downstream river can be reduced. At the end of a flood period, the reservoirs should ideally be filled. For defining the potential of flood retention of today's and the future hydropower scheme by preventive operation, several scenarios had to be tested. The following parameters have been analyzed:

- Two meteorological scenarios are chosen. The 2005 flood event corresponds by definition to a return period of about 100 years. To prove the reliability of the generated potential, a second 100 years event was simulated. To that end, the precipitation of 1987 was multiplied by an overall factor of 1.3, which generates also a flow of about 640 m³/s at Brienzwiler for the catchment area without hydropower plants.
- Three scenarios of filling degrees of the four main reservoirs Oberaar, Grimsel, Räterichsboden and Gelmer were defined, simulated and compared. Scenario 1 corresponds to the real levels of 2005 and 1987. Scenario 2 is a worst case scenario assuming full reservoirs on 18th of August 2005 and 23rd of August 1987. This quite hypothetical case is the upper limit of the sensitivity analysis. Scenario 3 presents average levels in August, calculated over the last 10 years, corresponding to the most likely filling degrees between 70 and 90%.
- Assuming, that flow can be adequately forecasted for a certain prediction time, preventive operation can be optimized. For the given cases, different combinations of prediction times of 24 or 48 hours for the turbine and bottom outlet operation are tested. For a prediction time X h for the turbines and Y h for the bottom outlets, the scenario is named Xh_TYh_B.

3.4 Simulations

The Oberhasli hydropower scheme comprises a large number of power houses and flood evacuation facilities. Table 1 shows the relevant elements and their admitted capacities for preventive operation. Water coming from the bottom of Lake Oberaar arrives in Lake Grimsel. The only outlet of this reservoir system is the basin of Handeck, where the water is either turbined by Innertkirchen 1 or released directly in the Aare River. The main goal is to retain the water in the reservoirs and to avoid turbining of Innertkirchen 1 during peak flow.

For an autonomous operation mode of the flow control elements (Tab. 1), an algorithm has been developed by *e-dric.ch* (Fig. 5). For a given prediction time Δt , the inflow to the reservoir, the volumes of the upper and lower lake, the flow at the critical point in the downstream river system and the electricity price at the time t' are compared to predefined threshold values. The algorithm considers the priority of the different variables defining the operation mode of each turbine and bottom outlet. The target level curve shows the annual filling cycle of the reservoir. Turbining should be achieved during peak price hours to generate maximum revenue.

Table 1. Turbine and bottom outlet capacities for preventive operation.

Power house	From	To	Today [m ³ /s]	KWOplus [m ³ /s]
Grimsel 1, Turbine 1	Oberaar	Räterichsboden	8	8
Grimsel 1, Turbine 2	Grimsel	Räterichsboden	20	20
Grimsel 2	Oberaar	Grimsel	93	93
Grimsel 3	Oberaar	Räterichsboden	–	130
Handeck 1	Gelmer	Handeck	18	18
Handeck 2	Räterichsboden	Handeck	32	55
Handeck 3	Räterichsboden	Handeck	14	14
Innertkirchen 1	Handeck	Aare River	39	64
Bottom outlet	From	To	Today [m ³ /s]	KWOplus [m ³ /s]
Oberaar	Oberaar	Grimsel	26	26
Grimsel	Grimsel	Räterichsboden	28	28
Räterichsboden	Räterichsboden	Handeck	35	35
Gelmer	Gelmer	Handeck	20	20

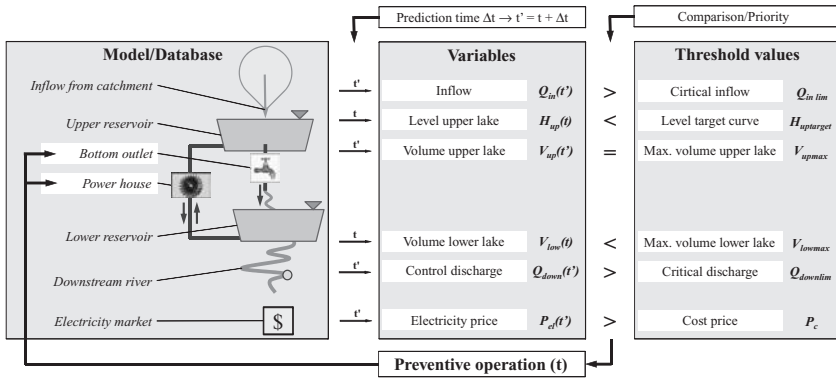


Figure 5. Flow chart of definition process for preventive operation.

4 RESULTS AND DISCUSSION

4.1 Results

Tables 2 and 3 show the peak flows and accumulated volumes in Brienzwiler for the two analysed flood events. The model allows the extraction of data for various river stations, turbines, spillways etc. In the following sections, the scenarios are compared for the Aare River at the Brienzwiler gauging station, where a high risk of flooding exists. The critical flood is assumed to be 400 m³/s.

4.2 Influence of initial reservoir level

The initial level in the main reservoirs is an important parameter, which influences directly the outflow of the system. Maximum reservoir levels without preventive operation produces 30% (Fig. 6a) to 17% (Fig. 6b) higher flows in the Aare River than the average August reservoir levels, which generate a discharge of 500 m³/s for both events, due to flood routing in the reservoirs. The accumulated volumes are also higher (Tab. 3), because of important flood release by the spillways, especially during increasing flows. Both downstream hydropower plants Innertkirchen 1 and 2 are operating on their maximum capacity.

4.3 Preventive operation

Preventive emptying of reservoirs leads to lower discharge in the Aare River. The peak flow of the 2005 flood could be reduced considerably from 605 m³/s, without preventive operation, to values between 535 m³/s for 24h_T0h_B and 500 m³/s for 48h_T48h_B (Tab. 2 and Fig. 7a). For the extended 1987 flood, the preventive turbinning scenarios are less efficient than the ones with bottom outlet operations (Tab. 2 and Fig. 7b). The reason is the lack of capacity of Innertkirchen 1, which does not allow the timely emptying of Lake Räterichsboden. The cumulated volumes are similar for all hydrographs (Tab. 3).

4.4 Potential of upgraded scheme KWOpplus

In spite of the 0h_T0h_B scenario for the extended 1987 flood, where results are not as pronounced, the upgraded scheme KWOpplus shows for all other scenarios with maximum initial reservoir levels much lower peak discharge than today's scheme, namely between 500 and 540 m³/s for 2005 (Fig. 8a) and 470 and 530 m³/s for 1987 (Fig. 8b). Considering scenarios 1 and 3, the maximum discharge for a flood with a return period of 100 years is 550 m³/s. The increased capacities of Handeck 2 and Innertkirchen 1 allow efficient water release in the pre-peak period, creating sufficient storage volume for avoiding turbinning during peak flow.

Table 2. Peak flow of Aare River in Brienzwiler of 2005 and extended 1987 flood event [m^3/s].

		Today's scheme					KWOpus				
		0h _T 0h _B	24h _T 0h _B	24h _T 24h _B	48h _T 0h _B	48h _T 48h _B	0h _T 0h _B	24h _T 0h _B	24h _T 24h _B	48h _T 0h _B	48h _T 48h _B
2005	1	501	507	507	502	502	539	544	508	530	509
	2	605	535	518	531	501	539	536	530	531	502
	3	513	501	501	507	507	539	535	508	530	509
1987	1	588	536	470	477	470	520	505	463	505	466
	2	620	608	506	608	473	593	529	475	519	466
	3	497	484	464	462	477	516	500	463	500	466

* Scenario 1: Observed level; Scenario 2: Maximum level; Scenario 3: Average level.

Table 3. Accumulated volume in Brienzwiler between 21st and 26th of August 2005 and 23rd and 28th of August 1987 [Mm^3].

		Today's scheme					KWOpus				
		0h _T 0h _B	24h _T 0h _B	24h _T 24h _B	48h _T 0h _B	48h _T 48h _B	0h _T 0h _B	24h _T 0h _B	24h _T 24h _B	48h _T 0h _B	48h _T 48h _B
2005	1	113	114	114	114	114	122	123	123	125	125
	2	150	153	154	152	156	146	148	150	150	155
	3	128	129	129	127	128	126	125	125	131	125
1987	1	83	83	84	81	87	72	72	72	72	74
	2	95	92	94	93	94	90	90	91	88	90
	3	73	74	74	76	75	71	72	72	72	74

* Scenario 1: Observed level; Scenario 2: Maximum level; Scenario 3: Average level.

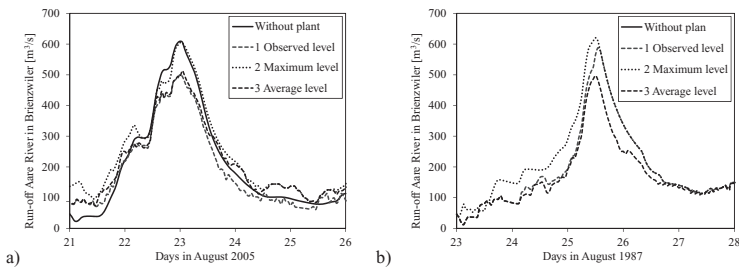


Figure 6. Hydrographs of 2005: (a) and extended 1987; (b) flood for different initial reservoir levels for today's scheme.

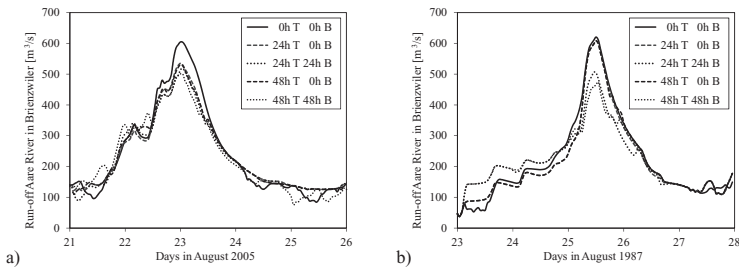


Figure 7. Hydrographs of 2005: (a) and extended 1987; (b) flood for different prediction times for preventive operation for maximum initial reservoir levels for today's scheme (T = turbine; B = bottom outlet).

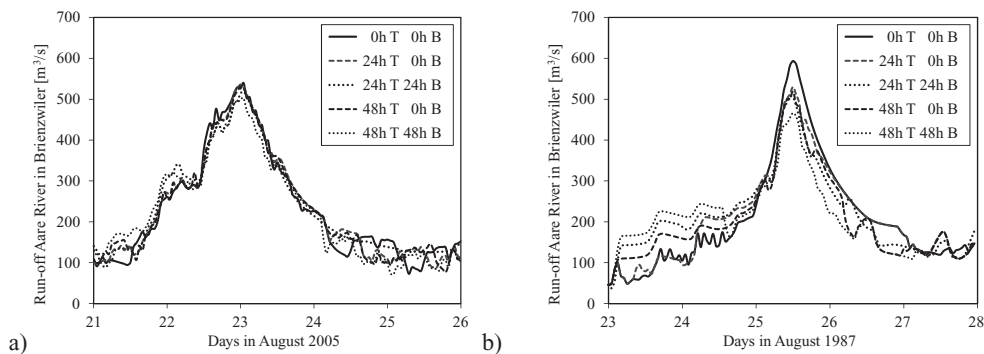


Figure 8. Hydrographs of 2005: (a) and extended 1987; (b) flood for different prediction times for preventive operation for maximum initial reservoir levels for KWOpplus (T = turbine; B = bottom outlet).

5 CONCLUSIONS

The presented model is robust and gives satisfying results for the observed flood events. The simulated hydrographs conform to the observed ones. By taking into account the influence of a hydropower scheme, different scenarios could be analysed. Constraints and initial conditions as well as input data can be adapted and their effects evaluated.

Even for today's scheme, preventive operation for lowering the reservoir levels can reduce the flood peak in the Aare River. Higher flood peak reduction is achieved by using not only the turbines but also the bottom outlets of the dams. Taking into account the upgraded scheme KWOpplus, the maximum flood peak with a return period of 100 years is $530 \text{ m}^3/\text{s}$ for most of the simulated scenarios, close to the observed value during 2005 flood event of $520 \text{ m}^3/\text{s}$. Even today's Oberhasli hydropower scheme has a retention effect of its reservoirs. Further simulations will be performed for flood scenarios with a return period of 300 years, the maximum event relevant for flood protection in this area.

An active flood management system, in collaboration with the local authorities, could reduce the risk of flooding. Therefore the model could be applied for real time simulations by using weather forecast data as input. An agreement between the plant owner and authorities, including a decision making strategy, would define the measures to be taken in the event of defined threshold values being exceeded during a flood.

REFERENCES

- Bieri, M., Schleiss, A.J. & Fankhauser, A. 2010. Modelling and simulation of floods in alpine catchments equipped with complex hydropower schemes. In A. Dittrich et al. (eds.), *River Flow; Proc. intern. symp., Braunschweig, 8–10 September 2010*. Karlsruhe: Bundesanstalt für Wasserbau.
- Dubois, J. 2005. Simulation des systèmes hydrauliques et hydrologiques complexe: Routing System II. In A. Schleiss (ed.), *Communication 21 du Laboratoire de Constructions Hydrauliques*. Lausanne: EPFL.
- García Hernández, J., Jordan, F., Dubois, J. & Boillat, J.-L. 2007. Routing System II: Flow modelling in hydraulic systems. In A. Schleiss (ed.), *Communication 32 du Laboratoire de Constructions Hydrauliques*. Lausanne: EPFL.
- Jordan, F., García Hernández, J., Dubois, J. & Boillat, J.-L. 2008. MINERVE: Modélisation des intempéries de nature extrême du Rhône valaisan et de leurs effets. In A. Schleiss (ed.), *Communication 38 du Laboratoire de Constructions Hydrauliques*. Lausanne: EPFL.
- Schaepli, B., Hingry, B., Niggli, M. & Musy, A. 2005. A conceptual glacio-hydrological model for high mountainous catchments. In *Hydrology and Earth System Sciences* 9: 95–109.

Controlled sediment flushing of Cancano reservoir

P. Espa, M.L. Brignoli & A. Previde Prato

Department Environment-Health-Safety, University of Insubria, Varese, Italy

E. Castelli & G. Crosa

Department of Structural and Functional Biology, University of Insubria, Varese, Italy

G. Gentili

Graia Srl, Varano Borghi (VA), Italy

F. Bondiolotti

A2A Spa, Grosio (SO), Italy

ABSTRACT: sediment flushing at Cancano hydropower reservoir (120 Mm³ storage, 1900 m AMSL top of active pool) aimed to start removal of a silty deposit (over 0.2 Mm³) burying the lower outlet of the dam by more than 15 meters. Operations were performed on March and April 2010 to get minimum seasonal storage and low enough temperatures, to prevent significant snow-melting inflows. Silt was displaced both by excavators and mud-pumps and by-passed downstream of the dam. The whole operation required almost fifty days. Attention was paid to the environmental sustainability of the flushing: limits for Suspended Solid Concentration (SSC) were fixed along the river below the dam, field surveys were carried out to quantify the impact on river habitats and biocenosis. Continuous turbidimeter measurements were employed to rule the works of mechanical means and the water diversion at high elevation intakes, achieving satisfactory control of SSC.

1 INTRODUCTION

In a world context characterized by increasing exploitation of water resources and attention to renewable energy (White, 2010), sustainable preservation of reservoirs storage is going to become crucial. Particularly if, as in Italy, building of new reservoirs is interrupted from decades.

Flushing may represent an effective technical alternative to desilt reservoirs (Morris & Fan, 1997), but operations should be managed aiming to reduce the impact on downstream ecosystems. This reduction can be actuated by limiting SSC of evacuated water. Careful evaluation of tolerable SSC values, as a function of the environmental quality of the impacted river, is therefore required. As obvious, SSC control while flushing a reservoir may be operationally difficult; moreover, ecologically sustainable thresholds of SSC, balancing technical and economical constraints, may be controversial. Only few technical and scientific works report on these subjects.

Sediment flushing at Cancano reservoir was carried out from March the 9th to April the 24th 2010, which represents a quite long time span in a quite unusual season: as well established, standard period for flushing is during high flows (i.e. between June and July in the investigated area), possibly during the falling limb of a flood hydrograph (White, 2001). In the discussed case, the presence of a low capacity bottom outlet (severely buried by the sediment deposit) and the following need to evacuate water from the working site led to prefer minimum seasonal storage, dry and cold climate. On the other hand, frequent problems connected to low temperatures affected the works and the limited water availability for transport and appropriate dilution of the sediment load resulted in a long lasting and thus expensive operation.

Desilting activities by mechanical means during daytime were alternated to nighttime releases of clean water and water diversion at high elevation intakes was calibrated to properly increase flow rate below the dam. Continuous SSC measurements as far as 65 km downstream of the reservoir were used both to manage dislodging activities and to verify respect of fixed thresholds. On the same river reach, pre and post ecological surveys were carried out to quantify flushing impact (at least the short term one) on river habitats and biocenosis.

Planning and control of the flushing works involved not only the licensee hydropower company, but also several local and regional Authorities under the framework of the Italy/Switzerland INTERREG project ECOIDRO (ID 7630754) whose main topics are water management and environmental safeguard.

2 INVESTIGATED SYSTEM AND MONITORING CAMPAIGN

Cancano reservoir (Fig. 1) is located on the upper course of the Adda river, Lombardy Alps, close to the border with Switzerland (at Schweizerischer Nationalpark). Cancano dam was closed in 1956. Dam crest is at 1902 m AMSL and the bottom outlet (a 1,2 m diameter steel pipe in the dam body) is at 1781 m AMSL. Cancano reservoir stores 123 Mm³; together with the slightly above San Giacomo reservoir (64 Mm³), it provides seasonal water storage in the upper Adda river basin. Catchment area at Cancano dam is 370 km², about 70 km² glacier covered. More than two thirds of this basin (275 km²) drains into San Giacomo reservoir, mainly through artificial connections of Spoel stream basin (105 km²) and upper Frodolfo and Braulio stream basins (150 km²)—Figure 2a. The Viola stream basin (75 km²) is artificially connected to the Cancano reservoir, whose natural basin has less than 20 km² area. Natural runoff is essentially snowmelt driven, with seasonal maximum values between late spring and early summer and minimum between January and February.

Main purpose of the mentioned reservoirs is hydropower. Cancano reservoir feeds Premadio powerhouse (230 MW installed capacity) and four smaller plants, located along the channel system and between the two contiguous reservoirs, install 30 further MW. Water discharged by Premadio powerhouse is then channeled to the Val Grosina reservoir to feed Grosio powerhouse (430 MW installed capacity), the larger plant of the area.

Monitored Adda reach is about 60 km long (Fig. 2b) and main sampling activities were carried respectively out at the following sites: Premadio (6.7 km below the dam, hereafter referred to as section I), Cepina (14.2 km below the dam, section II), Val Pola above the pond (16.4 km below the dam, section III), Val Pola below the pond (17 km below the dam, section IV), Le Prese (22.9 km below the dam, section V), Boscaccia (28.2 km below the dam, section VI), Sernio (42.7 km below the dam, section VII), Baghetto (64 km below the dam, section VIII). For the sake of brevity, results concerning the reach between sections VI and VIII, where SSC was very low and flushing effects were in practice negligible, won't be discussed herein.

From the dam to section I riverbed profile is very steep, with average slope of about 8.5%. Between sections I and II, main tributaries Viola (average natural discharge of 4.0 m³/s) and Frodolfo (average natural discharge of 5.8 m³/s) join the Adda river and the slope becomes significantly lower, with mean value of 1.3% in the reach between sections I and III. About

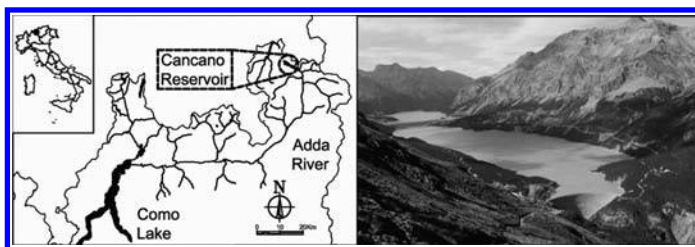


Figure 1. Position of Cancano reservoir (picture on the right) in the northern Italy and in the Adda river basin.

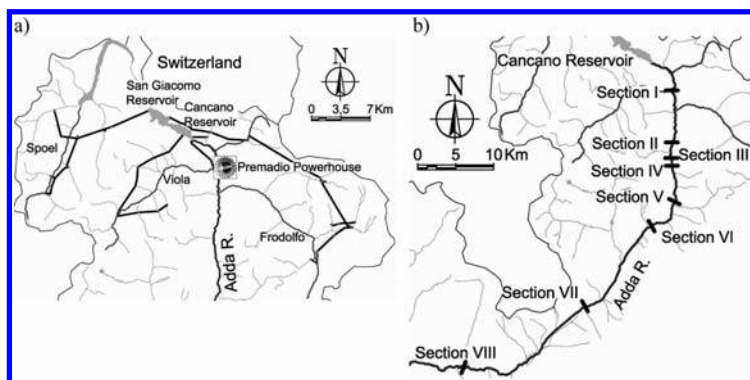


Figure 2. San Giacomo and Cancano reservoirs with main inflows from Spoel, Frodolfo and Viola stream basins (2a). Monitored Adda reach with main sampling stations indicated by Roman numerals (2b).

17 km below the dam, in the river area interested by the notorious Val Pola rock avalanche of July 1987, large river restoration works are taking place: here a 2 m tall check dam was built to develop a 500 m long backwater flow acting as a settling basin to decrease downstream SSC (Val Pola pond, 30,000 m³ estimated volume between sections III and IV). Below section IV, slope increases again, to an average value of about 2.3% almost constant until section VI.

As expected, discharges are highly regulated: average minimum flow of 0.2 m³/s (8% of mean annual) is released at section I, increasing to 0.25 m³/s from May to October and decreasing to 0.15 m³/s in the remaining six months. Modulated in the same way, the minimum flow at section V is 1.2 m³/s.

SSC was continuously measured at sections I, V, VII and VIII by one point sampling with Lange SC100 turbidimeters. Turbidimeters records were calibrated a posteriori by lab analyses of one liter samples as discussed in Espa et al. (2008). Analogous sampling was conducted by portable turbidimeters (Partech 740 and Insite 3150) on selected days and only during daytime at sections II, III and IV, with the main purpose of estimating sediment deposition between sections I and III and trap efficiency of Val Pola pond. Flow rate was continuously measured by stage record at sections I, II, V and VII.

Fish community was quantitatively sampled at sections II and V by electrofishing (removal method with two passes) before (Nov. 2009) and after (May 2010) flushing works; previous observations of spring 2009 are available at the same sites and will be used for comparison. Caught fishes were checked by species and measured by weight and length to estimate density (individuals/hectare) and biomass (kg/hectare) (De Lury, 1947) and to depict the age structure of the population. Only qualitative observations of this kind were possible below section VII because of larger river width and higher discharge. In the Adda reach between sections I and III, where maximum SSC values were expected, fish was prudentially removed by electrofishing, with the exception of the area round section II, where surveying of flushing effects was planned.

The quantitative measurement of macroinvertebrate community was carried out in February (pre-flushing), May (post-flushing) and July 2010, on sections I, II, V and VI. Macroinvertebrate samples were collected according to the AQEM strategy (Hering et al., 2004; Buffagni & Erba, 2007), a quantitative multi-habitat approach developed in accomplishment of WFD (Water Framework Directive 2000/60/EC). Ten quantitative sample units (area 0.1 m², 500 µm net mesh) were proportionately allocated in relation to the occurrence of microhabitats in the studied reaches. Collected macro-invertebrates were preserved in formalin (4%), identified to genus (*Plecoptera*, *Ephemeroptera*) or family level and counted. Quality classes (five in all, from high to bad status) were determined using the STAR_ICM index, the new official Italian method for classification based on macroinvertebrate communities, developed for WFD inter-calibration purposes (Buffagni et al., 2007; EC, 2008).

The STAR_ICM index is a multi-metric index, based on six different metrics (ASPT index, $\text{Log}_{10}(\text{sel_EPTD}+1)$, 1-GOLD, number of families of EPT, total number of families and Shannon-Weiner diversity index). The identification level required for calculation is family. After normalization by the median value of reference sites' samples, these metrics are combined into the STAR_ICM index. To classify samples, as far as the Biological Quality Element of macroinvertebrates is concerned, the official Italian boundaries were used (high-good 0.95; good-moderate 0.71; moderate-poor 0.48; poor-bad 0.24—EC, 2008).

3 FLUSHING OPERATIONS AND SSC MEASUREMENTS RESULTS

In the last forty years, the bottom outlet of Cancano reservoir was never opened and flushing operations were planned to start removal of a silty deposit close to the upstream face of the dam; this deposit (over 0.2 Mm^3) buried the lower outlet of the dam (1781 m AMSL) by more than 15 meters and begun to threaten the intake (1806 m AMSL) of Premadio powerhouse. As a consequence of supply characteristics, shortly described in previous paragraph, deposited sediment is mainly constituted by fines: sediment size analyses on samples collected after draw-down show that more than 80% was in the silt range (from 4 to $62 \mu\text{m}$) and the remaining 20% was clay.

Flushing period was selected between end of winter and beginning of spring to ensure minimum seasonal storage and optimal working temperature (i.e. low enough to prevent significant inflow due to snow melting). A small dyke was built on the reservoir bottom to preserve working area from flooding and to divert water to flush sediment. Silt was moved (both by excavators and mud-pumps) to the intake of Premadio powerhouse and evacuated downstream of the dam through a bypass.

Limits for SSC (average value on the entire works period) were fixed following prescriptions of Regione Lombardia (2008), in order to limit environmental damage:

- 3.0 g/l (i.e. 3.0 kg/m^3) in the reach between sections V and VII,
- 1.5 g/l below section VII (where quality achieves its highest standard in the Adda river).

The reach above section IV was left free of limits for general uncertainty about the development of the works. Control of the desilting activities was based on real-time rough (i.e. not calibrated) data of turbidimeter probes, while respect of previous constraints was verified a posteriori after probes calibration.

Flushing operations may be summarized as follows, subdividing them into three main phases:

- PH 1. 9–23 Mar.: draw-down of the reservoir at intake level, arrangement of the working site, beginning of the works by mud pumping, achievement of regime conditions.
- PH 2. 24 Mar.-15 Apr.: flushing was carried out at first by two mud pumps (PH 2a), then by a single pump and excavators plus lorries (PH 2b) and finally just by excavators and lorries (PH 2c); in the final days the level of the bottom outlet was approximately reached but further development of flushing works and full outlet opening was postponed to the next year.
- PH 3. 16–24 Apr.: cleaning of the intake tunnel and removal of working site equipment.

In general, considerable efforts were done to tackle difficulties due to adverse meteorological conditions (particularly low temperatures) and to evacuate water from the working site. Machines maintenance during nighttime (to avoid ice blocking) was necessary and no interruption for holidays was possible. [Table 1](#) reports temperatures measured at Cancano dam, averaged on the three previously mentioned working phases; mean temperature during the whole operation was -1°C .

[Table 2](#) reports main SSC and discharge data as detected at sections I and V, subdivided by operation phase. Best efficiency in terms of evacuated volume of sediment was achieved during phase PH 2a, with full mud pumping activity. SSC duration curves are given as well in tabular form ([Tab. 3](#)). SSC at section V only occasionally exceeded 2 g/l and the average value of 0.3 g/l was ten times smaller than the fixed limit; at section I mean SSC was 3.5 g/l and values over 10 g/l were detected for about four cumulative days.

Figure 3 displays time histories of SSC and flow rate at sections I and V during four days of phase PH 2c (Apr. 4 to 7). It provides an example of how SSC was controlled by executing dislodging works for approximately half of the day and releasing clear water during nighttime. SSC reduction along the Adda river is also noticeable: peaks of 20 to 30 g/l are quite regularly detected at section I as a result of daytime works while downstream increase of flow rate (more than threefold) and sediment deposition (particularly at Val Pola pond) determine SSC peaks reduction of about 90%.

As explained, SSC measurements at sections III and IV were not as detailed as for sections I and V; however they allow for a first approximation estimate of sediment deposition at different reaches as follows:

- 14,500 tons of sediment flowed through section I,
- about 2500 tons sedimented between sections I and III (a 10 km river reach at 1.3% average slope),
- about 7500 tons settled into the Val Pola pond (that cut off about 60% of inflowing sediment mass),
- negligible deposition was observed between sections IV and V.

Trap efficiency of Val Pola pond was computed by classical USBR method for settling basins design (Vanoni, 1975), adopting a schematic sediment size distribution based on sampling at section II during the flushing (20% with 30 μm diameter, 20% with 15 μm diameter, 30% with 8.5 μm diameter, 10% with 4.6 μm diameter and 20% with 0.8 μm diameter): computed efficiency of about 50% is reasonably close to the observed one.

Estimated unit cost was of about 50 €/m³, including both flushed sediment and displaced one into proper dead areas of the reservoir. This is a quite high value if compared to

Table 1. Phase averaged values of daily average (T_{DAY}), minimum (T_{MIN}) and maximum (T_{MAX}) temperatures at Cancano dam during flushing works.

Phase	Duration days	T_{DAY} (°C)	T_{MIN} (°C)	T_{MAX} (°C)
PH 1	15	-4	-9	5
PH 2	23	-1	-7	6
PH 3	8	3	-2	9

Table 2. Phase averaged values of flow rate (Q_{AVE}), SSC (SSC_{AVE}) and daily flowed mass (M_{AVE}) at sections I and V. Totally flowed mass per phase (M_{TOT}) and percentage sedimented mass (M_{SED}) between the two measurement stations.

Phase	Duration days	$Q_{\text{AVE,I}}$ (m ³ /s)	$Q_{\text{AVE,V}}$ (m ³ /s)	$\text{SSC}_{\text{AVE,I}}$ (g/l)	$\text{SSC}_{\text{AVE,V}}$ (g/l)	$M_{\text{AVE,I}}$ (t/day)	$M_{\text{AVE,V}}$ (t/day)	$M_{\text{TOT,I}}$ (t)	$M_{\text{TOT,V}}$ (t)	M_{SED} (%)
PH 1	15	0.8	2.6	1.5	0.05	110	12	1650	179	89
PH 2	23	1.0	4.0	5.5	0.5	498	167	11,461	3848	66
PH 2a	7	1.3	3.9	6.6	0.7	749	255	5246	1786	66
PH 2b	4	0.8	3.4	6.0	0.4	419	107	1676	428	74
PH 2c	12	1.0	4.3	4.6	0.4	378	136	4540	1635	64
PH 3	8	1.1	3.1	1.8	0.2	192	69	1538	554	64

Table 3. Duration (%) of SSC at sections I and V.

SSC (g/l)	20	10	5	2	1	0.5	0.2	0.1	0.05	0.02
Duration—Section I (%)	1.9	8.9	19.4	39.6	74.7	90.7	100			
Duration—Section V (%)	–	–	–	1.0	7.1	17.2	33.6	48.8	67.6	100

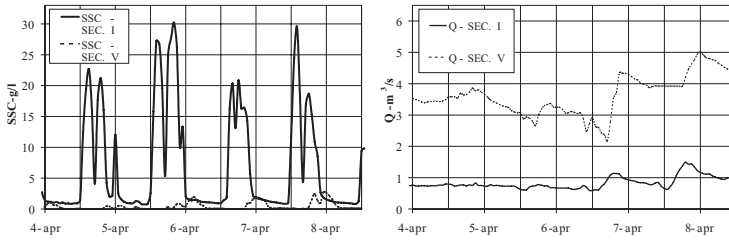


Figure 3. SSC (left) and discharge (right) time histories at sections I and V from April 4th to 7th.

5–50 USD/m³ reported by Morris & Fan (1997) for dry excavation by conventional earth-moving equipment in Los Angeles County and to 5 €/m³ reported by Espa et al. (2010) for free-flow flushing at a run-of-the-river intake on the Adda river, about 45 km below Cancano dam. It should be carefully considered the peculiarity of the discussed operation which required long time to achieve effectiveness and large costs to carry out and maintain working site (about 40% of the total). Water volumes loss to insure acceptable dilution resulted in energy loss representing about 60% of total cost. Working site charges are expected to decrease in March 2011, when the operation is planned to go on for a shorter period but with higher efficiency.

4 ENVIRONMENTAL EFFECTS OF FLUSHING

Fish data are provided at sections II and V (Figs 4 and 5). Comparisons between pre and post-flushing (Nov. 2009–May 2010) are in Figures 4a and 5a, while comparisons between same period, one year before (2009) and after the flushing are in Figures 4b and 5b. Both sites are characterized by a large predominance of brown trout which is therefore the represented species.

In general, flushing works impacted fish community, but also on the most exposed investigated reach (e.g. above the Val Pola pond) the impairment appears to be recoverable. Moreover, other disturbances (in particular activities connected to sport fishing) seem to bias the results, indicating the need of further investigation integrating the reported short-term impact data. More specifically, a drop in density (47%) and biomass (39%) was measured in section II. The same density decrease (48%) was detected at section V, but coupled with a slight increase in biomass (9%). Furthermore, at both sites no young of the year individuals, alevins of 30 mm expected length in that season, were visually detected in the course of the electrofishing surveys after the flushing works. Density reduction mainly affected the length class 100–150 mm (Figs 4a and 5a) which typically represents recruitment trout introduced for sport fishing purposes; as yet observed in a comparable context (Crosa et al. 2010), not wild fish is much more exposed to the stress represented by flushing operations. If post-flushing data are compared to the previous year ones, fish population looks basically unchanged at section II (Fig. 4b) while a drop, once again concentrated in the length class 100–150 mm (Fig. 5b), is noticed at section V, even if at this site SSC was sensibly lower than in the upstream one.

Main data of macroinvertebrate sampling are summarized in figure 6. As for previous fish data, some contradictions emerge, showing that the dynamics of macroinvertebrate assemblages are not only driven by the sediment flushing but also by other elements (seasonality, increase of discharge in late spring, ...), particularly in a so heavily regulated water system. For example, no meaningful change in quality was measured at section I before and after the flushing (figure 6b) and a good STAR_ICM status was preserved. On the other hand, a drop from good to moderate was detected in section II while in section V a drop was observed from May to July. Main conclusions concerning macroinvertebrate community sampling show substantial analogy to the ones concerning fish population:

- the short-term impact of flushing works on macroinvertebrate assemblages is clearly evidenced by a density drop at all investigated sites,

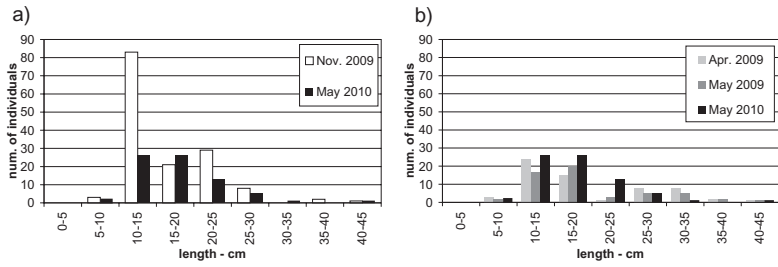


Figure 4. Brown trout population at section II before and after the flushing (4a), after the flushing and one year before (4b).

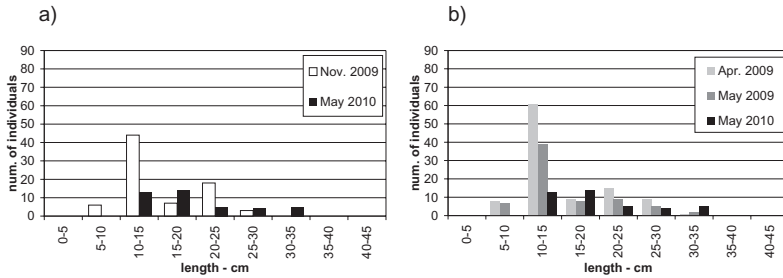


Figure 5. Brown trout population at section V before and after the flushing (5a), after the flushing and one year before (5b).

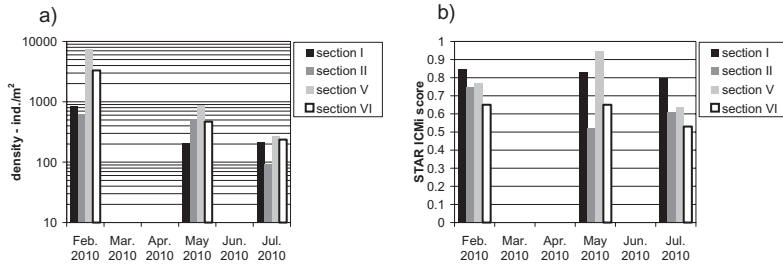


Figure 6. Main results of macroinvertebrate sampling campaign. 6a) Time history of macroinvertebrate density. 6b) Time history of STAR_ICM index.

- on the other hand, as shown by STAR_ICM values, good to moderate standards are generally preserved along the Adda river after the flushing,
- comparison between the available post-flushing values (May and Jul. 2010) demonstrates that further disturbs, both manmade and natural, superimpose over the flushing one, and that more reliable indications could be inferred only after further careful field investigation.

5 CONCLUSIONS

Sediment flushing at Cancano reservoir was carried out for 46 consecutive days, between end of winter and early spring 2010. SSC was continuously monitored on a river reach below the dam of approximately 60 km, but values became negligible for dilution and deposition after the first 25 km. In spite of operational difficulties connected to the selected season, control was successfully achieved and SSC values along the Adda river were well below fixed

thresholds. In particular, Val Pola pond turned out to be effective in lowering downstream SSC, although sediment was predominantly silt. Operation was quite expensive, but charges connected to arrangement and maintenance of working site would be amortized in next year analogous operation, which is expected to be shorter and more efficient.

The short term environmental impact of the flushing was quantified along the investigated Adda reach through pre and post sampling of fish and macroinvertebrates. Even if a drop was noticed on both communities, the impairment appears to be recoverable. Moreover, interpretation of so far available data is not straightforward, probably as a consequence of the high degree of hydraulic regulation on the studied basin and of human activities as sport fishing: further field sampling in the next months would possibly clarify the outline.

On the whole, the adopted procedure appears to represent a good compromise between technical-economical constraints and environmental considerations. Further improvements resulting in a significant reduction of the environmental impact of the flushing (i.e. significant reductions of SSC and/or of works duration), without compromising the feasibility of the operation, do not seem to be reasonably practicable.

ACKNOWLEDGEMENTS

An important part of the field sampling concerning the flushing of Cancano reservoir was financed by INTERREG Italy/Switzerland project ECOIDRO (*Water Use and Safeguard of Environment and Biodiversity in the River Basins of Adda, Mera, Poschiavino and Inn*—ID 7630754). DBSM (Department of Biotechnology and Molecular Sciences) of the University of Insubria is acknowledged for the activation of research contracts for paper coauthors M.L. Brignoli e A. Previde Prato.

REFERENCES

- Buffagni, A. & Erba, S. 2007. *Macroinvertebrati acquatici e Direttiva 2000/60/EC (WFD)*. Notiziario dei metodi Analitici. Roma: IRSA CNR.
- Buffagni, A., Erba, S. & Furse, M.T. 2007. A simple procedure to harmonize class boundaries of assessment systems at the pan-European scale. *Environmental Science and Policy* 10: 709–724.
- Crosa, G., Castelli, E., Gentili, G. & Espa, P. 2010. Effects of suspended sediments from reservoir flushing on fish and macroinvertebrates in an alpine stream, *Aquatic Sciences* 72(1).
- De Lury, D.B. 1947. On the estimation of biological populations. *Biometrics* 3: 145–167.
- EC, Commission of the European Communities 2008. *Commission Decision of 30 October 2008 establishing, pursuant to Directive 2000/60/EC of the European Parliament and of the Council, the values of the Member State monitoring system classifications as a result of the intercalibration exercise*. Brussels: Official Journal of the European Union.
- Espa, P., Compare, S., Crosa, G., Bondiolotti, F., Gentili, G. & Sibilla, S. 2008. Sediment flushing from an Alpine reservoir: hydraulic monitoring and biological impact. In Altinakar M.S. et al. (ed.), *River Flow 2008, International Conference on Fluvial Hydraulics. Proc. Intern. Symp., Çeşme, 3–5 September 2008*. Ankara: KUBABA Congress Department and Travel Service.
- Espa, P., Brignoli, M.L., Previde Prato, A., Castelli, E., Crosa, G. & Gentili, G. 2010. Rimozione di sedimenti per fluitazione dal serbatoio di Sernio (SO). *XXXII Convegno Nazionale di Idraulica e Costruzioni Idrauliche. Proc. Nat. Symp., Palermo, 14–17 September 2010*. Palermo: Walter Farina Editore.
- Hering, D., Moog, O., Sandin, L. & Verdonschot, P.F.M. 2004. Overview and application of the AQEM assessment system. *Hydrobiologia* 516: 1–20.
- Morris, G.L. & Fan, J. 1997. *Reservoir Sedimentation Handbook: Design and Management of Dams, reservoirs, and Watersheds for Sustainable Use*. New York: Mc Graw Hill.
- Regione Lombardia, 2008. *Definizione dell'impatto degli svassi dei bacini artificiali sull'ittiofauna e valutazione di misure di protezione*, Quaderni della ricerca, n. 90. Milano: Regione Lombardia.
- Vanoni, V.A. 1975. *Sedimentation Engineering*. New York: the American Society of Civil Engineers.
- White, W.R. 2001. *Evacuation of sediments from reservoirs*. London: Thomas Telford Publishing.
- White, W.R. 2010. *World water: resources, usage and the role of man-made reservoirs*. Marlow (UK): Foundation for Water Research.

Sediment bypass tunnel design—review and outlook

C. Auel & R.M. Boes

Laboratory of Hydraulics, Hydrology and Glaciology (VAW), ETH Zurich, Switzerland

ABSTRACT: Reservoir sedimentation is increasingly affecting the majority of reservoirs all over the world. As many dams are more than 50 years of age, this problem is becoming more and more serious nowadays. Reservoir sedimentation leads to various severe problems such as a decisive decrease of the active reservoir volume leading to both loss of energy production and water available for water supply and irrigation. These problems will intensify in the very next future, because sediment supply tends to increase due to climate change. Therefore countermeasures have to be developed. They can be divided into the three main categories sediment yield reduction, sediment routing and sediment removal. This paper focuses on sediment routing by means of sediment bypass tunnels. Sediment bypass tunnels are an effective measure to stop or at least decrease the reservoir sedimentation process. By routing the sediments around the reservoir into the tailwater in case of flood events sediment accumulation of both bed load and suspended load is reduced significantly. However, the number of sediment bypass tunnels in the world is limited primarily due to high investment and above all maintenance costs. The state-of-the-art design criteria of constructing bypass tunnels are summarized herein; major problems such as tunnel invert abrasion are discussed. The need for further research regarding sediment transport in bypass tunnels and invert abrasion is highlighted.

1 INTRODUCTION

Reservoir sedimentation is an increasing problem affecting the majority of reservoirs not only in Switzerland but worldwide. As many dams are more than 50 years of age, this problem is becoming more and more serious nowadays. Mean annual sedimentation rates of 0.2 to 2% of the reservoir volume led, and will lead in the very next future, to high aggradation (Schleiss & Oehy 2002, Sumi et al. 2004, Basson 2009, Schleiss et al. 2010). [Figure 1](#) gives an example for the Solis reservoir in Switzerland. The volume of this reservoir, commissioned in 1986, is reduced to less than 50% of its original volume during the last 24 years due to sediment aggradation (Auel et al. 2010).

Reservoir sedimentation causes various severe problems such as (1) a decrease of the active volume leading to both loss of energy production and water available for water supply and irrigation; (2) a decrease of the retention volume in case of flood events; (3) endangerment of operating safety due to blockage of the outlet structures; and (4) increased turbine abrasion due to increasing specific suspended load concentrations (Vischer 1981, Vischer 1996, Sumi et al. 2009). These problems will intensify in the very next future, as reservoir sedimentation will progress if no countermeasures are taken.

Sediment management or minimized sediment aggradation in reservoirs may be achieved with different measures as shown amongst others in Annandale (1987), Sloff (1991), Sumi (2000), Sumi et al. (2004, 2009), Mariño et al. (2009), Inoue (2009), Kantoush & Sumi (2010) or Schleiss et al. (2010). According to Sumi et al. (2004) and Kantoush & Sumi (2010) the type of measures can be divided into three main categories:

1. Sediment yield reduction.
2. Sediment routing.
3. Sediment removal.

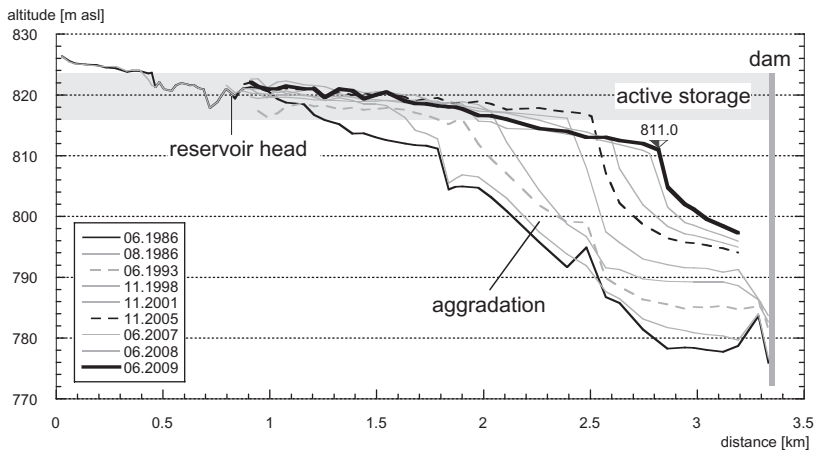


Figure 1. Longitudinal sections of the periodically surveyed reservoir bottom elevations in the Solis reservoir. Aggradation has led to a decrease of more than 50% of the original reservoir volume.

The first category refers to measures reducing the sediment inflow into the reservoir, i.e. erosion control in the catchment area such as reforestation or upstream sediment trapping.

The second category refers to measures that route sediments into the tailwater downstream of the dam. Within this category three effective measures can be applied: (2A) sluicing of sediments through the reservoir outlet structures by lowering the water level, (2B) venting of turbidity currents and (2C) routing of sediments through a sediment bypass tunnel.

Measures 2A and 2B are closely related. Depending on the reference sharp distinctions are difficult to make. The advantage of both measures is that incoming sediments are routed into the tailwater without settling in the reservoir (Sloff 1991, Müller & De Cesare 2009, Schleiss et al. 2010). Sluicing of sediments requires a partial water level lowering to transport incoming and to some extent accumulated sediments to the dam outlet structure, whereas venting of turbidity torrents can be performed without water level lowering. Sluicing of sediments mostly implies bedload and suspended load, venting of turbidity torrents focuses on suspended sediments transported within the current. One major disadvantage of sluicing sediments is that the routing through the outlet structure, mostly the bottom outlets, is operated under pressure conditions. Bottom outlets, if not reinforced, are not designed for high sediment or bed load concentrations. Flow velocities are very high and hence risk of damage due to blockage and abrasion is significantly increased. In contrast venting of turbidity torrents is possible not only through the bottom outlets but through the power intake (Schleiss et al. 2010). However, one major disadvantage is the possible turbine wear, depending highly on the sediment properties such as the quartz content or the specific sediment concentration. Thus this measure is not always suitable; having in mind that bed load inflow is not considered either. In contrast, routing sediments through a sediment bypass tunnel (2C) is very effective regarding bypassing of bed load material as well as suspended sediments (Vischer et al. 1997, Kashiwai et al. 1997, Sumi et al. 2004, Auel et al. 2010).

The third category refers to measures that remove accumulated sediments from the reservoir bottom. Typical measures are (3A) dredging of sediments during high reservoir levels, (3B) dry excavation of sediments during complete water level drawdown, or (3C) flushing of sediments through the reservoir outlet structures during high reservoir levels i.e. pressurized flushing or during complete water level drawdown.

The dredging of sediments is only applicable for small reservoir volumes, because mechanical removal is not economical for large reservoirs. Furthermore, dredging is always a limited countermeasure against one particular flood event; thus it has to be performed frequently. Dry excavation and sediment flushing during complete water level drawdown have a major disadvantage as they result in the complete loss of storage water for both energy production

and water supply. Furthermore, a complete drawdown is only reasonably applicable when the reservoir volume is small compared to the annual inflow, i.e. for low capacity inflow ratio. In case of annual storage reservoirs, refilling is a long-time process, depending essentially on the hydrologic conditions. Pressurized flushing is not very effective either, because of its local impact resulting only in a funnel shaped crater in the bottom outlet vicinity (Lai & Shen 1996, Meshkati et al. 2009). A second disadvantage of flushing sediments is the high quantity of eroded material that may lead to undesirable high ecological impacts on the downstream river reach. However, flushing of sediments is applied frequently in times of comparatively high reservoir inflow such as typically HQ_1 to HQ_2 , due to its easy applicability and economic reasons (Boillat et al. 2000, Sumi 2005, Inoue 2009).

Research on reservoir sedimentation and especially its countermeasures is still comparatively scarce. Especially the effective application of sediment bypass tunnels, i.e. category 2C, has not been completely investigated. Therefore, this paper summarizes the current knowledge regarding sediment bypass tunnel design and operation. Advantages and disadvantages of this type of measure are specified, discussed in detail, and the need for future research is highlighted.

2 SEDIMENT BYPASS TUNNELS

Sediment bypass tunnels are an effective measure to stop or at least decrease the reservoir sedimentation process. By routing the sediments around the reservoir into the tailwater during flood events, sediment accumulation in the reservoir due to both bed load and suspended load can be minimized significantly. A second advantage gaining in importance is the ecological and sustainable aspect of routing sediments. River bed erosion downstream of the dam is stopped or at least decelerated significantly and the morphological variability increases. Only sediments provided from the upstream river reach are conducted through the bypass tunnel, and no removal of already accumulated sediments in the reservoir occurs. The sediment concentration in the tailwater of the dam is not affected by the reservoir itself and therefore of natural character.

Nevertheless the number of realized sediment bypass tunnels in the world is limited primarily due to high investment and maintenance costs. Sediment bypass tunnels in operation are located mainly in Switzerland and Japan. In Switzerland there are five tunnels in operation and one under construction (Vischer et al. 1997, Auel et al. 2010). Referring to Sumi et al. (2004) there are three tunnels in operation in Japan, one under construction and one in planning.

2.1 *Sediment bypass tunnel design*

In a first step the tunnel intake location and the design discharge have to be defined. Thereafter the proper sediment bypass tunnel design can be projected in streamwise direction. A sediment bypass tunnel consists of a guiding structure in the reservoir, an intake structure with a gate, mostly a short and steeply sloped acceleration section, a long and smoothly sloped bypass tunnel section, and an outlet structure (Figure 2). The intake location, the tunnel operation and each individual bypass tunnel element are described in detail below.

2.1.1 *Intake location*

Two different locations are generally possible for the bypass tunnel intake, both affecting the entire bypass tunnel design and the reservoir operation during sediment routing. The most common location for the tunnel intake, applied in the majority of sediment bypass tunnels in Switzerland and Japan, is at the reservoir head (position A, Figure 2a). Another suitable intake location is somewhere downstream of the reservoir head closer to the dam (position B, Figure 2b).

The advantages of position A are the following: Firstly, the complete reservoir is kept free from sediments, and secondly, the reservoir level during bypass operation is independ-

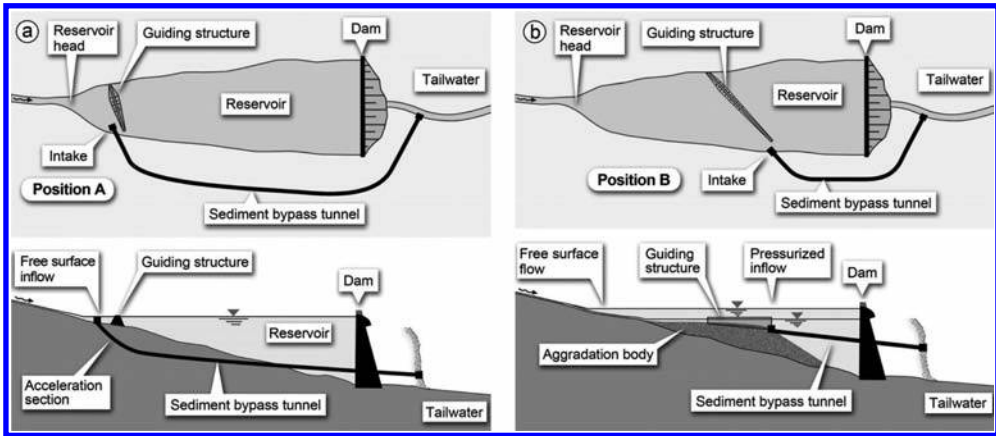


Figure 2. Sketches of two different sediment bypass tunnel systems. a) Position A: Location of the tunnel intake at the reservoir head; inflow under free surface conditions. b) Position B: Location of the tunnel intake downstream of the reservoir head; inflow under pressurized conditions.

ent from the upstream river reach and can be kept at full supply level. Disadvantages are, depending on the topography, the long distance from the reservoir head to the tailwater causing high tunnel construction costs, and the free surface flow conditions at the tunnel intake requiring a steep acceleration section which may provoke high abrasion at the tunnel invert due to high flow velocities (see parts 2.1.6 and 2.2.2).

Position B has the following advantages: Firstly, the distance between the tunnel intake and the tailwater is short causing low construction costs, and secondly, the intake inflow is under pressurized conditions so that an acceleration section can be waived. As a major drawback only the reservoir section downstream from the intake is kept free from sediment accumulation, and the reservoir level has to be lowered to a certain level to sustain sediment transport capacity in the upper reservoir reach upstream from the intake (see part 2.1.2).

The influence of the different intake locations on both bypass tunnel operation and each individual tunnel element are discussed below.

2.1.2 Operation

Depending on the tunnel intake location, the reservoir operation during sediment routing varies. If the tunnel intake is located at the reservoir head (position A), the gate is opened in case of flood events and the discharge is routed in free surface conditions through the tunnel. The reservoir level can be kept at full supply level. The incoming flow and the transported sediment are conducted independently from the reservoir level into the tailwater downstream of the dam.

If the intake is located downstream of the reservoir head (position B), the reservoir level has to be lowered prior to a flood event to a certain level depending on the distance of the reservoir head to the tunnel intake. It has to be secured that the reservoir reach upstream of the intake is subjected to free surface flow conditions so that incoming sediment is transported towards the intake. The reservoir level has to be kept at this certain level to avoid interruption of the sediment transport.

2.1.3 Design discharge

The determination of the design discharge depends first of all on an economic tunnel diameter and secondly on the given hydrological conditions in the catchment. According to Vischer et al. (1997) and Sumi et al. (2004) design discharges of sediment bypass tunnels in operation typically vary from a one to a ten year flood event. However, particularly for reservoirs with small catchments impounded by embankment dams, a higher recurrence interval of up to 100 years may be preferable to complement the service spillway capacity (Boes & Reindl

2006). When determining the design discharge one has to keep in mind that the surplus flow exceeding the design capacity has to be conducted to the downstream reservoir section. Thus a routing of all incoming sediments is achieved only up to the bypass tunnel design discharge. Sediment transported within the surplus flow accumulates to some extent in the downstream reservoir section. Hence a design discharge corresponding to a high flood return period should be aspired.

2.1.4 Guiding structure

The guiding structure also designated as diversion facility, check dam or partition dam has to lead both the incoming flood discharge and the transported sediment to the bypass tunnel intake. Referring to Vischer et al. (1997) and Sumi et al. (2004) in most existing bypass tunnels the guiding structure is located next to the tunnel intake crossing the reservoir from the intake to the opposite reservoir bank.

Some aspects have to be kept in mind when designing the guiding structure. On the one hand, the guiding structure should not be overtopped during bypass tunnel operation to avoid sediment accumulation in the reservoir. On the other hand, if the flood event exceeds the tunnel design discharge, the guiding structure has to be securely overtopped or openings in the guiding structure are to be designed to lead the surplus flow to the dam outlet structures. Depending essentially on the requested height, the guiding structure can be designed as a small dam or a vertical sheet pile wall. Detailed hydraulic studies of designing diversion facilities for sediment bypass tunnels are given in Kashiwai et al. (1997) and Auel et al. (2010).

2.1.5 Intake

The sediment bypass tunnel intake consists of an intake trumpet followed by a sluice or a radial gate. During normal reservoir operation the gate is closed. In case of flood events the gate is opened and the sediment-laden discharge is routed through the bypass tunnel. The design of the bypass tunnel intake depends directly on the selection of the intake location (compare part 2.1.1).

If the intake is located at the reservoir head (position A), the discharge is conducted under free surface conditions into the tunnel (Figure 3a). The tunnel invert level at the intake is constructed plain to the river bed. Downstream of the gate, the discharge has to be accelerated to generate supercritical flow conditions. This is achieved by a short and steep acceleration section (compare part 2.1.6).

If the intake is located further downstream (position B) the tunnel invert level can be situated lower than the river bed and the surrounding aggradation body, respectively. A certain energy head is thus generated and the discharge is conducted under pressurized conditions in the intake trumpet (Figure 3b). However, downstream of the gate the discharge is routed in free surface conditions through the tunnel. The flow velocity behind the gate is high due to the energy head; therefore an acceleration section can be waived (see part 2.1.6). One example is the sediment bypass tunnel Solis in the Canton of Grisons, Switzerland, which is currently under construction (Auel et al. 2010).

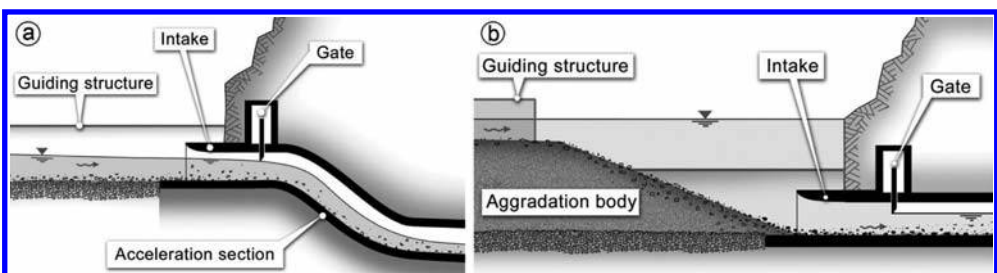


Figure 3. Sketches of the tunnel intake. a) Tunnel intake at position A; inflow under free surface conditions; b) tunnel intake at position B; inflow under pressure conditions.

2.1.6 *Steeply sloped acceleration section*

Referring to Chervet & Vischer (1996) and Harada et al. (1997) most bypass tunnels constructed in Switzerland and Japan include a short and steeply sloped acceleration section because of their intake location at the reservoir head. The aim of this steep section is to accelerate the discharge in order to achieve supercritical uniform flow. Fast velocities are required to ensure the requested sediment transport capacity in the upper tunnel section. Supercritical flow is desired to keep the tunnel cross section in an economical range (compare part 2.1.7). Typical slope values of the acceleration section range between 15 and 35%.

2.1.7 *Smoothly sloped bypass tunnel section*

The bypass tunnel connects the upstream tunnel intake with the downstream outlet structure located at the tailwater of the dam. Typical tunnel lengths according to Sumi et al. (2004) vary between 250 and 4300 m. The invert slope varies from 1 to 4%.

The cross section of most bypass tunnels is of archway shape (also referred to as hood shape) or horseshoe shape. Circular shapes are rare as the sediment transport is concentrated at the lowest invert point causing severe abrasion problems (see part 2.2.2). The second disadvantage compared to an archway shaped tunnel section is the round shaped tunnel invert leading to challenging trafficability during construction and maintenance.

The discharge is conducted under supercritical flow conditions to ensure both a sufficient sediment transport capacity and an economic tunnel cross section. The selection of the invert slope has to fulfill two contrary challenges: (1) The slope has to be steep enough so that even at minimum discharge sufficient shear stress is generated to transport all incoming sediments into the tailwater without sedimentation in the bypass tunnel itself. (2) The steeper the slope, the faster the flow velocities and consequently the higher the abrasion damages in the tunnel invert (see part 2.2.2).

2.1.8 *Outlet structure*

The outlet structure yields the sediment into the tailwater downstream of the dam. The following aspects regarding the outlet structure design have to be respected: (1) A sufficient transport capacity in the downstream river reach has to be secured to avoid sedimentation in the outlet vicinity and further downstream. This should typically be no problem because the sediment transport process in the entire river system is revitalized to its original condition before dam construction. (2) The tunnel outlet should not release sediments near the dam outlet structures to avoid sedimentation and backwater effects in the dam vicinity. (3) There should be a drop from the tunnel outlet into the river reach to avoid backward aggradation in the bypass tunnel itself. (4) The angle between the centerline of the tunnel outlet and the river thalweg should be kept small to reduce erosion impact on the opposite river bank. (5) Scouring due to the jet impinging from the tunnel outlet has to be monitored and resulting countermeasures have to be taken.

2.2 *Sediment bypass tunnel examples*

Excellent overviews of five existing sediment bypass tunnels located in Switzerland are given by Chervet & Vischer (1996) and Vischer et al. (1997). Another Swiss bypass tunnel currently under construction and presumably to be completed in 2012 is described by Auel et al. (2010). Sumi et al. (2004) and Kantoush & Sumi (2010) give a comprehensive overview referring, besides the five Swiss bypass tunnels, to additional three Japanese sediment bypass tunnels in operation, one under construction and one in planning. [Table 1](#) provides an overview of all sediment bypass tunnels summarized from the above mentioned references.

2.2.1 *Hydraulic design*

The maximum velocities in the sediment bypass tunnels, the velocities at the outlets, the uniform flow velocities and their corresponding Froude numbers at design discharge are presented in [Table 2](#) for all sediment bypass tunnels presented in [Table 1](#).

Table 1. Overview of sediment bypass tunnels in Switzerland and Japan.

No.	Country	Name	Completion [year]	Section shape	Section dimensions B × H [m]	Tunnel length* ¹ [m]	Slope* ² [%]	Op. Time [days/a]	Catchment [km ²]
1	CH	Pfaffensprung	1922	Horseshoe	4.70 × 5.23	25/282	35/3	ca 200	390
2	CH	Egschi	1949	Circul.* ⁴	D = 2.80	20/360	21/2.6	10	108
3	CH	Runcahez	1962	Archway	3.80 × 4.27	85/572	25/1.4	4	50
4	CH	Palagnedra	1978	Circul.* ⁴	D = 6.20	50/1760	29.6/2	2–5	140
5	CH	Rempen	1986	Horseshoe	3.45 × 3.42	22/450	25/4	1–5	25
6	CH	Solis	U.c.	Archway	4.40 × 4.68	8* ⁵ /968	0* ⁵ /1.9	1–10* ⁶	811* ⁷
7	J	Nunobiki	1908	Archway	2.90 × 2.90	n.s./258	n.s./1.3	n.s.	10
8	J	Asahi	1998	Archway	3.80 × 3.80	12/2384	20/2.9	13	39
9	J	Miwa	2004* ³	Horseshoe	D = 7.80	n.s./4300	n.s./1	n.s.	311
10	J	Matsukawa	U.c.* ³	Archway	5.20 × 5.20	n.s./1417	n.s./4	n.s.	n.s.
11	J	Koshibu	I.p.* ³	n.s.	n.s.	n.s.	n.s.	n.s.	n.s.

U.c.: Under construction; I.p.: In planning; n.s.: not specified. *¹First value: acceleration section length; second value: total length. *²First value: acceleration section; second value: smoothly sloped bypass tunnel section. *³Referring to Sumi et al. (2004). Data given in Kantoush & Sumi (2010) differ. *⁴Circular shape with plain invert. *⁵Horizontal invert slope. *⁶Estimated values. *⁷Effective value taking sedimentation in upper reservoirs into account; total value 900 km².

Table 2. Calculated hydraulic parameters of sediment bypass tunnels in Switzerland and Japan.

No.	Name	Design discharge* ¹ [m ³ /s]	Maximum velocity* ² [m/s]	Velocity at outlet [m/s]	Uniform flow velocity [m/s]	Froude number* ³ [-]
1	Pfaffensprung	220	17	15	14	2.4
2	Egschi	50	12	10	10	2.0
3	Runcahez	110	20	10	9	1.4
4	Palagnedra	220	19	13	13	2.4
5	Rempen	80	14	12	12	2.8
6	Solis	170	13* ⁴	11	11	1.7
7	Nunobiki	39	n.s.* ⁵	7	7	1.4
8	Asahi	120* ⁶	12	12	12	2.2
9	Miwa	300	n.s.* ⁵	10	10	1.7
10	Matsukawa	200	n.s.* ⁵	15	15	3.1

*¹Design discharge under free surface conditions. *²Maximum velocity at end of acceleration section. *³Froude number referring to the uniform flow velocity. *⁴Maximum velocity downstream of radial gate. *⁵No data for acceleration section length and slope given. *⁶Referring to Harada et al. (1997). Data given in Sumi et al. (2004) differ.

The values have been determined by a one-dimensional backwater curve calculation considering a constant tunnel cross section area and equal geometries for the intake as for the tunnel cross section. This simplification may lead to a slight overestimation of the maximum velocity. The equivalent sand roughness is assumed to $k_s = 3$ mm and the Froude number at the intake is assumed to approx. $Fr = 1$, taking into account that transition from subcritical to supercritical flow occurs at the tunnel intake. One exception is the Solis sediment bypass tunnel which is operated under pressure conditions at the intake. Therefore the water depth is given by the maximum gate opening.

The following conclusions can be drawn: (1) Uniform flow velocities vary between 9 and 15 m/s. (2) In every bypass tunnel outlet uniform flow velocity is approximately achieved. (3) Discharge is always conducted in supercritical flow i.e. $Fr > 1$. (4) Flow velocities are high at the end of the acceleration section, varying between 12 and 20 m/s.

Table 3. Geologic parameters of sediment bypass tunnels in Switzerland.

No.	Name	Geology	Quartz content	Grain diameter d_m/d_{90} [cm]	Abrasion damage
1	Pfaffensprung	Granite	High	25/270	Major
2	Egschi	Grisons schist	Low	10/30	Mean
3	Runcahez	Gneiss	High	23/50	High
4	Palagnedra	Gneiss	High	7.4/16	High
5	Rempen	Flysh/Nagelfluh* ¹	Low	6/20	Low
6	Solis	Grisons schist	Low	6/15	Low–Mean* ²

*¹ Conglomerate rock in the European Alps also designated as gompholite. *² Estimated data.

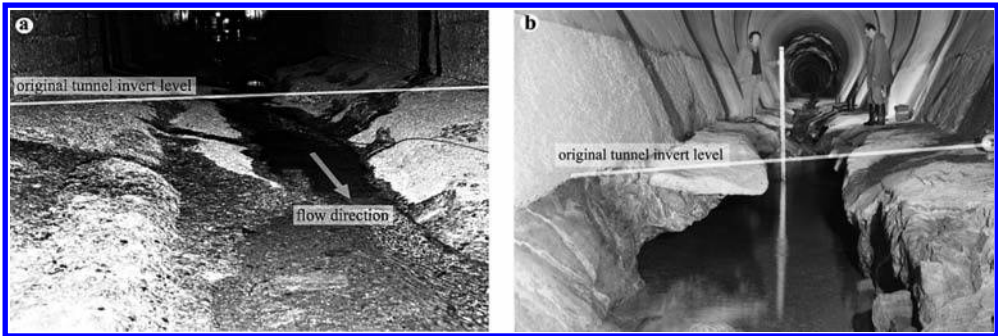


Figure 4. Severe abrasion damages at a) Runcahez bypass tunnel and b) Palagnedra bypass tunnel.

2.2.2 Abrasion problem

According to Chervet & Vischer (1996), Vischer et al. (1997), Sumi (2000, 2005), Sumi et al. (2004), and Inoue (2009) a severe problem affecting nearly all sediment bypass tunnels is the hydro-abrasion of the tunnel invert due to the combination of high flow velocities together with a great amount of transported sediment. Depending mainly on the geologic conditions in the catchment, the impact on the tunnel invert abrasion differs. Both high quartz content and high mean grain diameters contribute to high abrasion damages in the tunnel. Table 3 presents the geologic parameters of the Swiss bypass tunnels according to Chervet & Vischer (1996). It can be stated that hard rock like granite and gneiss combined with a high quartz content lead to high abrasion damages at the tunnel invert.

Figure 4 a shows an example of severe abrasion damage at the Runcahez bypass tunnel invert. The original tunnel cross section is of archway type implying a plain tunnel invert. Abrasion depths up to 1.20 m were measured (Jacobs et al. 2001). Figure 4 b shows severe abrasion damages at the Palagnedra bypass tunnel. Deep abrasion scour holes of several meters were observed after the extreme flood event in 1978 (Delley 1988).

3 FUTURE RESEARCH

Due to severe abrasion damages at the bypass tunnel invert the dam owners face, besides the construction costs, high investments for maintenance of the tunnel after almost every major flood event.

One effective approach to reduce hydroabrasive wear is the optimization of the hydraulic conditions in the sediment bypass tunnel. The basic hydraulic design neglecting the influence of sediment transport can be determined easily by analytical calculations or numerical simulations, respectively, but there is a major lack of knowledge when sediment transport

and abrasion are taken into account. An ongoing research project at VAW studies these processes and its decisive parameters by means of systematical hydraulic laboratory model tests. These are in detail the tunnel invert slope, the inflow conditions, the horizontal tunnel alignment, the tunnel cross section, and the sediment transport processes. Every parameter is varied systematically and flow velocities, invert shear stresses and invert abrasion are measured and compared with each other as well as with prototype data. The aim of this project is to establish general design criteria for optimal flow conditions where both sediment deposition in the tunnel is avoided and resulting abrasion damages are kept at a minimum.

Another possible approach to minimize abrasion damage is to strengthen the tunnel invert. Some fundamental research was done by Jacobs et al. (2001). Different invert materials, such as high cast basalt plates, standard concrete, steel fiber concrete, microsilica concrete, and polymer concrete were implemented and tested at Runcahez bypass tunnel and design recommendations are given. Unfortunately no direct correlation between the amount of transported sediment and abrasion depth was investigated due to the lack of sediment transport measurement techniques. Thus further research is needed to determine a direct correlation of transported sediment and abrasion depth, i.e. of impact and resistance. Therefore a research project will start in the next future at Solis bypass tunnel to fill this gap.

4 CONCLUSION

Reservoir sedimentation is a severe and increasing problem concerning nearly all reservoirs worldwide. The construction of a sediment bypass tunnel to route the sediments from the upstream to the downstream river reach is therefore a very effective countermeasure to stop or at least significantly decrease the sediment accumulation. Worldwide there are few bypass tunnels in operation up to date. Leading countries in sediment bypass tunnel construction are mainly Switzerland and Japan having eleven bypass tunnels in all.

In this paper, the state-of-the-art design of sediment bypass tunnels is presented. Descriptions of both tunnel operation and every individual sediment bypass tunnel element are given. These are namely the tunnel intake location, the method of tunnel operation, the design discharge, the guiding structure, the tunnel intake, the steeply sloped acceleration section, the smoothly sloped tunnel section, and the outlet structure.

Quasi all bypass tunnels in operation are facing an abrasion problem. Due to high flow velocities in combination with high sediment load abrasion of the tunnel invert is significant leading to major recurring maintenance costs. Having in mind that design of sediment bypass tunnels depends on both the hydraulic and the sedimentologic conditions a suitable layout is difficult. Whereas the basic hydraulic design is easy to determine, a crucial lack of knowledge exists in considering the sediment transport processes in the tunnel. Therefore a research project at VAW is launched focusing on sediment transport in bypass tunnels accounting for the invert abrasion.

ACKNOWLEDGMENTS

The authors would like to thank swisselectric research for their financial support.

REFERENCES

- Annandale, G.W. 1987. Reservoir sedimentation. *Developments in water science* No. 29. Elsevier Science Publishers B.V., The Netherlands.
- Auel, C., Berchtold, T. & Boes, R. 2010. Sediment management in the Solis reservoir using a bypass tunnel. *Proc. of the 8th ICOLD European Club Symposium*. Innsbruck, Austria.
- Basson, G.R. 2009. Management of siltation in existing and new reservoirs. General Report Q. 89, *Proc. 23rd ICOLD Congress*. Brasilia, Brazil.

- Boes, R. & Reindl, R. 2006. Nachhaltige Maßnahmen gegen Stauraumverlandungen alpiner Speicher [in German]. *Proc. Symposium "Stauhaltungen und Speicher—von der Tradition zur Moderne"*, Bericht 46/1, TU Graz, Austria: 179–193.
- Boillat, J.-L., De Cesare, G., Schleiss, A. & Oehy, C. 2000. Successful sediment flushing conditions in Alpine reservoirs. *Proc. Int. Workshop and Symposium on Reservoir Sedimentation Management*. 26–27 October 2000. Tokyo, Japan.
- Chervet, A. & Vischer, D. 1996. Geschiebeumleitstollen bei Stauseen; Möglichkeiten und Grenzen [in German]. *Int. Symposium: Verlandung von Stauseen und Stauhaltungen, Sedimentprobleme in Leitungen und Kanälen*, VAW-Mitteilung No. 143, ETH Zurich, 25–43.
- Delley, P. 1988. Erosionsschäden im Spülstollen Palagnedra und deren Sanierung [in French]. *Int. Symposium—Erosion, Abrasion und Kavitation im Wasserbau*, VAW-Mitteilung No. 99, ed.: D. Vischer, ETH Zurich, 329–352.
- Harada, M., Terada, M. & Kokubo, T. 1997. Planning and hydraulic design of bypass tunnel for sluicing sediments past Asahi reservoir. C. 9, *Proc. 19th ICOLD Congress*. Florence, Italy.
- Inoue, M. 2009. Promotion of field-verified studies on sediment transport systems covering mountains, rivers, and coasts. *Science & Technology Foresight Center, NISTEP*. Quarterly Review No. 33. 89–107.
- Jacobs, F., Winkler, K., Hunkeler, F. & Volkart, P. 2001. Betonabrasion im Wasserbau [in German]. *VAW-Mitteilung No. 168*, ed. H.-E. Minor, ETH Zurich.
- Kantoush, S. & Sumi, T. 2010. River morphology and sediment management strategies for sustainable reservoir in Japan and Switzerland. *Annuals of Disaster Prevention Research Institute*, No. 53 B. Kyoto, Japan.
- Kashiwai, J., Sumi, T. & Honda, T. 1997. Hydraulic study on diversion facilities required for sediment bypass systems. Q. 74, R. 59, *Proc. 19th ICOLD Congress*. Florence, Italy.
- Lai, J.-S. & Shen, H.W. 1996. Flushing sediment through reservoirs. *Journal of Hydraulic Research*: 34(2), 237–255.
- Mariño, J.J., Castro, H., Manjarrés, F., Gámez, J., Daza, A. & Alarcón, W. 2009. Sediment management at the Chivor hydroelectric project in Colombia. Q. 89 R. 15, *Proc. 23rd ICOLD Congress*. Brasilia, Brazil.
- Meshkati, M.E., Dehghani, A.A., Naser, G., Emamgholizadeh, S. & Mosaedi, A. 2009. Evolution of developing flushing cone during pressurized flushing in reservoir storage. *World Academy of Science, Engineering and Technology*: 58, 1107–1111.
- Müller, P. & De Cesare, G. 2009. Sedimentation problems in the reservoirs of the Kraftwerke Sarganserland—venting of turbidity currents as the essential part of the solution. Q. 89 R. 21, *Proc. 23rd ICOLD Congress*. Brasilia, Brazil.
- Schleiss, A. & Oehy, C. 2002. Verlandung von Stauseen und Nachhaltigkeit [in German]. *Wasser, Energie, Luft*, 94(7/8): 227–234.
- Schleiss, A., De Cesare, G. & Jenzer Althaus, J. 2010. Verlandung der Stauseen gefährdet die nachhaltige Nutzung der Wasserkraft [in German]. *Wasser Energie Luft*, 102(1): 31–40.
- Sloff, C.J. 1991. Reservoir sedimentation: a literature survey. *Communications on Hydraulic and Geotechnical Engineering Report No 91–2*, TU Delft, The Netherlands.
- Sumi, T. 2000. Future perspective of dam reservoir sediment management. *Proc. of Int. Workshop on Reservoir Sedimentation Management*. 145–156.
- Sumi, T. 2005. Sediment flushing efficiency and selection of environmentally compatible reservoir sediment management measures. *Int. Symposium on Sediment Management and Dams, 2nd EADC Symposium*. 25–26 October 2005. Yokohama, Japan.
- Sumi, T., Okano, M. & Takata, Y. 2004. Reservoir sedimentation management with bypass tunnels in Japan. *Proc. 9th International Symposium on River Sedimentation*. Yichang, China, 1036–1043.
- Sumi, T., Kobayashi, K., Yamaguchi, K. & Takata, Y. 2009. Study on the applicability of the asset management for reservoir sediment management. Q. 89 R. 4, *Proc. 23rd ICOLD Congress*. Brasilia, Brazil.
- Vischer, D. (ed.) 1981. *Int. symposium: Verlandung von Stauhaltungen und Speicherseen im Alpenraum* [in German]. VAW-Mitteilung No. 53, ETH Zurich.
- Vischer, D. (ed.) 1996. *Int. symposium: Verlandung von Stauseen und Stauhaltungen, Sedimentprobleme in Leitungen und Kanälen* [in German]. VAW-Mitteilung No. 142 & 143, ETH Zurich.
- Vischer, D., Hager, W.H., Casanova, C., Joos, B., Lier, P. & Martini, O. 1997. Bypass tunnels to prevent reservoir sedimentation. Q. 74 R. 37, *Proc. 19th ICOLD Congress*. Florence, Italy.

Numerical simulation of flow and sedimentation transport in the early stage of the Three Gorges Reservoir (TGR)

Renyong Huang, Xibing Zhang & Yue Huang
Yangtze River Scientific Research Institute, Wuhan, China

ABSTRACT: A numerical model for simulating unsteady flow and sediment transport in the mainstream and its tributaries at the TGR was presented in this paper. The validity of the model was checked with the observed data of the TGR from June 2003 to December 2009. Good agreement between the calculation and observed data was obtained. The simulation results show that this model could be used to simulate the flow and sediment transport at the TGR. The model can play its role in modeling and prediction about the optimal operation of the TGR in the future research work.

1 INSTRUCTIONS

Because sediment in the Three Gorges Project (TGP) is one of the key technical issues, TGP operators in china attach great importance to the issue. In the course of the sediment study of the TGP, the combining research methods of observation and investigation no the prototype, mathematical model and physical model tests were adopted, and a lot of research was achieved, it also promoted the development of the whole subject of sediment; Now the more mature 1-D mathematical models based on the non-equilibrium sediment transport theory were established by Yangtze River Scientific Research Institute and China Institute of Water Resources and Hydropower Research, and they played a basic and pivotal role in the sediment research of the TGP.

In previous research, most of the mathematical models were established based on the constant flow and sediment transport theory, which is reasonable and reliable for long period sedimentation processes of reservoir. however the river water sports and sedimentation processes of reservoir can not be reflected truly, because the unsteady processes of the water and sediment transport was overlooked. Therefore, it is necessary to study the sedimentation processes of the TGR with a mathematical model of unsteady flow and sediment transport. At the same time, the length of the TGR is about 700 km, and there are a lot of tributaries in the reservoir, because the inflow and the storage capacity of the tributaries are important too, in order to improve the calculated accuracy of reservoir, it is necessary to incorporated more tributaries into calculation. Based on these considerations, a 1-D numerical model of unsteady flow and sediment transport in the mainstream and its tributaries at the TGR was established and described in this paper.

Since June 2003 when the TGR has been commissioned, the Three Gorges Reservoir area had experienced significant changes in sedimentation characteristics of the reservoir and in sedimentation on the river from the basic balance of the overall shift continued siltation. In order to accurately understand the law of the flow and bed after the operation of the TGR, detailed observations were made by Hydrological Bureau of Changing Water Resources Commission. These data were valuable for the mathematical model validation and improvement. The validity of the model was checked with the observed data of the TGR from June 2003 to December 2009, including the simulation accuracy of the flood and sediment routing, water level variation and the silt evolvement. The reliability of predicted results was analyzed, and the new basis was provided for future improvement and application of the model.

2 MATHEMATICS MODEL

Because there are a lot of tributaries in the TGR, so the water and sediment movement of the mainstream and its tributaries should be considered when the 1-D numerical model of unsteady flow and sediment transport was established. If the mainstream and its tributaries were considered as a single river partly, and the river convergence point was named branching point, then the water and sediment mathematical model should include three parts of single river water and sediment movement equations and branching point connection equations and boundary conditions.

2.1 A single river water and sediment movement equation

The basic equations which describe water and sediment movement of a single river

Flow continuity equation:

$$\frac{\partial A_i}{\partial t} + \frac{\partial Q_i}{\partial x} = 0 \quad (1)$$

Momentum equation:

$$\frac{\partial Q_i}{\partial t} + \frac{\partial}{\partial x} \left(\frac{Q_i^2}{A_i} \right) + g A_i \left(\frac{\partial Z_i}{\partial x} + \frac{|Q_i| Q_i}{K_i^2} \right) = 0 \quad (2)$$

Sediment continuity equation:

$$\frac{\partial Q_i S_i}{\partial x} + \frac{\partial A_i S_i}{\partial t} + \alpha_i \omega_i B_i (S_i - S_{*i}) = 0 \quad (3)$$

Riverbed deformation equation:

$$\rho' \frac{\partial A_d}{\partial t} = \alpha_i \omega_i B_i (S_i - S_{*i}) \quad (4)$$

where ω = sediment velocity, corner i = section number, Q = discharge, A = the section area, t = time, x = the longitudinal coordinate, Z = water level, K = section discharge coefficient, S = sediment concentration, S_* = sediment carrying capacity, ρ' = the dry density of deposition, B = section width, g = gravity acceleration, α = coefficient of saturation recovery, A_d = river bed area.

2.2 Fork point connection equation

1. Water discharge convergence conditions

Discharge passing in and out must be corresponding with the practical water storage variety ratio.

$$\sum Q_i = \frac{\partial \Omega}{\partial t} \quad (5)$$

Ω represents the water storage of the fork point. Ω equals to zero when the point could be generated as a geometry point.

2. Dynamical joined condition

If fork point could be generated as a geometry point, the flow passing in and out the fork point is very slow, the water level turbulent condition is inexistent. The water level of each fork point section should be equal.

$$Zs_i = Zs_j = \dots = \overline{Zs} \quad (6)$$

2.3 Boundary condition

The boundary conditions were provided for the TGR when the mainstream and its tributaries were considered as a whole, but they will not be provided for a single river of the TGR. The water discharge process and sediment concentration process will be provided for the imports of the mainstream and its tributaries, and the water level process or the water discharge process or the relations of water level and discharge.

2.4 Treatment of the problem

1. Riverbed deposition distribution and gradation adjustment

Three-layer model was used to solve the mode of riverbed sediment exchange and gradation adjustment in this paper, so the riverbed deposition was generated as three layers of surface, middle and base. Surface is the sediment exchange layer, middle is the transition layer, and base is the sediment erosion terminal layer. The regulation is that the interface of each layer is fixed in each calculated period, sediment exchange is limited in the surface layer and the middle and base layer is not affected at this step. At the end of the time, the surface layer and middle layer would be removed up or down according to the erosion or deposition of the riverbed, and the thickness of the two layers retain fixed. Then the base thickness would change along with the thickness of scour and silting.

2. Sediment transport capacity calculation

Sediment transport capacity equations:

$$S_* = k \frac{u^{2.76}}{h^{0.92} \omega_m^{0.92}} \quad (7)$$

$$\omega_m^{0.92} = \sum_{L=1}^8 p_L \omega_L^{0.92} \quad (8)$$

where p_L = the size class L gradation, ω_L = the settling velocity of sediment particles of the size class L , S_* = sediment carrying capacity, u = the average velocity of flow, κ = sediment carrying capacity coefficient (reservoir is 0.03, natural river is 0.02).

3. Coefficient of saturation recovery α

Sediment saturation recovery coefficient is an important parameter in mathematical model, it is a comprehensive factor and need to deduce from the measured data. However, it can be influenced by many factors, such as flow and sediment conditions, and it changes all the time, in most of the sediment deposition calculations the sediment saturation recovery coefficient is assumed to be a positive constant, and gradually adjusted by verifying information. Sediment transport is calculated by sub-grain size in this model, the size of each group have taking the same value about α . As each group settling velocity difference between the sand is up to several times or even hundreds of times from the calculation result, small grain size relative to the large size group for the erosion and deposition volume is often negligible in the same section, then this often not match the actual from the measured data of sediment grain size entering into the TGR since the impoundment. The grain sizes of sediment sorting along the way are very prominent; there are many researches about the value of coefficient of saturation recovery nowadays, basically, having the following consensus: (1) Sediment in different size groups have different saturation recovery coefficient, (2) Coefficient of saturation recovery value should decreases with sediment grain size increases, (3) Coefficient of saturation recovery should vary with changes in space and time, the following experience formula was used in

this model for the calculation of the size of groups of different coefficient of saturation recovery:

$$\alpha_L = 0.25 * \left(\frac{\bar{\omega}}{\omega_L} \right)^\lambda \quad (9)$$

$$\bar{\omega} = \sum_{L=1}^8 p_L \omega_L \quad (10)$$

where $\bar{\omega}$ represents the average velocity of sediment in the entrance of the main stream of Zhuotuo station, settling velocity of the Group 5 is very close to the average velocity of sediment of Zhutuo station in 60 series and 90 series, the settling velocity of the Group 5 is used as the average velocity of sediment at last in order to be calculated easily. Index $\lambda = c/J$, in which J represents the hydraulic gradient, $c = 0.833 \times 10^{-10} \bar{Q}$, \bar{Q} represents the annual average flow at dam site.

4. Node sediment distribution

Node sediment distribution is determined by the boundary conditions of each reach section nearly the node, including riverbed landform condition and the angle of each river reach main stream and node main stream, and it is also affected by the sediment condition coming from the upstream. In this mode it is assumed that sediment distribution ratio equal to discharge distribution ratio.

$$S_{j,out} = \frac{\sum Q_{i,in} S_{i,in}}{\sum Q_{i,in}} \quad (11)$$

3 MATHEMATICS MODEL SOLUTIONS

3.1 Flow equation solution

A three-gradation method was applied to solve the flow governing equation. The equations (1) and (2) are difference equations which were created by four-point implicit Preissmann scheme.

$$B_{i1} Q_i^{n+1} + B_{i2} Q_{i+1}^{n+1} + B_{i3} Z S_i^{n+1} + B_{i4} Z S_{i+1}^{n+1} = B_{i5} \quad (12)$$

$$A_{i1} Q_i^{n+1} + A_{i2} Q_{i+1}^{n+1} + A_{i3} Z S_i^{n+1} + A_{i4} Z S_{i+1}^{n+1} = A_{i5} \quad (13)$$

In which the coefficient were all deduced from the practical conditions.

If section numbers of a river reach were m , and the equations (12) and (13) are self eliminated self, we would gain the water level and water discharge relations of river first section and last section after the all unknown quantities were expressed as one function of unknown quantities of nodes by recursive relations.

$$Q_1 = \alpha_1 + \beta_1 Z S_1 + \delta_1 Z S_m \quad (14)$$

$$Q_m = \theta_m + \eta_m Z S_1 + \gamma_m Z S_m \quad (15)$$

In which the coefficient of α_1 , β_1 , δ_1 , θ_m , η_m , and γ_m were all educed by the recursive relations.

The equations whose unknown quantities were node water level of the mainstream and its tributaries will be set with boundary conditions, water level and discharge relations of river first section and last section and the branching point connection equation then we would get the value of water level at each node by solving the set of equations. At last, we could get all unknown quantities of water level and discharge by generating back gradually.

3.2 Sediment solution

Obvious format was applied to create the equation (3) of sediment transport

$$S_i^{j+1} = \frac{\Delta t \alpha_i^{j+1} B_i^{j+1} \omega_i^{j+1} S_{*i}^{j+1} + A_i^j S_i^j + \frac{\Delta t}{\Delta X_{i-1}} Q_{i-1}^{j+1} S_{i-1}^{j+1}}{A_i^{j+1} + \Delta t \alpha_i^{j+1} B_i^{j+1} \omega_i^{j+1} + \frac{\Delta t}{\Delta X_{i-1}} Q_i^{j+1}} \quad (16)$$

We would obtain the equation (17) from the equation (4) of riverbed deformation equation.

$$\Delta A s_i = \frac{\Delta t (Q_{i-1}^{j+1} S_{i-1}^{j+1} - Q_i^{j+1} S_i^{j+1})}{\Delta X \rho'} + \frac{A_i^j S_i^j - A_i^j S_i^j}{\rho'} \quad (17)$$

We would get the sediment concentration of each section from top to bottom of each river reach according to equation (16) after the water level and water discharge of each section were obtained. In this model it is assumed that sediment distribution ratio is equal to discharge distribution ratio, then the riverbed deformation will be finally calculated according to equation (17).

4 MATHEMATICS MODEL VALIDATIONS

4.1 Calculated condition

The domain of calculation is from Zhutuo station of main stream to the dam of the TGR, its length is about 700 km (Figure 1). Including 14 tributaries as Jialing River, Wu River, Qi River, Mudong River, Dahong River, Longxi River, Quxi River, Long River, Xiao River (including tributaries as Nan River, Dong River and Puli River), Meixi River, Daning River, Yandu River, Qinggang River, Xiangxi River. The landform of Zhutuo station to Lidu station is the observed data in 1996, the landform of Lidu station to the dam of the TGR is the observed data in 2003 before storage of the TGR. Daily average discharge and sediment concentration from June 1, 2003 to December 31, 2009 of main stream Zhutuo station and Jialing River Beibei station and Wu River Wulong station were adopted as inlet condition, corresponding day by day average water level of Miaohe station was adopted as outlet condition. The interval flow was assigned to the tributaries of the TGR, and the interval sediment was not considered in calculation.

4.2 Validation of water level and discharge

According to available measured data, the measured water level and discharge process of some the hydrological stations from 2003 to 2004 were chosen to compare with the model calculation and the results were shown in Figure 2 and Figure 3, Table 1 is the highest flood level validation of the TGR in 2004. From the chart, the model simulation of the propagation of flood and

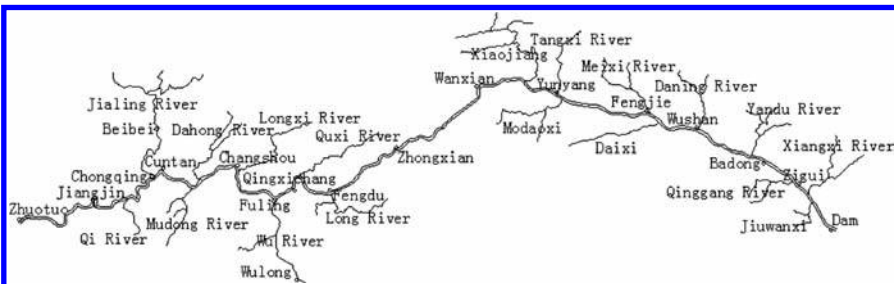


Figure 1. Schematic diagram of the TGR.

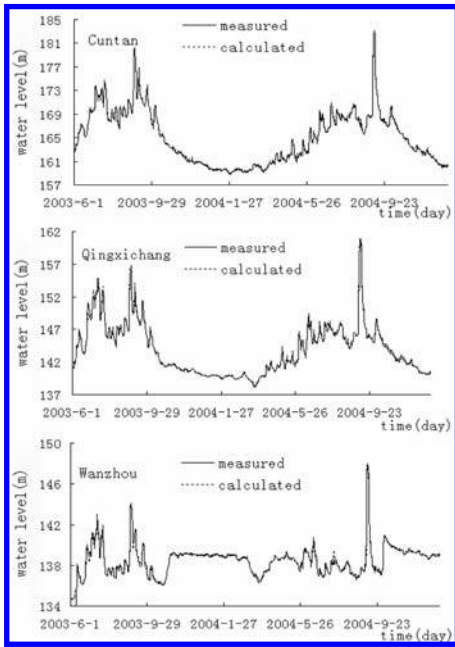


Figure 2. Validation of water level process.

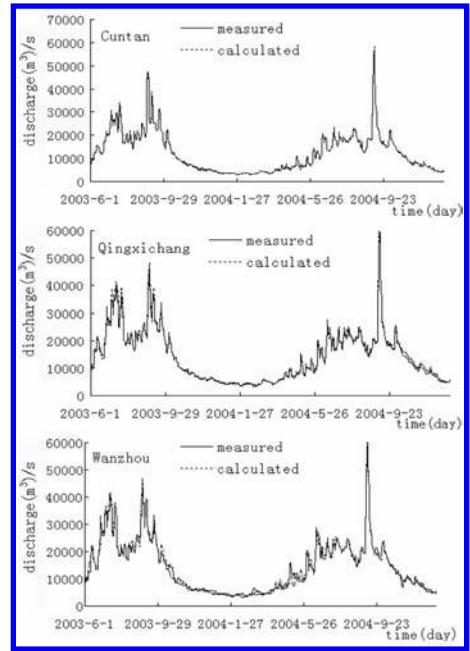


Figure 3. Validation of water discharge process.

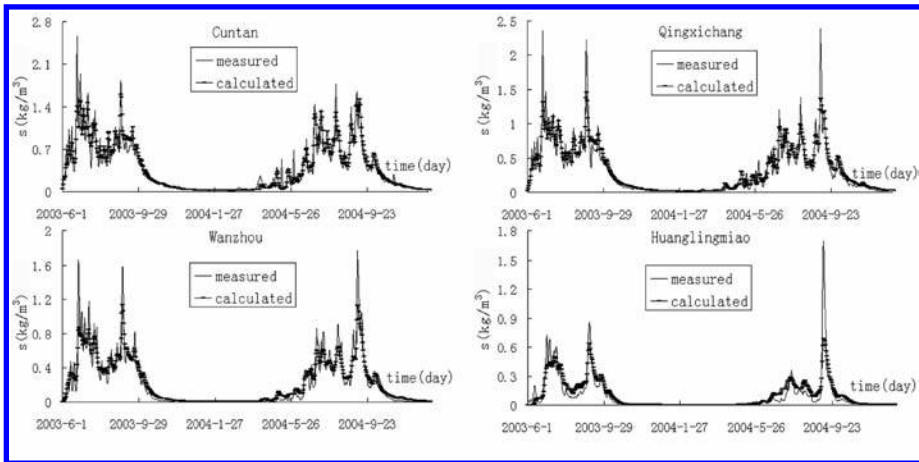


Figure 4. Validation of sediment concentration process.

water level change process is consistent with the observed situation along the hydrological stations, the highest flood peak water level calculated and measured values occurred almost simultaneously, the model validation results were in good agreement with the measured values.

4.3 Sediment transport volume validation of mainstream station

Fig. 4 is the validation of the sediment concentration process of some stations from 2003 to 2004. The calculation results of each station are consistent with the measured values basically. But the calculation of the peak sediment is smaller than the measured value, and the small flow calculation is slightly larger, since the calculated values were close to the measured values during most of the time. Therefore, the calculated values of cumulative sediment discharge throughout the year is still relatively close to the measured value (see Table 2).

Table 1. The highest flood level validation of the TGR in 2004 Unit: m.

Station	Water level (Wusong)		Level error	Date (month. Day)	
	Observed	Calculated	Absolute value	Observed	Calculated
Cuntan	183.14	183.20	+0.06	9.7	9.7
Changshou	171.44	171.43	-0.01	9.7	9.7
Qingxichang	160.81	160.83	+0.02	9.8	9.7
Zhongxian	151.54	151.23	-0.31	9.8	9.8
Wanzhou	147.92	147.98	+0.06	9.8	9.8
Fengjie	144.07	144.17	+0.10	9.9	9.9
Beibei	199.83	199.88	+0.05	9.6	9.6
Wulong	185.52	185.56	+0.04	6.24	6.24

Table 2. Sediment discharge validation of some stations Unit: a hundred million ton.

Year	Cuntan		Qingxichang		Wanzhou		Huanglingmiao	
	Observed	Calculated	Observed	Calculated	Observed	Calculated	Observed	Calculated
2003	2.03	2.14	2.08	2.08	1.58	1.58	0.84	0.85
2004	1.73	1.79	1.66	1.73	1.23	1.23	0.64	0.58
2005	2.70	2.67	2.54	2.53	1.85	1.85	1.03	1.00
2006	1.09	1.11	0.96	1.02	0.63	0.63	0.089	0.093
2007	2.10	2.20	2.17	2.08	1.29	1.29	0.51	0.46
2008	2.13	2.31	1.89	2.07	1.14	1.14	0.322	0.321
2009	1.73	1.89	1.82	1.85	1.00	1.00	0.36	0.29
Total	13.5	14.1	13.1	13.4	8.72	8.72	3.79	3.59

Note: 2003 equal to 2003.6.1–2003.12.31.

4.4 Validation of the deposition volume and the discharged sediment ratio

Table 3 and Table 4 present the siltation and discharged sediment ratio validation of the TGR respectively then from the deposition process, distribution and sediment deposition ratio calculation results; the calculated and measured values are in good agreement. Selected Zhutuo to dam as statistical range, and counted by sediment budget method, to the end of 2009, for the Section Zhutuo to Qingxichang, and Section Qingxichang to dam, and the whole reservoir area, the calculated deposition volume were 1.392×10^8 t and 9.773×10^8 t and 11.18×10^8 t respectively, they were close to the corresponding measured values of 1.631×10^8 t and 9.338×10^8 t and 10.97×10^8 t. From the view of the amount of accumulated sediment, the relative error of the whole reservoir cumulative deposition between the model calculation and measured values was 1.9%. From the view of the discharged sediment ratio validation, the relative error of the cumulative discharged sediment ratio between the model calculation and measured values was 1.4%. Satisfactory verification results was obtained not only for the year in which the discharged sediment ratio was relatively large (e.g. 2005), but also for the year in which the discharged sediment ratio was relatively small (e.g. 2006).

5 CONCLUSIONS

In previous research, most of the mathematical models were established based on the steady flow and sediment transport theory. Unsteady modelization of the water and sediment transport processes and taking into account of more tributaries were considered in this paper. Based on the basic idea of three-gradation method, a numerical model for simulating unsteady flow and sediment transport in the mainstream and its tributaries is presented in this paper, with an improved water and sediment calculated accuracy. The validity of the model was

Table 3. Calculated results of deposition volume and distribution Unit: a hundred million ton.

Year	Zhutuo to Qingxichang		Qingxichang to dam		The whole reservoir		err (%)
	Observed	Calculated	Observed	Calculated	Observed	Calculated	
2003	0.241	0.244	1.239	1.224	1.481	1.469	-0.8
2004	0.261	0.192	1.023	1.153	1.284	1.347	4.9
2005	0.241	0.249	1.510	1.529	1.751	1.780	1.7
2006	0.238	0.178	0.873	0.928	1.111	1.107	-0.4
2007	0.224	0.310	1.658	1.623	1.882	1.936	2.9
2008	0.421	0.243	1.571	1.752	1.992	1.998	0.3
2009	0.005	-0.024	1.464	1.564	1.469	1.544	5.1
Total	1.631	1.392	9.338	9.773	10.97	11.18	1.9

Table 4. Comparison between the calculated and observed data of Discharged sediment ratio Unit: a hundred million ton.

Year	Sediment storage a = Zhutuo + Beibei + Wulong			Sediment storage b = Storage control stations		
	Sediment storage	Discharged sediment ratio		Sediment storage	Discharged sediment ratio	
		Observed	Calculated		Observed	Calculated
2003	2.322	36.2%	36.6%	2.08	40.4%	40.9%
2004	1.923	33.3%	30.2%	1.66	38.6%	34.9%
2005	2.777	37.1%	36.0%	2.54	40.6%	39.4%
2006	1.19	7.5%	7.8%	1.021	8.7%	9.1%
2007	2.392	21.2%	19.2%	2.204	23.0%	20.9%
2008	2.314	13.9%	13.9%	2.178	14.8%	14.7%
2009	1.829	19.7%	15.9%	1.829	19.7%	15.9%
Total	14.747	25.7%	24.4%	13.512	28.0%	26.6%

checked with the observed data of the TGR from June 2003 to December 2009. The result indicates that the calculated water level process, the discharge process, the sediment volume and the discharged sediment ratio all agree well with the observed data. The validated results show that this model has good accuracy for the calculation of unsteady sediment transport, and it was suitable for the simulation of the flow and sediment transport at the TGR. The model would be able to provide technical support for erosion prediction and optimal operation at the TGR.

ACKNOWLEDGEMENT

This work is supported by the National Science and Technology Research Project Support Program (NO. 2008BAB29B08), and Ministry of Water Resources nonprofit industry-specific (NO. 200901002, 200901003).

REFERENCES

- Peng Yang and Zhang Hongwu, 2006. 1-D numerical simulation of unsteady flow and sedimentation transport at the TGR. *Journal of Hydrodynamics*, No. 6, pp. 285–292.
- Xie Jianheng, 1988. *River simulation*. Press of Water Resource and electricity, pp. 111–116.
- Zhang Ruijin, 1983. *River sediment dynamics*. Press of Water Resource and electricity.

Hybrid modeling of sediment management during drawdown of Räterichsboden reservoir

G. Möller & R.M. Boes

Laboratory of Hydraulics, Hydrology and Glaciology (VAW), ETH Zurich, Zurich, Switzerland

D. Theiner & A. Fankhauser

Kraftwerke Oberhasli AG (KWO), Innertkirchen, Switzerland

M. Daneshvari, G. De Cesare & A.J. Schleiss

Laboratory of Hydraulic Constructions (LCH), EPFL, Lausanne, Switzerland

ABSTRACT: The Swiss utility Kraftwerke Oberhasli AG (KWO) currently implements “KWO plus”, an upgrading program involving a large number of economical and ecological improvements of their hydropower schemes. A major project, the modification of the Handeck 2 power plant intake, requires total emptying of the Räterichsboden reservoir having an active volume of 25 million m³. In order to define the most efficient and ecological emptying process for these circumstances, KWO commissioned a hybrid modelling program of the sediment remobilisation processes during the planned reservoir drawdown. Hydraulic model tests were conducted at the Laboratory of Hydraulics, Hydrology and Glaciology (VAW) by means of a 1:35 scaled Froude model. Numerical simulations of sediment transport were performed by the Laboratory of Hydraulic Constructions (LCH) using the software FLOW-3D. A good agreement between both models was found for total values of the sediment concentration and its variation in time. Both the physical and the numerical model were validated by prototype data obtained during an annual functional test of the bottom outlet. These measurements were conducted at three downstream positions in the Aare River. The involved solution procedures provide the (1) sediment flux during pressure flushing, (2) influence of outlet gate opening height and opening velocity on sediment concentration, and (3) time-dependent distribution of sediment concentration along the Aare River.

1 INTRODUCTION

1.1 *Background and project context*

The Swiss utility Kraftwerke Oberhasli AG (KWO) currently implements “KWO plus”, an upgrading program involving a large number of economical and ecological improvements of their hydropower schemes. One major project involves upgrading the Handeck 2 and Handeck 3 power plants by enhancing the installed capacity from 145 to 230 MW, resulting in an increase in intake discharge from 42.5 to 65.5 m³/s.

In order to install preventive measures against vortices, the intake structure has to be modified. Also, because of the limited hydraulic capacity of the existing pressure tunnel with an inner diameter of 3.0 m, a second, parallel pressure tunnel with an inner diameter of 4.1 m will be constructed. Even if the power plant will remain in service for most of the construction time of the parallel headrace tunnel, the Handeck 2 intake will be out of service during the construction of the diversion between the two tunnels and the joint right before the surge chamber. For both constructive measures, i.e. the anti-vortex cover and the connections between the existing headrace tunnel and the new parallel tunnel, it is necessary to empty the Räterichsboden reservoir. All engineering works are to be completed in the period from mid 2012 to mid 2014.

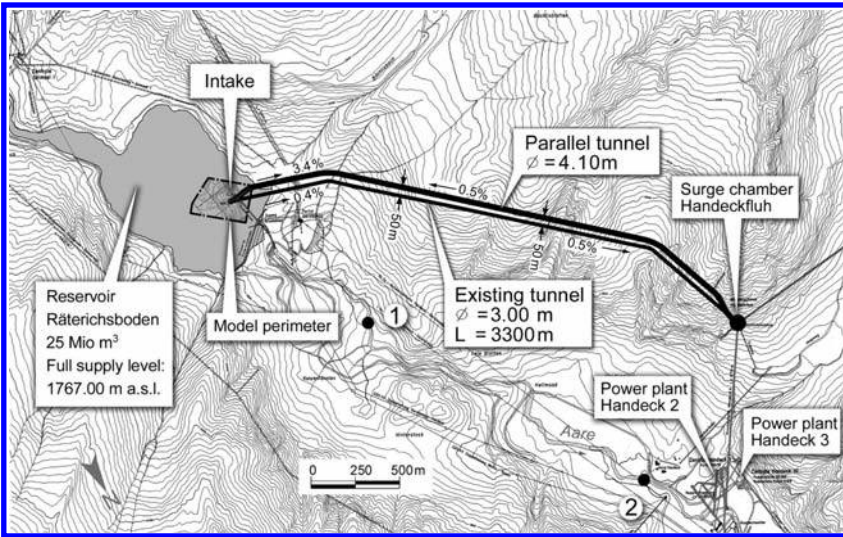


Figure 1. General arrangement of the hydropower plant including in-situ measurement sections no. 1 and 2 in the Aare river during flushing operation according to Table 1.

Using the bottom outlet for reservoir emptying, a certain sediment flushing is unavoidable during the process, with all its environmental impacts. During the last periodic yearly tests of the bottom outlet gate, recordings of sediment concentrations have been made. Also, in 1991 the Räterichsboden reservoir was totally emptied because of exceptional maintenance works. Sediment load and turbidity were registered downstream. Boillat et al. (2010) investigated the sediment flow out of the Grimsel reservoir, through the Aare reaches as well as inside the Räterichsboden reservoir by turbidity currents.

In the frame of elaborating documents for the environmental impact assessment, the question arose whether there are ways to reduce sediment concentration during the reservoir drawdown, for which two processes can be distinguished in general: (i) pressure flushing and (ii) free-flow flushing. Flushing under pressure is to release water through the bottom outlets by keeping the reservoir water level high. Free-flow flushing means releasing water by emptying the reservoir and also routing inflowing water from upstream through the reservoir by providing riverine conditions (Morris & Fan 1998).

This paper focuses on the study of the pressure flushing process, which was examined by (i) physical modelling, and (ii) numerical modelling. Both processes have been validated by measurements taken during the annual gate functional test in September 2010.

1.2 Description of hydropower plant

Both the Handeck 2 and the Handeck 3 power plants are fed by a common catchment area of about 52 km². Since the direct catchment area of the Räterichsboden reservoir comprises just about 9.5 km², most of the annual water volumes are conveyed through a subsidiary adduction tunnel from the Mattenalpsee reservoir (about 2 million m³), which is also fed, to smaller parts, by various other water intakes. The Räterichsboden reservoir has a storage volume of about 25 million m³, while annual inflow adds up to about 129 million m³. The average monthly inflow rates lie between 11 m³/s in July and less than 0.3 m³/s in the winter months.

The Handeck 2 and the later built Handeck 3 plant dispose of a common intake structure at the Räterichsbodensee reservoir. While the current structure is designed for an operating flow of $Q_d = 42.5$ m³/s, the Handeck 2 upgrading provides for an intake of $Q_d = 65.5$ m³. Model test showed that the installation of anti-vortex devices will be necessary.

Figure 1 depicts the general arrangement of the existing plant; Figure 2 shows the existing structure for the power and the bottom outlet intakes.

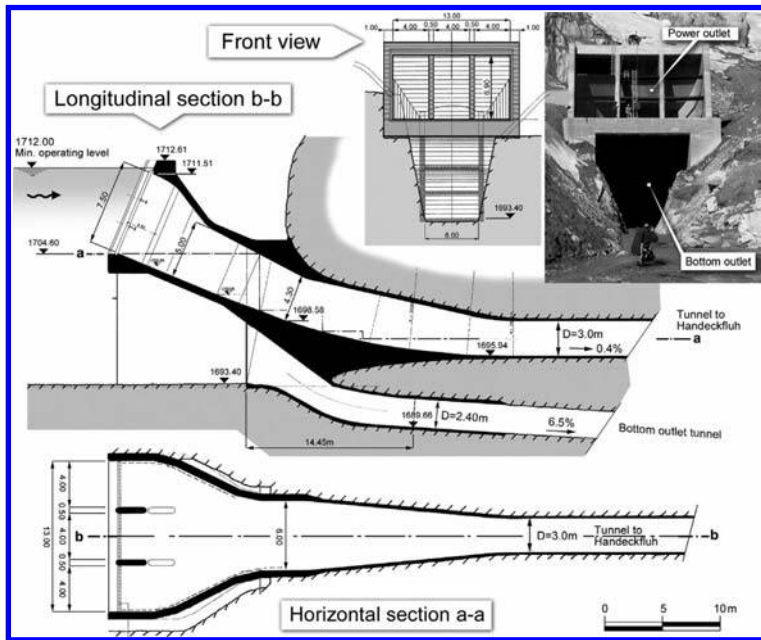


Figure 2. Intake structure of HPP Handeck 2 and 3 with power intake and bottom outlet.

1.3 Planned procedure based on experience from reservoir drawdown in 1991

The planned reservoir emptying should mostly be based on the experiences obtained during a similar operation in 1991, which had been rigorously monitored by limnologists. Foremost, the lowering of the water level will be obtained by turbinning, until the lower edge of the intake structure will be reached (1704.60 m a. s. l.). Below a critical water level, machine power output will be limited to avoid vortex formation. Subsequently, the bottom outlet will be opened and pressure flushing begins. Finally, free-flow flushing and erosion occurs, until the lake bottom and a constant slope of the flushing funnel are reached.

In a concept phase, KWO had also studied alternative measures as well as pre- and post-flushing operations. These studies led to the conclusion that reservoir dredging or pumping was not a viable alternative to desilt the vicinity of the intake structure because of the harsh climatic conditions during the emptying period in winter, the lack of landfill sites, and the low flows in the nearby tributaries. Experiences of KWO showed that costly damages occurred while turbinning sediment-laden water at the Innertkirchen plants, even if sediment concentrations were comparably low (around 1–1.5 g/l).

2 METHODS

For the reasons mentioned, a reservoir drawdown with subsequent flushing process is required. It is planned to start the flushing gradually with water of low sediment concentration. These preflushing operations allow the invertebrates in the downstream Aare river to enter into interstices in the riverbed where they find better shelter from the main flushing surge wave. Also, fish have the possibility to find suitable places where they can better withstand the increasing current and sediment load (Staub 2002). Moreover, post-flushing procedures are planned, in order to eliminate fine sediment deposits in the reaches downstream of the reservoir.

Clarifications had to be made to check whether the flushing process itself could be positively influenced and made as ecologically sound as possible. In order to define the most efficient and ecological emptying process for these circumstances, KWO commissioned a

hybrid modelling program of the sediment remobilisation processes during the planned reservoir emptying consisting of:

1. Hydraulic model tests,
2. Numerical simulations of sediment erosion and transport process,
3. Validation of both models by prototype data.

The hydraulic model tests were conducted at the Laboratory of Hydraulics, Hydrology and Glaciology (VAW) in a 1:35 scaled Froude model. Numerical simulations of sediment transport were performed by the Laboratory of Hydraulic Constructions (LCH) using the software FLOW-3D. Validation of both the hydraulic and the numerical model was done with prototype data obtained during an annual functional test of the bottom outlet. Measurements of sediment concentration were conducted at three downstream positions in the Aare River. The time-dependent sediment concentration was obtained by correlating continuous turbidity-sensor measurement data with laboratory results from conventional samples.

These procedures provide the (1) sediment flux during pressure flushing, (2) influence of outlet gate opening height and opening velocity on sediment concentration, and (3) time-dependent distribution of sediment concentration along the Aare River.

2.1 Hydraulic model tests (VAW)

KWO commissioned VAW in April 2009 with a physical model investigation on the designed hydraulic scheme. The model tests comprised the analysis of vortex formation at the intake structure and possible counter measures as well as the mobilisation and the transport of sediments through the bottom outlet.

The perimeter of the model around the intake structure reproduced a section of about 300×200 m of the Räterichsboden reservoir including the terrain topography and about 70 m of the tunnel system (cf. Figure 3). The model scale of 1:35 complies with common limit values of surface tension and viscosity of a Froude model for the investigation of vortex formation by intakes (Möller et al. 2010).

The bottom outlet is situated directly below the intake structure (Figure 2). The possible mobilisation of the deposited sediment will be tested in a subsequent project phase. The sediments in the Räterichsboden reservoir are very fine, thus having cohesive effects due to a considerable share of the sediment size below the silt limit (Figure 4). A transformation of the given sediment to the hydraulic model is therefore not possible for a scale of 1:35. In the frame of a preliminary sensitivity study VAW has tested several types of sediment material and size distribution in the model such as medium sand, quartz sand and plastic granular material. The results obtained regarding sediment release through the bottom outlet and cone formation in the reservoir were similar. The finest sediment (fine sand with $d_m = 0.17$ mm) was finally chosen for the main flushing experiments in view of the fact that the model only allows a qualitative prediction of the sediment movements. The initial sediment elevation

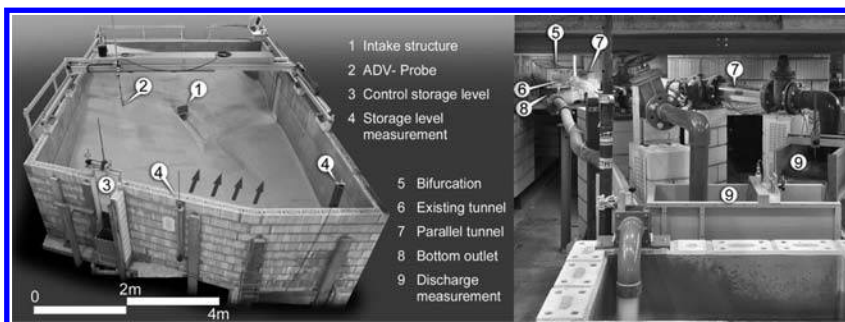


Figure 3. Hydraulic model at VAW. Left: view into the tank with partial reservoir topography; right: modelled tunnel system.

was defined as a constant surface all over the reservoir at 1704.60 m a. s. l. starting from the lower part of the power intake (see Figure 2). According to VAW's experience gathered with other projects on reservoir sedimentation, a funnel in the close-up range of the bottom outlet is expected to be formed and only a small amount of sediment would consequently be activated. This is in agreement with the findings of Meshkati et al. (2009) who analysed the effect of the water level and flow velocity in pressurized flushing operations. Sinniger et al. (2000) used an on-site bathymetric survey before and after pressure flushing operations at the Luzzone reservoir and observed similar flushing cone development.

2.2 Numerical simulation (LCH)

Numerical simulations of sediment transport were performed by the Laboratory of Hydraulic Constructions (LCH) using the software FLOW-3D. The numerical simulation was run by activating the sediment scour model in the program. The geometry of the Räterichsboden Reservoir (xyz file), intake gallery, bottom outlet and dam were inserted into FLOW-3D as a stereo lithography (stl) file created beforehand in several software packages. The geometry is based on the one realized at VAW. Figure 5 shows the created stl files for the reservoir and its outlets.

The water surface level was always held constant for the simulated scenarios. Sediment elevation was equal to the VAW model tests. The total number of cells in the computational space while modelling the reservoir reached some 2.1 million. The computational cells had a finer size (1 cm) around and in front of the intake and became coarser for the other regions with less importance in x-flow, y-flow and in z-vertical direction. With the intention of saving time and space for the result files, the meshing defined only the part of the reservoir directly concerned by the flushing process. Model simulation time was about 210 seconds corresponding to about 20 minutes at prototype scale. The output file size for each scenario was about 17 GB. In accordance with the hydraulic model (fine sand) the average diameter of the sediment was introduced as $d_m = 0.17$ mm with a density of 2707 kg/m³ and 32.4° as angle of repose in all the computed scenarios. The boundary conditions were defined as follows: symmetry in $Y_{\min, \max}$

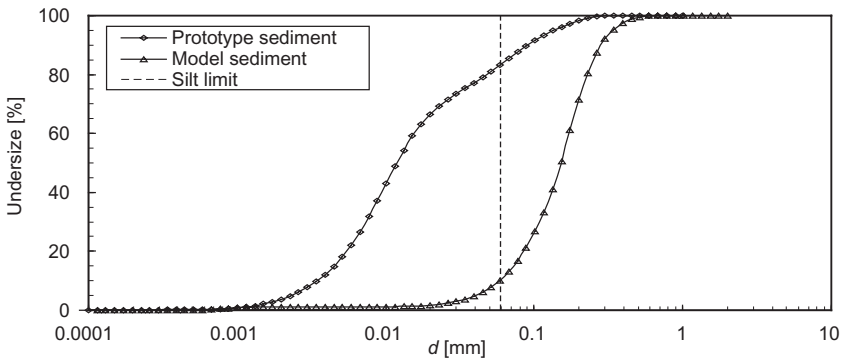


Figure 4. Particle size distribution from laser scattering of prototype and model sediment (fine sand).

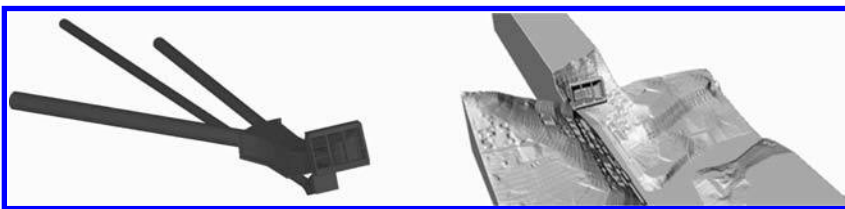


Figure 5. Intake structure and topography in numerical model, perspective of tunnel system (left); view of Räterichsboden reservoir (right).

Table 1. Measurement sections in the Aare river.

No.	Section name	Flow distance from bottom outlet
1	Bogenbrücke, Wanderweg	0.8 km
2	Gelmerbahnbrücke	3.1 km
3	Strassenbrücke Rotloui	8.0 km

and $Z_{\min, \max}$. The symmetric boundary condition implies no flux in any property across the boundary and no shear. The boundary condition at X_{\max} is defined as constant reservoir water surface level during flushing allowing water to flow in uniformly for mass conservation; at X_{\min} a volume flow rate was defined as discharge through the bottom outlet.

2.3 Model validation by prototype data (KWO)

Validation of both the hydraulic and the numerical models has been made using prototype data obtained during an annual functional test of the bottom outlet. Measurements of sediment concentration were conducted at three downstream positions in the Aare River during the 2010 functional test as given in Table 1 (cf. also Figure 1).

At all sections, turbidity measurements with scattered light photometer and receptor as well as sediment load measurements using Imhoff cone were made. Turbidity measurements at section 1 were performed with a probe recording not only turbidity but also the dissolved oxygen content (O_2) of the river flow. The turbidity sensors used are based on the backscattering method, operating with infrared light. Data was recorded at intervals of less than 1 minute. Since there is no universal relationship between turbidity (here NTU) and suspended sediment concentration (SSC) (Truhlar 1976), a gauging process is necessary. To correlate the turbidity measurements to the sediment load, water samples have been taken at intervals of about 2–5 minutes. Sediment load was to settle in the Imhoff cone, the declared settling time was 30 minutes.

The 2010 annual inspection of the Räterichsboden reservoir bottom outlet was conducted on 14 September 2010, starting at 09:00. The bottom outlet consists of a sluice gate with the main dimensions opening height $h = 1.3$ m and opening width $b = 1.0$ m. On the day of the functional test, the reservoir level was at 1760.49 m a. s. l., which equals to a pressure of 81.86 mWC above the bottom outlet invert. To allow for a better inspection, gate opening occurred stepwise until an opening of about 61% was reached (0.8 m), corresponding to a theoretical outflow of about 24.6 m³/s. After about 25 minutes, the gate was closed again.

3 RESULTS AND DISCUSSION

3.1 Hydraulic model (VAW) vs. numerical simulation (LCH)

All tests conducted in the hydraulic model study were also re-studied with the numerical model. Additionally the water level and the opening speed of the gate were also varied during the numerical model runs. Figure 6 shows two relatively identical test results of suspended sediment concentrations for fine sand sediment with rapid opening of the gate (VAW-LCH 1) and a prototype gate opening speed of about 0.25 m/min (VAW-LCH 2), respectively. The agreement of the peaks in terms of absolute value and timing is good. However, the decrease in concentration after the peak is different for lower water levels and slow gate opening (VAW-LCH 2). In contrast, at high water levels (VAW-LCH 1), the overall distribution curve agrees well except for the descending part with $t > 4$ min. e.g., after only 10 min (prototype value) the concentration reaches about 10 g/l in the hydraulic model, whereas the numerically simulated concentration value remains higher than 50 g/l.

So far, the comparison between hydraulic and numerical model results has generally shown good agreement. The outcome of some tests is therefore to some extent disturbing. While the result from the numerical simulation shows the expected behaviour, the concentration curve of the hydraulic model seems to be misleadingly delayed. Possible explanations are gallery

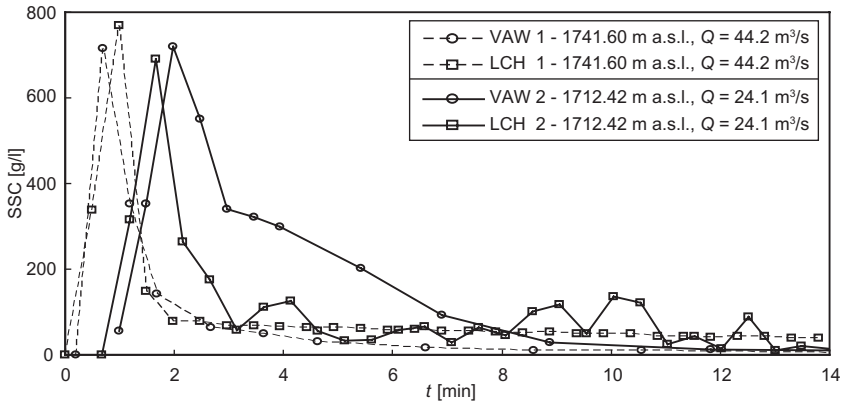


Figure 6. Suspended sediment concentration (SSC) over time t for fine sand at high water level with rapid gate opening (VAW-LCH 1) and low level with prototype gate opening (VAW-LCH 2).

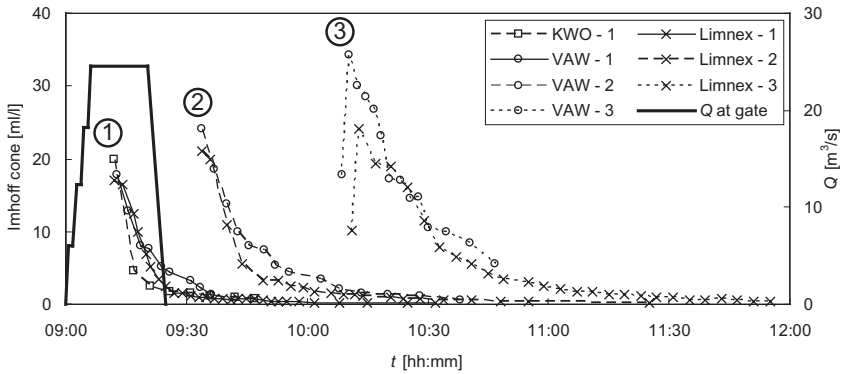


Figure 7. Comparison of sediment load determined by Imhoff cone in-situ measurements on 14 September 2010. The theoretical discharge Q due to gate opening value is shown. Sections according to [Table 1](#).

clogging, model scale effects, especially for low water levels as well as the initial boundary condition (compactness) of the sediment deposits that possibly mobilized only after a certain time. The shapes of both curves and removed volumes correspond well, however.

3.2 In-situ measurements on 14 September 2010

The sampling during the annual functional test of the bottom outlet was done at three locations (see [Table 1](#) and [Figure 1](#)). [Figure 7](#) shows the results of the in-situ measurements downstream of the Räterichsboden reservoir. The results of KWO and LimnEX refer to Imhoff cone measurements and are expressed by a volume concentration [ml/l]. Results of VAW measurements were determined as a mass concentration [g/l] from water samples. The conversion from a mass concentration [g/l] into a volume concentration [ml/l] has been done with a bulk density of approximately 2000 kg/m^3 (LimnEX 2010). The discharge was theoretically determined as a function of the gate position. The curves at the respective positions agree quite well. The peak concentration values follow the same trend for all measuring sections. It is noticeable that the peak concentration increases with distance from the bottom outlet; this is mainly attributed to a remobilization of bed material.

Whereas the temporal distribution of the sediment concentration is similar between model and prototype, the absolute values differ by an order of magnitude when comparing [Figures 6](#) and [7](#). The reason for this is supposed to be mainly due to (i) model and scale effects, because

the relevant sediment grain size distributions vary considerably between model and prototype, and (ii) to the different positioning of the measurement sections, i.e. immediately downstream versus 800 m and more from the bottom outlet.

4 SUMMARY AND CONCLUSIONS

To achieve a better estimation of the removed materials by pressure flushing from the Räterichsboden bottom outlet, a physical model was built at VAW. The physical model tests were simulated numerically with FLOW-3D at LCH. On-site measurements of flow turbidity downstream of Räterichsboden reservoir were recorded during the September 2010 flushing event and the suspended sediment concentration values compared to the results obtained both in the physical and numerical model.

Two major bottom outlet operation scenarios were defined: instantaneous and gradual slow gate opening. The physical model tests were performed with several types of sedimentary material such as quartz sand with various grains sizes and plastic granular material. The main tests were all conducted with fine sand. Numerical simulations using Flow-3D were run having the same initial and boundary conditions as the physical model. The simulated concentration curves match well with the physical model results. Some major differences can be observed with gradual opening and low water level, these are most likely due to potential scale effects or non homogeneous initial sediment deposits in the physical model. One has to bear in mind, however, that modeling two-phase water-sediment mixtures is always complex and source of uncertainties, both physically and numerically.

The on-site measurements confirmed the general shape of the suspended sediment release from the bottom outlet as obtained from the VAW and LCH tests, but with much lower concentration values than expected. As the first measurement section is already located some 800 m downstream, the short initial peak concentration value is possibly pronouncedly flattened and spread. The sampling method induces some lowering over time and space as well. Nevertheless, taking into account these uncertainties, the results of the monitored flushing event are in similitude with those of the physical and numerical models. These model tools can therefore be used to predict and estimate the flushed sediment from the reservoir.

REFERENCES

- Boillat, J.-L., De Cesare, G., Daneshvari, M. & Jenzer Althaus, J. 2010. Sedimentbewirtschaftung während der Grimselseeabsenkung im Rahmen der Erhöhung der Stauanlagen. [in German] *Proc. Internationales Symposium Wallgau, Lehrstuhl und Versuchsanstalt für Wasserbau und Wasserwirtschaft*, TU München. Bericht 124: 195–204.
- Limnex, 2010. *Funktionskontrolle NASS Grundablass Räterichsboden*. [in German] Limnex AG, Zurich, Switzerland.
- Meshkati, M.E., Dehghani, A.A., Naser, G., Emamgholizadeh, S. & Mosaedi, A. 2009. Evolution of developing flushing cone during the pressurized flushing in reservoir storage. *World Academy of Science, Engineering and Technology* 58: 1107–1111.
- Morris, G.L. & Fan, J. 1997. *Reservoir Sedimentation Handbook*. New York: McGraw-Hill Verlag.
- Möller, G., Pinotti, M. & Boes, R. 2010. Einlaufwirbeluntersuchung am Kraftwerk Handeck 2—Kritische Überdeckungshöhe und Wirbelunterdrückungsmassnahmen. [in German] *Proc. Internationales Symposium Wallgau, Lehrstuhl und Versuchsanstalt für Wasserbau und Wasserwirtschaft*, TU München. Bericht 124: 407–416.
- Sinniger, R.O., De Cesare, G. & Boillat, J.-L. 2000. Eigenschaften junger Sedimente in Speicherseen. [in German] *Wasser, Energie, Luft—Eau, Energie, Air* 92(1/2): 9–12.
- Staub, E. 2002. Effects of sediment flushing on fish and invertebrates in Swiss alpine rivers. *BUWAL, Fisheries Section*. Berne, Switzerland.
- Truhlar, J.F. 1978. Determining suspended sediment loads from turbidity records. *US Geological Survey, WRD, Hydrological Sciences-Bulletin des Sciences Hydrologiques* 23(4).

Aras transboundary river basin cooperation perspective

A. Heidari

Iran Water and Power resources development Company (IWPC)

ABSTRACT: Transboundary river management is a vital issue in terms of coordinating different water usage sectors and policies of states to achieve sustainable development. Aras river which shared between four states in the Caspian sea, is one of the important regional source of food production and hydro energy generation. There is already bilateral cooperation to develop infrastructures in the river but they are vulnerable to the policies of other upstream states. However, a full participation and cooperation of riparian countries is essential in sustainable, equitable, and reasonable water usage of the basin. This paper addresses important issues of the basin including conflicts and threads. On the other hand, opportunities of cooperation are identified and a framework is proposed to initiate the cooperation among four riparian countries. Moreover an action plan is proposed based on the identified opportunities and limitation to achieve river basin cooperation organization.

1 INSTRUCTION

Integrated water resources management and water efficiency planning is an essential element in all national or regional development strategies added this target to the list of Millennium Development Goals (MDGs) (UN, 2006). The concept requires that effective management of water resources demands and a holistic approach linking social and economic development with protection of natural ecosystems, and linking land and water uses across the whole of a catchment. In addition, agenda 21 of the Dublin Principles was also followed by the formulation of the Integrated Water Resources Management (IWRM) principles, commonly called Rio/Dublin Principles. IWRM imply fundamental change to the management and allocation of water.

The comprehensiveness of water resource planning and sharing has been the subject of much controversy and debate. It has been widely recognized that in order to maximize the benefits from any water resource project, a more systematic analysis of the broader environment is needed. In addition to a broadening of traditional management approaches, there are needed to increase sensitivity to decision-making that involves multi-purpose actions and multi-user considerations. There are many obstacles to achieve comprehensive approach in water resources management. Sources of potential water conflicts include the following items:

- Scarcity (permanent and temporary)
- Differences in goals and objectives
- Complex social and historical factors (including pre-existing antagonisms)
- Misunderstandings or ignorance of circumstances and data
- Asymmetric power between localities, regions or nations
- Significant data gaps or questions of validity and reliability
- Specific hydro-political issues at stake (dam construction or diversion of water) non-cooperative settings and value conflicts, especially in terms of water mythology, culture and water symbolism.

The aim of this paper is to focus on important issues of Aras river basin and provide general perspective for effective cooperation among riparian including Turkey, Azerbaijan, Armenia and Iran. The existing agreements for cooperation are mostly between Iran and

Armenia to develop hydropower plants in along the shared rive in the border of Iran and Armenia. In this paper, following subjects will be discussed:

- Identifying existing and future conflicts among the riparian
- Clarifying requirements of international cooperation
- Identifying water polices in the Aras river basin based on regional features
- Identifying the role of water in foster economic development of the region
- Clarifying threats and oppourtunities in regional cooperation
- The ways to reach participatory decision-making
- Proposing action plan toward regional cooperation

2 CASE STUDY FEATURE

The Aras river is one of the important transboundary river in north west of Iran. The river is originated from Turkey territory and flows to Caspian Sea via Iran, Azerbaijan and Armenia. The river makes borders of countries in some reaches. Water resources management is affected by four countries policies and plans. [Figure 1](#) shows Aras river where cross the riparian countries and flow to Caspian sea.

There are many dams and irrigation schemes under operation in riparian countries. In addition to the projects of each country, there are few joint projects which are mostly between Turkey—Armenia, Iran-Azerbaijan, and Iran—Armenia. For instance a runoff river hydropower projects in the border is under investigation and negotiation stage among two countries of Iran and Armenia. Constructing any infrastructure in the transboundary rivers between Iran and Armenia has been ratified by both parties to be based on international frameworks and mutual agreements. Armena has rejected construction of any kind of storage reservoir or regulation dam due to the inundation damages of roads, railway, and other facilities of the region in the boarder. However, Aras Hydropower Plant (HPP) project has been designed to utilize the Aras River potential for generating base load hydroelectric energy in the Iran-Armenia border. Installed capacity of HPP and annual power generation are 130 MW and 800 Gwh respectively for each country (IWPC 2008). Aras reservoir in upstream of projects sites (at Iran-Azerbaijan border) regulates annual runoff of river and makes it justifiable to develop run-of-river HPPs in downstream. There are many agreements among two riparian which emphasize on hydropower projects construction. Few of important agreements between Iran and Armenia are summarized as follow:

- Mutual agreement on construction of the projects (Mar 2007)
- 7th economical commission between Iran and Armenia (July 2007)
- 8th economical commission between Iran and Armenia (Dec 2008)
- Several technical agreement for project feature (2000 to 2009)
- At least 5 articles of memorandums of understanding (2000–2008)

Despite the great advantages and vital importance of the foregoing benefits of projects, cooperation among the riparian countries is generally obstructed by many barriers such as follow:



Figure 1. Location of Aras river basin in riparian countries.

1. Each country is generally inclined to optimize its benefits by considering national possibilities, resources and objectives regardless of the requirements and availability of the others opportunities. As a result, a few of optimum schemes which contradict with the interests of other countries might have been rejected.
2. Usually each country may adopt a policy to be self-sufficient and secured as much as possible in food and energy production. Such an approach may result in the development of infrastructures whose services may be related to non-water issues.
3. Definition of the relevant problems and misunderstanding may cause diverging opinion on cooperation and it becomes very difficult to create mutual trust.
4. Settlement of the water-related problems may be heavily obstructed by the inclusion of other unrelated issues and controversies which make agreement too difficult to be achieved.

3 COOPERATION PERSPECTIVE

3.1 *Formulation and principles*

Water policies are important in terms of water users, environmental conservation, and water governance in the transboundary river. Principles of water policy in Aras transboundary river are briefly presented in [Table 1](#).

Table 1. Principles of regional water policy in Aras transboundary river basin.

Item	Principles
Allocation and environmental issues	<p>Equitable and fare water distribution at the basin scale based on the agreed identified needs;</p> <p>Reasonable use of water in each riparian territories;</p> <p>Maintaining environmental sustainability;</p> <p>Food security in all riparian;</p> <p>Bottom up approach for decision-making process engaging all stakeholders participation;</p> <p>A common agreement accepted by the riparian to serve as the legal basis relying on international water law;</p> <p>Priorities for the “allocation” and “water quality” concerns:</p> <ul style="list-style-type: none"> – Accessing to salinity water; – A better status of natural resources; – Increasing irrigation efficiency and saving more water to allocate industrial demands; – Increasing GDP/capita in riparian countries by developing industries; – Environmental requirements and social vulnerability in high priority of water allocation criteria; – Water allocated to agriculture should ensure regional food security. A regional cropping pattern should be selected according to soil characteristics and land capacity. Modern irrigation techniques should be implemented to improve water productivity; – The amount of contamination released to the rivers should be controlled in upstream and downstream reaches;
Water Governance	<p>Water as a public good and as an economic good with a value in all its competing uses;</p> <p>Cooperation and collaboration instead of conflict over water;</p> <p>Information sharing and awareness sharing should be ensured;</p> <p>Water-related data should be collected and shared at the regional level;</p> <p>Stakeholder participation should be ensured by implementing consultation and active involvement mechanisms;</p> <p>Sharing the benefits of water allocation (hydropower, industry, domestic, environment and agriculture). The benefits should be valued economically, compared for each country and the gap between collective and individual benefits should be minimized;</p>

Table 2. Benefit sharing and identified opportunities in cooperation.

Identified opportunity	(Pre)-Investment studies	Institutional strengthening	Transaction services, financing	Notes
Regional management				
Regional development through economic cooperation in different aspects such as water, agriculture, energy, trade, ...	Study on regional economic relations and cooperation	Creating regional trade center; Facilitating goods export and import by related organization in each country	Unleashing the market forces that promote economic concentration and social convergence; Initiation of virtual water import and export among the countries	market access helps to remove barriers between the developing world's neighborhoods
Removing the barriers of commuting in the region	Study on possible negative effects such as increasing refugees	Cooperation cultural organization such as training centers, High education org.	Increasing Scientific cooperation and facilitating universities relation among the countries	The thickness of borders is proportional to each country's restrictions to the flow of goods, investments, people and ideas with all other countries
Maintaining ecosystem services through Cooperative management of common environmental assets	Study on regional water related ecosystems, key issues and management options	Getting agreed on environmental standards; Cooperation between countries to assess, investment by other countries	External funding necessary, agreement on moving forward is prerequisite for moving forward to unlock Financing for studies, assessments and investments; Donor funding, EU partnerships; Domestic financing, pooling resources	e.g. copper mine contamination sources in the region
Transboundary drought and flood mitigation	Assessment of drought and flood mitigation strategies at a regional scale; Implementing early flood forecasting systems	Strengthen, mechanisms, and facilities, investment facilities, special domestic issues; Bilateral agreements exists to build on, common management strategies, demand management strategies		Common early warning systems, models and scenarios; Stabilization of settlements during droughts; Creating permanent livelihood opportunities
Efficient use of transboundary groundwater resources	Assessment of transboundary groundwater sources	Considering ground water in shared water resources frameworks	Exchanging historical data records in existing gages	Role of Water User Associations (WUA)
Information and communication	Allocating common monetary fund to develop measuring networks			

Infrastructure

Food, water and energy security through developing joint infrastructures	Assessment on sharing the benefits of joint management of existing and new water and energy infrastructures; Strategic planning assessment; Identifying new projects of HPPs	Creating Shared Monetary Fund (SMF); Investing in regional development through SMF; Needs assessment of establishing a river basin commission for basin wide IWRM to strengthen 4 country water management policies	Financing the identified Projects e.g. Hydropower plants	Saving investment costs in water infrastructure from cooperation; Creating stable energy and power supply network; Trading energy based on differences of demand pattern in the countries
Reuse of wastewater for urban development through improved treatment technologies	Study on lessons learned from good water practices in reusing and treatment technologies in 4 countries			Preventing any loss in investment and insuring to achieve predetermined targets of projects
Strengthening livelihoods by improving domestic water infrastructure	Assessment of domestic water use, gender issues and water infrastructure investment			
Sustainable development of the region and minimizing the initial costs of infrastructures in full development situation	Identifying the potentials of the region for more development			

Knowledge

Mutual high educational and cultural cooperation	Identifying agendas based on regional needs	Initiation of Regional workshops and conference in different fields; Involving UNESCO committees and making regional committees;	Each country should pay the expenses	The workshop venue can change among the countries
Improved water use efficiency by building knowledge on land management, practices, and reclamation	Assessment of joint research on land management aspects, practices, land reclamation			
Improved irrigation through efficient use of water through training local water users	Study on lessons learned from good water practice and management in efficient irrigation			
Building expertise in IWRM in the region by strengthening regional training in water management	Assessment of long term training needs in IWRM and available training resources			
Improved water use efficiency and management by cooperative strategic planning through data sharing at the transboundary level	Transboundary Regional monograph study			Knowledge base on basin and sub-basin scale (naming issues to explore), water per capita issues, water for historic structures, climate change aspects

Table 3. Action plan for implementing foster IWRM in Aras river basin.

Goal	Implementation party	Action	Monitoring & Legislation	Remarks
Economic Cooperation Organization (ECO) water resources sub-commission	ECO	Establishing Sub—commission for water and energy cooperation	Worldwide trade rules	Iran has initiated hydropower workshop among the ECO members
Extending bilateral economical cooperation	Iran and Armenia	Inviting Turkey and Azerbaijan to join	Following ECO rules	4 riparian states are included in ECO which is regional organization among 10 countries
Initiating a joint basin cooperation commission including entire riparian	by the 4 states of Iran, Turkey, Armenia, Azerbaijan	Appointing representatives of politicians, experts, academics, NGOs, civil society	Legal modification at the national level; Monitoring poverty and welfare of the region specially in rural areas	Initiation by ministers of riparian during World Water Forum 2010 to discuss institutional framework; Agreement on time and venue of commissions and meetings
Data-collection & monitoring and implementing survey system	The joint commission	Current practice; Harmonizing; Common methodology; Web-based database	Same procedures applied by local authorities to collect data	A survey of all stakeholders needed
A list of potential joint projects for economic and social development		Comprehensive feasibility studies		
Operating hydropower potentials in the catchment	Joint technical commission in along with NGOs, world bank and Islamic bank	Establishing energy subcommittee under the supervision of technical committee; Identifying demand patterns of riparian countries;	Setting up power and energy market in the region; Monitoring the shared power net	Extending power network among neighbors
Identifying water demands, water rights, dependency based on the population growth, climate changes, economical development, water policies and equity in water usage	The joint commission with sub-commissions	Arranging technical meetings to identify requirements and barriers	Monitoring hydrological data, water withdrawal, crop pattern and water allocation to different users	Regular meetings of technical committees

(Continued)

Table 3. (Continued).

Goal	Implementation party	Action	Monitoring & Legislation	Remarks
Enhancing water efficiency by close cooperation of riparian considering the common responsibilities and benefits		Identifying virtual water trade through changing the crop pattern; Implementing highly efficient crop pattern and irrigation systems; Public awareness of efficient water usage by NGOs; Creating monetary fund to implement the strategies and policies; Implementing the strategy of high efficient water usage	Same procedures applied by local authorities to collect data; Ensuring food security in regional scale rather than national scale by politicians of riparian	Regular meetings of subcommittees and involving stakeholders
Carrying out environment evaluation for existing situation	The joint commission by formulating a technical committee	Working groups; field studies	Same procedures applied by local authorities to collect data	Regular meetings with various basin stakeholders
Developing flood & drought management plan		Working groups; field survey		Regular meetings with stakeholders

3.2 Implementing foster IWRM

It is difficult to implement whole aspects of IWRM even in a catchment inside a country territory. Due to the real facts, achieving to IWRM in transboundary rivers is an ambition of long term period. IWRM in such catchments can improve water usage in the whole basin dramatically, however, it would need a powerful backgrounds and hard working in regional and even international scales.

A hierarchy of institutions such as an international river basin organization, a national water management institution (ministry), a catchment organization, and sub-catchment forums and stakeholder councils/committees may be required to implement proposed IWRM components and achieve regional cooperation. Clear delineation of mandate, roles and responsibilities, and accountability between these organizations and institutions is imperative. The institutions, institutional arrangements and hierarchy should be dynamic and flexible, to adjust to the changing nature of the catchment (changing society, economy and natural environment) and to adapt to the lessons learned through the process. Table (2) shows mutual benefits and opportunities of cooperation in Aras river basin.

There need an action plan to achieve the foster IWRM and identified opportunities of cooperation. Table (3) indicates action plan to achieve the perspective and goals of cooperation.

4 CONCLUSION

The search for a typology for conflicts and appropriate responses in transboundary rivers has led to several conclusion and schemes. One conclusion is that it needs to pay particular attention to international river basins and aquifer systems, where confrontations and conflicts

can be far-reaching. Aras river which is one the main river basins shared between 4 riparian countries in Caspian sea, can potentially be in this category. There are a number of concerns for water management in the basin and cooperation ambitions among the riparian countries as follow:

1. To build on the water rights currently provided that they help achieving river-basin objectives.
2. To improve the system that fulfill both wet and dry seasons requirements, and that manages the switch in water availability and demand between the two seasons.
3. A further objective is to draw up an arrangement that incorporates without violating both formal and informal agreements.
4. In addition, it is necessary to look at water rights in design stage of the infrastructural so that water scarcity not exceeded and social requirement fulfilled.
5. National water policy should effectively be adopted based on targets of sustainable development.
6. To prioritize environmental issues in entire basin and to implement waste water treatment plants specially for industrial contamination in order to preserve safe and drinking water.
7. Equitable and fare water distribution at the basin scale based on the agreed needs and requirements.
8. Optimum utilization of available water resources in the basin.
9. Maintaining environment and ecosystem sustainable.
10. Developing potentials of hydropower generation by Clean Development Mechanism (CDM) and other financing mechanism.
11. Increasing gross domestic product (GDP) by enhancing the contribution of virtual water and industrial water allocation.
12. Promoting recreational and tourism industry.

A hierarchy of institutions and strong relationship among riparian countries is needed to implement foster IWRM components in transboundary rivers. Such an ambition needs hard working and permanent strategy not only in water related issues but also in other non-water related issues. A proposed action in the paper which initiates cooperation with very simple mutual benefits, can promote cooperation stages to higher levels in the future.

REFERENCES

- Andreas K.R., Zulma G.C., Ronaldo S.d.M., Clifford R. 2003. Environment Network.
- CIGB-ICOLD, 2008, Bulletin 132—Shared Rivers: Principles and practices.
- IPCC 2007. Climate change: Impacts, Adaptation and Vulnerability. Contribution of Working Group II to the Fourth Assessment Report of the Intergovernmental Panel on Climate Change. Cambridge, UK, Cambridge University Press. 976 pp.
- IWPC 2008. Aras HPPs feasibility studies reports, consultant engineer: Consultant engineer Mahab Ghodss company.
- UN water Report 2006. Water monitoring, Mapping existing global systems & initiatives.
- UNESCO 2008. Water is not a commercial product like any other, but rather a heritage that must be protected, defended and treated as such, Sharing water, Geothermal power plant with bathers enjoying, geothermally-heated water, Blue Lagoon, Iceland.
- World Wildlife Fund—UK 2006. Allocating Scarce Water, Review of Water Rights and Markets.

An example of sedimentation and proper management of flushing operation since 45 years: The Kashm El Girba reservoir on the Atbara river

C. Guilbaud, O. Cazaillet, P. Cochet & C. Odeyer

Sogreah Consultants, Grenoble, France

ABSTRACT: The Kashm el Girba (KEG) reservoir on the Atbara tributary of the Nile River in Sudan was impounded in 1964. The dam was built with large bottom sluices which ensure the possibility of carrying out flushing operations at low level during flood periods. Different operation rules have been used since the commissioning of the dam. Thanks to the past flushing operation, the reservoir is still fully operational and could be really perennial if flushing operation rules are maintained. The construction of the Dam Complex of Upper Atbara will create a new storage capacity upstream of KEG, will improve the efficient use of the water resources and will reinforce the role of the KEG dam as diversion structure to feed the New Halfa irrigation canal. The authors propose to describe the operating rules drawn up from the filling of the reservoir until now and the conclusions derived from the KEG experience.

1 INTRODUCTION

1.1 *Kashm El Girba dam construction*

The Kashm El Girba (KEG) dam construction started in 1960 and was completed on August 19th, 1964: the first impounding of the reservoir took place during the 1964 flood season.

The purpose of the dam was threefold: regulation of the Atbara floods, irrigation of the New Halfa scheme, and electricity production by power generation of the diverted water to the feeder canal of the irrigation scheme (El Sir, 1974). It is worth noting that the new irrigation scheme was so-called New Halfa, as it was designed to house the Halfawi nubian families who had lost their homes and lands as a result of the Aswan Dam construction in Egypt which flooded more than 150 km of the Nile valley in Sudan.

1.2 *Project location*

The dam is located on the Atbara river, which is one of the main tributary of the Nile downstream of Khartoum and the merge of the White Nile and the Blue Nile ([Fig. 1 Localization](#)).

The dam is close to two major towns of eastern Sudan: Kassala is 75 km east far from the dam near the Erythrean and Ethiopian borders and Gedaref, which is 120 km south far from the dam. Both cities are governorates of the eastern Sudan and have a strategic role in this part of Africa as they have welcomed refugees from Ethiopia after the large drought of the eighties or after the war between Erythrea and Ethiopia.

1.3 *Main features of the project*

Damming of the Atbara river was done by a 67 m high, 500 m long concrete buttress dam across the main stream of the river and by more than 3 km of earth fill embankments which

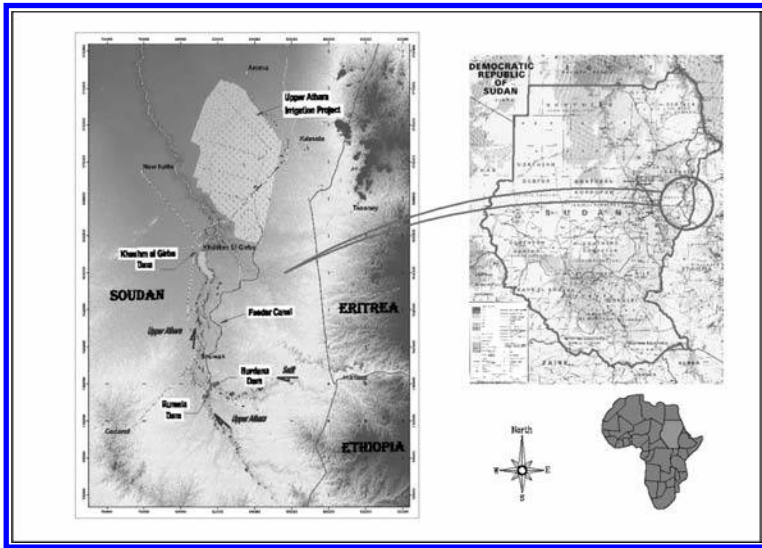


Figure 1. Localization.

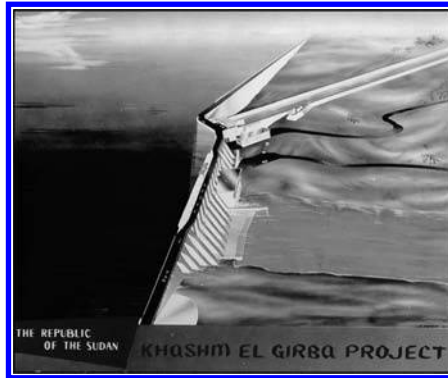


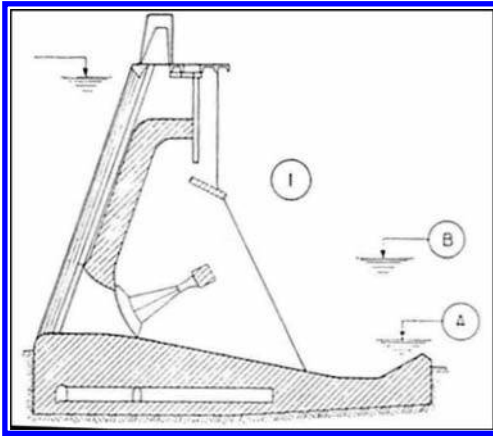
Figure 2. General view of the project.

allow for a total of 1.3 billion of cubic meters of water to be stored each year in view of irrigating the New Halfa scheme, over the 11.8 billion cubic meters which flow in an average year at the dam site (Fig. 2).

The normal operating water level of the dam was set at 473 m asl, whereas the elevation of 474.5 m was defined as the maximum of the reservoir level when a 1/5000 year flood occurred in either of the two main streams (Setit-Tekeze river or Upper Atbara) contributing to the Atbara flow upstream of the dam site.

The spillway is equipped with 7 bottom radial gates 7.00×7.30 m, able to evacuate $7,700 \text{ m}^3/\text{s}$ with the water level at 473 m asl in the reservoir, and 5 surface sliding gates $7.00 \text{ m} \times 7.10$ m with an additional discharge of $1,000 \text{ m}^3/\text{s}$ also at 473 m asl upstream in the reservoir. (Fig. 3).

Additional features of the project are the so-called downstream power plant equipped with 2 Kaplan turbines 3.9 MW each, with a net head of 40 m, maximum discharge of $10 \text{ m}^3/\text{s}$, and a pump turbine station, equipped with 3 bulb units, able to generate power from the $3 \times 34 \text{ m}^3/\text{s}$ diverted into the feeder canal of the New Halfa irrigation scheme when the reservoir level is offering a head above 2.0 m and operating as pumps when the level in the reservoir drops below 469.10 asl in order to supply the adequate amount of water to the feeder canal. An additional pumping station equipped with 4 vertical axis pumps, each having a



A : Minimum downstream Water Level
B : Maximum downstream Water Level
473 asl = Upstream Water Level Above Sea Level

Figure 3. Bottom outlet radial gates.

minimum discharge of 5 m³/s, operating at the maximum head of 20 m. enables the water supply to the feeder when the water level in the reservoir falls below 450 m asl.

2 BACKGROUND ON HYDRAULICS & HYDROLOGY

2.1 River discharge

KEG dam is located few tens kilometers downstream of the confluence of the Setit and Upper Atbara rivers. The catchment area of the upper Atbara is entirely situated in Sudan, while the Setit's catchment area is almost entirely situated in Ethiopia. Their respective catchment areas are some 70,000 km² and 30,000 km².

The average annual yield of water is in average 12 Billions of m³. The Setit River (called Tekeze in Ethiopia) contributes to about 60% of the average yearly liquid yield of the Atbara river flowing in KEG reservoir.

2.2 Sediment

Up to 1973, the only available data consisted in suspended sediment load measurement. The annual total loads evaluated on the basis of these measurements are compiled in the [Table 1](#).

No sediment measurement was carried out in the reservoir itself. Bathymetric surveys of the reservoir were periodically carried out. The computed evolution of the sedimentation in the KEG reservoir did not provide reliable information about sediment load in the Atbara River because of flushing operations carried out in a yearly basis. This monitoring mainly provides qualitative information on the flushing operation efficiency.

Nevertheless, suspension sediment measurements were carried out in the 70' on both Setit and Upper Atbara rivers, few kilometers upstream of their confluence.

Despite the poor quantity of sediment samples taken (47 in Setit River & 28 in the Upper Atbara river), the suspended sediment load was estimated for the two branches of the Atbara river. The [Table 2](#) presents the results of the sensibility tests carried out on Setit river inflow series.

Regarding the bed load component, no specific measurement was carried out on both Upper Atbara and Setit rivers. Nevertheless, on the basis of sediment investigation at Roseires Dam (Gibb and Coyne et Bellier, 1996) the bed load component could be assessed as some 25% of the suspended load.

The [Table 3](#) summarizes the annual average sedimentation expected in present condition for the Setit River and Upper Atbara close to their confluence and then at the entrance of

Table 1. Suspended sediment load measurement.

Year	River	Peak flood flow (m ³ /s)	Total sediment load (10 ⁶ tons)
1954	Main Atbara	3,700	85
1959	Main Atbara	4,500	86
1973	Setit	2,000	79
1973	Upper atbara	95	8

Table 2. Suspended sediment load estimation.

Setit River at Wad El Heliew—Suspended sediment load—Sensibility tests (1956–1972)

	Average yearly weight of sediment (10 ⁶ tons)	Average annual volume (d = 1.3) (10 ⁶ m ³ /year)
Setit River at Wad El Heliew	73	56
Upper Atbara at Kubur	11.2	9.6

Table 3. The annual average sedimentation.

Upper Atbara Dam complex: Annual average long term sediment loads (1956–1995 period)

Upper Atbara River	Suspended load	11 Mm ³ /year
	Total Sediment volume	14 Mm ³ /year
Setit River	Suspended load	65 Mm ³ /year
	Total Sediment volume	81 Mm ³ /year

KEG reservoir. The computations are based on reconstituted series of discharges (10 days-discharges) over the 1956–95 period.

3 THE EXPERIMENTAL “1974” SEDIMENT FLUSHING OPERATIONS

This operation at KEG was programmed on the basis of an analysis from Sogreah after the two experimental operations in 1971 and 1973. The programme was adjusted in accordance with comments and requirements of the Ministry of Irrigation.

3.1 *Sediment flushing operation programme*

3.1.1 *Initially proposed programme*

The initial flushing programme was proposed by SOGREAH (Johnson & Phelipon, 1974) on the basis that the 2 to 3 flushing events should be organized during the flood period early in August, with the last flushing operation as close as possible at the end of August. Prior to the each flushing, the removal of the timber accumulated by rising the level and spilled it.

It was considered that some of the inconvenience caused by cutting up the irrigation period into irregular intervals could be compensated by an increase in discharge during the normal operating level periods.

3.1.2 *Initially proposed programme*

Comments by the Ministry of Irrigation, made prior to the operation, and affecting its pattern, were as follows:

- In the view of the rhythm of planting and irrigation, there is no advantage in increasing irrigation supply discharge; By filling irrigation canals before the flushing operation, enough water for approximately four days could be available for irrigation (some

refilling could be undertaken by using the compensation pumps during long term low level operation);

- Two periods of twelve to fifteen consecutive days of water is required for cotton planting. Consequently the only way of obtaining this length of time would be with two operations;

3.1.3 Programme as executed

Finally the executed programme took into account the major comments from the Ministry as well as the natural condition encountered during the flushing period. The flushing sequences are shown in Figure 4, in terms of reservoir water level and outflow discharge.

The flushing sequences followed the steps:

1. By the 5th July 74, the reservoir was lowered to normal flood operating level at 462 m;
2. On 25th July the level was raised for timber spilling before lowering for flushing;
3. The drop was started on August 2nd, and the level was kept down longer than proposed in the initial programme, in accordance with the programme modification;
4. On August 4th, a visit was made to an accessible reach of the river at Manaba (7 km upstream of the dam) and revealed the lateral limit of the scour into the deep deposits. It revealed also the presence of slump and potential slips in the steep sediments faces.

With the idea of encouraging more material to slump into the flow, a rapid rise and fall in the reservoir was effected as shown on the graph;

5. After rising on August 6th, the normal operating level was maintained. An exceptional flood occurred from the 10th to the 14th of August. The outflow from the dam reached 6,500 m³/s on 12th and 13th August.

This flood brought large quantities of floating timber to the reservoir. New flushing operation was impossible before timber removal;

6. Consequently the level was raised to 469 m by August 17th, in order to spill the timber through the surface sluices gates until the 19th, when lowering started for the second flushing operation;
7. The second flushing was carried out on the 23rd and 24th of August.

3.2 Effectiveness of sediment removal

From the beginning of July the level in the reservoir was kept to the normal flood operation level (462 m). The Figure 5 presents the general view of the Dam Reservoir. The amount of sediment passing through the reservoir between the 1st of July to the 26th of July was evaluated (from Outflow Qs measurements) to 37×10^6 Tons. No measurements of sediment inflow were available for the period, but the estimated sediment transport of the river was well below the measured outflow.

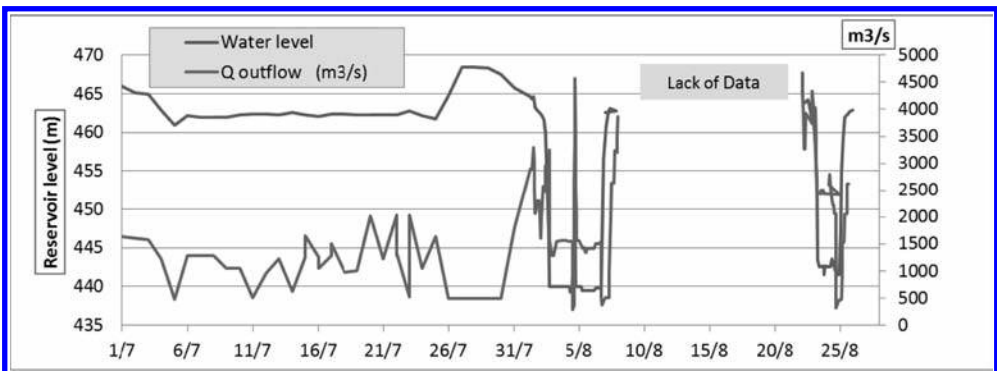


Figure 4. Flushing programme as executed: reservoir water level and outflow discharge.



Figure 5. General view dam and reservoir.

That suggests that a large part of this sediment load corresponded to the erosion of the previous years' deposits which were exposed to erosion when the reservoir is dropped to the normal flood season operating level.

The high sediment outflow during this period was indicative of the concentrated deposition of sediments in the main river channel as it raised above the normal flood operating level (462 m) in previous years.

Sediment outflow from the dam ceased when the reservoir was raised for timber removal (26th to 30th July). The [Figure 6](#) shows an example of timber accumulation at the turbine entrance.

The evolution in the sediment outflow from the dam during the flushing operation from the 1st to 7th August and during that from the 22nd to 25th August is similar.

The sediment concentration was very high at the beginning of the operation, ([Fig. 7](#)) but tailed off rapidly as shown in [Figure 8](#).

The stabilization value, towards the end of the six day period of the first flushing operation, was very similar to the measured and estimated average sediment inflow rates at that time. The rapid fall off in sediment concentration indicated the lack of usefulness in prolonging the low level period.

The [Figure 9](#) shows the reservoir during the flushing period, the main channel being well defined.

The short raising and lowering operation of the reservoir on 4th August, as shown in [Figure 10](#) below, with the idea of increasing the slumping of steep side slopes of deposits, as observed at Manaba, appeared to bring some increase in sediment concentration, despite the limited extent of the reservoir raising.

The total recorded sediment outflow from the dam for the two flushing periods was evaluated at 85.5 Million tons. Unfortunately no sediment outflow measurements were available for the period between the two flushing operations.

For further reference, the total mean annual sediment load of the main Atbara used in sedimentation studies for the Upper Atbara dam was evaluated to 84 Million tons. The total amount of sediment passing through KEG Dam would have been greater than this in 1974, with the two flushing operations.

It seemed reasonable to hope that two flushing operations, of 3 days duration each per year could be sufficient for maintaining an optimal state of the reservoir sedimentation equilibrium.

3.3 Lowering below level 462 and raising of the reservoir

The bottom gates were operated according to the inflow at Showak to maintain an emptying discharge of the reservoir (Outflow—Inflow) of about 1,000 m³/s. When the level is 448, all the gates are fully opened (10/10). Thus, the minimum level (440 to 445 depending of the flood) is reached in about eleven hours. It was expected that, during this period, the inflow would be less than 3,000 m³/s, so that the outflow would not exceed 4,000 m³/s.



Figure 6. Timber accumulation.



Figure 7. Downstream dam flushing.

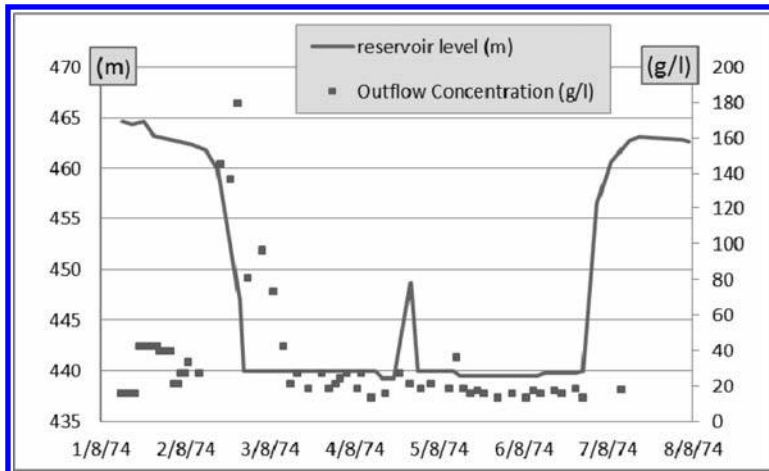


Figure 8. Detail of the first flushing period (reservoir water level and outflow concentration).

3.4 Conclusion of the sediment flushing operation in 1974

The estimated average annual sediment inflow was considered to be about 85 M tons (estimated from measurements up to 1973—Table 1—and from statistical analysis Tables 2 and 3), which represent the upper limit of the estimate in the sedimentation studies for the future



Figure 9. Upstream dam flushing.

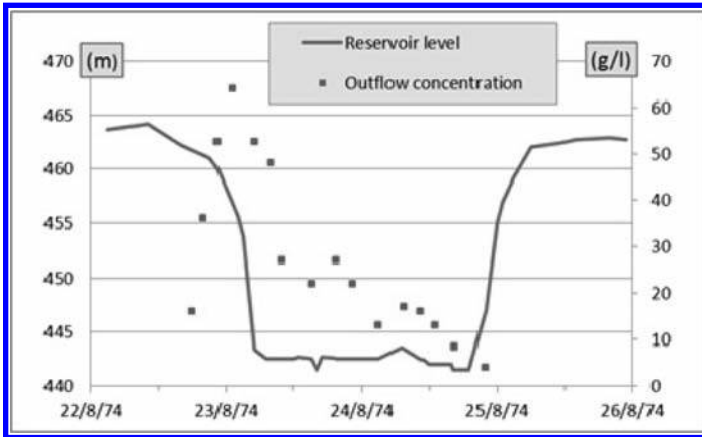


Figure 10. Detail of the second flushing period (reservoir water level and outflow concentration).

Upper Atbara Dams Complex. The total sediment outflow during the two flushing operations period in 1974 was evaluated to 85 M Tons.

Consequently, it might reasonably be expected that, two flushing operations a year, as in 1974, could be sufficient for maintaining a low sedimentation within the reservoir.

The two flushing operations ensured that the main stream in vicinity of the dam was kept clear from bed deposit. By maintaining a deep main channel is probably beneficial to concentrate the deposit of fine sediment into the channel during operation at level 462, during flood season. This deposit could be removed by subsequent low level operation.

The timing of the first operation at the beginning of August and the second towards the end of August appears to be the best arrangement with regard to sediment removal, as well as with regard to the satisfaction of irrigation requirements.

For timber removal the only reliable method available seems to be to raise the timber, and then to spill them with the water.

The methods developed for operation of electro-mechanical equipment during flushing operations appeared satisfactory.

4 LONG TERM RESULTS OF SEDIMENT FLUSHING OPERATIONS

The proposed flushing programme has been fairly followed by the KEG management.

It could be observed on the [Figure 11](#) the typical variation of water level in agreement with the typical reservoir operating programme for silt flushing from 1974 up to now:

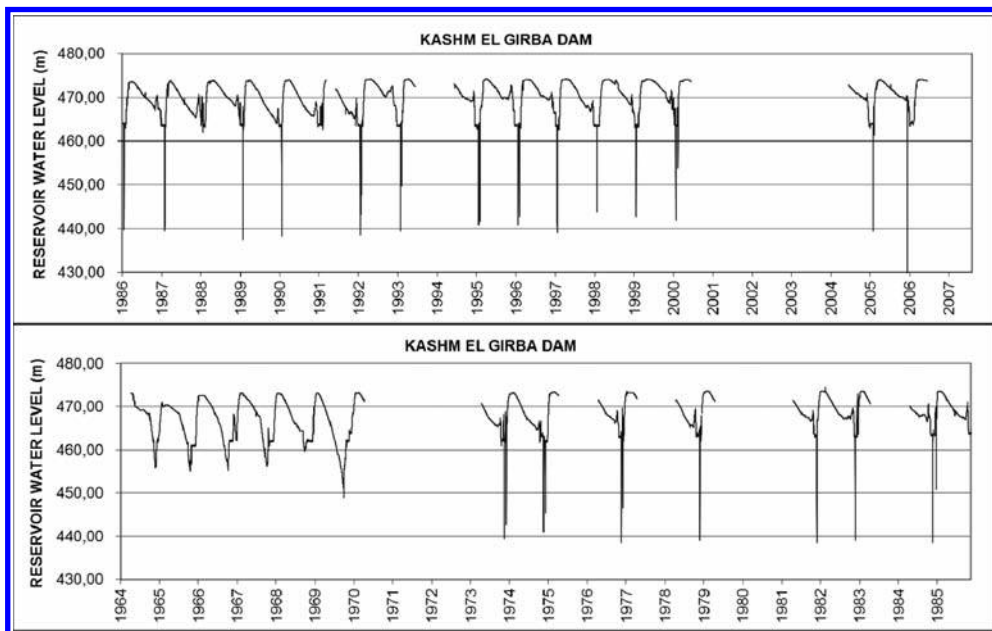


Figure 11. Water level in the reservoir periodical flushing operation.

Table 4. Analysis of the bathymetric surveys of the KEG reservoir.

Kashm El Girba reservoir—Bathymetric and topographic surveys				
Date	Survey carried out by:	Reservoir volume (Mm ³)	At level. (m)	Sediment rate (Mm ³ /year)
1964		1,300		
1969–1970		970	473.5	55
1972–1973	SOGREAH	840	473.5	43
1974	CGG	806	473.5	34
1985	DEMAS	660	473.5	13
1990	MOI & WR	611	473.5	10
2008	IGN	572	473.5	2.5

1. Beginning of July the reservoir was lowered to normal flood operating level at 462;
2. Then the level was raised for timber spilling before lowering for sediment flushing;
3. One or two rapid level drops to the level 440 were carried out at the end of summer.

The analysis of the different bathymetric surveys carried out in KEG reservoir can be summarized in the Table 4 (for the reservoir level fixed at 473.5 m) regarding the reservoir volume as well as the yearly sediment rate.

It is reported by several sources that a lot of problems relating to sedimentation have been identified after few years of operation of the KEG reservoir. A delta was created at the tail of the reservoir (see Fig. 12), above the normal level of the reservoir (i.e. 473.5 m).

Nevertheless, the sedimentation rate (Table 4) in the reservoir falls down drastically from about 50 to 10 Mm³/year after 1974 (starting of the proposed flushing operation).

These observations are confirmed by the evolution of the reservoir capacity (see Fig. 13).

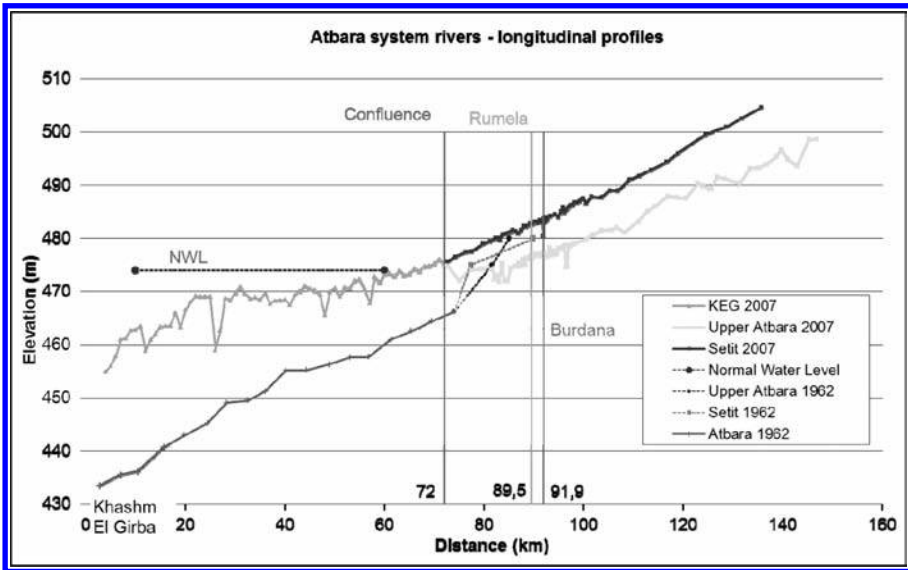


Figure 12. Bathymetric longitudinal profile—evolution of the KEG reservoir.

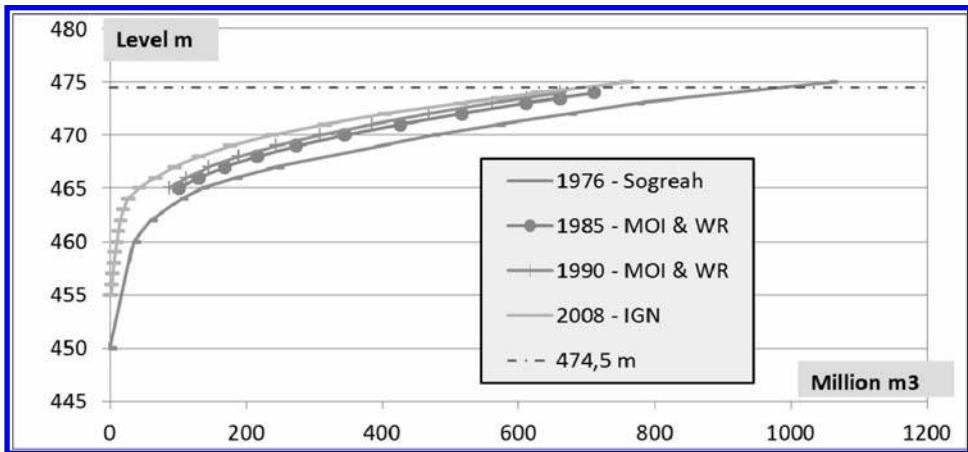


Figure 13. KEG reservoir capacity evolution.

5 PROPOSED PROGRAMME FOR THE NEW UPPER ATBARA COMPLEX

5.1 RUMELA and BURDANA reservoirs

Early after the start of the operation on the KEG dam, the rate of sedimentation in the reservoir was recorded to be rather critical, (refer to above Table 4), and rescue measures were considered necessary. As a consequence, the Upper Atbara Project was identified from the end of the seventies, less than ten years after the completion of the dam construction.

Few decades after, the project having been deeply revised to comply with the up-dated economical and technical criteria (Cazaillet, O., 2008), the project is presently about to be implemented and the construction has effectively started at the end of 2010.

The planned Atbara Dam Complex aims at supplying water to large irrigated perimeters. It will consist of three dams and reservoirs:

- The existing KEG dam and reservoir completed in 1964,
- Two dams forming a unique reservoir are now planned by the Republic of Sudan upstream from the KEG reservoir, across the upper Atbara River and its main tributary, the Setit River.

The main objective of the new dams is to develop another irrigation scheme and the secondary objectives are:

- To control the siltation problem in the KEG reservoir and consequently to increase water supply to the New Halfa irrigation scheme and,
- To generate electricity in addition to the existing power station at KEG dam,
- To improve the protection of the existing KEG dam against the extreme floods and in particular to reconstitute a consistency for the dams constructed on the Nile river (Merowe, High Aswan dam), or planned to be built in the near future (Sabaloka, Sherek, Dal dam, etc...) as regards to the flood control.

As a consequence, the new upper Atbara complex would allow transforming the KEG reservoir, in the new global scheme, into a derivation reservoir, with the main storage retained by the dams on the Upper Atbara and Setit rivers. Thus the future life time of the KEG will be increased, its sustainability will be restored and the irrigation associated scheme preserved for the future generations.

During the conceptual stage of the project up-dating, the designers have retained the lessons learnt from the KEG reservoir management: especially for the design of the spillways, the following overriding criteria were selected:

- The bottom outlets were over-sized in order to allow the flood routing of flows with return periods of 2 to 5 year to be routed through the radial gates without significant increase of the upstream head water,
- The surface spillway has to be equipped with flap gates, to evacuate without difficulty the floating logs and debris. In addition flap gates authorize the adjustment of the upstream level in the reservoir and possibly its progressive increase. In line with the development of the irrigation scheme, which will require the full amount of water to be stored, only after several years, when the full extent of the scheme is developed, the operating level in the reservoir has to be kept as low as possible.
- Over-sizing of the bottom outlets would allow also a better protection of the existing KEG dam downstream of the new dams. By the capacity of the new reservoir to store a large amount of water above the normal operating level, the extreme flows which could endanger KEG dam would be routed through the new reservoir and passed with a significant attenuation through either the surface or the bottom gates.
- Moreover, low level outlets equipped also with radial gates were designed to evacuate and floating debris at intermediate levels. The flow would also be, to a certain extent, able to mitigate the dissipation of the spilled water into the dissipation basin.

5.2 *New upper Atbara sedimentation study*

A detailed sedimentological study appears to be essential to secure the design and the operation of the new reservoirs and of the new irrigation water intake, in order to avoid the difficulties encountered with the New Halfa scheme (Sogreah, 2008).

Sogreah proposed a sedimentological study as followed:

- Defining possible further sedimentological investigations for the purpose of the study (sediment sampling with grain size analysis for non-cohesive sediment, possibly mud concentration and rheological analysis for cohesive sediment);
- Assessing the future sedimentation in the new reservoirs, taking into account the existence of the new dam and reservoir of Tekeze in Ethiopia on the upper Setit river;

- Defining the operation (particularly flushing) of the new reservoirs, to mitigate sedimentation, with the aim at improving, if possible, the KEG sedimentation. Operation of the reservoirs must consider irrigation and hydropower requirements.
- Assessing the possible evolution of the river bed just downstream of the Rumela and Burdana dam, according to the operation of the KEG, Rumela and Burdana reservoirs

6 PROPOSED PROGRAMME FOR THE NEW UPPER ATBARA COMPLEX

The KEG reservoir volume evolution from 1974 up to now, proves the efficiency of the design of the dam (large bottom sluices and spillway), on the proposed and executed flushing programs (Shahin, 1993).

The Upper Atbara Complex with two dams, on the Setit and Atbara rivers, will allow increasing the life time of the KEG.

The design of the new dams will take into account the experience of the KEG design as well as the basis of the sediment flushing operation.

In addition, a specific new sedimentation study on the global scheme of the Atbara Complex will ensure a sustainable sediment management not only for the new reservoir, but also for the KEG reservoir and the downstream stretches of the two rivers.

REFERENCES

- Cazaillet, O. 2008. Dam Complex of Upper Atbara Project, Sedimentology and flushing operation study, Internal report.
- El Sir, A. 1974. Khasham El Girba reservoir and silt control measures, *Sudan Engineering Journal*.
- Gibb, A. & Coyne Et Bellier. 1996. Physical Characteristics of Siltation of the *Roseires Dam* Reservoir, Ministry Irrigation and Water Ressources, Sudan.
- Johnson, G. & Phelipon, M. 1974. Khashm El Girba dam, Sediment flushing operation, 1974, *SOGREAH Internal Report*.
- Shahin, M.A. 1993. An overview of reservoir sedimentation in some African river basins, Yokohama symposium.

Future glacier evolution and impact on the runoff regime in the catchments of Alpine reservoirs: The Aletsch area, Switzerland

D. Farinotti, A. Bauder & R.M. Boes

Versuchsanstalt für Wasserbau, Hydrologie und Glaziologie (VAW), ETH Zürich, Switzerland

M. Huss

Department of Geosciences, University of Fribourg, Switzerland

G. Jouvét

Mathematics Institute of Computational Science and Engineering, EPF Lausanne, Switzerland

F. Widmer

Alpiq Suisse SA, Lausanne, Switzerland

ABSTRACT: The ongoing climate change is expected to have significant impact on the runoff regime of alpine catchments. Major changes are anticipated especially in glacierized basins where glacier retreat will alter the total runoff as well as its distribution in the course of the year. Projections of such changes are important for many fields of water resource management, especially the hydro-power industry. In this contribution, the expected changes and the potential impacts are quantified and presented for the hydro-power reservoir Gebidem, in the Aletsch area, Switzerland. In the projections, the uncertainty induced by the unknown climate evolution is taken into account by analyzing 10 different climate scenarios. According to the results, the area of the glaciers in the region will shrink by 70 to 90% by the end of the century whereas the runoff in the summer month will decrease by about one third in the same time.

1 INSTRUCTION

Glaciers are known to have a significant impact on the runoff regime of Alpine streams (Jansson et al., 2003; Hock et al., 2005). Ongoing climatic changes will lead to a substantial glacier retreat in the coming decades. With decreasing glacier area, the annual cycle of runoff is expected to change from an ice melt to a snow melt dominated regime (Horton et al., 2006). During the summer months glacial melt water may provide the only source of water in mountain regions. The reduction in ice volume will yield a significant increase in annual runoff for several decades, accompanied by a shift in the peak discharge towards early summer and spring, and followed by a decrease in total runoff (Braun et al., 2000; Huss et al., 2008b). The expected alterations in runoff characteristics of high mountain catchments will pose new challenges to water resources management in the Alps, in particular to the electric power supply (Schaeffli et al., 2007). The hydro-power sector is very important for the Swiss economy and represents an important source of revenue for the mountain Cantons (Romerio, 2008a,b). Thanks to their flexibility, hydro-power plants with reservoirs play an important role in ensuring the electric networks stability. Modified streamflow regimes caused by climate and glacier change will affect the supply security of electric power, the value of hydro installations as well as company returns and the regional economy. Future oriented investigations of these impacts require a broad spectrum of scenarios to be addressed, including changes in future electricity markets due to shifts and fluctuations in the generation mix and seasonal and daily demand.

In this contribution, the glacier and runoff evolution expected until the end of the current century is analyzed for the catchment basin of the hydro-power reservoir Gebidem (Aletsch area, Switzerland). The analysis is based upon the most recent climate projections, developed in the frame of the European ENSEMBLES project (van der Linden and Mitchell, 2009). Finally, the relevance of the glaciological and hydrological results presented will be assessed for hydro-power production.

2 THE WATERSHED AND PAST GLACIER CHANGES

The hydro-power reservoir Gebidem was built between 1964 and 1967 to dam the Massa River in the Aletsch area, Switzerland. The hydrological basin of the dam extends over 198 km² in total, of which 119 km² (60%) are glacier covered (Fig. 1).

The major glaciers in the watershed are the Grosser Aletschgletscher and the Oberaletsch- and Mittelaletschgletscher. With a total ice volume of 18 km³ (year 1999), the basin stores 25% of the glacier ice volume of the Swiss Alps (Farinotti et al., 2009). This is the largest amount of glacier ice actually present in a basin exploited for hydro-power production in Switzerland.

Long-term glacier observations have been carried out to document glacier variations in the Massa river watershed. The entire Aletsch area was mapped completely between 1846 and 1851. The first detailed map of the surface topography with modern precision (1:50,000, 30 m contour line interval) was produced in 1880. Two special high precision topographic maps covering the whole catchment area of the branched glacier system have been produced for the states of 1927 and 1957. The maps have been complemented by two photogrammetrical analyses of recent sets of aerial photographs dated 1980 and 1999. Variations in the front position have been recorded annually since 1880. Starting in 1918, the accumulation and mass balance has been measured on Jungfraufirn and was later on extended by several sites in the accumulation and ablation areas (Glaciological reports, 2009).

Volume changes of high spatial resolution were determined by comparing two consecutive surveys of the surface topography. Detailed volume and thickness changes for four multi-decadal periods are the result (Bauder et al., 2007). The mass balance has been reconstructed in seasonal (winter and summer) resolution since 1865 (Huss et al., 2008a). A retreat in length of Grosser Aletschgletscher of 2.9 km and a ice volume loss of -4.134 km³ in the entire watershed has been determined since 1900 (Fig. 2). The length variation is characterized

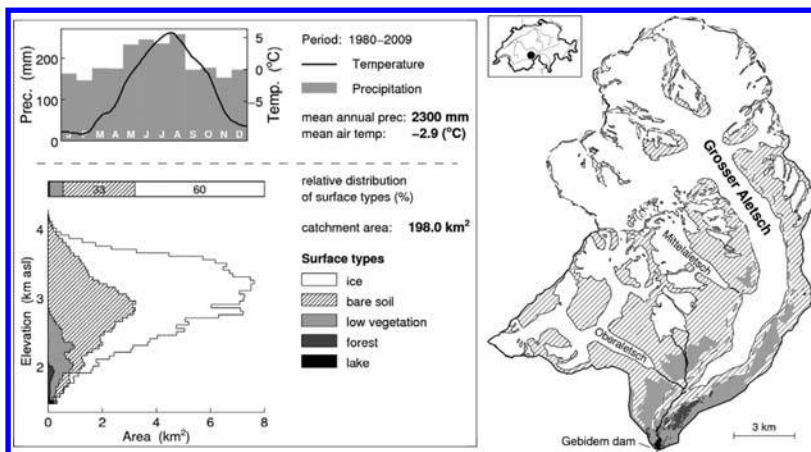


Figure 1. Location and characteristics of the Gebidem dam watershed. The left panel shows climate conditions during the 1980–2009 reference period, and the hypsometry of the surface types for 1999. The surface type distribution on the right panel refers to 1999 as well. Dashed outlines show the glacier extent in 1880.

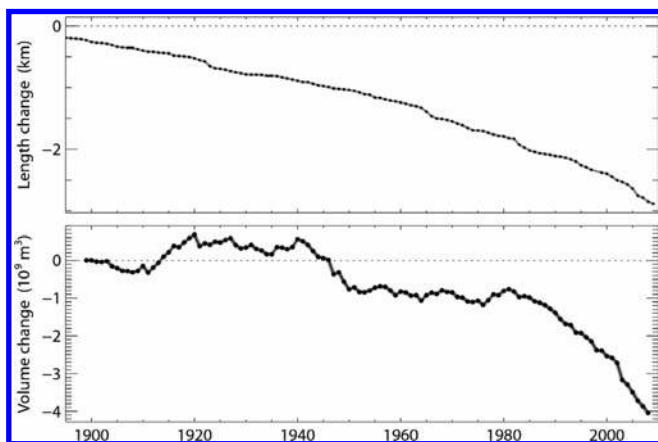


Figure 2. Past glacier evolution since 1900: length variation of Grosser Aletschgletscher (top) and cumulative volume change (bottom) in the entire watershed in annual resolution.

by a continuous retreat with a slight tendency to an increased rate in the second half of the twentieth century. More detailed insight is provided by the mass change: periods of higher mass losses in the 1940s and the last two decades are interrupted by two periods of reduced losses and even shorter decadal periods of mass gain in the 1910s and the late 1970s. These fluctuations were driven mainly by variations in the melting conditions visible in the summer balance (Fig. 2). While thickness changes are small in the accumulation area, large changes occur at the glacier snout.

3 METHODS FOR MODELING FUTURE GLACIER- AND RUNOFF-EVOLUTION

Hydrological modeling in high-alpine catchments presents a challenge: the large elevation range of the catchments and the pronounced spatial variability of meteorological phenomena require hydrological models to cope with a large number of processes. At high altitudes, components of the cryosphere as snow and ice play a determinant role in the water cycle and need to be represented adequately. Runoff modeling implies the linking together of different components of the water balance.

Our model is based on the approach presented by Huss et al. (2008b) and consists of five different modules coping with accumulation, ablation, glacier evolution, evapotranspiration and runoff routing. The model is fully distributed, designed for simulations at daily resolution and distinguishes six compartments (surface types): ice, snow, bare soil, low vegetation (pasture), high vegetation (forest) and open water (Fig. 1).

Accumulation is distributed over the catchment by adjusting the precipitation measured at the reference station with a correction factor accounting for the gauge catch deficit (Bruce and Clark, 1981) and a lapse rate prescribing a linear increase with altitude (Peck and Brown, 1962). Solid and liquid precipitation are distinguished by means of a threshold temperature. The fraction of solid precipitation decreases linearly from 0 to 1 in a range of $\pm 1^\circ\text{C}$ around this threshold (Hock, 1999). Solid precipitation is redistributed according to a spatially distributed factor (e.g. Tarboton et al., 2005; Huss et al., 2008a; Farinotti et al., 2010). Ablation is modeled with a distributed temperature-index approach (Hock, 2009). Melt is computed by using an empirical relation with average daily temperature and potential direct clear-sky solar radiation. The effect of radiation is assumed to be different for snow and ice, reflecting the differences in albedo of the two surfaces.

Modeling glacier evolution in a transient way is crucial for runoff projections in glacierized catchments. For this purpose a new state-of-the-art numerical model was developed recently,

coupling the described distributed mass balance model with a three-dimensional ice-flow model (Jouvet et al., 2009). The model calculates changes of the glacier geometry in response to a given mass balance. For practical reasons, the runoff projections presented in this study are based on a parametrization of the glacier evolution by Huss et al. (2010). The parametrization has been shown to agree well with the physical ice-flow model (Jouvet et al., 2009). In the parametric approach, glacier surface is updated annually by redistributing the annual mass balance according to a glacier-specific, elevation-dependent function derived from observations in the past.

Evapotranspiration is computed according to an empirical relation with temperature and the potential fraction of daylight per day (Hamon, 1961). The potential evapotranspiration is corrected for differences in the surface type. Runoff routing is based on the concept of linear reservoirs. The module distinguishes a snow and an interception reservoir, and two reservoirs representing slow and fast runoff components, respectively. The recession constant of the fast reservoir is surface type dependent and fixed for the slow reservoir. The snow reservoir is filled by solid precipitation, whereas the remaining ones are filled with both, liquid precipitation and melt. The interception and the slow reservoir have a maximal, surface type dependent capacity, whereas the capacity for the snow and fast reservoirs is not limited. The filling rates of the reservoirs with limited capacity are inversely proportional to their filling level (Schaeffli et al., 2005). Evapotranspiration is subtracted from the different reservoirs, depending on their filling level.

3.1 Calibration

The accumulation and ablation modules are calibrated according to the iterative calibration scheme described in Huss et al. (2008a). The scheme adjusts accumulation and melt parameters in order to match direct measurements of seasonal mass balance and glacier ice volume change, respectively. Mass balance measurements at selected points are available for the period 1921–2009. Ice volume changes are derived from digital elevation models (DEMs) of the years 1926, 1957 and 1999 according to the methods described in Bauder et al. (2007).

No direct measurements are available for calibrating the evapotranspiration module. The parameters are thus adjusted in order to match yearly evapotranspiration rates reported in the literature (e.g. Bernath, 1991; Verbunt et al., 2003).

The parameters of the runoff routing module are adjusted in order to maximize the agreement between calculated and measured discharge. Agreement is evaluated by considering daily, monthly and annual discharge, as well as comparing the modeled and observed distribution of runoff during the year. For the catchment concerned, measured runoff in daily resolution is available for the 1922–2007 period and provides an optimal basis for model calibration.

4 EXPECTED CLIMATE EVOLUTION

In order to assess the effects of climate change, projections for future climate play a key role. We rely on the most recent climate scenarios developed in the frame of the ENSEMBLES project (van der Linden and Mitchell, 2009). In this project, multiple model runs were performed coupling different general circulation models (GCMs) with different regional climate models (RCMs). The combination of a GCM with a RCM is usually referred to as ‘model chain’. The idea of ‘multiple runs’ is known to improve the accuracy and reliability of forecasts as the difference between individual results is useful for assessing which of the outcomes are more likely than the others.

In our study, we consider changes in temperature and precipitation and adopt the ‘delta change approach’. This approach describes the effects of climate change in terms of expected difference (‘delta’) in the mean of a given variable. The concept requires the definition of a ‘reference period’ (1980–2009 in our study) and a ‘scenario period’ of the same length (2021–2050 and 2070–2099 in our case). The ‘delta’ defines then the change in the mean

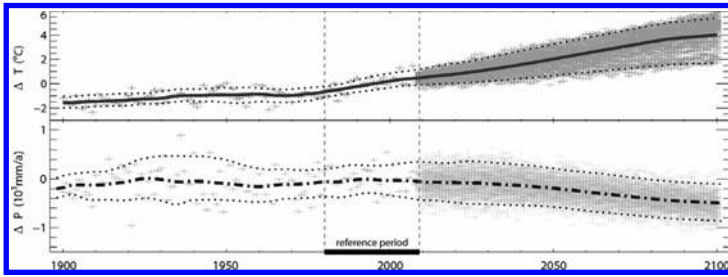


Figure 3. Evolution of mean air temperature T and annual precipitation sum P according to the climate scenarios. The deviation Δ from the mean of the reference period (black bar) is shown. For each year, all 100 realizations are displayed (gray crosses). The thick solid line shows the smoothed median deviation and the dotted lines contain 95% of the realizations. Smoothing is performed as 30-year moving average.

between the two periods. ‘Deltas’ do not need to refer to the annual mean but can have finer resolution. We use ‘deltas’ in daily resolution derived from 10 different model chains which all assume the SRES A1B emission scenario (Bosshard et al., in prep). ‘Daily resolution’ means that every day of the year has an individual ‘delta’.

For modeling the hydrological response of high-alpine catchments to climate change, transient simulations are necessary since the effect of glacier retreat needs to be represented continuously. In order to obtain transient scenarios from the ‘deltas’ described above, a linear interpolation is performed between the periods. This prescribes 10 different evolutions of the change in mean temperature and precipitation during the period 2010–2100.

However, meteorological variables are known to have a pronounced year-to-year variability, which is not accounted for in the delta-approach. In order to take into account this variability, we generate 10 different meteorological time-series for each of the 10 prescribed evolutions of the mean. This is done by repeating the following procedure for each year in the future for which a meteorological time-series is required: (1) randomly select a year in the past, (2) shift the mean of the selected year to the mean of the reference period, (3) add the interpolated, daily delta-change signal to the values thus obtained. The final result is a set of 100 possible realizations of mean daily air temperature and daily precipitation sum for the 2010–2100 period (Fig. 3).

For future projections of runoff and other variables of interest, we run our model with each of the 100 generated meteorological time-series. This provides the possibility of robustly assessing the uncertainty in the climate evolution.

5 PROJECTIONS OF GLACIER AND RUNOFF EVOLUTION TO 2100

We first present the glacier evolution towards the end of this century on the basis of the model presented in Jouvét et al. (2009) forced with the median of the climate scenarios (Fig. 3). The results show that the glaciers in the catchment will substantially retreat: the glacier surface area and the ice volume will decrease by 28% and 44%, in the middle, and by 68% and 89%, respectively, by the end of the century (Fig. 4).

While Grosser Aletschgletscher will only lose part of its tongue below Märjelen by the middle of this century, Ober- and Mittelaletschgletscher will have almost disappeared by then. The retreat of Oberaletschgletscher is probably overestimated since the melt reduction effect of the highly debris-covered tongue has not been taken into account sufficiently.

Figure 5 shows the evolution of runoff, precipitation, evapotranspiration, area covered by glaciers and the contribution of ice- and snow melt (ice melt: meltwater from snow-free, glacier covered area; snow melt: meltwater from snow, regardless of ground type) to the total runoff for the entire modeling period (1900–2100).

The importance of snow- and ice melt is clearly visible: on average over the past century, the contribution of the two components to annual runoff was about 50% and 30%, respectively.

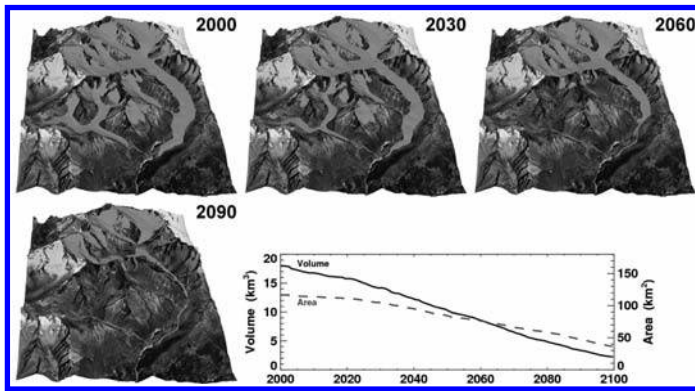


Figure 4. Glacier evolution in the Gebidem watershed until 2100 (snap shots for: 2000, 2030, 2060, and 2090). Time series of glacier surface area and volume until 2100 are shown in the lower right panel.

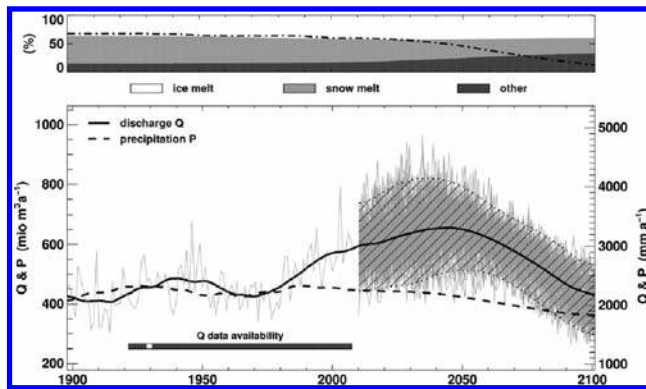


Figure 5. Evolution of annual discharge (Q, solid), precipitation (P, dashed), discharge components (ice melt, snow melt, other) and glacierization (dashed-dotted). For Q, the trajectories of all individual model realizations (gray lines), a smoothed confidence interval containing 95% of the data (dotted band) and the smoothed median of all realizations (thick solid line) is shown. For P, only the smoothed median is shown (dashed). The dark-gray bar displays the period in which measured data for Q are available. The relative contribution of the individual discharge components to total discharge is displayed in the top panel. The contribution from the non-cryosphere is summed up (labeled as “other”). Also shown is the glacierization. Smoothing is performed as 30-year moving average.

Since the last period of positive mass balances (in the late 1970s) the contribution of ice melt has steadily increased. This trend is expected to continue and reach a maximum during the period 2020–2070, when ice melt is expected to contribute to half of the annual runoff. This phase of increased ice melt and associated glacier retreat coincides with the phase in which the difference between annual precipitation and annual runoff is maximal. Considering the median of all realizations, annual runoff is expected to exceed annual precipitation by up to 58% in 2050. By the end of the century, however, annual runoff will almost coincide with annual precipitation, as it is expected for catchments with a small degree of glacier coverage and small evapotranspiration losses. Annual runoff has almost steadily increased in the last century. Although the scatter in the projections is large due to the uncertainty in future climate evolution, the trend is expected to continue and slightly accelerate until about 2030. Maximal annual discharges occur between 2020 and 2050 and will be about 25% higher than in the reference period. Beyond this period, annual discharge is expected to decrease, principally because of the diminishing ice melt contribution. The projected diminution of yearly

precipitation has a minor effect in the catchment but is not negligible. The median of all simulations forecasts a decrease in annual precipitation of about 20% compared to the reference period.

By the end of the century, glacier coverage is expected to decrease to about 18%. This does not affect the total annual runoff volume only, but also its distribution over the year. Figure 6 shows the temporal evolution of three selected quantiles of the annual discharge.

A significant change in the outer quantiles (i.e. 5 and 95% quantiles) is expected. This is a sign of the increase in runoff during the periods of the year which currently show very low runoff (i.e. winter months) and is attributed to two effects: (1) the prolongation of the melting season and (2) the warmer temperatures causing precipitation to occur as rain instead as snow during a longer period of the year. By the end of the century, the time by which 5% of annual runoff has occurred is expected to occur 30 ± 15 days earlier than in the reference period, whereas the 95% quantile is expected to occur 18 ± 10 days later in the season. However, the contribution of the winter months (Dec., Jan. and Feb.) to yearly runoff will remain insignificant until the end of the century. The changes in the central quantiles, in particular the median, are less pronounced. By the end of the century half of the yearly runoff is expected to have occurred 10 ± 8 days earlier. The time of maximal discharge is expected to occur about 40 days earlier, moving from late July/beginning of August to mid-June. The relative shift between the day on which the median and the maximal runoff occur is an additional indication of the regime curve becoming more asymmetric than in the reference period.

The projected rise in mean air temperature is reflected in two more variables of hydrological interest: glacier mass balance and duration of the snow cover season. The upper panel

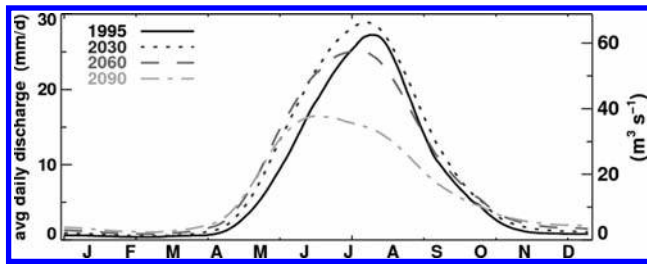


Figure 6. Evolution of runoff regime in the basin. Temporal evolution in 1995, 2030, 2060, and 2090 is shown.

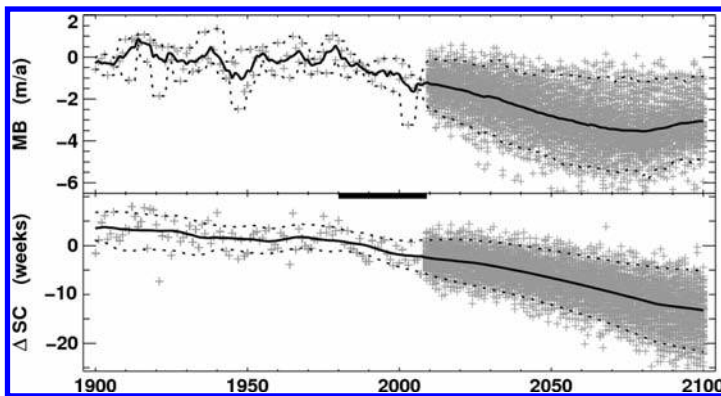


Figure 7. Evolution of glacier mass balance (MB, upper panel) and duration of the snow-cover season (SC, lower panel). The difference Δ of SC to the reference period (marked with the black bar) is shown. Individual data points (gray crosses) are yearly values. The smoothed median (solid line) and a confidence band containing 95% of the data (dotted lines) are displayed. Smoothing is performed as a 5- and 30-year running mean for MB and Δ SC, respectively.

in Figure 7 shows that positive mass balances are not expected during the whole century. Most negative mass balances are projected for the 2070–2090 period, when mass balance is expected to be as low as $-3.5 \text{ m w.e. a}^{-1}$ on a regular basis. This is in the order of the levels as experienced in the two extraordinary warm years 1947 and 2003 (Fig. 2).

The lower panel in Figure 7 shows the difference in the number of weeks in which the snow-covered fraction of the catchment is higher than in the average of the reference period. This measure is used as a proxy for quantifying the evolution in the duration of the snow-cover season. By the end of the century, the length of the snow-cover season is expected to have shortened by three months on average.

6 IMPACTS ON THE WATER MANAGEMENT FOR THE ELECTRA-MASSA POWER COMPANY

In order to assess the impacts of the projected changes in glacier volume and total runoff on the hydro-power generation processes, a comparison with the characteristics of the existing technical installations is required. The storage volume of the Gebidem reservoir amounts to $8.5 \times 10^6 \text{ m}^3$. The Bitsch power plant located 750 m below the reservoir is equipped with 3 Pelton turbines with a maximum capacity of $55 \text{ m}^3 \text{ s}^{-1}$. The mean annual production adds up to 470 GWh. Compared to 2010, the annual water inflow to the Gebidem reservoir is expected to increase by 9% until 2030 and decrease by 24% at the end of this century (Table 1).

The maximal average daily discharge is expected to rise by +5% in 2030 and decrease by 42% until 2100. This peak discharge will be progressively shifted from July 31 nowadays to June 23 at the end of the century (–38 days).

The reduction in glacier surface area will uncover large amounts of unconsolidated moraines and lead to an increase in sediment transport to the reservoir. This will make necessary more frequent purges and could accelerate significantly the wear on the equipment. The expected increased runoff will also have an impact on the hydrological dam safety, possibly requiring an adaptation of the spillway capacity, and on the flood risk of the Massa river downstream of the reservoir.

According to the runoff projections, different adaptations of the existing hydroelectric power plant may be considered in the time horizon 2050. Due to the expected increase in runoff for the next 3–4 decades, several extensions of the installations may be of interest in order to exploit in an efficient way the additional quantity of available water and renewable energy:

- Increasing the volume of the reservoir by elevating the existing dam and upgrading the discharge capacity of the pressure tunnel and shaft.
- Increasing the power of the installed turbines and generators and/or their number.
- Adapting the operating instructions using an energy optimization tool.

The choice of the extension of the hydro-power plant will be based on economic analysis and environmental parameters considering the more plausible long-term climate scenar-

Table 1. Projected evolution of annual discharge Q_a and maximal daily discharge Q_d^{\max} for selected points in time. Values are centered 30-year averages. ‘%’ indicate the relative change compared to 2010. ‘doy’ is the day of the year at which Q_d^{\max} occurs.

Year	Q_a				Q_d^{\max}			
	(mm a ⁻¹)	10 ⁶ (m ³ a ⁻¹)	(m ³ s ⁻¹)	(%)	(mm d ⁻¹)	(m ³ s ⁻¹)	(%)	(doy)
1995	2740	540	17.1	–8	26.7	61.2	–2	218
2010	2970	590	18.7	0	27.1	62.2	0	211
2030	3240	640	20.3	+9	28.6	65.6	+5	209
2060	3120	620	19.7	+5	24.6	56.5	–9	203
2090	2290	450	14.3	–24	15.8	36.2	–42	174

ios and the costs of the related investments. A preliminary requirement for this extension would be the reinforcement of the existing grid transport capacity between Mörel and Chippis.

7 DISCUSSION AND CONCLUSIONS

This study underlines that climate change will have major impacts on alpine hydrology and the water resources of highly glacierized watersheds. Glacier retreat and the consequent release of additional melt water are key processes in runoff projections from high-alpine basins over the next decades. An important condition to be fulfilled in modeling glacier retreat for hydrological purposes is mass conservation. The coupled distributed mass balance and ice-flow model presented here is a promising new approach.

The major source of uncertainty in models assessing future glacier- and runoff-evolution are the expected climatic changes and their impact on glacier mass balance. The large bandwidth of climate change projections is mainly due to the uncertainties in future evolution of anthropogenic greenhouse-gas emissions and the divergence of the results from different climate models. In this contribution, considerable effort was invested in assessing the uncertainties induced by such climate projections. A second type of uncertainty, linked to the parameters of the different modules of our model, was, however, not addressed. For all our simulations, we assumed constant parameters, i.e., a parameter set which remains unchanged for the whole modeling period. This choice may be questionable, as parameters may change over time but is a fairly common assumption, since the appropriateness of time-varying parameters is generally difficult to assess.

The conceptual models used in the study are a source of uncertainty as well. Aside from the module which deals with the glacier dynamics, all other approaches are based on empirical relations. Although all models have been shown to provide reasonable results in the past, there is a general question about their suitability for long-term projections. In many fields of natural sciences physically-based models become gradually more popular as it is suggested that such models may be better suited for projections in an environment for which one of the strongest drivers—the climate—is expected to change.

The future runoff from the drainage basin of the Gebidem reservoir was simulated for the 21st century. Runoff regime was simulated transiently by considering glaciers as a dynamically changing storage component of the watershed. Annual runoff is expected to increase by 9% until 2030 and to decrease by 24% by the end of the century. The annual runoff regime will shift progressively from a glacier-melt to a snow-melt dominated regime. Maximal average daily discharge will rise by 5% until 2030 and decrease by about 40% by the end of the century. This peak discharge will be progressively shifted from end of July to middle of June. Water resource management will have to adapt to this projected, major changes.

ACKNOWLEDGEMENTS

Support for this study was provided by the projects of CCHydro (Swiss Federal Office for the Environment, BAFU) and FUGE (Swiss national science foundation, NFP 61). Sincere thanks are extended to Electra-Massa SA, Moritz Steiner (Department of Energy and Hydro Power, Canton Valais) and Charly Wuilloud (Service of Forest and Landscape of the Valais) for their financial support. The delta-change scenario data were distributed by the Center for Climate Systems Modeling (C2SM) at the ETH Zurich. The data were derived from regional climate simulations of the EU FP6 Integrated Project ENSEMBLES whose support is gratefully acknowledged. The dataset was prepared by Thomas Bosshard at ETH Zurich, partly funded by swisselectric/Swiss Federal Office of Energy (BFE) and CCHydro. We acknowledge Stephanie Usselman for her contribution in the preparation of the Figures.

BIBLIOGRAPHY

- Bauder, A., Funk, M., & Huss, M. (2007). Ice volume changes of selected glaciers in the Swiss Alps since the end of the 19th century. *Annals of Glaciology*, 46:145–149.
- Bernath, A. (1991). Wasserhaushalt im Einzugsgebiet der Rhone bis Gletsch. Untersuchungen zu Niederschlag, Verdunstung und Abfluss in einem teilweise vergletscherten Einzugsgebiet. *Zürcher Geographische Schriften*, 43.
- Bosshard, T., Kotlarsky, S., & Schär, C. (in prep.). Spectral representation of the annual cycle in the climate change signal.
- Braun, L., Weber, M., & Schulz, M. (2000). Consequences of climate change for runoff from Alpine regions. *Annals of Glaciology*, 31(1):19–25.
- Bruce, J.P. & Clark, R.H. (1981). Introduction to hydrometeorology. *Pergamon Press*, Oxford.
- Farinotti, D., Huss, M., Bauder, A., & Funk, M. (2009). An estimate of the glacier ice volume in the Swiss Alps. *Global and Planetary Change*, 68(3):225–231.
- Farinotti, D., Magnusson, J., Huss, M., & Bauder, A. (2010). Snow accumulation distribution inferred from time-lapse photography and simple modelling. *Hydrological Processes*, 24:2087–2097.
- Glaciological reports (1881–2009). The Swiss Glaciers, 1880–2004/05. Technical Report 1–126, Yearbooks of the Cryospheric Commission of the Swiss Academy of Sciences (SCNAT). published since 1964 by Laboratory of Hydraulics, Hydrology and Glaciology (VAW) of ETH Zürich, <http://glaciology.ethz.ch/swiss-glaciers/>.
- Hamon, W.R. (1961). Estimating potential evapo-transpiration. *Journal of the Hydraulics Division*, 87(HY3):107–120.
- Hock, R. (1999). A distributed temperature-index ice-and snowmelt model including potential direct solar radiation. *Journal of Glaciology*, 45(149):101–111.
- Hock, R., Jansson, P., & Braun, L.N. (2005). Modelling the response of mountain glacier discharge to climate warming. In Huber, U.M., Bugmann, H.K.M., and Reasoner, M.A., editors, *Global Change and Mountain Regions (An Overview of Current Knowledge)*, volume 23 of *Advances in Global Change Research*, pages 243–252. Springer.
- Horton, P., Schaeffli, B., Mezghani, A., Hingray, B., & Musy, A. (2006). Assessment of climate-change impacts on alpine discharge regimes with climate model uncertainty. *Hydrological Processes*, 20(10):2091–2109.
- Huss, M., Bauder, A., Funk, M., & Hock, R. (2008a). Determination of the seasonal mass balance of four alpine glaciers since 1865. *Journal of Geophysical Research*, 113(F1):F01015.
- Huss, M., Farinotti, D., Bauder, A., & Funk, M. (2008b). Modelling runoff from highly glacierized alpine drainage basins in a changing climate. *Hydrological Processes*, 22(19):3888–3902.
- Huss, M., Jouvét, G., Farinotti, D., & Bauder, A. (2010). Future high-mountain hydrology: a new parameterization of glacier retreat. *Hydrology and Earth System Sciences*, 14(5):815–829.
- Jansson, P., Hock, R., & Schneider, T. (2003). The concept of glacier storage: a review. *Journal of Hydrology*, 282(1–4):116–129.
- Jouvét, G., Huss, M., Blatter, H., Picasso, M., & Rappaz, J. (2009). Numerical simulation of Rhonegletscher from 1874 to 2100. *Journal of Computational Physics*, 228(17):6426–6439.
- Peck, E.L. & Brown, M.J. (1962). An approach to the development of isohyetal maps for mountainous areas. *Journal of Geophysical Research*, 67:681–694.
- Romerio, F. (2008a). Hydroelectric resources between state and market in the alpine countries. In Wiegandt, E., editor, *Mountains: Sources of water, Sources of knowledge*, volume 31 of *Advances in Global Change Research*, 83–99. Springer, New York.
- Romerio, F. (2008b). Regional policy and hydroelectric resources. *Journal of Alpine Research*, 96(1):79–89.
- Schaeffli, B., Hingray, B., & Musy, A. (2007). Climate change and hydropower production in the Swiss Alps: quantification of potential impacts and related modelling uncertainties. *Hydrology and Earth System Sciences*, 11(3):1191–1205.
- Schaeffli, B., Hingray, B., Niggli, M., & Musy, A. (2005). A conceptual glacio-hydrological model for high mountainous catchments. *Hydrology and Earth System Sciences*, 9(1/2):95–109.
- Tarboton, D.G., Chowdhury, T.G., & Jackson, T.H. (1995). A spatially distributed energy balance snowmelt model. In Tonnessen, K.A., Williams, M.W., and Tranter, M., editors, *Biogeochemistry of Seasonally Snow-Covered Catchments, Proceedings of a Boulder Symposium*, pages 141–155. IAHS Publ. No. 228.
- van der Linden, P. & Mitchell, J.F.B. (2009). *ENSEMBLES: Climate Change and its Impacts: Summary of Research and Results from the ENSEMBLES Project*. Met Office Hadley Centre, UK. 160 pp.
- Verbunt, M., Gurtz, J., Jasper, K., Lang, H., Warmerdam, P., & Zappa, M. (2003). The hydrological role of snow and glaciers in alpine river basins and their distributed modeling. *Journal of Hydrology*, 282(1–4):36–55.

Decision Support System for the hydropower plants management: The MINERVE project

J.G. Hernández, A.J. Schleiss & J. Boillat

Laboratoire de Constructions Hydrauliques (LCH), Ecole Polytechnique Fédérale de Lausanne (EPFL), Lausanne, Switzerland

ABSTRACT: The MINERVE project was initiated for flood management in the Upper Rhone river basin. Its first goal is the prediction of floods. The second one is the optimum management of the complex system of hydropower plants located in the basin in order to diminish the peak discharge in the Rhone River and its tributaries. The MINERVE Interactive Decision Support (MINDS) proposes turbine and bottom outlet preventive operations before the flood peak, for having storage volume in the reservoirs during the peak flow. The *iterative ranking Greedy algorithm* allows successive resolutions for all the hydropower plants in an iterative way until reaching the optimum operations of the whole complex. The *multi-criteria analysis* optimises the start and the end of the preventive operations (turbine and bottom outlet operations) for the whole ensemble hydrological forecasts for a selected hydropower plant.

1 INTRODUCTION

Several flood events during the last decades have caused important disasters in the Upper Rhone River basin in Switzerland and have emphasized the need of dealing with catastrophic inundations. The MINERVE project aims to improve security by reducing damages in this basin (Boillat, 2009). The main objectives are to predict floods in advance for warning and to manage the multi-reservoir system of the existing hydropower schemes in order to gain a better flow control during floods.

The MINERVE system provides hydrological forecasts up to five days (García Hernández et al., 2010). It exploits flow measurements at river gauging stations, operation data from reservoirs and hydropower plants as well as deterministic (COSMO-7 and COSMO-2) and ensemble (COSMO-LEPS) meteorological forecasts from MeteoSwiss. The hydrological model is based on a semi-distributed concept and is completed by rivers and hydraulic structures such as water intakes, reservoirs, turbines and pumps. When the hydrological forecasts are simulated, a report provides the warning level (Notice, Alert or Alarm) at selected control points distributed over the whole basin, being a support to decision-makers for preventive actions.

The hydrological forecasts are also used for the evaluation of priority decisions concerning the safe management of the storage hydropower plants. A tool called MINDS (MINERVE Interactive Decision Support) has been developed for this purpose. Turbine and bottom outlet preventive operations can be proposed to the powerhouse operators, depending on observed discharge at control points, hydrological forecasts and reservoir levels. The goal is to store water inflows in the reservoirs and stopping turbines during the peak flow. Appropriate preventive operations can thus reduce the peak discharges in the Rhone River and its tributaries, limiting or avoiding damages.

Even if these preventive operations can be risky, good understanding and interpretation of the hydro-meteorological forecasts allow the identification of the potentially dangerous floods and the appropriate preventive interventions and manoeuvres.

2 HYDROLOGICAL FORECASTS

2.1 *Meteorological input data*

The MINERVE system exploits probabilistic COSMO-LEPS weather forecast as well as deterministic weather forecasts COSMO-7 and COSMO-2, all of them operated by MeteoSwiss.

COSMO-LEPS is the limited-area EPS (Ensemble Prediction System) developed within the COSMO consortium (Consortium for Small-scale Modeling) and combines the benefits of the probabilistic approach with the high-resolution detail of the model. Twice per day, COSMO-LEPS provides high resolution probabilistic forecasts (horizontal mesh-size of 10 km) based on a 16-member ensemble for central and southern Europe with a lead time of 120 h.

Deterministic forecasts COSMO-7 and COSMO-2 are a support of COSMO-LEPS. The regional COSMO-7 is driven by the global model of ECMWF (European Centre for Medium-Range Weather Forecasts) and covers most of western and central Europe. It is computed on a grid spacing of about 6.6 km and is calculated twice per day for 72 h lead time. The local COSMO-2, driven by COSMO-7, covers the Alpine region with Switzerland located at the center and is computed on a grid spacing of about 2.2 km. It is calculated 8 times a day for a 24 h lead time. Both of them allow the use of the most recent atmospheric conditions observed and the benefit of the short range forecasting.

2.2 *Hydrological model*

The catchment area of the Rhone River has about 5500 km² and has been divided in 239 sub-catchments taking into account all hydraulic structures of dams and hydropower plants. The hydrological concept used to estimate the discharge in the outlet of each sub-catchment is based on the GSM-Socont (Glacier & SnowMelt -SOil CONtribution) model (García H. et al., 2007).

For the hydrological part of modelling, each sub-catchment is divided into two parts, glacier and non-glacier, both divided in altitude bands. Precipitations and temperatures values are calculated from the meteorological input data for each one of these altitude bands. Then, a snow model follows the temporal evolution of the height and saturation degree of the snow. The snow melt produces an equivalent precipitation starting from a rate of saturation threshold.

In the case of a non-glacier band, this equivalent precipitation supplies the infiltration and the transfer model, composed by two parallel non-linear reservoirs, which produce the slow and fast components of the discharge going to the outlet of the sub-catchment.

In the case of a glacier band, the equivalent precipitation resulting from the snow melt is transferred to the outlet by a linear reservoir. When there is no more snow, a glacier model produces (when temperature is higher than zero) a discharge which is also transferred to the outlet of the sub-catchment by a linear reservoir behaviour.

2.3 *Hydrological simulations*

This semi-distributed hydrological model was built using the hydrological and hydraulic simulation tool Routing System II (García H. et al., 2007; Jordan et al., 2008). This software was designed to simulate the formation and the propagation of free surface flows in a complex system. It allows hydrological and hydraulic modelling by an oriented object approach, according to a semi-distributed conceptual scheme. It takes into account special hydrological processes such as snow and glacier melt, surface and sub-surface flows, routing in reservoirs, water transfer tunnels and rivers as well as the modelling hydraulic structures with valves, gates, water intakes, turbines or pumps.

An evolution of Routing System II tool provides a flood forecast in real-time, coupling the observed measurements and the weather forecast information with the hydrological model. Every time a new weather forecast is provided, the hydrological forecast is updated.

After the first developments of the project with deterministic forecasts until 2006 (Jordan, 2007), the MINERVE system is enhanced since 2008 by implementing new probabilistic forecasts (García H. et al., 2009a) as well as other improvements in other domains (García H. et al., 2009b) with the aim of providing better hydrological forecasts to the decision support system.

3 MINERVE INTERACTIVE DECISION SUPPORT

3.1 Hydraulic model

The hydraulic model of the Wallis and Vaud Cantons, developed for the optimisation tool MINDS (MINERVE Interactive Decision Support), is a simplified model of this complex river basin (Fig. 1). It contains the most important reservoirs RES (triangles), with its bottom outlets and spillways (square dotted lines), hydropower plants HPP (round dotted lines), as well as the main river network (solid lines) with the main control points CP (big circles).

In this model, the hydropower plants and reservoirs have been divided in independent groups (i.e. without any connexion between them). The characteristics of the groups and their reservoirs are presented in Table 1. Even if reservoirs are generally used to store water, several reservoirs operate without this function, just as a compensation basin. They work as elements where the inflow is derived to other reservoirs or rivers, or where pumping operations can be done.

The hydropower plants are also included in the model with their characteristics (discharge capacity, head, installed generation capacity,...). They connect two reservoirs or a reservoir to the river network. When a preventive operation of turbinage or pumping is proposed, the hydropower plant works with the maximum discharge capacity in order to have the best performance possible in terms of time, i.e. reducing the time for preventive operations as much as possible.

Finally, the main control points (CP) of the river network are assumed as the locations where optimisations can be done. The transit times between them are considered as constant.

For all the control points in Table 2, the discharge is given for the flood of October 15, 2000 (Q_{2000} in m^3/s , from which flooding are assumed), together with the extreme expected

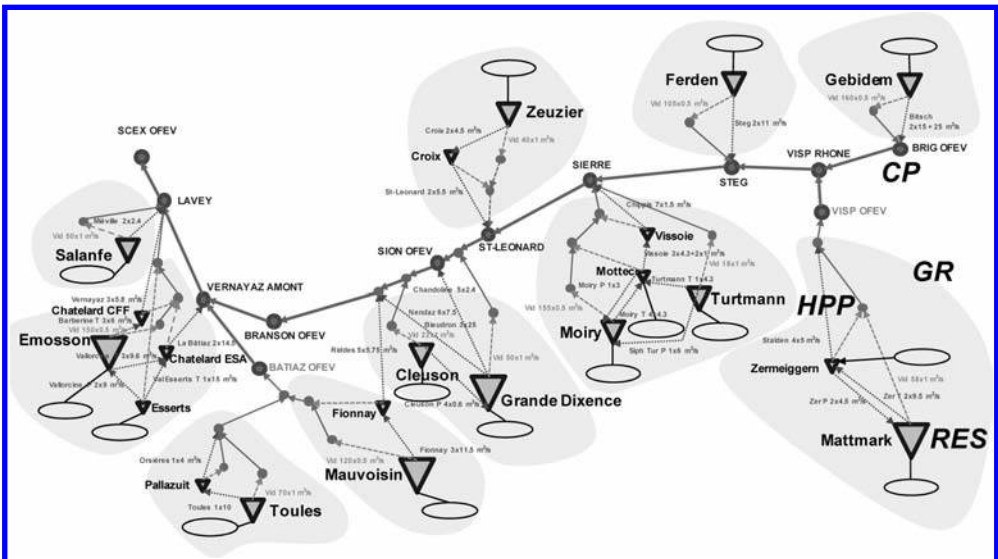


Figure 1. Scheme of the Upper Rhone River catchment with the MINDS model of the hydropower plants.

Table 1. Groups and reservoirs of the MINDS model (P for volume of punctual reservoirs).

Group (GR)	Reservoir (RES)	
	Name	Vol (Mm ³)
GD	Grande Dixence	422 · 10 ⁶
	Cleuson	28 · 10 ⁶
ESA	Emosson	255 · 10 ⁶
	Esserts	P
	Chatelard CFF	P
	Chatelard ESA	P
FMM	Mauvoisin	215 · 10 ⁶
	Fionnay	P
KWM	Mattmark	188 · 10 ⁶
	Zermeiggern	P
FMG	Moiry	83.3 · 10 ⁶
	Turtmann	0.844 · 10 ⁶
	Mottec	P
	Vissoie	P
EL	Zeuzier	61 · 10 ⁶
	Croix	P
SAL	Salanfe	43.6 · 10 ⁶
GSB	Toules	27.3 · 10 ⁶
	Pallazuit	P
EM	Gebidem	9.6 · 10 ⁶
KWL	Ferden	2.12 · 10 ⁶

discharge (Q_{ex}) associated with the expected costs of damages (10⁶ CHF, i.e. Swiss Francs) in the surrounding area.

The simplifications assumed in the model reduce the calculation time to a couple of minutes, without reducing the performance of the system. In fact, transit time has been estimated previously and reservoirs proposed as punctual elements have not enough volume to contribute to the preventive operations or to reduce significantly discharges in the river network. Thanks to these simplifications and the approach explained hereafter, the calculation time for optimisation has been reduced in order to use the software in real-time, updating the forecasts if necessary.

3.2 Optimisation objectives

The objective of the system is the minimisation of all the damages and production losses produced in Rhone River catchment area, upstream of the selected control point considered as the objective of the optimisation. All the damages and losses are calculated in economics values for comparison. Firstly, the damages expected in the studied catchment area are taken into account because of the flood. Secondly, the potential production losses in the hydropower plants because the proposed preventive operations are assessed.

Once a control point is selected as downstream objective (the selected point is usually the outlet of the catchment area), the objective function of the system is presented as the minimisation of both the expected damages and the potential costs of the preventive operations upstream of the selected control point. Then, the optimisation of the function searches the optimal sequences of turbine, emptying and pumping in each concerned hydropower plant. Thus, the variables of the system are the start and end for the expected sequences. Consequently, in the case that no damage is expected, the system does not propose any preventive operations.

Table 2. Characteristics of control points and areas related to them.

Control point (CP)	River	Q_{2000}	Q_{ex}	Maximum expected damages in the area
Brig OFEV	Rhone	560	750	207.9
Visp OFEV	Visp	190	590	441.0
Visp Rhone	Rhone	760	1380	2835.0
Steg	Rhone	779	1380	560.0
Sierre	Rhone	826	1480	1106.8
St-Léonard	Rhone	859	1520	50.4
Sion OFEV	Rhone	910	1580	896.7
Branson OFEV	Rhone	980	1600	452.3
Batiaz OFEV	Dranses	196	204	56.3
Vernayaz Am.	Rhone	1176	1804	8
Lavey	Rhone	1236	1913	313.16
Scex OFEV	Rhone	1370	2120	1936.44

The costs related to the preventive manoeuvre results, automatically and simultaneously, in a maximisation of the volumes in the reservoirs for the period of the optimisation. The reason is that preventive operations are done when they have an effect in the expected damages, and do not last more than is strictly necessary.

The inputs of the system are the hydrographs in the control points as well as the inflows and initial levels at the reservoirs. The constraints are the usual ones in this case of optimisations, such as the capacity of turbines, pumps and bottom outlets, the correct balance in the reservoirs volume, the emergency rules of reservoirs and the behaviour of the spillway.

To solve this objective function, the problem uses an *Iterative Ranking Greedy algorithm* (IRGA) and a *Multi-Criteria Analysis* (MCA). The IRGA allows the resolution in series for the hydropower plant groups. The MCA minimises the costs based on damages, losses and weights of the forecasts. Different MCA analysis methods have been implemented: Expected Risk, MinMax Regret (Savage, 1951), Hurwicz (Hurwicz, 1950) and Fuzzy logic (Cheng, 1999).

3.3 Damages and cost evaluation

For the estimation of the expected damages ED, the maximum discharge Q_{max} of the simulation period is calculated at each control point k , CP_k . According to Eq. 1, the theoretical discharge where severe flooding occurs (assumed to be the October 15, 2000 flood, Q_{2000}) and the considered extreme discharge Q_{ex} at the same control point are compared to Q_{max} .

If Q_{max} exceeds Q_{2000} , an initial damage (δED_{max} , $\delta \leq 1$) at the area surrounding the control point location is directly produced. The maximum damage ED_{max} is produced when it makes equal Q_{max} and Q_{ex} . The total expected damages are the addition of all the damages upstream of the selected objective location.

$$ED_{CP_k}(a_{i_{coll}} | f_j) = \begin{cases} 0 & \text{if } Q_{max_{CP_k}}(a_{i_{coll}} | f_j) \leq Q_{2000_{CP_k}} \\ \delta \cdot ED_{max_{CP_k}} + (1 - \delta) \cdot \left(\frac{Q_{max_{CP_k}}(a_{i_{coll}} | f_j) - Q_{2000_{CP_k}}}{Q_{ex_{CP_k}} - Q_{2000_{CP_k}}} \right)^{1-\lambda} \cdot ED_{max_{CP_k}} & \text{if } Q_{2000_{CP_k}} < Q_{max_{CP_k}}(a_{i_{coll}} | f_j) < Q_{ex} \\ ED_{max_{CP_k}} & \text{if } Q_{max_{CP_k}}(a_{i_{coll}} | f_j) \geq Q_{ex_{CP_k}} \end{cases} \quad (1)$$

where $a_{i_{coll}}$: collection i of preventive operations in all the reservoirs; f_j : forecast j ; δ : initial damage parameter, representing the percentage of initial damages compared to ED_{max} [-]; λ : power damage parameter [-]; Q_{max} : maximum discharge in the whole studied period [m^3/s];

Q2000: October 15, 2000 peak discharge, assumed to be the flooding discharge [m³/s]; Q_{ex}: extreme discharge related to maximum damages [m³/s]; ED_{max}: maximum expected damages [CHF].

For the potential preventive operations costs PPOC, installed capacity (P) and energy (E) are calculated depending on the discharge series Q and head H of the hydropower plant h HPP _{h} (Eqs. 2, 3). If a reservoir is connected to several hydropower plants, the same preventive operation is provided for all of them.

The potential costs of the preventive operations (energy sale losses) per reservoir r (RES _{r}) or group g (GR _{g}) are calculated based on the maximum price the energy could be sold (c_{\max}) in the energy market and the current estimated price (c_{current}) when preventive operations are realized (Eqs. 4, 5). Estimate price depends on time and day of the week and is obviously zero for bottom outlet operations.

$$P_{HPP_h}(a_{i_{RES_r}}) = \rho \cdot g \cdot H_{HPP_h} \cdot Q_{a_{i_{RES_r}}} \cdot \eta_{HPP_h} \quad (2)$$

$$E_{HPP_h}(a_{i_{RES_r}}) = \int_{t=t_a}^{t=t_b} \frac{P_{HPP_h}(a_{i_{RES_r}})}{1000} dt \quad (3)$$

$$PPOC_{RES_r}(a_{i_{RES_r}}) = \sum_{h=1}^{h=U} \int_{t=t_a}^{t=t_b} \frac{P_{HPP_h, HPP_h \in RES_r}(a_{i_{RES_r}})}{1000} \cdot (C_{\max} - C_{\text{current}}) dt \quad (4)$$

$$PPOC_{GR_g}(a_{i_{GR_g}}) = \sum_{r=1}^{r=h} PPOC_{RES_r, RES_r \in GR_g}(a_{i_{RES_r}}) \quad (5)$$

where ρ : water density, 1000 [kg/m³]; g : gravity, 9.81 [m/s²]; η : plant efficiency [-]; PHPP _{h} : installed capacity [W]; E: energy [kWh]; PPOC: potential preventive operation costs [CHF]; a_i RES _{r} : preventive operation i in the reservoir r ; a_i GR _{g} : collection i of preventive operations in the reservoirs of the group g .

3.4 Theoretical objective function

The Expected Risk criteria analysis (ERCA) is assumed for presenting the theoretical objective function. The ERCA identifies the ideal preventive operation for the whole ensemble hydrological forecasts based on a risk assessment which depends on expected damages, potential losses and weight of the forecasts taken into account, according to Equation 6.

$$\min \left[\alpha \cdot \frac{1}{n} \sum_{j=1}^{j=n} \left(\sum_{k=1}^{k=p} AD_{Cp_k}(a_{i_{collection}} | f_j) \cdot P(f_j) \right) + \beta \cdot \sum_{r=1}^{r=v} PPOC_{RES_r}(a_{i_{collection}}) \right] \quad (6)$$

where α : weight parameter for the expected damages, 1 [-]; β : weight parameter for the potential preventive operation costs, 1 [-]; $P(f_j)$: occurrence probability of forecast j ; n : total number of forecasts; p : total number of control points; v : total number of reservoirs.

Nevertheless, since calculation time increases considerably solving all the variables at the same time, the presented *iterative ranking Greedy algorithm* (Dechter and Dechter, 1989) is also used in order to be able to solve preventive operations reservoir by reservoir for decreasing the calculation time as much as possible for the real-time decision making task.

3.5 Iterative ranking greedy algorithm (IRGA)

The IRGA allows solving in series all the hydropower plants. First of all, a hierarchy of priority for the groups' management is defined. When a group is selected, the objective function searches the minimisation of the expected damages in the considered catchment as well as the potential costs of preventive operations in the group.

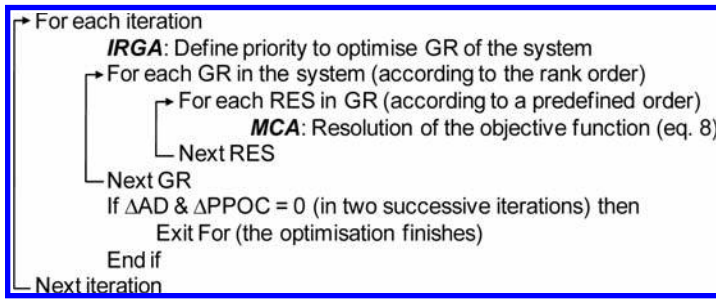


Figure 2. Scheme for the optimisation of the MINDS system.

The hierarchy of the groups is given by the efficiency of their reservoirs for storing water during a flood or by their location from upstream to downstream. Then, a pre-defined rank in the reservoirs of the group provides the position to optimise them. The theoretical objective function (Eq. 6), still assuming the ERCA methodology, becomes the objective function x (because it is related to the reservoir x of the group w) as presented in Equations 7 and 8.

$$\min \left[\alpha \cdot \frac{1}{n} \sum_{j=1}^{j=n} \left(\sum_{k=1}^{k=p} ED_{CP_k} (a_{i_{RES_x}} | f_j) \right) + \beta \cdot PPOC_{RES_x, RES_x \in GR_w} (a_{i_{RES_x}}) \right] + \zeta \quad (7)$$

$$\zeta = \beta \cdot \sum_{r=1}^{r=v} PPOC_{RES, r \neq x} \quad (8)$$

The optimisation is obtained by double scanning, searching the start and end for the preventive operations (turbine and bottom outlet operations) for the ensemble of the forecasts in the hydropower plants linked to the optimised reservoir. Firstly, the optimisation of the turbine sequence is done. Afterwards, if flood damages still occur in the basin, the bottom outlet sequence is optimised.

The first scan searches the sequence of the preventive operations with a bigger calculation step for the start and the end of the sequence (the parameters is pre-defined to four hours, but can be easily changed by the user). Once this solution is found, a second scan searches the optimal solution around this first one. The calculation step is then smaller, normally the same than data coming from hydrographs and inflows (one hour in our case).

This optimisation is carried out for each reservoir of all the groups (Fig. 2). When the preventive operations in the hydropower plants connected to the current reservoir are optimised, the operations of the hydropower plants of the other reservoirs are assumed known and established in advance. The potential costs PPOC of energy losses for the known operations are then ζ , as given in Equation 8.

The optimization is performed several times by iteration until the optimum is found and the results (expected damages in each sector and preventive operations costs in the reservoirs) do not vary anymore). Besides, before the next iteration, the *ranking* of the groups is recalculated and their hierarchy can be changed.

4 RESULTS

The initial results of the system reveal a reduction of the peak discharge and flooding in the Rhone River and its tributaries. The validation of the results is currently tackled but it is already clear that the system has a great performance and could be operated by the crisis task force in the Wallis Canton.

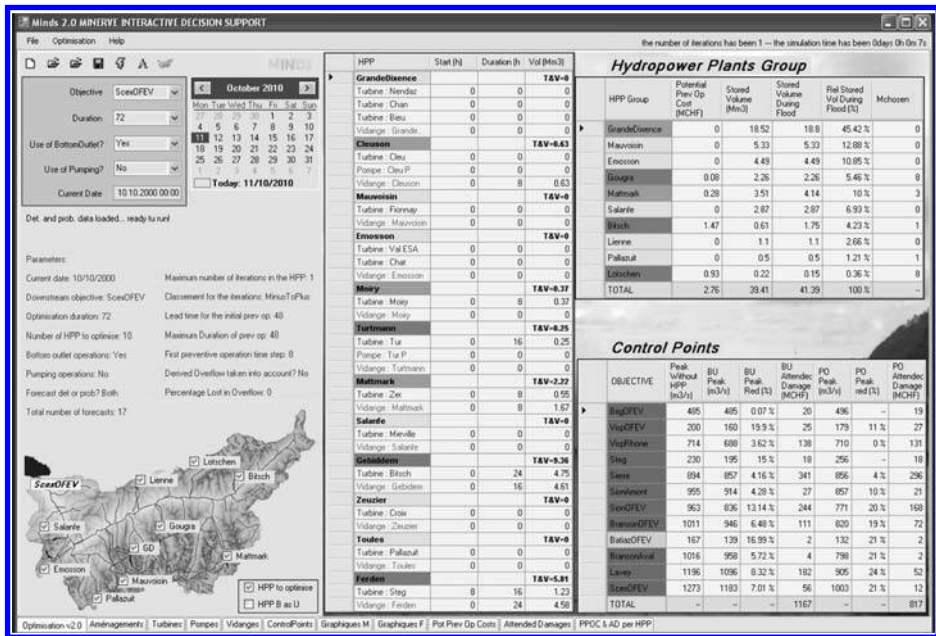


Figure 3. Interface of MINDS.

The first page of the MINDS interface (Fig. 3) presents preventive operations in the concerned hydropower plants as well as the control points with overflowing problems. Other pages of MINDS give the benefit of the preventive operations, the potential costs for the hydropower plants or expected damages in the control points, hydrographs with and without the preventive operations etc, always from a probabilistic point of view (e.g. with the help of box plots).

The MINDS interface which is still under development will give information on the probability damages before and after the optimisation of the preventive operations.

5 CONCLUSIONS

The MINERVE system developed for the Wallis and Vaud Cantons is already operational. It allows simulating the discharge in the river network of the Upper Rhone catchment area since it considers all hydraulic elements of the hydropower plants and dams, preventive turbine operations and water release for flood protection. The flood forecast and management system is the decision-making tool which is used by a crisis task force for limiting flood damages.

The program MINDS (MINERVE Interactive Decision Support) is the main development of the project for preventive operations at reservoirs located in the catchment area. A simple but robust procedure has been implemented for the optimization of this complex river basin.

The reservoirs and hydropower plants are organized in independent groups and are optimised in sequence based on a *Greedy algorithm*. The hydropower plant is optimised regarding its turbine and bottom outlet operations with an objective function which minimises expected damages and potential preventive operations costs upstream of the selected objective location.

The strength of MINDS is its flexibility and adaptability. If a river sector has a reduced flooding threshold because of ongoing construction works, a turbine is under maintenance and/or a bottom outlet gate is not operational, the program is able to recalculate the optimal

solution in real-time with the current characteristics of the rivers, reservoirs and hydropower plants.

The preventive operations are then transmitted to the crisis task force which decides whether or not to impose the hydropower plant operators to take actions. In this way, several agreements have been signed between the Wallis Canton and the hydropower plant operators for possible reimbursements when floods do not arrive and the energy sales benefits are reduced.

ACKNOWLEDGEMENTS

The MINERVE project is developed in partnership by the Swiss Federal Office for Environment (FOEV), Services of Roads and Water courses as well as Energy Water Power of the Wallis Canton and Service of Water, Land and Sanitation of the Vaud Canton. The Swiss Weather Service (MeteoSwiss) provides the weather forecasts and hydroelectric companies communicate specific information regarding the hydropower plants. Scientific developments are entrusted to two entities of the Ecole Polytechnique Fédérale de Lausanne (EPFL), the Hydraulic Constructions Laboratory (LCH) and the Ecohydrology Laboratory (ECHO), as well as to the Institute of Geomatics and Analysis of Risk (IGAR) of Lausanne University (UNIL).

REFERENCES

- Boillat, J.-L. 2009. Prévision hydrologique et aide à la décision. *Swiss Engineering* Vol. 7/8, p. 10.
- Cheng, C. (1999). Fuzzy optimal model for the flood control system of the upper and middle reaches of the Yangtze River. *Hydrological Sciences Journal*, Vol. 44 (4), 573–582.
- Dechter, A. & Dechter, R. (1989). On the Greedy Solution of Ordering Problems. *ORSA Journal on Computing*, Vol. 1, No. 3, 181–189.
- García Hernández, J., Jordan, F., Dubois, J., Boillat, J.-L., & Schleiss, A. 2007. Routing System II: Flow modelling in hydraulic systems. *Communication 32 du Laboratoire de Constructions Hydrauliques*, Ed. A. Schleiss, EPFL, Lausanne, ISSN 1661–1179.
- García Hernández, J., Boillat, J.-L., Jordan, F., & Hingray, B. 2009a. La prévision hydrométéorologique sur le bassin versant du Rhône en amont du Léman. *La Houille Blanche*, Vol. 5, 61–70.
- García Hernández, J., Horton, P., Tobin, C., & Boillat, J.-L. 2009b. MINERVE 2010: Prévision hydrométéorologique et gestion des crues sur le Rhône alpin. *Wasser Energie Luft*, Vol. 4, 297–302.
- García Hernández, Boillat, J.-L., & Schleiss, A.J. 2010. Flood forecast uncertainty and alert decision. Application to the Alpine Rhone River catchment. *Proceedings of Conference SimHydro “Hydraulic modeling and uncertainties”*. 198e session of Comité Scientifique et Technique de la Société Hydrotechnique de France, Nice, France, 2nd day, 3rd session.
- Hurwicz, L. (1951). Optimality criteria for decision making under ignorance. *Cowles Commission Discussion Paper 370S*, 16 p.
- Jordan, F. 2007. Modèle de prévision et de gestion des crues—optimisation des opérations des aménagements hydroélectriques à accumulation pour la réduction des débits de crue. PhD Thesis N°3711, Ecole Polytechnique Fédérale de Lausanne and *Communication 29 du Laboratoire de Constructions Hydrauliques*, Ed. A. Schleiss, EPFL, Lausanne, ISSN 1661–1179.
- Jordan, F., García Hernández, J., Dubois, J., & Boillat, J.-L. 2008. MINERVE: Modélisation des intempéries de nature extrême du Rhône valaisan et de leurs effets. *Communication du Laboratoire de Constructions Hydrauliques 38*, Ed. A. Schleiss, EPFL, Lausanne, ISSN 1661–1179.
- Savage, L.J. (1951). The theory of statistical decision. *Journal of the American Statistical Association* Vol. 46, 55–67.

Incorporating climate change scenarios into new operating rules for large reservoirs: A transnational assessment in the Meuse basin

B. Dewals, S. Detrembleur, P. Archambeau, S. Erpicum & M. Pirotton
HACH, University of Liege, Belgium

G. Demny, T. Rose, C. Homann & J. Lange
WVER, Düren, Germany

N.P. Huber, M. Kufeld, B. Sinaba & H. Schüttrumpf
IWW, RWTH Aachen, Germany

ABSTRACT: Opportunities for updating and optimizing current operating rules are being evaluated for the Vesdre reservoirs in Belgium (50 Mm³) and the Rur complex in Germany (300 Mm³). This assessment is conducted transnationally at the scale of the Meuse river basin. Common methodological approaches are followed in both countries and operating rules are analyzed in light of common climate change scenarios, recently defined for the whole Meuse basin. Similar risk-based approaches are used consistently in both countries to evaluate the performance of new operating rules in terms of risk reduction for floods and low flows.

1 INTRODUCTION

Water reservoirs are the most effective means for mitigating natural disasters such as floods or droughts. Therefore, existing reservoirs, especially those created by large dams, offer unique opportunities to mitigate hydrological impacts of climate change. Nonetheless, climate change scenarios must be incorporated into the development of enhanced operating rules for such reservoirs, in order to secure in the long term the achievement of goals in terms of flood damping and water resources management for low-flows.

Within the Interreg IVB project AMICE, involving 17 European partners, such studies are being conducted at the scale of the international catchment of river Meuse, with a focus on the Vesdre reservoirs in Belgium and the Rur reservoirs in Germany. The former consist of two large reservoirs with a combined capacity exceeding 50 Mm³, while the latter are six reservoirs with a total capacity reaching almost 300 Mm³. Their influence extends thus far in the downstream area, even transnationally on the lower Meuse in the Netherlands. All considered reservoirs are multi-purpose, serving for water supply as well as flood and low-flow control.

To guide the development of new operating rules for the reservoirs, an integrated methodology has been set up. In Germany, a modeling environment is available, consisting of hydrological models, a water management model for the reservoir control and 1D-2D hydraulic models for the determination of flood areas downstream. In Belgium, results of hydrological modeling will be exploited, together with a model for reservoir control as well as detailed 2D inundation modeling.

Climate scenarios derived earlier in the AMICE project (Drogue et al. 2010) are key inputs for the assessment. They were derived from existing regional and national scenarios within the international basin of river Meuse and include transnational scenarios both for floods and low flows. The scenarios have been developed for the time horizons 2021–2050 and 2071–2100.

The point of enhancing operating rules is twofold: reduce inundation impacts downstream and mitigate consequences of low flows. Therefore, the hydrologic-hydraulic assessment is

complemented by exposure modeling and risk analysis to be conducted in the downstream areas, based on outflows from the reservoir resulting from the new operating rules. To this end, existing and verified procedures will be exploited to assess socio-economic impacts of floods (e.g. Ernst et al. 2010), while an innovative approach will be elaborated for low-flows.

2 CONTEXT: THE AMICE PROJECT

The AMICE project (Adaptation of the Meuse to the Impacts of Climate Evolutions—AMICE) is a joint action of 17 partners from the four countries in the Meuse basin (France, Belgium, Germany, The Netherlands). The goal of the project is to develop a joint adaptation strategy to the flood and low flow situations expected to arise through climate change.

The structure of the AMICE project can be sketched by briefly representing the key objectives of the five work packages (WP) the projects consists of.

- WP 1 is on the technically and scientifically sound analysis of key characteristics and effects of flood and low flow events both for the current and future situation, taking into account climate change. Hydrologic and hydraulic loads and hazards, vulnerabilities of economy in the Meuse basin and finally effects and efficiency of risk mitigation and adaptation measures are addressed within the selected risk-based approach. Transnationality is clearly part of the analysis work which is performed on the basin scale. For example, this results in bringing together regional climate projections for the participating nations in order to derive a joint approach towards the assessment of effects of climate change on hydrology. Hydraulically modeling the Meuse from the source to the mouth requires harmonization and potentially extension of existing models at the model boundaries which can, but must not, agree with national political borders. Socio-economic data and methods used in flood and drought consequences assessment vary but have to be set on a common basis in order to not introduce bias into the analysis.
- WP 2 covers three selected natural water retention measures in the overall context of non-structural measures in the Meuse basin. Successful application of methods agreed upon will define the respective projects as valuable pilots for future planning of measures in the Meuse basin.
- Structural protection measures against floods and droughts are covered in WP 3. One out of three pilot projects is on dam and reservoir operational issues for the reservoirs located in the middle reaches of the Meuse, in particular the Rur reservoirs and, in the framework of WP1 (Ac 8), the Vesdre reservoirs.
- WP 4 is dedicated to preparedness measures, for example in the form of implementation of crisis management software; whereas transnational communication and dissemination of the results of the AMICE project are tasks which are followed in WP 5.

New operating rules will be developed for the Vesdre and Rur reservoirs and evaluated from the perspective of flood and low-flow risks on the Meuse basin level for specific scenarios developed in WP1 (Ac1 and Ac3). Additionally, the same methodologies as in WP 1, e.g. hydrologic and hydraulic modeling (Ac 6) as well as risk analysis (Ac 7), will be applied on the reservoirs in an extensive manner on a smaller, sub-catchment scale, aiming at the provision of a comprehensive set of scenario results by which a profound improvement of reservoir operation and climate proofing can be conducted. The conclusions of these studies will all be used in the elaboration of the strategy of adaptation as outcome (WP 1).

3 OVERVIEW OF VESDRE AND RUR RESERVOIRS

River Vesdre springs in the eastern part of Belgium, close to the border with Germany, and flows towards the west into river Ourthe, which is the main tributary of river Meuse in Belgium. River Vesdre is 70 km long, has a mean discharge of 12 m³/s at its mouth and the catchment area covers 700 km². The River Rur is one of the major tributaries of the Meuse, located to the east in the Ardennes and Eifel low mountain ranges. The catchment area covers 2,360 km². Major towns and cities in the Vesdre catchment are Verviers (55,000 inhabitants)

and Liege (200,000 inhabitants); while densely urbanized areas in the Rur catchment can mainly be found in Aachen, Düren, Mönchengladbach, Stolberg and Viersen.

Both Vesdre and Rur rivers show a distinct pluvial hydrological regime, since there are no glaciers and groundwater storage is limited. This results in a quick transformation of rainfall into surface runoff, as shown by Bogena et al. (2005) for the Rur catchment. The landscape of both catchments includes an upper part consisting of low mountains (Ardennes, High Fens, Eifel) and lowlands downstream. The Rur descends from an elevation of 660 m NHN at its spring in Belgium to 18 m NHN at the mouth in the Netherlands, in the city of Roermond. For river Vesdre, these figures are respectively 680 m DNG at the spring and 70 m DNG at the mouth. NHN and DNG refer respectively to the Belgian and German reference systems. This landscape results in strong precipitation gradients across both catchments. For river Vesdre, the gradient is west-east, with mean annual precipitations ranging between 700 mm/yr at the mouth and 1500 mm/yr in the upper part. Similarly, mean annual precipitation in the southern part of the Rur catchment is 1300 mm/yr, whereas in the northern lowlands it only reaches 550 mm/yr.

Two dams managed by the regional water authorities are located in the Vesdre catchment: the Vesdre masonry dam in Eupen (1950) and the La Gileppe dam (masonry dam heightened in 1971 with rockfill). They both have a storage capacity of approximately 25 Mm³ and were originally dedicated to the supply of drinking and industrial water. Operating rules for flood control have been introduced later. In 2003 a new agreement was reached between the dam operator and other stakeholders including a downstream municipality and a water supply company. Since then, a storage capacity of approximately 3.5 Mm³ has been kept available for flood storage, leading to enhanced flood control but also increased risk of shortages in water supply (Aubin 2007). This operating scheme has succeeded in limiting water level and avoiding flooding downstream. Indeed, although major floods occurred along river Vesdre in 2002 and 1998 with, respectively, peak hourly discharges of 160 m³/s and 275 m³/s (to be compared with a mean annual discharge of 11 m³/s in Chaudfontaine), they lead to flooding and significant damages only downstream from an uncontrolled tributary (river Hoegne, see Figure 1), the sub-catchment of which exceeds one third of total Vesdre catchment.

In the Rur catchment, high winter precipitation and low groundwater storage capacity in the mountainous area have led in the past to floods with estimated peak discharges of 450 m³/s in the middle reaches, while flow during summer month was often less than 1 m³/s. The economic development in the Rur basin was limited by these high fluctuations of water discharge. Therefore, a solution was sought in constructing reservoirs that would supply industries with water constantly and retain floods. The first reservoir to be built was the Urfttalsperre in 1905. Since then, more large dams have been built at the Rur and tributaries, with a total storage volume of 300 million m³. Links through pumping stations and galleries allow the distribution of water between the reservoirs and contribute to a complex multi-purpose scheme.

With today's system of interlinked reservoirs all floods on record would have been contained and peak discharges limited to 60 m³/s, while minimum summer flow is elevated to

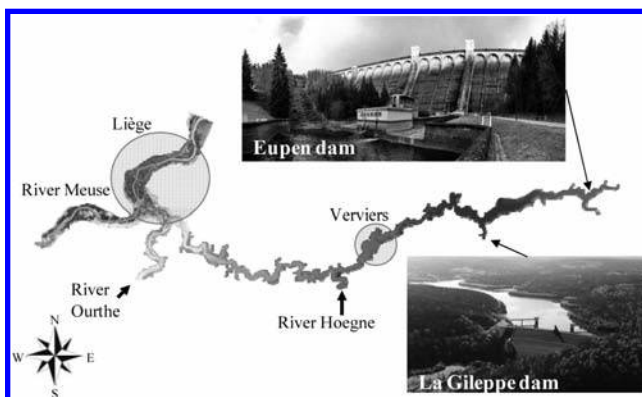


Figure 1. Vesdre valley from Eupen reservoir (east) to the mouth into rivers Ourthe and Meuse (west).

5 m³/s. Mean flow is 22 m³/s at gauging station Stah which is located close to the German-Dutch border. In absolute figures most of the water from the reservoirs is used as drinking water (for average hydrological conditions up to 80 million m³ per year) and to maintain minimum flow of 5 m³/s in the Rur for downstream water users. Water is released from the reservoirs through turbines that generate 60 million kWh per year on average. About 35 million m³ per year can be used by industry downstream of the reservoirs. The major share in water rights is kept by the paper industry. The agricultural sector does not use a significant amount of water. There is no commercial shipping on the Rur.

4 PLANNED ANALYSIS FOR THE VESDRE RESERVOIRS

In the current practice, water may be released from the Vesdre reservoirs in advance of floods, when heavy precipitations are monitored or forecast (Heuschling 2004). This enables to subsequently store in the reservoirs inflows from river Vesdre as well as from tributaries linked to the reservoirs by galleries, such as Helle and Soor; and thus to reduce discharge and water levels downstream. The part of the catchment controlled by the dams represents about half of the catchment upstream of the tributary Hoegne (Figure 1) and a quarter of the total Vesdre catchment.

It remains however unsure whether this current practice, particularly threshold values for triggering preventive water release, will turn out adequate in conditions of changing climate. Higher winter precipitations (AMICE dry scenario) and drier summers (AMICE wet and dry scenarios) are expected and might require adaptations of the operating rules of the reservoir in order to prevent increases in both flood risk and shortages of water resources available for domestic and industrial supply. Therefore, a model of the reservoirs is being setup and will be used to identify opportunities of adaptation and optimization of current operating rules, to cope with climate change as described in the common AMICE scenarios (Drogue et al. 2010).

The following paragraphs successively describe the evaluation of inflows to the reservoirs (§ 4.1) and outflows from them, the modeling framework for the reservoirs (§ 4.2), downstream flood propagation, inundation modeling and evaluation of flood risk downstream (§ 4.3) as well as the overall analysis to be performed (§ 4.4).

4.1 Inflows into the reservoirs and water uses

For the study of the hydrology of the reservoirs catchments, we will make use of the results of the integrated watershed model Mohican, incorporating rainfall-runoff modeling and run by Aquapôle at the University of Liege in the framework of the Amice project. This will provide us with the inflows to the reservoirs. Results of the same model will also be exploited in the impact analysis to evaluate inflows to the rivers located downstream of the reservoirs (§ 4.3).

As detailed in § 4.4, the rainfall-runoff model will be forced either with measured time series of precipitation and temperature or with perturbed time series to account for climate change scenarios. To this end, two different time horizons will be considered: 2020–2050 and

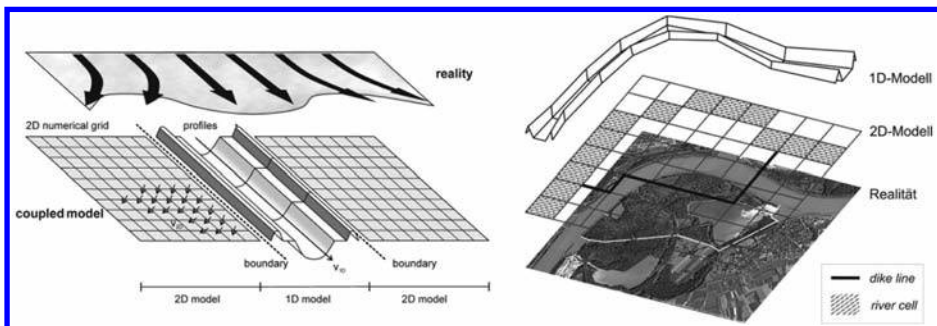


Figure 2. Coupled 1D-2D (storage cell) representation of river channel and floodplains.

2070–2100 and, to cope with uncertainty, both a wet and a dry scenario will be considered for each time horizon (Drogue et al. 2010).

Water from the Eupen reservoir is treated in a plant located at the toe of the dam. It is next sent for distribution in a large part of the region, including Liege except downtown, Spa and the Pays de Herve, through a water distribution pipeline between Eupen and Liege. The daily water supply is on average 75,000 m³/day (Ministère des Travaux publics 1986). Before reaching the treatment plant, water from the Eupen reservoir flows through turbines (max. discharge = 4.5 m³/s). Electricity produced is used for the local needs of the dam operation and the excess is sold to the electric network. This production in excess may reach 3 to 4 million kWh.

Water from La Gileppe reservoir is also first injected into turbines and next sent to the water supply network. Electricity is similarly used for the local needs of the dam operation and the excess is sold to the network. Water is treated for supply of drinking water in the town Verviers and partly sent to the water distribution pipeline Eupen-Liege.

During floods, the spillways of the Eupen and La Gileppe dams enable maximum releases of, respectively, 230 m³/s and 185 m³/s (Ministère des Travaux publics 1986).

4.2 Set up of the reservoirs model

A dynamic model of the reservoirs will be set up. The state of each reservoir j will be governed by its mass balance equation: $s_{t+1}^j = s_t^j + q_{t+1}^j - r_{t+1}^j$, where s_t^j is the storage in the j -th reservoir at time t ($j = V$ for the Vesdre reservoir in Eupen and $j = G$ for La Gileppe reservoir), q_{t+1}^j is the inflow volume in the interval $[t, t+1]$ and r_{t+1}^j is the release in the same interval. The time subscript of each variable denotes the time instant at which it assumes a deterministic value (Castelletti et al. 2008). For instance, inflow in the interval $[t, t+1]$ can be deterministically known at the end of the interval.

For the Eupen reservoir, the inflow volumes consist of the inflows a_{t+1}^V from river Vesdre and a_{t+1}^{Ge} from river Getzbach, a 9-km long tributary of river Vesdre, the mouth of which is located immediately upstream of Eupen dam. In addition, part of the discharge of river Helle is diverted through a gallery to the reservoir, providing an additional inflow a_{t+1}^H . Similarly, inflows into reservoir La Gileppe include not only the contribution of river La Gileppe (a_{t+1}^G) but also part of the discharge of river Soor which is diverted through a gallery (a_{t+1}^S). This leads to the following mass balance equations written out in full:

$$\begin{aligned} s_{t+1}^V &= s_t^V + q_{t+1}^V - r_{t+1}^V = s_t^V + (a_{t+1}^V + a_{t+1}^{Ge} + a_{t+1}^H) - (r_{t+1}^{V,d} + r_{t+1}^{V,r}), \\ s_{t+1}^G &= s_t^G + q_{t+1}^G - r_{t+1}^G = s_t^G + (a_{t+1}^G + a_{t+1}^S) - (r_{t+1}^{G,d} + r_{t+1}^{G,r}) \end{aligned} \quad (1)$$

in which superscripts d and r refer, respectively, to the outflows directed to the water distribution network and to the downstream river. Detailed sonar bathymetry of the reservoirs is available to convert pool elevation into storage and vice-versa.

4.3 Evaluation of downstream flood risk

The impact of each considered set of operating rules on downstream flood risk analysis will be evaluated. Conducted for each peak flood discharge, the assessment will rely on a micro-scale procedure, which involves hazard modelling by means of fully dynamic 1D flood routing (Khuat Duy et al. 2010) and detailed 2D inundation modelling as well as processing of high resolution land use and socio-economic database for vulnerability modelling.

The inundation modelling is conducted using the fully dynamic flow model WOLF 2D, entirely developed at the University of Liege. The model is run on a highly accurate DEM resulting from the combination of laser altimetry and, when available, sonar bathymetry. The typical grid spacing for the simulations is kept as low as 2 m, which is definitely fine enough to represent the complex flows occurring at the scale of individual buildings and streets in urbanized floodplains. This way, both the static and dynamic impacts of the flow may be characterized for all affected assets. This approach has been extensively applied since 2003 to issue inundation

maps throughout the Walloon region based on detailed 2D flow modelling of over 1,000 km of rivers, for which validation has been systematically conducted (Ercicum et al. 2010).

Consequently, the outcomes of such detailed inundation modelling constitute suitable inputs for the subsequent exposure analysis, performed at a micro-scale using detailed land use maps and geographic database (Ernst et al. 2010). Eventually, based on a multidisciplinary work, the procedure may incorporate social flood impact analysis and evaluation of direct economic damage to different categories of buildings and land use types. According to our experience, such risk-oriented analysis disclose findings which would not arise from a more standard hydraulic study such as based on design floods.

4.4 Analysis of operating rules and optimal control problem

The three-step analysis will include first a *control run*, during which flood risk and risk of water shortage will be evaluated under current climate conditions and operating rules. This step will simultaneously enable to validate the main model components.

Second, climate change scenarios will be incorporated in the rainfall-runoff simulations of a second run, which will lead to the evaluation of the *cost of inaction*, expressed as increased flood risk and increased risk of water shortage as a result of climate change. Two time horizons will be considered as well as two climate change scenarios, involving both drier summers. The analysis will incorporate reasonable assumptions concerning future trends in water demand.

Third, enhanced operating rules will be elaborated considering the same time horizons and climate change scenarios.

This may be formulated as an optimal control problem, in which the control variables u_t^j are the release decisions made at time t for the reservoir j . The release volumes are in turn functions of the release decision u_t^j , the storage s_t^j and the inflow q_{t+1}^j , which makes it possible for the actual release to differ from the release decision, e.g. when available water is not sufficient. A minimal environmental flow (MEF) \tilde{q}_t^j must be accounted for during each time interval $[t, t+1]$, as well as a regulation range on reservoir storage ($s_t^{\min,j}, s_t^{\max,j}$).

The control problem may be formulated in the following way (Castelletti et al. 2008): find optimal release decisions, such as to maximize avoided flood risk and revenue of hydropower production $\sum_{t=1}^N \vartheta_t^j \eta^j q_{t+1}^{d,j} H_t$, while minimizing the cost of supply deficit $\sum_{t=1}^N [w_t^j - q_{t+1}^{d,j}]^+$. w_t^j denotes the water demand, $q_{t+1}^{d,j}$ the flow supplied, ϑ_t^j the price of electricity, η^j an efficiency factor, $q_{t+1}^{d,j}$ the flow in the penstock, H_t the hydraulic head, N the number of considered time steps and $[\cdot]^+ = \max(\cdot, 0)$. Although specific methods exist for solving the optimal control problem, a preliminary assessment will rely on testing heuristically developed new operating rules (e.g. seasonal storage range), corresponding to either more “flood oriented” or more “low-flow oriented” policies. The problem may also be regarded as a cost-benefit analysis (CBA), in which the benefits arise from *avoided flood risk* and costs result from more frequent shortages in water supply and reduced hydropower production. Costs could also include investments in monitoring equipment to support real-time management of the reservoirs.

5 PLANNED ANALYSIS FOR THE RUR RESERVOIRS

5.1 Hydrologic modeling and flood routing

Flood routing is a key issue in transforming hydrological events to hazards and loads for humans and vulnerable assets, forming flood risk. A multitude of approaches, ranging from extrapolation of maximum flood water levels to numerical 2D (omitting 3D-approaches for the sake of representing common methods), the latter in the form of steady or unsteady modeling, are available for fulfilling the task of flood routing. Throughout recent years, approaches linking 1D channel flow and 2D modeling of the inundation of floodplains have increasingly been introduced to flood risk management, aiming at rather efficient modeling while not waiving desired detail. Kamrath et al. (2008) describes a linked 1D-2D storage cell approach which is characterized by an efficient handling of a large set of simulations.

The analysis and optimization of reservoir operations for different loading conditions, each of them representing a specific flood or low-flow event which is more or less triggered by climate change, is a time-consuming process which includes a large set of necessary analyses of loads and effects in the system. The true number of necessary runs and associated risk analyses (following the methodology developed in WP 1 of the AMICE project) is initially unknown. Thus, utilizing the efficient storage cell approach is a key prerequisite for performing a thorough optimization. In order to verify achieved results and increase trust in the overall work conducted, SOBEK Rural (Software developed by Deltares) is run parallel.

5.2 *Risk concept*

Choosing from the reservoir management options is performed on the basis of flood risk management approaches which are amended by specific means of assessing low flow risk. Risk management for the Rur catchment is seen as an issue linked to the whole catchment area. By stating this, one immediately has to depart from widely performed scenario based investigations in which a limited number of hazards and loads, i.e. very few selected flood events with associated recurrence intervals, and assessments of associated vulnerabilities and potential damage, probably at only few locations, are conducted. Risk estimates are therefore not fully representative of what might happen and fail to cover relevant contributions to risk by disregarding intermediate loads, i.e. a potentially high-risk 1 in 250 years event being framed by the 1 in 100 and extreme discharge event in common studies but not covered within the risk analysis.

The risk concept bases on an approximation of the overall hydrologic / hydraulic loads domain in the catchment by integrating a comprehensive set of events, also accounting for potential failures of flood protection measures, and calculating potential damages for the complete catchment. While flood risk analysis and assessment requires hydraulic modeling to estimate flood extents and inundations, assessment of risk related to low flows is more dependent on an elaborate estimation of potential damage. In order to work on a manageable, yet meaningful set of consequence categories, it has been decided to perform low flow risk assessment for four general economic fields: navigation, electric power generation, agriculture and drinking water supply. Flood and low flow risks will be weighted according to the implicit probability of occurrence of extreme events, thus facilitating an elaborate decision making on reservoir operations in the Rur catchment.

5.3 *Possible impacts on downstream reaches resulting from modified reservoir operations*

The operating policies were designed on the basis of measured data of past discharges. First results for the Rur reservoirs are showing that in future scenarios impacts in low-water enrichment can arise with the existing reservoir operating policies. Considering the low-water periods to get more intense in the future, the enrichment activities are to be worked over and optimized on the changed requirements. The focus of the underlying objective is widened from a former regional view to a transnational view with regard to the all parts of the Meuse catchment basin that can be influenced.

The first calculations for the Rur catchment basin are indicating higher reservoir levels and an increased frequency in reservoir spillover for some climate scenarios. The reviewed twenty year period does not allow an interpretation for infrequent floods, but for frequent floods increasing discharges have to be expected. Hence, optimizing the operation policies for the retention volumes in future scenarios, both, the low-water enrichment operations and the flood retention have to be taken into account. Unfortunately these two aspects are contradictory. For flood reduction sufficient retention volume has to be reserved in the reservoirs. The reservoir level has to be kept as low as possible for the maximum effect. In contrast to that, low-water enrichment needs stored volumes of water and accordingly high reservoir levels. Additionally, aspects like the provision of drinking water and hydropower production have to be taken into account too. An optimization of the reservoir operating policies on future scenarios has to find a compromise between all aspects based on carefully determined risk assessment. The coordinated adaptation of infrastructure and system utilizations can produce an evolution in the optimization objectives and provides new synergetic systems for water resources management.

5.4 *How to cope with decision and policy making in the transnational context?*

There are several levels of co-operation in the Rur-/Meuse-basin. The first level is the International Meuse commission (IMC), which is located in Liège. The main topics of the IMC are the adjustment of the commitments of the EU-Water Framework Directive, the apportionment of advice for better flood-protection, and the apportionment of advice for the prevention and abatement of water pollution due to accidents (warning and alarm systems). Each country in the Meuse-catchment is represented in the IMC. There are five permanent project groups for preparing the issues of the IMC. The next level is a bilateral co-operation between the Netherlands and Germany for the Rur-catchment. Here all relevant issues of the Rur-catchment are discussed in quarterly meetings between the water boards Roer and Overmaas (WRO) and Eifel-Rur (WVER). Hydrological and hydraulic issues are fixed in national agreements.

The project AMICE offers additional levels of co-operation. An Adjoint Expert Group (AEG) was formed to discuss all relevant themes concerning the risk-assessment for the Rur and the effects of changes in the operation of the Rur-reservoirs. The AEG consists of delegates from the state and regional governments, the adjacent water boards, the Aachen University, and the WRO and WVER. Moreover, several partners in AMICE, who are responsible for the flow-control at the river Meuse are forming a joint working group. This group works on a guideline for transnational cooperative water management with the focus on the coping with uncertainties related to climate change. Beside the EU-project AMICE, the WRO and the WVER co-operate in the transnational analysis of flood-risks due to the EU-Flood Risk Management Directive within the EU-project FLOODWISE. Here also the regional governments and the local people are incorporated in the full process of flood risk mapping and management.

The plurality in levels of co-operation in the Rur- and Meuse-catchments offers varying possibilities for recognizing and solving conflicts in the water management of the both river systems. Projects like AMICE or FLOODWISE help to strengthen the long-term existing collaborations and to establish new forms of co-operations.

6 CONCLUSION

Operating rules of the multipurpose Vesdre reservoirs in Belgium and Rur reservoirs in Germany are being reevaluated in the framework of the research project Amice, the aim of which consists in elaborating a common transnational adaptation strategy to cope with hydrological impacts of climate change in the Meuse basin. To avoid biases and enable sound comparisons, analyses of operating rules for the reservoirs are being conducted in both countries using the same climate change scenarios, the same time horizons as well as consistent approaches for hydraulic modeling and risk analysis.

Our end-to-end methodology, from climate scenarios to socio-economic risk analysis, provides an innovative insight into the influence of the reservoir control in Belgium and Germany on low-flow and flood impacts downstream. The transnational perspective of the assessment, accounting for impacts on downstream population of the lower Meuse in the Netherlands, constitutes clearly an added value. In particular, the increased water needs from downstream populations and activities will be included in the new operating rules. Lessons learned from comparative analysis of the updates needed in reservoir management practice in the two countries will contribute to the development of the Amice common transnational adaptation strategy.

ACKNOWLEDGEMENTS

This research is being carried out in the framework of the Amice project funded under the NWE Interreg IVB Program. The authors from ULg also gratefully acknowledge the “Service Public de Wallonie” (SPW) for the Digital Surface Model and other provided data.

REFERENCES

- Aubin, D. (2007). *L'eau en partage: l'activation des règles dans les rivalités d'usages en Belgique et en Suisse*, Peter Lang.
- Castelletti, A., Pianosi, F., & Rodolfo. (2008). "Water reservoir control under economic, social and environmental constraints." *Automatica*, 44(6), 1595–1607.
- Drogue, G., Fournier, M., Bauwens, A., Commeaux, F., De Keizer, O., François, D., Guilmin, E., Degré, A., Detrembleur, S., Dewals, B., Piroton, M., Pontegnie, D., Sohier, C., & Vaneuville, W. (2010). "Analysis of climate change high-flows and low-flows scenarios on the Meuse basin."
- Ernst, J., Dewals, B.J., Detrembleur, S., Archambeau, P., Erpicum, S., & Piroton, M. (2010). "Micro-scale flood risk analysis based on detailed 2D hydraulic modelling and high resolution land use data." *Nat. Hazards*, 55(2), 181–209.
- Erpicum, S., Dewals, B.J., Archambeau, P., Detrembleur, S., & Piroton, M. (2010). "Detailed inundation modelling using high resolution DEMs." *Engineering Applications of Computational Fluid Mechanics*, 4(2), 196–208.
- Heuschling, J. (2004). "La Gestion des barrages et les bassins écrêteurs." *Conférence sur le thème des inondations*, Pepinster, Belgium.
- Khuat Duy, B., Archambeau, P., Dewals, B.J., Erpicum, S., & Piroton, M. (2010). "River modelling and flood mitigation in a Belgian catchment." *Proc. Inst. Civil. Eng.-Water Manag.*, 163(8), 417–423.
- Ministère des Travaux publics. (1986). *Les Barrages belges*.

The flexible flood control capacity exploration and its relevant extra benefit estimation of lower Jinsha River cascade reservoirs

Xu Jijun, Chen Jin, Yin Zhengjie & Yang Chunhua

Water Resources Department, Yangtze River Scientific Research Institute, Wuhan, China

ABSTRACT: The large-scale reservoirs built on lower Jinsha River are not only the plants of hydropower output, but also the important part of Yangtze River's flood control system. How to balance the relationship between its hydropower benefit and the risk of flood control in flooding season is always an important issue, especially under new challenges due to the climatic change and increasing requirement of hydropower output, as well as ecosystem protection. It is not the best choice to reserve vast flood control capacity in flooding season of every year, to ready to store the possible floodwater for the safety of downstream. It will depress the benefit of hydropower generation in most years. In the paper, in order to carry out a flexible flood control capacity exploration of lower Jinsha River cascade reservoirs, some different schemes from the planning report have been evaluated by means of an optimization model of cascade reservoirs joint operation under new concept of downstream flood control and flood-plain ecosystem restoration. The extra benefit of flood control capacity changing has been also estimated. Results show, it is probable to get more hydropower output, through reducing flood control capacity and shortening the term of flood-limited level in flooding season.

1 BACKGROUND AND NEW CHALLENGES

A series of flood control engineering, dikes along river bank, flood diversion areas adjacent to mid-down stream and reservoirs in upper stream, had been constructed since 1950s, including Three Gorge reservoir (TGR). According to the planning of Yangtze River basin (1990), there are still some large-scale reservoirs which are going to be built in upper Yangtze River basin, including the four reservoirs (XJB, XLD, BHT and WDD) of lower Jinsha River, see Fig. 1. In flooding season, these reservoirs should run below flood-limited level, and reserve abundant flood control capacity to regulate flood peak (Ding Y. etc., 2006).

Along the mainstream of Yangtze River, the most dangerous reach of flood disaster is Jingjiang which locates in middle Yangtze River. Its maximum drainage capability of channel is much less than the discharge of floodwater coming from upper stream in flooding year. If flood peak was more than the drainage capability of channel, the excess floodwater would be guided into the flood diversion area, in order to avoid overflow. It needs to be mentioned here, the flood diversion areas of Jingjiang were formed gradually on the floodplain in the past, for making more farmland. It constricts river channel and reduces the drainage capability of river in a sense. Before the construction of TGR, even the flood of 10-year-return coming from upper stream, some lower flood diversion areas had to be inundated.

Usually, keeping adequate flood control capacity in upper stream to store floodwater will be an effective way to guarantee the safety of downstream, and also will lower the probability to use the flood diversion areas. Some experts thought, if more reservoirs were built in upper Yangtze River, the flood diversion areas would not be inundated frequently, and might become permanent farmland. Therefore in the past, the design principle of reservoir was focused on how to reserve flood control capacity as more as possible (Tan P.L. etc., 2000).

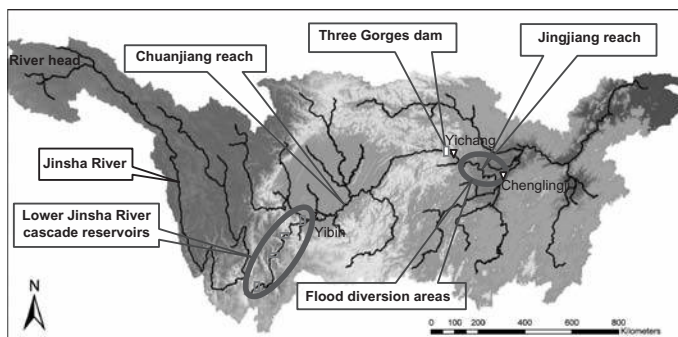


Figure 1. Sketch map of cascade reservoirs on lower Jinsha River and flood diversion areas of Jingjiang.

But at present, with the increasing demands of floodplain ecosystem restoration, more and more people think it is not good idea to keep floodwater out of flood diversion areas, it will drastically cut off the relationship between river system and floodplain, and destroy the ecosystem of wetland. The river has its natural life, and the floodwater need more room. We have to learn how to live with floodwater harmoniously. On the other hand, the shortage of energy has become crucial shade on Chinese economic and social development. The hydropower is regarded as a kind of re-cycle and clean energy.

It is no doubt to achieve two wins goal at hydropower benefit and eco-environmental protection, if we can make full use of upstream hydropower station to generate more hydropower, and simultaneously restore the ecosystem of flood diversion area in mid-stream. For example, according to flood control planning, the lower Jinsha River cascade reservoir should reserve vast flood control capacity in flooding season, for cooperating with TGR to protect the safety of Jingjiang reach. Recently, some experts propose a tentative suggestion that the flood control capacity of these reservoirs could be reduced. It may raise flood-limited levels, and correspondingly heighten the water head of hydropower generation, for getting more hydropower output (Lu Q.K., 2003). And then use the extra profit to compensate for the inundation loss of flood diversion areas. As viewed from the demand of hydropower output and eco-environmental protection, the suggestion proposes a new idea for balancing the systematic relationships among flood control, hydropower output and eco-environmental protection. The safety of flood control is important, but it isn't only one. The reasons of concept changing: one is due to great demand of hydropower; another is that the capability of flood control has been strengthened with more dams than before; and others are the technological development of non-engineering measures, such as flood forecast.

Therefore it is necessary to review our planning scheme again with new viewpoint. Here, some different schemes of flood control capacity will be discussed by means of an optimal model of cascade reservoirs joint operation under new concept of flood control and eco-system protection. The extra profit due to the adjustment of flood control capacity will be estimated for understanding the potential of hydropower output. Relevant influence of flood control capacity adjustment on the sedimentation in reservoir and the downstream safety of flood control will be discussed in other papers.

2 STUDY AREA

The Jinsha River is an important part of upper Yangtze River. From the riverhead to Yibin (see Fig. 1), the total length of Jinsha River is about 3500 km, with 5100 m elevation difference. The total drainage area of Jinsha River basin is $50 \times 10^4 \text{ km}^2$. The mean annual discharge of Jinsha River is $4920 \text{ m}^3/\text{s}$ with the mean annual runoff of $1550 \times 10^8 \text{ m}^3$, accounting for 1/3 of that observed at Yichang which is the exit of upper Yangtze River. According to the evaluation result of hydropower resources, the total hydropower resource of Jinsha River is about $1.2 \times 10^8 \text{ kW}$. The maximum potential of hydropower output could be up to $5927 \times 10^8 \text{ kW} \cdot \text{h}$.

The lower Jinsha River is from Yalong River estuary to Yibin city. The river length of this reach is 768.4 km and the fall head is 719.3 m. The river flows across many gorges, and the topographic and geologic conditions are suitable to build reservoirs with high dams. According to the planning report of Jinsha River (Proposed in 2006), four large-scale hydropower stations are being built here, including WDD, BHT, XLD and XJB whose total storage capacity is $414 \times 10^8 \text{ m}^3$ with the regulating storage of $204 \times 10^8 \text{ m}^3$.

From Yibin to Yichang, it is upper mainstream of Yangtze River, named by Chuangjiang reach. There is a national nature reserve zone of rare and endemic fish species established by the State Council in 2005. The operation of lower Jinsha River cascade reservoirs could bring about a significant impact on hydrological characteristics. Therefore, the constraints of environmental flow for the outflow of XJB should be taken into account.

When the Yangtze River flows from Yichang into the middle-lower plains, the slope of riverbed becomes small, and there are lots of dikes along river bank. Since 1950s, some flood diversion areas have been formed after years of reclamation and division in the original floodplain along both banks of Jingjiang reach. These flood diversion areas play a role of storing excess flood during extraordinary flooding year. In common year, it is used for farming activities. Half of century past, since some of them are rarely used for flood diversion, farming activities and grain production have been become normalizing, and more and more farmers are settled in these flood diversion areas. With the completion of TGR, the flood control capability of Jingjiang reach has been greatly improved from 10-years-flood to 50–100-years-flood (Jiang Z.Y. 2004). Therefore in common years, the probability of flood diversion is very low.

3 PLANNING SCHEME OF FLOOD CONTROL CAPACITY

According to the *Report on the Planning of Comprehensive Utilization of Yangtze River Basin* (Proposed in 1990 by CWRC), about 20 large-scale reservoirs/hydropower stations were planned to be built on the mainstream of Jinsha River. In order to meet the requirement of overall flood control of the Yangtze River, these reservoirs should not only control the flood of Chuanjiang reach which locates in the downstream of Jinsha River, but also play a certain role in the flood control of Jingjiang reach. Therefore, it was essential for them to reserve adequate flood control capacity in flooding season. In the report, the cascade reservoirs on the mid-lower of Jinsha River should reserve $270.4 \times 10^8 \text{ m}^3$ flood control capacity when operated separately, or $126 \times 10^8 \text{ m}^3$ when operated jointly in main flooding season (from Jul. to Sep. 02).

With the developing of economy and society since 1990, the demand for flood control safety had been once increased by the end of 20 Century, especially after 1998⁷ flood disaster. Relevant studies thought that the flood control capacity of $126 \times 10^8 \text{ m}^3$ in mid-lower Jinsha River can not meet the flood control strategic goal of Yangtze River basin. The flood control capacity should be enlarged further in flooding season. Thus, in the *Report on the Comprehensive Planning of the Mainstream of Jinsha River* (Proposed in 2006 by CWRC), a scheme of $249 \times 10^8 \text{ m}^3$ flood control capacity of cascade reservoirs in mid-lower Jinsha River had been suggested. Among them, the four reservoirs (XJB, XLD, BHT and WDD, see Fig. 2) which locates in lower Jinsha River were planed to reserve $145 \times 10^8 \text{ m}^3$ flood control capacity, accounting for 59% of the total. XJB and XLD have been building since 2008, and BHT, WDD are going to be built now. According to the planning report (2006), the total design installed hydropower

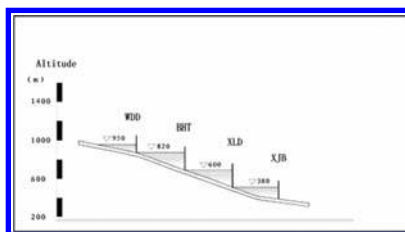


Figure 2. Cascade reservoirs in lower Jinsha River.

Table 1. Planning parameters of lower Jinsha River cascade reservoirs.

Item	Unit	WDD	BHT	XLD	XJB
Drainage area	10 ⁴ km ²	40.61	43.03	45.44	45.88
Normal water level	m	950	820	600	380
Normal storage	10 ⁸ m ³	39.41	179.24	115.7	49.77
Dead water level	m	920	760	540	370
Dead storage	10 ⁸ m ³	17.41	78.92	51.1	40.74
Flood-Limited level	m	930	780	560	370
Flood control capacity	10 ⁸ m ³	16.11	73.24	46.5	9.03
Regulation storage	10 ⁸ m ³	22.0	100.32	64.6	9.03
Installed hydropower capacity	MW	7400	13200	14400	7200
Design hydropower output	10 ⁸ kW · h	310.1	584.8	649.8	330.6

capacity of four reservoirs is about 40000 MW, the total design annual hydropower output is 1850×10^8 kW · h, and the total storage capacity is about 410×10^8 m³, including 145×10^8 m³ flood control capacity. The detailed planning parameters are shown as Table 1.

4 HYDROPOWER BENEFIT OF DIFFERENT FLOOD CONTROL CAPACITY

4.1 Model for joint operation of cascade reservoirs

In the mathematics model of cascade reservoirs joint operation, the optimization goal is to get the maximum of hydropower output. The input of model is the long series daily inflow (from 1951 to 2008) of cascade reservoirs. The control equations show as following:

1. Objective function

The total output of four hydropower stations is the optimization goal (Duan W.H., 2006).

$$\text{Max } W = \max \sum_{i=1}^N \sum_{t=0}^T P_{i,t} \Delta t \quad (1)$$

where T = number of operating days; $N = 4$, number of hydropower stations; $P_{i,t}$ = hydropower output of reservoir i at time step t .

2. Mass balance equation

$$\text{If } i = 1, \quad V_{i,t+1} = V_{i,t} + I_{i,t} - q_{i,t} - S_{i,t}, \quad \text{else} \quad V_{i,t} + I_{i,t} + q_{i-1,t} + S_{i-1,t} - q_{i,t} - S_{i,t} \quad (2)$$

where $V_{i,t}$ = storage in the reservoir i at time t ; $I_{i,t}$ = inflow; $q_{i,t}$ = flow discharge for power generation; $S_{i,t}$ = surplus water of reservoir i at time t .

3. The constraint of water level

$$\underline{Z}_{i,t} \leq Z_{i,t} \leq \overline{Z}_{i,t} \quad (3)$$

where $Z_{i,t}$ = water level of reservoir i at time t ; $\underline{Z}_{i,t}$ and $\overline{Z}_{i,t}$ are respectively the permissible lowest and highest water level, which are dead water level and normal water level in non-flooding season, and dead water level and flood-limited level in flooding season.

4. The average hydropower output

$$P_{i,t} = \begin{cases} AH_{i,t} Q_{i,t}, & \text{if } AH_{i,t} \leq \overline{N}_{i,t} \\ \overline{N}_{i,t}, & \text{else} \end{cases} \quad (4)$$

where $A = 8.7$, coefficient of hydropower output; $Q_{i,t}$ = flow for power generation; $N_{i,t}$ = permissible maximum output; $H_{i,t}$ = water head.

$$H_{i,t} = (Z_{i,t-1} + Z_{i,t})/2 - Zd_{i,t} \quad (5)$$

where $Z_{i,t}$ = water level of reservoir i at time t ; $Zd_{i,t}$ = downstream water level of reservoir i at time t , which can be attained through the characteristic curve between downstream water level and outflow of reservoir.

5. The permissible value of flow for power generation

$$\underline{Q}_{i,t} \leq Q_{i,t} \leq \bar{Q}_{i,t} \quad (6)$$

where $\underline{Q}_{i,t}$, $\bar{Q}_{i,t}$ = respectively permissible minimum and maximum flow for power generation

6. The permissible value of hydropower output

$$\underline{P}_{i,t} \leq P_{i,t} \leq \bar{P}_{i,t} \quad (7)$$

where $P_{i,t}$ = hydropower output of reservoir i at time t ; $\underline{P}_{i,t}$ and $\bar{P}_{i,t}$ are respectively the permissible minimum and maximum output hydropower of reservoir i at time t .

7. The characteristic curve of hydropower output

$$P_{i,t} = f_{i,t}(H, Q) \quad (8)$$

8. The permissible value of reservoir release flow

$$Q_{i,\min} \leq Q_{i,t} + R_{i,t} \leq Q_{i,\max} \quad (9)$$

where $Q_{i,\min}$ and $Q_{i,\max}$ are the permissible minimum and maximum release flow at time t .

The model of cascade reservoirs joint operation is a multi-stage decision process. In theory, the model can be solved by means of dynamic programming (DP) method proposed by Bellman in 1950's. Due to multi-state decision problems, the "dimension disaster" becomes the obstacle in solution when using DP (John W.L., 2003). So in this study, the POA (Progressive Optimization Algorithm) has been adopted to solve the model.

4.2 Environmental flow constraint

The Chuanjiang reach which below XJB dam is the nature reserve zone of rare and endemic fishes. The outflow of XJB will directly affect the hydrological process of reach. Therefore, the release of XJB should be controlled for the requirement of environmental flow (E-flow). In this study, the method of 7 days-smooth-average has been introduced into determine E-flow.

$$\bar{Q}_i = \sum_{k=i-7}^{i-1} Q_k / 7 \quad (10)$$

where \bar{Q}_i = average flow within 7d; Q_k is natural daily flow. The lower and higher bounds of daily E-flow are respectively $0.8 \bar{Q}_i$ and $1.2 \bar{Q}_i$ (see Fig. 3). If the flow of day i was within the range, the E-flow is satisfied. The ratio of the number of days when E-flow is satisfied to the number of total days is called "E-flow satisfiability".

The method of 7 days-smooth-average is based on the natural flow process. Its basic concept is that the effect of reservoir operation on flow is restricted in an acceptable range, in

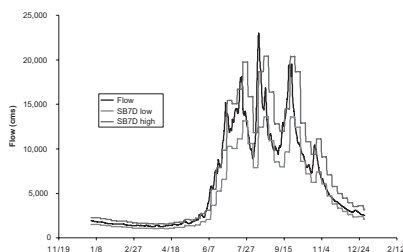


Figure 3. The constraint of E-flow determined by 7 days-smooth-average method.

order to avoid rough disturbance to natural flow. The method is quite simple to understand and calculate. But if the natural flow has a sharp change among seven days, the method will cause a deviation, namely, natural flow sometimes maybe not meet the demand of E-flow. By the method of 7 days-smooth-average, the E-flow satisfiability of natural flow has been tested using daily discharge observed at Pingshan gauge from 1951 to 2008. It is found that E-flow satisfiability of natural runoff cannot reach 100%. The average E-flow satisfiability of natural flow from 1951 to 2008 is 87.2%. The lower E-flow satisfiability mainly occurs in flooding season (June, July, August and September), because the daily flow is not stable. After October, the natural flow of Jinsha River tends stable, the value of E-flow satisfiability is above 90%.

In the model of cascade reservoirs joint operation, the lower and higher bounds of E-flow have been regarded as a potential constraint of the outflow of XJB. If the outflow cannot be satisfied with E-flow, the times of non-satisfaction will be counted.

4.3 Computing schemes

Referring to the planning parameters in the *Report on the Comprehensive Planning of the Mainstream of Jinsha River* (2006), a series of computing schemes for understanding the relationship between flood control capacity reducing and its extra benefit, have been assumed as following (also see Table 2).

Scheme Z: the flood control capacity of reservoir is same as the planning parameters.

Scheme A: 50% of flood control capacity for each reservoir is assumed to be cut down.

Scheme B: 75% of flood control capacity for each reservoir is assumed to be cut down.

Scheme C: it is assumed to cancel all of flood control capacity.

Scheme D: the computing condition is same as the scheme C, but total installed hydro-power capacity is 10% more than scheme C.

Scheme E: the constraint of E-flow is taken into account for the outflow of XJB. Scheme E_Z is a scheme comparing with scheme Z, namely, except for E-flow constraint to XJB, other computing conditions of scheme E_Z are same as scheme Z. Similarly, scheme E_A is the one comparing with scheme A, and so on.

Scheme F: some parameters of cascade reservoirs have been changed according to the latest feasibility design (2009). Especially the characteristic water level, storage capacity and installed capacity of WDD and BHT are different with those of planning report (2006). For example, in feasibility design, the normal water level of WDD is raised from 950 m to 975 m, correspondingly its dead water level is raised from 920 m to 950 m and its installed capacity is increased from 7400 MW to 8700 MW. The normal water level and dead water level of BHT are respectively raised 5 m, and its installed capacity is slightly decreased from 13200 MW to 13050 MW. The storage capacities and installed capacities of XLD and XJB remain unchanged. On the other hand, the term of flood-limited level has been shortened. For example, impoundment of WDD starts in early August, about 40 days early than that of planning report. For BHT, the beginning of flood-limited level is delay to July, about one month later than that of planning report. For XLD and XJB, the time of storing water starts in early September. The flood-limited level of each reservoir is raised step by step for impoundment after main flooding season, which will be favorable for improving hydropower benefit.

Table 2. Computing schemes.

Flood control capacity	WDD (10^8 m^3)	BHT (10^8 m^3)	XLD (10^8 m^3)	XJB (10^8 m^3)	Total flood control Capacity (10^8 m^3)
Scheme Z	16.11	73.24	46.50	9.03	144.88
Scheme A	8.05	36.62	23.25	4.52	72.44
Scheme B	4.03	18.31	11.63	2.26	36.22
Scheme C	0.00	0.00	0.00	0.00	0.00
Scheme D	0.00	0.00	0.00	0.00	0.00
Scheme E_Z	16.11	73.24	46.50	9.03	144.88
Scheme E_A	8.05	36.62	23.25	4.52	72.44
Scheme E_C	0.00	0.00	0.00	0.00	0.00
Scheme F	14.24	74.99	46.50	9.03	144.76
Scheme E_F	14.24	74.99	46.50	9.03	144.76

Table 3. Computing results of cascade reservoirs joint operation.

Scheme	Average annual hydropower output					Comparing with scheme Z			E-flow satisfiability %
	WDD ($10^8 \text{ kW} \cdot \text{h}$)	BHT ($10^8 \text{ kW} \cdot \text{h}$)	XLD ($10^8 \text{ kW} \cdot \text{h}$)	XJB ($10^8 \text{ kW} \cdot \text{h}$)	Total ($10^8 \text{ kW} \cdot \text{h}$)	Difference $10^8 \text{ kW} \cdot \text{h}$	Increment %	Benefit* 10^8 ¥ (RMB)	
Z	302.9	597.6	664.5	337.7	1902.7	–	–	–	56.9
A	310.3	616.9	694.6	347.8	1969.5	66.8	3.51	16.7	58.8
B	313.2	616.4	703.6	350.1	1983.4	80.7	4.24	20.2	62.9
C	315.3	621.9	710.2	352.4	1999.8	97.1	5.10	24.3	65.0
D	324.6	639.8	725.5	358.7	2048.6	145.9	7.67	36.5	69.0
E_Z	303.3	606.0	665.2	317.5	1892.0	–10.7	–0.56	–2.7	72.5
E_A	316.2	615.4	692.9	322.2	1946.7	44.0	2.31	11.0	72.4
E_C	316.4	626.0	707.5	322.6	1972.6	69.9	3.67	17.5	77.5
F	371.7	623.0	687.3	344.8	2026.8	124.1	6.52	31.0	48.7
E_F	372.1	626.7	683.8	321.2	2003.8	101.1	5.31	25.3	69.6

* The price of hydro-electricity is assumed to $0.25 \text{ ¥/kW} \cdot \text{h}$.

4.4 Analysis of computing results

The results of each scheme are listed in Table 3. For the planning scheme (scheme Z), the average annual total hydropower output of four reservoirs is $1902.7 \times 10^8 \text{ kW} \cdot \text{h}$, respectively $302.9 \times 10^8 \text{ kW} \cdot \text{h}$, $597.6 \times 10^8 \text{ kW} \cdot \text{h}$, $664.5 \times 10^8 \text{ kW} \cdot \text{h}$ and $337.7 \times 10^8 \text{ kW} \cdot \text{h}$ of WDD, BHT, XLD and XJB. The satisfiability of E-flow is only 56.9%, about 30% less than that of natural flow (87.2%). If half of flood control capacity (scheme A) is cut down, the average annual hydropower output will be $1969.5 \times 10^8 \text{ kW} \cdot \text{h}$. Comparing with scheme Z, the output of hydropower increases 3.51%, about $66.8 \times 10^8 \text{ kW} \cdot \text{h}$, which equals to $16.7 \times 10^8 \text{ ¥}$ (RMB) per year. With the reducing of flood control capacity, more extra profit would be gained from hydropower output. If there is no flood control capacity reserving in flood season (scheme C), the maximum hydropower output will be up to $1999.8 \times 10^8 \text{ kW} \cdot \text{h}$, and the maximum profit will be $24.3 \times 10^8 \text{ ¥}$ more than that of scheme Z. And if the hydropower installed capacity of these reservoirs is increased (scheme D), the extra profit will be increased further.

In scheme E_Z, the XJB has been undertaken the constraint of E-flow, and doesn't take part in the joint optimization operation of other three reservoirs. Comparing the result of scheme E_Z with that of scheme Z, the satisfiability of E-flow heightens to 72.5%, about 15% more than that of scheme Z. It is also found that the average annual hydropower output of WDD, BHT and XLD will be increased with a small increment. But the hydropower output of XJB reduces nearly $20.2 \times 10^8 \text{ kW} \cdot \text{h}$, which can be regarded as the cost for meeting the

demand of E-flow. The total hydropower output of scheme E_A is about 1% less than that of scheme A.

For the latest feasibility design (scheme F), the average annual total hydropower output of cascade reservoirs is 2026.8×10^8 kW · h, respectively 371.7×10^8 kW · h, 623.0×10^8 kW · h, 687.3×10^8 kW · h and 344.8×10^8 kW · h of WDD, BHT, XLD and XJB. Comparing with that of scheme Z, the hydropower output increases 124.09×10^8 kW · h (about 31.0×10^8 ¥). The WDD has the largest increment of 22.72%, and respectively 4.24%, 3.43% and 2.12% of BHT, XLD and XJB. There are two main reasons: one is the increase of installed hydropower capacity of WDD; the other is the term shortening of flood-limited level.

5 CONCLUSIONS AND RECOMMENDATIONS

- a. For the planning scheme, if the joint operation method is applied for lower Jinsha River cascade reservoirs, the total hydropower output will be 1902.7×10^8 kW · h. If all of flood control capacity were canceled, the maximum extra profit of hydropower output could be more than 24.3×10^8 ¥ per year. Therefore for the planning scheme, it is worthy to reduce flood control capacity. Of course, the decrease of flood control capacity will increase the inundation risk of flood diversion area in Jingjiang reach. Especially for the flood of once in 100 years or above, the impact on flood control safety need to be paid more attention.
- b. For the current feasibility design scheme, it is good attempt to shorten the term of flood-limited level in flooding season. This flexible adjustment of flood control capacity is benefit to get more hydropower output, especially in non-flooding year.
- c. By means of 7 days-smooth-average method, the E-flow satisfiability of planning scheme is evaluated as 56.9%, about 30% less than that of natural runoff (87.2%). In order to improve it, one way is to control the outflow of XJB reservoir to meet the demand of E-flow constraint. Under this kind of running mode, the E-flow satisfiability in the downstream of XJB will be increased to 70%. However, the hydropower output of XJB will be reduced. The total hydropower output will decrease 0.6%, about 3.0×10^8 ¥ per year.
- d. The adjustment of flood control capacity of lower Jinsha River cascade reservoirs is a complicated issue, which relates to flood control safety, sedimentation and river ecosystem. The study in this paper, only a preliminary estimate has been made. Further research will be more significant to understand the relationship between hydropower benefit and flood control safety as well as ecosystem restoration.

ACKNOWLEDGEMENT

The study was sponsored by the Yangtze River Project Team of TNC (The Nature Conservancy) and China Yangtze Three Gorges Project Development Corporation; 2009 National Public Research Institute Operating Expenses Special Project (No. YWF0901).

REFERENCES

- Ding Y. & Ji G.Q. 2006. Research on the scheme of flood control capacity in the upper Yangtze River basin (in Chinese). *Yangtze River* 9: 50–52.
- Duan W.H. & Mei Y.D. 2007. Long term optimal operation of Jinsha River cascade River (in Chinese). *Hydropower Automation and Dam Monitoring* 31(1): 17–20.
- Jiang Z.Y. 2004. Discussion on the flood control effect of Xiluodu reservoir of Jinsha River (in Chinese). *China Three Gorges Construction* 4: 40–42.
- John W.L. 2003. Optimal operation of multi-reservoir systems: State-of-the-Art Review. *J. Water Resour. Plng. and Mgmt.* 130(2): 93–111.
- Lu Q.K. & An S.Y. 2003. Discussion on the flood control capacity of Jinsha River (in Chinese). *Water Resources and Power* 21(2): 58–62.
- Tan P.L. & Jiang G.M. 2000. To understand correctly the relationship between hydropower generation and flood control of Xiluodu and Xiangjiaba hydropower stations (in Chinese). *Water Power* 4: 9–11.

Impact of climate change on the management of water resources in mountainous regions—case of the Lake Annecy basin in the French Alps

M. Cottet & C. Freissinet

*SOGREAH Consultants (ARTELIA Group), Water & Environment Department,
Water and Territorial Services Team, Echirrolles, France*

B. Graff

*Compagnie Nationale du Rhône, Engineering Department—River Systems and Climate
Hazards Division, Lyon, France*

*SOGREAH Consultants (ARTELIA Group), Water & Environment Department,
Water and Territorial Services Team, Echirrolles, France*

1 INTRODUCTION

Managing water resources in high-altitude lakes and reservoirs is a complex challenge for managers, developers and decision-makers, because it is difficult firstly to fully understand and predict the entire water cycle and its interactions with the various soil compartments and secondly to anticipate how certain poorly known phenomena such as climate change will evolve. These challenges are also the key subjects of study for ICOLD's Technical Committee on Global Climate Change, Dams, Reservoirs and Related Water Resources, created in 2008. Its forthcoming Bulletin on this subject is currently being written and will be presented at ICOLD's 2012 meeting in Kyoto.

Water resource managers are starting to take into consideration the potential impact of expected climate variations on resource availability (Leblois, 2002; Folton & Lavabre, 2007). The CLIMASILAC II research programme, backed by the Institut de la Montagne in Savoie (France) and implemented by Sogreah, focuses on a prospective modelling approach to draw up scenarios of changes reflecting the evolution of Lake Annecy and its catchment basin under the dual stresses of climate change and human activities. The aim is to develop decision-aid tools to be used by managers, developers and decision-makers in charge of all parts of the drainage network. Part of this applied research work will be presented in this article.

The impact of climate change on the water cycle of the Lake Annecy catchment basin was characterised in the framework of the CLIMASILAC II programme. The aim is to quantify seasonal variations in freshwater inflows into the lake as a function of various climate change scenarios. The impact of climate variations on flows is generally studied on the basis of statistics on long time series (Lang et al., 2002). In this case we attempted to quantify the impact of climate variations on a 2050 timescale obtained by regionalised climate models, by studying seasonal flow variations on the Ire, a river representative of the Lake Annecy tributaries. The MIKE SHE physically based, distributed hydrological model was applied to the Ire river basin and calibrated on the basis of available data. Temperature and precipitation change scenarios were then applied as model forcing conditions in order to measure the effects on seasonal flows in comparison with the calibration results obtained on the basis of the observed data.

2 METHODOLOGY AND IMPLEMENTATION OF THE MODEL

2.1 Presentation of the study area

The Ire is a tributary flowing into the south end of Lake Annecy. With a surface area of approx. 23 km², the Ire catchment basin represents 8% of the Lake Annecy basin, making it the third largest tributary in terms of surface area and the second largest in terms of lake inflows. The Ire is located in the mainly limestone and marl subalpine Bauges mountain range. The mountain-type climate of the basin is lessened by oceanic influences. Mean precipitation in Doussard is 1460 mm per year (1992–98). The river originates at an altitude of 1460 m and flows into Lake Annecy at Doussard at 450 m, after a 12.5 km course with an average gradient of 9.2%. The river is narrow upstream of the Combe de l'Ire, where it is surrounded by steep slopes covered with forests and pastures, and then widens downstream on reaching the plain formed of alluvium and Quaternary moraines. This downstream part has been transformed by human activity to a greater extent. The land is used for agriculture and property development (Figure 1).

The Ire catchment basin is located mainly in mountainous areas. A large proportion of precipitation is stored as snow in the winter and released during the spring thaw. Autumn rainfall also contributes to increased flows, so the flow regime of the lake tributaries is of the nivo-pluvial type (Figure 2). In view of its topography and climate, the Ire catchment basin is hence representative of the entire Lake Annecy catchment basin.

2.2 Methodology

To compare seasonal inflows from the Ire into Lake Annecy in the current state and the probable future states, the water cycle of the Ire catchment basin was modelled using the MIKE

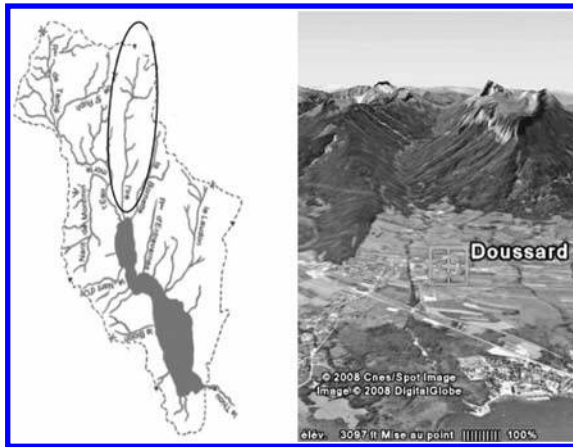


Figure 1. Location of the Ire catchment basin and indication of human activities.

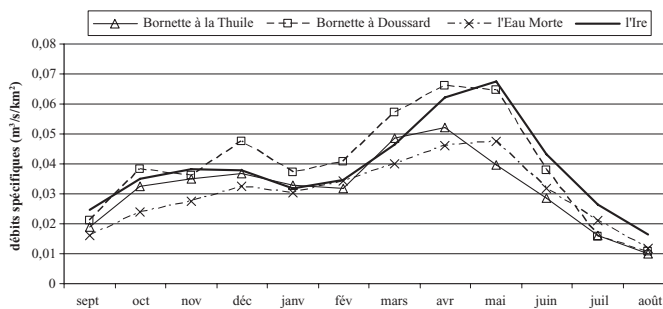


Figure 2. Specific discharges of instrumented Lake Annecy tributaries.

SHE software. This software can be used to represent the water cycle processes, especially evapotranspiration, which is likely to increase as the climate becomes warmer, and snow storage, which plays a vital role in an Alpine climate.

The model was implemented on the basis of available data observed in the Ire catchment basin. Since few soil and subsoil data are available, two sectors considered homogeneous were defined. This simplified representation explains the need for calibration in order to estimate the physical parameters of these two sectors. The model's input hydrometeorological data were the observed temperatures and precipitation. Calibration was carried out on the daily flows recorded at the Ire outlet. Calculation quality was assessed according to two criteria: the volume criterion and the Nash criterion described in section 3.1.

The model was then used in a prognostic manner, replacing the observed data with time series obtained from climate change scenarios. The scenarios were drawn from the results of a regional study based on the average from various climate models (section 4.1). These results were used to modify the input hydrometeorological data of the Ire basin model. Temperature and precipitation variations were then applied to the model, initially independently in order to understand their respective impacts and then simultaneously in accordance with the climate variation scenarios.

The climate change simulation results were then compared with the calibration based on observed data. The future simulations cannot be compared directly with the observations because the analysis would not take into account the model inaccuracies. Comparing the calibration results with the observations is a means of evaluating the model inaccuracies and analysing the future mean seasonal flow simulations. The climate change simulations were hence compared with the calibration results to identify the impact of the temperature and precipitation changes on the seasonal flows modelled on the Ire basin.

2.3 *Implementation of the Mike She model on the Ire basin*

With a view to conducting an integrated study of water resources on the Ire basin, we used the MIKE SHE software to model the following processes:

- surface runoff (storage in the microrelief, runoff and river flows),
- runoff in the unsaturated zone,
- groundwater flows in the saturated zone,
- evapotranspiration and rainfall interception by foliage,
- snow storage and melting.

In addition, in order to integrate the drainage system, MIKE SHE was coupled with MIKE 11, a 1D dynamic hydraulic model for simulating river flows.

The Ire basin, with a surface area of 23 km², was divided into square meshes with sides measuring 50 m.

The land use map obtained by the Corine Land Cover database was exploited to calculate evapotranspiration and rainfall interception by foliage. The land cover and root development indices are defined by vegetation type according to 3 categories: category 1 corresponds to urban areas, category 2 to agricultural areas and category 3 to natural areas.

Temperatures were distributed across the basin as a function of altitude in four zones between 450 m and 2200 m with an average gradient of 0.6°C/100 m. The temperature determines whether precipitation falls as rain or snow. If the precipitation falls as snow, it is stored until the temperature rises sufficiently for it to melt, at which point the water begins gradually being released and contributes to runoff.

Temperature was also used in the simulation to calculate evapotranspiration. On the basis of the hydrometeorological data and the land cover characteristics, MIKE SHE's evapotranspiration module determined the net rainfall resulting from the physical processes of rainfall interception and evaporation. The model calculated the actual evapotranspiration rate by estimating potential evapotranspiration (PET) (Freissinet, 1997). Oudin's formula (2006), which is a function of latitude and temperature, was used to estimate a PET

(mm/d) that varies as a function of temperature, which was essential for the climate change scenarios.

To represent orographic rainfall phenomena, precipitation was increased with altitude on the basis of the results of the studies performed in the Chartreuse mountain range by Desurosne et al. (1996). The study results were transposed to the nearby Bauges range.

The analysis of geology and topography revealed two distinctive sectors within which the hydrological behaviours of the unsaturated and saturated zones were considered homogeneous:

- A mountainous upstream sector with a thin soil layer and low permeability subsoil. Surface and sub-surface runoff is predominant in this sector;
- A downstream sector in the plain with a thicker soil layer and porous subsoil, likely to include an aquifer.

This simplified representation of the unsaturated and saturated zones as two sectors is the reason why calibration was necessary to estimate the physical parameters governing surface and sub-surface runoff and groundwater flows in the Ire catchment basin model.

3 MODEL CALIBRATION AND VALIDATION

3.1 Calibration

The calibration calculations were done over a two-year period between 1 September 1996 and 31 August 1998. The first year served to initialise the model. Modelling quality was judged on the results obtained during the second year, once the model was stabilised. Quality was judged on the basis of two criteria:

- The volume criterion (V), which represents the error measurement on the total runoff volume calculated by the model in relation to observations (the closer V is to 100%, the closer the calculated volume is to the observed volume).
- The Nash criterion, which takes into account the temporal nature of the inflows (it can vary between minus infinity and 100%. The higher its value, the better the calibration (Perrin, 2000))

$$V = \frac{\sum_{i=1}^n Q_{cal,i}}{\sum_{i=1}^n Q_{obs,i}} \times 100 \text{ and Nash} = 100 \times \left(1 - \frac{\sum_{i=1}^n (\sqrt{Q_{obs,i}} - \sqrt{Q_{cal,i}})^2}{\sum_{i=1}^n (\sqrt{Q_{obs,i}} - \sqrt{Q_{obs,i}})^2} \right) \quad (1)$$

The respective formulae of these criteria are as follows with i being the time step varying from 1 to n , $Q_{cal,i}$ being the flow calculated at time step i and $Q_{obs,i}$ being the flow observed at time step i .

The calibration results are given in [Figure 3](#). With respective values of 117% and 45%, the volume and Nash criteria are considered satisfactory. The daily hydrograph reproduces all the events observed concomitantly, but the amplitude of the flood peaks is insufficient, especially in the autumn and winter. In the spring, the modelled runoff is recorded earlier than the observed runoff, being high in March and lower in April and May. However, at the seasonal time step, these different inflows are balanced out and correspond to the observations. The model overestimates the low flow from June to November, which is why the runoff volume is too high.

3.2 Validation

Validation consists in checking that the model calibrated over one period produces satisfactory results over another period that was not used for calibration. Given the short period for

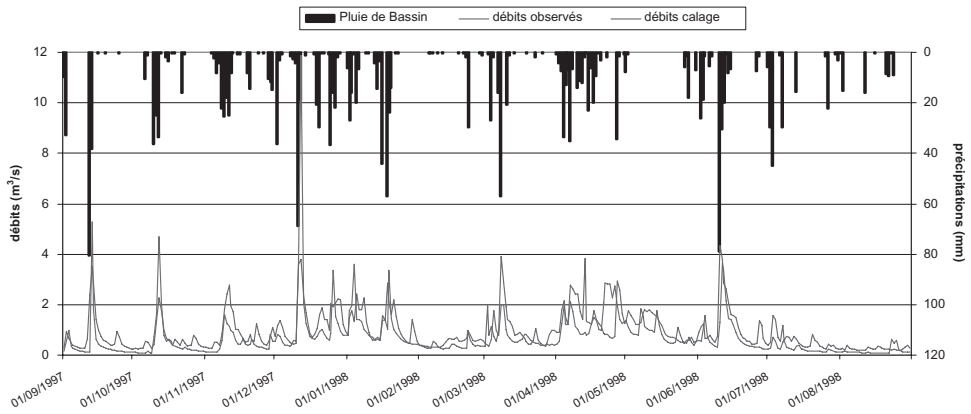


Figure 3. Hydrograph of daily flows observed and calculated following calibration.

which Ire basin data are available, validation was carried out on the complete data time series from 1993 to 1998.

V	93%	105%	110%	132%	123%	110%
	1993–94	1994–95	1995–96	1996–97	1997–98	total
Nash	41%	40%	44%	19%	37%	41%

First, the result quality is fairly good each year and throughout the time series. Second, each year the model presents the same qualities and flows as those described for the calibration:

- the flood events are concomitant. The major peaks are often underestimated, especially in the winter due to the storage of precipitation in the form of snow.
- the low flows in the summer and autumn are overestimated, as a result of which the total annual volumes are overestimated by 10%.

This calculation quality is considered satisfactory for the purpose of analysing the impact of climate change on seasonal inflows into Lake Annecy.

4 IMPACT OF CLIMATE CHANGE

It was hence possible to apply variations in temperatures and precipitation to the model input data. Next, the results for the seasonal volumes flowing through the outlet with the new input data were compared with the calibration results.

4.1 2050 climate change scenario

The climate variations applied to the model had to be adapted to the Ire basin, i.e. correspond to an Alpine climate. This type of climate is particularly sensitive to variations with amplitudes varying from one season to the next (Becker and Bugman, 1997; Beniston, 2001). Regional and seasonal data were hence needed. The Federal Office of Meteorology and Climatology MétéoSuisse has published a report on climate change in Switzerland in the 21st century (Frei, 2004). A regional climate scenario was calculated taking into account the results of the models from the PRUDENCE project (Christensen, 2002; <http://prudence.dmi.dk/>). This scenario offers the best estimation of the expected modifications with confidence intervals taking into account an understanding of the physical processes (model uncertainties).

The data are supplied in the form of temperatures and precipitation variations in relation to the present state. These variations are applied to the model input data and are presented in

Table 1. Modifications in temperature and precipitation made to the 1996–98 time series.

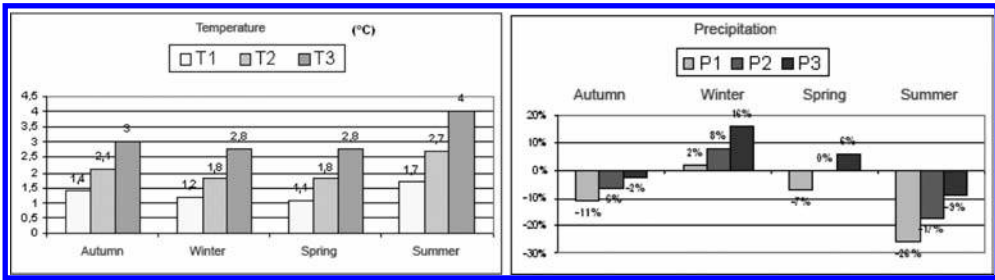


Table 1. T1 represents the 10% quantile temperature variation, and T3 the 90% quantile temperature variation. The confidence interval from T1 to T3 is shared by the T2 median, which is the most probable temperature variation. Similarly, P1, P2 and P3 are the 10%, 50% and 90% quantile precipitation variations.

The results are given per season for the northern and southern slopes of the Alps. The Ire basin is in the Haute Savoie department, on the northern slopes of the Alps according to the authors' distinction. These results are appropriate. Since they come from several climate models comprising regional and seasonal characteristics, they are supplied with confidence intervals. The scenario predicts temperature rises in all seasons and with all probabilities. The precipitation variations depend on the probabilities. On the whole, precipitation is expected to increase in the winter and decrease in the summer and autumn.

Insofar as we wished to analyse the impact of climate change on river Ire seasonal flows, the 1996–98 temperature and precipitation time series were modified taking into account the variations supplied by the Swiss scenario for 2050. The new temperature and precipitation series thus obtained formed the forcings for the climate change simulations.

As was the case with calibration, these simulations were conducted over a two-year period. The first year served to initialise the model with the new forcings; only the results from the second year were analysed.

4.2 Impact of climate variations on seasonal volumes

4.2.1 Impact of temperature variations

First the model was used in a prognostic manner, modifying only the temperatures and keeping the precipitation observed between 1996 and 1998 as inputs.

In the winter, the temperature rise will cause flows to increase by up to +29% in relation to the calibration. The rain/snow line is higher, so less precipitation is stored as snow. Furthermore, the higher temperatures lead to faster snowmelt. Since winter precipitation makes such a large contribution, spring and summer runoff will fall significantly, by up to –28% in the summer in relation to the calibration.

The decrease in runoff volumes in the spring and summer is accentuated by an increase in evapotranspiration in line with temperature. Indeed, evapotranspiration represents 27% of total precipitation in the case of the calibration compared with 33% in the case of the simulation due to the larger temperature increase. As a result of the temperature increase the annual runoff volume could fall by up to –5% in relation to the calibration (Figure 4). The larger-scale study performed by Barnett et al. (2005) obtained similar results in terms of the impact of temperature increases on water cycle variations on rivers with nival regimes.

4.2.2 Impact of precipitation variations

The effect of precipitation variations was then tested keeping the temperatures observed between 1996 and 1998 as inputs.

The climate variation scenario predicts that precipitation will increase in the winter and decrease in the summer and autumn. The seasonal volume variations follow the precipitation

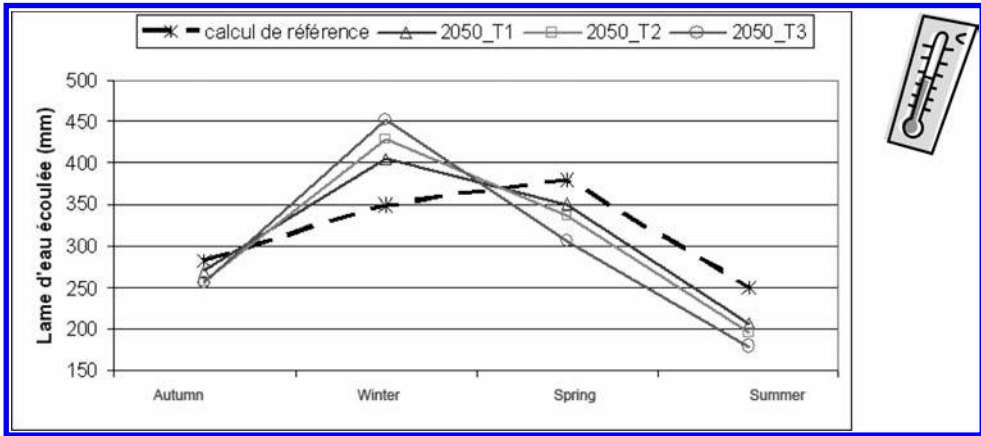


Figure 4. Impact of temperature increase on seasonal discharges.

variations. The volumes increase in the winter by up to +11% in relation to the calibration and decrease in the summer by up to -26%.

In some cases a time lag between the precipitation variations and the flow variations is observed. This lag is due to a buffer effect exerted by the ground, which dries out or becomes waterlogged depending on the new precipitation forcings applied. The state of the ground hence either slows down or accelerates runoff, contributing to flow variations and explaining the time lag between the precipitation variations and the flow variations.

The variation in runoff volume over the year decreases by up to -13% or increases by +5% in relation to the calibration depending on the precipitation variation probabilities being considered (Figure 5).

4.2.3 Impact of combined temperature and precipitation variations

The combinations of temperature and precipitation variations produced nine climate change scenarios, which are listed in the left-hand column of Table 2. This table summarises the seasonal and annual volume variations of the nine simulations in relation to the calibration. When the volume is higher than the calibration, the background is grey. In addition, the largest variation in each column is indicated in bold.

When the temperature and precipitation variations are combined, the seasonal volume variations are greater because the two parameters act in conjunction (Zierl and Bugmann (2005)). Our simulations revealed similar results. Indeed, the increase in winter volumes is accentuated (by up to +46% in the case of simulation T3_P3). Both the increased precipitation and the temperature rises lead to increased runoff volumes in the winter. The decreases in volume in the summer and autumn (up to -47% in the case of simulation T3_P1) are also accentuated by the combined action of temperature and precipitation variations. First, there is less precipitation. Second, the temperature rise increases evapotranspiration losses and accelerates snowmelt, reducing the contribution from snow in the early summer. The temperature and precipitation variations thus act in the same way to reduce runoff volumes in the summer and autumn. The springtime runoff volumes decrease in most cases (by up to -27% in the case of simulation T2_P1). During this season the melting snow mantle makes the largest contribution. With the increasing temperatures, the mantle is thinner, thus producing smaller runoff volumes as it melts. Only the runoff volume from simulation sim_T1_P3 increases slightly during the spring, because this simulation combines a slight temperature rise with increased precipitation. The effects of increased volumes during the winter and reduced volumes the rest of the time compensate for each other over the year, making the annual balance variations smaller than those of the seasonal balances

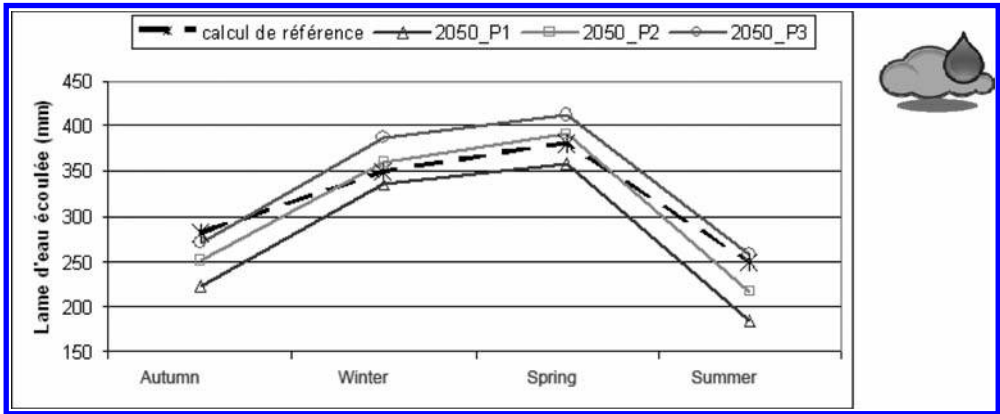


Figure 5. Impact of increased precipitation on seasonal flows.

Table 2. Flow ratios between the simulations with temperature and precipitation variations and the calibration.

	Autumn	Winter	Spring	Summer	Annual
sim_T1_P1	-25%	+14%	-12%	-41%	-13%
sim_T1_P2	-17%	+18%	-5%	-32%	-6.50%
sim_T1_P3	-10%	+33%	+0.3%	-20.50%	+3%
sim_T2_P1	-27%	+16%	-16%	-43%	-15%
sim_T2_P2	-16%	+25%	-11%	-37%	-7%
sim_T2_P3	-9%	+38%	-4%	-30%	+1%
sim_T3_P1	-30%	+24%	-27%	-47%	-17%
sim_T3_P2	-24%	+35%	-21%	-44%	-11%
Sim_T3_P3	-14%	+46%	-12%	-31%	-0.2%

(+3% to -17%). Nevertheless, at the scale of a year a runoff deficit is generally observed in relation to the calibration.

4.2.4 Comments on the model characteristics

The previous section compares the model results obtained using the observed data with the data affected by climate change. In comparing the 2050 climate change simulation results with the observations, the model inaccuracies must be taken into account. Calibrating and validating the model enabled us to demonstrate that the model always overestimates low flows. For example, the mean summertime flow with simulation sim_T2_P2 is 0.45 m³/s. If, as is the case with the calibration, this flow is overestimated by 67%, it would only be approx. 0.27 m³/s. According to the Banque Hydro data concerning minimum flows over 90 consecutive days, a 0.27 m³/s flow currently has a return period of 5 to 10 years on the Ire basin. On the other hand, the model always underestimates wintertime flood peaks. The climate variation simulations indicate that runoff volumes will increase at this time of year. If the flow increases simulated in 2050 are applied to the observed values, heavy flooding will occur during the winter.

Moreover, in order to apply the climate change scenarios to the model, the input data were modified by adding temperature and precipitation variations to the observed time series. This method is appropriate for temperatures, but has drawbacks when it comes to precipitation. These variations modify the cumulative precipitation recorded but do not modify the number

of days of precipitation. Some studies foresee longer periods without rainfall during the summer and autumn coupled with more frequent extreme events. However, the current climate models are not capable of quantifying these phenomena (Frei et al.; 2006). The climate variation data are hence supplied season by season, making it possible to study variations in seasonal runoff volumes.

5. CONCLUSION

In this study, the MIKE SHE water cycle modelling software was applied to the catchment basin of the Ire, a tributary of Lake Annecy. The aim of this study was to characterise the impacts of climate change on the hydrological conditions of the Ire.

At the end of the study, the results of the simulations incorporating the climate changes expected in 2050 can be used to quantify seasonal volume variations on the Ire for different temperature and precipitation variation scenarios. Overall the results indicate increased runoff volumes in the winter, and decreased runoff volumes in the summer and autumn. These contrasting seasonal variations indicate a general decrease in the annual balance of runoff volumes. The flow conditions of the Ire are representative of the other lake tributaries. The variations in the Ire hydrological conditions caused by climate change will hence probably be reflected throughout the Lake Annecy catchment basin. In particular, our study indicates that summertime lake inflows will decrease substantially whatever the probability of the temperature and precipitation variations selected. This decrease could affect the quantity and quality of the lake's water resources at the time when it is most heavily used.

Using the integrated hydrological model on the Ire catchment basin enabled us to quantify variations in Ire flows under various climate change scenarios. These flow variations may then be extrapolated to a scale of the entire Lake Annecy catchment basin. This tool is therefore of interest for lake catchment basin managers, with a view to managing water resources in an integrated, concerted manner against the backdrop of climate change.

Methodologies of the same type could be used to assess the potential consequences of climate change for hydropower production or for other uses of water resources.

ACKNOWLEDGEMENTS

The authors are greatly indebted to Pierre Cochet and Stéphane Duflo from SOGREAH for their active participation in reading through and editing the final version of this article.

BIBLIOGRAPHY

- Barnett, T.P.; Adam, J.C. & Lettenmaier, D.P. (2005)—Potential impacts of a warming climate on water availability in snow-dominated regions. *Nature*, Vol. 438/17, p. 303–309.
- Becker, A., & H. Bugmann (eds.), (1997)—Predicting Global Change Impacts on Mountain Hydrology and Ecology: Integrated Catchment. *Hydrology/Altitudinal Gradient Studies*. IGBP Report 43, International Geosphere-Biosphere Programme, Stockholm.
- Beniston, M., & P. Junco, (2001)—Shifts in the distributions of pressure, temperature and moisture in the alpine region in response to the behaviour of the North Atlantic Oscillation. *Theor. Appl. Climatol.*, 71, 29–42.
- Christensen, J.H.; Carter, T. & Giorgi, F. (2002)—PRUDENCE employs new methods to assess European climate change. *EOS*, 87, 147.
- Desurogne, I.; Ribot-Bruno, J.; Watremez, S. & Oberlin, G. (1996)—Guide pratiques des données pluviographiques et des résultats d'un réseau préalpin, le TPG (période 1987–1995). Cemagref Lyon, Laboratoire de Météorologie Physique de Clermont-Ferrand, p. 115.
- Folton, N.; & Lavabre, J. (2007)—Approche par modélisation PLUIE-DEBIT pour la connaissance régionale de la ressource en eau: application à la moitié du territoire français. *La Houille Blanche*, no. 3–2007; 64–70.

- Frei, C. (2004)—Die Klimazukunft der Schweiz—Eine probabilistische Projektion. (www.occc.ch/Products/CH2050/CH2050-Scenarien.pdf).
- Freissinet, C (1997) Estimation des imprécisions dans la modélisation du devenir des produits phytosanitaires dans les sols: une méthode fondée sur la logique floue”.Thèse de Doctorat de l’Université Joseph Fourier-Grenoble I.
- Lang, M.; Naulet, R.; Recking, A.; Cœur, D.; & Gigon, C. (2002)—Etude de cas: l’analyse des pluies et crues extrêmes observées depuis 200 ans dans un bassin cévenol, l’Ardèche. *La Houille Blanche*, no. 6–7 2002, 131–138.
- Leblois, E. (2002)—Evaluation des possibles impacts du changement climatique par modélisation distribuée. *La Houille Blanche*, no. 8–2002, 78–83.
- Oudin, L. (2006)—Une formule simple d’évapotranspiration potentielle pour la modélisation pluie-débit à l’échelle du bassin versant. *La Houille Blanche*, no. 6–2006, 113–120.
- Perrin, C. (2000)—Vers une amélioration d’un modèle global pluie-débit au travers d’une approche comparative, thèse de doctorat de l’Institut National Polytechnique de Grenoble.
- Zierl, B. & Bugmann, H. (2005)—Global change impacts on hydrological processes in Alpine catchments. *Water Resour. Res.*, 41, 1–13.

Optimized and adapted hydropower management considering glacier shrinkage scenarios in the Swiss Alps

S. Terrier, F. Jordan & A.J. Schleiss

Ecole Polytechnique Fédérale de Lausanne (EPFL), Laboratory of Hydraulic Constructions (LCH), Lausanne, Switzerland

W. Haerberli, C. Huggel & M. Künzler

Geography Department, University of Zurich, Switzerland

ABSTRACT: Global warming is an alarming reality and likely leads to an increase of multiple pressures on socio-economic systems. However, in high-mountain regions it might also become an opportunity to adapt existing hydropower schemes and future projects to this new reality. In the Alps, the melting of glaciers first produces over the near future an increase of the average annual discharge depending on glacier and catchment characteristics, especially during the summer season. Nevertheless after a certain time, significant decrease of runoff related to glacier melting must be considered for hydropower management. Moreover, the melted glaciers free new alpine valley areas, which have a potential for the construction of new dams and reservoirs.

The opportunity to build new dams and hydropower plants downstream of retreating glaciers is studied systematically in Switzerland within the framework of the National Research Program on Sustainable Water Management (NRP61) under the project “New lakes in deglaciating high-mountain areas: climate-related development and challenges for sustainable use (NELAK)”. The developed methodology is based on several prediction models. Regional climate models provide spatially distributed rainfall and temperature scenarios for the next 50 years. The RS3.0 CLIMATE rainfall-runoff hydrological model computes the glacier evolution, the river discharge at the outlet of the catchment area as well as the hydropower production of the new lakes. Another model (GlabTop) is used to predict the future topography and geomorphology underneath the melting glaciers, in order to define the optimal locations of the future dams and reservoirs.

As a case study the Corbassière glacier near the Mauvoisin reservoir in Valais is presented. The opportunity of the construction of a new dam and a hydropower plant is studied, as well as its economic benefit and its impacts on the environment. The result of the case study provides a basis to assess the potential of investing in such projects to ensure the Swiss hydroelectricity production also in future.

1 INTRODUCTION

With the climate change, the mean temperature is rising globally and also in the Alps. One of the most visible consequences of this change is strong glacier shrinkage (UNEP 2007, Zemp et al. 2008).

Due to glacier retreat, each year, new glacier-free areas are revealing a topography carved by glaciers. In some locations, where a depression was present under the glacier, new lakes may be appearing with various sizes and depths. Sometimes they may form on unstable geology and be impounded by moraine dams, and thus representing a threat for the people living downstream (Clague & Evans 2000, Haerberli et al. 2001, 2010, Huggel et al. 2004). However, they might also be an opportunity for hydropower production.

A second impact is a change in the hydrological regime of the Alpine rivers. As the glaciers are readjusting to the rising temperature, they may provide a higher discharge during the summer for a limited number of years and depending on glacier size, hypsography and catchment characteristics. However, this process is probably only temporary, as the glaciers either find a new equilibrium state or disappear. As a consequence the hydrological regime and the annual inflow volume will change, causing an important impact on the existing hydropower schemes.

In this contribution, the evolution of the glaciated catchment area of the *Forces Motrices de Mauvoisin* (FMM) hydropower scheme is studied. More precisely, an important depression currently lies under Corbassière Glacier and in the future could represent an opportunity to adapt the hydroelectric scheme to the changing situation.

2 DESCRIPTION OF THE UPPER BAGNES VALLEY BASIN

2.1 *Forces Motrices de Mauvoisin (FMM) hydropower scheme*

The FMM scheme lies in the upper Bagnes Valley in Valais, Switzerland. It is designed around the Mauvoisin reservoir (204 hm³) which was created by the construction of the Mauvoisin arch dam (height of 250 m) on the Dranse de Bagnes River (Figure 1).

The natural catchment area of the reservoir is 112 km². Additional water is transferred from intakes on the left and right bank of the Bagnes valley, increasing the contributive area by respectively 35 and 19 km². The elevation of the catchment area ranges from 1976 m a.s.l. (Mauvoisin dam crest level) to 4315 m a.s.l. 37.1% of the total catchment area of 166 km² is covered by glaciers. Therefore the hydrologic regime is glacial.

The average annual inflow in the Mauvoisin reservoir reached 280 hm³ in the recent years. 76% of this inflow is produced by the natural catchment area. The remaining part is brought by the left and right side tunnels with a proportion of 18% and 6% respectively. As 90% of the inflow occurs in the summer months and the peak electricity demand is in winter, the 204 hm³ capacity of the Mauvoisin reservoir is used as a seasonal storage.

The total head between the Mauvoisin reservoir and the tailrace in the Rhone River varies between 1498 and 1361 m, and is divided into two different stages. The two corresponding power plants are Fionnay (138 MW) and Riddes (225 MW). A smaller run-of-river power

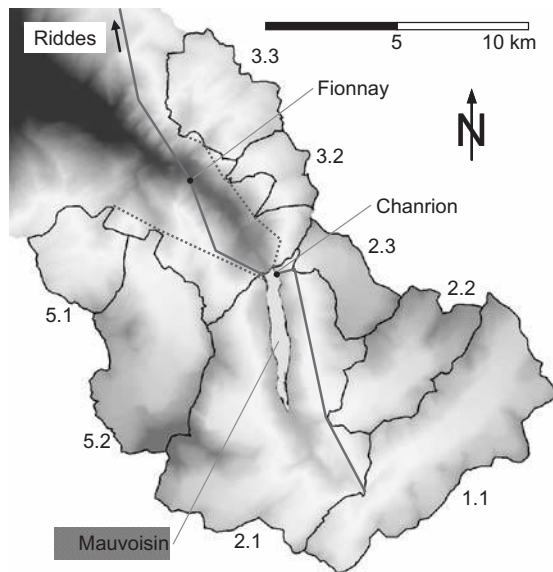


Figure 1. Catchment areas and FMM hydroelectric scheme.

plant (Chanrion 28 MW) was built upstream of the Mauvoisin reservoir to produce energy with a part of the natural inflows coming from the right side water transfer tunnel.

2.2 Corbassière Glacier

The Corbassière Glacier is the 5th longest glacier in Switzerland with a length of 9.8 km and an area of 17.4 km². It is located on the west side of Mauvoisin reservoir and is part of the left bank tunnel.

An analysis of the topography currently covered by glaciers shows that an important depression is present under the tongue of the Corbassière Glacier. The methodology to assess the glacier bed topography is based on a model estimating the glacier thickness using an inverse ice flow law together with a shallow ice approximation (Haerberli & Hoelzle 1995; Linsbauer et al. 2009). Since the basic parameter that influences ice thickness is surface slope, the method explores the variability of glacier thickness for glacier parts with variable surface inclination in a spatially explicit way. Subtracting the ice thickness grid from the input DEM yields a DEM without glaciers. We consider the overdeepenings (depressions) in the modeled glacier beds as potential sites for new glacier lakes. We furthermore use a simplified model of future glacier retreat (Paul et al. 2007) to roughly classify the potential lakes by their mean depth and their time period of appearance. The likelihood of actual lake formation is

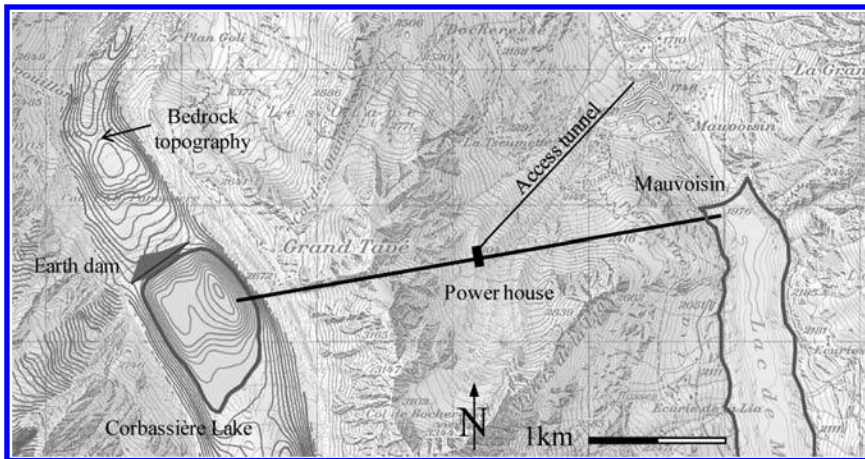


Figure 2. Plan view of the new lake Corbassière and pumped-storage scheme.

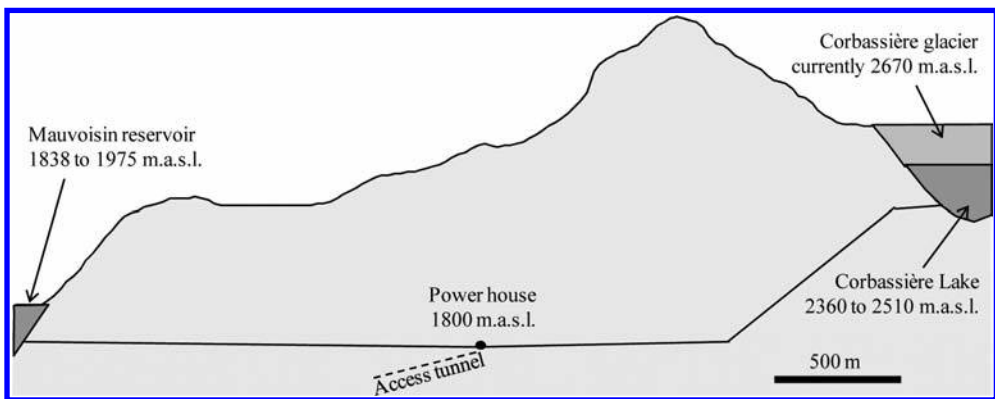


Figure 3. Longitudinal profile of the pumped-storage scheme project Corbassière.

probably high but currently remains difficult to assess safely due to a number of uncertainties with respect to future drainage patterns.

Based on this method, we assess that a lake of 0.64 km² might appear at 2500 m a.s.l. Having a depth of 200 m, the estimated new lake volume is 51.6 hm³, which is about 25% of the Mauvoisin reservoir. This potential depression is currently located 2 km upstream of the tongue's end and underneath about 120 m of ice.

2.3 Potential future hydroelectric projects

In the 1990's, the "Mauvoisin II" project was developed. The idea was to build a new underground power house of 550 MW in parallel of the existing two stages system directly from the Mauvoisin reservoir to Riddes. With this new plant, the total FMM installed capacity could have been increased from 390 to 940 MW and the energy production could be concentrated on a few peak hours per day. For the time being, this project was not followed up for economical reasons, but could be reactivated in future.

With the creation of a new lake at Corbassière due to glacier retreat, a new pumped-storage scheme of 500 MW could be installed between this lake and the Mauvoisin reservoir (Figures 2–3). As these two lakes have a significant volume of 204 hm³ and 51.6 hm³ respectively, this high capacity power house can be used to regulate the electricity grid at hours of peak demand. The energy produced by renewable sources such as a wind power during low demand could be pumped in order to transfer it to peak energy. Based on the topographic assessment, the new reservoir Corbassière would need the construction of an earth fill dam (eventually concrete faced rockfill dam) of about 40 m height.

3 MODELLING

3.1 RS3.0 Software

3.1.1 Rainfall-runoff

The rainfall-runoff model used in the RS3.0 hydrological software (Keller 2009, Garcia et al. 2007) is based on GSM-SOCONT (Glacier-Snow Melt Soil CONTRIBUTION). This semi-distributed conceptual model is able to consider numerous hydrological processes determining the river flows (Schäfli et al. 2005, Jordan 2007). The basins are subdivided into 300 m elevation bands in order to take into account the influence of the temperature evolution with altitude. When necessary, the elevation bands include a glacier melt model in addition to the soil infiltration model.

The considered hydrological processes in the GSM-SOCONT model are the spatial interpolation of the precipitation and temperature, the evapo-transpiration, the snow melt, the glacier melt, the soil infiltration, the surface runoff and the river routing, as well as the hydraulic transfers and storage functions due to the hydropower plants and natural lakes.

3.1.2 Glacier

The purpose of the glacier melt model is to simulate the glacier evolution and the discharge at its outlet over a long period. The focus is more on the precision of the discharge than on the glacier evolution (surface and height modifications during time).

In each glacier elevation band, the glacier is modeled as a simplified rectangular cuboid with a surface S and a thickness h (Figure 4b). The melt V_{out} depends on a melt parameter A_{GL} , on the temperature and on the surface. If a snow height H_N is present above the glacier, it gradually transforms into ice (V_{GL}) depending on a controlling parameter A_{GLN} . The ice flow between the elevation bands V_{down} is taken into account with a flowing speed U and the glacier width L . After each time step, the volume balance dV is either added or subtracted to the ice volume.

When the volume changes, part of it is transformed to glacier height, the other contribution to the glacier area. The parameters A_{GL} and A_{GLN} are calibrated for an observed reference period (see section 3.2).

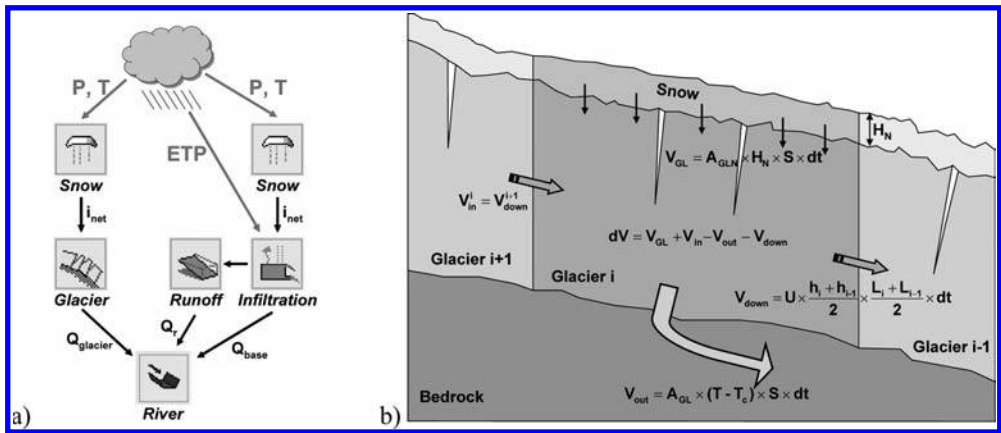


Figure 4. RS3.0 software: a) Structure of the hydrological model, example of a basin with one glacier (left) and one non-glacier (right) elevation zone; b) Functioning and equations of the glacier model.

3.1.3 Energy production algorithm

An energy production algorithm is used to simulate the hydropower plants. To perform an optimization of the income, it takes into account the hourly electricity prices and reservoir target curve to simulate the seasonal level variations. At each time step, depending on these parameters and the reservoir filling percentage, the algorithm chooses if the power plant is turbinning or not (Jordan & Heller 2010).

3.2 Calibration

The model was calibrated in order to reproduce the measured discharges as close as possible. For the period from October 2002 to October 2004, Figure 5 compares the observed and simulated discharge in the left bank collector which is mainly fed by the Corbassière sub-basin.

3.3 Climate scenarios

Different climate models and scenarios were considered. They are all based on temperature and precipitation measurements made at different weather stations in the vicinity of the study area during the period from 01.10.1981 to 30.09.2009.

The first scenario is considered as a reference (also named 0°) and represents the climate of the past 30 years, reproduced during the next 100 years. The data from 1981 to 2009 are simply repeated each 28 years until 2100.

The second and third scenarios are modifications of the first one, with a linear temperature increase and no precipitation change. The scenario +4° adds 4°C linearly until 2100 and the -2° scenario subtracts -2°C until 2100.

The last scenario, called ETHZ, modifies the temperature and the precipitations. This scenario is based on a model from the recently completed EU-ENSEMBLE project and was provided by the Center for Climate Systems Modeling (C2SM) at the ETH Zurich. The results are derived from the Regional Climate Model (RCM) CLM, driven by the General Circulation Model (GCM) HadCM3Q0. The model and the respective method assess the relative difference between the future climate and a reference observation period, and add the difference to the reference period (Bosshard et al. 2010). The difference is a value to add to the reference for the temperatures and a coefficient to multiply for the precipitations. The differences are given for every weather station and for two periods: 2021–2050 and 2070–2099. Between these periods, a linear interpolation is applied. Compared to the +4° scenario, the temperature rises faster, especially in the summer months.

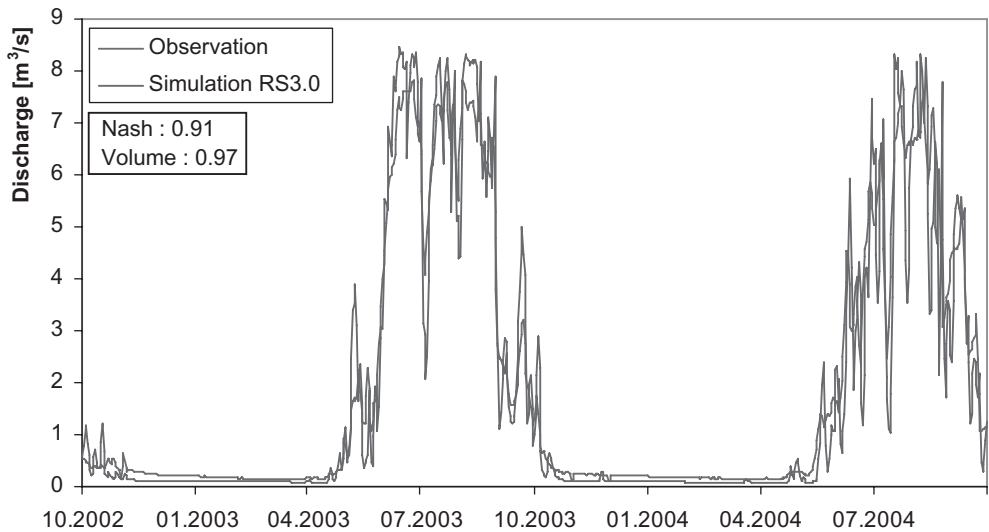


Figure 5. Observed and simulated outflows in the left bank water transfer tunnel.

3.4 Electricity prices

The energy production algorithm needs a future price curve to compute the expected incomes. For the pump-storage scheme, this information is important as it is used to determine the benefits and the operation time.

The spot market prices from 01.01.2004 to 31.12.2008 are used as a reference and repeated every 5 years. Of course they do not represent fully the reality, but can be used to optimize the power production of the scheme. Moreover, an important part of the electricity production is sold at higher prices by mid-term and long-term contracts which guarantee beside energy also firm power during a certain time. In the economical analysis this is considered by a multiplication factor of the spot market price proportional to the guaranteed firm power.

4 RESULTS AND DISCUSSION

4.1 Corbassière Glacier

Figure 6 shows the evolution of the thickness of the Corbassière Glacier's lower elevation band for the different climate scenarios. The lowest elevation band will disappear during the next 40 years, regardless of the climate scenario.

The second band, which covers the new Corbassière Lake, is also decreasing. But there are important differences between the climate scenarios. For the scenario ETHZ and the scenario +4°, the second band is disappearing in 2075 and 2089 respectively. Although the mean temperature is about the same in 2100 with these two scenarios, the ETHZ scenario has a mean temperature that rises more rapidly than the linear increase in the +4° scenario. This explains why the glacier band is melting sooner in this case. In the reference scenario, the band is losing 70% of its thickness, and probably disappears around 2150. With the cooling scenario -2°, the glacier band is losing 50% of its thickness, but is almost stabilized in 2100.

Finally, the climate scenarios have a major impact on the third band. In the scenarios ETHZ and +4°, this glacier band is disappearing between 2100 and 2130. In the reference scenario, the thickness is slowly decreasing during the whole 21st century. And in the -2° scenario, the glacier is growing in the second half of the century.

For the power production analysis, the date of 2075 is considered as the emergence of the new Corbassière Lake. Important uncertainties are related to this estimation, as the model was primarily developed to simulate the inflows and not to simulate the glacier evolution in detail.

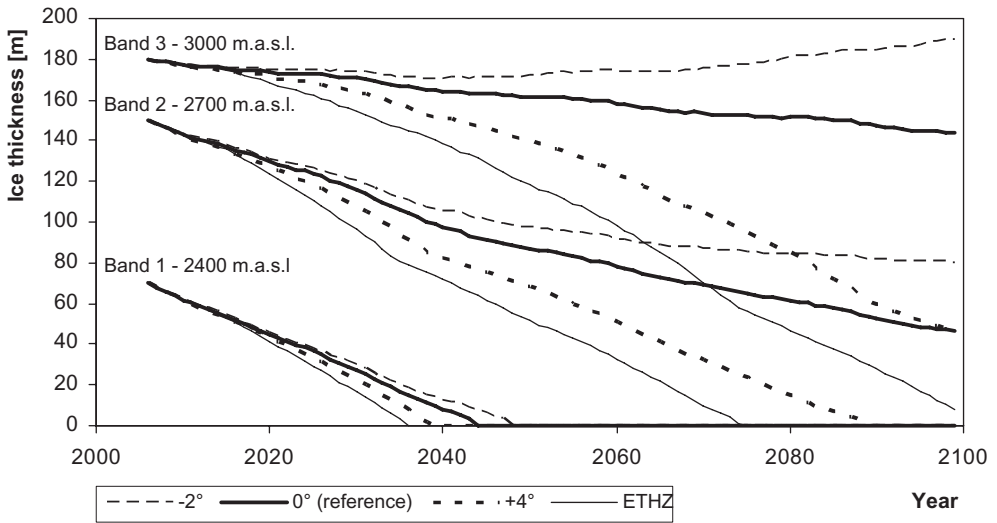


Figure 6. Ice thickness of the 3 lower bands of Corbassière Glacier simulated for the 4 climate scenarios.

4.2 Inflows

Figure 7 shows the annual inflow into Mauvoisin reservoir. A 5 years average was used to smooth the high annual variability (showed with dashed line for the measured values) and therefore having a better vision of the trends.

For the measured values, an increase of the inflow occurred since 2000 which can be explained by an increased temperature. The summer of 2003 was the hottest ever recorded in Switzerland, and the annual inflow into Mauvoisin was 339 hm³.

For the reference scenario, the annual inflow volume remains constant at about 270 hm³/year until 2030. After this date, it decreases slowly until reaching 210 hm³/year at the end of the century. For the -2° scenario, the annual volume decreases from the beginning and is reaching 185 hm³/year in 2100.

For the +4° scenario, the inflow does not vary much until 2035 and then decreases to 220 hm³/year in 2100. For the other rising temperature scenario of ETHZ, the inflow keeps rising and reaches often the 2003 peak annual inflow. After reaching a peak around 2020, the inflow decreases faster than the other scenarios, and reaches 195 hm³/year at the end of the century. This annual volume in 2100 for the ETHZ scenario is lower than the volume for the reference and for the +4° scenarios.

It is important to note that whatever the scenario is, there will be a decrease in the annual inflow volume in the second part of the century compared to past years. This is partly related to the response time of a large glacier like Corbassière to current climate (i.e. it is in a state of imbalance with current climate). To better understand the driving processes we analyze here the origin of the inflow.

Figure 8 shows the inflow predicted by the ETHZ scenario. As it can be expected, an important part is coming from non-glacial flow (snow melt, runoff, and groundwater base flow). Currently, a volume of about 12% of the annual precipitation is coming from a sustainable glacial melt (renewed). This means that the ice volume melted in the lower part of the glacier is in the same year formed by snow fall in the upper part of the glacier. The third type of flow is also coming from glacial melt, but it is not renewed as it comes from the readjustment of the glaciers. The proportion of this inflow is very important in the first 50 years with an average of 48% of the precipitation volume. In the second part of the century, as the glaciers increasingly lose their mass, this inflow will decrease down to 13% in 2100 and when the glaciers will be in equilibrium, this inflow will not exist anymore. Currently the glacier melt coming from the existing mass is about a third of the total inflow.

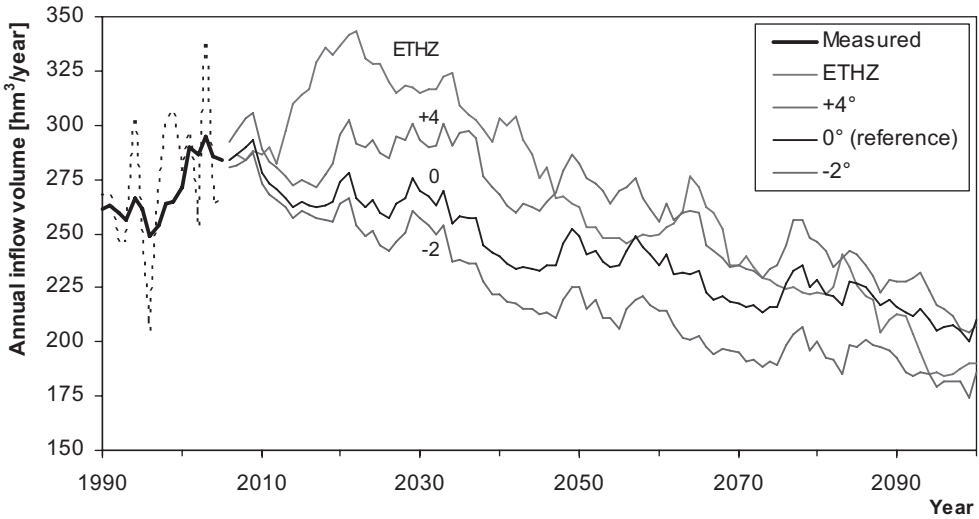


Figure 7. Annual inflow volume (5-years average) in the Mauvoisin reservoir.

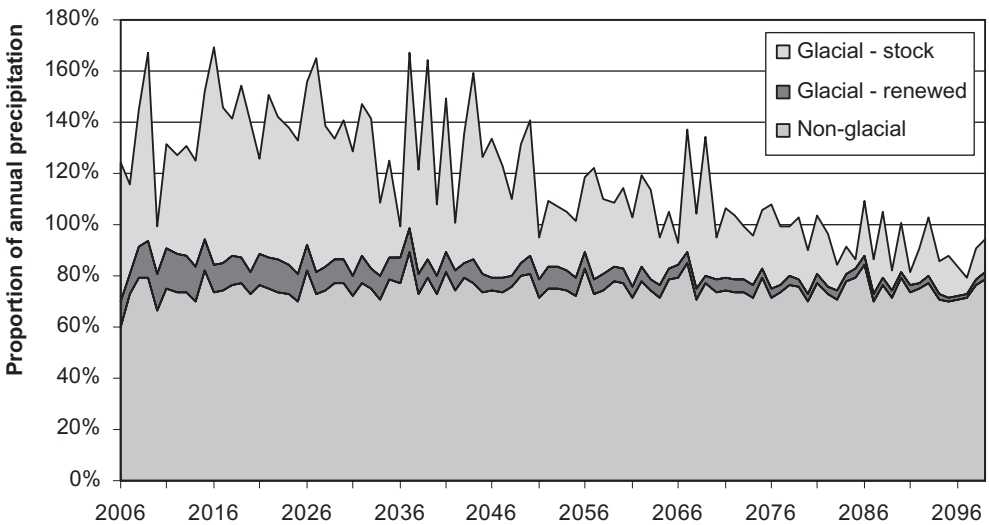


Figure 8. Origin of the inflow into Mauvoisin reservoir (ETHZ scenario).

The evaporation (not represented on the graph as it is not entering the Mauvoisin reservoir) doubles from about 12% in 2010 to 25% in 2095. When neglecting the inter-annual mass differences, the evaporation, the non-glacial and sustainable glacial flow are equal to the precipitation.

As the glacier melt volume will change during the 21st century, the inflow regime will also change, especially in the summer months. Figure 9 shows the hydrological regime for the ETHZ scenario for 4 different periods (average of 5 years). The regime of 2005–2010 is mainly glacial, with a high discharge between June and September. After 35 years, the snow melt will start earlier in spring and the peak discharge of the glacier melt during July will be reduced as the glacier has already lost a significant part of its surface. In 2075–2080 and 2094–2099, the regime is significantly changed, with highly reduced glacier melt, thus decreasing also the annual inflow.

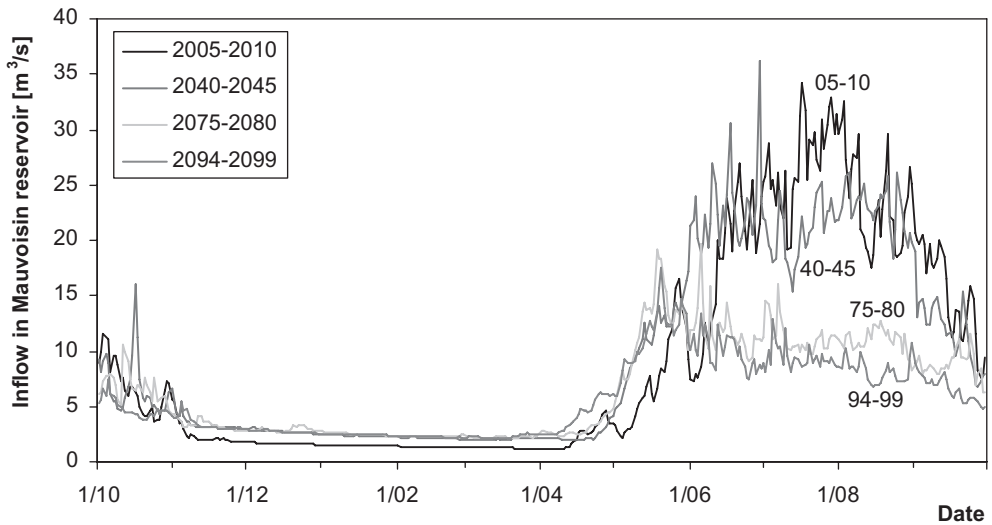


Figure 9. Inflow regime (5-year average) into Mauvoisin reservoir (ETHZ scenario).

4.3 Energy production and economical analysis

The energy production is studied for 3 periods with the ETHZ scenario: 2005–2010 to have a reference situation, 2075–2080 when the Corbassière pump-storage scheme could go into operation and 2094–2099 to have the lowest inflows in the 21st century. Over these 3 periods, different states of the schemes are analyzed: the actual scheme (FMM) alone, with Mauvoisin II project, with Corbassière pump-storage project and a combination of the two projects. The results are shown in Table 1.

During the 21st century, the inflows will probably decrease from 290 hm³/year in 2005–2010 to 216 in 2075–2080 and to 178 in 2094–2099. As a consequence, in 2074 and 2094 the Mauvoisin reservoir cannot be filled anymore according to the actual annual curve. The reservoir can be used to regulate the inter-annual inflow changes. In the model, the minimum operation level at the end of winter was raised from 1840 m a.s.l. in 2005 to 1880 in 2075 and to 1900 in 2099.

Table 2 summarizes the results for the different scenarios. With the Mauvoisin II capacity extension of 550 MW, there is only a small increase in production due to increased plant efficiency. About two third of the production from the Mauvoisin reservoir is generated in winter time. This proportion, given by the production algorithm, could be increased but at the cost of losing high price hours in summer.

The construction cost of Mauvoisin II was estimated to 650 mil. CHF in 1994 which is equivalent of 495 mil. EUR today (with an exchange rate of 1.3 EUR/CHF). For the Corbassière pumped-storage scheme, a preliminary cost analysis resulted in a construction cost of 450 mil. EUR. The annual installment considered is 5.48% of the construction cost (5% loan for 50 years) and the annual operation costs assumed with 2% of the investment.

The annual benefits are estimated with the EEX energy prices. As mentioned before, the income might be higher because of price of the guaranteed power. With these EEX spot market prices only, the Corbassière pumped-storage scheme is economical, but the Mauvoisin II extension not yet. Nevertheless if this guaranteed power can be sold at a 47% higher price than the short-term spot market in 2005, or 63% in 2075 and 76% in 2094, the Mauvoisin II capacity extension would be economical compared to today's scheme. In the case of Corbassière pumped-storage scheme it would be economical already if the energy would be sold on the spot market only.

A more accurate economical value is the cost of the produced energy (Figure 10). The inflow reduction in the 21st century has a clear impact on the production cost: the expenditures

Table 1. Summary of energetical and economical results for the different schemes at 3 periods.

Period		2005-2010		2075-2080				2094-2099				
Mauvoisin II		-	yes	-	yes	-	yes	-	yes	-	yes	
Corbassière P-S		-	-	-	-	yes	yes	-	-	yes	yes	
Power	Run-of-the-river	28	28	28	28	28	28	28	28	28	28	MW
	Storage	363	913	363	913	863	1'413	363	913	863	1'413	MW
Production	Corbassière					1'126	1'091			1'040	1'024	GWh/year
	(winter)					51%	50%			51%	50%	-
	Mauvoisin	1'001	1'021	755	768	762	771	617	624	619	626	GWh/year
	(winter)	65%	57%	71%	70%	70%	71%	68%	67%	68%	68%	-
Pump energy	Corbassière	0	0	0	0	-1'399	-1'352	0	0	-1'372	-1'348	GWh/year
Expenditures	Energy purchase	0	0	0	0	44	42	0	0	44	42	mil. EUR/year
	Annual installment	29	60	29	60	56	88	29	60	56	88	mil. EUR/year
	Operation costs	14	26	14	26	24	36	14	26	24	36	mil. EUR/year
Production costs	Corbassière					72	73			78	78	EUR/MWh
	Mauvoisin	43	84	57	112	57	112	70	138	70	137	EUR/MWh
Income	Energy sale EEX 0%	71	86	58	71	140	152	50	62	128	139	mil. EUR/year
Benefits		27.3	0.2	14.7	-15.3	15.6	-13.7	7.2	-24.3	3.3	-26.7	mil. EUR/year
Income	Guaranteed power	84	127	72	115	224	300	66	109	219	302	mil. EUR/year
EEX multiplication factor		19%	47%	25%	63%	60%	98%	30%	76%	72%	118%	-
Benefits		40.4	40.7	29.2	29.2	99.2	134.5	22.5	22.7	95.1	136.4	mil. EUR/year

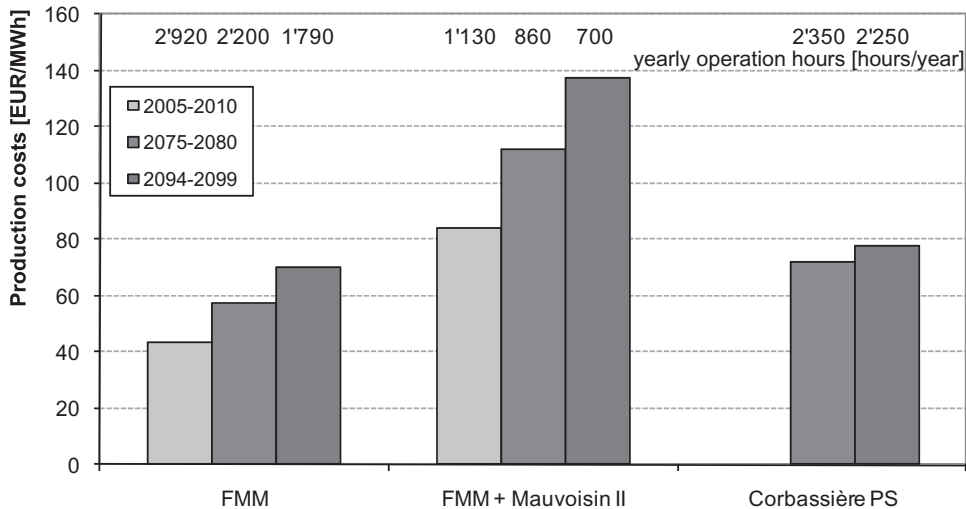


Figure 10. Production costs and yearly operation hours of the different schemes.

are the same, but less energy is produced which leads to an increased cost. Nevertheless at the same time, the yearly operation hours are also reduced. Thus the production could be more concentrated on the peak hours, leading to a higher average sell price. For Corbassière P-S, the production cost of the water in the Mauvoisin reservoir is the same as the FMM scheme alone. The production cost of the lake Corbassière pumped-storage is between 70 and 75 EUR/MWh for 2300 h/year.

5 CONCLUSIONS

At strongly glacierized catchments such as Corbassière, glaciers retreat is producing an increase of runoff for the next few years, resulting in larger inflows to reservoirs in alpine basins. By the end of the 21st century, the inflows will probably return to a balanced situ-

ation (the precipitations minus the evaporation). However, the hydrological regime will be significantly modified as the melt of the remaining glaciers will be very small. With retreating glaciers and this decreasing inflow, new lakes will appear at locations currently covered by glaciers. In addition to potential new hazards of such lakes, they may also represent an opportunity to extend the existing hydropower schemes. In the case of the Corbassière glacier, an economically interesting pumped-storage scheme could be built between the new lake Corbassière and the existing Mauvoisin reservoir. Our study shows that with the significant volume of the lower Mauvoisin reservoir of 204 hm³ and the new upper Corbassière reservoir 51.6 hm³, this pump-storage power scheme could play an important role in the regulation and safety of the European electricity grid.

ACKNOWLEDGEMENTS

The presented study has been funded by the NELAK project of the Swiss National Research Program NRP61.

The delta change scenario data were distributed by the Center for Climate Systems Modeling (C2SM). The data were derived from regional climate simulations of the EU FP6 Integrated Project ENSEMBLES (Contract number 505539) whose support is gratefully acknowledged. The dataset has been prepared by Thomas Bosshard at ETH Zurich, partly funded by swisselectric/Swiss Federal Office of Energy (BFE) and CCHydro/Swiss Federal Office for the Environment (BAFU).

REFERENCES

- Clague, J.J. & Evans, S.G. 2000. A review of catastrophic drainage of moraine-dammed lakes in British Columbia. *Quaternary Science Reviews* 19(17–18): 1763–1783.
- Bosshard, T. et al. Spectral representation of the annual cycle in the climate change signal, in preparation.
- Garcia, J., Jordan, F., Dubois, J. & Boillat, J.-L. 2007. Routing System II, Modélisation d'écoulements dans des systèmes hydrauliques. In A. Schleiss (ed.), *Communication LCH n° 32*. Lausanne: EPFL.
- Haerberli, W. & Hoelzle, M. 1995. Application of inventory data for estimating characteristics of and regional climate-change effects on mountain glaciers: a pilot study with the European Alps. *Annals of Glaciology* 21: 206–212.
- Haerberli, W., Kääh, A., Vonder Mühl, D. & Teyssiere, P. 2001. Prevention of outburst floods from periglacial lakes at Grubengletscher, Valais, Swiss Alps. *Journal of Glaciology* 47(156): 111–122.
- Haerberli, W., Clague, J.J., Huggel, C. & Kääh, A. 2010. Hazards from lakes in high-mountain glacier and permafrost regions: Climate change effects and process interactions. In X. Úbeda, D. Vericat, R.J. Batalla (eds), *Avances de la Geomorfología en España 2008–2010—XI Reunión Nacional de Geomorfología; Proc., Solsona, 20–24 september 2010*. Salsona:CTFC.
- Huggel, C., Haerberli, W., Kaab, A., Bieri, D. & Richardson, S. 2004. An assessment procedure for glacial hazards in the Swiss Alps. *Canadian Geotechnical Journal* 41(6): 1068–1083.
- Jordan, F. 2007. Modèle de prévision et de gestion des crues - optimisation des opérations des aménagements hydroélectriques à accumulation pour la réduction des débits de crue, In A. Schleiss (ed.), *Communication LCH n° 29*. Lausanne: EPFL.
- Jordan, F., Heller, P. 2010. Swissrivers.ch—a tool for predicting the mini-hydropower production of Switzerland. In *Hidroenergia – Small streams make rivers; Proc. CD, Lausanne, 16–19 June 2010*.
- Keller, R. 2009. Le débit des rivières au peigne fin. *Revue Technique Suisse* 2009(7/8): 11.
- Lemke, P., Ren, J., Alley, R., Allison, I., Carrasco, J., Flato, G., Fujii, Y., Kaser, G., Mote, P., Thomas, R. & Zhang, T. 2007. Observations: Changes in Snow, Ice and Frozen Ground. In S. Solomon, D. Qin, M. Manning, Z. Chen, M. Marquis, K.B. Averyt, M. Tignor and H.L. Miller (eds), *Climate Change 2007: The Physical Science Basis. Contribution of Working Group I to the Fourth Assessment Report of the Intergovernmental Panel on Climate Change*: 337–383. Cambridge: Cambridge University Press.
- Linsbauer, A., Paul, F., Hoelzle, M., Frey, H. & Haerberli, W. 2009. The Swiss Alps Without Glaciers - A GIS-based Modeling Approach for Reconstruction of Glacier Beds. In *Proceedings of Geomorphometry, Zurich, 31 August-2 September 2009*.

- Paul, F., Maisch, M., Rothenbühler, C., Hoelzle, M. & Haerberli, W. 2007. Calculation and visualisation of future glacier extent in the Swiss Alps by means of hypsographic modeling. *Global and Planetary Change* 55(4): 343–357.
- Schaepli, B., Hingray, B., Niggly, M. & Musy, A. 2005. A conceptual glacio-hydrological model for high mountainous catchments. *Hydrology and earth system sciences* 9: 95–109.
- UNEP 2007. *Global outlook for ice & snow*. Arendal:UNEP/GRID.
- Zemp, M., Haerberli, W., Bajracharya, S., Chinn, T.J., Fountain, A.G., Hagen, J.O., Huggel, C., Käab, A., Kaltenborn, B.P., Karki, M. & others. 2007. Glaciers and ice caps. Part I: Global overview and outlook. Part II: Glacier changes around the world. In UNEP (ed.), *Global outlook for ice & snow*: 115–152. Arendal:UNEP/GRID.
- Zemp, M., Roer, I., Käab, A., Hoelzle, M. Paul, F. & Haerberli, W. 2008. *Global glacier changes: facts and figures*. Zurich:UNEP / WGMS.

Future challenges for dams under climate change

D.-K. Koh & J.-H. Park

Water Resources Research Center, K-water Institute, Daejeon, Republic of Korea

ABSTRACT: Water issues due to climate change require new strategies for water resources development and management. The purpose of this study is to suggest a methodology to evaluate hydrological change at the dam watershed due to climate change in the future so that the adaptive measures could be developed. In this study, weather series data including air temperature and precipitation projected to the future until the year 2100 were used, that are disseminated officially by the Korea Meteorology Agency. The data were generated by MM5 Regional Circulation Model (RCM) based on A1B Scenario using the results of ECHO-G model as the boundary condition. For the daily runoff prediction from the dam watershed for the study period from 2000 to 2100, a semi-distributed runoff model, SWAT (Soil and Water Assessment Tool) was selected. The SWAT model which is based on GIS can simulate temporal and spatial distributions of surface and subsurface flows. The weather series was fed into the SWAT to simulate the streamflows associated with other hydrologic components such as subsurface flow, soil moisture contents, and etc. This approach is applied to the Yongdam Dam and Daechung Dam in Geum River Basin, Korea. The results show that annual mean inflow to the dam reservoirs will be decreased by 7.6% compared to the recent 10 years observations. Regarding the seasonal variation, dam reservoir inflows during winter and autumn are going to be increased, while in summer less inflow was predicted. It is necessary to conceive a strategy for the dam development and management adapted with the climate change.

1 INTRODUCTION

The water-related disasters such as drought and flood have occurred more frequently than ever before all over the world. A report from the IPCC stated that the climate change in the water sector are already observed, and predicted that the impact of climate change would significantly increase.

Because of recent climatic change by global warming, the management of water resources in Korea is gradually becoming more difficult. Global mean temperature has increased by about 0.74 degree since the late 19th century. Increase of temperature during recent 50 years is almost twice as past 100 years. Particularly, change of mean temperature in Korea is higher 2 times than the change of the global mean temperature. According to report of KMA (Korea Meteorology Agency) Institute, it is anticipated to further increase by 5 degree in temperature and 17% in precipitation over the next 100 years in Korea.

In respect of flood about impacts of climate change in water resources of Korea, the localized rainfall frequency over 100 mm/day is anticipated to increase 2.7 times. And extreme event over 1000 mm/day and super typhoon over 70 m/sec may frequently cause because of rise of surface temperature of the sea. The existed daily maximum rainfall was 870 mm in 2002 by typhoon RUSA. According to research in Japan using earth simulator, two huge typhoons simultaneously may cause in Korea peninsula and Japan. Particularly, flood protection capacity of the existed banks designed with 100 years may decrease in half. In respect of drought, the number of drought occurrence may increase 3.4 times. At present, seasonal rain front moves up and down in normal condition. But, it simulates the rain front stays in

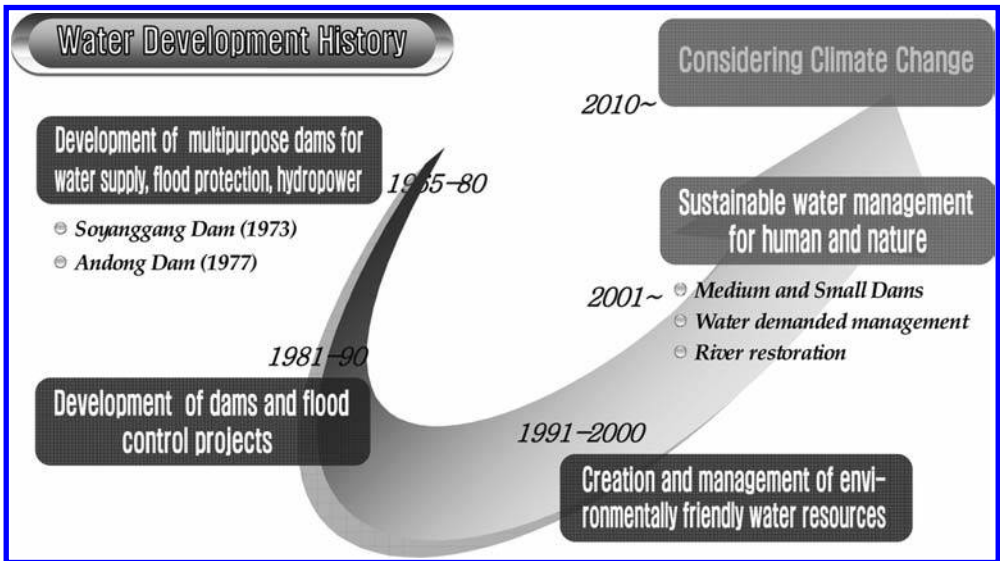


Figure 1. The history of water development in K-water.

southern sea of Korea. So, drought is getting worse in the East-Northern countries. Also, stream discharge may decrease 5.7% during drought season because although the yearly rainfall will increase due to temperature increase.

In other words, since its establishment in 1967, K-water has been implementing national water resources management policies regarding multi purpose dams, water supply dams and regional water supply systems. It is also making a great contribution toward the development of the national economy and improving the quality of life for local people. Currently K-water has launched the new strategy considering climate change in our water resources systems and policies. It is required to prepare more definite action plan in the field of vulnerability assessment, adaptation policy, and improvement of laws.

In this paper, we are trying to propose future plan through quantitative evaluation of variability for dam watersheds under climate change. ECHO-G model was provided from KMA as an optimized GCM model on the Korean peninsula. And MM5 model based on A1B scenario with 27 kilometers of space resolution that exploits dynamic downscaling technique was used for producing future rainfall data on a regional scale. And the weather series fed into a semi-distributed hydrological model called SWAT to simulate the streamflows associated with other water resources. This approach is applied to the Yongdam Dam and Daechung Dam Basin in southern part of Korea.

2 STUDY AREA

The Geum River is located in the middle part of the Korean peninsular. The river is 401 km long, making it the third longest in South Korea. The basin area is 9805 km² equivalents to 10% of this country. There are several big cities in the river basin including Daejeon, Cheongju and Jeonju. The Daechung Dam is located at 150 km upstream from the estuary of the Geum River which flows into the Yellow Sea.

Principal facilities of the dam include a main dam and reservoir, a re-regulation dam, three saddle dams, a hydropower plant, and two water supply systems to the Daejeon and Cheongju areas. Yongdam Dam is located at Jinan-Gun, Cheonbuk Province, which is known as an uncontaminated area. Yongdam Dam diverts the water of the Geum River, where relatively abundant water flows, into the Mankyung River Basin Area, which lacks municipal and industrial water. There are Jeonju City, Nonsan City and Gunsan City, etc. in

the Mankyung River Basin. Total capacity of the reservoir is 815 million m³, and part of this reservoir's water flows through a diversion tunnel whose length and diameter are 21.9 km and 3.2 m, respectively. This dam is to supply about 500 million m³ of water per year solving the water deficit problem until 2023. A hydropower plant is constructed at the outlet side of the diversion tunnel to utilize the high head difference.

3 STATISTICAL ANALYSIS OF HYDROLOGIC TIME SERIES DATA

It has been attempted to quantitatively assess the influences of climate changes by means of statistical analyses such as basic statistics, analyses of limiting values, tendency analysis based on Mann-Kendall test, correlations among the elements, and variance of the moving average by 10 year-period, which have been available through time series data of the weather & hydrology for Geum River for the last thirty years. Climate and hydrologic data for analyzing time series trend was provided by KMA (Korea Meteorology Agency) and K-water. According to Fig. 2, temperature and rainfall is increasing during last 30 years for Geum River. Annual average temperature is increasing 0.6°C during last 30 years, especially winter temperature is increasing 1.1°C. And annual rainfall is increasing 152.9 mm compared with 30 years ago. This means that variation of temperature and rainfall by climate change will be directly affect water resources field. According to the report of KMA institute, it is anticipated to further increase by 5 degree in temperature and 17% in precipitation over the next 100 years in Korea. According to the outlook of climate change in water resources of Korea, localized rainfall frequency over 100 mm/day is anticipated to increase 2.7 times. And extreme event over 1000 mm/day and super typhoon over 70 m/sec may frequently cause because of rise of surface temperature of the sea.

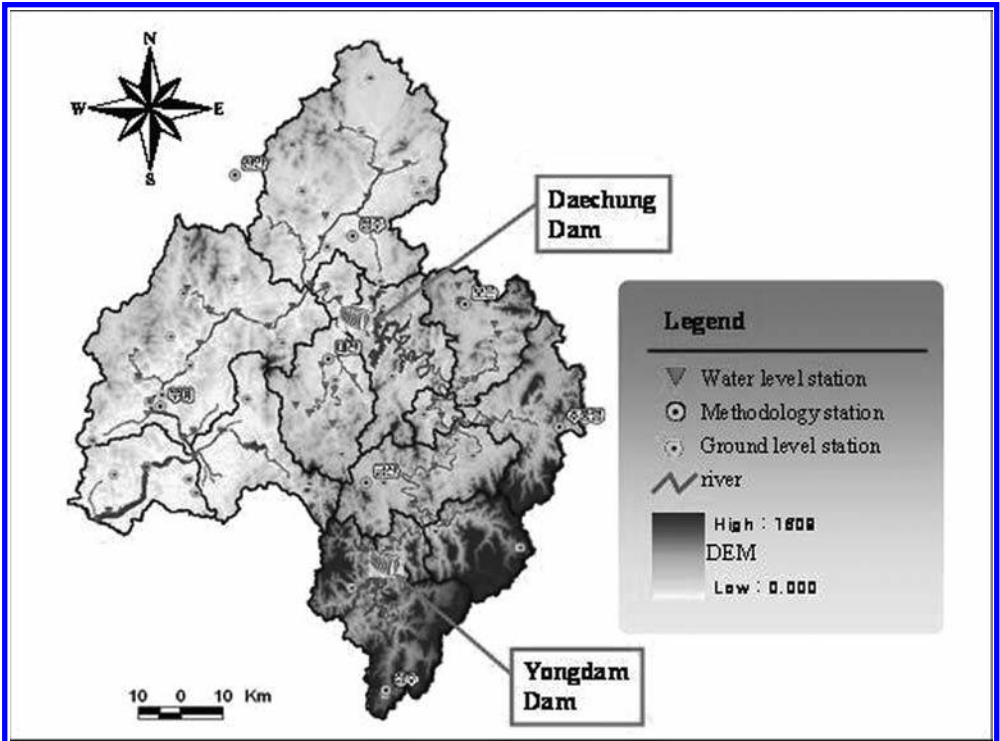


Figure 2. Location of Daechung Dam (up) and Yongdam Dam (down).

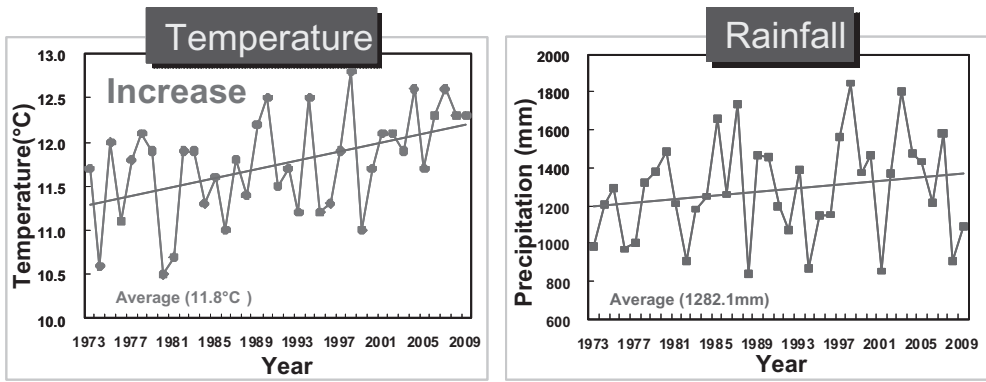


Figure 3. Analysis results for time series trend of temperature and rainfall.

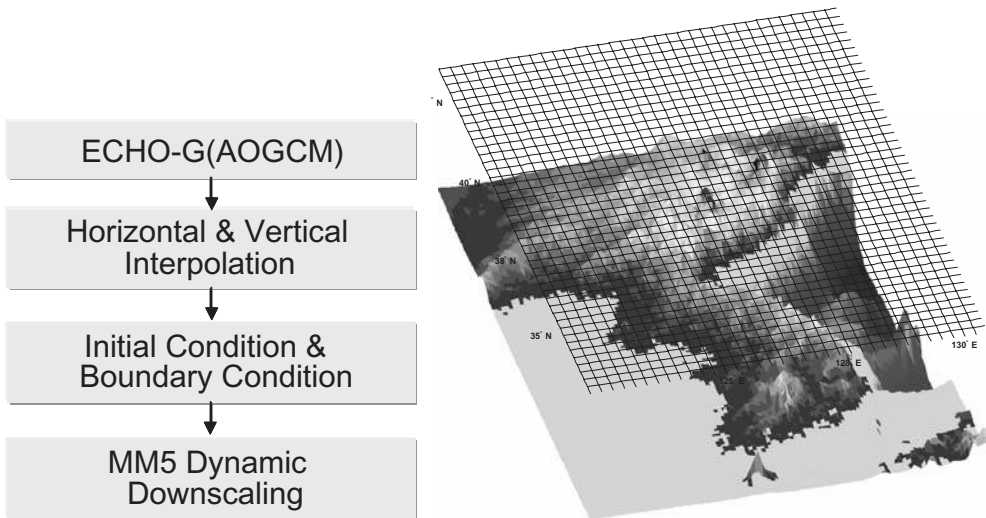


Figure 4. Downscaling process based on A1B scenario.

4 DOWNSCALING OF CLIMATE DATA

ECHO-G model has the resolution of 400 km as an optimized GCM model on the Korean peninsula. And MM5 model based on A1B scenario with 27 kilometers of space resolution that exploits dynamic downscaling technique was used for producing future rainfall data of regional scale.

Seen from an aspect that GCM and RCM are not likely to be directly utilized because of the differences in their respective scale in terms of temporal and spatial factors, the RCM grid data have been downscaled spatially from basins to spots for rainfall-observatories, and problems related with the scale of time & space, as they are stemming from the downscaling of RCM data from on a monthly basis to a daily basis, have been resolved in this research. Thus, the seasonal precipitation scenarios related with climate changes have been temporally downscaled to daily precipitation series, and the RCM climate-changes scenario by grid have been spatially downscaled to accord the standards set up by precipitation observatories. The A1B scenario has been exploited as basic input data for multi-spots irregular downscaling

• Runoff Simulation by climate change (SWAT model)

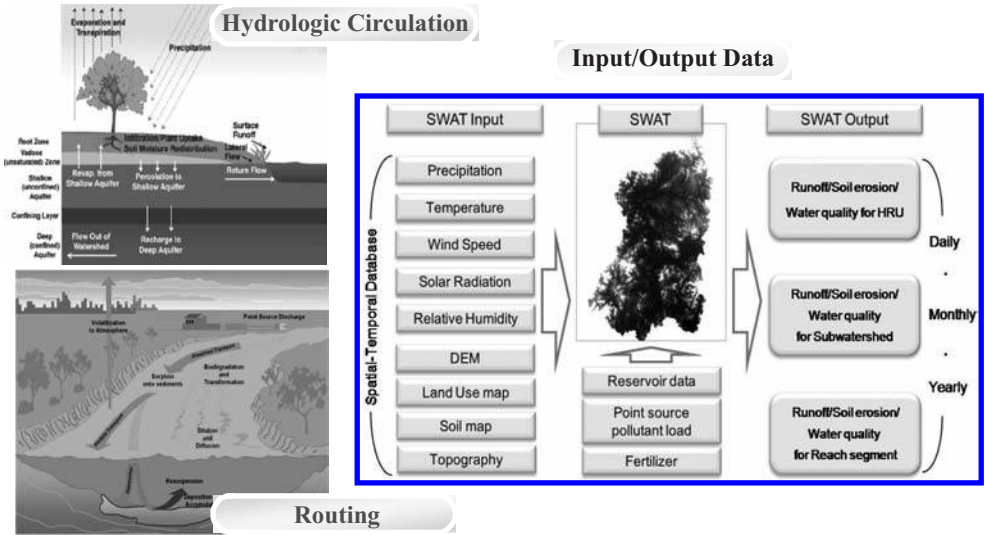


Figure 5. Structure of SWAT model.

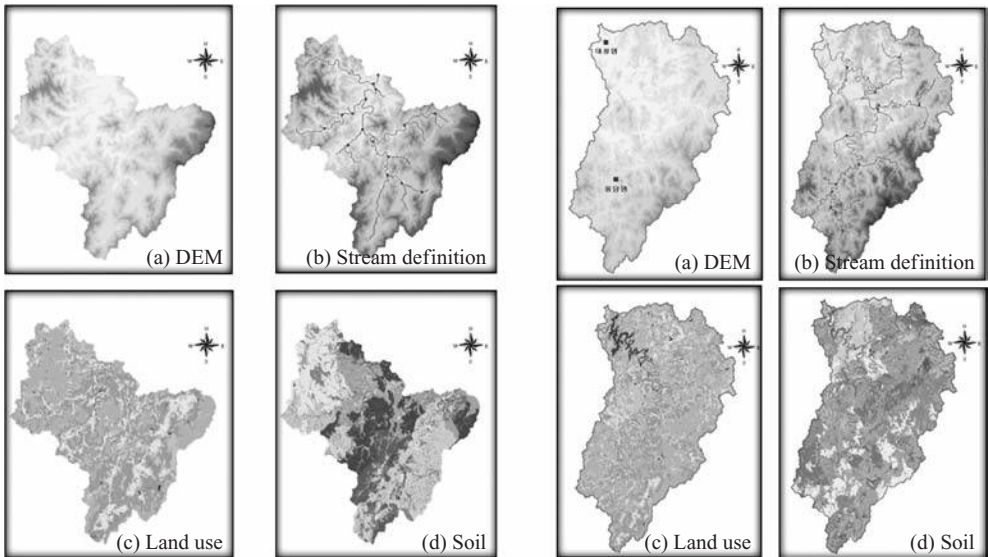


Figure 6. GIS data of Daechung Dam(left) and Yongdam Dam(right).

methods, and the time series of daily precipitation reflecting influences of climate changes have been analyzed by major spot along the Geum River.

Also, variability in the precipitation events with regard to the future climate changes have been examined by diverse methodologies in consideration of irregularity overlooked by the existing daily precipitation simulation skills and by multi-spots irregular downscaling technique in order to produce detailed hydrology scenarios by river basin. Analysis periods including the reference period from 1970 to 2000 were as follows; 2015s (2001~2030), 2045s (2031~2060), and 2075s (2061~2090).

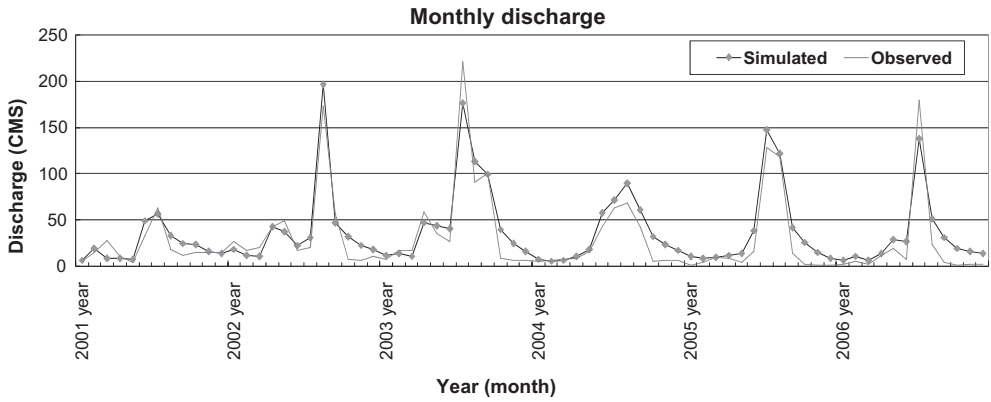


Figure 7. Hydrograph of comparison between simulated and observed values (Yongdam dam).

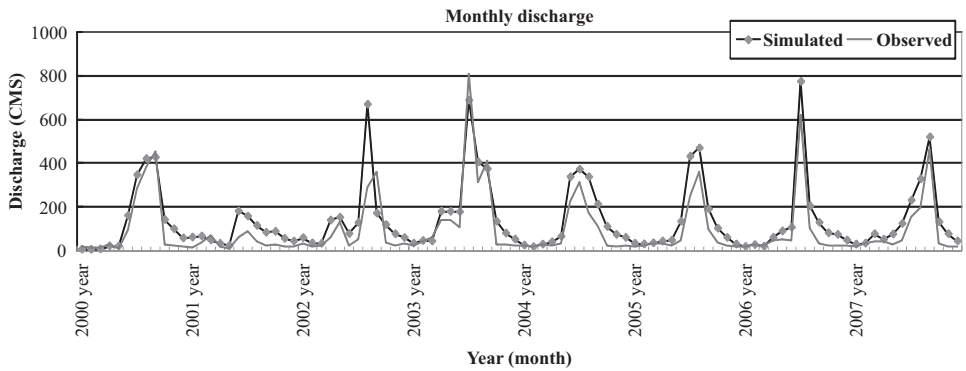


Figure 8. Hydrograph of comparison between simulated and observed values (Daechung dam).

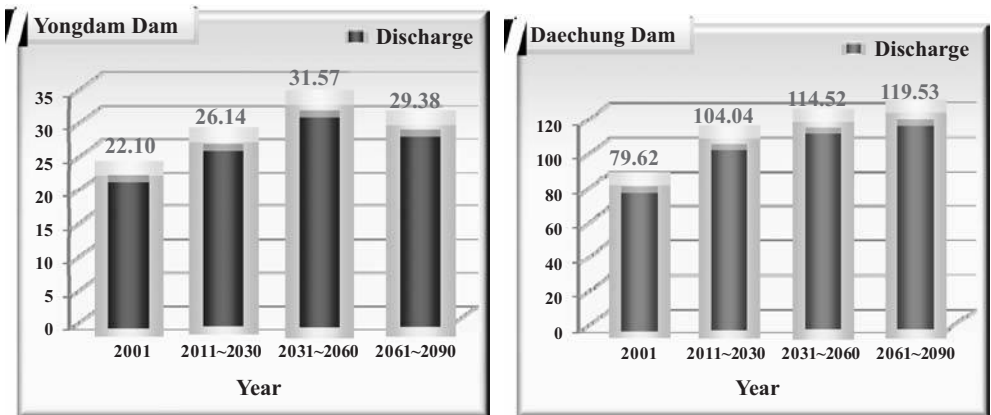


Figure 9. Simulation results of discharge for next 90 years.

5 OUTLOOK OF FUTURE DISCHARGE

As the tool of daily runoff simulation, a semi-distributed runoff model, SWAT (Soil and Water Assessment Tool) has been selected out of six models reviewed in full consideration of existing model awareness, research outputs, and suitability for researches.

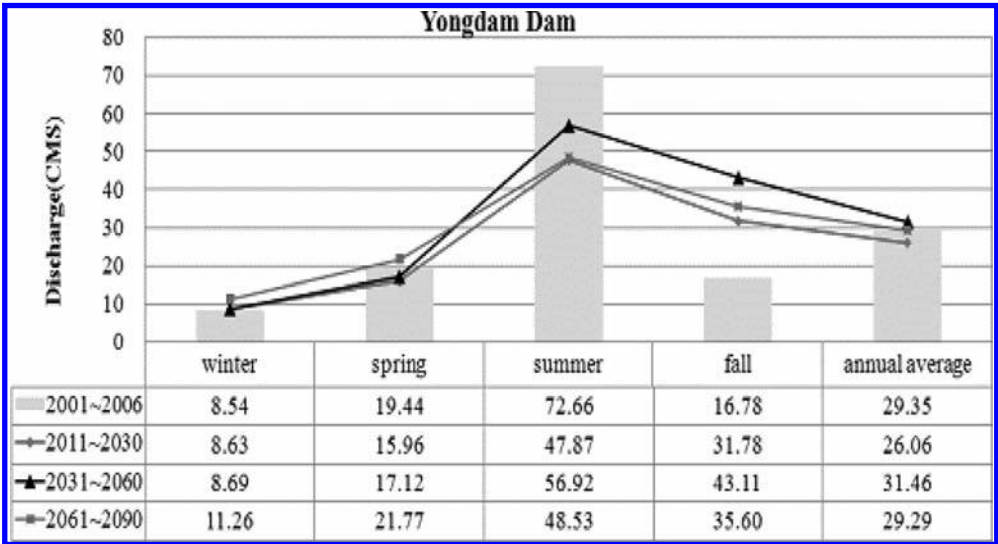


Figure 10. Outlook of the future discharge per season (Yongdam Dam).

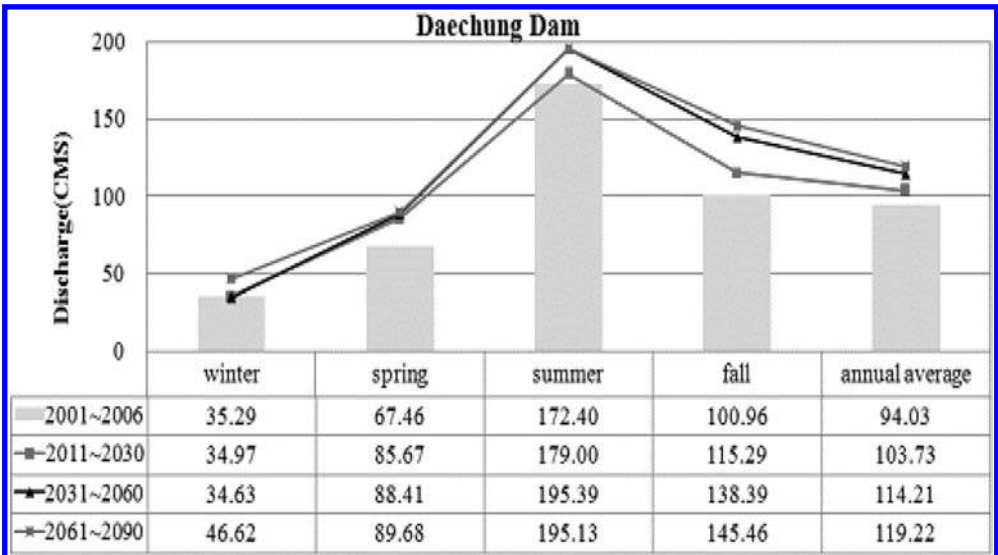


Figure 11. Outlook of the future discharge per season (Daechung Dam).

SWAT is a river basin or watershed, scale model developed by Dr. Jeff Arnold for the USDA Agricultural Research Service (ARS). SWAT was developed to predict the impact of land management practices on water, sediment and agricultural chemical yields in large complex watersheds with varying soils, land use and management conditions over long periods of time.

The SWAT model which is based on GIS can simulate temporal and spatial distribution of surface flow and sub-surface flow per small basins, and input parameters such as DEM, land use and soil as pre process can be extracted.

Using the SWAT model from 2001 to 2006, the comparison of the discharge at a spot of Yongdam Dam in the Yongdam basin and a final outflowing spot has showed 90.1% coinciding with each other, and the other results from a comparative analysis of a discharge

at Cheonchun water-level observatory as opposed to that gained from a simulation by the SWAT model have also indicated 91.3% of coincidence of values. Therefore, the outputs as to discharge analysis for Yongdam dam and Daechong dam at the Geum River have validated that SWAT model has a high applicability.

The 80 years of period ranging from 2011 to 2090 has been set up to facilitate the analyses of climate changes. The outcome of the analyses has predicted that the amount of run-off will increase by 18% between 2011 and 2020. The results show that about 7.6% of annual mean streamflow is reduced when it is compared with the observed one under A1B scenario. And while Seasonal streamflows in the winter and autumn are increased, a streamflow in the summer is decreased. However, the seasonality of the simulated series is similar to the observed pattern.

Through the result of this research, it can be reviewed the change of dam management pattern from seasonal water system to use water for drought season to annual water storage system to distribute water by necessity in the future.

6 CONCLUSIONS

In this paper, we are trying to propose future plan through quantitative evaluation of variability for dam watersheds under climate change.

ECHO-G model was provided from KMA as an optimized GCM model on the Korean peninsula. And MM5 model based on A1B scenario with 27 kilometers of space resolution that exploits dynamic downscaling technique was used for producing future rainfall data on a regional scale. The SWAT model which is based on GIS can simulate temporal and spatial distribution of surface flow and sub-surface flow per small basins, and input parameters such as DEM, land use and soil as pre process can be extracted. The weather series fed into a semi-distributed hydrological model called SWAT to simulate the streamflows associated with other water resources. This approach is applied to the Yongdam Dam and Daechung Dam Basin in southern part of Korea. The results show that annual mean flow is reduced by about 7.6% compared to the observed one observed under A1B scenario. While Seasonal streamflows during winter and autumn increased, simulated summer streamflow was found to be less compared to observed values. The seasonality of the simulated series is similar to the observed pattern.

Additionally, a master-plan and strategies for the dam watershed management considering climate change were proposed.

REFERENCES

- K-water Institute, A study for the generation of corresponding plan on climate change for future water resources management, 2010.
- Korean national committee on large dams, <http://www.kncold.or.kr/>
- S.L. Neitsch, J.G. Arnold, J.R. Kiniry, & J.R. Williams, 2001. Soil and water assessment tool theoretical documentation.

Study on rational control model for excess flood by utilizing rainfall prediction

A. Yamamoto, S. Mitsuishi & T. Ozeki

River Department, National Institute for Land and Infrastructure Management (NILIM), Ministry of Land, Infrastructure, Transport and Tourism (MLIT), Tsukuba, Ibaraki, Japan

T. Sumi

Water Resources Research Center, Disaster Prevention Research Institute, Kyoto University, Uji, Kyoto, Japan

ABSTRACT: The construction of new flood control facilities has been slow due to various constraints despite a steady increase of the phenomenon of extreme precipitation associated with climate change. With this status, the more efficient and effective operation of existing dams are essential. This study examined the applicability of a rational method for flood control, including excess flood, while utilizing rainfall prediction by the weather research and forecasting model (WRF), the accuracy of which has significantly improved in recent years. The study also examined a range of ideas for more effective flood control operation, including the handling of errors of rainfall prediction by the WRF model, risk management with due consideration of flood control and water use and the effect of the remodelling of spillways.

1 INTRODUCTION

The Intergovernmental Panel on Climate Change (IPCC) (IPCC, 2007) points out the strong likelihood of the continual occurrence of heavy precipitation events as an outcome of climate change. It is now imperative for the world to come up with suitable measures to deal with such likelihood. In Japan, the number of dams newly constructed by the Ministry of Land, Infrastructure, Transport and Tourism has been declining since the peak year of 1993 while the number of dams managed by the Ministry has increased to 532. Under these circumstances, it is requested that the functions of existing dams should be further strengthened.

In this study, rainfall prediction was conducted using the WRF model which has significantly improved recently in terms of accuracy to the extent that the model now offers highly reliable rainfall prediction for up to 48 hours (Toyoda, 2009). This exercise was followed by the simple calculation of the lost amount of rainfall in a basin to establish the total volume of inflow to a dam for the purpose of examining an efficient flood control method utilizing the dam capacity to the maximum. The applicability of this method was then examined with actual flood events, including those of excess floods. The purpose of this exercise was to establish integral operation utilizing the capacity for water use and the flood control capacity of a dam for efficient flood control through preliminary discharge operation in tandem with operation to supply water for productive use and utilization of the total dam capacity. The ultimate aim was to minimize flood damage downstream.

2 FLOOD CONTROL METHOD UTILIZING RAINFALL PREDICTION BY WRF METHOD

In the study, the volume of inflow to a dam was predicted based on rainfall prediction by the WRF model and the reduction of the maximum discharge rate below the discharge rate

stipulated in the dam operation rules for the purpose of establishing a more effective flood control method. This simulation was conducted for 12 existing dams in Japan.

Figure 1 is a flow diagram of the flood control method examined by the study. In consideration of the duration of design rainfall, the rainfall for the next 48 hours was predicted using the WRF model.

This method using rainfall prediction data can be expected not only to improve the positive effects of flood control but also carry risks because of errors in prediction. To determine the impacts of rainfall prediction errors on such risks for dam management as an insufficient flood control capacity and unfulfilled water use capacity, an error range where the actual rainfall level is either above or below the predicted level was set in addition to the rainfall prediction value by the WRF model. Given the fact that the rainfall prediction errors of the WRF model were not clearly established, in this study the error rates for 48 hour accumulative rainfall were based on the study by the Japan Meteorological Agency (Wada, 2006). The predicted rainfall range was estimated by multiplying the predicted rainfall calculated by the WRF model, by the error rate defined as the ratio between the predicted rainfall and the actual one where the maximum and the minimum values are 1.43 and 0.714 respectively. In this study, it was presumed that the actual rainfall level fell within this predicted rainfall range as the first step to analyze the impacts of ranged rainfall prediction on flood control operation. The rainfall prediction value was renewed every six hours in accordance with the acquisition of initial condition data for calculation by the WRF model. Flood control simulation was conducted to determine the hourly dam operation shown in Figure 1 according to the level of inflow every hour.

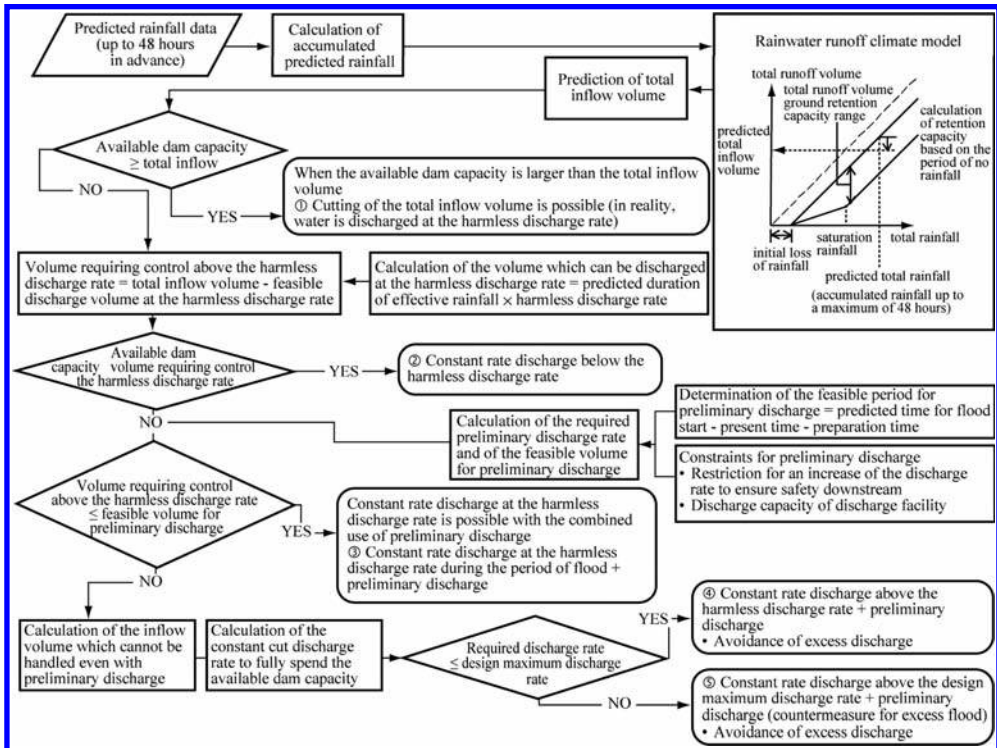


Figure 1. Flow diagram of the proposed flood control method.

3 RESULTS OF SIMULATED DAM OPERATION UTILISING RAINFALL PREDICTION BY THE WRF MODEL

Using the method described in chapter 2, flood control simulation was conducted for 69 actual floods experienced by 12 dams. Table 1 shows the number of discharge operations to reach the harmless discharge rate, number of preliminary discharge operations implemented, number of discharge operations at the maximum design discharge rate and other data which were necessary for these simulations. The simulated flood control effects vary depending on

Table 1. Summary of simulation results.

Name of dam	Number of cases examined	Value used to judge suitable operation	Number of cases						
			The discharge operation at a constant rate upto the harmless discharge rate was conducted*	Preliminary discharge took place	The discharge operation above the harmless discharge rate took place	The discharge rate exceeded the design maximum discharge rate	The dam capacity was completely used up	delayed operation took place	The water use capacity was not fully restored ****
Hoheikyo	12	maximum prediction	11	0	1	1	1	0	9 (0)
		minimum prediction	11	0	1	1	1	0	9 (0)
		Actual operation	9	0	3	1	0	0	9 (0)
		maximum prediction	6	4	1	0	0	1**	4 (2)
Shijyushida	7	minimum prediction	6	2	1	0	0	0	4 (0)
		Actual operation	7	0	0	0	0	0	4 (0)
		maximum prediction	4	0	3	0	0	0	1
		Actual operation	6	0	0	0	0	0	5 (0)
Kawamata	6	minimum prediction	6	0	0	0	0	0	5 (0)
		Actual operation	6	0	0	0	0	0	5 (0)
		maximum prediction	5	0	1	1	0	0	3
		Actual operation	13	10	1	0	0	0	13 (9)
Yahagi	14	minimum prediction	13	1	1	0	1	0	12 (1)
		Actual operation	14	0	0	0	1	0	12 (0)
		maximum prediction	8	0	6	1	0	0	8
		Actual operation	4	0	0	0	0	0	1 (0)
Nukui	4	minimum prediction	4	0	0	0	0	0	1 (0)
		Actual operation	3	0	1	0	0	0	1 (0)
		maximum prediction	9	1	1	0	1	8***	4 (0)
		Actual operation	9	0	1	0	1	7	4 (0)
Sameura	10	minimum prediction	9	0	1	0	1	7	4 (0)
		Actual operation	5	0	5	0	0	0	4
		maximum prediction	3	11	8	1	1	1	1 (1)
		Actual operation	7	9	4	1	2	1	1 (1)
Tsuruda	11	minimum prediction	5	3	6	1	5	0	1 (0)
		Actual operation	0	0	11	1	0	0	1
		maximum prediction	0	1	1	1	1	0	0
		Actual operation	0	0	1	1	1	0	0
Nibutani	1	minimum prediction	0	0	1	1	1	0	0
		Actual operation	0	0	1	1	1	0	0
		maximum prediction	0	1	1	0	0	1	0
		Actual operation	0	0	1	0	1	1	0
Kanogawa	1	minimum prediction	0	0	1	0	1	1	0
		Actual operation	0	0	1	0	1	0	0
		maximum prediction	1	1	0	0	0	0	1 (1)
		Actual operation	1	1	0	0	0	0	0
Nomura	1	minimum prediction	0	0	1	0	0	0	0
		Actual operation	0	0	1	0	0	0	0
		maximum prediction	0	1	1	1	0	1	0
		Actual operation	0	0	1	1	0	1	0
Dokawa	1	minimum prediction	0	0	1	1	1	1	0
		Actual operation	0	0	1	1	1	1	0
		maximum prediction	0	0	1	1	1	0	0
		Actual operation	0	0	1	1	1	0	0
Hohri	1	minimum prediction	0	0	1	1	1	0	0
		Actual operation	0	0	1	1	1	0	0
		maximum prediction	0	0	1	1	1	0	0
		Actual operation	0	0	1	1	1	0	0
Total	69	maximum prediction	53	30	16	5	5	12	38 (13)
		minimum prediction	57	13	12	5	8	10	36 (2)
		Actual operation	56	3	13	5	12	9	36
		Actual operation	34	0	35	7	3	1	26

* The number of cases with a constant discharge rate of up to the harmless discharge rate includes those cases where the flood inflow rate failed to reach the harmless discharge rate (not depending on the set prediction error range). The actual number of such cases was 2 for Shijyushi Dam, 2 for Kawamata dam, 1 for Yahagi Dam and 2 for Nukui Dam.

** Delayed operation was due to lowering of the water level, in turn caused by preliminary discharge.

*** Because of the absence of a conduit gate, Sameura Dam experiences operational delay when the water level is below the control level (crest gate bed height). Although the August, 2004 flood exceeded the crest gate bed height, the discharge capacity was not raised due to the deep water depth.

**** The number of cases where flood control operation ended with the reservoir level remaining below the control level (of these, the number of cases where preliminary discharge was conducted).

Table 2. Comparison between simulated operation based on the WRF model and actual operation performed.

Name of dam	Flood	Maximum inflow rate (m ³ /s)	Maximum discharge rate (m ³ /s)		Reduction (m ³ /s)
			Actual	WRF model	
Yahagi	Sep. 2000	2993	2378	974	1404
Nibutani	Aug. 2003	5959	5489	5000	489
Dokawa	Aug. 2004	1005	827	712	115

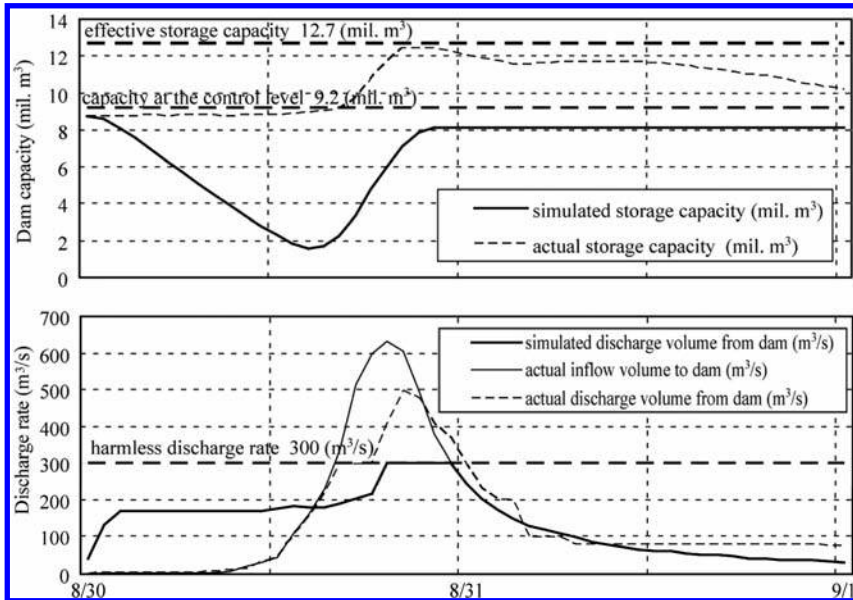


Figure 2. Case of maximum value (1.43 times higher than the WRF predicted value) for the August, 2004 flood involving Nomura dam.

the use of the predicted rainfall value by the WRF model, maximum value or minimum value. Analysis of the simulation results has clarified the following points.

1. In the case of an excess flood, the damage can be minimized by means of deciding appropriate preliminary discharge operation and maximum discharge rate based on rainfall prediction. On the three excess floods flooded downstream of dams, the respective predicted rainfall values by the WRF model in Table 2 suggest the maximum discharge rate is significantly reduced and a substantial alleviation of the flood damage.
2. The general trend is that preliminary discharge operation or discharge more than the harmless discharge rate was often conducted in those cases where the maximum value was used. Regarding many of those cases where the minimum value was used, the entire dam capacity is completely spent.
3. Of the 69 floods involving 12 dams used for simulation, only harmless discharge rate operation as a result of preliminary discharge, etc. was required for 50 plus smaller floods regardless of either the maximum value or minimum value being used. In reality, discharge operation at or below the harmless discharge rate was conducted with only 34 floods.
4. In the case of using the maximum value in August, 2004 flood at Nomura Dam, the excessive level of predicted rainfall necessitated massive preliminary discharge operation, resulting in failure to fulfill the full capacity for water use in the aftermath of the flood as

shown in Figure 2. When the predicted value by the WRF model or the minimum value was used for the same flood, no such negative effect from the viewpoint of water use occurred.

4 IMPROVEMENT OF THE METHOD FOR ITS PRACTICAL APPLICATION TO DAM MANAGEMENT

The simulations described in chapter 3 established that errors in rainfall prediction can result in the prediction of a much higher or lower volume of inflow to a dam reservoir than the actual volume and affect the performance of such dam functions for flood control and water use as preliminary discharge and fulfillment of the unfulfilled water use capacity. For practical dam management, it is essential to accurately understand possible errors in rainfall prediction by the WRF model and to formulate appropriate responses, considering the risks posed by prediction errors (response to deal with excess flood which may result from an actual rainfall level exceeding the predicted level or a need to fulfill the unfulfilled water use capacity as a result of a lower than predicted actual rainfall level). To be more precise, the following improvement and clarification are required.

4.1 Improvement of the operation method

When a prediction range is set for actual dam operation in consideration of rainfall prediction errors, there can be cases where such contradictory operation as preliminary discharge operation and harmless discharge rate operation are judged to be necessary according to the flow diagram shown in Figure 1. To be more precise, there are four different cases as shown in Figure 3 when the normal dam operation rules are followed. In Figure 3, the inferred reservoir

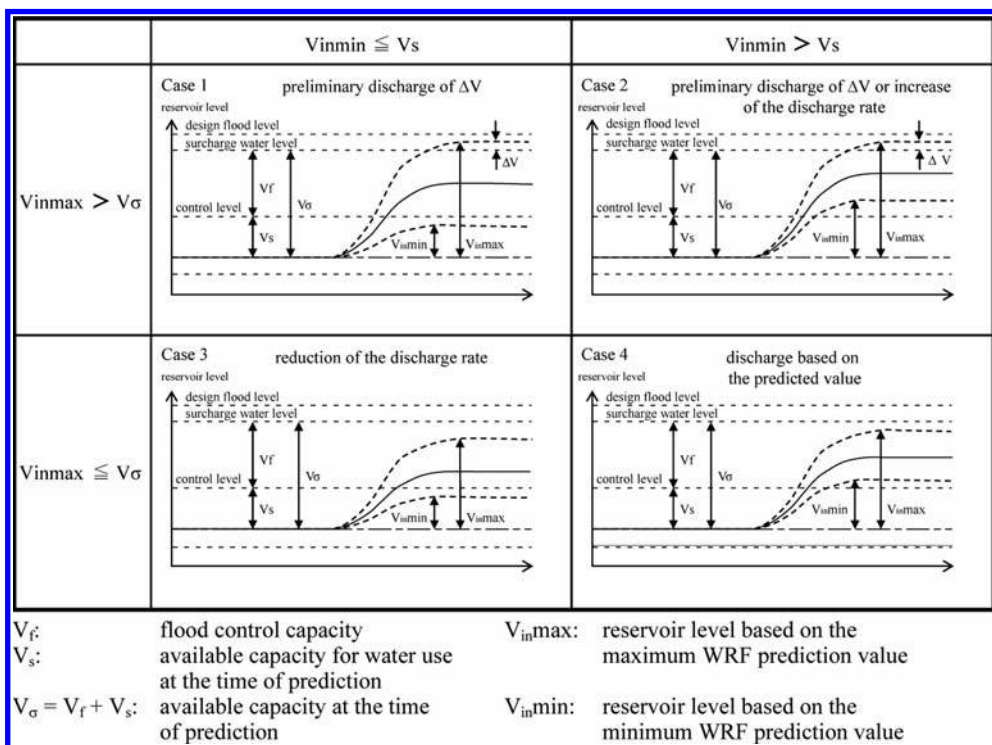


Figure 3. Classification of reservoir water level and discharge operation based on rainfall prediction errors.

water level is shown for each of the predicted, maximum and minimum rainfall levels when normal dam operation stipulated by the dam operation rules is conducted. In Case 1, rainfall at the maximum value causes an insufficient flood control capacity while rainfall at the minimum value causes non-fulfillment of the water use capacity. In this scenario, the flood control function and water use function work against each other. Assuming that the actual rainfall is within the prediction error range used in this paper, it must be realized that discharge above the design discharge rate could cause serious damage while non-fulfillment of the unfulfilled water use capacity does not necessarily cause immediate damage apart from a negative impact on power generating operation. The highest priority should, therefore, be given to the alleviation of likely flood damage downstream. Once the priority of flood control over water use is accepted, preliminary discharge corresponding to the volume ΔV , which is above the flood control capacity, should be conducted as indicated in [Figure 1](#). In Case 2, preliminary discharge corresponding to the volume of ΔV is necessary as in Case 1. In Case 3, rainfall at the minimum value causes disruption to water use. Here, even if rainfall at the maximum value occurs, the required dam operation is to try to restore the unfulfilled water use capacity so long as the available flood control capacity does not become insufficient. No operational problems are experienced with Case 4. For practical dam management, adequate judgment must be made in consideration of such possible negative impacts as an insufficient flood control capacity and the non-fulfillment of the unfulfilled water use capacity due to rainfall prediction errors of the WRF model on the flood control and water use functions.

4.2 Clarification of rainfall prediction errors of the WRF model

The study results on error rates (Wada, 2006), which are referred to in [chapter 2](#) and used for convenience for the simulations described in [chapter 3](#), indicate the maximum and minimum values of the error range for rainfall predictions made by the Japan Meteorological Agency for actual rainfall levels observed by using a 20 km mesh static model which features a limited number of observation stations and precipitation events. In contrast, the WRF model is non-static and involves down-scaling to a minimum 1 km mesh. Because of these differences, it is necessary to clarify the characteristics of prediction errors through comparison of the predicted rainfall levels of the WRF model and actual rainfall levels for as many dams and floods as possible prior to the application of the WRF model to practical dam operation management.

4.3 Improvement of facilities

In case that the discharge capacity of dams is small under low water levels because of the limitation of discharge capacities of bottom outlets, it is difficult to conduct smooth operation to increase the discharge rate to meet the inflow rate or preliminary discharge which mitigates flooding at the time of excess flood effectively and the expected positive effects of the simulation exercise described in [chapter 3](#) cannot be fully materialized. With these dams, remodelling, such as installing an additional bottom outlet, can be expected to improve their flood control function.

5 CONCLUSIONS

The study has proposed a simple flood control method in order to minimize flood damage downstream by the integrated operation of the flood control and the water use capacities of dams by forecasting the total inflow volume to a dam using the rainfall prediction method based on WRF techniques which have significantly improved in recent years. The effectiveness of this method was examined using actual data on rainfall, flood and dam operation events. Assuming that the rainfall prediction errors of the WRF model are within the error range used by the study for convenience, the following conclusions are presented.

1. The proposed method enables the prediction of the total inflow volume to a dam within a certain period of time. It is, therefore, possible to alleviate flood damage in many cases by means of conducting preliminary discharge, etc., to lower the maximum discharge rate than the discharge rate stipulated by the existing exceptional rule for dam operation even if an excess flood has taken place.
2. For many smaller floods, the application of the new method can prevent flood damage downstream as the discharge rate remains below the harmless discharge rate.
3. The actual use of rainfall prediction by the WRF model can enhance the effectiveness of flood control function but there are also risks posed by prediction errors. It is necessary to accurately understand the characteristics of the new model, including possible rainfall prediction errors. To minimize these risks any judgment on the flood control operation should reflect the characteristics.
4. For those dams where the capacity of the crest spillway gates and other flood control facilities is insufficient, their remodelling can be expected to achieve certain positive results to ensure the effective implementation of preliminary discharge and other operations. It is, therefore, desirable to conduct adequate remodelling, taking into consideration the flood control capacity, water use capacity and situation of flood damage occurrence downstream.

REFERENCES

- IPCC. 2007. The AR4 Synthesis Report. *Climate Change 2007*. Geneva: IPCC.
- Toyoda, Y. 2009. Development of hydrological model with meteorological forecast model. *Civil Engineering Research Laboratory Report 8058*. Tokyo: Central Research Institute of Electric Power Industry (CRIEPI).
- Wada, K. 2006. The study on applicability of precipitation forecasting information for river management report. *Technical Note of NILIM 329*. Tsukuba: NILIM.

Effective flood control through integrated and collaborative dam operation at three dams in the upper Nabari River

T. Matsumura, H. Kamiya & N. Yoshida

Japan Water Agency (JWA), Mie, Japan

ABSTRACT: Heavy rain with the 18th typhoon threatened the Nabari River Basin, Kansai region with causing inundation early in the morning on 8th October, 2009. The Nabari River is a tributary of the Yodo river basin which contains Osaka and Kyoto and runs through Nabari City which is a residential zone as commutable distance area from Osaka city. In the upper reach of the Nabari, there are three multi-purpose dams; Shorenji Dam, Hinachi Dam, and Murou Dam, which are operated by Kizugawa Integrated Dam Control and Management Office (KIDCMO), branch office of Japan Water Agency (JWA). Since it rained heavily in the downstream of the three dams, the regular operation by three dams complying with the given flood control regulation seemed not to be able to prevent Nabari City from inundation. Therefore, JWA and Ministry of Land, Infrastructure, Transport and Tourism (MLIT) conducted collaborative operation of the three dams to avoid the inundation in the city area.

In this case, flood control operation of three dams commenced in early stage before the inflow reached the defined flood discharge in consideration of the water level of the Nabari River, rainfall condition and capacity of the reservoirs. During the operation, discharge from the dams was changed timely and appropriately through the collaborative work of the three dams in order to maximize the effectiveness of all flood control capacities of the reservoirs according to the latest rainfall forecast technology and runoff analysis.

The use of improved rainfall forecast technology and runoff analysis model enabled the effective application of this flexible operation protocols. It is estimated that this operation has resulted in 1.5 m decrease of the water level at Nabari design control point, and prevented approximately 1200 households from inundation.

Considering the recent climate change, it is possible to have extreme rainfall more often. The proof of adaptability of this flexible operation is quite meaningful not only for flood damage mitigation in the downstream, but also for future prospects of flood control by dams.

1 INTRODUCTION

The River Bureau of Ministry of Land, Infrastructure, Transport and Tourism, Japan (MLIT) is in charge of flood management and mitigation. Particularly, 109 large scale river systems are directly managed by the Ministry. Japan Water Agency (JWA) is constructing dams, estuary barrages, facilities for lake and marsh development, and canals in seven major and legally designated river basins out of above 109 river systems. Also, it is operating, managing and reconstructing completed facilities. The mandate of JWA is based on the Water Resources Development Promotion Law and Japan Water Agency Law. The Yodo river is one of seven basins and covers Osaka and Kyoto cities.

October 13th, 2009, the typhoon 18th with heavy rain came closest to Kansai and Tokai area. Its rain ranged all over Japan and caused lots of casualties and damages. As of 15:00 on October 8, the Fire and Disaster Management Agency reported five people killed, 127 people injured, and 4328 houses damaged.

Early morning on October 8th, the heavy rain threatened Nabari city in Mie Prefecture with causing significant inundation. Nabari city locates in commutable area to Osaka and

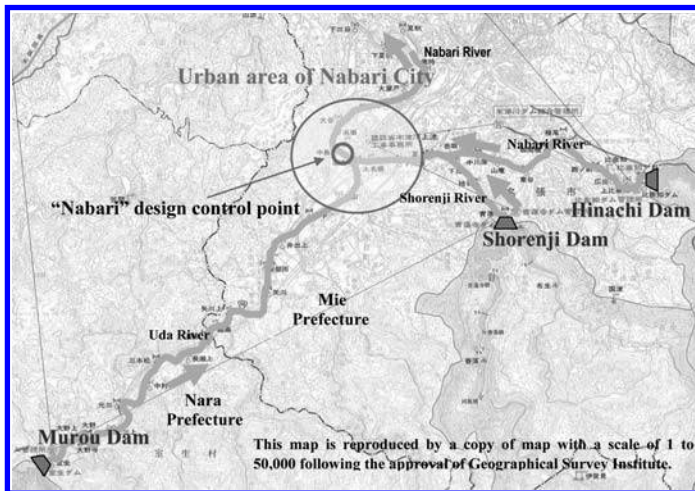





Figure 1. The location of three dams in the upper Nabari River.

Table 1. Specifications of three dams in the Nabari River upstream.

Shorenji Dam	Hinachi Dam	Murou Dam
<p>Shorenji Dam</p> <p>【Dam Data】 Type: Concrete arch dam Dam height: 82.0 m Dam crest length: 275.0 m Catchment area: 100 km² Effective capacity: 23,800,000 m³ Flood control capacity: 8,400,000 m³ Start of management: July, 1970</p> <p>【Purposes of dam】 1. Flood control 2. Maintenance of normal function of flow 3. Water supply 4. Agricultural water 5. Power generation</p> 	<p>Hinachi Dam</p> <p>【Dam Data】 Type: Gravity concrete dam Dam height: 70.5 m Dam crest length: 355.0 m Catchment area: 75.5 km² Effective capacity: 18,400,000 m³ Flood control capacity: 9,000,000 m³ Start of management: April, 1989</p> <p>【Purposes of dam】 1. Flood control 2. Maintenance of normal function of flow 3. Water supply 4. Power generation</p> 	<p>Murou Dam</p> <p>【Dam Data】 Type: Gravity control dam Dam height: 63.5 m Dam crest length: 175.0 m Catchment area: 136 km² Effective capacity: 14,300,000 m³ Flood control capacity: 7,750,000 m³ Start of management: April, 1974</p> <p>【Purposes of dam】 1. Flood control 2. Maintenance of normal function of flow 3. Water supply</p> 

has eighty thousand populations. The Nabari River which is a tributary of the Yodo river runs through the city center. Since it rained heavily, the regular flood control operation based on management rules by three dams; Shorenji Dam, Hinachi Dam, and Murou Dam in the upper Nabari River, managed by Kizugawa Integrated Dam Control and Management Office (KIDCMO), branch office of JWA, might not prevent inundation.

Therefore, KIDCMO and Yodogawa Integrated Dams Control Office (YIDCO), branch office of MLIT conducted the collaborative operation of the three dams to avoid inundation in the city area.

The integrated flood control operation of the three dams started before the volume of runoff reached the flood discharge; taking then water level in the Nabari River, rainfall intensity,

and the capacity of the three dams into considerations. During flood control operation, outflow discharge from the dams was under timely and appropriate control by the operations to make the most of storage capacities and collaborative operations of the three dams employing the latest rainfall forecast technology and runoff analysis.

The latest rainfall forecast technology and runoff analysis model enabled the effective flood control operation of the three dams. The effect of the operations was estimated to lower the water level in the Nabari River by 1.5 m and prevent inundation of approximately 1,200 households comparing with the case without the dams.

Considering the recent climate change, heavy rains are more likely to occur than before. The proof of the adaptability of flood control operation to reduce damages in the downstream means not only the prevention of the flood damage in the downstream, but also the future prospects for flood control for dams.

This report shows the state of implementation and effects regarding to flood control operation (three dam integrated operation)

The locations of the three dams in the Nabari River upstream are shown in [Figure 1](#) and principal features in [Table 1](#).

2 SUMMARY OF THE FLOOD CONTROL BY JWA

Incorporated administrative agencies are established and given objectives and missions by the national government to carry out "administrative tasks and projects, where implementation should ensure public benefits such as stable public life and social and economic activities." JWA is one of this type of agencies and mandated to construct and manage the facilities for water resource development such as dams for water supply and flood control, and canals in seven water systems (Tone River/Ara River/Toyo River/Kiso River/Yodo River/Yoshino River/Chikugo River) based on Japan Water Agency Law.

As for dams, JWA carries out flood control following the management rules of each dam based on Japan Water Agency Law. Each management rule has two types of operations; one is a regular operation that regulates outflow discharge from dams to cope with an expected large scale flood in the dam basins, and the other is a special operation that carries out the most suitable flood control considering the situation of the rain and the downstream rivers.

As for the special operation, the management rule doesn't have any rule regarding the outflow discharge from the dam, but when JWA carries out special operation, an instruction from the Integrated Dam Control and Management Office (MLIT) is necessary. This cooperative flood control operation of the three dams on this report was carried out following the instruction from YIDCO after KIDCMO and YIDCO thoroughly examined and adjusted.

3 FLOOD CONTROL OPERATION

3.1 *The day before the typhoon 18 hit Nabari*

From the afternoon on October 7, in order to prepare for the approach of the typhoon 18, KIDCMO inspected discharge facilities and warning facilities of dams and started forecasting the rainfall and the amount of inflow in each dam based on the typhoon course forecast.

With the increase of the amount of inflow to the dams, KIDCMO started contacting to the related institutions and patrolling the down stream river sequentially from 18:00 at Murou Dam, and from 20:30 at Shorenji Dam and Hinachi Dam. One hour later, each dam started discharging from spillways facilities.

When each dam started discharging from spillways facilities, the typhoon 18 was heading more easterly which meant it wouldn't rain heavily in the Nabari River basin according to the typhoon course forecast.

3.2 Rise of the Nabari River water level

A rain forecast changed significantly around 2:00 on October 8. The forecast showed that the water level in the Nabari River, in the downstream of the dams, would exceed flooding attention water level, and continue rising. [Figure 2](#)

For this reason, MLIT instructed KIDCMO to start operation to prevent the inundation in the city area by controlling the water level in the Nabari River. In order not to raise the water level in the Nabari River, three dams in the Nabari River upstream were required to reduce the outflow discharge to the downstream of the dam. In this case, the outflow discharge from the dam was carefully arranged because storage capacity for flood control would be filled up if heavy rain continued.

Although the speed of the typhoon was accelerated, still it was forecasted that heavy rain would continue. So it was necessary to adjust the outflow discharge based on the observed precipitation and changing forecast.

At 3:15, KIDCMO started special operation to keep the outflow discharge (Shorenji Dam 250 m³/s, Murou Dam 250 m³/s, Hinachi Dam 150 m³/s) less than the outflow discharge during regular operation that means increase the outflow discharge of Shorenji Dam 450 m³/s, Murou Dam 300 m³/s, Hinachi Dam 300 m³/s in consultation with the Nabari City. [Figure 3](#)

Following operations were implemented by KIDCMO under the instructions from MLIT after their close consultation.

Prediction of water level at Nabari

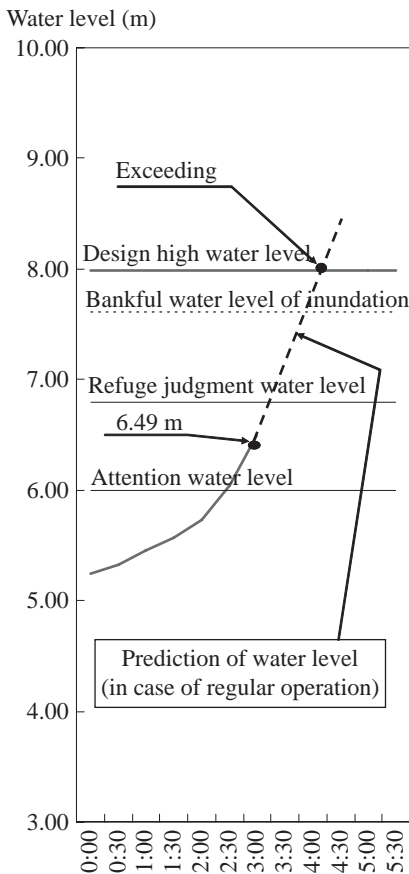


Figure 2. Prediction and judgment at 3:00.

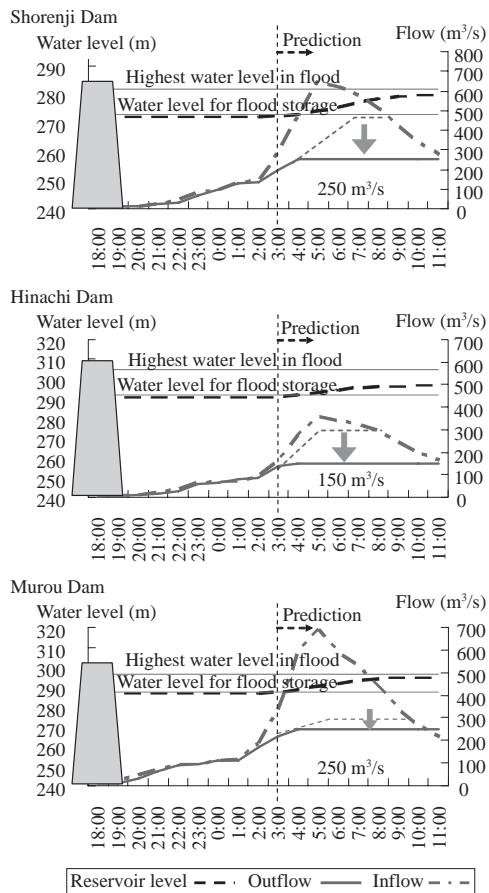


Figure 3. A prediction and the dam operation at 3:00.

3.3 Integrated and collaborative dam operation at the three dams in the Nabari River upstream

At 3:40, Shorenji Dam's storage capacity for flood control might possibly be filled up if Shorenji Dam continued to store up the water without increasing the outflow discharge in this heavy rain. On the other hand, the water level in the Nabari River continued rising, and it was forecasted that if this continued, the water level in the Nabari River would reach the bankful water level of inundation and bring an inundation damage to the city area. For this reason, it was difficult to increase the outflow discharge from the dams although inflows to the dams largely increased. **Figure 4**

At 4:00, the water level in the Nabari River was expected to rise not too quickly due to the gradual increase of outflow discharge from Shorenji from current 250 m³/s to 450 m³/s. After considering the rainfall forecast, the water level prediction in the Nabari River, the flood control capacity and the inflow prediction of the three dams, it was decided that the outflow discharge from Hinachi Dam would be reduced by 100 m³/s to 50 m³/s, instead of increasing the amount of discharge from Shorenji gradually. **Figure 5**

3.4 Decline of water level in the Nabari River

At 4:40, since the rainfall in Murou Dam basin was less than forecasted, it was decided to make the water level in the Nabari River lower by decreasing the outflow discharge from

Prediction of water level at Nabari

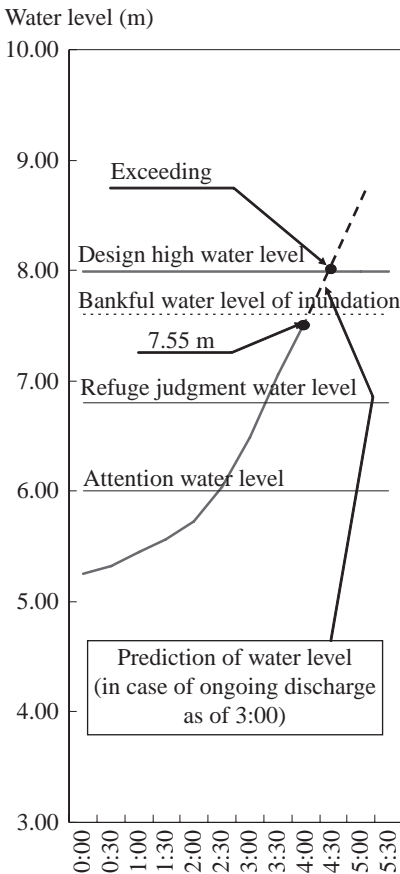


Figure 4. Prediction and judgment at 4:00.

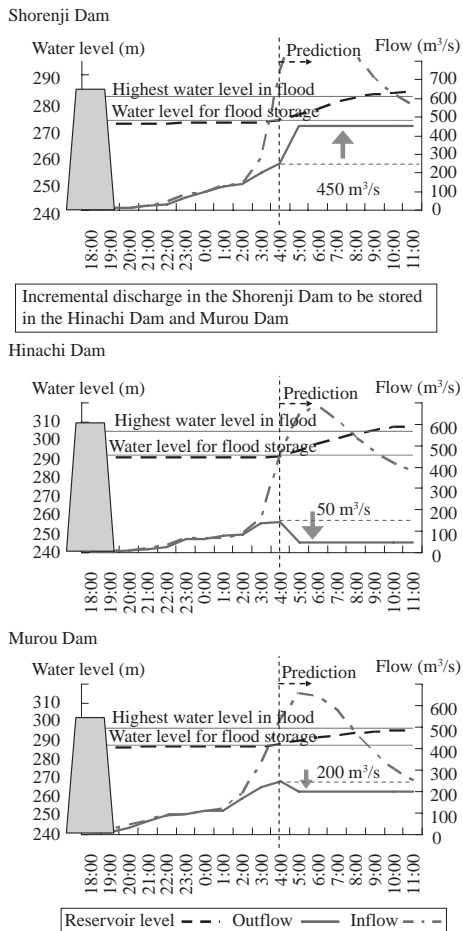


Figure 5. A prediction and the dam operation at 4:00.

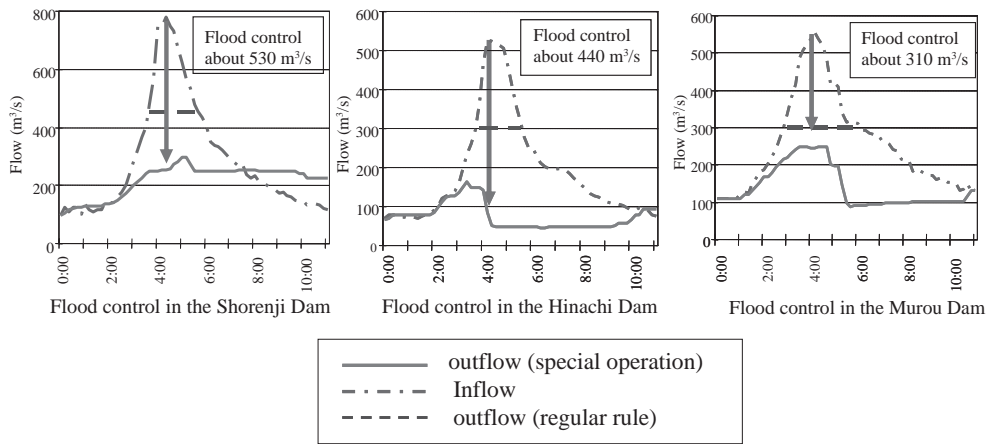


Figure 6. The flood control operation of three dams.

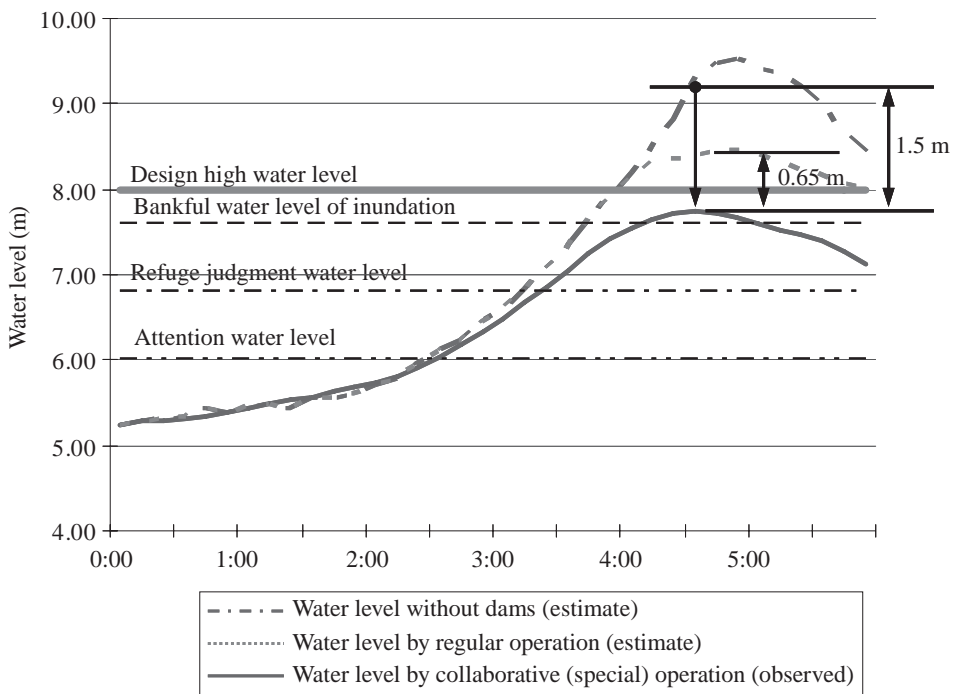


Figure 7. Water level at Nabari design control point.

Murou Dam to $200 \text{ m}^3/\text{s}$ by the smart examination based on observed data and the amount of inflow, because there is no time to examine with considering the rainfall forecast.

As a result of repeated examinations and operations with forecasting the water level in the Nabari River and so on, the outflow discharges were finally decreased to $250 \text{ m}^3/\text{s}$ from Shorenji Dam, $100 \text{ m}^3/\text{s}$ from Murou Dam, and $50 \text{ m}^3/\text{s}$ from Hinachi Dam. This operation made the water level at Nabari design control point lower than bankful water level at 5:00 and lower than refuge judgment water level at 6:20.

Table 2. Comparison with the Isewan Typhoon in 1959.

Details		Typhoon No.18, 2009	Isewan Typhoon, 1959
Scale	Period	Sep 29 (21:00) to Oct 9 (15:00)	Sep 21 (21:00) to 27 (21:00)
	Lowest pressure	910 hPa	895 hPa
	Maximum wind	55 m/s	75 m/s
At landfall	Central pressure	955 to 960 hPa	925 hPa
	Maximum wind	40 m/s	50 m/s
	Radius storm wind	220 km (SW), 170 km (NW)	250 km
Rainfall in the upper Nabari	1-hour rainfall	65 mm	58 mm
	3-hour rainfall	145 mm	137 mm
	Cumulative rainfall	315 mm	393 mm
Nabari city			
Rainfall	1-hour rainfall	41 mm	43 mm
	Cumulative rainfall	239 mm	342 mm
Damage	Death	–	11
	Missing	–	1
	Swept houses	1	102
	Demolished houses	–	180
	Partially destroyed	–	525
	Inundated floor level above	1	1434
	Inundated floor level below	27	848

Reference: Meteorological Agency, History of the Kizu River (1980), Interviews by Nabari City Material about flood in the Yodo River and the Yamato River (liaison council of flood forecasting, August 1960).

Afterwards, the flood control operation was continued till the water level in the Nabari River became lower than warning water level, and flood control operation was shifted to the integrated control operation to decrease the water level in each three dam in order not to raise the water level in the Nabari River. [Figure 6](#)

4 FLOOD CONTROL EFFECT

This flood control regarding special operation by the three dams in the Nabari River upstream made the water level for approximately 1.5 m lower than the water level without the three dams, and for approximately 0.6 m lower than the regular operation. With this special operation, it is assumed that approximately 1200 households in Nabari City area were saved from inundation damage. [Figure 7](#)

There is a comparison between typhoon 18 and Isewan typhoon that hit the Nabari City 50 years ago in the damages in the Nabari City area. Despite the rainfall in three hours this time was equal to that of Isewan typhoon, the damages the Nabari City suffered were completely different. [Table 2](#)

5 CONCLUSION

KIDCMO received a letter of appreciation from the mayor of Nabari City on October 20, 2009 due to the “Great contribution for reduction of the flood damage in the Nabari River by quick and appropriate flood control operation”. In fact, during the special operation, outflow discharge was arranged ten times in only 2 hours by getting and considering data observed in every ten minutes.

In addition, this flood control operation was highly evaluated by Japan Society of Civil Engineers (JSCE) because of its crisis control ability and operating performance. KIDCMO and YIDCO won the Outstanding Civil Engineering Achievement Award of 2009 from JSCE on May 28, 2010. It was the first splendid achievement that the operation of the dam won the JSCE Award.

This special operation was able to be carried out by understanding the capacity of flow in the river in downstream of the dams, and using the outflow forecast system based on the observed rainfall and forecasted rainfall. KIDCMO will improve the outflow prediction system, in order to aim the higher stage of flood control operation in the future.

Global warming and design flood: The case study of Bagatelle dam, Mauritius

S. Le Clerc & H. Garros-Berthet

TRACTEBEL ENGINEERING—Coyne & Bellier, Gennevilliers, France

ABSTRACT: Global warming is expected to cause significant changes to climate, but some uncertainties remain about nature and extent of these changes. This is particularly true with regard to possible changes at regional or local level and to changes in the extremes that produce floods. Any assessment of the effect of climate change on flooding must start with its effects on rainfall. The intensity of extreme rainfalls is associated with temperature increases. This paper focuses on hydrological outcomes related to flood estimation at Bagatelle dam site in Mauritius.

During Bagatelle studies, Coyne & Bellier has taken into account an increase of temperature for the assessment of the design floods.

The influence of temperature increase on the probable maximum precipitation (PMP) estimation is evaluated. PMP is assessed using storm transposition and maximization. Such an approach involves moisture adjustment with the basic assumption that a storm would have produced maximum precipitation with maximum moisture available.

After estimating the change in rainfalls, probable maximum flood PMF is computed using SCS approach.

1 INTRODUCTION

This paper presents the main results of the PMP/PMF estimation carried out by Coyne & Bellier during the detailed design studies (Coyne & Bellier—SJP, 2009) of Bagatelle dam project. Bagatelle dam site is located in Mauritius Island in the Grand River North West catchment on Terre Rouge River. The objective of the Bagatelle Dam Project is to meet the present and future water demand of the Port Louis and Lower Mare aux Vacoas (MAV) Water Supply Systems up to 2050 as well as to increase water availability for irrigation to the maximum possible extent.

Classical methods of design flood estimation have been applied combining statistical and deterministic approaches for the purpose of this study. Only deterministic features of rainfall—runoff transformation by unit hydrograph technique and storm maximization are discussed here in order to be compared to PMP/PMF estimates of previous hydrological studies carried out on Mauritius Island (ABM, 1978; SMEC & Mega Design, 2004).

In what follows, after a brief description of the climate of the studied area and of the hydrological database used to compute design floods are presented, methods and main results of PMP computation are detailed. PMP is assessed using two approaches: (i) Hershfield's formula according to statistical patterns of the Mauritian maximum rainfall database and (ii) Storm maximization by dew point analysis on 15 observed storm events. The influence of temperature increase is analyzed in the dew point analysis carried out for the PMP estimation by storm maximization.

For the estimation of the probable maximum flood (PMF), the computation of flood hydrographs is based on a rainfall-runoff analysis of the major observed floods and the application of a unit hydrograph technique. Computed PMF results are then compared to the previous results estimated on Bagatelle dam site.

2 CLIMATE AND DATABASE

2.1 *Climate description*

The climatology of the study area is characterized by the following aspects (Mauritius Climate, 1972):

- Mauritius lies 20° south and 57° east near the edge of the tropical belt. Being an isolated is-land, it has a tropical maritime climate. Topographic features affect the rainfall pattern over the island;
- The southeast trade winds dominate in winter, but winds are light and variable during summer;
- Frequent tropical cyclones occur mainly between December and March. These cyclones and other tropical depressions during summer can produce very heavy precipitations.

These aspects have an important bearing on the flood potential. Design flood conditions can result either from the occurrence of a tropical cyclone or from the occurrence of a thunder-storm.

A synthesis of the main Mauritian recent climate trends has been presented in (Mc Sweeney and et al., 2008) and summarized below:

- Mean annual temperature has increased by 0.6°C since 1960, an average rate of 0,13°C per decade. This increase in temperature is most rapid in JFM (0.16°C per decade) and least rapid in OND (0.10°C per decade);
- The large inter-annual and inter-decadal variations in rainfall in this part of the world mean that it is difficult to identify long term trends. Whilst there is no evident trend in annual rainfall, OND rainfall has declined over the period 1960 to 2006, at an average rate of 7.7 mm per month (8.7%) per decade;
- There are insufficient daily temperature data available from which to determine trends in daily temperature extremes and insufficient rainfall observations available to identify trends in daily rainfall extremes.

2.2 *Flood database*

The database for flood analysis comprises rainfall information inferred from a regional data sample based upon several stations located in Mauritius and hydrograph shape analysis using a selection of observed floods. The flood estimation is based on the use of:

- Climatological data: temperature and relative humidity during storm events;
- Rainfall data: maximum daily precipitation from 30 Mauritian raingauge stations during storm events, storm profiles;
- Stream flow data: maximum instantaneous and daily discharges observed on Terre Rouge Rivers.

3 PMP COMPUTATION

The Australian Bureau of Meteorology (ABM, 1978) estimated the PMP for the Champagne Project (SMEC & Mega Design, 2004). These estimates were based on rainfall data recorded during the passage of the most severe cyclones over Mauritius.

In this paper, the synthesis of the PMP estimation analysis carried out by Coyne et Bellier during the Detailed Design Studies of Bagatelle Dam Project (Coyne et Bellier & SJP, 2008) are compared to the PMP estimated by ABM (ABM, 1978).

Two methods have been used by Coyne & Bellier to compute PMP: (i) Hershfield estimation based on statistic patterns of the observed maximum precipitations and (ii) Storm maximisation by the dew point approach based on the analysis of 15 storm events.

The third part of the PMP computation deals with storm profiles definition.

3.1 PMP computation by Hershfield's approach

Maximum daily precipitation data from 30 raingauges covering the whole Mauritius Island have been criticized and analyzed. From this database, statistical patterns (M , mean of maximum daily precipitation and S , standard deviation) from 12 rainfall stations in the vicinity of the project area have been extracted in order to compute PMP according to Hershfield's formula (Hershfield, 1961), as follows:

$$PMP = M(P) + K.S(P) \tag{1}$$

With $\sqrt{K} = 4.851 - 0.09995\sqrt{M}$

The 12 selected rainfall stations are located nearby Terre Rouge catchment. A PMP estimate according to Hershfield's approach is given in the [Table 1](#):

3.2 PMP computation by storm maximization

The estimation of the PMP based on the World Meteorological Organization, "Manual for estimation of PMP" (WMO, 1986) deals with dew point analysis and storm maximization approach. Storm maximization involves moisture adjustment with the basic assumption that a storm would have produced maximum precipitation with maximum moisture available. The method of moisture adjustment commonly used involves the estimation of air-mass moisture content, taken as the precipitable water, from dew-point observations.

3.2.1 Dew point analysis

Climatological data related to dew points at Pamplemousses, Medine and Vacoas for the period 2004–2008 have been provided by Mauritius Meteorological Services for the purpose of Bagatelle dam project flood study. These data concerned two daily estimates: one during morning (AM) and one during afternoon (PM).

The analysis carried out by ABM was based on a 22 years period (1951–1973) at Pamplemousses, Plaisance and Vacoas stations. The dew point analysis of the present period (2004–2008) has revealed some differences with the analysis conducted by ABM:

- The maximum dew point line deduced from Sea Surface Temperature is about 28°C for the present period a maximum line of 26,5°C have been considered by ABM;
- The present data provide such estimate for March and December at Pamplemousses and Medine stations. ABM analysis depicted a maximum occurring in February;
- Coyne & Bellier proposed a dew point value of 29°C for PMP computation when ABM had selected a dew point of 27,5°C, corresponding to the increase of maximum observed dew points.

3.2.2 Storm maximization

Storm maximization approach has been applied to 15 daily observed storms ([Table 2](#)) by considering only the dew point adjustment. For each of these storms, dew point has been computed according to Murray's formula related to relative humidity (RH), and air temperature (T). Using the dew point value (T_{dew}), the precipitable water, or water content of the atmosphere (PW), has been assessed (Howell, Dusek, 1995).

Table 1. Hershfield's PMP estimation of the rainfall stations around Bagatelle catchment.

Code	Station	PMP (mm)	Code	Station	PMP (mm)	Code	Station	PMP (mm)
W6.MDA	Minissy	1470	W1.H	Bega	1490	W8.H	Highlands	1340
W18.MDA	Beau Bois	1500	W2.H	Ebene	1400	W9.H	Bagatelle	1390
W19.MDA	Alma	1510	W5.H	Mon Reve	1370	W11.H	Cote d'Or	1490
W17.MDA	Valetta	1410	W7.H	Minissy	1460	W14.H	Hermitage	1360

For $T_{\text{dew}} = 29^{\circ}\text{C}$, $\text{PW} = 115.5 \text{ mm}$ ($T_{\text{dew}} = 27,5^{\circ}\text{C}$, $\text{PW} = 102.5$), the dew point maximization factor is given by $\text{MF} = 115.5 / \text{PW}$ (Obs. storm).

For the 15 selected storms, the maximization factor MF varies from 1.64 to 2.06. The mean value is 1.81, with a coefficient of variation of 0.08.

The maximization factors found by ABM have been rescaled from $T_{\text{dew}} = 27.5^{\circ}\text{C}$ to $T_{\text{dew}} = 29^{\circ}\text{C}$. The corresponding rescaling ratio $\text{PW}(29^{\circ}\text{C})/\text{PW}(27,5^{\circ}\text{C})$ is about 1,13. The rescaled maximization factors are fully consistent with the ones obtained previously.

Using the results of the [Table 2](#), a regional sample of data related to 240 observed rainfall occurred during the 15 selected storm events have been maximized. For five of the maximized storm events, PMP estimates exceed 800 mm/24 h:

- Beryl (25/12/1961) provides PMP candidates in the range of 819 to 1211 mm/24 h.
- Danielle (19/1/1964) gives candidates from 839 to 1220 mm/24 h.
- Gervaise (7/2/1975) yields possible PMP between 803 and 1432 mm/24 h.
- Hollanda (9/2/1994) results in one candidate at 931 mm.
- Dina (20/1/2002) leads to possible PMP in the range of 844 to 1267 mm.

The rescaling of ABM's PMP estimates is in accordance with those findings. Finally, a PMP value of 1430 mm/24h appeared relevant for design purposes, ABM estimate was about 1280 mm/24h.

3.3 Storm profiles

When determining a flood hydrograph from a rainstorm event, it is necessary to know or specify how the intensity of rain varies during the period of the storm. In this part, a database of 6 storm profiles describing temporal distributions of adopted PMP is provided in the following:

- Observed storm profiles from three major storms in Mauritius have been analyzed: the storm of December 1961, Beryl and Gervaise. These storm profiles are based on 3 or 6 hours time steps;
- A composite profile deduced from Gervaise storm by grouping two sub storms;
- Two 24-hour duration design storms based on the use of rainfall world records and near records information. These storm profiles are based on hourly time step.

3.3.1 Storm profiles derived on observed events

To define relevant storm profile, observed storm profiles from three major storms in Mauritius have been analysed: the storm of December 2 and 3, 1961, Beryl (December 1961) and Gervaise (February 1975). The corresponding storm profiles are given in [Table 3](#).

In addition to these profiles, we considered one profile deduced from Gervaise profile by grouping the two sub storms into a unique storm.

On a 24-hour basis, Gervaise and Beryl have similar amounts. The storm of December 1961 has a 24-hour amount of almost 700 mm to be compared to about 550 mm for the two other storms.

Table 2. Computed maximization factors of the 15 selected storm events.

Storm	Date	T (°C)	RH (%)	T _{dew} (°C)	MF	Storm	Date	T (°C)	RH (%)	T _{dew} (°C)	MF
Carol	25/02/1960	25,4	75,0	20,6	2,06	Gilberte	11/01/1967	25,6	82,5	22,3	1,76
Danielle	17/01/1964	24,3	80,0	20,6	2,06	Gervaise	05/02/1975	25,5	83,0	22,3	1,76
Alix	16/01/1960	24,7	80,0	21,0	1,98	Helga	04/02/1971	25,1	85,0	22,4	1,75
Beryl	22/12/1961	23,9	87,0	21,6	1,87	Hennie	22/03/2005	25,1	87,0	22,7	1,70
Dina	20/01/2002	24,5	84,0	21,6	1,87	Claudette	21/12/1979	25,4	82,5	22,1	1,65
Fleur	18/01/1978	25,1	83,0	21,9	1,82	Hollanda	09/02/1994	25,5	86,5	23,1	1,65
Davina	08/03/1999	25,4	82,5	22,1	1,79	Louise	27/03/1970	25,5	87,5	23,2	1,64
Gerry	12/02/2003	25,1	84,3	22,2	1,78	Average		25,1	83,3	22,0	

Table 3. Observed storm profiles for 3 major storms.

t (h)	Gervaise (mm)	Ptot (mm)	t (h)	Beryl (mm)	Ptot (mm)	t (h)	2-3/12/1961 (mm)	Ptot (mm)
3	3	3	6	22	22	6	3	3
6	0	3	12	22	44	12	3	6
9	0	3	18	25	70	18	5	11
12	6	9	24	25	95	24	5	16
15	6	15	30	28	123	30	11	27
18	6	21	36	39	162	36	16	43
21	15	36	42	67	229	42	22	65
24	12	48	48	151	380	48	43	108
27	66	114	54	246	625	54	140	248
30	96	210	60	89	715	60	425	673
33	150	360	66	45	759	66	81	754
36	84	444	72	28	787	72	22	775
39	12	456	78	11	798			
42	102	558	84	6	804			
45	24	582	90	3	807			
48	6	588						
51	3	591						
54	3	594						
P24	546			P24	553	P24	689	

In addition to these profiles, we considered one profile deduced from Gervaise profile by grouping the two sub storms into a unique storm.

On a 24-hour basis, Gervaise and Beryl have similar amounts. The storm of December 1961 has a 24-hour amount of almost 700 mm to be compared to about 550 mm for the two other storms.

3.3.2 Storm profiles derived from world records

Since the previous storms were defined with time steps of three (3) and six hours (6), two design storms of 24-hour duration have been delineated on hourly time step.

Available information about world and near world records of rainfall and about world envelope curves approach, both 24-hour storm profiles have been delineated in the [Table 4](#) considering the following analysis:

- The 15th March 1952, a rainfall world record of 1870 mm/24 hours has been observed at Belouve (La Reunion). This record is a little bit higher than the estimates given by World envelope in [Table 4-\(1\)](#);
- The application of the quasi world envelope ([Table 4-\(2\)](#)) provides a 24-hour precipitation of 1240 mm and a 6-hour precipitation of 600 mm. The 2nd and 3rd of December 1961 storm gave a 6-hour precipitation of 425 mm.

Finally, a PMP value of 1430 mm/24 hours has been recommended for the PMF computation and two storm profiles ([Table 4-\(3\)](#) & [\(4\)](#)) have been deduced from the observations above and adopted for PMP computation.

4 PMF COMPUTATION

Methods of estimating PMF have been evolving as a result of increased data, an improving understanding of, and a greater ability to model, meteorological and hydrological processes.

The computation of PMF flood hydrographs deals with:

- A flood shape analysis based on rainfall-runoff data of several floods of importance. An estimation of a CN value required on SCS method (Ven Te Chow, 1964) for PMF estimation is deduced from this analysis;

Table 4. Rainfall envelope curves.

World envelope	Near world envelope	Adopted storm profiles	
		High intensity storm	Low intensity storm
(1) 359.D ^{0.49}	(2) 230.D ^{0.53}	(3) 275.D ^{0.52}	(4) 200.D ^{0.62}

Table 5. Selected flood events on Terre Rouge catchment.

	Gilberte 14/1/67	Gervaise 06/02/75	Claudette 23/12/79	Hollanda 10/02/94
V(Storm)	1 504 333	1 977 297	1 209 391	1 217 014
Qd	17,4	22,9	14,0	14,1
Qp	43,2	114	36,8	94,6
Qp/Qd	2,5	5,0	2,6	6,7
RO	92	154	69	122
CN	62,7	35,3	43,7	50,2

Table 6. Results of PMP/PMF computations based on 6 storm profiles.

Storm	dt (h)	Qp (m ³ /s)	V (m ³)	RO tot (mm)	Rain (mm)	CRO	Qp/Q24	D (h)
Storm 1	1	600	16,23	1131	1430	0,79	3,54	24
Storm 2	1	479	16,29	1135	1430	0,79	2,81	24
Gervaise 1	3	437	18,13	1264	1556	0,81	2,17	54
Gervaise 2	3	435	18,13	1263	1556	0,81	2,23	54
Beryl	6	473	25,98	1811	2087	0,87	2,16	90
December 1961	6	591	18,97	1322	1609	0,82	2,87	72

- PMP storm profiles defined in 3.3 are used to compute PMF flood hydrographs.
- PMF results are compared to corresponding PMF estimate of Bagatelle dam Project Feasibility Study.

4.1 Flood shape analysis

Four observed major flood events recorded on Terre Rouge River catchment have been analysed to estimate flood characteristics. For each observed event, several flood characteristics are summarised in the Table 5: storm volume V, maximum daily discharge Qd and peak discharge Qp, the peak ratio Qp/Qd, the runoff value RO and the computed CN value from SCS method.

This flood shape analysis concluded on recommended CN value of 45,4 is recommended for the PMF computation according the above computed results and their flood magnitude.

4.2 Combination of PMP/PMF approach

The PMF hydrographs at Bagatelle dam site have been computed by the use of the 6 PMP storm profiles defined in 3.3 and a CN value of 45,4 for the SCS method application. Synthetic results are given in the Table 6.

Finally, the PMF of 600 m³/s based on the Storm 1 patterns is proposed by TE—Coyné & Bellier to provide the basic data needed for sizing the spillway. The PMF computation based on a 24-hour PMP design storm profile of 1129 mm (ABM, 1978) and carried out during the feasibility study of Port Louis Water Supply (SMC & Mega Design, 2004) at Bagatelle dam sitewas about 500 m³/s.

The South African National Committee on Large Dams (SANCOLD) regional maximum flood has been computed on Bagatelle dam site. The SANCOLD uses the concept of regional maximum (RMF) in determining the spillway design floods. The Terre Rouge catchment fell into the Region 5 (Kovacks, 1988) with the following envelope curve:

$$RMF = 100. A^{0.68} \quad \text{with } A, \text{ the catchment area} \quad (2)$$

The computed RMF is about 611 m³/s. This value confirms the magnitude of the above assessed PMF.

5 CONCLUSION

In this paper the probable maximum precipitation has been assessed using statistic and deterministic approaches. A database of 6 PMP storm profiles has been defined for PMP computation of PMF hydrographs.

A PMP of 1430 mm/24 h associated to a storm profile characteristic of the high intensity storms given in the Table 4-(3) is recommended for PMF assessment. The recommended PMF peak discharge is of 600 m³/s.

The influence of recent climate trends has taken into account in this analysis. The comparison of the PMP/PMF computation between Coyne & Bellier results (Coyne et Bellier & SJP, 2009) and ABM-SMEC results (ABM, 1978; SMEC & Mega Design, 2004) has revealed that temperature increase involves differences on dew point analysis, storm maximisation factor and PMP estimates.

The occurrence of the maximum values has also changed, moving from February—in the previous studies—to March and December in the recent period.

As a synthesis of results characterising both periods, main flood results are:

For the period 1951–1973, $T_{\text{dew}}(\text{PMP}) = 27,5^{\circ}\text{C}$, PMP = 1280 mm/24 h, PMF = 505 m³/s
 For the recent period, $T_{\text{dew}}(\text{PMP}) = 29^{\circ}\text{C}$, PMP = 1430 mm/24 h, PMF = 600 m³/s

REFERENCES

- Australian Bureau of Meteorology, (ABM), 1978. Feasibility study on L'Etoile, Cascade Diamond and Champagne hydroelectric project, SMEC & Mega Design.
- Coyne et Bellier—Servansingh Jadav & Partners, 2009. Consultancy Engineering Services for the Detailed Design and Construction supervision of the proposed Bagatelle Dam Project—Lot 1—Detailed Design—Flood Study, Mauritius.
- Hershfield D.M., 1961. Estimating the probable maximum precipitation. *J. Hydraul. Div. ASCE*, 87: 99–106.
- Howell T.A. and Dusek D.A., 1995. Comparison of Vapor-Pressure Deficit Calculation Methods - Southern High Plains. *Journal of the ASCE—Irrigation and Drainage Engineering*, 121(2): March/April 1995, p. 191–198.
- Kovacks Z.P., 1988. Regional Maximum Flood Peaks in Southern Africa, Technical Report TR137, Department of Water Affairs, Directorate of Hydrology, Pretoria.
- Mauritius Climate/Mauritius Meteorological Services, 1972.
- McSweeney C., New M. and G. Lizcano, 2008—UNDP climate change country profiles—Mauritius <http://country-profiles.geog.ox.ac.uk>
- SMEC & Mega Design, 2004. Feasibility Study of Port Louis and Lower Plains Wilhems Water Supply Project (Bagatelle Dam Project)—Phase I Studies (Final).
- Ven Te Chow, 1964. Handbook of applied hydrology—Section 20—Hydrology of Agricultural Lands. Mac Graw Hill.
- World Meteorological Organization, 1986. Manual for estimation of probable precipitation. *Second Edition, WMO*. No. 332–1986.

Study on the Pan-basin optimization of West route engineering of South-to-North water transfer

J. Zhang, S. Peng & Y. Wang

Yellow River Engineering Consult Co. Ltd, Henan, Zhengzhou, China

H. Wang

China Institute of Water Resource and Hydropower Research, China

ABSTRACT: Pressure index of supply-demand balance of regional water resources is introduced to assess the security situation in the Yellow River, and the incentives of water resources crisis are analyzed. Based on the safety assessment of water resources, the potential water receiving areas of the Western Route project of South-to-North Water Transfer are selected. For the conditions of water resources and ecological environment are different between the water transfer areas and the water receiving areas and the level of economic and social development varies greatly, we put forward multidimensional simulation and optimization for pan-basin water resources on the basis of inter-basin water transfer, and establish a system which links water transfer areas and water receiving areas together and contains a space-time optimization module and a model of three-layer structure for water resources allocation. Technology of decomposition and coordination of large system and nested searching RAGA (real code genetic algorithm) are adopted to solve the problem of water resources optimal allocation of the super large system of inter-basin water transfer. Through the model optimization, we get the scale and layout of the project and a scenario of space allocation of inter-basin water transfer, thus a scenario of appropriate water transfer scale and rational allocation is put forward.

1 INTRODUCTION

According to the extent of water receiving areas, the major water receiving areas of the western route project are 6 provinces of the upper and middle reaches of the Yellow River. In 2030, the water deficit is 12.44 billion m³, and it will exceed the maximum transferable water volume 9.45 billion m³~10.21 billion m³, which means that the water transfer scale is impossible to meet all the water demand of the water receiving areas. Based on this, the allocation scenario for diverted water along the river is mainly determined by the economic and social goal of water allocation, the supply-demand balance of water resources in the related water allocation regions and the differences of marginal benefits of water use in different time and sectors.

The scale and the feasibility study of inter-basin water transfer involve many factors such as economic society and ecological environment etc. On the condition that the market economic system and the project investment are taken as the main body, the major influence factors of regional water transfer decision are the water demand of water receiving areas and the transferable water volume of the water transfer areas, and the economic and social goal is also an important influence factor.

2 ANALYSIS OF POTENTIAL WATER RECEIVING AREAS

The measurement of water resources security is a significant and theoretical problem far from being solved. Here the ratio between demand and supply of water resources is defined

Table 1. Grades of regional water resources security.

Grade	Security	Comparative security	Critical state	Unsafe	Extreme unsafe
W_{ds}	(0–0.5)	(0.5–1)	(1–1.15)	(1.15–2)	(2–∞)

as the pressure index of supply-demand balance of regional water resources bearing capacity W_{ds} :

$$W_{ds} = \frac{W_d}{W_s} \quad (1)$$

where W_s is the regional available water and W_d the total regional water demand.

According to Equation 1, it is observed that when the regional available water is less than the water demand of social-economic system, that is $W_{ds} > 1$, the regional available water is not enough to support the social-economic system of such scale and the pressure of the water resources is greater than the bearing capacity; otherwise the regional water resources can provide the bearing capacity. In accordance with the relationship between the pressure index of water resources balance and the water resources security, 5 grades are divided (see Table 1).

With the result of supply-demand analysis of the regional water resources, the insecure regions ($W_{ds} \geq 1.15$) caused by water scarcity are selected as the potential water receiving areas and the selection of them can be seen in Table 3.

3 ESTABLISHMENT OF MODEL

Water transfer will have great effect on the future development of the water transfer areas and the water receiving areas. Therefore, the rationality analysis of the inter-basin water transfer involves every aspect such as the water resources of the water transfer areas and the water receiving areas, society, economy and ecological environment etc., of which the essence is a multi-goal decision making problem. The study on the establishment of an optimal system of water resources in Pan-Basin which is based on inter-basin water transfer is a research on water transfer scale and rational water allocation of the western route project of the south-to-north water transfer, carried out respectively from the angles of the optimization of total diverted water volume, the scale of water transfer, the optimization of project layout and water allocation.

3.1 Goals of model optimization

3.1.1 Goal of minimum integrated water deficit

The comprehensive allocation model of pan-basin water resources built under the condition of inter-basin water transfer connects all of the potential water receiving areas and water transfer areas as a unified whole. Take the minimum integrated water deficiency ratio of the pan-basin system (or the highest security degree of integrated water resources) as the goal:

$$\min f = \sum_{i=1}^n \left[\omega_i \left(\frac{W_d^i - W_s^i}{W_d^i} \right)^\alpha \right] \quad (2)$$

where ω_i is the weight of sub-region's contribution to the goal, decided by AHP method on the basis of the criteria of economic development goals, population, economic scale, environmental condition; W_d^i , W_s^i are regional water demand and water supply volume; α ($0 < \alpha \leq 2$, taking value of 1.5) is power exponent used for reflecting the principle of water resources allocation. If α increases, the water deficiency degrees in sub-regions become more

approximate to others and the water allocation is more equitable; otherwise, the allocation is more efficient.

3.1.2 Maximization of integrated net benefit of water transfer

The integrated benefit of water transfer includes the profits of water receiving areas and the loss of water transfer areas. The maximization of integrated net benefit of water transfer is the maximum difference between the profit and the loss after water transfer.

$$B = \text{Max} \left(\sum_{i=1}^2 \sum_{j=1}^J \sum_{k=1}^K TB(Q(i,j,k)) - \sum_{n=1}^N \sum_{m=1}^{12} TC(Q(m,n)) \right) \quad (3)$$

where $TB(Q(i,j,k))$ is the profit of water allocation in water receiving area with certain volume of $Q(i,j,k)$, and $TC(Q(m,n))$ is the loss of water transfer area with diverted volume of $Q(m,n)$.

3.1.3 High as possible of water transfer guaranteed rate

Many factors of the complicated water resources system have the property of uncertainty, and the uncertain change from a single factor or from the combination of multiple factors could cause target risk of water transfer project. With certain diverted water volume, the highest guaranteed rate of water transfer should be satisfied.

$$\text{Pr} = \text{Max}(1 - (P(Q < Q_0))) \quad (4)$$

where Pr is the probability when the diverted water volume satisfies the designed volume, and $P(Q < Q_0)$ is the probability when diverted water volume Q is less than the designed volume Q_0 . The diverted water volume and project scale which satisfy the three goals are the optimal diverted water volume and project scale.

3.2 Constraints and principles of model

3.2.1 Water transfer areas use water first

In order to keep the stability of water resources system and guarantee the safety of water transfer areas, the usage of water should be prior in water transfer areas.

$$W_{dsd} < KW_{dsr}, \quad \text{and} \quad K \leq 0.5 \quad (5)$$

where W_{dsd} , W_{dsr} are pressure index respectively in water transfer areas and receiving areas.

3.2.2 Keep the stability of water resources system

In order to maintain the stability and harmony, each unsafe water resources area will be out of unsafe state after water transfer, and the pressure indexes will approximate to others.

$$W_{ds} = w_d/w_s < 1.2 \quad (6)$$

$$w_{ds}^i \approx w_{ds}^j \quad (7)$$

where w_{ds}^i , w_{ds}^j are pressure indexes in different areas respectively; The pressure index is the ratio between practical bearing status and water resources bearing capacity.

3.2.3 Supply water to instream first

Water utilization in the Yellow River Basin has exceeded its bearing capacity for a long time, and has caused a series of ecological environment problems. After water transfer, it should be guaranteed that the ecological environment has the priority of water supplement.

$$W_{dsor} \geq \gamma W_{dsir} \quad (8)$$

where W_{dsor} , W_{dsir} are respectively the pressure indexes in and out of the river course, and $\gamma(\gamma > 1)$ is multiple proportion. The bearing capacity of the in-stream water resources should be no less than the bearing capacity of off-stream water resources in a certain multiple proportion, and the water resources pressure in the river course should be no more than the pressure out of the river course, otherwise the diverted water should be supplied to in-stream first.

3.2.4 Use water efficiently

The allocation of diverted water is realized by weight ω_i under the principle of efficiency priority. According to the water deficiency analysis in unsafe areas in the Yellow River Basin, the levels of ω_i determined by AHP method are as follows: the first level is metropolitan city in which water deficiency effect is severe and affects domestic water use, its importance is 9 and weight $\omega_i = 1.9$; the second level is large city in which water deficiency of key industry affects industrial development and eco-environmental water consumption of instream, its importance is 7 and weight $\omega_i = 1.7$; the third level is small city in which water deficiency affects water consumption of general industrial development, its importance is 3 and weight $\omega_i = 1.3$; the fourth level is country in which water deficiency affects agricultural irrigation and the development of irrigated areas, its importance is 1 and weight $\omega_i = 1.1$.

3.3 Establishment of model system

The model system consists of a three-layer framework in whole-part structure and goes deep into the problem layer upon layer. First it solves the water transfer problem on macro level, and then it solves the problems such as project layout for water transfer and water allocation in sectors etc. on medium level, finally it solves the problem of rational water resources regulation of water transfer project and the problem of optimal water allocation in water receiving areas on micro level. In the model, solutions of upper layer will be input to lower layer as inner parameters, and by parameter transfer the model is nested layer upon layer.

According to Table 2, it shows that from model 1~3 the degrees of freedom and the space for optimal operation increase, thus it can be expected to obtain a better optimal result and a higher target value. Meanwhile the difficulty of operation especially of the symbolic solution (analytical solution) increases greatly.

Model M0, coordinating water transfer areas and water receiving areas, determines the total diverted water volume Q_{sum} based on optimization of minimum goal of integrated water deficit. On the basis of water transfer scale given by M0 and in accordance with the layout and the scale of each project which are optimized by the water transfer guaranteed rate and investment scale, M1 satisfies the constrains of project optimization $Q_{sum} = \sum_{n=1}^N \sum_{m=1}^{12} Q(m,n)$ and $P(Q) > P_0$. Model M2 is a time-space operation model which on the basis of benefit maximization of water allocation, optimizes the allocation of total diverted water and satisfies the constrain of diverted water volume $Q_{sum} = \sum_{i=1}^2 \sum_{j=1}^J \sum_{k=1}^K Q(m,n)$, where $i = 1, 2$ is water allocation in and out of river course, $j = 1, 2, \dots, J$ is water receiving areas, $k = 1, 2, \dots, K$ is water allocation sectors, i, j, k are all free variables. Thus, the essence of M2 is the optimization of

Table 2. Water resources optimization model system of water transfer projects.

Sub-model	Model objective	Model function	Fixed parameters	Variables
M0	overall coordination model	water transfer project scale optimization, water allocation optimization	α	Q_{sum}
M1	water transfer projects optimization	water transfer projects layout and engineering scales optimization	n	$Q(m,n)$
M2	water allocation for water receiving areas	water allocation for river In and Off stream	γ	$QP(i,j,k)$
M3	Input-output optimization	Model solution module	$\lambda(i,j,k), \theta(m,n)$	B

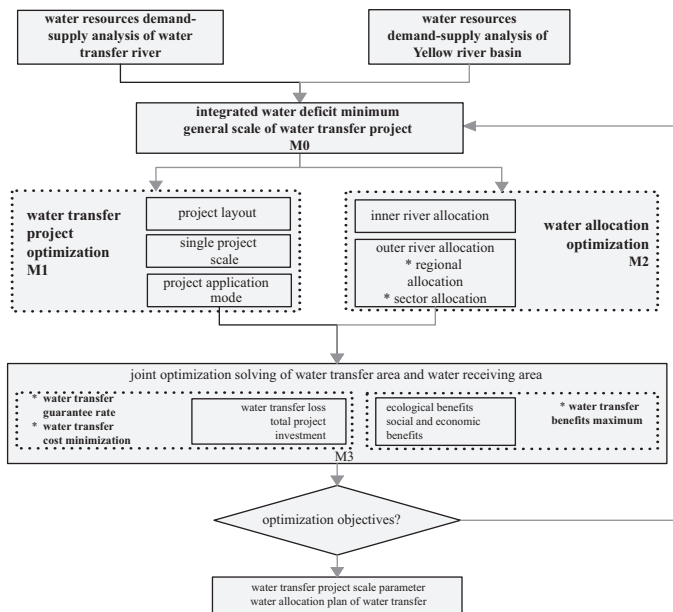


Figure 1. Model structure and flow chart.

water resources $QP(i,j,k)$ in three-dimensional space. Model M3 is a decision support module of interval analysis of solving model, which through the analysis and comparison of the marginal input of each engineering, marginal cost of water transfer areas and marginal benefit of water receiving areas, operates the analytical subprogram to determine the optimal scenario.

4 GENERALIZATION OF PAN-BASIN WATER RESOURCES SYSTEM

The western route of south-to-north water transfer diverts water from the main stream and tributaries of Yalong River and Dadu River. The engineering consists of 7 reservoirs and many water conveyance tunnels, with which the water conveyance sub-tunnels connect at each diversion junction. The diverted water flows into the Yellow River from its headwater and is allocated to water receiving areas through the major reservoir in the main stream of the Yellow River. In order to generalize the pan-basin system, the entities can be abstracted and simplified as conceptual elements expressed by parameters, and a framework is established to describe the hydraulic connection and water transportation in and between every kind of elements, which lays a foundation for mathematical model of the system. In accordance with the adjusting and storing of diverted water and the hydraulic connection of water supply in the Yellow River Basin, the inter-basin water transfer system can be generalized as six kinds of basic elements including water transfer river, water transfer project, water transfer channel, water receiving river, water receiving reservoir and water receiving unit. According to the water system characteristics of the project layout, the water resources allocation system in pan-basin is generalized as a relationship as below.

5 THEORETICAL BASES FOR MODEL OPTIMIZATION

5.1 Principle of decreasing marginal benefit of water resources utilization

Marginal benefit is a useful and significant concept in economical analysis and is a critical parameter for optimal decision-making in the field of economy. According to Western

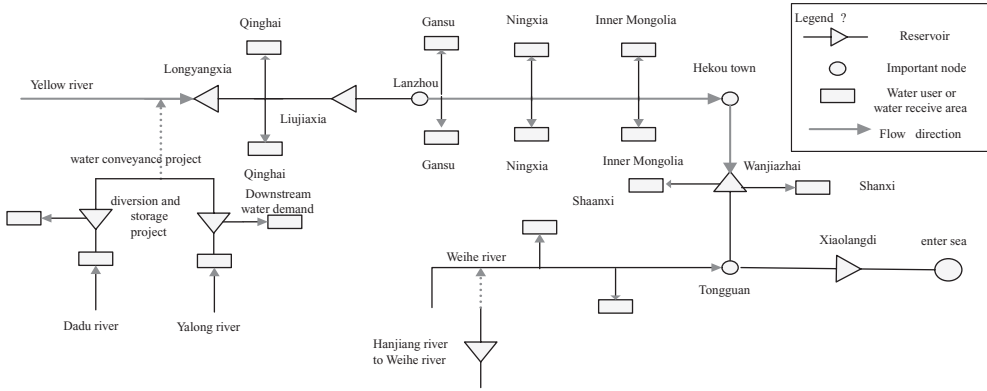


Figure 2. Pan-basin water resources allocation node generalization of south to north water transfer west route project.

Economics, the basic principle for benefit maximization of manufacturers is that the marginal benefit equals to the marginal cost.

The marginal benefit of water utilization means the profit increment brought by increasing every unit of water consumption on the basis of present water consumption under the condition of a certain technical level and the other productive input factors unchanged. Economic principle shows that with unchanged technical level, if one input factor increases continuously and the others keep unchanged, the marginal output will decrease at last.

5.2 Principle of increasing marginal cost of water resources utilization

According to western economics, when the utilization volume of certain rare resources increases, the marginal cost will be caused to rise, which is a semi-U-shape curve. If the utilization volume increases in water shortage area, it will lead to the accretion of marginal cost, that is, the marginal cost MC_w will increase progressively.

The determination of diverted water volume in water transfer areas is based on marginal net profit (NMP_w). The dual action of decreasing marginal profit and increasing marginal cost will cause the marginal net profit to realize a balance at last. According to the maximization goal of net profit in Equation 3, it can obtain by solving the Lagrange extremal function:

$$NMP_w = MP_w - MC_w = 0 \quad (9)$$

where NMP_w , MP_w , MC_w are respectively the marginal net profit, marginal profit and marginal cost. Equation 10 matches the profit maximization condition.

6 SOLUTION OF MODEL OPTIMIZATION

6.1 Solution method of model

In order to solve the super large system problem of optimal water resources allocation in pan-basin, Technology of large system decomposition, progressive optimal algorithm and genetic algorithm are adopted and meanwhile the time-space correlation of flow is properly simplified to overcome the problem of “dimensionality curse”.

From Figure 3, we can see that the model nests two layers of real coding genetic algorithm in the method of decomposition and coordination of large system. The super system is decomposed into two parallel parts, water transfer area and receiving area, and the two parts are decomposed into several sub-problem, every sub-problem is a single object or

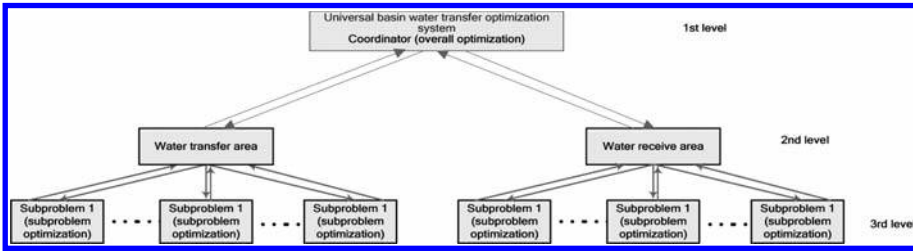


Figure 3. Pan-basin water resources allocation model large-scale system decomposition and coordination.

Constraint for the system. It solves the optimal allocation problems respectively on the levels of pan-basin and water receiving areas and adopts POA method to optimize the problem of reservoir operation mode (see Figure 4).

6.2 Results of model optimization

According to the maximum transferable water volume 10.21 billion m³ of the water transfer rivers, the valid value of water transfer scale is settled as 0~10.21 billion m³, and the GA module of model M0 presently generates the first population of diverted water volume, and iterates them on the basis of crossover, mutation, evolution to solve Equation 1. The total diverted water volume satisfies the maximum transferable water volume and the diverted water volume of each water diversion dam satisfies the transferable water volume constrains:

$$\left. \begin{aligned}
 0 &\leq \sum_{n=1}^7 \sum_{m=1}^{12} Q(m,n) \leq 102.5 \\
 0 &\leq \sum_{m=1}^{12} Q(m,1) \leq 52.7 \\
 0 &\leq \sum_{m=1}^{12} Q(m,2) \leq 7.97 \\
 0 &\leq \sum_{m=1}^{12} Q(m,3) \leq 9.43 \\
 0 &\leq \sum_{m=1}^{12} Q(m,4) \leq 3.23 \\
 0 &\leq \sum_{m=1}^{12} Q(m,5) \leq 12.42 \\
 0 &\leq \sum_{m=1}^{12} Q(m,6) \leq 11.13 \\
 0 &\leq \sum_{m=1}^{12} Q(m,7) \leq 5.17
 \end{aligned} \right\} \quad (10)$$

In accordance with the first population, the model system starts the decomposition and coordination of large system and the model system establishes two parallel models M1 and M2 to calculate respectively the optimal diverted water volume in each water transfer area and the optimal distributed water volume in water receiving area. Based on the long series runoff and the POA method, M1 sets an initial curve V_t^k ($t = 1, 2, \dots, n-1, n$) within the allowed scope of water level amplitude of reservoir. It fixes V_{t-1}^k , V_{t+1}^k and adjusts V_t^k (by 0.618 method), which makes the project cost C_d lowest and solves Equation 4. M2 is regional optimization RAGA module. It operates the optimization of diverted water volume

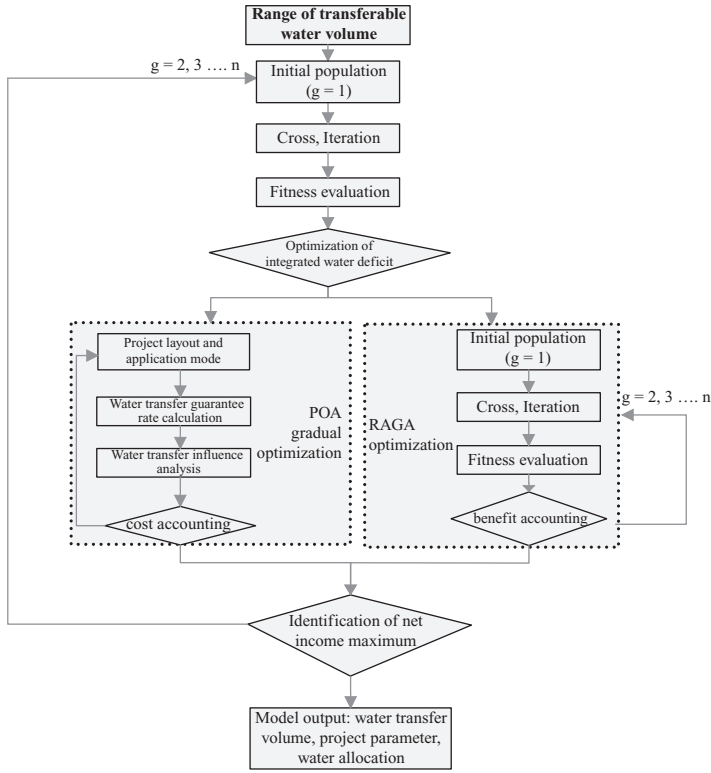


Figure 4. Pan-basin water resources allocation model solving flowchart.

and allocated space, and the volume of water allocation in water receiving areas satisfies the model constrains:

$$\begin{cases} 0 \leq \sum_{i=1}^2 \sum_{j=1}^J \sum_{k=1}^K Q(i, j, k) \leq QS(i, j, k) \\ 0 \leq Q(i, j, k) \leq QS(i, j, k) \\ w_d(i, j, k) / w_s(i, j, k) < 1.2 \\ w_d(1, j, k) < w_d(2, j, k) \end{cases} \quad (11)$$

M3 is economic analysis and optimization of space. The model satisfies the constrains of (3)~(5) and (6), and the model optimization realizes the maximization of Equation 3, which satisfies Equation 10 that the marginal cost of water transfer equals to the marginal profit.

Through the decomposition and coordination of model system and the solution with methods of two-layer nested RAGA and POA, the optimal water transfer scale is 8.23 billion m³.

6.3 Allocation of diverted water

Through the coordination and solution of pan-basin model system, The result of the supply-demand analysis is that in 2030, the diverted water volume in the first stage of the western route project will be 8.23 billion m³, with 5.66 billion m³ water allocate to off-stream and 2.57 billion m³ water to instream. 5.66 billion m³ water of the off-stream will first guarantee the water demand of important cities and energy industrial bases and solve the water resources insecurity problem in major water receiving areas, so the pressure index of water resources demand and supply balance decrease from 1.34 to 1.04, get to a safe level. 2.57 billion m³ water of the in-stream will enhance the condition of ecological and environment of river

Table 3. Water supply and demand balance of Yellow River Basin in 2030 level year after Western Route Water Transfer Project (unit 10^8 m^3).

Water receiving sector	Water receiving area	Water demand	Water supply	Water deficit	Water added	Water shortage	Added water consumption
Off-stream	Qinghai	22.62	16.54	6.56	5.41	1.08	4.35
	Ganshu	47.85	32.85	15.00	13.16	1.85	11.19
	Ningxia	81.41	60.19	22.91	21.91	1.01	13.13
	Inner Mongolia	59.66	43.02	17.03	15.34	1.71	12.52
	Shanxi	23.59	21.80	5.11	4.48	0.63	2.88
	Shaanxi	80.18	60.64	21.89	18.61	3.29	12.55
	Total	315.31	235.04	88.50	78.91	9.57	56.62
In stream		220.00	185.46	34.54	25.66	8.88	25.66

course. Therefore after 8.23 billion m^3 water transfer of west route project of South to North water transfer, situation of the water resources security will improve greatly both in river course and out of stream (see Table 3).

7 CONCLUSIONS

The optimal allocation of diverted water of the western route project is a global problem, and the key technical problems of the western route project of south-to-north water transfer are the selection of diverted water volume and timing for water transfer, the greatest elaboration of water transfer benefit and the rational allocation of diverted water. From the angles of the economy and the society of the basin and the harmony between ecological environment and water resources, the study analyzed the coupling relationship of water resources system, made a research on the conjunctive operation mode of inter-basin super large system and multi water resources, and put forward a scenario about rational scale and optimal allocation of the western route water transfer, which can provide technical reference for the macro decision-making of the western route project of south-to-north water transfer.

REFERENCES

- Feng Yaolong, Lian Jijian, Wang Hongjiang, et al. An Analysis of Rationality of Interbasin Water Transfer by Water Resources Carrying Capability[J]. Journal of Tianjin University, 2004, 37(7): 595–599.
- Gao Hongye. Western Economics[M]. Beijing: China Renmin University Press, 2000: 42–47.
- Lei Shenglong Qin Qiangrong Guo Yuanyu. Self-optimization simulation and its application in the Project of South-to-North Water Transfer[J]. Journal of Hydraulic Engineering, 1989,(5): 1–13.
- Liu Jianlin, Ma Bin, Xie Jancang, et al. Simulation Model of Multi-reservoir and Multi-consumer and Multi-workfor Water Unite Regulation of Cross-drainage Basin—For example of the east route of the south-to-north water transfer project[J]. Journal of Soil Water Conservation, 2003, 17(1): 75–79.
- LongAihua, Xu Zhongmin, Zhang Zhiqiang, et al. Analysis on Marginal Revenues Model of Water Resource Spacial Balanced Allocation —Take Zhangye Prefecture as a Case[J]. Journal of Glaciology and Geocryology, 2002, 24(4): 407–413.
- Shao Dongguo. Study on Optimization Decision Models of Interbasin Water Transfer Engineering[J]. Journal Of Wuhan University Of Hydraulic And Electric Engineering, 1994, 27(5): 500–505.
- Wang Jinfeng, Liu Changming, Yu Jingjie, et al. Theoretical models for space and temporal distribution of water resources[J]. Journal of Hydraulic Engineering, 2004, (4): 7–14.
- Yin Hongwei, Li Yong, ZHENG Cuiyong. Water resources allocation model of water receiving area[J]. Statistics and Decision, 2007(23): 38–41.
- You Jinjun, Wang Zhongjing, Gan Hong, et al. Stepwise compensatory allocation of inter-basin water diversion[J]. Journal of Hydraulic Engineering, 2008, 39 (7): 870–876.

Impact of climate change on hydro-energy systems: An overview

R.P. Brenner

Consulting Engineer, Weinfelden, Switzerland

ABSTRACT: Increasing concentrations of the greenhouse gases CO₂, CH₄ and N₂O in the atmosphere, caused by anthropogenic activities, lead to an increase in global surface temperature, which can produce wide-ranging impacts on natural systems, such as the hydrologic cycle. The paper reviews the various consequences of global warming for the Alpine region, namely changing patterns of precipitation (i.e. more in winter and less in summer), reduced total mean annual precipitation, melting of glaciers, and more frequent occurrence of earth surface processes (rock slides, debris flows, larger volumes of transportable materials) in higher altitude catchments, posing serious hazards to storage facilities of hydropower plants (dam, spillway, intakes, communication lines, etc.). Modelling of the discharge from eleven catchments shows a decreasing trend of annual runoff. Compared to the period 1961–1990, hydropower plants are therefore expected to have a reduced energy output in the order of 7% to 11% by 2050, and 20% to 30% by the end of the 21st century.

1 INTRODUCTION

Global warming, attributed mainly to greenhouse gas emissions caused by human activities, is today an accepted fact and believed to have wide-ranging impacts on natural systems, especially also on the hydrologic cycle, which includes precipitation, evaporation, soil moisture, melting of glacier ice, and river flow. Hydropower is a renewable energy source exploiting the head potentials along rivers and is therefore likely to be affected by changes in river flow caused by climate change.

After a review of the salient facts of climate change, this paper addresses the projected impacts of climate change on hydropower facilities and energy production, including a brief look at attempts to model the complex system of climate change and hydrology. The impacts of an increasing temperature on the hydrological system vary from location to location. There are significant differences between, for example, the Alpine and the Mediterranean region or a large tropical catchment. The projections presented here are valid mainly for the Alpine region (e.g. Switzerland and Austria) with partially glaciated catchments and with a snow cover during winter time.

The number of publications on global warming and the projected impacts and risks to the environment and society is overwhelming but there is not much specific information on the impacts of climate change on hydropower (Hänggi & Plattner 2009; ProClim/OcCC 2003). In 2004, larger hydropower plants with a generating capacity of over 10 MW accounted worldwide for over 2800 TWh/yr of consumer energy (i.e. 90% of the renewable electricity) (IPPC 2008). Another 6000 TWh/yr could be obtained from new projects, mainly in developing countries. Hence, hydropower is by far the most important renewable energy and in many countries, i.e. those with mountains and sufficient water, this form of power generation is the principal contributor to the national energy production. Switzerland has 543 hydropower plants with a capacity of at least 300 kW, producing around 35,600 GWh per annum which account for about 56% of domestic electricity production (49% are from storage power plants, 47% are from run-of-river plants along major rivers, such as the river Rhine, and 4% come from pumped storage power plants). Preparations for adaptive measures to cope

with the projected impacts of climate change have therefore a high priority in the politics of energy.

2 FACTS ON CLIMATE CHANGE

2.1 *Greenhouse gases*

Global warming is believed to be the outcome of an increase in the atmospheric concentrations of greenhouse gases (GHGs), resulting mainly from anthropogenic activities. GHGs are heat absorbing gases and the Earth is actually shielded by a natural greenhouse effect keeping the average mean temperature at around 13.5 to 14°C. Without these gases the temperature would be about -19°C. The major component of the natural greenhouse gases is water vapour (H₂O) and it makes the largest contribution to the natural greenhouse effect. The greenhouse gases produced by humans are carbon dioxide (CO₂), methane (CH₄) and nitrous oxide (N₂O). Through the addition of these gases, additional heat can be absorbed, which alters the magnitude of the greenhouse effect. The amount of water vapour in the atmosphere is regulated by the temperature on the Earth's surface. Hence, when the temperature increases additional water vapour will enter the atmosphere, thus amplifying the warming of the atmosphere induced by the anthropogenic GHGs. This causes a feedback effect. Another important feedback is related to natural "carbon sinks", processes that absorb CO₂ from the atmosphere. Land and ocean CO₂ sinks are able to remove about one half of the CO₂ emitted to the atmosphere by fossil fuel combustion and land use change. But it has been observed that the fraction that has been removed by these sinks has decreased over the past 50 years. There are indications that this decrease will continue further under high future emission scenarios. This means that more gases will remain in the atmosphere and even stronger reduction targets must be envisaged (Univ. of Copenhagen 2009).

Greenhouse gases are also emitted from some of the reservoirs of hydropower plants. GHG emissions have been measured since 1993 on reservoirs from different climates (i.e. from cold regions to humid tropical). Relevant is the "net emission" of GHGs, which is the difference in the emissions of the present reservoir and those of the ecosystem before creation of the reservoir. Important are emissions of methane because the global warming potential of CH₄ is much stronger than that of CO₂. Some reservoirs, particularly in Brazil, have indicated rather high gross emissions, but it turned out later that in general the emissions are about the same as from floodplains of similar area as the reservoir. There are also numerous studies claiming that reservoirs actually sequester large amount of carbons, i.e. they are carbon sinks (Tremblay et al. 2004).

The CO₂ content of the atmosphere has increased from a pre-industrial value of 280 parts per million (ppm) to 385 ppm in 2009. The pre-industrial value has been deduced from drill cores in the ice of Antarctica. Switzerland has currently a CO₂ emission of 1.5 per mille of the global total amount. But to this figure about another 70% should be added to account for the so-called "embedded" emissions, which are associated with goods produced abroad and later imported for consumption in Switzerland. At present, the per capita emissions vary widely from country to country. In a world with a global population of 9 to 10 billion people by the year of 2050, the per capita emissions will have to be about 1 tonne of CO₂ per annum to meet the emission reduction targets established to avoid dangerous climate change scenarios. For comparison, the United States have a per capita emission of over 20 tonnes, China has 3.1 tonnes and India 1.2 tonnes of CO₂ per year. Switzerland has about 6 tonnes, and 10.7 tonnes when including embedded emissions (SCNAT 2007).

2.2 *Temperature projections*

The surface temperature of the Earth has increased on all the continents. In the last 50 years the mean global surface temperature has risen by 0.6°C. However, in continental inland regions and in mountainous areas the temperature increase is considerably higher than over the oceans. For example, in Switzerland the temperature increase during the last 100 years

was 1.6°C. The projections for 2050 are a warming of 1.8°C in winter and of 2.7°C in summer. The zero degree isotherm will move up to a 360 m higher elevation (BAFU 2010). The projected temperature increases published in different reports vary to some extent depending on the GHG emission scenario adopted. Projections are usually made for the middle and the end of the 21st century. The difficulties to make such projections stems from the great uncertainties in the future economic and social developments and whether society will abide by the restrictive energy policies which are needed to arrest climate change.

The 4th report of the Intergovernmental Panel on Climate Change (IPCC 2007) assumes a global increase of the mean surface temperature for the next 100 years of between 0.6°C and 4.1°C and expects a significant change in the water resources in different parts of the world. Other predictions foresee for 2100 a temperature increase in summer by 3.5°C to 7°C compared to the control period 1980–1999, assuming the GHG emissions will not be reduced rapidly (OcCC 2007). A major problem is also the persistence of the GHGs. Their concentration will not decrease suddenly when man-made emission are cut to zero; they will decrease very slowly (Univ. Copenhagen 2009).

Warming in Switzerland, up to the year 2050 is expected to amount to 2°C in winter and 2.5 to 3°C in summer. The target set by the Swiss Government, however, is to limit the temperature increase to 2°C compared to pre-industrial conditions.

2.3 *Precipitation and runoff*

Predictions of changes in the amount (volume), form (rain or snow) and distribution pattern in mountainous regions (e.g. the Alps) are difficult because of variable and complex topographic conditions (Hänggi & Plattner 2009). Up to about the year 2000, there was a general consensus in Switzerland that there would be an increase in total precipitation which could result in an increase of the hydro-electric potential. Records of the 20th century actually showed that the winter precipitation in the northern and western parts of the country had clearly increased. Based on this trend, a potential increase in production of 26% was projected for the hydro-electric scheme of Grand Dixence, for the period 2031–2060 (Westaway 2000). Some years later, however, new climate models became available and it was realized that total annual precipitation would decrease (Frei 2004). For the year 2050 a reduced hydro-electric potential of about 7% was then projected (Horton et al. 2005). According to OcCC (2007) projected changes in precipitation for the year 2050 are: winter +8% and +11%, and summer –17% and –19% for the regions north and south of the Alps respectively. By the year 2100, the mean summer precipitation could reduce by as much as 30%. Hence, hydropower plant operators will have to make arrangements for living with a reduced availability of water. The reduced total annual precipitation is attributed to increased evapotranspiration caused by the higher temperature. Changing patterns of precipitation in Switzerland are recognized only slowly and up to now there are no clear trends indicating a decrease in the mean annual precipitation, which is 1240 mm. This is the same as in the control period of 1961–1990. This amount corresponds about to the volume of Lake Constance with 48 billion cubic meters (OcCC 2008).

On a global scale an increase in the volume of precipitation was observed in northern Europe, in the East of North and South America and also in parts of Asia. Reductions in rainfall were recorded in the already dry areas of the Mediterranean region and in the Sahel zone.

The greatest changes in the hydrological conditions can be expected for catchments in Alpine regions located at medium to high altitudes. These are areas which are partially covered with glacier ice and which are alimented with a significant volume of snow during the winter season. Melting ice and snow contribute a fairly large amount of water to the catchment discharge. As a result of global warming, precipitation in winter will increasingly be in the form of rain. Hence, runoff will increase in winter, i.e. the runoff regime changes from nival to nivo-pluvial.

Climate change will also bring an increase in extreme precipitation events accompanied by floods in the lowlands. The prediction of the timing and location of such events is very difficult. Available statistics clearly indicates that the mean rainfall intensity has increased and that since the begin of the 20th century the frequency of intense rainfall events north of the Alps has grown by 15% to 70% (OcCC 2007).

2.4 *Snow and ice resources*

Extensive regional investigations have revealed that the ablation and deterioration of alpine glaciers has accelerated. Since the historically highest advance of the glaciers in 1850, the alpine glaciers have lost about 0.5% of their volume every year. Between 1980 and 2000 the losses increased to 1% per year and meanwhile they have grown to between 2 and 3%. In the extremely warm summer of 2003 an estimated 8% (5 to 10%) of the glacier ice in the Alps was lost (ProClim/OcCC 2005). In particular, the firn regions of some smaller and medium-sized glaciers also disappeared (firn is a material that is transitional between snow and glacier ice, being older and denser than snow but not yet transformed into glacier ice). Subsequently, the remaining ice surfaces were covered by rock dust and turned into a dark colour. This caused a reduction in their ability to reflect solar radiation and the additional heat amplified the melting process. Model calculations predict that by the year 2050 about 75% of the glacier mass will have disappeared.

Global warming will shift the start of snow pack melting to an earlier date, i.e. at the present estimate by about half a month. This will contribute to the diminished runoff predicted for the summer months (July to September). But an additional reduction in runoff will come from the additional evaporation over the areas freed from the ice by the retreating glacier.

2.5 *Sea level rise*

Sea level rise has two components, namely thermal expansion of the sea water (when the oceans become warmer) and melting of the ice sheets in the polar regions and in Greenland. The rate of sea level rise has increased from 1993 to present largely due to the contributions of the ice loss from Greenland and Antarctica. Models to predict the future behaviour of the polar ice sheets are not yet well developed and projections of the amount of sea level rise by the end of the 21st century are highly uncertain. The Greenland ice sheet is losing mass at a rate of 179 Gt/yr since 2003. This rate corresponds to a contribution to global mean sea level rise of 0.5 mm per year. The current rate of total global mean sea level rise is 3.1 mm/yr. New observations on the increasing loss of mass from glaciers result in more pessimistic estimates for the end of the 21st century, i.e. a total rise in the range of 1 m (± 0.5 m) (Univ. Copenhagen 2009).

A dramatic development seems to have taken place in the Arctic in the summers of 2007 and 2008. The surface of the ice-covered area has lost about 2 million km². This creates a feedback effect because the ice sheet will reflect the solar radiation while the ocean water absorbs most of the radiation it receives from the sun. It is believed that changes in ocean heat content will continue to affect sea-level rise for several centuries.

2.6 *Earth surface processes*

2.6.1 *Permafrost*

Warming of the atmosphere also causes the thawing of permafrost areas, also known as perennially frozen ground. Through permafrost thawing, global warming controls slope stability, landscape evolution and the natural hazard potential in mountainous regions (Gruber & Haeberli 2007). In Switzerland permafrost can be expected in regions above about 2500 m asl. According to observed temperatures in boreholes in high altitude permafrost regions, the atmospheric temperature increase has warmed up steep bedrock slopes to a depth of 60 to 70 m (Harris et al. 2003).

In bedrock with permafrost, fractures and joints are usually filled with ice. Warming causes loss of bonding by the ice, hydrostatic pressures, and a reduction in shear strength. As a result large rock slides can develop which will travel down the slope far into the protecting forest. Permafrost degradation is faster and deeper near a ridge or a peak than in a slope. Forecasting destabilization of a permafrost steep slope is difficult because of the heterogeneity of its surface and the variable subsurface conditions. Also, contrary to glaciers, permafrost disappears only slowly, even if the surface has warmed to positive annual temperatures.

Thawing of permafrost in gently sloping areas of a catchment will liberate previously frozen loose material and increases the volume of materials transportable by water. This will augment sediment transport into reservoirs.

2.6.2 *Mass movements (debris flows, landslides), erosion and sedimentation*

Mass movements occur in various forms. Most devastating are debris flows. They can be triggered by extremely heavy rainfall, whereas landslides need a longer period of cumulative rainfall of medium intensity. Debris flows can be described as a flowing slurry composed of various proportions of granular soils, clay, organic material, and water. Their travel distance depends on the availability of water. They not only leave an ugly scar along their travel path but they can, when entering from a side valley, block the flow of the river in the main valley either upstream of a dam or downstream. This will create a lake which when left unattended will eventually be breached and release a flood wave travelling into the reservoir or down the valley. Lakes from mass wasting can also be created in a side valley when at the toe of a landslide sufficient debris has accumulated. Also broken off ice can block a river and impound a glacier lake, which eventually may be subject to a glacier-outburst flood.

Another hazard with mass movements is the sudden plunging of rock- snow- or ice masses into the reservoir or into a landslide lake in the catchment. This will rise the lake level by a few centimetres and the resulting impulse waves travelling to the shoreline and towards the dam can cause substantial damage. The most severe scenario would be an overtopping of the dam. Calculation methods to estimate the height of such waves are available (e.g. Huber 1982, 1984).

The increased availability of loose material in the catchment above a storage facility will enlarge the transported volume of bed load and floating debris, leading to accelerated reservoir sedimentation. The active storage volume will gradually be diminished. Also, when atmospheric warming will push the snowfall to higher altitudes, the area previously covered by snow will become exposed to erosion by rainfall. The eroded material will contribute to a larger suspended sediment load from tributaries. Particularly troublesome are turbidity currents. They occur regularly with flood events and transport large volumes of already deposited sediment masses along the thalweg of the reservoir, as far as the dam where they can impair the operation of the outlet facilities (bottom outlet and power intake). Oehy & Schleiss (2003) tested some innovative methods to disperse or re-direct turbidity currents in the reservoir. Considered were devices such as a floating geotextile curtain, a vertical bubble curtain, but also an inclined water jet on the reservoir bottom and an obstacle.

An additional factor which can generate difficulties at dam sites and should not be overlooked is hurricane-force wind. It can cause extensive damage in forests and the tree logs felled by the storm will later turn up as drift wood in the reservoir and block the spillway gates.

3 MODELLING CLIMATE CHANGE IMPACTS

For hydropower owners or stakeholders and plant operators the assessment of climate impacts from relatively simple global climate models are not very useful, because the results are expressed only as trends or mean values. For example, the coarse resolution Atmospheric Ocean General Correlation Models (AOGCMs) are not able to resolve spatial scales of less than about 300 km. This is far too coarse for realistically simulate events and the detailed spatial structure of variables like temperature and precipitation over heterogeneous surfaces, such as the Alpine region. In addition, stakeholders require integrated studies of the complex interrelationship climate change—hydropower production, taking into account hydrology and topography of the region and as well power plant-specific aspects. The results of such model experiments will then furnish the basis for decision makers regarding investments for possible adaptive and/or mitigating measures. More information is also desirable on the frequency and magnitude or the duration of extreme events (floods, droughts, extremely cold weather, and vigorous atmospheric motion (hurricane-force winds).

The European Union has initiated the research project PRUDENCE (Prediction of Regional Scenarios and Uncertainties for Defining European Climate Change Risks and Effects) to provide high-resolution climate change scenarios for 2071–2100. These Regional Models (RCMs) have a resolution of about 50×50 km. For making climate change projections, these RCMs are driven by the global AOGCMs. The combination of several different climate models will allow a quantifications of uncertainties.

The Laboratoire Hydrologie et Aménagement (Hydram) of the Federal Institute of Technology in Lausanne, Switzerland, has conducted a study with the objective to obtain information on the impact of climate change on the supply of energy from hydropower. They developed one of the most advanced models for the alpine region and tested it in eleven different catchments located in seven different hydrologic regions (Horton et al. 2005; Piot, 2005; Schaepli 2005; Schaepli et al. 2005). These catchments have at present a glaciation between 0 and 50%. Their areas are between 39 and 185 km², and their average altitudes are between 1340 and 2940 m asl. The hydrological response of a catchment to a given climate scenario was simulated through a conceptual reservoir-based precipitation runoff transformation model (Schaepli 2005). The simulation was carried out in two steps. In the first step historical data were used to calibrate and validate the model before it was applied to the control period of 1961 to 1990. In a second step, the climatic models were established. Nine state-of-the-art RCMs driven by three coupled global AOGCMs gave twelve climate scenarios for the Alps. These were then coupled with two GHG emission scenarios, namely B2 and A2. Scenario A2 represents a heterogeneous world with preserving local identities and a continuously growing population. This emission scenario can be regarded as pessimistic. Scenario B2 also has a growing population but at a slower rate than A2. Emphasis is on the local and regional level taking into account environmental protection and social justice. This scenario can be viewed as optimistic. The projections were made for the periods 2020–2049 and for 2070–2099. Since there was hardly any difference in the results for the earlier period, an additional scenario corresponding approximately to a global warming of +1°C was introduced. Scenarios A2 and B2 were then employed for the period 2070–2099.

The results obtained from these simulations demonstrate the following: In the alpine region the +1°C global temperature increase corresponds to a rise in regional temperature by 1.2 °C. Precipitation will increase by 6% in winter (Dec.–Feb.) and decrease by 8% in summer (June–August). This means that the discharges will be reduced in summer and slightly increased in winter. Increased melt water flow from glaciers cannot compensate for the diminished precipitation. Peak discharge will be shifted by about half a month to an earlier date. For the 2070–2099 period, precipitation decreases significantly compared to the control period. Changes in the mean discharge are in the range of –12% to –26% for the B2 scenario and –14% to –30% for the A2 scenario. Projections varied greatly between the various climate models considered, which demonstrates that projections based on only one model cannot give a meaningful result (Schaepli et al. 2005).

4 IMPACTS ON DAM SITE AND POWER PRODUCTION

The impacts of global warming to dam sites and hydropower production can basically be divided into two groups, namely (1) hazards to plant components by natural processes intensified by the temperature increase in the atmosphere, and (2) loss in energy production caused by a reduced availability of water. The first group may invoke some adaptive measures to better cope with possible accelerated natural processes or also to mitigate the occurrence of extreme events, i.e. usually floods. Hydropower dams already play an important role in flood control and protection. Power plant operators must foresee higher maintenance costs to adapt to the changing natural conditions in the catchment. Also dam safety inspections must put enhanced emphasis on natural hazards in the area of the dam site.

Natural hazards have been addressed in Section 2.6 and they will affect mainly dam sites in the Alps. Run-of-river power plants in the lowlands may be plagued by sedimentation problems. Table 1 summarizes the more common natural hazards in the Alpine region which are expected to become more frequent due to the thawing of permafrost, melting of glaciers and more rainfall of higher intensity.

Regarding the reduction in electricity production, some projections are rather pessimistic. For example, Piot (2005) reports a production loss for the storage power plants in the period 2020–2049 of 7% caused by the reduced water discharge and Schaepli et al. (2007) show that for the Mauvoisin hydropower scheme, which has the highest arch dam in Switzerland, the expected production loss for the period 2070–2099 amounts to as much as 36%. The operation of the hydropower plants will have to adapt to the changed water availability over the year.

Table 1. Impacts from natural hazards on power plant facilities in the Alpine region.

Natural hazard	Possible impact on dam, appurtenances and reservoir	Possible protective or mitigating measures
Rock fall on parts of the storage scheme	Damage to dam crest, spillway gates, outlet facilities	Application of slope protection measures, removal of loosened rock blocks, monitoring of cracks and possible movements
Rock/earth slides or snow avalanches into reservoir	Generation of impulse waves travelling to shoreline and dam, overtopping hazard, rise in lake level by a few centimetres	Removal of potentially unstable zones, drainage of unstable earth masses, monitoring of movements
Broken off ice blocks from glacier impounding a lake	Flood wave travelling down the catchment when ice dam bursts	Removal of water, e.g. by draining it through an access tunnel driven to the lake
Debris flow	Can block tributary valley or main valley and cause landslide lake which eventually may become overtopped	Construction of check dams in the catchment, afforestation where possible, water withdrawal by iron bar screen in the river bed
Increased sediment accumulation in catchment	May later turn into debris flow during periods of heavy rainfall, or transported into the reservoir during periods of high flow, reducing the storage volume	Retention and/or stabilization of sediments by check dams, wire nets, vegetation, etc. Removal where feasible.
Turbidity currents in reservoir	Blocking outlet facilities (bottom outlet, power tunnel intake, etc.) at the dam	Installation of technical devices, e.g. check dam in reservoir, geotextile or bubble curtains
Erosion of ice-free previously glaciated areas	Generation of fine material which can lead to denser turbidity currents	Stabilization with pioneer plants to create a natural protective carpet of humus and roots

5 CONCLUSIONS

Global warming causes wide-ranging impacts on natural, economical and social systems. This also applies to the hydrological cycle and water resources. Although atmospheric warming has been going on since the start of industrialization in the middle of the 19th century, the impact of the small temperature rise by less than 1°C was hardly felt and the release of greenhouse gases caused by human activities was still quite insignificant. Population density was also much smaller. But this scenario has now changed and in recent time CO₂ concentrations in the atmosphere have grown at an alarming pace. Signals of climate change in Alpine catchments are becoming noticeable from the comparison of present data with long-term measurements. Particularly the loss of ice from alpine glaciers is quite dramatic.

Projections for temperature increase have been made until the end of the 21st century using different combinations of climate models and coupling them with GHG emission scenarios. For the alpine region results show a clear increase in atmospheric temperature. This causes a decrease in water availability, especially in the second half of the 21st century. The reduced discharge from alpine catchments will have a distinct impact on both hydropower plants with storage and run-of-river plants, causing a production loss of electric energy.

In the alpine catchments of storage power plants, temperature increase can lead to an intensification and enhanced frequency of earth surface processes, such as the thawing of permafrost, and as well terrain instabilities with mass movements and sediment transport into the reservoir. To protect the dam and appurtenances from such adverse impacts, maintenance efforts around the dam site are required and protective measures may need additional investments. However, it is believed that hydropower stations will be able to adapt to the changes imposed by the global warming.

REFERENCES

- BAFU 2010. *Schweizer Klimapolitik auf einen Blick*. Kurzfassung des klimapolitischen Berichts 2009 der Schweiz an das UNO-Klimasekretariat. Bundesamt für Umwelt, Bern, 19 pp.
- Frei, Ch. 2004. *Die Klimazukunft der Schweiz—Eine probabilistische Projektion*. Inst. f. Atmosphäre und Klima, ETH Zürich, 8 p.
- Gruber, S. & Haeberli, W. 2007. Permafrost in steep bedrock slopes and its temperature-related destabilization following climate change. *J. Geophys. Research*, 112, F02S18, doi:10.1029/2006 JF000547, 10 pp.
- Hänggi, P. & Plattner, Ch. 2009. *Projekt Klimaänderung und Wasserkraftnutzung—Schlussbericht der Vorstudie*. Geographisches Inst. Univ. Bern & Netzwerk Wasser im Berggebiet, WLS Institut, Davos, 42 pp.
- Harris, C., Vonder Mühll, D., Isaksen, K., Haeberli, W., Sollid, J.L., King, L., Holmlund, P., Dramis, F., Guglielmin, M. & Palacios, D. 2003. Warming permafrost in European mountains. *Global Planet. Change*, 39(3–4): 215–225.
- Horton, P., Schaefli, B., Mezghani, A., Hingray, B. & Musy, A. 2005. *Prediction of climate change impacts on Alpine discharge regimes under A2 and B2 SRES emission scenarios for two future time periods*. Bundesamt für Energie, Bern, 84 pp.
- Huber, A. 1982. Impulse waves in Swiss lakes as a result of rock avalanches and bank slides. *Trans. 14th Int. Congress on Large Dams*, Rio de Janeiro, Q. 54, R. 29, 3: 455–476.
- Huber, A. 1984. Mögliche Auswirkungen von Schneelawinen und Gletscherabbrüchen auf künstliche und natürliche Seen. *Int. Symposium Interpraevent*, Villach, 2: 49–59.
- IPCC 2007. *Synthesis Report of the IPCC Fourth Assessment Report*. Metz, B. Davidson, O.R., Bosch P.R., Dave, R. & Meyer, L.A. (eds.), Cambridge Univ. Press, Cambridge, UK.
- IPCC 2008. *Climate change and water*. Bates, B., Kundzewicz, Z.W., Wu, S. & Palutikof, J. (eds.) IPCC Technical Report VI, IPCC Secretariat, Geneva, 210 pp.
- OcCC 2007. *Climate change and Switzerland 2050: Expected impacts on environment, society and economy*. Organe consultatif sur les changements climatiques (OcCC), Bern, 170 pp.
- OcCC 2008. *Das Klima ändert sich—was nun?* Der neue UN-Klimabericht (IPCC) und die wichtigsten Ergebnisse aus Sicht der Schweiz. OcCC—Organe consultative sur les changements climatiques, Bern, 47 pp.
- Oehy, Ch. & Schleiss, A. 2003. Beherrschung von Trübeströmen in Stauseen mit Hindernissen, Gitter, Wasserstrahl- und Luftblasenschleier. *Wasser Energie Luft*, 95(5/6): 143–152.
- Piot, M. 2005. Auswirkung der Klimaerwärmung auf die Wasserkraftproduktion in der Schweiz. *Wasser, Energie, Luft*, 97(11/12): 365–367.
- ProClim/OcCC 2003. *Wasserkraft und Klimawandel in der Schweiz—Vision 2030*. Climate Talk—Dialog zwischen Wissenschaft und Wirtschaft. Tagungsunterlage, Februar, 24 pp.
- ProClim/OcCC 2005. *Hitzesommer 2003: Synthesebericht*. Forum for Climate and Global Change (ProClim), Bern, 28 pp.
- Schaefli, B. 2005. *Quantification of modelling uncertainties in climate change impact studies on water resources: Application to a glacier-fed hydropower production system in the Swiss Alps*. Doctoral Thesis No. 3225, Ecole Polytechnique Fédérale de Lausanne, Lausanne, 209 pp.
- Schaefli, B., Horton, P., Hingray, B., Mezghani, A. & Musy, A. 2005. Impacts potentiels d'un changement climatique sur les régimes hydrauliques alpines. *Wasser, Energie, Luft*, 97(11/12): 346–351.
- Schaefli, B., Hingray, B. & Musy, A. 2007. Climate change and hydropower production in the Swiss Alps; quantification of potential impacts and related modelling uncertainties. *Hydrology and Earth System Sciences*, 11: 1191–1205.
- SCNAT 2007. *Denk-Schrift Energie*. Energie effizient nutzen und wandeln; Beitrag zur nachhaltigen Entwicklung in der Schweiz. Akademien der Wissenschaften Schweiz (SCNAT), Bern.
- Tremblay, A., Varfalvy, L., Roehm, C. & Garneau, M. (eds.) 2004. *Greenhouse gas emissions: fluxes and processes. Hydroelectric Reservoirs and Natural Environments*. Environmental Science Series, Springer, New York, 731 pp.
- Univ. Copenhagen 2009. *Synthesis Report from climate change—global risks, challenges & decisions*. March 10–12, Copenhagen, 39 pp.
- Westaway, R. 2000. Modelling the potential effects of climate change on the Grand Dixence hydroelectricity scheme, Switzerland. *J. of the Chartered Institution of Water and Environmental Management*, 14(3): 179–185.

The Upper Paunglaung RCC dam—design and construction

U. Myint Zaw & U. Thuang Han

Department of Hydropower Implementation, Ministry of Electric Power (MOEPI), Nay Pyi Taw, Union of Myanmar

Ch. Rohrer & K.M. Steiger

Hydropower Plants, AF-Colenco, Baden, Switzerland

ABSTRACT: The paper gives an overview of the Upper Paunglaung project layout and the current situation of the construction and describes how the dam design was adapted for a rapid dam construction. It also describe the challenges of flood protection during construction, the unfortunate weather condition during the wet season, the challenging access to the site for transportation of the construction materials, as well as the initial stages of the RCC mix design and the performance of the RCC full Scale trial embankment in May 2010.

1 INTRODUCTION

The 140 MW Upper Paunglaung hydropower project is owned by the Ministry of Electric Power No. 1 and comprises a 103 m high RCC (roller compacted concrete) gravity dam with Powerhouse located on the left bank at the toe of the dam. It will be the second RCC dam constructed in Myanmar and the first built by local contractors. An ungated spillway is located in the central section of the dam for flood water discharge. The Project situated on the Paunglaung River upstream of the existing Paunglaung Hydropower plant (280 MW) is located 50 km east of the Capital Nay Pyi Taw, in Mandalay Division, Myanmar (Fig. 1).

The purpose of the project is the production of hydro-electric power. The large reservoir with a capacity of 1.3 Mia. m³ represents a seasonal storage and increases the energy production potential of the existing power plant.



Figure 1. Project map.

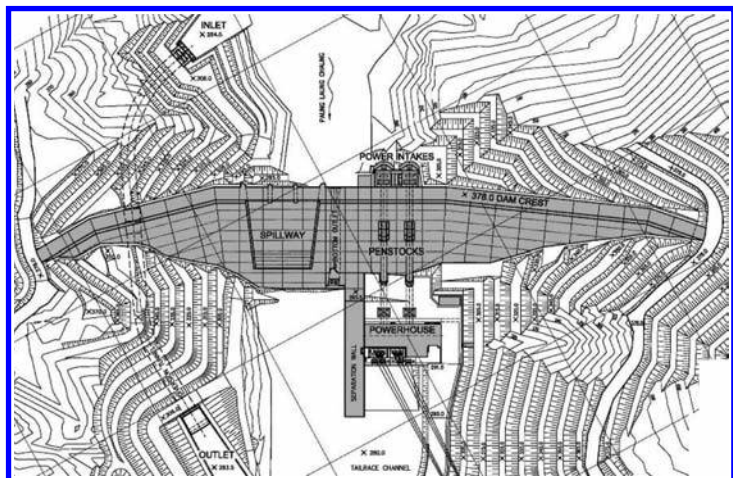


Figure 2. General layout of the Upper Paunglaung hydropower project.

2 PROJECT LAYOUT

2.1 General layout

The general layout of the project is shown in [Figure 2](#). The project essentially comprises a 103 m high RCC gravity dam with an ungated spillway and a bottom outlet, both integrated into the dam body. Two power intakes are placed on the upstream face of the dam. Two penstocks pass through the dam body, which are connected by steel penstocks on the downstream face leading to the powerhouse. A separation wall separates the powerhouse from the spillway and river section. A diversion tunnel is located in the right bank. It will be plugged prior to impounding.

2.2 River diversion

The Paunglaung River is diverted through a 290 m long and 10 m diameter concrete lined tunnel arranged in the right abutment. At the upstream portal an inlet structure with stoplogs is built to close the tunnel under flow. The diversion tunnel will finally be closed with a 20 m long grouted concrete plug before impounding. The diversion tunnel and the 24 m high upstream cofferdam with clay core are designed for flood discharge of 1100 m³/s which correspond to a 10 years flood return period ([Figs. 3, 4](#)).

For higher floods, the advantage of the over-topping capability of an RCC dam and arrangement of its construction sequences is taken into account to keep the work site safe against major damages by floods passing over the river section of the RCC dam. As shown in [Figure 3](#) and [4](#) the diversion tunnel and cofferdams have been constructed and river diversion took place successfully in December 2008.

2.3 Main dam

The main dam is a RCC gravity dam of 103 m height, with a vertical upstream face and a stepped 1:0.8 sloped downstream face. The axis of the dam shows four kinks due to the complicated geological foundation condition. The dam has horizontal inspection and drainage galleries at three elevations, as well as an abutment gallery for grouting, drainage and inspection purpose. The dam is divided into 27 RCC blocks with maximum block spacing of 20 m. The total RCC volume of the dam is 0.95 Mio m³.

Consolidation grouting is foreseen in the entire dam footprint with drilling spacing from 6 m to 3 m. A grout curtain with 10° inclination towards upstream and maximum dept of 80 m is the main feature to prevent seepage though the underground composed of metasandstone and granite. A drainage curtain will be executed downstream of the grout curtain.



Figure 3. Diversion inlet under construction.

Figure 4. U/s cofferdam with clay core.

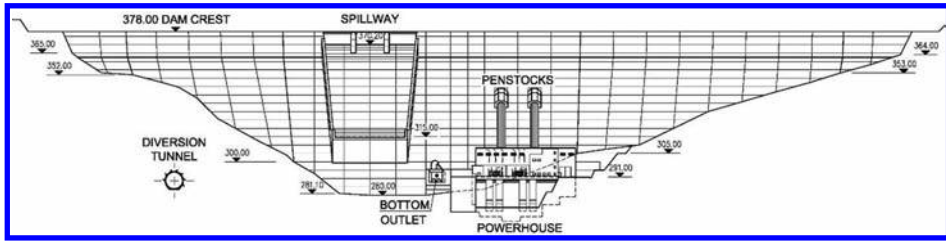


Figure 5. Downstream view of the dam.

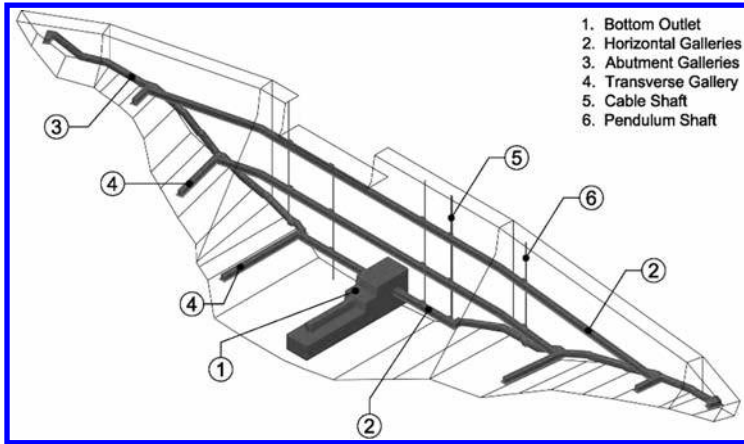


Figure 6. Dam view with grouting and drainage galleries.

For the RCC gravity dam stability analysis as well as detailed finite element analysis has been carried out. The static, dynamic and thermodynamic conditions of the dam body were analyzed.

2.4 Spillway and bottom outlet

The spillway, with a maximum width of 67 m at the ogee crest and a design discharge of 1750 m³/s is integrated in the dam body at the river section. The spillway chute is 75 m long with convergence of 7° on both sides towards downstream and has a flip bucket at its downstream end. The Bottom Outlet with two openings of 3 m × 2 m each is equipped with radial and sliding gates. They are also integrated into the dam body enabling reservoir drawdown or maintaining of riparian discharge during impounding and in the case of both turbines being shut down. The maximum capacity of the Bottom Outlet is 360 m³/s.

2.5 Power intakes and penstocks

The power generation facilities comprise 2 power intakes, 2 steel penstocks and 2 vertical axis Francis turbine and generator units with associated electro-mechanical and auxiliary equipment installed in the open air powerhouse. A section through the dam and power generation system (Fig. 7) indicates that the Power Intake is placed in front of the dam with emergency closure gates and maintenance gates operated from the dam crest. The steel penstocks of 4.8 m diameter are passing through the dam and are connected to the inclined steel penstock on the downstream face of the dam leading to the spiral casings of the 70 MW turbines in the open-air powerhouse just beyond the toe of the dam. The maximum discharge of one penstock is 100 m³/s.

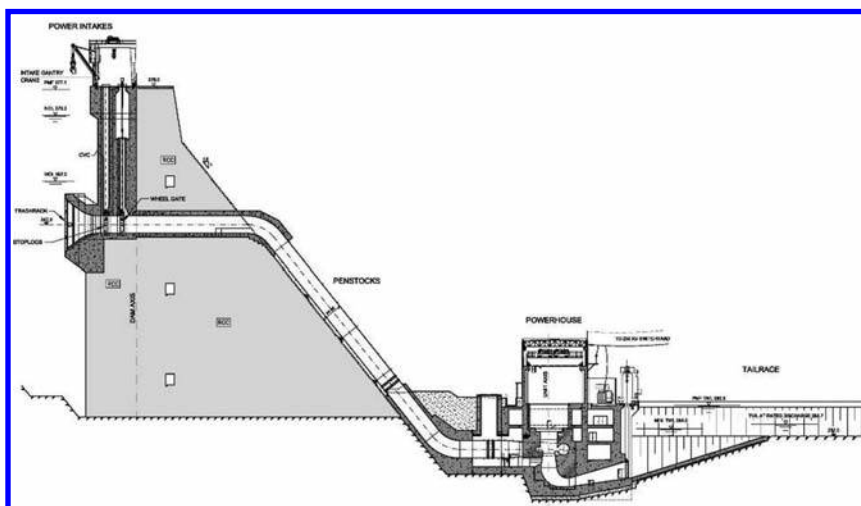


Figure 7. Section through the intake, dam and powerhouse.

3 RCC DAM DESIGN

3.1 *RCC Dam layout and construction sequences*

The RCC dam is divided into right and left part to limit the RCC placing volume per layer and to allow flood protection during construction. An overtopping of the dam in case of high floods during the wet season shall be allowed on the right side of the dam. The left side of the dam where the power generation facilities are located shall never be overtopped. Therefore the left side of the dam is always built ahead of the right side. At the downstream toe of the dam in the river section the separation wall and the downstream cofferdam are protecting the powerhouse construction site. The RCC construction sequences also have to take into account the incorporated structures such as bottom outlet, embedded penstock, spillway and the gallery system. The ideal scenario against risk of thermal cracking of the RCC is the high quality of horizontal joints as well as rapid construction progress within continuous placing. Hence, the planning of the construction sequences of the RCC dam is of utmost significance. The construction sequences of the Upper Paunglaung RCC dam are shown in Figure 8.

Taking into account the local conditions and capability of the contractor, the RCC sequences are defined as follows: RCC stage 1, 2 and 3 are to be built first with short interruptions for the construction of the horizontal galleries. This also allows the contractor to construct the bottom outlet next to RCC stage 1. After completion of stage 3, the intake towers and penstocks will be built, while RCC stage 4 and 5, in the centre of the river will be built. As soon as the upper, horizontal penstock encasement is built, RCC stage 6 shall be constructed. Thereafter RCC stage 7, 8 and 9 will follow, keeping the rule that the left side of the dam is always built ahead of the right side to guarantee flood protection of the powerhouse area.

3.2 *Weather condition*

The weather conditions at Upper Paunglaung site are quite challenging. The mean annual rainfall is in the range of 1700 to 1800 mm. In contrast to the months November to April which are very dry, the months of July to September are affected by heavy monsoon with precipitation almost every day. Hence, appropriate site installations, care of water and especially all-weather access roads are essential for the project. The main tasks are to assure reliable material production and transportation, good quality of work on the dam site and the safety

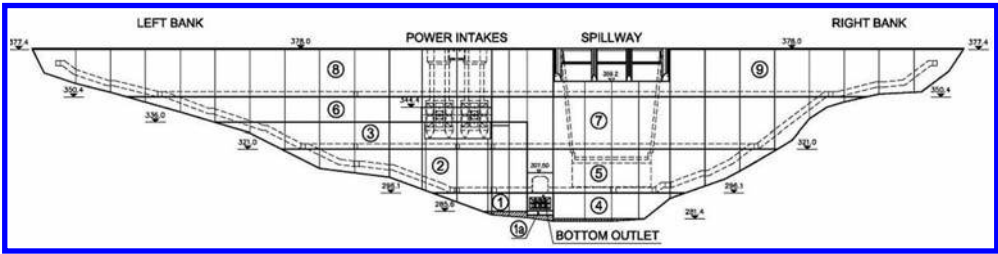


Figure 8. RCC construction sequences.

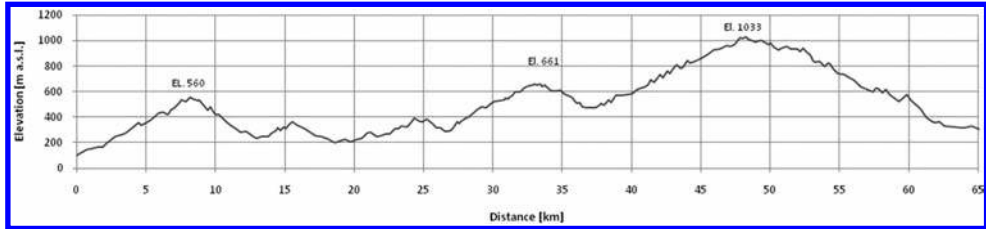


Figure 9. Profile of the access road from Paunglaung Plant to Upper Paunglaung construction site.

for the people on site. One of the goals is to speed up production and construction during the dry season. All the important, critical and difficult structures shall be built during this time and as much preparation works and material storage shall be completed before the heavy rain starts. During the rainy season the progress will slow down or even stop during some time for some of the works like the RCC placing.

3.3 Access and transport

Due to the fact that the project is located some 50 km east of Paunglaung Power Plant in a hilly, sparsely populated area of deep jungle, the access to the construction site is very difficult. The whole area is characterized by deeply weathered rock covered by thick vegetation. The initial construction, the continuous development as well as the maintenance and repair works after the wet season of the 65 km long access road detain a lot of resources, which is the Achilles heel of the whole project. In addition all roads on the construction site as well as the 15 km long road to the quarry need the same attention as the access road.

To emphasize the importance of a proper access road some material flow data over the year is presented. The RCC dam with a concrete volume of approximately 950,000 m³ shall be built within 17 months. That means on average 120,000 tons of aggregates per month have to be transported from quarry to the batching plant. 12,300 tons of cementitious materials (cement and natural pozzolan) have to be transported over the 65 km long access road every month. Assuming the use of 20 ton trucks, an average of 20 trucks journeys are required every day.

3.4 Material management

To ensure a continuous RCC placing, the material transportation and storage has to be planned very carefully. Due to the difficult topographical and weather conditions as well as the long transport distances, interruptions of the material flow have to be anticipated. For each material, storage capacities have to be provided to guarantee a continuous RCC placing. As a result of the hilly and narrow construction site, space is very limited. To provide sufficient stockpile area for the aggregates, several platforms at different locations have to be built. A time span of three months for ordering spare parts, shipment, custom clearance and repair



Figure 10. Aggregates 20 mm-10 mm.



Figure 11. RCC trial mix in the laboratory.

works is assumed to overcome possible problems of equipment in the aggregate production line and to return to full operation again. Therefore a three months aggregate stockpile shall be provided which is at least 360,000 tons. For cementitious materials which will be transported several 100 km to reach the construction site intermediate storage facilities have been installed near the existing Paunglaung plant.

3.5 *Mix design and trial mix program*

Aggregate for the dam construction is limestone from two quarries approximately 15 km upstream of the project. This material has been used for the trial mix program. For the RCC-mix four aggregates proportions are used: one fine aggregate proportion and three coarse portions with a maximum aggregates size of 40 mm. The same Portland cement and natural pozzolan sources as successfully used previously for Yeywa RCC dam have been chosen.

The trial mix program was carried out in two stages at DHPI's (Department of Hydro-power Implementation) Concrete and Soil Laboratory in Paunglaung. The first stage of testing started in September 2009 (Figs. 10, 11), where different cement sources, aggregates materials, various mix proportions and admixtures were tested. At this stage the final quarries and crushing plants for the aggregates production were not yet fully developed. The aggregates had been taken from the rock surface and had been crushed in a temporary plant. Nevertheless the results of the testing program were quite promising. The Stage 2 trial mix program concentrated on the optimization of the mixture proportion as well as testing of leveling concrete mixes. The RCC mix which will most likely be selected is in the order of 70 kg of cement and 160 kg of natural pozzolan.

3.6 *Full scale trial embankment*

A full scale trial embankment was constructed on site in May 2010 (Fig. 12). The purpose of the embankment is to confirm the quality of the RCC mix, in particular the horizontal joints, the performance of the admixtures as well as the workmanship and the reliability of the RCC equipment which will be used for the dam construction. The full scale trial was carried out under very difficult conditions. The first stage of the trial was affected by very hot temperature, shortage of power, problems with the batching plant and lack of ice to keep the RCC placing temperature low. The second stage was characterized by a temperature drop of almost 10°, frequent rain and consequently by contaminated aggregates and finally shortage of aggregates. Despite of this, solutions to all the operating problems could be found. In September 2010 several cores were extracted from the 90 day old trial embankment and tested in compression, tension and also for modulus of elasticity (Fig. 13), indicating acceptable values.



Figure 12. RCC FST embankment.



Figure 13. Tensile testing of RCC cores.

4 CONSTRUCTION IMPLEMENTATION

4.1 Separation wall

In parallel with dam and powerhouse excavation works, site installations and concrete testing, the construction activities continued. After river diversion in December 2008 the excavation in the river bed started and the construction of the separation wall followed. The separation wall is located in the river bed downstream of the dam toe, between the powerhouse and the impact area of the spillway. It is 100 m long, 15 m wide and 25 m high. For ease of construction, to save time and to use the opportunity to use the structure as a first RCC trial, it has been decided to build the wall in RCC (Fig. 14) and not with conventional concrete. The design of the wall has been adapted to correspond with RCC placing. Typical RCC features such as block joints, waterstops and drainage pipes and a gallery system have been introduced for training the RCC laborers. As result, the construction of the separation wall built by DHPI was a great success (Fig. 15).

4.2 Leveling concrete and bottom outlet

Excavation in the riverbed started during the last dry season (2009/2010) and was progressing with the powerhouse excavation. After the excavation, placing of leveling concrete started in the dam footprint. It is the base upon which RCC placing will commence and acts as counterweight for the consolidation grouting. The leveling concrete is built in 20 m wide blocks as for the RCC dam. Leveling concrete placing and consolidation grouting is almost completed at the left side, and placing of RCC can start at beginning of the dry season. At RCC block 15, where the Bottom Outlet is located, a 3 m thick RCC placement has been constructed as base of the Bottom Outlet reinforced concrete structure (Fig. 16). It could also have been built in conventional concrete but the experience has shown that the quality of RCC is as good as conventional concrete and placing is much quicker.

4.3 RCC conveyor system

The concrete plant is located on the left abutment near the dam crest. The plant consists of four twin-shaft batch type mixers, each with a capacity of 3 m³. The theoretical peak concrete production is 500 m³/h. It will be used for conventional concrete and for RCC. A special delivery system has been introduced to allow discharge of the mixer either to trucks or to the RCC conveyor belt. The conveyor belt is the main delivery system to the dam, and runs on the upstream side of the dam axis from the abutment to the centre of the dam. The conveyor is supported by self raising posts. At the end of the system a swinger is installed for loading the RCC onto the dump truck on the placement. At some RCC stages vacuum chutes, short



Figure 14. Separation wall under construction.



Figure 15. Separation wall completed.



Figure 16. Leveling concrete and RCC.



Figure 17. Conveyor belt foundation.

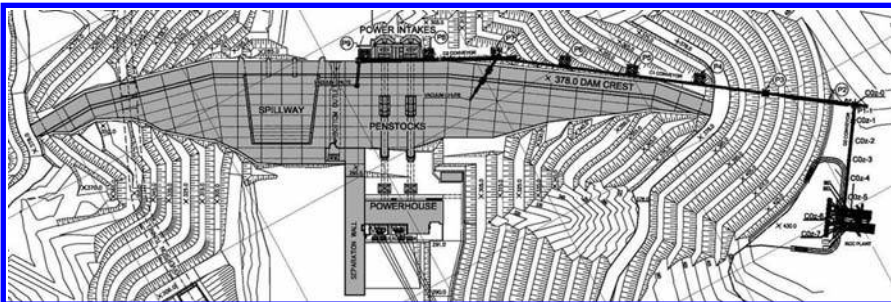


Figure 18. Layout of the RCC conveyor system.

conveyors or temporary trucks will be used in addition. The concrete foundation and post installation of conveyor system has already started (see [Figure 17](#) and [Figure 18](#)).

5 CONCLUSION

The design and construction planning of the Upper Paunglaung RCC dam is based on well established methods, on the experience made in Myanmar and on the experience of the local contractors who have already been involved in a similar project. The original design has been adjusted to suit the local conditions, the available equipment and other limitations. Importance has been given during the design to allow construction of the RCC dam as simple as possible and to assure continuous RCC placing with the aim to guarantee a high quality of the RCC.

Theme C: Dams and natural hazards



Contra Dam, Switzerland (220 m, 1965).

Damage to the Ishibuchi dam by the Iwate-Miyagi Nairiku earthquake in 2008 and seismic assessment

H. Yoshida, A. Nakamura & N. Matsumoto

Japan Dam Engineering Center, Tokyo, Japan

T. Kasai

Tohoku Regional Bureau, MLIT, Sendai, Miyagi, Japan

ABSTRACT: The Ishibuchi Dam is a dumped rock CFRD with height of 53 m, completed in 1953. During the Iwate-Miyagi Nairiku Earthquake in 2008, a seismograph installed on the crest of the Ishibuchi Dam, which was located 9.4 km from the epicenter, recorded maximum acceleration of 14.61 m/s^2 horizontally and 20.70 m/s^2 vertically. However, the concrete facing was largely unaffected, the water storage function of the dam was completely maintained, and the damage to the dam body and the appurtenant structures remained within a repairable range.

This paper presents the damage to the Ishibuchi Dam by the Iwate-Miyagi Nairiku Earthquake in 2008. The paper also introduces the results of performing a dynamic deformation analysis of the rockfill dam, and analyzing contributing factors which could maintain the seismic stability of the dam under such strong motion.

1 INTRODUCTION

The Iwate-Miyagi Nairiku Earthquake in 2008 (JMA magnitude 7.2) occurred at a depth of 8 km under southern Iwate Prefecture (North latitude $39^{\circ}1'7''$, east longitude $140^{\circ}52'8''$) at 8:43 a.m. on June 14, 2008. The earthquake records show 14.33 m/s^2 (EW direction) at the station Ichinosekinishi (IWTH25) of the digital strong-motion seismograph network, KiK-net near the epicenter, while at the Ishibuchi Dam, 20.97 m/s^2 (dam axis direction) was observed on a terrace located just downstream from the Ishibuchi Dam.

2 OUTLINE OF THE ISHIBUCHI DAM

The Ishibuchi Dam, located 9.4 km from the epicenter, nearer than any other dam in the affected area. The Ishibuchi Dam, which is a dumped rock CFRD, was completed in 1953 as a multipurpose flood control, power generation, and water supply dam with height of 53 m, a 345 m long crest, and total reservoir capacity of $16,150,000 \text{ m}^3$. The Ishibuchi Dam is the first concrete face rockfill dam (CFRD) in Japan.

The concrete facing using 10 m by 10 m reinforced concrete slabs is 40 cm, 50 cm, or 60 cm thick depending on the depth of the reservoir. The upstream and downstream sides of the rock zone are made of rubble work compacted adequately to thickness of 5 m and 1.5 m, respectively. [Figure 1](#) shows the standard cross-section.

The reservoir's water level at the time of the earthquake was EL. 314.41 m, which was about 4 m below the full reservoir level (EL. 318 m). A seismometer installed on the crest recorded maximum accelerations of 14.61 m/s^2 in the upstream-downstream direction, 9.34 m/s^2 in the dam axis direction, and more than 20.70 m/s^2 (measured upper limit) in the vertical direction.

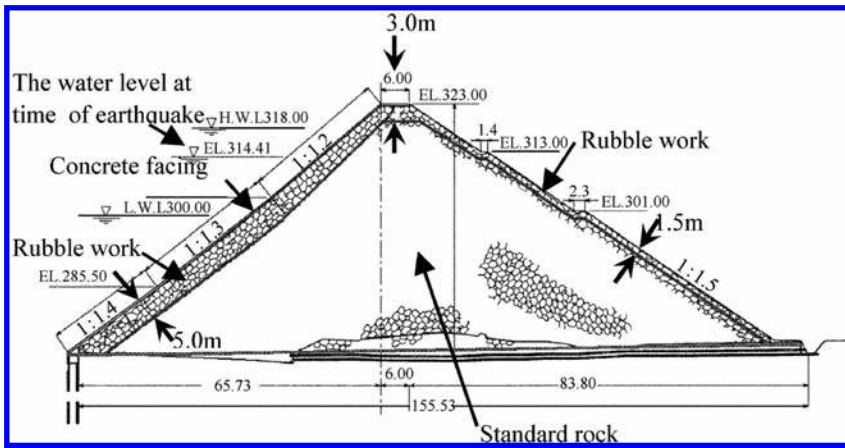


Figure 1. Cross-section of the Ishibuchi CFRD.

The seismograph on the crest is installed on the downstream side shoulder of the crest. This earthquake caused movement in the surrounding rock, which might have impacted the values measured by the seismograph.

3 DAMAGE TO THE ISHIBUCHI DAM

3.1 Concrete facing

According to the emergency inspection of the concrete facing after the earthquake, as shown in Photo 1, no damage was found at either the reinforced concrete slabs or its joints.

An emergency discharge was performed immediately after the earthquake, lowering the reservoir level by about 3 m. In order to determine whether or not the concrete facing was deformed below the reservoir water level, a diver conducted an underwater inspection to check for suction by injecting a tracer along the surface of the concrete facing. The underwater inspection was accompanied by the performance of a boring inspection of the concrete facing to obtain a core sample and a fiber scope was inserted to make sure that the rock behind the concrete slab adhered to the concrete slab. The results of the above inspections did not detect any abnormality on the concrete slabs or its joints.

3.2 Crest

As shown by Photo 2, on the pavement on the dam crest, wavy deformation and cracks were found, there was a gap on the boundary between the handrail and pavement on the downstream side, and a waving level difference of about 50 cm formed on the waves on the crest pavement. Rocks from part of the rubble fell from the edge of the crest on the downstream side.

Piers under the trolley track used to dump the rock during construction of the Ishibuchi Dam were left standing inside the dam body. It was hypothesized that the waving on the downstream edge of the crest formed because the earthquake caused the dam body to settle while the piers did not settle. When locations of the waving were excavated, as expected, piers were discovered.

3.3 Spillway

The radial gate of the spillway was free of damage, even though the water level at the time of the earthquake was EL. 314.41 m at foundation elevation of EL. 312 m. No damage



Photo 1. Concrete facing after the earthquake.



Photo 2. Deformation at the dam crest.

was found on the conduit gate. Horizontal cracks formed on the side of the gate columns at both ends and on the left and right banks. Cracks also formed at the point where the gate column tops were connected to the operating bridge, as well as on the spillway training wall.

4 DAM BODY OBSERVATION RESULTS

4.1 Leakage

Amount of leakage on the riverbed part nearly doubled, from 42 to 98 liters per second, in the aftermath of the earthquake, but later, it stabilized to follow the reservoir water level. And immediately after the earthquake, turbidity of the leaked water was observed, then a few days later, it disappeared.

As shown by [Figure 2](#), leakage on the riverbed part increased after the earthquake, but it was smaller than the leakage measured in 1954 immediately after completion of the Ishibuchi Dam. The relationship between the leakage that occurred after the earthquake and the reservoir water level stabilized at almost the same state as it was in the late 1950s, a few years after completion of the dam.

4.2 Deformation

[Figure 3](#) shows the cumulative settlement along the crest occurring between the completion of the dam and the occurrence of the earthquake. The maximum settlement after the earthquake was about 55 cm at the crest of cross-section No. 20, which is the maximum cross-section. An examination of change in the cross-section shape of the maximum cross-section reveals that, generally speaking, the deformation was large near the crest. Moreover, the entire dam body was deformed toward the downstream side, while the crest was displaced by about 53 cm in the downstream direction.

Focusing on the middle elevation reveals settlement of about 60 cm near the berm on the downstream side and displacement of about 72 cm in the downstream direction. However, on the upstream side, settlement was only about 16 cm and downstream direction displacement was only about 13 cm. Only small deformation occurred on the upstream side, presumably because the rock material was constrained by the concrete slab and the water pressure. This is consistent with the observation that while there was almost no deformation of the concrete facing on the upstream side, unevenness appeared on the downstream side rubble.

Observation of dam body deformation was done later by introducing a GPS based displacement measurement system, thereby strengthening the observation system.

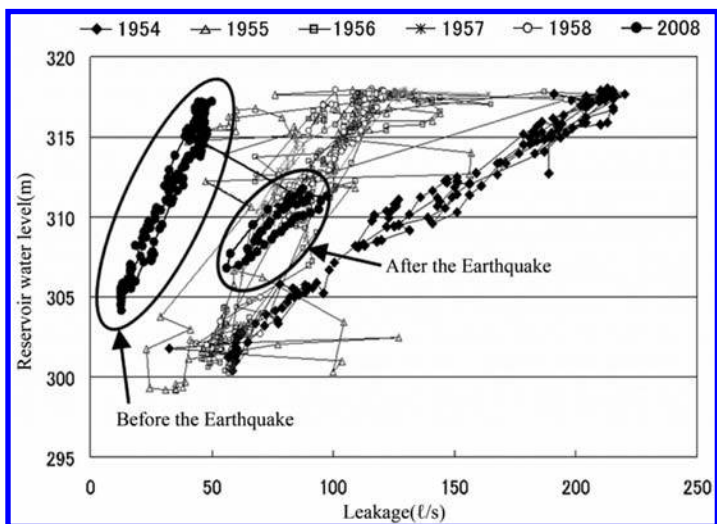


Figure 2. Reservoir water level and leakage history.

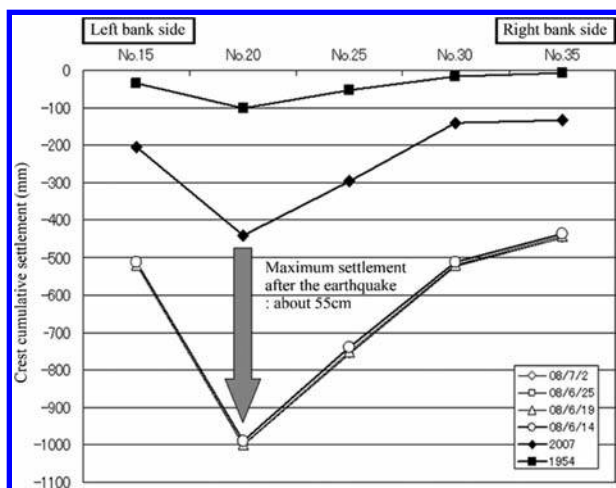


Figure 3. Changing cumulative settlement at dam crest.

4.3 Evaluation of safety

The Ishibuchi Dam Function Evaluation and Inspection Study Committee, consisting of dam experts, was formed after the earthquake to inspect deformation of the dam, evaluate its safety, and to study restoration methods and the impoundment test to confirm safety.

Although the crest and downstream side of the dam body were deformed, large deformation was limited to the higher elevation near the crest. And the concrete facing was free of any serious problems. Moreover, although leakage on the riverbed part increased, after the earthquake its behavior stabilized to follow the reservoir water level. For the above reasons, it was judged that no problem seriously impacting the safety of the Ishibuchi Dam had occurred.

5 RESTORATION WORK AND IMPOUNDMENT TEST TO CONFIRM SAFETY

5.1 *Restoration work*

The Isawa Dam, a central clay core type rockfill dam with height of 132 m, currently under construction approximately 1.8 km downstream from the Ishibuchi Dam, is scheduled to be completed in 2013. The Ishibuchi Dam will be submerged after the Isawa Dam is completed, so the minimum necessary measures were adopted as damage restoration works.

Restoration work was also executed at locations where cracks had formed: the crest, the sides of the gate columns at both the left and right bank ends, the tops of the gate columns, joints of the operating bridge, and so on.

5.2 *Impoundment test to confirm safety*

The reservoir water level at the dam was EL. 314.40 m when the earthquake occurred. Emergency discharge immediately after the earthquake lowered the reservoir level to the normal water level (NWL, EL. 311.00 m), but the impoundment test to confirm safety was done after completion of the repair of the dam crest. The impoundment test was performed by raising the reservoir water level to EL. 317.50 m which is nearly the design high water level (HWL), then lowering the reservoir water level to EL. 314.40 m, which was the reservoir water level at the time of the earthquake. In the meantime, amount of leakage and dam body displacement were monitored and observed, confirming that there were no abnormalities, so the impoundment test was concluded.

The riverbed leakage during the impoundment test found no abnormality. An underwater inspection was done at the maximum reservoir water level to check for locations of suction on the joints or the concrete slabs of the concrete facing. But the quantity of suction was extremely minor, and no evidence of any change of leakage was obtained. These locations were repaired after the reservoir water level was lowered.

6 DYNAMIC ANALYSIS

6.1 *Outline*

The Iwate-Miyagi Nairiku Earthquake in 2008 caused the crest of the Ishibuchi Dam to settle a maximum of 55 cm, which corresponds to about 1% of the dam height. As the Ishibuchi Dam is a dumped rock CFRD, the dam body was not roller compacted. So it is assumed that its settlement would be a little large. At the crest, waviness and cracking of the pavement were observed, but the concrete facing was undamaged, confirming the seismic performance of the dam.

The following is a report on the results of plastic deformation analysis based on dynamic analysis performed in order to discover the reasons why the Ishibuchi Dam escaped serious damage despite being hit by such strong motion.

6.2 *Analysis method*

The dynamic analysis of the residual deformation of the Ishibuchi Dam after the earthquake was performed using the Fast Lagrangian Analysis of Continua (FLAC) (Cundall 1992), to analyze the factors which ensured its seismic performance.

FLAC is a numerical analysis program based on a finite analysis method that can be used to analyze large deformation behavior of embankments. FLAC expresses balance in the form of an equation of motion to obtain nodal velocity based on nodal force, and at the same time, consecutively renews the coordinates of nodes in large deformation analysis. Additionally, FLAC applies the differential method based on the explicit method to achieve an extremely small time step Δt , thereby preventing calculation errors.

6.3 Analysis model, deformation modulus, shear strength

The Ishibuchi Dam analysis model considered only the dam body, handling the water blocking concrete face and the dam body as an integrated body because of computation restrictions.

The maximum section of the dam body was modeled by zoning it into the rubble work installed on the upstream and downstream surfaces and the standard part consisting of the normal rock zone. In case 1 and 2, the rubble work was considered, but in Case 3, it was hypothesized that the dam body was comprised entirely of standard parts in order to study the impact of the rubble work of the dam body, obtaining the dam body displacement in the absence of rubble work by analysis.

The embanking analysis was performed in 14 steps, followed by the filling analysis in 6 steps. Physical values were calculated at each step and the calculated stress was used as the initial stress for the following step.

The Ishibuchi Dam is a dumper rock CFRD, so its density and other deformation modulus and its shear strength are not clearly known. Thus, the deformation modulus and shear strength were set based on the relationship of the shear strength and void ratio of the Isawa Dam (which was constructed using similar rock) obtained by estimating the void ratio based on Ishibuchi Dam work reports.

6.4 Input earthquake motion

The input earthquake motion was the earthquake motion estimated by the PWRI (Yamaguchi et al. 2008). The PRWI estimated the main earthquake motion at the foundation bedrock of the Ishibuchi Dam, by employing the acceleration response spectrum ratio of the right bank terrace/dam foundation based on records of after-shocks in the Ishibuchi Dam observed during the Iwate-Miyagi Nairiku Earthquake in 2008.

The maximum acceleration at the dam foundation was estimated at 4.65 m/s² in the upstream-downstream direction, 6.57 m/s² in the dam axis direction, and 6.21 m/s² in the vertical direction. The measured maximum acceleration at the dam crest was 14.61 m/s² in the upstream-downstream direction, 9.34 m/s² in the dam axis direction, and 20.70 m/s² in the vertical direction.

6.5 Analysis results

The input earthquake motion was 100% and 90% of the earthquake motion which the PWRI estimated in Case 1 and in Cases 2 and 3, respectively. The shear strength of the standard part of the dam body was $\phi_0 = 54.1^\circ$ which is equivalent to void ratio $e = 0.3$. The shear strength of the rubble work was $\phi_0 = 62.0^\circ$, which is higher than that of the standard part. Regarding the damping ratio for the dynamic analysis, considering the radiation damping and material hysteresis damping, radiation damping was set as 10%.

Table 1 shows the results of a comparison of measured and analytical values of maximum acceleration (center of the crest) and dam displacement (dam crest).

In Case 1, the maximum acceleration of the crest was nearly identical to the estimated earthquake motion, but the analytical value of displacement of the crest was higher than the measured values.

In Case 2, the analytical values of the maximum acceleration at the crest were smaller than the observed values because the input earthquake motion was lowered to 90%, but the analytical values of the crest displacement, and the crest settlement in particular, were almost identical to the measured values. Therefore Case 2 was regarded as the results of calculations to reproduce the dam body behavior during the earthquake.

Next, in Case 3, the upstream-downstream displacement of the crest was 0.59 m and settlement was 0.85 m, which was almost 0.3 m larger than the settlement of the crest in Case 2.

The dam body deformations observed in both cases after the earthquake at the Ishibuchi Dam are shown in Figure 4 (Case 2) and in Figure 5 (Case 3). A close examination of the

Table 1. Comparison of measured values and analytic values according to FLAC.

Analysis cases	Input earthquake motion/ shear strength	Maximum acceleration (crest)		Dam body displacement (crest)	
		Horizontal (m/s ²)	Vertical (m/s ²)	Up/ downstream	Vertical (m)
Measured values	–	14.61	20.70	0.53	0.56
Case 1 (Rubble work considered)	Input earthquake motion 100% Shear strength (e = 0.3)	11.12	12.85	1.05	0.77
Case 2 (Rubble work considered)	Input earthquake motion 90% Shear strength (e = 0.3)	8.36	12.76	0.81	0.56
Case 3 (No Rubble work)	Input earthquake motion 90% Shear strength (e = 0.3)	8.85	11.90	0.59	0.85

1 Radiation damping = 10%.

2 Measured value of dam body displacement (crest) is difference between 2007 measured value and post-earthquake measured value.

3 Analytic values of maximum acceleration are output values at each 1000 steps.

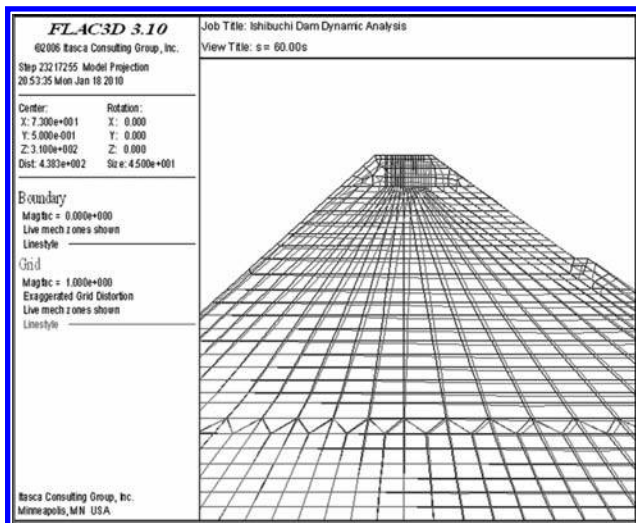


Figure 4. Results of analysis of dam body deformation after the earthquake (Case 2).

dam body deformation after the earthquake shows that in Case 3, deformation was greater than it was in Case 2, with (1) large settlement and deformation near the upstream edge of the crest, and (2) more conspicuous deformation in the downstream direction of the high elevation parts of the downstream side. However, as in Case 2, the dam body deformation after the end of the earthquake was small in parts below the reservoir water level on the upstream side.

The stresses in the upstream rockfill beneath the concrete facing are far below the Mohr failure envelope due to effective confining stress of water pressure and hence the residual strains by cyclic loading are unlikely to occur in this portion (Matsumoto et al. 2000).

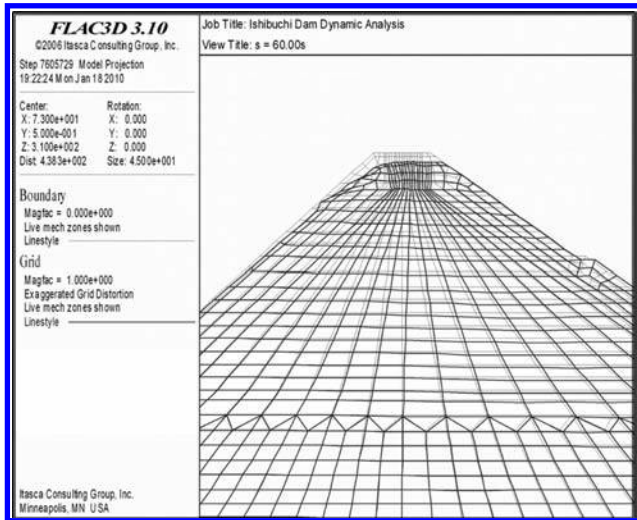


Figure 5. Results of analysis of dam body deformation after the earthquake (Case 3).

For the above reasons, it can be said that the rubble work that was installed on the upstream and downstream sides played an important role in sparing the Ishibuchi Dam severe damage despite the large scale of the earthquake motion that struck it.

7 CONCLUSIONS

1. The Iwate-Miyagi Nairiku Earthquake in 2008 caused the crest of the Ishibuchi Dam to settle a maximum of 55 cm, which corresponds to about 1% of the dam height. At the crest, waviness and cracking of the pavement were observed, but the concrete facing was undamaged.
2. The dynamic analysis of the permanent deformation of the Ishibuchi Dam was conducted to assess the factors which played important role in its seismic performance. The confinement of the upstream rockfill due water pressure and the rubble work both of upstream and downstream are considered to restrict the permanent deformation of the dam body resulting in Ishibuchi Dam sustaining to minimal damage.
3. The friction angle of the materials has much effect on the permanent displacements of rockfill dams subjected to earthquake shaking. Placing the high strength materials in the shallow portion near the downstream face reduces the settlement in this portion.

REFERENCES

- Cundall, P.E. 1992. FLAC, Fast Lagrangian Analysis of Continua, *Itasca Consulting Group, Inc. Minneapolis, Minnesota.*
- Matsumoto, N., Yamabe, K., Sakamoto, T. & Hojo, K. 2000. Seismic Response Analysis of CFRD, *Proc. International Symposium on CFRD, Beijing, ICOLD-CHINCOLD*, pp. 351–359.
- Yamaguchi, Y., Iwashita, T., Hayashi, N., Mitsuishi, S., Otani, T. & Sasaki, S. 2008. Report on Damage to Infrastructures and Buildings by the 2008 Iwate-Miyagi Niriku Earthquake, *Technical Note of Public Works Research Institute*, No.4120, pp. 90–137 (in Japanese).

Effects of vertical earthquake motions on deformation of Newmark sliding analysis

N. Matsumoto, T. Sasaki & K. Shimamoto

Japan Dam Engineering Center, Tokyo, Japan

Y. Sugiura & H.Q. Zhao

CREARIA, Tokyo, Japan

ABSTRACT: Newmark procedure is one of the methods to predict earthquake-induced deformations of embankment dams. It assumes that the sliding mass is rigid and the mass begins to move when the safety factor of the sliding mass becomes less than 1.0 and cease to move when the velocity of the sliding mass becomes equal to the rest of the embankment. Most of the Newmark procedures are based on the equilibrium equation of one-dimensional horizontal motion ignoring the vertical component. According to recent strong motion monitoring, large vertical accelerations were recorded. Hence the inertia force of vertical component is introduced in the paper. By using sinusoidal and recorded earthquake acceleration records, the earthquake-induced deformations were computed and the effects of vertical motion on permanent deformation of embankment dams are described.

1 INTRODUCTION

Newmark proposed the deformation based procedure for the assessment of the seismic stability of embankment dams (Newmark, 1965). In his procedure, an earth mass sliding over a shear surface was modeled as a rigid block sliding over a plane assuming the stress-strain relationship to be rigid-plastic. In reality, embankment materials show volumetric strain and softening property to cyclic loading, so the Newmark procedure is considered as a tool for the first approximation. But in this method input parameters are identical to those of the slope stability analysis and it provides relatively reasonable results which are easily interpreted with clear assumption.

Modifications have been proposed to Newmark's sliding block procedure since its first formulation. In most cases, however, only horizontal accelerations were included with a few exceptions. Yan proposed a rigid block on an inclined plane slip surface and also a rigid block on a circular arc slip surface and in both cases vertical motions are included (Yan, 1991). Later, Yan et al. computed the effects of vertical motion on permanent displacements for two slopes and two earthquake records (Yan et al., 1996). Their results indicate that the introduction of the vertical component can both increase (11%) and decrease (−4%) the calculated displacements. Tateyama et al. introduced the idea of the rotating block (Tateyama et al., 1998) as shown in [Figure 1](#). They gave the equation of motion for the rotating block considering horizontal earthquake inertia force by [Equation 1](#).

$$-J\ddot{\theta} + M_{DW} + M_{DKh} - M_{RW} - M_{RKh} = 0 \quad (1)$$

where θ = angle of rotation; J = Inertia moment; M_{DW} = Driving moment due to gravity; M_{DKh} = Driving moment due to horizontal earthquake inertia force; M_{RW} = Resisting moment due to gravity; M_{RKh} = Resisting moment due to horizontal earthquake inertia force.

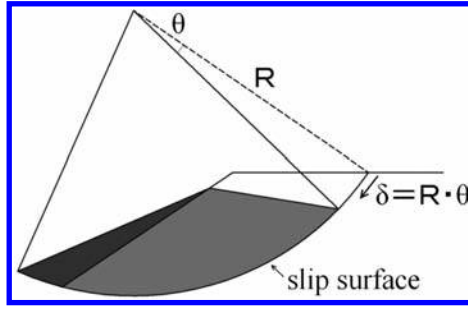


Figure 1. Rotating block.

If we take the vertical earthquake acceleration into consideration, Equation 1 is modified as follows:

$$-J\ddot{\theta} + M_{DW} + M_{DKh} + M_{DKv} - M_{RW} - M_{RKh} - M_{RKv} = 0 \quad (2)$$

where M_{DKv} = Driving moment due to vertical earthquake inertia force; M_{RKv} = Resisting moment due to vertical earthquake inertia force.

The driving moments M_{DKh} and M_{DKv} can be computed from the acceleration distribution of the sliding block directly, or by using the average absolute acceleration k_h and k_v (Eq. 3). Comparing the driving moment from the average acceleration and the inertia force of each element, the difference was recognized as insignificant. Therefore, the average acceleration is used for obtaining the driving moment, hereafter.

$$k_h = \frac{\sum \rho_i \alpha_{hi}}{\sum \rho_i} \quad k_v = \frac{\sum \rho_i \alpha_{vi}}{\sum \rho_i} \quad (3)$$

where k_h = average horizontal acceleration in g; k_v = average vertical acceleration in g; ρ_i = mass of element i ; α_{hi} = absolute acceleration of horizontal component of element i in g; α_{vi} = absolute acceleration of vertical component of element i in g.

The safety factor, F_s , during shaking is given by

$$F_s = \frac{M_{RW} + M_{RKh} + M_{RKv}}{M_{DW} + M_{DKh} + M_{DKv}} = \frac{(1 + k_v)M_{RW} - k_h M_{Rh1}}{(1 + k_v)M_{DW} + k_h M_{Dh1}} \quad (4)$$

where M_{Rh1} = Resisting moment when average horizontal acceleration is 1.0 g; M_{Dh1} = Driving moment when average horizontal acceleration is 1.0 g.

Resisting moment M_{Rh1} , M_{Rv1} can be obtained from the resisting force using normal stresses on the slip surface of the finite element or from ordinary method of slice of the block. Here, the latter procedure is adopted.

In Figure 2, when F_s becomes 1.0, the rotation of the block begins at $t = t_b$ and continues until the driving moment falls below the resisting moment and ends when the velocity falls to zero at $t = t_e$. The angular acceleration can be calculated by Equation 5.

$$\ddot{\theta} = \frac{(1 + k_v)M_{DW} + k_h M_{Dh1} - (1 + k_v)M_{RW} - k_h M_{Rh1}}{J} \quad (5)$$

The displacement or angular rotation of the block will be obtained by integrating the angular acceleration twice.

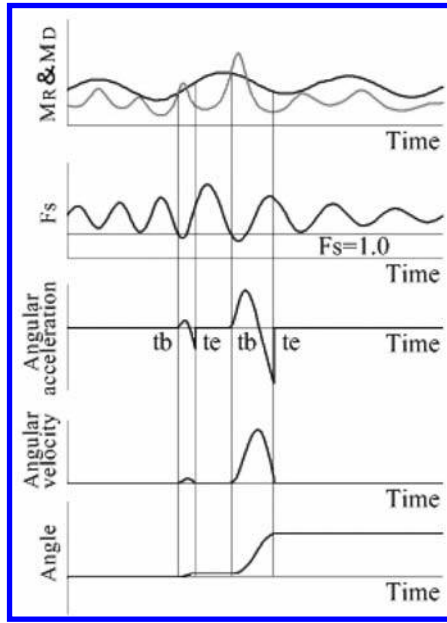


Figure 2. Stick-slip rotation of block mass.

2 ANALYTICAL MODEL AND MATERIAL PROPERTIES

Figure 3 is the finite element mesh used for the two-dimensional dynamic analyses to assess the earthquake-induced deformations. In this figure, 10 circular sliding blocks on the downstream side are shown. The dynamic material properties for each zone are shown in Table 1. Figure 4 shows the normalized modulus reduction ratio of filter and rockfill materials. Poisson's ratio is derived from Equation 6.

Core	$\nu = 0.450 - 0.006Z^{0.60}$	
Filter and rockfill	$\nu = 0.375 - 0.006Z^{0.58}$ (above the seepage surface)	(6)
	$\nu = 0.490 - 0.001Z^{0.95}$ (beneath the seepage surface)	

Where, Z is the depth from top surface of the dam body (m).

The strength for each zone used to calculate the sliding safety factor and sliding deformation are shown in Table 1. The shear strength of rockfill is assumed according to the curved failure envelope formula of $\tau_f = A(\sigma_n)^b$ and the shear strength of the core is expressed as cohesion concept c' and friction angle ϕ' .

3 YIELD ACCELERATION

The combination of the horizontal yield acceleration and vertical yield acceleration when F_s equals 1.0 computed from Equation 4 is shown in Figure 5. It suggests that the deeper the sliding surface is, the smaller the yield acceleration is. This is because of the curved shear strength envelop of the materials which means the internal friction angle decreases with the increase of the confining pressure. The vertical acceleration has greater effects on shallow sliding blocks than on deep ones. This is because the upward seismic inertia force reduces the resisting moment and the friction angle decreases more in the low confining pressure range of the curved failure envelope.

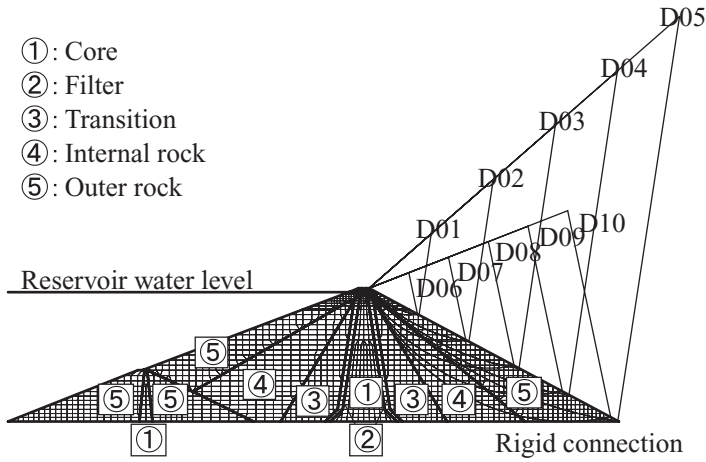


Figure 3. Finite element mesh with material zones and assumed sliding blocks with centres D_{01} – D_{10} .

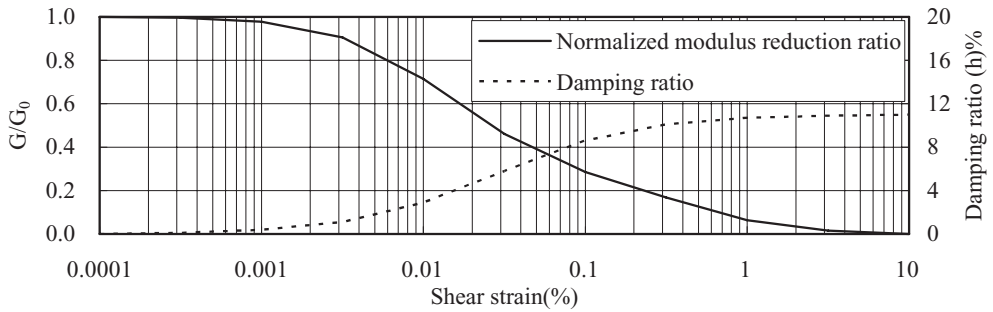


Figure 4. Normalized modulus reduction ratio and damping ratio used for analysis.

Table 1. Material properties for dynamic analysis and strength parameters used to calculate the sliding safety factor and earthquake-induced settlements.

Zone	Total unit weight (kN/m ³)	Shear modulus G_0 in MPa V_s in m/s Z in meter	Shear strength in kN/m ²			
			c' (kN/m ²)	ϕ' (°)	A	b
Core	22.5	$G_0 = 1.3 \times (\gamma_t \times V_s^2 / 9800)$ $V_s = 6.4Z + 314$	12.5	36.5	–	–
Filter	21.8	–	–	–	3.075	0.817
Transition	21.1	$G_0 = 1.3 \times (\gamma_t \times V_s^2 / 9800)$	–	–	3.482	0.805
Internal rock	21.2	$V_s = 5.1Z + 342$	–	–	4.039	0.777
Outer rock	20.8	–	–	–	3.769	0.792

4 EFFECTS OF INPUT VERTICAL MOTION

The response was compared for the case of horizontal motion input only and the case for both of horizontal and vertical motion input. Figure 6 shows the maximum acceleration distribution in the center of the dam with and without vertical motion input using acceleration record of Hitokura Dam in Table 2. The vertical input motion has

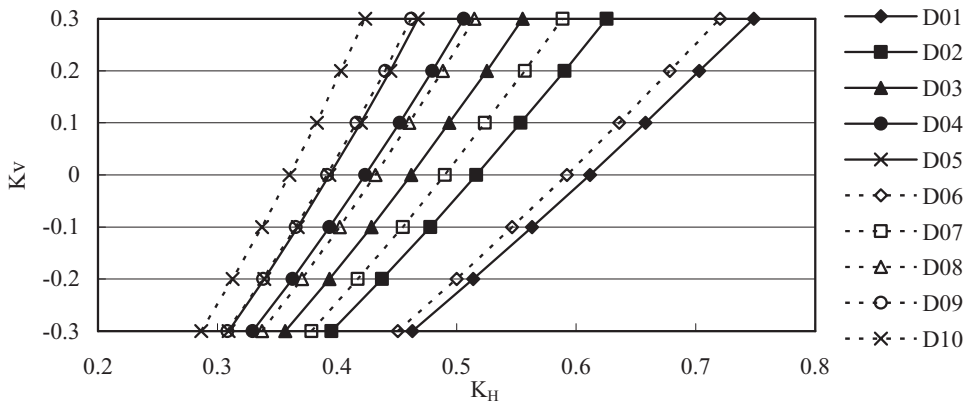


Figure 5. Relation of yield acceleration K_v and K_H .

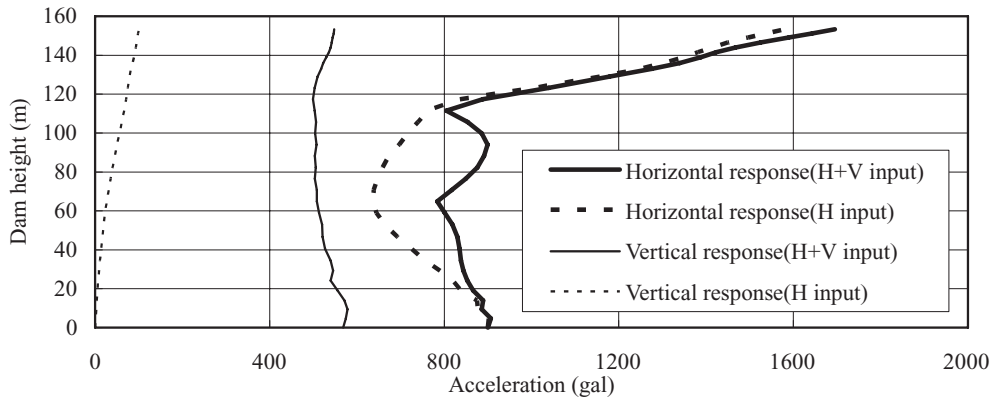


Figure 6. Maximum acceleration with and without vertical motion input.

Table 2. Acceleration records used for the analysis.

Earthquake	Dam	Year	Magnitude	Duration (s)	PGA (gal)			Case no
					Up-down stream	Cross canyon	Vertical	
Kobe	Hitokura	1995	M7.3	10.48	182	168	63	CASE01
Kobe	Gongen			24.00	104	90	66	CASE02
Kobe	Mino			59.21	135	128	80	CASE03
Tottori	Gasho	2000	M7.3	60.00	494	569	485	CASE04
Tokachi	Urakawa	2003	M7.9	173.68	103	100	66	CASE05
Tokachi	Takami			70.41	56	-	41	CASE06
Chuetsu	Sabaishi	2004	M6.8	15.12	230	231	213	CASE07
Noto	Hakkagawa	2007	M6.7	100.00	167	203	167	CASE08
Chuetsu	Kakizaki	2007	M6.8	120.00	170	143	76	CASE09
Iwate-Miyagi	Kurikoma	2008	M7.2	100.00	461	276	402	CASE10

more effects on the vertical response than on the horizontal one. Therefore, when the vertical response is taken into Newmark sliding block analysis, vertical motion input is a must.

5 RESPONSE AND SETTLEMENT TO SINUSOIDAL INPUT MOTION

To study the effect of the phase difference of horizontal and vertical input motions, the sinusoidal motion was used for the analytical model of Figure 3. The period of sinusoidal motion is 0.5 s ($f = 2$ Hz) for both of horizontal and vertical input and maximum acceleration of horizontal and vertical is 0.75 g and 0.5 g, respectively. The phase was staggered by $\pi/4$ for horizontal and vertical inputs.

Horizontal input: $A_h(t) = 0.75g \sin(2\pi ft)$

Vertical input: $A_v(t) = \sin(2\pi ft + n\pi/4)$

where, $n = 0, 1, 2, 3, 4, 5, 6, 7$ and $A_v(t) = 0$

The duration of the motion is 5.12 s and the envelope coefficient was multiplied by the sinusoidal input. Figure 7 shows the vertical input motions in the cases, $n = 0$ (phase difference 0) and $n = 4$ (phase difference π).

Figure 8 shows the settlements of sliding block D03. Here, the settlement is defined as the vertical displacement at the upper tip of the sliding block as a result of its rotational

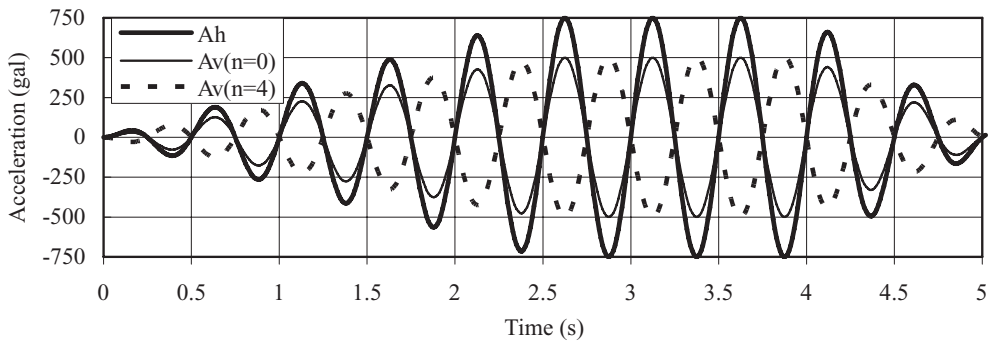


Figure 7. Sinusoidal input motion with phase difference.

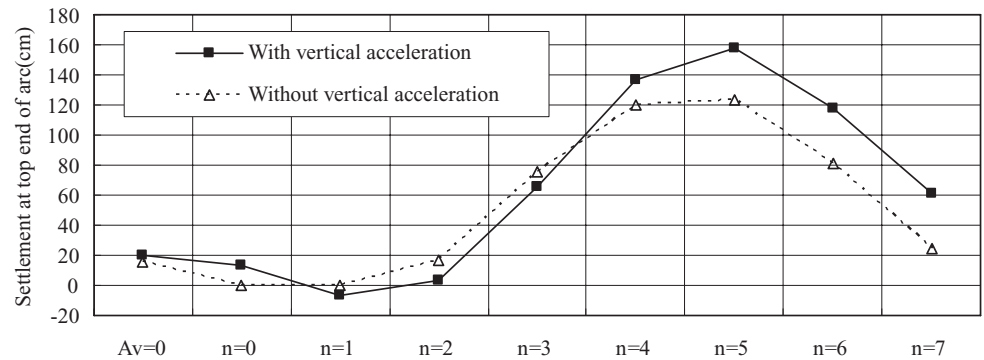


Figure 8. Settlement of sliding block D03 to different phase vertical motions.

movement. This figure indicates that settlement varies with the vertical motions of different phases regardless of whether or not the vertical response acceleration is taken into account. This is due to the vertical motion input of different phase affecting the horizontal response acceleration. In cases $n = 4$ to 7 (phase difference π to $7\pi/4$), the settlement was greater when the vertical response acceleration is considered. The case $n = 5$ gives the maximum settlement of 160 cm when horizontal and vertical acceleration are taken into account and 120 cm without vertical acceleration.

6 RESPONSE AND SETTLEMENT TO EARTHQUAKE INPUT MOTIONS

The acceleration time histories recorded at foundations of 10 dams as shown in [Table 2](#) are used to perform dynamic analyses. Here the Tokachi Earthquake is an earthquake with hypocenter on the subduction plate boundary. The other earthquakes occurred in the shallow crust.

The acceleration time histories are normalized to a maximum acceleration of 0.75 g. Their frequency characteristics are distributed in a wide range. [Figure 9](#) shows the time histories of the resisting moment and driving moment for sliding block D09 in CASE06, which gives relatively large settlement. The top figure shows the moment with horizontal and vertical response acceleration while the bottom gives the moment with horizontal response acceleration only. Comparing the top and bottom, the vertical response acceleration seems to have less effect on the driving moment and more effect on the resisting moment. This diagram also shows that the duration the driving moment exceeds the resisting moment becomes longer for taking the vertical response into consideration into account, resulting in larger settlement.

The correlation of settlements with and without vertical accelerations is depicted in [Figure 10](#). The figure shows that the ratio of the settlement with and without vertical acceleration varies from 0.6 to 1.4 excluding cases of very small settlements and uppermost slip surfaces of D01 and D06.

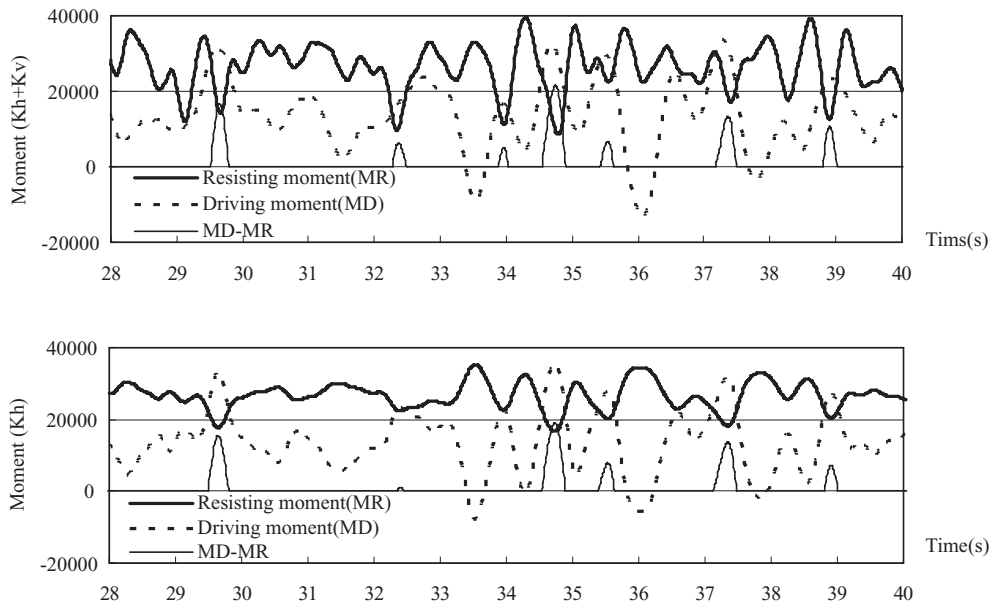


Figure 9. Time histories of resisting and driving moments (CASE06 in [Table 2](#)).

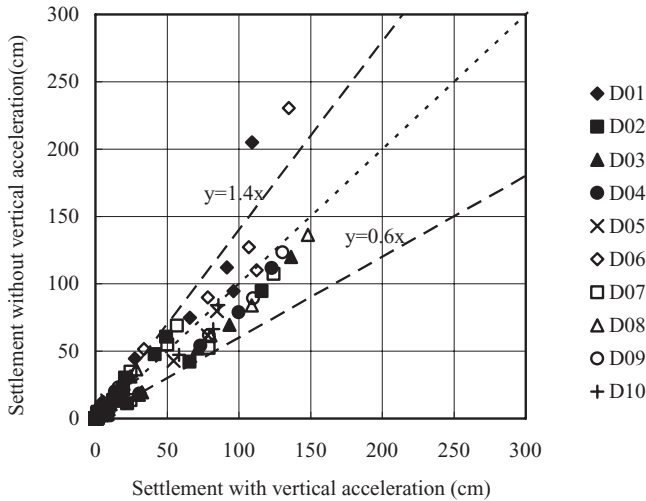


Figure 10. Settlements with and without vertical acceleration for slip surfaces D01 to D10 (Fig. 3).

7 CONCLUSIONS

The following conclusions can be drawn from this study:

1. When the curved failure envelope is used for the strength evaluation of the slip surface, the deeper the sliding surface is, the smaller the yield acceleration is. In this case, the larger and deeper the arc is, the smaller the effect of the vertical seismic coefficient on the sliding safety factor is.
2. In the case of the sinusoidal acceleration input with the period of 0.5 sec and the duration of 5.12 sec, the maximum settlements with the vertical acceleration and without are 160 cm and 120 cm, respectively. This effect of vertical acceleration varies with its phase of input vertical motions.
3. In the case of earthquake input motions the ratio of settlement with and without vertical acceleration is mostly in a range of approximately 0.6 to 1.4.

REFERENCES

- Newmark, N.M. 1965. Effects of earthquakes on dams and embankments. *Geotechnique*, 15(2): 139–160.
- Tateyama, M. Tatsuoka F. Koseki J. & Horii K. 1998. Studies on Seismic Design Method of Soil Structures. Railway Technical Research Institute, Vo. 12, No. 4: 7–12.
- Yan, L. 1991. Seismic deformation analysis of earth dams: A simplified method, Soil Mechanics Laboratory Report, No. SML 91–01: California Institute of Technology.
- Yan, L. Matasovic N. & Kavazanjian E. 1996. Seismic response of a block on an inclined plane to vertical and horizontal excitation acting simultaneously. Proceedings of 11th Conference on Engineering mechanics, ASCE, Fort Lauderdale, FL: 1111–1113.

Earthquake-induced settlement analysis for rockfill dams using cumulative damage theory

Y. Yamaguchi, H. Satoh & K. Shimoyama

Dam Structure Team, Public Works Research Institute (PWRI), Tsukuba, Japan

ABSTRACT: According to “Guidelines for Seismic Safety Evaluation of Dams (Draft)” in Japan, the seismic safety of rockfill dam is basically evaluated based on the sliding deformation due to large earthquake motion. But, during the Niigata-ken Chuetsu Earthquake in 2004, relatively large settlements without sliding were observed at rockfill dams at which consolidation settlement thought to have almost finished before the earthquake. Thus, to accurately estimate the settlement due to large earthquake motions, the settlement should be reproduced by other methods, such as deformation analysis based on cumulative damage theory. We clarify the dynamic strength of construction materials for rockfill dams from the results of cyclic triaxial tests under various conditions, and execute earthquake-induced deformation analysis.

We conduct dynamic laboratory tests for construction materials and evaluate differences of dynamic properties due to the confining pressure and the saturated/unsaturated conditions. We calculate settlements induced by large earthquake motions using cumulative damage theory and evaluate differences due to the confining pressure and saturated/unsaturated conditions. We find that it is very important for accurate evaluation of earthquake-induced settlement to use the laboratory test results considering confining pressure and saturated/unsaturated conditions.

1 INTRODUCTION

In the “Guidelines for Seismic Safety Evaluation of Dams (Draft)” issued by the River Bureau of the Ministry of Land, Infrastructure, Transport and Tourism in March, 2005 (MLIT, 2005), seismic performance of embankment dams is basically evaluated based on sliding deformation. This evaluation method stands on technical and empirical judgments that earthquake-induced settlement without accompanying sliding formation due to a large earthquake motion is about equal to future consolidation settlement (JDEC, 2001) and that earthquake-induced settlement is smaller than the settlement by sliding deformation. Nevertheless, post surveys of rockfill dams that had been damaged in the Niigata-ken Chuetsu Earthquake in 2004 revealed that relatively large-scale settlements occurred without sliding deformation (JR East Co., 2006). So, we should investigate other evaluation methods such as cumulative damage theory analysis (hereafter, CDTA) in addition to the sliding deformation analysis to accurately evaluate earthquake-induced settlement of rockfill dams due to large earthquake motions.

In this study, dynamic strength tests for construction materials were conducted under various conditions in terms of confining pressure and saturated/unsaturated conditions and the previous test results were reviewed to evaluate the effects of those conditions on the dynamic strength. Furthermore, we calculated earthquake-induced settlements by CDTA using the dynamic strength properties in order to examine the effects of the confining pressure and saturated/unsaturated conditions.

2 EFFECTS OF CONFINING PRESSURE AND SATURATED/UNSATURATED CONDITIONS ON DYNAMIC STRENGTH

When a rockfill dam is constructed and impounded, there are saturated/unsaturated areas in dam body and the confining pressure distribution in the dam body varies according to the depth from the surface. The dynamic strength properties of rockfill dam materials can be assumed to be subject to such factors as confining pressure and saturated/unsaturated conditions.

In this chapter, we review the previous test results of dynamic strength tests for rockfill dam materials under various conditions regarding confining pressure and saturated/unsaturated conditions and evaluate the effects of those conditions on dynamic strength properties. Further, we carry out dynamic strength tests in saturated/unsaturated conditions using rock materials of a rockfill dam that is currently under construction.

2.1 Effects of confining pressure

Matsumoto *et al.* (Matsumoto, 1991) conducted cyclic triaxial tests on the rock materials of the Sagurigawa Dam by applying several levels of mean effective stress, σ'_m . Figure 1 illustrates the cumulative strain for each σ'_m value. As the value of σ'_m becomes smaller, the shear stress ratio that generates the same level of strain in the same number of cycles increases. This indicates that dynamic strength increases as the confining pressure decreases.

2.2 Effects of saturated/unsaturated conditions

Satoh and Yamaguchi (Satoh, 2007) conducted cyclic triaxial tests in saturated/unsaturated conditions on the core materials of Dam A (an earth core rockfill dam (ECRD)), which is currently under construction. Figure 2 illustrates the cumulative strain in saturated/

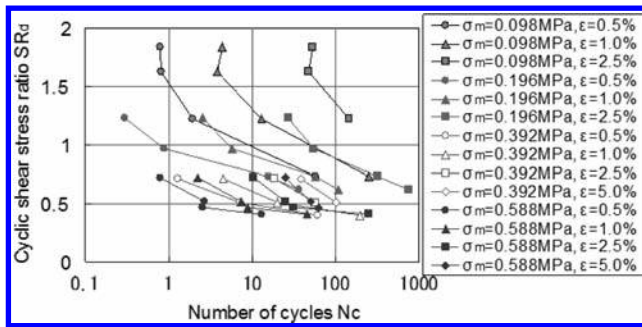


Figure 1. Cumulative strain of the rock materials of the Sagurigawa Dam by cyclic loading.

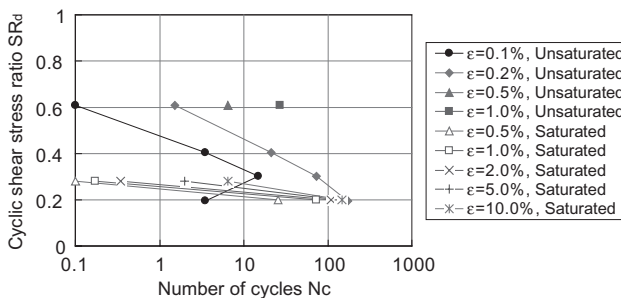


Figure 2. Cumulative strain properties of the core materials of Dam A.

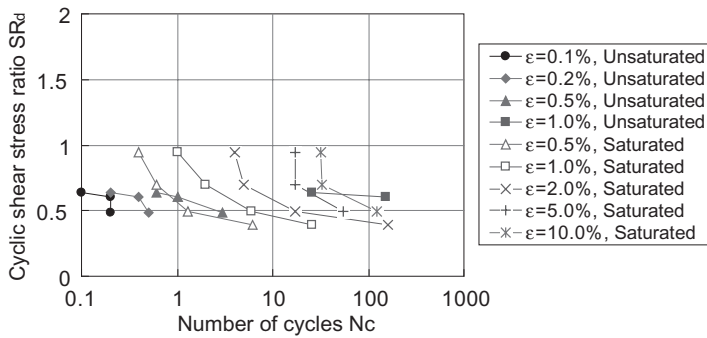


Figure 3. Cumulative strain of the rock materials of Dam A.

unsaturated conditions and indicates that the dynamic strength in unsaturated condition is larger than that in saturated condition.

2.3 Dynamic strength tests on rock materials in saturated/unsaturated conditions

Cyclic triaxial tests on the rock materials of Dam A were carried out in saturated/unsaturated conditions.

The rock materials of Dam A were dacites.

The rock materials were compacted in a relative density of $D_r = 85\%$.

The lateral stress of σ_r in a saturated condition was decided based on the normal minor principal stress in the upstream rock zone of a 100-meter-high rockfill dam model during impounding period. The lateral stress of σ_r in an unsaturated condition was decided based on the normal minor principal stress in the downstream rock zone. The consolidation stress ratio of σ_r/σ_3 was set at 2.0.

Figure 3 shows the cumulative strain in both saturated and unsaturated conditions. Very small strain is generated in unsaturated conditions in comparison with that in saturated conditions.

3 SEISMIC DEFORMATION ANALYSIS OF AN EARTH CORE ROCKFILL DAM (ECRD)

Based on the test results in Chapter 2, we decided the dynamic strength properties of the dam body materials taking into account the confining pressure and saturated/unsaturated conditions during the impounding period, and performed cumulative damage analysis. Effects of these conditions on the earthquake-induced settlement of an ECRD were investigated.

4 OUTLINE OF ANALYTICAL PROCEDURE

In this study, the static stress distribution within a dam body was calculated by static analyses including embanking and impounding processes. Based on this as the initial stress, a dynamic analysis was conducted to evaluate the effect of an earthquake on the dam (Inomata, 2005). As for the embankment analysis, the nonlinear elasticity analysis based on the Duncan-Chang model was employed. The stress at impounding was calculated taking into consideration the effect of the seepage force on the core zone and of the buoyancy on a submerged section. In the dynamic analysis, the complex response analysis based on the equivalent linearization method was adopted, where only the dam body was modeled and the benthic boundary was fixed. Therefore, energy dissipation in the foundation was considered with a dissipation damping

ratio. CDTA is based on the concept that a permanent displacement caused by an earthquake can be attributed to residual strain that occurs under the influence of cyclic loading.

4.1 Analytical conditions

The analytical model, an ECRD with a height of 100 m is shown in Figure 4. The water level was determined to be 92 m on the assumption of a normal water level for a common rockfill dam in Japan. The physical properties used in the dynamic analysis based on the equivalent linearization method are shown in Figure 5.

Table 1 summarizes equations concerning the cumulative strain properties, which were formulated from the dynamic strength tests for each material.

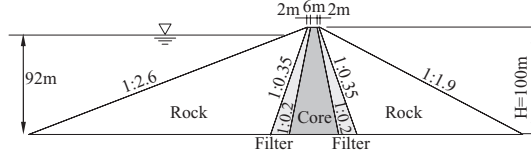


Figure 4. Analytical model.

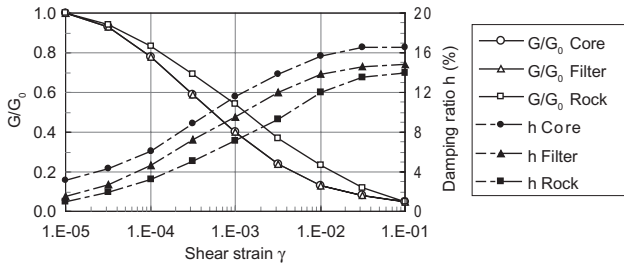


Figure 5. Relationship between G/G_0 , h and γ .

Table 1. Cumulative strain properties.

Property	Zone	Equation
T	Core	$SR_d = 0.43\epsilon^{0.50} \times Nc^{-0.33} + 0.16$
	Filter	$SR_d = 0.59\epsilon^{0.47} \times Nc^{-0.33} + 0.16$
	Rock (i)	$\sigma'_m > 0.196 \text{ MPa}$ $SR_d = 0.65\epsilon^{0.50} \times Nc^{-(0.34\epsilon^{0.01})} + 0.20$
	Rock (ii)	$0.098 < \sigma'_m \leq 0.196 \text{ MPa}$ $SR_d = 1.05\epsilon^{0.70} \times Nc^{-(0.25\epsilon^{0.01})} + 0.25$
	Rock (iii)	$\sigma'_m \leq 0.098 \text{ MPa}$ $SR_d = 2.00\epsilon^{0.80} \times Nc^{-(0.28\epsilon^{0.01})} + 0.26$
A	Core	Unsaturated $SR_d = 2.15\epsilon^{0.90} \times Nc^{-(0.51\epsilon^{0.08})} + 0.19\epsilon^{0.25}$
		Saturated $SR_d = 0.23\epsilon^{0.60} \times Nc^{-(0.40\epsilon^{0.33})} + 0.19\epsilon^{0.21}$
	Filter	Unsaturated $SR_d = 0.44\epsilon^{0.07} \times Nc^{-0.17} + 0.06\epsilon^{1.46}$
		Saturated $SR_d = 0.22\epsilon^{0.87} \times Nc^{-(0.45\epsilon^{0.09})} + 0.21\epsilon^{0.15}$
	Rock	Unsaturated $SR_d = 0.47\epsilon^{0.07} \times Nc^{-0.17} + 0.37\epsilon^{1.46}$
		Saturated $SR_d = 0.57\epsilon^{2.01} \times Nc^{-(0.96\epsilon^{0.17})} + 0.38\epsilon^{0.03}$

* SR_d : Cyclic shear stress ratio, Nc : Number of cycles, ϵ : Axial strain (%).

In the CDTA, we used Property T in Table 1 to examine the effects of confining pressure and Property A in Table 1 to examine the effects of the saturated/unsaturated conditions.

The results of the undrained cyclic triaxial tests carried out by Yonesaki *et al.* (Yonesaki, 2000) on the core materials and sand-gravel filter materials of ECRD were employed for the core materials and filter materials of Property T. As shown in Chapter 2, on the rock materials, Matsumoto *et al.* (Matsumoto, 1991) performed undrained cyclic triaxial tests, where various values of confining pressures were examined for the ECRD rock materials. Among these values, the effective mean stresses of $\sigma'_m = 0.098, 0.196$ and 0.588 MPa were employed. Figure 6 illustrates the cumulative strain properties of Property T.

Property A was derived from the results of cyclic triaxial tests that were carried out on the construction materials used for Dam A. However, no cyclic triaxial tests were performed in unsaturated condition on the filter materials of Dam A. Thus, the cumulative strain properties of the filter materials in saturated condition were estimated from (1) the cumulative strain properties of the filter materials in unsaturated condition and (2) the cumulative strain properties of the rock materials in saturated/unsaturated condition. Figure 7 shows the cumulative strain properties of Property A.

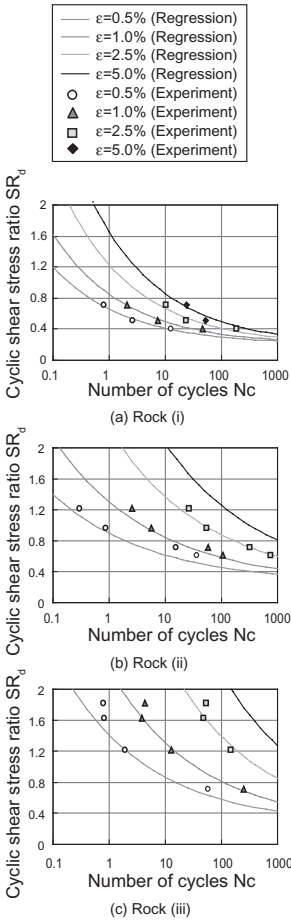


Figure 6. Cumulative strain properties of Property T (rock materials).

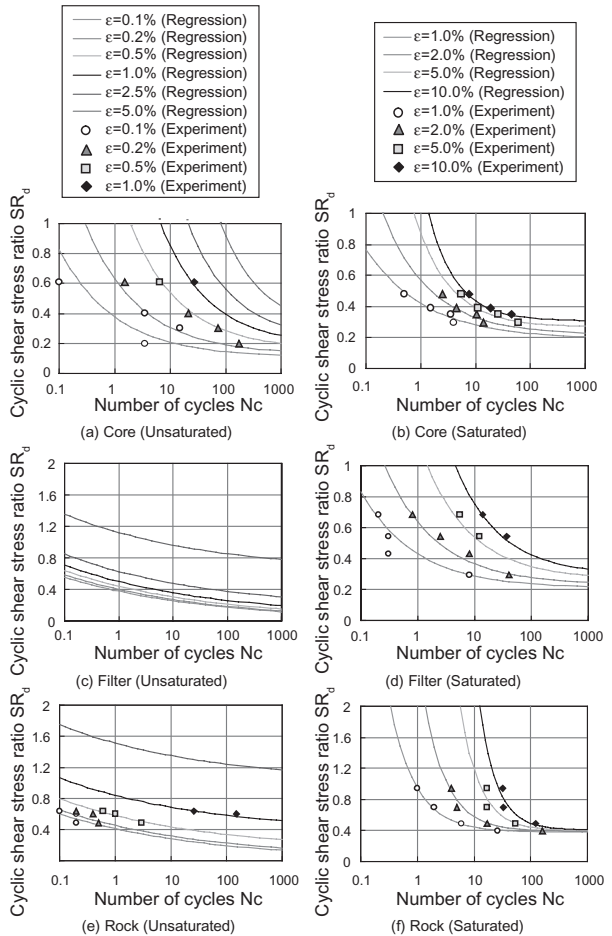


Figure 7. Cumulative strain properties of Property A.

The input earthquake motions were prepared based on the observed waves at dam foundations during the 1995 South Hyogo Prefecture Earthquake, namely the Hitokura Dam Wave, the Minoogawa Dam Wave, and the Gongen Dam Wave. The maximum horizontal accelerations of three waveforms were adjusted as 7.20 m/s^2 simply by increasing those amplitudes in proportion to the observed maximum accelerations. Figure 8 shows the time histories of the horizontal accelerations of the three input waves. Figure 9 illustrates the acceleration response spectra of these three waveforms.

Analytical cases are listed in Table 2. The analytical cases were intended to evaluate effects on the CDTA of dynamic strength properties considering effective confining pressure and saturated/unsaturated conditions.

Cases 1 and 2 show examinations of the effects of the mean effective stress during the impounding period. In Case 1, the value of $\sigma'_m = 0.588 \text{ MPa}$ for Property T was applied to the entire rock zone, and in Case 2 cumulative strain properties of the rock zone were assigned in response to the initial mean effective stress. In Cases 3 and 4, the effects of saturated/unsaturated conditions are examined. Case 3 deals with Property A only in a saturation condition whereas Case 4 deals with physical properties in both saturated/unsaturated conditions.

4.2 Analytical results

The analytical results are summarized in Table 3.

The maximum settlement in the CDTA increases in an ascending order of: Hitokura Dam.

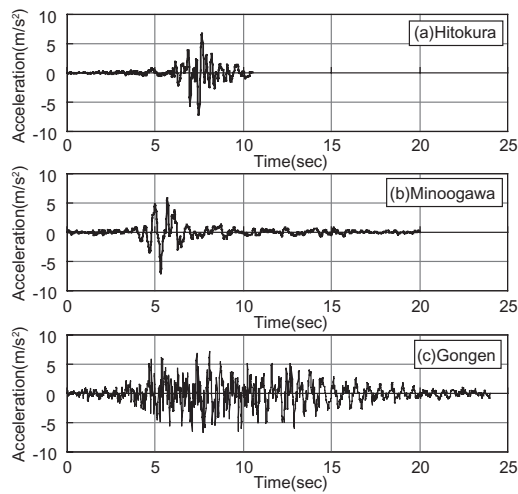


Figure 8. Time histories of accelerations of the input motions (upstream-downstream direction).

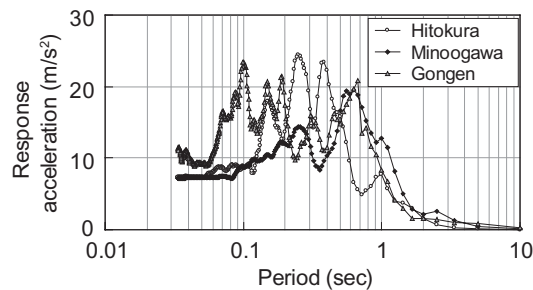


Figure 9. Acceleration response spectra (upstream-downstream direction).

Table 2. Analytical cases.

Case	Input waveform	Maximum acceleration m/s ²	Dynamic strength	How to assign the dynamic strength			Remarks
				Core	Filter	Rock	
1-1	Hitokura	7.20	T	Property T		Rock (i) was applied to the entire rock zone	Effects of mean effective stress
1-2	Minoogawa						
1-3	Gongen						
2-1	Hitokura	7.20	T	Property T		Assigned in response to the initial mean effective stress	Effects of saturated/unsaturated
2-2	Minoogawa						
2-3	Gongen						
3-1	Hitokura	7.20	A	Deals with Property A only in a saturated state			Effects of saturated/unsaturated
3-2	Minoogawa						
3-3	Gongen	states					
4-1	Hitokura	7.20	A	Deals with Property A in both saturated/unsaturated conditions			
4-2	Minoogawa						
4-3	Gongen						

Table 3. Analytical results.

Case	Natural period		Maximum acceleration at crest		Cumulative damage analysis*1)					
					Maximum settlement			Maximum horizontal displacement*2)		
	Initial rigidity (s)	Convergent rigidity (s)	horizontal (m/s ²)	vertical (m/s ²)	U (cm)	C (cm)	D (cm)	U (cm)	C (cm)	D (cm)
1-1	0.572	0.838	13.51	11.68	75.6	72.4	36.7	-107.7	-38.0	-13.9
1-2		0.908	13.94	10.03	142.3	139.1	98.6	-44.7	-47.4	-21.0
1-3		0.851	10.57	6.36	226.7	212.8	123.4	-275.4	-101.1	-49.9
2-1	0.572	0.838	13.51	11.68	50.8	55.4	30.5	-35.0	-16.0	-10.4
2-2		0.908	13.94	10.03	109.1	112.8	85.5	-47.3	-14.7	-12.0
2-3		0.851	10.57	6.36	157.6	161.7	105.4	-76.9	-31.3	-24.4
3-1	0.572	0.838	13.51	11.68	117.4	122.3	86.8	-68.7	-31.8	-27.3
3-2		0.908	13.94	10.03	189.3	193.8	159.6	-75.0	-49.4	-48.0
3-3		0.851	10.57	6.36	368.3	377.5	243.4	-169.8	-120.5	-107.7
4-1	0.572	0.838	13.51	11.68	100.6	96.6	69.6	-69.7	-44.9	-38.6
4-2		0.908	13.94	10.03	171.4	171.0	145.8	-75.8	-57.6	-56.1
4-3		0.851	10.57	6.36	295.0	273.2	190.4	-173.0	-148.7	-142.2

*1) C: 10 m section at crest, U: entire upstream slope excluding the crest, D: entire downstream slope excluding the crest.

*2) Positive values are given to the downstream side.

Wave, Minoogawa Dam Wave, and Gongen Dam Wave in all cases.

The maximum horizontal displacement in the CDTA was always on the upstream side, increasing in an ascending order of: Hitokura Dam Wave, Minoogawa Dam Wave, and Gongen Dam Wave in all cases except for the displacement at the crest in Case 2.

We then focused on the analytical results of the Gongen Dam Wave, which generated the largest settlement and horizontal displacement, to examine the effects of initial mean effective stress and saturated/unsaturated conditions on the dam body deformation. Figures 10 through 13 show the distributions of the dam body settlement and horizontal displacement under each comparative condition.

4.2.1 Effects of confining pressure

The horizontal displacement as well as the settlement of a dam body surface tends to decrease with the consideration of effects of confining pressure on dynamic strength. The degree of decrease in deformation is large on the upstream side.

According to the vertical distribution of settlements in the bottom of Figure 10, in large confining pressure areas, the settlements for Case 1 and Case 2 are almost same. But, the difference between Case 1 and Case 2 becomes large near the surface where the confining pressure is small. Particularly, because of decrease in effective stress due to impounding, the difference in settlement is large near the surface of an upstream rock zone where the confining pressure is small.

Regarding the vertical distribution of horizontal displacement illustrated in the bottom of Figure 11, the horizontal displacements in both cases are almost same at large confining pressure area, but difference of the horizontal displacements is large near the surface in small confining pressure area.

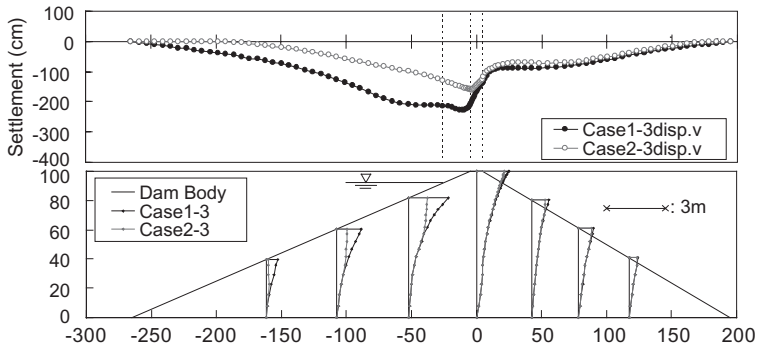


Figure 10. Effects of mean effective stress (confining pressure) on settlement. (Top: settlement of dam body surface, Bottom: vertical distribution of settlement).

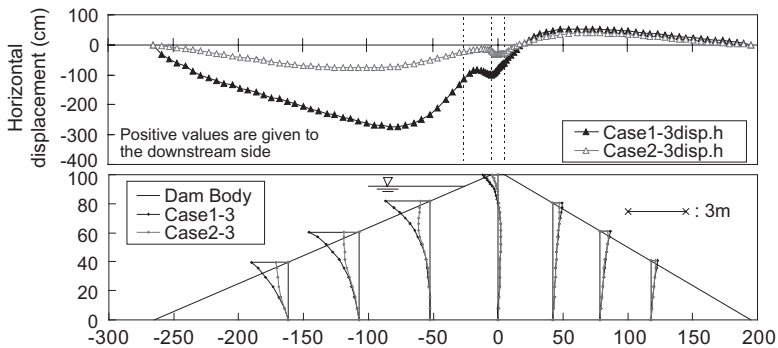


Figure 11. Effects of mean effective stress (confining pressure) on horizontal displacement. (Top: horizontal displacement of dam body surface, Bottom: vertical distribution of horizontal displacement).

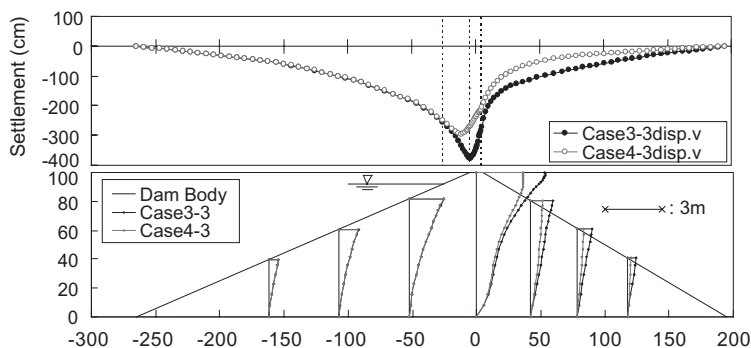


Figure 12. Effects of saturated/unsaturated conditions on settlement.
(Top: settlement of dam body surface, Bottom: vertical distribution of settlement).

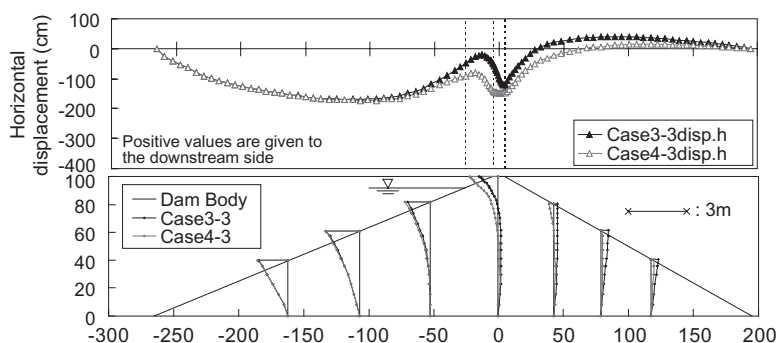


Figure 13. Effects of saturated/unsaturated conditions on horizontal displacement.
(Top: horizontal displacement of dam body surface, Bottom: vertical distribution of horizontal displacement).

4.2.2 Effects of saturated/unsaturated conditions

Little difference was seen between Case 3 and Case 4 in horizontal displacement as well as settlement of dam body surface in upstream side below the reservoir water level. Regarding the unsaturated area above a reservoir water level, as the vertical distribution of horizontal displacement in the bottom of Figure 13 indicates, the distribution of horizontal displacement in Case 4, which considers an unsaturated condition, appears to be affected by the deformation in downstream rock zone to downstream direction. Settlement in unsaturated area in Case 4 is smaller than that in Case 3.

In the bottom of Figure 12, a comparison of the settlements in the saturated areas between Case 3 and Case 4 reveals that they are almost same. In the unsaturated area (above El. 92 m) and the downstream zone, however, the settlement in Case 4, where the unsaturated area was taken into account, is smaller than that of Case 3.

5 CONCLUSIONS

1. We carried out cyclic triaxial tests to evaluate the effects of mean effective stress (confining pressure) and saturated/unsaturated conditions on the dynamic strength properties of rockfill dam materials. As a result, we found that the dynamic strength of dam materials becomes large with a decrease in the mean effective stress, and that the dynamic strength in an unsaturated condition is large in comparison with that in a saturated condition.

2. We used the dynamic strength properties obtained in [Chapter 2](#) to the CDTA of a 100-meter-high ECRD model. As a result, we found that the initial mean effective stress and saturated/unsaturated conditions had significant effects on the settlement and displacement.

REFERENCES

- East Japan Railway Company (JR East Co.), 2006, Report of Technical Specialist Committee on the Shinano River Power Plant Restoration Works, pp. 69–101. (in Japanese).
- Inomata, J., Nagayama, I. et al., 2005, Technical Report on Seismic Performance Evaluation of Dams against Large Earthquakes, in Journal of National Institute for Land and Infrastructure Management, No. 244/ Technical Memorandum of PWRI, No. 3965. (in Japanese).
- Japan Dam Engineering Center (JDEC), 2001, Sectional Meeting Report on Rationalization of Embankment Dam Design. (in Japanese).
- Matsumoto, N., Yasuda, N., Okubo, M., & Yoshioka, R. 1991, Monotonic Loading Tests and Cyclic Loading Tests for Rock Materials, Technical Memorandum of PWRI, No. 2996. (in Japanese).
- River Bureau, Ministry of Land, Infrastructure, Transport and Tourism (MLIT), 2005, Guidelines for Seismic Performance Evaluation of Dams During Large Earthquakes (Draft). (in Japanese).
- Satoh H. & Yamaguchi Y. 2007, Dynamic strength of core materials with compaction degree, Engineering for Dams, No. 252, pp. 42–53. (in Japanese).
- Yonesaki, F., Sato, N., & Someya, T. 2000, Study on Seismic Design for Structures—Seismic Diagnosis for the Tokuyama Dam against Level 2 Ground Motions, Research Institute, Water Resources Development Public Corporation, No. 99213, 2000. (in Japanese).

Shaking table test of concrete dams with penetrated cracks and DEM analysis simulation

T. Iwashita, T. Kirinashizawa, Y. Yamaguchi & H. Kojima

Public Works Research Institute, Tsukuba, Japan

Y. Fujitsuka

CTI Engineering Co., Ltd., Fukuoka, Japan (Former Public Works Research Institute)

ABSTRACT: To evaluate the seismic performance of concrete gravity dams subjected to strong earthquakes such as the maximum credible earthquake, it is necessary to evaluate the seismic stability of the detached block of the dam body when tensile cracks in the dam body are predicted to penetrate from the upstream face to the downstream face. In this study, shaking table tests of a dam-shaped model specimen with penetrated cracks were performed considering hydraulic loading from the reservoir. The dynamic behavior of the detached block was analyzed using the pictures captured by a high-speed camera. The shaking table tests under two load conditions, with and without uplift pressure acting on the penetrated cracks, clarified the impact of uplift pressure on the behavior of the detached block. Numerical simulations of the dynamic behavior of the detached block during the shaking table tests were performed based on the Distinct Element Method (DEM).

1 INTRODUCTION

The Ministry of Land, Infrastructure, Transport and Tourism (MLIT) of Japan enacted “Guidelines for Seismic Performance Evaluation of Dams Against Large Earthquakes (Draft)” (River Bureau of the MLIT, 2005), which systematically regulates the method of evaluating the seismic performance of dams under the Level 2 earthquake, which is equivalent to the maximum credible earthquake, and has tentatively applied the guidelines to the dams under the jurisdiction of the MLIT. Under the guidelines, a dam is evaluated by confirming two seismic performance functions: (1) the storage function of the dam is maintained and (2) damage which has occurred is limited to a range which can be repaired. Regarding Function (1), earthquake response analysis considering the damage process is performed for a concrete dam, confirming that the damage which occurs is limited. In the case of a concrete gravity dam, conditions for tensile failure are generally critical for Function (1), which is considered to be satisfied if the tensile cracks generated in the dam body do not penetrate completely between the upstream and downstream faces. However, the guidelines also state that even when tensile cracks penetrate from the upstream to downstream faces of a dam body, if the upper detached block of the dam body is not unstable, it can be assumed that Function (1) is satisfied. Therefore, in a case where the earthquake response analysis shows that cracks penetrate from the upstream face to the downstream face, a more detailed evaluation by assessing the stability of the dam body after the dam body is separated by penetrated cracks.

Some researchers have studied the seismic performance of concrete dam bodies separated by the penetration of cracks. Malla & Wieland (2006), Zhu & Pekau (2007) and Wang (2008) used finite element analysis, and Pekau & Cui (2004) used the distinct element method (DEM) analysis, to evaluate the stability of dams separated by penetrated cracks by analyzing dynamic behavior, including rocking and sliding, of the upper detached concrete block. Most of these analyses were based on a case study of the Koyna Dam, which was a concrete gravity dam in which cracks penetrated between the upstream and downstream faces at the elevation

of the downstream gradient of the dam body changed due to the Koyna Earthquake of 1967. However, there have been almost no experimental studies, including shaking table tests, on the dynamic behavior of detached blocks due to penetrated cracks.

In this study, to clarify the seismic behavior of the detached block of a crack-penetrated dam body, shaking table tests were performed using a dam-shaped model specimen. The behavior of the upper detached block of the model in the shaking table tests was reproduced by DEM analysis.

2 SHAKING TABLE TESTS FOR DAM MODEL

2.1 Experimental apparatus

A water tank (1.25 m long, 0.5 m wide, and 0.8 m deep) was installed on the shaking table (8 m long and 8 m wide) and a dam-shaped model mortar specimen that had already been separated into two blocks was placed inside the water tank. The reservoir water level was kept at a constant depth of 465 mm during each shaking test by injecting water using a pump and letting it overflow from the weir as shown in Figure 1.

The dimensions of the dam model specimen are 515 mm in dam height, 318 mm in base length in the upstream-downstream direction and 300 mm in thickness in the dam axis direction. The upstream face of the specimen was vertical and the downstream slope had a gradient of 1:0.8. The model specimen assumed that cracks were generated along a horizontal construction joint at the lower elevation of the dam, where large tensile stress is generated during shaking, and that the cracks penetrated from the upstream to downstream face. The model specimen was made of mortar with a maximum aggregate size of 0.75 mm. The specimen was made by the following process. First, the lower part with a layer thickness of 115 mm was placed. One day later, after laitance clearance by wire brushing, remover was applied to the construction joint. Next, the upper part of the model specimen was placed. Seven days later, the model specimen was split into two blocks along the construction joint with remover.

The scale factor ($1/\lambda$) of the model specimen with a height of about 0.5 m corresponds to 1/30 for a prototype dam with a height of 15 m, and 1/200 for a 100 m-high prototype dam. Table 1 shows the relations of the properties of the prototype dam converted to the model scale based on the similarity rule with the material properties of the model specimen. The compressive strength of the mortar specimens was 3.94 N/mm^2 , despite efforts to make low-strength mortar because of the limitation of removal of forms. The compressive strength and elastic modulus of the specimen are somewhat larger than those of prototype dams according to the similarity rule based on scale.

2.2 Methodology of shaking table tests

The shaking table tests were carried out for two cases with water pressure acting directly from the reservoir inside the penetrated crack of the model specimen (Cases-UPL-a and -b) and for one case in which water pressure acting directly from the reservoir was prevented (Case-N-UPL), as shown in Table 2. In Case-N-UPL, a latex sheet was loosely pasted on the upstream side of the penetrated crack, preventing reservoir water flowing from the upstream face into the penetrated crack and water pressure directly from the reservoir.

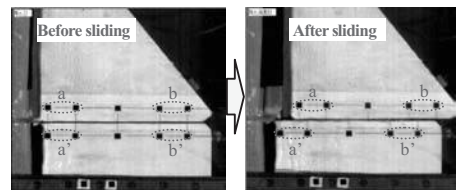
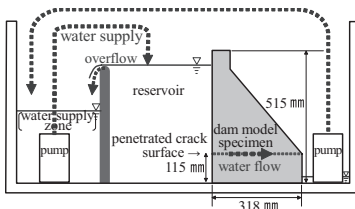


Figure 1. Schematic figure of the experimental apparatus.

Photo 1. Pictures captured by a high-speed camera before and after sliding of the upper detached block.

Table 1. Relations of the similarity rule and material properties of the dam model specimen.

	Range of properties of prototype dam	Similarity ratio	Range of properties of prototype dam converted to model height of 0.5 m based on the similarity rule	Dam model specimens used for experimental tests
	(For dam height of 15 to 100 m)	($\lambda = 30$ to 200)		(Dam model height of about 0.5 m)
	(a)	(b)	(a) \times (b)	
Dam height	15 to 100 m	$1/\lambda$	–	About 0.5 m
Elastic modulus	20,000 to 30,000 N/mm ²	$1/\lambda$	100 to 1000 N/mm ²	6675 N/mm ²
Compressive strength	20 to 30 N/mm ²	$1/\lambda$	0.1 to 1.0 N/mm ²	3.94 N/mm ²

The shaking table was shaken with a sinusoidal acceleration with a frequency of 50 Hz which is equivalent to the range of 3.5 to 9.1 Hz for a prototype dam with a height of 15 to 100 m based on the similarity rule. The duration of the shaking acceleration was 5.5 seconds, and the acceleration amplitude increased linearly during the initial period of 0.5 second. The shaking test was performed as a series, with the amplitude of shaking increasing in steps of approximately 100 gal until reaching 800 to 1000 gal. The maximum input acceleration amplitude was equivalent to out of the range of Level 2 earthquake motions.

2.3 Results of shaking table tests

2.3.1 Sliding displacement at each shaking step

Photograph 1 shows pictures captured by a high-speed camera before and after sliding of the upper detached block. Figure 2 shows the relationship between the input shaking acceleration amplitude and residual horizontal relative displacement of the upper detached block relative to the lower block for each shaking step in all test cases. In Cases-UPL-a and -b, the sliding of the upper detached block significantly increases toward the downstream face when the input acceleration amplitude was 700 to 800 gal. But in Case-N-UPL in which water pressure from the reservoir was prevented from directly acting in the penetrated cracks, the sliding of the upper detached block significantly increased at the shaking step of 900 gal amplitude. When the upper detached block slides downstream in Case-N-UPL, the uplift acting on the penetrated crack surface near the upstream side is so small compared with that in Cases-UPL-a and -b that the upper detached block resists sliding, as mentioned in the next section.

2.3.2 Behavior mechanism of upper detached block

The typical dynamic behavior of the upper detached block was analyzed from observations of the final shaking step (input amplitude acceleration of about 970 gal) in Case-UPL-b. Figure 3 shows the horizontal acceleration time history of the lower block of the model specimen and the horizontal relative displacement time history at the bottom of the upper detached block relative to the lower block. The upper detached block slid gradually downstream after the acceleration time history of the lower block reached a constant amplitude of the shaking.

Figure 4 shows an enlargement for the period from 4.0 to 4.1 seconds in Case-UPL-b shown in Figure 3. Figure 5 shows the behavior of the detached block in the period from 6.0 to 6.1 seconds in Case-N-UPL. Tracking analysis using the pictures captured by a high-speed camera with a shutter speed of 1000 frames per second was performed to obtain the dynamic 2D-behavior of the rigid upper detached block. Comparing the vertical relative displacement of the upper detached block on the upstream side (DH-Y1 indicates vertical length between

Table 2. Test condition of shaking cases.

Case	Uplift pressure acting on the penetrated crack surface	Frequency of sinusoidal acceleration input
Case-UPL-a	With uplift pressure	50 Hz
Case-UPL-b	With uplift pressure	50 Hz
Case-N-UPL	Without uplift pressure*	50 Hz

*Water pressure from the reservoir was prevented from acting directly on the penetrated crack surface.

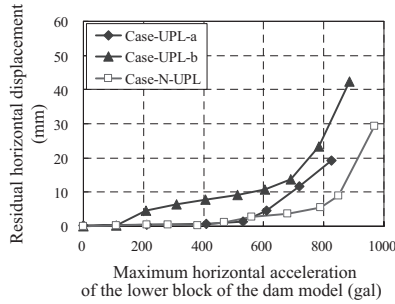


Figure 2. Residual horizontal relative displacement at each shaking step.

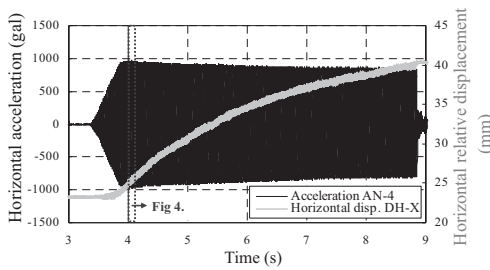


Figure 3. Horizontal acceleration time history of the lower block and horizontal relative displacement time history of the upper detached block (Final shaking step in Case-UPL-b).

a-a' in Photo. 1) with that on the downstream side (DH-Y2 indicates vertical length between b-b' in Photo. 1), we can see the displacement time histories of DH-Y1 and DH-Y2 with a reverse phase. We can thus identify the rocking of the upper detached block. The rocking motion was partitioned into tilting toward the downstream side (rocking motion I) and toward the upstream side (rocking motion II). Figures 4 and 5 are hatched to distinguish the period during rocking motions I and II. While rocking in the upstream and downstream directions, the upper detached block slid downstream a little at a time, as clearly shown by the horizontal displacement time history of DH-X. While the hydrodynamic pressure acting on the upstream face increased, the upper detached block slid downstream, with the penetrated crack on the downstream side closed and the detached block tilted downstream.

Next, the effect of the uplift pressure acting on the penetrated crack surface on the behavior of the model specimen is considered. In the test case in which water is permitted to flow from the reservoir into the penetrated surface (Case-UPL-b shown in Fig. 4), when the inertia force acted on the upper detached block in the downstream direction, uplift pressure of about 8 to 10 kPa acted instantaneously at PB-1 and PB-2 on the penetrated surface. In the same period, the upper block returned to its original position after tilting upstream (rocking motion II),

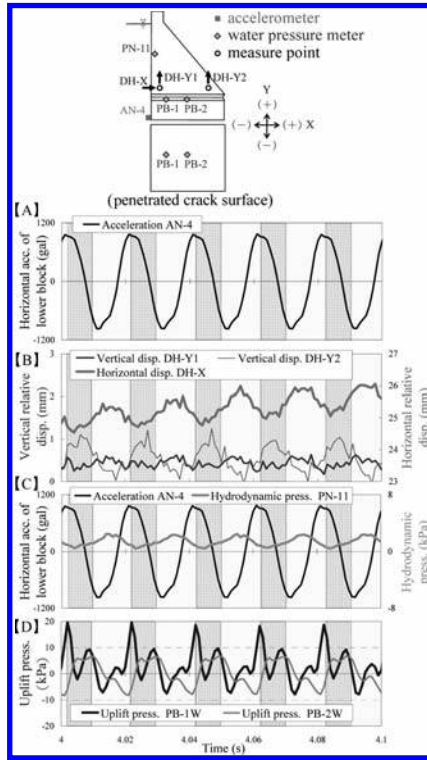


Figure 4. Measured value time histories of the behavior of the upper detached block (Final shaking step in Case-UPL-b).

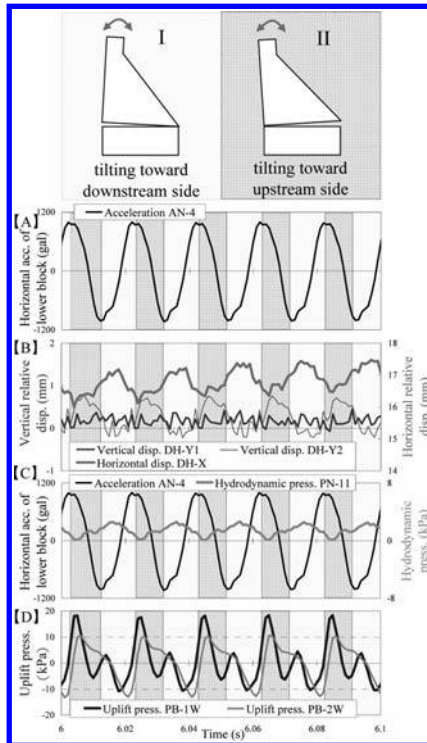


Figure 5. Measured value time histories of the behavior of the upper detached block (Final shaking step in Case-N-UPL).

the penetrated crack closed, and rocking motion I started to occur. It is assumed that because the action of this uplift pressure reduced the frictional resistance between the penetrated crack surfaces, the upper detached block slid easily downstream. On the other hand, in the case in which water pressure from the reservoir was prevented from acting on the penetrated crack surface (Case-N-UPL shown in Fig. 5), water gathered between the crack surface, even though direct seepage flow was prevented. Therefore, the rocking behavior of the upper detached block caused the pore water pressure between the penetrated surfaces as shown in Figure 5 [D]. When the inertia force acted on the detached block in the downstream direction, the uplift pressure near the upstream side in Case-N-UPL was significantly smaller than that in Case-UPL as shown in Figures 4 [D] and 5 [D]. As a result of this effect of uplift pressure, the sliding displacement in Case-N-UPL is seemed to be smaller than that in Case-UPL.

3 NUMERICAL SIMULATION

3.1 Methodology of numerical analysis

Numerical simulation of the dynamic behavior of the upper detached block during the shaking table tests was performed using the distinct element method (DEM) with the UDEC code (Itasca, 2004). The analysis model mesh is shown in Figure 6. Table 3 shows the material properties of the analysis model. The material properties were set from the experimental tests for mortar specimen with the same mix proportion and age as the dam model specimens used for the shaking table tests.

Interface elements were set in the normal direction and in the tangential direction as the joint model between the penetrated crack surfaces of the analysis model. While the upper detached block and the lower block are in contact, the normal stress σ_n acting between the upper and lower blocks is transmitted through a constant normal stiffness k_n . This is the soft contact assumption. The constant normal stiffness k_n was set based on the elastic modulus of the mortar of the specimen. In the shear direction along the penetrated surface, the Coulomb slip model was adopted in UDEC. The shear stress τ_s is limited by the shear strength τ_f which is a combination of cohesive (C) and frictional (φ) strength and is controlled by a constant shear stiffness k_s :

$$\text{If } \tau_s < C + \sigma_n \tan \varphi = \tau_f \quad (1), \text{ then } \Delta \tau_s = -k_s \Delta u_s^e \quad (2)$$

$$\text{and if } \tau_s \geq \tau_f \quad (3), \text{ then } \tau_s = \tau_f \quad (4)$$

where Δu_s^e is the elastic component of the incremental horizontal relative shear displacement.

The cohesion C , frictional coefficient $\tan \varphi$ and constant shear stiffness k_s were obtained from the box shear tests of the specimen made using the same mortar mix proportion and age, as shown in Table 3.

A combination of Rayleigh damping and stiffness damping force was adopted as damping. The Rayleigh damping factor of 15% or 20% was given at the predominant input frequency of 50 Hz considering radiation damping due to the boundary condition with a rigid basement. The method of setting the stiffness damping forces gives greater control for simulating the block bounce including rocking motion. The equation for the stiffness damping force is:

$$f = -\beta \times K \times l \times \Delta v \quad (5)$$

where f is the damping force; β is the damping factor; K is stiffness; l is length of contact on the penetrated surface; and Δv is change in velocity. The damping factor of 1.0×10^{-4} or 1.2×10^{-4} was given in the numerical analyses.

The sinusoidal velocity, which was integrated from the input acceleration wave with a frequency of 50 Hz in the shaking table test, was input. The numerical analysis at all the shaking steps was continuously performed starting from an input acceleration with amplitude of 300 gal. Hydrodynamic pressure acting on the upstream face of the model specimen was calculated using Westergaard's added mass method.

The analysis cases are shown in Table 4. The damping factor was adjusted by the numerical analyses of Cases N-1 to N-3 which were performed without uplift pressure on the penetrated crack. Cases U-1 to U-3 were performed with uplift pressure acting on the penetrated crack

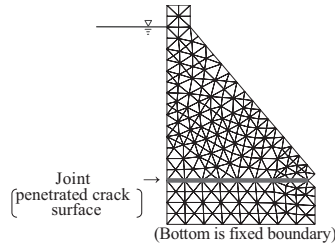


Figure 6. DEM analysis mesh of the model.

Table 3. Material properties of the analysis model.

Material properties		
Upper and lower blocks	Density ρ	2090 kg/m ³
	Dynamic elastic modulus E	6700 N/mm ²
	Poisson's ratio ν	0.2
Penetrated crack surface	Cohesion C	0.0304 N/mm ²
	Coefficient of friction $\tan\phi$	0.82
	Normal stiffness k_n	6700 N/mm ² /m
	Shear stiffness k_s	590 N/mm ² /m

Table 4. Cases of numerical analysis.

Case	Condition of uplift	Rayleigh damping factor	Stiffness damping factor
Case N-1	Without uplift pressure	15%	1.0×10^{-4}
Case N-2		15%	1.2×10^{-4}
Case N-3		20%	1.0×10^{-4}
Case U-1	With uplift pressure*	15%	1.0×10^{-4}
Case U-2		15%	1.2×10^{-4}
Case U-3		20%	1.0×10^{-4}

*Static uplift pressure was made to act on the nodes of the penetrated crack joint.

surface. The triangle-shape distribution of static uplift pressure measured on the penetrated surface in the model specimen before shaking was given instead of the dynamic uplift pressure for the numerical analyses of Cases U-1 to U-3.

3.2 Results of numerical analysis

3.2.1 Rocking motion of the upper detached block

Figure 7 shows a part of the time history results of the experimental shaking table test (Case-N-UPL) and the numerical analyses (Cases N-1 to N-3) performed without uplift pressure for the final shaking step of 900 to 970 gal. The experimental test results in Figure 7 (1) show that the rocking motion of the upper detached block was such that the upper block tilted upstream and returned to the normal position (the penetrated surface of the downstream side closed) and then the block tilted downstream (the penetrated surface of the upstream side opened), while the upper block slid downstream. In the numerical analysis results in Figure 7 (2) and (3), the time histories of vertical displacement of the detached block on the upstream side are reverse phase with those on the downstream side. The behavior of the detached block in the numerical analyses reproducibly simulated the rocking behavior observed in the experimental test Case-N-UPL. The vertical displacement amplitudes of the block, which is the opening gap of the penetrated surface, of the analyses Cases N-2

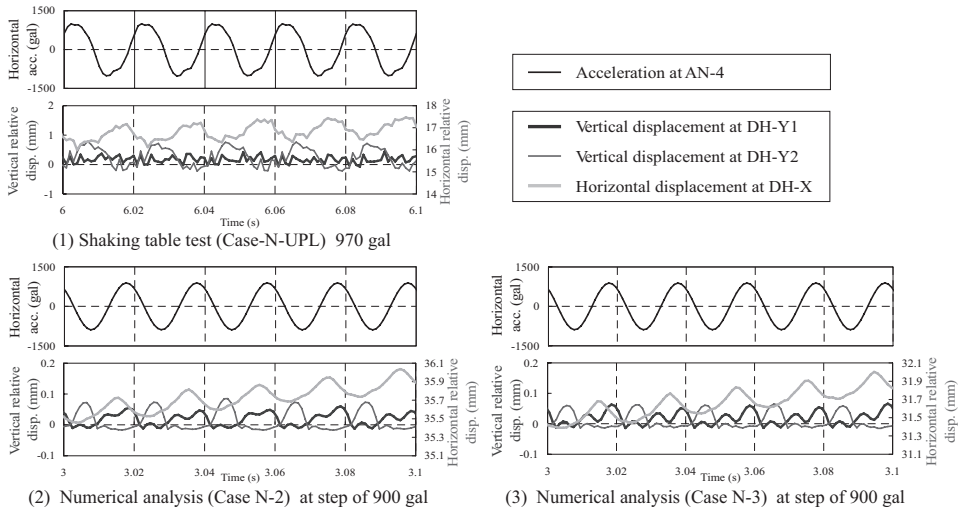


Figure 7. Measured value time histories of the behavior of the upper detached block.

and N-3 in Figure 7 (2) and (3) are quantitatively smaller than that of the experimental test Case-N-UPL in Figure 7 (1). The reason is expected to be because of the modeling of the penetrated surface of the specimen. The penetrated surface of the specimen has asperities due to the mortar aggregate. These asperities caught the upper detached block during rocking, causing the rocking amplitude to increase. On the other hand, the penetrated surface in the numerical analysis was modeled as a flat surface with frictional resistance based on the soft contact assumption.

3.2.2 Horizontal displacement of the upper detached block

The upper detached block slid toward the downstream side, vibrating in the upstream-downstream directions in both of the experimental shaking test (Case-N-UPL) and the numerical analyses (Cases N-2 and N-3) in Figure 7. The amplitudes of horizontal displacement time histories of the block in the numerical analyses were about half those of the experimental test results.

Figure 8 shows the residual horizontal displacement at each shaking step for numerical analyses Cases N-1 to N-3 without uplift pressure. In the numerical analysis results, the upper block started to slide at the shaking step with an acceleration amplitude of about 600 gal, which is similar to the behavior during the experimental test of Case-N-UPL. Though the residual horizontal displacements in Cases N-1 to N-3 become slightly larger than in the experimental test Case-N-UPL with subsequent shaking steps, the increase tendency for the residual displacement in Cases N-2 and N-3 to increase with larger damping factor is similar to that in Case-N-UPL.

Figure 9 shows the experimental results of Cases-UPL-a and -b, and numerical analysis results of Cases U-1 to U-3, in which uplift pressure acted on the penetrated crack surface. In Cases U-1 to U-3, the upper block started to slide at the shaking step with an acceleration amplitude of about 600 gal, which is similar to the behavior during Case-UPL-a. The residual horizontal displacements in Cases U-1 to U-3 become slightly larger than those in Cases-UPL-a and -b with subsequent shaking steps. Regarding the numerical analysis cases with uplift pressure (Case U series) in Figure 9 compared with the cases without uplift pressure (Case N series) in Figure 8, the residual horizontal displacements for Cases U series are somewhat larger than those for Cases N series in each case under the same damping conditions. The uplift pressure acting on the penetrated crack surface reduce the frictional resistance acting on it. The distribution of the static uplift pressure measured on the penetrated surface before shaking was given to the nodes of the penetrated surface of the DEM analysis model. Because the dynamic

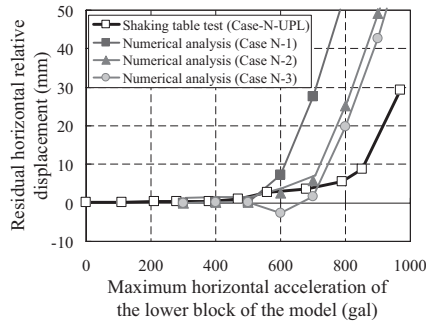


Figure 8. Residual horizontal relative displacement at each shaking step (Without uplift pressure).

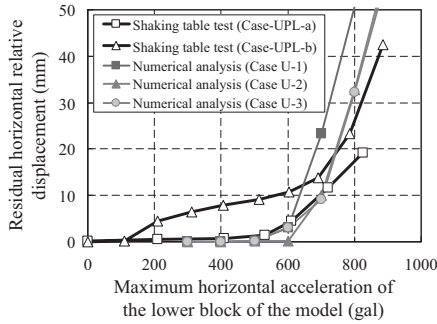


Figure 9. Residual horizontal relative displacement at each shaking step (With uplift pressure).

uplift pressure acts on the penetrated surface in the experimental tests Cases-UPL-a and -b shown in Figure 4, the uplift pressure input in the numerical analysis was different from the uplift pressure time history in the experimental tests. This is assumed to be one of the reasons for the difference of the residual horizontal displacements between Cases-UPL-a and -b and Cases U-1 to U-3, though the damping factors affect the results of the numerical analysis.

In the next step of this study, it will be necessary to improve the setting of input uplift pressure, stiffness and strength on the interface of the penetrated crack for DEM analysis.

4 CONCLUSIONS

To evaluate the ultimate seismic resistance of a concrete gravity dam which cracks formed and penetrated the horizontal construction joint separating it into two parts, shaking table tests were performed using dam-shaped model mortar specimens. The following results were obtained by the experimental shaking table tests. Numerical simulations of the behavior of the detached block during the shaking table tests were performed by DEM analysis.

- The dynamic behavior of the upper detached block during strong shaking was measured and analyzed by the shaking table tests. When shaking acceleration in the upstream direction acted on the lower block, inertia force in the downstream direction acted on the upper detached block. Therefore, the upper detached block slid downstream, accompanying the rocking motion as the behavior changed from upstream side tilting to downstream side tilting. Conversely, when the inertia force in the upstream direction acted on the upper detached block, the detached block returned slightly upstream, accompanying the contrary rocking motion as the behavior changed from downstream side tilting to upstream side tilting. During shaking, horizontal relative displacement of the upper detached block

relative to the lower block occurred gradually in the downstream direction, with the upper block repeating the above-mentioned behavior.

- Comparable shaking table tests were performed under the loading conditions with or without uplift pressure acting on the penetrated crack surface. When the inertia force acted on the detached block in the downstream direction, the uplift pressure on the penetrated crack surface acted near the upstream face side. As a result, the shear resistance of the penetrated surface decreased and the upper detached block could easily slide in the downstream direction.
- A DEM simulation analysis of the dam model with a penetrated crack during the experimental shaking table tests was performed. The numerical analysis results roughly reproduced the rocking motion and residual horizontal displacement of the upper detached block during shaking, even though simple procedures were used, such as joint modeling for the penetrated surface and uplift pressure loading methods.

REFERENCES

- Itasca Consulting Group, Inc. 2004. *Universal Distinct Element Code (UDEC) Theory and Background*.
- Malla, S. & Wieland, M. 2006. Dynamic stability of detached concrete blocks in arch dam subjected to strong ground shaking. *First European Conference on Earthquake Engineering and Seismology, Geneva, 4–8 September 2006*: K10.
- Pekau, O.A. & Cui, Y.Z. 2004. Failure analysis of fractured dams during earthquakes by DEM. *Engineering Structures* 26: 1483–1502.
- River Bureau, Japanese Ministry of Land, Infrastructure, Transport and Tourism. 2005. Guidelines for Seismic Performance Evaluation of Dams against Large Earthquakes (Draft).
- Wang, H. 2008. Seismic stability of detached concrete block of concrete gravity dam. *The 14th World Conference on Earthquake Engineering, Beijing, 12–17 October 2008*: S13–030.
- Zhu, X. & Pekau, O.A. 2007. Seismic behavior of concrete gravity dams with penetrated cracks and equivalent impact damping. *Engineering Structures* 29: 336–345.

Effects of the Iwate-Miyagi Nairiku earthquake in 2008, Japan, on a central clay core rockfill dam

T. Ohmachi

Japan Dam Engineering Center, Tokyo, Japan

T. Tahara

Tokyo Institute of Technology, Tokyo, Japan

ABSTRACT: The effect of the Iwate-Miyagi Nairiku earthquake in 2008 (M_j 7.2), Japan on the Aratozawa dam which is a 74.4 m high rockfill dam with a central clay core is studied with a main focus on the change in the vibration period, shear wave velocity, shear modulus, and pore-water pressure. During the main shock, the acceleration exceeded 10 m/s^2 at the gallery, inducing large shear strains in excess of 10^{-3} and a sudden build-up of the excess pore water pressure in the core. Due to the large strains, the shear wave velocity and shear modulus showed a significant decrease from their initial values and the vibration period was elongated. The full recovery of the wave velocity was found to take at least one year, while the dissipation of the excess pore water pressure seemed faster than the recovery of the wave velocity.

1 INTRODUCTION

The Iwate-Miyagi Nairiku earthquake (M_j 7.2) occurred at 8:43 on June 14, 2008 under southwestern Iwate Prefecture, Japan (Japan Meteorological Agency 2008). The Aratozawa dam which is a 74.4 m high rockfill dam constructed mainly for irrigation and flood control purposes, is located 15 km south of the epicenter of the main shock.

During the main shock, strong motion accelerometers installed at the Aratozawa dam registered a peak acceleration of 10.24 m/s^2 at the bottom gallery. Despite such a high acceleration, the dam continued to be in a safe and stable condition for operation because of little damage only. At the dam, the earthquake motion acceleration has been well recorded not only during the main shock of the 2008 earthquake but also during smaller earthquakes before and after the main shock. The total number of the observed earthquakes used in the present study is 189 which consisted of 3 in 1996, 172 in 2008, and 14 in 2009. [Table 1](#) shows

Table 1. Examples of 10 earthquakes out of 189 used in the present study.

No	Date (time)	Magnitude (M_j)	Peak acceleration at gallery (m/s^2)
1	1996.8.11 (3:12)	5.9	0.28
2	1996.8.11 (8:10)	5.7	0.33
3	1996.8.11 (15:01)	4.8	0.30
4	2008.6.14 (8:43)	7.2	10.24
5	2008.6.14 (9:00)	4.7	0.99
6	2008.6.14 (9:01)	4.0	4.82
16	2008.6.14 (12:10)	4.7	0.79
19	2008.6.14 (19:11)	4.1	2.29
183	2009.7.1	3.2	0.02
189	2009.8.4	1.6	0.02

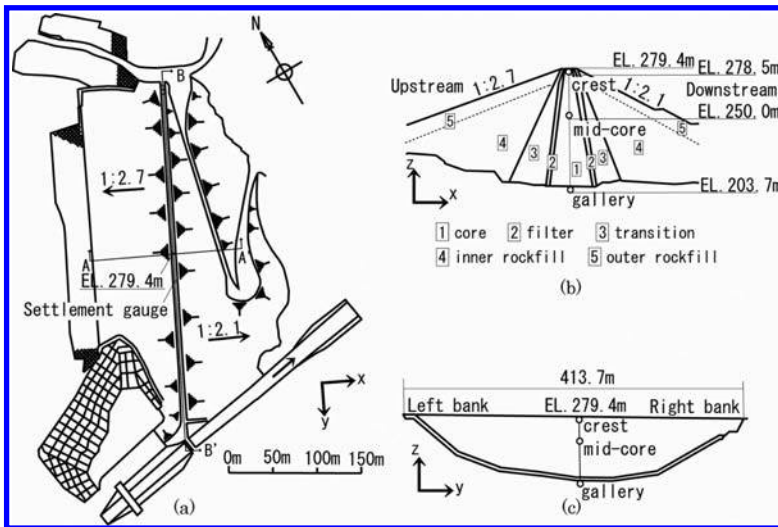


Figure 1. (a). Plan, (b). Cross section A-A' and (c). Cross section B-B' of the Aratozawa dam with seismometers located at crest, mid-core and gallery. Arrows with x, y and z indicate positive directions of observed accelerations.

10 selected earthquakes out of the 189, where all recorded earthquakes used in the present study are numbered from 1 to 189 in chronological order (year/month/day).

2 MAIN FEATURES OF ARATOZAWA DAM AND RESIDUAL DISPLACEMENTS DUE TO THE MAIN SHOCK

The plan and cross sections of the Aratozawa dam are shown in Figure 1. The dam has a central clay core and side slopes of 1:2.7 and 1:2.1 on the upstream and downstream sides, respectively. The seismic coefficient method with a horizontal coefficient of 0.15 was used for the seismic design of the dam. Embankment work of the dam body which was nearly complete in 1991, was followed by construction of appurtenant structures and impounding tests, and the dam was finally completed in 1998. The dam has a crest length of 413.7 m, a crest width of 10 m and the dam body consists of the 5 zones; core, filter, transition, inner rockfill, and outer rockfill zones.

Due to the main shock of the 2008 earthquake, the dam underwent large residual displacements. The residual displacements at the crest shoulder evaluated from the difference between the original design and the survey conducted after the main shock, was 19.8 cm settlement, 4.3 cm towards the upstream, and 6.0 cm to the left at the middle cross section. In the meantime, the top of a plastic pipe of a differential settlement gauge whose location is indicated in Figure 1(a), was observed protruding about 40 cm. According to the measurements of the settlement gauge, the top gauge at EL.275 m showed a settlement of 37.9 cm due to the main shock, which was consistent with the observation of the protruding pipe. In addition, minor cracks in the asphalt pavement were also observed at the right bank corner of the crest.

3 STRONG MOTION RECORDS

Three-component strong motion seismometers (accelerometers) are installed at three locations, i.e. the dam crest, mid-core and bottom gallery (see Fig. 1). The acceleration time histories of the main shock are shown in Figure 2. The peak accelerations observed during the main shock are also shown in Figure 2 where it is seen that, in each direction, the peak

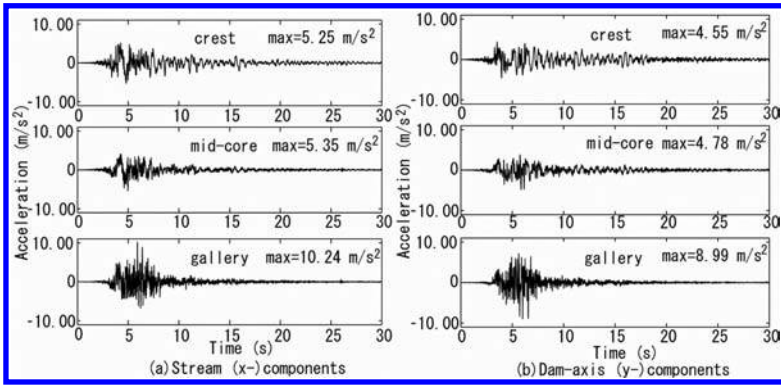


Figure 2. Acceleration time histories of the main shock.

acceleration at the bottom gallery was the largest among the three locations. This fact seems unusual, because earthquake acceleration at a dam crest is usually the largest due to amplification effects of the dam body. The acceleration time histories were sampled at 100 Hz with a frequency range of 0.1–30 Hz and a dynamic range of $\pm 10 \text{ m/s}^2$.

In what follows, the vibration components in the stream, dam-axis and vertical directions are referred to as x-, y- and z-components, respectively, as shown in Figure 1, where the positive directions of those components are also indicated with arrows.

4 VIBRATION PERIODS OF THE DAM

First the vibration periods of the dam were analyzed using spectral ratios (or transfer functions) between the crest and gallery based on the earthquake records Nos. 1–4. The spectral ratios of the x- and y- components are shown in Figure 3, where the horizontal and vertical axes are vibration period and spectral ratio, respectively. The longest of the peak periods in the spectral ratios for the 1996 earthquakes are $T = 0.33\text{--}0.35 \text{ s}$ and $T = 0.32\text{--}0.33 \text{ s}$ for x- and y- components, respectively.

For the Aratozawa dam with $H = 74.4 \text{ m}$, empirical equations for the fundamental period T (Okamoto 1984) yields $T = 0.37 \text{ s}$ and $T = 0.34 \text{ s}$, for the stream and dam-axis directions, respectively. Since the longest peak periods of $T = 0.33\text{--}0.35 \text{ s}$ and $T = 0.32\text{--}0.33 \text{ s}$ for the 1996 earthquakes are consistent with the periods obtained from the equations, the longest peak periods are thought to be the fundamental period of the dam in each direction. On the other hand, for the main shock, the longest two peak periods are $T = 0.65 \text{ s}$ and 1.20 s for the x-component, and $T = 0.56 \text{ s}$ and 0.98 s for the y-component. These periods are significantly longer than the fundamental periods from the 1996 earthquakes, implying nonlinear response of the dam due to the main shock.

When it comes to the nonlinear response of the dam, it is natural to expect that the spectral ratio varies with time during the main shock. The time-varying spectral ratio can be obtained from a ratio of running spectra of the time histories observed at the dam crest and bottom gallery. The running spectral ratio was calculated with a temporal window of $\tau = 5.12 \text{ s}$ with the result shown in Figure 4, where the broken line in the darkest band indicates the most predominant period. The predominant period of the x-component was suddenly elongated to $T = 1.20 \text{ s}$ at around 4 s when the intense motion was input at the gallery, shortened again to $T = 0.65 \text{ s}$ at around 8.0 s when the intense motion started to decay, and finally approached $T = 0.5 \text{ s}$. Likewise, the predominant period of the y-component was suddenly elongated to $T = 0.98 \text{ s}$ at around 4 s, shortened to $T = 0.56 \text{ s}$, and finally approached $T = 0.4 \text{ s}$.

Hence, both peak periods of $T = 0.65 \text{ s}$ and 1.20 s of the x-component, and $T = 0.56 \text{ s}$ and 0.98 s of the y-component are found to appear separately corresponding to the start and end of the intense motion input at the gallery, and are closely related to the fundamental vibration

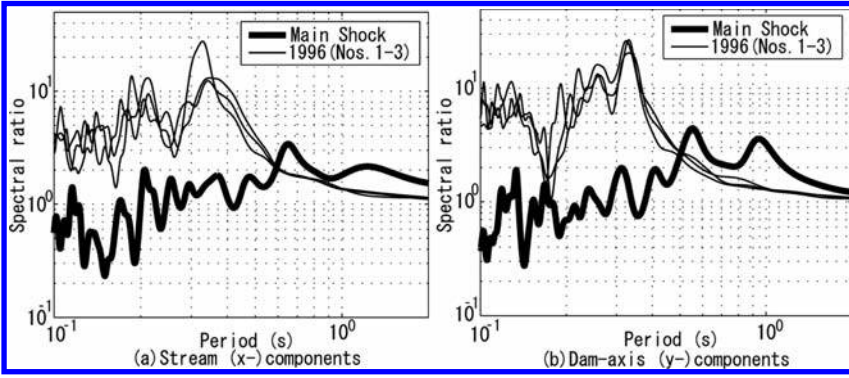


Figure 3. Spectral ratios between the crest and gallery.

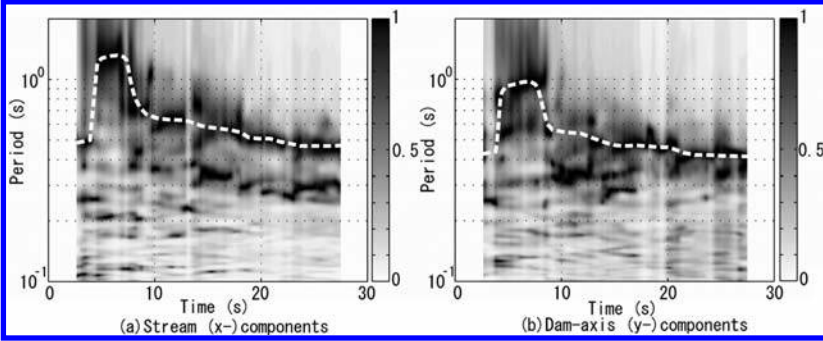


Figure 4. Running spectral ratios between the crest and gallery.

periods of the dam in both horizontal directions. Since the change in the vibration periods during the main shock implies a change in the seismic wave velocity within the dam body, the wave velocity will be discussed next.

5 ESTIMATION OF SEISMIC WAVE VELOCITY

The seismic wave velocity between a pair of the seismometers is estimated from the Fourier phase spectra of the acceleration time histories. When a seismic wave observed at seismometer A is propagated to seismometer B, the arrival time at seismometer B is delayed from that at seismometer A by $\Delta t = l/v$ where l is the distance between the two seismometers, and v is the wave velocity. With Fourier phase θ_A at seismometer A and θ_B at seismometer B, the phase difference $\theta = \theta_B - \theta_A$ is expressed as

$$\theta = 2\pi l / \lambda, \quad (1)$$

where λ is the wave length expressed as $\lambda = vT$ with period T . Substitution of $\lambda = v/f (= vT)$ in Eq. (1) leads to

$$\theta = 2\pi f l / v. \quad (2)$$

Hence, when the phase difference θ is plotted against the frequency f , the velocity v can be estimated from the slope of the plots.

Since the seismometers are installed at 3 locations on a vertical line (see Fig. 1), the wave velocity is estimated for the 3 sections shown in Table 2, where distances l of the sections are also shown. The stream (x-) component of the seismic wave velocity that is estimated from 1996 earthquakes is given in Table 3. All the estimated velocities seem to be reliable (Sawada & Takahashi 1975).

Table 2. Sections where wave velocity is estimated and their distance.

Section	Terminal observation points (A/B)	Distance l (m)
U	Mid-core/Dam-crest	29
M	Gallery/Dam-crest	75
L	Gallery/Mid-core	46

Table 3. Wave velocity of stream (x-) component from 1996 earthquakes.

	Section U (m/s)	Section M (m/s)	Section L (m/s)
Earthquake No. 1	429	496	564
Earthquake No. 2	424	487	565
Earthquake No. 3	435	501	573

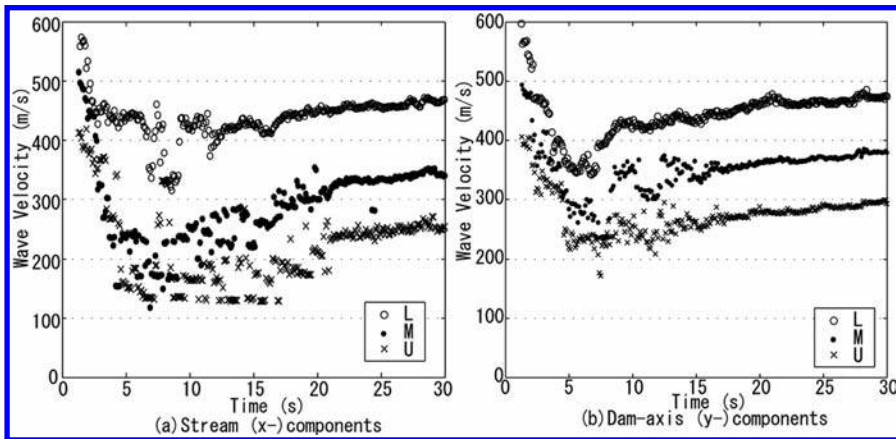


Figure 5. Wave velocities of 3 sections during main shock.

Using the same procedure, the seismic wave velocity during the main shock was estimated from Fourier phases of the acceleration time histories. Since the wave velocity was expected to change with time, the estimation procedure was applied in succession with a 2.56 s long moving temporal window. Figure 5 shows the time-varying wave velocities at the 3 sections estimated from the stream (x-) and dam-axis (y-) components, respectively. Although there is scatter in the estimated velocities, it can be observed that,

- Due to the intense shaking during the first 8 s, the wave velocities at all 3 sections showed a sudden decrease with time.
- The decrease in the velocity was more conspicuous in the upper part (section U) than in the lower part (section L) of the core zone.
- After the strong shaking, the wave velocity increased gradually with time.
- Initially both horizontal components at a particular section had the same velocity, but after the intense shaking, the stream (x-) component tended to exhibit a smaller velocity than the dam-axis (y-) component, especially for sections M and U.

6 STRAIN-DEPENDENCY OF DYNAMIC SOIL PROPERTIES

The acceleration time histories were integrated twice to obtain displacement histories. From the displacement time histories, relative displacements between the two ends of each section shown in Table 2 were obtained and divided by the distance between a pair of installations in order to calculate the mean shear strain of each section.

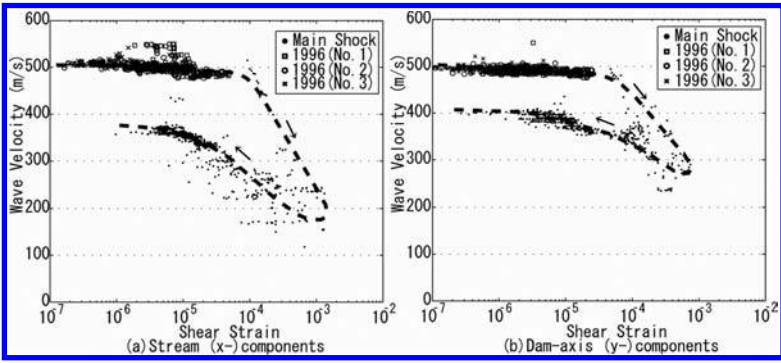


Figure 6. Strain-dependent wave velocity evaluated for horizontal components.

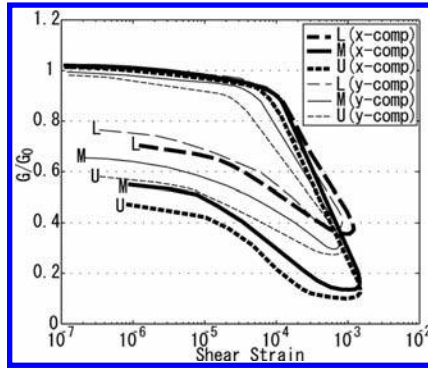


Figure 7. Strain-dependent shear modulus ratio.

Next the time-varying positive envelope of the mean shear strain which is regarded as a reference shear strain and the corresponding time-varying wave velocity shown in Figure 5 are plotted in Figure 6. In addition, the wave velocity-shear strain data from the 1996 earthquake records are also plotted, and an outline of the strain history during the main shock is shown with a dashed line and arrows. In Figure 6, when the shear strain exceeds 10^{-4} , the shear wave velocity shows a sudden decrease, and then increases again with the decrease in the strain level.

It is assumed that the shear wave velocity V_s and the shear modulus G are related by,

$$V_s = (G / \rho)^{1/2} \quad (3)$$

where ρ is mass density. As the change in mass density is negligibly small in comparison with the change in shear modulus, the above mentioned strain-dependent wave velocity V_s is converted to a strain-dependent shear modulus G , as shown in Figure 7 in which G_0 denotes the initial shear modulus at low strain. It should be noted in Figures 6 and 7 that at the end of the main shock the shear wave velocity V_s and shear modulus G remained considerably smaller than their initial values. In Figure 7, the six lines associated with the gradual increase are almost parallel to each other. Due to the parallel increase in the ratio G/G_0 , the modulus G in the core becomes anisotropic during the increasing process including the final state.

7 LONG-TERM RECOVERY OF DECREASED WAVE VELOCITY AND ISOTROPY

Acceleration time histories of 185 earthquake events at the dam which were recorded after the main shock of the 2008 earthquake were analyzed. Among these events, the largest peak acceleration recorded at the gallery was 4.82 m/s^2 corresponding to event No. 6 which was an aftershock occurring 18 minutes after the main shock (see Table 1).

The recovery process of the decreased wave velocity was investigated, with the result shown in Figure 8 for section M. It can be said that, in general the decreased wave velocities have almost recovered to the initial values by August, 2009, and the anisotropy in the wave velocity has also disappeared by then.

8 PORE WATER PRESSURE BEFORE AND AFTER MAIN SHOCK

The pore water pressure distribution in a vertical section was estimated from daily readings of the meters at 9:00 AM before and after the main shock, as shown in Figure 9 where small circles

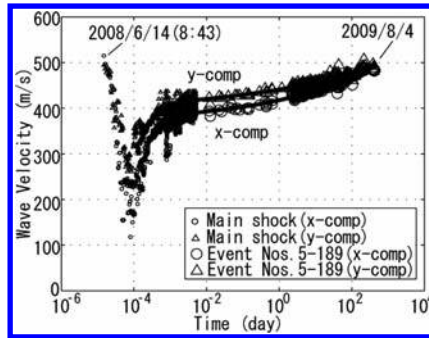


Figure 8. Long-term recovery of the decreased wave velocity and isotropy of section M.

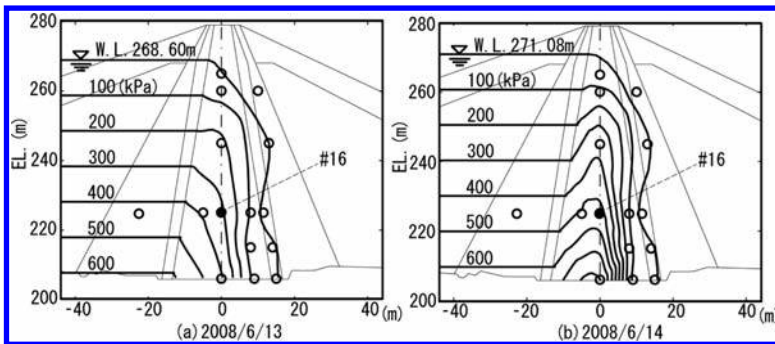


Figure 9. The generation and dissipation of excess pore water pressure in the core. Small circles indicate location of pore water pressure meters. The solid circle indicates the location of pore water pressure meter #16.

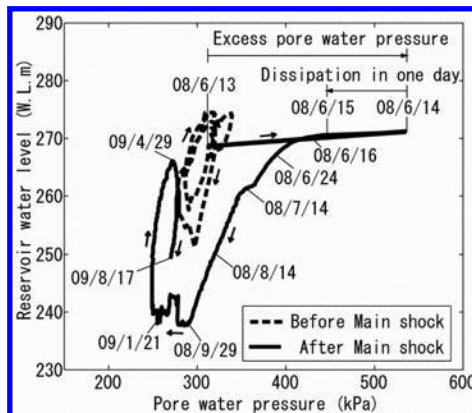


Figure 10. Time history of pore water pressure at meter #16.

indicate locations of the meters and a simple distribution is assumed on the upstream side. The section is the cross section A-A' shown in Figure 1(b) where the seismometers are installed.

The pore water pressure of June 13, 2008 (denoted by 2008/6/13) was distributed in the typical pattern of a normal steady state condition, although the estimated phreatic line was not so smooth as expected, maybe due to some mechanical errors included in the readings. On June 14, seventeen minutes after the main shock, the distribution pattern had changed to exhibit a sudden build-up of excess pore water pressure especially at the lower part of the core zone, while the build-up was not so obvious in the other zones such as filter and transition zones.

Figure 10 shows a series of the daily readings of the pore water pressure meter #16 whose location is shown with a solid circle at EL.225 m in Figure 9. It can be seen that after the main shock, with a continuous drawdown of the reservoir water level to W.L.237.7 m, the pore water pressure showed a monotonous decrease. The readings on June 13, 14 and 15 were 314, 535 and 442 kPa, respectively. Hence, the excess pore water pressure produced by the main shock was dissipated by 42% within a single day after the main shock. The dissipation of the excess pore water pressure seems faster than the long-term recovery of the decreased wave velocity.

9 CONCLUSIONS

Conclusions drawn from the present study are:

- During the main shock of the 2008 earthquake, the acceleration of the stream component exceeded 10 m/s^2 at the gallery, but did not exceed 5.3 m/s^2 at the dam crest.
- The intense shaking of the main shock induced large shear strains in excess of 10^{-3} in the stream direction and a little below 10^{-3} in the dam-axis direction.
- Due to the large strains in the horizontal directions, the shear modulus G exhibited a remarkable decrease from the initial shear modulus G_0 by 90% in the upper part and 60% in the lower part of the core.
- As a result of the decrease in G , the shear wave velocity V_s in the core was significantly reduced and the fundamental period of the dam was elongated to $T = 1.20 \text{ s}$, which lead to the attenuation of the earthquake response of the dam.
- Towards the end of the main shock, the modulus G in the core showed a gradual increase, but remained below G_0 and was anisotropic.
- The decreased shear wave velocity continued to recover and the anisotropy decreased with the passage of time, and the full recovery of the wave velocity to the initial one of isotropy was found to take at least one year.
- During the main shock, excess pore water pressure was also induced in the core. The dissipation of the excess pore water pressure seemed faster than the recovery of the decreased wave velocity.

ACKNOWLEDGEMENTS

The authors would like to express their thanks to the civil engineers in Miyagi Prefecture for providing information about earthquake response of the Aratozawa dam.

REFERENCES

- Japan Meteorological Agency. 2008. Iwate-Miyagi Nairiku earthquake in 2008. http://www.seisvol.kishou.go.jp/eq/2008_6_14_iwate-miyagi/index.html
- Okamoto, S. 1984. Earthquake resistance of embankment dams. *Introduction to Earthquake Engineering 2nd Edition*. Japan: University of Tokyo Press.
- Sawada, Y. & Takahashi, T. 1975. Study on the material properties and the earthquake behavior of rockfill dams. *Proc. 4th Japan Earthquake Engineering Symposium*: 695–702.

Seismic stability of a Peruvian tailings earth-rockfill dam with liquefiable foundation

M. Seid-Karbasi, H. Hawson & U. Atukorala

Golder Associates Ltd, Vancouver, BC, Canada

ABSTRACT: Earthquake remains a direct threat to the stability of earth structures and life-lines. Liquefaction of water-saturated soils is one of the major risks that affect the safety and post-earthquake stability of dams and in particular tailings dams. Although, notable advancements have been made over the past several decades on the understanding of soil liquefaction mechanism, the advancements are confined to assessing the likelihood of triggering of liquefaction. Only limited progress has made on the consequences of soil liquefaction i.e. induced ground movements, which ultimately have a significant impact on the overall stability of dams.

Dam crest displacements and the intactness of the seepage control system under strong ground shaking have substantial effects on the global stability of the dam and the potential for release of its contents. This paper describes the results of dynamic analyses conducted as part of closure design for an existing 72 m high earth-rockfill dam retaining tailings founded on thick interlayer strata, which in turn, is underlain by limestone bedrock. The key objective of the analyses was to assess the potential for release of toxic mine tailings to the environment immediately downstream of the dam following closure of the facility. The dam is classified as a “*High Consequence*” structure under the 2007 Canadian Dam Association Guidelines (CDA). Coupled stress-flow analyses were carried out utilizing *FLAC* computer code and the user-defined constitutive models *UBCSAND* and *UBCHYST* to model the liquefiable soils and to account for the hysteretic and nonlinear behavior of the non-liquefiable soils, respectively. The results show that the presence of the liquefied alluvium leads to a significant deformations of the overlying dam with risk of global instability and loss of freeboard.

1 INTRODUCTION

The seismic safety of embankment dams is controlled by the permanent deformations induced as a result of strong shaking and the intactness of the seepage control system. If the prime concern is the dam crest post-earthquake displacements, there are a number of simplified pseudo-static methods of analyses (e.g. Newmark 1965, Sarma 1975, Makdisi & Seed 1978, Bray 2007 among others) along with data from past earthquakes that can be utilized to evaluate the anticipated overall performance of the dam under seismic loading conditions. These observations indicate that the induced seismic deformations are commonly manifested as dam crest deformations and bulging of the dam body (e.g. Seed 1979 & Marcuson et al., 2007).

Therefore, as far as the freeboard of dam reservoir is concerned the dam crest permanent deformations is a good measure to assure safe post-shaking dam performance, also this is an index that represents the general response of a dam to a given earthquake. There are a few correlations to estimate dam crest settlement suggested by a number of people (e.g. Swaisgaard 2003, Singh & Roy 2009 and Ishihara 2010 among others).

However, when liquefiable materials are present in the dam body or its foundation the simplified pseudo-static methods analyses and those correlations based on past observations data cannot be relied upon, and more rigorous procedures should be employed. The performance of embankment dams during past earthquakes indicates that occurrence of liquefaction in foundation soils and/or the dam body plays a key role in the stability of the dams (Seed 1979, Marcuson et al., 1996 & 2007). The incidents in tailings dams and impoundments are more

frequent (*ICOLD* 2001). Data from *USCOLD* (1994) also indicate that earthquakes are one of the major causes of failure of tailings dams.

In most cases, damage has occurred as a result of a large drop in the stiffness and strength of soil resulting from liquefaction. Two tailings dams within the Mochikoshi gold mining complex in Japan failed due to liquefaction of tailings from the 1978 Izu-Ohshim-Kinkai earthquake. One dam failed at the end of earthquake whereas the other one failed about 24 hours later. Information on the failure of Mochikoshi tailings dams can be found in a number of publications (e.g. Ishihara 1984, Seid-Karbasi & Byrne 2004).

In general, two types of factors control the response of an earth structure to earthquake excitation, namely:

- Mechanical conditions
- Flow/Hydraulic conditions.

Mechanical conditions include soil density, stiffness and strength, static stress state, and earthquake characteristics (amplitude, No. of cycles, etc.) and are responsible for the generation of excess pore pressures during cyclic loading. Flow conditions include drainage path, soil hydraulic conductivity (permeability) and its spatial variation within the soil medium (permeability contrast) and are responsible for the re-distribution and dissipation of excess pore pressures both during and after earthquake shaking. Detailed discussions regarding these factors may be found in Seid-Karbasi & Byrne (2006a and 2007). Although, notable advancements have been made over the past several decades in understanding the mechanism of soil liquefaction, much of the progress was limited to assessing the likelihood of triggering liquefaction focusing primarily on the mechanical conditions.

From a geotechnical engineering point of view, the earthquake-induced deformations are often the prime concern if significant zones of foundation soils and/or soils comprising the dam body are prone to liquefaction. To accurately predict the induced deformations, it is necessary to employ a coupled stress-flow analysis procedure. This paper describes the results of a fully coupled stress-flow dynamic analysis procedure used to predict seismic deformations and stability of an existing 72 m high tailings dam. The procedure captures the sand element behavior observed in cyclic laboratory tests, and has been verified by comparisons with physical model tests and field experience. The dam is to be constructed to retain tailings during mining and also following closure. The fully coupled stress-flow analysis has been carried out using the constitutive model *UBCSAND* that captures the liquefiable soil response. The nonlinear behavior of non-liquefiable materials was accounted for by employing the model *UBCHYST*. These user-defined constitutive models are incorporated into the commercially available computer code *FLAC* (*Itasca*, 2005). The dam specifications, foundation characteristics and predicted behavior are discussed in the following sections.

2 DAM DESCRIPTION AND SITE CONDITIONS

The Tlacayan tailings dam is located 8 km north of the main complex site of Atacocha Mining Company (*Compania Minera Atacocha, CMA*) in the Rio Huallaga valley, Peru. Dam construction was started in 1988 and the dam has been raised in several stages since 1995 up to 2004 to retain tailings from copper mining operation.

Tailing Storage Facility (*TSF*) comprises a “High Consequence” based on Canadian Dam Association guidelines (*CDA* 2007) tailings dam that is 72 m in height (at closure condition) with upstream and downstream slopes of 0.5H: 1V and 1.4H: 1V, respectively. The dam is founded directly on a 15 m soil foundation underlain by limestone bedrock. The dam comprises of tailings sand zones in upstream and downstream shells. The downstream shell has also an external zone of rock-fill material composed of waste mine rocks retained by a 12 m high reinforced concrete wall with counterfort at 5 m spacing that accommodates a main road at the downstream (D/S) dam toe aligned parallel to the dam crest. The dam has a central core of gravelly clay soils which is protected by filter layers at upstream and downstream sides. There is an incomplete parapet wall at the upstream (U/S) dam crest which does not provide any additional freeboard. [Figure 1](#) shows the maximum cross section of the dam.

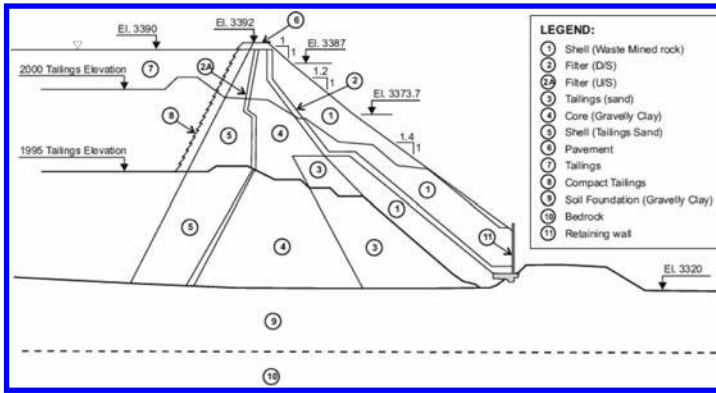


Figure 1. Current typical maximum cross-section of the Tlacacayan Tailings dam.

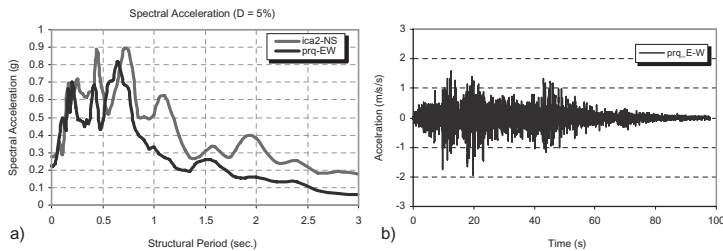


Figure 2. Ground motion, a) Spectral acceleration, b) Typical acceleration time history.

The foundation conditions at the dam site have been established based on available site investigations data indicates the presence of 15 m of foundation soil composed of coarse materials with variable fines contents over limestone bedrock.

2.1 Seismicity and ground motion parameters

The Tlacacayan dam site is located in a complex, geologically active region east of a major plate boundary where numerous damaging historical earthquakes have occurred. Peru, as with most of western South America, is situated along the western edge of the convergent plate boundary between the South America plate in the east and Nazca plate to the west. The eastern edge of the oceanic Nazca plate in this region is marked by the deep Peru-Chile Trench (PCT) offshore. The western edge of the continental South America plate is marked by broad, high mountains of the Western and Eastern Peruvian Cordillera, and the numerous folds and faults that mark the eastern boundary of the Andes Range.

The horizontal peak firm-ground acceleration of 0.35 g. was established for the dam site for *MDE*. Figure 2 shows the spectral accelerations and a typical time-history of the firm-ground acceleration records of the earthquakes (applicable components) considered for dynamic analyses of the Tlacacayan dam for the closure condition. The records are long with different initial *PGAs*. The input motions applicable at the base of the models of the pond and soil foundation were derived from a 1-dimensional soil column taken near the upstream and downstream toe of the dam using the public domain computer code *ProShake* (*EduPro Civil Systems* 2003), where the bedrock *PGA* was scaled to 0.35 g.

3 ANALYSIS PROCEDURE

The response of the dam-foundation and impounded tailings to earthquake shaking has been analyzed in two stages. In the first stage, the dam body and its foundation has been analyzed

under gravity loads (static mode) with drained conditions to establish the pre-earthquake stress state. Thereafter, the analysis was switched to the dynamic mode with undrained properties for fine-grained soils (i.e. dam core).

The analysis outlined above has been conducted using the computer program *FLAC* (Version 5.0, *ITASTCA*, 2005). This is a commercial, finite difference analysis code capable of coupled stress-flow analysis under static and dynamic loading conditions. The earthquake motions were applied as a time history of excitation at the model boundaries. As the earthquake motions were “outcrop” records (i.e. without any overburden effects) and the dam is not founded directly on bed rock, the earthquake motions were converted to “within” motion. This process was undertaken by site response analysis employing the 1-D computer code *ProShake* (Civil Systems, 2001) and taking into consideration the modulus reduction and damping behaviour of the foundation soils as documented in the literature (i.e. Seed and Idriss 1986; Vucetic and Dobry 1991 and Yasuda et al., 1993 & 2003).

To model sandy soil behavior and account for shear induced (excess) pore pressures and the effects of pore water pressure redistribution and dissipation during and after seismic shaking, a dynamic coupled stress-flow analysis was employed. In such an analysis, the volumetric strains are controlled by the compressibility of the pore fluid and flow of water through the soil elements. An effective stress-based elasto-plastic constitutive model (*UBCSAND*) was used in the coupled dynamic analysis. The model has been calibrated using laboratory test data as well as centrifuge data and is described below briefly.

3.1 Constitutive model for sands

The *UBCSAND* constitutive model is based on the elasto-plastic stress-strain model proposed by Byrne et al. (1995), and has been further developed by Beaty & Byrne (1998) and Puebla (1999). The model has been previously used in analyzing the *CANLEX* liquefaction embankments (Puebla et al., 1997) and predicting the failure of Mochikoshi tailings dam (Seid-Karbasi & Byrne 2004). It has also been used to examine partial saturation conditions on liquefiable soil response (Seid-Karbasi & Byrne 2006b) and to predict centrifuge model tests under dynamic loading (e.g. Byrne et al., 2004 & Seid-Karbasi et al., 2005). It is an incremental elasto-plastic model in which the yield loci are lines of constant stress ratio ($\eta = \tau / \sigma'$). Plastic strain increments occur whenever the stress ratio increases. The flow rule relating the plastic strain increment direction is non-associated. A detailed description of the model may be found elsewhere (e.g. Byrne et al., 2004 & Puebla et al., 1997). The constitutive behaviour of sand is controlled by the soil skeleton. The pore fluid (e.g. water) within the soil mass acts as a volumetric constraint on the skeleton if drainage is fully or partially curtailed. This model has been incorporated into the *FLAC* code as a user-defined model.

The key elastic and plastic parameters for the *UBCSAND* constitutive model were developed based on empirical correlations between the parameters and relative density, D_r , or normalized Standard Penetration Test values, $(N_1)_{60}$. The model parameters were chosen so as to simulate the behavior of sand under monotonic and cyclic loading conditions as observed in the laboratory (e.g. Byrne et al., 2004 & Seid-Karbasi et al., 2005). Currently, the constitutive model can be used to simulate the behavior of soils with a range of relative density or N values. The model has also been calibrated to reproduce the *NCEER 97* (Youd et al., 2001) liquefaction-resistance chart, which in turn is based on field data collected from past earthquakes and is expressed in terms of Standard Penetration Test, $(N_1)_{60}$ values.

3.2 Dam-foundation model and input parameters

The 72 m high dam and the impoundment tailings were discretized using a finite difference grid comprising 88×188 zones in the vertical and horizontal directions, respectively. The nominal thickness of zones within the dam body was 1.0 m. The model extended about 225 m from the upstream toe area of the dam over a total length of about 500 m. The pond tailings were assumed to be horizontal where the phreatic surface within the tailings tends to the impoundment surface at about 350 m from *U/S* edge of the dam crest. The built-in *Mohr-*

Coulomb model with stress-level dependent parameters and *UBCSAND* constitutive model were applied to liquefiable and non-liquefiable zones (e.g. tailings and rockfill, respectively).

The strength parameters of the rockfill were estimated based on data from similar cases found in the literature (e.g. Leps 1970, Marsal 1973, Indraratna et al., 1993 & Charles 2008). Similar stress level dependent strength and moduli of deformation have been used in the dynamic analysis of other dams (Seid-Karbasi et al., 2008a). The estimated parameters are listed in [Table 1](#). The parameters are comparable to the lower-bound values complied by Leps (1970). The small-strain shear modulus, G_0 and friction angle, ϕ were estimated based on Seed & Idriss (1970), Seed et al. (1986) and, Barton & Kjaersnli (1981), respectively.

$$G_0 = 21.7 (k_{2-\max}) P_a (P'/P_a)^{0.5} \quad (1)$$

$$\phi = \phi_1 - \Delta\phi \log(\sigma'_3 / P_a) \quad (2)$$

where, $k_{2-\max}$, P_a , P' , σ'_3 , ϕ_1 , and $\Delta\phi$ are stiffness parameter, atmosphere pressure (100 kPa), effective mean stress, minor principal effective stress, reference friction angle (at $P' = P_a$), and friction angle reduction for every log cycle of stress level increase, respectively. The soil foundation was characterized based on $(N_1)_{60}$ corrected for fines content inferred from data obtained from downstream drilled boreholes ([Figure 3b](#)).

For seismic loading the non-linearity of material stiffness in the core and rockfill zone was modeled using the user-defined subroutine *UBCHYST* model developed at the University of British Columbia (Byrne 2006). Other materials within the foundation and dam body (e.g. foundation soil, tailings, zone 3 and zone 5) were inferred that would respond as sand-like material during earthquake shaking and develop excess pore water pressures and/or likely undergo liquefaction. To take into consideration the seismic pore pressure generation of these types of soils, *UBCSAND* constitutive model was used to model the constitutive behaviour of these materials. The tailings were represented in the model with a variable $(N_1)_{60}$ with vertical effective stress as depicted on (see [Figure 3a](#)).

The 12 m retaining concrete wall and its base at the downstream dam toe were represented as elastic beam elements connected/interacting with the main dam model through interface elements. The elastic properties of the structural elements for the concrete retaining wall were as: $E = 2.5e7$ kPa, $I_{\text{wall}} = 0.0095$ m⁴, $I_{\text{base}} = 0.0504$ m⁴. The 3-D stiffening effect of the wall but-

Table 1. Material properties used in *FLAC* analyses.

Soil type	$\gamma_{(\text{dry})}$ (kN/m ³)	ϕ' (°)	$\Delta\phi^1$ (°)	G^2 (kPa)	B^3 (kPa)	$(N_1)_{60}^4$
ROCKFILL (zone 1)	2.4	40.0	6.0	3e4	8e4	–
D/S shell tailings SAND (zone 3)	2.15	35.2	–	–	–	22 ⁵
Gravelly core (zone 4)	2.0	30.0	–	1.9e4	4.8e4	–
U/S shell tailings SAND (zone 5)	2.15	35.2	–	–	–	22
TAILINGS (zone 7)	1.7	–	–	–	–	Variable (see Figure 3a)
FOUNDATION soil	2.0	–	–	–	–	Variable (see Figure 3b)

- Friction angle reduction for one-fold of confining stress increase.
- Static shear stiffness at $\sigma'_m = 100$ kPa was taken as $G = G_0/9$, where G_0 is the small strain shear modulus of materials (e.g. rockfill) estimated as $G_0 = 21.7(k_{2-\max}) \cdot \text{Pa} \cdot (\sigma'_m / \text{Pa})^{0.5}$ with $(k_{2-\max}) = 125$ for rockfill (see Vrymoed, 1981, Seed et al., 1985, and Uddin & Gazetas, 1997). The parameters are listed for a reference confining stress (100 kPa).
- Bulk modulus, B calculated from G for $K_o = 0.5$ ($K_o = \sigma'_x / \sigma'_y$).
- Pond tailings, dam body sandy zones (i.e. 3, 5) and soil foundation were modeled as soils susceptible to seismic excess pore water pressure generation using the user-defined constitutive model *UBCSAND* with (see [Figure 3 & 4](#)) varying $(N_1)_{60}$ with depth estimated.
- Estimated based on construction data indicating compaction ratio more than 95% (modified proctor).

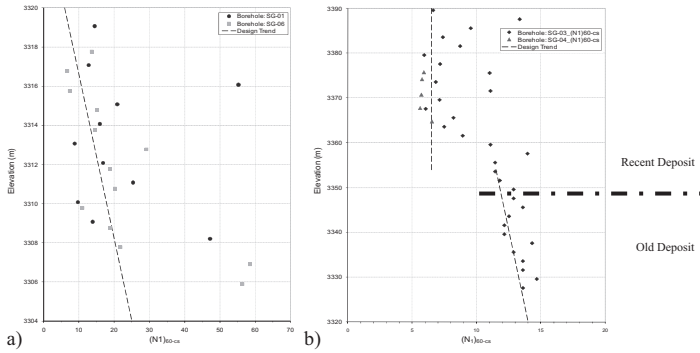


Figure 3. Materials characterization, a) Soil foundation, b) Impoundment tailings.

tresses was accounted for by an increase in the section moment of inertia “I” as of a 2-way slab supported in 3 sides with fixity which is controlled by width/length ratio of the slab.

4 RESULTS AND DISCUSSION

The dynamic analysis was carried out following establishing the equilibrium conditions under gravity loading (static condition) and steady-state flow condition that determines the pre-earthquake stress state. Then the computations continued in the dynamic mode which the results are discussed in the followings.

The predicted seismic response of the pond tailings-dam-foundation system when subjected to the *MDE* ground motion (labeled as “*prq*” earthquake record, E-W component, see Figure 2) is described in this section.

Figure 4 shows a typical analysis results in terms of the seismic-induced excess pore water pressure ratio, R_u , after 20 s of shaking. The results indicated that the tailings (below the pond water level) develop high excess pore water pressures at an early stage of earthquake shaking and they occur over the full depth of the tailings. Also, it was observed that high excess pore water pressures are built-up in the soil foundation and in particular at the *D/S* dam toe. The global stability of the dam is essentially controlled by the *D/S* soil foundation strength with low confining stresses behind the *D/S* toe retaining wall. The analysis suggested that the downstream shell of the dam undergoes large deep seated movements (>1.5 m) that leads to general instability of the dam-foundation system. Therefore it was decided that to examine the effects of dam height reduction as depicted in Figure 5 to enhance the dam seismic safety.

Figure 6 shows the lateral displacement contours for the case of the modified dam subjected to the *MDE* ground motions (“*prq*” earthquake record, E-W component) after end of shaking (100 sec.). Also, it shows the time histories of the top and bottom of the *D/S* wall. As may be seen, large lateral displacements extend from the dam crest to the *D/S* slope toe that is controlled by the *D/S* retaining wall displacements with more than 3.5 m movement. The predicted vertical displacement for the *D/S* crest edge for the modified dam section is still large (>1.5 m) however, the crest width in this case is large enough to reduce the vertical displacement at the upstream edge of the crest to lower 0.5 m. Hence, it can be inferred that the risk of loss of freeboard is not significant particularly with respect to the low water level in the pond. The analysis indicated that the wall rotates largely at the end of shaking while it also moves translational to downstream during the strong shaking. The analysis predicted that the wall moves in phase with the soil mass and the differential velocity at 100 sec. is negligible and overturning of the wall is unlikely, however its distortion is quite large.

In regard to large distortion of the wall and deep seated dam movements pattern that endangers the post-earthquake service of the downstream road, it was decided to relocate the road.

It should be noted that prediction of such behavior involving soil-structure interaction using conventional simplified procedures is not feasible.

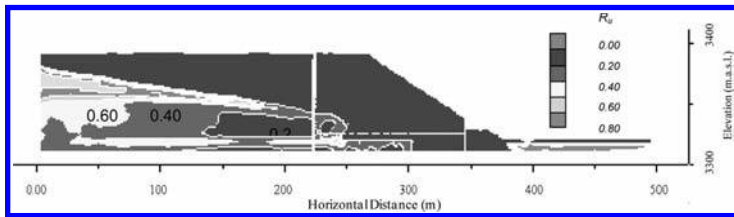


Figure 4. Contours of excess pore water pressure ratio, R_u at 20 sec. of shaking.

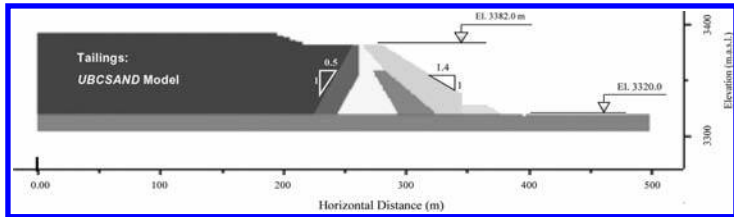


Figure 5. Tailings-dam-foundation system model used in analysis.

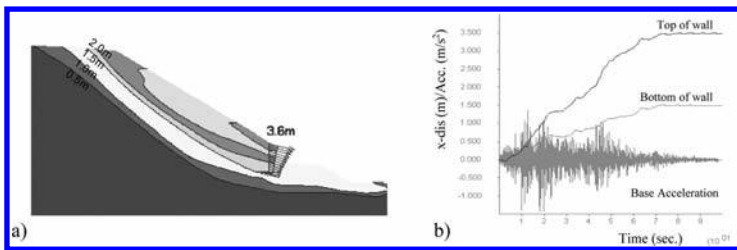


Figure 6. Modified dam lateral displacements, a) D/S shell, b) Wall movement time histories.

5 CONCLUSIONS

A fully coupled stress-flow procedure was applied to predict the behavior of a tailings dam founded on liquefiable soil foundation for the closure condition subjected to *MCE* motion. The following can be construed from the study:

- The seismic behavior of earth structures is controlled by two key factors: Mechanical factors and Hydraulic/Flow factors;
- Rigorous methods are efficient tool to provide an insight into the earth structures seismic behavior and to optimize remedial measures.
- The tailings dam for closure, will require some toe buttressing to accommodate predicted *MCE* ground motion.

REFERENCES

- Barton, N. & Kjaersli, B. 1981. Shear Strength of Rockfill, *ASCE J., Geotech. Eng. Div.*, V. 107(GT7): pp. 873–891.
- Beatty, M.H. & Byrne, P.M. 1988. An Effective Stress Model for Predicting Liquefaction Behavior of Sand. *Proc., Conf., Geotech. Eq. Engg. & Soil Dyn. III*, ASCE GSP No. 75, V1, pp. 766–777.
- Bray, J.D. 2007. Simplified Seismic Slope Displacement Procedures. In *Proc., Earthq. Geotech. Engg.*, pp. 327–353.
- Byrne, P.M. 2006. Personal Communications.
- Byrne, P.M., Roy, D., Campanella, R.G. & Hughes, J. 1995. Predicting Liquefaction Response of Granular Soils from Pressuremeter Tests. *ASCE National Convention, ASCE, GSP. 56*, pp. 122–135.
- Byrne, P.M., Park, S., Beatty, M., Sharp, M., Gonzalez, L. & Abdoun, T. 2004. Numerical Modeling of Liquefaction and Comparison with Centrifuge Tests, *Can. Geotech. J.*, V. 41, pp. 193–211.

- Candaian Dam Association Guidelines, 2007. *CDA*.
- EduPro Civil Systems, 2001. Proshake, Ground Response Analysis. Version 1.1, *User's Manual*, EduPro Civil Systems Inc. Redmond, Washington.
- ICOLD 2001. Tailings Dams, Risk of Dangerous Occurrences. Bul. 121, *Int. Commiss., Large Dams, Paris*. p. 144
- Ishihara, K. 2010. Performances of Rockfill Dams during Recent Earthquakes. In *Proc., 5th Int. conf., Recent Advances in Geotechnical Engg. And soil Dynamics*. Paper No. IMI 5.
- ITASCA, 2005. Fast Lagrangian Analysis of Continua (FLAC), V.5. *User's Guide*. Itasca Consulting Group, Inc.
- Leps, T.M. 1970. Review of Shear Strength of Rockfill. *ASCE J., Soil Mech. & Found. Engg. Div.*, V. 96(SM4), pp. 1159–1170.
- Makdisi, F.I. & Seed, H.B. 1978. Simplified Procedure for Estimating Dam and Embankment Earthquake-Induced Deformations. *J. Geotech. Eng.*, 104(7), pp. 1427–1434.
- Marcuson III, W., Hadala, P. & Ledbetter, R. 1996. Seismic Rehabilitation of Earth Dams, Design and Analysis of Embankment Dams, *J. Geotech. Engg., ASCE*, 122(1), pp. 7–20.
- Marcuson III, W., Hynes, M. & Frankin, A. 2007. Seismic Design and Analysis of Embankment Dams: State of Practice. *Burmister Lecture*, available at: www.civil.columbia.edu/ling/burmister
- Newmark, N.M. 1965. Effects of Earthquakes on Dams and Embankments. *Geotechnique*, 15(2), pp. 139–160.
- Puebla, H. 1999. A Constitutive Model for Sand Analysis of the CANLEX Embankment. *PhD. Thesis*, Civil Engg. Dept., Un., British Columbia, Vancouver, B.C.
- Puebla, H., Byrne, P.M. & Phillips, R. 1997. Analysis of CANLEX Liquefaction Embankment: Prototype and Centrifuge Models. *Can. Geotech. J.*, 34, pp. 641–654.
- Saboya J.F. & Byrne, P.M. 1993. Parameters for Stress and Deformation Analysis of Rockfill Dams. *Canadian Geotechnical J.*, V. 30, pp. 690–701.
- Sarma, S.K. 1975. Seismic Stability of Earth Dams and Embankments. *Geotechnique*, 25(4), pp. 743–761.
- Seed H.B. & Idriss, I.M. 1970. Soil Moduli and Damping Factors for Dynamic Response Analyses. *Report No. EERC 70-10*, Earthquake Engineering Research Center, University of California, Berkeley.
- Seed, H.B., Wong, R.T., Idriss, I.M. & Tokimatsu, K. 1986. Moduli and Damping Factors for Dynamic Analyses of Cohesionless Soils. *ASCE J., Geotech. Engg.*, V. 112(GT11), pp. 1016–1032.
- Seed, H.B. 1979. Considerations in the Earthquake-Resistant Design of Earth and Rockfill Dams. *Geotechnique J.*, V. 29(3), pp. 215–263.
- Seed, H.B., Idriss, I.M., Lee, K.L. & Maksidi, F.I. 1975. Dynamic Analysis of the Slide in the Lower San Fernando Dam during the Earthquake of February 9, 1971. *ASCE J., Geotech. Engrg.*, V. 101(GT9), pp. 889–911.
- Seed, H.B., Seed, R.B., Lai, S.S. & Khamenehpour, B. 1985. Seismic Design of Concrete-Face Rockfill Dams. In *Proc., Symp., Concrete-Face Rockfill Dams- Design, Construction and Performance*, ASCE, N.Y. pp. 459–478.
- Seid-Karbasi, M. & Byrne, P.M. 2004. Embankment Dams and Earthquakes. *Hydropower and Dams J.*, V.11(2), pp. 96–102.
- Seid-Karbasi, M., Byrne, P.M., Naesgaard, E., Park, S., Wijewickreme, D. & Phillips, R. 2005. Response of Sloping Ground with Liquefiable Materials during Earthquake: A Class A Prediction. In *Proc., 11th Int. Conf., Int. Ass., Computer Methods & Advances in Geomechanics, IACMAG*, Turin, V. 3, pp. 313–320.
- Seid-Karbasi, M. & Byrne, P.M. 2006a. Significance of Permeability in Liquefiable Ground Response. In *Proc., 59th Canadian Geotechnical. Conf.*, pp. 580–587.
- Seid-Karbasi, M. & Byrne, P.M. 2006b. Effects of Partial Saturation on Liquefiable Ground Response. In *Proc., ASCE 2006 Geo-Congress, Geotechnical Engineering in Information Tech. Age*, Atlanta, Georgia, Paper No. 11803.
- Seid-Karbasi, M. & Byrne, P.M. 2007. Seismic Liquefaction, Lateral Spreading and Flow Slides: A Numerical Investigation into Void Redistribution. *Canadian Geotechnical J.*, V. 44, pp. 873–890.
- Swaigood, J. 2003. Embankment Dam Deformations caused by Earthquakes. In *Proc., Pacific Conference on Earthquake Engineering*, Paper No. 14.
- USCOLD. 1994. Tailings Dam Incidents. *US. Committee on Large Dams*, p. 82
- Uddin N. & Gazetas, G. 1997. Dynamic Response of Concrete-Faced Rockfill Dams to Strong Excitation. *J. Geotech. Engg. Div.*, ASCE, V. 1210(GT2): 185–197.
- Youd, T.L., Idriss, I.M., Andrus, R., Arango, I., Castro, G., Christian, J., Dobry, J., Finn, L., Harder Jr., L., Hynes, H.M., Ishihara, K., Koester, J., Liao, S.S., Marcuson III, W.F., Martin, G., Mitchell, J.K., Moriwaki, Y., Power, M.S., Robertson, P.K., Seed, R.B. & Stokoe II, K.H. 2001. Liquefaction Resistance of Soils: Summary Report from the 1996 NCEER and 1998 NCEER/NSF Workshops on Evaluation of Liquefaction Resistance of Soils. *J. Geotech. and Geoenviron. Engg.*, ASCE, V. 127, pp. 817–833.

Simplified methodology for estimating seismic coefficients for the pseudo-static slope stability analysis of earth dams

A.G. Papadimitriou

Department of Civil Engineering, University of Thessaly, Greece

K.I. Andrianopoulos & G.D. Bouckovalas

Geotechnical Department, School of Civil Engineering, National Technical University of Athens, Greece

K. Anastasopoulos

Public Power Corporation S.A., Greece

ABSTRACT: This paper presents a simplified methodology for the estimation of seismic coefficients for pseudo-static slope stability analysis of earth dams and tall embankments. This methodology is based on a statistical analysis of numerical results from 110 non-linear seismic response analyses of 2D cross sections with height ranging from 20 to 120 m. The peak value of the seismic coefficient is estimated as a function of: (a) the peak ground acceleration at the free field, (b) the predominant period of the seismic excitation, (c) the non-linear (first) eigen-period of dam vibration, (d) the stiffness of the foundation soil, and (e) the geometrical characteristics and the location (upstream or downstream) of the failure surface. The effective value of the seismic coefficient is estimated as a percentile of the peak ground acceleration, on the basis of the allowable permanent seismic displacement.

1 INTRODUCTION

It is well known that the pseudo static stability analysis of earth dams leads to the estimation of a Factor of Safety FS_d against seismic “failure” of its slopes. The described problem is illustrated in Fig. 1, which also depicts critical problem parameters like the peak values of the seismic acceleration at the crest, $a_{\max, \text{crest}}$, at the outcropping bedrock PGA_1 and in the “free-field” of the foundation soil, PGA . The critical measure of the whole analysis is the value of the horizontal inertial force F_h that is applied at the center of gravity of the sliding mass and equals to the weight of the mass W multiplied by a dimensionless seismic coefficient k_h . Therefore, the selection of an appropriate value for k_h is critical for the estimation of FS_d and of exceptional importance for the rational and safe design of an earth dam.

In any case, the value of k_h should reflect the vibration of the sliding mass during the design earthquake. Given that the sliding mass is not rigid, different locations within the mass do not vibrate in phase (especially deep sliding masses in tall dams) and their vibration is not of equal intensity (e.g. it intensifies near the surface of the dam). Therefore, and as a first approximation, the value of k_h could be selected to correspond to the peak value of the resultant (“average”) acceleration time history of the sliding mass. Yet, such a value of k_h is only observed momentarily and therefore the design of earth dams using this value along with a requirement for $FS_d \geq 1.0$ leads to an over-conservative approach. Hence, common practice dictates the use of an “effective” value of the seismic coefficient k_{hE} (a percentile of k_h) in combination with the foregoing requirement, at the expense of the occasional development of generally small permanent slope displacements after the end of the design earthquake.

Despite the wide use of the pseudo-static method of limit equilibrium of slopes, there is still no widely accepted methodology for estimating seismic coefficients for the design of

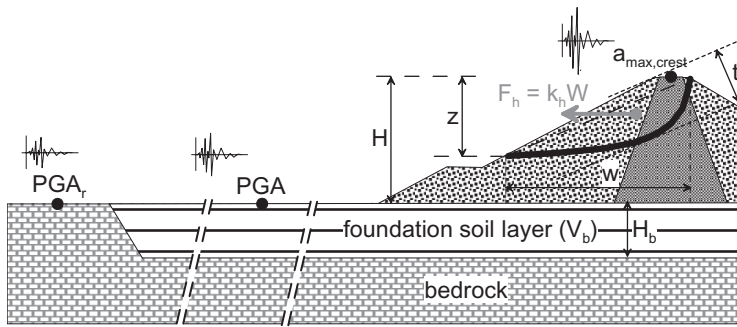


Figure 1. Definition of critical parameters for seismic slope stability of earth dams.

earth dams. This paper aims at filling this gap, by proposing a rational and user-friendly methodology for estimating seismic coefficients, taking into account performance-based criteria on the basis of allowable slope displacements.

2 LITERATURE REVIEW

Based on Kramer (1996) and the detailed presentation of Papadimitriou et al (2010), the existing methodologies for estimating seismic coefficients may be divided roughly into three (3) categories, i.e. on the basis of: a) local seismicity (e.g. Terzaghi 1950, old guidelines of the US Corps of Engineers), b) the PGA (e.g. USCOLD 1985, British Standards: Charles et al 1991), and c) the $a_{\max,crest}$ (e.g. Makdisi and Seed 1978, Marcusson 1981). As concluded by Papadimitriou et al (2010), the usually selected values of effective seismic coefficients ($k_{hE} = 0.10$ to 0.20) are found to be safe choices for cases of $PGA \leq 0.30$ g, but may prove severely unconservative for cases designed for higher intensity earthquakes. In parallel, the correlation of seismic coefficients to the value of $a_{\max,crest}$ is theoretically sound, but creates a practical problem of estimating $a_{\max,crest}$, a parameter for which there is no established user-friendly estimator procedure. Furthermore, the ratio of the effective over the peak value of the seismic coefficients k_{hE}/k_h ranges significantly in the literature (i.e. from 0.5 to 0.8), with no direct correlation to specific values of permanent slope displacements.

Given the foregoing problems, Papadimitriou et al (2010) proposed a simplistic methodology that was based on a statistical analysis of input data and results from already performed numerical analyses of real earth dams owned by the Public Power Corporation S.A. of Greece (ΔΕΗ Α.Ε.) and other Greek Agencies. This methodology had the benefit of completeness (it provides estimates of the seismic coefficients, requiring seismological data and the geometry of the earth dam), user-friendliness (may be programmed in a worksheet) and led to increased accuracy in comparison to existing methodologies from the literature. Yet, it suffered from a rather narrow range of applicability defined from the range of variation of important problem parameters in the analyses on which it was based.

3 NEW METHODOLOGY

The hereby proposed methodology is based on the basic principles of the methodology of Papadimitriou et al (2010), but has a quite wider range of applicability. More importantly, it takes into account in a systematic manner parameters like the stiffness of the foundation soil (introduced via the shear wave velocity V_b in the respective layer), the exact geometric characteristics (z , t , w in Fig. 1) and the location (upstream or downstream) of the failure surface. It was based on 110 two-dimensional (2D) seismic response analyses of earth dams that yielded results for 1084 potential failure surfaces. The analyses were performed using the finite difference code FLAC (Itasca Inc 2005) in which the geomaterials obeyed a (Ramberg-

Osgood type) non-linear hysteretic constitutive law. The analyses studied parametrically the effects of:

- Intensity and frequency content of the seismic excitation
- Foundation conditions
- Existence of (large) stabilizing berms
- Reservoir impoundment, and
- The geometric characteristics of the potential failure surface.

In order to provide for the greatest possible applicability of the methodology, the response of four (4) cross sections was analyzed, namely cross sections of:

- H = 20 m, that simulates the response of a tall earth embankment
- H = 40 m, that simulates the response of a rather short earth dam
- H = 80 m, that simulates the response of a medium height earth dam, and
- H = 120 m, that simulates the response of a tall earth dam.

The slope inclinations of the earth dams ranged from 1:2 to 1:2.5 (vertical: horizontal). In the cases of H = 40, 80 and 120 m the earth dam possessed a clay core with slope inclinations ranging from 4:1 to 5:1, while for the case of H = 20 m the embankment was considered uniform. In addition, and in order to investigate the effect of (large) stabilizing berms on the response, variations of the foregoing sections were studied that possessed berms of height and width equal to H/3 and 2H/3 respectively on both sides of the body of the dam.

The remainder of this paper presents the new methodology in a step-by-step manner, providing evidence of the accuracy provided in each step. In particular, the seismic coefficients may be estimated in five (5) successive steps, as follows:

Step 1: Estimation of PGA and predominant period T_e of the seismic excitation

The seismic hazard study for an earth dam proposes values for the peak ground acceleration (PGA_p) and the elastic response spectrum (for 5% damping) at the outcropping bedrock for the various design earthquakes (MDE, OBE, RIE). For any of the design earthquakes, the predominant period T_e may be estimated as the structural period (or the range of structural periods) leading to the peak spectral accelerations. The estimation of PGA is based on PGA_p , but should take into account the potential local amplification due to the foundation soil. Therefore, one may outline two cases:

- a. the earth dam is founded on rock, and therefore $PGA = PGA_p$,
- b. the earth dam is founded on a soil layer overlying rock (e.g. as shown in [Figure 1](#)).

In the second case, the estimation of PGA may be performed either via a numerical analysis [e.g. the equivalent-linear method employing SHAKE91 (Idriss & Sun 1992)] or using an approximate methodology, as for example the multi-variable relations of Bouckovalas & Papadimitriou (2003), or their simplified version as presented by Papadimitriou et al. (2010).

Step 2: Estimation of the non-linear (first) eigen-period T_o of dam vibration

The so-called non-linear (first) eigen-period T_o depicts the fundamental eigen-period of dam vibration under intense shaking, which is generally larger or equal to its elastic counterpart, denoted as T_{oe} , that is observed under very low intensity shaking. The increase in value from T_{oe} to T_o is due to the non-linear soil response (e.g. shear modulus reduction) exhibited under high intensity shaking. Hence, in order to estimate the non-linear (first) eigen-period T_o of the dam vibration, one needs to first estimate the elastic value, T_{oe} , according to Eq. (1), that is a simplification of the proposals of Dakoulas & Gazetas (1985):

$$T_{oe} = 2.6 \frac{H}{V_s} \quad (1)$$

where H is the height of the dam and V_s is the average shear wave velocity within the body of the dam. Based on the results of the parametric analyses, the value of V_s entering Eq. (1) ranges from 230 to 360 m/s for a dam with a clayey core, with the higher values corresponding

to the taller dams. The following relation is proposed for the direct estimation of the elastic (first) vibration eigen-period T_{oe} of the earth dam, on the basis of the same analyses:

$$T_{oe}(s) = 0.024H(m)^{0.75} \quad (2)$$

The accuracy of Eq. (2) is evident from Fig. 2a, which illustrates the effect of the height H on the value of the elastic eigen-period T_{oe} , on the basis of the numerical results. In the sequel, the value of the non-linear (first) eigen-period T_o of the dam vibration is estimated by:

$$\frac{T_o}{T_{oe}} = \begin{cases} 1 + 1.76 \left(\frac{V_b(m/s)}{1000} \right)^{0.25} \left(\frac{PGA}{g} \right)^{0.75} \left(\frac{T_{oe}}{T_c} \right)^{-0.80} & , T_{oe} > T_c \\ 1 + 1.76 \left(\frac{V_b(m/s)}{1000} \right)^{0.25} \left(\frac{PGA}{g} \right)^{0.75} & , T_{oe} \leq T_c \end{cases} \quad (3)$$

The increasing effects of PGA and V_b in Eq. (3) depict the increase of the non-linear eigen-period as compared to its elastic value due to increased non-linearity of the response, originating from hysteretic damping of the geomaterials (resulting from PGA) but also due to the reduction of the radiation damping at the base of the dam (via V_b). The introduction of T_c in Eq. (3) illustrates that for high frequency (and out-of-phase) seismic excitations, the non-linearity predicted by the second relation in Eq. (3) is too severe and its effect should therefore be reduced (leading to the proposal of the first relation for $T_c < T_{oe}$). The overall accuracy of Eq. (3) is investigated in Fig. 2b against the numerical results on which it was based, and leads to a standard deviation of the relative error equal to $\pm 16\%$.

Step 3: Estimation of the peak seismic acceleration at the dam crest, $a_{max,crest}$

The value of $a_{max,crest}$ is practically analogous to the intensity of the shaking, PGA , and therefore the estimation of the former is based on the value of the ratio $a_{max,crest}/PGA$, that practically reflects the amount of the seismic amplification within the body of the dam. This amount is primarily a function of the proximity of the non-linear eigen-period T_o of the dam to the predominant period of the seismic excitation T_c . Hence, the ratio of $a_{max,crest}/PGA$ is given by:

$$\frac{a_{max,crest}}{PGA} = \begin{cases} 2.7 \left(\frac{V_b(m/s)}{1000} \right)^{0.52} & , 0.5 \leq \frac{T_o}{T_c} \leq 1.5 \\ 2.7 \left(\frac{V_b(m/s)}{1000} \right)^{0.52} \left(\frac{2T_o}{3T_c} \right)^{-0.7} & , 1.5 \leq \frac{T_o}{T_c} \end{cases} \quad (4)$$

Based on Eq. (4), the correlation of $a_{max,crest}/PGA$ to T_o/T_c takes the form of code-like design spectrum, i.e. it has a maximum value in a range of predominant periods T_c close to

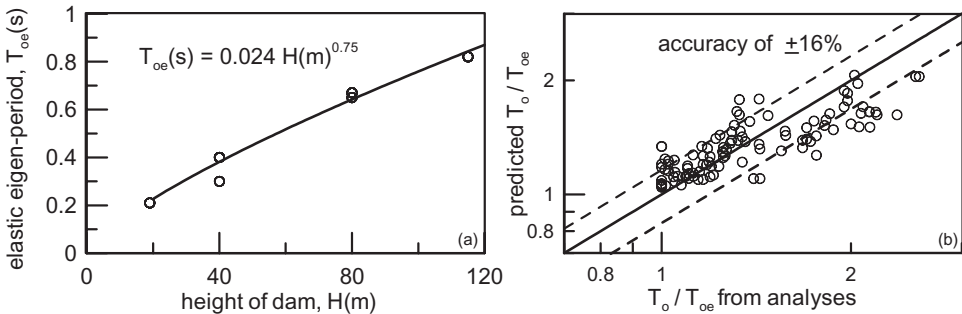


Figure 2. a) Effect of height H on the elastic (first) eigen-period T_{oe} of the dam, b) Prediction accuracy of the increase ratio of the dam eigen-period (T_o/T_{oe}) due to non-linearity.

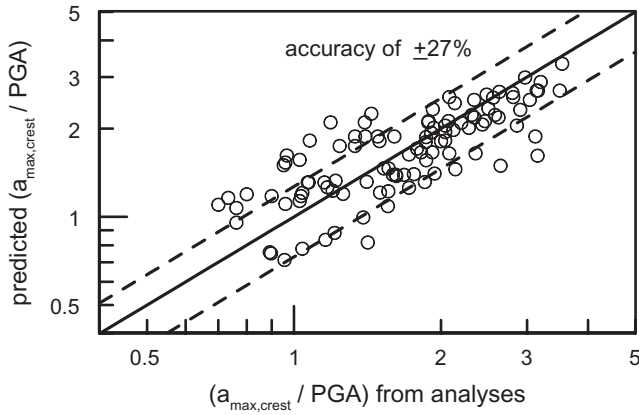


Figure 3. Prediction accuracy of $a_{\max,crest}/PGA$ ratio for all numerical data.

the eigen-period of the dam T_o , and its value reduces for increasing dam heights (that vibrate out-of-phase to the base excitation).

In addition, according to Eq. (4) the value of this maximum amplification ratio is a function of the stiffness of the foundation soil, via V_b , thus reflecting the favorable effect induced by a “soft” foundation layer to the seismic amplification within the body of the dam. The accuracy of Eq. (4) is illustrated in Fig. 3, in comparison to the numerical results on which it was based (standard deviation of the relative error equal to $\pm 27\%$, see dashed lines).

Step 4: Estimation of the peak seismic coefficient k_h as a function of $a_{\max,crest}$

The value of k_h for any sliding mass is practically a percentile of $(a_{\max,crest}/g)$, and therefore it is estimated using the ratio $k_h/(a_{\max,crest}/g)$. It was Makdisi & Seed (1978) who first showed that this ratio reduces with an increase of the maximum depth z (measured from the crest, see Fig. 1) of the failure surface. Statistical analysis of the numerical data clearly verifies this reducing effect, but also leads to a more elaborate estimating equation:

$$\left(\frac{k_h}{a_{\max,crest}/g} \right) = C_w - 1.18C_b C_f C_g \left(\frac{z}{\lambda_d} \right) \quad (5a)$$

$$\text{with } 1.0 - 0.65C_b C_f C_g \leq \left(\frac{k_h}{a_{\max,crest}/g} \right) \leq 1.0 \quad (5b)$$

where λ_d is the predominant wavelength of shear waves in the body of the dam.

The normalization of depth z with λ_d , and not with the height H as proposed by Makdisi & Seed (1978) and adopted by Papadimitriou et al (2010), is a significant novelty of the hereby proposed methodology, which reduces significantly the scatter in the estimation of $k_h/(a_{\max,crest}/g)$. This because Eq. (5) takes into account not only the intensity of the vibration (via $a_{\max,crest}$), but also the fact that relatively large predominant wavelengths λ_d lead to in-phase vibration of different locations within a sliding mass and therefore larger values of $k_h/(a_{\max,crest}/g)$. The estimation of λ_d may be approximately performed by assuming that the dam vibrates at a period T_{ave} whose value is the average between its eigen-period T_o and the predominant period of the excitation T_e . Given this assumption:

$$\lambda_d = V_s T_{ave} = \frac{2.6H}{T_o} \left(\frac{T_o + T_e}{2} \right) \quad (6)$$

Figure 4 illustrates the “fundamental” relation of $k_h/(a_{\max,crest}/g)$ reduction with the normalized maximum depth z/λ_d of the failure surface that is based on, the also presented,

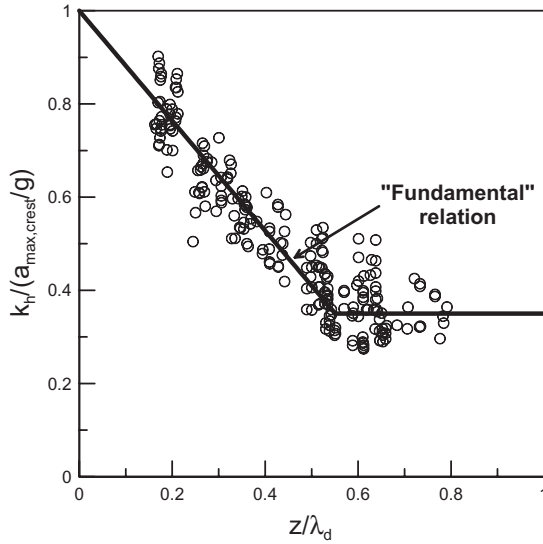


Figure 4. Indicative comparison of $k_h/a_{\max,crest}$ versus z/λ_d ratios as per Eq. (5) (for $C_w = C_b = C_f = C_g = 1.0$) against numerical data.

pertinent numerical data. The term “fundamental” relation used here denotes that in Fig. 4 all C coefficients of Eq. (5) are taken equal to 1.0, thus leading to presentation of only the pertinent numerical data in Fig. 4, that correspond to cases where the dam is founded on stiff soil or rock ($V_b > 500$ m/s) and does not have large stabilizing berms (or if it does the failure surfaces studied do not contain them, practically leading to $z < 0.67H$). In addition, the presented data correspond to “rotational” failure surfaces, which are not influenced by the reservoir water, (i.e. they are not valid for “planar” failure surfaces as well as for upstream surfaces in the case of a full or partially-filled reservoir).

In more detail, Eq. (5) includes the following C coefficients that play the role of “correction factors” to the foregoing “fundamental” relation. In particular:

- C_w is the *location coefficient*, that takes a value of 1.08 for upstream failure surfaces of an impounded dam, and a value of 1.00 in any other case
- C_b is the *berm coefficient*, that takes a value of 0.96 if the sliding mass includes a large stabilizing berm, and a value of 1.00 in any other case
- C_f is the *foundation coefficient*:

$$C_f = \begin{cases} 0.38 + 1.24 \left(\frac{V_b}{1000} \right), & V_b < 500 \text{ m/s} \\ 1.00, & V_b \geq 500 \text{ m/s} \end{cases} \quad (7a)$$

- C_g is the *geometry coefficient* of the sliding mass:

$$C_g = \begin{cases} 0.91, t/w \leq 0.14 & \text{ (“planar” surface)} \\ 1.00, t/w > 0.14 & \text{ (“rotational” surface)} \end{cases} \quad (7b)$$

with the w and t being geometrical characteristics of the sliding mass, corresponding to its width (in the horizontal direction) and its depth, as these are defined by the maximum distance between two lines that are parallel to the points of entry and exit of the failure surface and adjoin the sliding surface (see Fig. 1).

Figure 5 presents the overall accuracy in the prediction of the peak seismic coefficient k_h for all cases in the numerical database, based on which a satisfactory accuracy is depicted with a standard deviation of the relative error equal to $\pm 27\%$ (see dashed lines).

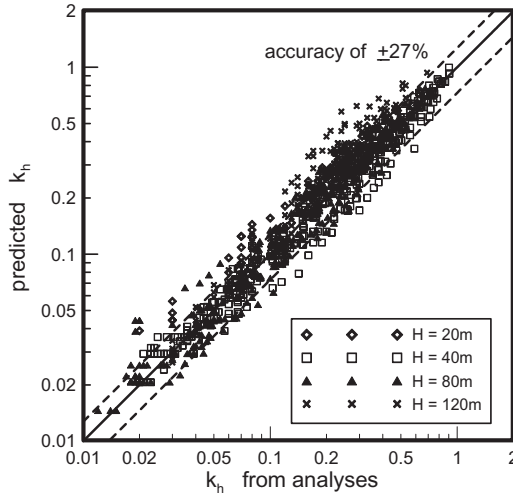


Figure 5. Prediction accuracy of k_h for all numerical data.

Step 5: Estimation of the k_{hE} as a function of the allowable slope displacement d_{all}

The value of k_h that is calculated from Eq. (5) corresponds to the peak acceleration of the sliding mass. Therefore, it is appropriate for estimating seismic displacements using the “sliding block” theory (e.g. Newmark 1965, Richards & Elms 1979), but not for performing pseudo-static slope stability analyses with a requirement of $FS_d \geq 1.0$. For the latter calculations, the effective value k_{hE} of the seismic coefficient should be used, that is given by:

$$k_{hE} = k_h / q \tag{8}$$

where $q (\geq 1)$ is the *sliding coefficient* of the slope, that may be related to the allowable displacements d_{all} on the basis of the well-known conservative relations of Newmark (1965) and Richards & Elms (1979). More specifically, the coefficient q in Eq. (8) may be set equal to the ratio of the peak acceleration $a_h (= k_h g)$ of the sliding mass over the yield acceleration a_y , a ratio that is included in both of the foregoing relations from the literature. Setting $q = k_h / k_{hE} = a_h / a_y$ implies that the slope is designed to be at a state of limit equilibrium ($FS_d = 1.0$) when the acceleration is equal to $k_{hE} g$ (and hence $a_y = k_{hE} g$) and is allowed to develop seismic displacements (of a maximum of d_{all}) if the peak acceleration a_h takes the value of $k_h g$ (corresponding to $FS_d < 1$). In such a way, by solving the foregoing literature relations for a_h / a_y , one may conservatively define q as:

$$q = \max \left\{ \left[\frac{d_{all}}{0.5(k_h g)} \left(\frac{v_h}{a_h} \right)^{-2} \right]^{0.5}, \left[\frac{d_{all}}{0.087(k_h g)} \left(\frac{v_h}{a_h} \right)^{-2} \right]^{0.25} \right\} \geq 1.0 \tag{9}$$

The only parameter not quantified in Eq. (9) is the value of the ratio (v_h / a_h) , i.e. the ratio of the peak velocity over the peak acceleration of the sliding mass (in sec), whose value was also estimated on the basis of the numerical data as:

$$\frac{v_h}{a_h} (\text{sec}) = 0.071 \left(1 + 0.74 [T_o + T_e] \right) \left(\frac{Z}{\lambda_d} \right)^{0.12} \tag{10}$$

where values of periods T_e and T_o (see Steps 1 and 2, respectively) are set in sec (relative error equal to $\pm 19\%$).

4 ACCURACY—LIMITATIONS

Based on the contribution above, the proposed methodology is complete, simple (may be programmed in a worksheet) and leads to satisfactory accuracy in the estimation of the peak seismic coefficient k_h with a standard deviation of the relative error equal to $\pm 27\%$ in comparison to case-specific non-linear numerical analyses of seismic response of earth dams. In addition, the methodology allows for the performance-based seismic design of earth dams, as a function of the allowable slope displacements d_{all} that lead to a prescribed decrease of the seismic coefficient from its peak value k_h to its effective value k_{hE} , which is to be used with a requirement of $FS_d \geq 1.0$. The proposed simplified methodology is considered reliable for use in the preliminary design of:

- a. Tall embankments or earth dams, with height H ranging from 20 to 120 m, of triangular or trapezoidal cross section, with or without large stabilizing berms, for end of construction and steady state seepage conditions, that are founded on soil layers of shear wave velocities V_b higher than 250 m/s (firm soil or rock),
- b. Seismic excitations with predominant periods $T_g = 0.14$ to 0.50 s and peak accelerations PGA at the free-field of the foundation soil reaching up to 0.50 g.

Given that the methodology was based on plane strain analyses, the dams in question should be sufficiently long as to allow for an accurate 2D approximation.

ACKNOWLEDGMENTS

The authors would like to thank Public Power Corporation of Greece S.A. for funding this research, as well as Civil Engineers Angelos Zographos, Sofia Tsakali and Stavroula Stavrou for performing the numerical analyses on which the new methodology was based.

REFERENCES

- Bouckovalas G.D. & Papadimitriou A.G. (2003), "Multi-variable relations for soil effects on seismic ground motion", *Earthquake Engineering and Structural Dynamics*, 32: 1867–1896, Wiley.
- Charles J.A., Abiss C.P., Gosschalk E.M. & Hinks J.L. (1991), "An engineering guide to seismic risk to dams in the United Kingdom", *Building Research Establishment Report*.
- Dakoulas P. & Gazetas G. (1985), "A class of inhomogeneous shear models for seismic response of dams and embankments", *Soil Dynamics and Earthquake Engineering*, 4(4): 166–182.
- Idriss I.M. & Sun J.I. (1992), "SHAKE91: a computer program for conducting equivalent linear seismic response analyses of horizontally layered soil deposits", University of California at Davis.
- Itasca Consulting Group Inc (2005), "FLAC – Fast Lagrangian Analysis of Continua", Version 5.0.
- Kramer S.L. (1996), *Geotechnical Earthquake Engineering*, Prentice Hall.
- Makdisi F.H. & Seed H.B. (1978), "Simplified procedure for estimating dam and embankment earthquake-induced deformations", *Journal of Geotechnical Engineering Division*, ASCE, 104(7): 849–867.
- Marcusson W.F., III (1981), "Moderator's report for session on 'Earth dams and stability of slopes under dynamic loads', *Proc. Intl Conf. on Recent Advances in Geotechnical Earth-quake Engineering and Soil Dynamics*, 3, p. 1175.
- Newmark N. (1965), "Effects of earthquakes on dams and embankments", *Geotechnique*, 15(2): 139–160.
- Papadimitriou A.G., Andrianopoulos K.I., Bouckovalas G.D. & Anastasopoulos K. (2010), "Improved methodology for the estimation of seismic coefficients for the pseudo-static stability analysis of earthdams", *Proc., 5th Intl. Conf. on Rec. Advan. in Geotech. Earthq. Eng. and Soil Dynamics*, May 24–29.
- Richards R. & Elms D.G. (1979), "Seismic behaviour of gravity retaining walls", *Journal of Geotechnical Engineering Division*, ASCE, 105(4): pp. 449–464.
- Terzaghi K. (1950), "Mechanisms of landslides", *Engineering Geology* (Berkey) Volume, Geological Society of America.
- USCOLD (1985) "Guidelines for selecting seismic parameters for dam projects", *Report of Committee on Earthquakes*, U.S. Committee on Large Dams.

Dam shape adaptation resulting from strong earthquake context

B. Tardieu

French Committee on Dams and Reservoirs, France

A. Si-Chaib

Tractebel Engineering-Coyne et Bellier, France

M. Marouk & M. Bibi

National Agency of Dams and Transfers ANBT, Algeria

ABSTRACT: The Tabellout Roller Compacted Concrete dam in Algeria creates an intermediate reservoir, as part of the “Setif-Hodna” transfer project. With a maximum height of 121 m and a length of more than 360 m, the Tabellout dam has a 294 million m³ capacity to provide irrigation and drinking water for the El-Eulma region. Three regional potentially seismogenic faults have been identified in close proximity to the dam. The purpose of the paper is to introduce the measures adopted to adapt the Tabellout dam’s shape to this context. Dam stability is checked based on irreversible sliding calculated based on the Newmark approach. The stability condition can be improved by enlarging the gravity dam profile. An additional measure to minimize irreversible displacement is to adopt a curved shape, taking advantage of the arch effect. The admissible irreversible displacement should be defined based on the geotechnical characteristics of the rock on site.

1 INTRODUCTION

1.1 *Geological context*

After analyzing different geological maps related to the site of the future dam of Tabellout, a seismotectonic studies are performed (Bès de Berc & Winter 2009, Bès de Berc et al., 2009). The conclusions indicate the presence of three regional potentially seismogenic faults in close proximity to the dam with a significant probability of generating an earthquake. One of these seismogenic sources is the main thrust of Little Kabylia.

Afterwards and in order to refine the location of the fault and its activity, a geological survey (lithology, structures and fracturing) was necessary to complete the first observations. Carried out in October 2009, it shows that the main thrust of Little Kabylia, bring into contact the volcano-sedimentary complex (greenstone) constituting the foundation of the dam, and the more recent (Cretaceous) marl-sandstone flysch formations that constitute the basin of the reservoir (Bougdal 2009). It is observed that the major thrust contact lies within about 200 m upstream from the dam axis and forms a large deformation zone of several tens of meters, marked by slickenside fault planes, drag folds, and sometimes quartz veins and lenses.

The greenstone metamorphic complex constituting the foundation of the dam is attributed to a Jurassic (Djellit 1987). Considering the regional geological setting, this necessarily implies the presence, downstream from the site, of another major tectonic contact, overlapping Kabyle Paleozoic substratum over Jurassic. Accordingly, the search for an alternative site downstream would be pointless, because geological conditions would not be better. The retained solution is the adaptation of the dam shape to the actual, newly determined seismic load.

Table 1. Magnitude & PGA in the site of Tabellout.

Sismogenic source	OBE		MDE		MCE	
	Mw	PGA (g)	Mw	PGA (g)	Mw	PGA (g)
Offshore thrust	6.3	0.14	7.1	0.22	7.4	0.26
Little Kabylia thrust	5.5	0.30	6.5	0.47	7.2	0.70

1.2 New seismic data

According to ICOLD recommendations, the structure has to be designed for various levels of ground motion. These levels at the dam site depend on the geological conditions and seismotectonic frame in the region including the dam site and potential earthquake sources. Consequently the various levels of ground motion depend on released energy, source mechanism, related attenuation and surface geology of the dam site.

The seismic hazard studies (Bès de Berc & Winter 2009, Bès de Berc et al., 2009) has shown that the critical PGA (Peak Ground Acceleration) for the Tabellout dam site is controlled by the Little Kabylia thrust. According to ICOLD recommendations, the PGA was calculated for three different earthquakes (ICOLD. 1989; EM 1110-2-6053):

Operating Basis Earthquake (OBE): The OBE is a level of ground motion that is reasonably expected to occur within the service life of the project, that is, with a 50-percent probability of exceedance during the service life. (This corresponds to a return period of 144 years for a project with a service life of 100 years).

Maximum Design Earthquake (MDE): The MDE is the maximum level of ground motion for which a structure is designed or evaluated. As a minimum, for other than critical structures, the MDE ground motion has a 10 percent probability of being exceeded in a 100-year period, (or a 1000-year return period). For critical structures, the MDE ground motion is the same as the maximum credible earthquake (MCE) ground motion.

Maximum Credible Earthquake (MCE): The MCE is defined as the largest earthquake that can reasonably be expected to be generated by a specific source, based on seismological and geological evidence. It represents an upper bound of expected magnitude intensity.

The seismic hazard approach predicts a MCE of $M_w = 7.2$ (SMP) with a vertical displacement of 0.70 m in case of pure overlapping displacement and an average horizontal displacement of 1.4 m for pure strike-slip displacement. The corresponding horizontal Peak Ground Acceleration (PGA) is 0.70 g. The values to be taken into account for the Tabellout dam calculations are summarized in the following table.

The new ground acceleration values are larger than the value taken into account in the tender design (0.2 g). These will have a significant impact on a straight dam profile, designed originally with upstream slope of 0.1/1 and downstream slope of 0.8/1 (Fig. 1).

These new seismic data do not menace the existence of the Tabellout project. However, the selected site can be conserved by taking into account special provisions in the dam design by:

- Keeping the dam shape straight with softening slopes (Enlarging the dam cross section)
- Curving dam shape with adapted cross section taking the advantage of arch effect.

2 INITIAL APPROACHES

2.1 Defining key data

With the lack of site investigations, and taking into account both; results of geological survey and feedback from different sites, the material characteristics can be taken into account as follow:

- Foundation: $c = 0$ MPa and $\varphi = 40^\circ$
- RCC mass density: $\gamma = 2.35$ t/m³
- RCC dynamic elastic modulus: $E_d = 35,000$ MPa (Zdiri et al., 2007)
- Damping coefficient $\xi = 3\%$ under OBE and $\xi = 7\%$ under MDE.

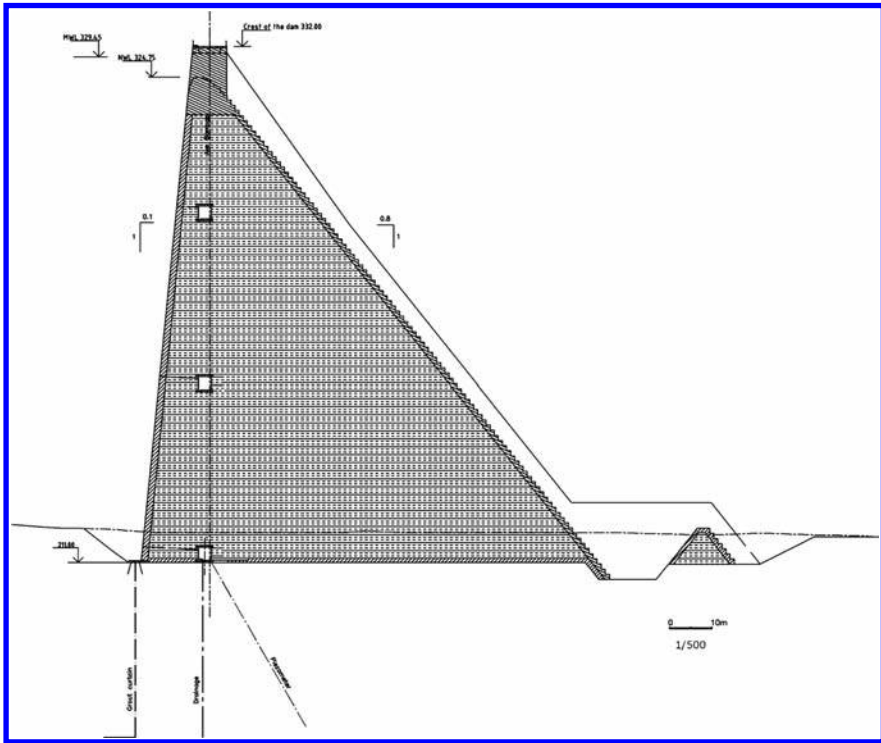


Figure 1. Dam profile in tender design.

These material characteristics are used to perform several computations to obtain the response of a dam with a straight shape.

2.2 Preliminary calculations

Several calculations are performed, in preliminary design stage. The first approach is a simplified method for pre-dimensioning gravity dams in seismic areas (Tardieu et al., 1993). The main assumptions adopted for this method are the following:

- The dam is considered as a simple resonator (triangular prism) with two degrees of freedom (translation and bending parallel to the dam axis).
- The height of the prism “H” is the height of the normal water level
- The dam is founded on rigid bedrock.
- The effects of earthquake bank-to-bank horizontal component are not taken into account.
- The hydrodynamic effect is taken into account using Westergaard’s analysis.

Taking into account the first vibration mode, the simplified method gives the vibration frequency as follows:

$$\text{Empty dam reservoir } N = 0.23 \text{ S/H} \quad (1a)$$

$$\text{Full dam reservoir } N = 0.17 \text{ S/H} \quad (1b)$$

where S = the shear wave velocity; H = normal water level immediately upstream of the dam.

For an elastic modulus of Roller Compacted Concrete (RCC) equal to 35,000 MPa, the S wave velocity is 2486 m/s. The frequencies of the Tabellout dam will be respectively 4.7 Hz for the empty dam reservoir and 3.5 Hz for the full dam reservoir. The projection of these

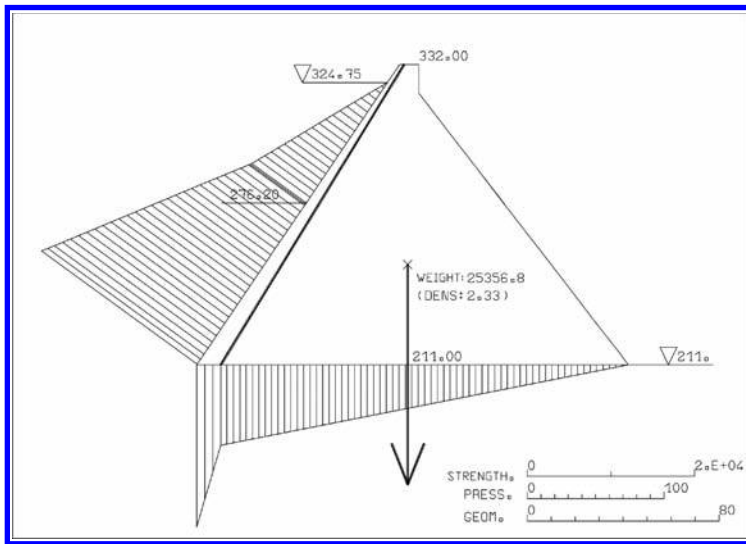


Figure 2. New straight shape of dam (0.7Up/0.8Dw).

frequencies on the Boumerdes earthquake spectrum of May 21, 2003, shows that they are very close to the plateau, which varies according to acceleration and damping values between 4 Hz and 11 Hz. This implies that under Boumerdes earthquake response spectrum, the induced Tabellout dam response is not well damped. The total dam slope “ f ” can be written as a simplified formula, relating acceleration at the dam foundation \ddot{U}_f , dam height H , and the efficiency of drainage:

$$f = aA_g\ddot{U}_f + b \quad (2)$$

where $A_g = 7.7 \cdot 10^{-3} H + 1$ is the variation of the amplification at the gravity centre of the dam as a function of height; a and b = scalars depending on joints efficiency.

In the second approach, the Tabellout dam is modelled as a rigid body using STABCON software, taking into account sliding at the dam-foundation contact. Different load cases are taken into account and seismic solicitations given in Table 1 are introduced in pseudo-static analysis.

The results of the two initial approaches are close to each other and the obtained shape of the straight dam is a profile defined by an upstream slope of 0.7/1 and a downstream slope of 0.8/1 (see Figure 2).

3 DYNAMIC APPROACH

The steps of this approach are initially used to perform pseudo-static calculations for different dam profiles. Then the critical acceleration is determined for the profiles assuring stability. The last step is to calculate using transient dynamic the dam irreversible displacements at the contact dam-foundation using Newmark’s method.

3.1 Critical acceleration

The critical acceleration of the dam is defined as the value that would cause the mass to move relatively to the ground. The critical acceleration depends mainly on the shape of the dam and the critical friction angle in the dam-foundation contact. The calculation of the critical acceleration is performed with STABCON software developed by Coyne et Bellier as follows:

1. Find the profiles of the dam assuring stability with (Shear Friction Factor) $SFF = 1.1$ for an earthquake acceleration $OBE = 0.3$ g. These conditions verify that the dam remains operational after the OBE.
2. Perform other calculations for the obtained profiles and find the critical acceleration that gives a safety factor of 1.0 SFF.

The obtained profiles fulfilling the above mentioned requirements are defined by the following slopes:

0.4 Upstream/0.9 Downstream and 0.3 Upstream/1.0 Downstream.

Table 2. Obtained critical acceleration.

Profile	Critical acceleration
0.4Up/0.9Dw	0.250 g
0.3Up/1.0Dw	0.257 g

3.2 Dynamic transient calculus

The transient dynamic calculus is performed using the ASTER finite element software, adopting 2D plane strain assumptions. The foundation is assumed to behave rigidly. The steps of computations are defined as follows:

- Perform a dynamic analysis by applying accelerogram at the dam foundation.
- Record the resulting acceleration at the gravity centre of the dam.
- Apply Newmark's method to calculate the cumulative displacement by integrating the part of acceleration exceeding the obtained critical acceleration.

Two accelerograms are obtained starting from Boumerdes accelrogram (Tardieu et al., 2009), which is adjusted with respect to the two maxima site acceleration values of OBE and MDE given in Table 1. The results are illustrated in Figure 3.

The sliding displacement is obtained using Newmark approach (Newmark 1965) assuming rigid body motion with friction developing on the contact surface. The irreversible displacement is calculated by integrating pulse areas exceeding the critical acceleration.

After several calculations, it appears that the suggested profile in tender design (0.1 Up/0.8 Dw) was undersized compared to the new seismic data. The use of Newmark

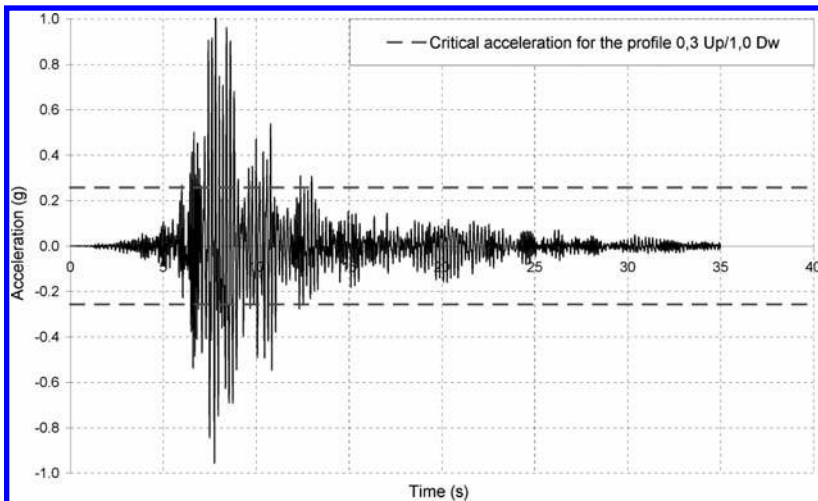


Figure 3. Dam acceleration response at the gravity centre.

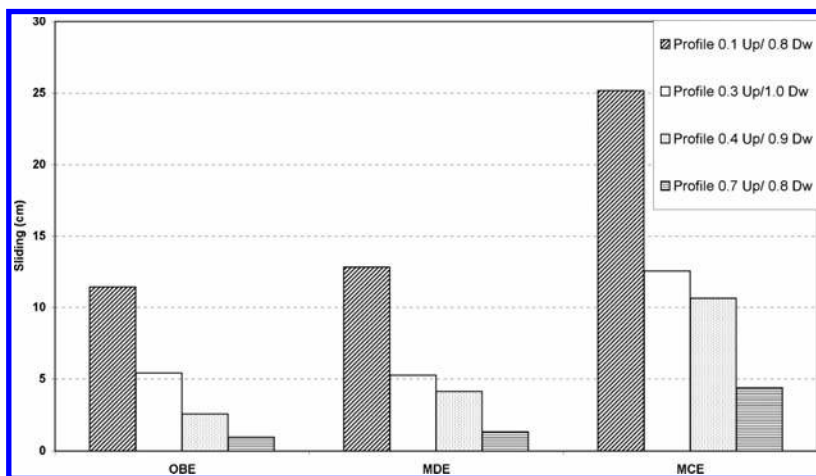


Figure 4. Dam sliding for different profiles.

method with the profiles assuring stability (0.3 Up/1.0 Dw) and (0.4 Up/0.9 Dw) under OBE gives sliding displacement values which are not negligible (respectively 5.42 cm and 2.57 cm).

To ensure dam behavior without major permanent damage under OBE, the sliding displacement expected must be very low or does not exist.

Under MCE the two profiles (0.3 Up/1.0 Dw) and (0.4 Up/0.9 Dw) show that the irreversible displacement exceed 10 cm. This value leads a significant deterioration of the rock foundation characteristics and an apparition of high leak flow rates. An increase of profile is needed to ensure stability of the dam, with acceptable sliding displacement under MDE and MCE.

Further calculations were conducted with dam profile of (0.7 Up/0.8 Dw). The sliding displacement values obtained under OBE, MDE and MCE, are respectively, 0.95 cm, 1.34 cm and 4.38 cm. These results, illustrated in Figure 4, show that the profile 0.7 Up/0.8 Dw is giving an acceptable sliding displacement under MCE (<10 cm). This new dam cross section induces about 75% of increase in RCC volume comparing to the profile suggested in tender design.

A possible alternative to design a dam which resists the new earthquakes acceleration values with less changes on RCC volume is to arch dam shape in order to mobilize the arching effect during the earthquakes. This solution will be discussed hereafter.

4 ALTERNATIVE DAM PROFILE

A curved RCC dam mobilizes the arch effect and transmits by its curvature the water pressure to the foundation rock edges. It is therefore possible for Tabellout gravity dam to operate partly as an arch dam during strong earthquakes. The mobilization of the arch effect assumes that the joints can be grouted. This implies that the provided joints are equipped with suitable devices to be injected before the application of water pressure once the temperature in the concrete mass has reached the final temperature of the structure.

It is therefore suggested to create a vertical upstream face and to optimize the downstream face (0.75/1) by finding a good compromise that guarantees the stability of the structure while avoiding additional costs. The calculations on the arched profile are performed and will be communicated soon.

It should be noted that arching the dam is actually effective if the construction joints of the dam are grouted after completion of the concreting in order to create a unique body behaviour. Various techniques have been used, for example in the Moula dam project in Tunisia where grouting has been proved efficient.

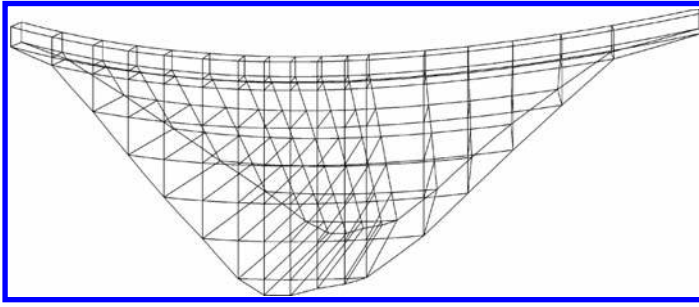


Figure 5. New dam arched shape.

5 CONCLUSION

The present paper introduces the measures adopted to adapt the Tabellout dam's shape to highly seismic context ensuring stability and safety.

Two main approaches are used to define the straight dam profile. The initial approaches with simplified method and pseudo-static method performed with STABCON software, give relatively the same profile (0.7 Up/0.8 Dw). The dynamic approach using Newmark method and performed using ASTER finite element software confirms the obtained profile. This solution ensures the stability of the dam under strong earthquake motion but induce an important increase in RCC volume, which will affect the total project costs.

The alternative solution that reduces the RCC volume and guarantees robust dam behaviour is to adopt a curved shape, taking advantage of the arch effect. The results of calculus with this new shape will be obtained soon and the admissible irreversible displacement will be defined based on the geotechnical characteristics of the rock on site.

REFERENCES

- Bès de Berc, S. & Winter, Th. 2009. Evidence d'activité récente le long du système de chevauchements de Petite Kabylie (Algérie). *Report of Tractebel Engineering—Coyne et Bellier*. France.
- Bès de Berc, S. Winter, Th. & Auclair, S. 2009. Evaluation de l'aléa sismique au droit du site du barrage de Tabellout. *Report of Tractebel Engineering—Coyne et Bellier*. France.
- Bougdal, R. Mission sur site du 06 au 13 Octobre 2009, Géologie, géomorphologie et caractéristiques géotechniques de deux sites de barrage a Tabellout. *Report of Tractebel Engineering—Coyne et Bellier*. France
- Djellit, H. 1987. Evolution tectono-métamorphique du socle Kabyle et polarité de mise en place des nappes de flysch en petite Kabylie occidentale (Algérie). *Thèse de docteur en sciences de l'université Paris XI*. France.
- EM 1110-2-6053. 2007. Earthquake Design and Evaluation of Concrete Hydraulic Structures. *US Army Corps of Engineers*. Washington.
- ICOLD. 1989. Selecting Seismic Parameters for Large Dams. *ICOLD Bulletin 72*: 1–73.
- Newmark, N.M. 1965. Effects of earthquakes on dams and embankments, 5th Rankine Lecture, *Geotechnique 15* (2): 139–160.
- Tardieu, B. Zghal, H. Aubry, D. & Ozanam, O. 1993. Méthode simplifiée de prédimensionnement des barrages poids en zone sismique. *AFPS*.
- Tardieu, B. Bousquet, C. & Goguel, B. 2009. Dynamic response of dams. Example of Taksebt, Algeria. *Géosciences 9*: 104–113.
- Zdiri, M. Ben Ouedzou, M. & Abriak, N. 2007. Prediction and measurement of the elastic modulus of the RCC: Case of the low cement proportioning; *International Journal of Physical Sciences 2* (12): 331–339.

Seismic safety of Chancy-Pougny dam

M. Ferrière & J.-P. Person

Compagnie Nationale du Rhône, France

H. Charif

ESM Sarrasin Ingénieurs SA, Saint-Sulpice, Switzerland

O. Vallotton

Stucky SA, Renens, Switzerland

S. Rossier

Scia Group SA, Gurmels, Switzerland

P. Lestuzzi

Résonance Ingénieurs-Conseils SA, Carouge & EPFL-ENAC-IIC-IMAC, Lausanne, Switzerland

ABSTRACT: The Chancy-Pougny hydropower development scheme, located on the French-Swiss Rhone, is a gate structure dam made of masonry and reinforced concrete. In the framework of renewing the concession, the seismic behaviour of the dam is investigated. Initially, methodological approach was linked to usual standards. A heavy reinforcement solution was defined with long anchors for piers rocking behaviour and overall stability and big cross bracings for superstructures behaviour in cross-stream direction. A new approach consisting of a pushover analysis which takes into account the deformation capacity of the structure and includes possible dynamic crack at the base of superstructure piers is proposed. The results show a very favourable seismic situation, related to a relatively stiff structure associated with an A class soil. The seismic safety of the upper bridge is already satisfactory for the current state (without reinforcement). Consequently, the proposed costly reinforcement for the upper bridge may be significantly reduced.

1 INTRODUCTION

1.1 *Context*

The Chancy-Pougny hydropower development scheme is located on the French-Swiss Rhone. It is a gate structure dam made of masonry and reinforced concrete constructed in 1925 to supply Schneider plants in Le Creusot (France). Its main characteristics are a head of 10 m, 4 bays equipped with Stoney type gates with 12 m openings, one bay with a reservation for a future lock, a tower and an upper bridge to carry the cables from the plant to a power substation, and a partial lower bridge.

In the framework of renewing the concession, the French-Swiss supervisory authorities, i.e. direction régionale de l'environnement, de l'aménagement et du logement (DREAL) and Swiss federal office of energy (OFEN), requested the owner of the structure, the Société des Forces Motrices de Chancy-Pougny (SFMCP), to carry out a study on the dynamic behavior of the dam under seismic loads.

The assessment of the dam's dynamic behavior was performed in conformity with the directives of the two supervisory bodies. Given the characteristics of the development scheme, an earthquake loading with a return period of 5000 years was taken into account.



Figure 1. Chancy-Pougny hydroelectric development.

The entire structure was modelled with three dimensional finite elements, taking into account dynamic soil-structure interaction (mixed rock-alluvial soil foundations) and the structure-mass of entrained water interaction. Model resolution consisted of linear dynamic analysis using the acceleration response spectra method completed with a pseudo-static analysis that cumulated load cases. Verifying the internal resistance of the structure demanded knowledge of existing conditions, especially the mechanical characteristics of the concretes used. The integrity of the gates was studied by using a specific finite elements model.

After revealing structural deficiencies, choosing the solution of reinforcement entailed a compromise between several criteria including severe operating constraints, safety considerations during works, architectural constraints, technical feasibility, cost and lead-time objectives.

This leads to a major and costly project. Consequently, an alternative approach is proposed to the supervisory authorities that takes into account a displacement-based analysis that allows for ductile behaviour of concrete structures. The paper focuses on the description of this alternative approach and on the related results.

1.2 Dam description

The Chancy-Pougny development scheme straddles the French-Swiss frontier. It is equipped on the Swiss left bank with an electrical power plant with 5 Francis turbine units of 7.7 MW each. The initial design flow is 520 m³/s. The refurbishment project includes the complete replacement of the 5 existing Francis turbine units by Kaplan turbine units of 12 MW each, turbinning 140 m³/s under a mean head of 10 m. This project is associated with compensatory measures, namely a fish pass on the right bank. The electric substation is located on the French right bank with a 123 kV power line to Swiss.

Each gate is composed of a 60 t lower part and a 15 t upper part, operated by chains from the upper bridge. A lock for navigations is provided for a reservation in the additional bay.

Five concrete piles support the equipments: they are composed of a lower part (pillars) 21.7 m high made of reinforced concrete with stone facing and an upper part (piers) 12.4 m high made of lightly reinforced concrete with cement coating. The piles are founded on caissons sunk into a molasse substratum. An intermediate 4 m thick foundation slab guarantees the dam against hydraulic erosion between piles.

A 26 m high cable tower is used to route the electrical power cables from the plant to the substation: a gallery in the upper bridge completes this routing between the two banks, more precisely between the cable tower and the right abutment. This bridge is made of isostatic beams simply supported at the top of the piers. It allows the circulation of a Titan gantry crane with a 600 kN dead weight used for bulkhead gate installation.

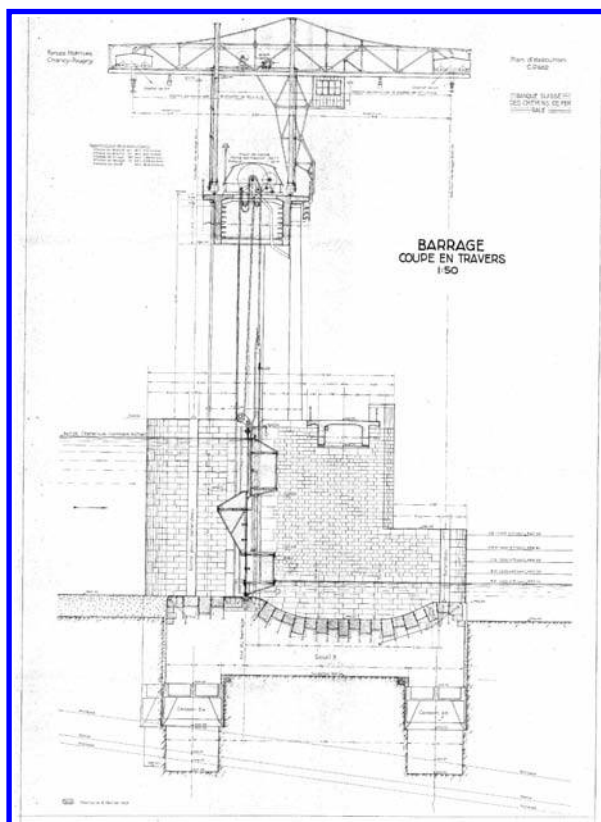


Figure 2. Cross-section of the Chancy-Pougny dam.

2 INITIAL SEISMIC ANALYSIS

2.1 *Seismic parameters*

The assessment of the dam's dynamic behavior was performed in conformity with the OFEN directives. Given the characteristics of the development scheme, the dam was classified as class II. An earthquake loading with a return period of 5000 years was taken into account.

The methodology was taken from the OFEN chapter relating to barrages. The OFEN 5000 years spectrum was adopted as a checking signal. For a 5% damping ratio and class soil A, the response spectrum is characterized by a peak ground acceleration of 0.23 g and a maximum plateau acceleration of 0.58 g horizontally.

2.2 *Linear dynamic analysis*

The first approach consisted of a linear dynamic analysis using the response spectrum method. The OFEN response spectrum was applied in the two main horizontal directions and in the vertical direction with an attenuation factor.

Scia Engineer software was used to model the entire structure with three dimensional finite elements: beam elements for piers, cable tower, upper and lower bridges; shell elements for piles; thick plates for foundation slabs. Particular attention was given to the dynamic soil structure interaction of the abutment foundation: a system of springs and masses was modelled to take into account phase shifts and amplification between the bedrock and the top of alluvial column.

The results showed that the main deficiencies appear in the cross-stream direction which is not mobilized under service conditions. Excess tensile stresses (up to 10 MPa) were

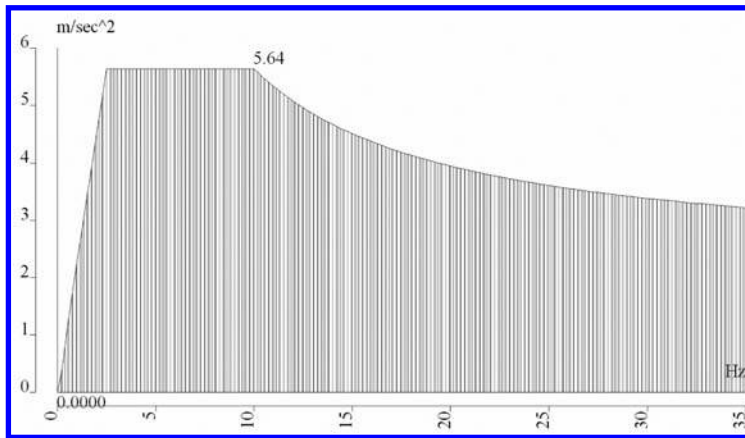


Figure 3. OFEN spectrum with a return period of 5000 years—A class soil—Damping ratio 5%.

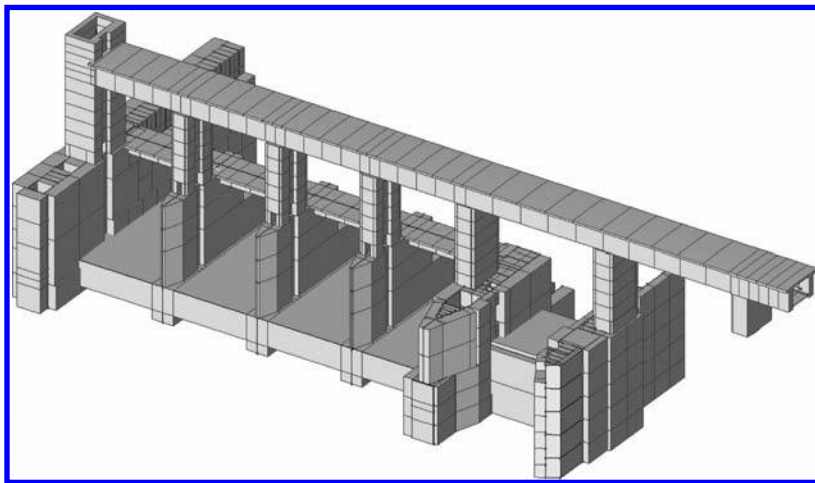


Figure 4. Chancy-Pougny dam—3D finite elements model.

determined in the cable tower and upper part of the piles due to cross-stream excitation. For the lower part of the piles, conventional tensile resistance was also exceeded due to entrained water in the along-stream direction. Regarding global stability, given the fact that passive earth pressure was minimized in the superficial molasse, thus stability against sliding and overturning was not guaranteed.

2.3 Initial proposed reinforcement

The choice of the initial proposed reinforcement solution was a compromise between:

- Severe operating constraints: e.g. no simultaneous blocking of two gates during works,
- Safe working conditions, e.g. the proximity of HV cables inside upper bridge,
- Architectural constraints: the plant is listed as a historic monument,
- Expected low quality concrete in the pillars identified by local investigation,
- The technical feasibility of long anchors to ensure the overall stability of the structure.

The principles adopted were:

- St Andrew steel cross braces to resist cross-stream excitation (Fig. 5),
- Abutment on the right bank slope: ground anchors to stabilize in the cross-stream direction,

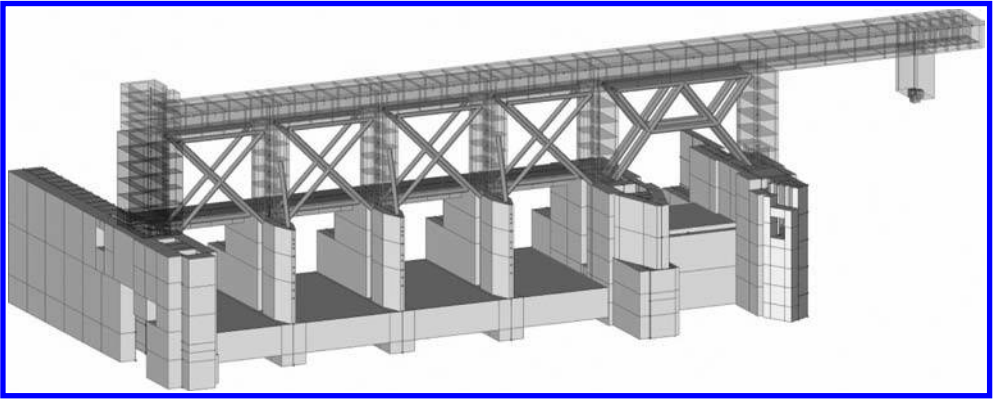


Figure 5. Chancy-Pougny dam—Seismic initial proposed reinforcement project.

- Piles: vertical anchors 38 m in length to counteract along-stream overturning of piles,
- Piles: inclined anchors 38 m in length to counteract sliding of piles,
- Cable tower: vertical anchors 40 m in length and thickening of the concrete at its base.

The initially adopted methodology leads to a major reinforcement project that is also complex in terms of feasibility, particularly for long drilled tensioned anchors in old concrete structures. As a consequence, an alternative is proposed to the supervisory authorities. This alternative approach is based on a “push-over” analysis of the upper part of dam. This method may not be applied to the lower part of the dam because of its role in hydraulic retention.

3 DISPLACEMENT-BASED APPROACH

3.1 Methodology

The structural characteristics of the upper part of the dam are similar to the ones of conventional bridges. Therefore it was proposed to apply modern seismic assessment methodologies, now usually involved in case of existing structures, to the upper bridge. These modern methodologies are displacement-based approaches. Compared to conventional force-based approaches, they consider the seismic behavior more realistically. More specifically, they allow taking into account the actual “plastic” displacement capacity after reaching the strength of the structure.

In the case of Chancy-Pougny dam, the displacement-based approach allows to consider the rocking behavior of the 12.4 m high piers of the upper bridge. This means that, compared to the initial approach, the condition of avoiding cracking at the base of the piers is no more considered. By contrast, cracking at the base is used since it leads to a seismic satisfactory rocking behavior, generally associated with relatively large displacement capacity. Furthermore, preliminary investigations, considering only one pier, with the related portion of the upper bridge, showed that this displacement-based approach is very favorable for the upper part of the dam because of its relatively high stiffness, leading to small displacement demand.

3.2 Displacement-based method

The used methodology was developed for seismic assessment and design of buildings and bridges (Priestley et al., 2007). This is a nonlinear—static method, oriented in deformation, which generally leads to more favorable results than conventional force-based methods. This method applies to deformable structures, i.e. to structures which behavior is not governed by

fragile collapse. This method should not be confused with the capacity design method which is more restricting and only concerns new structures.

Generally in the displacement-based method, a capacity curve is first determined for each element of the lateral stabilization (shear wall, frame, etc.). The capacity curve is defined by three points: the lateral strength of the element, the yield displacement, and the ultimate displacement. The global capacity curve for the structure is obtained by the addition of the individual elements capacity curves. The strength and the displacement capacity (ultimate displacement) of the structure are determined by the global capacity curve. The seismic safety is then evaluated by the comparison of structural displacement capacity with the displacement demand associated with the related response spectrum. This comparison is generally graphically illustrated with a diagram called ADRS spectrum.

3.3 Assumptions

The capacity curves of the piers were determined based on the three following parameters: the top displacement when uplift appears at the base, the lateral strength corresponding to a rocking failure mode and the ultimate drift. The rigidity is the ratio of the uplift displacement to the associated lateral strength. Lateral strength by rocking constitutes the plateau of the capacity curve.

Based on the values of deformation capacity for masonry shear walls proposed by Eurocode 8 (EC 8, 2005), i.e. 0.4% in case of shear failure and 0.8% for rocking failure, a value of 0.8% was considered as ultimate drift. The very low reinforcement (near no reinforcement) at the base of the piers leads to a rocking behavior characterized by a bending strength only due to the normal compression force at the base. Moreover, shear failure mode may be excluded because of the high slenderness (height/length ratio) of the piers and the fact that they are made of reinforced concrete. Note that the adopted value for ultimate drift may be considered as very careful because EC 8 allows for the masonry shear walls governed by a rocking failure mode to increase the basic value of 0.8% through its multiplication by the corresponding slenderness ratio.

3.4 Results

Figure 6 shows the capacity curve of the upper bridge in the cross-stream direction for the current state (without reinforcement). In this direction, the upper bridge is analyzed globally because the connection by the gallery leads to an identical top displacement for all elements. The individual curves for each element (tower and piers I to V) are first determined. The global capacity curve is obtained by adding up all individual curves.

In the cross-stream direction, lateral strength of the upper bridge is about 6400 kN. The yield displacement at the top is approximately 6 mm. The fundamental period is about 0.4 s. According to the assumption of a value for ultimate drift of 0.8%, the top displacement capacity is approximately 110 mm.

In the stream direction, the piers may be analyzed independently because, in this direction, the connection by the gallery does not lead to an identical top displacement for the elements. The piers resist in their larger cross-section dimension. Therefore, the fundamental periods are much smaller than the one in the cross-stream direction and do not exceed 0.2 s.

Figure 7 shows the seismic evaluation of the upper bridge for the cross-stream direction in the usual ADRS format. According to the EC 8 procedure, the fundamental period just enter the validity domain of the equal displacement rule. As a consequence, displacement demand does not depend on the strength of the structure. For the fundamental period of the upper bridge, the top displacement demand is about 23 mm, which is much smaller than the top displacement capacity of 110 mm.

However, the seismic rocking behavior is associated to a low energy dissipation capacity which leads to an increase of the displacement demand compared to the usual behavior of reinforced concrete corresponding to the equal displacement rule. Displacement demand

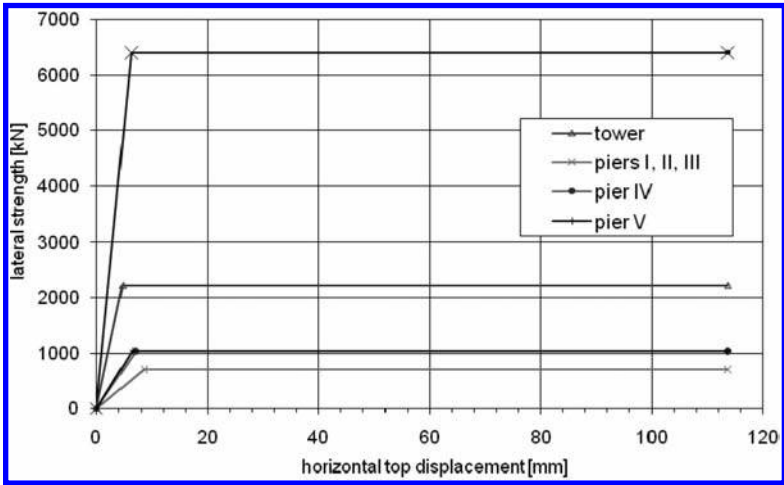


Figure 6. Capacity curve of the upper bridge for the cross-stream direction.

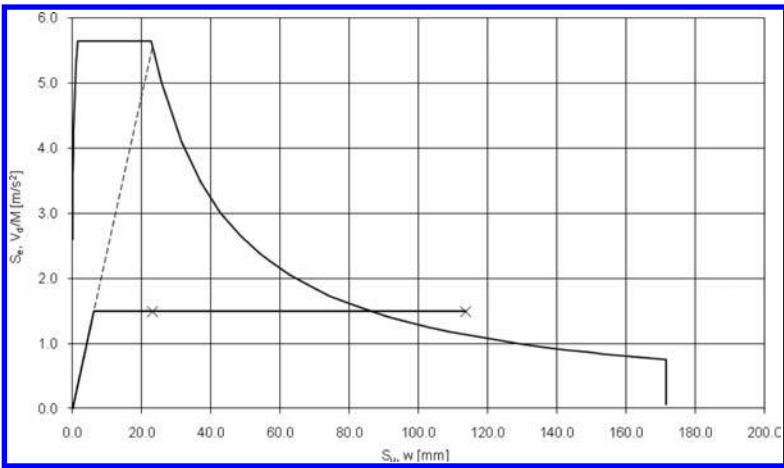


Figure 7. Seismic evaluation of the upper bridge for the cross-stream direction.

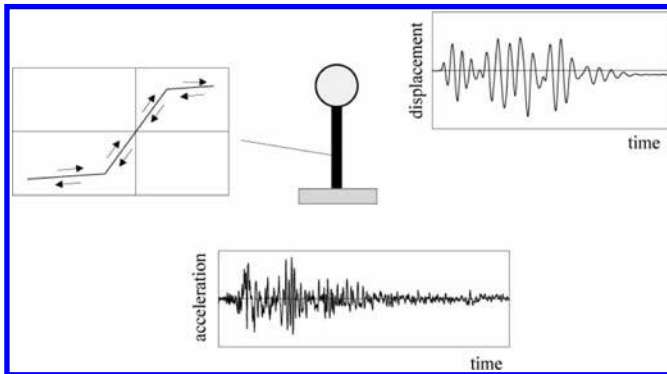


Figure 8. Schematic description of the performed non linear time history analysis.

should be, therefore, increased to account for this amplification. An increase of about 25% of the displacement demand was recently proposed, based on extended numerical results (Lestuzzi et al., 2007).

Nonlinear time-history analyses were achieved in order to determine an accurate value of this amplification for the upper bridge of Chancy-Pougny dam. The numerical analyses were performed with equivalent SDOF and a specific hysteretic model, simulating an “S” shape. Stationary synthetic accelerograms, compatible with the prescribed response spectrum are specified by the Swiss supervisory body. In total 33 accelerograms with different durations were used. Obtained results for the cross-stream direction indicate a larger increase of the displacement demand than the one proposed in the literature, with a magnitude of about 50% for mean values. A peak value of 42 mm was obtained. Even this maximum displacement demand is clearly smaller than the displacement capacity.

In the stream direction, limited amplifications of the displacement demand corresponding to the ones of the literature were obtained. Moreover, the situation in this direction is not significant because the smaller fundamental periods are related with much smaller displacement demand than the ones in the cross-stream direction.

4 CONCLUSIONS

Displacement-based approach for the superstructure piers of the Chancy-Pougny allows pointing out a very favorable seismic situation. This situation is related to a relatively stiff structure associated with an A class soil. The results show that the seismic safety of the upper bridge is already satisfactory for the current state (without reinforcement). Consequently, the proposed costly reinforcement for the upper bridge may be significantly reduced.

REFERENCES

- Eurocode 8. 2004. “Design of structures for earthquake resistance - Part 1: General rules, seismic actions and rules for buildings”, Comité Européen de Normalisation, Bruxelles.
- Eurocode 8. 2005. “Design of structures for earthquake resistance - Part 3: Assessment and retrofitting of buildings”, Comité Européen de Normalisation, Bruxelles.
- Lestuzzi, P., Belmouden, Y. & Trueb, M. 2007. “Non-linear seismic behavior of structures with limited hysteretic energy dissipation capacity”. *Bulletin of Earthquake Engineering*. Vol 5/4, 2007, pp. 549–569.
- Priestley, M.J.N., Calvi, G.M. & Kowalsky, M.J. 2007. “Displacement-Based Seismic Design of Structures”. IUSS Press, Pavia, Italy.

Behavior analysis of soil-structure interaction of a composite dam using geo-centrifuge test

J.Y. Lim & I.S. Ha

K-water Institute, Daejeon, Republic of Korea

ABSTRACT: Existing dams are an important part of the safety problems. Because of climate change is due to the increased earthquakes magnitude and the PMP and PMF. Dam safety problems are no exceptions. Especially, the composite dam which is constructed other dam types has characteristic of different behavior during the earthquake. In the evaluation of the seismic stability of a composite dam, besides others, the main problem is the dynamic interaction between concrete gravity dam and soil embankment. In this study was analyzed dynamic behavior characteristic of composite dam, which is composed of concrete gravity dam and embankment section, using centrifuge (including shaking table test). In this test, prototype model was 1/40 scale model of the existing composite dam and the test condition was centrifugal a 40 g. In addition, the Hachinohe (long-period) and Ofunato (short-period) waves were applied. The characteristics of dynamic behavior were compared with those obtained by the centrifuge test which was carried out in the earthquake wave of Korea earthquake conditions. Furthermore, the results obtained in this the centrifuge test were compared with the 3D numerical analysis of the composite dam.

1 INTRODUCTION

In this experiment test which is compared with centrifuge scale model test and numerical analysis results for dynamic behavior characteristics of composite dam in contact with concrete gravity dam and embankment. Also, centrifuge shaking table test for composite dam consisted on concrete gravity dam and embankment was carried out.

The stability analysis of soil-structure such as dam and embankment are applied theoretical method and experimental method usually.

There were various experimental methods for seismic stability evaluation, but that was not able to presented characteristics of behavior same as a real structure.

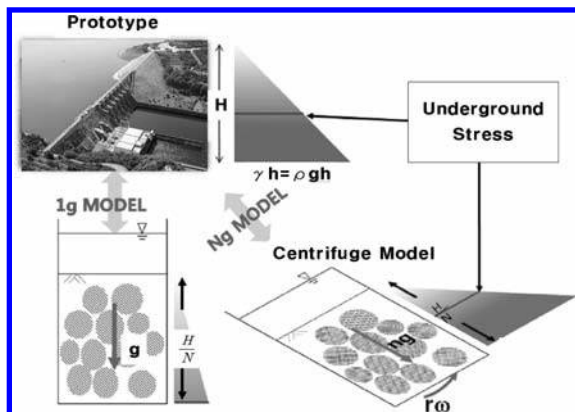


Figure 1. Basic concept of centrifuge.

Table 1. Similitude laws of centrifuge (scaling factor).

Quantity	Scaling factor
Stress	1
Density	1
Length	1/N
Acceleration	N
Dynamic acceleration	N
Dynamic time	1/N
Strain	1
Force, Load	1/N ²

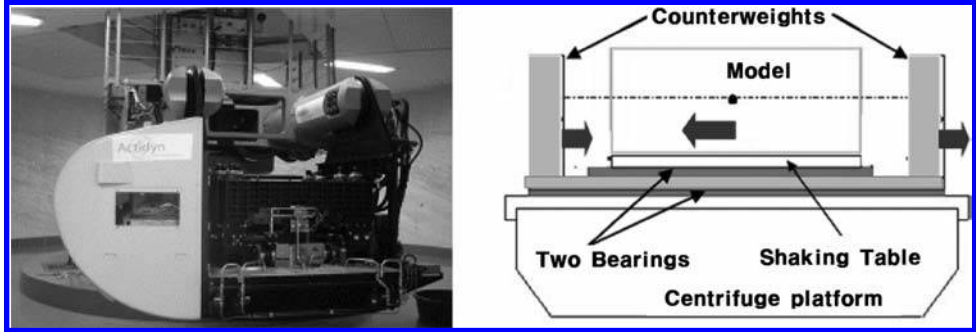


Figure 2. Centrifuge and 2D shaking table.

Also, the 1 g ($g = 9.8 \text{ m/s}^2$) model tests had not reproduce state of stress about self-weight among the most important element of ground motion. So, to solve this problem usually centrifuge model tests were carried out.

The basic concept of a centrifuge model test on structure was reduced to size by $1/N$ for prototype and the acceleration of gravity increased N times, ground depth to simulate closely the actual state of stress.

The scale model was used same density (ρ) of prototype in N g-level conditions and the case which was carried out a centrifuge model test in the scale model. Normal stress σ_{vp} from of prototype depth h_p , the normal stress σ_{mp} from of depth h_m of model with is expressed. If h_m/h_p comes to make with N ratio, the normal stress from each representative depth makes come to be same.

$$\sigma_{vp} = g\rho h_p, \quad \sigma_{mp} = gN\rho h_m \quad (1)$$

2 RESULTS BY CENTRIFUGE TESTING

2.1 Centrifuge experimentation

In this study, centrifuge test used by accelerator of beam form, it was radius of rotation 5.0 m, tester of validity radius 4.5 m and maximum capacity 240 g-tons because of maximum 2,400 kg of model loads was possible to acceleration to 100 g.

In this research, shaking table test used by stiffness soil box that was made to utilize centrifuge shaking table and measured acceleration, displacement etc.

2.2 Test section

The only one type of dam model was tested in the centrifuge. The wrap-around sections are the transitional sections of a dam where it changes from concrete dam to embankment dam.

Soil-concrete interface area between concrete dam and both upstream and downstream embankment wing dams are also illustrate in Figure 3, Figure 4. Figure 4 shows a typical two dimensional composite section in the wrap around region.

2.3 Material

Materials used in this test conditions were as follows:

- Concrete section: Proportion mortar
- Embankment section: Dry unit weight 2.02 g/cm^3 , Moisture content 4%.

2.4 Test model and sensor

Figure 5 shows the test model of composite dam in shaking table and Figure 6 shows the install of sensor (high speed camera, accelerometer) and measurement point of composite dam section.

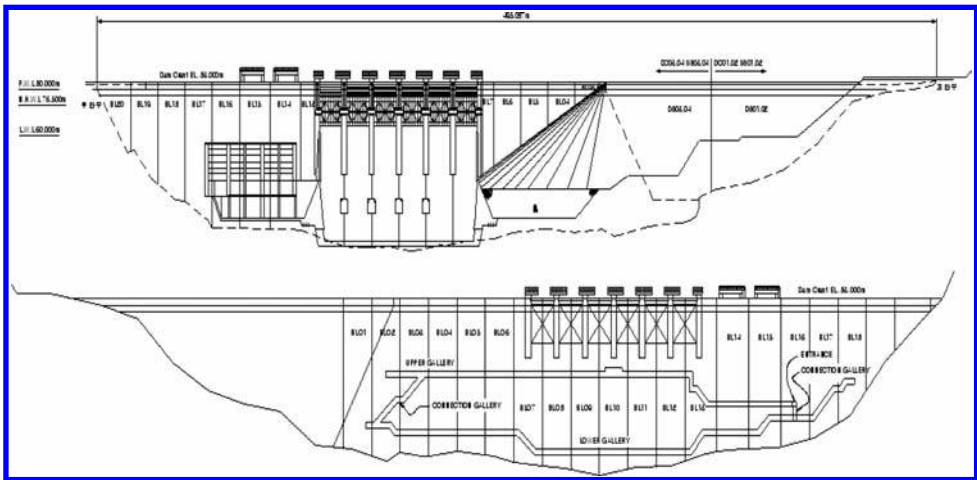


Figure 3. Plane and longitudinal section of composite dam.

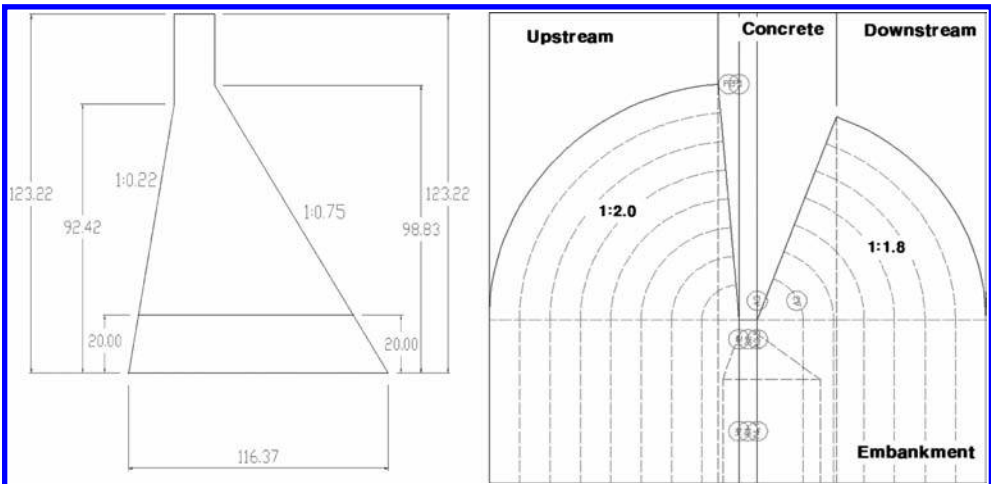


Figure 4. Concrete dam and composite dam section of test model.

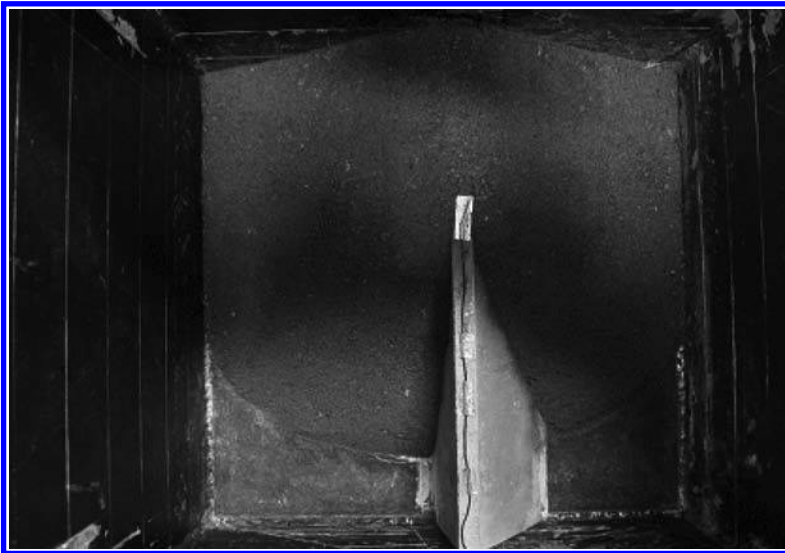


Figure 5. Test model of composite dam.

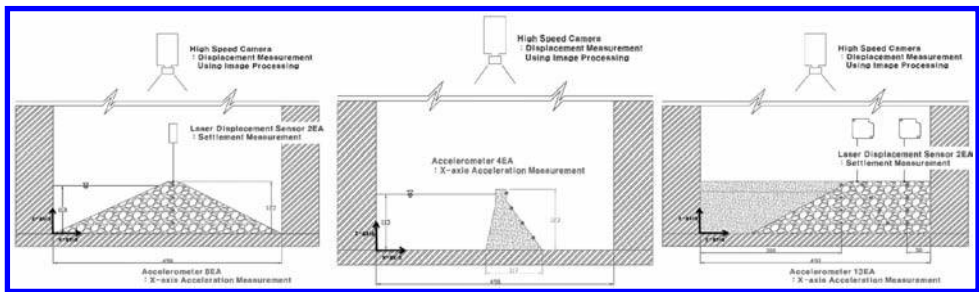


Figure 6. Sensor and measurement point of composite dam section (embankment, concrete, interface).

Table 2. Test condition (Applied by centrifugal acceleration 40 g).

Earthquake	Max. Acc. (Empty)	Max. Acc. (N.H.W.L)	Max. 0.5 g (N.H.W.L)
Hachinohe	0.098	0.120	0.113
	0.159	0.165	0.169
	0.218	0.227	0.281
	0.216	0.300	0.480
Ofunato	0.085	0.109	0.105
	0.275	0.164	0.160
	0.341	0.174	0.275
	—	0.232	0.456

The composite dam consists of concrete gravity section, embankment section, and interface section, as shown in [Figure 6](#).

2.5 Put earthquake wave

Due to the magnitude of the event, it was considered necessary to evaluate the dynamic behavior of the composite dam for more than one seismic record. Therefore, horizontal

time history accelerations from two seismic events—Hachinohe and Ofunato—were used to evaluate the dam. The studies scaled the time history accelerations from the seismic events to match the Korea site criteria.

2.6 Centrifuge test condition

The purpose of this study is to evaluate the applicability of a centrifuge test for maximum credible earthquake in the Korean dam sites. In this centrifuge test, water level conditions were empty and N.H.W.L. And bedrock acceleration was applied bedrock maximum acceleration which was modified (0.12 ~ 0.542 g) via 0.154 g. In this experiment test was carried out empty 7 times, at the N.H.W.L 8 times, and until the destructive at the time of 17 times (maximum earthquake acceleration).

3 RESULTS AND DISCUSSION

3.1 Empty and N.H.W.L conditions

The results of experiment test, earthquake response acceleration of dam crest with input earthquake was showed the result which is similar. Figure 7 show the result of concrete, interface and embankment (rockfill) response acceleration.

Table 3 and Table 4 show the information of target dams and acceleration condition in empty and N.H.W.L. A total of four earthquake accelerations were case-studied.

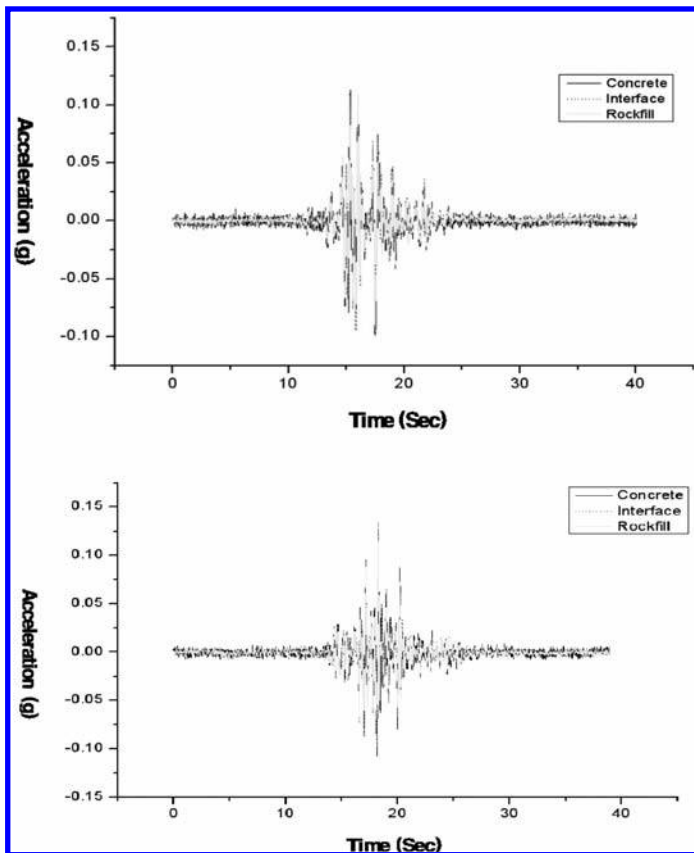


Figure 7. Time history acceleration of transverse (empty condition).

Table 3. Response acceleration of dam crest.

Division		Bedrock	Concrete	Interface	Embankment
Hachinohe (0.098 g)	Acceleration(g)	0.098	0.113	0.107	0.108
	Amplification ratio	1	1.153	1.087	1.105
Ofunato (0.085 g)	Acceleration(g)	0.085	0.113	0.107	0.108
	Amplification ratio	1	1.489	1.578	1.337

Table 4. Response acceleration of dam crest.

Division		Bedrock	Concrete	Interface	Embankment
Hachinohe (0.202 g)	Acceleration(g)	0.202	0.275	0.272	0.264
	Amplification ratio	1	1.361	1.347	1.309
Ofunato (0.204 g)	Acceleration(g)	0.204	0.215	0.234	0.224
	Amplification ratio	1	1.053	1.145	1.098

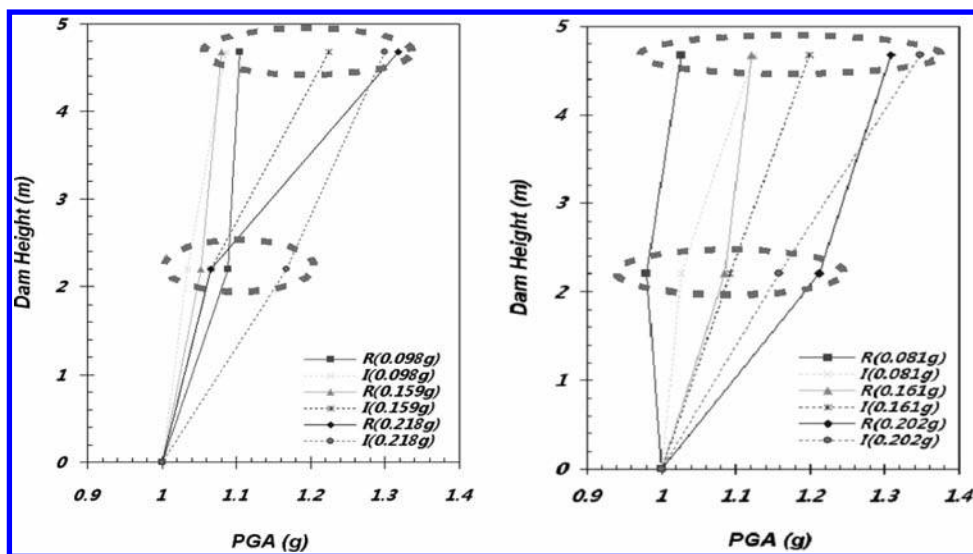


Figure 8. Comparison response acceleration results between embankment and interface section (Hachinohe, Empty, N.H.W.L.).

3.2 Analysis of experimental results

In general, dynamic behavior characteristic of existing composite dam interface was analyzed as embankment section for response acceleration and behavior. In this experiment, and the interface of composite dam compared to the response characteristics which was the interface effect was not considering.

Figure 8 shows that compared to response acceleration results between embankment and interface section. In this result, earthquake response acceleration was amplified to dam 2/3 point and dam crest amplification increases greatly at 0.218 g application, but interface section was more amplified to dam 2/3 point than embankment section.

Table 5 shows the result of the compared to the embankment and interface amplification ratio at the dam crest. Until the 2/3 point of the dam height was increased embankment amplification ratio than the interface.

Table 5. Amplification ratio of embankment vs. interface (Ofunato-empty).

Height	0.085 g	0.275 g	0.341 g
4.7 m	1.180	0.905	0.888
2.2 m	0.932	0.964	0.783

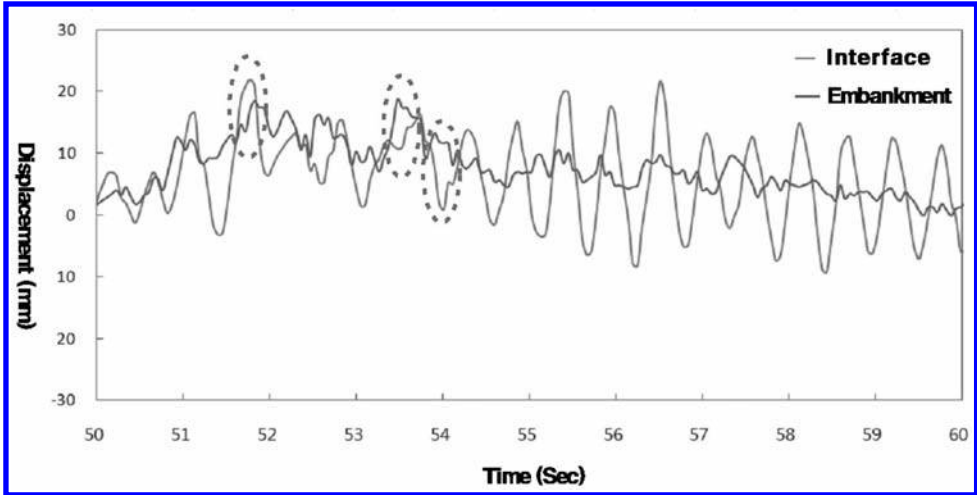


Figure 9. Comparison of lateral displacement (Hachinohe 0.202 g).

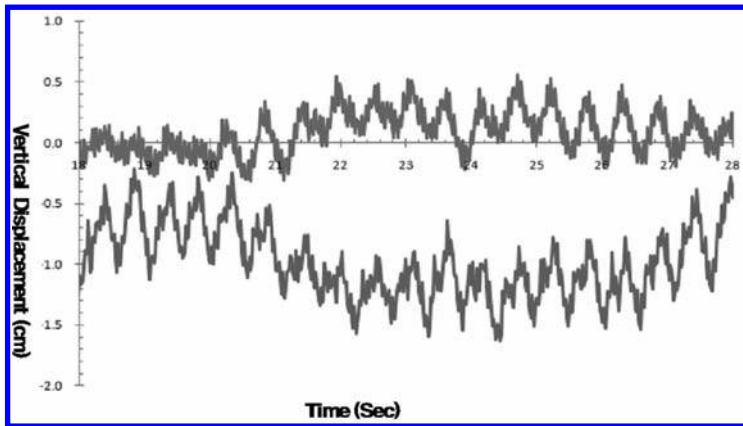


Figure 10. Comparison of settlement between embankment and interface section.

Also, in this study to evaluated later displacement between embankment (rockfill) section and interface section. Composite dam lateral displacement by earthquake magnitude compared to each seismic wave in case of empty and N.H.W.L of reservoir.

Figure 9 show lateral displacement of embankment and interface section of composite dam. In this study, the displacement result different between embankment section and interface section because of interface effects.

Composite dam settlement compared to each seismic wave at in case of empty and N.H.W.L of reservoir. In this test purpose, dynamic behavior of composite dam to compared with between embankment and interface section for earthquake wave. The result of test, embankment section was settlement and interface section was uplift (Figure 10).

4 CONCLUSIONS

The purpose of this study is to analyze the dynamic behavior characteristic of composite dam using centrifuge model test. In this study, using centrifuge model tests to characterize the dynamic behavior of composite dam. From the results of this research, the following conclusions are made:

1. In this research, the response relative displacement and settlement patterns of composite dam shows the same amplitude and phase trend in the initial response, but the interface and embankment section shows at the time of the phase difference, respectively.
2. In this research, the lateral displacement of embankment and interface section shows the different behavior pattern. Furthermore, the interface section of composite dam has to be considered to relative critical area.

REFERENCES

- Asteris, P.G. & Tzamtzis, A.D. 2003. Nonlinear Seismic Response Analysis of Realistic Gravity Dam-Reservoir System. *International Journal of Nonlinear Sciences and Numerical Simulation* (4): 329–338.
- Nien-Yin Chang Oncul, 2000. A Parameter Study on Seismic Behavior of a Composite Dam. *Journal of Geotechnical engineering Geotechnical special publication* (107): 178–190.
- Stavridis, L.T. 2002. Simplified Analysis of Layered Soil-Structure Interaction. *Journal of Structural Engineering* 128(2): 224–230.

Swiss expertise in North Africa focusing on flood protection

Nima Nilipour & Khalid Essyad

BG Consulting Engineers, Lausanne, Switzerland

ABSTRACT: Due to the population growth, social and land usage changes, consequences of natural disasters have been constantly increasing over the past decades. North Africa is also affected by natural disasters, particularly by flood events and drought. Algeria, Morocco and Tunisia are the most vulnerable both in terms of flood mortality and economic losses.

In this region, dams play an important role in flood protection reducing losses and recharging the ground water, leaving hydropower production as a secondary purpose of these structures. Traditionally, Swiss engineers, as pioneers in the construction of large dams, used to focus more on the hydropower benefits of dams. Working in different countries around the world, this point of view has been drastically changed since golden era of dam construction in Switzerland, 50 s to 70 s. Most of the time local restrains and standards are quite different and some important design data are not available. This requires pragmatic design concepts by making simple and realistic assumptions guarantying the safety while avoiding unnecessary costs due to overdesigned structures.

BG has been actively participating in flood protection program in the north of Algeria together with local partners. Solutions range from high dams including hydropower plant to small embankments and levees according to the project context. In this paper two particular projects are described, flood protection of M'Zab Valley and Bouhdid dam.

M'Zab Valley is located in the northern part of the Algerian Sahara where flashfloods caused important destructions and damages in the past. A global program has been implemented to define the flood protection scheme for the whole valley. Beside protection measures such as restructuration of the river course in the urban area, three embankments at upstream of the populated area were proposed with particular design adapted to the local context. One of the embankments has been completed in 2007, and its efficiency was clearly observed during the catastrophic flood of October 2008. The other two embankments are under construction and the completion is foreseen in early 2011.

Annaba region is located in the north of Algeria close to the Mediterranean Sea. Bouhdid RCC dam has two main objectives, providing enough storage volume in case of flood in order to protect the downstream population in the Annaba region and creating a permanent recreation lake. One of the main challenges of this project is the lack of seismic data. Recent seismotectonic studies show existence of active offshore faults potentially causing large earthquakes in the dam site, requiring a seismic resistance dam design. Complementary geological investigation and final design of the dam is ongoing and the construction is to be started in 2011.

1 INTRODUCTION

Nowadays the natural disasters are of main concerns in the world. Due to population growth, social and land usage changes, consequences of natural disasters have been constantly increasing over the past decades. The risk related to the natural hazards is usually measured by the mortality rate and economic losses as a proportion of gross domestic product. The critical natural hazard is different depending on the region. While in some regions earthquakes or

cyclones are the most critical natural hazards, in other region as North Africa, flood and drought are the main causes of mortality and economic loss. In the northern part of Algeria, Morocco and Tunisia the flood is the most critical natural hazard both in terms of mortality and economic loss (Dilley 2005).

In this region, dams play an important role in flood protection reducing human and economic losses and recharging the ground water to avoid drought, leaving hydropower production, if any, as a secondary purpose of these structures. Traditionally, Swiss engineers as pioneers in the construction of large dams, used to focus on the hydropower benefits of dams. Working in different countries around the world, this point of view has been drastically changed since golden era of dam construction in Switzerland, from 50 s to 70 s. Most of the time local restrains and standards are quite different and some important necessary design data are not available. This requires pragmatic concepts by making simple and realistic assumptions for design to guarantee the safety while avoiding unnecessary cost due to overdesigned structures.

BG has been actively participating in different flood protection programs and dam construction projects in the north of Algeria and Morocco working closely with local partners. According to the project context, solutions range from high dams including hydropower plant to small embankments and levees. In this paper two projects focusing on flood protection in the north of Algeria are described, flood protection of M'Zab Valley and Annaba Region Bouhdid dam.

2 RELABLITATION AND FLOOD PROTECTION M'ZAB VALLEY

2.1 *Context*

M'Zab Valley is located in the northern part of the Algerian Sahara 700 km south of Algiers. The annual mean precipitation is about 70 mm, however, the extreme precipitation (100-year rainfall event) could be of the same magnitude leading extremely severe flashfloods.

Inhabited since the 12th Century, traditional settling organised in 5 Ksour (fortified towns) along 30 km of M'Zab Valley, the principal being the well-known Ghardaïa. Actual population is around 200'000 and is estimated to reach 330'000 in 2030.

The main water resource of the region is the periodical floods of M'Zab River with a catchment area of 1'200 km², flooding palm groves located in the flood plain. Traditional small dams were used to slow down the flashfloods in order to recharge the phreatic aquifer, which was later used for irrigation.

Due to the attractiveness of this desert area, nowadays the palm grove is being densely urbanized, however, it is still potentially flooded, as it was sadly happened during the recent flood events in 1991 and 2008 causing major losses.

Since 90 s BG Consulting Engineers has been working on the rehabilitation and flood protection measures to be implemented in this region. A global program has been implemented to define the flood protection scheme for the whole valley.

2.2 *Flood protection scheme*

Since the very beginning of the project, it was clear that the increase of the flood-passing capacity in the urban area alone would not be sufficient to manage major floods. The flood protection scheme was therefore developed as an optimization between two following main flood protection concepts:

- Active measures: Upstream flood retention by dams,
- Passive measures: Riverbed widening and increasing the flood-passing capacity in the urban area.

After sites investigations and characterization and several optimizations the flood protection scheme proposed by the study comprises:

- three embankments at the upstream to reduce the 100-year flood discharge peak from 700–750 m³/s to 250–300 m³/s, [Figure 1](#) and [Table 1](#).
- Rehabilitation over a total length of 30 km by approximately doubling the riverbed capacity through a combination of bottleneck removal such as old bridges, widening and creating new dikes. One of the main challenges of the project was to preserve and integrate historical and patrimonial hydraulics structures.

2.3 Design principles of the embankments

The sites conditions are quite similar for the three embankment sites. The geology of the foundation is mainly composed of limestone covered by the alluvial deposit of around 20 m-thick at the bottom of the valley.

The main concept is to have a robust design requiring minimum maintenance during operation with reasonable cost in terms of construction material. The embankments are designed as homogeneous earthfill with chimney drain and particular care in terms of filtering. This has been carried out by selective placement of the material in course of the construction in order to maximize and to improve the filtering effect and to reduce the risk of internal erosion. The seismic activity of the region is quite low and therefore, seismic design of the embankments was not a major issue in terms of stability and liquefiable materials. The typical cross section is shown in [Figure 2](#).

The reservoir is almost empty in normal conditions. The average annual flood lasts typically four hour and the reservoir emptying takes one to five days. The emptying is done through an



Figure 1. El Abiodh, Bou Brik, El Haimeur embankments to protect the M'Zap populated area.

Table 1. Embankment characteristics.

	El Abiod	El Haimeur	Bou Brik
Embankment height [m]	18	22	8
Embankment volume [m ³]	700'000	500'000	200'000
Crest length [m]	1'100	430	880
Spillway capacity [m ³ /s]	475	455	200
Reservoir capacity [Mm ³]	19.0	15.7	1.2
Bottom outlet capacity [m ³ /s]	20	20	5

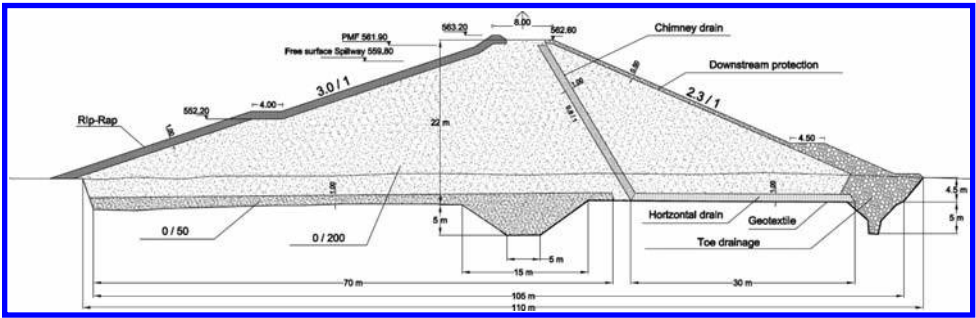


Figure 2. Cross section of El Haimeur embankment.

ungated outlet and a free flow spillway with low specific discharge. Cares have been taken in the hydraulic design to minimize the maintenance requirement and the risk of blockage and by floating bodies.

El Abiod embankment was completed in 2007, and its efficiency was clearly observed during the catastrophic flood of October 2008. The reduction of the peak discharge in the agglomeration was estimated as 35%. The other two embankments are under construction and the completion is foreseen in early 2011.

3 ANNABA VALLEY FOOD PROTECTION, BOUHDID DAM

3.1 Introduction

Annaba region is located in the north of Algeria close to the Mediterranean Sea. Bouhdid River takes its sources in Edough and Bougantas mountains and crosses the alluvial plane of Annaba before flowing into the Mediterranean Sea and its catchment area is around 14.85 km². In the past, flood events made important damages to the area and to the city of Annaba, particularly during the 1982 flood.

In the framework of the rehabilitation program of Annaba Region, studies have been conducted in order to prepare a general plan for flood protection of the central Annaba region. These studies showed the necessity of constructing a flood routing scheme. The main objectives of the scheme are:

- Flood protection: flood routing to reduce the 100-year flood to maximum 10 m³/s requiring a flood retention volume of 500'000 m³,
- Recreation: providing a recreation activities focusing on water and environmental topics,
- Sediment management: allowing sediment management and extraction of materials.

Based on the topography of the valley and geological and hydrological aspects, the dam axis has been selected at around 2 km upstream of the city towards southwest. Another two studied axes have been discarded. The upstream alternative axis has a smaller catchment area and presents some geological issues, mainly the presence of landslide and poor quality of the foundation. At the downstream alternative axis, the valley is wider and there are some restrictions of the land use.

3.2 Dam site conditions

Dam site on the selected axis presents the following conditions:

- Valley shape: the valley is relatively wide. The crest length/dam height ratio at the selected dam axis is around 9. Therefore, the only alternatives would be a concrete gravity dam or an earth dam.

- Geological conditions: the rock is visible in the river bed, therefore, a concrete gravity dam can be considered as an alternative. However, the bedrock quality and the thickness of alluvial sedimentation on the sides of the valley should be verified. The rock is composed of gneiss and schist with vertical joints and presenting local important fracturing and surface weathering.
- Hydrological data: the rainfall records are available for only 16 years giving an average annual rainfall of 660 mm mostly fell in during winter months. Flood with different return period are estimated using rain-flow Chicago type model. The peak flows are 60, 127 and 207 m³/s corresponding to 100, 1'000 and 10'000-year floods.
- Seismic activity: several studies have been conducted on the seismic hazard assessment of the northern part of Algeria. Historically and based on instrumental seismicity, seismic activity of Annaba Region has been evaluated as moderate by the past studies (Harbi 1996, Harbi et al. 2003a, b, Boughacha et al. 2004). Even if this region did not experience any important seismic activity, the occurrence of large earthquakes cannot be ruled out. Indeed a new research, based on recently available data, revealed the development of young, active fault-related folds at the foot of the Algerian margin off the Annaba region (Kherroubi et al. 2009). Therefore, in the dam design seismic aspects should be carefully dealt with. (Figure 3)
- Construction material: investigations are ongoing to find a proper nearby borrow area for construction materials such as clay, rockfill material and concrete aggregate. The comparison of alternative and design are based on the assumption that the construction material should be brought from other sites.

3.3 Bouhdid Dam alternatives

Different alternatives have been studied and compared for the selected axis of Bouhdid Dam:

- Embankment dam: based on the preliminary site investigation, there is no proper borrow area for clay material to be used as impervious core. Therefore, the embankment alternative

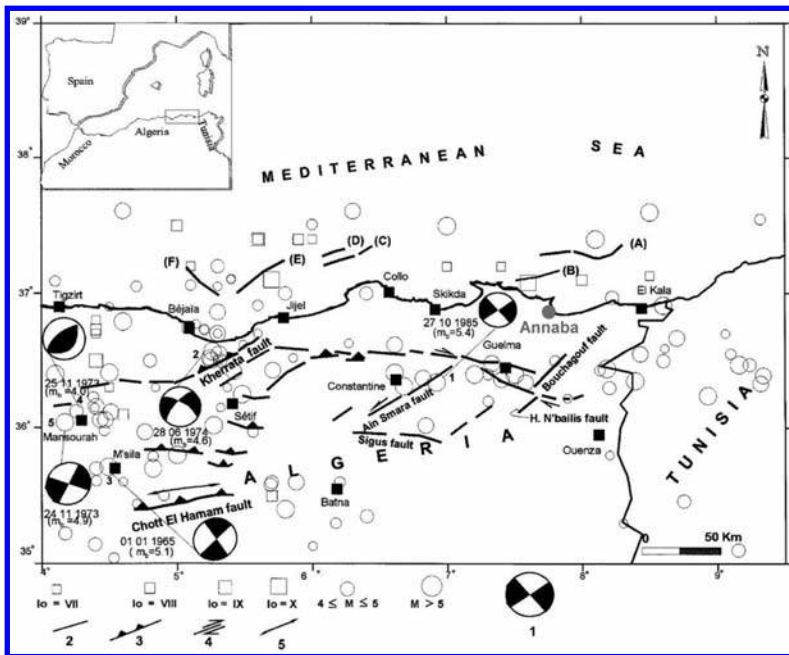


Figure 3. Seismotectonic map of northeast of Algeria. Squares: historical earthquakes (1357–1910)—circles: instrumental seismicity (1911–1996), (A to F): recent offshore faults, Harbi et al. 1999.

should be designed considering an impervious upstream membrane or concrete or asphalt core. Due to the high seismic activity of the region, care should be taken regarding the use of potentially liquefiable soils.

- Concrete gravity dam: in order to reduce the cost of this alternative, Roller-Compacted-Concrete (RCC) is foreseen. Both upstream and downstream faces are made on conventional vibrated concrete. The main issue of this alternative is the quality of the rock foundation and required grouting works.
- Concrete faced rockfill dam (CFRD): flexibility and low vulnerability to internal erosion due to post earthquake conditions made this type of dam the most suitable for seismic areas. Many recent experiences have been made for CFRD dams smaller than 200 m. However, the availability of the rockfill material is the main concern. The construction of upstream concrete slab and its connection to the plinth are also important technical and construction issues.

The RCC gravity dam alternative has been adopted for Bouhdid Dam. The main advantages of this alternative are:

- a. Easier integration of appurtenant structures, i.e. free flow spillway, bottom outlet,
- b. Less vulnerable to flooding during the construction period. Due to limited hydrological available data, this is an important issue which reduces considerably the costs of diversion system compared to the other alternatives,
- c. Lower dam volume. Since most probably the construction material should be transported from other sites, low dam volume is an advantage for the RCC alternative,
- d. Less impact on the site as the dam footprint is smaller,
- e. easier to adapt the design in the course of the project, by concrete strength zoning, if seismic loads are revealed to be higher,
- f. No significant difference in the total cost between alternatives.

3.4 *Bouhdid RCC dam design*

The design and construction of the dam are influenced by two main uncertainties: a) construction flood b) design earthquake. While the former has an impact on the construction planning and diversion concept, the latter influences the design hypotheses and the dam geometry. The main section of the dam enjoys a conventional geometry with 1:10 slope for the upstream face and 1:0.9 for the downstream face ([Figure 4](#)).

Static analyses are performed for normal flood water levels combined with corresponding temperature loads. Due to the rather conservative section, low maximum compressive and tensile stresses are locally obtained for static loads, 3.3 MPa and 0.3 MPa, respectively. This rather conservative section provides enough reserve in terms of concrete strength for dynamic loads.

Dynamic analyses were conducted to verify the design for peak ground acceleration (PGA) ranging from 0.6 to 0.8 g corresponding to the verification earthquake level. These high PGA values are obtained based on newly available data and hypotheses on the seismic activity of two nearby offshore faults, [Figure 3](#). Although these PGA values should be confirmed by further studies, the dam design at this stage takes them into account. First natural frequency of the dam is computed as 8 Hz meaning the acceleration amplification would be maximum based on the European standard elastic response spectra. Due to uncertainties on the seismic loads, the dynamic analysis at this stage is conducted with pseudo-static approach. Computed dynamic stresses are combined with thermal stresses and normal water level load case. The maximum obtained compressive stress is 11.3 MPa corresponding to the combination of PGA towards downstream and 2/3 downward with summer temperature stresses. The maximum computed tensile stress is 2.8 MPa corresponding to the combination of PGA towards upstream and 2/3 upward with winter temperature stresses. Both maximum values occurred on the dam faces, where conventional concrete is foreseen. The concrete zoning will be detailed on the final phase and based on the detail dynamic analysis. Most probably the thickness of conventional vibrated concrete will be increased on both upstream

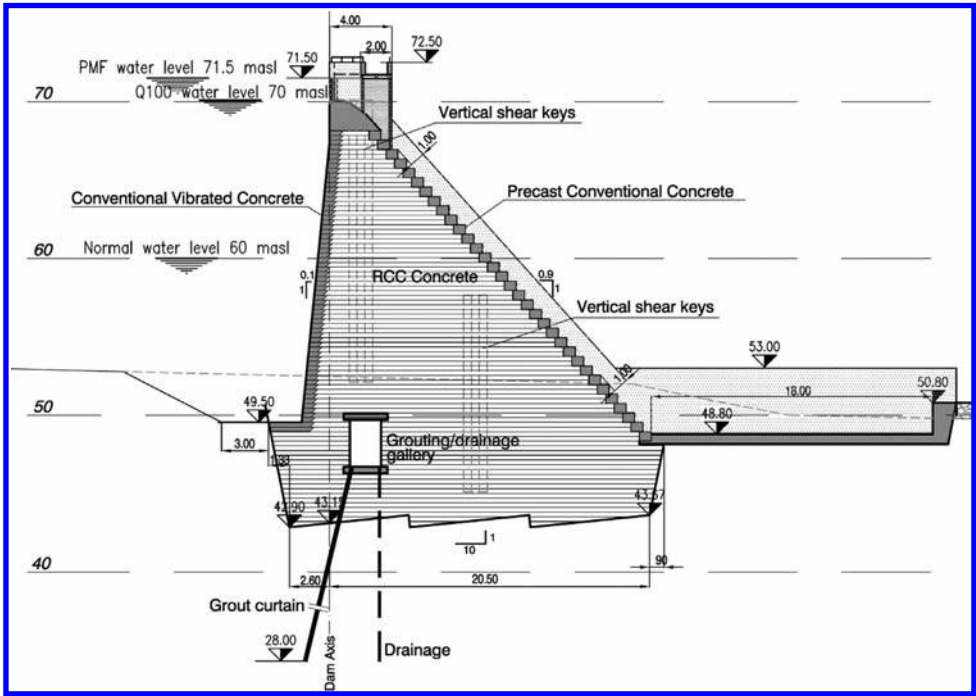


Figure 4. Main vertical section of Bouhdid RCC gravity dam.

and downstream faces close to the foundation level where maximum stresses were obtained. At this stage of the project a nominal concrete strength of 10 MPa for RCC and 25 MPa for the conventional concrete are adopted.

Vertical shear keys are foreseen in the vertical RCC cut joints in order to improve the stability of the concrete blocks and to benefit from the three dimensional behavior of the structure during the earthquake.

The overall dam stability was verified for both overturning and sliding modes for static and dynamic load cases. Obtained safety factors for static loads are largely above the required level for both sliding and overturning. Whereas for the dynamic load cases, safety factors could be instantaneously below 1 for sliding for PGA higher than 0.6 g, and for downstream-upstream overturning for PGA higher than 0.7 g. The stability has been improved for downstream sliding by giving an upward slope of 1:10 to dam-foundation contact with particular shape. The displacement of the dam due to sliding should be computed in a later phase and using more precise dynamic loads and analyses. The downstream-upstream overturning can potentially cause some cracks on the hill of the dam for very high PGA. These cracks are not critical as they are on the hill of the dam and would be closed under normal static loads, therefore there is no risk for post earthquake condition. Using higher strength concrete at this zone reduces the risk of cracking.

4 CONCLUSIONS

The flood and drought are the main natural disaster in the northern part of Algeria both in terms of mortality and economic losses. BG Consulting Engineers have been actively participating in development of flood protection general plans in collaboration with local partners.

M'Zab Valley flood protection program enjoys active and passive measures. As active measures three embankments have been foreseen at the upstream to reduce the peak flood discharge. Increasing the riverbed capacity through a combination of bottleneck removal

such as old bridges, widening and creating new dikes in urban areas have been used as passive measures. El Abiodh embankment was completed in 2007, and its efficiency was clearly observed during the catastrophic flood of October 2008. The reduction of the peak discharge in the agglomeration was estimated as 35%. The other two embankments are under construction and the completion is foreseen in early 2011.

City of Annaba was frequently flooded during the past heavy rainfalls. In the framework of the rehabilitation program of Annaba Region, studies have been conducted in order to prepare a general plan for flood protection of the central Annaba region. These studies showed the necessity of constructing a flood routing scheme. Bouhdid dam allows reducing the maximum flow during the flooding events and creates a permanent lake for recreation purposes. The adopted alternative consists of a RCC gravity dam with specific design to withstand a high level of seismic activity of the region revealed by recent researches on the offshore nearby faults and the development of young, active fault-related folds. Complementary geological investigations and the final design of the dam are ongoing and the construction is to be started in 2011.

REFERENCES

- Dilley, M., Chen, R.S., Deichmann, U., Lerner-Lam, A.L., Arnold, M., Agwe, J., Buys, P., Kjekstad, O., Lyon1, B. & Yetman, G. *Natural Disaster Hotspots: A Global Risk Analysis, Synthesis Report, 2005.*
- Kherroubi, A., Déverchère, J., Yelles, A., Mercier de Lépinay, B., Domzig, A., Cattaneo, A., Bracène R., Gaullier, V. & Graindorge, D. 2008. Recent and active deformation pattern off the easternmost Algerian margin, Western Mediterranean Sea: New evidence for contractional tectonic reactivation. *Marine Geology* 261(1–4): 17–32.
- Harbi, A., Benouar, D. & Benhallou, H. 2003a. Re-appraisal of seismicity and seismotectonics in the north-eastern Algeria Part I: Review of historical seismicity. *Journal of Seismology* 7(1): 115–136.
- Harbi, A., Maouche, S. & Ayadi, A. 1999. Neotectonics and associate seismicity in the Eastern Teelian Atlas of Algeria. *Journal of Seismology* 3: 95–104.
- Harbi, A., Maouche, S. & Benhallou, H. 2003b. Re-appraisal of seismicity and seismotectonics in the north-eastern Algeria Part II: 20th century seismicity and seismotectonics analysis. *Journal of Seismology* 7(2): 221–234.

Risk assessment for the critical regimes of Chaira dam stilling basin

J. Tadjer

RILRAM, Sofia, Bulgaria

H.T. Falvey

Henry T. Falvey & Associates, Inc., Conifer, Colorado, USA

ABSTRACT: The estimation of potential hazardous operations of the stilling basin can be obtained after determining their critical regimes. The processes definition can be understood from the power point of view with a relative ease. At times, however, there is the possibility to observe several critical regimes for varying discharges. These regimes govern the design defining the dimensions of the stilling basin.

The stilling basin of Chaira Dam Bulgaria is a good example demonstrating these different governing regimes. Several unfavourable effects are observed at different working regimes. This authors' work shows that predictions of the negative effects at the stilling basins is possible and necessary.

This paper describes how the current Chaira Dam construction allows a unique possibility to observe and document extreme regimes for discharges less than the maximum level possible. These regimes, obtained for both small and large openings of the gate, are explored and explained in detail.

1 INTRODUCTION

The stilling basin of the Chaira Dam shown in [Figure 1](#) was changed several times during the construction. The initial conceptions are changed during the time of building. The numbers of outlets was varied and finally one outlet was selected in the final design. That leads to the bed configuration of the basin and to the no satisfaction power dissipation. Despite that, the configurations presented the possibility of observing interesting effects and critical regimes that were different from the maximum discharge and maximum head.

Some authors such as Chow (1974) and Stanchev (1957) show that adverse stilling basins operating modes may exist at less than the maximum discharge. The existing of adverse operating regimes at less than the maximum discharge can be shown with the help of the power equation. The power E , is denoted by

$$E_i = \rho \cdot Q_i \cdot v_i^2, \quad (1)$$

and for the full opening $k_i = 1$

$$E = \rho \cdot Q \cdot v^2,$$

where k = percent gate opening; Q = discharge; v = velocity; and ρ = density.

For the case of stilling basin downstream of a bottom outlet is considered, [Equation 1](#) may be written for the power at the entrance of the basin with relative gate opening $k_i < 1$, for any $Q_i < Q$ as;

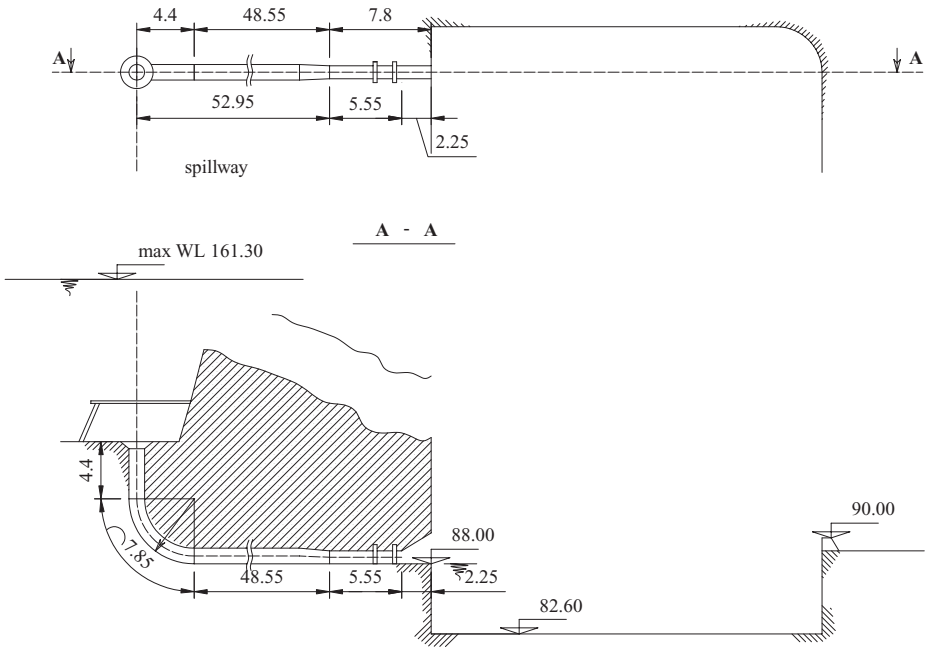


Figure 1. Stilling basin of Chaira Dam.

$$\rho Q_i v_i^2 = \rho S_i v_i v_i^2 = \rho k_i S_i \left(\frac{2 \cdot g H}{k_i^2 \cdot p^2 \cdot \Sigma \xi + \xi_i + \alpha} \right)^{\frac{3}{2}}, \quad (2)$$

where g = the acceleration of gravity; k = percent gate opening, p = the ratio of the cross section of a full open valve and the cross-section of the pipe; H = head between the WL of the dam and the axe of the gate; S = the cross section of the full opened valve; ρ = density of water; α is the Coriollis' coefficient; ξ_i = head losses of the valve at the relative opening k_i ; and $\Sigma \xi$ = sum the pressure head losses between the derivation entrance and the gate. For full opening $Q = Q_{\max}$ (1) can be written as

$$\rho Q v^2 = \rho S \cdot v^3 = \rho S \cdot \left(\frac{2 \cdot g H}{p^2 \cdot \Sigma \xi + \xi + \alpha} \right)^{\frac{3}{2}}. \quad (3)$$

To compare the energies (per sec), the expressions (2) and (3) must be balanced

$$\frac{k_i^{\frac{2}{3}}}{k_i^2 \cdot p^2 \cdot \Sigma \xi + \xi_i + \alpha} \geq \frac{1}{p^2 \cdot \Sigma \xi + \xi + \alpha} \quad \text{or} \quad \frac{k_i^{\frac{2}{3}}}{k_i^2 \cdot p^2 \cdot \Sigma \xi + \xi_i + \alpha} < \frac{1}{p^2 \cdot \Sigma \xi + \xi + \alpha} \quad (4)$$

In some cases the left part of the relationship given in Equation 4 is greater than the right side. This indicates that part gate openings can have more power entering the stilling basin at part gate than at full gate.

The critical part gate regime can be determined from plots of Equation 1 with different relative gate openings. The maximum value of the plot is the critical regime. This condition is the design condition used in design. Critical regimes are defined by the parameters of the structure, or for the constant values of Q and H these regimes depend on the head losses $\Sigma \xi$ and the valve characteristics $\xi_i = \varphi(k_i)$.

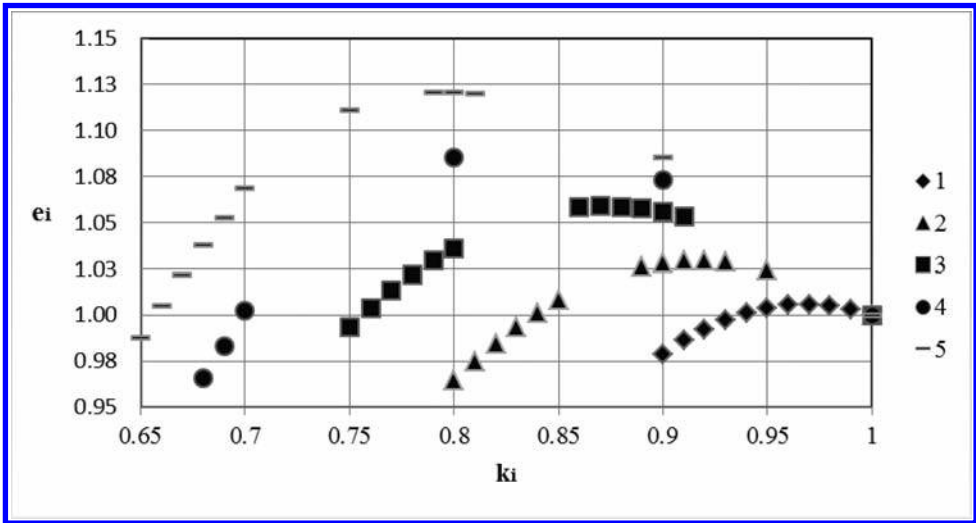


Figure 2. Values of relative power parameter $e_i = E_i/E$, depending on the relative opening k_i and different head losses $\Sigma\xi = 1, 2, 3, 4$ and 5 for gate.

Any derivation at the end of which is mounted gate with known characteristics is examined. For different head losses in the derivation the relationship between the power of the flow after the gate, related to the power of the flow of the maximum discharge, can be given in graphical form in Figure 2. This can be accepted as a model scheme of derivation with gate and it is valid for any derivation with known head losses and characteristics of the valve mounted at the end of it.

2 CRITERION FOR DETERMINING THE CRITICAL REGIMES OF STILLING BASINS FOLLOWING BOTTOM OUTLETS

This section examines how the critical regime influences the design of a sample stilling basin. In addition the effect of the structure parameters on the formation of various critical regimes is investigated.

The ratio between the power at part gate opening and the full gate opening from Equation 1 is defined as relative power (power) parameter given by;

$$e_i = \frac{E_i}{E} = \frac{Q_i \cdot v_i^2}{Q \cdot v^2} \quad (5)$$

The variation in this parameter for various values of the summation of the power loss is given in Figure 2 for Gate. The maximum of e_i shows is for critical regime which is greater than different than the maximum discharge and maximum head.

In case of different valve—perhaps Hollow Jet Valve for the roughly estimation of the critical regimes have to be taken in account Figure 3. Here for $\Sigma\xi = 2$ the different critical regime will not be observed.

For the purposes of the preliminary estimation and design of the stilling basin is good to be tested for the critical regime for the 0.92 opening, Figure 2. If the valve is different, for instant Howell-jet, see. Figure 3 the critical regime will be the same as for the maximum discharge. The different critical regimes will be more evident for $\Sigma\xi > 3$. On Figures 4–6 are shown the different positions of the water jet.

The value of e_i is a preliminary assessment of the possibility of the different critical regime appearance. Stilling basins are traditionally calculated by Bernouli's equation, hydraulic jump

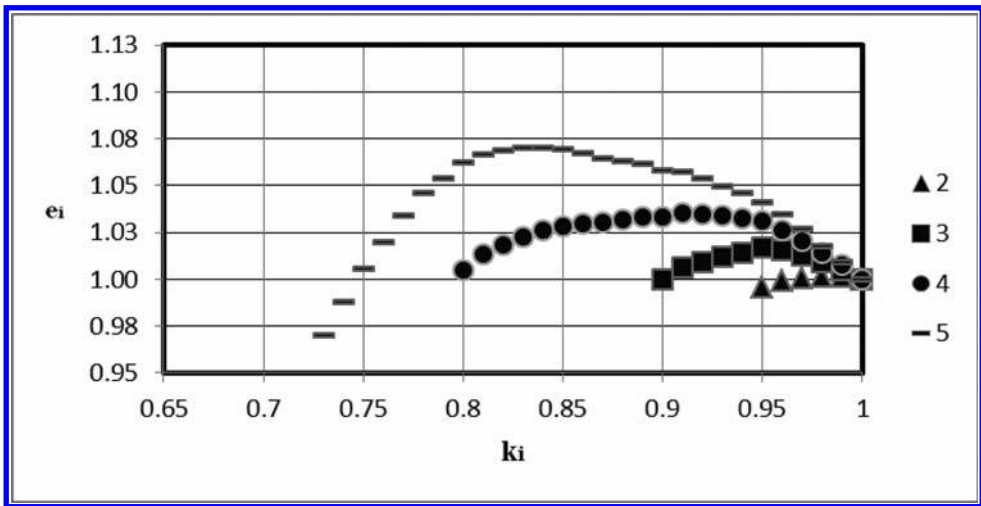


Figure 3. Values of relative power parameter e_i , depending on the relative opening k_i and different head losses $\Sigma\xi = 2, 3, 4$ and 5 for Hollow-jet valve.

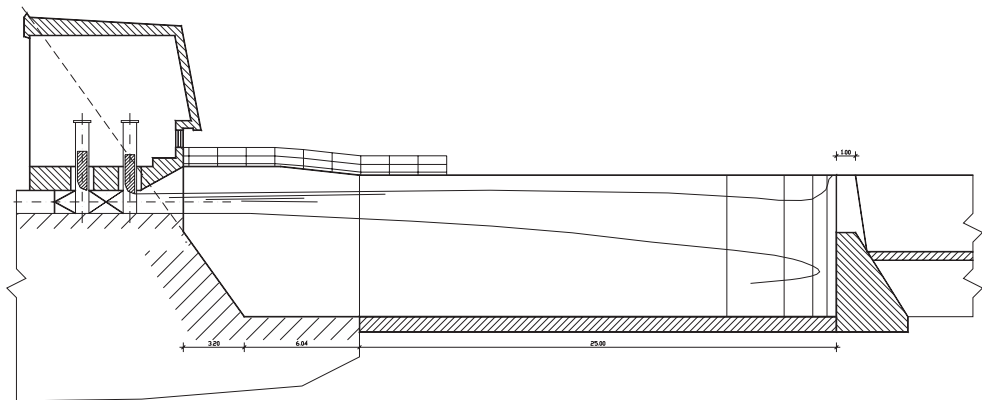


Figure 4. Working regime for 85% opening of the gate.

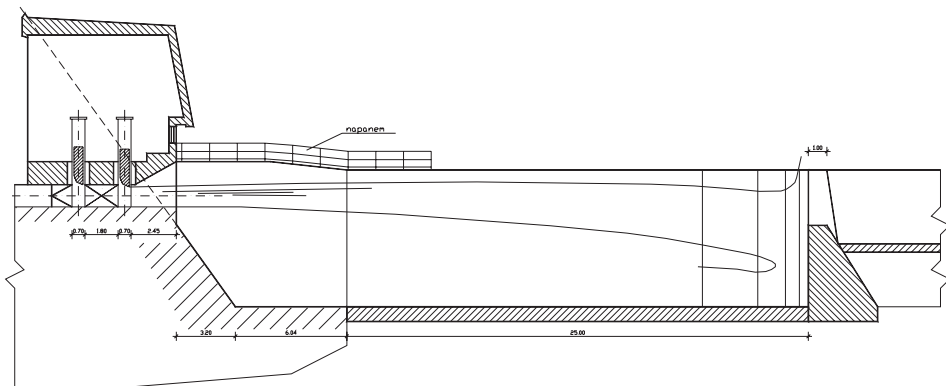


Figure 5. Working regime for 90% opening of the gate.

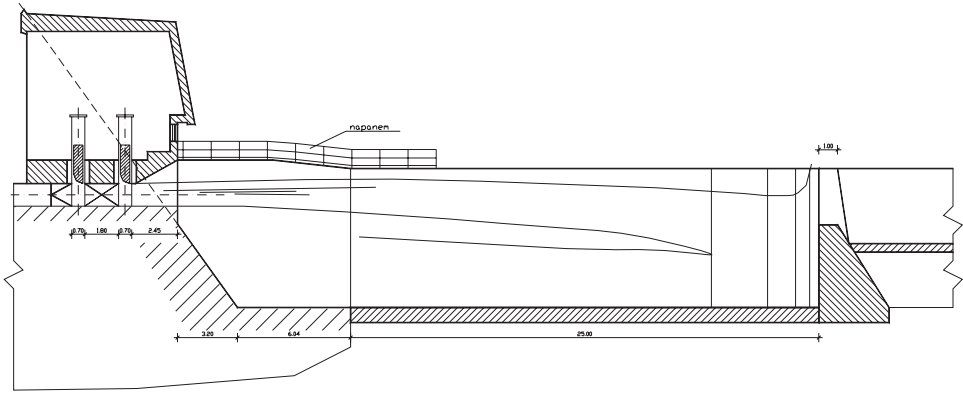


Figure 6. Working regime for 100% opening of the gate.

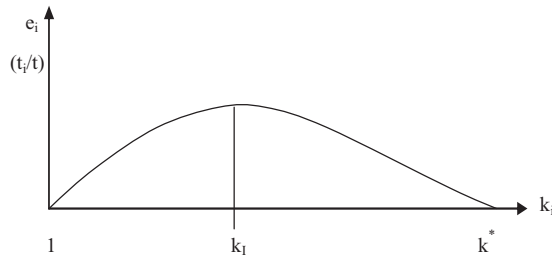


Figure 7. Relationship between relative opening and k_i power parameter e_i .

and the formula for spillways. The height of the baffle wall is determined by the difference of the sequent depth and the head on crest of the threshold at the end of the stilling basin. The estimation with line of influence can be found in details in Tadjer (2001), Tadjer (2002) and Tadjer (2005).

By looking at Figure 2 and Figure 5, when the presence of critical regime is observed that the power parameter e_i given in (6) is maximum. These values define the interval on the axis k_i —Figure 7, which contains two values of the relative opening (with the exception of k_i —the relative opening for which e_i reaches its maximum) there are two values with power greater than that of $Q = Q_{\max}$. Naturally, the question arises, is it possible to exclude one part of these two areas and the zone of critical regimes to be limited only by $k_i < k_i < 1$ or $k_i^* < k_i < k_i$, where k_i^* is the relative opening. If it is possible to exclude one area, this would significantly limit the critical regimes.

The concern about critical regime, from the power dissipation point of view, is considering the operational (cavitation and vibration) safety.

The critical regime related to the first area $k_i < k_i < 1$ should take into account the possibility of power dissipation in the borders of the basin. The second area $k_i^* < k_i < k_i$ could be omitted having in mind e_i and t_i/t —the relation between the heights of the baffle wall calculated for different discharges Q_i and Q . Occasionally, there are exceptions of course—see splash problem Figure 8 at “Chaira” Dam.

At the second area $k_i^* < k_i < k_i$, it must consider the effect of cavitation, vibration and even abrasive hazards. In these cases the large volume of basin or inadequate structure can lead to closing the areas with cavitation close to the valve, especially if the free aeration is not implementable.

The process can be observed by the movie about the gate operation of Chaira Dam made on 6 April 1995. The opening time is 170 s, while the close time is 140 s. If the movie is

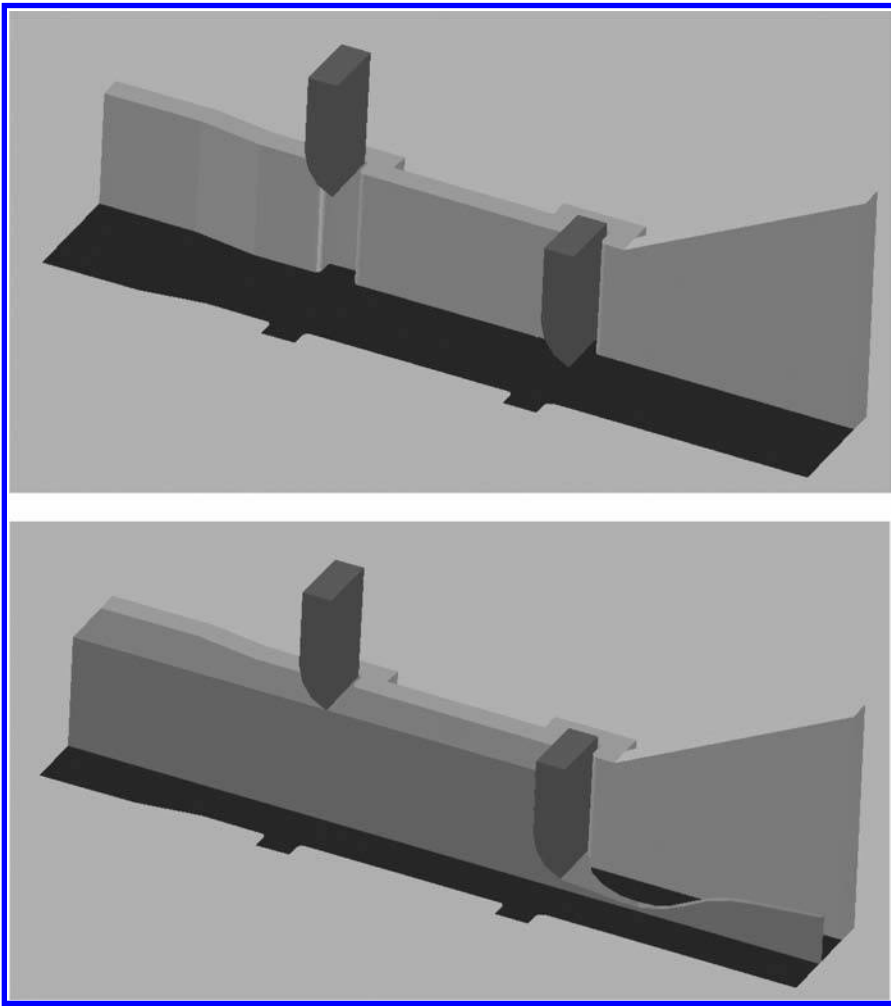


Figure 8. Splash effect generation.

watching carefully it can be seen that the worst regime is realized at about 90% opening. The head losses in the derivation can be assessed as $\Sigma\xi = 2$. For this value according to the [Figure 2](#) the critical regime has to be at 0.92 see [Figures 4–6](#). After several time the volume of the stilling basin become full and the jet from the outlet collaborate with the water surface. These different regimes can be observed when the gate is closing. This can reproduce the regime worst than the 90% the effect of the free jet effect striking on the baffle wall before collaboration can be assessed by the power criterion (6).

3 EFFECTIVE POWER DISSIPATION BY MODIFYING THE SHAPE OF THE GATE-SLOTS

In addition, the splash effect for the very small opening of the same construction is observed. During the model tests was accepted that this effect is generated by the shape of the gate-slots see [Figure 8](#).

Possible correction of the shape of the gate-slots of the bottom outlets of the “Chaira” Dam is available. For small gate openings the streams formed into the gate-slots run into

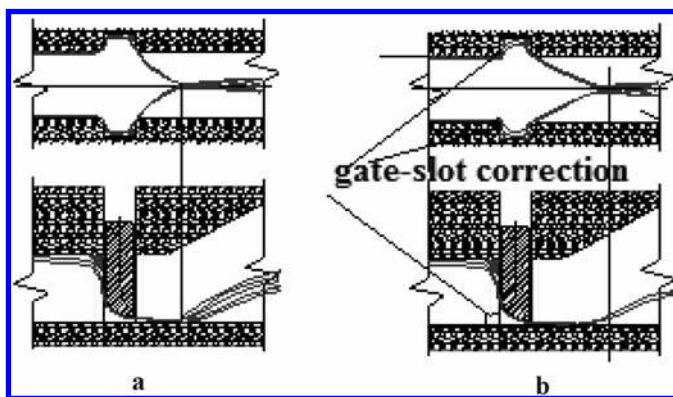


Figure 9. Possible correction of pressure side of the gate-slots. a) Without correction—a strong contracted flow, b) with the improved form of recesses in the lower 0.2 meters.

each other. They meet in crash zone and splash pass over the stilling basin dimensions. If a gate-slot form of Figure 9a is changed as figure—shown on Figure 9b, the crash zone of two opposite streams will be displaced downstream, and the splash will be diminished respectively. It was found that the effect can be substantially reduced after modification of the gate-slots for the lower 0.2 m.

4 CONCLUSIONS

The paper argued that stilling basins optimization should be done according to their cavitation, vibration and erosion (abrasion) reliability. Based on this it is recommended to identify the purpose, shape and dimensions of the structure. Optimization does not necessary require a reduction of dimensions, but requires a choice suitable structure.

In the present work is given an original methodological approach to assess the stilling basin structure according to availability events occurring where it does not work effectively. The suggested vision allows to predict unfavourable regimes, defined as critical.

Proposes a methodology for stilling basin designing. As first step is make prediction of the critical regimes and the possible conditions under which they exhibit. The next step is to evaluate the design according to the possibilities of described negative events.

The splash effect can be avoided with the help of a correction of pressure side of the gate-slots.

REFERENCES

- Chow, W. 1974. *Open Channel Hydraulics*, New York: McGRAW-HILL Book Company, INC.
- Stanchev, St. 1954. On the design of the stilling basins situated after the standard crest shaped spillways. *Proceedings of the Institute of Civil Engineering and Architecture*, v. VI, Book II, (Annuaire de l'Institut du Genie Civil, Facultes des Constructions, d'Architecture et d'Hydrotechnique, Annee 1954, tome VI, Livre II).
- Tadjer, J. 2001. Review of some unfavorable regimes in the stilling basins and concepts for their definition. *Proceedings of the UACEG vol. XL 1999–2001*, 207–215.
- Tadjer, J. 2002. Extending the interpretation of the criteria for determining the critical regimes in the stilling basins. *Разширяване тълкуването на критерия за определяне на меродавните оразмерителни режими при енергогасителите*. *Proceedings of the UACEG Jubilee*, 403–411.
- Tadjer, J. 2005. Design Criterion for Authoritative Regimes of the Bottom Outlet Stilling Basins Determination. *10TH JUBIL. NAT. CONGRESS OF THEORETICAL AND APPLIED MECHANICS*, Varna, Sept.

Design and hydraulic modelling of a fuse plug spillway

L. Schmocker, E. Rühli, V. Weitbrecht & R.M. Boes

Laboratory of Hydraulics, Hydrology and Glaciology (VAW), ETH Zurich, Zurich, Switzerland

P.A. Mayor & S.M. Springman

Institute for Geotechnical Engineering (IGT), ETH Zurich, Zurich, Switzerland

ABSTRACT: Flood events during the last two decades led to increased design flood definitions that require the provision of additional spillway capacity for dams and river flood protection systems. A fuse plug is an earth and rockfill embankment designed to wash out completely in a predictable and controlled manner, when the spillway capacity of the service spillway and of additional outlets, such as the bottom outlet, is exceeded. Furthermore, a fuse plug can be used as a side spillway along rivers to prevent uncontrolled overtopping of the embankments during extreme floods. So far, only limited knowledge is available on the design and operation mode of fuse plugs. Therefore, a series of laboratory tests has been conducted at the Laboratory of Hydraulics, Hydrology and Glaciology of ETH Zurich to examine: 1) the design of the fuse plug, e.g. grain size distribution, zoning, core, filter, surface protection; 2) the breach process; and 3) long term behaviour. Both small and large scale experiments have been carried out, modelling a projected fuse plug along the Aare River in Switzerland. In this case, the fuse plug is designed with an inclined, impermeable core to prevent early and uncontrolled failure for water levels below the crest. Sand and gravel form the main portion of the fuse plug and lead to fast breach enlargement when overtopping starts. A riprap surface protection prevents erosion due to wind, waves and rain. The fuse plug breaching can be initiated using a pilot channel with a lower elevation than the fuse plug crest. The breach process is dominated by erosion of the highly erodible embankment material followed by undercutting and collapse of the impermeable core.

1 INTRODUCTION

A fuse plug, or a breaching section, is an erodible predetermined separate section of a dam, designed to wash out when the reservoir or the river reaches a specific level (Khatsuria 2005). Fuse plugs for reservoir dams are mostly used as additional spillways when the spillway capacity of the service spillway and of possible additional outlets, such as the bottom outlet, is exceeded. Along rivers, fuse plugs can provide a side spillway to prevent uncontrolled overtopping of the embankments. In both cases, the fuse plug collapses gradually over a reasonable time when overtopped, releasing surplus flood without endangering the safety of the main dam and levees, respectively. Erosion of a fuse plug enables large overflow depths and a high spillway capacity to be achieved, compared to side spillways with a fixed crest. The wash out of a fuse plug begins at a preselected location, e.g. a low spot in the embankment, called a pilot channel. The breaching of the pilot channel will occur rapidly and the rest of the fuse plug embankment will breach and wash out laterally.

1.1 *Flood control plan Hagneck Channel*

The Hagneck Channel provides the man-made diversion of the Aare River from Aarberg to Lake Biel in Switzerland. The channel was built between 1875 and 1878 to improve the flood

control along the Jura waterways in Switzerland (Minor and Hager 2004). Today, the 140 year old channel needs to be upgraded as the design flood of $1500 \text{ m}^3/\text{s}$ can not be discharged without causing major problems. The 2005 flood event demonstrated that dam overtopping may already occur for a discharge of $1300 \text{ m}^3/\text{s}$. Further problems exist regarding seepage, internal erosion and slope failure as the dams were constructed without an impermeable core. Therefore, the dams are refurbished and elevated to assure a discharge capacity of $HQ_{100} = 1500 \text{ m}^3/\text{s}$, including a freeboard of 1 m.

To prevent uncontrolled dam overtopping in case of extreme flood scenarios ($HQ_{300} = 1800 \text{ m}^3/\text{s}$), a side spillway will be constructed at the beginning of the upgraded dam section. The fixed weir sill is located 1.7 m below the crest of the new levee (Fig. 1) to ensure sufficient spillway capacity can be provided. To activate the spillway as late as possible during a flood event, a fuse plug is placed on top of the fixed weir sill (Fig. 1). If the fuse plug is overtopped during an extreme flood event, it should erode fast and entirely. An impermeable core prevents an early failure for water levels below the activation point. The fuse plug, constructed as an earth embankment, is 1.2 m high, 300 m long and provides a spillway capacity of approximately $300 \text{ m}^3/\text{s}$. The surplus water is discharged into a destined flood plain with comparatively low damage potential.

1.2 State of the art

In total, not more than about 20 fuse plugs had been constructed by 2005 (Khatsuria 2005), and even fewer have actually been in operation. A general fuse plug spillway design can be found in the literature (Chee and Zaghoul 1971, Pugh 1985, Engels and Sheerman-Chase 1985, USBR 1985, Gosschalk 1988). The principal features are: (1) pilot channel, (2) impervious core, (3) filters, (4) composition of sand and gravel, and (5) slope protection. The first fuse plug model tests were conducted for the emergency spillway of the Oxbow Dam (Tinney and Hsu 1961). The fuse plug consisted of rock fill along with an inclined impervious core that was 8.5 m high and 130 m long. The erosion process was modelled at 1:40, 1:20 and 1:2 scales and the erosion was initiated using a pilot channel. Another detailed work on fuse plugs was carried out by Pugh (1985). He establishes a general design and describes the erosion process in detail. Wahl (1993) conducted hydraulic model tests for the Horseshoe dam fuse plug. A system consisting of three fuse plugs separated by concrete walls was tested at small scale and one or more fuse plugs are activated, depending on the required spillway discharge. All studies in the past concluded that the lateral erosion rate is primarily a function of the erosion rate of the embankment material and not of the resistance of the impermeable core. General work on dam breaching due to overtopping were conducted by e.g. Coleman et al. (2002), Chinnarasri et al. (2003), Project DIFUSE (2004), Schmocker and Hager (2009) and Pickert et al. (2011).

Despite this research, detailed design guidelines for a fuse plug are still missing. The work conducted and described above is mostly limited to a specific application or a special fuse plug design. Most laboratory tests described in literature were performed using uniform embankment materials. The hydraulic model tests presented herein are therefore essential to guarantee correct operation of the fuse plug at the Hagneck Channel.

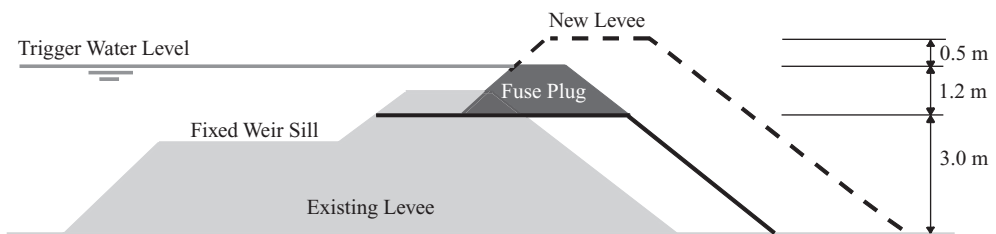


Figure 1. Dam cross section along the side spillway section with planned fuse plug.

1.3 Goal of hydraulic model tests

The design and feasibility of the fuse plug was investigated using hydraulic model tests. Of special interest are: (1) fuse plug design, e.g. grain size distribution, zoning, core, filter, surface protection; (2) breach process and breach time; and (3) long term behaviour. Both small scale and prototype experiments have been carried out. A systematic parametric investigation of the fuse plug design and the general functionality is achieved through the small scale experiments. The final design is tested next, at prototype dimensions using prototype materials to minimize possible scale effects. The erosion process of the fuse plug may be either 2-dimensional or 3-dimensional. The latter case normally occurs in nature and includes both vertical and lateral erosion. In the hydraulic model tests, the erosion process is investigated primarily 2-dimensionally. Therefore, the tractive forces in the river mainstream are neglected. An additional small scale test is conducted to investigate the 3-dimensional erosion process. Long term behaviour and durability of the fuse plug and its material cannot be modelled properly in hydraulic model tests. The stabilising effect of vegetation is not part of this study.

2 FUSE PLUG DESIGN AND MATERIALS

The design of a fuse plug does not differ fundamentally from the design of a normal zoned dam. The fuse plug section must remain stable for all conditions up to the design discharge, in particular for all water level variations, including rapid draw-down. Special constraints have been taken into account for the design of the Hagneck Channel project. The slopes are comparatively steep as the fuse plug width is limited due to space constraints. In ensuring that the long term behaviour is guaranteed, core material that is not susceptible to shrinkage cracking must be used, since it will be exposed to long periods of desaturation as the water level may seldom reach the elevation of the fuse plug. In addition to these geotechnical considerations, the choice of the building materials depends also on the availability of a sufficient quantity of material of suitable quality to achieve the construction.

The fuse plug was designed in collaboration with the Institute for Geotechnical Engineering of ETH Zurich and is based on experience from previous investigations (Pugh 1985) and physical model tests. Figure 2 shows the fuse plug cross section with four different zones. The impermeable core (1) is inclined in the downstream direction. It prevents washout of the fuse plug for discharges smaller than the design discharge and collapses under its own weight when the embankment body is eroded below the core. Achieving collapsibility demands a soil with a limited stiffness, even in a dry state, so that a material with a grain size in the range of silt and with optimal shrinkage characteristics has been chosen. The core is covered with a suitable filter to prevent piping (2). The thickness of the filter layer was chosen large enough to prevent segregation during construction and to provide a self-healing effect in case of cracks, especially in the core.

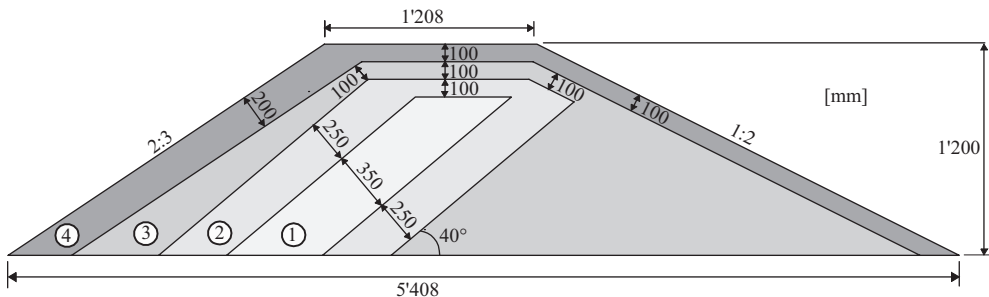


Figure 2. Fuse plug design and dimensions with (1) impermeable core, (2) filter, (3) embankment body, (4) slope protection.

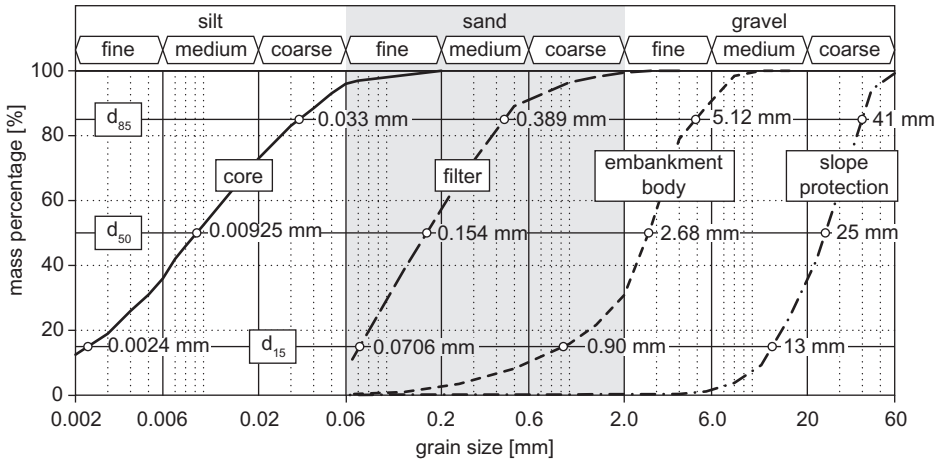


Figure 3. Grain size distribution for the four different fuse plug materials.

The major part of the fuse plug embankment is made of a highly erodible sandy gravel (3). The washout rate is primarily dominated by the sediment size and gradation of this material. Finally a slope protection consisting of coarse gravel (4) is provided on both the upstream and downstream slope to protect the fuse plug against wind, waves and rainfall.

Figure 3 shows the grain size distribution for all materials used in the Hagneck Channel fuse plug. The filter criteria (as given by the Swiss Standard on material for filters) are followed for the four material types to prevent internal erosion and sediment washout (SN 670 125a). The material will be placed and compacted at optimal water content to reduce shrinking, deformation and to achieve the required long term durability. These conditions were reproduced in the prototype model tests as well.

3 HYDRAULIC MODEL

Two different flumes were used for the model tests. The small scale experiments were conducted in the 0.20 m wide and 8 m long horizontal glass-sided VAW dike-breach channel, with a discharge capacity of 70 l/s. The existing flood levee was not modelled and the fuse plug was directly erected on the channel bottom, close to the channel end. This guaranteed complete erosion of the material and prevented backwater effects. The approach flow discharge was automatically regulated to obtain steady reservoir conditions after initial overtopping. Given the channel width of 0.20 m, the discharge overtopped the dike on its entire width resulting in a two-dimensional (2D) erosion. The advance of the streamwise erosion surface across the channel sidewall was therefore representative for the entire fuse plug width. Only minor side wall effects are present for this width (Schmocker and Hager 2009). Both the water surface and the sediment surface were recorded during each test, using a 30 Hz CCD camera with a resolution of 1034(H) × 778(V) pixels.

To analyze possible scale effects the fuse plug was tested for two scale factors of $\lambda = 2.5$ and $\lambda = 5$. As erosion due to overtopping is a free surface process dominated by gravity, Froude similitude was applied. The slope protection was geometrically scaled and the embankment body material was scaled according to Zarn (1992). In this approach, the natural grain size distribution is downscaled geometrically with the scaling factor in a first step. In a second step, the finer fractions of the grain size distribution with grain size related Reynolds numbers between 2 and 200 have to be adapted. The characteristic dip in the Shields diagram with varying dimensionless bed friction between 0.03 and 0.047 can be found in this domain. To compensate for the effect of the ‘Shields dip’ and to achieve the same transport rate in nature and in the scale model, the finer fractions of the model sediment have to be coarsened.

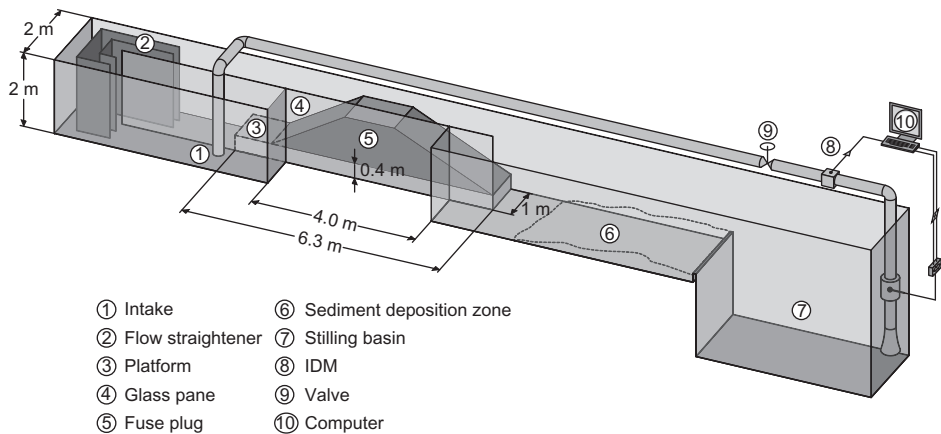


Figure 4. Schematic side view of the hydraulic model test setup for prototype experiments.

The filter and core material were not scaled, given the already very small diameters in prototype. To compensate the resulting overestimation of the core stability at small scale, the core width was reduced as $d_{\text{core, model}} = 1/\lambda^{3/2} \cdot d_{\text{core, prototype}}$, thus achieving equal section modulus as in the prototype.

The prototype tests were conducted in a 15 m long, 2 m high and 1 m wide channel with a discharge capacity of 300 l/s. The fuse plug was erected on a small platform, to prevent back-water effects (Fig. 4). The erosion process could be observed through the channel side wall or from above. Given the limited discharge of 300 l/s, it was not possible to obtain a constant reservoir water level during the breach test. In addition the channel was used for small scale 3D experiments, investigating the lateral breaching and erosion process.

4 RESULTS

4.1 2D erosion process—small scale

First of all, it should be noted that the following observations, made for the small scale experiments, are very similar to the prototype experiments. Figure 5 shows a typical temporal advance of the fuse plug breach for $\lambda = 5$. The inflow discharge results in a slow filling of the reservoir volume. As soon as the water level rises above the impermeable core, seepage through the downstream embankment body is initiated. The water level further increases until overtopping starts and the downstream slope protection becomes destabilised and starts to slide down the slope. This initiates the breach process for an overflow depth of 0.05 m ($t = 0$ s). The embankment body is then exposed due to erosion and sliding failure of the slope protection zone ($t = 8$ s). The highly erodible sediment is removed fast due to the increased overtopping discharge until the impermeable core partly collapses due the undercutting process and its own weight ($t = 34$ s). This process is repeated until the fuse plug is completely eroded after approximately $t = 105$ s. This corresponds to a prototype erosion time of about $t = 235$ s. However, compared to the prototype, the small scale model lacks additional slope protection like a thin grass layer or similar. The erosion will therefore be initiated for slightly higher overflow depths. Furthermore, the prototype erosion process is mainly depending on sediment properties and compaction methods that differ from the small scale experimental conditions.

4.2 3D erosion process—small scale

The fuse plug erosion typically starts at a preselected location. Overtopping of the entire fuse plug in the initial phase of breaching is not intended. The preferred method to initiate breaching is the provision of pilot channels with a lower elevation than the fuse plug. Overtopping

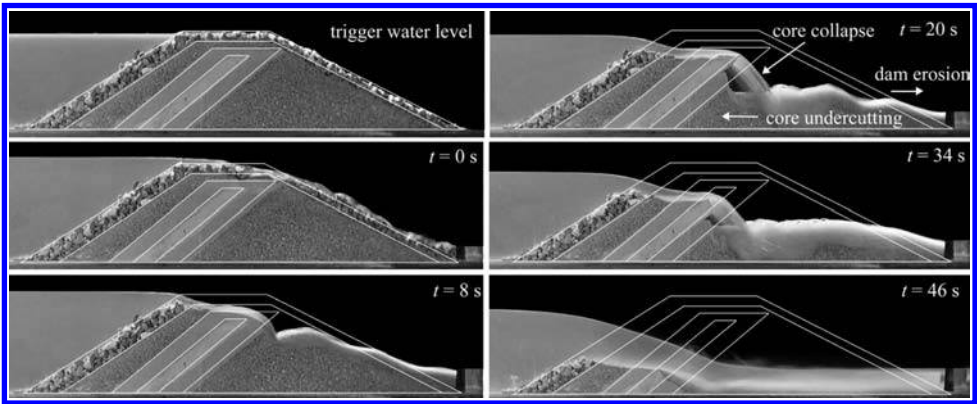


Figure 5. Advance of fuse plug erosion at different model times t for small scale experiment with $\lambda = 5$.

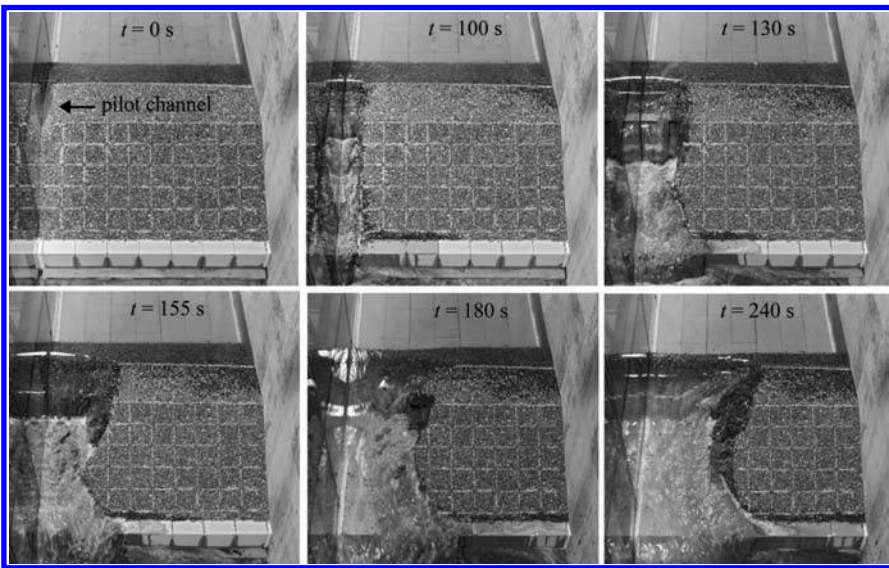


Figure 6. Advance of 3-dimensional fuse plug erosion at different model times t for small scale experiment with $\lambda = 5$.

of a pilot channel leads to a fast vertical erosion and the rest of the fuse plug will washout laterally without overtopping. The lateral erosion rate is therefore of high importance for the design as it determines the spillway capacity during the breaching process of the fuse plug.

To investigate the lateral erosion, the model fuse plug, with $\lambda = 5$, was built over 1 m length. A triangular pilot channel was cut in the embankment crest along the channel sidewall, to initiate the breach process, with the channel wall simulating the breach centreline. Figure 6 shows the temporal advance of lateral erosion. The breach process initiated at time $t = 0$ s with discharge entering the pilot channel. The breach then develops both in vertical and lateral directions with time. After $t = 100$ s, the downstream embankment body at the channel sidewall is completely eroded, and the core is fully exposed after $t = 130$ s. The core collapses after $t = 155$ s. The lateral erosion advances fast and additionally undercuts the core. Half of the fuse plug is almost completely eroded after $t = 240$ s. Assuming that the channel wall represents the breach centreline and the breach will develop in both directions, the lateral erosion in the prototype can therefore be roughly estimated to about 0.5 m/min. The impermeable core has only a minor impact on the lateral erosion process.

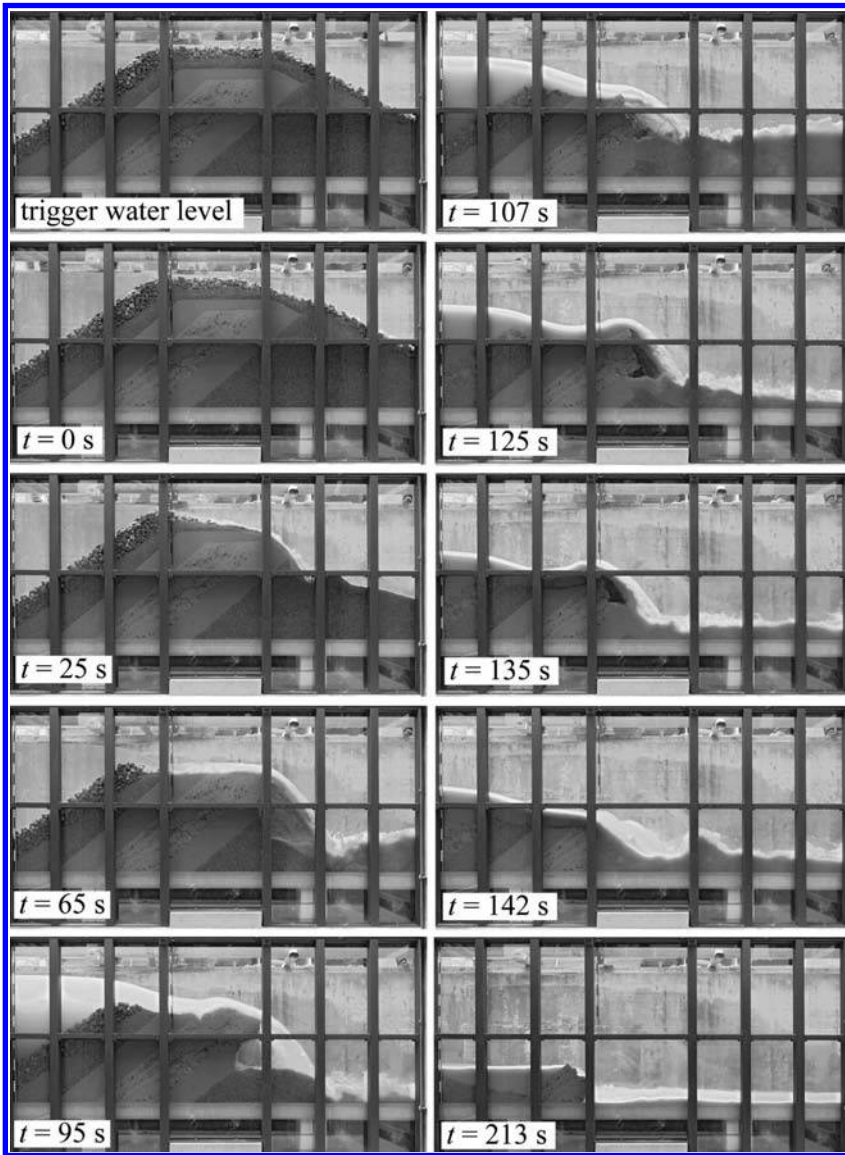


Figure 7. Advance of prototype fuse plug erosion at different times t .

4.3 2D erosion process—prototype

The prototype tests at full scale demonstrate the feasibility of the fuse plug design, because scale effects are minimized. The prototype material is built in taking into account correct water content and compaction factor. Figure 7 shows the advance of the breach. The erosion process observed, and especially the undercutting and collapse of the core, were similar to the small scale tests. The core will probably remain largely unsaturated on the downstream face, and will be mobilising suctions that both increase the internal effective stresses and hence the strength. This will explain the mode of failure as the core broke and collapsed in three major pieces. Due to the reservoir drawdown during the test, the erosion time was around $t = 15$ min. Furthermore, due to the limited inflow discharge, it was not possible to erode the fuse plug entirely. A small portion of 0.2 m height remained intact, as the core could not collapse any further and the erosion only advanced slowly (Fig. 7, $t = 213$ s).

5 CONCLUSIONS

Future extreme flood events along the Hagneck Channel shall be controlled by means of a side spillway using a fuse plug embankment. The fuse plug is placed on the existing flood levee and should erode fast and completely for a design water level slightly above the dam crest. The fuse plug design was investigated at VAW and the general feasibility could be demonstrated using both small scale and prototype model tests. The main fuse plug body consists of highly erodible material and is covered with a coarse slope protection. An inclined impermeable silt core prevents seepage and internal erosion for water levels below the trigger water level. The breach process is dominated by erosion of the highly erodible embankment body material followed by undercutting and collapse of the nominally impermeable core. The dam breaching can be initiated using a pilot channel with a lower elevation than the fuse plug crest. The erosion will proceed vertically at first, and the fuse plug will breach primarily due to lateral erosion.

Further open questions regarding the long term behaviour, especially with respect to developing vegetation or how to treat the connection between the fixed weir and the fuse plug, still remain. Other aspects for future research are alternative trigger mechanisms to strengthen the initial breach process, when the design water level is reached.

REFERENCES

- Chee, S.P. & Zaghoul, N.A. 1971. Erosion of fuse plug embankments. *Transactions of the Engineering Institute of Canada* 14(1), 1–4.
- Chinnarasri, C., Tingsanchali, T., Weesakul, S. & Wongwises, S. (2003). Flow patterns and damage of dike overtopping. *Intl. Journal Sediment Res.* 18(4), 301–309.
- Coleman, S.E., Andrews, D.P. & Webby, M.G. (2002). Overtopping breaching of noncohesive homogeneous embankments. *Journal Hydr. Engng.* 128(9), 829–838.
- Engels, E.T. & Sheerman-Chase, A. 1985. Design and operation of a fuse-plug spillway in Swaziland. *Water Power and Dam Construction* 37(6), 26–28.
- Gosschalk, E.M. 1988. *Reservoir Engineering: Guidelines for practice*. Thomas Telford Books, Reston, USA.
- Khatsuria, R.-M 2005. *Hydraulics of spillways and energy dissipators*. Dekker, New York, USA.
- Minor, H.-E. & Hager, W.H. 2004. *Flussbau in der Schweiz*. Stäubli Verlag, Zürich (in German).
- Pickert, G., Weitbrecht, V. & Bieberstein, A. (accepted for publication). Breaching of overtopped river embankments controlled by apparent cohesion. *Journal of Hydraulic Research*.
- Projet DIFUSE Volet A, B, C et D/ CTI 4898.1 2004. Dignes fusibles et submersibles pour la protection contre les crues. *Report*. Laboratoire de Constructions Hydrauliques – EPFL, Ecole d'ingénieurs et d'architectes de Fribourg, Ecole d'ingénieurs du Canton de Vaud, Ecole d'ingénieurs de Genève (in French).
- Pugh, C.A. 1985. Hydraulic model studies of a fuse plug embankment. REC-ERC-85-7, USBR, USA.
- Scheidig, A. 1934. *Der Löß und seine geotechnischen Eigenschaften*. Verlag Th. Steinkopf. Dresden (in German).
- Schmocker, L. & Hager, W.H. 2009. Modelling dike breaching due to overtopping. *Journal of Hydraulic Research* 47(5), 585–597.
- SN 670 125. Swiss standard. Mineral construction material, quality requirements: filter material, quality specifications.
- Tinney, E.R. & Hsu, H.Y. 1961. Mechanics of washout of an erodible fuse plug. *Journal of the Hydraulics Division ASCE* 87(3), 1–29.
- USBR 1985. Guidelines for using fuse plug embankments in auxiliary spillways. U.S. Department of the interior, Bureau of Reclamation, USA.
- Wahl, T.L. 1993. Hydraulic model study of horseshoe dam fuse plug auxiliary spillway. R-93-10, USBR, USA.
- Zarn, B. 1992. Lokale Gerinneaufweitung, eine Massnahme zur Sohlenstabilisierung der Emme bei Utzendorf. *Mitteilunge* 118, VAW, D. Vischer, ed., ETH Zurich (in German).

Inflow Design Flood and dam safety

P.A. Zielinski

Ontario Power Generation, Toronto, Ontario, Canada

ABSTRACT: The paper provides a brief history of establishing design flood criteria for dams in North America. The concept of the Probable Maximum Flood (PMF) in all cases where dam failure may result in fatalities or significant damage is present in classification systems almost everywhere in North America. Many countries on other continents followed the same pattern, but with few exceptions, countries in Europe have chosen a different approach and preferred the use of flood frequency analyses as a basis for design flood criteria. Selection of a specific design flood, irrespective of the general approach, historically rested with experts from the engineering community, and this has never been examined from the perspective of general, national safety policies, societal desires and preferences with respect to individual and group safety.

1 INTRODUCTION

The current dam safety assessment methodology of spillway capacity is based on design flood criteria (often called incorrectly ‘design standards’) associated with classification systems reflecting either hazard potential or consequences of dam failure. The spillway system is of critical importance in ensuring that the dam is safe and its safety can be compromised if the system is inadequate. Available information on dam failures indicates that overtopping resulting from spillway system inadequacy or unavailability accounts for over 40% (the number may differ slightly depending on the sources and the length of available record) of all failures. A simple fault tree illustrating overtopping failure mechanism is displayed in [Figure 1](#). It can be noted that “Inadequate freeboard” failure mode can be included in the failure mode “Inadequate available spillway capacity” but for the focus of this paper is on the failure mode “Inadequate installed spillway capacity”. The sizing of the flow discharge equipment is usually carried out through establishing the Inflow Design Flood (IDF) or Safety Check Flood (SCF). Which one of these two design values is used to determine the flow discharge capacity depends on the philosophy of the design and the safety assessment process.

The following section provides a brief history of establishing flood design criteria for dams in North America. Traditional approach to solving the dilemma of design criteria (it applies not only to floods but to earthquakes as well) has been to link its values to dam safety classification systems. Such systems based either on dam failure consequences or on the dam hazard potential, link different classes or categories of dams with the design values deemed to be appropriate. How the “appropriateness” has been determined is the subject of this paper.

At the foundation of the IDF selection almost everywhere in North America is the belief that Probable Maximum Flood (PMF) is the most appropriate design flood in all cases where dam failure may result in fatalities or significant damage. Australia and New Zealand followed the same pattern, but recognizing shortcomings and limitations of design standards, regulatory frameworks have promoted and implemented a risk-informed approach to decision making in all areas of dam safety. Many other countries around the world accepted the concept of the PMF and have been using it in their dam safety requirements for spillway capacity. With the exceptions of United Kingdom and Norway, countries in Europe have chosen a different approach and preferred the use of flood frequency analyses as the basis for design flood criteria.

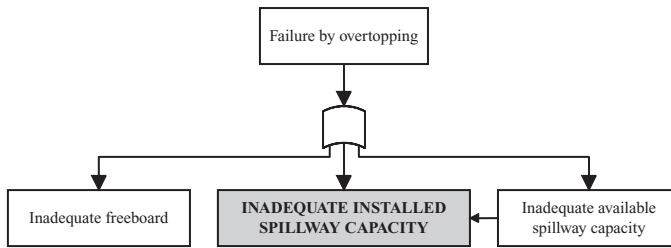


Figure 1. Overtopping failure mode.

Historically, the selection of a specific design flood, irrespective of the general approach, rested with experts from the engineering community, and this has never been examined from the perspective of general safety concepts, national safety policies and societal desires and preferences with respect to individual and group safety.

2 ORIGINS AND HISTORY OF PMF

Dam design has a long history and its beginnings were founded on a predominantly empirical basis. Traditional methods for selection of what we define today as the SCF or the IDF have always been prescriptive. As late as at the end of the 19th century a simple up-scaling of the highest flood on record by some arbitrarily selected factor greater than one was considered to be adequate. Development of rational spillway flood design criteria has remained largely unaddressed until in 1955 the ASCE Task Force on Spillway Design Floods (Banks, 1964) took the position that the spillway design practice influenced by a variety of complex political, ethical, economic and technical factors has been as a result guided by “experience and judgment rather by rigid technical procedure”.

In 1964 one of the members of the ASCE Task Force (Franklin Snyder) proposed a classification of dams with reference to spillway design floods and danger potential (Snyder, 1964). The proposal included two main categories where failure either could or could not be tolerated, and further subdivision of the first category into two sub-categories based on economic and policy considerations (Table 1). Snyder stated that selection of the Probable Maximum Flood as the SDF was “essential where complete protection against the possible failure of the dam is considered mandatory” and that “the mathematical probability of occurrence of a probable maximum flood on any particular drainage basin is very small, not evaluable and without significance in any event”. According to Snyder a complete protection against overtopping failure could have been achieved if the spillway were capable of safe passing of “the most severe flood considered reasonably possible of occurrence”, which is how the PMF has been defined. It is not entirely clear whether Snyder’s proposition was in the agreement with the general thinking of the broader dam engineering community at that time or it was just a new concept of defining safety goals for dams. However, it is important to recognize that Snyder’s proposal has constituted, with some minor differences, the informal basis for deriving technical guidelines for selection of the SDF or IDF.

In 1972 the US National Dam Inspection Act was enacted and the US Army Corps of Engineers (USACE) was given the responsibility for implementation of the Act. The exact mandate of USACE was to “carry out a national program of inspection of dams for the purpose of protecting human life and property”. In Phase 1 of the program USACE had as the main objective the quick identification of these dams that could have posed hazards to human life or property (USACE, 1975). For that purpose, USACE developed a classification system (USACE, 1979) based on the dam size and its hazard potential (Tables 2 to 4). It is quite clear that the approach followed very closely Snyder’s proposal from 1964.

In view of the developments that followed USACE classification it has to be stated very clearly that the original mandate was to develop means to prioritize/screen the US portfolio of dams in order to identify these structure that required more attention than others. USACE’s undertaking was not supposed to provide the framework for assessing and judging safety of individual dams.

Table 1. ASCE Classification of dams and Inflow Design Flood.

Category	Impoundment danger potential		Failure damage potential		Inflow Design Flood
	Storage acre-feet	Height feet	Loss of life	Damage	
Major (failure cannot be tolerated)	>50,000	>60	Considerable	Excessive or as matter of policy	Probable maximum; most severe flood considered reasonably possible
Intermediate	1,000 to 50,000	40 to 100	Possible but small	Within financial capability of owner	Standard project; based on most severe storm or meteorological conditions considered reasonably characteristic of specific region
Minor	<1,000	<50	None	Same magnitude as cost of dam	Frequency basis; 50–100 year recurrence interval

Table 2. USACE Spillway design criteria (USACE, 1979).

Hazard classification	Dam size		
	Large	Intermediate	Small
High Significant	PMF PMF	PMF 1/2 PMF to PMF	1/2 PMF to PMF 100-year flood to 1/2 PMF
Low	1/2 PMF to PMF	100-year flood to 1/2 PMF	50- to 100-year flood

Although the guidelines received input and support from other US Federal and State agencies, professional engineering organizations and consulting companies, USACE was well aware of its inadequacy for making decisions with respect to safety individual dams and explicitly stated that:

“Conditions found during the investigation which do not meet guideline recommendations should be assessed by the investigator as to their import from the standpoint of the involved degree of risk. Many deviations will not compromise project safety and the investigator is expected to identify them in this manner if that is the case. Other will involve various degrees of risk, the proper evaluation of which will afford a basis for priority of subsequent attention and possible remedial action”.

It is unfortunate that this very clear and accurate statement has been entirely disregarded. Following the issuance of the guidelines, many US agencies adopted the requirements in the USACE classification as design safety criteria. This action had a profound influence on development of dam safety guidelines and design criteria both in the United States and elsewhere.

It should be also noted that the adoption of USACE guidelines well beyond their original mandate went also against recommendations of American Society of Civil Engineers report (ASCE, 1973) of the Task Committee on the Reevaluation of the Adequacy of Spillways of Existing Dams of the Committee on Hydrometeorology of the Hydraulics Division. Among the most important findings and recommendations the Committee included in the report were the following observations:

- There is a tendency within the engineering community to avoid difficult decisions by applying blanket standards in situations where the dam failure may result in loss of life. Use of the PMF as the only available standards, without appropriate discrimination between the cases when a single or few lives are lost as opposed to many fatalities, is inappropriate.
- Pre-planned measures such as flood proofing, emergency planning and evacuation should not be disregarded in assessment of safety when loss of life is being considered.

Table 3. USACE Size classification (USACE, 1979).

Dam size	Storage acre-feet	Height feet
Small	Between 50 and 1,000	Between 25 and 40
Intermediate	Between 1,000 and 50,000	Between 40 and 100
Large	>50,000	>100

Table 4. USACE Hazard potential classification (USACE, 1979).

Hazard classification	Loss of life	Economic loss
Low	None expected (no permanent structures for human habitation)	Minimal (undeveloped to occasional structures or agricultural)
Significant	Few (no urban development and no more than a small number of inhabitable structures)	Appreciable (notable agriculture, industry or structures)
High	More than a few	Excessive (extensive community, industry or agriculture)

- Engineering profession should actively promote the use of financial evaluation of loss of life as a necessary tool for appropriate and economic design of spillways.
- On the issue of life safety, instead of hiding behind a subjective standard, any decision should be fully transparent and should provide complete disclosure of costs necessary to reduce the risk of life loss.

It seems that the visionary report of the ASCE Task Committee was too revolutionary for the dam engineering community at the time and the recommendations of the Committee were rejected. As a result, for the next 2 decades, hazard potential philosophy and use of physical limits of natural hazards as design standards were very firmly entrenched in the North American approach to safety assessment of dams.

3 EUROPEAN APPROACH TO DESIGN FLOODS

Most of the European countries that have formal dam safety assessment programs which specify design floods use results of flood frequency analyses for that purpose. [Table 5](#) illustrates how the IDF or SCF are defined in various countries in Europe.

Out of eleven countries listed in the table only two adopted the PMF as a design requirement and in addition one of these two (UK) allows in certain cases to reduce this requirement to a 10,000-year flood. None of the other countries uses the design requirement more stringent than the 10,000-year flood while some of the countries impose the requirements as low as 1,000-year flood. One may argue that a 10,000-year flood does not necessarily have to be lower than the PMF but theoretically any flood with a given return period has to be lower than the limiting event that is the PMF. Since in applications one uses operationalized value of the PMF it may indeed be lower than the true limiting value (it may also be higher) but the practical experience indicates that the 10,000-year flood is generally equivalent to about ½ of the PMF (Zhou et al., 2009).

What is important to observe when comparing spillway discharge requirements in Europe and in North America is that North American dam safety practices aim at physical limits of floods as opposed to European practice which stays away from limiting events and uses very rare floods instead.

4 THE PRINCIPLE OF ABSOLUTE PROTECTION AND PMF

Although the reasons for using the PMF as a design flood for dams with potentially serious consequences of failure have never been properly discussed at the time when the concept was born, it seems that such discussion is worthwhile since it may help in understanding how

Table 5. Dam safety requirements for discharge capacity in some European countries.

Country	Category	Category description	Required spillway capacity
Austria	Dams higher than 15 m or reservoirs larger than 500,000 m ³	One additional outlet work may be taken into account, some overtopping of concrete dams allowed depending on the specific circumstances No damages allowed, only spillway (without any outlet works) taken into account, no overtopping (including wave action)	5,000-year flood about 1.3 to 1.5 times 5,000-year flood
Finland	Risk class P	Demonstrated endangerment of life/health and/or environment	5,000 to 10,000-year flood
Germany	Large dams	The effect of retention of the storage may be considered and discharge through (n – 1) bottom outlets too. Damage to the dam is not permissible during the discharge of the design flood All outlets of the dam are available. In case of emergency valves of outlets can be opened by means of force (including blasting). Damage to some parts of the dam is allowed if it does not influence the stability of the dam	1,000-year flood 10,000-year flood
Italy	Large dams	H > 15 m, V > 1,000,000 m ³	1,000-year flood
Norway	High—3	More than 20 houses affected	PMF
Spain	High consequences—A		10,000-year flood
Sweden	High hazard	Significant risk of human loss of life or injury. Considerable risk of extensive damage on infrastructure, or on nature. Evident risk of considerable economic loss	Swedish Design Flood
Switzerland	N/A	Flood can be passed safely with the largest capacity outlet unavailable Reservoir level should not rise above the so-called danger level. In the case of concrete dams this level is usually higher than the crest (controlled dam overtopping), but for embankment dams it corresponds at the most to the crest level or is even lower	1,000-year flood 1.5 × 1000-year flood
Portugal	High potential hazard	h ≥ 50 m (embankment dams) h ≥ 100 m (concrete dams)	5,000 to 10,000-year flood
UK	Category A	Breach could endanger lives in a community (general) Breach could endanger lives in a community (if overtopping tolerable)	PMF 10,000-year flood

the alternatives should be constructed. Closer examination of Snyder's statement justifying the selection of the PMF as a design standard for spillways reveals the unstated principle which has been underlying the philosophy of dam safety in North America for the past several decades. This principle, followed by many jurisdictions around the world, can be defined as the principle of absolute protection. The intention of it was to design or retrofit the spillway system to such a standard that it would be capable of safe passage of any flood that can occur at the dam site. If the dam had discharge capacity equal to the highest physically possible flooding event then it would be capable of handling the flood which in the limit had zero probability of occurrence and therefore such dam could be deemed as risk-free from overtopping.

At the foundation of the no-risk concept is the belief that the public should be exposed to no additional or unnecessary risk and even if the risk appears to be small no exposure should be tolerated. The no-risk concept has great appeal as rhetoric since it is difficult to argue that people do not necessarily have to have absolute protection and it is also convenient since it requires less effort in collecting information and carrying out analyses. The major deficiencies of the no-risk approach are possible misallocation of society's resources and unavoidable inconsistencies in overall government risk policies. However the public exposed to industrial risks is increasingly realizing that conveniences and benefits from technological progress can introduce new hazards threatening not only property and environment but also lives. The risks resulting from these hazards can usually be reduced but the reduction of risk almost always entails some reduction of benefits by incurring additional costs. This poses a serious dilemma for society as a whole and for decision makers in particular. The dilemma can be best illustrated by the following question: Is the proposed or existing technology acceptably safe? (Or alternatively, how safe is safe enough?) To answer these questions in a coherent manner, some kind of weighing of risks and benefits would have to be performed but the no-risk framework does not allow for that. The position of risk-free policy proponents effectively negates the presence of the cost trade-offs involved and thus, what the no-risk policy in fact means is that the risk has to be eliminated entirely and the costs of risk elimination action are irrelevant.

The principle of absolute protection as postulated by Snyder was embraced by the dam safety professional community without any major disagreements. However as early as in the beginning of the 70's and before the USACE guidelines were developed and implemented it was pointed out that there were basic fallacies and inconsistencies in both the concepts and practices of applying limiting events as the basis for safety requirements (Benson, 1973). In his paper Benson pointed out that:

- The widely used argument used to support the concept ("human risk is intolerable") was equivalent to putting an infinite value on human life and that has always been contrary to what was indicated by expenditures for safety in all areas of hazardous industrial activities.
- Original, logically consistent concept of 'maximum possible flood' (it presupposes the simultaneous occurrence in one area of every possible natural factor in such a manner as to create the theoretically maximum possible flood) has been for pragmatic reasons replaced by the 'probable maximum flood' (the most severe flood considered reasonably possible of occurrence) which had virtually no meaning being neither scientific nor engineering statement.
- The only reason that the method has been used and accepted was not because of its merits but because it provided a solution that removed responsibility for making important decisions as to the degree of risk or protection. It implied absolute protection when in reality the actual degree of residual risk remained unknown.

The notion of 'putting infinite value of human life' in dam safety decision making has been a crucial one because the engineering community has always been extremely reluctant to pursue the estimates of a monetary value that society would be willing to spend in order to prevent fatalities from human-created hazardous installations. Such decisions are being made routinely across different hazardous industries and regulatory agencies. There is an advantage in making implicit figures explicit because it is a necessary first step to achieve consistency across the full spectrum of decisions affecting public health and safety.

Although the critique by Benson has remained almost entirely ignored by the engineering community, it should be recognized that it was the first one which identified important ethical and moral issues with the foundation of the decision making framework based on arbitrarily imposed design criteria. Benson warned that the serious ethical dilemma it created was caused by the implied message that the design can be virtually free of risk. In support for Benson's position (Fahlbusch, 1979) stated that such approach misleads the public in that it implies absolute safety when in reality this goal cannot be guaranteed due to the present limitations of our knowledge of natural processes causing flood formation.

Dubler (1996) pointed out another problem with the PMF-based design criteria indicating that since the use of the PMF creates an illusion of absolute safety it diverts attention from less extreme but more likely events that could also lead to overtopping. Salmon and Hartford

(1995) warned that the obsession with “safe design” for selected design floods often results in neglect for other flood-related. Their point is clearly illustrated by the simple fault tree introduced before (Fig. 1) which demonstrates that inadequacy of spillway capacity is only one of several possible failure modes.

5 THE RIGHT TO IMPOSE SAFETY GOALS

History of dam building spans thousands of years and until recently the entire dam design, build and operation process was exclusively in the domain of dam engineering. It originated in the tradition of the engineering profession and re-confirmed the long-standing position of engineers that technical experts not only know how to design safe structures but are also in the best position to decide on behalf of society what the appropriate safety goals should be. For the lack of a better term it can be called the principle of the right to impose the safety goals.

In the 1960's and 1970's when the concept of the PMF as the design standard was first introduced there were no clearly articulated societal expectations with respect to acceptable political decisions affecting health, safety and well-being of individual citizens and the society as a whole. The processes of arriving at the decisions on acceptable safety levels were not consistent with the requirements of modern democracies. Such consistency would require that public preferences were considered in the context of informed consent where conflicting interests were identified and debated. Since the public at that time was not capable of informing itself and of meaningful participation in the decision making process, its rights were assumed by the legislators and dam safety regulators. However the complexity of technical issues related to safety of dams and high levels of uncertainty involved were of such magnitude that the policy makers transferred their responsibilities into the hands of technical experts.

The public of the 21st century wants to be involved in decisions affecting their everyday lives and demands transparency in making these decisions. The traditional position of the engineering profession that it has all necessary information and knowledge to decide on matters of public safety goes contrary to these expectations and does not serve well the engineering community in establishing the necessary trust. These profound changes in public awareness increasingly require that transparent decision-making processes be considered as necessary conditions for the working of a representative democracy. The public demands access to information and participation in the decision processes in order to be able to make informed choices. Transparency understood as such requires a different approach to the decision-making process from the authorities, technical experts and scientific advisors. The old argument that ‘the experts know’ what they are doing and are better equipped than anybody else to arrive at the best decisions is now being questioned and often is not acceptable anymore.

In view of these considerations, it is not difficult to conclude that the current dam safety practice (at least on the subject of design criteria selection) is far from meeting transparency criteria. It presumes that the technical expertise whose judgment is invaluable in analyzing and assessing technical problems can also be extended to political and social arenas. This assertion logically leads to the next step, which claims that technical experts can single-handedly determine what is right for the society and what safety goals are appropriate (the principle of the right to impose safety goals). Such an approach is in disagreement with the growing demand on technical and professional communities to consult with the public and all parties who can be directly and indirectly affected by the decision. This fact is increasingly being acknowledged and new processes recognizing explicitly that risk and uncertainty are key aspects of any engineering activities are being developed. If implemented, risk analysis and assessment not only contributes to a better and safer design but also offers valuable information on likelihoods and consequences of hazards. This in turn leads to better informed politicians, stakeholders and decision makers and to increased capability to arrive at sound and responsible policy choices, priorities and decisions.

Implementation of risk analysis in the area of dam safety assessment is not a simple task. Inadequacy in flow discharge capacity is only one failure mode within a set of potential failure modes. Risk analysis brings significant analytic complications that were not present in the traditional dam safety assessments. One of these complications arises from the fact that the

characterization of risk requires estimation of probabilities. In terms of the failure mode discussed in this paper it requires probabilistic characterization of inflows. It seems that the path chosen by the majority of European countries to characterize these type of loadings with the help of flood frequency analysis is better suited to meet the requirements of risk analysis.

6 CONCLUSIONS

The original flaw in Snyder's reasoning came with the preconception that dam engineers who have a specialized knowledge about dam safety should have the right to unilaterally impose safety goals for dams. The current views on the subject of safety of hazardous installations are very different from popular concepts applied in the 1960s. Development of risk assessment and risk management methodology aimed at providing support to rational decision making in conditions of uncertainty was very helpful in systematic delineation of boundaries of authority between engineers, analysts, the public and the decision makers. The solution for hazardous installations which are capable of providing generally acceptable safety levels have to consider all relevant factors and that includes not only technical but also social, administrative, political, legal and economic ones. The risk informed approach, with all its imperfections caused by knowledge and data limitations, is capable of providing insight into the interaction of all these factors, and thus provides a venue to different segments of the society to reach decisions.

Is the PMF too conservative for a spillway design flood? The answer depends on the circumstances; it may be too conservative in some cases but it may as well be not conservative enough in other cases, since what is being presented as the 'flood upper limit' may be underestimated. The important fact is that the use of PMF as a spillway design flood is simply not meeting today's criteria of professional integrity and transparency in decision making. The way the PMF is often being portrayed might be considered misleading to the unsuspecting public and other stakeholders of dam safety. The unknown size of the gap between what the PMF claims to be and what in fact it is makes it unsuitable as a safety target for dam safety. The only indisputable fact is that the PMF methodology can deliver a large number but still there is no a scientific, political or socioeconomic justification to use it as a safety target and to claim that this target is technically sound, credible and appropriate.

REFERENCES

- ASCE (American Society of Civil Engineers). 1973. Reevaluating spillway adequacy of existing dams. *Journal of Hydraulic Division* 99(2): 337–372.
- Banks, H.O. 1964. Hydrology of spillway design: introduction. *Journal of Hydraulic Division* 90(3): 235–237.
- Benson, M.A. 1973. Thoughts on the design of design floods. *Proc. 2nd int. symp. in hydrology*. Fort Collins, CO: Water Resources Publications.
- Dubler, J.R. 1996. Dam safety policy for spillway design floods. *Journal of Professional Issues in Engineering Education and Practice* 122(4): 163–169.
- Fahlbusch, F.E. 1979. Optimum design flood for spillways. *International Water Power & Dam Construction*. November: 79–84.
- Salmon, G.M. & Hartford, D.N.D. 1995. Risk analysis for dam safety. *International Water Power & Dam Construction* 7(3): 42–47.
- Snyder, F.F. 1964. Hydrology of spillway design: large structures—adequate data. *Journal of Hydraulic Division* 90(3): 239–259.
- USACE (United States Army Corps of Engineers). 1975. National program of inspection of dams—Volume 1. Vicksburg, MS.
- USACE (United States Army Corps of Engineers). 1979. Recommended guidelines for safety inspection of dams. Engineering Regulation ER 1110-2-106. Vicksburg, MS.
- Zhou, R.D., et al. 2008. On the relationship between 10,000 year flood and the Probable Maximum Flood. *Proc. Hydrovision 2008 conf...* Sacramento, CA.
- Zielinski, P.A. 2009. Safety of dams, Probable Maximum Flood and the selection of inflow design floods. *Proc. CDA 2009 Annual Conference*. Whistler, British Columbia.

Combinations of earthquake and flood hazards together with other factors

D.N.D. Hartford

BC Hydro, Burnaby, British Columbia, Canada

ABSTRACT: The paper makes a case for a “refined” philosophy of dam safety for ICOLD based on a risk-informed functions and services philosophy for engineering design, performance, and safety assessment of “dam-reservoir-downstream systems”. The paper goes beyond the contemporary practical application of this philosophy which generally focuses on the sustainability of the dam and does so under the assumption that by focusing on withstanding (albeit in a damaged state) the extremes of natural hazards, and particularly earthquakes and floods. Under these conditions, the safety and therefore the sustainability of the dam are considered to be assured. This paper challenges this practical interpretation of the implementation of the contemporary philosophy and explains why the focus on the extremes of natural hazards is non-conservative from the perspective of risk to; the dam, the reservoir and their functions, as well as the public, the environment, the infrastructure and the social fabric at risk from dam failure.

1 INTRODUCTION

In terms of the ICOLD philosophy (Bulletin 61), the objective of design is to create a “structural form together with the foundation and environment that will, most economically: a) perform satisfactorily its function without appreciable deterioration during the conditions expected normally to occur in the life of the structure and, b) will not fail catastrophically during the most unlikely but possible conditions which may be imposed”. The philosophy implies consideration of the many factors, including human factors, managerial controls and operational considerations that should be considered in dam design. Despite this, the majority of the literature, conferences, technical committees and industry discussions on design and performance criteria for dams focus on natural hazards individually; earthquakes, floods, reservoir landslides, etc. Further, the majority of the focus on performance of dams pertains to the performance of individual elements of the dam, such as spillways, foundations, embankments, etc. Thus, while the ICOLD philosophy is clearly focused on ensuring the “sustainability” of dams, it is less clear that the philosophy is also focused on the “sustainability of the functions” of the dam-reservoir system.

2 ESTABLISHED PRACTICE

Established practice, the fundamentals of which have been utilised since ancient times has proved to be a sound basis for establishing a design basis and management framework for dams that has served the industry and society well over the ages. The general principles are to ensure that the dam can withstand the physical loads normally expected to occur over the operating life of the dam and to be able to accommodate the effects of large abnormal floods (in comparison to what might be normally expected) which may possibly occur during this period. Since the early 1920’s basic consideration of the effects earthquakes on dams has been available, although it was largely applied in terms of a “nominal capacity”. Towards the

end of the 20th century, the effects of large earthquakes have received greater consideration. Guidance as to the application of the philosophy described in Bulletin 61 in practice is provided in ICOLD Bulletin 59 in terms of general considerations rather than guidance as to the nature and form of physical controls.

Fundamentally, the philosophy has been that the dam should have the capacity to pass large floods and withstand the effects of large earthquakes. In this context, the passage of floods fundamentally requires an adequately large spillway and withstanding the effects of large earthquakes entails possibly sustaining damage, but having adequate residual strength not to collapse catastrophically and release the contents of the reservoir. These fundamental considerations are obviously eminently sensible and this paper does not in any way intend to suggest either de-emphasising their value or replacing them with any alternative; rather the purpose is to embody these fundamental principles in a broader more comprehensive framework that captures the modern complexity of “demands on dams” which includes demands from natural loads, combinations of natural loads; operational loads and combinations of natural and operational loads; demands and loads due to mis-operation of various systems such as discharge and production systems; and demands on the dam and its appurtenant structures to cope with emergent upstream and downstream conditions.

3 MOTIVES FOR BROADER CONSIDERATIONS APPROPRIATE FOR THE DAMS IN THE MODERN CONTEXT

The functional and operational demands on dams in the modern context are far more varied and complex than the demands of physical loads under “normal static operating conditions” and the effects of large abnormal floods and earthquakes. There is considerable variation and complexity over the operating life of the dam that arises from many sources including management and procedural sources, and societal expectations with respect to minimising downstream damages resulting from releases from dams. The old philosophy that “the dam will be safe if it can pass the inflow design flood and withstand the design earthquake without collapsing catastrophically” is too narrow in the modern context. Rather in the modern context, the performance objective of the dam is better described in terms of “the capacity to retain the stored volume and to pass flows through (e.g. seepage) and around (through production facilities, outlets and spillways) in a controlled manner” (Fig. 1).

The notion of transforming the practical implementation of the existing philosophy from “prevention of the dam from failing during an extreme natural event”, to one where dam safety embodies the concepts of “retaining the stored volume and passing all flows through and around

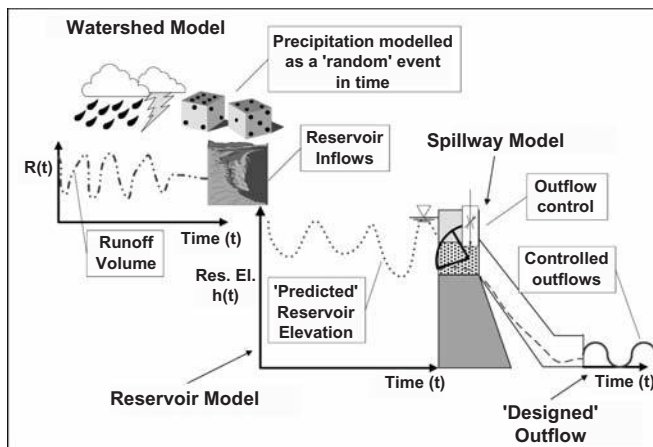


Figure 1. Functional model of watershed, reservoir and dam system (ICOLD, B130).

the dam in a controlled manner over the whole life of the system” is central to the expanded philosophy proposed here. The practical implementation of this expanded philosophy is through the process of “systems engineering” which finds widespread application in other industries and endeavours where complexity and competing multi-purpose demands are normal features of the system, its functions and the services that it provides. In providing for such an integrated approach across multiple objectives, this expanded philosophy and its practical implementation preserve the established notion of the sustainability of dams while providing a transparent means of securing stakeholder inputs, determining expectations, and providing sustainable functions and services that can be explained and justified. This is set within the broader societal context within which dams are now expected to function and provide useful services for humanity.

Importantly, in terms of the traditional practice philosophy, it was considered that extreme floods and earthquakes should not be considered in combination (that is extreme floods occurring at the same time as extreme earthquakes) because the possibility of joint occurrence of these two random events in space and time could be considered to be so remote as to be effectively negligible. However, this philosophy while mathematically correct has a very serious flaw, because regardless of how low the joint frequency of occurrence of extreme floods and earthquakes together might be, the possibility that a large earthquake might be followed in the same year by a moderate or even very large flood (not necessarily the extreme) is a great deal higher. Thus, while the frequency of the joint occurrence of floods and earthquakes in time might be very low, with a correspondingly very high joint probability of non-occurrence, the probability of occurrence of a damaging earthquake followed by a substantial inflow requiring spillway operation is significantly higher.

Rather than focusing on joint occurrence of two random infrequent events, it is necessary to consider how the combination of damaging earthquakes preceded or followed by the occurrence of inflows ranging from the annual inflow to much larger flows can be safely controlled within the dam-reservoir-production and discharge system. In addition to performance demands from natural phenomena, operational factors including unplanned operational disturbances can create demands on the dam system to retain an elevated volume and/or to pass flows unrelated to any natural flow demand. These demands need to be included in the suite of total functional demands on the system. Further, emergent conditions downstream may also impose demands on the dam and reservoir such as surcharging the reservoir to permit evacuation to occur or, in coastal regions to accommodate the effects of high tides. Environmental considerations such as short-term (a week or two) fish-migration considerations might also create demands for storage or release on the dam/reservoir system.

With reference to [Figure 1](#), the modern expectation is that the outflows from a dam should be within previously agreed limits with agreed ramping (up or down) rates. In other words, in the modern context there are much greater demands for “outflow from dams to be controlled” than was previously the case. Similarly, there are also increasing demands for reservoir levels to be controlled within certain limits of elevation with fluctuations in reservoir level also occurring in terms of pre-defined targets. At a fundamental level the observable measures of hydraulic control are the depth (a scalar parameter) and velocity (a vector parameter); where the depth refers to the elevation of the water (in the reservoir or downstream of the dam) and velocity refers to the speed of movement in any spatial direction; up and or down in the reservoir, and up, down, forward, left or right in the downstream river channel. Together, depth and velocity provide a measure of the disturbing force of the moving water, which in turn can be related to the degree of control over the hazard (the water and its intrinsic energy).

Obviously there are physical limits to the extent to which the owner (operator) of a dam/reservoir/hydro-production system can control the upstream and down-stream water levels and their fluctuations. However, the operating environment now is different to that which prevailed when dams were constructed for a single purpose such as hydroelectric generation, water supply or irrigation, or some combination of the these functions.

Dams that were or are required to pass the so-called “probable maximum flood” and “maximum credible earthquake” for whatever reason (e.g. regulatory requirement or national precedent) fall under the philosophy of “prevention of dam failure”, at least in principle. However, in practice, a spillway crest capable of passing very large floods is not in itself

sufficient to ensure that the overtopping failure mode cannot occur; especially if the spillway is of the gated variety or if the spillway is susceptible to blockage by debris, or both. Thus, prevention of failure by flow induced failure modes demands rather more in the way of control than can be provided by simply constructing a sufficiently large spillway crest.

Similarly, a dam with a capacity to retain the stored volume despite the damaging effects of large earthquakes, albeit sustaining some degree of damage while possibly successful in the immediate term may not be successful in the near or intermediate term as the damaged dam may not have the capacity to withstand increased hydraulic demands associated with the flow that occur when the system is in the post-earthquake damaged state (seismically damaged dams can require several years before complete repair and functional restoration can be accomplished). Importantly, spillway function is arguably one of the most important functions of a dam system that should be secure and functional post earthquake. In this respect, spillway function, which is what can traditionally be considered to be the “safety valve for floods”, is also a key “safety valve” post earthquake, albeit in this case to relieve the hydraulic pressure from behind the damaged dam. There are other instances such as production disturbances or unplanned outflows from upstream dams or high reservoir levels due to reservoir landslides when the spillway function is also the critical safety function.

Against this background, there are clearly interdependencies between the different parts of the dam-reservoir-production-discharge systems; interdependencies that need to be accommodated in the operation and safety management of the dam and reservoir. In addition, there are interdependencies between the downstream demands, the operational/production demands and the reservoir and upstream demands that must also be accommodated. Thus, the matter is rather broader than simply extending the established philosophy of not combining floods and earthquakes to one of considering “combinations of floods and earthquakes”. Rather, it is necessary to consider the full suite of “demands for hydraulic functionality” where “hydraulic functionality” involves both “controlled retention of the stored volume” and “controlled passage of all flows through and around the dam”. The interdependencies between these “control functions” are not simply linear cause-effect relationships; rather in general they are non-linear relationships, with the degree of non-linearity depending on the complexity, configuration and functions of the “system”.

4 DAMS AND RESERVOIRS AS SYSTEMS

The term “system” is often a convenient term to describe dams and reservoirs and their associated production facilities. While in its simplest form a “system” can be considered as simply a “collection of parts”, more commonly there is typically some form of orderly association between the parts according to some scheme established in a way that forms a complex unity that achieves one or more functions. The collection of parts, by themselves are not sufficient to achieve one or more functions, rather the way that they are designed; configured relative to each other; and made to function in harmony with each other are collectively what gives the system its “properties” and its “functionalities”. These properties and functionalities are not self sustaining; they must be constantly “maintained” through application of appropriate procedures which are of three general forms; operations; maintenance; and monitoring. “General Systems Theory” as first formalised by von Bertalanffy in 1928 (von Bertalanffy, 1968) provides a means of addressing this problem.

In general, the system will comprise a great deal more than the dam, reservoir, production facility, and spillway (Fig. 2). The actual definition of the “system” is generally controlled by the purpose for which the representation is intended to serve. Where relevant, the definition of the system can and should include a series of dams in “cascade” on the one river basin. “System” refers to a group of interacting, interrelated, and interdependent elements that form the complex whole. In the context of performance, system function is defined in terms of performance parameters or “functional requirements”. In the context of safety analysis, system failure means the cessation of proper functioning or performance, or non-performance of what is required or expected of the system as a whole to function safely. Individual parts

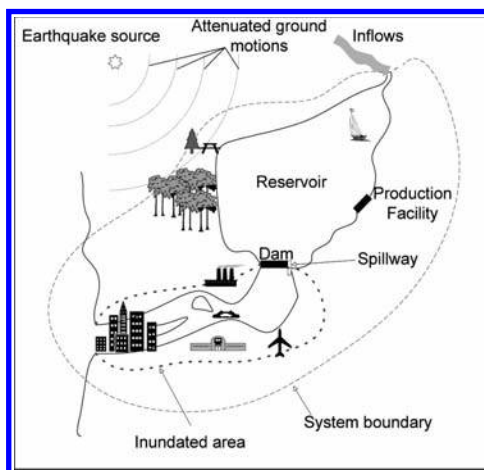


Figure 2. Schematic of a dam-reservoir system (after ICOLD, B 130).

of the system (e.g. the dam) can also be represented as systems, and even subdivided into sub-systems (e.g. earth dam or concrete gravity spillway alone). Further sub-division all the way down to basic components (e.g. earth core, rip-rap protection) is also possible and is sometimes necessary. Since the function of a dam structure is to retain water (with some allowable seepage), the functional failure of a dam occurs when, for example, the system ceases to adequately retain water (which can include severe leakage).

5 DAMS AND RESERVOIRS AS “HYDRAULIC CONTROL SYSTEMS”

The term “control” features prominently in all of the above, in a way that is not typical in established dam safety philosophy, which as mentioned previously typically focuses on preserving the ability of the dam to retain the stored volume and dispose of any excess inflow through the spillway. For some reason, and while the necessity for spillway gates to be functional is explicitly considered, established dam safety guidelines and practices typically do not explicitly refer to the “reliability or availability” of the spillway to perform its function and particularly the reliability with which gated spillways are required to function; specifically to remain closed when required to be closed and to open as required when called into service to discharge flows. Typically, it is assumed that provided the gates are operational when inspected and tested that the spillway sub-system will be fully functional when called into service. In addition, the hydraulics of the spillway and the interaction of spillway flows with other flows or parts of the dam or spillway may require operational controls with respect to gate opening and closure.

In the following, the terms “open system” and “closed system” are used in the sense of “control systems” and not in the strict interpretation of the terms as used in thermodynamics. Figure 3 illustrates in system analysis block diagram in terms an “open system”, a “dam-reservoir-production-spillway” system modelled as an “open system” and the domain of established dam safety practice modelled as an “open system” with the emphasis being on the “inflow”; the “integrity of the water barrier (dam)”; and the “spill capability” to maintain the reservoir elevation within pre-defined limits.

Dams and reservoirs with free overflow spillways where the production discharges are insignificant in comparison to the stored volume and/or the inflows can be modelled as represented in Figure 3. Such an “open system” with a free overflow spillway is generally considered to be “operationally very safe”. However, although the functional representation is simple and generally valid, the occurrence of an earthquake which damages but does not fail either the water retaining barrier of the spillway, but causes damage to one or both structures exposes one fundamental weakness of the system; specifically the capacity to control the “hydraulic hazard”

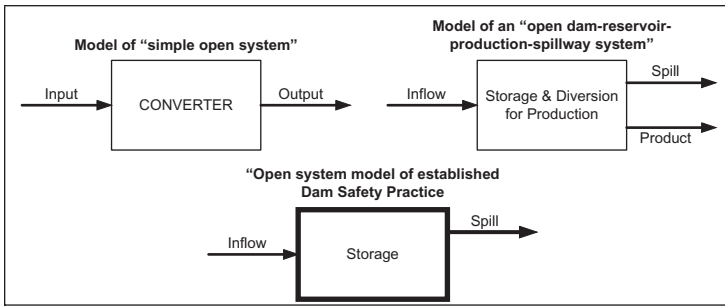


Figure 3. “Open system” representation of dam safety (adapted from Ryder and Bennett, 1990).

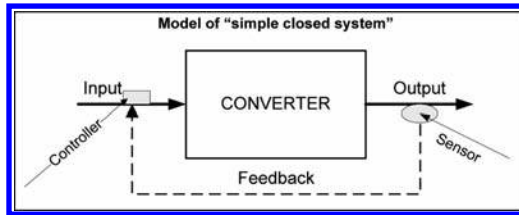


Figure 4. “Closed system” representation.

which is the stored volume and any inflow that might arise post earthquake and pre any repairs. A second fundamental weakness in the system function would be the occurrence of significant cavitation damage due to a prior discharge event. In fact, the entire system while elegant in its functional simplicity when functioning properly is rendered hazardous in an uncontrolled way as a result of earthquake or cavitation damage. Thus, the safety of the “operationally very safe system” if functionally deficient is transformed to a “very unsafe” system, with no obvious means of lessening the hazard (degree of danger) pending repairs. While there are many dams where the above model applies, discharge release control facilities provide greater control over the inflows and stored volume; although the degree of control is limited by a number of physical factors such as reservoir volume, size of production discharge facilities, level of top of spillway sill, etc. In simple terms, the application of such controls can be modelled in terms of a “closed system” (Fig. 4). When represented in terms of the “closed system” concept, the simple “open dam-reservoir-production-spillway system” illustrated in Figure 3 becomes as in Figure 5.

Ensuring full functionality of the system illustrated in Figure 5 involves rather a lot more than maintaining the physical (and therefore functional) integrity of the water barrier (dam) and the spillway. However, gated spillways function in this way and full functionality of the control systems must be maintained along with the structural integrity. The interdependencies between functions during “normal operation” become important with the strengths of the interdependencies being additional factors to be considered. With reference to Figure 1, the functions of the system can be modelled in terms of control functions as illustrated in Figure 6.

When viewed in this way, the engineering of dams and reservoirs and therefore their safe management demands that an appropriate balance be struck between expected outflow characteristics, and the essentially random inflows over the full spectrum of operating conditions over which “hydraulic control” can be exercised through manipulation of the system characteristics over time (and usually to a lesser degree over space). Loss of hydraulic control, be it due to an internal failure or an external hazard, involves loss of control of the hazard (the stored volume and inflows) thereby rendering the system potentially unstable and therefore unsafe.

In terms of this view, safe operation of dams and reservoirs entails maintaining hydraulic control over the full range of operating conditions. This includes being able to either withstand

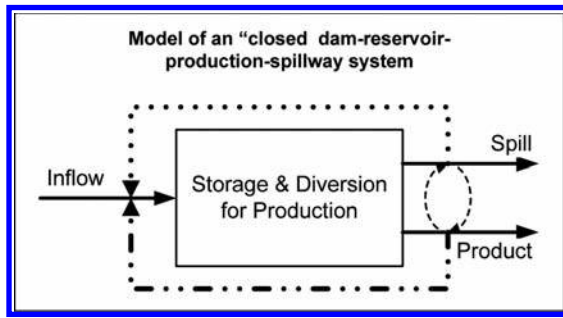


Figure 5. “Closed system” representation of “dam-reservoir-production-spillway” system.

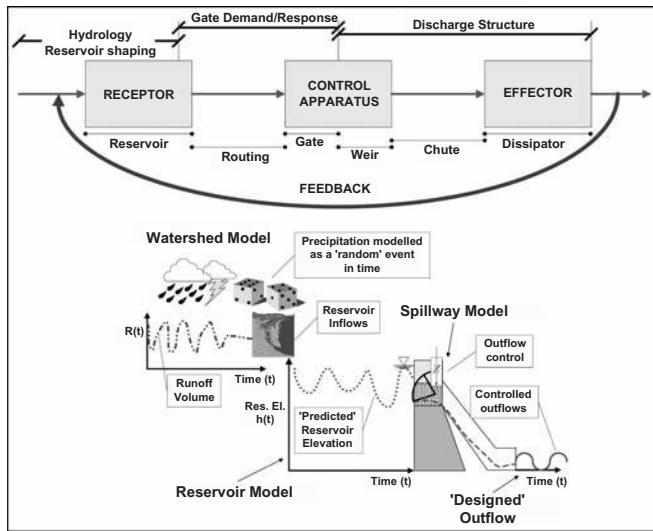


Figure 6. Dam-reservoir-spillway as a “hydraulic control system”.

the effects of external system disturbances such as earthquakes or to have the capacity to regain hydraulic control after the event without having lost control of the outflows to any appreciable degree (e.g. within operating envelope). This “maintenance of hydraulic control” encompasses all of the traditional aspects of dam safety which typically focus on the ability to withstand “normal” loads over the life of the dam; and physically withstand exceptionally large floods (by passing the flood) and comparably large earthquakes (by having sufficient resistance to prevent catastrophic collapse). The proposed broader interpretation encompasses and assures a great deal more of the functionality of dams and reservoirs, and doing so imposes management controls over the vast majority of conditions that can create risk in the system. Combinations of conditions lesser than either extreme natural floods or earthquakes, and including management and procedural factors associated with operation, maintenance, and monitoring contribute a great deal more to the total risk than the extreme natural events individually or collectively.

6 DAMS AND RESERVOIRS AS “LOW-PASS FILTERS” FOR FLOOD

While dams are often built for a sole purpose such as power generation or water storage for irrigation, they are also often built to provide a number of functions including flood control. However, a dam that impounds a storage reservoir of any significant volume necessarily has the effect of absorbing the smaller more frequent floods before passing larger floods. In terms

of the physics of filtration, the reservoir serves as a “low pass flood filter” in that it absorbs the “high frequency” floods and passes the “low frequency floods”. The “bandwidth” of the filter is determined by the range of flood frequencies that can be absorbed by the reservoir within the operating limits of the reservoir. If the reservoir has a wide operating range, that is both a large total storage volume and a large reservoir level operating range, and where the operators have a range of options available for optimising production by controlling the pre-inflow season reservoir elevation based on forecasts of both inflow supply quantities and production demand, the bandwidth of such a dam reservoir system is not only very large, but also equipped with a high degree of controllable variability. As such, the flood filtration capability is not only very large, it can be finely “tuned” or operated with a high degree of control.

Thus, in general, a dam and storage reservoir can be considered to be a “variable bandwidth low-pass flood filter”. The physics of the situation mean that the construction of storage reservoirs necessarily means that the owner/operator is involved to some degree in flood management. Traditionally, owners of “single purpose” dams such as dams constructed for hydropower production or irrigation do not consider themselves to be in the “flood control business” even though the physics of the situation inevitably means that they are involved in flood control by virtue of their “low-pass variable bandwidth flood filters” that are necessary for the success of their production processes. From a production perspective, capitalising on the flexible flood filtration capability of a dam and storage reservoir makes eminent sense in that the maximum possible amount of flood water is captured and used for production. This is obviously an important operational and licensing matter. However, comprehensive consideration of the dam, reservoir, production facility and spillway together with the downstream environs as a “multi-purpose multi-functional system” with the hydraulic and production control sub-systems as the critical controlling features of the system, together with comprehensive functional analysis of these hydraulic controls, provide a robust, scientific basis for establishing and negotiating “operating regimes” over the full spectrum of flows.

One by-product of considering the dam, reservoir, production facility and spillway as a “variable bandwidth low-pass filter” is that what constitutes “normal operation” can be defined in terms of physically controllable functional parameters of the hydraulic control system. Thus, rather than defining “normal operation” in terms of “annual average inflows” which is quite typical, with anything else being considered abnormal to some degree, normal operation can be defined in terms of the controllable bandwidth of the reservoir storage, subject to a previously agreed (with other stakeholders) antecedent reservoir and river conditions, prior to the onset of what is generally considered (for that basin) the inflow season.

7 CONCLUSIONS

It is proposed that the philosophy outlined above is more relevant to the operation of dams and reservoirs in the modern context than traditional dam safety practice which focuses on a limited set of “applied loads and withstand capacities for “normal and extreme floods and earthquakes”. If the focus of dam safety is expanded to include “retaining the stored volume and passing all flows through and around the dam in a controlled manner”, then the concepts and philosophy presented here apply directly. The most fundamental shift in thinking involves considering the dam-reservoir-production facility and system and spillway as a dynamic (in space and time) functional system rather than as a collection of static parts (or pseudo static form).

REFERENCES

- ICOLD (1988). Dam Design Criteria: The philosophy of their selection. Bulletin 61.
- ICOLD (1987). Dam Safety Guidelines. Bulletin 59.
- ICOLD (2005). Risk Assessment in Dam Safety Management: A Reconnaissance of Benefits, Methods and Current Applications. Bulletin 130.
- von Bertalanffy, L. (1968). General Systems Theory. George Braziller, Inc.
- Ryder, G.H. and Bennett, M.D. (1990). The Mechanics of Machines, Macmillan.

Measures to reduce dynamic plunge pool pressures generated by a free jet

Th. Berchtold

Laboratory of Hydraulics, Hydrology and Glaciology (VAW), ETH Zurich, Zurich, Switzerland

M. Pfister

Laboratory of Hydraulic Constructions (LCH), Ecole Polytechnique Fédérale de Lausanne (EPFL), Lausanne, Switzerland

Formerly: VAW, ETH Zurich

ABSTRACT: Spillways often include a flip bucket as terminal energy dissipator, combined with a plunge pool. To prevent scour at the river bed for large jet fall heights additional measures are required, such as terminal chute widening or increase of the plunge pool depth. The effect of these measures was investigated in hydraulic modeling. The dynamic plunge pool bottom pressures in the jet footprint area were systematically recorded. Both, the time-averaged and the fluctuating dynamic pressure heads are considered as references for the jet scour potential, beside the related pressure coefficients. The investigated measures were proven to be effective in terms of reduced pressures, especially in combination. The relevant parameters of the herein presented measures were systematically varied. This research relates to the Kárahnjúkar spillway model investigation, in which the principal working conditions as canyon topography, jet fall head and discharge spectrum were determined.

1 INTRODUCTION

Most reservoirs include a spillway to convey floods, thereby avoiding dam overtopping. They typically spill extreme discharges with a large head, resulting in high-velocity flows. Chute flows have a considerable energy at the spillway end, which has to be adequately dissipated upstream of the receiving waters (Fiorotto & Rinaldo 1992, Lopardo 1988, Puertas & Dolz 2005, Khatsuria 2005). Otherwise, large scour emerges which may destabilize the dam foundation or erode adjacent valley flanks, and generate sediment deposits further downstream. High-head spillways therefore often include a flip bucket with a plunge pool (Vischer & Hager 1998).

Despite of jet disintegration and diffusion within the plunge pool (Ervine et al. 1997), jets may provoke unacceptable scour for a large fall height combined with a limited plunge pool depth (Bollaert & Schleiss 2003a, b). Additional measures are then necessary to enhance the jet disintegration process, thereby minimizing its energy entrainment into the plunge pool (Ervine & Falvey 1987, Annandale 2005, Bollaert & Schleiss 2005, Pagliara et al. 2006, Li & Liu 2010). These additional measures normally include elements to increase jet turbulence, such as terminal spillway width increase to generate thinner jets. Jet disintegration, spreading and aeration are thereby enhanced (Canepa & Hager 2003, Schmocker et al. 2008, Pfister & Hager 2009), reducing specific energy density at the jet footprint on the plunge pool bottom. Ervine et al. (1997) mention that jet diffusion in the plunge pool is furthermore relevant for limited pressure fluctuations on the pool bottom, and that air entrained by the jet reduces bottom pressure amplitudes. Manso et al. (2007) show that dynamic pressures at the bottom of shallow and deep pools often follow a Gaussian distribution.

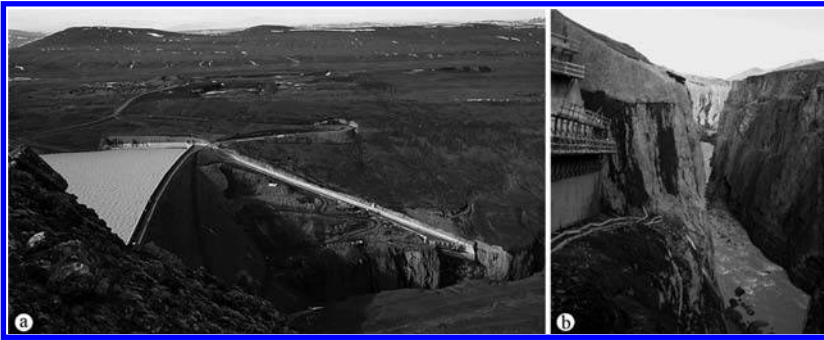


Figure 1. a) Overview of Kárahnjúkar Dam and spillway above canyon (courtesy Landsvirkjun), and b) canyon in flow direction with chute end at left; tailwater dike was not yet constructed.

This research presents measures affecting a free jet issued from a spillway to reduce plunge pool pressures. The results were derived from a physical model investigation conducted at the Laboratory of Hydraulics, Hydrology and Glaciology (VAW), ETH Zurich. This project was initiated by the related Kárahnjúkar spillway investigation (VAW 2006, Pfister et al. 2008), in terms of topography, net fall head and discharge spectrum. However, the relevant parameters of this work were systematically varied in a wide range, independent of the original project.

The national power company of Iceland, Landsvirkjun, took the 690 MW Kárahnjúkar Hydroelectric Project in Eastern Iceland in 2008 into service for the electric supply of an aluminium smelter. It includes three dams storing the Háslón reservoir with a water volume of $2.1 \cdot 10^9 \text{ m}^3$. An unregulated spillway is located at the left embankment of the 198 m high main dam (Fig. 1a), consisting of a side channel, a transition bend and a 419 m long chute. It was designed for a discharge of $1350 \text{ m}^3/\text{s}$, and evacuates a PMF of $2250 \text{ m}^3/\text{s}$ (Tómasson et al. 2006). At the chute end, the water falls as a free jet into a narrow canyon with almost 100 m high vertical rock flanks (Fig. 1b). These are unstable due to cracks and soft rock, such that measures to reduce the scour potential of the jet were sought. A tailwater dike resistant to overflow erosion stores a plunge pool on the riverbed.

2 CHARACTERISTIC PLUNGE POOL PRESSURES

The following pressure heads in [m] water column are considered:

- Effective (subscript *e*) measured, instantaneous (subscript *i*) transmitter pressure head P_{ei} .
- Hydrostatic pressure head Y defined as vertical elevation difference between the transmitter-level and tail water dike crest. This simplification overlooks the high degree of turbulence and air entrainment within the plunge pool which inhibits the recording of a precise hydrostatic pressure head.
- Dynamic (subscript *d*) instantaneous pressure head $P_{di} = P_{ei} - Y$.
- Time-averaged (subscript *a*) dynamic pressure head P_{da} and respective average dynamic pressure coefficient C_{da} as

$$P_{da} = \frac{\sum P_{di}}{N} \quad (1)$$

$$C_{da} = P_{da} \left(\frac{v_j^2}{2g} \right)^{-1} \quad (2)$$

with N as number of pressure head records, and g as acceleration of gravity. The jet impact velocity v_j on the plunge pool water surface was derived from the hydraulic model using high-speed particle tracking and from energy considerations.

- Fluctuating dynamic pressure head P'_d and respective fluctuating dynamic pressure coefficient C'_d as

$$P'_d = \sqrt{\frac{\sum (P_{da} - P_{di})^2}{N}} \quad (3)$$

$$C'_d = P'_d \left(\frac{v_j^2}{2g} \right)^{-1} \quad (4)$$

3 HYDRAULIC MODEL

The physical model was built for the Kárahnjúkar investigation with a scale factor of 45 and operated using Froude similitude (Fig. 2a, VAW 2006). It reproduced a sector of the Háslón reservoir, the entire spillway, a section of the canyon and the complete plunge pool including the tailwater dike. The canyon bed was rigid, i.e. no scour occurred in the model thereby allowing for dynamic pressure measurements. The vertical extension of the Kárahnjúkar plunge pool depth is limited because: 1) plunge pool bottom elevation is restricted to avoid extensive excavation works and instability of the adjacent rock flanks, and 2) high water levels are excluded to avoid a submerged bottom outlet. The plunge pool width is 70 to 90 m restricted by the canyon dimensions (Figs. 1 and 2), and its length is some 400 m. The main dam toe is located 250 m upstream and the tailwater dike 150 m downstream of the jet impact. Given the narrow canyon and high discharges, a distinctive longitudinal flow component is established in the plunge pool toward the tailwater dike.

The take-off lip at the chute end is oblique relative to the flow direction, following the canyon edge. Furthermore, no flip bucket is installed, such that the chute end has the same slope of 20% as the chute. Beside constructional advantages, this design rotates the jet foot-print and adjusts it to the plunge pool shape (Pfister et al. 2008).

The discharge was determined by Inductive Discharge Measurement to $\pm 3\%$ accuracy. The pressure head P_{ei} was recorded in the model using transmitters, typically over 120s. BAUMER relative sensors were used for pressure measurements. These sensors have a flush-mounted diaphragm of diameter 17.5 mm with a relative measurement range between 0 and 1 bar and a precision of $\pm 0.5\%$ of the full scale output. The sampling rate during dynamic acquisitions was

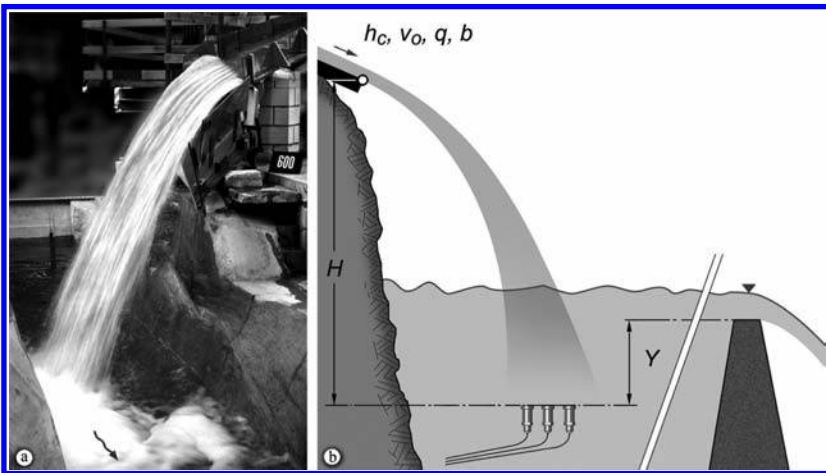


Figure 2. a) Lower part of model spillway with canyon and plunge pool, $Q = 600 \text{ m}^3/\text{s}$, $b = 30.6 \text{ m}$ and $Y = 5.2 \text{ m}$, and b) definition plot.

Table 1. Test program with systematic parameter variation including Tests 1–27, and Tests 28–30 related to Kárahnjúkar project, all in prototype dimensions.

Test Nr.		1	2	3	4	5	6	7	8	9	10	11	12
Q	[m ³ /s]	400	600	800	400	600	800	400	600	800	400	600	800
b	[m]	17.0	17.0	17.0	17.0	17.0	17.0	17.0	17.0	17.0	23.8	23.8	23.8
Y	[m]	5.2	5.2	5.2	10.2	10.2	10.2	15.2	15.2	15.2	5.2	5.2	5.2
P_{daM}	[m]	15.3	19.5	21.3	7.4	9.2	13.5	2.6	5.1	10.5	12.8	15.7	18.8
Test Nr.		13	14	15	16	17	18	19	20	21	22	23	24
Q	[m ³ /s]	400	600	800	400	600	800	400	600	800	400	600	800
b	[m]	23.8	23.8	23.8	23.8	23.8	23.8	30.6	30.6	30.6	30.6	30.6	30.6
Y	[m]	10.2	10.2	10.5	15.2	15.2	15.2	5.2	5.2	5.2	10.2	10.2	10.2
P_{daM}	[m]	3.8	7.5	8.3	2.4	3.2	4.5	8.1	11.9	13.3	2.6	5.2	7.6
Test Nr.		25	26	27		28	29	30					
Q	[m ³ /s]	400	600	800		600	950	950					
b	[m]	30.6	30.6	30.6		30.6	30.6	30.6					
Y	[m]	15.2	15.2	15.2		6.5	6.5	11.5					
P_{daM}	[m]	2.4	2.5	3.1		12.7	12.0	3.4					

200 Hz and the transmitters were calibrated before each test. A movable plate with eight transmitters was fixed on the river bed to detect jet-generated pressures and their fluctuations. The entire jet footprint was thereby covered with a prototype grid spacing of 2.25 m.

The width b of the chute end perpendicular to the flow direction was varied between 17.0 and 30.6 m, the hydrostatic plunge pool pressure head Y between 5.2 and 15.2 m, the discharge Q between 400 and 800 m³/s, and the jet impact head H as elevation difference between the jet take-off level and the transmitter-level was kept constant at 92.5 m, all in prototype dimensions (Fig. 2b). Small discharges as compared to PMF were tested to keep the footprint on the riverbed, thereby avoiding an effect of the canyon flanks. Discharges are expressed with the critical flow depth $h_c = (q^2/g)^{1/3}$, where $q = Q/b$. In total, 27 tests were conducted with $1.1 \leq b/Y \leq 5.9$ and $0.2 \leq h_c/Y \leq 1.2$. The present results therefore by far exceed the test program of the original spillway investigation including a systematic parameter variation, as noted from the test program (Table 1, Tests 1–27). Test series were conducted by varying one parameter, e.g. Q , and keeping the other two parameters constant, e.g. b and Y . As a consequence, the isolated effect of each parameter on P_{da} resulted. Furthermore, selected tests of the Kárahnjúkar investigation (Tests 28–30) were considered with Q up to 950 m³/s, yet with isolated pressures affected by the opposite rock flank and the chute aerator, such that these were excluded for the data analysis.

4 JET FOOTPRINT

The grid for pressure measurements on the riverbed covered the entire canyon width, i.e. the entire jet footprint as the zone of notable jet-induced dynamic pressures. To define the footprint area, two criteria were applied: 1) $P_{da}/H \geq 0.1 h_c/Y$, and 2) $P_{da} \geq 2.0$ m in absolute terms for model measurement reasons. The pressure head of criterion (1) corresponds to half of the maximum value detected within the footprint, as shown below. Transmitters whose measured heads satisfied both criteria were considered located within the jet footprint. The two criteria resulted from an extensive data analysis; absolute offset values as a function of e.g. H resulted in poorly-defined footprint areas, especially for tests with small Q and large b and Y .

Figure 3 shows an example of three footprints, where b was varied, for otherwise constant parameters. The streamwise axis x corresponds to the chute centre line, with the transverse coordinate y perpendicular to x . Note that the footprint spreads with increasing b , is U-shaped and relevant pressures are concentrated laterally. The U-shaped footprint originates from a slightly

smaller lateral chute velocity due to wall friction, with a reduced jet take-off velocity generating shorter lateral jet trajectories as compared to the chute centre flow. The relative thickness of a narrow jet is larger than of a wide, such that the footprint concentrates near the chute axis around $y=0$. In contrast, the jet is thinner for a wide chute end, such that the footprint locally even disappears close to $y=0$. In parallel, small chute flow depths imply higher energy losses, such that the jet take-off velocity slightly decreases, shifting the footprint towards the chute end.

The individual P_{da} of all transmitters located within the footprint were summed up to ΣP_{da} and divided by the transmitter number n located within the footprint. The data were then normalized with the jet impact head H and plotted versus h_c/Y . Consequently, the footprint area-averaged dynamic pressure head is

$$\frac{\Sigma P_{da}}{nH} = 0.15 \frac{h_c}{Y} \quad \text{for } 0 < h_c/Y < 1.2 \quad (5)$$

with a coefficient of determination of $R^2 = 0.95$ between the model data and Eq. (5). The lower limit was set to $h_c/Y = 0$, whereas the data only include $h_c/Y \geq 0.17$, because $P_{da}(h_c/Y \rightarrow 0) \rightarrow 0$. Figure 4 compares the measured data with Eq. (5). Note that the footprint is located close to the opposite canyon flank for large discharges. Then, a distinction between footprint and wall effect was difficult, such that unfiltered data may include small wall effects in Eq. (5).

5 EFFECTS OF CHUTE END WIDTH, DISCHARGE AND PLUNGE POOL DEPTH

5.1 Individual effect

The characteristic pressure heads P_{da} were derived for all grid points, of which the maximum (subscript M) P_{daM} within the footprint area was selected for further analysis to investigate the

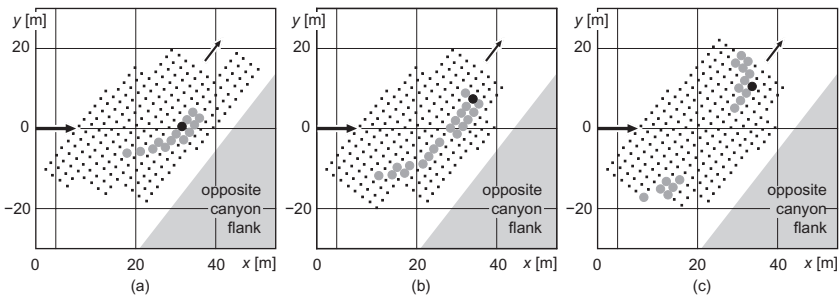


Figure 3. Footprint example of Tests (a) 3, (b) 12, and (c) 21, i.e. for increasing b , with (·) transmitter location, (◐) footprint area, and (●) maximum P_{daM}

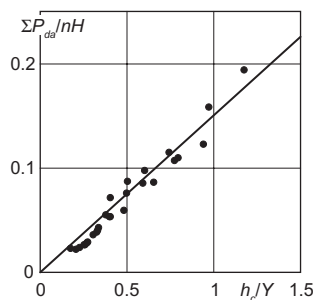


Figure 4. Footprint area-averaged dynamic pressure head $\Sigma P_{da}/nH[h_c/Y]$ with (—) Eq. (5).

effects of b , Q , and Y . The long chute upstream of the take-off generates fully developed turbulent approach flow with uniform flow conditions for the tested discharges. The measured average maximum P_{daM} of all tests was 21.3 m (Table 1), corresponding to 23% of H . This is a relatively small value, pointing at pronounced jet disintegration. Almost immediately beyond take-off, the jet is fully-aerated below some 3 to 7% of H (Pfister & Hager 2009), and breaks up at 14 to 22% of H (Ervine et al. 1997), reducing pressures drastically in the plunge pool.

Figure 5 shows the un-normalized isolated effects of Q , Y , and b on P_{daM} in prototype dimensions. Within a series consisting of three tests, only the discussed parameter varies, while the others remain unchanged. Note from Figure 5a that P_{daM} almost linearly increases with Q . However, this effect is relatively small, as P_{daM} only slightly increases with Q . More relevant is Y (Fig. 5b), involving a strong decrease of P_{daM} for large Y , similar to Ervine et al. (1997). The effect of b on P_{daM} is shown in Figure 5c, indicating reduced pressures as b increases. The maximum time-averaged dynamic pressure head P_{daM} measured within the jet footprint therefore increases with discharge, but decreases with chute end width, and with deep plunge pools. The jet impact head H further affects plunge pool pressures, yet this parameter was kept constant herein.

5.2 Normalized results

The dynamic plunge pool pressures were normalized as P_{daM}/H and P'_{daM}/H to include the jet impact head (Khatsuria 2005). The additionally investigated parameters affecting the plunge pool pressures were normalized as $h_c/Y = [(Q/b)^2/g]^{1/3} Y^{-1}$ thereby including Q , b and Y . The model data of P_{daM} collapse with a linear trend line as (Fig. 6a)

$$\frac{P_{daM}}{H} = 0.20 \frac{h_c}{Y} \quad \text{for } 0 < h_c/Y < 1.2 \quad (6)$$

with $R^2 = 0.93$ between the model data and Eq. (6). The latter may be expressed as $P_{daM} = 0.2 H Y^{-1} Q^{2/3} b^{-2/3} g^{-1/3}$ to assess the effect of the single variables, indicating that the jet impact head H and the plunge pool depth Y are significant, whereas the chute end width b and the discharge Q are less relevant. Dividing Eq. (5) by Eq. (6) results in $(\Sigma P_{daM}/n)/P_{daM} = 0.75$. Accordingly, the area-averaged footprint pressure head is equivalent to some 75% of the local maximum P_{daM} , independent of b , Q and Y . The individual measured data include a ratio of 60 to 100%, with an average around 77%.

The same abscissa normalization as for P_{daM} was used for P'_{daM} again resulting in a linear trend as

$$\frac{P'_{daM}}{H} = 0.23 \frac{h_c}{Y} - 0.03 \quad \text{for } 0 < h_c/Y < 1.2 \quad (7)$$

Figure 6b compares the data and Eq. (7), with $R^2 = 0.89$. Note that $P'_{daM}/H = 0$ for $h_c/Y < 0.13$. Accordingly, fluctuating pressures are absent if h_c is sufficiently small, i.e. for

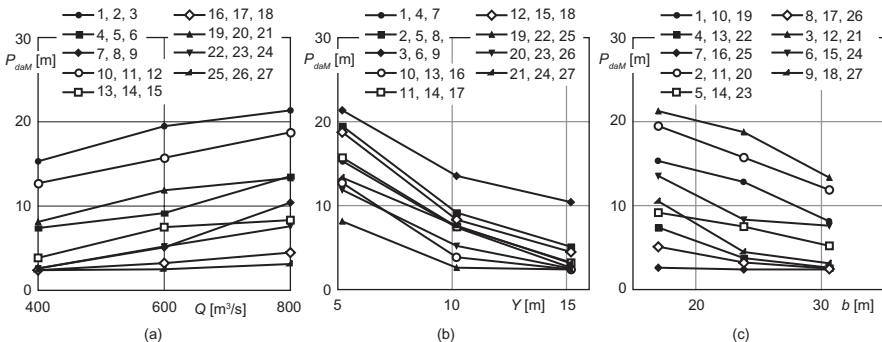


Figure 5. Individual effect of (a) Q , (b) Y , and (c) b on P_{daM} test number according to Table 1.

a small q combined with large values Y corresponding to ‘deep’ plunge pools, resulting in small P_{daM} , combined with $P'_{dM} = 0$. The jet momentum affects the plunge pool bottom, while the jet fluctuations are fully damped by the water cushion.

As explained, P_{daM} refers to the transmitter with the maximum measured average value of the entire footprint. To ensure its relevance, the next smaller maxima M2 and M3 were considered, with M1 representing the maximum P_{daM} , and M2 as well as M3 the next smaller values at a different transmitter. These are shown in Figure 6c, which corresponds basically to Figure 6a plus the further maxima. All values M1 to M3 almost collapse, such that recording errors may be excluded. In parallel, linear best fits were added to the figure, indicating a slight decay of the gradients for M1→M3. Accordingly, M2 and M3 are marginally lower than the absolute maximum M1.

The pressure coefficients were again derived as a function of h_c/Y . The dynamic coefficient collapses with a linear trend line as ($R^2 = 0.93$).

$$C_{da} = 0.15 \frac{h_c}{Y} \quad \text{for } 0 < h_c/Y < 1.2 \quad (8)$$

The fluctuating coefficient was expressed as ($R^2 = 0.84$)

$$C'_d = 0.18 \frac{h_c}{Y} - 0.03 \quad \text{for } 0 < h_c/Y < 1.2 \quad (9)$$

The data of both coefficients are shown in Figure 7 including Eqs. (8) and (9), indicating good agreement between measurements and predictions. Again, the fluctuating pressure coefficient is zero for $h_c/Y < 0.13$, as the fluctuating pressure head was.

Dividing Eq. (8) by Eq. (6) results in $C_{da}/(P_{daM}/H) = 0.75$. Accordingly, the dynamic pressures coefficients are 75% of the relative dynamic pressure head, independent of b , Q and Y . From Eq. (2) then follows the jet net head $v_j^2/2g = 1.3 H$. For the present tests, the gross jet energy head at impact on the plunge pool water surface is H plus the velocity head at take-off, which is between

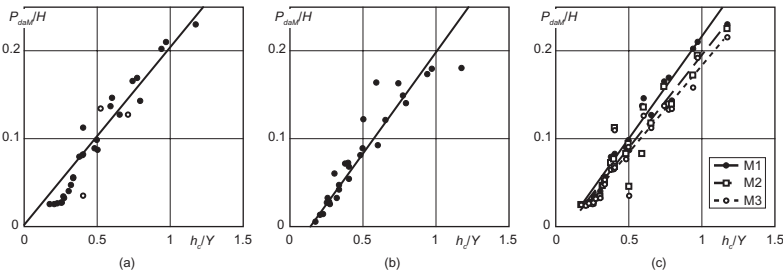


Figure 6. a) $P_{daM}/H[h_c/Y]$ with (–) Eq. (6) and (c) Tests 28–30, b) $P'_{daM}/H[h_c/Y]$ with (–) Eq. (7) and c) maxima M1 to M3 of $P_{daM}/H[h_c/Y]$ with trend lines.

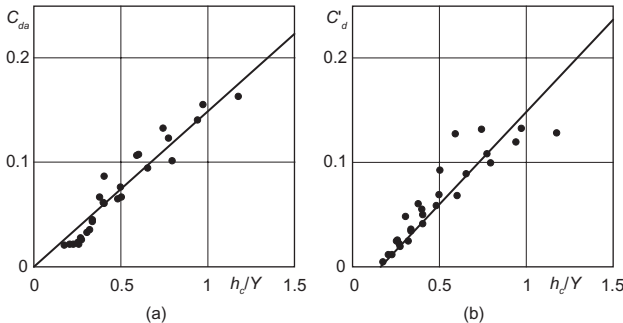


Figure 7. a) $C_{da}[h_c/Y]$ with (–) Eq. (8), and b) $C'_d[h_c/Y]$ with (–) Eq. (9).

0.3 and 0.5 H . Accordingly, the difference of the gross jet head equivalent to 1.3 to 1.5 H and the net jet head with 1.3 H ranges between 0 and 0.2 H , probably related with jet dissipation effects.

6 CONCLUSION

Measures to reduce dynamic plunge pool pressures generated by a free jet are discussed, including jet expansion by terminal chute widening and increase of the plunge pool depth. The effect of these parameters was investigated using a hydraulic model with a systematic parameter variation. The dynamic and fluctuating pressure heads on the plunge pool bottom were thereby considered as reference values. For the present case study, the jet impact head H and the plunge pool depth Y are relevant, whereas the chute end width b and the discharge Q are of lower significance. Equations were derived to predict the determining pressures within the limitations of the model investigation. The model limitations relate to the jet fall height, the discharge spectrum and the plunge pool arrangement, resulting from the Kárahnjúkar spillway investigation, for which the model was initially erected.

REFERENCES

- Annandale, G.W. 2005. *Scour Technology*. McGraw-Hill, New York.
- Bollaert, E.F.R. & Schleiss, A.J. 2003a. Scour of rock due to the impact of plunging high velocity jets Part I: A state-of-the-art review. *Journal of Hydraulic Research* 41(5), 451–464.
- Bollaert, E.F.R. & Schleiss, A.J. 2003b. Scour of rock due to the impact of plunging high velocity jets Part II: Experimental results of dynamic pressures at pool bottoms and in one- and two-dimensional closed end rock joints. *Journal of Hydraulic Research* 41(5), 465–480.
- Bollaert, E.F.R. & Schleiss, A.J. 2005. Physically-based model for evaluation of rock scour due to high velocity jet impact. *Journal of Hydraulic Engineering* 131(3), 153–165.
- Canepa, S. & Hager, W.H. 2003. Effect of jet air content on plunge pool scour. *Journal of Hydraulic Engineering* 129(5), 358–365.
- Ervine, D.A. & Falvey, H.T. 1987. Behavior of turbulent water jets in the atmosphere and in plunge pools. *Proc. Instn Civ. Engrs* 83(2), 295–314, Paper 9136.
- Ervine, D.A., Falvey, H.T. & Withers, W. 1997. Pressure fluctuations on plunge pool floors. *Journal of Hydraulic Research* 35(2), 257–279.
- Fiorotto, V. & Rinaldo, A. 1992. Turbulent pressure fluctuations under hydraulic jumps. *Journal of Hydraulic Research* 30(4), 499–520.
- Khatsuria, R.M. 2005. *Hydraulics of spillways and energy dissipators*. Dekker, New York.
- Li, A. & Liu, P. 2010. Mechanism of rock-bed scour due to impinging jet. *Journal of Hydraulic Research* 48(1), 14–22.
- Lopardo, R.A. 1988. Stilling basin pressure fluctuation. *Proc. Intl. Symposium on Model-Prototype Correlation of Hydraulic Structures*, Colorado Springs, USA, 56–73.
- Manso, P.A., Bollaert, E.F.R. & Schleiss, A.J. 2007. Impact pressures of turbulent high-velocity jets plunging in pools with flat bottom. *Experiments in Fluids* 42(1), 59–60.
- Pagliara S., Hager, W.H. & Minor, H.-E. 2006. Hydraulics of plunge pool scour. *Journal of Hydraulic Engineering* 132(5), 450–461.
- Pfister, M., Berchtold, T. & Lais, A. 2008. Kárahnjúkar dam spillway: Optimization by hydraulic model tests. 3rd IAHR *International Symposium in Hydraulic Structures*, Hohai University, Nanjing (Cn), VI, 2106–2111.
- Pfister, M. & Hager, W.H. 2009. Deflector-generated jets. *Journal of Hydraulic Research* 47(4), 466–475.
- Puertas, J. & Dolz, J. 2005. Plunge pool pressures due to a falling rectangular jet. *Journal of Hydraulic Engineering* 131(5), 404–407.
- Schmocker, L., Pfister, M., Hager, W.H. & Minor, H.-E. 2008. Aeration characteristics of ski jump jets. *Journal of Hydraulic Engineering* 134(1), 90–97.
- Tómasson, G.G., Garðarsson, S.M., Petry, B. & Stefánsson, B. 2006. Design challenges and solutions for the Kárahnjúkar spillway. *Hydropower & Dams* 13(5), 84–88.
- VAW 2006. Kárahnjúkar HEP Iceland; Physical model investigation on the Kárahnjúkar dam spillway. *VAW Report 4203*, ETH: Zurich [unpublished].
- Vischer, D.L. & Hager, W.H. 1998. *Dam hydraulics*. John Wiley & Sons, Chichester, UK.

Impulse waves at Kühltai reservoir generated by avalanches and landslides

H. Fuchs & R.M. Boes

Laboratory of Hydraulics, Hydrology and Glaciology (VAW), ETH Zurich, Zurich, Switzerland

M. Pfister

Laboratory of Hydraulic Constructions (LCH), Ecole Polytechnique Fédérale de Lausanne (EPFL), Lausanne, Switzerland

Formerly: VAW, ETH Zurich

ABSTRACT: The Kühltai reservoir is planned as an addition to the existing Sellrain-Silz group of HPPs. Two natural hazards relevant in terms of potential impulse wave impact on the dam were identified: a snow avalanche near the dam axis and a possible landslide further upstream. A preliminary analytical evaluation of impulse wave heights and wave run-up based on empirical equations showed that dam overtopping could not be excluded. However, several limitations of this evaluation were not satisfied, resulting in a reduced validity of the prediction. Thus, impulse wave generation was investigated in a 1:130 hydraulic scale model. Beside tests related to the relevant events, an additional systematic parameter variation validated the quality of the results. However, as no overtopping occurred even for the parameter variation, no measures such as breakwater or increase of the freeboard were required. The model test results are compared to a further analytical evaluation based on the recently published VAW-manual on landslide generated impulse waves.

1 INTRODUCTION

In addition to the existing Sellrain-Silz group of HPPs the Kühltai reservoir is currently planned by the Tyrolean Hydropower Company TIWAG-Tiroler Wasserkraft AG in order to increase the total storage volume (Boes et al. 2007). During load determination, two hazards relevant in terms of potential impulse wave impact on the 140 m high dam were identified (Fig. 1):

1. A snow avalanche zone close to the dam axis. Since the reservoir is located in the Alps at high altitude, intense snowfall and steep topography may result in a variety of avalanche events possibly impinging the reservoir. Governing avalanche parameters were evaluated by numerical simulations and provided by TIWAG. The gross avalanche volume was estimated to 90,000 m³.
2. An unstable jointed beak of rock about 300 m upstream of the dam possibly provoking landslides. A survey and evaluation of rock fissures resulted in two possible failure scenarios, one with a gross volume of 5000 m³ and another with 10,000 m³ slightly further upstream. Both are initiated directly above the Full Supply Water Level (FSL). For further comparisons only the scenario generating larger waves will be considered hereafter.

Both events are expected to transmit a certain impulse to the water and thus generate impulse waves when impinging the reservoir. A preliminary estimation of the expected waves resulted in a possibility for dam-overtopping, representing a potential dam safety risk. The Laboratory of Hydraulics, Hydrology and Glaciology (VAW) was therefore assigned to physically model relevant avalanche and landslide impact into a laboratory scale reservoir.

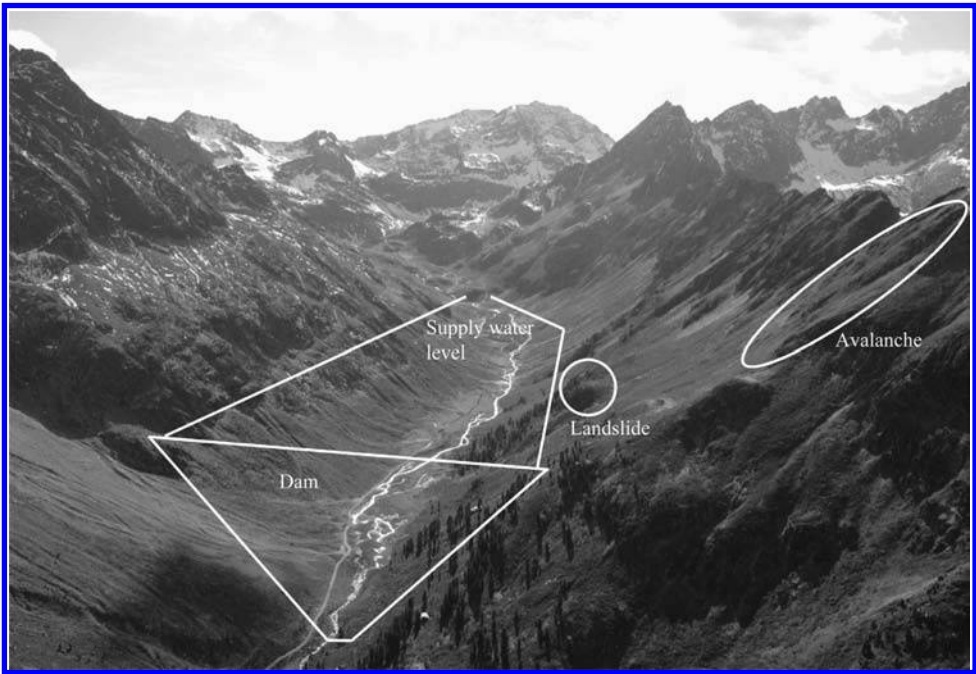


Figure 1. Planned Kühtai reservoir including dam contour, full supply water level and landslide as well as avalanche zones (courtesy of TIWAG).

2 PHYSICAL MODEL

The 1:130 physical scale model includes the complete dam, both valley flanks and roughly half of the reservoir length (Fig. 2). The model thus represents a 500 m wide and 600 m long section of the prototype. The complete height reaches from the reservoir bottom at 2030 m a.s.l. up to an elevation of 2200 m a.s.l., i.e. 60 m above FSL. The FSL is defined at an elevation of 2140 m a.s.l., thereby ensuring a freeboard of 5.0 m along the dam crest at 2145 m a.s.l. With a reservoir depth of 110 m, equivalent to a model depth of 0.85 m, relevant scale effects regarding wave generation and propagation are small (Heller et al. 2008, Dean & Dalrymple 2008). To reduce wave reflections and thus avoid model effects a wave absorber is located at the upstream model boundary corresponding to roughly half of the prototype reservoir length. The spillway located at the left dam embankment has been modeled only qualitatively including an increased hydraulic capacity, since the model scale did not allow for correctly scaled flow conditions. The volume of the unsteady spillway flow was determined by continuously weighing the impulse wave induced discharge.

The avalanche was modeled using a generator-chute hinged on top of the left model valley flank. With variable bottom slope, generator-flap elevation and opening a large variety of avalanche parameters could be generated. A granulate material consisting of white polypropylene (PP) with a grain diameter of 2 to 3 mm was filled in the load zone behind the generator-flap. With a porosity of 39% the grain density of 900 kg/m^3 reduces to a bulk density of 550 kg/m^3 . The density of the propagating avalanche is estimated to 400 kg/m^3 . The avalanche was released by suddenly opening the flap. The model avalanche propagated down the chute slope and followed the local topography when leaving the generator-chute at 2200 m a.s.l.

The granulate material used for landslide modeling had a diameter of 8 mm and consisted of 13% polypropylene (PP) compounded with 87% of barium-sulfate, increasing both density and roughness. With a porosity of 45%, the grain density of 2430 kg/m^3 reduces to a bulk density of 1340 kg/m^3 . During slide propagation the density further decreases to an

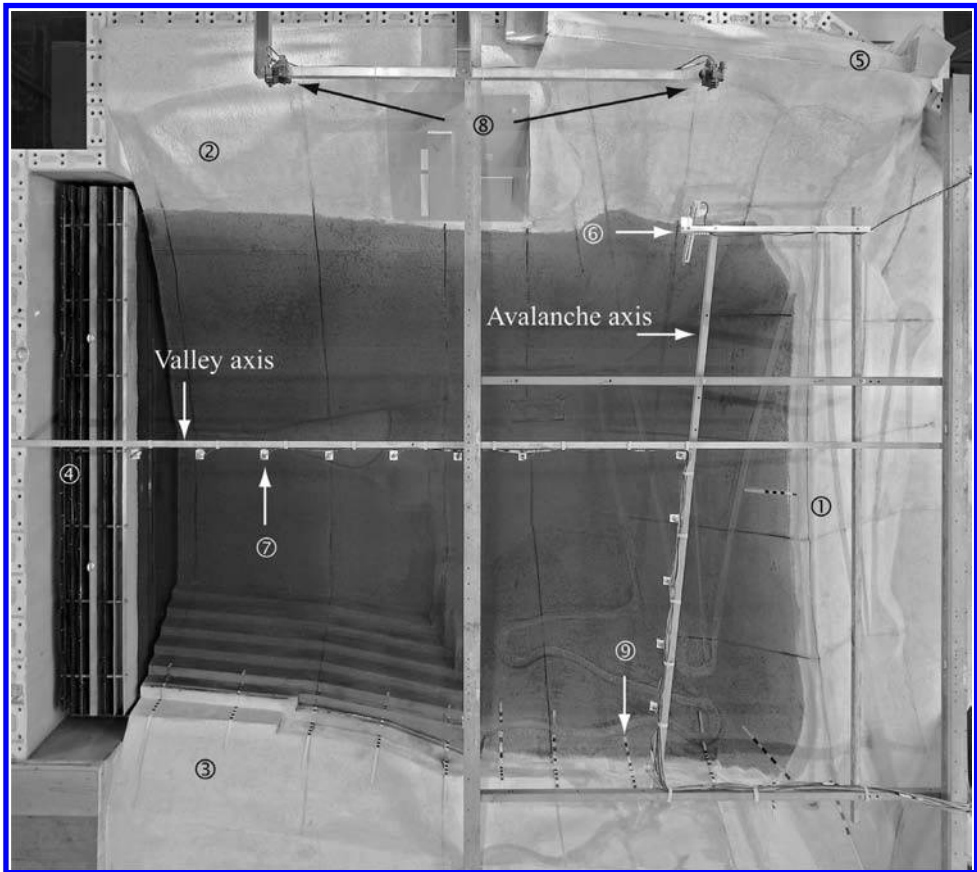


Figure 2. Situation of the physical model including ① dam, ② left valley flank, ③ right valley flank with stepped quarry, ④ wave absorber, ⑤ bearing of the avalanche generator-chute, ⑥ LDS, ⑦ UDS, ⑧ Video Cameras, ⑨ run-up markers.

estimated value of 1100 kg/m^3 . A box equipped with a flap was used to keep the granulate on the topography until release. Specific wedge shaped insets configured the initial slide shape according to shear planes evaluated from numerical simulations. The slide was again released by suddenly opening the flap.

3 INSTRUMENTATION

Three measurement systems were applied (Fig. 2): 1) Laser Distance Sensors (LDS) to scan the avalanche shape prior to impact into the reservoir, 2) Ultrasonic Distance Sensors (UDS) to record the water surface elevation and 3) Digital Video Cameras to capture the wave run-up at the opposite shore-line and wave overtopping over the dam crest.

The LDS were mounted at an individual distance of 0.2 m and measured with a sample frequency of 100 Hz. By correlating the two slide profiles, the temporal offset was derived, relating to the slide impact velocity. Furthermore, the time origin $t = 0$ was specified for which the slide front impinged the reservoir surface.

The individual UDS were installed along two axes. During tests related to the snow avalanches, those axes were the main direction of the transferred impulse and the valley axis (Fig. 2). For landslide testing the wave properties were measured in the landslide axis as well as along an axis from the impingement point to the right dam abutment. Wave characteristics

resulted from a correlation of single wave profiles of adjacent sensors. The UDS were operated with a sample frequency of 50 Hz.

Markers were attached on the topography along the right valley flank to allow for wave run-up height determination (Fig. 2). The exact values were derived visually by analyzing video sequences. The three cameras installed were connected to individual computers but controlled simultaneously with the further instrumentation, thus ensuring a thorough time assignment for all measurement systems.

4 SLIDE PARAMETERS

Since avalanche or landslide propagation may not be modeled correctly for the present model scale using the above described granular material, the impact parameters at FSL were considered exclusively. Those parameters were extracted from numerical simulations for the relevant avalanche and landslide (i.n.n. 2009), as listed in Table 1.

According to an evaluation conducted by TIWAG, the relevant avalanche has a gross volume of 90,000 m³, of which roughly 80,000 m³ enter the reservoir. The remaining volume deposits on the valley flank and on the dam embankment. The relevant avalanche has a density of 300 kg/m³, a thickness of 2 m and a front velocity of 23 m/s at FSL. During physical model tests, 15% of the material remained on the topography, the dam crest and the downstream dam face, resulting in 77,000 m³ eventually impinging the reservoir. The filtered avalanche profile scan is shown in Figure 3a. The lower profile was already shifted for 1.14 s, such that its front coincides with the upper profile, resulting in a slide front velocity of roughly 23 m/s. The average slide thickness is assumed to be 2.0 m. Figure 3b compares the relative mass flux of the relevant avalanche at FSL with the mass flux derived from the numerical simulation, showing a good agreement.

Table 1. Relevant slide parameters of avalanche and landslide modeling, defined at reservoir impact.

Scenario	(1) Snow avalanche	(2) Landslide
Slide volume [m ³]	90,000	5000
Initial slide width [m]	260	31
Slide front velocity [m/s]	23	16
Slide thickness [m]	2	not specified

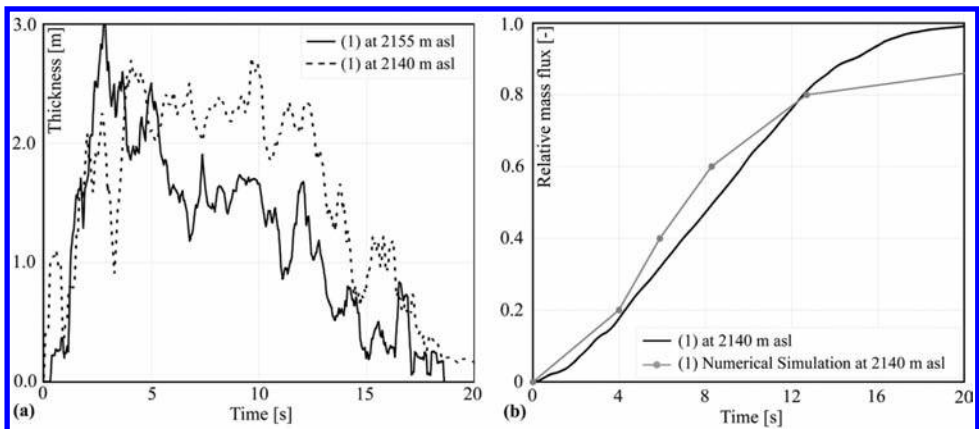


Figure 3. (a) Avalanche profile scans and (b) relative mass flux at FSL.

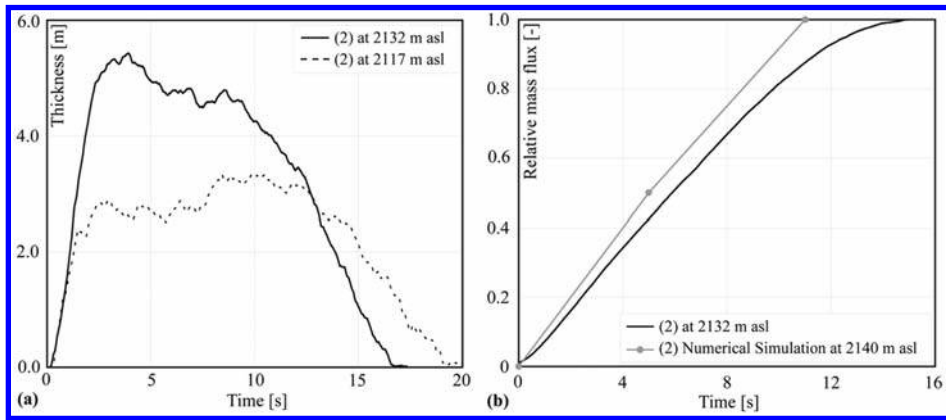


Figure 4. (a) Landslide profile scans and (b) relative mass flux at roughly FSL.

No precise values for landslide thickness and velocity were derived by TIWAG, hence modeling characteristics were compared to the numerical simulation in both, the relative mass flux and the slide width at roughly FSL. Since the unstable rock part is situated right above FSL, and LDS measurement is not applicable through the water surface, the slide characteristics were deduced from separate dry testing. The upper LDS was then installed at 2132 m a.s.l. and the lower at 2117 m a.s.l. Again, the slide front velocity was determined by slide front correlation of the two laser scans resulting in 17.6 m/s for the landslide event. The slide thickness is about 5.5 m (Fig. 4a) and the deduced mass flux coincides well with the numerical simulation (Fig. 4b). Whereas the slide propagated down to the reservoir bottom during dry testing, it remained on the valley flank due to buoyancy if the reservoir was filled. Reproducibility of the slide scenarios was verified by repetition of each test. Both slide and wave characteristics were found to be nearly identical.

5 RESULTS

5.1 Impulse waves

The resulting impulse waves are non-linear Stokes-type waves of transitional water-depth. With a wave length ranging from 200 to 500 m they have a celerity between 10 and 25 m/s. Due to the large width of the avalanche of 130 m, and the dam confining lateral wave propagation on the left side, a rather linear wave front is generated by the avalanche impact. Wave propagation thus occurs mainly two-dimensionally in the direction of the avalanche axis, with significantly smaller waves in the valley axis (Fig. 5). However, waves resulting from landslide impact propagate three-dimensionally and with significantly smaller heights, for instance $H_{(x=200\text{ m})} = 0.5\text{ m}$ for the landslide compared to $H_{(x=200\text{ m})} = 1.6\text{ m}$ of the avalanche generated waves, with H as the primary wave height and x as the radial distance to the impact point. Further wave parameters such as celerity or length are similar for both events.

Consecutive waves propagate with different celerity such that they tend to superpose each other resulting in increased wave height (see Fig. 5, e.g. (1) valley axis, $x \approx 500\text{ m}$). The decreasing reservoir depth at the opposite shoreline results in increased impulse wave heights as a result of shoaling (Fig. 5, (1) avalanche axis, $x \geq 350\text{ m}$).

5.2 Overtopping

Dam overtopping was not observed for any scenario, neither for avalanche nor for landslide impact. Solely at the right dam abutment a sparse wetting of the horizontal dam crest occurred. The downstream dam face remained completely dry throughout model test series of the relevant events.

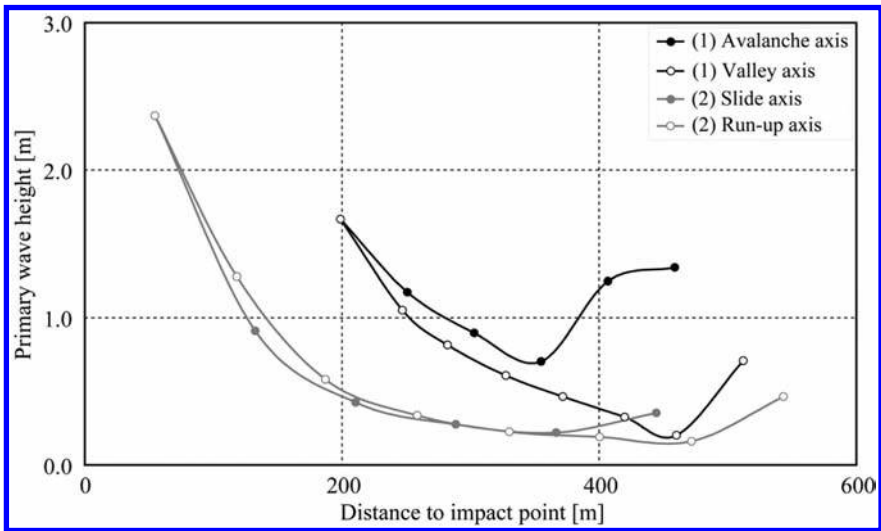


Figure 5. Measured primary wave heights for both measuring axes for (1) avalanche and (2) landslide scenario.

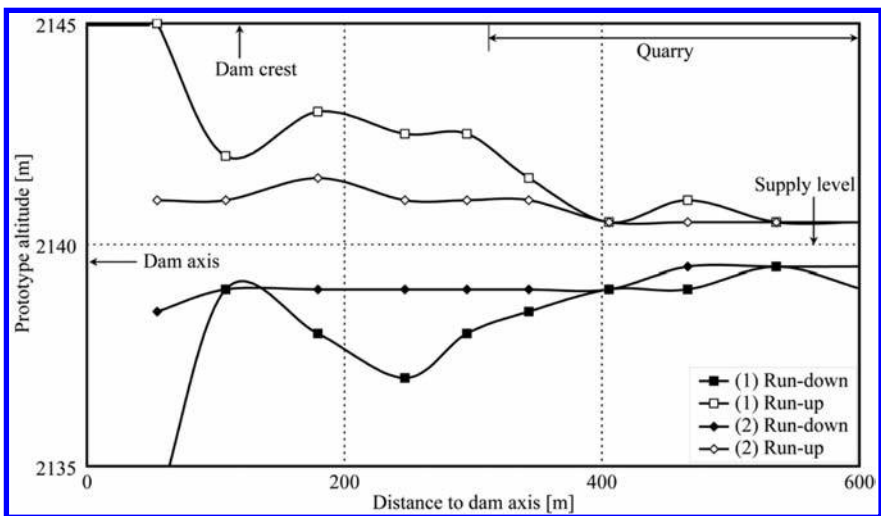


Figure 6. Maximum wave run-up and run-down measured at opposite shoreline during entire test period for (1) avalanche and (2) landslide scenario.

5.3 Wave run-up

Wave run-up and run-down were measured along the right shoreline using digital video recording. The maximum and minimum water levels within the observed period are shown in Figure 6 and refer to FSL. The abscissa represents the distance to the dam axis along the opposite shoreline with $x = 0$ at the dam; a planned quarry for dam construction material will be located at $x > 300$ m (Fig. 2, Fig. 6). The graphs represent maximum values observed during the test period of 170 s and do not stringently result from the primary wave. As described above, wave superposition may result in increased or decreased water levels, respectively. The maximum wave run-up of the relevant avalanche test was measured up to 5.0 m at the right dam abutment having the smallest slope angle of $\beta = 22^\circ$ of the investigated shore section. The deepest run-down reached to 2134 m a.s.l., i.e. was equivalent to 6.0 m below FSL.

The steep shore slope at the quarry further upstream, in combination with the smaller wave heights in the valley axis, result in significantly lower values for both run-up and run-down.

Due to the smaller height of landslide induced waves, wave run-up was smaller as well. The maximum values were measured to 1.5 m for both run-up and run-down.

6 COMPARISON TO PREDICTIONS

In order to facilitate a comparison, the analytical evaluation of impulse wave heights conducted by TIWAG was adapted to the specific physical model test conditions. This evaluation based on a VAW impulse wave guideline (Heller et al. 2009) is subdivided into three regions: 1) generation, 2) propagation and 3) run-up. The maximum wave height during wave generation is determined independently of 2D or 3D geometry. Thereafter, a distinction between 2D and 3D wave propagation is necessary, since for radially unconfined propagation the wave energy spreads in all directions, leading to smaller wave heights. The final computation of wave run-up is only dependent on wave parameters and the run-up shore angle. For the prediction of wave heights according to Heller et al. (2009), the slide centroid velocity is required in place of the slide front velocity deduced from numerical simulation or LDS scans. Following Volkart (1974), a reduction factor of 0.63, unfavorably selected on the safe side, was therefore applied to the slide front velocity of both events to estimate the slide centroid velocity.

As described above, avalanche generated impulse waves appeared to be mainly 2D and thus were compared to a 2D computation. The point of the maximum computed wave height ($H_M = 2.9$ m at $x_M = 75.4$ m) was beyond the instrumentation range, avoiding a direct comparison of measured and computed values. However, the extrapolated origin of the measured wave height roughly coincides with the computed maximum wave height (Fig. 7). The measured wave heights are significantly smaller than analytically predicted for the entire propagation area. Whereas the analytically estimated wave height is almost constant over the propagation distance, extensive wave height decay is observed in the model tests. The smallest wave height along the avalanche axis was measured to $H = 0.7$ m at $x \approx 350$ m, compared to a computed value of $H = 2.5$ m. A wave height increase due to shoaling is clearly visible in both graphs of Figure 7, though the measured wave height in front of the opposite shore at $x \approx 450$ m is only $H = 1.34$ m compared to $H = 3.4$ m resulting from computation.

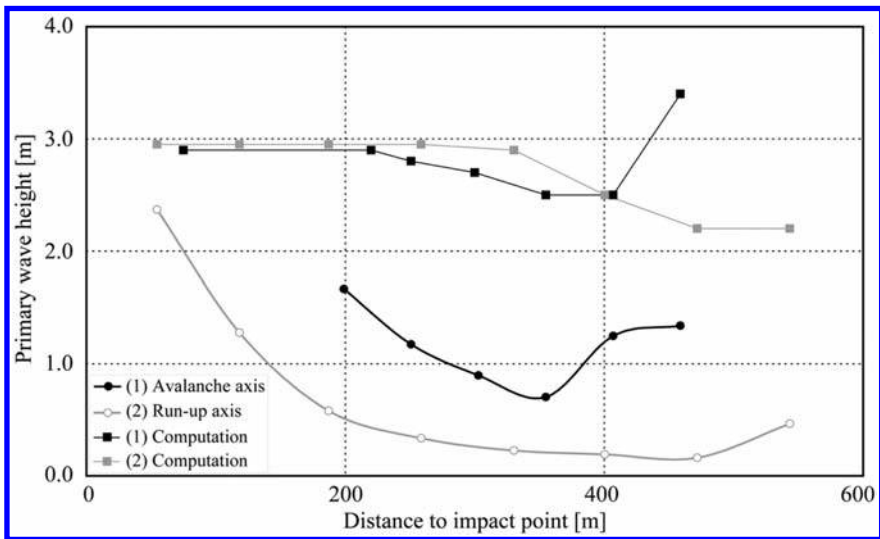


Figure 7. Comparison of computed and measured primary wave heights for (1) avalanche and (2) landslide scenario.

Since the landslide has a small width compared to the reservoir geometry, waves propagate unconfined, i.e. three-dimensionally. Measured wave heights were thus compared to a computation based on 3D propagation. Close to the impact point at $x \approx 50$ m a good correlation of measured ($H_M = 2.4$ m) and computed ($H_M = 3.0$ m) maximum wave heights in the generation zone is visible. Similar to the avalanches, the computed wave heights remain constant, contrary to the measured wave heights strongly decaying. The largest difference occurs at $x \approx 470$ m where the measured $H = 0.16$ m is about 14 times smaller than the predicted $H = 2.2$ m.

The wave run-up for avalanche impact was calculated to $R = 7.0$ m compared to $R = 5.0$ m measured during model testing (Fig. 6). For the landslide event the maximum run-up was calculated to $R = 4.2$ m contrary to the measured $R = 1.0$ m.

These relevant differences between estimation and measurements may be due to a number of not satisfied boundary conditions or so-called limitations of the computation according to Heller et al. (2009), resulting in a reduced validity of the prediction. Furthermore, effects of the complex highly 3D topography are difficult to include in the analytical evaluation.

7 CONCLUSIONS

The Kühltai reservoir in Tyrol, Austria, is planned in addition to the Sellrain-Silz group of HPPs. Due to its high alpine location, snow avalanche impact and resulting impulse waves must be considered in the dam safety assessment. Furthermore, a potential landslide region also possibly provoking impulse waves was determined. Since dam overtopping could not be excluded as a result of a preliminary analytical analysis, VAW was assigned to perform physical model tests.

These tests of the relevant scenarios showed that impulse wave run-up may reach the dam crest, however without dam overtopping even at full supply water level. The downstream dam face remained completely dry for the relevant avalanche and landslide tests. The results of the analytical evaluation were thus complemented, as a number of limitations were not satisfied during the computation procedure.

Eventually, TIWAG decided to further apply a 1.5 m high rock breakwater at the upstream dam crest, increasing the upstream dam slope to 1:1 in the upper part.

ACKNOWLEDGEMENTS

The authors kindly thank TIWAG for this interesting mandate and for the fruitful cooperation.

REFERENCES

- Boes, R., Hofer, B. & Perzlmaier, S. 2007. Planung eines 120 m hohen Steinschüttdammes im Zuge des Wasserkraftausbaus im Tirol. *Wasserwirtschaft* 97(10): 72–74 (in German).
- Dean, R.G. & Dalrymple, R.A. 2008. *Water wave mechanics for engineers and scientists*, Advanced series on ocean engineering—2. Singapore: World Scientific.
- Heller, V., Hager, W.H. & Minor, H.-E. 2008. Scale effects in subaerial landslide generated impulse waves. *Experiments in Fluids* 44(5): 691–703.
- Heller, V., Hager, W.H. & Minor, H.-E. 2009. *Landslide generated impulse waves in reservoirs: Basics and computation*, Mitteilungen 211. R. Boes (ed.), Zurich: VAW, ETH Zurich.
- i.n.n. Ingenieurgesellschaft für naturraum-management mbH & Co KG 2009. *Lawinenmassendurchgang für eine Lawinenrutschdichte von 300 kg/m³*. Innsbruck: unpublished (in German).
- Volkart, P. 1974. Modellversuche über die durch Lawinen verursachten Wellenbewegungen im Ausgleichsbecken Ferden im Lötschental. *Wasser- und Energiewirtschaft* 66(8/9): 286–292 (in German).

Numerical simulations of water waves due to landslides

Jiang Zhibing, Han Jibin & Cheng Zibing

Department of Hydraulics Research, Changjiang River Scientific Research Institute, Wuhan, Hubei, People's Republic of China

ABSTRACT: Water waves due to landslides belong to local flood disaster induced by geological debacle. Research on landslide-generated wave formation and spreading pattern can provide scientific basis for their forecast and risk assessment. In this paper, a numerical model is established to simulate landslide-generated waves by adopting the finite volume method to make control formulas discrete in space and adopting improved MacCormack prediction-correction format to achieve time discretization. TVD technology makes the model possess a strong discontinuity wave capturing ability. Equipped with a dynamic boundary treatment technology based on unit attribution and interface attribution, the model can simulate surges and wave runups rationally which are very unsteady processes involving strong dry-wet alteration. This numerical simulation of prototype landslide reveals surged waves formation and its spreading pattern magnificently. It can be used as an effective tool for forecasting landslide-generated waves and disaster mitigation.

1 INTRODUCTION

Water waves due to landslides belong to a kind of local secondary flood disaster induced by geology debacle, which can cause more serious damage than the original landslide. After the landslide mass slips into the reservoir or river due to its instability, a great water wave appears, its spreading can worsen navigation conditions and threaten ship safety. If the landslide happens near the dam, the water waves caused by it will produce a great pushing force to the dam body in horizontal direction, which may threaten the dam body stability. When the water wave's runup height is greater than the freeboard of the dam, water will overflow the dam crest and rush into the downstream area, the safety of the dam and its downstream structures may be threatened. Therefore, the research of landslide-generated wave formation and spreading pattern can provide scientific basis for its forecast and precaution and is very important to reservoir bank protection, wave proofing project design and reservoir dispatching.

Mathematical modelling is one of the effective methods to research landslide-generated wave problems. During numerical simulation, there are still some important and difficult problems that to be solved, such as the landslide mass's sliding process, wave formation, impact wave capturing and the treatment of the dry-wet boundary.

2 MATHEMATICAL MODEL

2.1 *The basic equations*

The basic control equations are the water depth integral equations for which unit width discharge $\vec{q} = (uh, vh)$ is introduced:

$$\frac{\partial z}{\partial t} + \nabla \cdot \vec{q} = 0 \quad (1)$$

$$\frac{\partial \vec{q}}{\partial t} + \nabla \cdot \left(\frac{\vec{q}\vec{q}}{h} - \nu \nabla \vec{q} \right) = -gh(\nabla z + \vec{S}_f) \quad (2)$$

where z = water level; h = water depth; ν = coefficient of turbulence viscosity; \vec{S}_f = bottom resistance force of the channel, which can be computed by $\vec{S}_f = \vec{q}|\vec{q}|/(C^2h^3)$ (C refers to the Chezy coefficient) or $\vec{S}_f = n^2\vec{q}|\vec{q}|/h^{10/3}$ (n refers to the Manning coefficient).

Equations 1 and 2 are used for flow movement control outside the landslide mass action zone, and they can be used for flow movement control after the landslide mass stops its movement.

2.2 Some assumptions

In the ideal condition, if the landslide mass does not break up when sliding into the water, it will produce an active force to the water body through its surface only, transfer its momentum and energy to the water body and occupy the water body's position. However, in the actual condition, the landslide mass may break up, some pieces fill up the lower river bed area and stop their movement early after leaving their parent body, some pieces just mix into the water and transfer their energy to the water body directly. In addition, due to the drive of the momentum of the landslide mass, loose material in the river bed may move.

In order to deduce the control equations of the wave formation area, it is assumed that the landslide mass will keep the conservation of its volume, its thickness distribution will not change in the process of sliding, that it will not drive loose substance in the river bed and that its momentum acting on the water body will be achieved only by its surface pressure and friction force.

2.3 The control equations in wave formation area

After the landslide mass slides into water, river bed is lifted due to landslide's filling up effect, water level of local river bed rises, which causes the formation of water level gradient. Due to water body of high water level zone flowing to the surrounding area of low water level in landslide's filling up area, Equation 1 changes as follows:

$$\frac{\partial z}{\partial t} + \nabla \cdot \vec{q} = \frac{\partial z_B}{\partial t} \quad (3)$$

where z_B = river bed elevation. According to the assumptions mentioned above, the change of z_B is only caused by the filling up action of the landslide, so Equation 3 can be transformed into Equation 4:

$$\frac{\partial h}{\partial t} + \nabla \cdot \vec{q} = 0 \quad (4)$$

In addition to the landslide volume occupying the water body, its surface pressure and friction force give momentum acting on the water body. Due to the friction force between the landslide mass and the water body being far less than the surface pressure, its contribution will be neglected in the following derivation. By adding momentum source S_H into Equation 2, this equation is changed to:

$$\frac{\partial \vec{q}}{\partial t} + \nabla \cdot \left(\frac{\vec{q}\vec{q}}{h} - \nu \nabla \vec{q} \right) = -gh(\nabla z + \vec{S}_f) + \vec{S}_H \quad (5)$$

Inspecting the infinitesimal landslide slice between section a and b in Figure 1, its area is expressed as ΔA_s , its horizontal projection area is expressed as ΔA and water body mass ΔM

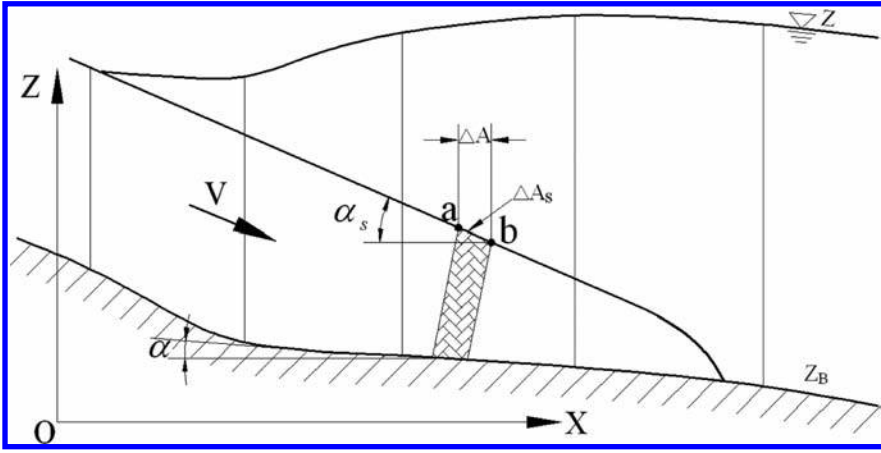


Figure 1. Landslide mass movement schematic illustration.

on its top is computed as $\Delta M = \rho h \Delta A$. Projecting the infinitesimal landslide acting on the infinitesimal water body to the horizontal plane, expressed as $\Delta \vec{F} = (F_x, F_y)$, the following equation can be established:

$$\vec{S}_H = h \frac{\Delta \vec{F}}{\Delta M} = \frac{\Delta \vec{F}}{\rho \Delta A} \quad (6)$$

For simplicity and convenience, inspecting the component in some direction, the projection of $\Delta \vec{F}$ is ΔF , the projection of \vec{S}_H is S_H , the landslide's velocity component in horizontal direction is assumed as V_s and the angle of the sliding plane is expressed as α , as shown in Figure 1. Using ΔA_N to represent the projected area of the infinitesimal landslide area ΔA_s perpendicular to the sliding direction, the corresponding coefficient of form resistance force is expressed as C_D , the following relationship can be established in sliding direction:

$$\frac{\Delta F}{\cos \alpha} = C_D \rho \left(\frac{V_s}{\cos \alpha} \right)^2 \Delta A_N \quad (7)$$

The surface angle of infinitesimal landslide is expressed as α_s ,

$$\Delta A = \Delta A_S \cos(\alpha_S); \quad \Delta A_N = \Delta A_S \sin(\alpha_S - \alpha) \quad (8)$$

Equations 7 and 8 can be substituted into Equation 6.

$$S_H = C_D \frac{V_s^2 \sin(\alpha_S - \alpha)}{\cos \alpha \cos(\alpha_S)} = C_D V_s^2 (\tan \alpha_S - \tan \alpha) \quad (9)$$

Using α_v to represent the angle between the sliding direction's horizontal projection and x direction, based on Equation 9, the following equations can be established:

$$S_{Hx} = C_D (V_s \cos \alpha_v)^2 (\tan \alpha_{Sx} - \tan \alpha_x) \quad (10)$$

$$S_{Hy} = C_D (V_s \sin \alpha_v)^2 (\tan \alpha_{Sy} - \tan \alpha_y) \quad (11)$$

If original river bed elevation is expressed as z_{B0} , and the elevation of river bed filled up by the landslide is expressed as z_B , Equations 10 and 11 are changed as follows:

$$S_{Hx} = C_D (V_S \cos \alpha_V)^2 \left(\frac{\partial z_B}{\partial x} - \frac{\partial z_{B0}}{\partial x} \right) \quad (12)$$

$$S_{Hy} = C_D (V_S \sin \alpha_V)^2 \left(\frac{\partial z_B}{\partial y} - \frac{\partial z_{B0}}{\partial y} \right) \quad (13)$$

Finally, Equations 4, 5, 12 and 13 are used as the control equations of flow movement in the landslide affected area.

2.4 Solution method

The basic control equations and the control equations of flow movement in the landslide acting area can be integrated to the following conservation form.

$$\frac{\partial U}{\partial t} + \nabla \cdot F(U) + \nabla \cdot T(U) = S(U) \quad (14)$$

where U = conservation variable, $U = (h, hu, hv)$; F = convection subitem; T = diffusion subitem.

The computation area is divided into anomalistic quadrangular meshes, the finite volume method is adopted to make control equations discrete in space, the improved MacCormack prediction-correction format is adopted to achieve time discretization, the obtained solutions of predicting step and correcting step are as follows:

$$U^p(t + \Delta t) = U(t) - \frac{\Delta t}{\Delta V} \left(\sum_{k=1}^4 F \cdot A + \sum_{k=1}^4 T \cdot A \right) + \Delta t S(t + \Delta t) \quad (15)$$

$$U^c(t + \Delta t) = U(t) - \frac{\Delta t}{\Delta V} \left(\sum_{k=1}^4 F^p \cdot A + \sum_{k=1}^4 T^p \cdot A \right) + \Delta t S^p(t + \Delta t) \quad (16)$$

$$U(t + \Delta t) = \frac{1}{2} [U^p(t + \Delta t) + U^c(t + \Delta t)] \quad (17)$$

where p = predicting step; c = correcting step; F = interface flux; A = interface area; Δt = time step; ΔV = the control body's volume.

In the process of obtaining the flux of the convection subitem, in order to assure the symmetry of forward and backward difference in two directions, the cycle period adopts 4 steps, the predicting and correcting steps adopt forward and backward difference alternately. In the process of obtaining the flux of the diffusion subitem, in order to assure the computation's rationality and anti-interference, the velocity gradient and water level gradient are obtained by integral averaging the interlaced meshes of a single direction.

Due to unsteady flow and greater water level gradient, it is necessary to introduce a greater numerical viscosity to keep the format's numerical stability. But increased numerical viscosity will result in a weakened wave peak value and bring a negative effect on simulating precision. In order to increase computational stability and wave simulating precision, an impact wave capturing format is introduced. Such formats as TVD, ENO, AUSM etc. are applied widely. In this article, a second-order upwind TVD scheme is introduced to make flux revision to correcting step, which was originally developed by Harten and later modified

and generalized by Yee (Yee, H.C. 1985–2008). So Equation 16 is changed to Equation 18 as follows:

$$U^c(t + \Delta t) = U(t) - \frac{\Delta t}{\Delta V} \left(\sum_{k=1}^4 F^p \cdot A + \sum_{k=1}^4 T^p \cdot A + \sum_{k=1}^4 D^p \cdot A \right) + \Delta t S^p(t + \Delta t) \quad (18)$$

$$D_{k+1/2}^p = R_{k+1/2}^p \Phi_{k+1/2}^p \quad (19)$$

where $R_{k+1/2}$ = right characteristics vector matrix; $\Phi_{k+1/2}$ = dissipation column vector, its single element $\phi_{k+1/2}$ is defined as follows:

$$\phi_{k+1/2} = \frac{1}{2} \psi(a_{k+1})(g_{k+1} + g_k) - \psi(a_{k+1/2} + \gamma_{k+1/2}) \alpha_{k+1/2} \quad (20a)$$

where $a_{k+1/2}$ = right characteristics value; $\alpha_{k+1/2}$ = characteristics column vector. The function ψ is an entropy correction to $a_{k+1/2}$. One possible form is

$$\psi(a_{k+1}) = \begin{cases} |a_{k+1}|, & |a_{k+1}| \geq \delta, \\ [(a_{k+1})^2 + \delta^2]/2\delta, & |a_{k+1}| < \delta. \end{cases} \quad (20b)$$

In this equation, δ is an infinitesimal positive number. In Equation 20a, $\gamma_{k+1/2}$ can be expressed as follows:

$$\gamma_{k+1/2} = \begin{cases} \frac{1}{2} \psi(a_{k+1})(g_{k+1} - g_k) / \alpha_{k+1/2}, & \alpha_{k+1/2} \neq 0, \\ 0, & \alpha_{k+1/2} = 0. \end{cases} \quad (20c)$$

In Equations 20a and 20c, restriction function g_k adopts min mod limiter:

$$g_k = \min \text{mod} \left[2\alpha_{k-1/2}, 2\alpha_{k+1/2}, \frac{1}{2}(\alpha_{k-1/2} + \alpha_{k+1/2}) \right] \quad (20d)$$

2.5 Dry-wet boundary

In the process of water wave formation and its spreading, the wave will make the dry-wet boundary of the shallow water zone near the river bank change vigorously. In order to simulate the wave formation and wave runoff process reasonably, according to the numerical solution adopted in this article, a moving boundary treatment technique is developed, which is based on unit attribute and interface attribute.

Defining two water depth threshold values H_{dry} and H_{wet} , by comparing the unit depth of both sides of the target interface with the water depth threshold values, considering the relationship between unit water level and unit bed elevation of both interface sides, according to the principle of preventing water to flow into an adjacent dry unit (its bed elevation is higher than the target unit's water level), the interface attribute can be defined as 0 and 1, 1 representing that flow can pass, 0 representing that flow passing is not allowed.

Considering the relationship between water depth of target unit and water depth threshold values, considering every interface attribute, the unit can be defined as 3 kinds, namely marked as 0, 1 and 2. The units marked as 1 will not be computed. For the units marked as 2, only mass flux is computed. For the units marked as 0, mass flux and momentum flux are computed.

3 MODEL TEST

A river course of about 4 km length is chosen for mathematical model testing, with a landslide mass located on its right bank. A landslide mass of regular shape is adopted, a few measuring points are installed to monitor wave formation in the river course and on the river bank, as shown in Figure 2.

The landslide mass is 120 m long, 80 m wide and 40 m thick, the slide face angle is 35° and water level is 180 m. The river bed elevation is about 20 m where the landslide mass slides into water. The landslide mass's sliding velocity is 20 m/s and its sliding process lasts 17 s.

The wave formation processes obtained from the measuring points are shown in Figure 3. The water surface changes at particular times are shown in Figure 4.

According to Figures 3 and 4, after the landslide mass slides into water, it pushes away the water body, occupies its position to form the first wave and the ring-shaped wave marches

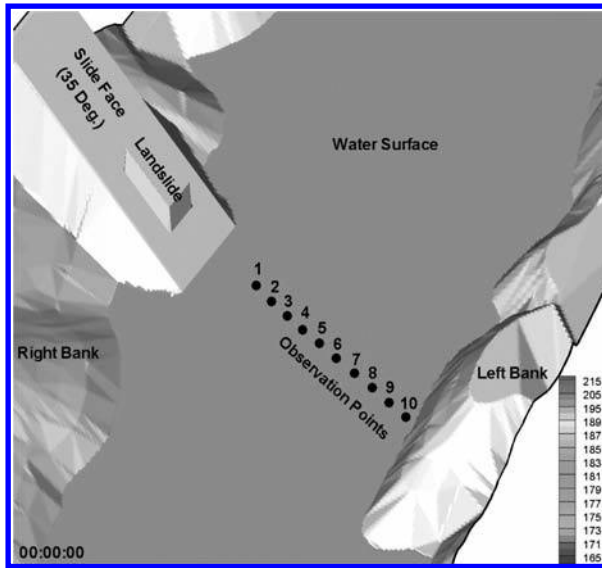


Figure 2. Model arrangement drawing.

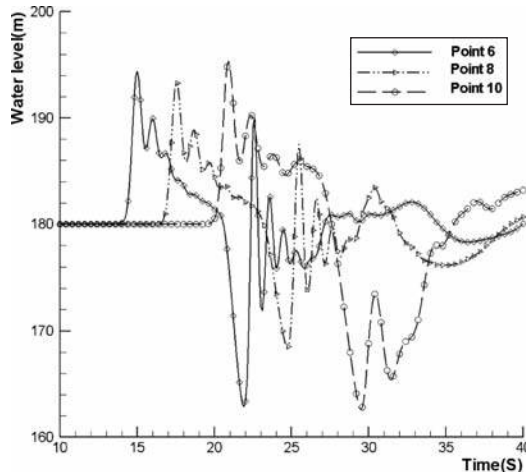


Figure 3. Wave formation process.

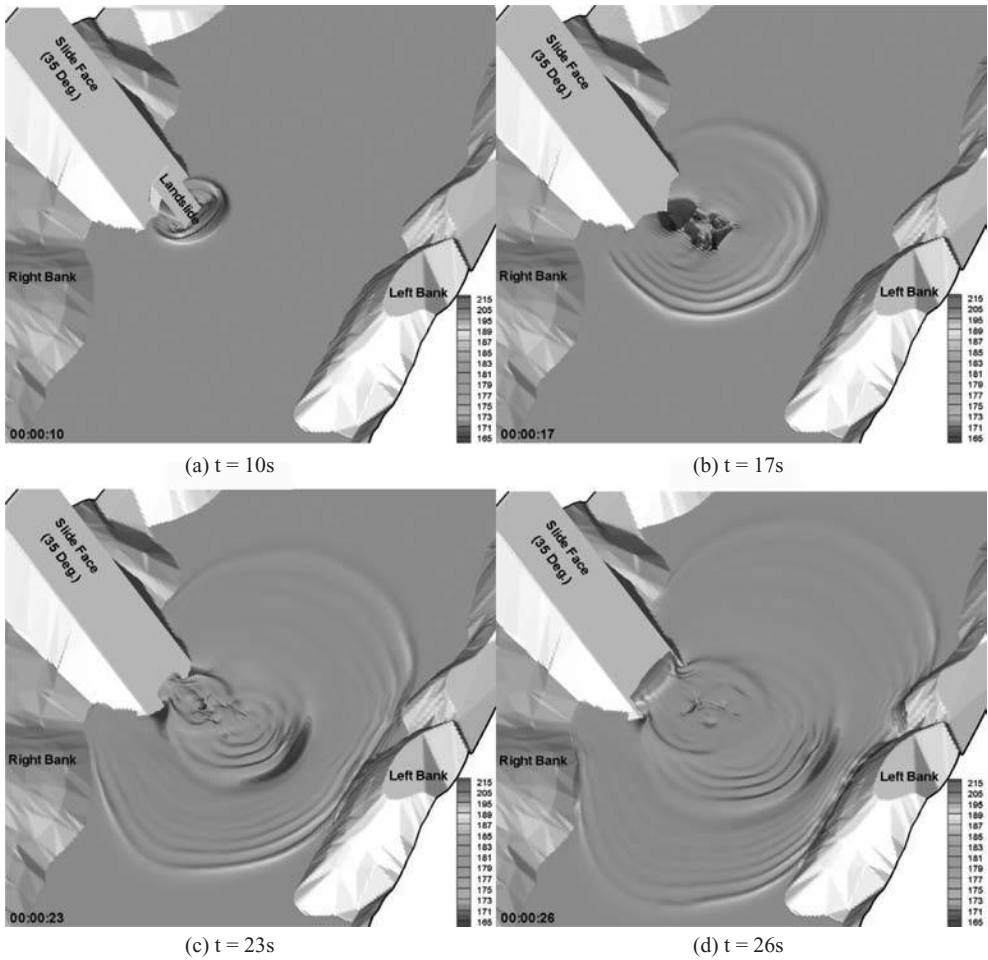


Figure 4. Water surface changes at particular times.

around (Fig. 4a). After the landslide mass stops its movement, the local water surface caves in (Fig. 4b), the surrounding water bodies flow into and collide with each other to form the second wave, which runs up on the slope of the slide (Figs. 4c, d). In the mean time, the first wave arrives at the opposite bank and climbs up the bank slope. According to Figure 3, the wave height decreases gradually in its spreading to the opposite bank process. When the wave arrives at the measuring point on the bank side (Point 10), its height increases a little due to bank slope effect.

4 CONCLUSIONS

The preliminary test result indicates that the mathematical model introduced in this article simulates the landslide-generated wave formation and wave spreading process rationally, and reveals the wave formation mechanism. The model shows good discontinuity wave capturing ability, shows good simulation ability of shallow water zone which is near bank and involves violent dry-wet changes. It can be used as an important tool for landslide-generated wave forecast.

The next work in this research is to improve the mathematical model according to the physics model test result, so as to increase its precision and reliability.

REFERENCES

- Prestininzi, Pietro. 2008. Suitability of the diffusive model for dam break simulation: Application to a CADAM experiment. *Journal of Hydrology* 361(1–2):172–185.
- Tseng, Ming Hseng. 2004. Improved treatment of source terms in TVD scheme for shallow water equations. *Advances in Water Resources* 27(6):617–629.
- Tseng, Ming Hseng. 2000. The simulation of dam-break flows by an improved predictor–corrector TVD scheme. *Advances in Water Resources* 23(6):637–643.
- Vimmr, Jan. 2007. Modelling of complex clearance flow in screw-type machines. *Mathematics and Computers in Simulation* 76(1–3):229–236.
- Yee, H.C. 2000. Entropy splitting and numerical dissipation. *Journal of Computational Physics* 162(1):33–81.
- Yee, H.C. 1997. Explicit and implicit multidimensional compact high-resolution shock-capturing methods: Formulation. *Journal of Computational Physics* 131(1):216–232.
- Yee, H.C. 1985. Implicit total variation diminishing (TVD) schemes for steady-state calculations. *Computational Physics* 57(3):327–360.
- Yee, H.C. 1999. Low-dissipative high-order shock-capturing methods using characteristic-based filters. *Journal of Computational Physics* 150(1):199–238.
- Yee, H.C. & Sjögren, B. 2008. Adaptive filtering and limiting in compact high order methods for multiscale gas dynamics and MHD systems. *Computers & Fluids* 37(5):593–619.
- Yee, H.C. & Sjögren, B. 2007. Development of low dissipative high order filter schemes for multiscale Navier–Stokes/MHD systems. *Journal of Computational Physics* 225(1):910–934.

Hazard and risk assessment of rock slide tsunamis in lakes and reservoirs

C. Harbitz, F. Løvholt, U. Domaas & S. Glimsdal

NGI, Oslo, Norway

B. Romstad

Cicero Centre for Climate Research, Oslo, Norway

ABSTRACT: Tsunamis generated by rock slide impact in reservoirs and lakes constitute a serious threat, as exemplified by the disastrous 1963 Vaiont dam event in Italy and the 1905 and 1936 Loen events in Western Norway, causing altogether more than 2000 fatalities. This paper gives a brief overview of different methodologies for the quantification of the tsunami hazard and risk, exemplified by tsunami hazard assessments in Norway. The first part of the paper presents a regional evaluation of rock slide tsunami hazard applied on a nationwide scale to Norwegian lakes as a first phase screening study. The analysis results in a potential score that indicates the relative hazard in each lake, enabling the possibility of distinguishing between lakes with high and low hazards. The method is implemented in a GIS tool, and the results reveal a clustering of exposed lakes in parts of Western Norway as well as some locations in Northern Norway. The method is also capable of producing more detailed local hazard maps that may be useful for field campaigns or for designing scenarios for numerical simulations of tsunamis in a given lake or reservoir. It should be emphasized that the rock slide potential reported for each lake is based on the topographical setting alone and hence, does not represent the actual probability of rock slides into the lakes. For a given area, more detailed investigations of the geology, triggering factors, and frequency of previous rock slide events should be carried out before definite statements about the actual hazard can be made. The second part of this paper demonstrates tsunami generation, propagation, and run-up from laboratory tests and numerical simulations. Finally, numerical simulations of tsunami generation, propagation, and run-up should be applied in order to quantify dam overtopping if unstable rock masses are proven tsunamigenic.

1 INTRODUCTION

Rockslides plunging into lakes, reservoirs, or fjords can generate huge, destructive waves. Such waves may endanger reservoirs due to the potential overtopping of the dam crest, and cause floods in the down stream valley. Norway is a mountainous country with a record of devastating rock slide tsunamis impacting its many fjords and lakes that goes back many centuries. This is demonstrated further by the fact that Norway comprises more than 200,000 lakes and 25,000 km of coastline (numbers based on 1:50,000 digital maps). While the need for managing the risk towards this tsunami threat is obvious, it seems equally clear that the topographic extent of the problem necessitates a simple procedure (i.e. covering an area and a number of lakes that are too large to be analyzed by e.g. numerical simulations). To this end, this paper presents a method towards regional hazard mapping of rock slide tsunamis in reservoirs.

Examples of well documented events are the 1905 and 1936 Lake Loen events (Jørstad, 1968; Furseth, 2006) and the 1934 Tafjord event in Norway (Harbitz et al., 1993), the 1958 Lituya Bay event in Alaska (Miller, 1960), as well as the disastrous 1963 Vaiont dam catastrophe

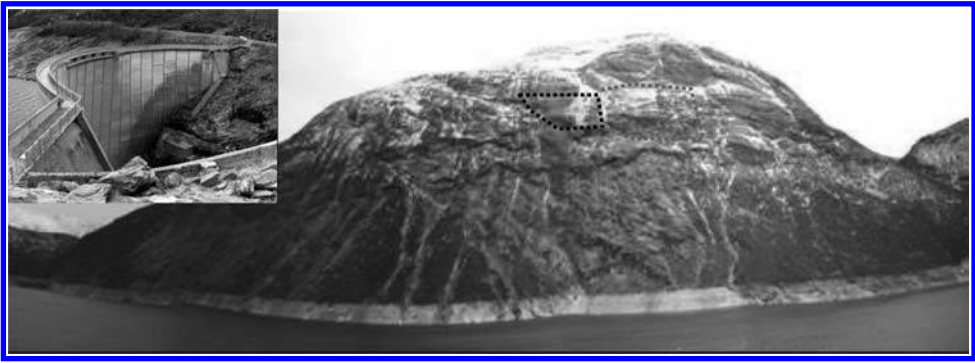


Figure 1. The rock slope to the north of Lake Zakariasvatnet, Norddal, western Norway. Possible rock slides identified. The dam (inserted) is located in the leftmost part of the picture (from NGI, 2004).

in Italy (Kiersch, 1964; Müller, 1964, 1968). Maximum run-up heights for these events were between 40 and 500 m. The present risk related to rock slide tsunamis is probably increasing as a result of more human activity and presence in mountain regions, an increasing number of hydropower reservoirs (see Fig. 1), and a higher population density along the fjords. It is further expected that possible future climate changes with corresponding changes in temperature and precipitation will increase the rock slide frequency.

The first and main part of this paper is the description of the method for regional hazard mapping in Section 2. The method is implemented in a GIS framework, developed and applied to assess the topographical potential of tsunami generating rock slides in all Norwegian lakes and reservoirs. It is further revealed how the method may be used for more detailed analysis around a given lake (or fjord).

The second part of the paper deals with numerical simulations of rock slide tsunamis in reservoirs and is given in Section 3. Finally, a short review of computational methods for dam overtopping is briefly described.

2 GIS METHODOLOGY TO IDENTIFY LAKES AT RISK

2.1 *Regional assessment of the potential for tsunami generating rock slides*

Rock slope release depends on conditions such as geological, geotechnical, and hydrological properties along with triggering factors such as climatic conditions or earthquakes. In order to assess the hazard from rock slides it may be appealing to apply physically based models to predict slope instability and travel distance. However, if the area of analysis is a large region such models are often not applicable, mainly because they require data that are not available on a suitable scale. The availability of intermediate to high resolution Digital Elevation Models (DEMs) is the fortunate exception from this situation. Such DEMs contain detailed information about the topography, which controls both rock slide release and dynamics. Basically, rock slides can only be released when the local slope is steep enough, and the path of a rock slide is mainly governed by the underlying topography. Romstad et al. (2009) utilized these facts in a simple method for simultaneous quantification of the topographic potential of tsunami generating rock slides around a large number of lakes. The method requires only a DEM of intermediate resolution (10–30 m cell size) and a map of lakes as input data.

The run-out ratio of a rock slide is defined as the height difference (H) divided by the horizontal distance (L) between crown and toe. The general idea of the methodology is to analyze the topographic position of potential rock slide release areas relative to the lakes. When solely considering the topography it is assumed that rock slides released from areas that have a large run-out ratio relative to the lake have a higher probability of reaching the lake and create a tsunami than rock slides released from areas with a smaller run-out ratio.

In the absence of any further information relevant for rock slope failure than the surface topography it is assumed that the probability of rock slide release is equal for all cells where the local slope is above a given threshold (e.g. 30°). Several studies have shown that the magnitude frequency distribution of rock slide events follows a power law distribution (e.g. Guzzetti et al., 2002; Hergarten, 2003; Hergarten, 2004; Malamud et al., 2004). This can be applied to make the assumption that for any of the potential release cells the probability of a given volume, V , is:

$$P(V) = V^{-\beta} \quad (1)$$

where the exponent β is typically in the range 0.5 ± 0.2 on a 10^{-3} m^3 to 10^{10} m^3 volume range (Dussauge et al., 2003).

For rock slides with a volume smaller than about 10^5 m^3 the run-out ratio (H/L) is governed by the dry friction. Hence, the maximum run-out angle of the slide is restricted by the friction angle of the material in question (usually around 30°–40°) and is not dependent on volume (e.g. Scheidegger, 1973; Hsü, 1975; McEwen, 1989; Legros, 2002). However, for larger slide volumes the run-out angle may become smaller as the volume increases. Empirically it has been shown that there is a fairly robust statistical relationship between rock slide volume (V) and rock slide mobility (H/L), as suggested by Scheidegger (1973):

$$\log_{10} \frac{H}{L} = a \log_{10} V + b \quad (2)$$

where V is in m^3 and the constants a and b are set to -0.157 and 0.624 , respectively. Equation 2 can be rearranged to solve for volume:

$$V_{\min} = \left(\frac{H}{10^b L} \right)^{\frac{1}{a}} \quad (3)$$

This relationship can be used to define the minimum required volume, V_{\min} , for a rock slide released at any cell in order to reach a given lake. If the angle between the release cell and its candidate lake is steeper than the friction angle, any slide may reach the lake regardless of volume. For smaller run-out angles only slides larger than V_{\min} will be mobile enough to reach the lake.

The topographic potential for a rock slide released at any given cell and reaching a lake is termed the Topographic Tsunami Generating Potential (TTGP), which is estimated by substituting the volume V in Equation 1 with Equation 3. Since Equation 3 is invalid when the run-out ratio H/L corresponds to a run-out angle steeper than the internal friction angle it will overestimate the minimum required volume in these areas. Consequently the TTGP will be underestimated if Equation 3 is used unmodified. In addition the minimum required volume, V_{\min} , should be constrained downwards by a minimum damaging volume, V_d , which is here the minimum volume required for a rock slide to create a destructive tsunami. Hence, TTGP is defined as:

$$TTGP = \begin{cases} \max(V_{\min}, V_d)^{-\beta} V_d^{\beta}, & \frac{H}{L} < f \\ V_d^{-\beta} V_d^{\beta}, & \frac{H}{L} \geq f \end{cases} \quad (4)$$

When H/L is smaller than the internal friction angle, f , TTGP is obtained by applying Equation 1 to the maximum of V_{\min} and V_d and then normalizing it so that TTGP has a maximum value of 1.0 where V_{\min} equals V_d . When H/L is larger than or equal to f , V_d should replace V_{\min} with TTGP will always be 1.0. A friction angle, f , of 0.7 (about 35°) was applied.

V_d was set to a conservative estimate of 5000 m³ and β , the parameter that controls the slope of the expected magnitude–frequency distribution, was set to 0.7, which is in the upper range of reported values for rock falls and in the lower range of reported values for mixed landslide types (Dussauge et al., 2003; Hergarten, 2003).

For any given lake a score value can be calculated that indicates how favorable the topographical setting of the lake is for tsunami generating rock slides. This score value is termed the Topographic Rock Slide Potential (TRSP) and is calculated adding the TTGP values computed for all steep cells (>30°) in the catchment area of the lake. When applied to a larger region the final output of the analysis is thus a list of TRSP scores for all lakes in the study region. The list indicates the hazard in each lake relative to the other lakes and it can be used as it is, or be manipulated further and presented e.g. as in Figure 2.

It is important to keep in mind that the method implicitly assumes equal conditions of all geological and triggering factors for the whole study area, which is of course a gross simplification. Due to the large variability in observed maximum rock slide velocities, and the corresponding uncertainties in rock slide impact velocities, it is simply assumed that every slide that reaches the shore line with a volume larger than the required minimum will also have an impact velocity large enough to generate a tsunami. This is a conservative assumption, not excluding any potential tsunami generating rock slide due to low velocity. In an enclosed water body such as a lake, a reservoir, or a fjord, even quite small rock slide volumes may cause devastating tsunamis, thus the relatively low estimate of 5000 m³ was used as the minimum damaging volume V_d . Obviously, a large tsunami may be more destructive than a smaller one, but this is not taken into account in this analysis.

2.2 Local assessment of an individual lake

The method developed by Romstad et al. (2009) may also be used to produce more detailed maps of the potential release areas around individual lakes (or fjord sections) where the volume required in order to reach the lake (fjord) from any location is indicated (Fig. 3). For lakes that are given preference for further investigations, such maps may serve as a guide when carrying out field campaigns to establish the likelihood of the required volumes based on geological/geotechnical criteria for release (see e.g. Harbitz et al., 2010), and when designing rock slide scenarios as input to numerical simulations of the resulting tsunamis.

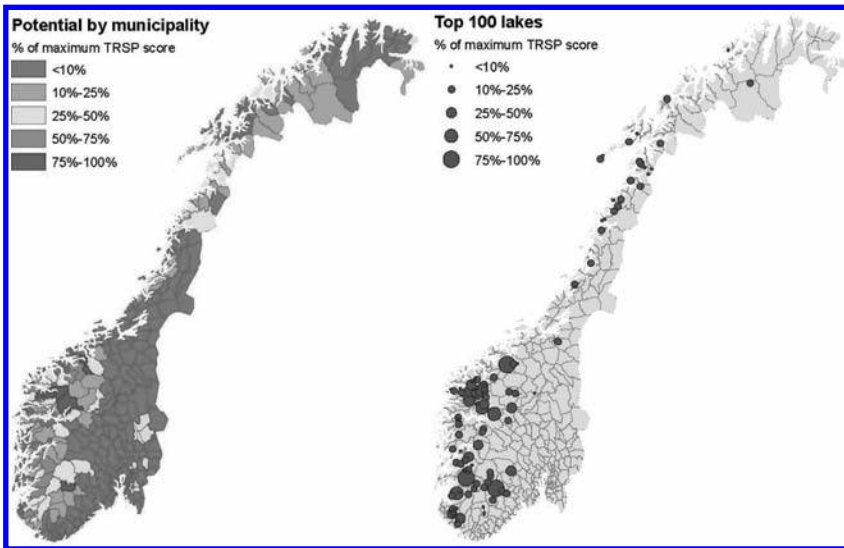


Figure 2. Geographical distribution of rock slide potential within municipalities (left) and the 100 lakes with highest rock slide potential (right). The potential is expressed in percent of the maximum value for both maps.

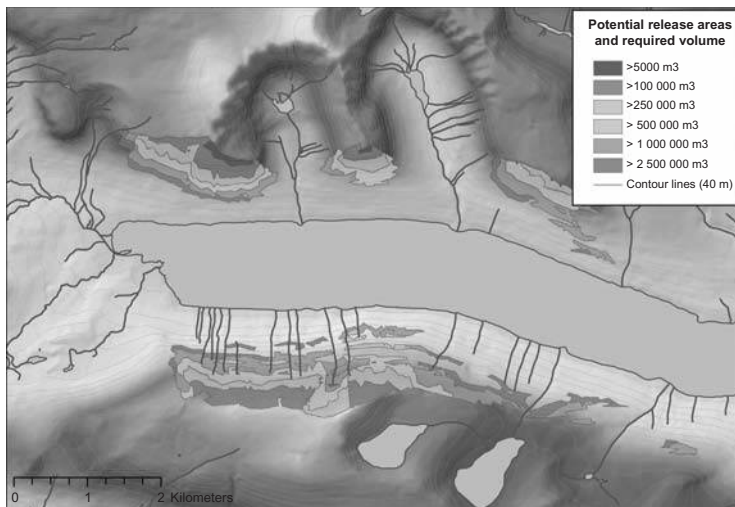


Figure 3. Gjevilvatnet in Oppdal, Norway. The figure shows areas with a slope steeper than 30 degrees (potential release areas) and the minimum volume required for slides to reach the lake.

2.3 Prospects of the method

The advantage of this method is that it requires a minimum of data and that it can be applied over large areas. The model has only a few parameters that do not require expert knowledge to adjust. It is emphasized that the result reveals only what areas are safe and what areas should be investigated further, rather than what areas are hazardous. Altogether this makes the model a convenient tool for focusing further research as well as for authorities and decision makers who need an overview of the hazard situation in an area before resources are allocated to specific tasks. The topographically most critical areas can be highlighted and subsequently be combined with expert knowledge about the geological situation, previous rock slide activity in the area, etc.

In spite of its limitations, it is possible already today to perform regional/national analyses and produce precautionary maps for rock slide tsunamis in lakes, reservoirs, and fjords with the existing tool. The method should preferably be developed further to reduce the number of exposed/critical areas by implementing simple geological criteria and rough estimates of run-up heights (based on volume of rock slide volume, configuration and size of water body), and by including maps of exposed objects and population (i.e. exclude areas with low vulnerability and risk).

2.4 Possibilities to combine with risk models

It is possible to combine the GIS method described above with tools for local tsunami vulnerability and risk assessment that enable more detailed mapping of the elements at risk (population, buildings, infrastructure, etc.). Run-up simulations may be applied for a more accurate description of the flow field and the inundated area, i.e. the hazard. The following examples illustrate alternative approaches.

Eidsvig et al. (2009) apply a simple and practical method for estimating the risk due to a potential tsunamigenic rock slide at Aknes, western Norway, by assessing quantitatively hazard, vulnerability, and elements at risk. The proposed method introduces empirical relations between the risk components and illustrates the uncertainty propagation through the steps in the risk analysis. The risk assessment considered two hazard conditions: One based on historical data, and another based on the expert's beliefs for the slope stability (site dependent).

Eidsvig and Medina-Cetina (2008) followed an approach based on Bayesian Network which incorporates causal effects. An important feature of the Bayesian Network approach

is the capacity to back-propagate evidence to generate a diagnosis based on current evidence. Diagnosis analysis results for prescribed risks could be a useful tool during operation of an early warning system.

Lacasse et al. (2008) describe risk assessment by event tree analysis. This approach is especially useful for geotechnical problems that involve large uncertainties. The probability of occurrence and the risk were obtained through a consolidation of all the branches of the event tree.

NGI (2009) combines a manifold of methods, including structural vulnerability, population exposure, and mortality, as well as the framework to combine these elements. For simplicity, NGI (2009) represents the tsunami hazard for a given scenario with a corresponding return period by the flow depth during inundation rather than other tsunami metrics such as the momentum flux (normally considered the best “damage indicator”). With respect to structural vulnerability, the model operates with building scores (based on height, barrier, material, and use) according to their ability to withstand wave load and to protect people.

3 NUMERICAL MODELLING OF ROCK SLIDE TSUNAMIS AND DAM OVERTOPPING

3.1 *Numerical modeling*

Tsunami modelling can be split into three stages: generation, propagation, and inundation. For the generation, it is critical whether the rock slide reaches the lake (or fjord) as one block or as a series of minor (retrogressive) events. The physical dimensions of the rock slide (especially the cross sectional frontal area) is the most important parameter, but the permeability, the impact velocity, the velocity progression, and the run-out distance of the rock slide as well as the water depth also play a role for the height and the shape of the initial wave.

Rock slide tsunamis plunging into hydropower reservoirs, lakes, or fjords are mostly huge and destructive as the rock slides are most often super-critical (i.e. the slide speed-to-the wave celerity-ratio, the Froude number, is larger than unity at impact). The build-up of the wave persists as long as the rock slide motion is still near critical (i.e. the Froude number is close to unity).

A simple way to model the generation is to define the rock slide as a rounded box with prescribed dimensions; more advanced methods comprises numerical modeling resulting in deformable slide bodies fed directly into the model. To determine the run-out distance the H/L ratios (see above) may be applied. The velocity progression fitting the prescribed run-out may be found through an energy-line approach, or determined through numerical rock slide (block) models.

Rock slide tsunamis are often too short or too high to be modeled by the standard Linear Shallow Water (LSW) approximation; i.e. they may be influenced by non-linear effects such as steepening and breaking, as well as by frequency dispersion. To include the effects of dispersion and non-linearity, models based on the Boussinesq equations are applied (Løvholt et al., 2008; Løvholt et al., 2010). For the process of tsunami inundation, non-linear shallow water models incorporating bore capturing are best suited, as elaborated in Section 3.2. Generally, the inundation process exhibits large local variations of the maximum inundation height (and the maximum current velocity). The topography may guide, channelize, and focus the wave leading to higher current velocities, increased loads, and stronger erosion e.g. in (narrow) river valleys. Such effects are important to take into account when designing physical mitigation measures.

3.2 *Dam overtopping*

In many cases, dam overtopping, possible dam break, and subsequent downstream flooding may constitute the largest tsunami risk for a reservoir. The well known and devastating example of the Vaiont rock slide (Müller, 1964) demonstrates this. Analyses of the dam overtopping prior to the downstream flooding, largely resembles any inundation process

and may be analyzed with conventional numerical tools for computing tsunami inundation. Previous studies of rock slide tsunami final run-up often comprise empirical formulas from general numerical simulations or laboratory experiments, e.g. Osavatnet (NGI, 1999), Mysevatnet (NGI, 2003), and Zakariasvatnet (NGI, 2004, see Fig. 1). However, a difference from the randomly shaped terrain encountered in nature, is the relatively simple geometry constituting the dam and the fact that overtopping will not cause any backwash.

Wave run-up and overtopping of dams by impact generated waves has been thoroughly investigated by Müller (1995). Although his work concerning tsunamis still lacks confirmation by other authors, the process of run-up and overtopping by ordinary waves has been studied by numerous authors and is thought to be well understood. A model study should therefore concentrate on examining different design strategies for embankment dams with special focus on the stability of the downstream slope and thus the whole dam. Different parameters could be investigated, including the shape of the wave as it passes the crest; the overtopping volume; the dam geometry (e.g. the upstream and downstream slope and the crest length); as well as the size, shape, amount, and riprap pattern of protective stones.

Although there are fewer examples from literature, recent developments of numerical inundation models have simplified the procedure for computing dam overtopping numerically. The tsunami inundation may be computed by nesting it with a numerical wave propagation model, e.g. given as forced input along the boundary for a non-linear inundation model (e.g. ComMIT, 2010). Close to the dam, the tsunami may also be focused due to bathymetric/topographic effects and amplified due to shoaling, leading to wave steepening and possible wave breaking. It is emphasised that standard inundation models like ComMIT (2010) are less suited for modeling the subsequent downstream inundation, where other models must be used.

4 CONCLUDING REMARKS

Quantification of rock slide tsunami hazard and risk in lakes and reservoirs is a complex problem. A multi-disciplinary approach is presented including: 1) a GIS tsunami hazard analysis for identification of endangered lakes, hydropower reservoirs, and fjords; 2) geological, geotechnical, and geophysical investigations to study rock slope stability, triggering factors, and probability of release (see e.g. Harbitz et al., 2010); 3) numerical simulations of rock slide, wave dynamics, and overtopping; and 4) methodologies to assess fatal consequences or mortality risk.

A proper quantitative description of rock slides and their tsunami generation requires general hydrodynamic computational tools, like Navier–Stokes type models, with modified rheology for the rock slide masses. Today, three-dimensional models of this kind are so computationally demanding that simulations with sufficient resolution are difficult to perform.

ACKNOWLEDGEMENTS

The authors are indebted to Unni Eidsvig for contributions to the described work on rock slide tsunami risk models. We acknowledge financial contributions to this paper from the International Centre for Geohazards (ICG), the Norwegian Geotechnical Institute (NGI), and the Research Council of Norway (NFR). This is contribution no. 332 of the International Centre for Geohazards.

REFERENCES

- ComMIT, 2010. ComMIT package. URL: <http://nctr.pmel.noaa.gov/ComMIT/>.
- Dussauge, C., Grasso, J.R., & Helmstetter, A.S. 2003. Statistical analysis of rockfall volume distributions: Implications for rockfall dynamics. *Journal of Geophysical Research-Solid Earth*, 108: 2286.
- Eidsvig, U., & Medina-Cetina, Z. 2008. Quantitative Risk Assessment for Tsunamigenic Rock slides: The Aknes Case Study. *ICG report 2006-2-3 for the EU project IRASMOS*.

- Eidsvig, U., Medina-Cetina, Z., Kveldsvik, V., Glimsdal, S., Harbitz, C.B., & Sandersen, F. 2009. Risk Assessment of a Tsunamiogenic Rockslide at Aaknes, *Natural Hazards*, 10.1007/s11069-009-9460-6.
- Furseth, A. 2006. Skredulykker i Norge—En historisk dokumentar om de mest alvorlige leirskred, snøskred og fjellskred som har rammet oss de siste 500 år (in Norwegian). *Tun Forlag AS*. ISBN(10): 82-529-3043-3, ISBN(13): 978-82-529-3043-6.
- Guzzetti, F., Malamud, B.D., Turcotte, D.L., & Reichenbach, P. 2002. Power-law correlations of landslide areas in central Italy. *Earth and Planetary Science Letters*, 195(3–4): 169–183.
- Harbitz, C., Pedersen, G., & Gjevik, B. 1993. Numerical simulations of large water waves due to landslides. *Journal of Hydraulic Engineering*, 119: 1325–1342.
- Harbitz, C.B., Romstad, B., Glimsdal, S., Domaas, U., & Løvholt, F. (2010). Hazard and risk assessment of rock slide tsunamis in lakes and fjords. *Proceedings of the International Conference Mountain Risks: Bringing Science to Society*, 24–26 November 2010, Firenze, Italy.
- Hergarten, S. 2003. Landslides, sandpiles, and self-organized criticality. *Natural Hazards and Earth System Sciences*, 3(6): 505–514.
- Hergarten, S. 2004. Aspects of risk assessment in power-law distributed natural hazards. *Natural Hazards and Earth System Sciences*, 4(2): 309–313.
- Hsü, K.J. 1975. Catastrophic Debris Streams (Sturzstroms) Generated by Rockfalls. *Geological Society of America Bulletin*, 86(1): 129–140.
- Jørstad, F.A. 1968. Waves generated by landslides in Norwegian fjords and lakes. *Norwegian Geotechnical Institute Publ.* 79.
- Kiersch, G.A. 1964. Vaiont reservoir disaster. *Civil Engineering*, 34: 32–39.
- Lacasse, S., Eidsvig, U., Nadim, F., Høeg, K., & Blikra, L.H. 2008. Event tree analysis of Aknes rock slide hazard. *4th Canadian Conference on Geohazards*, Quebec Canada, May 2008.
- Legros, F. 2002. The mobility of long-runout landslides. *Engineering Geology*, 63(3–4): 301–331.
- Løvholt, F., Pedersen, G., & Gislser, G. 2008. Oceanic propagation of a potential tsunami from the La Palma Island. *Journal of Geophysical Research—Oceans*, 113: C09026.
- Løvholt, F., Pedersen, G., & Glimsdal, S. 2010. Coupling of dispersive tsunami propagation and shallow water coastal response. In Zahibo, N., Pelinovsky, E., Yalciner, A., & Titov, V. (eds.). *Proceedings of the “Caribbean Waves 2008” workshop in Guadeloupe Dec. 2008*. The Open Oceanography Journal special volume.
- Malamud, B.D., Turcotte, D.L., Guzzetti, F., & Reichenbach, P. 2004. Landslide inventories and their statistical properties. *Earth Surface Processes and Landforms*, 29(6): 687–711.
- McEwen, A.S. 1989. Mobility of Large Rock Avalanches—Evidence from Valles Marineris, *Marine Geology*, 17(12): 1111–1114.
- Miller, D.J. 1960. Giant waves in Lituya Bay, Alaska. *Prof. Paper 354-C, U.S. Geological Survey*, 51–84.
- Müller, L. 1964. The rock slide in the Vaiont Valley. *Rock Mechanics and Engineering Geology*, 2: 148–212.
- Müller, L. 1968. New considerations on the Vaiont slide. *Rock Mechanics and Engineering Geology*, 6: 1–91.
- Müller, D.R. 1995. Auflaufen und Überschwappen von Impulswellen an Talsperren (Run-up and overtopping of impulse waves at dams). *Dissertation 11113. Eidg. Technische Hochschule ETH, Zürich* (in German).
- NGI 1999. Osavatnet, Osterøy—Vurdering av skredfare og flodbølger. *NGI report 994090-1* (in Norwegian).
- NGI 2003. Mysevatnet, Kvinnherad—Flodbølger etter fjellskred. *NGI report 20031139-1* (in Norwegian).
- NGI 2004. Hotell og glassbjelke ved Zakariasdemningen—Vurdering av skredfare og skredgenererte bølger. *NGI report 20031673-1* (in Norwegian).
- NGI 2009. Local Tsunami Risk Assessment Approach—The Bridgetown Demonstration Project. *Norwegian Geotechnical Institute report no. 20081430-2*.
- Romstad, B., Harbitz, C.B., & Domaas, U. 2009. A GIS method for assessment of rock slide tsunami hazard in all Norwegian lakes and reservoirs. *Natural Hazards and Earth System Sciences*, 9(2): 353–364.
- Scheidegger, A., 1973. On the prediction of the reach and velocity of catastrophic landslides. *Rock Mechanics and Rock Engineering*, 5(4): 231–236.

Characteristics study of Gorge reservoir landslide

X.L. Tang

*State Key Laboratory of Geohazard Prevention and Geoenvironment Protection,
Chengdu University of Technology, Chengdu, China*

X.L. Tang, D.Y. Liu & H.B. Feng

Hydrochina Kunming Engineering Corporation, Kunming, China

ABSTRACT: Gorge reservoir bank areas are usually featured by strongly dissected topography, with steep mountains and deep valleys of large relative height. Geologic strike of the valleys and mountains is obviously controlled by regional fault. Complex geological setting and strong activity of new tectonic in such areas contribute to well-developed physical-geological phenomenon. Genesis and instability model of potential landslide of reservoir bank slope are complex. Landslides formed by reservoir impounding or after impounding lose stability at high speed or in progressive form. Based on case studies of bank slope losing-stability when and after impounding reservoirs running for many years, this article reaches the conclusion that the main factors leading to various types of landslides diversify greatly. The article analyses the geological structure characteristics of bank slope in landslide and instability phenomena, and studies landslide genesis mechanisms, bank slope instability models and the main stability-controlling factors. Finally it proposes the characteristics of gorge reservoir landslide and explores the corresponding prediction method.

1 INTRODUCTION

Chinese water power resources are mainly distributed in high mountain and deep valley area of Southeast China, where many large-scale gorge reservoirs were built or are building, such as Manwan Reservoir, Xiaowan Reservoir, Luozhadu Reservoir, Ertan Reservoir, Xiluodu Reservoir, and Baozhusi Reservoir. The gorge reservoir bank areas are usually strongly dissected, with steep mountains and deep valleys of large relative height. Geologic strike of the valleys and mountains is obviously controlled by regional fault. Complex geological setting and strong activity of new tectonic in such areas contribute to well-developed physico-geological phenomenon. As reservoir impounding may potentially leads to ancient landslide re-sliding in bank slope region, or even cause new slide occurrence, it remains a threat to the security of the lives and property of the residents in the reservoir area, and there are not few such occurrences at home and abroad. On March 6th, 1961 in China, when at the beginning of impounding, there occurred 1.65×10^6 m³ landslide at high speed on the right bank slope of Tuoxi Reservoir, and the slide mass fell into water violently, caused serious damages. This is the first Chinese instance of large-scale landslide caused by reservoir impounding (Xiao, S.R. & Liu, D.F. 2010). In Italy, After impounding Vaiont Reservoir, a slide with volume of 2.7×10^8 m³ happened on October 9th, 1963, which destructed the project and caused over 3000 casualties (Tika, T.E. 1999 & Semenza, E. & Ghirotti, M. 2000 & Wang, L.S. 2007). After the two occurrences, especially Vaiont accidents, people throughout the world began to place more importance on slide prevention in reservoir areas, and enhanced survey and research of slide genesis and prediction (Xiao, S.R. & Liu, D.F. 2010). Till now, the genesis research of reservoir type landslide, especially, the research on slide genesis, slide instability model in gorge reservoir still remains one of the advanced subjects in academic and engineering circles.

Through examining landslide characteristics in gorge reservoir area, typically as in Ertan Reservoir, Baozhusi Reservoir, Manwan Reservoir, and Xiaowan Reservoir, the article analyses the geological structure features of bank slope in landslide and instability phenomena, and studies landslide genesis mechanisms, bank slope instability models and the main stability-controlling factors. Finally it proposes the characteristics of gorge reservoir landslide and explores the corresponding prediction method.

2 SURVEY AND ANALYSIS OF BANK COLLAPSE AND LANDSLIDE CHARACTERISTICS IN GORGE RESERVOIR

2.1 Characteristics of the typical reservoir bank collapse and landslide

2.1.1 Manwan reservoir area in Lancang River

Normal storage level of the Manwan Reservoir reaches 994 m, while its dead storage level is 982 m. The reservoir has been in normal running for over 17 years. Lancang River winds its way in the reservoir area within 66 km diameter. Varied angles between the river and strata strike of the area form different type of valleys, of which most are longitudinal ones with rock strike parallel to bank slope. In the valleys, there are well-developed Quaternary colluvial deposits and residual-slope accumulations. After impounding the reservoir, there are totally 107 occurrences of bank collapse and 14 landslides, each with 2000–20,000 m³ volume, and 9 of the occurrences are caused by deep-thick deposits sliding, 3 by sliding along bedrock cover and 2 by ancient landslide re-sliding. In terms of form and rule of bank collapse development in the area, the height is usually smaller than the width. The former ranges from 3 m to 20 m, while the latter from 12 m to 38 m. Totally speaking, medium and small-sized bank collapse occurred there. In terms of bank collapse volume, 76.1% is with volume smaller than 1000 m³, 20% between 1000 m³ and 10,000 m³, and 3 of the occurrences with volume larger than 10,000 m³, accounting for 2.9%. Statistics shows that about 52.3% bank collapse developed in soil slope, 44.9% in rock-and-soil mixed slope, and only 2.8% in rock slope. Roughly speaking, there are 3 types of bank collapse, namely, collapsing, sliding and wash and abrasion type (Table 1).

2.1.2 Xiaowan reservoir area in Lancang River

Xiaowan Reservoir with a dam of largest height 294.5 m has a total storage capacity of 15,000,000,000 m³. Its normal storage level reaches 1240 m, while its dead storage level is 1160 m. During the process of impounding at EL.1160 m water level, there were 103 occurrences of bank collapse, among which are 10 landslides, 7 sliding along bedrock cover, 1 sliding in deep-thick deposits, 1 re-sliding of ancient landslide, and 1 sliding along bedrock weak surface. Among these occurrences, “7.20” Landslide and the slide happening in Xinming Plain are large-scale slides. In terms of form and rule of bank collapse development in the area, the width is usually bigger than the height. The latter ranges from 5 m to 30 m, while the former from 20 m to 60 m. On the whole, medium and small-sized bank collapse occurred there. In terms of bank collapse volume, 32 of the occurrences are with volume smaller than 1000 m³, accounting for 43.8%, 35 with volume between 1000 m³ and 10,000 m³, accounting for 47.9%, and 6 with volume larger than 10,000 m³, accounting for 8.3%. Statistics shows that about 38.3% of the bank collapse developed in colluvial deposits soil slope, 35.6% in fully severely-weathered rocky slope, and 13.7% in fully weathered rock slope.

2.1.3 Baozhusi reservoir area in Bailong River

Baozhusi Reservoir with a dam of largest height 132 m has a total storage capacity of 2.5×10^{10} m³. Its design water level reaches 588 m, and its dead storage level is 558 m. The reservoir has been in normal running for over 14 years. According to relevant research documents, there are over 80 landslides on different scale in the reservoir, 20 of which are large-scale slides distributed mainly in river reaches with phyllite bedrock and broad or relatively broad valleys. According to its composition and genesis, landslide in reservoir may falls into three basic types, namely, ancient landslide re-sliding, residual-slope deposits instability deformation

Table 1. The statistics of bank collapse type in Manwan Reservoir.

Type	Subtype	Diagrammatic cross-section	Quantity	(%)
Collapsing	Collapsing recession		88	82.2
	Block collapsing		3	2.8
Sliding	Shallow-sliding in deep-thick deposits		9	8.4
	Sliding along bedrock cover		3	2.8
	Ancient landslide re-sliding		2	1.9
Wash and abrasion	Wash and abrasion		2	1.9

sliding, and artificially-excavated-and-filled slope deformation sliding. According to different kinds of instability caused by slope sliding, landslides in reservoir may fall into 3 types, front-slop-edge-pulled slide, rear-slop-body-pushed slide, and pulled-and-pushed complex slide. Artificially-excavated-and-filled slopes, washed by storm rainfall, usually deform and slide fast. Whereas, most of ancient landslide bodies and residual-slope deposits, under the influence of reservoir water, deform and slide slowly, keeping pace with water level falling (Deng, R.G. & Fu, X.M. 2005). Through detailed study of the slides and deformation bodies in Fenjiaba Plain, Jintong Town, Dongshan Village, Dingjiaba Plain, and Zuojiaba Plain, it is revealed that the bank slope bedrock is mainly composed of Siluric phyllite, muscovite-quartz schist, quartz-bearing dolomite, and slate, Which bears weak resistance to weathering and

poor interlayer bonding, with various well-developed Quaternary deposits such as residual-slope deposits and ancient landslide. The creeping deformation mass in Fenjiaba Plain and the ancient landslide body in Zuojiaba Plain mainly are characteristic of “creeping-cracking” deformation, while landslide in Jintong Town and Dongshan Village, and the deformation body in Dingjiaba Plain mainly are featured by “sliding-cracking” deformation.

2.2 Characteristics of the typical landslide

2.2.1 Laoyingyan landslide

Laoyingyan Landslide is an ancient landslide in Ertan Reservoir in the Yalong River, with three sides of the slide body exposed in the air. When impounding, cracking deformation appeared on top of the slope. As water level fell from normal storage level to dead storage level, crack developed quickly and cause obvious shake. A single crack spread as long as over 20 m with 0.2 m tensile deformation, and the slope body exposed in the air was raised up to 0.6 m as it deformed on the outer side of the crack. Then, when water level fell steeply for several times, slope experienced no obvious macro-deformation. In the early 2003 reservoir water level fell to 1160 m, bank slope slid from front edge to rear edge and cracked up to 8 m, 43 m, 40 m, and 25 m gradually, with a total volume of 1,700,000 m³. The deformation developed in relatively steep ancient landslide deposits with formation. Influenced by water infiltration and sharp fluctuation of water level, slope deformed, toward exposed part, from shear creep to loosening dilatancy along maximum shearing stress plane. Deformed mass developed from surface to depth into tensile splitting, and when it reached potential shear plane, shearing stress concentrated on the plane and enhanced shearing deformation. Then the slope disintegrated gradually from front edge to rear part. The deformation development belongs to typical “sliding to pull-splitting” retrogressive landslide.

2.2.2 “7.20” landslide

“7.20” landslide happened on both sides of the bank slopes in the upper reach of Lancang River, 9 km away from Xiaowan Reservoir (Fig. 1). On July 20th, 2009, successive heavy rainfall caused both sides of the hill body to slide suddenly and form a 500 m wide, 350 m high large landslide, with a total volume of 3,000,000 m³. About 1,000,000 m³ hill body fell into the water thunderingly, throwing up 30 m high spray. The landslide is a deep-thick deposit, steep in the upper part and gentle in the lower part. After impounding, the rock-earth mass in the foot bank slope immersed in water, which raised the ground water level in the bank slope. For one thing, the strength of the rock-earth mass reduced; for another, the uplift pressure caused by the rise of ground water level weakened effective stress in the foot rock-earth mass, decreasing sliding resistance. Furthermore, successive heavy rainfall triggered losing stability and sliding and formed high-speed landslide.

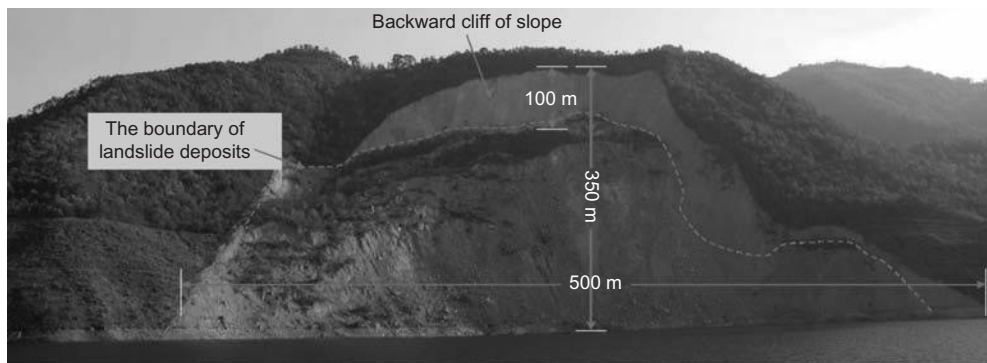


Figure 1. Panorama of the “7.20” landslide.

3 ANALYSIS OF INDUCING FACTORS OF BANK COLLAPSE AND LANDSLIDE IN RESERVOIR AREA

Previous cases show that most landslides in gorge reservoir area develop in loose colluvial deposits, ancient landslide deposits, and in bedrock slide with combination of adverse geological structural planes. Adverse bank slope structure is the internal cause. Under pure natural condition, even influenced by heavy rainfall, slope still keeps stability. On the contrary, after impounding, bank slope of reservoir area loses stability. This shows that water level rise and fall are main inducing factor of landslide, whereas rainfall and other factors are secondary.

1. Adverse material composition and poor bank slope structure lay foundation for landslide: Loose colluvial deposits, ancient landslide deposits, consequent-slope bank slope with interlayer-shear disturbed belt or weak zones, and bedrock slope with adverse combination of weak structural layers usually lose stability. Under pure natural condition, slope may keep relatively lower stability, but if influenced by impounded water, may lose stability and slide.
2. Uplift water pressure when impounding reservoir: When impounding, the ground water level rises rapidly in the sliding resistant section of bank slope. That increases uplift water pressure in sliding resistant slope body, lightens the weight of that slope part, weakens sliding resistance, and finally results in sliding.
3. Softening and Clayer by immersion in water: When immersed in water, soil mass in loose deposits softens easily, which reduces shearing strength in that mass. Weak structural layer in rock mass, especially that with clay minerals, is easy to bulge, soften and Clayer when the mass is immersed in water. That must decrease shearing strength on weak structural layer and induce landslide.
4. Osmotic pressure caused by rapid water rise and fall in reservoir: When water rises and falls rapidly in reservoir, ground water in slope body can't be discharged timely. That produces strong osmotic pressure, enhances rock mass to slide down and results in stability loss of bank slope.
5. Erosion and under-washing by wave: When materials in slope bottom are carried away by wave, upper slope body will lose balance and that will lead to rupture in lower part or even whole slope collapse.
6. Earthquake or induced earthquake by reservoir: Earthquake will decrease bank slope stability and strong quake usually causes lots of slope to lose stability.
7. Rain falling: Heavy or excessive rainfall will increase the volume-weight of rock-soil mass, produce strong penetration, and speed up the process of slope-stability loss.

4 MECHANISMS AND MODES ANALYSIS ON BANK SLOP DEFORMATIONAL FAILURE

Apart from the major factor that bank slope has special material composition and structural features, reservoir landslide will be induced by other important factors such as impounding, rain falling, earthquake and etc. Through above studies on bank-caving and landslide in gorge reservoir area, modes of slope deformational failure can be generalized as follows.

4.1 *Bank collapse*

4.1.1 *Slumping or collapsing*

Slumping or collapsing refers to that kind of slope deformational failure mode when soil slope bottom softens for long time, or when influenced by under-washing, upper slope body loses balance, lower slope body ruptures or even whole slope collapses. Usually the mode takes on the two forms, slump and collapse and its striking points are that in deformation, vertical displacement is larger than horizontal displacement, and failure is directly related

with soil mass self-weight. In the mode, bank slope reformation involves wide distribution range and long reach of bank line, and usually occurs in relatively steep soil slope. The reformation, as a mode with great paroxysm, is most likely to happen in storm or when water level in reservoir changed dramatically. It is the main and most frequent bank slope reformation mode in gorge reservoir area.

4.1.2 Wash and abrasion type

The wash and abrasion type refers to the bank slope reformation mode under the influence of reservoir water, surface water, wind and other external agents, materials in bank slope are carried away by erosion, abrasion, or weathering, and thereby bank slope recedes slowly. The mode of bank collapse usually happens in gentle soil slopes, residual soft rocky deposits, or strongly-weathered zones, but rarely seen in gorge reservoir area. Such kind of deformational failure develops slowly in quite long time and on small scale. It is not directly dangerous, but as a basic mode exists widely.

4.2 Landslide

4.2.1 Ancient landslide re-sliding

Ancient landslide deposits, commonly seen in gorge reservoir area, are clay soil-block rock mixed deposits with loosely-structured slope body. Under pure natural condition, the deposits keep stability well, but under the condition of water immersion or strong water level fluctuation, the deposits tend to re-slide wholly or partially. The deformational failure mode develops well in Three Gorges area, Ertan region, and Baozhusi Reservoir. When front edge of ancient landslide deposits is at a low elevation, it mainly takes on the form of gradual failure such as Laoyingyan landslide in Ertan reservoir area (Fig. 2).

If the failure mechanism of ancient landslide is bedding slip, or original slide surface is steep in the upper part and gentle in lower part and has exposed front edge, when impounding, front slope body influenced by uplift pressure will see its volume-weight decrease, and slide surface will soften, then shear strength reduces sharply. In that case high-speed landslide would happen, causing serious disaster.

4.2.2 Loose accumulative formation slide

Loose accumulative formation slide develops in kinds of thick deposits. Influenced by water infiltration and sharp fluctuation of water level, slope body controlled by maximum shearing stress plane, experiences continual shear creep toward exposed part. Deformed mass develops

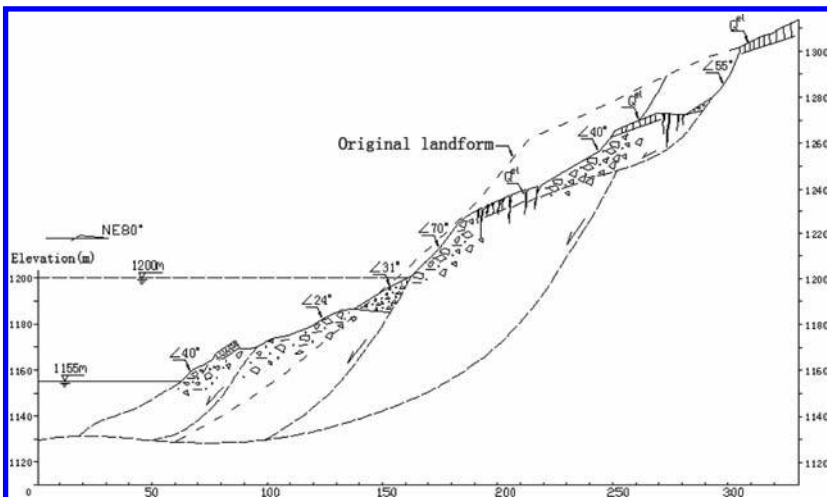


Figure 2. Measure profile of Laoyingyan ancient landslide.

from surface to depth into tensile splitting, and along potential shear plane develops into slipping disintegration year by year. Broken-stone deposits formed in disintegration slides along underlying bedrock layer; deposits composed of weathered granite crust and residual sedimentary mass slides on shallow superficial capping; silt bank slope of alluvial-proluvial deposits, influenced by longtime sharp fluctuation of water level, undergoes small bank collapse; discarded mass after excavation and landfill tend to form secondary slide, such as the “7.20” Landslide in Xiaowan reservoir (Fig. 3).

4.2.3 Bedding slipping

Compared to ancient landslide in reservoir area and accumulative formation slide, bedding slipping including wedge slipping is characteristic of great qualities of concealment, destructiveness, paroxysm, and large scale. It develops in consequent rocky slope with tilt angle smaller than slope angle. Such landslide usually has the following geological structure features: 1) there are consequent weak structural surfaces in slope body; 2) front edge and weak structural surface are exposed in the air, or front edge exposed but weak structural surface not, and rock mass on weak structural surface, with poor strength is weathered seriously; 3) weak structural surface tends to soften in water; 4) lateral boundary is exposed or steep and tilting structural plane cutting, such as Wanzihe Landslide in Erntan and Xiaowan Landslide in Xinming Plain (Fig. 4). Special attention should be paid to the concave-down landslide, with steep upper part and gentle lower part, chair-like potential sliding surface, and upper consequent body and lower cutting layer. Once such landslide occurs, it slips at high speed and brings about large disaster, as in Italian Vaiont Landslide and Chinese Tangyanguang Landslide in Tuoxi, Hunan province.

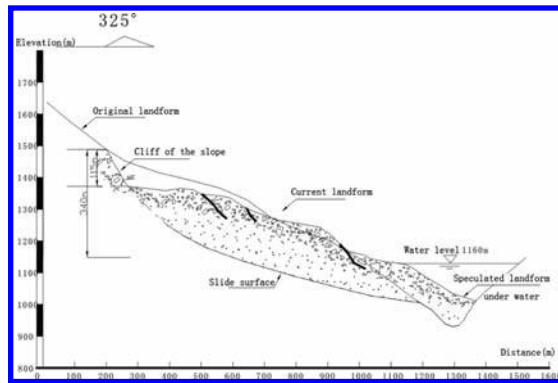


Figure 3. Profile of “7.20” landslide in Xiaowan reservoir.

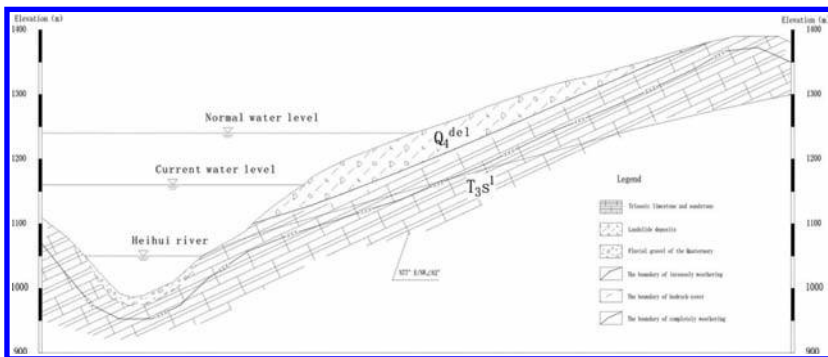


Figure 4. Profile of Xiaowan landslide in Xinming Plain.

5 PREDICTION RESEARCH ON BANK COLLAPSE AND LANDSLIDE

Based on above analysis and examination of engineering cases, It may be concluded that the internal factors to controlling stability of bank slope include bank slope structure features and rock-soil mass structure features, while the main inducing factors of landslide include water uplift pressure in rock-soil mass, softening and argillization by immersion, erosion and corrosion, and hydrodynamic pressure. Therefore, to predict slope stability, focus should be placed on studies of slope structure features, rock-soil mass structure features, and the dynamic response process of slope seepage field under the influence of reservoir water.

To predict bank collapse, E. Г. Качугин method, Зоро Башня Королёв graphic method, two-stage method, slope structure caving predicting method can be used to determine the height and width of bank collapse. According to field investigation, the prediction results is Generally Biased safe to gorge reservoir by the stable slope angle underwater, above water and in under-washing zone. Above mentioned parameters should be modified according to practical investigation of the slope angle in nearby place of exact water level height, so to keep results close to actual states. Comparison may also be made according to similar bank slope characteristics and rock-soil composition features of established reservoir under proper running for years.

To predict ancient landslide re-sliding and stability of potential unstable slope, the same methods can be used as in common slope prediction. The main differences lie in that not only slope structure features and rock-soil mass structure features, but the dynamic evolution and response process of slope rock-soil mass and groundwater seepage field under the influence of reservoir water, should be studied so as to evaluate and predict slope body stability under various reservoir-operation conditions. What's more attention should also be paid to possible impact by induced earthquake on slope stability. Corresponding engineering measures should be made according to prediction results so as to guarantee security of the lives and property of people and better environmental protection.

6 CONCLUSION

The slope deformational failures developed in gorge reservoir area mainly fall into three modes, bank collapse, ancient landslide re-sliding and new slide, which are mainly determined by bank slope structure features, rock-soil mass structure features, and the dynamic response process of slope and groundwater seepage field under the influence of reservoir water. Emphases of the prediction lie in coupling between rock-soil mass and ground water, and dynamic response process of slope rock-soil mass under various reservoir-operation conditions.

REFERENCES

- Xiao, S.R. & Liu, D.F. 2010. Engineering geologic study of three actual dip bedding rockslides associated with reservoirs in the world. *Journal of Engineering Geology* 18(1): 52–59.
- Tika, T.E. 1999. Hutchinson. Ring shear tests on soil from the Vaiont Landslide slip surface. *Geotechnique* 49(1): 59–74.
- Semenza, E. & Ghirotti, M. 2000. History of the 1963 Vaiont slide: the importance of geological factors. *Bulletin of Engineering Geology and the Environment* 59(2): 87–97.
- Wang, L.S. 2007. Review of Vajont reservoir landslide in Italy. *The Chinese Journal of Geological Hazard and Control* 18(3): 145–150.
- Deng, R.G. & Fu, X.M. 2005. Fuzzy clustering analysis and stable degree of landslides and landslide distribution feature along the bank of Baozhusi Reservoir on Bailongjiang River in Sichuan Province. *The Chinese Journal of Geological Hazard and Control* 16(4): 24–28.

Goescheneralp dam—impact of natural hazards on construction site and freeboard optimisation

T. Dietler

Pöyry Energy AG, Zurich, Switzerland

ABSTRACT: The borrow areas, where the material for the heightening of the Goescheneralp dam is taken from, and parts of the dam construction site, are highly threatened by different types of natural hazards. To analyse the situation adequately and to design appropriate mitigation measures for a safe construction site, the standardised methodology prepared by the relevant Federal Offices of the Swiss Government was applied. Furthermore, the analysis was geographically extended around the entire reservoir for use as basic input data for the optimisation of the new freeboard. The relevant natural hazards to be considered are rock falls, rock avalanches, debris flows and snow avalanches.

1 INTRODUCTION

1.1 *Location and layout of the construction site*

The Goescheneralp Dam and reservoir are located in central Switzerland, in a typical alpine mountain valley on a western tributary of the Reuss River (Fig. 1).

The existing Goescheneralp Dam (Fig. 2) will be heightened by 8 m to increase the storage volume by 14%. It is planned to take the rock fill material from the old borrow areas at the downstream foot of the dam. The new fill material will be taken from old debris fans along the southern slope of the valley. Processing and interim storage areas for the material will be located in the same area. For the transportation of the fill materials to the dam crest, a new access track must be constructed, due to the old track from the previous construction period being partly eroded and exposed to natural hazard events. The public road is not suitable for heavy transportation.

The construction site on the dam is only exposed to natural hazards in its southern part (right abutment). The left abutment (northern side) is not affected by such events and has therefore been chosen as the location for the main installation areas (offices, camp, etc.). The construction site will be in operation during the summer period (May to October) only.

1.2 *Geological situation in the project area*

The morphology of the wider project area is characterised by a typical U-shaped valley eroded by glaciers. The highest mountain around the reservoir is the glacier covered Dammastock with a peak elevation of 3630 m a.s.l. (Fig. 2).

The tectonic and geological framework is the Central Aar-Massive, the backbone of the Swiss Alps, with its huge granite body. Within the project area the texture of this whitish granite varies from massive to gneissic in slightly sheared zones and chlorite shists in strongly sheared zones. Together with the foliation of the partly sheared granite, major joint-sets with more or less orthogonal orientations, form a blocky to platy fabric of rock bodies.

1.3 *Principles of the applied methodology*

Due to numerous and severe events during the 1980s and early 1990s, with many fatalities and much damages (amounting to billions of Swiss Francs), the relevant offices of the Swiss Government established a standardised methodology for the documentation and assessment



Figure 1. Location of the project area in Switzerland (B: Berne, G: Geneva, L: Lucerne, Z: Zurich).



Figure 2. Goescheneralp dam and reservoir with Dammastock mountain in the background (view from East to West).

of natural hazard events, including standardized parameters and symbols for classification and mapping (BUWAL 1997):

- Step 1: Identification of hazards: “What can happen where?” (Documentation of events and mapping of phenomena).
- Step 2: Assessment of hazards: “How often and with what effect will it happen?” (Analysis of risks and mapping of hazard zones).
- Step 3: Planning of mitigation measures: “How can we protect ourselves?” (Implementation of measures in the fields of land use planning, defensive structures and contingency planning).

Following this methodology, the identification and assessment of the situation becomes traceable and transparent. [Chapter 2](#) briefly describes the comprehensive assessment of the natural hazards performed in the project area (Pöyry Energy 2009).

2 COMPREHENSIVE ANALYSIS OF THE NATURAL HAZARDS

2.1 *Identification and assessment of hazardous events*

For the identification of possible natural hazards old topographic maps and documents were consulted and the surface was carefully mapped. Since the topography is very steep and

exposed, different ways of mapping were applied. The lower parts of the slope were observed during walkover surveys, and the middle and higher elevations of the slope were mapped from the opposite side of the valley. During these activities sketches and wide angle and close-up photographs were taken. Furthermore, a reconnaissance flight by helicopter was undertaken to inspect the area from the air and to get closer to the highest peaks. During the flight, photographs and short landings enabled the identification of potential hazards.

The field mapping, photographs and information from old documents were then used to draw a series of large scale thematic maps providing 1) a topographic map indicating the morphological situation before the construction of the existing dam focussing on the numerous debris fans. 2) A geological overview, visualizing areas of compact and fractured bedrock as well as the different types of loose overburden material (in-situ or transported). 3) A map of natural hazard phenomena, documenting areas of origin, corridors of transportation and areas of deposition of rock fall and debris flows (Fig. 3). 4) A map documenting the envelope of all known snow avalanche events.

The dominant processes identified in the investigated area that occur during the summer period are 1) Rock fall of small dimensions <0.5 m. 2) Rock fall of large single boulders up to several metres in diameter. 3) Rock avalanches with a total volume of a few hundred to tens of thousands of cubic metres, and 4) Debris flows with a volume of a few thousands of cubic metres. During winter time, different types of snow avalanches transport a considerable amount of boulders with varying sizes down the slopes. To enable statements about the frequency to be made, old documents reporting past events were consulted, and the observations made by local people were registered. Events with large single blocks must be expected once or several times each year, rock avalanches with a large volume must be expected every second to fourth year (often reaching the bottom of the valley). Finally, debris flows reaching the valley bottom can occur annually during heavy rainstorms.

For further assessment of the hazards, 10 different transportation routes were selected and their various flow paths were listed by slope angle and type of surface material (e.g. bedrock, block fields, vegetation, etc.). Using a commercial rock fall simulation software, the extend of transportation (endpoints) and the expected kinetic energy in the final part of the path were calculated for different block volumes and elevations of origin.



Figure 3. Map of rock fall, debris flow and selected transportation channels using standardized symbols and colours.

Based on this information, maps of hazards for the summer and the winter periods were produced, covering the complete area of the construction site. This type of map, well known in Switzerland for many decades with regard to the documentation of snow avalanches, consists of three different colours, defining areas of different hazard potentials: yellow = low hazard, indicating possible occurrence of hazards; blue = medium hazard, request for mitigation measures; and red = extensive hazard, indicating areas of ban. According to this hazard map, important parts of the borrow areas for the new rock fill material, areas for the crushing plant and interim storage, transportation route to the dam crest and the southern most part of the dam's right abutment are located within red and blue hazard areas (Fig. 4).

2.2 Definition of scenarios and risk analysis

To plan adequate and effective mitigation measures, construction related scenarios were defined and their potential risks were analysed. In a first step the relevant construction site sectors were defined as follows. 1) Material borrow areas. 2) Crushing/screening plant. 3) Interim storage areas. 4) Transportation route to dam crest. 5) Right dam abutment area, and 6) Construction areas near the reservoir water level. For each site sector typical scenarios were defined for subsequent risk analysis. Typical scenarios include large single blocks hitting excavators/trucks and the operator in the borrow area, or rock avalanches hitting trucks and drivers along the transport route to dam crest.

In a second step a risk assessment for each defined scenario was performed using event trees (Fig. 5). Considering the probability and the size/consequences of an event, the potential of risk was estimated using five to six different steps within a scenario, as follows. 1) Event occurs? 2) Construction site closed (in expectation of debris flows)? 3) Block reaches construction site? 4) Evacuation of personnel possible? 5) Block hits equipment/operator? and 6) Severe injury or fatality?

The highest risk potentials of the different scenarios represent the worst cases, which, considering the experience in the area, are quite likely to occur. The risks were then entered into sensitivity analysis to estimate the variation of the potential, in a similar way to cautious optimistic estimation. Values for the worst, but still realistic case and the optimistic estimation were then plotted in a risk matrix (Fig. 6). On the X-axis of this diagram the

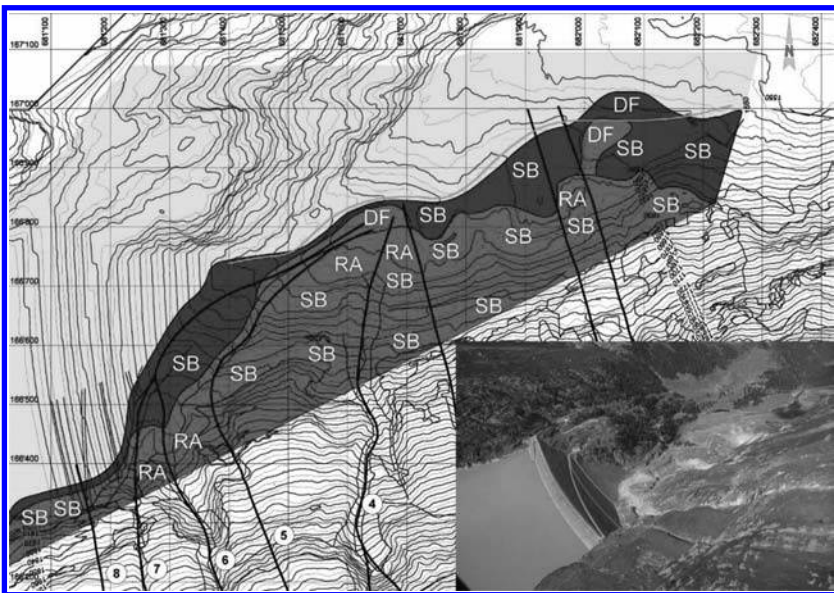


Figure 4. Hazard map covering the entire construction area (yellow = low hazard potential; blue = medium hazard; red = extensive hazard). SB: single blocks, RA: rock avalanches, DF: debris flows).

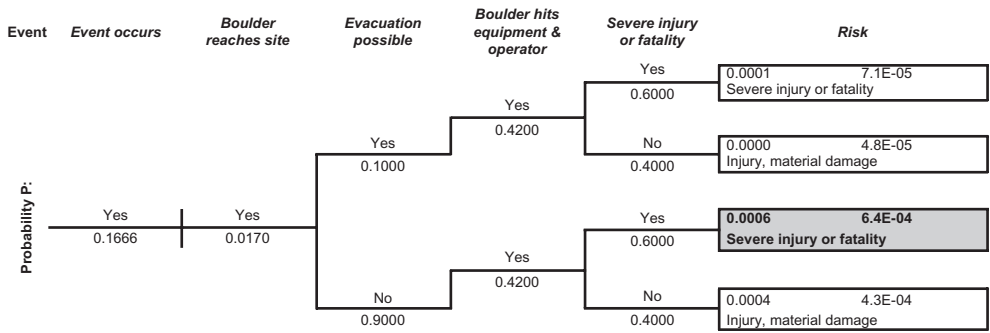


Figure 5. Risk analysis of defined hazard scenario using event trees (the path of the highest risk potential is marked in bold).

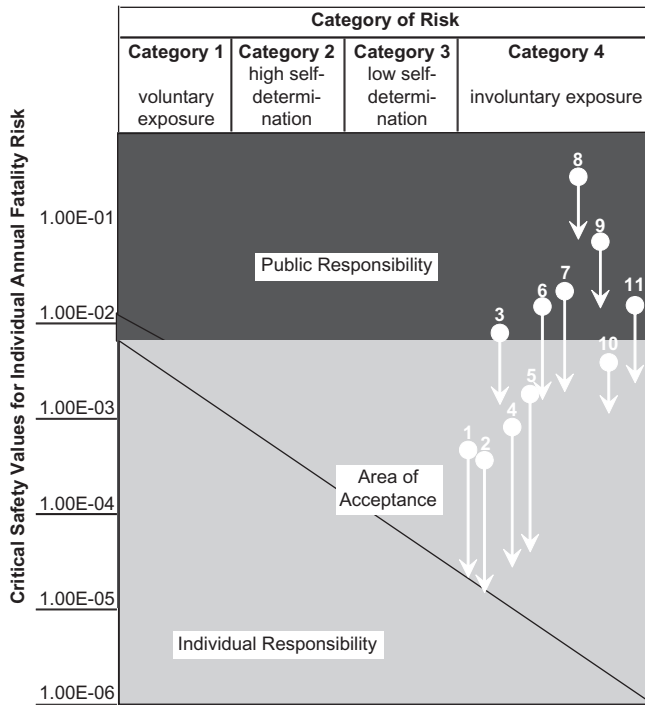


Figure 6. Worst case (circles) and optimistic (arrows) values of risk potentials plotted in the risk matrix with different sectors of acceptance and responsibilities.

different categories of risks for an individual person are marked as follows. 1) Voluntary exposure. 2) High amount of self-determination. 3) Low amount of self-determination, and 4) Involuntary exposure. According to the Swiss working laws and insurance regulations, construction site workers have to be classified in (4). On the Y-axis the critical safety values for an individual fatality risk per year are plotted. In Switzerland, the critical safety value for involuntary fatality risks is defined as 10^{-5} to 10^{-6} . The risk matrix in Figure 6 indicates that all worst case values determined are located in the dark grey sector of public responsibility, which means they are unacceptable (white circles in Fig. 6). When the values of cautious optimistic estimations are considered (arrows in Fig. 6), only four out of eleven scenarios are translated into the grey sector of public acceptance. The bright grey sector of individual responsibility is not entered.

2.3 *Conclusions of the assessment*

The conclusion of the investigations for natural hazards and their risk analysis are briefly summarized as follows:

- Considerable sectors of the construction site will be severely and acutely endangered by natural hazards, originating from the southern valley slope.
- From the northern slope no risk is to be expected.
- Since it is a high alpine area, the construction site will be closed during winter time. Thus the hazard of snow avalanches is only relevant for construction equipment remaining on the site during this time.
- The priority for protection of the different site sectors with mitigation measures was defined as 1) Area of right dam abutment: Small area with highest density of personnel, equipment and temporary occupation. 2) Transportation route to dam crest: Slow traffic with no possibility for evacuations. 3) Borrow areas, crushing plant and interim storage: Only a few persons present and moving around.
- Hazards from debris flows are more predictable than rock fall or rock avalanches, since they are connected to heavy rainfall periods. Under such weather conditions the process of rockfill placement will be stopped and time will be available to evacuate personnel and mobile equipment.
- The potential of natural hazards may be reduced to a generally acceptable level by means of mitigation measures. However, in mountainous regions such as Goescheneralp, a residual risk is always present.

2.4 *Planned mitigation measures*

While planning adequate mitigation measures against the natural hazards, different options were discussed and designed:

- *Areal organisation* of the construction site: All installation areas and equipment not tied to specific construction locations will be situated in the yellow sectors.
- *Advance warning* of events: Debris flows are the only hazardous event that can be foreseen within enough time for evacuation. Direct communication procedures already existing with the relevant authorities for such events in the Canton of Uri will be implemented.
- *Active measures* at the source of hazards: The area where natural hazards may originate from is very extensive. Such measures are not efficient and are therefore not considered.
- *Passive measures* near the impact of the hazards: All facilities tied to areas with medium (blue) and extensive (red) hazard potential will be protected with physical structures to reduce the risk to a generally accepted level in mountainous regions.

The specific mitigation measures to reach the level of accepted risk are defined below for the different site areas (Fig. 7):

- *Right dam abutment*: A 128 m long, 3 m high flexible protection fence will be installed a few metres above this area. If required, rock outcrops below this structure will be cleaned of loose blocks. Due to the high pressure of snow masses during wintertime, this structure must be removable during winter periods.
- *Transportation route to the dam crest*: The safest way for to transport rock fill material to the dam crest will be on a new track along the foot of the dam, and then using existing tracks on the downstream face of the dam body. The new track will be located in the prolongation of two gullies, prone to rock fall, rock avalanche and debris flow. Protection of the smaller gully will consist of a 30 m long, 3 m high fence. At the larger, more important gully a 75 m long, 2 to 4 m high rock fill diversion wall will be constructed. During wintertime, the fence must be removed.
- *Area of borrow material, crushing plant and interim storage*: These areas in the bottom of the valley will be protected by approximately 2 m high rock fill walls, erected 5 to 10 m

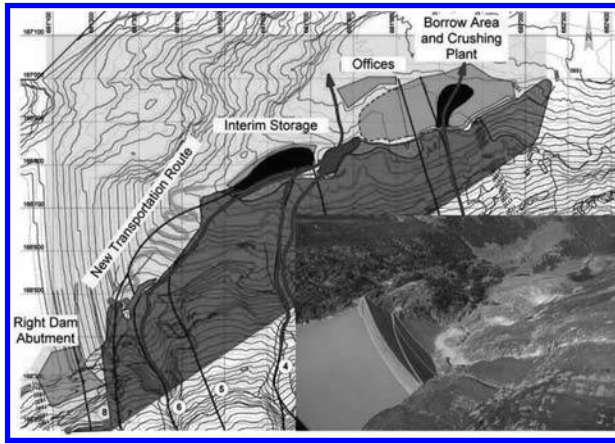


Figure 7. Map with main affected construction sectors, protection measures and reduced areas of hazard potential.

away from the toe of the valley slope. These protection walls must have adequate openings for small gullies, prone to debris flows.

All of the above defined protection structures must be in place before construction activities behind them can commence.

3 NATURAL HAZARDS INFLUENCING FREEBOARD OPTIMISATION

3.1 Introduction

The freeboard of the existing Goescheneralp dam is five metres. The project under discussion foresees the full supply reservoir level being increased by eight metres. Every metre of additional dam height makes the construction more expensive and thus the investment less economic. Therefore, a scientific study for the optimisation of the freeboard was performed to minimise the required dam heightening e.g. only 4.5 m freeboard instead of 5.0 m.

The parameters influencing waves on the reservoir and thus determining the minimum freeboard are 1) Slope instabilities around the reservoir. 2) Snow avalanches reaching the reservoir, and 3) Wind generating waves in the reservoir. These basic studies were performed by Pöyry Energy for the slope instabilities (Pöyry Energy 2010), Wasser/Schnee/Lawinen for the snow avalanches (WSL 2010) and the Swiss Federal Institute of Technology in Lausanne (EPFL) for wind induced waves (LCH 2009). The numeric simulation of the induced waves and their run-up on the dam body were also carried out at the EPFL (LHE 2010).

3.2 Slope instabilities

The geological-tectonic disposition in the slopes around the reservoir is in such a manner that wedge like gliding of compact rock masses along discrete gliding planes can be excluded. However, due to partly high density joints, rock avalanches of to a few tens of thousands of cubic metres, reaching the reservoir level, must be expected during the lifetime of the scheme.

Figure 8 shows the reservoir area and the valley slopes around it. Eleven areas where rock avalanches and two areas where debris flows may originate and reach the reservoir could be identified. The numerical simulation revealed that only in an event with a volume more than 50,000 m³ from Location 1 (which is designated as extremely rare) will induce critical waves with respect to the freeboard determination. In this extreme case, a single wave of 0.7 m would run over the dam crest (roughness of 0.5 m from the upstream dam face is ignored in the calculation).

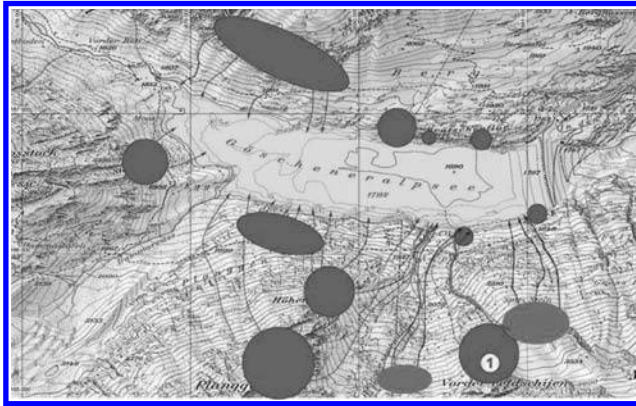


Figure 8. Topographic map of reservoir area and indicated locations of sources for rock avalanches, debris flows and their transportation routes to the reservoir.

3.3 Snow avalanches

Similar to the rock avalanches, 17 different areas of origin for snow avalanches were identified and analysed. Again, critical events have to be expected from the area around Location 1 in Figure 8, which is in the south-eastern corner of the reservoir. An extreme event would induce a run-up wave which would over top the dam crest by 0.5 m; however, with only a small volume of water. The existence of an ice cap on the reservoir, which would dampen the waves, was ignored in the calculation. Lowering the water level in the reservoir during critical winter periods by 1.5 m or artificially releasing avalanches before snow masses reach a critical volume, will decrease the risk considerably.

3.4 Wind waves

Since the surface area of the reservoir is only moderately large (2.3 km long by 500 m wide) and because the reservoir is surrounded by high mountains, wind induced waves are small (<0.35 m) and cause a run-up of <1 m, insignificant in the determination of freeboard.

4 CONCLUSIONS

Based on the scientific studies performed, a reduction of the freeboard from 5.0 to 4.5 m at Göscheneralp Dam is justifiable in connection with the current dam heightening.

REFERENCES

- BUWAL Bundesamt für Umwelt, Wald und Landschaft Bundesamt für Wasserwirtschaft & Bundesamt für Raumplanung 1997: *Berücksichtigung der Massenbewegungsgefahren bei raumwirksamen Tätigkeiten*. Bern: EDMZ.
- LCH Laboratoire de Constructions Hydrauliques 2009: *Rehaussement du barrage de Göscheneralp—Etudes des vagues dues au vent*. Rapport LCH Nr. 19/2009. Lausanne: EPFL (unpubl.).
- LHE Laboratoire d'Hydraulique Environnementale 2010: *Dammerhöhung Göscheneralp—Untersuchungen zur Freibordauslegung—Numerische Berechnung von Impulswellen*. Bericht LHE Nr. 1/2010. Lausanne: EPFL (unpubl.).
- Pöyry Energy 2009: *Dammerhöhung Göscheneralp—Analyse der Naturgefahren*. Bericht 300893.04a. Zürich: Pöyry Energy AG (unpubl.).
- Pöyry Energy 2010: *Dammerhöhung Göscheneralp—Geologische Grundlagen zur wissenschaftlichen Studie der Freibordauslegung*. Bericht 300893.04b. Zürich: Pöyry Energy AG (unpubl.).
- WSL Wasser/Schnee/Lawinen 2010: *Dammerhöhung Göscheneralpsee—Beurteilung der Lawinengefährdung*. Bericht 100111. Brig: Ingenieurbüro A. Burkard (unpubl.).

Design and construction of asphalt facing in cold heavy snow region

S. Abe, H. Seto & H. Watanabe

First Civil Engineering Section, Kyogoku Project Office, Hokkaido Electric Power Co., Inc., Kyogoku, Hokkaido, Japan

ABSTRACT: The upper reservoir of the Kyogoku Hydroelectric Power Plant is a pool-type reservoir and the application of the asphalt facing to the entire inner surface of this reservoir is planned. This reservoir is located in one of the coldest regions in Japan and also has much snowfall. Because of the limited period available for civil engineering work, it is important to do the work efficiently. Therefore, Hokkaido Electric Power selected the cold-lay foamed asphalt mixture for the base layer of the asphalt facing because of its characteristics to allow laying at normal temperature and the work is currently in progress. This paper reports on the design and construction of the cold-lay foamed asphalt mixture for the project as well as the properties of this mixture after construction.

1 INTRODUCTION

Hokkaido Electric Power is currently constructing the pure pumped storage-type Kyogoku Hydroelectric Power Plant (maximum output of 600,000 kW, maximum utilizable flow of 190.5 m³/s and effective head of 369.0 m). The four sides of its square-shaped upper reservoir are approximately 440 m in length with rounded corners. Three sides are embanked using excavated materials. It is planned to construct asphalt facing to cover the entire inner surface of approximately 180,000 m². [Table 1](#), [Figures 1](#) and [2](#) show the specific data, plan and standard cross-section of this pool-type reservoir respectively.

The levelling macadam layer using a coarse graded asphalt mixture has been traditionally used in Japan for the base layer of the asphalt facing. The Kyogoku project site experiences such severe weather conditions as a minimum temperature of -25°C and snow cover of approximately 5 m in thickness in winter. Therefore, term of the construction work is restricted between late May and mid-October, making the selection of a highly efficient construction method essential. Hokkaido Electric Power took notice of the foamed asphalt mixture used for the upper base layer of roads and decided to adopt an improved mixture

Table 1. Specific data of the upper reservoir.

Item	Data
Type of dam	Rockfill dam with asphalt facing
Total Crest length	1464.1 m
Total area of asphalt facing	178,000 m ²
Available depth	45.0 m
Reservoir area	0.16 km ²
Maximum water level	EL. 890.0 m
Minimum water level	EL. 845.0 m
Gross storage capacity	4,400,000 m ³
Effective storage capacity	4,120,000 m ³

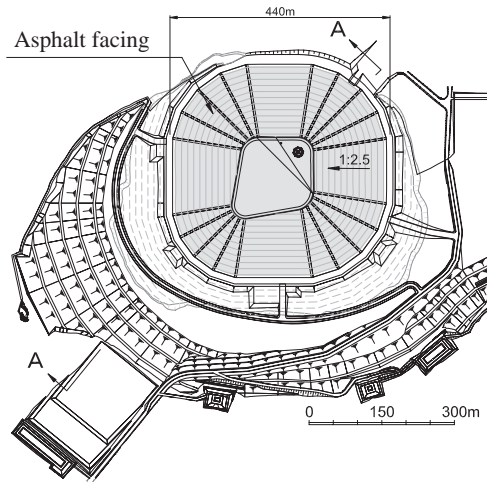


Figure 1. Plan of the upper reservoir.

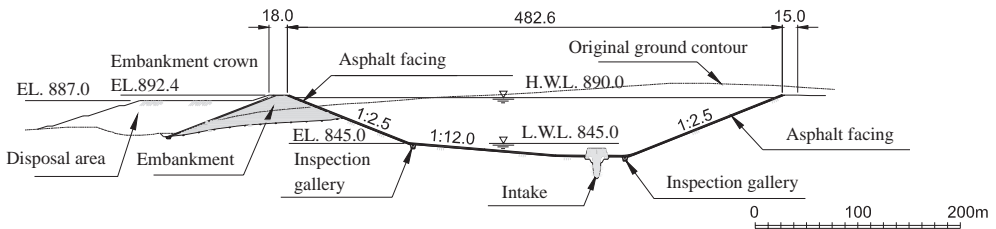
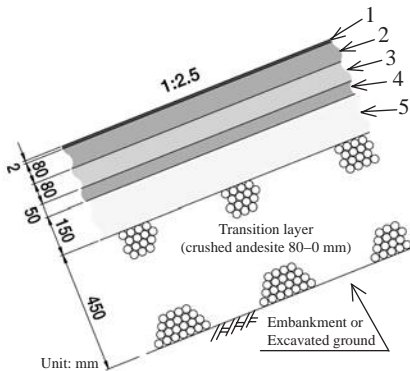


Figure 2. Standard cross-section of the upper reservoir (A-A).



Name of layer and material used	
1	Protection layer
2	Asphalt mastic
3	Upper impervious layer
4	Dense graded asphalt mixture
5	Intermediate drainage layer
	Open graded asphalt mixture
	Lower impervious layer
	Dense graded asphalt mixture
	Base layer
	Foamed asphalt mixture (FAM)

Figure 3. Configuration of asphalt facing.

(cold-lay foamed asphalt mixture, hereinafter referred to as “FAM”) for the base layer of the asphalt facing. Compared to a coarse graded asphalt mixture, FAM is less likely to be affected by the weather conditions during construction work, can be applied at normal temperature and does not require an asphalt finisher and other special machinery. In this project, the thick lift placing of a single 8 cm thick layer is used to form the upper impervious layer instead of the conventional double layer construction for the suppression of inter-layer blistering and cost reduction. This paper reports on the design and construction of FAM and the properties of FAM after construction. Figure 3 shows the configuration of the asphalt facing.

2 OUTLINE OF FAM

Figure 4 shows the fundamentals of the foamed asphalt and the manufacturing process of FAM. When water and air are sprayed into hot asphalt (around 150°C), foamed asphalt is created. The volume expands by 10 to 20 times and the resulting fall of the viscosity makes it possible to mix foamed asphalt and wet aggregates at normal temperature. Foamed asphalt does not completely cover coarse aggregates unlike a hot asphalt mixture but it adheres to fine aggregates and eventually combines with coarse aggregates after compaction. As FAM possesses the characteristics listed in Table 2, its use for the asphalt facing produces a great effect.

3 PERFORMANCE REQUIREMENTS OF FAM FOR THE BASE LAYER

The base layer should meet such performance requirements as durability (protection of the transition layer), deformation performance (structural coherence from the asphalt facing to the embankment) and flatness (base for the asphalt facing and adjustment of the unevenness to ensure the sufficient thickness of the lower impervious layer). The results of the test established in advance confirm that these performance requirements of the base layer will be met as long as the void of the FAM to be used for the base layer does not exceed 20%. Table 3 and Figure 5 show the specified mix proportion and specified gradation respectively. The aggregates come from fresh and hard andesite which is produced by the excavation work of the upper reservoir and is crushed to the predetermined grain size. To produce FAM of uniform quality, slaked lime is added as it can improve the homogeneity of the asphalt.

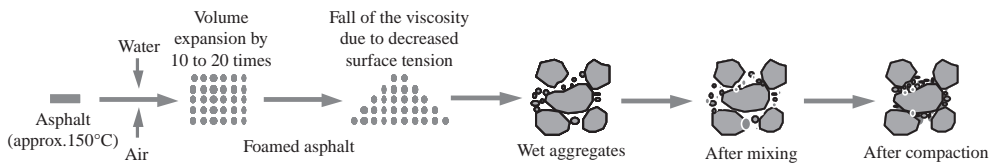


Figure 4. Fundamentals of foamed asphalt and the manufacturing process of FAM.

Table 2. Characteristics of FAM.

Characteristics	Description
Workability	Compared to a common hot asphalt mixture, there are noticeably fewer work restrictions, making rapid work execution possible (shorter construction period)
Environmental impacts	The environmental impact (CO_2) can be reduced as FAM is produced at normal temperature
Effective use of local materials	The effective use of local materials is possible

Table 3. Specification mix proportion for FAM.

Composition by weight (%)		
Asphalt	Aggregate	Dispersibility improver
4.5	94.5	1.0
Maximum grain size (mm)	Water content	Water-asphalt ratio (W/As, %)
40	7.0 (OMC*)	2.0

*Optimum Moisture Content.

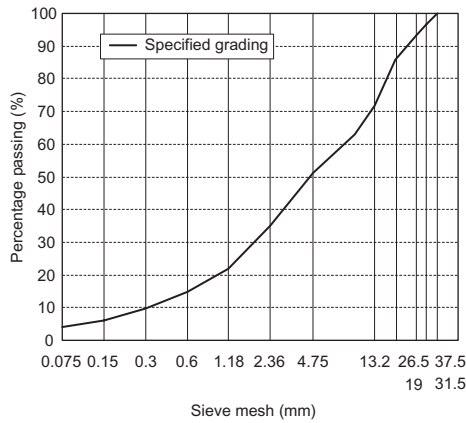


Figure 5. Specified gradation.

Table 4. Exposure test.

As content	Void	Emulsion
4.5%	15%, 20%	With, without

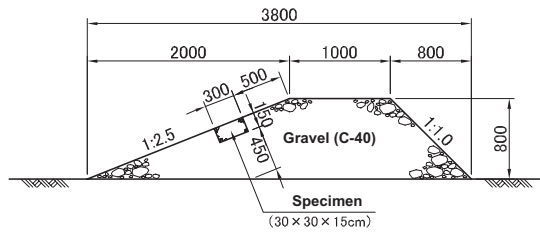


Figure 6. Condition of the test.

3.1 Durability (frost damage resistance)

Because the construction site is located in a heavy snow area, the transition layer requires protection against the erosion due to avalanches or melting snow. A long-term exposure test using FAM specimens was conducted to evaluate the durability (frost damage resistance).

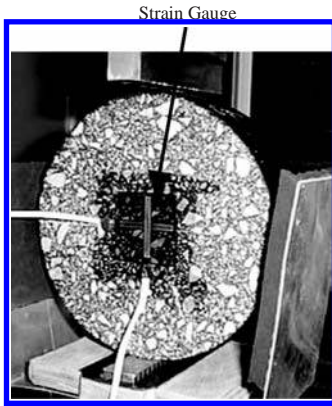
This exposure test was conducted with the conditions shown in Table 4 as the durability was expected to depend on different void and the presence of asphalt emulsion (sprayed for the protection of the base layer surface). The test commenced in March, 2002. Figure 6 shows the condition of the test.

Visual observation of the specimens exposed for three and a half years could not identify any clear differences between the specimen of 15% void and that of 20% void. In the case of the specimen without emulsion, the fine grain content on the surface gradually decreased, exposing the coarse aggregates. The specimen with emulsion did not show such a tendency.

These results seem to indicate that sufficient frost damage resistance can be secured with void of 20% or lower and that asphalt emulsion protects the surface of the base layer.

3.2 Deformation performance

A gyratory compactor was used to make the specimens, based on the specified mix proportion. These were subject to an indirect tensile test to evaluate the deformation performance of FAM. The indirect tensile test used an Instron universal testing machine as the loading device and applied a load diametrically to the cylindrical specimen (80 mm in thickness and 150 mm in diameter) inside a thermostatic oven at a predetermined temperature. Photograph 1 shows the specimen of the indirect tensile test. Based on the results of the creep test, the modulus of deformation was calculated. Figure 7 shows the test results (Takano et al. 2004).



Photograph 1. The specimen of indirect tensile test.

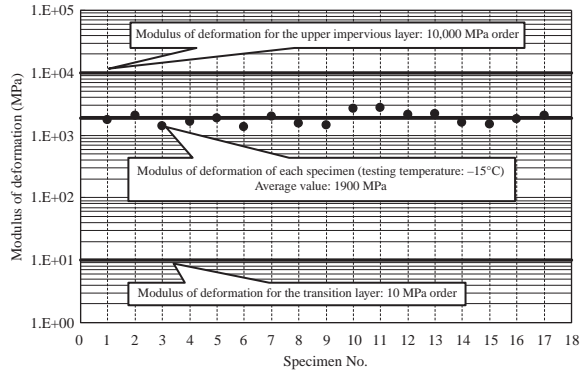


Figure 7. Indirect tensile test results.

Table 5. Conditions of dynamic analysis.

Model	Two-dimensional Finite Element Method
Seismic waves	Kaihoku-Brige Wave (1978.6.12) Minohgawa Dam Wave (1995.1.17)
Maximum horizontal acceleration	220 gal (Magnitude 6.5 at the nearest fault, considering the distance from the source)

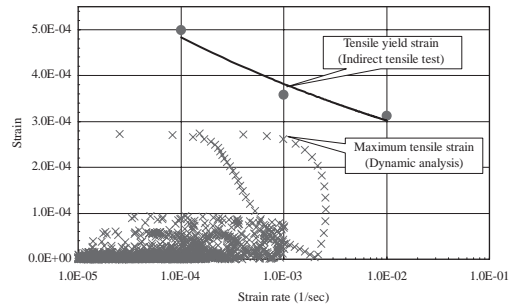


Figure 8. Safety evaluation result (upper impervious layer).

The modulus of deformation of FAM is in the range of 1000~3000 MPa, which is between the relevant modulus for the upper impervious layer and that for the transition layer.

The seismic safety of the asphalt facing was evaluated by means of dynamic analysis. Table 5 shows the conditions of dynamic analysis. This analysis found that the maximum tensile strain at the upper impervious layer occurred at the upper part of the cut boundary of the embankment provided that the water level was its lowest. Because of the external exposure of this area, the satisfaction of the required safety factor (1.1) was checked and confirmed by comparison with the tensile yield strain under the design temperature of -20°C for the upper impervious layer in winter. Figure 8 shows the results of the analysis.

3.3 Flatness

The base layer functions as the foundation for the asphalt facing and the unevenness adjustment layer to ensure the sufficient thickness of the lower impervious layer. As such, it should have adequate trafficability for construction machinery. Evaluation of the trafficability was based on the residual deformation of the base layer after the running of a dump truck (vehicle delivering a mix) on the base layer constructed for the slope paving test in 2002. Two loading cases, i.e. with the maximum load (17.7 ton) and with no load (7.7 ton), were used and the number of running was set at 15 for both cases. The results of the test appear to indicate the sufficient level of trafficability as the residual deformation with the maximum load was approximately 2 mm.

4 CONSTRUCTION OF THE BASE LAYER

Figure 9 shows the flow of the construction of the base layer of FAM and the construction machinery to be used. As FAM is a normal temperature mixture, it can be laid by means of levelling by a bulldozer and compacting by a vibration roller as in the case of the transition layer unlike the case of a hot asphalt mixture. The daily rate of the base layer laying work using FAM by one party is approximately 2000 m². The overall construction period is shorter than that of conventional levelling and macadam layer work (using a coarse graded asphalt mixture) as the work with FAM is less likely to be affected by the weather conditions (outside temperature and rain).

The number of compaction operations for the base layer is 4 passes. The compacted surface will get the unevenness (around 3 cm in size) caused by the caterpillar of the vibration roller (14 ton class), and this unevenness is eradicated with the use of a smaller vibration roller (2.5 or 2.8 ton class) for finishing compaction. As the finished elevation is within 25 mm of the design elevation, the accuracy of the work is sufficient for the base layer.

5 PROPERTIES OF THE COMPLETED BASE LAYER

5.1 Slackness

The construction of the base layer using FAM commenced in September, 2005 and approximately 107,000 m² of the base layer has been completed as of September, 2010. As some sections of this base layer are exposed for a long time until the laying of the lower impervious layer, the completed base layer has been monitored for the purpose of checking its properties. This follow-up monitoring found that the base layer laid in autumn suffered the softening of FAM (this phenomenon is described as “slackness” hereinafter), primarily at the embankment top, after winter. The check of the specimens collected from an area of the slackness found that the slackness is confined to the surface. The embankment top area is the first area to experience the melting of snow in spring as shown in Photograph 2. This exposed area receives a constant supply of melted snow while the ambient temperature often drops below 0°C. The decrease of the adhesive strength between the asphalt and coarse aggregates by the cycle of freezing and melting causes this slackness (Seto et al. 2010).

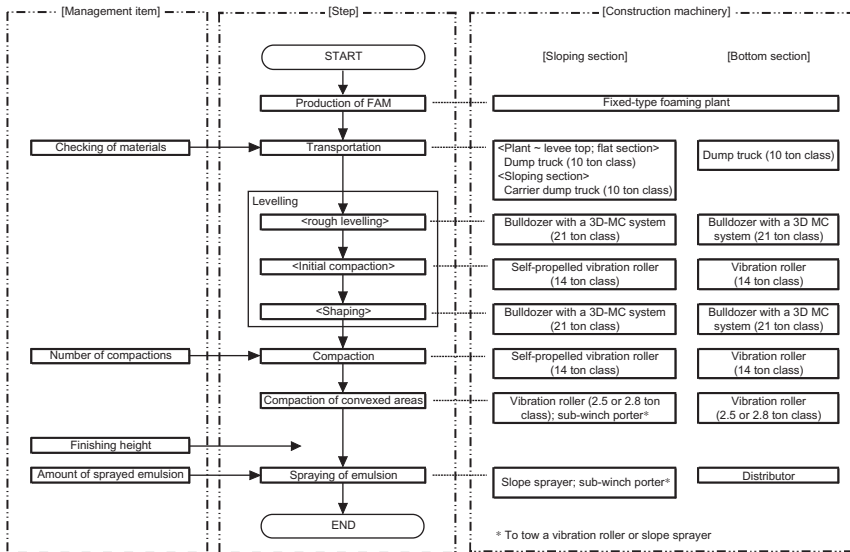


Figure 9. Construction flow of the base layer and construction machinery to be used.

5.2 Measuring of the slackness by the yamanaka-type soil hardness meter

The slackness of the base layer was measured using the Yamanaka-Type Soil Hardness Meter to quantify the slackness. With this meter, a cone of 18 mm in diameter and 40 mm in height was vertically inserted into the soil to measure the non-penetration amount (0~40 mm, a larger value means greater hardness) to determine the level of the soil hardness. Photograph 3 shows the meter. For this measuring operation, nine measured values were obtained at each point to calculate the average value. Figure 10 shows the results of the measurement.

The following knowledge has been acquired from the results of the measurement using the said meter.

- The slackness of the base layer observed after the first winter tends to disappear (the non-penetration amount increase, suggesting harder) towards summer.
- The disappeared slackness does not reappear from the second winter onwards.
- The non-penetration amount after the first winter is highly dependent on the temperature. It tends to become smaller when the surface temperature of the base layer rises and larger when the said temperature drops. This dependence on the temperature is less evident from the second winter onwards.

The reason for the disappearance of the slackness may well be an increase of the adhesive strength of the coarse aggregates as a result of an increased contact area between the asphalt and aggregates, in turn caused by an increased surface area of asphalt in the base layer due



Photograph 2. Melting of snow at the base layer.



Photograph 3. Yamanaka-Type Soil Hardness Meter.

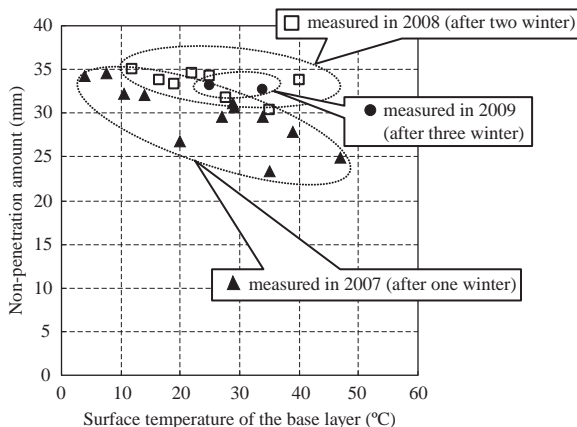


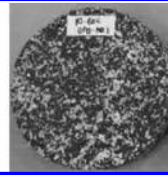
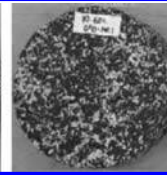


Figure 10. Measurement results of the base layer laid in 2006.

Table 6. Observation of specimen dried at 60°C.

Drying time (hours)				
0	12	24	48	
				

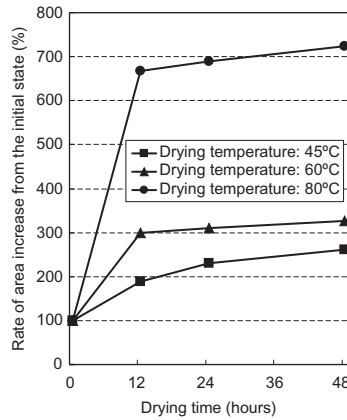


Figure 11. Rate of increase of asphalt mortar area.

to its growing viscosity facilitated by a higher ambient temperature (this phenomenon is described as “re-expansion of asphalt cover by temperature” hereinafter).

5.3 Re-expansion of asphalt cover by temperature

To ascertain the re-expansion of the asphalt cover by temperature in the base layer, FAM specimens (80 mm in thickness and 150 mm in diameter) were created using a gyratory compactor and were observed. These specimens were dried in an oven at 45°C, 60°C or 80°C after aeration for one week at a constant temperature (20°C). The changes of each specimen were observed after 12, 24 and 48 hours. Table 6 shows the observation results of the specimen dried at 60°C. Figure 11 shows the rate of increase of the asphalt mortar area from the initial state (i.e. 0 drying hours) for each case of the drying temperature. The observation results confirm that the asphalt in FAM will begin to show the property of a viscous substance when it exceeds its softening point (around 45°C), expanding its surface area. It was confirmed that the high temperature of asphalt reveals its viscosity more prominently. Therefore, the extent of asphalt cover re-expansion will be larger with a higher drying temperature.

6 INFORMATION TECHNOLOGY CONSTRUCTION SYSTEMS

Information Technology (IT) construction system has been greatly increasing the efficiency and effectiveness of civil engineering work. The system enables one to have centralized management of an enormous amount of three-dimensional data.

An IT system using Real Time Kinematics Global Positioning System (RTK-GPS) and Total Station (TS) is used throughout the construction of the upper reservoir. The IT system



Photograph 4. Levelling by a bulldozer Withures a 3D-MC system.

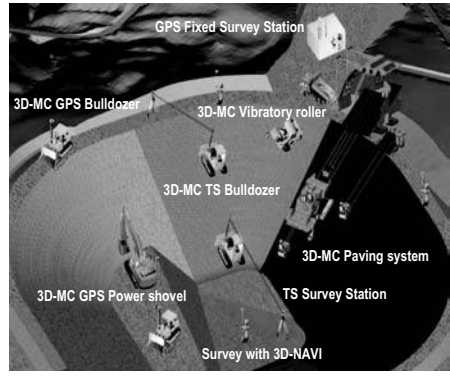


Figure 12. Civil engineering work with the IT system.



Photograph 5. Situation of the impervious layer.

greatly increased the construction efficiency. Photograph 4 shows scenes of levelling FAM by a bulldozer with a three-dimensional Machine Control (3D-MC) system, which is capable of automatically controlling the blade operation using three-dimensional design data. Figure 12 shows the civil engineering work with the IT system at the upper reservoir.

7 CONCLUSION

This report compiles the design, field construction and post-construction properties of FAM used for the base layer of the asphalt facing. FAM has such positive effects as cost reduction and a shorter construction period. Even though it partially slackens after winter, the slackness is gradually eradicated through the re-expansion of the asphalt cover, proving its value as a material which sufficiently satisfies the required performance of the base layer. As shown in photograph 5, Laying of the impervious layer was commenced in 2010, in addition to the laying of the base layer. And all possible measures will be taken to ensure proper quality control and schedule control as has been the case so far.

REFERENCES

- Seto, H. et al., 2010. Design and Construction of the Cold-Lay Foamed Asphalt Mixture at Kyogoku Project; The 11th International Conference on Asphalt Pavements, 1–6 August 2010. Nagoya: Japan.
 Takano, J. et al., 2004. The Rational Design and Construction System of Asphalt Facing in a Cold Heavy Snow Region; International Conference of Hydropower, 24–26 May 2004. Yichang: China.

Theme D: Dams in a sound environment



Emosson Dam, Switzerland (180 m, 1974).

Identification of hazardous zones for development of tourism industry: A case study in Taleghan dam catchment area

N. Ahmadi & H. Ahmadi
Tehran University, Tehran, Iran

ABSTRACT: Regarding the interactive effects of dam and tourism, one of the most important studies required prior to determination of dam structure location the local zone for settling, is to identify the conditions of tourism industry.

The Taleghan basin is one of the sub-watersheds of Sefidrood River basin. Construction of Taleghan Dam has resulted in great development of tourism industry in the region. Despite the notable environmental and economical potential, tourism because of inappropriate development process has caused irremediable damages to natural tender mountainous ecosystems and destructions of the region. This region is accepting a large number of tourists because of its attractive mountain ecosystem and its location which is near large cities such as Tehran and Karaj.

The research is performed in two scales: micro scale that consists of sub-watersheds corresponding directly to the reservoir and macro scale that includes the total catchment area.

Sensitive issues such as soil erosion, degradation and fragmentation of vegetation cover, settlement of population, geological and etc. have been identified through field studies and literature reviews in eighteen sub-watersheds of the area. Afterwards, by choosing the indicating, giving weightiness to them and finally overlaying them observed results were analyzed based on the implemented classification and then compared with the results of the degradation model. Finally, the map of hazardous region zones was prepared in order to plan tourism development on the basis of interactive effects of dam and environment. Study results show that no change has occurred within at most eastern limits of Taleghan watershed as well as the highest elevations of the watershed. On the other hand, sub-watersheds which more condensed population are encountered with more changes. Moreover, the development of population centers, adjacent to streamlines and construction towards the riversides has caused the entrance of pollution into the reservoir.

Therefore, the result of the study shows that eastern boundaries have a high potential of recreation development in a concentrated and expanded way. Also, some of the central and western sub-watersheds are capable of developing tourism industry by considering the environmental aspects. However, the development of tourism has been very rapid in the region, such that unfortunately development has occurred in places where their suitable potential capability is conservation or expanded recreation. Therefore by the increase of the construction and decrease of permeability of soil and also the senility of the lands to slipping because of the special geological structure and tectonic specification the ecological balance will encounter with sever irremediable effects. Regarding the coincidence of the developing area with hazardous zones of tourism development, if development continues in this way, we will the region will face with an environmental disasters and many tragic social and economical results.

1 INTRODUCTION

The land of Iran is located in an arid to semi-arid region and has always faced water shortages due to temporal and spatial imbalance of water supply and demand. The old history of

our civilization shows that, many centuries ago, our ancestors embarked on construction of hydraulic structures such as storage and diversion dams to optimize utilization of the limited fresh water resources available in the country. Notably, a corollary opportunity that develops after construction of a dam is the touristic attraction of the lake view in the region that helps in the development of the tourist industry.

Although tourism activities and visiting natural scenery and cultural and human-made attractive features are necessary for the leisure and vacation times of the people, the intensive concentration of such activities in one region and lack of due attention to the carrying capacity and ecological tolerance and sensitivities of the environment will have deteriorating and undesirable consequences and impacts (UNEP, 1992).

The relationships between tourism and environment are complex. On the decision making one hand, tourism has positive impacts such as economic development, prosperity, and job creation. On the other hand, it could also have negative quality effects on air, soil, and water resources, destruction of wild life habitats, degradation of natural vegetation, as well as damages due to intensified hunting and illegal trade of extinct species. Tourism could also have undesirable effects on social behavior and cultural values of a society and could create fake or “pseudo”-jobs” (Page et al., 1996).

In addition to the main objectives of water supply for residential and industrial purposes and generation of hydroelectric power, construction of large dams and development of reservoir lakes behind these structures has special aesthetic attraction for tourists. Lack of tourist management plans in the dam basin and site could cause problem for proper management of the dam and lead to increased environmental risks. These risks are intensified in mountainous basins with environmental sensitivities due to slope, rainfall, and geological aspects that make them susceptible to erosion. Therefore, any plan for development of tourism in the basin of the large dams needs detailed feasibility studies and identification of management priorities.

For the purpose of designing development plans for tourism, Dowling (1993) proposed an environmentally-based framework, or Environmentally Based Tourism Planning (ETP), which is based on environment and one of its main pillars is determination of the “critical locations” i.e. locations where environmental safety and tourism will cross and oppose each other. According to him, in tourism development, achieving sustainability and equilibrium is possible only when a strong relation is established between environmental conservation and tourism development.

2 NECESSITY OF SELECTING THE RIGHT LOCATION

Taleghan Catchment is located in a mountainous and elevated area in Central Alborz, about 140 km northwest of Tehran. This is one of the SefidRudRiver sub-basins or catchments with north latitudes of 36° 5' 40" to 36° 21' 5" and east longitudes of 50° 36' 40" to 51° 11' 16" as shown in [Figure 1](#). This catchment covers an area of about 960 km² with a perimeter of 161 km, a length of 51 km, average elevation of 3045 m, and the lowest point, located at the Taleghan Dam site, is 1688 m while the highest elevation is 4402 m in the northern highlands of the catchment (Bazabm 2001).

Climate of Taleghan is of cold mountainous type. The Taleghan River is the main stream of the study site that flows east-west and branches from the northern and southern slopes join the main stream. This catchment is located in the Central Alborz, which is tectonically active. Although it constitutes two third of SefidRudBasin, erosion and sediment yield in Taleghan catchment are higher than those of the other catchments in the basin. Using PSIAC method, the total sediment yield of Taleghan watershed has been estimated at 1086 tons per km² per year.

According to the statistics of the latest census of 2006, there are a total of 81 residential sites or villages in the Taleghan Catchment. In this study, 58 villages located in the upstream of the Taleghan Dam site are considered and include 4 villages of the Lower Taleghan District together with the villages of the Middle and Upper Taleghan Districts (Ahmadi, 2008).

Taleghan Storage Dam, that has a height of 103 m and a crest length of 111 m, has a lake area of 12.8 km². Construction of this dam has led to drastic changes in landscape, land use,

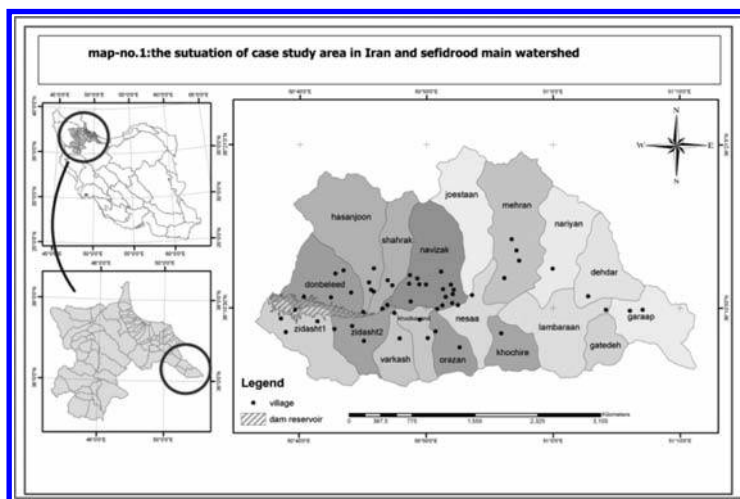


Figure 1. The project area situation in Iran.

tourism development in the region, and severe irreversible damages to the ecosystem of the catchment. After the dam was built, the original conditions of this mountainous area that had a rural economy dependent on agriculture and livestock production has changed to what is now a summer resort with a lot of gardens and an ever-growing touristic industry and the related services.

The catchment is now receiving many tourists from the nearby megacities of Tehran and Karaj who come to enjoy the attractive mountainous ecosystems, natural landscape, special habitats, the flora and fauna, and the lake behind the dam. Also, according to some documents, one of the priorities in development plans for the dam surroundings is promotion of tourism and tourist attraction programs (Ahmadi, 2008).

However, absence of development plans for construction of the infrastructures needed for expansion of tourism in the region and lack of due attention to the ecological carrying capacity of the area have resulted in extensive degradation and pollution of soil and water resources as well as visual pollution. Continuation of this trend will lead to destruction of the natural habitats and loss of the remaining ecotourism values of the region.

In order to improve the abovementioned situation and make optimum use of the tourism potential of this basin, it is necessary to determine the tourism management and planning priorities at sub-basins scale, taking into consideration the natural capabilities of the environment. The objectives of the present research were to determine these priorities and identify the critical and hazardous zones, as the first step toward reforming the ecotourism structure in the basin while keeping it in line with the objective of supplying drinking water from Taleghan Dam. It is to be noted that being oblivious to environmental risks and dangers of tourism industry, especially water pollution in the reservoir of the dam, can bring about secondary and indirect problems for the users.

3 METHODOLOGY

In order to determine the tourism management priorities in Taleghan Watershed and to study the trend of changes over the basin, the existing conditions were used as the baseline and three study methods were employed, namely, Degradation Model, Overlaying of Index (criteria) Layers, and prioritization on the basis of Fragmentation of Vegetation Cover. Using the available data, each of these three methods was used to analyze the conditions of the region. Finally, the output of each method was drawn as a catchment management priority map and was compared with the others. The results are presented in the following sections.

3.1 Prioritization method based on ecological parameters of the landscape

The main steps for determination of fragmentation of the vegetation cover in this method are as follows:

1. Selection of criteria for studying the changes
2. Determination of the zones that had undergone changes, using ArcGIS 9, Arcview 3.1
3. Analysis of the research results by using comparative method and system analysis
4. Determination of the catchments management and planning priorities.

In this study, the existing vegetation cover has been used as the index of the ecological resources i.e. vegetation type in each location/zone is indicator of the soil and climate of that area and soil type and texture is a function of the land morphology, parent material, bedrock characteristics, and its interaction with climate. Besides, vegetation type of an area affects the wild life and fauna and, depending on its use and quality, it can affect social environment of the human communities and the way they use the vegetation: this can be one of the reasons for the development of a special livelihood structure in a particular region.

Construction of a dam and its related structures bring about great changes in the landscape, such as the access roads. Thus, the changes in the characteristics of the patches of vegetation cover (as indicators of ecological resources) were studied in two periods: before and after dam construction.

The most important landscape parameters used in this study are as follows:

TA: Total area of the landscape, NP: number of patches, MPS: mean patch size, and richness of the patches.

In order to sum up the above-mentioned parameters, they were compared with the elevation layers, the existing ecosystems in the studied basin, land use plan, rangelands status and trends, and population centers. This comparison was carried out with the intention of comprehensive analysis and interpretation of the reasons for the changes that occurred and their effects on other ecosystems. The result is shown in [Figure 2](#).

3.2 Method of overlaying

This method was first used by McHarg (1969). In the present research, layers of habitats, slope, and erosion were overlaid to identify the locations with the maximum and the minimum environmental sensitivity. The habitats layer contains the sensitivity of the region from the standpoint of wildlife and vegetation type. Selection of the erosion layer was due to the fact that, in PSIAC method, erosion is estimated by making use of 9 physical parameters of the environment and, practically, erosion map reflects these nine parameters. The slope layer was

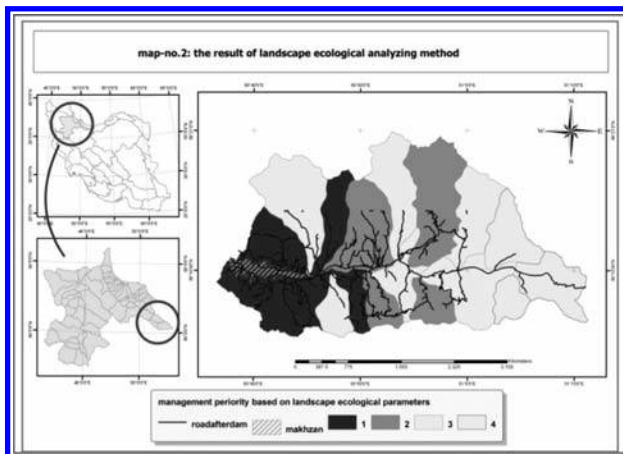


Figure 2. The result of landscape analyzing method.

used by taking into consideration the classification criteria needed for the tourism ecological model (Makhdoom, 2005).

To achieve quantitative results for the purpose of classification of the sensitivities, in the habitat and slope layers, three classes were considered, namely, 1) small, 2) medium, and 3) high. In the case of the slope layer, however, four classes were chosen: 1) slight, 2) medium, 3) high, and 4) very high. In the slope layer, weighting was based on the proper slope percentage used in the class 1 of the tourism ecological model.

After carrying out the quantitative classification in each layer, the information layers were multiplied by using the tools available in GIS. The resulting figures could vary between 0 and 36. Considering the different possible cases resulting from multiplication of the layers, Table 1 was developed for classification of the sensitivities. The result map is shown in Figure 3.

3.3 Method of degradation model

This model was first developed by Makhdoom in 1992 and was used in assessing environmental impacts of development. The method uses linear models to show the degradation in the target units, which can be watershed, sub-basin or catchment, ecological/environmental unit, or a network (Makhdoom 1992).

The model used is shown below:

$$D \cdot Ci = \frac{\left(\sum Ai \cdot Ii + D \cdot Pi \right)}{E \cdot Vi} \quad (1)$$

where, $D \cdot Ci$ = Degradation Coefficient; Ai = Agent of Degradation; Ii = Intensity of Degradation Agent; $D \cdot Pi$ = Density of Population; EVi = Environmental Vulnerability Code; i = Number of the Target Unit.

Table 1. Classification of the sensitivities of different parts of the study site based on the results of multiplication of the layers.

Results obtained from multiplication of layers	Sensitivity assessment class
0–3	Low
4–6	Medium
7–9	High
10–36	Very High

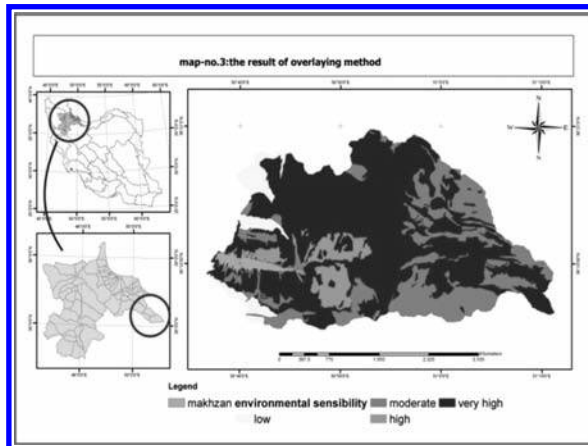


Figure 3. The result of overlaying method.

In this method, the first step is field identification of all degradation factors in each target unit and their qualitative classification in one of the following four classes: Code 1—slight degradation, Code 2—medium degradation, Code 3—severe degradation, Code 4—very severe degradation. In the next step, physiological density is calculated for each unit by determining the area of agricultural lands and population and using the following equation

$$D \cdot Pi = \frac{Pi}{Ari} \quad (2)$$

where, $D \cdot Pi$ = Physiological density in unit i ; Pi = Population in unit i ; Ari = Area of agricultural lands in unit i .

Then, environmental vulnerability is calculated using the map of the ecologically/environmentally effective factors affecting degradation such as slope elevation, climate, soil susceptibility, etc. Vulnerability is then grouped in four classes based on the number of factors and the ranges of the figures calculated. Table 2 shows the definitions for the four environmental vulnerability classes (Makhdoom 1992).

In the next stages of this method, a degradation model is developed for each target unit. This is done by adding the physiological density to the sum of the intensities of degradation factors in the numerator of the fraction in Equation 1 and the environmental vulnerability code is used as the denominator. The result is a figure that reflects the degree of degradation in each unit (Maladil 1992).

In the final stage of the method, degradation coefficients are grouped into six classes as shown in Table 3.

In Taleghan watershed studies, degradation factors have been identified and recorded in 18 catchments (sub-basins). The most important of these are over-exploitation of the natural resources, land use change, over-grazing, plowing along the slope, soil and water pollution, and habitat destruction. These factors were used as model inputs and in each catchment the degradation intensity was assessed by considering these factors and extensive field observations.

Environmental degradation was also determined using the information on maps of slope, erosion, vegetation cover, and geology. Overall, based on all the aforementioned factors and calculations of physiological density and considering the cultivated areas of agricultural lands, the final map of areas suitable for (tourism) development, or those that require conservation and protection, was drawn by the model. The map was verified by ground trusting and its reliability was assured.

Table 2. Environmental vulnerability classification.

Code	Degree of vulnerability
1	Vulnerable
2	Sensitive
3	Semi-sensitive
4	Tolerant

Table 3. Classification of degradation coefficients and decision making on suitability for development.

Suitability for development	Range of degradation coefficient	Class
1	1.33–4.99	Suitable for further development
2	5–14.99	Needs rehabilitation
3	15–19.99	
4	20.56–29.98	
5	30–47	Needs conservation actions
6	47.21–73–49	

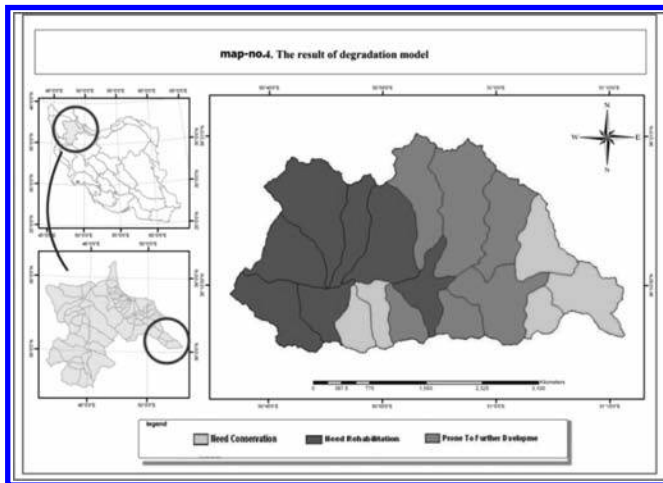


Figure 4. The result of degradation model.

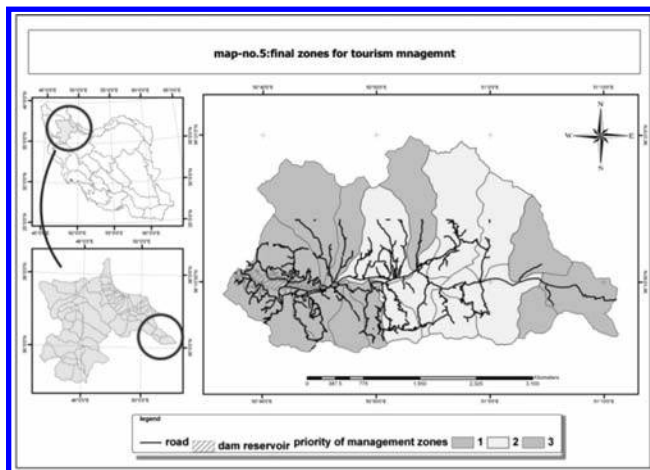


Figure 5. Final zones for tourism management.

4 CONCLUSION AND SUM UP

The results of the study show that, within the east end of Taleghan watershed and the highest elevations of this part, no significant change has taken place. Furthermore, with increasing distance from the dam reservoir, the changes have decreased. On the other hand, the catchments that have more population centers have undergone more changes. Besides, next to the sensitivity of the mountainous ecosystem of the region, the hills ecosystem, as a transitional eco-tone, is susceptible to the greatest losses and degradation. Also, development of population centers next to the waterways and construction of buildings within the river frontage lands intensify water pollution of the dam lake. Additionally, destruction of the natural vegetation cover increases soil erosion and transfer of sediments to the dam reservoir. The susceptibility of the geological formations around the lake to land slide poses a great challenge and risk to land use change.

Therefore, the results obtained in this study show that the eastern parts of the region are suitable for recreational developments. Also, some catchments in the central and western sections of the watershed have potential for tourism development, though considerations

should be given to environmental criteria. Nevertheless, it should be stated that, presently, tourism development in this basin is too rapid and, unfortunately, this development has been in areas that are only suitable for recreation or need conservation and protection. Increase in construction activities and decrease in soil infiltration will have irreversible damages to the ecological equilibrium of the basin. Considering that the present developmental activities overlap the high risk zones for tourism development, continuation of the prevailing trends will soon lead to an ecological catastrophe, with grave socio-economical consequences. By the result of method no. 1, four sub watershed which are adjacent to dam reservoir have the most fragmentation by considering the landscape ecological parameters. In the map no. 1 which is the result of applied method no. 1 these sub watersheds are the first priorities of zoning management program for tourism development.

The results mentioned above are compiled with the result of degradation model which introduce them for rehabilitation. In fact these sub watersheds are the most crisis zones in Taleghan watershed.

In the map resulted from method no. 2. Mountains ecosystems and Hills ecotones which are adjacent to dam reservoir have more and the most environmental sensibility and any shape of development should be based on intelligent and accurate programming for tourism.

The sub watersheds which are introduced capable for future developments in degradation model by considering the result of method no. 1 are zones with lower degradation and are remained some safe from unplanned developments after dam construction.

In the sensibility map these watersheds have very high sensibility and are suitable for outdoor recreation based on conservation methods and some other places with moderate sensibility are suitable for intensive tourism developments in case of complementary studies.

The eastern zones need to be conserved based on result of degradation model and have very high and moderate sensibility. These zones have the lowest degradation and fragmentation so are not the priority of the management programming comparing to other places with more crisis situation in Taleghan watershed.

REFERENCES

- Ahmadi, N. 2008. Analyzing the effects of Taleghan dam by landscape ecological parameters; Master degree thesis. Tehran University.
- AzariDehkordi, F., Makhdoum, M.F., & Nakagoshi, N. 2003. Sefiedrood River Sub Watershed-dam-estuary and degradation model: A holistic approach in Iran. *Chinese Geographical Science*, 13(4): 328-333.
- Baazab Consulting Engineers Company. 2000, Taleghan dam reservoir project study.
- Botequilha, A. & Ahrea, J. 2002. Applying landscape Ecological Concepts and Metrics In Sustainable Landscape Plannin. *Landscape and Urban Planning Journal*, 59(2002): 65-93, Elsevier Pub.
- Dowling, R.K. 1993. An environmentally based planning model for regional tourism development; *journal of sustainable tourism*, 1(1): 17-37.
- Farina, A. 1998. *Principles and Methods in Landscape Ecology*. London: Chapman & Hall 234 pp.
- Forman, R.T.T. 1995. *Land Mosaics: The Ecology of Landscapes and Regions*. USA: Cambridge University Press 632 pp.
- Madadi, H. 2004. Development of GIS for automatic environmental impact assessment. Master degree thesis. Tehran University.
- Page, R., Bayley, S., Cook, D., Green, J.E., & Brent, J.R. 1996. *Bnaff-BowValley: At the crossroads*. Prepared for the honorable minister of Canadian heritage, Ottawa.
- Rezvani, A. 1995. *Geography and tourism Industry*. Payam Noor Univerity Publishing pp. 225 (In Farsi).
- Soltani, M. 2000. *Tourism and Environment*. *Environment Periodical*. Vol 32. pp. 39-43.
- UNEP. 1992. *Tourism and the environment: fact and figures; Industry and environment*. 15(34): 3-5.

How to maintain the bad reputation of dam projects

R. Zwahlen

Pöyry Energy AG, Zurich, Switzerland

ABSTRACT: Hydropower and dam projects are either considered as a sustainable and environmentally friendly way of producing energy, or as devastating, environmentally and socially disruptive projects. This bad reputation (which is the one the public usually gets from newspaper articles) continues to thrive in spite of all efforts of the recent past to improve environmental and social acceptability of such projects. It is argued here that this is the case because there is still a continuous flow of high-impact projects, which are not acceptable from an environmental or social point of view, reaching the project pipeline, providing arguments against dam projects. The way to address this problem would be to include social and environmental considerations already in the very earliest steps in project identification, i.e. long before the EIA process starts, and then to accept that not every technically feasible project is necessarily a sustainable one. This approach, besides reducing anti-dam arguments, would also save costs involved in planning of projects which will then be abandoned at a later stage due to environmental or social reasons.

1 INTRODUCTION

One striking issue about hydropower and dam projects is the fact that they continue to receive two completely contradictory qualifications: On the one hand, hydropower is praised as “clean, renewable, and sustainable energy resource” or “the most environmentally friendly option for power generation”, on the other hand we read about “environmentally and socially devastating dam projects” or, as Leslie (2005) puts it, “dam’s monumental destructiveness”. This paper tries to show why, despite all the efforts made so far (WCD 2000), the bad reputation of dam projects is being maintained, and what we might be able to do about it.

2 MAIN IMPACTS OF DAMS

It is an obvious fact that every dam project—like any other human activity—has effects on the environment. Very shortly, the main negative environmental impacts which to some degree every dam project has are the following (Zwahlen 2003):

- Interruption of a river continuum. A dam built across a river will always interrupt a system that used to be an entity. Direct consequences of this interruption are a change in river flow patterns, a change in sediment transport (sediment retention in the reservoir, risk of increased erosion downstream), an interruption of fish migration (complete for upstream migration; obstacle and risk for downstream migration, since this has to go through the turbines or the spillways), and the interruption of drift (i.e. the more or less passive displacement of various organisms downstream).
- Change in river discharge pattern downstream of the dam. This effect is closely related to the first one. In this respect, two main parts of the river can be identified: 1) between the dam and powerhouse outlet, where discharge is reduced, in extreme cases to zero, and 2) downstream the power house outlet, where river discharge is influenced by plant operation. These changes can also affect floodplain dynamics in the downstream area.

- Change from river to lake conditions in a part of the former river at the formation of the reservoir. Water quality will change due to this effect, and the new lake is a habitat very different from that of the former river.
- Destruction of terrestrial habitats. Terrestrial habitats within the reservoir area will be permanently destroyed, because they are going to be covered with water. This has effects on vegetation and fauna, as well as on the human population living in this area.
- Access to the area provided by new access roads. Although the direct impact of the roads (e.g. on vegetation) might be rather small, the roads can trigger a development, especially in cases when hitherto inaccessible areas are opened in this way, which can have very considerable environmental effects.
- Social impacts. These can be manifold. The most important in many cases is the involuntary resettlement as a consequence of a dam project, but there are also other socio-economic effects, such as effects on the population in the downstream area (through disruption of river floodplain dynamics, groundwater table changes, etc.); immigration into the area, especially during the construction phase, as a consequence of job opportunities; and effects on the host population for the resettlers.

The magnitude and the importance of these impacts can be very different from one project to another and need to be assessed for every case. When it comes to sustainability, there is also a controversy on whether hydropower as such is a sustainable way of producing energy, or if this is only the case for small hydro (whereby it is not quite clear what “small” in this context exactly means, see e.g. Scudder (2005), Frey & Linke (2002).

This question cannot be answered on a mere principle of size, but has to be checked on a case by case basis. In this discussion, alternatives have to be taken into consideration. Hydropower will continue to play an important role, and this also in view of the “demystification” of alternative energy sources. While solar and wind energy, a short while ago, were still considered as the sustainable answer to energy production, at closer scrutiny it became clear—not surprisingly—that they also have their drawbacks, like noise and danger to birds and bats for wind farms, occupation of large areas of land and interference with different, also desert, ecosystems for solar panels, and impacts on landscape for both systems (see e.g. Barrios & Rodriguez 2004, Gill 2005, Johnson et al. 2002, Kunz et al. 2007, Leitner 2009, Reynolds 2006, SL 2001, Stewart et al. 2007).

3 CASE STUDIES

The purpose is to discuss situations that can lead to projects considered as socially or environmentally unacceptable. However, the aim is not to point the finger at certain organisations, projects or even persons. Therefore, the “case studies” are fictional, although based on real cases.

3.1 *Case 1: Resettlement*

Here, the project is a high dam in a remote mountainous area, difficult to access. The high dam will submerge a narrow valley, forming a long, deep and rather narrow reservoir. An EIA (Environmental Impact Assessment) had to be prepared for this project as part of the feasibility study. When establishing the scope for this EIA (or better: ESIA, Environmental and Social Impact Assessment; see below) the information available (from persons who had visited the site already) was that “nobody lives in the reservoir area”.

As it turned out, there were several villages within the reservoir area: The winter quarters of a tribal population of semi-nomadic herdsman who spend the summer with their livestock at higher elevations, but depend on this low lying valley as a winter quarter for their herds and themselves, when the summer pastures are covered with snow. Obviously, their livelihood and lifestyle depends on the availability of both summer pastures and winter quarters.

The fact that the project area is actually inhabited in the described way does not necessarily mean that this has to be considered as a reason for abandoning the project. However, not taking into account the resettlement issue—or not to a sufficient degree—is a very sensitive issue, which can cause a very negative image of the project. Besides, in this case the affected population being a rather marginalised ethnical minority (differing from the mainstream population in lifestyle, language, traditions and self-identification) this also triggered WB OP 4.10, and there is a high risk of drawing attention to the project, again as a bad example. According to all internationally accepted guidelines, at the very least the standard of living of the affected population should be kept at its pre-project level. This can obviously only be achieved if the situation is known and if the resettlement and compensation issue is planned and implemented very carefully.

3.2 *Case 2: Biodiversity*

In another mountainous and rather remote area, all relevant tributaries of a major river had been earmarked for hydropower development. The general plan was to have cascades of 2 to 4 dams and hydropower plants in each of these valleys. In the steep and narrow valleys, reservoirs would be rather small, but given the high head of all these projects, energy production would be quite high in spite of the fact that discharge of the harnessed streams is rather modest.

In a valley which was one of the first to be selected for this type of development the feasibility study revealed that, a number of years ago, this very site had been identified as a biodiversity hotspot. It is a suitable habitat of a number of endangered species, and it harbours the largest population of one very rare and highly threatened species. The main reason for this is the fact that, unlike most of the other valleys in this area, it is covered to a large degree with almost intact and so far not exploited forests. This is due in part to climatic reasons, since because of its location it receives slightly more rain than the other valleys, but at least as much also to the fact that there is no access road, which under these topographical conditions makes logging almost impossible; the small amount of logging done by the local population for their own needs can (still) be considered as a sustainable use of the forest. Since more than 10 years, a number of international organisations (NGOs as well as state agencies) had different programs under way in this valley which aimed at sustainable development, integrating the protection of the remarkable biodiversity with an improvement of the economic situation of the population.

The dams foreseen by the project were certainly high dams according to ICOLD definitions, but the reservoirs, given to the steep and narrow valley, would have been rather small. Besides, neither dams nor reservoirs would affect any core habitats; mainly, they were not located within or close to the ecologically important forests. The main problem there would be the access road, without which construction of these dams and appurtenant structures would not be possible. Inevitably, the access road would make the valley accessible for heavy vehicles, and would make logging—whether legal or illegal—possible. With the high and increasing demand for timber, there is no doubt that these forests would come under heavy pressure. The importance of roads for deforestation has been shown in many different regions of the world (e.g. Ali et al. 2005, Cropper et al. n.d., Michalski et al. 2008, Khan & Khan 2009).

3.3 *Case 3: Protected areas*

A site selection study for hydropower plants had identified 5 potential sites on one river (Fig. 1). The study had been done exclusively taking into account engineering (topography, hydrology) and economic criteria.

Subsequently, site No. 2 was selected as the first site to be developed. It turned out that not only this site was located within a national park (a fact which the site identification study had not mentioned), but that it was in a core area of this park, affecting one of its main attractions. Furthermore, it required an access road of about 60 km through dense forest, 40 km of which within the national park.

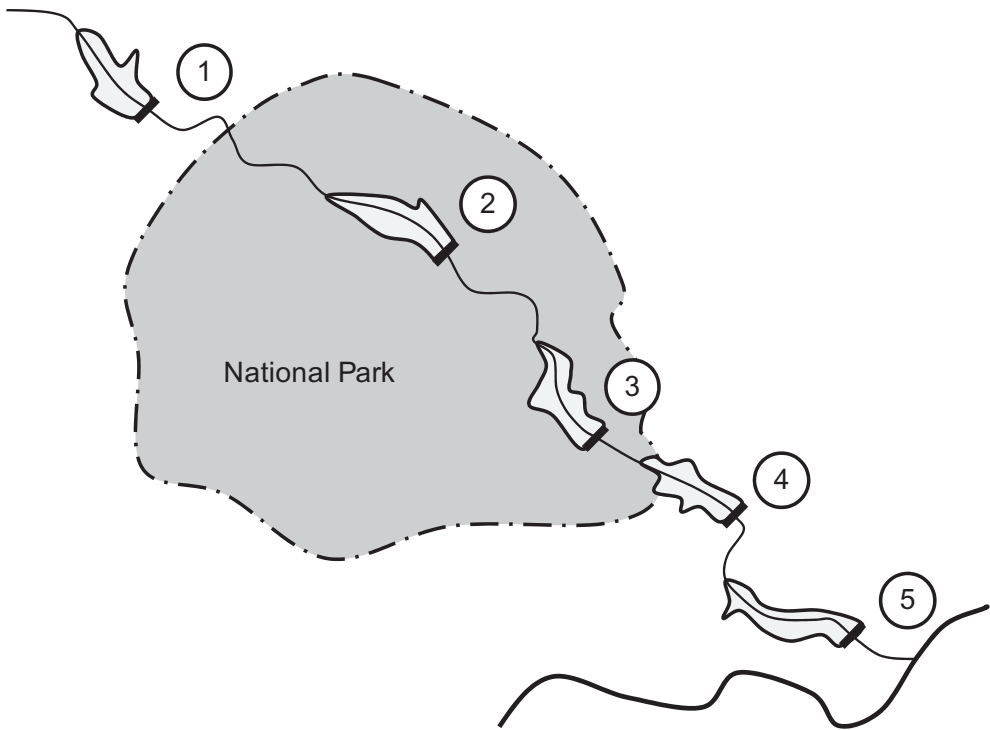


Figure 1. Sites identified as suitable for hydropower development.

A comparison of the alternatives showed the following:

- None of the projects would have required any resettlement. While all reservoir areas contained some resources used by the local population, none of them was inhabited.
- No. 3 is also located within the park, although in a much more marginal area, not affecting the core values of the park, and requiring a substantially shorter access road.
- No. 4 is mostly outside the park, only a small part of the reservoir still reaching it. Access does not affect the park.
- Nos. 1 and 5 are entirely outside the national park, access does not affect the park.

The recommendation of the ESIA was to abandon site No. 2 and to develop site No. 5, which had the additional advantage of being more easily accessible.

4 CONCLUSIONS

There is a long history of dam projects which have been contested, more or less vehemently, by NGOs and civil society. Murchison Falls HPP in Uganda, planned in the late 1960ies, might have been one of the first hydropower projects which experienced resistance on grounds of nature protection, but there have been many others, rather well documented in an extensive literature either focussing on single projects (Hong 1987, Khagram 2004) or on a more general level (Goldsmith & Hildyard 1984, McCully 1996, Leslie 2005, Scudder 2005). In all these projects, public discussion was never about technical details, but always about environmental and social impacts. Major topics in these discussions are either impact on nature (landscapes, habitats, protected areas, endangered species) or social impacts (displacement, loss of resources).

Dam induced resettlement is an especially important and sensitive topic. While other projects (roads, railways, mining etc.) can also lead to forced displacement of a considerable

number of people, reservoirs were—and will continue to be—at the forefront of this discussion, due to the often large areas they cover and due to the fact that people tend to concentrate in river valleys, which offer important resources as water, fertile alluvial soils, and transport routes. Unfortunately, this is exactly where dams and reservoirs are located.

The problem is well known, and so are the ways how to deal with them, at least in principle (e.g. Cernea & McDowell 2000, De Wet 2006). Internationally accepted guidelines, as e.g. the World Bank's OP 4.12 on resettlement, the Equator Principles and others show the way. Unfortunately, the reality shows another picture. Scudder (2005) analysed the results of resettlement programs of 50 dam projects, with resettlements from less than 1000 to more than 50,000 people. Out of 44 projects for which the required data were available, 3 had been classified as good (improving living standards for the majority), while 31 were unsatisfactory (worsened living standards for the majority). This shows two things: First, that it is possible to reach good results in a resettlement program; second, that the result does not necessarily depend on the size of the project. One of the 18 projects in the category of resettling between 10,000 and 50,000 people achieved a good result, showing that this is feasible even for large projects. On the other hand, in one case out of three where less than 1000 people were resettled, the result was unsatisfactory (and in one case good, but for reasons not related to the project), which shows that even the seemingly easy task of resettling a small number of people can be done badly.

Obviously, Scudder's sample contains a number of projects which have been carried out rather a long time ago. However, and without having a statistical evidence for this, I have the feeling that if a similar sample of projects presently under way or recently accomplished would be analysed, the result would not be fundamentally different.

The Environmental Assessment, which is the procedure developed for dealing with these issues, consists in the following phases (see e.g. IHA 2004):

1. Environmental screening: Preliminary identification of potential impacts and risks (IEE, Initial Environmental Examination).
2. Scoping: Definition of the scope of work for the preparation of the ESIA Report (definition of TOR, Terms of Reference).
3. Preparation of the ESIA Report and associated documents. Carrying out of field studies (according to TOR); description of the prevailing situation, identification of impacts, definition of required measures; preparation of the Environmental and Social Management Plan (ESMP) and, if required, the Resettlement Action Plan (RAP).
4. Appraisal: This is done by the competent authority. It is about acceptability of the ESIA report (done according to TOR, relevant standards and requirements of the authority), completeness and plausibility (identification of impacts), and finally a decision on acceptability of the project which also includes a statement on measures proposed in the ESIA that are a condition for project implementation.
5. Implementation: During the construction phase of the project, and to some extent during the operation, ESMP and RAP have to be implemented.
6. Monitoring: Surveillance of ESMP and RAP implementation, and identification of corrective measures in case of non-compliance.

In current projects, screening and scoping is usually done rather well. Potential impacts are usually addressed in the TOR, and these are mostly realistic. One point that in my experience is often not really well judged in this phase—obviously with consequences for the subsequent steps—is the issue of public participation. Too often the TOR—correctly—ask for a comprehensive public participation process, but the available budget does not take into account that this is a time consuming process.

Considerable improvement has been reached in the preparation of ESIA Reports. Usually, the relevant topics are covered in the reports, and the important impacts are usually identified. Still, there are reports which ignore certain important topics, or come to wrong (or strange) conclusions where impacts are concerned. The most frequent problem with many reports is probably the fact that sometimes the part of identifying mitigation measures is rather weak; this can be in the form that measures are proposed which are not justified by the expected impacts, or that proposed measures are strictly not feasible.

The appraisal process of such studies and projects is not always without problems. Too often, still now, comments by the authority in question insist on purely formalistic issues, or unrealistic measures are not identified as such. This is obviously related to the lack of experience of some of these authorities, and possibly sometimes also to their rather weak position in the process of decision making.

In an ex-post study of environmental effects of a Brazilian hydropower project Barrow (1988) came to the conclusion “that there is a need for more study of impacts downstream ... , and for an examination of *why some predicted difficulties have not in practice been avoided*” (emphasis added). My impression is that a closer look at many dam projects put in operation since then might come to the same conclusion. Undoubtedly, implementation of ESMPs and RAPs has improved and is well handled in a number of projects, and this especially in cases where an external monitoring is being carried out, as it is now the rule for projects financed by multilateral funding agencies. Nevertheless, this is often still a weak point, too many of these plans still end up in the bottom drawer once the project has received the “green light”. Implementation and monitoring still needs to be improved.

5 RECOMMENDATIONS

However, the weakest link in the whole project chain is still the earliest stage of project development, the identification of suitable project sites. Still now, such evaluations are often being done based solely on technical and economic criteria.

I very strongly suggest that no such evaluation should be done without duly taking into consideration environmental and social issues.

The most critical points to be considered at this early stage are the following:

- presence of and impacts on a national park or a similar protected area;
- impacts on special (rare, highly diverse, very sensitive ...) ecosystems or habitats;
- densely populated area, high number of people to be relocated; and
- area inhabited by an ethnic minority.

Not all of these characteristic are equally easy to identify, and the magnitude of the expected impact will again depend on the project. Therefore, these conditions do not necessarily mean an “early out” for a project; however, their presence should raise an alarm at an early stage, the earlier the better.

Costs as the reason for not including environmental and social considerations at this early stage is not a convincing argument. If a project is being investigated through a number of stages, from pre-feasibility through feasibility to detailed design, including geological investigation, ESIA etc., and then has to be abandoned due to reasons of environmental or social impacts which would have been obvious right from the start, if only somebody had looked at them, then this is a waste of money. Undoubtedly, the Pareto Principle (according to which 20% of invested input is responsible for 80% of the results obtained) can be applied here as well: A short (and therefore not very costly) site visit by an experienced ESIA expert will, as a rule, provide most of the information required for correctly addressing the main impacts of a project. Discussions with selected stakeholders, like NGOs, already at this stage can also be very helpful (Zwahlen 2007). The time consuming and costly part is then to go into details, namely, carrying out all the work which is required for preparing the ESIA for the project and should only be done for projects which have a high chance of success. The same, obviously, is true for the engineering part of a project. We have to accept the fact that not every technically feasible project is necessarily a good project (in the sense of sustainability), and that in some cases “no” has to be accepted as an answer.

Not considering environmental and social issues in the very early stages of a (potential) hydropower project can easily result in a considerable waste of time and money. It is also the best guarantee for maintaining a steady stream of environmentally and/or socially unacceptable dam projects getting into the project pipeline and then into the public discussion. In this way the bad reputation of dam projects will be maintained.

REFERENCES

- Ali, J., Benjaminsen, T.A., Hammad, A.A., and Øystein, B.D., 2005: The road to deforestation: An assessment of forest loss and its causes in Basho Valley, Northern Pakistan. *Global Env. Change Part A* Vol. 15, 4:370–380.
- Barrios, L., and Rodríguez, A., 2004: Behavioural and environmental correlates of soaring-bird mortality at on-shore wind turbines. *Journal of Applied Ecology* 41(1):72–81.
- Barrow, C., 1988: The impact of hydroelectric development on the Amazonian environment: With particular reference on the Tucuruí project. *Journal of Biogeography* 15:67–78.
- Cernea, M.M., and McDowell, C. (eds.), 2000: *Risks and reconstruction. Experience of resettlers and refugees*. World Bank, Washington DC., 487 pp.
- Cropper, M.L., Griffiths, C., and Mani, M., (n.d.): Roads, population pressures, and deforestation in Thailand, 1976–1989. *World Bank Policy Research Working Paper Series* No. 1726.
- De Wet, C., 2006: *Development-induced displacement: Problems, policies and people*. Studies in Forced Migration Vol. 18. Berghahn, New York, Oxford, 218 pp.
- Dorcey, T., Steiner, A., Acreman, M., and Orlando, B. (eds.), 1997: *Large Dams: Learning from the past, looking at the future*. Workshop Proceedings, Gland, Switzerland, April 11–12, 1997. IUCN/The World Bank, Gland and Washington, 145 pp.
- Frey, G.W., and Linke, D.M., 2002: Hydropower as a renewable and sustainable energy resource meeting global energy challenges in a reasonable way. *Energy Policy* 30(14):1261–1265.
- Gill, A.B., 2005: Offshore renewable energy: ecological implications of generating electricity in the coastal zone. *Journal of Applied Ecology* 42(4):605–615.
- Goldsmith, E., and Hildyard, N., 1984: The social and environmental effects of large dams. Vol. 1: Overview: 346 pp. Vol. 2: Case Studies: 331 pp. Vol. 3: A Review of the Literature: 243 pp. Wadebridge Ecological Centre, Camelford, UK.
- Hong, E., 1987: Natives of Sarawak. Survival in Borneo's vanishing forests. Institut Masyarakat, Malaysia, 265 pp.
- IHA, 2004: *Sustainability Guidelines*. International Hydropower Association, February 2004, 24 pp.
- Jia, J., 2010: *Rethinking the role of dams and hydropower in sustainable development*. World Atlas 2010, The International Journal of Hydropower & Dams: 8–9.
- Johnson, G.D., Erickson, W.P., Strickland, M.D., Shepherd, M.F., et al., 2002: Collision mortality of local and migrant birds at a large-scale wind-power development on Buffalo Ridge, Minnesota. *Wildlife Society Bulletin* 30(3):879–887.
- Khagram, S., 2004: Dams and development. Transnational struggles for water and power. Cornell University Press, Ithaca, 270 pp.
- Khan, S.R., and Khan, S.R., 2009: Assessing poverty-deforestation links: evidence from Swat, Pakistan. *Ecological Economics* 68(10):2607–2618.
- Kunz, T.H., Arnett, E.B., Cooper, B.M., Erickson, W.P., et al., 2007: Assessing impacts of wind-energy development on nocturnally active birds and bats: a guidance document. *Journal of Wildlife Management* 71(8):2449–2486.
- Leitner, P., 2009: The promise and peril of solar power. *The Wildlife Professional* 3(1):48–53.
- Leslie, J., 2005: *Deep Water*. The epic struggle over dams, displaced people, and the environment. Picador, New York, 352 pp.
- McCully, P., 1996: *Silenced rivers*. The ecology and politics of large dams. Zed Books, London, 350 pp.
- Michalski, F., Peters, C.A., and Lake, I.R., 2008: Deforestation dynamics in a fragmented region of southern Amazonia: evaluation and future scenarios. *Environmental Conservation* 35(2):93–103.
- Reynolds, D.S., 2006: Monitoring the potential impact of a wind development site on bats in the Northeast. *Journal of Wildlife Management* 70(5):1219–1227.
- Scudder, T., 2005: *The future of large dams*. Dealing with social, environmental, institutional and political costs. Earthscan, London, 389 pp.
- SL, 2001: Windenergie im Konflikt mit dem Landschaftsschutz. Mit der Masthöhe und dem Durchmesser der Rotoren weiten sich die Konflikte um die Landschaft aus. *Landschaftsschutz 2000*. Jahresbericht der Stiftung Landschaftsschutz Schweiz: 20–25.
- Stewart, G.B., Pullin, A.S., and Coles, C.F., 2007: Poor evidence-base for assessment of windfarm impacts on birds. *Environmental Conservation* 34(1):1–11.
- WCD, 2000: *Dams and development. A new framework for decision-making*. The Report of the World Commission on Dams. Earthscan, London, 404 pp.
- WWF, 1999: *A place for dams in the 21st century? A WWF International Discussion Paper*. WWF International. Gland, 108 pp.

- Zwahlen, R., 2003: Identification, assessment and mitigation of environmental impacts of dam projects. In: Ambast, R.S. (ed.): *Modern Trends in Applied Aquatic Ecology*. Kluwer Academic Publishers, New York, 281–370 pp.
- Zwahlen, R., 2006: The value of talking to NGOs: A case study. Proceedings, Asia 2006, *International Symposium on Water Resources and Renewable Energy Development*, Bangkok, Nov. 30 and Dec. 1, 2006.

Measures for vegetation restoration on modification sites at Takizawa dam

N. Takemoto

Japan Water Agency, Arakawa Dam Integrated Management Office, Chichibu, Saitama, Japan

Y. Takahashi & M. Hirose

Japan Water Agency, Environmental Department (Head Office), Saitama, Saitama, Japan

ABSTRACT: Takizawa Dam is located in Chichibu-Tama-Kai National Park in Saitama Prefecture, Japan. Since the national park is rich in nature, it was aimed to reduce impact on ecosystem in the area and downstream during the construction of the dam. Measures for vegetation restoration were taken on all modification sites as the quarry site, cut slopes of the road, and cut slopes near the dam body generated by the dam construction projects. The total area of vegetation restoration is about 130,000 m². The materials used for the restoration were the surface soil near modified sites and purchased soil, seeds gathered near the modification sites, seedlings grown from the gathered seeds, and trees going to be underwater by the appearance of the dam lake. Especially, in the quarry site, the seeds of pioneer trees were sprayed with soil on slopes by seeding work (double layer spraying and seed spraying, etc.), and the seedlings of native species were planted on the berms and platforms. Measures for vegetation restoration began in 2001 and completed in 2007. The monitoring survey has been carried out at regular intervals to investigate the degree of germination and restoration. This report shows the present states of vegetation restoration and the imported alien species on the quarry site among the measures of vegetation restoration at Takizawa Dam.

1 INTRODUCTION

In Japan, a lot of legal systems and measures have been enacted for the conservation of the biological diversity which has been taken into considerations in a variety of discussions and suggestions on re-vegetation matter as well (Fukunaga et al. 2008, JSORT 2002, Kobayashi and Kuramoto 2006, MOTEIJ et al. 2006). However, in Japan, design and construction of re-vegetation to conserve biological diversity have been carried out without a collective view of concrete method (DMOROS 2004). In order to solve this problem, an accumulation of data on survey, design, construction, and monitoring regarding to re-vegetation, data sharing and an appropriate evaluation of those data are essential. In addition to an improvement of present situation by making up a gap between the policy and on site technical capability, an immediate countermeasure against negative influence on local ecosystem by alien species should be carried out at each site.

Located in Chichibu in Ara River System in Japan, Takizawa Dam is a multipurpose dam constructed and completed by Japan Water Agency in 2008. Vegetation restoration has been executed since 2001 based on a policy of natural recovery without alien species that have negative influence in the area and downstream but with native species collected near the dam sites (Inaba et al. 2004). Vegetation restoration, whose area is approximately 130,000 m², is carried out in such modification sites due to dam project as the quarry site, cut slopes of the road and cut slopes near the dam body. Vegetation restoration used the seeds collected around the dam and seedlings grown from them, trees grown up in the area that was going

to be underwater because of the dam lake, and materials available in the basin such as soils of modification sites (Inaba et al. 2004). In the quarry site, the seeds of pioneer trees were sprayed with soil on slopes by seeding work (double layer spraying and seed spraying, etc.), and the native seeds and seedlings were planted on the berms and platforms by planting work. Vegetation restoration was completed in 2007. The monitoring survey has been carried out at regular intervals to investigate the degree of vegetation growth.

In measures for vegetation restoration using native species in Takizawa dam, we report the present states on the quarry site. And we discuss the factors of difference of states of vegetation restoration and imported alien species on both slopes sprayed with soils by seeding work and piled with the surface soil.

2 OVERVIEW OF TAKIZAWA DAM

Takizawa Dam is a concrete gravity dam located at the upstream part of Ara River System in Chichibu, Saitama Prefecture, Japan. Ara River System, whose basin area is approximately 3,000 km², has Tokyo Metropolis in its downstream area, leaving it one of Japan's major river systems in terms of population and assets in estimated flood area. The river water is used in a highly complicated way. Figure 1 shows the location and Picture 1 shows a bird's-eye view of Takizawa Dam.

The upstream area of Takizawa Dam is located in the rich natural region designated as Chichibu-Tama-Kai National Park. Since the region is inland and high in elevation, it's cool all year around. The average annual temperature is approximately 11 degrees Celsius and the average annual rainfall is 1,370 mm (Average value from 1999 to 2003).

3 THE EXECUTION OF VEGETATION RESTORATION ON THE QUARRY SITE

The aggregates of concrete of Takizawa Dam were collected from the quarry site around the dam from May, 2001 to June, 2004. The quarry site is located in the left bank of Nakatsu River, a branch of Ara River. Its elevation is in between approximately 930 and 1,100 meters.

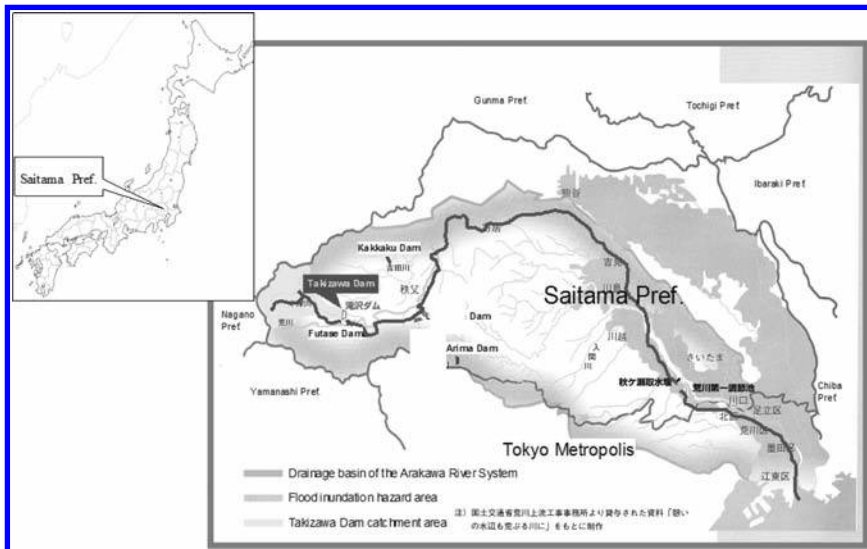
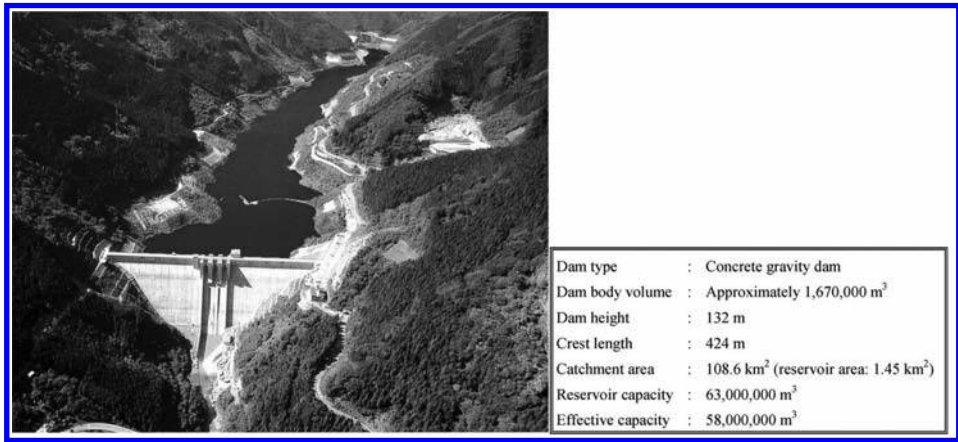


Figure 1. The location of Takizawa Dam.



Picture 1. A bird's-eye view of Takizawa Dam.



Figure 2. The location of the quarry site.

It consists of cut slopes of approximately 29,000 m² facing to southeast and berms and a platform of approximately 60,000 m². Figure 2 and Picture 2 show the location of the quarry site. Picture 3 shows a bird's-eye view of quarry site.

Two types of soil for vegetation restoration were used. On mild gradient (1:1.2) slopes, the surface soil of the quarry site was piled to aim at restore vegetation by buried seeds (referred to as “surface soil area”). On steep gradient (1:0.8) slopes, purchased soil, brought from out of the region, and seeds of native pioneer trees, gathered near the modification sites, were mixed and sprayed by seeding work called double layer spraying (referred to as “double layer spraying area”). The compound of seeds used in the double layer spraying area was reviewed since the number of collected species and amount differed every year. Table 1 shows the compound of seeds on the double layer spraying area. On the berm and the platform, the surface soil was also piled and native seeds and seedlings, and seedlings of native trees were planted. The native seeds and seedlings were raised in a premeditated way since 2001 (Inaba et al. 2004).

As a result of these executions, the following transitions are expected; the formation of pioneer tree communities (e.g. *Rhus javanica var. chinensis* (Sumac)) in the first step, followed by the growth of deciduous broad-leaved forest (e.g. *Quercus mongolica ssp. crispula*), which is common in the region, in the end of the process of succession.



Picture 2. A bird's-eye view of the quarry site & Picture 3. A bird's-eye view of quarry site.

Table 1. The compound of seeds on the double layer spraying area.

Execution	1,2,3		4,5		6,7,8,9		10,11,12,13,14,15,16	
Slope No.	3-1	3-2	5-1	5-2	6	8-1	12	13
Quadrat No.								
Execution Period	Nov.2001	Nov.2001	Apr.2002	Apr.2002	Dec.2002	Apr.2003	Feb.2004	Apr.2004
Slope Direction	SE	SE	SE	SE	SE	SE	SE	NE
Slope Gradient	1:1.2	1:1.2	1:0.8	1:0.8	1:0.8	1:0.8	1:0.8	1:0.8
Soil type (Soil Depth)	Surface soil of quarry site (30cm)	Surface soil of quarry site (30cm)	Mixture of purchased soil and seeds of native pioneer trees	Mixture of purchased soil and seeds of native pioneer trees	Mixture of purchased soil and seeds of native pioneer trees	Mixture of purchased soil and seeds of native pioneer trees	Mixture of purchased soil and seeds of native pioneer trees	Mixture of purchased soil and seeds of native pioneer trees (5cm)
Execution Method	Piling	Piling	Double layer spraying	Double layer spraying	Double layer spraying	Double layer spraying	Double layer spraying	Double layer spraying
Species of seed								
<i>Miscanthus sinensis</i>			0.239	0.239				
<i>Abies firma</i>						0.072	0.016	0.041
<i>Betula platyphylla var japonica</i>							0.022	0.038
<i>Deutzia crenata</i>					0.062	0.188	0.059	0.066
<i>Deutzia scabra</i>						0.033	0.023	0.026
<i>Mallotus japonicus</i>					0.118	0.042	0.078	0.134
<i>Rhus javanica var chinensis</i>			0.078	0.078	1.875	3.125	0.364	0.63
<i>Suchyarus praecox</i>			0.079	0.079	0.167			0.042
<i>Aralia elata</i>			0.009	0.009	0.1	0.075	0.007	0.011
<i>Clethra barbinervis</i>			0.019	0.019	0.187	0.125	0.08	0.09
<i>Clerodendrum trichotomum</i>					0.141	0.05	0.081	
<i>Buddleja japonica</i>						0.008		
<i>Weigela decora</i>						0.006		
Total weight(g/m2)			0.424	0.424	2.65	3.724	0.73	1.078
No. of species	0	0	5	5	7	10	9	9

4 MONITORING SURVEY

4.1 Survey area

8 quadrates, divided depending on execution method and year, were set on slopes in the quarry site (Table 1) to record the growth of plants in each quadrate. Figure 3 shows the survey area.

4.2 Method

Main monitoring survey items were the composition of plant species, the percentage of vegetative covers, cover degree, sociability, and the height of plants in the quadrates. Within the first three years after the execution (until 2005), the size of quadrate was one square meter (1 m × 1 m) to record the germination mainly. After three years from the execution (on and after 2006), the quadrates were expanded to 25 square meters (5 m × 5 m) because of the growth of plant communities, and vegetation was recorded by Braun-Blanquet method (Suzuki 1971) (referred to as “detailed survey”). In addition to “detailed survey”,

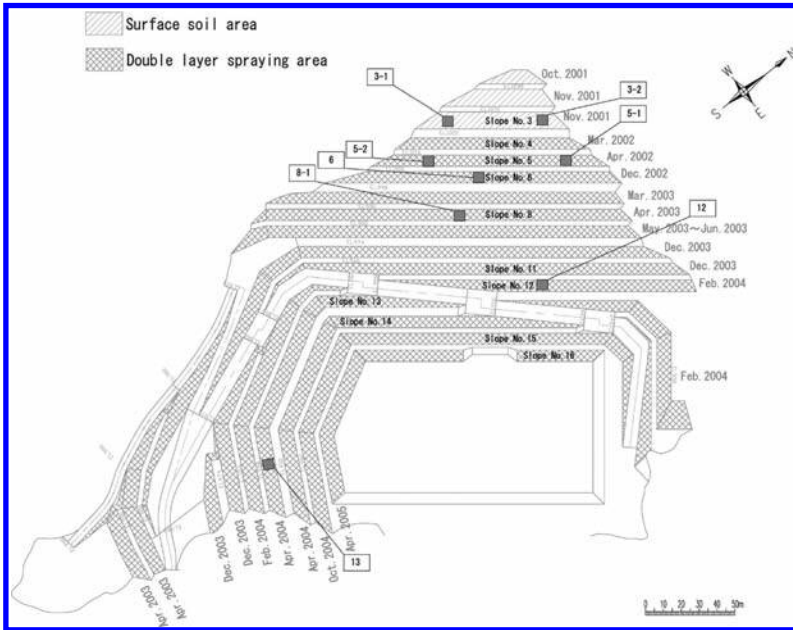


Figure 3. The survey area of quarry site.

the percentage of vegetative covers, the height of plant communities and dominant species were recorded on each slope (referred to as “wide survey”).

5 RESULTS

5.1 *The percentage of vegetative covers, the height of plant communities, dominant species*

Picture 4 and Picture 5 show the view of the quarry site in August, 2003 and August, 2010. From these pictures, it is confirmed that all slopes were getting covered with plants, and vegetation restoration occurred.

Figure 4a, Figure 4b and Table 2 show changes in the percentage of vegetative covers, the height of plant communities and dominant species in each quadrat over the years. The percentage of vegetative covers increased in every quadrat. In the double layer spraying area, the percentage of vegetative covers reached 60 to 80% in the first 3 or 4 years after the execution. Later on it kept over 80% although there was a period when the percentage was slightly low. In the surface soil area, the percentage of vegetative covers was as low as 50% in the first 5 or 6 years after the execution, but it finally reached 80% after 8 years. The height of plant communities increased in every quadrat over the years. In the double layer spraying area, where grasses such as *Miscanthus sinensis* (Eulalia) were dominants, the height of plant communities was around 1 to 2 meters. The dominant species differed depending on quadrates. In the double layer spraying area, species such as *Miscanthus sinensis* (Eulalia), *Rhus javanica var. chinensis* (Sumac) and *Buddleja japonica* (Japanese buddleja) sprayed by seeding work grew and became dominants just after execution. In the surface soil area, species such as *Miscanthus sinensis* (Eulalia) and *Weigela decora* finally became dominants after a short period when *Macleaya cordata* (Plume poppy) was a dominant.

5.2 *Secular changes of number of species and the percentage of alien species*

Figure 4c and Figure 4d show changes in number of species and the percentage of alien species in each quadrat over the years. The definitions of alien species (species, subspecies or



Picture 4. The view of the quarry site in Aug. 2003. & Picture 5. The view of the quarry site in Aug. 2010.

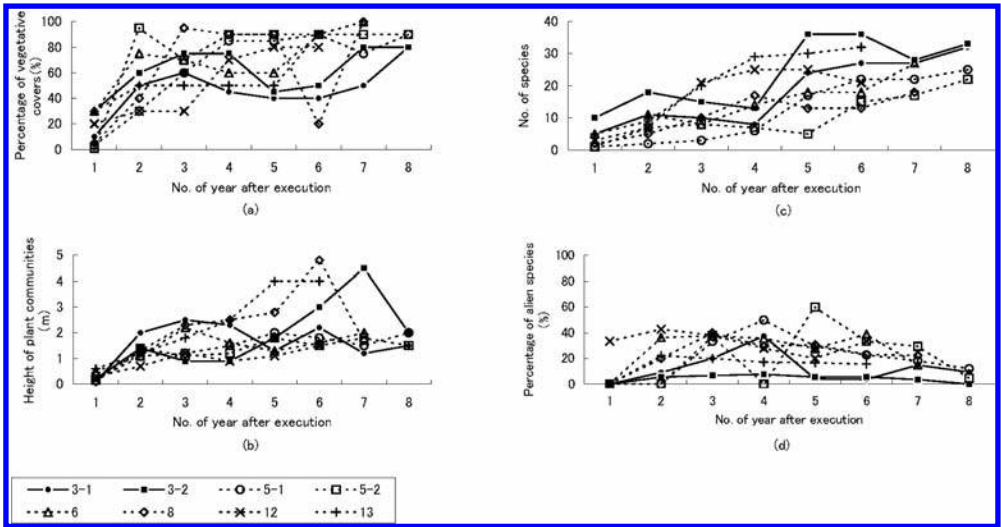


Figure 4. Changes in the percentage of vegetative covers, the height of plant communities, number of species and the percentage of alien species in each quadrate.

Table 2. Changes in dominant species in each quadrate.

Quadrates No.	No. of year after execution							
	1	2	3	4	5	6	7	8
3-1	-	<i>Macleaya cordata</i>	<i>Macleaya cordata</i>	<i>Miscanthus sinensis</i>	<i>Miscanthus sinensis</i>	<i>Miscanthus sinensis</i>	<i>Alnus firma var. hirtella</i>	<i>Miscanthus sinensis</i>
3-2	<i>Youngia denticulata</i>	<i>Reynoutria japonica</i>	<i>Weigela decora</i>	<i>Weigela decora</i>	<i>Weigela decora</i>	<i>Weigela decora</i>	<i>Weigela decora</i>	<i>Miscanthus sinensis</i>
5-1	-	<i>Miscanthus sinensis</i>	<i>Miscanthus sinensis</i>	<i>Miscanthus sinensis</i>	<i>Miscanthus sinensis</i>	<i>Miscanthus sinensis</i>	<i>Miscanthus sinensis</i>	<i>Miscanthus sinensis</i>
5-2	-	<i>Buddleja japonica</i>	<i>Miscanthus sinensis</i>	<i>Miscanthus sinensis</i>	<i>Miscanthus sinensis</i>	<i>Miscanthus sinensis</i>	<i>Miscanthus sinensis</i>	<i>Miscanthus sinensis</i>
6	<i>Rhus javanica var. chinensis</i>	<i>Rhus javanica var. chinensis</i>	<i>Rhus javanica var. chinensis</i>	<i>Rhus javanica var. chinensis</i>	<i>Rhus javanica var. chinensis</i>	<i>Miscanthus sinensis</i>	<i>Miscanthus sinensis</i>	-
8	-	<i>Rhus javanica var. chinensis</i>	<i>Rhus javanica var. chinensis</i>	<i>Rhus javanica var. chinensis</i>	<i>Rhus javanica var. chinensis</i>	<i>Rhus javanica var. chinensis</i>	<i>Miscanthus sinensis</i>	-
12	-	<i>Digitaria ciliaris</i>	<i>Oenothera biennis</i>	<i>Artemisia indica</i>	<i>Miscanthus sinensis</i>	<i>Miscanthus sinensis</i>	-	-
13	-	<i>Buddleja japonica</i>	<i>Alnus firma var. hirtella</i>	<i>Alnus firma var. hirtella</i>	<i>Alnus firma var. hirtella</i>	<i>Alnus firma var. hirtella</i>	-	-

Table 3. The list of alien species confirmed.

Species	Surface soil area	double layer spraying area	Selected as reminded species in	Habitat
<i>Pleuropterus multiflorus</i>		○		Urban area
<i>Phytolacca americana</i>	○			Low land, uncultivated land
<i>Stellaria media</i>				Low land, cultivated land
<i>Chenopodium ambrosioides</i>				shoulder of road, uncultivated land
<i>Trifolium repens</i>				Low land, shoulder of road, grassland, farmland
<i>Oenothera biennis</i>	○	○	●	shore
<i>Symphytum x uplandicum</i>				Shoulder of road, grass land
<i>Solanum nigrum</i>				uncultivated land
<i>Buddleja davidii</i>		○		Shore
<i>Verbascum thapsus</i>				Shore, uncultivated land, shoulder of road
<i>Veronica persica</i>		○		Low land, cultivated land, shoulder of road
<i>Bidens frondosa</i>	○	○	●	uncultivated land, wetland
<i>Bidens pilosa</i>	○	○	●	Urban area, uncultivated land, shore
<i>Comiza sumatrensis</i>	○	○	●	uncultivated land, shoulder of road
<i>Cosmos bipinnatus</i>				Bare ground, shore
<i>Crassocephalum crepidioides</i>				Low land, cleared section of forest
<i>Erechtites hieracifolia</i>	○	○		cleared section of forest, shoulder of road, uncultivated land, landfill
<i>Erigeron canadensis</i>	○	○	●	cultivated land, uncultivated land, shoulder of road
<i>Erigeron philadelphicus</i>	○	○	●	cultivated land, shoulder of road, urban area
<i>Gnaphalium pensylvanicum</i>		○		cultivated land
<i>Solidago altissima</i>			●	Low land, Excessively fertilized land
<i>Sonchus asper</i>	○	○		cultivated land, shoulder of road
<i>Stenactis annuus</i>	○	○	●	cultivated land, shoulder of road
<i>Taraxacum officinale</i>	○	○		Urban land, cultivated land
<i>Agrostis alba</i>		○		Shoulder of road, grassland
<i>Eragrostis curvula</i>		○	●	Farmland, shoulder of road, uncultivated land, shore
<i>Festuca arundinacea</i>			●	playground, house garden, shoulder of road, cultivated land, uncultivated land
<i>Panicum dichotomiflorum</i>				Low land

any taxonomic unit introduced to outer area of natural distribution and carrying any organs, gametes, seeds, eggs capable of sexual and/or asexual reproduction) followed the handbook of alien species (ESOJ 2002). Table 3 shows the list of alien species confirmed. The number of species increased over the years in almost all the quadrates. The number of species in the double layer spraying area was less than 10 in the first 1 or 2 years after the execution. On and after 5th year, the number of species differed from 5 to 30 depending on quadrates; the quadrate with 32 species was confirmed on the north-east slope on and after 6th year. The number of species in the surface soil area was 10 to 20 in the first 4 years after execution, and then increased to 25 to 40 on and after 5th year. The percentage of alien species differed depending on execution method. In the double layer spraying area, the percentage of alien species was low just after execution, but then it shifted to around 20 to 60%. In the surface soil area, that was lower than 20%, even though that recorded 40% in the 4th year. 19 alien species such as *Oenothera biennis* (Evening primrose) were found in the survey area. They were commonly seen in areas as cultivated land and shoulder of road. Even though invasive alien species was not found, 9 species designated as dangerous alien species in Japan were found.

6 CONCLUSIONS

Conclusions based on the results of survey and states on the quarry sites are shown below.

- In the double layer spraying area, native pioneer tree communities of 2 to 3 m in height were formed in the first 3 to 4 years after execution. The percentage of vegetative covers was 60 to 80%. However, the area where *Miscanthus sinensis* (Eulalia) was mixed in to be a dominant had slower formation of pioneer tree communities.
- The number of species or diversity, and the dominant species in the double layer spraying area seemed to be strongly related to the species and amount of seeds mixed in.
- Since the seeds of alien species were not distributed in the double layer spraying area, they could have been originally contained in the purchased soil material.
- In the surface soil area, because of the buried seeds, the number of species was larger while the percentage of alien species was lower than those in the double layer spraying area. From this reason, native pioneer tree communities were formed in the first 3 to 4 years after execution.

The soil materials need to be treated carefully before seeding work (double layer spraying) since the number of collected species and amount differ every year and also there is a high percentage of alien species mixed in. Role of vegetation restoration is to make a chance to put a natural ecological succession on track (DMOROS 2004).⁶ At Takizawa Dam, the formation of pioneer tree communities such as *Rhus javanica* var. *chinensis* (Sumac) was expected as the first step of the vegetation restoration. It was confirmed that this step was achieved within 3 to 5 years after execution by using the surface soil. The “ecological succession” seemed to be continued at Takizawa Dam since invasive alien species, such as *Pueraria lobata* (Kudzu-vine), have not been found yet. The monitoring survey will be continued to confirm an indication of formation of a deciduous broad-leaved forest, a common forest type in the region, which is the final step.

ACKNOWLEDGMENT

We would like to express our heartfelt appreciation to Mr. Jiro Otsubo (IDEA Consultants) and Mr. Daichi Fujita (OYO CORPORATION) for valuable advices and great contributions to our work.

REFERENCES

- Departmental meeting of revegetation on slopes of Society of Revegetation Technology of Japan. 2004. Summary of basic idea of natural revegetation on slopes. *J. Jpn. Soc. Reveget. Tech.* 29(4):509–520.
- Ecological Society of Japan. 2002. Handbook of alien species in Japan. Chijinshokan. 372 pp.
- Fukunaga K, Yoshida H, Yamada M, Nakano Y. 2008. A special feature article “Problems and views in the future of natural revegetation of slopes around construction sites” the handling policy of plants for revegetation by four ministries. *J. Jpn. Soc. Reveget. Tech.* 33(3):453–473.
- Inaba E, Fujita D, Suzuki K, Urayama S, Marutani S. 2004. Measures for vegetation restoration used native species at Takizawa Dam. *J. Jpn. Soc. Reveget. Tech.* 29(4):477–481.
- Japanese Society of Revegetation Technology. 2002. The suggestion of the handling policy of plants for revegetation for the biological diversity. *J. Jpn. Soc. Reveget. Tech.* 27(3):481–491.
- Kobayashi T, Kuramoto N. 2006. The handbook of the revegetation for the biological diversity. Chijinshokan. 323 pp.
- Ministry of the Environment in Japan, Ministry of Agriculture, Forestry and Fisheries in Japan, Forestry Agency in Japan, Ministry of Land, Infrastructure, Transport and Tourism in Japan. 2006. The report of the handling policy of plants for revegetation considered influence of alien species. 283 pp.
- Suzuki T (translator). 1971. Braun-Blanquet social studies of plants I, II. Asakurashoten. 865 pp.

Building dams in a sound environment: Development of La Romaine HEP, situated in Northern Québec, Canada

B. Soucy & V. Alicescu

Planning of Power Generation Projects, Hydro-Québec, Production Division

J.-P. Tournier

Expertise HEP, Hydro-Québec, Equipment Division

ABSTRACT: Hydro-Québec is developing the hydroelectric project of La Romaine, situated on the North shore of the St Lawrence River, in Quebec, Canada. The project consists in building 4 generating stations with a total installed power of 1550 MW and an annual output of 8.0 Twh. In order to increase significantly the production and the export of clean and renewable electrical energy, the Government of Québec, recommended in its strategic guide lines the construction of new hydroelectric projects, one of the most important being the La Romaine Complex. The electricity produced in the four power plants of the Complex will help to avoid new emissions of gas with greenhouse effect in North America with approximately 3 million tons, if that energy would have been generated with natural gas and with about 7,5 million tons, if coal would have been used for the same purposes.

1 INTRODUCTION

1.1 *General description of Hydro-Québec*

Hydro-Québec generates, transmits and distributes electricity. Its sole shareholder is the Québec government. It uses mainly renewable generating options, in particular hydroelectricity, and supports the development of wind energy through purchases from independent power producers. It also conducts research in energy-related fields, including energy efficiency. The company comprises four divisions:

Hydro-Québec Production generates power for the Québec market and sells its surpluses on wholesale markets. It is also active in arbitraging and purchase/resale transactions.

Hydro-Québec TransÉnergie operates the most extensive transmission system in North America for the benefit of customers inside and outside Québec.

Hydro-Québec Distribution provides Quebecers with a reliable supply of electricity. To meet needs beyond the annual heritage pool which Hydro-Québec Production is obligated to supply at a fixed price, it mainly uses a tendering process. It also develops initiatives for encouraging its customers to make efficient use of electricity.

Hydro-Québec Équipement and Société d'Énergie de la Baie James (SEBJ), a subsidiary of Hydro-Québec, design, build and refurbish generation and transmission facilities.

1.2 *The Strategic Plan 2009–2013 and the Sustainability report 2009*

Few electricity companies can boast as high a level of profitability and as small an environmental footprint as Hydro-Québec, who owe this performance in large part to the abundant, powerful hydraulic resources available in Québec and the vision shown by past generations who successfully tapped this potential.

Hydro-Québec's employees are following in their footsteps, and the *Sustainability Report 2009* gives concrete evidence of their achievements in the area of sustainable development.

In keeping with the Québec government's environmental policy, Hydro-Québec is working to reduce its greenhouse gas emissions by focusing on the three priorities laid out in its Strategic Plan: energy efficiency, renewable energies and technological innovation. The economic slowdown in 2009 resulted in a somewhat lower rate of participation by business customers in our energy efficiency programs, but we noticed a great success with residential customers. Overall, the programs generated new energy savings of 946 GWh over the year. The challenge for 2010 was to encourage the building industry to incorporate energy efficiency measures right from the design stage. The year also featured the commissioning of the Rupert diversion and the launch of construction on La Romaine hydropower complex, an important addition to Hydro-Québec's energy reserves. We have completed the draft-design stages, in consultation with the host communities, and signed a number of partnering agreements with Native people and other local communities. Environmental studies and measures carried out before, during and after construction will cost over \$300 million altogether. In addition to generating approximately \$3,5 billions in economic spinoffs in Québec, including \$1.3 billion on the North Shore region, La Romaine complex will provide a reliable supply of electricity that will allow Hydro-Québec to increase its exports to markets outside the province.

The electricity produced in the four power plants of the Complex will help to avoid new emissions of gas with greenhouse effect in North America with approximately 3 million tons, if that energy would have been generated with natural gas and with about 7,5 million tons, if coal would have been used for the same purposes.

2 LA ROMAINE HYDROELECTRIC COMPLEX

2.1 Introduction

Hydro-Québec is developing the hydroelectric project of La Romaine, situated on the North shore of the St Lawrence River, in Quebec, Canada. The project consists in building 4 generating stations with a total installed power of 1550 MW and an annual output of 8.0 Twh (see Fig. 1). Hydro-Québec conducted extensive environmental assessment studies and deposited in January 2008 the Environmental Assessment Report to the provincial and federal governments. The formal environmental assessment process was completed by the spring of 2009 and the project started with the construction of the access road. Romaine 2 is the first facility to be developed and the first kilowatt is expected to be produced by the end of 2014. The project will continue with the construction of Romaine 1 and Romaine 3 facilities and finally, Romaine 4, who must produce its first kilowatts by the summer of 2020 (see Table 1 and Figs. 1 & 2).

The total cost of the power generation project (without transmission grid) is estimated at 6,5 billion \$CAN.

2.2 Description of the project

The four facilities of the project consist of a generating station with two Francis turbines, a rockfill dam and dikes (except for Romaine 4), a spillway and a diversion tunnel. The total area of inundated land will be 279 km² at full supply level of the 4 reservoirs.

2.3 Romaine 2 HEP

The project consist in a dam, 5 dykes, a spillway, an intake, a 5,5 km long headrace tunnel, a surge shaft, 2 pressure shafts, a diversion tunnel, a tunnel for the ecological flow outlet, and a power plant (see Table 1). The total cost of this project is estimated at 2,5 billion \$CAN.

La Romaine Complex is located in a region of Québec with low seismic activity and the anticipated earthquake shaking is assumed to have no noticeable effect on the design of the rockfill embankments. The Complex is situated in a region with an iso-acceleration of 14% g

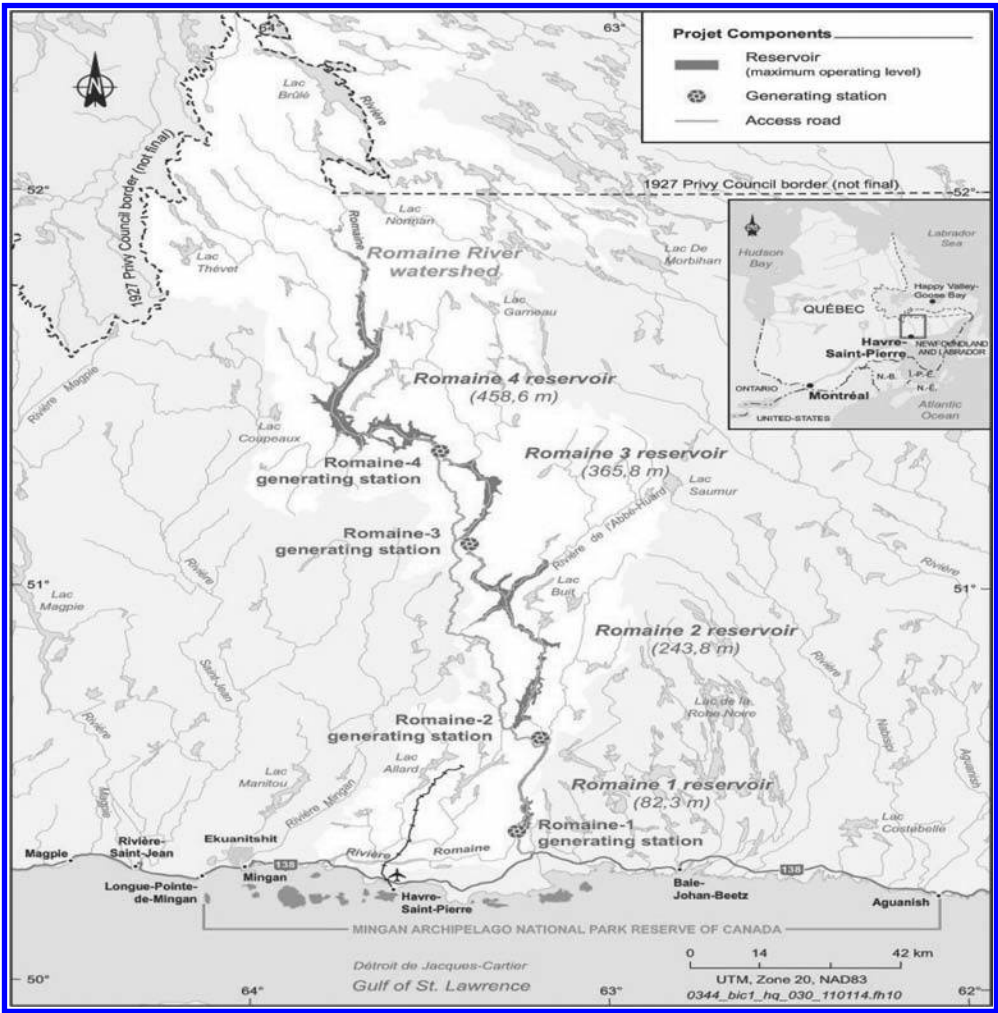


Figure 1. La Romaine Hydroelectric Complex, with its 4 facilities, Romaine 1, Romaine 2, Romaine 3 and Romaine 4.

Table 1. Characteristics of La Romaine Hydroelectric Complex.

Characteristics	RO-1	RO-2	RO-3	RO-4	Complex
Dam (PK)	52,5	90,3	158,4	191,9	–
Maximum flow (m ³ /s)	289,4	272,4	223,2	184,5	–
Maximum operating level (m)	82,3	243,8	365,8	458,6	–
Area of inundated land at max. operating level (km ²)	12,6	85,8	38,6	142,2	279,2
Net hydraulic head (m)	62	158	119	88	427
Turbines (number and type)	2 Francis	2 Francis	2 Francis	2 Francis	8 Francis
Installed power (MW)	270	640	395	245	1 550
Annual output (TWh)	1,4	3,3	2,0	1,3	8,0
Dams and dykes (number)	2	6	2	1	11
Year of completion	2016	2014	2017	2020	

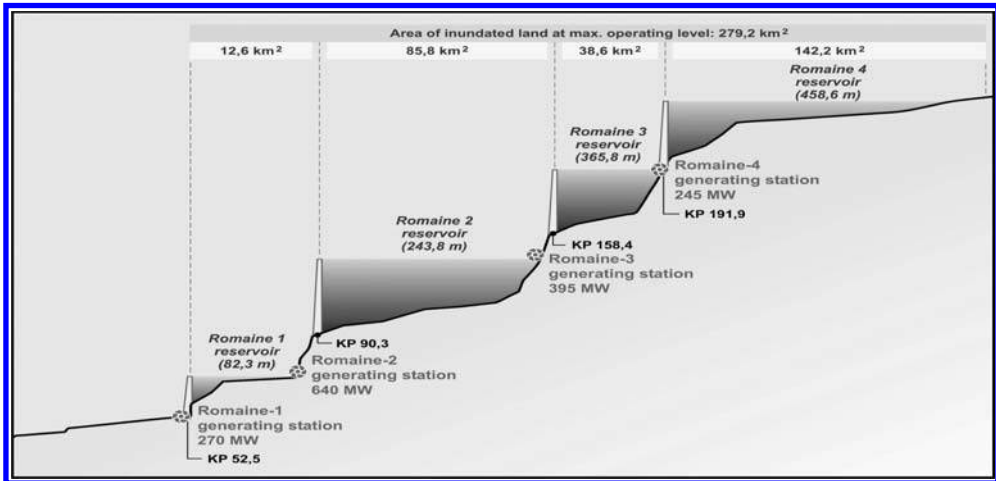


Figure 2. The longitudinal profile (scheme) of La Romaine Hydroelectric Complex.

(period of return—1:2 500 years and an exceeding probability of 2% in 50 years). According to Hydro-Québec’s seismic guidelines, the seismic coefficient for a pseudo-static analysis is 0,1.

2.4 Design of the retaining structures

The design of the retaining structures of the Romaine 2 HEP was an interesting and challenging task. After using for more than 50 years the glacial till as waterproofing material for its embankment dams, Hydro-Québec was looking forward to develop new dam concepts, mainly for the zones where natural waterproofing materials do not exist or are of poor quality.

Romaine 2 is one of those particular zones with very limited quantities of natural impervious material on site. The nearest significant till deposit is situated at 45 km North, with a very high natural water content. The bedrock consists of solid granitic gneiss which is only weathered down to fairly shallow depths. Generally, beneath the weathered zone, RQD values of 80–100 were reported. The overburden of silty sand and gravel is fairly shallow in all locations except under one dyke (F2) and upstream toe of the Main Dam.

Based on the information about the site conditions and lack of suitable earth core material, CFRD (Concrete Face Rockfill Dam) and ACRD (Asphalt Core Rockfill Dam) options were considered for the Main Dam (Figure 4). The overburden under the upstream toe of the Main Dam is 10 to 11 m in the river section. However, under the centerline, the overburden in the river is only 2–3 m, which should be excavated under the ACRD core. For the CFRD option, the best solution was to excavate the 10 to 11 m deep overburden under the upstream toe, and construct the plinth on the rock foundation. The cost criteria and some other particular issues like maintenance, behaviour, construction difficulties, etc. have made the difference between the two variants and finally, the ACRD variant was chosen.

The main characteristics of the retaining structures of Romaine 2 HEP are presented in Table 2.

The ACRD design is very suitable for the 5 dykes of the Romaine 2 facility. For example, dykes D2 and E2 are very long compared to their heights and this makes the machine placing of the asphalt core particularly efficient. Furthermore, both dykes have bends (“knees”) in the embankment axis alignment. This may easily be accommodated for an asphaltic concrete core, but is harder to handle for a concrete facing. The ACRD design is also a good option for the dike F2 (see the cross section on Fig. 5) and there is significant economy (lower unit price of compacted asphalt concrete in place) if a common asphalt mixing plant and quality control program may be used for all six embankments.

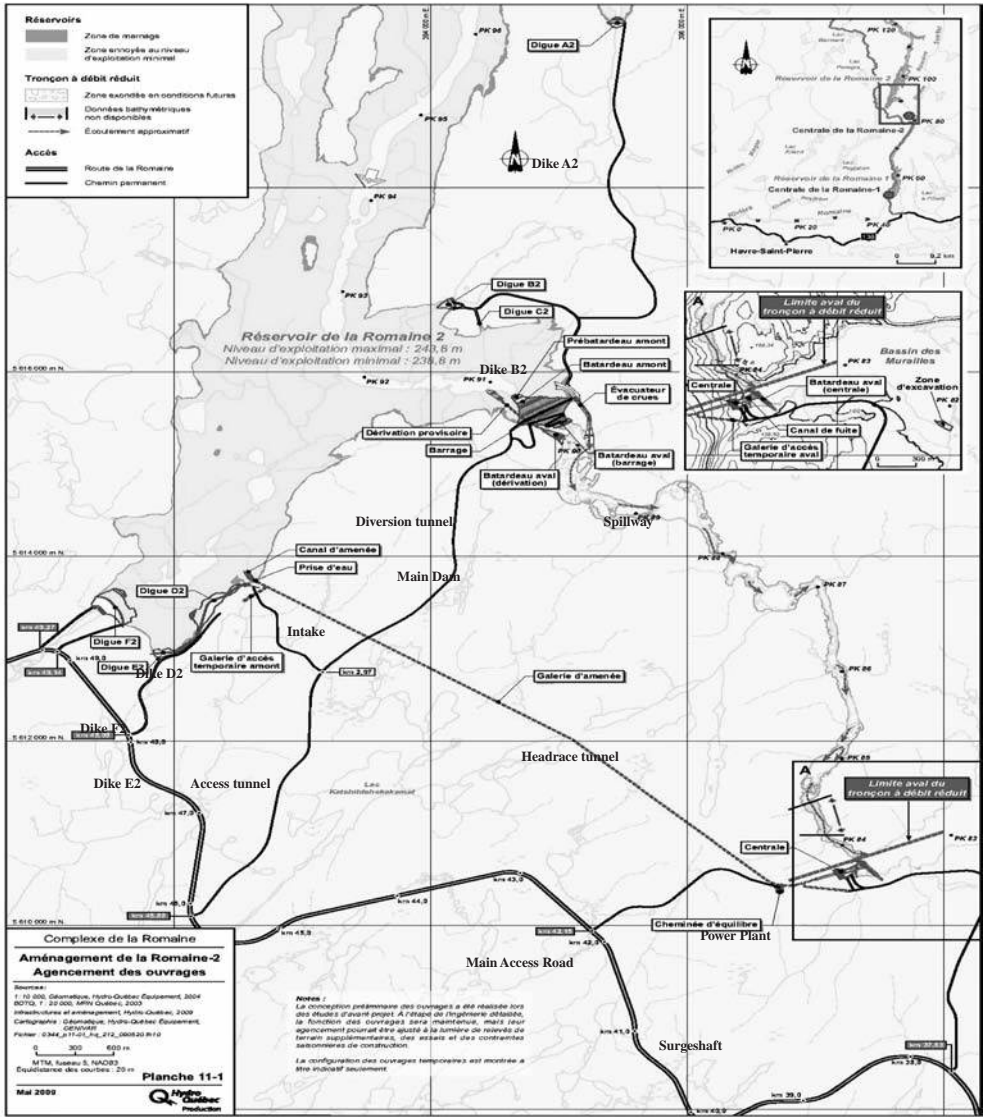


Figure 3. The Romaine 2 HEP, general view.



Figure 4. Romaine 2 Main dam and spillway (CATIA simulation).

Table 2. Characteristics of Romaine 2 Dam and dykes.

Structure	Type	Height (m)	Crest length (m)	Asphaltic concrete core volume (m ³)
Dyke A 2	ACRD	31	144	1040
Dyke B 2	ACRD	26	115	790
Dyke D 2	ACRD	45	728	6330
Dyke E 2	ACRD	38	407	2470
Dyke F 2	ACRD	80	423	10700
Main Dam	ACRD	109	496	18850
TOTAL				40180

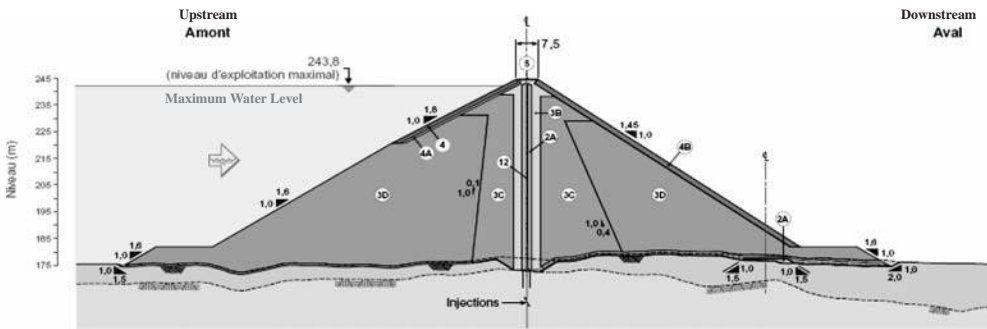


Figure 5. Romaine 2 HEP, Dyke F2, cross section.

3 DESIGN AND CONSTRUCTION OF NEMISCAU-1 DAM, THE FIRST ASPHALT CORE ROCKFIL DAM IN NORTH-AMERICA

3.1 Scope

Through the design and construction of the Nemiscau-1 Dam, Hydro-Québec wanted to gain experience with asphalt concrete core construction, before proceeding with the final design and construction of the much larger dams or dykes for La Romaine Complex. Hydro-Quebec has extensive and successful experience with the design and construction of Earth Core Rockfill Dams (ECRD) and wanted to use as much as possible of that practice, with respect to types of materials, dam zoning, compaction procedures, upstream slopes related to the riprap design, but adapt the design to the special features and requirements of the ACRD concept. The construction of the Nemiscau-1 Dam (see cross section on Fig. 6) started in May, 2008 and was completed by October, 2008.

3.2 Results and recommendations for La Romaine retaining structures

Nemiscau-1 ACR Dam was designed according to higher standards, used on similar projects in Europe or elsewhere and the construction of the dam was completed before the schedule. Quantities of works for the core, transition zones and rock excavations were less than the calculated ones at design stage. For other ACRD projects, the longitudinal profile of the rock excavation and concrete plinth must be optimized, with an optimum balance between the rock excavation, the volume and shape of the concrete plinth and finally, the placement of the asphalt core with the manual method. Placement of the asphalt concrete in 3 or even 4 layers (on specific conditions) of 22,5 cm per day, instead of 2 layers of 20 cm (ancient traditional practice) is feasible and the results are satisfactory. Given its self-compaction and self-healing

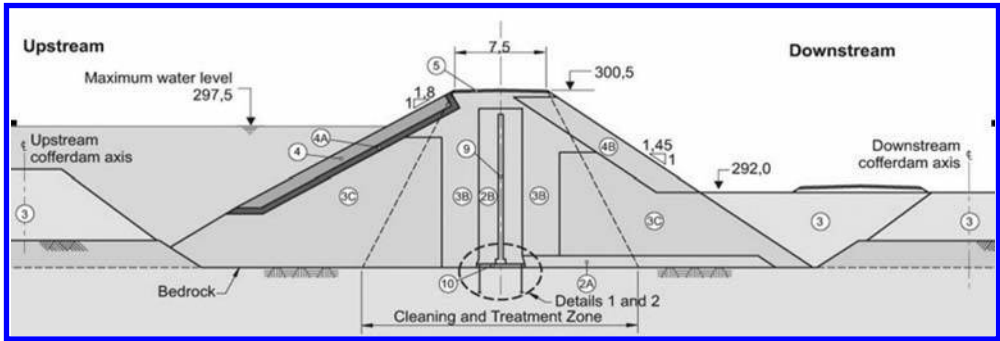


Figure 6. Nemiscau-1 Dam, cross section.



Photo 1. Des Murailles camp (near Romaine 2 site) in November, 2010.

properties, imperviousness, flexibility and ductile behaviour, the asphalt mix design with a Quebec bitumen type PG 52-34 (similar to the Norwegian bitumen type B 180, used at the construction of Storglomvatn Dam, $H = 125$ m, the highest ACRD in the world) and, an average bitumen content of 7,0% to 7,3%, is an interesting and effective option for the construction of the dam and dikes of Romaine 2 facility and other ACRD retaining structures.

4 CONCLUSIONS

La Romaine Hydroelectric Complex is one of the most important development projects in Canada. The project started with the construction of Romaine 2 facility and more than 1 100 workers are now on duty on the field (Photo 1). The draft-design stages were carried out in consultation with the local communities and the Native people, several partnering agreements being signed for the construction of the Complex. Environmental studies and attenuation measures carried out before, during and after construction will cost over \$300 million.

In addition to generating approximately \$3,5 billions in economic spinoffs in Québec, including \$1.3 billion on the North Shore region, and with an average of 975 jobsite workers per year for 11 years, La Romaine Hydroelectric Complex will provide a reliable supply of clean an renewable energy that will allow Hydro-Québec to increase its exports and will help to avoid new emissions of gas with greenhouse effect in North America.

As mentioned in its Strategic Plan 2009–2013, Hydro-Québec considers that the technological innovation is a powerful engine for growth and performance. Trough the design and construction of the Nemiscau-1 Dam, the first Asphalt Concrete Rockfill Dam in North-America, Hydro-Québec wanted to gain experience with asphalt concrete core construction, before proceeding with the final design and construction of the much larger dams or dykes for the La Romaine Complex. With its 6 Asphalt Core Rockfill Dams, Romaine 2 will be the largest HEP in the world, using this type of rockfill retaining structure.

Methodological approach and artificial intelligence application as a solution for environmental conflict related to large dams

S. Stevovic

Faculty for Ecology and Environmental Protection, Belgrade, Serbia

M. Stamatovic

Faculty of Information Technology, Belgrade, Serbia

G. Ivanovic

Faculty of Mechanical Engineering, Belgrade, Serbia

ABSTRACT: This paper presents methodological approach to defining an optimal hydro development concept which mathematically considers technical, economical, and environmental and socio political inputs, at the same time. The proposed model gives the answer to the question what is optimal dam height that will not affect the environment? When and how to incorporate non technical, but important impacts in the decision making process when selecting an optimal heights of large dams and pertaining technical parameters? It also answers the question as to what are the input variables. How to quantify the environmental impacts or historical-political factors? The fuzzy logic and expert systems are applied on a dam height definition case study which has existed for more than 60 years on a Drina river dam project, at the borders of three countries: Serbia, Montenegro and Bosnia and Herzegovina.

1 INTRODUCTION

Hydropower is clean and renewable energy. Construction of large dams and reservoirs takes a significant position in an overall hydropower system, by its importance and role in management over hydro potential and sustainable development of any country. However, the construction of large dams and reservoirs causes considerable disturbances in the environment and provides serious discussions in the local community.

That's why it is really difficult today to find a suitable profile for construction of large dams. Most of the river valleys are populated, and if not, it is quite complicated to find capital investments, while the electric energy requirements are constantly growing. In many countries different movements for environmental protection, for safeguarding cultural and historical monuments, for preservation of various plant and wildlife species are more influential (Banner 2000). The optimal technical and economical solutions are not the only ones sought when designing and constructing the hydropower structures. The suggested schemes must respect both ecological and legal aspects; otherwise the adopted technically and economically proved alternatives will not be implemented.

The decision makers and designers are sometimes faced with the situations in which, even after the millions are spent on preparation of necessary technical documentation, the designed and approved techno economical optimum solutions for large dams are not be realized on site because of the environmental, social, or political problems.

HPP Buk Bijela (with normal high water level of 500.00 m asl.) a large dam and its accumulation have been planned on the borders between three countries: Serbia, Montenegro and Bosnia and Herzegovina. Investigation works and construction of the dam and HPP "Buk Bijela" started immediately after the World War II. For surrounding population that

meant that the hydropower structure “Buk Bijela” would be constructed on the river Drina. Although construction was only foreshadowed at the time it has already made certain impacts on the population and planning of housing development in the potential flood zone.

The first serious designs were made back in 1957, when RO “Energoprojekt” from Belgrade produced the first variant solution.

From then to 1968, a series of variant solutions were made, also by “Energoprojekt”, and since 1968 “Energoinvest” from Sarajevo overtook designing, and by 1970 the conceptual design was completed and adopted in December of the same year. The concept included a fill dam with underground plant and two spillways.

Finally, in 1975, almost 20 years after the first variant solution, the works started on breaking of diversion tunnels, yet, in 1976, the works were stopped, and the site was brought to a standstill.

More than 50 million dollars (\$) have been spent on all designs, modifications and amendments to technical documents, because the project of the Drina hydro potential utilization was not managed properly, with equal representation of all relevant criteria and limitations. This is a complex issue and it requires multi-criteria consideration, with control and monitoring of all relevant parameters.

HPP Gorazde (with normal high water level of 383.00 m asl.) has been designed as concrete arch dam downstream of the HPP Buk Bijela, on river Drina, at the stretch extending from the town of Foca to the town of Gorazde. Within this part of the river according to the available Preliminary Design adopted even in 1978, a large arch dam and a power station Gorazde were foreseen. The accumulation has flooded the walleys, the only road, villages, cemetery and affected the environment. The large dam and its accumulation have been placed on river Drina, at the border between Serbian and Muslim entities and it is not yet realized.

2 IMPERATIVE OF NEW METHODOLOGICAL APPROACH

Above mentioned case studies and alarming environment degradation by large dam constructions yielded the imperative of researching a new methodological approaches to defining an optimal hydro development (Borri et al. 1998).

The existing methods for evaluation and selection of an optimal hydropower system are mainly based on standard techno-economic analyses (Perace et al. 2002). These methods can hardly include the parameters such as the reservoir influence on modification of climate, detachment of diluvia cover resulting from oscillations of the reservoir water level, impact on natural resources (e.g., the Pancic spruce), possible flooding of mosques or old orthodox cemeteries, etc. (Borri et al. 1998, Passarella et al. 2002, Zalewski et al. 2001).

The real problems in practice require a new methodological approach to the question of optimal selection for hydro power development solution. This paper presents an option for modelling of environmental impact elements, while selecting the optimal technical solution by fuzzy-expert approach. A series of technical alternatives among which the optimal one is to be chosen, may be presented in a standard way, or as a part of an expert system. Environmental impact elements are quantified or defined as functions of input variable.

The essence and novelty of this methodology lies in the fact that environmental impact elements are introduced to the decision-making process as mathematical fuzzy values, at the very beginning of optimal technical solution selection.

The new methodological approach will be presented on large dam and HPP Gorazde case study.

3 TECHNICAL DESCRIPTION OF HPP GORAZDE AND ALTERNATIVES

Large dam and HPP Gorazde and belonging accumulation are situated in the Drina River valley, between the towns of Foca (18° 47' East longitude and 43° 30' North latitude) and Gorazde (18° 59' East longitude and 43° 40' North latitude). Due to environmental, political and cultural constrains in this particular section of the river Drina, it is necessary to search

for a particular solution that will respect the circumstances (Harley et al. 2002). In theory it is possible to construct seven hydropower plants: HPP Gorazde 383, HPP Gorazde 375, HPP Gorazde 362, HPP Gorazde 352, HPP Sadba 362, HPP Ustikolina 373 and HPP Paunci 384. Numbers are associated to the names of each of these plants (e.g., HPP Gorazde 375), marking the backwater level in the corresponding reservoir (375 m asl, meters above sea level). Given the geographic restraints, it is not possible to construct all the seven hydropower plants, but instead one of six combinations should be selected, implying one, two, three or four of the named hydropower plants. The following alternative solutions of hydropower utilization of the Drina River are possible.

- A – HPP Gorazde 383: one concrete dam at the Gorazde II profile, with a plant by the dam and reservoir at the normal backwater level of 383.00 m asl.
- B – HPP Gorazde 375: one concrete dam at the Gorazde II profile, with a hydropower plant by the dam and backwater level of 375.00 m asl.
- C – HPP Gorazde 352, HPP Sadba 362, HPP Ustikolina 373, HPP Paunci 384: four concrete spillway dams in the riverbed, with backwater levels of 352.00 m asl, 362.00 m asl, 373.00 m asl and 384.00 m asl, respectively
- D – HPP Gorazde 375, HPP Paunci 384: consists of two hydropower plants at the Gorazde II and Paunci profiles, with normal backwater levels of 375.00 m asl, and 384.00 m asl, respectively
- E – HPP Gorazde362, HPP Ustikolina 373, HPP Paunci 384: this alternative refers to a cascade consisting of three concrete dams with run-of-the-river hydropower plants, namely: Gorazde II, Ustikolina and Paunci, with backwater levels of 362.00 m asl, 373.00 m asl and 384.00 m asl, respectively.
- F – HPP Sadba 362, HPP Ustikolina 373, HPP Paunci 384: (Fig. 1) this possible technical solution is a cascade consisting of three uniform concrete dams and hydropower plants in the Drina riverbed, at the profiles of Sadba, Ustikolina and Paunci, with backwater levels of 362.00 m asl, 373.00 m asl and 384.00 m asl, respectively, and with approximately equal heads and uniform equipment.

4 RELEVANT INPUT VARIABLES IN FUZZY OPTIMIZATION MODEL

The model for hydropower plants evaluation, proposed in this paper, operates with five input fuzzy variables (Kandel 1992). These fuzzy variables with corresponding membership

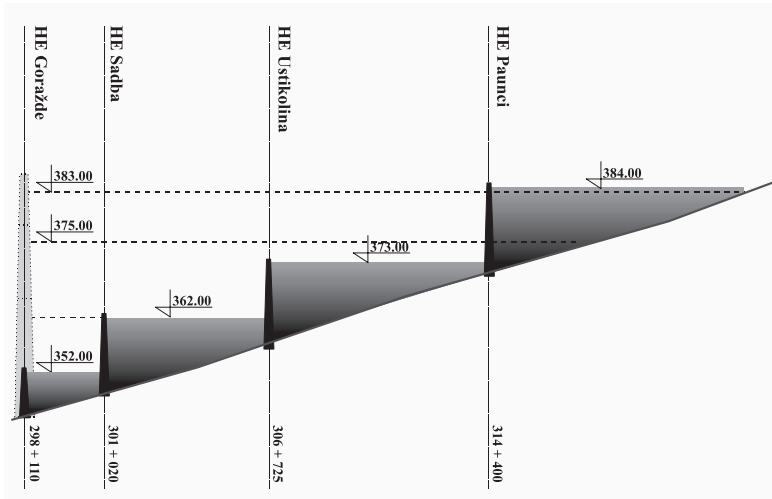


Figure 1. HPP Gorazde with the normal backwater level of 383.00 m asl. and possible alternatives.

functions are chosen so as to describe both techno-economic and environmental parameters together with historical and political ones. These variables are defined as follows.

The first input variable is B/C (Benefit/Cost) ratio. In this model all fuzzy input variables have arbitrarily been scaled in the interval [0, 1]. Therefore the first input variable for each of the analyzed plants, x_1 , is calculated by the following relation:

$$x_1 = \max(0, B/C - 0.8) \quad (1)$$

wherein B/C marks the benefit/cost coefficient for considered hydropower plant. This input is characterized through two attributes: *profitable* and *unprofitable*, and these two properties are defined as fuzzy sets with corresponding membership functions, which has been defined applying the so called bell function.

The second input variable is the investment quotient, one of the important techno-economic parameters. Two linguistic variables are attributed to this variable: *acceptable* and *expensive*, and again, corresponding membership functions are used to define these attributes. The value of the second fuzzy variable, x_2 , is calculated based on actual *investment quotient* according to the following relation:

$$x_2 = \min(1.43 \times (Inv\ quot.) - 0.43, 1) \quad (2)$$

wherein (*Inv.quot*) marks the actual *investment quotient of considered plant*.

The third variable is peak energy productivity of the hydropower system. It is defined as a ratio of peak energy produced during the increased consumers consumption and total annual energy. It is already scaled within 0 to 1 interval, and described by fuzzy attributes: *moderate* and *high capacity*.

The fourth variable is the quantified environmental impact. In order to find a way to quantify the environmental impact, and to determine the numerical values of the fourth input variable, x_4 , five significant environmental impacts have been considered and taken into account: the area which must be flooded, the number of households which must be relocated, the number of public facilities and cemeteries which will be flooded due to the plant construction, as well as the effect of groundwater level raising.

Finally, the fifth variable is the historical-political impact and, by this criteria, the hydropower solutions may be (in fuzzy terms) *acceptable* or *unacceptable*. This choice of linguistic attributes is a consequence of the present political relations between the neighbouring national entities. At the moment, these relations exclude the possibility of building a hydropower system in the territory of both entities. Accordingly, the input variable, x_5 for considered hydropower plant may be 1 or 0, depending on whether it is to be constructed in the territory of one or two entities, respectively.

Based on numerical values of input variables, x_i , $I = 1, 2, \dots, 5$, the fuzzification process calculates the values of membership function $\mu_i^j(x_i) = 1, 2, \dots, 5, j = 1, 2$ (where index i denotes the variable and index j the attribute addressed to that variable). These membership functions values represent the inputs for the inference decision engine. Based on the set of fuzzy rules, the inference decision machine generates the values of membership functions adjoining the output variable called the *grade* of hydropower solution.

5 FUZZY RULES AND THE TRAINING OF THE FUZZY EXPERT SYSTEM

The system for evaluation of hydropower systems, presented in this paper, is formed using 10 'if-then-else' rules, covering the all possible situation in the practice. These rules are enough to support the final decision and they are formed based on experience, but they also represent and materialize the logical and expected influence of input variables on the final grade of hydropower systems. The applied rules are as follows:

1. If peak energy productivity is moderate, the grade is y_5 (the weight of this rule is 0.8)
2. If peak energy productivity is high, the grade is y_7 (the weight of the rule is 0.8)
3. If B/C is unprofitable the grade is y_1 (the weight of the rule is 1.0)

4. If B/C is profitable the grade is y_9 (the weight 1.0)
5. If a historical-political factor is unacceptable the grade is y_4 (the weight 1.0)
6. If a historical-political factor is acceptable the grade is y_8 (the weight 1.0)
7. If environmental influence is bad the grade is y_2 (the weight 1.0)
8. If environmental influence is acceptable the grade is y_6 (the weight 1.0)
9. If the investment quotient is acceptable the grade is y_{10} (the weight 1.0)
10. If the investment quotient is expensive the grade is y_3 (the weight 1.0)

The listed rules are applied with the corresponding weights that are taken into account when the defuzzification process is formed. Weights attributed to particular rules are not identical. Rules 1 and 2, which define the importance of peak energy for selection of the optimal hydropower solution, have a lower weight (0.8) than other rules. By such selection of weights, the authors of fuzzy-evaluation model wishes to emphasize that this is one of the techno-economic criteria which are not crucial in the decision making process. For this model a Sugeno fuzzy inference system has been applied. Defuzzification is performed using the centroid method (Lin and Lee 1996).

The training of the expert system means the tuning of the adopted parameters that define the membership functions of the input variables and position of the singletons adjoined to the output variable and definition of the fuzzy rules set (Liebowitz 1997). The training process must fulfil two different criteria. The main one is the expert system to behave according to the experts' experience. The other one is more formal and it requires the quantified grade to be continuous function of each of the input variables excluding the first-type breakpoints. For the training process the eleven particular hydropower plants where used.

6 OPTIMAL TECHNICAL SOLUTION SELECTION BASED ON FUZZY MODEL

The final goal of the fuzzy model is to choose the optimal hydropower alternative on the River Drina (Stevovic 2000), between the towns of Foca and Gorazde. The values of input variables and final grades for the alternatives A, B, C, D, E and F and input variables for these technical solutions are calculated by analogous procedure, as well as the final grades of these alternatives. All the values are scaled to the interval [0,1].

Analyzing the final grades of the alternatives, one can conclude that the results are quite logical and consequent, yielding the alternative F with a grade of $y = 0.724$, as the optimal solution. This alternative consists of three almost uniform plants: Sadba 362, Ustikolina 373 and Paunci 384. This uniformity of plants (because of the standardized equipment and common spare parts) causes 30% lower costs of hydro, mechanical, and electrical equipment and lowers the maintenance cost, as well. The structures are low concrete dams with spillways which are also used as bottom outlets. Each structure has five spillways with radial gates featuring protection flaps. Hydropower plants are located in the blind part of the dam and they are equipped with horizontal bulb turbines. This type of solution has the minimal environmental impact and its hydropower facilities satisfy the criteria pertaining to particular national entities. HPP Paunci belongs to one national entity, while HPP Sadba and HPP Ustikolina belong to the other.

The optimal solution of the expert system points out the following facts:

- The characteristics of the considered area, regarding the defined criteria, require several small cascade structures in the riverbed, instead of one structure with a large reservoir, since small structures do not have such an intensive environmental impact and it is also possible to adjust their location according to the political constraints;
- Obviously the structures of HPP Ustikolina 373 and HPP Paunci 384 must be included in the optimal solution scheme;
- Community will decide later on whether the lowest reservoir with a normal high water level of 362.00 m asl will be formed with a dam and hydropower plant at the profile of Sadba or Gorazde (Stevovic 1999);
- The alternative solution involving construction of hydropower plant HPP Sadba 362 also includes the option of total usage of the river Drina head between the towns of Foca and

Gorazde by constructing the forth small cascade, a concrete dam in the riverbed at the Gorazde profile with a normal high water level of 352.00 m asl. HPP Gorazde 352 is not a profitable structure at the moment. This will change after growth of consumers' demand and adequate appreciation of clean and renewable energy (Stevovic 2002).

7 CONCLUSION

Application of modern techniques of artificial intelligence is also possible in the fields of the environment and sustainable development. This paper is dealing with the modern methods of artificial intelligence, where the fuzzy expert system is developed and applied in the decision making process. When a decision to build a large dam is made, it is not enough to consider only techno-economical criteria and prepare separate environmental impact assessment studies. Environmental parameters have to be incorporated in the decision-making process from the very first planning step, simultaneously and equally with other relevant values. This paper offers a new methodology based on the fuzzy expert system developed for the selection of the technical solution optimal for the environment as well. Environmental, historical, political, various technical and economic parameters are treated as input fuzzy variables. The idea of equal incorporation of environmental parameters in the fuzzy expert system for decision-making has been tested and proved on a real example in practice: hydropower exploitation of the Drina River between Foca and Gorazde towns in Bosnia and Herzegovina. Experts system is trained on 11 different Hydro-Power-Plants (HPP) on the Drina River. The applied methodology gives us grades that change the conclusion obtained when standard techno-economic analysis is applied. The fuzzy expert system enables a linguistic depicting of specified impacts and their presence in the decision-making system, and by an appropriate defuzzification procedure, a numerical evaluation of each of the possible hydropower solution variants is obtained again as the output. The fuzzy expert system is functioning with five input fuzzy variables: Benefit/Cost ratio, investment quotient, peak energy productivity, quantified environmental and historical-political impacts. These fuzzy variables with corresponding membership functions are chosen in such a way to describe both: techno-economic and environmental with historical and political parameters. The practical implications of the results are seen in the technical solutions of hydro development composed of cascades instead of a large dam.

REFERENCES

- Banner, N. (2000). *Environmental Compliance Policies And Tools*, Environment, Orlando.
- Borri, D., Concilio, G. and Conte, E. (1998). "A fuzzy approach for modelling knowledge in environmental risk system". *Computer, Environment and Urban Systems*, 22, 299–313.
- Harley, N., Shogreen J.A., and White, B. (2002). *Environmental Economics in Theory and Practice*, Macmillan, Houndmills Hampshire UK and New York.
- Kandel, A. (1992). *Fuzzy Expert Systems*, CRC-Press, Florida, USA.
- Liebowitz, J. (1997). *The Handbook Of Applied Expert Systems*, CRC—Press, Florida, USA.
- Lin, C.T., and Lee, C.S.G. (1996). *Neural Fuzzy Systems: A Neuro-Fuzzy Synergism to Intelligent Systems*, Prentice-Hall.
- Passarella, G., Vurro, M., D'Agostino, V., Giuliano, G., and Barcelona, M.J. (2002). "A probabilistic methodology to assess the risk of groundwater quality degradation". *Environmental Monitoring and Assessment* 79, 57–74.
- Perace, D. (ed.), Perace, C., and Palmer, C. (2002). *Valuing the environmental in developing countries*, Edvard Elgar, Chaltenham, UK.
- Stevovic, S. (1999). "Priority to hydro power plants", *Proc., Updating and Refurbishing Hydro Power Plants Conf.*, Berlin, vol 1. pp. 325–330.
- Stevovic, S. (2000). "Optimization and evaluation of hydro development", *Proc., Millennium Congress on Energy and Environment*, Geneva, vol 1. pp. 78–89.
- Stevovic, S. (2002). "Small scale hydropower plants as renewable energy sources in FR Yugoslavia", *Proc., Med. Power Conf.*, Athens, vol 2. pp. 124–129.
- Zalewski, M. (ed.), Janauer, G.A., and Jolankai, G. (2001). *A new paradigm for the sustainable use of aquatic resources*, UNESCO, UNDP.

Introduction of cost-benefit evaluation of the environmental impacts and mitigation measures in hydropower production and water supply service sectors

A. Kryžanowski

Faculty of Civil and Geodetic Engineering, University of Ljubljana, Ljubljana, Slovenia

M. Gorišek

Urban Planning Institute of Ljubljana, Ljubljana, Slovenia

ABSTRACT: In almost all European Union countries, the full cost recovery principle is implemented during the decision making process of planning and defining the most adequate technologies of energy production. This principle defines that the price of the final product is calculated by taking into account two components, the production and the external costs, which are caused by the parallel activities of installing the structure in the social and nature environments. The external costs can be negative, expressed as damage to the environment, but in most cases, when the adequate planning process is implemented, the external costs are positive and improve the social and nature environment, by introducing the added value to both. The main issue of this article is to present the demonstration of the developed methodology of cost-benefit evaluation of the environmental mitigation measures, separately from the total investment costs of the installations in the hydropower production sector in practice of planning and designing of hydropower plant installations and as a pilot case of planning and designing of water supply infrastructures.

1 INTRODUCTION

The methodology of cost-benefit evaluation of the environmental impacts and the corresponding mitigation measures were developed to provide the unification of financial evaluations of the environmental components of hydropower constructions and a transparent overview of the short and long term economical efficiency of the planned investments for hydropower energy production (full cost recovery analyses). On the basis of environmental impact assessment report, the different technically possible solutions of hydropower elementary construction elements and the corresponding environmental mitigation measures were defined. The cost-benefit analysis of different solutions of the elementary hydropower installation elements connected with the corresponding environmental mitigation components provides the economically most cost-effective solution of the investment as a whole, as well as the environmental part of the investment. In sense of minimising the impact to the environment as well as the costs of environmental mitigation measures, the final solution of the investment project in hydropower production sector is defined on the bases of a transparent financial evaluation of various technically possible solutions. The implementation of the full cost recovery principle in hydropower energy production planning process was regulated by the Slovenian national legislation on efficient management of public finances like state, local, public institution and enterprise budgets, recommended by various European guidelines and more and more dictated by the national and the international market requirements in electricity production sector (Gorišek & Kryžanowski 2001). The developed methodology was tested in the water supply sector also and the final solution of the investment projects in this sector could be optimised on the bases of a transparent financial evaluation of various technically possible solutions.

2 OBJECTIVES

The main issue of this article is to present the demonstration of the developed methodology of cost-benefit evaluation of the environmental mitigation measures, separately from the total investment costs of the installations in the hydropower production sector in practice of planning and designing of hydropower plant installations and as a pilot case of planning and designing of water supply infrastructures. The methodology was used on the practical case of upgrading the Moste hydropower plant installation and tested on the practical case of Integral Water Supply System for Slovenian Istra and hinterland Karst region. When distinguishing between the elementary and environmental parts of the investment only, the cost-benefit evaluation procedure is composed of the following steps (Gorišek & Kryžanowski 2001):

- Inventory or specification of the investment elements that are directly related to the intent of the investment (energy, water supply, ...), and additional, environmental elements arising from site selection of the investment
- Economic and financial evaluation of the investment expressed as the unit of the product (electric energy, drinking water, ...)
- Financial and economical analyses of costs and benefits caused by the environmental mitigation measures—cost-benefit analyses
- Separate presentation of the costs of elementary investment and environmental costs and benefits.

3 DESCRIPTION OF THE EVALUATION PROCEDURE

3.1 *Breakdown of investment elements*

The breakdown of the investment elements was the following: 1) the elementary part of the investment related to ensuring the primary purpose of the investment (e.g. structures for electric energy production and water supply, respectively) and 2) environmental part of the investment arising from the additional elements of investment tied to reduction of impacts to the environment and incorporation of the investment into space (environmental mitigation measures). The inventory of the elements for the elementary part of the investment is based on the design documentation (technical documentation, detail designs, ...), while the inventory of the environmental part of the investment is based on the Environmental Impact Assessment Report (EIA Report). The environmental part of the investment is composed of the following:

- Measures for reducing the environmental impacts of the investment, defined as the benefits of the investment or external costs that can be evaluated quantitatively (water management, preservation of biotopes, ...) or qualitatively (impacts to the living and social environments, ...);
- Measures capping the irreversible impacts to the environment defined as opportunity costs of the investment that can be evaluated qualitatively (replacement of utilisation of natural resources, economic use, ...) or qualitatively (loss of natural surface, restricted use of natural resources, ...). The principles and standards of evaluation of the financial and economic efficiency of the elementary investments are defined by the adopted national and EU legislation and guidelines.

3.2 *Economic and financial evaluation of the elementary part of the investment*

The evaluation of financial and economical efficiency of the elementary structures (hydropower plant structural elements, water supply installations) based on detail designs (bill of quantity) of the planned structures can be calculated by static and dynamic financing methods.

The indicators of the financial and economical efficiency of the investments evaluated by the static financing methods are the return period, the investment profitability rates, the productivity and the economical efficiency and the average yearly rate of return per unit of the investment costs. The indicators of the financial and economical efficiency of the investments evaluated by the dynamic financing methods are the net present value, the discount rate of return, the profitability index, the yearly profitability equivalent and the internal rate of return.

3.3 *Methods of financial evaluation of the environmental part of the investment*

The financial evaluation of the impacts to the environment and environmental mitigation measures is based on Environmental Impact Assessment Reports (EIA Reports), which have provided the quantitatively (where possible) or qualitatively evaluated impacts to the environment and corresponding mitigation measures for reduction of these impacts. As mentioned, the evaluation methods introduced by the developed methodology are quantitative and qualitative, in case when the value of the impacted environment cannot be expressed in monetary units. The indicators of the financial and economical efficiency of the mitigation measures, evaluated by the quantitative method, are discount rate of return, criteria of sustainable development and environmental accountancy. Two basic qualitative methods were introduced by the developed methodology:

- Methods based on public opinion: 1) description of the planned activity including the values that are being protected, 2) public presentation of the evaluation system of protection, and 3) registering the response of the public
- Preference (indirect) methods:
 - travel expenses method: 1) zoning of impacted area, 2) sampling of visitors and assessment of frequency of visits, 3) estimation of travel expenses, 4) analysis of statistical data and 5) analysis of estimations of public interest
 - critical circumstances behaviour method: 1) assessment of impacts, 2) identification of exposed population and 3) assessment of population reception regarding changes
 - hedonistic method: 1) assessment of state of environment, 2) assessment of real property price, inclusive the environmental surrounding, 3) collection and disposition of data on real property, 4) correlation of parameters of real property in relation to the environment and 5) assessment of population willingness for covering the environmental costs.

3.4 *Cost-benefit analysis*

3.4.1 *Economic evaluation of the investments*

The cost-benefit economical evaluation of the investments is expressed by the unit of produced energy in energetic supply system or unit of water supplied to the final consumer in the water supply system. In reference to the Slovenian legislation on efficient management of public finances, the technically and financially optimal solution of the planned infrastructure investment is identified by the prescribed procedure for elaboration of the pre-feasibility and feasibility studies including an investment programme for identified optimal solution, which includes the definition of the objectives of the planned investment, identification of various technical solutions of the structures, definition of valuable and physical extent of costs and benefits for various solutions, sensitivity analysis of various technical solutions, selection of optimal solution, and elaboration of an investment programme for the selected solution.

3.4.2 *Analysis of the impacts to the environment*

All additional costs of the elementary investment structure, caused by environmental mitigation measures, which affect indirectly and directly, in short and long term, the costs and benefits in economic and public (state and municipality budget) sectors, are defined by environmental impact assessment reports. These documents represent quantitatively and

qualitatively evaluated environmental mitigation measures of the investment. Regarding this, the additional costs are broken down as follows:

- Environmental mitigation measures which cause the external costs and benefits of the investment (construction adaptation of individual structures in sense to reduce the impacts to the environment, construction of additional structures of installation or structures, which enable the development of other activities in the area, ...)
- Environmental mitigation measures which cause irreversible changes to the nature and social environment and determine the opportunity costs of the investment only (reduced use of the nature resources and space, compensations, ...)

3.5 *Financial analysis of total costs and benefits*

The final financial analysis of the total costs and benefits caused by the environmental mitigation measures for the reduction of the impacts to the environment consists of:

- financial analysis of different technically possible solutions for reduction of environmental impacts
- determination of financially optimal solution
- economic analyses (evaluation of external costs and benefits expressed in monetary units, evaluation of opportunity costs, evaluation of imported substitution impact)
- evaluation of indirect impact to the environment
- sensitivity and risk assessment analyses

3.6 *Presentation of the investment cost*

The methodology of cost-benefit evaluation of the environmental impacts and the corresponding mitigation measures was developed on the case of upgrading the Moste HPP in order to unify the financial evaluations of the environmental components of hydropower constructions and a transparent overview of the short and long term economical efficiency of the planned investments for hydropower energy production in Slovenia. In reference to the pertaining Slovenian administrative act, the use of water potential is defined as specific use of water resources, for which the mode and conditions are specified. In addition, the design of hydropower plant installations, constructed for electric power production, must enable the protection of water damage effects. In this context the installations are considered as incorporated structures of water management infrastructure in way to enable the use of water potential. Taking into consideration this fact, the costs of construction of the hydropower installations are divided into:

- construction costs of water management infrastructure, which incorporate the costs of environmental mitigation measures
- costs directly tied to the construction of power plant installation

3.6.1 *Case I—Upgrading the Moste HPP*

The Moste hydro power plant is the only storage power plant in Slovenia that contributes a considerable portion to peak energy generation. A revitalisation of the hydro energy system is urgent in view of the power plant's age and obsolescence of the equipment. Within the project the following activities are planned: to construct a new intake structure; a head-race tunnel with a diameter of 4.9 m in the length of 2600 m; a surge tank; a powerhouse Moste II containing two units (installed discharge $2 \times 35 \text{ m}^3/\text{s}$, peak load 42 MW and output 69.2 GWh). A downstream compensation reservoir with a weir will be provided for flow compensation and a smaller powerhouse Moste III containing two units (installed discharge $2 \times 20 \text{ m}^3/\text{s}$, peak load 4.8 MW and output 8.9 GWh) with spillway openings. The existing dam (60 m high concrete arch-gravity dam) with storage reservoir remains a part of the system. Total investment value amounts to EUR 75 million (Kryžanowski & Somrak 1997, Kryžanowski 2000). The revitalization project commenced in 1996. The refurbishment of the existing dam was done and nature conservation measures in the area of the existing reservoir

were taken. However, the works on the compensation reservoir have been suspended due to the special nature conservation requirements.

Table 1 shows the main construction elements in the Moste HPP project including the proportion of the total investment costs independently as part of the energy infrastructure (83% of the total investment) and water management infrastructure (3% of the investment), and separately energy production structures as part of water management infrastructure (14% of the investment), also showing the corresponding cost breakdown into energy production (93% of the investment) and environment structures (7% of the investment). The compensation reservoir area turned out to be the most sensitive part of the project while the preference methods were used in the evaluation. In later discussions the expectations and requirements of the interested public became unacceptable in terms of costs compared to the costs during evaluation and economical assessment of the project, which led to temporary suspension of the project.

The methodology was later successfully used as the model of funding the project of building the HPP chain on the Lower Sava. When justifying the project feasibility a consensus was reached regarding the funding of the investment by introducing a breakdown of proportions of the energy production part of investment costs (concessionaire), represented by the corresponding energy infrastructure, and the environment part of investment costs (awarding authority) as part of public and economic infrastructure (Širca et al. 2008).

3.6.2 Case II—Integral Water Supply System for Slovenian Istra and hinterland Karst region

The successful application of the methodology for evaluating investments in the energy sector provided the incentive to use a similar principle in other cases of evaluating investments into public infrastructure. The method was modified so that it could be used in the water supply sector and practically tested on the case of Water Supply System for Slovenian Istra and hinterland Karst region—the Padež project.

The Slovenian Coast and Karst region is the largest water-deficient region in the country. In order to ensure a permanent water source for a population of 150,000 of the region, a regional water supply system has been planned, which includes: the building of over 60 m dam of the Suhorica with a reservoir capacity of 13.1 hm³, connecting regional pipeline in a length of 27 km and a comprehensive raw water treatment system for potable water supply from the Suhorica reservoir of an additional capacity up to 7 hm³ in a dry year, which

Table 1. Moste project: Representation of cost distribution.

Padež project	Part of total invest. costs	Energy production	Environment structures
Energy infrastructure:			
Moste II—energy production structures	71%	100%	
Moste III—energy production structures	12%	100%	
Energy production structures as a part of water management infrastructure:			
Environmental protection measures in Moste reservoir area	1%	8%	92%
Environmental protection measures in Moste II powerhouse area	1%	66%	34%
Moste III dam structure	11%	80%	20%
Environmental protection measures in Moste III dam area	1%	54%	46%
Water management infrastructure:			
Environmental protection measures in compensating reservoir area	3%		100%

Table 2. Padež project: Representation of cost distribution.

Padež project	Part of total invest. costs	Water supply service	Environment structures
Water supply infrastructure:			
Water conditioning structures	10%	100%	
Transport pipelines for drinking water	25%	100%	
Water supply structures as a part of water management infrastructure:			
Suhorica dam structure	48%	90%	10%
Intake tower with access bridge	5%	90%	10%
Environmental protection measures in Suhorica reservoir area	7%	50%	50%
Water management infrastructure:			
Environmental protection measures in hinterland area	5%		100%

would cover the increasing needs until 2060. The total investment value amounts to EUR 70 million. The Padež project was, due to its broad regional and national significance, listed as one of the environmental projects to be nominated for financing from the EU Cohesion Fund (Krajnc et al. 2010).

Table 2 shows the main construction elements pertaining to the Padež project with the portion of total investment costs independently as the part earmarked for water supply (35% of investment) and water infrastructure (5% of the investment) and separately for water supply structures as a part of water management infrastructure (60% of the investment), also showing the corresponding cost breakdown of water supply service (86% of the investment) and environment structures (14% of the investment). A substantial part of environmental costs is earmarked for remedial measures in the hinterland of the reservoir in order to preserve the good condition of waters in the influence area of the reservoir. In the hinterland active conservation measures are used: refurbishment of water and sewage pipelines, protection of streams using barriers against pollution, as well as passive protection measures introducing extensive agriculture in the hinterland and partial reimbursement of costs due to loss of agricultural production. The reservoir also provides a unique nature conservation measure in the hinterland of the Škocjan Caves Park, which has been entered on UNESCO's list of natural world heritage sites, under extreme hydrological conditions ensuring minimum flow in the underground cave, which could otherwise dry out during dry periods of today.

4 CONCLUSIONS

The paper aimed to represent the methodology of cost-benefit evaluation developed to provide the unification of financial evaluations of the environmental components of hydropower constructions and a transparent overview of the short and long term economical efficiency of the planned investments for hydropower energy production (full cost recovery analyses). This was later, with small modifications, successfully applied to the evaluation of viability of investments in the water supply sector.

When choosing the evaluation method it is important that the calculative costs of the production unit (electric energy or quantity of drinking water) are presented transparently, showing the breakdown of setting up the necessary elementary, sector infrastructure and the costs of incorporating the structures into space, including all environmental costs (external costs and opportunity costs), which are usually never fully included into the evaluation of investment costs. At the same time the short and long time benefits of new constructions to the nature and social environment are evaluated in a way that the construction of hydropower

plant installation or water supply infrastructure can provide an added value to the nature and social environments.

REFERENCES

- Gorišek, M. Kryžanowski, A. 2001. Introduction of cost-benefit evaluation of environmental impact and mitigation measures in hydropower production sector. *Methodology, focalization, evaluation and scope of environmental impact assessment. Seventh report, Water management and assessment of water systems, Report, No. 249*. Antwerpen: University of Antwerp. 128–135.
- Krajnc, U. Kryžanowski, A. Somrak, D. 2010. Padež Project: A case study of strategically planning of water resources for water supply. *Proc. intern. Symp: "Dams and Sustainable Water Resources Development", VNCOLD*. Hanoi.
- Kryžanowski, A. Somrak, D. 1997. Upgrading of the Moste HPP. *Proceedings of the 2nd IHA Conference, Portorož, 15–17 September 1997*. 623–627.
- Kryžanowski, A. 2000. Benefits of the Moste HPP Renovation project in the regional Development. *Proc. 20th Congress on Large Dams, Beijing*. Q77. R2.
- Širca, A. Josipovič, Z. Kvaternik, K. Močnik, I. Somrak, D. 2009. A Multipurpose Lower Sava River Project in Slovenia. *Proc. 23rd Congress on Large Dams, Brasilia*. Q88. R5.

Environmentally rehabilitation of dam Bitdalen

A.M. Ruud

Statkraft Energy

L. Lia

Norwegian University of Science and Technology

ABSTRACT: The dam Bitdalen is a rockfill dam completed in 1971. The support fills are a mix of gravel and rock. Previously the dam was covered with grass on downstream slope. The reassessment in 1997 identified a required rehabilitation of the dam. In addition to the project's primary goal of increased dam safety, it has been focused on landscaping and an environmentally friendly solution since the dam is located in a vulnerable area at an altitude of 1000 masl. Statkraft has recognized in retrospect that these measures have not led to additional cost, when the matter is the strict environmental requirements for structures in sensitive natural areas. After rehabilitation dam Bitdalen today stands out as a clearly constructed element with precise transition to natural terrain.

1 BACKGROUND

The dam Bitdalen is located in a mountainous area in the southern part of Norway in Telemark county.

The embankments in the dam are constructed from a mix of gravel and rock and previously the dam was covered with grass on downstream side. Dam Bitdalen has a moraine imperious core.

The dimensions of the dam:

Height:	46 m
Length:	540 m
Max/Min Water level:	masl 974,00/939,00
Dam crest:	masl 979,0
Slope of dam: Upstream and downstream slope:	1: 1,6

The fixed crest spillway, located in the rock on the dam's left hand side, has a concrete weir structure with flood discharge through a shaft and tunnel. The weir and tunnel was extended in 1995.

During the years after commissioning, there have been leakages at several spots in horizontal layers over shorter periods. The cause is believed to be incomplete injection of the core foundation. It still seems to be some open cracks in the rock foundation (Ødemark 1997).

In 1981 the upstream face of the dam was improved. Also the height of the core was extended due to later requirements for the freeboard.

2 THE NECESSITY OF REHABILITATION

Due to the Norwegian dam safety regulations, a dam owner has to do reassessment every 15th year. A part of the reassessment is to do control calculations of the dam in accordance with applicable regulations. Many dams do not meet today's formal dam safety requirements. This was also the case for dam Bitdalen.

The reassessment in 1997 identified a required rehabilitation of the dam. The basic intention was to meet new governmental requirements. In particular the drainage capacity of the dam was unsatisfactory in relation to the legal framework. It was further emphasized to upgrade the leakage measurement systems.

3 THE REHABILITATION WORK

Statkraft considered several alternatives to satisfy the requirements. What is presented here is the chosen solution which was approved by the authorities, NVE (Norwegian Water Resources and Energy Directorate).

Statkraft conducted the extensive rehabilitation of the dam in the years 2006–2008.

There is limited time for construction work in this mountainous area with snow 7 months a year.

The main upgrading issues were (Søreide 2008):

- Excavation of vegetation cover on the downstream slope
- New dam toe
- New rip rap structure on downstream side
- Monitoring systems for leakages and settlement

The width extension work on the downstream side of the dam was started with excavating the existing vegetation and soil covering. The green slope was removed and humus containing soil was excavated down to rock fill. The top layer and the underlying masses were stored separately downstream of the dam. The masses were later used for revegetation in affected areas in the construction area, and for revegetation of the quarry.

After excavating soil and vegetation masses, a new slope protection was established with rip rap structure on the underlying support of rubble. The new damtoe was built with block size from 600 to 1000 mm. The slope protection was performed with block size from 450 to 800 mm. Blocks in the existing crest were removed and replaced with two layers of rip rap structure of size 600–1000 mm and more. The new extension have a width of 6 m which consists of a transition zone as a filter between the existing downstream embankment of gravel and the rip rap structure on downstream side. Top level of the dam was not changed. The crest of dam was completed by a 4 m wide roadway and curbs on both sides of the dam's entire length.

Leakages are collected by a drainage system throughout the length of the damtoe and collected at 3 different places. Small buildings for leakage measurement were built in the damtoe. Measured leakage is transferred to Statkraft's regional dispatch center. Bolts are installed in the downstream slope and on top of the core to measure horizontal and vertical settlement.

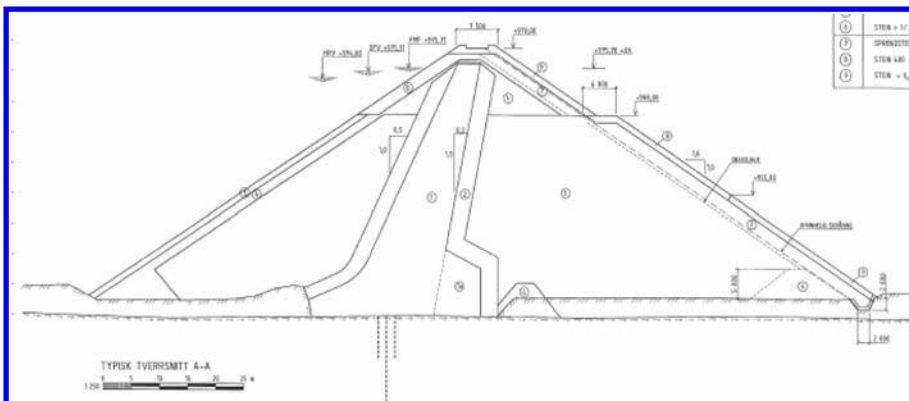


Figure 1. A typical cross section of dam Bitdalen.



Figure 2. Excavation of vegetation and soil masses and establishing new rip rap structure. (Photo: Pedersen).

The construction site was safeguarded and controlled by daily presence, as well as an extended control of the environment within a two weeks lap. In addition, the HSE has been the first issue on the agenda on all construction meetings and no major injuries have occurred.

4 LAND USE AND LANDSCAPE PLAN

Besides the required technical improvement of the dam, Statkraft found it expedient at same time to upgrade the landscaping.

A plan for landuse and landscape was prepared to provide recommendations on how the dam and the area close to the dam should be renewed in terms of an esthetic and landscape adaptation (Aarbakk 2006). The landuse plan shows how the area should be handled in the construction phase and the landscape plan how the area should be returned to fit into the environment in this open and vulnerable landscape.

The landscape plan was prepared in cooperation with different actors: Norwegian University of Life Sciences, Norwegian Water Resources and Energy Directorate, landscape architect, Vinje municipality, landowners and Statkraft.

4.1 *Landscape measures*

Prior to the rehabilitation of dam Bitdalen, there has been a major change concerning the views on the exposure of a dam. From being a big grassy area that almost disappeared within the terrain, the dam after rehabilitation became “flashy” with big grey stones. The dam has now emerged as a structure with distinctive form. It has been a main principle from the

landscaping point of view to make interventions as limited as possible and allow the dam to stand out as a clearly constructed element with precise transition to natural terrain.

The first years after rehabilitation the rip rap structure of the dam will be of light grey rocks. As the years go by, these rocks will become darker gray and take the same colour as elsewhere in this mountainous landscape.

4.2 *The quarry*

The quarry is also an intervention in the landscape. The location of existing quarry was rated as the best in terms of stone deposits and also how it is exposed in the landscape. The quarry is modelled after the natural valley in the northwest direction.

Today the replacing of the masses and revegetation of the quarry appears as a natural part of the landscape. This is shown in Picture 6.

4.3 *Cultural heritage*

Some investigations on cultural heritage were done in the valley near dam Bitdalen. The County Governor of Telemark has registered protected cultural relics in the form of coal pits in the area to be used for quarry. A dispensation was given to remove directly affected coal pits. Since there are many similar coal pits in the area.

4.4 *Elements from the land use plan*

There were several requirements to the contractor in the construction phase in relation to perform the work in an environmentally sensitive manner. It was required that the barracks should be placed within the agreed range. A program for sorting of all waste was carried out and hazardous waste was delivered to approved sites. All repair and maintenance work on construction equipment should be carried out without spoil of any oil or fuel.

It was also implemented measures taken against dust pollution from construction traffic on roads and dust from drilling in the quarry. Irrigation was used in both cases. A reasonable bonus would take effect if the contractor fulfilled the contract in an environmentally good way. Opposite the contractor would be fined for a sloppy performance.



Figure 3. The quarry during construction periode (Photo: Skrindo).

5 REVEGETATION

In addition to the project's primary goal of increased dam safety, it has been focused on landscape design and environmentally friendly solutions. The dam is located in a vulnerable area in the border zone of Hardangervidda National Park at an altitude of 1000 masl. The required rock quarry was planned located in an undisturbed area and it was thus important to re-establish the area after the dam was completed.

There are several challenges concerning natural revegetation in vulnerable areas. Erosion and landslides is a couple of the biggest challenges. In many areas, including Bittdalen, there is poor soil. In highland areas as for this rehabilitation project, there are few suitable seed mixtures available.

At Bittdalen peats were removed from the dam and quarry. After 2 years storing, they were transplanted in the quarry and other affected areas.

5.1 Restored quarry at Bittdalen

The quarry is at the end of construction period returned to a natural terrain (Rosef 2009). The transition to the existing terrain has been shaped as natural as possible and the sides of the quarry is gentle with slopes no steeper than 1:3. The quarry is designed as a continuation of the natural valley.

In this sensitive area it has been important to follow the principle of preserving the local soil and vegetation. Peats with vegetation were removed from the surface of the quarry; respectively with and without birch and stored separately (Hansen 2007). Peats and birch trees were tagged and recorded for later follow-up. Some of the tagged peats are shown in [Figure 4](#).

Masses were also removed; respectively topsoil, humus and inorganic soil. These were also stored separately in piles at a temporary storage site by the dam. Cover quantities from the



Figure 4. Revegetation in the quarry (Photo: Søreide).



Figure 5. Revegetation in the quarry (Photo:Søreide).



Figure 6. The quarry after revegetation (Photo: Søreide).

dam were stored by the downstream side of the dam. In addition varying sizes of natural stones were removed and stored. As part of the revegetation process the peats with vegetation, the unprocessed stones and masses were moved back into the quarry.

Peats were transplanted back in the quarry in such a way that “a desired vegetation structure was achieved in terms of aesthetic and ecological vegetation conditions” (Aarbakk 2006). They were also planted back at a time suitable for the growing season. For revegetation to be as natural as possible, the peats were replaced in a random pattern. A total of 126 peats with mountain birches were transplanted. 60% of the transplanted birch trees survived the first year after transplanting (Pedersen 2009).



Figure 7. Bitdalen dam after rehabilitation (Photo: Søreide).

Another example of measure for revegetation is the replacement of stones. Several natural stones in varied size from 0.5 to 2.5 m in diameter were stored and replaced in a natural pattern as shown in Figure 6.

6 CONCLUSION

In the project planning and execution stages Statkraft had main focus on the landscape design work in order to achieve such quality that the affected areas over time, should fall naturally into the surrounding landscape. From the very start of the project it was an integrated process between the technical and environmentally disciplines to find the best solutions for the rehabilitation.

Statkraft has recognized in retrospect that these measures have not led to additional cost, when the matter is the strict environmental requirements for structures in sensitive natural areas. In the last decades the environment has been focused in all rehabilitation projects and we assume that the increased costs due to environmental friendly solutions has increased the total project cost about 5–10% within a 40 year period.

It was estimated a total project cost of 5,8 million Euro. Final work is still going on, but the total cost tends to be less than estimated.

REFERENCES

- Aarbakk, J, Telnes, T., Pedersen, P.A. & Bardal, R. 2006. Land scape plan (in Norwegian).
- Hansen, S. 2007. Restoration of Bitdalen dam—revegetation and landscape adjustment after nature disturbance (in Norwegian).
- Pedersen, P.A. & Rosef, L. 2009. Ecological restoration of disturbed nature sites. Development of ecologically sound methods for revegetation following hydropower development and large road projects *Restaurering av natur i Norge*. (in Norwegian).
- Rosef, L. 2009. Ecological restoration of natural environment in the mountains. Rauland, 25–26 June (in Norwegian).
- Søreide, A. & Aarbakk, J. 2008. Bitdalen dam reconstruction. Final report 2006–2008 (in Norwegian).
- Ødemark, E, Østerbø, J. & Steine, H. 1997 Dam Bitdalen Reassessment (in Norwegian).

The conservation measures on rare and endemic fish during the construction of cascaded hydropower projects in downstream of Jinsha River

Xiujiang Zhao

China Three Gorges Corporation, Yichang, Hubei, China
Institute of Hydrobiology, Chinese Academy of Sciences, Wuhan, Hubei, China

Zhiyu Sun & Yongbo Chen

China Three Gorges Corporation, Yichang, Hubei, China

Ding Wang

China Three Gorges Corporation, Yichang, Hubei, China
Institute of Hydrobiology, Chinese Academy of Sciences, Wuhan, Hubei, China

Yong Gao

China Three Gorges Corporation, Yichang, Hubei, China

ABSTRACT: The downstream area of Jinsha River is significantly rich in both waterpower resources and fish biodiversity. The constructions of the cascaded hydropower projects (Xiluodu, Xiangjiaba, Baihetan, Wudongde) in this area may cause negative impacts on the fish biodiversity. China Three Gorges Corporation pays great attention to the conservation of fish at all times, and have been carrying out series of ecological mitigation measures. The conservation measures mainly consist of: Firstly, establishment of the “Rare and Endemic Fish National Reserve in Upstream of the Yangtze River”; The infrastructure construction, capacity building and the management capacity of the reserve has been greatly strengthened. Secondly, to carry out long-term investigation on resources, environments and social development by long-term systematic monitoring, i.e. fishery resources and environments monitoring system. Large quantities of information are collected accordingly including the knowledge of life history, population structure, population dynamics and genetic dynamics of endemic fish. All these information is integrated into one standardized fish database to facilitate the analysis and decision making significantly. Thirdly, to carry out scientific research on specific problem emerging stochastically based on a number of research institutes. Fourthly, captive breeding has been promoted substantially for reserving a collection of fish germplasm resources; Meanwhile, artificial propagation and restocking has been systematically and continuously implemented. This paper also illustrates the future conservation plans of the corporation.

1 GENERAL INTRODUCTIONS

1.1 *Hydropower resources in Jinsha River*

Jinsha River is the alias of upper reaches of the Yangtze River covering the section from Batang River estuary in Qinghai to Minjiang River estuary in Sichuan Province. Jinsha River is extremely rich in hydropower resources. Theoretically, it has the potential of 1.124×10^5 MW waterpower resources, which accounts for about 16.7% of total deposits in China. Particularly, the lower reach of Jinsha River (i.e. section from Panzhihua to Yibin) is the most abundant area of the whole river, accounting for more than 80% of the deposits of Jinsha River.

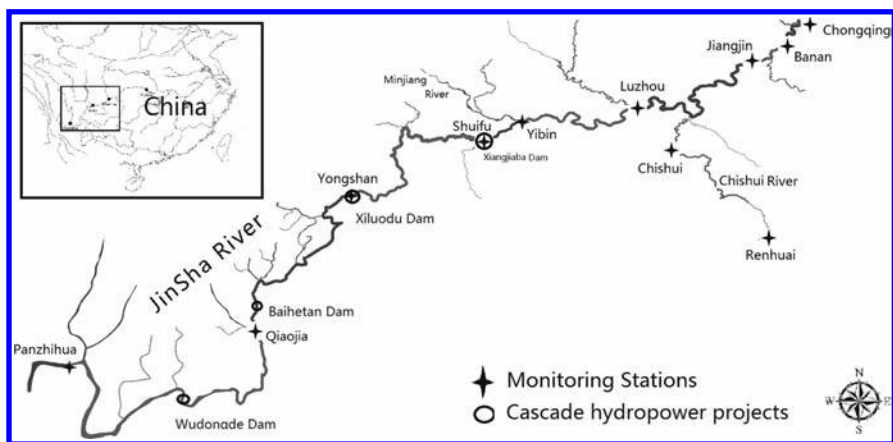


Figure 1. The sketch map of downstream of Jinsha River and “rare and endemic fish national reserve in upstream of the yangtze river”.

The exploitation of hydropower resources in this area will considerably alleviate the energy shortage in China, and accordingly has important economic and strategic significance for the country. In 2002, China Three Gorges Corporation (CTGPC) was authorized by government to exploit four cascade hydropower stations in this section, i.e. Wudongde, Baihetan, Xiluodu and Xiangjiaba hydropower stations. Two of them, the Xiluodu and Xiangjiaba, commenced in 2005 and 2006, successfully dammed in 2007 and 2008, and will impound in 2013 and 2012, respectively. Baihetan and Wudongde Hydropower Stations are currently in the phase of pre-feasibility.

1.2 Rich biodiversity in Jinsha River

Based on the Statements of Environment Impact of Xiangjiaba and Xiluodu, habitats of sections up and downstream of the dams would be changed due to the construction and running of hydropower stations. This section accommodates more than 69 endemic fish species, while the total endemic fish species in the Yangtze River is 142. Due to barrier effect of cascade hydropower stations, the continuity and integrity of habitats would be fragmented and weakened. Consequently, the survival of fish species here is greatly threatened.

1.3 Purpose of the paper

For purpose of keeping well balance between hydropower exploitation and environmental conservation, an overall scheme has been made by CTGPC to preserve fish species in all water areas affected by the cascade hydropower projects both in downstream of Jinsha River and “Rare and Endemic Fish National Reserve in Upstream of the Yangtze River”. In this paper, the background, implement and corresponding outputs of the conservation scheme were described. Meanwhile, the future conservation plan was also briefly described. Considering of significance of keeping harmony of development and conservation, a dilemma present worldwide and has to be addressed very carefully, the experiences acquired by CTGPC may provide a mirror for fish conservation in similar hydropower projects.

2 CONSERVATION SCHEME AND ACTIONS

2.1 Establishment of the reserve

To promote the conservation of endangered fish species, a national reserve “Rare and Endemic Fish National Reserve in Upstream of the Yangtze River” was established in April 2005.

This reserve was dedicated for the protection of 69 endemic fish species including Chinese paddle fish (*Psephurus gladius*), Yangtze sturgeon (*Acipenser dabryanus*), Chinese sucker (*Myxocyprinus asiaticus*) and so on. The reserve covered a total length of 1162.6 km river section in Sichuan, Yunnan, Guizhou and Chongqing, including the section between Xiangjiaba hydropower station and Masangxi (a small town nearby Chongqing) in the mainstream of Yangtze, the Chishui River (including some tributaries), and downstream of Minjiang River (including some tributaries).

For better operation and management of the reserve, CTGPC designed overall scheme for the reserve including: 1) Construction of infrastructure of the reserve, allowance of fisherman and support on the operation and management of reserve administrations, etc.; 2) Artificial restocking, including the construction of restocking stations, catchment and maintenance of parental fishes, fingerling rearing and releasing, etc.; 3) Scientific research, including research on conservation techniques, the evaluation of ecological impacts and research on new conservation strategies; 4) Monitoring of aquatic environments, including construction of electronic telemetry networks, capacity building of reserve administrations (Cao et al. 2007). The details of the scheme mentioned above generally covered three traditional conservation measures, i.e. in-situ conservation, ex-situ conservation and artificial breeding.

An administration office was specially set up for the operation and management of the overall scheme.

2.2 Infrastructure construction and capacity building of the reserve

CTGPC have been made regular investments on the infrastructure construction and capacity building of the reserve. On one hand, the facilities of reserve were constructed and renovated, including the infrastructure of reserve and three fish breeding releasing stations (Yibin, Chishui and Chongqing Restocking stations). Currently, the basic office space and subsidiary facilities of the reserve have been generally completed. Yibin Restocking Station

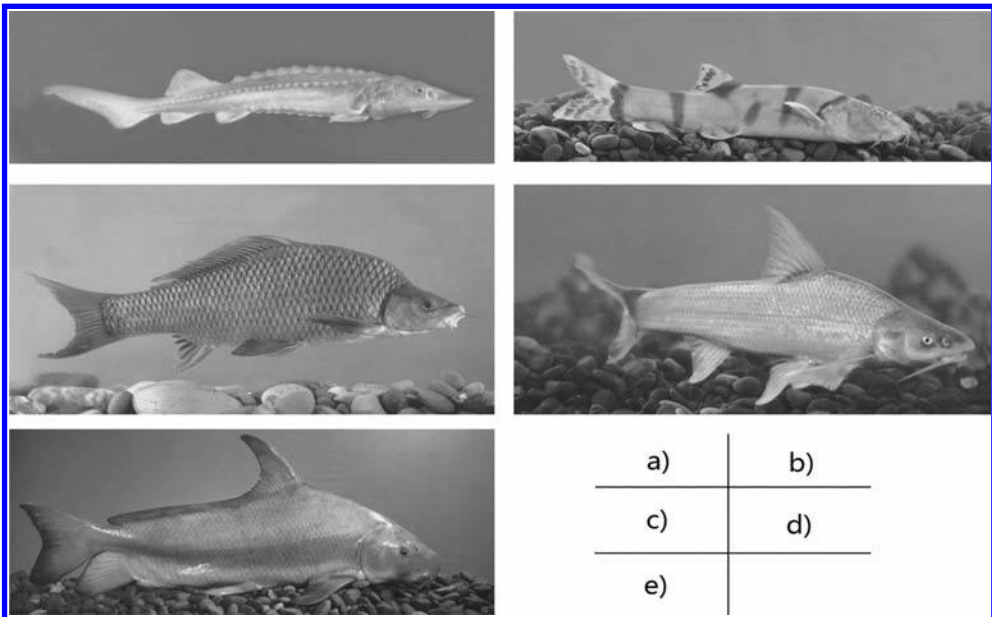


Figure 2. Some rare and endemic fish species inhabiting the downstream of Jinsha River, a) Yangtze sturgeon (*Acipenser dabryanus*), b) elongate loach (*Leptobotia elongate*), c) rock carp (*Procypris rabaudi*), d) Largemouth Bronze Gudgeon (*Coreius guichenoti*), and e) Chinese sucker (*Myxocyprinus asiaticus*). (Courtesy of Institute of Hydrobiology, Chinese Academy of Sciences, available at <http://www.ihb.ac.cn/kxcb/wsszg/>).

was completed and put into trial operation in 2008. The construction of Chishui Restocking Station has been mostly finished and will be put into operation. Chongqing Restocking Station will be expanded based on the Wanzhou Fisheries Research Institute in 2010, and expected to finish in 2012. On the other hand, efforts were made by buying or updating new technological equipments, as well as training staff regularly for the capacity building of the reserve.

2.3 *Systematic monitoring*

For understanding of the background information of the reserve, a full range investigation of fish resources, environments and society has been carried out. During the environmental impact assessment of the Xiluodu and Xiangjiaba, CTGPC has pre-launched the specialized studies “the impacts of water temperature and water quality” and “impacts on rare and endemic fish”. In 2005, conservation of rare and endemic fish and the reserve projects was fully launched. The long-term monitoring has been conducted. Relying on related research institutes and reserve administration networks, the long-term monitoring shall cover: Rare and endemic fish resources, commercial fishes resources, early resources of fishes and fishery environment. The monitoring sites were located respectively in Panzhihua, Qiaojia, Yongshan, Shuifu, Yibin, Luzhou, Jiangjin, Banan, Chishui and Renhuai. The direct output of this monitoring is an intergraded database consisting of a massive collection of information. This database thereafter was employed to evaluate the health of reserve from a macro-scale. Such kind of analysis and evaluation were conducted annually by a couple of institutes and the evaluation results would be reported to the Ministry of Agriculture, Ministry of Environmental Protection of China through annual formal report. These kind of information would facilitate the management and decision-making of governmental departments.

The monitoring was considered as a regular task and would continue quite a long time in future. In order to guarantee all the institutes involving this monitoring project would follow same standards and use same methodology, a research program was commissioned to compile a unified standard action plan, thus the standardization and unification of monitoring results were achieved. Furthermore, for better and effective management of the monitoring data, a rare and endemic fish database was developed. This database could integrate fish biology, fish population genetic, early resources of fishes, ecological environment and basic geographic information on a high degree of information platform, which greatly facilitates the compilation, storage, and analyses of monitoring data.

2.4 *Scientific research*

Beside long-term systematic monitoring, CTGPC also initiated scientific researches aiming at specific interested problem. These programs were launched based on a number of the scientific research institutes. Programs generally consist of four categories as follows according to the research subjects.

First of all is to develop the technology of rearing and artificial propagation. For example, in order to protect the critically endangered paddle fish, three trial capture operations were launched to hopefully get the paddle fish for genetic studies. Currently, the fourth and fifth capture action plan is now in preparation. Once the paddle fish is captured, the artificial propagation experiment will be conducted accordingly in terms of prearranged planning. Other ongoing similar programs include the rearing of mature and artificial propagation of fingerling technology of Largemouth Bronze Gudgeon (*Coreius guichenoti*), and the rearing technology of rock carp (*Procypris rabaudi*) and elongate loach (*Leptobotia elongate*).

The second subject is to study the habitats variation after the impoundment of the cascade reservoirs and corresponding impacts on the endemic fishes. The main purpose of this subject is to predict the trends of hydrological factors (e.g. water velocity, temperature, etc.) and water quality (e.g. gas super-saturation, heavy metals, organic contaminant etc.) of the river. Subsequently, with the aim of understanding the corresponding impacts, countermeasures

and mitigation plans of these environmental factors, simulation experiments have been conducted in the laboratory to study the mechanism of physiological impacts.

The third subject is to investigate the biological background information of the endemic fishes, and evaluate the conservation effects of relevant measures. For example, in order to probe into the relationship between project construction and the age structure, growth, feeding habitats, reproduction, life history characteristics of endemic fish before and after the operation, 21 endemic species, including rock carp, elongate loach and *Megalobrama pellegrini*, were selected as specific study objects for basic biological investigations. For the analysis of fish population structure, abundance and trends of population, a series of ecological surveys were conducted. For the purpose of understanding the impacts manner, extent, trends and response of genetic structure under the cascade hydropower stations, background information of genetic structure was collected and genetic diversity analyses were conducted. For the comprehensive assessment of the habitats changes of reserve, an evaluation of the ecological integrity of the reserve is now in preparation. This work will evaluate the ecological integrity of the reserve from the physical integrity, chemical integrity and ecosystem integrity.

The fourth is to carry out development policy study. For example, to conduct case studies home and abroad to look into experience and lessons from the other projects.

2.5 Captive breeding, artificial propagation and restocking

CTGPC launched the captive breeding and artificial culture of rare and endemic fish, therefore reserved a number of fish germplasm resources. These resources are mainly distributed as follows. Firstly, the parental resources of rare and endemic species are reared by Chinese Sturgeon Research Institute, an institute affiliated to CTGPC and professional on the research of Chinese sturgeon. Secondly, Yibin Restocking Station, a restocking station affiliated to CTGPC, reserved lots of parental resources such as rock carp, *Megalobrama pellegrini*, *Spinibarbus sinensis* and *Onychostoma simus*. The number of Yangtze sturgeon, elongate loach and other fish in captive for breeding is over thousands of individuals. In 2010, the total number of fingerling currently in artificial propagation reached up to 200,000 including the Chinese sucker, rock carp, *Megalobrama pellegrini*, and *Spinibarbus sinensis*. Chongqing Restocking Station and Chishui Restocking Station, which are expected to finish in 2012, will play similar role soon. Thirdly, a number of research institutes funded by the Three Gorges Corporation also reserve a huge number of parental resources and fingerling resources, including the largemouth bronze gudgeon, elongate loach and so on. Moreover, CTGPC is now constructing new breeding base for in the Three Gorges Dam area for expanding production of fingerling. When this base is finished, it will greatly strengthen the rearing capability of the institute.

Artificial propagation is also one important means, especially for the conservation of critically endangered species. A number of other fishes, like Yangtze sturgeon, Chinese sucker, *Largemouth bronze gudgeon*, *Leptobotia elongate*, *Megalobrama pellegrini*, and *Ancherythroculter nigrocauda* are also successfully artificially propagated funded by CTGPC. The artificial breeding of Yangtze sturgeon and Chinese sucker could even fulfill the requirements of continuous restocking already. Although Chinese sturgeon is actually not impacted by the cascade stations, it is noteworthy to mention one great progress on the artificial propagation of this unique species. The institute of CTGPC succeeded in complete artificial propagation of Chinese sturgeon in October, 2010. This successful event stands for the achievement of large-scale artificial restocking of sturgeon species without loss of wild sturgeon resources, and consequently has positive significance in the artificial propagation of other sturgeon species, such as paddle fish. So far, the new born second generation individuals are in very good conditions.

Restocking is now conducted regularly in the downstream of Jinsha River taking advantage of the captive breeding facilities. An overall restocking framework was accordingly urgently needed for comprehensive planning of restocking activities. Hence a specific study was

carried out by overall consideration of fish distribution, abundance, research progress, fish fry production, parental fish resources and facilities conditions. Accordingly, a framework involving the restocking stations, restocking species, restocking quantity etc., was established. Up until now, more than 200,000 endemic fish (rock carp, elongate loach, etc.) have been released only in Yibin restocking station. In order to assess the contribution of released populations to the restoration and maintaining of the wild populations, CTGPC launched evaluation program at both population and genetic levels. When all the cascade stations are finished, CTGPC will extract a certain proportion of electricity profits as conservation funds for the conservation of the rare and endemic fish in upper stream of Yangtze River (Cao et al. 2007). By doing so, CTGPC will keep doing restocking activities for a long time even after all the hydropower stations were finished.

3 CONCLUSION

This paper has concluded the conservation schemes, plans, documents, actions, and measures of CTGPC in fish conservation. The corporation will continue to adhere to the philosophy of “building a power station, promoting the local economic, improving the environment and benefiting the local people” in the continuous endeavor to promote the Jinsha hydropower development process. The corporation is committed to achieving the harmonization of economic, social and ecological benefits (Cao et al. 2007), to promoting harmonious balance between hydropower development and conservation, and ultimately, to achieving eco-friendly hydropower development.

REFERENCES

Cao G.J., Sun Z.Y., Chen Y.B. 2007. To fully promote the conservation of biological resources of the Yangtze River during the construction of hydropower development. *China Three Gorges Journal*, 6.

Application of MIKE 11 model in the prediction of water pollution accident in the Three Gorges Reservoir

Y. Fang

China University of Geosciences, Wuhan, Changjiang Water Resources Protection Institute, Wuhan

Y. Min

Changjiang Water Resources Protection Institute, Wuhan

ABSTRACT: After the impoundment of the Three Gorges Reservoir in June 2003, the water quality of Three Gorges Reservoir has been an focus worldwide. The generalized river network of the whole main stream and its tributaries has been constructed with the water characteristics of the Three Gorges Reservoir Area. On the basis of HD module and AD module from MIKE 11 Model, HD model and AD model of Three Gorges Reservoir are established. And it proves that these models have comparably ideal simulating effects by conducting calibration and verification. Under the condition of 175-meter water-impoundment and running of the Three Gorges Reservoir, The above mentioned models are used to simulate and calculate the diffusion and transference of pollutants after the water pollution accident in the reservoir area. Meanwhile, quantitative simulation is carried out to test the time and concentration value of the pollutants downstream in different places of Cuntan section, moreover, the quantitative forecast is made, concerning the range of influence, extent and time of sudden risk accidents.

1 INTRODUCTION

The Three Gorges Project is a key backbone project for harnessing and developing the Yangtze River. Having tremendous comprehensive benefits in flood prevention, power generation, shipping and etc., the Three Gorges Project plays a very important role in the economic and social sustainable development in China. Since the establishment of the Three Gorges reservoir, the hydraulic regime of some part of the reservoir has changed, therefore, people pay high attention to water resource protection and the reliability of water supply.

With the rapid development of the economy in the Three Gorges Reservoir Area, chemical industrial enterprises, with high risk rate for environmental security, are gradually becoming major hazardous sources along the Yangtze River. These enterprises constitute a big threat to the water quality of the reservoir and downstream of the dam because of the high risk of water pollution caused by hidden danger in the production and potential accident. Besides, the gradually heavy water and land transportation, as well as the growth of dangerous chemicals transportation increase the possibility of pollution accident. The water pollution accident, which is unexpected, diffused and dangerous, poses an enormous threat to people's lives and property as well as the ecological environment. The Three Gorges Reservoir is such an important strategic water source and ecological shelter for the middle and lower reaches of the Yangtze River that high standard should be set for the water environment quality and great attention should be given to the increasing risk of water pollution accident and difficult task of tackling emergency.

With the help of MIKE 11 model, one-dimension HD prediction model was established for the whole main stream and tributaries of Yangtze River in the Three Gorges Reservoir area. Assuming the Three Gorges Reservoir operates at the storage level of 175-meter, the

diffusion and transference of pollutants after the water pollution accident in the reservoir area is simulated and calculated with the HD prediction model, to provide technical support and scientific basis for the prediction, warning of water pollution accident and emergency response.

2 ABOUT MIKE 11

MIKE 11, developed by DHI Water & Environment, is a professional engineering software package for the simulation of flows, water quality and sediment transport in estuaries, rivers, irrigation systems, channels and other water bodies.

MIKE 11 is a user-friendly, fully dynamic, one-dimensional modeling tool for the detailed analysis, design, management and operation of both simple and complex river and channel systems. With its exceptional flexibility, speed and user friendly environment, MIKE 11 provides a complete and effective design environment for engineering, water resources, water quality management and planning applications.

The MIKE 11 Hydrodynamic (HD) module solves the vertically integrated equation for the conservation of continuity and momentum (the 'Saint Venant' equation). The MIKE 11 Hydrodynamic module (HD) uses an implicit, finite difference scheme for the computation of unsteady flows in rivers and estuaries. MIKE 11 one-dimensional hydrodynamic control equation is as follow:

$$\begin{cases} \frac{\partial Q}{\partial x} = \frac{\partial A}{\partial t} \\ \frac{\partial Q}{\partial t} + \frac{\partial(\alpha \frac{Q^2}{A})}{\partial x} + g \cdot A \cdot \frac{\partial h}{\partial x} + \frac{gQ|Q|}{C^2 A \cdot R} = 0 \end{cases} \quad (1)$$

where, Q is the discharge, A the flow area, q the lateral inflow, h the stage above datum, C the Chezy resistance coefficient, R the hydraulic or resistance radius, α the momentum distribution coefficient.

The primary feature of the MIKE 11 modeling system is the integrated modular structure with a variety of add-on modules each simulating phenomenon related to river systems. MIKE 11 includes add-on module for Advection-Dispersion. The advection-dispersion (AD) module is based on the one-dimensional equation of conservation of mass of dissolved or suspended material, i.e. the advection-dispersion equation. The module requires output from the hydrodynamic module, in time and space, in terms of discharge and water level, cross-sectional area and hydraulic radius.

The advection-dispersion equation is solved numerically using an implicit finite difference scheme which, in principle, is unconditionally stable and has negligible numerical dispersion. A correction term has been introduced in order to reduce the third order truncation error. This correction term makes it possible to simulate advection-dispersion of concentration profiles with very steep fronts.

The one-dimensional (vertically and laterally integrated) equation for the conservation of mass of a substance in solution, i.e. the one-dimensional advection-dispersion equation reads:

$$\frac{\partial AC}{\partial t} + \frac{\partial QC}{\partial x} - \frac{\partial}{\partial x} \left(AD \frac{\partial C}{\partial x} \right) = -AKC + C_2q \quad (2)$$

where C is the concentration, D the dispersion coefficient, A the cross-sectional area, K the linear decay coefficient, C_2 the source/sink concentration, q the lateral inflow, x the space coordinate and t the time coordinate.

3 ESTABLISHED MODEL

3.1 Establishment of hydrodynamic model

The simulation covers: From the dam site to Zhutuo at the storage level of 175 meters; and the main backwater areas of tributaries, especially Jialing river, Wujiang river, Xiaojiang river, Daning river, Xiangxi river. [Figure 1](#) presents the scope of simulation.

According to the different hydrologic condition and upstream inflow, the boundary condition of water flow (and water level) was defined for the hydrodynamic model. The water level and flow quantity for the rivers and streams in Three Gorges Reservoir Area were simulated using Mike 11 Hydrodynamic Model, providing basis for the follow-up water quality simulation.

1. The Model Simulation needs some data, including: Network editor(.Nwk11), cross editor (.xns11), boundary editor(.bnd11), parameter editor(.hd11) and time series editor(.dfs0).

2. Calibration of the hydrodynamic model.

Bed Resistance is the key calibration parameter for hydrodynamic model. There are many ways to estimate this parameter. According to the typical hydrological observation data of water flow (and water level) of the year 2006, the bed resistance was calibrated to satisfy the accuracy requirement. Base on the observation data of Hydrological Station of the Three Gorges Reservoir from 2000–2009, the simulated water level value was in agreement with the actual measured result when the bed resistance reaches 35. But about 95% trace data really follow the corresponding stochastic distribution in each state and 90% of predictions are correct with the probability of 0.8 or 0.9, and the relative error is lower than 15% for backbone networks. The river system in the Three Gorges Area, which is fully developed with large number of tributaries, is the main reason for the error. While the hydrodynamic model only took into account of five tributaries, namely Jialingjiang River, Wujiang River, Xiaojiang River, Daning River and Xiangxi River. And no consideration was given to regional rainfall runoff.

3. Verification of the hydrodynamic model.

With the observation data of Hydrological Station of 2009, the hydrodynamic model was further verified. The simulated water level and discharge value were basically in agreement with the actual measured result with relative error of less than 10%, which can satisfy the precision requirement of the model. [Figure 2](#) presents the comparison between the simulated and the observed of discharge of Qingxichang section in 2006. [Figure 3](#) presents the comparison between the simulated and the observed of water level of Fengjie section in 2006.

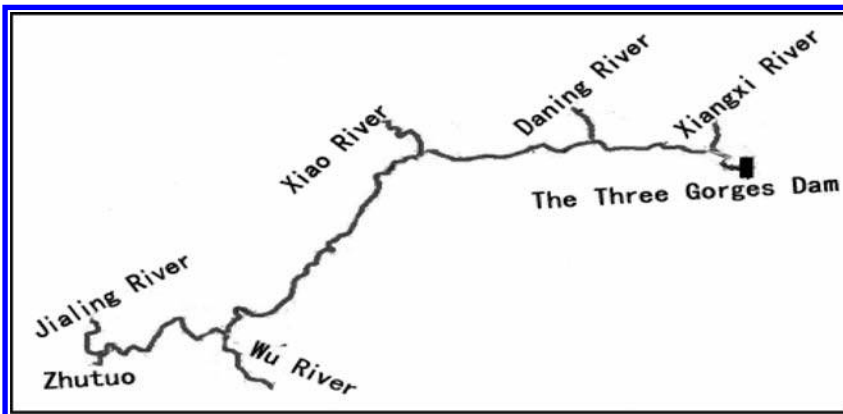


Figure 1. The scope of simulation.

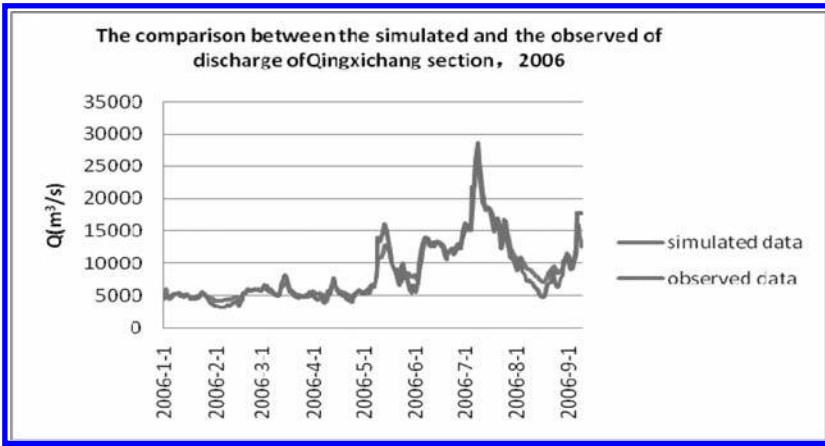


Figure 2. The comparison between the simulated and the observed of discharge of Qingxichang section, 2006.

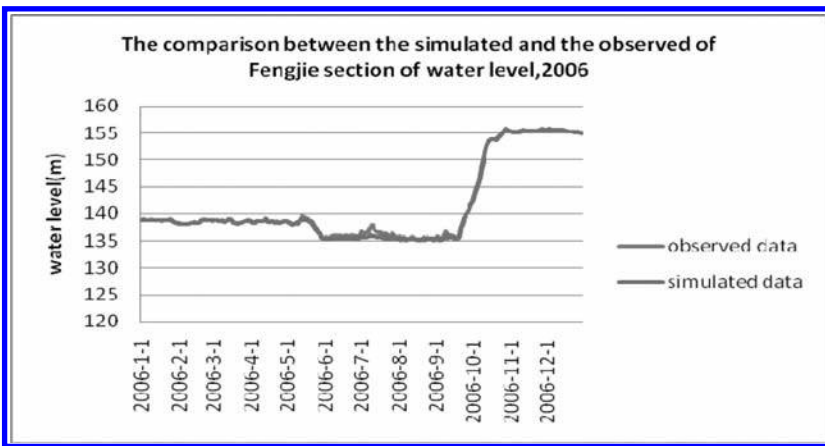


Figure 3. The comparison between the simulated and the observed water level of Fengjie section of water level, 2006.

3.2 Establishment of advection-dispersion model

Mike 11 Advection-Dispersion module could satisfy the need for simulation of the diffusion and transference of pollutants and the site analysis of water pollution accident for water pollution accidents usually occur with large quantity of high concentration pollutants.

1. Based on current situation of the reservoir water environment, COD_{Mn} was selected as the simulation factor, using the average of the monitoring data of Zhutuo section as the initial concentration of Advection-Dispersion model.
2. Calibration of the advection-dispersion model.

The main Calibration parameters need to be calibrated for advection-dispersion model are D the dispersion coefficient and K the linear decay coefficient. Linear decay coefficient was very difficult to be determined for many factors, such as the local natural condition, the water pollution extent, the flow velocity and air temperature, and etc., could influence the coefficient.

On the basis of drawing lessons from past research results and the water quality monitoring data from 2000 to 2009 in the Three Gorges Reservoir, the main parameters

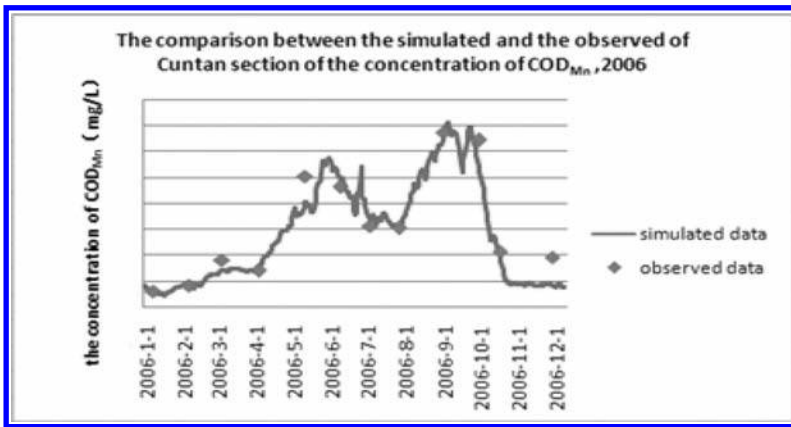


Figure 4. The comparison between the simulated and the observed of Cuntan section of the concentration of COD_{Mn}, 2006.

calibrated in the model are dispersion, the dispersion coefficient ($D = 10$) and the linear decay coefficient ($K_{\text{COD}_{\text{Mn}}} = 0.06$).

3. Verification of the advection-dispersion model.

The advection-dispersion model was verified with the water quality monitoring data of the main sections of the Three Gorges Reservoir. The simulated concentration of COD_{Mn} was basically in agreement with the actual measured result. The result shows that their relative error is within 20%, which can satisfy the precision requirement of the model.

Figure 4 presents The comparison between the simulated and the observed concentration of COD_{Mn} of Cuntan section in 2006.

4 SIMULATION

On the basis of the working condition of 175-meter water-impoundment and running of the Three Gorges Reservoir and the flow condition of the main and tributary streams, the HD model has been used to simulate the diffusion and transference of the pollutants in case of water pollution accident.

Supposing water pollution accident occurs in up, middle and down reaches of the main stream respectively during the dry period (in February), flood period (in July) and impounding period (in September) in Cuntan section, Qingxichang section and Fengjie section. Different pollution load is given according to different pollution level. The assumed emission of water pollution accident is as in Table 1.

The range of influence is different in different periods because of different hydraulic and hydrological regime. Table 2 lists the simulative characteristics of the pollution influence in each period.

Table 2 presents the diffusion and transference of pollutants in Cuntan section, Fulin section and Fenjie section. It shows that the time and distance are dramatically different in the same section during different periods, which is determined by the operating characteristics of the Three Gorges Reservoir. As a seasonal regulating reservoir, the drifting distance and time are much longer at the upper reaches due to the high flow velocity and the push of the flow in the flood period with a water level of 145-meter before the dam. However, the range of influence becomes much smaller at the middle and lower reaches because of large water volume and sluggish water flow. In the low water period with a water level of 175-meter before the dam, the influencing distance becomes even smaller. Anyway, there is more prone to pollution accident at the up reaches with larger coverage range.

Table 1. The assumed emission of water pollution accident.

No.	Flow of pollutants (m ³ /s)	COD _{Mn} (mg/L)	Duration (h)	COD _{Mn} overall load (t)
1	20	10000	2	1440
2	20	7000	2	1008
3	20	3500	2	504

Table 2. The predictive range of influence and influencing time (take COD_{Mn} for instance).

Assumed accident location	Time of accident	Program	Influence distance (km)	Influencing time (h)	
Cuntan section	Dry period	1	77	81	
		2	54	49	
		3	14	10	
	Flood period	1	199	44	
		2	137	25	
		3	20	1	
	Qing xichang section	Impounding period	1	253	83
			2	149	40
			3	98	19
Dry period		1	14.6	8	
		2	2.8	6	
		3	—*	—	
Fengjie section	Flood period	1	94	29	
		2	33	7	
		3	21	7	
Fengjie section	Impounding period	1	126	60	
		2	62	26	
		3	21	7	
Fengjie section	Dry period	1	7.5	4	
		2	13.5	5	
		3	15	7	

*Note: “—” Shows that the result of the simulate is within the standard (GB3838-2002) (COD_{Mn} = 6 mg/L).

Table 3. Program 1 the prediction of water pollution accident cuntan section (low water period, dry period).

Lower reaches x (km)	Arriving time	Time of maximum concentration (h)	Maximum concentration (mg/L)	Duration of pollution
Accident area		1	27.7	2h 45min
5	After 2h 45min	5	17.1	5h
10	After 6h	8	16.4	6h
15	8h 45min	12	14.2	5h 45min
20	After 12h 15min	15	12.7	6h 15min
25	After 17h 20min	20	11.3	6h 25min
30	After 22h 30min	26	10.5	6h 30min
35	After 27h	30	10.4	6h 20min
40	After 31h 30min	35	9.9	6h 50min
50	After 43h 20min	46	8.0	6h 25min
60	After 53h 50min	57	7.2	6h 10min
70	After 69h	71	6.4	4h
77	After 81h	81	6.0	

The dynamic calculative process of HD model makes it possible to show the drifting time and peak value of the pollutants all the time since the outbreak of the accident, therefore, the administrators can monitor the harm degree. The following will take Cuntan section for example, as is shown in Table 3.

From Table 3, when the accidental pollution takes place, we can get the arriving time, peak concentration and lasting time by using the one-dimension model. As a result, the decision-makers can make emergency plan to cope with this problem and issue warning objectively and scientifically within a short time.

5 CONCLUSION AND SUGGESTION

According to the working condition of the Three Gorges Reservoir and flow condition of its main streams and tributaries, a one-dimension HD model is established to effectively simulate the pollution extent and trend of pollution accident in any section of the reservoir, including the maximum time and distance the pollutants take to float downstream and the specific arrival time, pollution extent and time of duration. Therefore, the decision makers of management can work out emergency plans and measures, provide technical support and improve the ability of management decision support while handling water pollution accident.

The application of the one-dimension model has somewhat practical significance; however, the more exact simulation of pollution influence can be got if the two-dimension model is adapted. In a word, the combination of the one-dimension model and two-dimension model will provide scientific support for those decision-makers to make scientific and accurate judgment on the damage level of the water pollution accident.

ACKNOWLEDGMENT

This project has been supported by scientific and technological major special project in state water pollution control and management—"The prevention and control of water pollution and the control technology of water bloom of the Three Gorges Reservoir" (2009ZX07104-006).

REFERENCES

- Danish Hydraulic Institute (DHI). MIKE 11: A Modeling System for Rivers and Channels, Reference Manual[R], DHI. 2009.
- Danish Hydraulic Institute (DHI). MIKE 11: A Modeling System for Rivers and Channels, User Guide[R], DHI. 2009.
- Danish Hydraulic Institute (DHI). MIKE 11: A Modeling System for Rivers and Channels, Short Introduction Tutorial[R], DHI. 2007.
- R.Z. Li, C. Wang and J.Q. Wang, "Study on Simulation and Prediction of River Water Quality based on Unascertained Information". *Advances In Water Science*, vol. 15, Jan. 2004, pp. 35–39.
- J.Q. Wang, Z. Chen and J. Wu, "Stream Water Quality Models and Its Development Trend". *Journal of Anhui Normal University (Natural Science)*, vol. 27, Mar. 2004, pp. 242–247.
- B.Q. Tan and G.P. Zhang, "Water Quality Management Model for Huaihe River Basin". *Water Resources Protection*, vol. 46, Mar. 2001, pp. 15–18.
- W. Liu, H.C. Liu and H.Y. Xu, "Calculation Method of Water Environment Capacity for Water Function Area Based on MIKE 11 Model". *Water Resources & Hydropower of Northeast China*, vol. 8, 2009, pp. 69–70.

Protection of the National Mayanghe Natural Reserve in development of Wujiang Penshui Hydropower Station

Guzheng Jiang, Hongqing Li & Yingxi Li

Changjiang Water Resources Protection Institute, Wuhan, Hubei Province, China

ABSTRACT: Pengshui Hydropower Station, the tenth power station on Wujiang River, is one of the key projects for water resources development of the river. The major purpose of the station is to generate power with comprehensive uses of navigation, flood control and etc. The storage level is 293 m high with reservoir volume of 1.212×10^9 m³. The National Mayanghe Natural Reserve is the sensitive receiver of the project. During the environmental impact assessment, environmental research of special subject has been carried out about the natural reserve. Based on technical code of environmental impact assessment and the requirements of the environmental protection laws and regulations concerning natural reserves, the advantaged and adverse impacts on Francois's leaf monkeys and their habitats, the ecological integrity of the natural reserves, the structure and the functions of the natural reserve have been analyzed with adoption of various analytic methodologies, such as ecological mechanism method and map overlay method, through comprehensive investigation & evaluation of the present environmental condition of the natural reserve and analysis of the effects of reservoir inundation. At the same time, the food habit and the home range of Francois's leaf monkeys (*Prsbevtis francoisi*) have been thoroughly investigated.

1 BACKGROUND

1.1 Project description

Pengshui Hydropower Station, which is located on Wujiang River, in a comprehensive large-scale facility with main purpose of electricity generating, as well as other objectives, such as navigation and flood prevention. The station is a Class I water project, with the normal storage level of 293 m, reservoir capacity of 1.212×10^9 m³. The dam is of concrete gravity type with the dam-top height of 301.5 m. The tallest dam height is 116.5 m. The installed capacity is 1750 MW with firm output of 371 MW. The power generating units consume 3629 h each year with mean multi-year energy yield of 6.351×10^9 kWh. The construction of this project uses 68 months.

When storage level reaches 293 m, the backwater spreads 117.0 km during 20-year occurrence flooding. The reservoir is a year-regulated water pool with storage coefficient of 1.26%. The normal storage level, the dead water level, the flood prevention limiting water level are 293 m, 278 m, 287 m respectively. And the regulating storage capacity is 5.18×10^8 m³.

The Pengshui Reservoir is of valley type. When the normal storage level reaches 293 m, an area of 46.77 km² will be impounded, including water surface of 16.35 km² and land of 30.42 km². 21,781 people will be affected with 43977.3 mu farmland submerged, involving Pengshui County, Youyang County of Chongqing Municipality and Yanhe County of Guizhou Province. In National Mayanghe Natural Reserve, 1728.8 mu farmland will be flooded, involving 4 groups of 3 villages in 3 townships. 15 persons from 4 families have to be relocated.

1.2 Research background and methodology

The impacts arising from Pengshui Hydropower Station on National Mayanghe Natural Reserve are mainly displayed on the influences on the land of the Reserve and on the population relocation when reservoir storage level is raised.

According to investigation, the total land which will be flooded reaches 1728.8 mu in the Reserve, including 279.4 mu farm land, 1230.1 mu forest land for special purposes, 2.8 mu cartilage base and 216.5 mu non-used land. The river reaches which will be affected within the Reserve includes main stem of Wujiang River, the middle and lower river reaches of Hongdu River and the estuary of Mayang River, among which Hongdu River is the stream to be submerged. Francois's leaf monkeys (*Presbytis francoisi*) and their habitats are the protected objectives. There are altogether 6 herds of 42 to 78 Francois's leaf monkeys living in Hongdu River, which will be impounded by the reservoir backwater and on the steep cliffs by the Wujiang River. The habitats for the monkeys face the risk of flooding. It should be clarified whether there is any influence on the structural functions of the Reserve and the characteristics, the scope and the extent of the influence should be determined. For the core area, the buffer zone and the experimental area of the Reserve will be submerged.

Treatment for impoundment and population relocation should be planned as some farmland, population and houses within the Reserve will be affected by the impoundment. According to the national and local regulations concerning the protection of natural reserves, the principle, which population relocated due to work opportunity losses and living environment change should be resettled outside natural reserves, should be followed to mitigate and eliminate the potential long term adverse impacts on natural reserves, for the good of management and protection of natural reserves. The moving and relocation of the population will possibly impose disturbance on the wild animals within the Reserve.

The main impacts on the natural reserve comprise the influences arising from the reservoir impoundment on the land along both Hongdu River and Siqu River within the Reserve. Therefore it should be analyzed whether impoundment gives rise to influence on the regional eco-integrity of the Reserve. The impacts on eco-structure and the function as well as Francois's leaf monkeys and their habitats should be investigated and examined. Priority method has been employed for the analysis of eco-integrity and the maintenance. For the influence on the eco-structure and the functions, map overlay method has been introduced. Ecological mechanism method and map overlay method are mainly applied in the analysis of influence on Francois's leaf monkeys and their habitats. And the influence on home range, food habit and food source for the monkey has been analyzed.

2 ENVIRONMENTAL SITUATION OF THE RESERVE

2.1 Basic situation

Entrusted for the protection of national Class I protected animal Francois's leaf monkeys (*Presbytis francoisi*) and their habitats, the National Mayanghe Natural Reserve, a protected area for wild animals and forests, is located in the north-west of the Yanhe County (Fig. 1), covering an area of 31,113 hm², of which the core area is 10,543 hm², the buffer zone is 15,022 hm², and the experimental area is 5,548 hm². The Reserve is an area most densely populated nationwide with altogether 78 herds of 652 Francois's leaf monkeys.

The county level Mayanghe Natural Reserve was established in September 1987 with total area of 4,308 hm², encompassing two sub-areas of Mayanghe and Hongduhe. 38 herds of 395 Francois's leaf monkeys were populated in the Reserve. In August 1994 the Reserve was upgraded to provincial level, and the protected area was enlarged to 20,515 hm², with 67 herds of 630 monkeys. Authorized by People's Government of Guizhou Province in March 2002, the Juchishan Natural Reserve of Francois's Leaf Monkey, located in Wuchuan County of Zunyi City, was incorporated into the Provincial Mayanghe Natural Reserve for protection of the species and the integrity of their habitats. Consequently the protected area

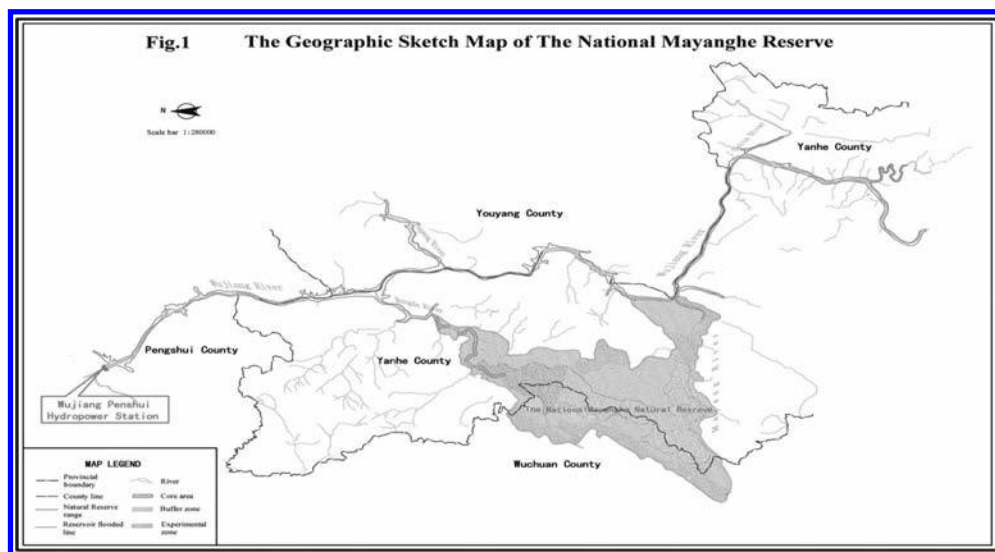


Figure 1. Geographic sketch map of the Mayanghe Reserve.

was extended to 31,113 hm² with 78 herds of 652 monkeys populated. In June 2003, the Reserve was authorized to upgrade to national level.

2.2 Environmental background

The natural reserve is a limestone mountainous area with cuesta and box valley fully developed. The banks of Wujiang River is at an altitude of 1,441 meters while the most lower part is 280 meters high with a wide disparity of more than 1100 meters in the height above sea level. Valleys are much distributed in the tributaries of Mayang River and Hongdu River, the valley bottom is normally 350 meters high and the height of the mountain top is more than 1100 meters. The area lower than 800 meters is strongly cut precipitous cliffs. The area between 500 to 1000 meters above sea level are distributed with shallow strip eroded terraces, forming layer mountain landscape and the deep cut valley landscape with solution structure.

The National Mayanghe Natural Reserve is located in the middle humid subtropical climate zone with abundant rainfall and intense heat. It is hot in summer and cool in winter with long frost free period and duration of growth. The annual temperature varies much greatly with annual mean temperature of 16.7°C, extreme high temperature of 41.0°C and the lowest one of -6.0°C. The accumulated temperature higher than 10°C varies from 3500°C to 5500°C with the change of altitude. The annual mean rainfall in the area is 1158.7 mm.

The main streams in the Reserve are Mayang River, and Hongdu River, the Class I tributaries of Wujiang River. Completely located in the Reserve, Mayang River is 30 km long. To west it drains in Juchishan Mountain in the territory of Wuchuan County, and to the east it joins the Wujiang River at Siqu Township of Yanhe County. Steep cliffs are distributed on both banks of the river with great disparity of altitude varying from 330 meters to 750 meters. In the middle and lower river reaches of Hongdu River, the stream flows southwest to northeast through the north part of the Reserve with an little disparity of altitude varying from 280 meters to 350 meters. As the tributary of Hongdu River and the trans-boundary river between Yanhe County and Wuchuan County, Hongsi River is 15 km long, flowing south to north from the core area of the Reserve and joining the Hongdu River at the river mouth of the two rivers.

Mainly distributed on the steep cliffs $>70^\circ$ and the top on both sides of the valley where bushes and grass are distributed, the typical vegetation in the National Mayanghe Natural Reserve is subtropical evergreen broad leaf forest. Besides the trees which are calcivorous, the vegetation in the Reserve does not completely possess any characteristics of that of typical karst landform, though the vegetation covers on the eroded structure morphology and the soil is neutral and slightly acid. Most of the native vegetation are destroyed due to terrain change and human activities. The present vegetation is secondary except some native vegetation is kept in very few places. According to survey, there are altogether 266 species of vertebrates, including 17 families of 37 species of animals, 40 families of 149 species of birds, 12 families of 32 species of amphibian and reptilian, and 10 families of 48 species. In the Reserve 29 species are key national protected animals, among which 3 species are on the national Class I animal list, namely bear, leopard and musk deer (*Moschus berezovskii*) and 26 species are on the national Class II animal list.

The National Mayanghe Natural Reserve covers but not limit to 7 townships of 40 villages belonging to Yanhe County and Wuchuan County of Guizhou Province. According statistics 2002, 22816 individuals of 5040 families were uneven populated in the Reserve with population density of 73 people/km². The population resided in the protected area is mainly living in the adjacent area, leaving the core area less populated. The minorities make up 94% of the total population. Since the Reserve was established, administrative system had been set up progressively with almost shaped preliminary infrastructure. At the same time basic tourism facilities have been constructed and ready for visitors.

3 ENVIRONMENTAL IMPACT ANALYSIS AND PROTECTION MEASURES

3.1 *Impacts on Francois's leaf monkeys and their habitats*

3.1.1 *Ecological characteristics of Francois's leaf monkey*

3.1.1.1 *Activities and habits*

Locally know as “rock spider monkey” or “rock cat”, the Francois’s leaf monkeys, mainly inhabiting in dense forests and caves on steep rock, are very alert and resourceful animals that are good at climbing and jumping. Francois’s leaf monkeys are group living animals. Headed by a strong adult male, a group may comprise 7 to 13 individuals. They normally go out the caves, hunt for food, play, rest, groom, drink water and sleep according to certain time schedule. Each group normally has definite activity range. Natural caves, cracks or rock cells constitute their main sleep grounds. Each group has more than two sleeping grounds, shifting for 3 to 5 days. The play ground, influenced by food hunting range, is usually centered on the sleeping ground with a radius of approximately 800 meters.

3.1.1.2 *Food habit*

Francois’s leaf monkeys prefer fruits, leaf and flower of plants, while the parts of plants which the monkeys prefer may vary with season shifting. According to the survey on the diet for the monkey distributed along Mayang River and Hongdu River, there is discrepancy for the type, distribution and abundance of food for the monkeys in different seasons. In spring shoots and tender leaves constitute their main diet, while flowers and fruits of some plants make up for their second preferences. In hot Summer Francois’s leaf monkeys eat flowers and fruits of some kinds of plants. During fall season they mostly feed on fruits and seeds. When winter comes, fruits and leaves are their diet. Sweet potatoes are their important food source.

3.1.1.3 *Habitat*

The National Mayanghe Natural Reserve is mostly lime rocky mountain area with many caves. The river beds of Mayang River and Hongsi River, the tributary of Hongdu River, are flat; with considerable height difference from the mountain top as much as to more than 1000 m. Steep cliffs are distributed on both sides of Mayang River and Hongsi River.

The slope from the cliff top to mountain top is mainly $>60^\circ$. The Francois's leaf monkeys mostly inhabit on the steep cliffs with woodland.

3.1.2 *Impact assessment*

3.1.2.1 *Home range*

Home range is a land often used for food finding, multiplication and rearing. The research of home range is the key study on animal activities. The choice of the habitats is closely related to the food abundance, vegetation, obscurement of habitat, and the physical condition of the animals. The size of home range varies with food habit, season, in-community relation, relationship between herds and physical condition of animal itself.

According to the scientific survey on National Mayanghe Natural Reserve and Francois's leaf monkeys' habits, the home range for each herd is approximately 2–3 km², holding 7–13 monkeys. The home range and the caves (rock cell) are comparatively stable. The home ranges for different herds sometimes are overlapping, while not for a day. Occasionally the Francois's leaf monkeys behave unusually, such as howling, attacking or moving very fast, when two herds of monkeys are approaching.

3.1.2.2 *Impact on the home range arising from impoundment*

Impact on the distribution of Francois's leaf monkeys: According to the impounded scope by backwater, some land in the bordering area to Wujiang River, Hongdu River and Mayang River will be flooded. Based on the field survey of the areas which are involved in the impoundment within the Reserve, 6 herds of Francois's leaf monkeys are distributed in the Pengshui Reservoir Area encompassing Hongdu River, Mayang River and main stream of Wujiang River. Assumed each herd has 7 to 13 individuals, altogether 42 to 78 monkeys will be influenced by backwater, whose activity range is normally on the steep cliffs in the main stream of Wujiang River, Hongdu River and Mayang River will be influenced by backwater.

The impacted habitats: In the analysis of the influence, projected area shall not be the only consideration for the impacted habitats, for Francois's leaf monkeys mainly inhabit on the steep cliffs along the rivers. The vertical area, which is also the habitat and will be submerged by raised water, should be taken into account. The impacts arising from sedimentation and backwater jacking have been considered in the estimation.

From [Table 1](#) it could be seen that normally the habitats for the 6 herds of Francois's leaf monkeys which would be impacted within the backwater area would not exceed an area of 0.017 km², a land that would turn out to be waters. While the structure of the habitats has changed to some extent though the habitats lost constitute no more than 1% of the home range. Therefore the habitats will be affected after the impoundment, for some habitats in the reservoir area will lose due to impoundment, with shrinking home range for the 6 herds of Francois's leaf monkeys.

Impact on the food source: Francois's leaf monkeys have abundant food source in Spring and Autumn, mainly feeding on shoots, leaves and fruits. In winter and summer crop, such peanuts are their prime food source. Besides some ever-green broad leaves, shrubs, such as *Pyracantha fortuneana* and *Rubus* (*Rubus saxatilis* L.) are the diet for Francois's leaf monkeys. After the reservoir impoundment, some vegetation, mainly shrub, farmland vegetation and woodland, in the natural reserve covering Hongdu River, Mayang River and along the Wujiang River will be submerged due to water level raised. The farmland at lower elevation above sea level is not the food ground for Francois's leaf monkeys, while the shrub and woodland are mostly the food source. At the same time, it takes relative long time to restore the vegetation on the lime rock. Therefore, temporary impacts on the food source growing on lime rock will arise due to impoundment.

3.2 *Impacts on other rare animals*

Sparsely distributed in the Reserve with relative large disparity of height above sea level, the key protected animal present relatively large number. Most habitats of the rare animals in the

Table 1. Impacts on the home range of Francois's leaf monkey.

No.	Location	River reaches	Water level raised by (m)	Submerged habitats		The backwater section location referred
				Area (km ²)	Percentage of the home range (%)	
1	Houchayuan	Tributary of Hongduhe R.	6	0.011	0.44	17.7 km to Hongduhe River mouth
2	Chiya	Hongduhe R.	5	0.008	0.32	21.4 km to Hongduhe River mouth
3	Huangquan	Hongduhe R.	5	0.008	0.32	The opposite bank of Chiya
4	Siqu	Mayanghe R.	7.5	0.012	0.48	Anxigou on the main stream of Wujiang River
5	Liangqiao	Mayanghe R.	0.5	0.001	0.04	Backwater end of Mayanghe River
6	Yintongzi	Rujiang R.	10.5	0.017	0.68	Yintongzi on the main stream of Wujiang River

Notes: The home range for Francois's leaf monkey is 2–3 km². In the analysis, the value of 2.5 km² is compared. The raised water level is from the reservoir backwater estimation output.

Reserve inhabit in areas at higher altitude. According to the analysis on the composition and distribution of the rare animals in the Reserve, these rare animals are mainly distributed in core area upstream of Hongsi River and Hongdu River and in areas higher than 350 meters. Therefore little impact will be imposed on the rare animals.

Among the special protected animals for National Mayanghe Natural Reserve, 10 species are wild animals, 5 species are wild birds and 4 species are aquatic organisms. Black bears were not found in the last decades though they were reported in 1950's. Leopards are distributed sparsely and were occasionally found in Juchishan Range within the Reserve. Both bears and leopards are not distributed in the submerged area in Pengshui Reservoir Area and will not be influenced by population resettlement. Besides Francois's leaf monkeys, the other key national protected animals are common Otter (*Lutra lutra*) and Macaca (*Macaca mulatta*)

Some habitats for the otters probably will be submerged for few otters are distributed around the backwater line. The otters are very active and inhabit near the streams and rivers. They will move upward to the water front and find new habitats when the water level is raised. The impacts on the habitats for otters are limited. On the other hand, the habitats and food ground will be enlarged due to reservoir impoundment, which help increase their communities. Otter deserves more attention in the population resettlement.

The National Mayanghe Natural Reserve has many rare birds. The increase of the water surface and improvement of local climate are favorable for the growing of food ground and habitats as well as the increase of their communities.

3.3 Impact on terrestrial plant

According to the overall distribution characteristics of the vegetation in the Reserve, we could find no significant difference between vegetation communities and there is no distinguished pattern for vertical and horizontal distribution.

According to the field survey over the typical vegetation within the range of the backwater of Hongdu River and Mayang River in the Reserve, we could find that box-type valleys dominate the mountain range on both sides of Hongdu River with larger gradient

(generally $>70^\circ$), where the primary vegetation has been seriously destroyed. And the present vegetation are more distinguished secondary type with brushwood and bare hills. The steep cliffs, high and precipitous mountain top, valleys with larger gradient, and the eroded land and slopes are usually not suit for farming. The plants which are distributed on river banks of Hongdu River and Mayang River generally grow in the rock cracks on the steep cliffs and abrupt slopes with thin layer of soil.

The impacts arising from the Pengshui Hydropower Station on the natural reserve comprise flooding the land in the Reserve due to the rise of water level after the impoundment. The natural reserve is mainly located in the dissected valleys along Mayang River and Hongdu River which are distinguished with valleys with bottom elevation of 350 m and hill top elevation of more than 1100 m. Perilous cliffs and precipices are mostly distributed on the steep slopes lower than height of 800 m above sea level.

The normal storage level is 293 m for Pengshui Reservoir. The water depth and surface area of Hongdu River will increase with the reservoir impoundment. According to the analysis on the backwater of Hongdu River, the water level will rise by 18 m at the location with a distance of 9.4 m to the river mouth under 5-year flooding reoccurrence.

According to the scientific field study on Mayanghe Natural Reserve, the backwater area for Hongdu River is mostly perilous cliffs and steep slopes. Natural vegetations are normally distributed in the valleys over 300 m high above sea level, due to steepness, bare rocks and eroding. The top water level reaches 301 m under normal storage level of 293 m with consideration of the influence of backwater. Furthermore the water level, from Gongxikou to Dayanmen (the end of the backwater), may vary between 282.2 m to 302 m during 10-year reoccurrence flooding. The natural vegetation is sparsely distributed on both sides of Hongdu River under natural circumstance. Therefore the impacts on the vegetation arising from reservoir impoundment are limited.

3.4 *Impacts on the structure and function of the reserve*

The submerged land in the core area of the Reserve is 35.1 hm² after the impoundment, accounting for 0.1% of the total area of the Reserve and 0.3% of the core area. The lost land uses are mainly farmland of 10.5 hm², special purpose woodland of 21.1 hm². The core area which will be influenced by flooding is located outside of the center area of the natural reserve, bordering the buffer zone with frequent human activities.

According to the field survey and investigation, the total area that will be submerged is 115.2 hm², accounting for 0.37% of the protected area. The total acreage of core area and buffer zone is 254.57 km². Assumed that the home range for each herd of Francois's leaf monkeys is 2 to 3 km², the total home range for the 76 herds of Francois's leaf monkeys reaches 152 to 228 km² after the impoundment. Some habitats will turn into waters which still fall into the protected area. The interior function will not change. With impoundment, the proportion and the components of the landscape will not change; no isolated island will be formed. The transportation and communication of species will receive no influence from habitat fragment and smashing.

Generally, the protected species will not change due to reservoir impoundment with little influence on the structure and function of the Reserve. While impoundment will give rise to reducing and shrinking of habitats for the 6 herds of Francois's leaf monkeys, this problem will get eased with proper mitigation measures.

3.5 *Environmental protection measures*

3.5.1 *Creation of food woodland*

According to the eco-environmental protection targets, 300 mu food woodland should be created to guarantee that the eco-environmental quality is not worse than present or even better. The creation of the food woodland should be coordinated with the overall plan of the Reserve—that is both scattered distribution and concentrated small piece should be considered for reasonable management of the natural reserve.

3.5.2 *Establishment of emergency center for rare and endangered wild animals*

An emergency center in Gongxikou for rare and endangered wild animals has been planned for the Reserve to temporary caring for the disturbed and injured animals during the initial stage of impoundment and population resettlement, and for the starving animals which are short of food due to impoundment. Those animals will be released to the nature after the injures are cured or favorable habitats are located.

3.5.3 *Orientation and education*

Teach the local people and the resettled population to protect the Francois's leaf monkeys and other rare and endangered wild animals through broadcasting, TV, wall papers, poster, orientation car, workshops and etc., on village fair. The participants to the workshops should be the managers from the townships and villages which will be submerged or get involved in population resettlement, and the primary and middle school teachers whose townships will be submerged. Permanent instruction and stands should be set up in the key crossings, main entrance to the mountain and the reserve boundary.

3.5.4 *Eco-environmental monitoring*

The capacity building should be improved to accelerate the protection of Francois's leaf monkeys in the Reserve. The survey shall focus on the quantity, activity range and the habitats of the 6 herds of monkeys.

3.5.5 *Launch research programs*

In the view of the specialty and sensitivity of National Mayanghe Natural Reserve, environmental change and the countermeasures, and the eco-environment to the reservoir response research program has been proposed for the habitats of the Francois's leaf monkey after reservoir impoundment.

REFERENCES

- Chen, Z.R., Luo, Y., Wang, S.X. 2001. The Primary Study on the Impact Factors of the Francois's leaf monkeys Inhabiting in Mayang River of Guizhou Province, Guizhou Frest Science and Technology 29(2):34-37.
- Chen, Z.R., Luo, Y., Wang, S.X. 2000. Obsevation on Food Habit of the Francois's leaf monkeys Inhabiting in Mayang River of Guizhou Province, Chinese Journal of Zoology 35(3):44-49.
- Fang, J.Y. Liu, G.H. 1996. The Biomass and Net Production of National frest vegetation, Acta Ecologica Sinica 16(5):497-508.
- Fenjingshan Natural Reserve Administrative, Forest Department of Guizhou Province. 1994. Proceeding of Scientific Survey of the Mayanghe Natural Reserve for Francois's leaf monkeys. Guiyang: Guizhou National Press.
- Guizhou Forest Survey and Design Institute. 2002. The Overall Planning for Mayanghe Natural Reserve, Feburary 2002.
- Li, M.J., et al. 1994. Wild Animal Resources in Guizhou. Beijing: China Forest Publish House.
- Li, M.J., Ma, J.Z. 1989. The Primary Survey on the Ecology and Ammount of Francois's leaf monkeys in Mayanghe Natural Reserve, Chinese Wildlife (4):13-15.
- Li, M.J., Lei, X.P. 1989. Primary Study on the Ecology of Francois's leaf monkeys in Mayanghe Natural Reserve. Guizhou Forest Science and Technology (4):85-90.
- Li, M.J., Huang, S.Q. 1993. Report on Wild Primates in Guizhou. Guizhou Science 11(3):68-74.
- Li, B.G., Liu, A.H. 1994. Study on Home Range of Primates. Chinese Journal of Ecology 13(2):61-65.
- Natural Ecological Protection Department of National Environmental Protection Agency. 1999. Guidelines for Non-pollution Ecological Impact Assessment. Beijing: Chinese Environmental Science Publish house.
- Wu, B.Z., Wang, Y.H. 1994. The Primary Report on the fishery Resources in Mayanghe Natural Reserve, Guizhou Science 12(3):45-49.

Implement water diversion measures to ease the ecological water demand of the Yellow River Delta

Li Xining, Sun Lijuan & Meng Xiangwen
Yellow River Shandong Bureau, YRCC, Jinan, China

ABSTRACT: The Yellow River Delta is China's the most complete and most young native wetland ecosystems. Yellow River Delta National Nature Reserve is located at the new silt zone on both sides of the Yellow River, with a total area of 153,000 hectares. There are large variety of plants and migratory birds. Due to the development of the area, land and oil exploring, and water flow decreasing, the wetland scope is becoming smaller and the biodiversity is threatened. During the two years from 2008 to 2009, YRCC implemented two times of Yellow River water and sediment regulation practices to supply water into the wetland. But there are still many problems to keep the substance development of the delta wetland, such as serious lack of water resources, no water supply flow guarantee for delta ecology and so on. According to these problems and the present situations and effects of the eco-water-supply practices, the author point out some measures and opinions to keep a long term effect eco-water-supply.

1 AN OVERVIEW

The Yellow River Delta National Nature Reserve is the transit station, wintering and breeding grounds for the migratory birds of the Northeast Asian inland, and the Western Pacific. It plays a very important position in the biodiversity conservation and wetlands research and is one of the most representative examples of the worldwide wetland ecosystems. There are two components of the reserve area, one located in the present water course and the surrounding area; the second is the previous water course of Diaokou River estuary mouth and the surrounding area, with a total area of 153,000 ha, of which the core area of 58,000 ha, buffer area of 13,000 ha, and experimental area of 82,000 ha (See Fig. 1). According to comprehensive scientific investigation of the area, there are 393 kinds of plants including 116 kinds of two grade national protection wild plants, 1543 kinds of wild animals including 418 kinds of marine aquatic animals of which there are 6 kinds of state grade protection animals, 108 kinds of fresh water fish of which there are 3 kinds of state grade protection, and 283 kinds of birds including 9 kinds of state grade protection birds like white crane, red-crowned crane, black stork, and etc.

The Yellow River Delta wetlands are rich in biological species and diversities, and the ecological environment is very fragile influenced by the terrestrial and marine combined power function. For a long time, the main consideration of the Yellow River water utilization has been focused on agricultural, industrial and domestic water demands. However the water demands for maintaining an ecological balance has been ignored. Because of the neglect, intentionally or unintentionally, people begin to interference on the river and estuary ecosystems, large-scaled, sustained and severely. In the process of water resources development and utilization, we have created serious environmental and ecological problems to the downstream river and estuary area, such as ecological degradation, intensified environmental crisis, increased ecological security risk, and others.

Especially since the 90's of the 20th century, due to sharp drop of the Yellow River water flow running into the sea, the Yellow River Delta wetlands ecological system is faced with

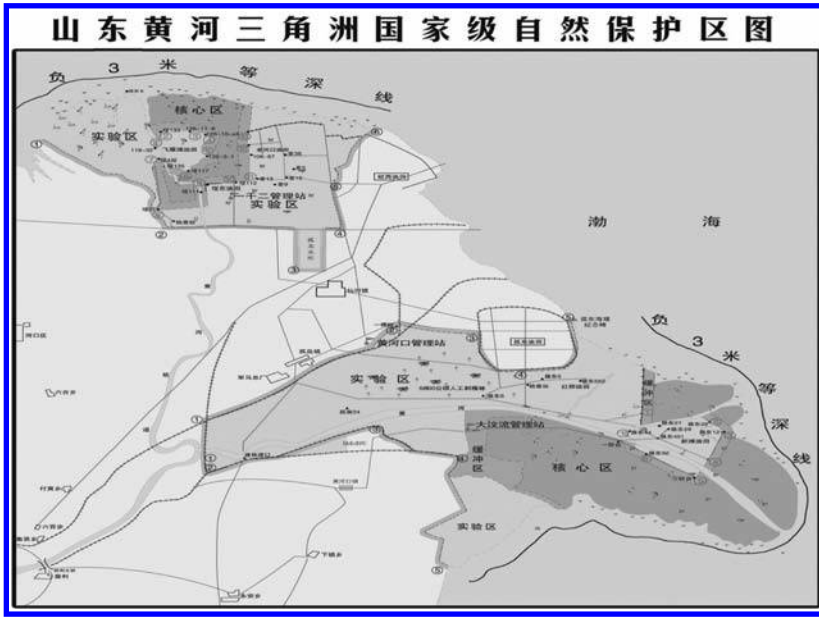


Figure 1. Distribution map of the Yellow River Delta Nature Reserve.

series serious problems like large-scaled wetland area shrinking, biodiversity and marine biological resources decaying, and so on, which have seriously influenced the ecosystem stability and sustainable economic and social development of the Yellow River Delta. Since the Yellow River water unification management and dispatch comes into truth in 1999, cutting-off of the river has not taken place for 10 years from 2000 to 2009. However, due to the overall severe shortage of the Yellow River water resources, the ecological water demands of the estuary area can not be guaranteed, especially in the old Diaokou river course Nature Reserve, wetlands area shrinking is even more serious without Yellow River water supplement for many years.

On November 23, 2009 the State Council officially approved the “Development Plan of Eco-efficient Economic Zone in Yellow River Delta”, which indicates that the development of the Yellow River Delta has been raised to the grade of national strategies to become an important component of the national regional development strategies. The Plan is required to be implemented as a main line of efficient utilization of resources and ecological environment improvement. To maintain the healthy ecosystem maintenance of the Yellow River Delta has a great importance to the construction of economic zone.

2 MAIN PROBLEMS OF THE YELLOW RIVER DELTA

2.1 Significant reduction of freshwater wetlands

Since the 80's, 20th century, the Yellow River Delta's natural wetlands area began to rapidly decline, and large areas of natural wetlands depredated to salinization influenced by wetlands development, occupation and destruction and steady reduction of Yellow River runoff and sediments. From 1993 to 2005, the natural wetland area has been decreased by nearly 40%.

2.2 Severe land salinization

In addition to area of the south of Xiaoqing River, the land of the Yellow River Delta is a new-born land formed by Yellow River sand and silt deposition. There are mainly two types

of the soil, damp and saline. From inland to offshore, the type of the soil gradually changes from damp to saline. Most of the land reserve resources have the characteristics of high salt content, shallow depth of groundwater, and vulnerable to secondary soil salinization. From the salinization evolution of the Yellow River Delta, the alluvial soil formed in 20's and 30's of 20th century has been severe salivated and is not suitable for farming, and the soil formed in 40's and 50's is also gradually becoming into salinization stage with a large scale.

2.3 *Water pollution, reduction of the Yellow River runoff flowing into the sea, coastal environment affected*

Every year, as a certain amount of leakage of oil and sewage running into the sea at the tidal estuaries, the shallow waters area has been polluted, the beach near the sewage estuary has also been seriously polluted by the oil, and the permanganate index there exceeded the rate of 11.1%. The total inorganic nitrogen in the shallow water is far exceeded the normal index, and the nutrients concentrations is in a high level. Since 1989, "red tides" have occurred many times, marine life and aquatic resources have been greatly influenced, and the potential risk of eutrophication has been exposed increasingly.

Due to the sharp reduction of the Yellow River water and sand flowing into the sea, the main evolution type of the Yellow River Delta coast has changed from deposition to retro-gradation. According to some observation data, since 1996, the Yellow River delta coast has been negative growing with an average annual land area reduction of 7.6 km². Meanwhile, the reduction of the Yellow River water flowing into the sea not only makes the coastal salinity, but also makes a large number of organic matter sharply reduction which results in degradation of the marine environment.

2.4 *Severe water resources shortage, ecology water supplement shortage in the estuary area*

There is only a small amount of shallow fresh groundwater in the region at south of the Xiaoqing River. The local river is short in river course with a little runoff of only about 47 million m³ a year. And the customer rivers have little water resources for utilization. 90% of the water demands of the estuary region are supplied by the Yellow River water resources. Every year in the estuary region there's about 1.5 billion m³ water cultivated from the Yellow River for utilization, but there is still a shortage of about 0.5~0.8 billion m³. Recently with the development and construction of the Yellow River Delta efficient ecological economy zone, water demand would further increase and the development of the estuary would strongly depend on the Yellow River Water Resources. On the situation of terrible shortage of water resources, the contradiction between water utilization for ecological protection economic and social development will get even more and more sharp. And in the Yellow River Water Allocation Plan approved by the State Council in 1987 there is no water use index for ecology water utilization in the estuary.

3 IMPLEMENT ECOLOGICAL WATER SUPPLY METHODS AND GRADUALLY INCREASE ECOLOGY WATER SUPPLEMENT FOR THE DELTA REGION

3.1 *Combining with the Yellow River water and sediment regulation to supply water for ecological use*

In 2008, the eighth Yellow River water and sediment regulation started. This is the first time to combine with the water and sediment regulation to implement ecological water diversion. By observation, about 13.56 million m³ of fresh water has been supplied to the 10 thousand ha of the Delta with 0.3 m water depth rising in the core wetland. In 2009 about 15.08 million m³ of fresh water has been supplied to the wetland by 10 days' eco-water regulation from June 24 to July 3. According to the two times of satellite remote sensing monitoring on June 19, and July 4 in 2009, the core area of wetlands has increased 3480 ha, and average water depth of

the wetland has increased about 0.4 m. And the biodiversity has been significantly improved by the eco-water regulation practice. In addition, in recent years, during the critical period of April and May in estuary area, We appropriate to increase the amount of water flow running into the estuary to reduce degree of soil salinity, and to promote the restoration of vegetation, fish Class of migratory spawning and healthy development of wetland ecosystem.

3.2 *Implement the test of ecological water supplement in the Yellow River delta and diaokou river course recovering water flow, supply water demand of the diaokou river course wetland*

From June to July in 2010, combining with the Yellow River water and sediment regulation we operated a test of eco-water supplement in the Yellow River Delta and river course of Diaokou recovering water flow. The water course of Diaokou is the previous river course of the Yellow River which has been protected as a spare river course with no water flow again for 34 years after the Yellow River changed to flow into the sea through the Qingshuigou river course in May 1976. According to the problems like river course shrinking, estuary coastal retrogradation, coastal ecosystems deterioration and so on, our Yellow River Conservancy Committee decides in time to implement a test to supply ecological water and recovery water flow in river course of Diaokou. During the Yellow River water and sediment regulation from June 19 to July 18, 2010 water flow run through the whole course of the Diaokou River with a total water volume flowing into the river course of 23.09 million m³ till July 20.

3.3 *Ecological and environmental protection measures in Dongying City achieve effect*

There are significant developments in ecological environment protection and construction of Dongying City. During the “Tenth Fifth” period the effective ecological economy zone has been finished construction. On the side of natural ecology protection there is two natural reserve recovering engineering being constructed in 2000 and 2005 with a total area of 10000 ha. And in 2005, the Overall Construction Planning of Ecological City of Dongying (2003–2020) has been worked out.

4 SUGGESTIONS

4.1 *Properly handle the relationship between ecological protection and estuary harnessing*

The economy development and ecology environment healthy maintenance of the estuary region needs comprehensive harnessing methods to properly handle the relationship among flood protection, river course running into the sea, water resources and ecological environment protection. According to the present situation of the estuary wetland, as a precondition to ensure the flood protection security of the Yellow River Estuary, we should strictly follow the natural law to protect and appropriate rehabilitation the wetland, properly handle the relationship among flood protection, river course running into the sea and the contradiction between supplement and demand of water resource, and reasonably regulate and dispatch water resources of the Yellow River region to supply enough ecology water for the Yellow River Delta to achieve the aim of estuary ecological environment restoration and healthy maintenance in the Yellow River Delta region.

4.2 *Actively undertake research on eco-water demand of the Yellow River Delta to acquire a water distribution indicator*

It is the basis of improving the ecological environment of estuary and remaining the virtuous cycle of environment to put the ecological water demand volume of the estuary into the whole Yellow River water resources unified regulation goals. But till now there has been no a well-recognized data of eco-water demand of estuary. So that it is urgent and important

for us to actively undertake the research on eco-water demand of the Yellow River Delta and to work out a well-recognized water demand data. With the data we can call on the higher authorities to put the estuary eco-water demand data into the whole Yellow River water resources regulation goals, and allocate a water use indicator to ensure the eco-water demand of the estuary area.

4.3 *Increase the intensity of eco-water regulation*

First is to continue to implement eco-water regulation combining with the Yellow River water and sand regulation just like in the year of 2008 and 2009, and change the eco-water supplement time from July and August to April and May to meet the growing demand of the plants in the wetland. Second is to propose that the state increase investment, further improve the water diversion facilities and water transfer program, implement long-term water supplement practice for the Diao kou river course, gradually restore the wetland function of the Diaokou river course, and improving the ecological environment in the region constantly.

4.4 *Strengthen research on theoretical system of water demand and health standards of estuary ecological environment*

Water demand of the estuary ecological environment is a new concept proposed according to problems like eco-environment protection while water resources development and utilization, scientific eco-environment reconstruction and improvement and so on. And there are no clear definition and scientific distinction for the words of environment water demand and ecology water demand, and no systematic and deeply analysis and research on mechanism and principle of ecological environment water demand. Therefore it is necessary to carry out large number of works like site investigation, data survey and analysis about the ecological environment of estuary. Meanwhile in the Yellow River efficient ecological economy zone construction plan the ecology water demand volume should be considered enough to ensure the water supplement for ecology environment in estuary.

Study on river ecological compensation of China

B. Ruan & Y. Fu

China Institute of Water Resources and Hydropower Research, Beijing, China

ABSTRACT: On the basis of generalizing the conception of river ecological compensation (eco-compensation) reasonably, according to river characteristics and people's practice experience, the paper gives discussion on river eco-compensation mechanism from the angle of coupling system. By analyzing the characteristics during theoretical study and practical experience of river eco-compensation, to ameliorate the limitations, the paper describes the framework of effective river eco-compensation mechanism. For Xin'an River as an example, in the light of the present compensation theory, the author gives river eco-compensation mechanism overall framework based on co-construction and sharing ideas. Learning from the research progress and achievement of different areas, the paper gives typical examples analysis about trans-boundary river eco-compensation implementation on water quantity and quality joint operation level. Finally, the paper puts forward the improvement measures and further research emphasis of river eco-compensation in China.

1 RIVER ECO-COMPENSATION

Eco-compensation is an economy measure to realize the internalization of externalities for the deeds of damaging the ecological environment. Eco-compensation, as an effective measure to balance efficiency and equity during economic developing, has been adopted in many countries and proved to be a good approach to protect environment (Gong 2002; ACCA21 2007). Before the 1990s, the river in China is the resources tool only to be used and harnessed. At that moment, the engineering means to treat river is the main method, abandoning the ecological factors, which makes a serious disturbance to ecological protection. Late 1990s, with the rapid development of economic society, the river ecology system bears the great stress coming from water pollution, river underlying surface "distortion", river shape artificialization, river ecological system deterioration and river function linearization. To recover the bio-diversity and river natural sceneries to polluted river, so implementing the river eco-compensation mechanism becomes more important at present. Using the former research achievement as reference, the author gives the conception of river eco-compensation: river eco-compensation is a mechanism, which puts the whole function of river ecology as the basis, according to the ecological cost-benefit brought by damaging river ecology as well as ecological gain-benefit brought by protecting the river ecology, taking material flow, energy flow, information flow, value of ecosystem services, cost of ecological protection, opportunity cost of development and risk assessment of ecological restoration as logical proofs, depending on government supervision, markets spontaneous adjustment and people's broad participation, to realize the sustainable development in coordinated way of river eco-environment and economic society.

River ecosystem is an open complex system consisting of water, biology and riparian zone. The integrity, dynamic continuity makes river own multi-objective and multi-level social economy function, as well as the ecological service function of leisure entertainment for people, purifying wastewater, cleaning up the environment and regulating climate. Therefore, the formulation of river eco-compensation mechanism should contain a variety of ecological factors, such as water quantity, water quality, water temperature, biology and landscape.

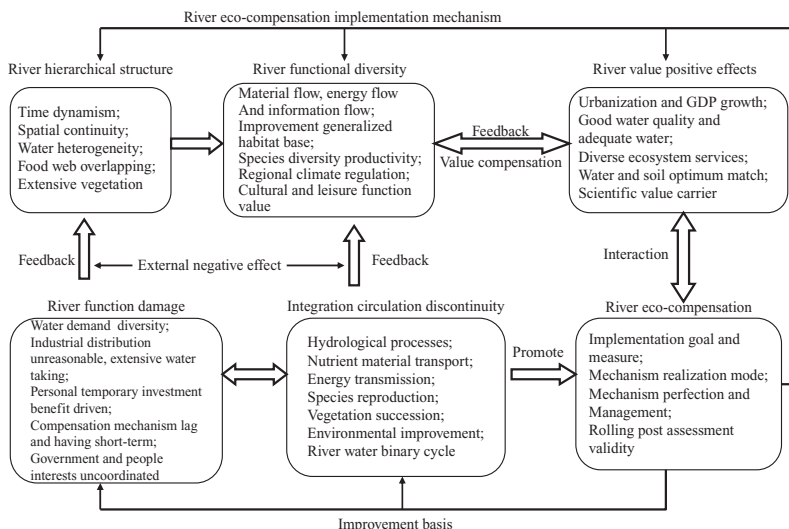


Figure 1. The overall framework of river eco-compensation.

Above all, the researcher should put river ecological factors of the living space of many kinds of living creatures as the core. Starting from the angle of river hierarchical structure, function diversification, value and holistic circle, considering the specific attribute and limitation factors of different modules, the paper depicts the overall framework of river eco-compensation from system integrity and variant coupling (Liu 2008, Fig. 1).

The template is used to format your paper and style the text. All margins, column widths, line spaces, and text fonts are prescribed; please do not alter them. You may note peculiarities. For example, the head margin in this template measures proportionately more than is customary. This measurement and others are deliberate, using specifications that anticipate your paper as one part of the entire proceedings, and not as an independent document. Please do not revise any of the current designations.

2 RIVER ECO-COMPENSATION MECHANISM IMPLEMENTATION

On the basis of river continuum concept, flood pulse concept and river water system theory, the paper puts sustainable development, externality, eco-capital and water resources public-goods theory as compensation basis, with the help of economic and legal administrative means, and makes the ecological function recovery of degraded river as the goal to implement river eco-compensation.

The ecological environment of river has value and capital attribute. Based on the principle of equal value exchange, following benefit overflow effect, the paper proposes river eco-compensation mechanism to eliminate the phenomenon of “free rider” during consuming river ecology service product by persuading “the beneficiary” who enjoys river ecological protection achievement to pay certain compensation to the protectors for their use behavior. By doing this, the government can encourage people to enlarge the investment to the river ecological protection behavior, to realize “Pareto Optimality” of protecting river ecology.

Under diverse biophysical and social contexts, Gretchen C et al. thought if payments for ecosystem services are not carefully designed, they may yield minimal gains in services of interest, and may well harm the production of other services and biodiversity conservation (Gretchen 2008). Therefore, to implement river eco-compensation successfully, we should adjust the relational balance: marginal personal payment of protecting river ecology equals to marginal social payment, marginal personal benefit from river ecological protection equals to marginal social benefit. Taking this as foundation, we can achieve the balance of protecting

the river system “external economy and external diseconomy”, also can realize internalization of external effects (Fig. 2).

Based on the above-mentioned presentation as foundation, to realize the restoration of destroyed and polluted river body, China starts positive exploration from theory research to practical integration of ecosystem services in a credible, scalable and sustainable way.

Zheng et al. applied ecosystem engineering theories to discuss river ecological restoration mechanism, and pointed out to satisfy the demand of river ecological water requirement is the key in water scarcity area, which laid the foundation for the implementation of river eco-compensation mechanism (Zheng 2002). Yang et al. proposed the coastal zone ecosystem restoration of degraded river should contain contents, provided the reference for river eco-compensation mechanism perfect (Yang 2004). Dong proved the feasibility of implementing eco-compensation to dammed rivers in view of the disadvantage of tradition hydraulic engineering to river ecosystem, and described the dammed rivers eco-compensation mechanism (Dong 2006). By analyzing the negative influence to the river brought by human activity, Chen et al. gave the method of river ecological rehabilitation from the aspects of soil and water conservation and management, eco-hydraulic engineering and water body pollution sources control (Chen 2006). In China, to reinstate the original function of destroyed and polluted the rivers water body, different areas carried out a series of practice studies. Han et al. propounded river ecological rehabilitation principles of Zhejiang province, discussed the practice achievement by using plant measures and the biochemistry technology (Han 2008). Wang et al. put forward river ecological rehabilitation overall strategies on the basis of analyzing the living environment of benthic macroinvertebrate (Wang 2007). Wu et al. offered the basic methods to perfect eco-compensation system in Suzi River basin (Wu 2008). Xu et al. presented the calculation method

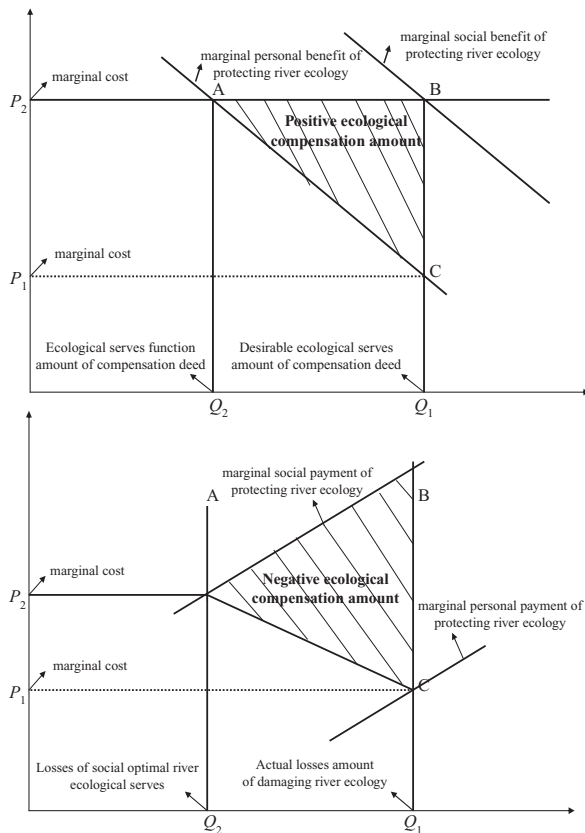


Figure 2. The compensation of external economy and diseconomy.

of eco-compensation based on the water quantity and quality of trans-boundary river combining with practice (Xu 2008). Therefore, reference to international successful experience, China caught out a system of theory, method and practice research, which is helpful for restraining water pollution and ecological degradation state of river.

3 EFFECTIVE ECO-COMPENSATION MECHANISM

China has achieved a series of successful cases of river eco-compensation, while existed many disadvantages in the respects of eco-compensation basis research, policy formulation, implementation, management, monitoring and evaluation. Such as lacking laws and regulations on eco-compensation, outdated overview of methodologies for compensation foundation, the ambiguity of river eco-compensation scope and the uncertainty between duties and rights of all stakeholders. To ameliorate the limitations, The paper discussed the framework of river effective eco-compensation mechanism from the angle of river eco-compensation implementation, theory and management basis (Fig. 3).

4 XIN'AN RIVER ECO-COMPENSATION

Xin'an River originates from Xiuning County of Anhui Province, and flows into Thousand Islands Lake (Xin'an River reservoir) of Chunan County the Zhejiang Province from west to east. Xin'an river and Lan river converges in Meicheng of Jiande city (named Fuchun River), at last, pours into Hangzhou bay. The catchments area of Xian'an River in Huangshan city, Chun'an County and Jiande County is 6002 km², 4427 km² and 13 km² respectively. The average flow from Huangshan city to Thousand Islands Lake is 6.53 billion m³ every year, accounting for 60% of the total inflow in Thousand Islands Lake. Chun'an County has done great effort to make the water quality flowing into downstream Huangshan city reach at or above class III. Therefore, to protect river surrounding environment, Chun'an County loses many opportunity costs, the economic level of Chun'an County is lower than downstream areas. According to the principle of "sharing of water resources co-conservation", Xin'an River downstream Huangshan (Zhejiang province) city requires the establishment of river eco-compensation mechanism to pay for the loss of Chun'an County (Zheng 2006).

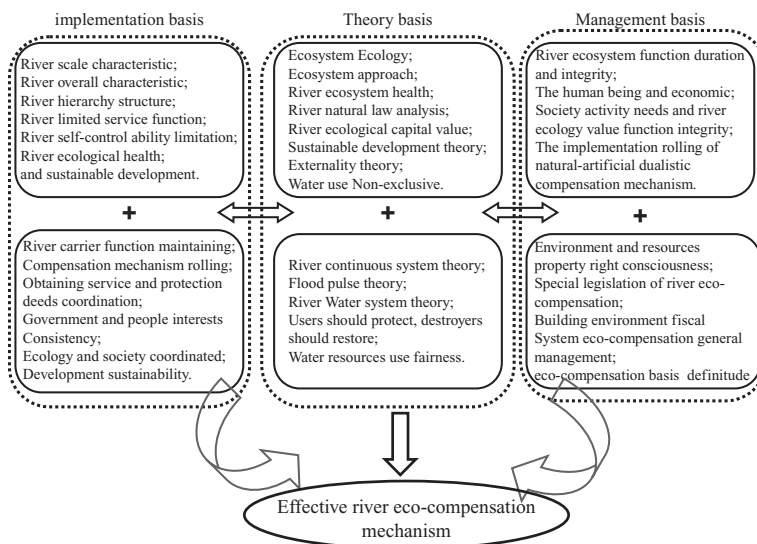


Figure 3. Effective river eco-compensation mechanism framework.

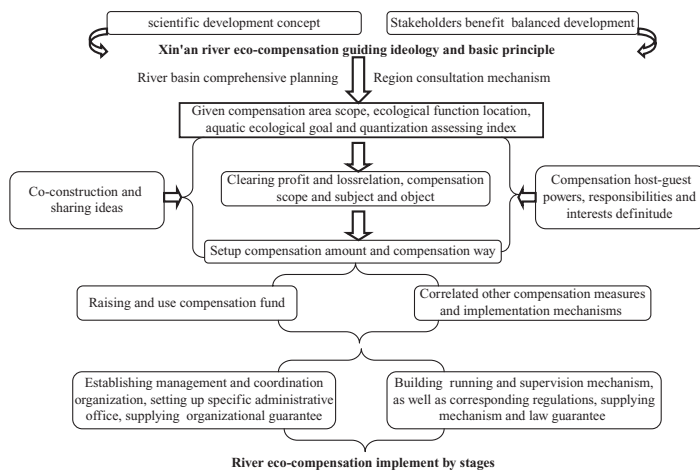


Figure 4. The overall framework of Xin'an river eco-compensation mechanism.

In 2006, the actual investment of Xin'an river basin be used for water resources and water environmental protection is 439 million Yuan. Based on the principle that the allocation of water resources benefit among beneficiaries shall be determined according to their corresponding input proportion, the conservation cost is allocated to water users or governments in whole sharing area according to the proportion of benefits sharing (Xu 2010). By calculation and regional coordination, Anhui province, Chunan County, Xin'an river reservoir dam downstream Hangzhou city and Xin'an river reservoir management department should share the investment respectively of 87 million Yuan, 154 million Yuan, 183 million Yuan and 15 million Yuan. For the effective protection by Xin'an river upstream people, the proportion of basin water resources benefit (the total of national economy and ecological benefit is 7.5 billion Yuan) and the actual protection investment is about 17:1.

Joint regulation of water quantity and quality is the basis of managing and using water resources efficiently. River eco-compensation will be made based on water quality and quantity or catchments area in the upstream according to monitoring the quality of outflow in the inter-section (Zheng 2006). At present, Chun'an County has done good work to control the polluted things flowing into Thousand Islands Lake, to make 80% of the domestic sewage in towns around the Thousand Islands Lake has been treated. As a result, water from Chun'an County is basically class I, which is better than the order of the government of Zhejiang including Hangzhou city.

The rate of water resources development in Xin'an river is low, so the competition is not obvious arising from water quantity problem, but focusing on water quality issues. On the basis of acquiring the data of Xin'an river different sections water quantity and quality, according to the orders of water functional zone water quality, the Anhui and Zhejiang province put class III as Xin'an river upstream and downstream area water quality compensation judgment standard. In 2004, Huangshan city and Chunan County of Xin'an river basin got compensation 258 million Yuan, 300 million Yuan respectively for reducing pollutant discharge of COD_{Mn} and $\text{NH}_3\text{-N}$.

According to effective river eco-compensation mechanism framework, to solve the exposed questions during former river eco-compensation implementation, Xin'an river basin eco-compensates overall framework supplies a good way (Fig. 4).

5 TRANS-BOUNDARY RIVER ECO-COMPENSATION

Based on river water body fluidity, river upstream protectors offers effort to protect eco-environment, and the whole basin can share the economic, social and environmental benefits

from nice eco-environment. According to the public products attribute and externality theory of water resources, the trans-boundary river downstream beneficial area should take in hand the ecological construction obligation with river upstream. When the water quality of river upstream and downstream interfaces reaches to both agreed water quality standard (For example, both parties can put “Environmental quality standards for surface water” (GB3838-2002) class III as the judgment standard), the upstream area shouldn’t compensate downstream area; when river downstream area taking extra quantity from upstream area, the upstream area can get compensation regards downstream water quality requirement and water intake variation as basis. From the aspects of water quantity and quality, the paper gives the river downstream should pay compensation determination method (Table 1, taking class III as the water quality judgment standard).

$$C = \frac{W_d}{W_t} \cdot V \pm D_q \cdot M_q \quad (1)$$

where C is the compensation river downstream should pay for upstream (10^4 Yuan); W_d is the extra water quantity river downstream get from upstream (10^8 m³/a); W_t is the total flows river upstream (10^8 m³); V is the total compensation total amount (10^4 Yuan); D_q is river upstream contaminant emissions below (above) standard (t); M_q is the investment to treat unit contaminant (10^4 Yuan/t).

By virtue of “Capital water resources sustainable use plan in 21 century” and Beijing water resources supply and demand state analysis, put water quantity and quality as the mainline to calculate Beijing-Tianjing and Northern Hebei region eco-compensation standard located in Guanting reservoir up-down stream, Zhou et al. proposed that Yongdinghe River downstream Beijing city should compensate the upper Zhangjiakou city 598 million Yuan annually. By doing this, Yongdinghe watershed can increase high-quality water 1.5 billion m³/a, also can decrease upstream wastewater discharge 1.02 billion m³/a (Zhou 2009).

Dongjiang River is one of three main streams in Zhujiang river basin, which originates from Xunwu county of Jiangxi province. Dongjing River water resources total volume is 4.4 billion m³, and the amount flowing into Guangzhou province is 2.92 billion m³. For sufficient water quantity, good water quality, Dongjiang River also is the water source area of Shenzhen City and Hong Kong Special Administrative Region. Dongjiangyuan area makes great effort to protect the water quality, such as source area has invested 22.693 million Yuan to control pollution during the Tenth Five-year Plan period, and invested 1.42 billion Yuan during the Eleventh Five-year plan Period. To compensate the loss of Jiangxi province, Jiangxi province and Guangdong province made protocol that: Guangzhou province would extract 1% from hydropower overall benefit as source area soil and water conservation capital input; HongKong would take out 260 million Yuan as eco-compensation tax to support source area eco-construction (CCICED 2006). On the basis of following in order and advance step by

Table 1. Trans-boundary river downstream compensation standard determination.

Type		Compensation			Explanation
Interface	Judgment standard	Water quantity	Water quality	Add up	
I, II	III	$(W_d/W_t) \cdot V$	$D_q \cdot M_q$	$(W_d/W_t) \cdot V + D_q \cdot M_q$	Positive water quantity and quality compensation
III	III	$(W_d/W_t) \cdot V$	0	$(W_d/W_t) \cdot V$	Positive water quantity compensation only
IV, V	III	$(W_d/W_t) \cdot V$	$-D_q \cdot M_q$	$(W_d/W_t) \cdot V - D_q \cdot M_q$	Positive water quantity and negative water quality compensation

step and consultation, Dongjiangyuan area eco-compensation can encourage both source area people to strengthen eco-environment protection and river downstream people to treasure and save water resources.

6 RIVER ECO-COMPENSATION STUDY PROSPECTS

The paper gives a elaboration of river eco-compensation theory and methodology, and then establishes trans-boundary river eco-compensation mechanism based on water quantity and water quality joint regulation combining with domestic successful cases and effective river eco-compensation implementation framework. However, there are still a lot of questions existing in river eco-compensation implementation processes. Firstly, the law basis of compensation mechanism is deficient, and related legislation forecast at present is weak, lagging actual river eco-construction and protection progress. Secondly, river eco-compensation range underextension, and the compensation style is singleness, which makes the helpful deeds of ecology protector can't acquire valid requital, as a result, decreasing the enthusiasm of participants. Thirdly, eco-compensation fund management is confused. Finally, lack of a long-term dynamic transformation mechanism.

In allusion to above-mentioned deficiencies, the paper gives some suggestion:

1. Strengthening resources property right consciousness, establishment effective assessment mechanism.
2. Making river eco-compensation special legislation, perfecting financing system to promote financing market development.
3. Enhancing eco-compensation comprehensive management to realize compensation mode diversification.
4. Setting up water environment financial system to prefect resource environment compensation policy.
5. Enacting desirable river eco-compensation standards, making compensation priority order scientifically.
6. Perfecting foundation supporting institution gradually, adjusting industry structure, and quickening manpower resources developing to change "blood transfusion" to "blood production" to solve eco-compensation funds insufficient.
7. Perfection compensation management system, improving public participation consciousness, promoting eco-compensation mechanism implementation sustainability.

In the future, to realize economy, society and eco-environment all-round, coordinated and sustainable development, implementing eco-compensation is an emergent and important issues in China. To change the "treatment after pollution" situation, China should protect river ecology, enhance the river ecosystem utility value, regard the restoration of the whole river channel, estuary region, river floodplain and wetland, and realize the unification of eco-compensation area target, special target and ecological target (Fu 2009). Therefore, the river management department will strengthen the followed work:

1. Defining scientific management model. Perfecting financing channels, management system and resources environment compensation policy, establishing valid assessment mechanism and public participation mechanism.
2. Selecting ecological restoration integrated template. On the basis of giving appropriate ecological water demand, by studying stream segment restoration integrated template, establishing exact eco-economy correlation model to realize the coupling between economic system input-output and the positive-negative externalities of river ecosystem protection.
3. The determination of compensation recovery target. By analyzing present situation assessment of degenerated river and the risk analysis of ecology restoration degree, to determine suitable recovery target and direction.

4. The determination of compensation post-evaluation system. Referencing multi-object fuzzy comprehensive evaluation method, genetic algorithm, Analytical Hierarchy Process (AHP) and neural network method, to analyze the comprehensive relationships between evaluation indexes and evaluation results. Besides that, we also should bring ecological risks into river effective compensation mechanism, to establish practical post-evaluation object system.

ACKNOWLEDGEMENTS

The paper is funded by National Natural Science Foundation of China (Grant No 50979114) and “Key Project of the National Eleventh-Five Year Research Program of China” (Grant No 2007BAB28B02).

REFERENCES

- ACCA21 (The Administrative Center for China's Agenda 21), 2007. Eco-compensation: International experiences and China's practices. Beijing: Social Sciences Academic Press.
- CCICED (Task Force on Eco-Compensation Mechanisms and Policies). Eco-Compensation Mechanisms and Policies in China. Beijing: Science Press.
- Da-jie ZHOU, Yan-hong SANG, Hui-ming LI, et al. Research on standard for watershed ecological compensation. *Journal of Agricultural University of Hebei*, 2009, 1(1):10–14.
- Da-wei XU, Hai-xia ZHENG, Min-quan LIU. Measuring Method of River Basin Ecological Compensation Based on River Water Quality and Its Water Quantity About Across Administration Area. *China Population Resources and Environment*, 2008, 18(4):189–194.
- Feng-ran XU, Ben-qing RUAN, Dang-xian WANG, et al. Model for calculating benefit and cost sharing of water resources co-conservation in a river basin. *Journal of Hydraulic Engineering*, 2010, 41(6):665–670.
- Gretchen C. Daily, Pamela A. Matson. Ecosystem services: From theory to implementation. *Proceedings of the National Academy of Sciences*, 2008, 15(28):9455–9456.
- Hai-jun YANG, UCHIDA Taizo, Lian-xi SHENG, et al. Advances in studies on the restoration of the damaged riparian ecosystem. *Journal of Northeast Normal University (Natural Science Edition)*, 2004, 36(1):95–100.
- Hai-xia ZHENG, Lu-biao ZHANG. Chinese Practices of Ecological Compensation and Payments for Ecological and Environmental Services and its Policies in River Basins, 2006.
- Li-qiang WU, Jun-shi HE. The study of eco-compensation in Suzi River basin. *China Rural Water and Hydropower*, 2008(9):45–47.
- Min-fen CHEN, Jiang-cai MAO, Yong WANG. Ecological Restoration of Rivers. *Journal of Zhejiang Water Conservancy and Hydropower College*, 2006, 18(2):38–40.
- Tian-zhu ZHENG, Jian-ren ZHOU, chao WANG. Study on mechanism of ecosystem rehabilitation of polluted riverbed. *Environment and Sustainable Development*, 2002, 23(12):115–117.
- Ya-zhen Gong. Experiences of eco-compensation in the world and their uses for reference to China. *Management of Forestry Sciences*, 2002(3):19–22.
- Yi-cheng FU, Chuan-jiang WEI, Rui-nian WANG, et al. Research on River Ecological Compensation. *Water Resources and Power*, 2009, 27(3):31–35.
- Yong LIU, Huai-cheng GUO. The study of lake and basin ecosystem management. Beijing, science press, 2008.
- Yu-ling HAN, Li-ping SHAO, SHeng-jun ZHANG, et al. The practice of river ecological rehabilitation in Zhejiang province. *China Rural Water and Hydropower*, 2008(8):25–28.
- ZHao-yin WANG, Dong-sheng CHENG, Xue-hua DUAN, et al. Assessment of ecological system in East River and corresponding ecological restoration strategies. *Journal of Hydraulic Engineering*, 2007, 38(10):1228–1235.
- ZHe-ren DONG. Eco-compensations for Dammed Rivers. *Engineering Science*, 2006, 8(1):5–10.

Impacts of dam on Key Biodiversity Area in southwest China based on integrated map

L. Chong & P. Jing

China Institute of Water Resources and Hydropower Research, Beijing, China

W. Hao

The School of Life Sciences, Peking University, Beijing, China

ABSTRACT: Based on fruitful database and joint research from hydrologist and ecologist, impact of hydropower development in southwest China on Key Biodiversity Area (KBA) was studied. Public DEM (USGS 90 m DEM) was adopted to extract river network in southwest China, which compare well with rivers in national digital map. Due to lack of latitude and longitude coordinates for part of dams, three methods, such as manual seek via Google Earth map, steepest gradient in river slope, comprehensive approach, were used to locate the dam location in extracted river network. Digital rivers with near 300 located dams were integrated into KBA digital map. From the integrated map, it shows there isn't clear overlap between dams and KBA, except part of small dams, which brings about impact on protection of KBA. So, it is light impact to dams on KBA, for it extracted mainly from terrestrial animal.

1 INTRODUCTION

China is main nation with huge hydropower. Up to the end of 2007, there were 86,353 reservoirs, including 26581 reservoirs with height more than 15 m, 70 reservoirs with height more than 60 m (IWHR, 2009a, b). As a developing country, the need on water resources and energy is increasing. The developed percentage of waterpower utilization is only 21 percents at present stage, lower than 70% in the developed country (Li Jugen et al. 2006). So for a long time in the future, the development for hydropower is still a basic strategy for China national energy development.

However, the problem of the ecological and environment effects caused by hydropower development is becoming main restrictive factor for hydropower development (Wang shucheng, 2004). In the southwest of China, hydropower resource is abundance and plays an important role in energy optimal allocation strategy, such as West-to-East electricity transmission projects. It is one of the world's most biologically diverse regions in China's southwest mountainous region, also one of 34 biodiversity hot spots delimited by Conservation International (CI), and a part of Yangtze River upstream ecological zones which is one of 200 global important ecological zones recognized by World Wildlife Fund (WWF) (Myers et al. 2000; Olson et al. 1998, 2002). According to partial statistics, there are 12,000 kinds of higher plants and 1141 kinds of vertebrate animals in the area, which is an international recognized region with peculiar species intensive distributing and has an irreplaceable value in biodiversity, among them, 3500 kinds of higher plants and 178 kinds of vertebrate animals are regional peculiar species (Myers et al. 2000; Stattersfield et al. 2000; Lei et al. 2003, 2006; Orme et al. 2005). It ranges west from southeast of Tibet, the western Sichuan Province and extends to the south to northwest of Yunnan Province, the north to Qinghai Province and southern Gansu Province, which accounts for 10% of national land areas with distribution of 30% higher plant species totally and 50% birds and mammal, including some

endemic and rare species such as *giant panda*, *Ailurus fulgens*, *Tamarin*, *snow leopard*, *takin* and *Crossoptilon crossoptilon*. As a stress factor for regional biodiversity, the hydropower construction and development aroused broad attention.

Biodiversity protection has been a national commitment to the international community after 153 countries had signed in “Convention on Biological Diversity” in 1992. As a large scale ecotope indicator, biodiversity has been used to reflect species composition and degree of variation of ecosystem and do some numerical analysis for ecosystem ranking and tendency. The international study of the water ecological and environment effect of hydropower have two aspects. One is focus on the theory and technology of aquatic response and water quality alteration in micro-scale, the other in watershed macro-scale developed from reach, corridor. But as the impact is persistent and comprehensive, the scientific understanding of the real ecological and environment effect of hydropower is not in-depth, especially the large-scale study is not sufficient, the quantitative relationship between hydropower and regional biodiversity are lack. Due to unavailability of basic data, regional biological achievement can't compromises the hydro-science well and be integrated in the same space information platform to support further study and to form the cross-disciplinary basic.

So, based on the coordinated needs for hydropower and regional ecological and environment protection, this study with a scientific integration of biological data into hydrological data forms a relevant map between dams and Key Biodiversity Area (KBA). From the digital map, it can provide intuitionistic relationship on regional hydropower and biodiversity.

2 MATERIAL AND METHODS

2.1 Data

2.1.1 Dam data

This study gathers more than 4000 built or to be built dams with height more than 30 m in mainland of China, including more than 200 located in southwestern. The data is available from the China branch of International Commission on Large Dams and the Hydro-science Data Share Centre. Additionally, part of the reservoir data with height less than 30 m is available from China branch of CI.

2.1.2 Key Biodiversity Area digital map in southwest region

Dividing key biodiversity area is a global-scale protection action promoted by CI. It provided foundation of decision for global and regional protective strategy (Langhammer et al. 2005). There are 3 characters in the divided KBA: 1) It's of great importance for these areas in global biodiversity protection. The protective value of endangered species or regional endemic species with special protective significance in these areas is much higher than that in the surrounding areas. 2) These regions are actual protected areas or potential protected areas and themselves are protected and managed unites. 3) These areas themselves could support survival resources for protective species.

According to the international standard of dividing KBA (Langhammer et al. 2005), Peking University makes KBA map merged into the expert knowledge based on the map of the distribution of 314 kinds of endangered vertebrate, 213 higher plants and southwest montanic nature preservation zones (Fig. 1). 199 key biodiversity areas including 141 biodiversity areas and 58 candidate key biodiversity areas are defined in southwest of China. Of the whole areas, 176 are defined by global endangered Animals, 138 by global endangered, distribution limited or mass migration, 8 by global endangered reptiles, 171 by global endangered amphibians and 54 by global endangered plants. These areas show the protective value of key biodiversity in view of present knowledge and are the subset of real existent key biodiversity areas.

2.1.3 DEM data and digital river network

Digital river network and divided sub-region was extracted from USGS 90 m DEM by using developed software (Li chong et al. 2004) in the southwest China. The result compares well with 1:250000 digital river network.

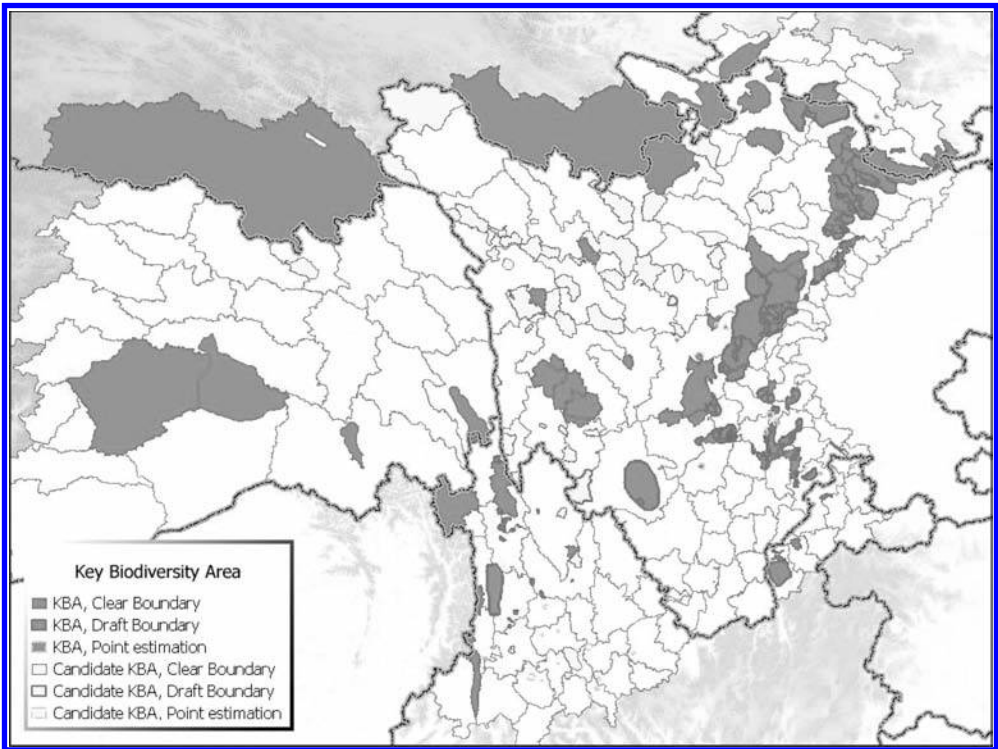


Figure 1. Key Biodiversity Area (KBA) in southwest China.

2.2 Method

In this study, the information of the dam and backwater areas are integrated into KBA, then the map of relevancy of location of dam and biodiversity are generated.

Due to the insufficiency of dam information, especially accurate site coordinate data, how to check the obtained dam coordinate data to locate it on the digital river network or complement the data using the space technology, such as DEM or remote sensing data, is a basic and critical point in map integration. There are 3 requirements on dam relocation, 1) dam should be located on the river; 2) it could reflect the longitudinal gradient of rivers; 3) there should be a backwater areas with light gradient in the upstream of dam. Three methods, such as manual seek via Google Earth map, steepest gradient in river slope, comprehensive approach, are used to locate the dam location in extracted river network. In the first method, Google Earth are used as a background application, the dam location are searched in the Google map, the latitude and longitude are noted and then the DEM map is compared with, and then give a precise location. In the second method, it is supposed that dam locates in the steepest gradient site along river reach, which is available from extracted digital river network (Li chong et al. 2007). In comprehensive approach, dam is relocated by steepest gradient in river slope first, then check it via Google Earth map.

3 RESULTS

3.1 Dam in southwest China and its relocation

293 hydropower stations from upstream of the Yangtze River, Lantsang River and Nu River are relocated through the above 3 methods. River gradient and possible backwater length in the upper reach above every dam are extracted from DEM, then backwater length and

possible backwater surface areas are calculated in GIS map with consider dam attributes. The distribution of hydropower stations of all rivers shows in [Table 1](#).

3.2 Integrated map between dam and KBA in southwest China

The above relocated dams are integrated into the KBA digital map ([Fig. 2](#)). 105 hydropower stations locate within KBA. From [Figure 2](#), there are few characters: 1) there isn't clear overlap between dams and KBA; 2) the intersections between dam backwater surface areas and KBA is small, due to KBA locates mainly in lands, especially in riverhead zone without close relation to river wate; 3) Few dams are located in KBA, for example, more than 10 dams, among which are middle or small hydropower stations with height less than 30 m, are located in the KBA in Min River. It illustrates that the conflict between Dams and KBA is really exits although few dams in KBA.

A firm positive conclusion whether the impact of dams on regional biodiversity is profound is still difficult to draw, in spite of the weak relevancy between dam and KBA in the

Table 1. Dam distribution in the upper reach of Yangtze river, Lantsang river and Nu river.

River	Jinsha river	Yalong river	Min river	Jia-ling river	Wu river	The upper reach of the Yangtze river	Lantsang river and Nu river
Number of dams	46	22	66	73	25	50	11

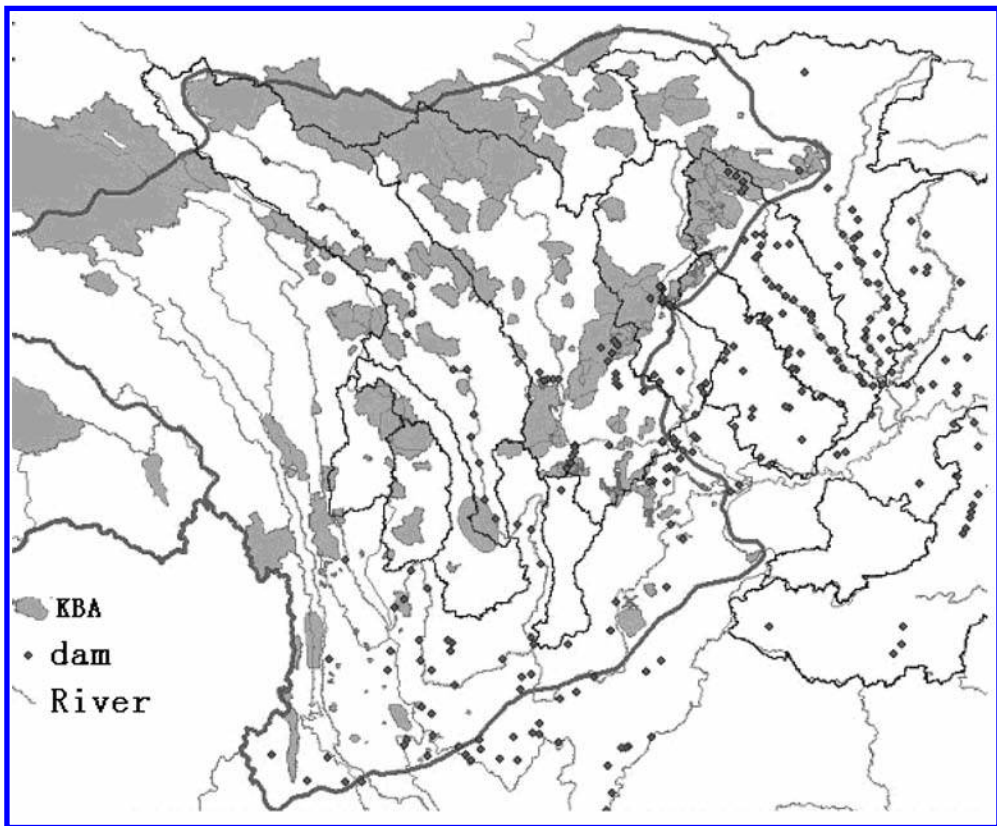


Figure 2. Integrated map of dam and KBA in southwest China.

aspect of their distributions. It is because: 1) the construction of dam reflects the human activities of river development, the impact of its backwater areas and length on KBA where terrestrial organism mainly lived in is limited but is profound for river ecosystem. The present KBA is identified mainly based on terrestrial organism due to lacking aquatic lives data. An objective assessment of the impact of dam on biodiversity will be given after adding aquatic into KBA. 2) The regions with rich biodiversities always are where human activities are difficult to stretch into, such as riverhead in alpine region. It is not an appropriate space for a large-scale hydropower development in the perspectives of economics and environments. The intersection between dam and KBA is small as the large-scale hydropower stations in southwest China is mainly focus on the easily developed areas. The study on relation of KBA and middle and small hydropower stations is needed to give a more comprehensive assessment of impact of dam on biodiversity. 3) Additionally, as the development continues, large new dam construction will appear in the KBA and its impacts should be given precisely.

4 CONCLUSION

Southwest China is the base for national hydropower development and one of the global biodiversity protective hotspot. Integrating dam into KBA digital map based on the same space information platform is a basic and interdisciplinary job. Based on knowledge of biology and hydrology, public DEM (USGS 90 m DEM) and dam database are used to extract river network and relocate the dam location. A GIS map integrated the Dam map into KBA map is made. It shows there isn't clear overlap between large dams and KBA, except part of mid or small dams, which brings about impact on protection of KBA. So, it is light impact to large dams on KBA, for it extracted mainly from land-based lives. When aquatic lives are adopted in KBA, the impact for dams on KBA is significance. This research will provide technological and reference supports of macro-decision-making for river development and regional ecotope protection.

ACKNOWLEDGEMENTS

This research was sponsored and supported by the Chinese National 11th Five-Year Plan major scientific and technological issues (2008BAB29B09), and the Critical Ecosystem Partnership Fund (CEPF). Thanks to all of them.

REFERENCES

- China Institute of Water Resources and Hydropower Research (IWHR). 2009a. Survey on dam option. IWHR report (in Chinese).
- China Institute of Water Resources and Hydropower Research (IWHR). 2009b. Study on the development of Large dams in the world. IWHR report (in Chinese).
- Langhammer PF, Bakar MI, Bennun LA, et al. 2005. Identification and gap analysis of key biodiversity areas: targets for comprehensive protected area systems. The World Conservation Union.
- Lei FM, Qu YH, Tang QQ, An SC. 2003. Priorities for the conservation of avian biodiversity in China based on the distribution patterns of endemic bird genera. *Biodiversity and Conservation*. 12: 2487–2501.
- Lei FM, Zhao HF, Yin ZH. 2006. Distribution pattern of endangered bird species in China, *Integrative Zoology*. 1: 162–169.
- Li Chong, Yang Dawen. 2004. Deriving drainage networks and catchment boundaries from grid DEM. *J. China Institute of Water Resources and Hydropower Research*. 2(3): 208–214 (in Chinese).
- Li Chong, Wan Hao and Peng Jing. 2007. Approach on making dam location clear based on grid DEM. *Chinese Environment Resources and Hydroelectric Engineering* 306–309 (in Chinese).
- Li Jugen, Shi Lishan. 2006. Brief Description of Hydropower Resources in China, *Water Power*. 32(1): 3–7 (in Chinese).

- Myers N, Mittermeier RA, et al. 2000. Biodiversity hotspots for conservation priorities. *Nature*. 403(6772): 853–858.
- Olson DM, Dinerstein E. 1998. The global 200: A representation approach to conserving the Earth's most biologically valuable ecoregions. *Conservation Biology*. 12(3): 502–515.
- Olson DM, Dinerstein E. 2002. The Global 200: Priority ecoregions for global conservation. *Annals of the Missouri Botanical Garden*. 89(2): 199–224.
- Orme CDL, Davies RG, et al. 2005. Global hotspots of species richness are not congruent with endemism or threat. *Nature*. 436(7053): 1016–1019.
- Stattersfield, Alison J, Capper, David R. 2000. *Threatened birds of the world: the official source for birds on the IUCN red List*, BirdLife International. Cambridge.
- Wang Shucheng. 2004. On dams and ecology. *Water Power*. 30(4): 1–4. (in Chinese).

A model for the dry closure of tailings dams

J.L. Justo, P. Durand, M. Vázquez & A. Morales

Department of Continuum Mechanics, University of Seville, Spain

F.A. Jiménez

Egmasa, Spain

ABSTRACT: An original model for the dry closure of Almagrera tailings dam is being developed. This model includes the cleaning of the neighbouring Las Viñas mine. The toxic coarse Las Viñas material, deposited in waste embankments, is being thrown on the tailings inside the reservoir. A preliminary model has been presented by Justo et al. (2010). With this tool, the first closure phase has been successfully completed and is described here. A detailed study of cap and landscaping of the cleaned Las Viñas area will be undertaken, seismic calculations will be improved and the behaviour of large mobilized masses of fluidized soils, as it has happened in catastrophic tailings dams' failures, will be introduced in the model.

1 INTRODUCTION

In Europe, there are many abandoned mines. Nowadays, when permission is granted for opening a mine in any country of the EU, a closure plan (including financing) must be presented by the mining company (ITC, 2000), but it was not so in the old times. Whichever has visited an abandoned mine will be aware of the environmental devastation surrounding the site and the contrast with zones where no waste dumps have been thrown (Fig. 1). In some cases, vegetation has nearly disappeared.

In this context, the authority is faced with the task of closing many abandoned mines and the corresponding tailings dams or ponds. The point is that, up to now, only a small amount of the possible closures has been undertaken owing to economic reasons.

The recent (5 October) Ajkai Timfoldgyar dam failure poured 700,000 m³ of bauxite ore and formed a flow that struck three villages in Hungary.

This accident, jointly with the catastrophic failures of Stava, Los Frailes and Baia Mare tailings dams, has emphasized the catastrophic consequences that tailings dams' accidents in EU and the rest of the world might cause, and the need for safer design methods.

Rico et al. (2008) have compiled a corpus of 147 cases of worldwide tailings dam disasters, from which 26 are located in Europe. Many of these failure events have resulted in massive damage, severe economic impact and, in several cases, loss of life (Davies, 2002).

There is no technical guideline that would provide a focus on the tailings dam closure phase (Szymanski and Davies, 2004), although many publications indicate the sustainable closure principles. An object of this paper is to highlight the points that should underpin this guide and present a model with improved construction and calculation methods. Another object is to describe a closure that will contribute to recover neighboring degraded mining zones.

2 TAILINGS DAMS INVENTORIES AND FAILURES

Table 1 shows a summary of the inventory of tailings dams and ponds in extractive industry in Spain (Rodríguez and Gómez de las Heras, 2006).



Figure 1. Las Viñas abandoned mine (13 September 2010). 400,000 m³ of waste embankments have been thrown into Almagrera reservoir.

Table 1. Inventory of tailings dams and ponds in extractive industry in Spain.

Volume of residues (m ³)		322.878.8000
Number of structures		986
Structures	Dams	610
	Ponds	378
Present state	Active	385
	Abandoned	535
	Restored	54
	Closed	24

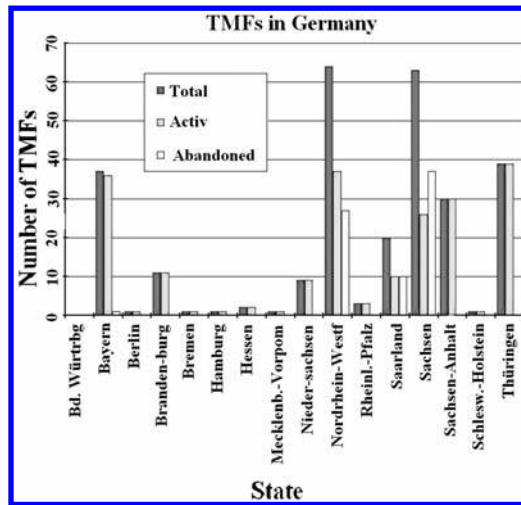


Figure 2. Number and state of tailings management facilities in Germany (courtesy of Karl Kast).

Figure 2 shows the number of tailings management facilities in Germany. It may be seen that 75 are abandoned.

Davies and Martin (2000) estimate there are 3500 appreciable tailings dams worldwide. According to Davies (2002) during the last years, there have been 2 to 5 “major” tailings dam failure incidents. Referred to the worldwide inventory of 355 tailings dams, equates to an

annual probability between 1/1750 and 1/700, compared with 1/10000 for conventional dams. Furthermore, these failure statistics are for physical failures alone. Tailings impoundments can have environmental “failure” (e.g. leaks) while maintaining sufficient structural integrity.

The recent dam failures have produced enormous environmental, human and economic losses, and have struck the awareness of citizens with respect to the sword of Damocles hanging over their heads.

3 ALMAGRERA DAM

Egmasa is the public enterprise, which has been entrusted by the Junta de Andalucía (regional Andalusia government in Spain) with the dry closure project of the abandoned Almagrera tailings dam, 37.5 m high, partly financed with FEDER funds. Figure 3 shows an aerial view of the dam before the closure operations started. The closure is being carried out in three phases.

Figure 4 shows the central cross-section at the end of the first closure phase. It has an upstream sloping core, and the foundation is formed by alternation of volcanic and inter-stratified sedimentary rocks, including lava, clayey phillite and shale. The dam corresponds to the downstream borrow material type, and it was raised 5 times adding material on the downstream side. The downstream slope was 1.7 (H):1 (V) up to the third phase, but it was changed to 2 (H):1 (V) for the last two phases. According to a report by Knight Piésold Ltd, delivered before the 5th phase construction, the sandy filter placed below the core was much too coarse. The filter criterion to avoid fines migration was not fulfilled between the sandy filter and the selected rockfill placed below either. This way, after the 4th phase, the dam rather behaved as a homogeneous dam. During the 5th phase, an inclined sand and gravel filter was placed between the 4th and 5th phase shells using normalized filter criteria.

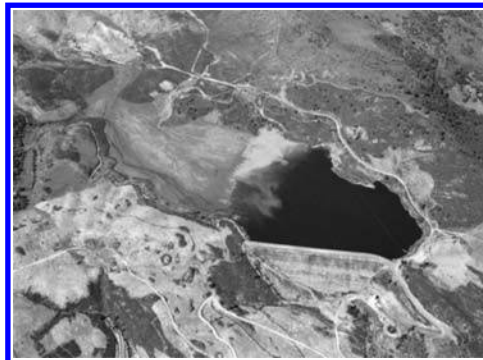


Figure 3. Aerial view of Almagrera dam, showing the reservoir and tailings to the left.

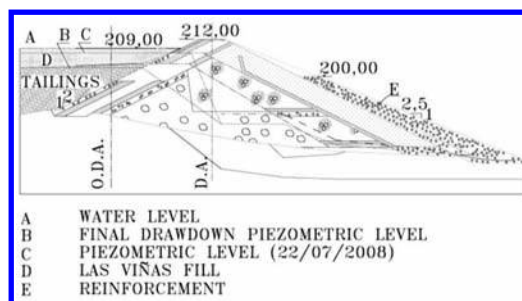


Figure 4. Final state of dam with downstream rockfill reinforcement.

The reinforcement to fulfil the safety factors required by the Spanish guide (ITC, 2000) for closure is shown in the Figure.

4 THE MODEL

In 2007, the first author was charged with the elaboration of a model to simulate the dry cap closure of this dam.

The model should include as well some measures to improve the environmental conditions in the neighboring site of Las Viñas abandoned mine, introducing coarse toxic waste material inside the reservoir. The cleaned zones will be later landscaped.

The results of a preliminary model were delivered in January 2009. The model has two distinct phases: The closure of Almagrera dam and the cleaning and landscaping of Las Viñas site.

4.1 *The model for closure*

An important consideration is that Almagrera dam had been abandoned, and the problem for the closure of abandoned tailings dams is quite different to a closure foreseen at the beginning of mine exploitation.

Up to now only one third of the project (about 7,000,000€) has been executed using this preliminary model. The intention is to improve the construction methods for the remaining two phases.

The first problem with many tailings dams, compared with hydraulic dams, is that, in general, few tests have been carried out during its design and construction. Some problems arise during the site investigation.

In the case of Almagrera dam, the following phases have been followed for closure. Most of them will be simulated in the model.

1. Site investigation, as the reconnaissance made before construction was scarce. Many problems had to be solved to bore upstream and downstream boreholes.
2. Construction of lateral drainage channels to hinder the entrance of runoff and stream water into the reservoir.
3. Pumping of the reservoir toxic water to be deperated and sent downstream.
4. Reinforcement of dam, if the results of the model indicate it is necessary.
5. Placement of coarse waste material retired from Las Viñas mine on the tailings, inside the reservoir.
6. Construction of special deep wells or band-shaped drains to accelerate the tailings settlements.
7. Construction of cap, when the remainder tailings settlement will be allowable.
8. Detailed study of cap.
9. Landscaping of Las Viñas site, once the coarse toxic waste materials will be retired.

Figure 5 shows the rockfill reinforcement at the end of the first phase closure. The acceleration of tailings consolidation under the weight of Las Viñas material is necessary to prevent damage to the cap that must be placed after an acceptable time.

There are two possible procedures: band-shaped drains or drainage wells. Band-shaped drains should be driven before placing coarse Las Viñas material, because later is more difficult. To make that possible, a method of mixing the tailings with cement to form a resistant crust may be proved (v. Burgos and Samper, 2006).

In the first phase of Almagrera closure, deep drainage wells have been used. The performance has not been good.

The result of pumping and drainage is that Acid Rock Drainage (ARD) that often emerges downstream will disappear. This way, measures difficult to carry out, such as grouting, will be avoided. This procedure will improve the dam safety, as the piezometric level will decrease inside the dam.



Figure 5. Almagrera closure reinforcement (13 September 2010).

Table 2. Safety factors (F) in LE and FE calculations. Maximum displacement (δ_{max}) in FE calculations.

Phase	F in limit equilibrium method		Finite elements	
	Upstream	Downstream	δ_{max} (mm)	Safety factor
Initial	2.00	1.70		1.44
Drawdown	2.17	1.70	193	1.47
Fill	0.74 (tailings)	1.35	1300	1.36
Long term	2.70	1.71	206	1.79
Earthquake and liquefaction	1.76 (tailings)	1.35	278	1.19 (tailings)

As the access of water inside the reservoir is hindered, the pumping needed during post-closure will be small. For the success of this technique, it is completely necessary that drainage will work properly.

According to the European legislation, the dam must fulfill certain conditions, among them safety factors, at closure. The finite element model reproduces all the steps that are being taken during closure:

1. Finding the initial safety factor.
2. Upstream water drawdown.
3. Upstream filling with coarse tailings.
4. Settlement of tailings.
5. Long term stability including earthquake loading.

5 RESULTS

The NCSR-2002 considers that large dams (height greater than 15 m) are *constructions of special importance*, which should be calculated for a return period of 1,000 years. The seismic acceleration for pseudo-static calculation was 0.08 g. The reinforcement has been calculated using this acceleration. The ITC (2000) requires a safety factor of 1.3.

Both Limit Equilibrium (LE) and Finite Element (FE) calculations were carried out (v. Justo et al., 2010). For FE calculations, Plaxis 2D program and Mohr-Coulomb material model were used, and the safety factors (F) indicated in Table 2 were obtained using the *FI-C reduction* method. The factors of safety prescribed don't need to be fulfilled when failure is produced inside the tailings as it happens under earthquake loading. Very large settlements were produced when the toxic Las Viñas material was placed on the tailings. Band-shaped drains are needed if the remaining settlement after one year is to be acceptable (40 cm).

This way the cap may be placed in an acceptable time (one year after placing the waste material in the reservoir).

6 NEW SEISMIC CALCULATIONS

With the new model, a dynamic calculation will be carried out. A method to select accelerograms for the closure calculation has been developed based on *uniform seismic hazard response spectra* (Morales-Esteban, 2010).

First of all, the seismic hazard at the location is calculated according to the Gutenberg-Richter (1954) law. The seismogenic areas defined by Martin (1984) were used. The Gutenberg-Richter law can be expressed as:

$$\log_{10} N(M) = a - bM \quad (1)$$

where a and b are constants, M the magnitude and N the number of earthquakes with $M \geq 3$.

A high b -value implies that small earthquakes are predominant. However, a low value indicates that there is a lower difference between the relative number of large and small earthquakes. Udías and Mezcua (1997) estimate a value of b between 0.6 and 1.5 for global seismicity.

The b -value has been estimated according to the maximum likelihood method for the seismogenic area where the dam is located. The following results were obtained:

- Annual rate per square km of earthquakes of magnitude larger than 3.0: 1.63×10^{-3}
- b -value = 2.33

Next, the uniform seismic hazard response spectra are calculated.

The arrival of earthquakes to the site that exceed a reference value $\log S_0$ is modelled as a Poisson stationary process, defined according to the Gutenberg-Richter law.

For source i , the average number of events per year is:

$$\lambda_i = v_i \int_M^{M_{\max}} P(\log S \geq \log S_0 / M, D) f(M) dm \quad (2)$$

where:

v_i is the seismic rate of earthquakes of the individual source

P is the probability for $\log S$ to exceed the reference value, $\log S_0$, for an earthquake of magnitude M that occurs at a distance D from the site

$f(M)$ is the magnitude probability density function between the minimum and maximum magnitudes considered.

If N individual seismic sources act simultaneously, the rate λ of arrivals at the site of earthquakes that exceed the reference value, $\log S_0$, is:

$$\lambda = \sum_{i=1}^N \lambda_i \quad (3)$$

The return period, T , is the average time interval between events and its value is:

$$T = 1/\lambda \quad (4)$$

The probability of exceeding the reference value $\log S_0$ during the period of time, t , owing to the simultaneous action of N individual seismic sources is:

$$P(\log S \geq \log S_0; t) = 1 - e^{-\lambda t} \quad (5)$$

With this procedure, uniform seismic hazard response spectra can be created for the site according to the period of exposure, the probability of exceeding the design spectrum and the type of soil. Then, real design accelerograms can be selected following these steps:

- The period of exposure of structure is established according to its estimated lifetime.

- The probability of exceeding this level is established according to the seismic hazard required. In this case, as the return period is established (1000 years), the probability is calculated using equations (4) and (5).
- For the type of soil at the site, the uniform seismic hazard response spectra are calculated according to the required seismic hazard level.
- From the database of accelerograms, those recorded at the same type of soil are selected.
- They are multiplied by a scale factor so as to reduce the standard deviation, between their spectra and the one of the uniform seismic hazard response spectrum, to a minimum.

The standard deviation is defined as:

$$S = \left(\frac{\sum [\log(f \cdot S_R - \log S_C)]^2}{n} \right)^{1/2} \quad (6)$$

and:

$$f = \left(\frac{\sum \log S_C - \sum \log S_R}{n} \right) \quad (7)$$

where S_R are the values of the response spectrum corresponding to the real register (multiplied by a scale factor), S_C are the values of the calculated response spectrum and n is the number of intervals considered in the calculation.

This methodology has been applied to the site of Almagrera Dam, founded on rock, for a damping ratio of 5%, considering a return period close to 1000 years (Figure 6). The accelerograms have been selected from the European Strong Motion Database that can be obtained from Internet at <http://www.isesd.cv.ic.ac.uk/>.

From the database, the accelerograms that have a scale factor near to 1, and a smaller standard deviation between spectra are finally selected. One of these accelerograms is included in Figure 7.

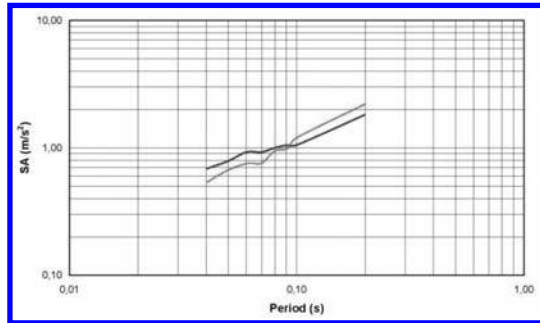


Figure 6. Comparison between the response spectrum calculated for Almagrera dam, in rock, for 1000 years return period, and the response spectrum from the selected accelerogram. SA = acceleration spectrum. —uniform seismic hazard response spectrum. —spectrum for accelerogram 7488.

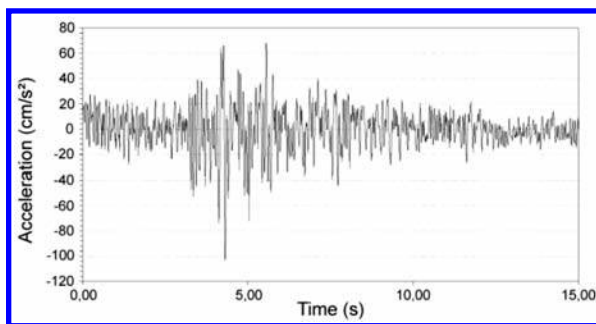


Figure 7. Accelerogram No. 128. Scale factor for all periods 0.99.

The last step will be to carry out a dynamic calculation of the dam, with different accelerograms and check the final displacements and stress states.

7 CONCLUSIONS

A model has been presented to reproduce all the operations needed for the dry closure of tailings dams. The model includes the cleaning of a neighbouring mine (Las Viñas). A rockfill reinforcement had to be placed so as to accomplish with the required safety factors. Closure will be executed in three phases. The first phase, including dam reinforcement, pumping and loading the tailings with 400,000 m³ of waste material has been successfully ended.

The model will be substantially improved in the future, in several aspects as dynamic calculation and static liquefaction. The model is being validated with monitoring, but at present the measurements are in an early stage.

ACKNOWLEDGEMENTS

This work has been financed by the Spanish Ministerio de Ciencia e Innovación (Project BIA 201020377).

REFERENCES

- Burgos, M. & Samper, F. 2006. Geotechnical characteristics of a very soft dredged silty clay and soil-cement mix in Valencia (Spain). Fourth International Conference on Soft Soil Engineering, Vancouver, British Columbia, Canada, Taylor & Francis Group plc, 427–435.
- Davies, M.P. 2002. Tailings impoundments failures: Are geotechnical engineers listening? *Geotechnical News*, September: 31–36.
- Davies, M.P. & Martin, T.E. 2000. Mine tailings dams: when things go wrong. *Tailings dams 2000*, Proceedings ASDSO Conference, Las Vegas.
- Gutenberg, B. & Richter C.F. 1954. *Seismicity of the Earth*, 2nd ed., Princeton University, Princeton, New Jersey.
- ICOLD (2010). Sustainable design and post-closure performance of tailings dams. Draft 20100615, ICOLD Committee on Tailings Dams, ICOLD.
- ITC 2000. Instrucción Técnica Complementaria 08.02.01 del capítulo XII del Reglamento General de Normas Básicas de Seguridad Minera Depósitos de lodos en procesos de tratamiento de industrias extractivas. BOE de 9 de mayo de 2000, 17235–17244. Ministerio de Industria y Energía.
- Justo, J.L., Jiménez, F.A., Durand, P. & Vázquez, M. 2010. The dry closure of Almagrera tailings dams. *International Symp. Dams and Sustainable Water Resources Development*, Hanoi.
- Martín, A.J. 1984. Riesgo sísmico en la Península Ibérica. Tesis doctoral. Ph. D. Thesis, Politechnical University of Madrid.
- Morales-Esteban 2010. Peligrosidad Sísmica. Leyes de Atenuación y Análisis de las Series Temporales de los Terremotos. Aplicación al Tajo de San Pedro de La Alhambra de Granada. Ph. D. Thesis, University of Seville.
- NCSR 2002. Norma de Construcción Sismorresistente NCSR-02. Parte General y Edificación. BOE, 244:35898–35967.
- Rico, M., Benito, G., Salgueiro, A.R., Díez-Herreros, A. & Pereira, H.G. 2007. Reported tailings failures. A review of the European incidents in the worldwide context. *J. of Hazardous Materials*, 152:846–852.
- Rodríguez, R. & Gómez de las Heras, J. 2006. Los problemas de la industria extractiva en España. Distribución geográfica y problemática ambiental asociada. *Los Residuos Minero-metalúrgicos en el Medio Ambiente*. Instituto Geológico y Minero de España, 3–25.
- Szymanski, M.B. & Davies, M.P. 2004. Tailings dams. Design criteria and safety evaluations at closure. *Proc. BC Reclamation Symposium*, 1–12.

A holistic approach to reduce negative impacts of hydropeaking

W. Gostner & C. Lucarelli

Patscheider & Partner Engineers Ltd., Mals, South Tyrol, Italy

D. Theiner

AF-Colenco Ltd., Baden, Switzerland

A. Kager & G. Premstaller

Sel Plc, Bozen, South Tyrol, Italy

A.J. Schleiss

EPFL ENAC IIC LCH, Lausanne, Switzerland

ABSTRACT: Hydropeaking is a common phenomenon of water courses that are affected by peak energy production of hydro power plants. It may cause severe impacts on the biodiversity of a stream. In fact, due to hydropeaking fishes, macroinvertebrates and aquatic plants undergo a major stress and frequently they are not able to survive these frequent water level fluctuations. In this paper a case study is presented where several mitigation measures for an affected river are evaluated. Abiotic indicators representing the hydropeaking phenomenon and responsible for an impaired biodiversity are calculated and compared. Furthermore a cost-benefit analysis of the mitigation measures is carried out allowing to define the measures to be realized. Facing the challenge of a holistic approach the study is embedded in a project with public participation of all concerned stakeholders addressing also the need of flood protection and ecologically sound river restoration.

1 INTRODUCTION

1.1 *Motivation of the study*

Hydropeaking is a common problem of water courses that are affected by production of peak energy in hydro power plants. The hydropeaking phenomenon is characterized by rapid changes in discharge (Locher, 2005, Schneider & Noack, 2009). In order to meet peak electricity demand, hydropower stations alter their discharge several times a day, resulting in the alteration of hydrological characteristics of downstream flow, including magnitude, duration, timing, rate of change (upramping and downramping rate) and frequency of changes in flow (Céréghino & Lavandier, 1998, Marty et al., 2009).

Hydropeaking may cause severe impacts on the biodiversity of a stream. In fact, due to hydropeaking the abiotic environment in a stream is strongly altered. As a consequence many fishes, macroinvertebrates and aquatic plants undergo a major stress and very often they are not able to survive these frequent water level fluctuations (Vehanen et al., 2003, Meile, 2006).

Water policies, for example the European Water Framework Directive (EU, 2000) require a good ecological status of rivers to be re-established. The Swiss Federal Law for water protection is even more straightforward in forcing the owners of hydropower plants, responsible for hydropeaking, to realize structural or—in exceptional cases—non-structural mitigation measures.

In this paper a case study is presented where different solutions to mitigate the impacts on stream ecology due to hydropeaking are evaluated. With the help of abiotic indicators representing the hydropeaking phenomenon the present status of habitat conditions in the affected river system is examined. By analyzing costs and benefits of technically feasible solutions and judging the effect on river ecology the best variants can be determined.

In order to provide a holistic understanding, the analysis is deepened with the help of the Gomez and Probst (Gomez & Probst, 1995) method. This method was developed in order to analyze complex problems including the construction of a network between elements forming the system. However, integrated analysis for problem solving provides only the fundamentals for discussion of the issues in the public. Thus, the present case study was embedded in an integrated river management concept with public participation where other topics like flood protection, aquatic and terrestrial ecology, land use planning were also considered.

1.2 *Physical indicators of hydropeaking*

Due to hydropeaking the hydrological regime of a river is altered with a direct impact on the abiotic environment of a river such as hydraulics and sediment transport. The abiotic environment exerts his impact on the biotic environment of the aquatic system, i.e. on its long term ecological functionality. In order to describe the short term impacts and assess the hypothetical effect of mitigation measures several physical indicators might be used (Schweizer, 2009). They are briefly described here:

- Absolute flow change rate ($Q_{\max/\min}$): depending on this relation and on the characteristics of the artificially added discharge water temperature and turbidity in the affected river reach might change, causing negative impacts for aquatic animals. However, peak flow Q_{\max} is responsible for others of the following indicators, too.
- Frequency of bed mobilization: if the river bed is mobilized at each hydropeaking cycle, macroinvertebrates and fish eggs in the hyporheic zone are moved. Consequently, in these river reaches reproduction activity for fishes is barely possible.
- Rate of change on the rising limb of the hydrograph: A too high rate of change causes the drift of macroinvertebrates as there isn't given enough time to them to budge into zones where shear stress is low. This happens rather in channelized rivers than in other river types.
- Rate of change on the falling limb of the hydrograph: this relation influences mainly the variation of river width, but also the variation of flow depth and velocity, creating a stress on aquatic animals. If variation of river width happens too fast, there is the risk that fishes during the decrease of discharge remain in water ponds that are separated from the main flow. In rivers with a natural morphology this risk is higher than in channelized rivers.
- Variation of Reynolds number and shear stress: these indicators have a direct influence on the resistivity of macroinvertebrates against being drifted downstream.

For some of these indicators clear quantitative predefinitions and thresholds for ecologically compatible values are available in literature, whereas for other indicators only qualitative considerations can be found.

1.3 *The study area and hydropeaking issues*

The Etsch has its source on the main chain of the Alps closed to the boarder between Italy and Austria and is, in terms of length, the second largest, and, in terms of watershed surface, the third largest river in Italy. Mainly the headwaters of the Etsch are intensively exploited for hydropower production. In the XXth century several dams were constructed for the seasonal storage of water in order to produce peak energy.

In the extended project area (Fig. 1) there are two power plants which produce peak energy, namely the power plants of Glurns and Kastelbell. The power plant of Glurns is supplied by water from the Reschen lake that has a reservoir volume of 120 mio · m³. Downstream of the power plant in Glurns there is an intermediate reservoir. From there water is artificially

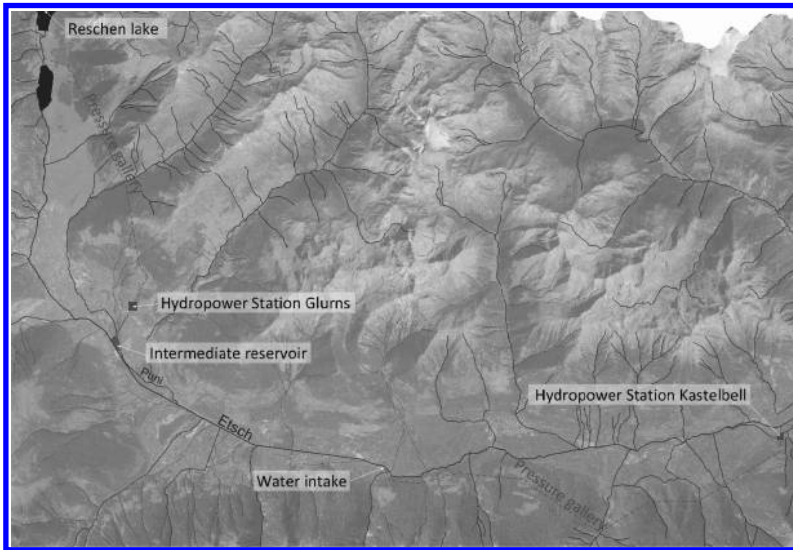


Figure 1. Extended project area with key elements.

Table 1. Key data of the Glurns and Kastelbell power plant.

Plant	Net head (m)	Design discharge (m ³ /s)	Installed capacity (MW)	Energy production/year (GWh)
Glurns	586	18	90	291
Kastelbell	294	30	93	438

released in order to allow peak production also for the run of river plant in Kastelbell who's water intake is situated around 12.5 km downstream of the intermediate reservoir, creating hydropeaking effects on the river courses in between. Table 1 reassumes the key data of the Glurns and Kastelbell power plant.

Peak energy usually is produced on working days between 8:00 to 18:00. However, in the last years due to changes on the energy market (liberalization, increase in energy demand during weekends) the operation of the plants has undergone some modifications.

In order to follow the daily peak demand, Kastelbell power station that during the night works as run of river plant requires water released from the intermediate reservoir in Glurns. Thus the discharge in the affected rivers Puni and Etsch in the reach between Glurns and Laas is rapidly rising from a low to a high stage corresponding to a flood discharge. When the power stations are turned off, the river discharge returns back to a residual flow, which is often very low because of the large quantities of water that are diverted into the Reschen lake. The result of this operating mode is a high and, more important, rapid variability in flows. Figure 2 shows a typical discharge curve on the Etsch river for a two week period. It can clearly be noticed that there is kind of an artificial flood every day from Monday to Friday due to hydropeaking whereas on the weekends (in the center of the graph) energy need is lower and thus the power stations don't produce peak energy.

There are two rivers affected by hydropeaking in the study area (Fig. 4). From the intermediate basin water is released into the Puni river. After around 3.54 km of flow length downstream of the point where water is released the Puni confluent with the Etsch river. The length of the Etsch between the confluence of Puni and Etsch and the water intake for the Kastelbell power plant is 8.91 km.

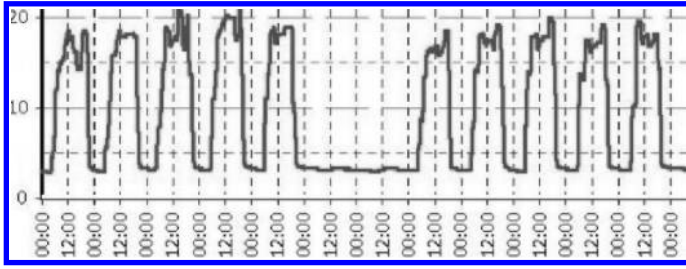


Figure 2. Discharge fluctuations due to hydropeaking in the Etsch river.



Figure 3. The affected rivers during peak flow due to hydropeaking. Left: Puni (note that hydropeaking causes a discharge almost equal to bank full flow). Right: Etsch (note the artificial river morphology).

During the years from 1819 to 1825 the Etsch river has been entirely channelized in the project area whereas the Puni river is characterized by a rather natural morphology with diverse habitats that are favorable for the aquatic community (see also Fig. 3). When dealing with hydropeaking it is of primary importance to consider also the morphology of the concerned stream. Depending whether the stream is channelized with a regular section or the stream has a natural, pristine morphology the impacts of hydropeaking on the aquatic ecology can be significantly different.

2 CONDUCTED STUDY

2.1 Present state

In order to assess the present state, the following indicators have been considered at three control sections: i) hydropeaking ratio Q_{\max}/Q_{\min} , ii) rate of change on the rising and falling limb of the artificially created hydrographs (dP/dt), iii) near bottom shear stress (τ), iv) dimensionless critical shear stress ($\theta - \theta_c$). The control section P1 (Fig. 4) is situated at the Puni river, the control section P2 at the Etsch river immediately downstream of the confluence with the Puni river, whereas the control section P3 is at the Etsch river around 2 km downstream of the inflow of the Sulden river which in the study area is the most important tributary of the Etsch.

Analyzing in detail the discharges from 1996 to 2004 at the control section P2 (situated near a gauge station), the duration curve for the hydropeaking ratios Q_{\max}/Q_{\min} (Fig. 5) shows that a hydropeaking ratio $>1:5$ at the Etsch is exceeded for not more than 16.5% of the time, whereas a hydropeaking ratio $>1:8$ is an exceptional event that occurs in average once or twice per year. Comparing hydropeaking ratios between river Etsch and river Puni (Fig. 5) it can be concluded that a hydropeaking ratio of 1:5 at the Etsch is corresponding to a ratio of 1:25 at the Puni.

When considering up-ramping and down-ramping rates at the control sections (Fig. 6), it can be observed that at river Puni the change of water depth is 29 cm/hour at the rising limb

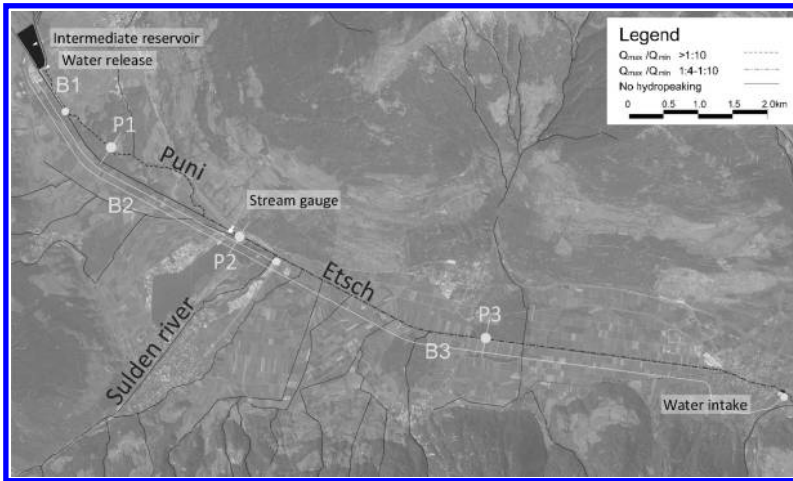


Figure 4. Study area with key elements, control sections P1–P3 and structural project variants B1–B3.

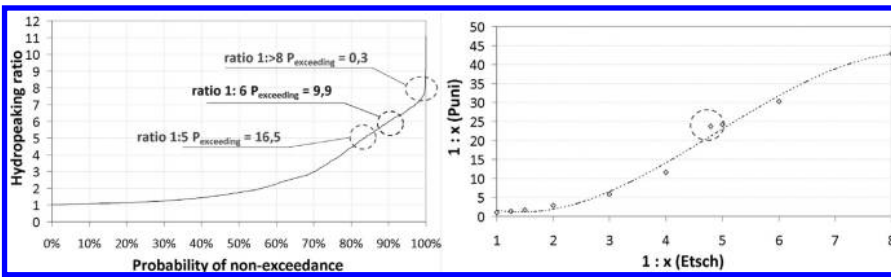


Figure 5. Duration curve for hydropeaking ratio in the Etsch (left) and correlation of hydropeaking ratio between Etsch and Puni.

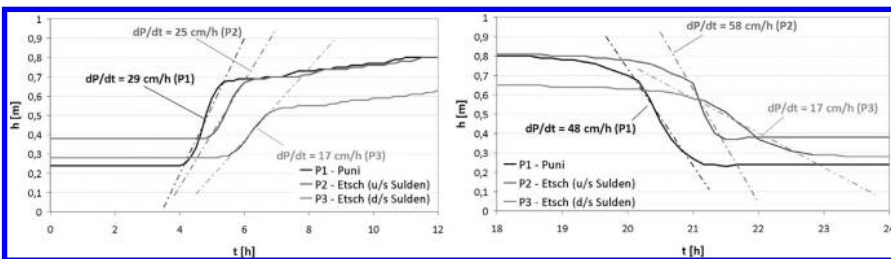


Figure 6. Up-ramping (left) and downramping rate (right) at control sections.

of the hydrograph and 58 cm/hour on the falling limb of the hydrograph, whereas at P2 and P3 these values are slightly lower. In literature different threshold values are given (Saltveit et al., 2001, Halleraker et al., 2002, Baumann, 2004). An average value of 12–18 cm/hour for the downramping rate is generally seen as an ecologically acceptable value.

If bottom shear stress is looked at, in Figure 7 can be seen that during maximum discharges bottom shear stress is always above 10 N/m² which in literature (Baumann, 2004, Gibbins et al., 2007) is indicated as maximum tolerable shear stress for most of the macroinvertebrates. The combination of fast up-ramping rates and high bottom shear stresses for macrobenthos in the Puni and Etsch causes life conditions being far from the ideal. However, due to the channelized morphology of the Etsch bottom shear stress is higher than 10 N/m² even in low flow conditions.

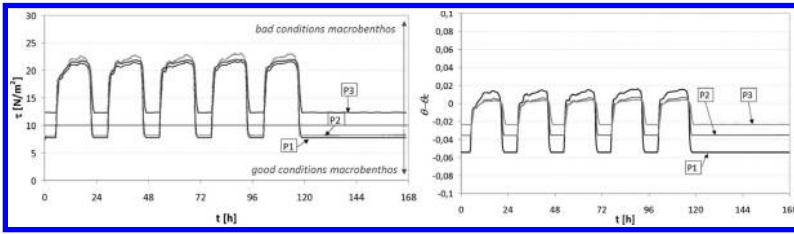


Figure 7. Bottom shear stress (left) and difference of shear stress θ and critical shear stress θ_c for incipient bed load motion (right).

The right imagine on [Figure 7](#) states that during maximum flow critical shear stress for the commencement of bed mobilization is reached. Therefore additional stress during the spawning season might be caused due to partial movement of the river bed.

The analysis of the present situation allows the conclusion that the rivers in the project area are strongly affected by hydropeaking operations leading to losses in biomass and consequently an impairment of biodiversity. However, mainly in the Etsch also the channelized river morphology is a factor responsible for biodiversity decline. Therefore, mitigation measures to improve the present situation have to be planned considering both hydropeaking and morphology.

2.2 Definition of mitigation measures

2.2.1 General considerations

Mitigation measures for hydropeaking are subdivided into two concepts, namely operational (non-structural) measures and structural measures. If at the first glance operational measures seem to be realizable quite easy, it is important to be aware that hydropeaking operations are necessary to cover the peak electricity demands. Peak load power plants are, besides gas turbine and pump storage plants, the most effective way to produce peak energy. When a peak load power plant changes its operational rules by reducing hydropeaking in scale and/or time, consequences for national economies are to be faced as other sources have to cover the loss in peak energy production.

2.2.2 Operational measures

For the present case two major groups of operational measures have been considered:

- the complete elimination of peak production in the power plant of Kastelbell (A1) and
- the reduction of the hydropeaking ratio to maximum ratios of 1:4, 1:3, 1:2, 1:1.5 and 1:1.25 (A2).

If peak production in the power plant of Kastelbell was completely given up and from the intermediate basin a constant discharge was released, the power plant in Glurns would also have to modify his operational rules and would reduce drastically the duration of peak production. The volume of the intermediate basin is in fact large enough to temporarily store the water that has been turbined in the power plan of Glurns only for two hours before being filled. Also when hydropeaking ratio is reduced, both power plants have to adapt their operational modes.

2.2.3 Structural measures

Several structural measures for the present case were discussed. They focus on realizing an artificial subterranean channel that runs parallel to the affected rivers and transports the hydropeaking discharges downstream. To transport the peak flows of maximum 20 m³/s the channel will be realized as a rectangular concrete profile with a width of 7 m and a height of 3.15 m. The channel will be pressurized, therefore allowing for a low head power plant to be installed at its downstream end. The three variants B1, B2 and B3 ([Fig. 4](#)) only differ in the lengths of the channel.

In variant B1 the artificial channel has a length of only 0.5 km. It allows to release water alternatively into the Etsch or into the Puni. At the intermediate reservoir water can only be released into the Puni, because there the river bed of the Etsch is at a higher level than

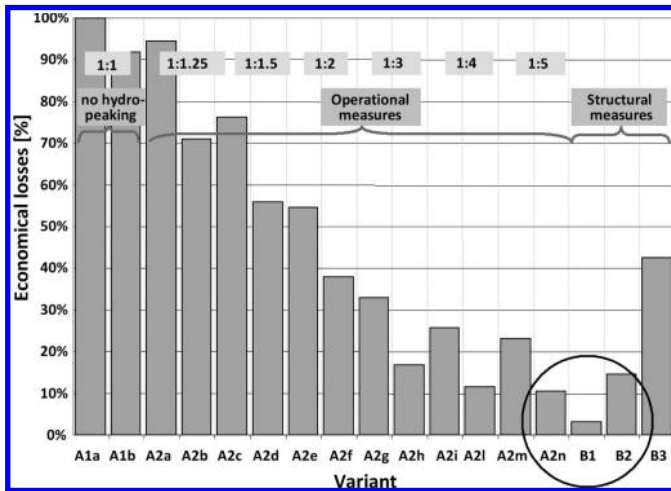


Figure 8. Graphical representation of the cost-benefit analysis.

the bottom of the intermediate reservoir. In variant B2 the channel has a length of around 4.5 km is extended until the mouth of the Sulden river and the water is released at this point into the Etsch. In variant B3 the channel, having a length of 12.5 km, covers the whole length of the study area and releases water directly into the water intake in Laas.

2.2.4 Cost-benefit analysis

A cost-benefit analysis has been conducted in order to compare operational with structural measures. When operational measures are adopted, besides of the fact that peak energy has to be provided elsewhere, the plant owner has to face economical losses. A complete elimination of hydropeaking for example would lead to an average loss of selling price of more than 10% at the Glurns power plant and around 5% at the Kastelbell power plant. In Figure 8 the cost-benefit analysis is represented graphically. The total abandonment of hydropeaking is taken as reference scenario where the expected losses in 30 years are assigned a value of 100%. For each of the operational measures always two scenarios were calculated: one scenario with the actual volume of the intermediate basin (150.000 m³) and one scenario with the hypothesis that the volume of the intermediate basin is increased to 400.000 m³. The left column beneath the indication of the hydropeaking ration (f.i. 1:2) shows the scenario with the actual volume and the right column with the increased volume of the intermediate basin. The three columns on the right end of the graph show the structural variants B1 to B3.

The graph puts in evidence that the variant B1 generates the least economical losses in 30 years (only 3% of the losses in comparison to a total elimination of hydropeaking). Also variant B2 is an economically valid variant as the economical losses are at a level of around 15% in comparison to a total hydropeaking abandonment. Concerning the operational measures, it results that after an increase of the volume the intermediate reservoir is suitable for being used as detention reservoir. If hydropeaking ratio is limited to 1:5 in the Etsch river and the volume increased, economical losses are around 10% in comparison to no hydropeaking.

Consequently, a combination of variant B1 or B2 and A2n is the best solution to mitigate the harmful impacts of hydropeaking without major losses for the plant owner and with an acceptable loss of available peak energy.

3 DECISION FINDING PROCESS

3.1 Establishment of a holistic decision supporting network

When complex problems have to be solved, holistic and integrated approaches that consider all the critical elements involved in a decision taking process are needed. Mitigation of

hydropeaking impacts concerns not only the plant owner, but also different other stakeholders having an interest on a sustainable use of the water resources.

In the present case, the variant analysis described in the preceding chapter, is deepened with the help of the Gomez and Probst (Gomez & Probst, 1995) method. This method was developed in order to analyze complex problems where a high number of factors with strong interactions and high dynamics are present. The core of the method includes the construction of a network forming the system. The network is set up by defining all the factors that are concerned by a problem, and subsequently establishing where relations between the factors exist and in which way the factors influence each other, i.e. evaluating in a relation which is the influencing (active) element and which is the influenced (passive) element. A matrix is then built, attributing weights to every link, allowing to obtain an integrated view of the functioning of a system.

In an expert assembly a total number of 64 factors that are relevant for the study area have been defined. After establishing direct relations, and also indirect relations of the first and second order, Figure 9 that shows the significance of the considered factors was elaborated. Hydropeaking and peak energy production obtain the highest active sums and are therefore motors of the system. Therefore the decision to analyze in detail hydropeaking in the project area was more than correct. Reactive elements can be used as indicators for the problems created by the situation. As expected, biodiversity and cash flow for the plant owner are important variables that are strongly influenced by hydropeaking. Surprisingly, also the attractiveness for tourism is an important reactive element demonstrating that the status of running waters is a key element for the prosperity and image of a region.

3.2 Public participation

As the issues in the study area are not only limited to hydropeaking, but also to flood protections, to land use management, irrigation for agriculture, tourism, biodiversity conservation and enhancement, in 2008 an integrated river management project was launched with the participation of the concerned stakeholders.

In regular sessions detailed information about ongoing studies was given as a base for working groups where directives for a guiding image (“Leitbild”) were elaborated. Also the measures to mitigate hydropeaking impacts were discussed either in working groups or open panel discussions. After the working process the defined measures were approved by the plenum.

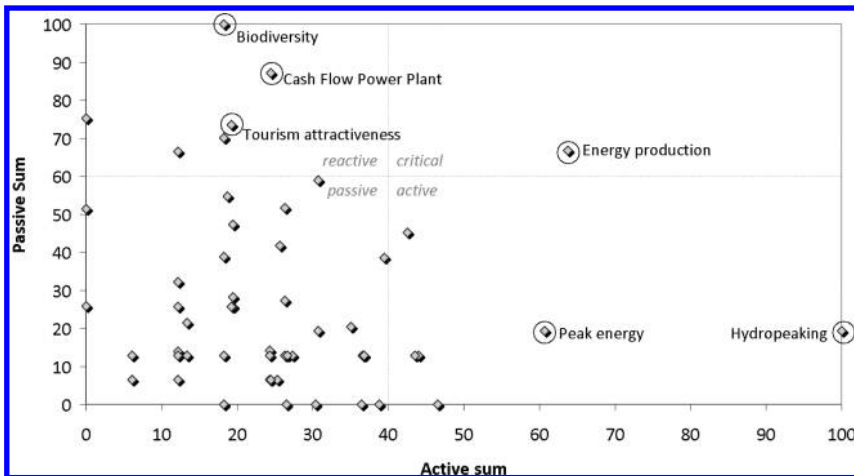


Figure 9. Graphical representation of influence matrix with active, critical, reactive and passive elements.

4 CONCLUSION

The present study shows that hydropeaking causes significant alterations of the abiotic environment. However, evaluation of physical indicators revealed that the strongly altered morphology of the affected water courses also plays an important role for the impaired biodiversity.

In order to define mitigation measures a variant analysis was carried out with the result that operational measures should be adopted in a very limited way as they cause not only economical losses for the plant owner, but also losses of peak energy that has to be produced elsewhere to cover electricity demands. A combination of operational adaptations together with structural measures such as a pressurized conduit running in parallel to the rivers and releasing water at a point where absolute flow rate change might be ecologically acceptable is the solution to be realized.

An integrated decision supporting network clearly showed that hydropeaking is a lever of the system. Therefore, planning and realizing measures to mitigate negative hydropeaking impacts is an important step to allow a sustainable development of the region also in the future. In order to realize the mitigation measures detailed feasibility studies are now on the way.

ACKNOWLEDGMENTS

The present study has been carried out within the frame of the integrated river management concept “Flussgebietsplan Oberer Vinschgau” (www.etschdialog.it). It was financed by the plant owner Seledison Plc and by the Public Authority for Water Protection of the Autonomous Province of South Tyrol.

REFERENCES

- Baumann, P. 2004. *Revitalisierung und Benthos der Rhone*. Schlussbericht SP I-6, Rhone-Thur Projekt, EAWAG, WSL, LimnEX AG.
- Céréghino, R. & Lavandier, P. 1998. Influence of hypolimnetic hydropeaking on the distribution and population dynamics of Ephemeroptera in a mountain stream. *Freshwater Biology* 40: 385–399.
- EU WFD. 2000. Establishing a framework for Community action in the field of water policy. *Directive 2000/60/EC of the European Parliament and of the Council of 23 October 2000*. The European Parliament and the Council of the European Union.
- Gibbins, C.N., Vericat, D. & Batalla, R.J. 2007. When is stream invertebrate drift catastrophic? *Freshwater Biology* 52: 2369–2384.
- Gomez, P. & Probst, G. 1995. *Die Praxis des ganzheitlichen Problemlösens*. Verlag Paul Haupt, Bern.
- Halleraker, J.H., Harby, A., Hessevik, T. & Saltveit, S.J. 2002. Individual response of juvenile atlantic salmon and brown trout to rapid and frequent flow fluctuations. Abstract, 4th Symp. Ecohydraulics, Cape Town.
- Marty, J., Smokorowski, K. & Power, M. 2009. The influence of fluctuating ramping rates on the food web of boreal rivers. *River Research and Applications* 25: 962–974.
- Meile, T. 2006. Hydropeaking on watercourses. *Eawag News* 61e.
- Saltveit, S.J., Haug, I. & Brittain, J.E. 2001. Invertebrate drift in a glacial river and its non-glacial tributary. *Freshwater Biology* 46 (12): 1777–1789.
- Schneider, M. & Noack, M. 2009. Hydropeaking, environmental impact and mitigation in Germany and Switzerland. Universität Stuttgart, Germany. *EnviPeak 24.03.2009*, Trondheim.
- Schweizer, St. 2009. Bewertung von Schwall/Sunk—Herleitung eines ökologisch abgestützten Bewertungskonzepts. *Wasser—Energie—Luft* 3: 194–202.
- Vehanen, T., Huusko, A., Yrjänä, T., Lahti, M. & Mäki-Petäys, A. 2003. Habitat preference by gray (Thymallus thymallus) in an artificially modified, hydropeaking riverbed: contribution to understand the effectiveness of habitat enhancement measures. *J. Appl. Ichthyol.* 19: 15–20.

The new Mutsee dam (Switzerland)

F. Tognola

Lombardi Engineering Ltd, Minusio, Switzerland

M. Balissat

Stucky Ltd, Renens VD, Switzerland

ABSTRACT: The new Mutsee Dam is part of the new pumped-storage power plant Limmern, presently under construction. With his 1000 MW installed capacity, this plant will be the largest pumped-storage power station in Switzerland. The plant includes a new underground powerhouse located close to the existing Limmern Arch Dam, at an altitude of about 1700 m a.s.l., and uses the about 600 m gross head between the Limmern reservoir (92 mio m³) and the existing Mutsee natural lake. With the new dam at Mutsee the maximum water level of this natural lake will be raised up by 28 m. The live storage of the reservoir will be so increased from 9 mio to 24 mio m³. The new dam is designed as a conventional gravity dam with 68 blocks of 15 m width each. The dam reaches a maximum height of 35 m, while the total concrete volume is 250'000 m³. An ungated spillway extends over 5 dam blocks and is designed in order to release the maximal pumps discharge (160 m³/s). The particular location of the dam in a high mountain area and the fact that the excavation material of the powerhouse shall be transported to the dam site by a cableway is particularly challenging from the logistic point of view.

1 INTRODUCTION

The Linth-Limmern Scheme has been under operation for more than 40 years. It consists of a 120 m high arch dam impounding a reservoir of 92 mio m³, a headrace tunnel and a pressure shaft leading to an underground powerhouse with two units at Tierfehd. The gross turbined head is 1050 m. A compensating basin allows regulation of the discharge for the downstream course of the Linth River and the next scheme plant in Linthal. Water of the natural lake of Mutsee located 630 m higher than the Limmern Lake is collected and turbined in a small underground powerhouse next to the main reservoir.

The actual development plan under the name of Linthal 2015 (Fig. 1) consists in establishing a high capacity pumped storage scheme (1000 MW) between the Mutsee and the Limmern lakes. For this purpose the capacity of the Mutsee reservoir will be increased from 9 mio to 24 mio m³ by raising the level of the natural lake by 28 m. This will be achieved by erecting a more than 1 km long gravity dam along a smooth ridge on the South side of the natural lake. The new scheme consists of a water intake and a 500 long headrace tunnel leading to two large diameter pressure shafts. An underground powerhouse with 4 reversible pump-turbines (4 × 250 MW) will be built next to the Limmern reservoir. Access to the powerhouse shall be provided from downstream by an inclined gallery (inclination: 23%) equipped with a cable-railway.

The new Mutsee Dam is located at a high altitude with severe climatic conditions as they prevail at this elevation in the Alps. The area is situated well above the limit of trees and is characterized by a sensitive environment with long winter periods and relatively short summers. These conditions have also a significant impact on the material supply and the construction program.

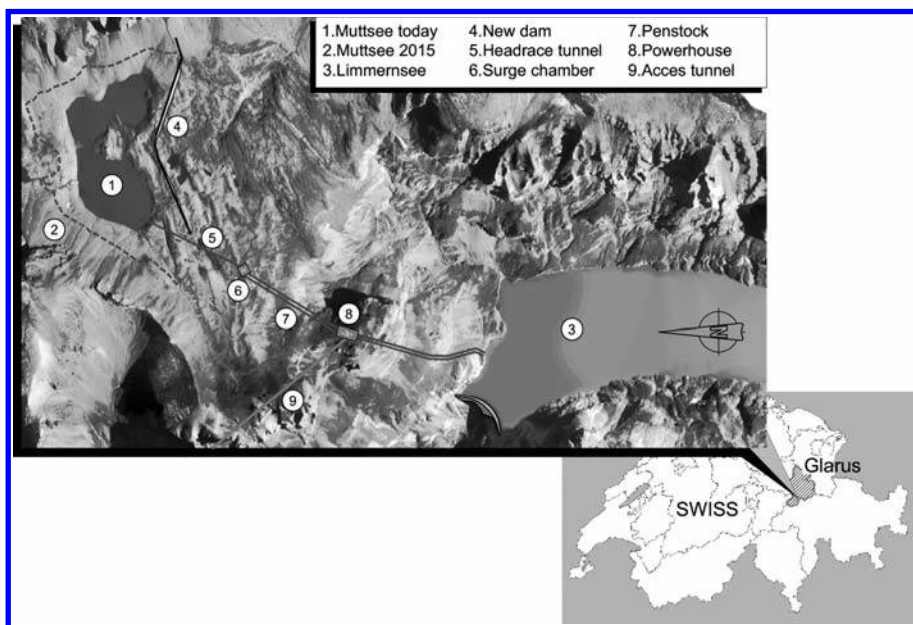


Figure 1. The new pumped storage scheme of Linthal 2015.

2 GEOLOGICAL CONDITIONS

The Muttsee Dam site is located on sedimentary rocks which are disposed in successive scales. The geological layers (Fig. 2) rise slightly from the South towards the dam site, lie at the dam site almost horizontally and fall down within some 100 m steeply towards North as they form a brow wrinkle. The upper layers in the dam area consist of tertiary sediments (so called Pectinit schists, sandstone and Discocycline limestone) covering the underlying rocks made of sediments of the Chalk and Malm periods (various types of limestone).

One of the main issues is the water tightness of the dam foundation. Beside some disturbed and sheared zones the tertiary sediments are generally impervious. However the protective layer of rocks resisting to karstification is relatively thin (only 20 to 50 m thick). The rock in the first 15 m is often loosened up and exhibits fissures and shear planes that can carry water. The main water carrying feature is formed by a ESE-WNW cleavage system that plunges nearly vertically. Furthermore the shear and disturbed zones such as the Muttsee Bruch can be considered as water carrying too. Two ground depressions have been noticed in the dam area. They can be considered as sinkholes (dolines) caused by an underlying karst system.

On the East side of the dam the Chalk layers that are prone to karstification lie at a deeper level. The rock mass is however characterized there by overtopping and shearing of several layers and is highly fissured. It may be therefore locally less watertight.

3 THE LAYOUT OF THE NEW DAM

3.1 General requirements for the dam concept

The relative remoteness of the dam site calls for a limited volume of construction material to be brought up by cableway from a lower level since environmental considerations do not allow operation of a quarry next to the lake. Essentially selected muck of the excavation works for the powerhouse cavern and access galleries shall be transported to the dam site. Other environmental considerations request also to limit the extension of the dam footprint. These various constraints led to the early choice of a concrete gravity dam.

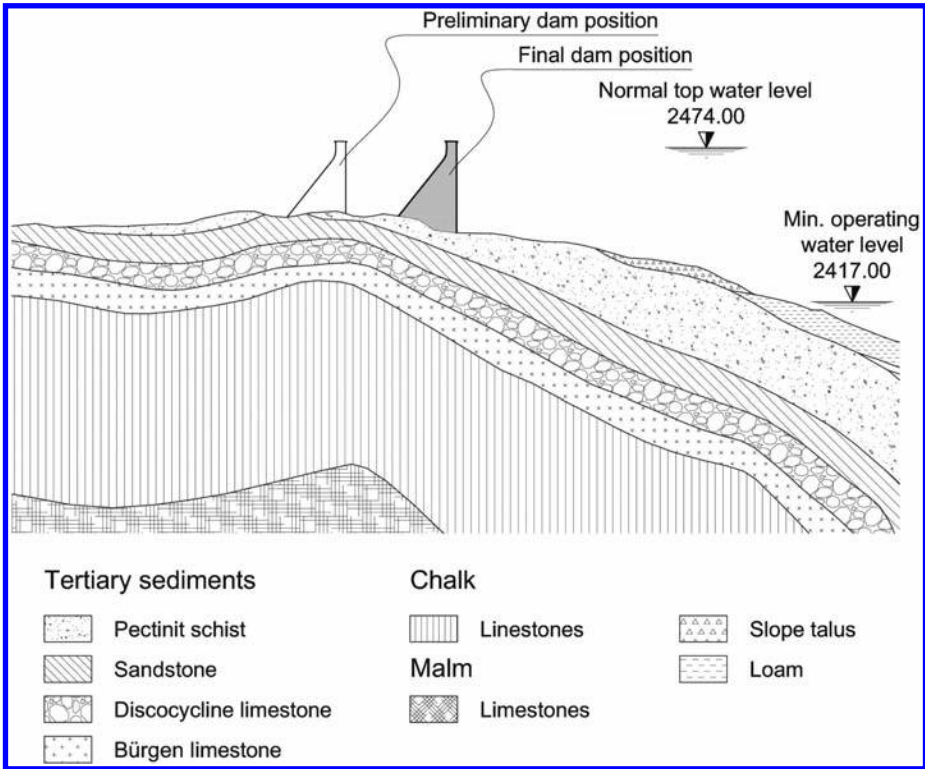


Figure 2. Geological cross-section of the Muttsee Dam site.

The foundation rock exhibits generally a good strength and as the height of the dam will not exceed 35 m induced stresses will remain relatively low. The main problem lies with the permeability of the foundation that is linked on one hand to single fracture zones in the upper rock layers and on the other hand to the deeper karstified rock formation. The first aspect shall be treated by constructional measures such as blanketing and grouting, while the second one will influence the location of the dam axis that shall take into account a sufficient thickness of the upper rock layers because of their relative imperviousness. Appropriate grouting and drainage works in the dam foundation shall complete the underground treatment.

The Muttsee lake as upper reservoir of a pumped storage scheme will be subjected to rapid water level variations. Stability of the lake shores and watertightness of the foreland on the upstream side of the dam have therefore to be carefully examined.

Construction of the Muttsee Dam is not on the critical path of the Linth-Limmern 2015 project. Nevertheless the construction schedule shall take into account the restricted supply chain of materials (mainly cement and aggregates) and the limited length of the construction periods per year (5 to 6 months). Low temperatures especially during night will have also an influence on concrete curing procedure.

3.2 *Alignment of the dam axis*

Several dam axis alignments have been examined in a preliminary design phase (Fig. 3). The criteria considered for the definition of these alignments may be summarized as follows:

- a minimum thickness of the Pectinite schists (and other surface rock types) to benefit of their imperviousness as upper foundation layers;
- some distance to the small ponds on the South side that are under environmental protection;
- a geometrical alignment as simple as possible.

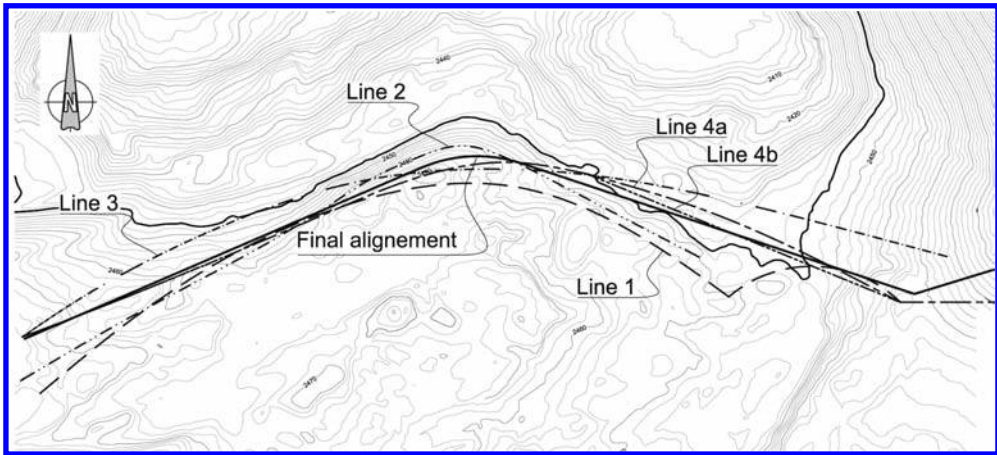


Figure 3. Alternative dam axis alignments.

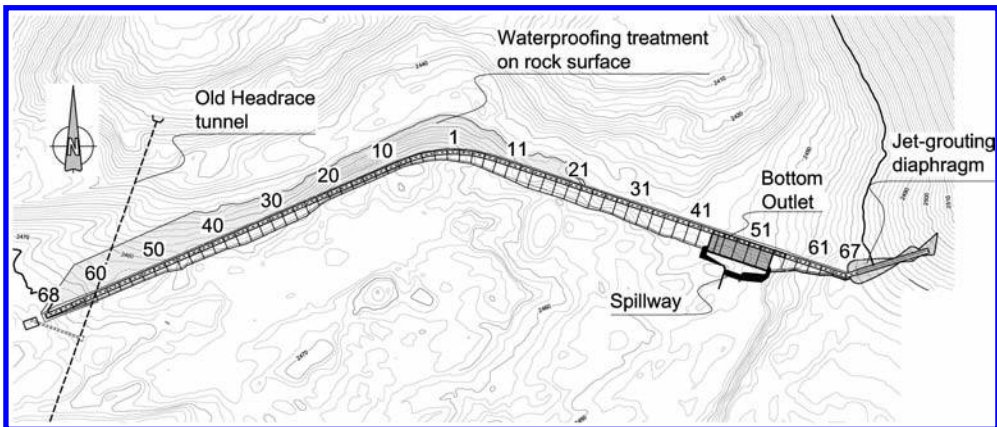


Figure 4. Plan view of the Muttsee Dam.

The *line 1* corresponds to a preliminary approach with a composite concrete dam consisting of a gravity section in the center and on the West side and an arch dam section on the East side where the dam is the highest. This solution was discarded as the apparent economy of concrete will be ousted by the volume required for the abutment blocks of the arch dam. Furthermore the dam axis was too close to one of the doline that was found in the subsequent investigations.

The *line 2* was an attempt to place the dam further North and to take advantage of a maximum thickness of the relatively impervious surface rock layers. Nevertheless this alternative was discarded as the right abutment could not be properly imbedded in the rock and the thickness of the talus deposits on the left abutment was excessive.

The *line 3* corresponds to a dam with a continuous curved alignment without a sharp bend. This was selected to avoid possible abnormal behavior of the dam as it sometimes occurs with a composite axis. This solution was eventually not retained as it crossed the left bank scree with a significant thickness of deposits and would have required a larger volume of concrete.

The *lines 4a and 4b* represent the last optimization steps for the location of the dam axis. Crossing of the talus deposits at the left bank has been moved 50 m further South in order to intercept the minimum thickness of these deposits. Eventually the line 4b has been retained with some minor geometrical simplifications as the definitive alignment of the dam axis.

The final dam plan view is presented in [Figure 4](#).

4 CHARACTERISTICS OF THE DAM

4.1 Generalities

From a structural point of view the new Muttsee Dam is a conventional gravity dam with 68 independent blocks, whose length is generally 15 m at the dam axis. The 1054 m long dam crest is located at 2476 m a.s.l., and the maximal dam height from the foundation is 35 m. The normal water level is designed at 2474 m a.s.l., allowing a total storage volume of 26.53 mio m³, while the live storage volume by a minimum operating level of 2417 m a.s.l. is 23.43 mio m³.

As shown in Figure 5, the typical cross section of the dam is designed with vertical upstream face and an inclination of the downstream face of 1:0.8 (V:H). The maximum width at the foundation reach 27 m, while the minimum width of the crown blocks is typically 4 m. Only for the first four blocks on the right bank, which have a very small height, the thickness had to be increased to 6 m for static reasons. The total volume of concrete used for the dam is about 250,000 m³.

On the left bank, where the bedrock is covered with talus deposits reaching locally a depth of 20 m, a watertight diaphragm is foreseen (Fig. 6). This diaphragm will be made by jet-grouting columns arranged in three rows in the sections with higher depth and only two rows in shallow part. Consolidation grouting at the intersection of the jet-grouting columns is planned in order to further increase the imperviousness of the diaphragm.

An inspection gallery with relatively large dimensions to allow for the carrying out of grouting work in the foundation is located at the upstream toe of the dam. This gallery continues

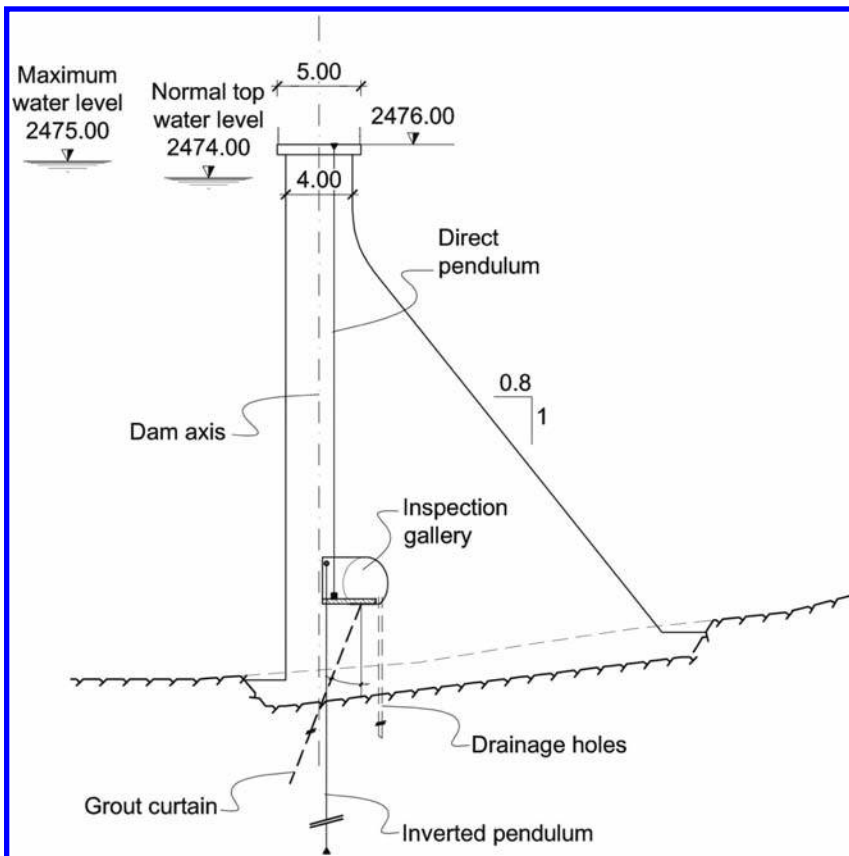


Figure 5. Muttsee Dam standard cross section.

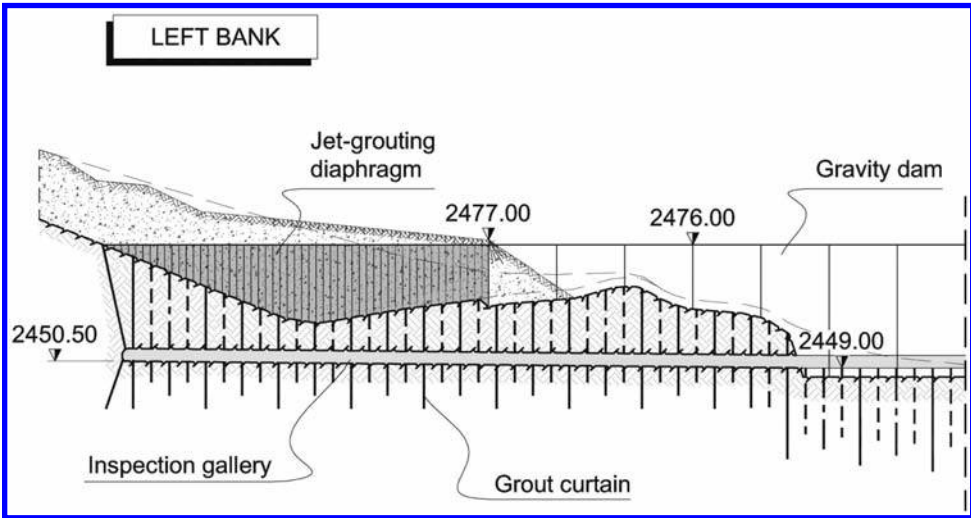


Figure 6. Diaphragm wall on the left bank.

in the foundation rock of the left bank up to the end of the diaphragm. The inspection gallery is accessible from the downstream toe of the dam through five adits located at low points of the ground.

On the right bank the construction of the dam will make it impossible for surface waters (rainwater and water resulting from the melting of snow) to naturally flow towards the lake. Therefore this water shall be collected and channelled through the access adits into the inspection gallery. From here, the water is evacuated together with the leakage water through a inclined borehole towards the old headrace tunnel. The latter is closed with a concrete plug below the dam axis and used as a winter access to the dam. An elevator installed in a vertical shaft is connecting the access gallery to the service house on the right bank. From here, it is also possible to directly access the dam's inspection gallery through an underground passage.

4.2 The spillway and the bottom outlet

The spillway of the dam extends over five blocks to the left bank, where the dam reaches its maximum height. The spillway is made up of five ungated sills at elevation 2474.60 m a.s.l. (Fig. 7). Four of these sills are 14.40 m wide and the fifth has a width of 15.0 m. Thus, the total effective length of the spillway reaches 72.60 m. A stilling basin is designed at the downstream end of the spillway in order to improve the energy dissipation.

The maximum peak during the design flood (1000 years return period) is relatively small ($40 \text{ m}^3/\text{s}$) because of the very small size of the catchment area. On the other hand, the spillway is designed for the worst scenario of over-pumping at maximum capacity of the plant ($160 \text{ m}^3/\text{s}$) over the normal top water level. It should be noted that in order to reduce the risk of over-pumping two independent water level measuring systems are provided. This load case may therefore be considered as an exceptional operational case.

Since the design flood volume ($245,000 \text{ m}^3$) is smaller than the storage volume between the normal top water level and the spillway elevation ($380,000 \text{ m}^3$), it is expected that the water level will not reach the spillway elevation during flooding. Nevertheless for safety reasons the spillway is designed in order to allow the passage of the peak flow of $40 \text{ m}^3/\text{s}$ without exceeding the maximum water level (2475.00 m a.s.l.). In case of over-pumping the water level reaches 2475.60 m a.s.l. and is still 0.40 m lower than the dam crest elevation.

The bottom outlet is located in one of the spillway blocks. The bottom outlet is designed as an horizontal square conduit with a section of 1.44 m^2 and a total length of 25 m.

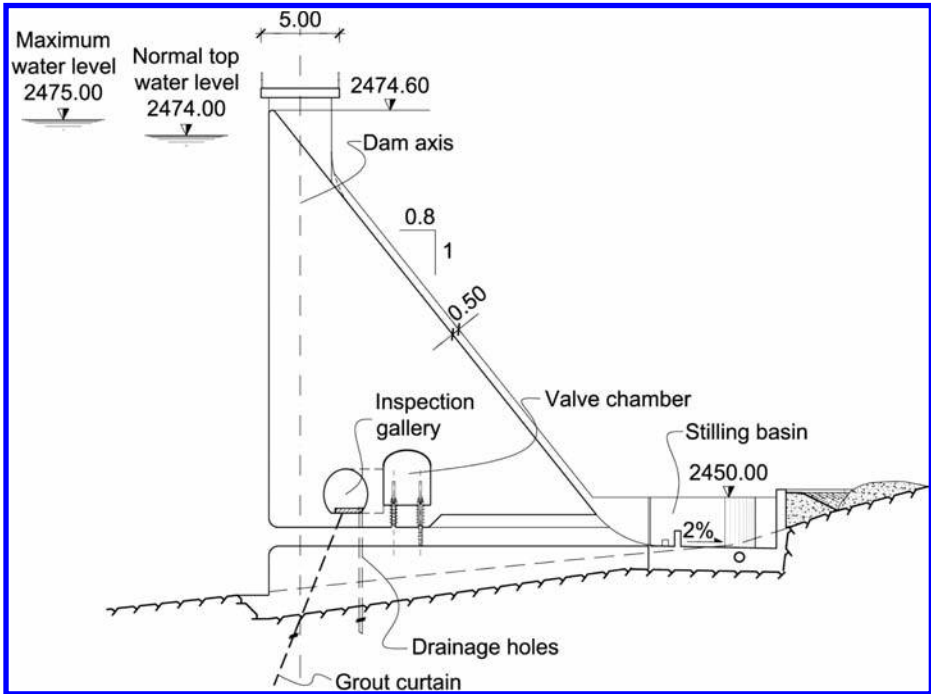


Figure 7. Cross section of the spillway and of the bottom outlet.

The upstream stretch, up to the two identical siding gates (for revision and service), is entirely steel lined whereas the downstream stretch is made of an open channel. At the end of the channel a concrete block allows energy dissipation before releasing the water in the stilling basin of the spillway. The access to the valve chamber is given through the inspection gallery of the dam. It has to be noticed, that the relatively high location of the bottom outlet only allows a partial emptying of the Muttsee reservoir. For achieving a complete lowering of the water level a valve will be provided in the concrete plug in the old headrace tunnel.

4.3 Grouting works

Contact grouting is provided on the entire surface of the dam foundation to a depth of 3 m in the rock. A grout curtain down to a depth of 20 m is also envisaged at the upstream toe of the dam to reduce seepage and uplift pressure (Figs. 5 and 7). The grout curtain extends on the left bank under the jet-grouting diaphragm. The grouting works are generally carried out from the inspection gallery. Once the grouting works are completed, drain holes will be drilled from the gallery to further reduce the uplift in the foundation.

In order to prevent seepage through fissures in the bottom of the new impounding, which are difficult to seal by local treatments, it is envisaged to provide the rock surface with a waterproof lining (Fig. 4). This consists of a layer of reinforced shotcrete with an approximate thickness of 15 cm. Since the imperviousness of the natural lake is considered satisfactory, the waterproofing treatment only affects the new submerged surfaces between the maximum water level of the natural lake and the new dam over a surface of approximately 15,000 m².

4.4 Monitoring instrumentation

The displacements of the dam are measured in five sections by means of a direct and an inverted pendulum, both provided with a reading station at the level of the inspection

gallery (Fig. 5). This system allows to measure absolute displacements at two different levels of the dam. Furthermore, thermometers to determine the thermal state of the dam are installed at each measuring section. The monitoring equipment is completed by measures of uplift pressure in the foundation and seepage in the inspection gallery. Geodetic measurements and a levelling of the dam crest are also included in the monitoring program.

5 DAM CONSTRUCTION PROGRAM AND PROCEDURES

Given the severe weather conditions and the short summer working seasons, the construction of the new dam is planned over a period of six years between 2010 and 2015. The work program provides for the preparation of the job site installations during the first two seasons (2010 and 2011). The start of the excavation for the dam foundation and casting of a few small blocks are also envisaged during these seasons. The main blocks of the dam are casted throughout three seasons between 2012 and 2014, during which the average volume of concrete placed per season is 80,000 m³. The maximum daily casted volume is expected to reach about 2000 m³. The completion of the crest and other finishing operations are envisaged during the last working season in 2015.

In addition to job site installations, it is foreseen to install an aggregate crushing plant and two concrete batching plants at the dam site. All material used for the preparation of the concrete comes from underground excavation of the powerplant and appurtenant galleries and is transported from the Limmern reservoir to Mutsee with the use of a cableway.

Preliminary tests have been carried out on aggregates coming from an exploratory tunnel in the powerhouse area. This allowed to design a concrete mix containing 150 kg/m³ CEM I and 100 kg/m³ of fly ash. Final testing to confirm the final concrete mix-design is currently under way.

Despite the fairly low average temperatures at the job site, a post-cooling of concrete with the use of coils is suggested. This procedure is limited to the lower lifts of the higher blocks, where the dam width is the largest. In fact, while the maximum temperature of the concrete should not be a problem during the hydration phase, numerical analyses indicate that the thermal gradient between centre and facing of the blocks could reach critical values during the winter months following casting. It is considered that cooling of the concrete is simpler and less expensive compared to other procedures such as thermal insulation of the blocks during winter months.

Post-audit of Alqueva reservoir's water quality: Lessons learned with the comparison between forecast and reality

P.A. Diogo, A.C. Rodrigues, P.S. Coelho & M. Almeida

New University of Lisbon, Faculty of Sciences and Technology, Department of Science and Environmental Engineering, Portugal

ABSTRACT: Eight years after the construction of the Alqueva dam in southern Portugal, creating the largest European artificial lake, a comparison is made between the water quality forecasts before the construction and the actual reservoir behavior. Water quality problems in the Portuguese-Spanish Guadiana basin have been a determinant issue hence one of the main discussion topics around the Alqueva project. The main goal of this study is to compare and discuss modeling results obtained before the existence of the reservoir with prototype observed data. This may contribute to learn a number of lessons. Alternative pump storage operation scenarios and reservoir filling period were some of the issues addressed before the dam was concluded, on the basis of predefined operation rules for the dam's hydraulic system and water quality monitoring data collected in the Guadiana river. Post-evaluation of simulation forecasts indicate that, if adequate assumptions are considered, reservoir modeling can indeed be used as a tool for dam project design analysis and the study of reservoir water quality issues enabling anticipatory measures towards an adequate water quality management.

1 INTRODUCTION

The Multipurpose Alqueva Project was developed for the Alentejo region, comprising irrigation, hydropower and urban water supply for a vast area in southern Portugal and also strategic water storage. First planned in 1957, the final construction decision was taken in 1995 and gates were closed in 2002. The project is yet under development as it includes water transfers among other reservoirs and most irrigation infrastructures are still under construction.

Considering its location in the Guadiana river, the Alqueva reservoir catchment area is mainly located in Spanish territory, enhancing the need for transboundary cooperation regarding the assurance of affluences (Guadiana river is highly regulated by a series of dams in Spain), both in terms of quantity and quality. Agreement was finally achieved in 1998 with the Albufeira Convention, addressing all water related activities with potential transboundary impacts.

Nutrient loading represents one major problem and eutrophication has in fact been recognized as a serious water quality problem. The Alqueva reservoir also shows evidence of nutrient related water quality problems, including oxygen depletion and algal blooms, leading to its designation in 2004 as a Sensible Area according to the Urban Waste Water Directive 91/271/EEC.

Dams are in fact, among the many factors leading to the degradation of watershed ecosystems, the main physical threat fragmenting and transforming aquatic and terrestrial ecosystems with a range of effects that vary in duration, scale and degree of reversibility (WCD, 2000). According to He et al. (2004) dam construction is considered the major factor contributing to significant modifications of river ecosystems. Thus the growing awareness of environmental and social issues involved in the construction and operation of hydropower facilities demands for an anticipatory debate of possible water allocations, for which scenarios of reduced or altered future river flows must also be accounted for (Lehner, 2005).

As for hydropower, the ideal conditions for electrical energy production can contribute to excessive algae growth, which may be considered one of the symptoms of eutrophication (Valle et al., 2008), one of the most serious problems affecting the quality of water in multireservoir systems (Sechi and Sulis, 2009). Water quality management is therefore a critical component of overall integrated water resources management and modeling can be used to assess future water quality situations resulting from different management strategies (Loucks and Van Beek, 2005).

According to Garrido et al. (2009) there are strong reasons for modeling and simulating: testing and optimizing the design of a system before its construction, preventing design errors, improving quality, reducing costs, evaluating performances and predicting behaviors.

The main goal of this study is to compare and discuss modelling results obtained before the existence of the reservoir with real data from the prototype. This may contribute to learn a number of lessons. First, it's important to perform a critical evaluation of the modelling options initially adopted, aiming the improvement of modelling strategies in future applications regarding reservoir water quality assessment. Second, it is relevant to make a post-evaluation of different issues like dam design, reservoir operation, monitoring and compliance with the international agreement or water resources policies carried out within the basin.

2 BACKGROUND

2.1 Study site

The Multipurpose Alqueva Project has been studied for a long time as a response to the severe drought problems affecting one of the largest regions in Portugal (Fig. 1). As an important agricultural area, water shortage has been a serious problem not only in terms of urban water supply but also in terms of economics as crops are consecutively depleted.

The Alqueva dam is located at the Guadiana river, which is about 810 km long, including 550 km in Spanish territory, corresponding to 83% of the river basin, which totals around 67,000 km². The Alqueva reservoir is considered the largest artificial lake in Europe, being 83 km long and with a surface area at maximum pool level of 250 km² (Diogo et al., 2008). It includes hydropower production with a pump storage scheme, enabled by an afterbay—Pedrógão. Pumped storage plants, in contrast to conventional ones, reuse water as after water initially produces electricity, it flows from the turbines into a lower reservoir and during off-peak hours some of the water is pumped back into the upper reservoir to be reused during periods of peak-demand (Mahmoud et al., 2004).

As 40% of Portuguese water resources drain from Spanish territory (Albergaria and Fidelis, 2006) the strategic value of the Alqueva project is obviously enhanced, not only in terms of water storage but also as a flow control infrastructure.



Figure 1. Location of Alqueva reservoir.

2.2 Previous modeling studies

First modeling results were reported by Rodrigues (1995) and were obtained during the environmental assessment studies. The one dimensional model WQRRS (HEC, 1978) was then used. This model implementation, more than associating pollution sources and expected reservoir water quality, allowed the establishment of reference water quality characteristics, including stable seasonal thermal stratification, this usually leading to a summer hypolimnion virtually isolated from the atmosphere (Marcé et al., 2006) and consequently oxygen depletion and phosphorous related eutrophication problems.

During a period of vivid public debate regarding the project, alternative solutions and dam project design, the two-dimensional water quality model CE-QUAL-W2 was implemented to simulate water quality under maximum pool levels scenarios of 147 m and 152 m (Diogo and Rodrigues, 1997). Also addressed at this time was the question whether multilevel abstraction for urban supply should be used and how pump storage operations could affect water quality.

In 2003, when reservoir elevation was about 147 m, Diogo et al. (2003) presented calibration for the first filling period of the Alqueva reservoir, between 2002 and 2003, but simulations were limited to temperature and dissolved oxygen. Following this study the first filling of the Pedrógão reservoir was also simulated (Diogo et al., 2004), aiming to evaluate water quality relationships in both reservoirs. As expected and considering that releases from the upstream reservoir are located deep into the water column, the downstream reservoir was directly affected by the upstream reservoir. These last simulations were though not included in the present analysis.

Following the adoption of the Water Framework Directive (WFD), the CE-QUAL-W2 model was calibrated for the Alqueva reservoir and used to evaluate effects on water quality resulting from potential phosphorous removal from urban waste water discharges in the Portuguese drainage area of the reservoir (Diogo et al., 2008).

3 METHODS AND DATA

3.1 Water quality model

CE-QUAL-W2 (here designated as W2) is a two dimensional, laterally averaged hydrodynamic model developed at the U.S. Army Corps of Engineers, considered best suited for relatively long and narrow water bodies exhibiting longitudinal and vertical water quality gradients (Cole and Wells, 2002). W2 models eutrophication processes such as temperature–nutrient–algae–dissolved oxygen–organic matter and sediment relationships and hydrodynamic calculations include predictions of water surface elevations, velocities and temperature (Ostfeld and Salmons, 2005).

Table 1. Main characteristics of Alqueva project.

<i>Alqueva Dam:</i>	
Height	96 m
Length	458 m
Maximum pool level	152 m
Total storage capacity	4 150 hm ³ (152 m)
Dead storage volume	1 000 hm ³ (135 m)
Surface area	250 km ² (152 m)
Reservoir length	83 km
Reservoir perimeter	1 160 km
Hydropower capacity	260 MW
<i>Multipurpose Alqueva project:</i>	
Pedrógão afterdam maximum pool level	84,8 m
Total irrigation area	115 000 ha
Total number of complementary dams	15
Main pumping stations	9
Secondary pumping stations	56

Implementation of the W2 model to the Alqueva system was subjected of successive improvements along the various studies. First applications only included the Alqueva reservoir which was conceptually represented as a grid of 20 layers and 46 segments, with 3 upstream branches, one withdrawal located at branch 3, one dam discharge and one back pumping represented as a tributary entering the reservoir at dam site.

According to Diogo et al. (2003) when calibration of the model during first filling of the Alqueva reservoir was pursuit, the grid resolution had to be increased to insure stability of the model. The fast changing volumes during this filling period resulted in model crashing and model grid was therefore changed to accommodate 75 segments and 83 layers.

Model grid was further incremented in 2004 (Diogo et al., 2004) in order to include the Pedrógão afterbay. Two additional branches were also included: main Pedrógão branch and Ardila river branch (Fig. 2). Filling of this smaller reservoir was then simulated but results were not compared with prototype data, as actual filling only took place in 2006.

3.2 Model performance evaluation approach

Typical modeling studies include model calibration, model verification and only then, scenarios simulation. This is the case when simulations are meant to analyze alternative scenarios regarding the forcing variables of an existent system under analysis. When modeling tools are used to study a non existent system calibration is not possible hence modeler's expertise assume more importance for the analysis of results. In this case, the modeler should be able to encompass in the simulation methodology a broad selection of alternatives regarding state variables and possible future scenarios, and results must be analyzed taking into account all the uncertainty associated with the required assumptions.

Project development has continued and both the Alqueva and Pedrógão reservoirs and respective hydraulic circuits are now fully operational. This means a great part of the simulations previously performed can now be reevaluated and results compared with observed data. The present work aims not only to achieve that comparison but also to assess previous conclusions and assumptions on which simulations were based on.

For that purpose previously forecasts are compared with observed field data, not as an objective evaluation of simulation results but more as a way to verify assumptions and considered scenarios, trying to determine which could now be considered the right options and the wrong ones. Future developments should include new simulations using alternative assumptions, limited to those which could have in fact been previously used.



Figure 2. Conceptual representation of the system.

Table 2. Historic mean monthly inflow to Alqueva (m³/s) (Diogo and Rodrigues, 1997).

	Jan	Feb	Mar	Apr	May	June	July	Aug	Sept	Oct	Nov	Dec
1982	274	45	21	9	2	1	1	2	3	2	26	4
1987	79	359	101	304	4	0	1	2	2	0	56	611

3.3 Data

During design, flows were designated according to historical flow records and operational stage of the hydraulic infrastructures. Water quality simulation scenarios result therefore from crossing historical hydrological year with operations stages (EDP, 1993). For the simulations carried out before 2002, records of 1982 and 1987 were selected as representative of dry and average hydrological years. Stages designated as 2001 (the project was delayed in relation to previously defined projects), referring to an operational stage without afterbay and as 2015, this describing a fully operational stage were then crossed with the historical flow data. These same scenarios were considered in all simulations developed before the first filling of Alqueva, in 2002 (Rodrigues, 1995, Rodrigues and Diogo, 1997, Diogo and Rodrigues, 2000).

Water quality monitoring at the Alqueva and Pedrógão reservoirs has been in course and continuously improved since 2002, including during the first filling periods. These data sets have been considered for simulations developed after 2002 (Diogo et al., 2003, 2004, 2006, 2008).

4 RESULTS AND DISCUSSION

4.1 Pump storage operation simulations before dam construction

As a part of the environmental impact studies carried out by Rodrigues (1995), the use of the WQRRS model was focused on the quality of the Alqueva reservoir and the operation of hydraulic system of the dam. Pump storage was then simulated using monthly flow values, enabling a first glimpse of what was then expected to be the future water quality in the Alqueva reservoir: typical behavior of temperate lakes with strong stratification occurring during warm periods.

Eutrophication problems were identified, associated with high nutrient inputs from the upstream inflows, mainly Phosphorous (P). The increase in nutrients leads to greater productivity of the water system which may lead to excessive increase in algal biomass or other primary producers such as macrophytes (Sechi and Sulis, 2009). As the Guadiana river basin is under the influence of a dry climate interrupted by significant strong precipitation events, periods of high flows represent the major source period of pollutants. Located in a strong agricultural region, these intense precipitation events enhance phosphorus transport into the river system via surface runoff, either as Particulate Phosphorus (PP) bounded to soil particles in connection with erosion or as dissolved phosphorus (Rode and Lindenschmidt, 2001).

First simulations of pump storage operation using the W2 model were presented by Diogo and Rodrigues (1997) and Rodrigues and Diogo (2000), and a possible positive effect was then mentioned as a result of high pumped flows: induced mixing of reservoir water may increase water temperature in deeper reservoir layers thus decreasing thermal stratification with consequent increase of dissolved oxygen. Although simulations showed thermocline collapse was not achieved, some water quality improvements were nevertheless anticipated, mainly when low flow scenarios were considered (Diogo and Rodrigues, 1997). These effects could nevertheless be localized in time as oxygen levels tend to decrease right after the back pumping period (Fig. 3) and its magnitude was considered dependent from operational flows in the hydraulic circuit.

It was also concluded that the use of selective withdrawals could be useful, but this suggestion was not considered in the final design. These results were obtained assuming back pumping would occur during the weekends (off peak time periods) and turbined flows during week days (high peak time periods). Also, the concentration of pumped flows during weekend determines a much higher effect at the upstream reservoir resulting from the associated reaeration effect. Results from this study haven't been reevaluated yet.

4.2 Pump storage operation simulations after initial filling of Alqueva

After the filling of the reservoir, new simulations of the pump storage scheme using W2 model were developed (Diogo et al., 2003, 2004), using inflow data from 2002 and 2003. For this purpose reservoir levels (Alqueva and Pedrógão) were assumed constant and upstream flows turbined downstream. Half of these volumes were discharged downstream and the other half

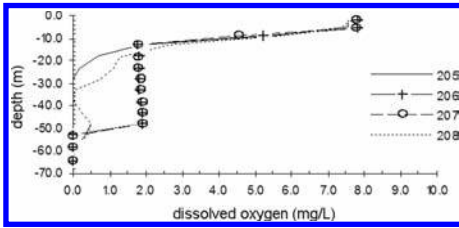


Figure 3. Dissolved oxygen showing variations induced by back pumping (days 206 and 207) from afterbay (Diogo et al., 1997).

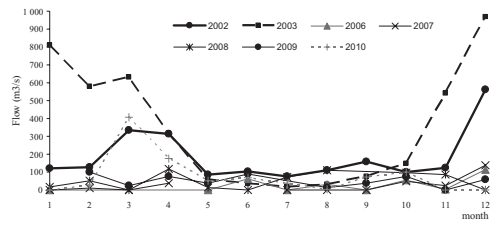


Figure 4. Simulated (2002 and 2003) and observed turbined flows at the Alqueva Dam.

Pump storage temperature (°C) simulations. Location: Alqueva, 1 km from dam. Input data from 2002/2003; field data from 2006/2007

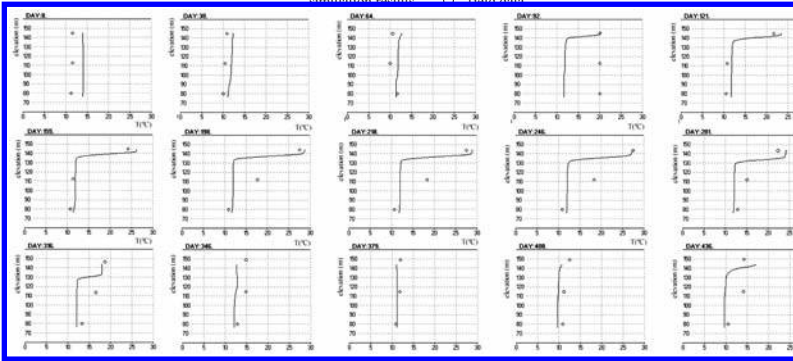


Figure 5. Pump storage simulations in 2004 and observed data in 2006/2006—Temperature.

pumped back into the Alqueva reservoir. Results were considered consistent with previous simulations, and back pumping associated to induced temperature elevation in deep reservoir layers.

Pump storage simulations were performed after the calibration of the W2 model for the period of first filling, which was yet not concluded by the end of 2004. According to Diogo et al. (2003, 2004) calibration results agreed with observed data for temperature, dissolved oxygen and phosphorous although unsatisfactory results were obtained for nitrogen.

Adequate assessment of these results was only made possible after pump storage operation of the Alqueva system was in fact implemented. This operation started in 2006, shortly after the Pedrógão dam was concluded and the reservoir filled (first filling also previously simulated but not included in the present study). For a post evaluation of the results presented in Diogo et al. (2003, 2004), one must certainly consider the simulated flow regimes and how they match with flows occurred during pump storage operation. Figure 4 shows that previously simulated turbined flows were much higher during winter months (December to March) than those later observed. For the rest of the year flows are similar. It is relevant to notice that main water quality influence from pump storage is expected to happen during the low-flow months.

This may be a reason for the significant similarity between simulated temperatures using flows from 2002/2003 and observed temperatures in 2006/2007 showed in Figure 5, although the model seems to overestimate summer stratification. Considering all the assumptions, results are considered quite satisfactory and potentially adequate for decision support.

Dissolved oxygen simulations did not perform as well as temperature (Fig. 6) as the model appears to have overestimated oxygen depletion with depth when compared with field data in 2006/2007. To better understand this situation results were also compared with data from 2004 (Fig. 7) where a much better agreement is observed between simulated and field data. Joint analysis of Figures 6 and 7 suggests the possibility that the impact of settled organic matter has significantly decreased between 2004 and 2006, resulting in the reduction of sediment oxygen demand. This could justify better accordance with field data collected in 2004

Pump storage simulations. Location: Alqueva, 1 km from dam. Input data from 2002/2003; field data from 2006/2007
 simulation results ○ - field data

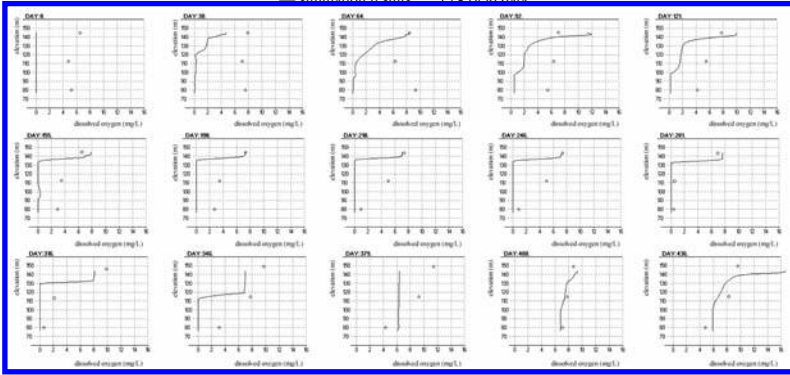


Figure 6. Pump storage simulations in 2004 and observed data in 2006/2007—dissolved oxygen.

Pump storage simulations. Location: Alqueva, 1 km from dam. Input data from 2002/2003; field data from 2004/2005
 simulation results ○ - field data

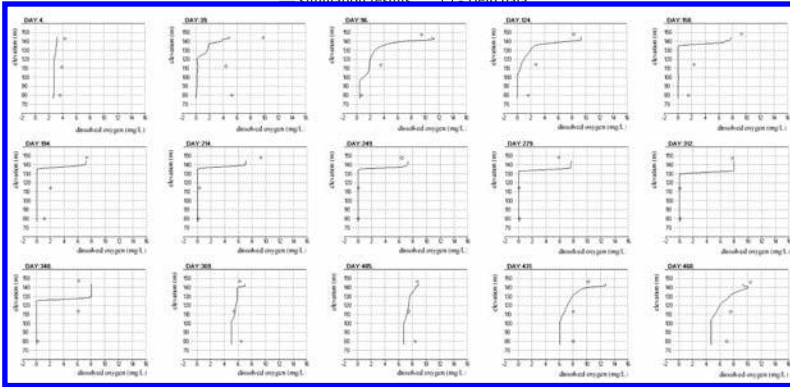


Figure 7. Pump storage simulations—2004—and observed data from 2004/2005—dissolved oxygen.

(Fig. 7), closer to the first filling period, as the model was previously calibrated for this initial period. The same effect was also observed with P.

5 CONCLUSIONS

Water quality problems have been a determinant issue around the Alqueva project. Nutrient loading and eutrophication have been in fact recognized as serious water quality problems. In times when hydropower and pump storage are regaining importance, fundamental problems that researchers and managers involved in dam construction will face in coming decades will be the adequate design of structures devoted to water quality supply and management (Marcé et al., 2010). For the case of the Alqueva project it was shown that modeling results obtained with W2 reasonably agree with observed data. Also, pump storage may play an important role on water quality management but adequate assessment of possible effects is yet to be established.

The ability of the CE-QUAL-W2 model to simulate the Alqueva reservoir and its afterbay Pedrógão has previously been established. With the present study it was demonstrated that, despite the relative scarcity of data, the use of simulation models may be a useful and reliable tool, enabling anticipatory measures towards an adequate water quality management, as long as adequate assumptions are taken into account during the design of the project.

Models are very often used as decision support tools, but results and conclusions drawn are seldom post evaluated. Future modeling studies may benefit from the identification of mistakes, wrong options or misjudged assumptions.

REFERENCES

- Albergaria, R., Fidelis, T. 2006. Transboundary EIA: Iberian experiences. *Environmental Impact Assessment Review*, 26, 7, October, 614–632.
- Cole, T.M., Wells, S.A. 2004. CE-QUAL-W2: A Two Dimensional, Laterally Averaged, Hydrodynamic and Water Quality Model, Version 3.2. User manual. Instruction Report E-95-1. U.S. Army Engineer Waterways Experiment Station, Vicksburg, Miss. USA, March.
- Diogo, P.A., Rodrigues, A.C. 1997. Two Dimensional Reservoir Water Quality Modelling Using CE-QUAL-W2, Conference Proceedings, Reservoir Management and Water Supply—an Integrated System, IAWQ-IWSA Joint Specialist Conference, Prague, Czech Republic, 19–23rd May.
- Diogo, P.A., Coelho, P.S., Almeida, M., Serrazina, N., Rodrigues, A.C. 2003. Simulação da qualidade da água durante enchimento da albufeira de Alqueva. 6 ° Simpósio de Hidráulica e Recursos Hídricos Países de Língua Oficial Portuguesa, Cidade da Praia, Cabo Verde, 10–13th November.
- Diogo, P.A., Coelho, P.S., Almeida, M., Serrazina, N., Rodrigues, A.C. 2004. Simulação da qualidade da água na albufeira de Alqueva: a fase de enchimento e a importância do contra-embose de Pedrógão; 8th National Environment Conference, Lisbon, Portugal, 27–29th October.
- Diogo, P., Fonseca, M., Coelho, P., Almeida, M., Mateus, N., Rodrigues, A.C. 2006. Reservoir Phosphorous Sources Evaluation and Water Quality Modeling in a Transboundary Watershed, 10th Int. Specialized Conf. on Diffuse Pollution and Sustainable Basin Management, Istanbul, Turkey, 18–22 September.
- Diogo, P., Fonseca, M., Coelho, P., Almeida, M., Mateus, N., Rodrigues, A.C. 2008. Reservoir Phosphorous Sources Evaluation and Water Quality Modeling in a Transboundary Watershed, *Desalination*, 226, 200–220.
- EDP, Electricidade de Portugal, S.A. 1993. Quantificação da Valia Eléctrica do Aproveitamento de Fins Múltiplos de Alqueva, EDP, Direcção Central de Planeamento, Porto, Portugal, September.
- Garrido, J., Zafra, A., Vázquez, F. 2009. Object oriented modelling and simulation of hydropower plants with run-of-river scheme: A new simulation tool. *Simulation Modelling Practice and Theory*, 17, 1748–1767.
- He, D.M., Zhao, W., Chen, L., 2004. The Ecological Changes in Manwan Reservoir Area and its Causes. Asian International Rivers Centre, Yunnan University, Kunming, Yunnan, China, Accessed on October 2010: <http://www.lancang-mekong.org/Upload/upfile/200563018926705.pdf>.
- HEC. 1978. Water Quality for River-Reservoir Systems. Computer Program Description, Hydrologic Engineering Center, United States Army Corps of Engineers, Davis California, USA.
- Lehner, B., Czisch, G., Vassolo, S. 2005. The impact of global change on the hydropower potential of Europe: a model-based analysis, *Energy Policy*, 33, 839–855.
- Loucks, D.P., Van Beek, E. 2005. Water Resources Systems Planning and Management—An introduction to Methods Models and Applications. UNESCO.
- Mahmoud, M., Dutton, K., Denman, M. 2004. Dynamical modelling and simulation of a cascaded reservoirs hydropower plant. *Electric Power Systems Research*, 70, 129–139.
- Marcé, R., Moreno-Ostos, E., Ordóñez, J., Feijoo, C., Navarro, E., Caputo, L., Armengol, J. 2006. Nutrient fluxes through boundaries in the hypolimnion of Sau Reservoir: expected patterns and unanticipated processes. *Limnetica*, 25, 527–540.
- Marcé, R., Moreno-Ostos, E., Garcia-Barcina, J.M., Armengol, J. 2010. Tailoring dam structures to water quality predictions in new reservoir projects: Assisting decision-making using numerical modeling. *Journal of Environmental Management*, 91, 1255–1267.
- Ostfeld, A., Salomons, S. 2005. A hybrid genetic—instance based learning algorithm for CE-QUAL-W2 calibration. *Journal of Hydrology*, 310, 122–142.
- Rode, M., Lindenschmidt, K.E. 2001. Distributed Sediment and Phosphorus Transport Modeling on a Medium Sized Catchment in Central Germany. *Physics and Chemistry of the Earth, Part B: Hydrology, Oceans and Atmosphere*, 26, 7–8, 635–640.
- Rodrigues, A.C. 1995. Aproveitamento Hidroeléctrico do Alqueva e Açude de Pedrógão—Estudos de qualidade da água. EDIA S.A., December.
- Rodrigues, A.C., Diogo, P.A. 2000. The Alqueva reservoir in the Guadiana river. Water quality simulation. II Assembleia Luso-Espanhola de Geodesia e Geofísica. Lagos. Portugal, 8–12th February.
- Sechi, G.M., Sulis, A. 2009. Dynamic attribution of water quality indexes in a multi-reservoir optimization model. *Desalination*, 237, 99–107.
- Valle, A.C.M., Aguiar, M.A.A., Cruz Jr, G. 2009. The impact of water quality as an environmental constraint on operation planning of a hydro-thermal power system. *Renewable Energy* 34. pp. 655–659.
- WCD—World Commission on Dams. 2000. Dams And Development—A New Framework for Decision-Making. The Report Of The World Commission on Dams, Earthscan Publications Ltd, London and Sterling, VA.

Keyword index

- Abrasion 403
ACRD 777
Aged dam 19
Aging 297
Alkali aggregate 171
Alkali content 163
Alkali-silica reaction 163, 187
Alluvial foundation 305
Alpine character 255
Alpine environment 867
Alpine reservoir 449
Anchor 195
Arch dam 59, 73, 287
Arch-gravity dam 99
Artificial intelligence 785
Asphalt facing 741
Avalanches 701
- Base layer 741
Behaviour 59
Benefits 791
Biodiversity 843
Buttress dam 51
Bypass tunnel 403
- Cascade reservoir 479
CFRD 65, 91, 569
Chaira Dam 661
Chancy-Pouigny Dam 637
Characteristics 725
Chemical expansion 115
Climate change 487, 509, 525, 551
Clogging drainage 51
Coagulation treatment 363
Compensation 835
Composite dam 645
Concrete dam 115
Conservation 807
Consolidation 263
Construction logistics 867
Construction site 733
Corrosion 195
Cost analysis 791
- Cost-benefit 857
Crack model 99
Crack monitoring 35
Cumulative damage 585
- Dam 203, 551, 629, 761
Dam deformation 79, 297
Dam heightening 229, 255
Dam monitoring 65, 73
Dam operation 517, 525
Dam project 769
Dam rehabilitation 271
Dam safety 137, 279, 677
Data evaluation 73
Decision making 153
Decision support 459
Delta formation 379
DEM 595
Design floods 677
Digital camera 35
Dry closure 849
Dynamic pressures 693
Dynamics 629
- Earth dam 271, 621
Earthquake 569, 585, 605, 621, 685
Earthquake motion 577
Ecology 829
Economic study 791
Elasto-plastic model 27
Embankment 653
Embankment dam 247, 305
Emergency 123
Environment 785
Environmental impact 395, 479, 821
Environmental screening 761
Ermenek Dam 3
Expanding concrete 179
- Fibre optic 107
Filter material 229
- Finite element 99
Fish 807
Flood control 479, 517, 525
Flood Hazards 685
Flood protection 653, 669
Flood retention 387
Flood risk 469
Flushing 437
Foamed asphalt 741
Foundation 263
Function test 421
Fuse plug 669
- Geo-centrifuge 645
Geo-membrane 203
Glacier retreat 449
Glacier shrinkage 497
Global warming 533
Gravity dam 867
Grouting 219, 263, 271
- Hazard assessment 717
Hazardous zone 753
Hydraulic modelling 669
Hydrological modelling 387
Hydrology 487
Hydro-peaking 857
Hydropower 449, 551
- Impounding 3, 27
Impulse waves 701
Internal erosion 305
IWRM 429
- Jet 693
Jinsha River 807
- Landscaping work 799
Landslide 701, 709, 725
Leakage 297
Leakage detection 107
Life safety 153
Liquefiable foundation 613
Long term 115

Maintenance 19
 Management 123
 Methodological approach 785
 MIKE 11 813
 MINERVE 459
 Mitigation measures 733
 Mitigation method 163
 Modelling 875
 Modification 769
 Monitoring 11, 107, 137
 Morning glory 239
 Morphology 345

 Natural hazards 733
 Natural reserve 821
 Network analysis 857
 Numerical analysis 321
 Numerical modelling 379, 709, 717

 Operation 91

 Pan Basin 541
 Pengshui HPP 821
 Permanent deformation 577
 Peruvian Dam 613
 Photographic measurement 35
 Plastic deformation 569
 Plunge pool 693
 PMF 533, 677
 Pollution 813
 Post-audit 875
 Pressure flushing 421
 Pump storage 211

 Rainfall prediction 517
 RCC 313, 559, 653
 Reactivity 171

 Regional cooperation 429
 Rehabilitation 247, 279, 287, 799
 Reinforcing technology 43
 Remedial works 51
 Renewable energy 211, 777
 Reputation risk 761
 Reservoir 3, 363, 701
 Reservoir accumulation 339
 Reservoir bottom 219
 Reservoir capacity 339
 Reservoir control 469
 Reservoir sedimentation 353, 403
 Reservoir sustainability 353
 Re-vegetation 799
 Risk analysis 19
 Risk assessment 661
 River ecology 835
 Rock treatment 239
 Rockfill dam 27, 79, 229, 585, 605

 Safety improvement 145
 Safety management 129
 Sediment concentration 421
 Sediment flushing 395
 Sediment removal 371
 Sediment replenishment 353
 Sediment supply 371
 Sedimentation 339, 345, 371, 379
 Sedimentation transport 413
 Sefidrud Dam 239
 Seismic coefficients 621
 Seismic performance 595
 Seismic safety 637
 Seismic stability 613
 Settlement 65

 Shaking Table 595
 Simulation model 849
 Site logistics 255
 Slab movement 79
 Slab rupture 91
 Slide 247, 629
 Sliding block 577
 Small hydropower 211
 SSC control 395
 Stability 195
 Storage HPP 387
 Storm maximisation 533
 Strengthening 287
 Submerged 219
 Supervision 137

 Tailings dams 849
 Taleghan Dam 753
 Technological innovation 777
 TGP 413, 725
 Tourism industry 753
 Transboundary river 429
 Transfer 345
 Tsunami 717
 Turbid water 363

 Unpredictable 59

 Value of life 153
 Vegetation restoration 769
 Versetal Dam 321

 Warning 123
 Water quality 813, 875
 Water resource 469, 487, 829
 Waterproofing 203
 Wave velocity 605
 Wetland 829

Author index

- Abe, S. 741
Ahmadi, H. 753
Ahmadi, N. 753
Alicescu, V. 777
Almeida, M. 875
Amberg, F. 115
Anastasopoulos, K. 621
Andrianopoulos, K.I. 621
Arai, N. 211
Archambeau, P. 469
Ariga, S. 19
Atukorala, U. 613
Auel, C. 403
Aufleger, M. 107
- Baldovin, E. 247
Baldovin, G. 247
Balissat, M. 99, 867
Bashash, A. 239
Bauder, A. 449
Berchtold, Th. 693
Bettzieche, V. 321
Bibi, M. 629
Bieri, M. 387
Boes, R.M. 403, 421, 449, 669, 701
Boillat, J. 459
Boldea, L.I. 187
Bondiolotti, F. 395
Bouckovalas, G.D. 621
Brenner, R.P. 551
Brignoli, M.L. 395
- Castelli, E. 395
Cazaillet, O. 437
Charif, H. 637
Charlwood, R. 179
Chen, J. 479
Chen, Y. 807
Cheng, Z. 709
Chong, L. 843
Cochet, P. 437
Coelho, P.S. 875
Constantinescu, A. 51
- Cottet, M. 487
Crosa, G. 395
- Daneshvari, M. 421
Dashui, G. 43
De Cesare, G. 421
Demny, G. 469
Deng, G. 91
Detering, M. 345
Detrembleur, S. 469
Dewals, B. 469
Dietler, T. 733
Diogo, P.A. 875
Doi, M. 297
Domaas, U. 717
Dornstädter, J. 107
Dunstan, M.R.H. 313
Durand, P. 849
- Erpicum, S. 469
Eslamian, F. 271
Espa, P. 395
Essyad, K. 653
- Faghihimohaddess, A. 239
Falvey, H.T. 661
Fang, Y. 813
Fankhauser, A. 421
Fankhauser, A.U. 387
Farinotti, D. 449
Feng, H.B. 725
Ferrière, M. 637
Freissinet, C. 487
Friedrich, M. 279
Fu, Y. 835
Fuchs, H. 701
Fujitsuka, Y. 595
- Gabl, W. 255
Gao, Y. 807
Garros-Berthet, H. 533
Gentili, G. 395
Glimsdal, S. 717
Godart, B. 187
- Goltz, M. 107
Gorišek, M. 791
Gostner, W. 857
Graff, B. 487
Guilbaud, C. 437
Güven, S. 3
- Ha, I.S. 645
Haeberli, W. 497
Hakoishi, N. 363, 371
Han, J. 709
Han, L. 171
Hao, W. 843
Harbitz, C. 717
Hartford, D.N.D. 687
Hattingh, L.C. 59
Hawson, H. 613
Heidari, A. 429
Heidarzadeh, M. 271
Heinrichs, P. 129
Hernández, J.G. 459
Herweynen, R. 195
Hirose, M. 769
Hofmann, T. 255
Homann, C. 469
Huang, R. 413
Huang, Y. 413
Huber, N.P. 469
Huggel, C. 497
Huss, M. 449
Hyakutake, T. 163
- Jacob, I.D. 123
Ivanovic, G. 785
Iwashita, T. 595
- Jia, J. 331
Jiang, G. 821
Jiang, Z. 709
Jie, Y. 171
Jiexiong, T. 43
Jikan, S. 27
Jiménez, F.A. 849
Jing, P. 843

- Jordan, F. 387, 497
 Jouvet, G. 449
 Justo, J.L. 849
- Kager, A. 857
 Kaleli, M. 263
 Kamiya, H. 525
 Kantoush, S.A. 353
 Kasai, T. 569
 Kasana, A. 137
 Katayama, M. 19
 Kawashima, F. 219
 Khamwongkhong, P. 79
 Kikuchi, T. 297
 Kimura, Y. 219
 Kirinashizawa, T. 595
 Kita, Y. 19
 Kloze, J. 339
 Kobelt, A. 145
 Koga, H. 163
 Koh, D.-K. 509
 Kohler, R. 3
 Kojima, H. 595
 Koliji, A. 99
 Kono, Y. 35
 Kosik, A. 339
 Kryżanowski, A. 791
 Kufeld, M. 469
 Künzler, M. 497
- Lançon, H. 11
 Lange, J. 469
 Le Clerc, S. 533
 Leroy, R. 187
 Lestuzzi, P. 637
 Li, H. 821
 Li, X. 829
 Li, Y. 821
 Lia, L. 799
 Lim, J.Y. 645
 Ling, W. 171
 Linortner, J. 3
 Lins, Y. 321
 Liu, D.Y. 725
 Løvholt, F. 717
 Lucarelli, C. 857
- Ma, J. 331
 Mairaing, W. 79
 Mangarovski, O. 107
 Marouk, M. 629
 Matsumoto, N.
 569, 577
 Matsumura, T. 525
 Mayor, P.A. 669
- Mellal, A. 99
 Meng, X. 829
 Messerklinger, S. 229
 Min, Y. 813
 Mirghasemi, A. 271
 Mitsuishi, S. 517
 Moll, S. 65
 Möller, G. 421
 Morales, A. 849
 Morelli, G. 247
 Müller, O. 287
 Müller, R.W. 145
 Myint Zaw, U. 559
- Naghibian, R. 239
 Nakamura, A. 569
 Nilipour, N. 653
 Nishigaki, M. 219
- Odeyer, C. 437
 Ohmachi, T. 605
 Ohmori, K. 27
 Ohta, H. 27
 Oosthuizen, C. 59
 Ozeki, T. 517
- Panenka, P. 137
 Papadimitriou, A.G. 621
 Park, J.-H. 509
 Peng, S. 541
 Person, J.-P. 637
 Pfister, M. 693, 701
 Piot, S. 11
 Piroton, M. 469
 Pougatsch, H. 145
 Premstaller, G. 857
 Previde Prato, A. 395
- Rodrigues, A.C. 875
 Rohrer, Ch. 559
 Romstad, B. 717
 Rose, T. 469
 Ross, K.A. 263
 Rossier, S. 637
 Ruan, B. 835
 Rühli, E. 669
 Ruud, A.M. 799
- Sakamoto, T. 163
 Sakurai, T. 371
 Sarghiuta, R. 51
 Sasaki, T. 577
 Sato, N. 27
 Satoh, H. 585
 Schanz, T. 321
- Schleiss, A.J. 387, 421, 459,
 497, 857
 Schmocker, L. 669
 Schüttrumpf, H. 345, 469
 Scrivener, K. 179
 Scuero, A.M. 203
 Seid-Karbasi, M. 613
 Seignol, J.-F. 187
 Seto, H. 741
 Shimamoto, K. 577
 Shimoyama, K. 585
 Shisheng, L. 171
 Shourijeh, P.T. 305
 Si-Chaib, A. 629
 Sinaba, B. 469
 Soda, H. 27
 Sonderegger, T. 145
 Sorgenfrei, A. 279
 Soroush, A. 305
 Soucy, B. 777
 Springman, S.M. 669
 Stahl, H. 73
 Stamatovic, M. 785
 Steiger, K.M. 559
 Stematiu, D. 51
 Stevovic, S. 785
 Straubhaar, R. 65, 229
 Sugiura, Y. 577
 Sumi, T. 353, 517
 Sun, L. 829
 Sun, Z. 807
- Tadger, J. 661
 Tahara, T. 605
 Takahashi, Y. 769
 Takemoto, N. 769
 Tang, X.L. 725
 Tang, X.L. 725
 Tardieu, B. 629
 Teal, M.J. 379
 Terrier, S. 497
 Thuang Han, U. 559
 Theiner, D. 421, 857
 Tognola, F. 867
 Tomida, N. 27
 Tournier, J.-P. 777
 Tsukada, T. 297
- Umino, H. 363
 Ursin, M.H. 387
 Üzüceck, E. 3
- Vallotton, O. 637
 Vaschetti, G.L. 203
 Vázquez, M. 849

Wada, S. 35
Wang, D. 807
Wang, H. 541
Wang, Y. 541
Watabe, H. 211
Watanabe, H. 163, 741
Weitbrecht, V. 669
Wickenhäuser, M. 255
Widmer, F. 449
Wita, A. 339
Wohnlich, A. 287

Xingping, L. 171
Xu, J. 479
Xu, Z. 91

Yamaguchi, Y. 585, 595
Yamamoto, A. 517
Yang, C. 479
Yin, Z. 479
Yoshida, H. 569
Yoshida, N. 525
Yoshizawa, K. 297

Zachia, D. 123
Zhang, J. 541
Zhang, X. 413
Zhao, C. 91
Zhao, H.Q. 577
Zhao, X. 807
Zheng, C. 331
Zhiqing, C. 171
Zielinski, P.A. 153, 677
Zimmerer, M.M. 321
Zwahlen, R. 761